Proceedings of the European Conference on Agricultural Engineering AgEng2021

4 – 8 July, 2021
Évora, Portugal

Proceedings of the European Conference on Agricultural Engineering AgEng2021

4 – 8 July, 2021
Évora, Portugal

Title: Proceedings of the European Conference on Agricultural Engineering AgEng2021

Edited by:
José Carlos Barbosa
Luis Leopoldo Silva
Patrícia Lourenço
Adélia Sousa
José Rafael Marques da Silva
Vasco Fitas da Cruz
Fátima Baptista

Please, use the following format for paper citation:
Author(s) (2021). Title. In: Barbosa, J. C., Silva, L.L., Lourenço, P., Sousa, A., Silva, J.R.,Cruz, V.F., Baptista, F., (Eds.) Proceedings of the European Conference on Agricultural Engineering AgEng2021. Évora, Universidade de Évora, pp. xxx-xxx.

Cite Proceedings as:
Barbosa, J. C., Silva, L.L., Lourenço, P., Sousa, A., Silva, J.R.,Cruz, V.F., Baptista, F., 2021. Proceedings of the European Conference on Agricultural Engineering AgEng2021, 4-8 July, Évora, Portugal. Universidade de Évora. 852 pp

Presentation

This proceedings book results from the AgEng2021 Agricultural Engineering Conference under auspices of the European Society of Agricultural Engineers, held in an online format based on the University of Évora, Portugal, from 4 to 8 July 2021.

This book contains the full papers of a selection of abstracts that were the base for the oral presentations and posters presented at the conference.

Presentations were distributed in eleven thematic areas: Artificial Intelligence, data processing and management; Automation, robotics and sensor technology; Circular Economy; Education and Rural development; Energy and bioenergy; Integrated and sustainable Farming systems; New application technologies and mechanisation; Post-harvest technologies; Smart farming / Precision agriculture; Soil, land and water engineering; Sustainable production in Farm buildings.

We would like to thank all the participants who made this conference possible, despite the constraints in which it took place.

Also thanks to the sponsors and members of the scientific committee, for their important and fundamental contribution to this congress

Organising Committee

Prof. Fátima Baptista	Universidade de Évora/MED - Chair
Prof. Adélia Sousa	Universidade de Évora /MED
Prof. José Carlos Barbosa	Instittuto Politécnico de Bragança
Prof. José Rafael Marques da Silva	Universidade de Évora /MED
Prof. Luís Leopoldo Silva	Universidade de Évora /MED
Dr. Patricia Lourenço	AgroInsider, Universidade de Évora /MED
Prof. Vasco Fitas da Cruz	Universidade de Évora /MED

Organization

Universidade de Évora
EurAgEng

Supporters

Scientific committee with reviewers of abstracts

Adélia Sousa	Universidade de Évora, MED, Portugal
Adriana Guimarães	University of Valladolid , Spain
André Aarnick	Wageningen University, The Netherlands
Andreas Meyer-Aurich	Leibniz-Institute for Agricultural Eng. and Bioeconomy, Germany
António Castro Ribeiro	Instituto Politécnico de Bragança, Portugal
António Comparetti	University of Palermo, Italy
António Dias	Universidade de Évora, MED, Portugal
Arlindo Almeida,	Instituto Politécnico de Bragança, Portugal
Athanasios Balafoutis	Institute for Bio-Economy & Agro-Technology of CERTH, Greece
Bill Day	Biosystems Engineering, UK
Claus Gron Sorensen	Aarhus University, Denmark
Coral Ortiz Sánchez	Polytechnic University of Valencia, Spain
Daniele De Wrachien	State University of Milan, Italy
Daniele Torreggiani	University of Bologna, Italy
Danilo Monarca	University of Tuscia, Italy
Diego Valera	University of Almeria, Spain
Edmund Lorencowicz	University of Life Sciences in Lublin, Poland
Evelia Schettini	University of Bari, Italy
Fabrice Béline	IRSTEA, France
Fátima Baptista	Universidade de Évora, MED, Portugal
Florentino Juste	Polytechnic University of Valencia, Spain
Francisco Ayuga Téllez	Polytechnic University of Madrid, Spain
Francisco Lúcio Santos	Universidade de Évora, MED, Portugal
Francisco Rodríguez Díaz	University of Almeria, Spain
Franz Handler	HBLFA Francisco Josephinum, Austria
George Papadakis	Agricultural University of Athens, Greece
Gonçalo Rodrigues	ISA, Universidade de Lisboa, Portugal
Guoqiang Zhang	Aarhus University, Denmark
Hugo Emmanuel	Centre de recherche Clermont-Auvergne-Rhône-Alpes, France
In-Bok Lee	Seoul National University, Republic of Korea
Ir Antti Peltola	Häme University of Applied Sciences, Finland
Isabel Ferreira	ISA, Universidade de Lisboa, Portugal
Ivo Hostens	European Society of Agricultural Engineers, Belgium
Jan Harms	Bavarian State Research Center for Agriculture, Germany
João Rolim Lopes	ISA, Universidade de Lisboa, Portugal
João Serrano	Universidade de Évora, MED, Portugal
Jorge Sánchez Molina	University of Almeria, Spain
José Blasco	Instituto Valenciano de Investigaciones Agrarias, Spain
José Boaventura-Cunha	Universidade de Trás-os-Montes e Alto Douro, INESC TEC,Portugal
José Carlos Barbosa	Instituto Politécnico de Bragança, Portugal
José Manuel Gonçalves	Instituto Politécnico de Coimbra, ESA, Portugal
José Maria Camara Zapata	University of Miguel Hernández, Spain
José Maria Tarjuelo	University of Castilla La Mancha, Spain
José Rafael Marques da Silva	Universidade de Évora, MED, Portugal
Karel Charvat	Czech Centre for Science and Society, Czech Republic
Luis Alcino Conceição	Instituto Politécnico de Portalegre, Portugal
Luís L. Silva	Universidade de Évora, MED, Portugal
Luis Manuel Navas	University of Valladolid, Spain
Maria do Rosário Cameira	ISA, Universidade de Lisboa, Portugal
Martin Kremmer	John Deere European Technology Innovation Center, Germany
Melynda Hassouna	INRAE, France
Miguel Angel Muñoz Garcia	Polytechnic University of Madrid, Spain
Nikolaos Katsoulas	University of Thessaly, Greece
Nills Bjugstad	Norwegian University of Life Sciences, Norway

Paolo Balsari	University of Torino, Italy
Patrícia Lourenço	AgroInsider, MED, Portugal
Patrizia Tassinari	University of Bologna, Italy
Peter Demeyer	Institute for Agricultural and Fisheries Research, Belgium
Peter Groot Koerkamp	Wageningen University, The Netherlands
Peter Schulze Lammers	University of Bonn, Institut fuer Landtechnik, Germany
Pierluigi Febo	University of Palermo, Italy
Pietro Picuno	University of Basilicata, Italy
Pilar Barreiro	Polytechnic University of Madrid, Spain
Rasmus Nyholm Jørgensen	Aarhus University, Denmark
Reiner Brunsch	Leibniz institute for agricultural engineering and bioeconomy, Germany
Ricardo Serralheiro	Universidade de Évora, MED, Portugal
Rosario Castro Abengoza	University of Leon, Spain
Sabine Schrade	Agroscope, Switzerland
Salvador Calvet	Polytechnic University of Valencia, Spain
Stefan Böttinger	University of Hohenheim, Germany
Steve Parkin	Biosystems Engineering, UK
Szalay Kornél	NAIK Institute of Agricultural Engineering, Hungary
Teresa Afonso do Paço	ISA, Universidade de Lisboa, Portugal
Teresa Batista	Universidade de Évora, MED, Portugal
Thomas Bartzanas	Agricultural University of Athens, Greece
Vasco F. Cruz	Universidade de Évora, MED, Portugal

Table of Contents

Sustainable Production in Farm Buildings 727

Artificial Intelligence, data processing and management

Deep Learning and IoT Technology Applied to Monitor the Growth of Tea Trees Indoors Under Artificial Lighting

Cheng-Cheng Huang, Hung-Wen Chen, Chung-Liang Chang[*]

Department of Biomechatronics Engineering, National Pingtung University of Science and Technology, Taiwan, R.O.C.

* Corresponding author. Email: chungliang@mail.npust.edu.tw

Abstract

The tea tree (Camellia sinensis (L.) O. Kuntze) was suitable for being grown under the humid and warm climate. This growth environment can result in a high risk of infestation of tea trees. The use of pesticide to prevent and control disease of tea tree was usually needed during cultivation. However, such a method also indirectly destroyed the soil quality and causes the environmental damage to land. This research proposed a multiple sensing and control system based on the artificial intelligence of things (A-IoT), which was applied to the cultivation and management of indoor tea seedlings with LED lighting. The system included multi-sensor modules, environmental control devices, and feature of tea leaves recognition devices. Among them, multiple sensors were used to collect environmental parameters of different cultivation areas. The environmental control device included an atomization device and circulating fans, which was utilized to adjust the temperature and humidity of each cultivation area. The recognition device was used to identify the traits of tea trees, including the number of leaves and the diseases of tea leaves. An image processing algorithm based on morphological operations was employed to identify three types of tea disease characteristics, including brown blight, white scab, and algal spot disease. The samples of tea leaves disease were provided to the YoLov3 network model for training. The recognizer had been implemented in an embedded device, where the average recognition rates of the number of tea leaves and diseases were 94% and 83%, respectively. The performance of the proposed system had been verified during the cultivation of two different varieties of tea trees. The obtained environmental data, number of tea leaves and diseases of tea could be used to analyze and evaluate the health of tea trees during seedlings cultivation. These data could also be displayed in the application (APP) interface of the mobile phone. Early warning information about the environment and the growth status of tea trees could also be displayed in this interface. Using this system could reduce the number of people entering and leaving the cultivation room and reduce the risk of tea trees infection. The proposed system could provide tea factory producers with a reference template for designing smart plant factories.

Keywords: Image processing, YoLov3 network, classification, plant factory, internet of things, tea disease.

1. Introduction

Extreme climate and environmental changes have caused uncertain crop harvesting periods and yields, which indirectly caused insufficient or excessive food, supply and even motivated consumers to pay attention to food safety issues. Food safety was most important item for those engaged in agricultural production. During the planting process of tea tree (Camellia sinensis (L.) O. Kuntze), many external disturbance factors affected its growth quality, such as pests and diseases, air or water pollution (Genshenga et al., 2019). In order to save costs, farmers often applied pesticides frequently to maintain good growth quality of tea trees. This would undoubtedly cause damage to the soil ecosystem as well as an additional source of environmental pollution.

In recent years, many studies have pointed out that plant factory can replace traditional agricultural farming methods, mass-produce crops and save resources (Bontsema et al., 2011), be friendly to the environment, and save carbon emissions. It's practice greatly reduced the environmental pollution caused by planting (Wang et al., 2020). Relying on the advancement of digital technology and chip process technology, wireless transmission and remote-control technology are fully developed. In 2010, PRIVA, located in the Netherlands, proposed an advanced greenhouse cultivation technology plan, which covered the establishment of a crop growth optimization system (PRIVA, 2010); therefore, in order to achieve the optimization and standardization of crop yield and quality, a more complete environmental control strategy should be introduced. In addition to basic environmental parameters, including air temperature, humidity (Kalia et al., 2020), luminosity, and carbon dioxide concentration (Quan et al., 2018), the physiological state of plants still needs to be considered.

In the past few decades, the Internet of Things (IoT) had been widely used in various fields and places (Tzounis et al., 2017), such as hospitals, factories, etc., especially in the industrial field (Dobrescu et al., 2019). In recent years, it has also been widely used in agriculture (Hajjaji et al., 2021), such as greenhouses (Wang et al., 2020), farmland or fish farms, and animal husbandry and other different types of fields (Popovic et al., 2017). The sensor receives data (Lee et al., 2019), the camera takes photos (Hatou et al., 2000), transmits this information through the network, and then sends signals to different actuators, such as fans, motors, or sprayers (Kumara et al., 2020). All environmental data from planting

to harvest was stored in the cloud, including temperature, humidity, light intensity, and even the location of the field (Kamilaris et al., 2017).

In addition, with the improvement of high-speed image processing technology, many artificial intelligence technologies have been introduced into industry (Zhang et al., 2018), people's livelihood and agricultural applications. Using image processing technology could perform non-destructive processing on images of different plant parts such as leaves (Chaudhary et al., 2012), flowers, and fruits, the image of the leaves could be used to observe the health of the plant from the image (Sahu et al., 2019), and to identify plant defects (Karmokar et al., 2015), such as diseases or insect pests (Ampatzidis et al., 2020). It could solve the quality problems of agricultural products early, which not only reduced human resources, but also assisted the accuracy of judgment (Kumar et al., 2018) in proposing the use of graphics algorithms, colors and Hough element transformation to calculate the number of leaves. If the plant to be detected was green and the shape was round or oval, this method could effectively extract the leaf area and calculated the number of leaves, with an accuracy of 95.4%. Chen et al. (2019) proposed a convolutional neural network model (CNN) to visualize tea disease identification, and developed a CNN model named LeafNet, which had feature extractor filters of different sizes. The characteristics of tea tree disease could be automatically extracted from the image. What's more, image processing technology could not only identify the current plant health status, it could also inform the monitoring system of information. The system drove the equipment to control environmental factors (Muangprathub et al., 2019), and could even predict the health status of crops in advance (Lokers et al., 2016).

This research proposes an IoT-based tea growth monitoring platform. The environmental factors in the cultivation space will compare the climate of the hilly land to simulate an environment suitable for tea growth. Different sensors are installed on the platform, which can detect the environmental factors of each cultivation area in real time. Through the Internet of Things technology, the environmental factors of each cultivation area are controlled within a certain range. At the same time, the cloud database was used to store the growth data of tee tree, and the user could also uilize the mobile application (APP) to view the environmental data in real time. The image monitoring device allows users to remotely observe the growth and appearance of tea trees. The YoLov3-based machine learning technology was employed to identify trait of tea tree and detect three types of diseases of tea leaves.

2. Materials and Methods

In order to monitor the environmental data of tea trees in different planting areas in real time, an artificial Internet of Things (AIoT) platform was established (see Figure 1). A small organic light-emitting diode (OLED) panel was used to display current environmental data in real time, including illuminance, temperature, humidity, CO_2, and soil moisture content. The embedded system was used to upload various environmental factors to the cloud database for storage. The data would be compiled by the ThinkSpeak open-source platform and presented as a useful curve. Through the curve, the user could observe whether the environmental changes were in line with expectations. This system could also drove dripper, water atomizers, CO_2 supplier and fans. In addition, users could use APP to view historical environmental data of different cultivation areas. In order to be able to automatically recorded the growth of tea trees for a long time, a camera device was installed on the side of each cultivation area, which can periodically photograph the side growth appearance of the tea seedlings and upload the images to the cloud at the same time. These images are used to detect tea diseases through image processing technology or YoLov3 network. The detection results can provide users to observe the relationship between environmental factors and diseases of leaves of tea.
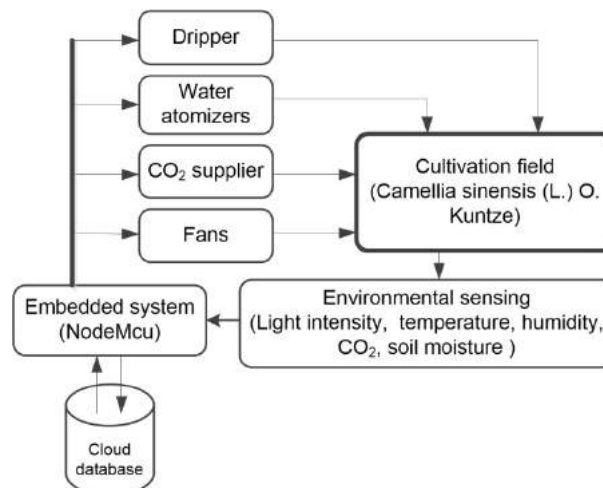
Figure 1. Flow chart of sensing system architecture.

2.1. Sensing and monitoring platform

a.   IoT-based environmental sensing

The platform included NodeMcu v3 (NodeMCU V3, Espressif Systems Co., Ltd., Shanghai, China), illuminance sensor module (BH1750FVI, ROHM CO., Ltd., Tokyo, Japan), environmental sensor (BME280, Bosch Sensortec GmbH, Reutlingen Germany), carbon dioxide sensor (MH-Z19B, Winsen Electronics Technology Co., Ltd, Zhengzhou, China) and capacitive soil moisture sensor. In order to view environmental data on site, each group of sensors was equipped with a small OLED display (Figure 2), which could display the data of each sensor. The bottom of the interface displayed the fan opening and closing status and the data upload time.
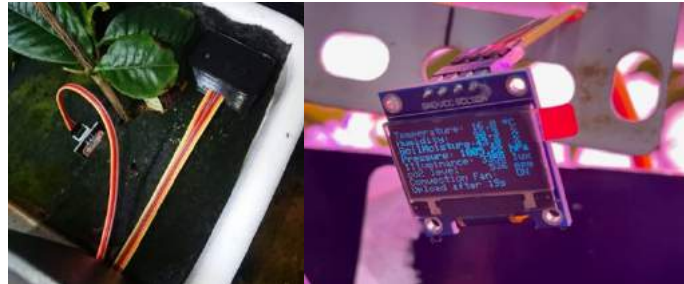
Figure 2. The position of the soil moisture sensor and sensor box (left); OLED display interface (right).

b.   Image capturing

In this experiment, four sets of embedded chips (Raspberry Pi Zero W, Raspberry Pi Foundation) were used to photograph the growth of all tea trees in each layer of the planting frame (Figure 3a), and four sets of cameras (Figure 3b) photographed the growth status of individual tea trees in each layer of the planting frame (Figure 3c), then upload the captured pictures and environmental data to Google Cloud hard drive and local server database SQL, the process was shown in Figure 4.

Figure 3. Camera placement for experiment; (a) Respberry pi (RPi Zero W, Respberry foundation) with camera installed on the side of the cultivation area, (b) Camera device (RPi 3B+, Respberry foundation) for photographing single plant, (c) Snapshot of seedling of tea tree.
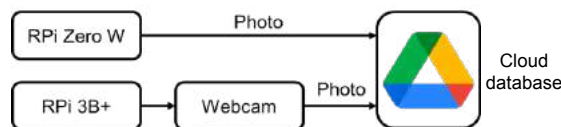
Figure 4. Image capture and storage process.

c.   Cloud storage and APP

Use ThingSpeak database was used to store sensing data. ThingSpeak can integrate heterogeneous environmental data and display graphs. The user can clearly see the distribution of environmental data, and the user can set the data display range to filter out unreasonable sensor data. ThingSpeak has two built-in functions, ThingHTTP and TalkBack. Among them, ThingHTTP sets the type of sensor data that needs to be notified, and TalkBack's notification robot can periodically send environmental data. Once the alarm system detects abnormal values, such as high/low temperature, humidity, and soil moisture. When the measured value exceeds the interval set by the user, the TalkBack robot will send a notification to the user (Figure 5).
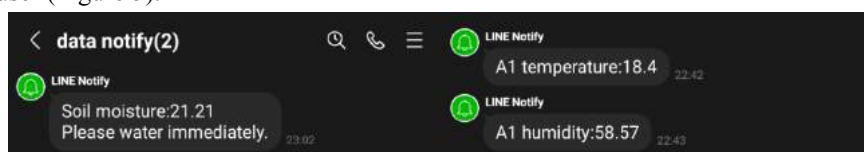
Figure 5. Alarm message notification (left); notify messages at a fixed time (right).

MIT App Inventor software was employed to design data display APP, users could view the data without using a browser. The program would display the environmental data, the latest sensed data would be displayed by numbers, and the fan's activation status would be displayed by lights. After slide down the APP interface, the change curve of each environmental data in the last 8 hours would be displayed (Figure 6).
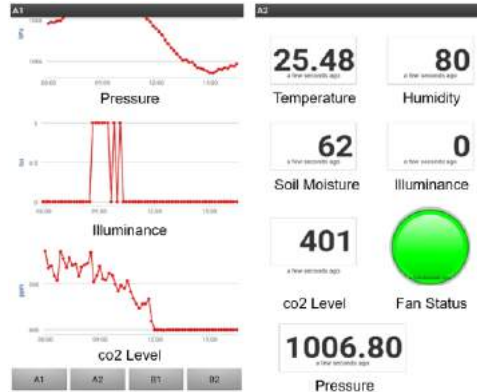
Figure 6. Switch node button at the bottom of the APP (left); Sensing data of a specific cultivation area (right).

d.　Environmental control

In order to provide a suitable tea tree planting environment, the air-conditioning devices was utilized to lower the indoor temperature, and design a fog-making device to regulate the humidity of the cultivation environment. The main principle of the fog generation was the application of ultrasonic waves to resonate with RO water, which allows liquid water to form mist-like water vapor particles with smaller particles (Figure 7).
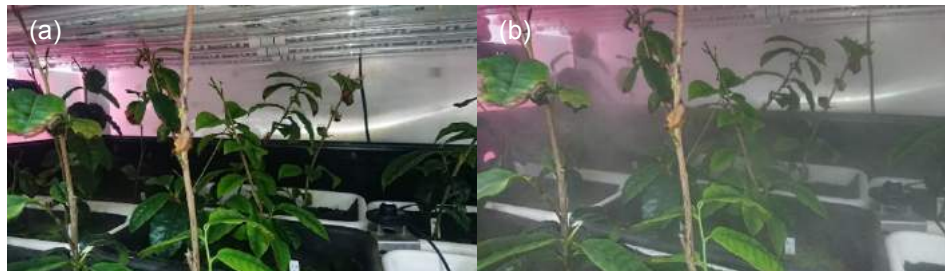
Figure 7.　The appearance of the cultivation area before and after atomization; (a) Before starting the atomization device, (b) After starting the atomization device.

In order to prevent the leaves of tea seedlings on the outlet side of the mist pipe from being excessively damp and causing diseases, a set of fans were installed on the side of the planting area. The fans could be started and stopped by the controller and a control rule library (Figure 8). This fan group could also reduce the temperature around the LED tube. In the Figure 8, the X-axis represents humidity, and the Y-axis was temperature. The yellow square indicated that when the temperature is too high and the humidity was too low, the water mist system and convection fan would be turned on; the green square indicated that only the water mist system would be turned on when the humidity was too low; the blue square indicated that the temperature and humidity were within the proper range, and there was no need to turn on the water mist system and the convection system. The pink area indicated that the humidity was too high, so start the convection fan to avoid condensation.
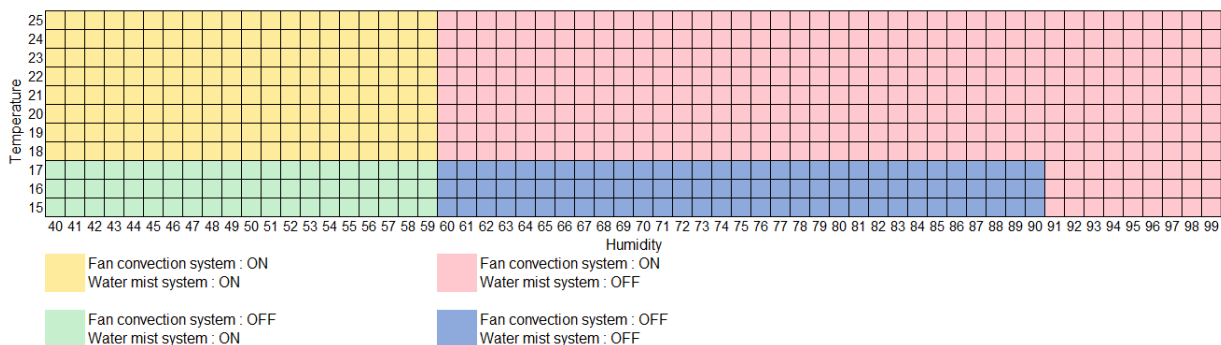
Figure 8. Actuator start and stop rules.

2.2. Identification methods of tea plant diseases

A. Image processing

The disease detection device can detect brown blight, leaf spot and white scab of tea trees. The image processing algorithm flow was shown in Figure 9. In order to improve the contrast and eliminate noise, we first preprocess the image. The main purpose was to enhance the object of interest in the image. This processing can improve the success rate of object recognition. Because the red, green and blue (RGB) images taken by digital cameras are easily affected by light, the image processing algorithm cannot detect object features. Therefore, we use Hue-Saturation-Value (HSV) color images (Sharma, 2003) to improve the success rate of object detection. First, the original RGB image was converted to HSV image, and then the image was masked and median filtering operation (Huang et al., 1979) to reduce the influence of noise on the image. However, the processed image still contains background or extraneous objects. Therefore, we use threshold segmentation method or adaptive threshold segmentation method to distinguish feature objects and background. This method was to first set the color space range value of each layer of HSV (the threshold setting principle can be defined according to the Otsu's method (Otsu, 1979)).

First, set the HSV detection threshold of the original image (orange: [11 43 46], [27 255 255], white: [0 0 221], [180 30 255]). Then, HSV conversion was used on the original image, and the converted image was subjected to median filter processing. After that, the image was binarized and the roundness detection method was used to determine whether it was algae leaf spot or white scab. The brown blight detection did not require the use of roundness detection.
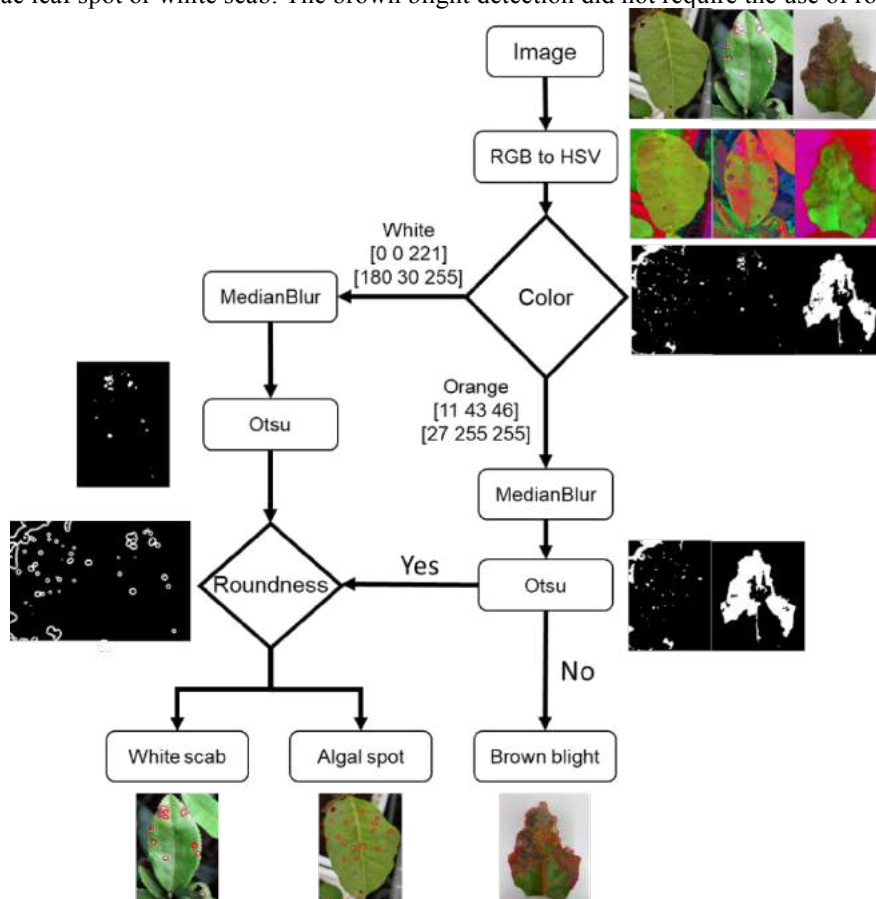
Figure 9. Disease of tea leaves recognition process

B. Object detection (YoLov3) in tea disease identification

At present, the most well-known deep learning tool was the YoLo toolbox designed by Joseph Redmon. The research team has successfully used the YoLov3 tool to perform AI recognition on red quinoa crops in the previous research (Chang and Chung, 2020). The steps of using YoLov3 deep learning for tea tree disease feature recognition include:

1) Collect samples

Collecting samples was a very important thing for deep learning training. Since this moment we mainly detect the characteristics of tea leaves, we are in the process of planting tea trees. The tea tree photos are collected every day, and the collected photos are classified into the early middle and late stages, and the diseased leaves are classified by

6

characteristics.

2)   Labeling of disease sample categories

Manual labeling was carried out based on the color, shape and extent characteristics of the leaf disease. The steps to label tea tree disease samples are as follows:

a) Input the image into the LabelImg labeling tool.

b) Set the storage location of the labeling result.

c) Carry out disease feature labeling, and add 3 types of disease names, namely brown blight disease, algal leaf spot and white scab disease.

3)   Adjust the internal parameters of YoLov3.

Before deep learning training, you need to adjust some parameters, you can do data adjustment in the settings file (.cfg), such as: photo rotation, exposure, saturation, hue, and Yolov3 learning rate. The parameters of this study are set as: (angle)=0, (exposure)=1.5, (saturation)=1.5, (hue)=0.1, and (Learning rate) =0.001.

4)   YoLov3 network training

This training was performed on Windows 10 and the environment with Python3, OPENCV, CUDA10.2, and CUDNN10.2. The training was performed on Intel Core i7-8750H@ 2.20GHz processor and GeForce GTX1050ti.

After the above steps are completed, the test samples can be used to identify disease features and evaluate its recognition performance.

3.   Results and Discussion

3.1. Implementation field and cultivated products

The experimental field was located in the laboratory in the Agricultural Machinery Center of the National Pingtung University of Science and Technology. There are two sets of three-dimensional planting racks in the laboratory, with a length of 120 cm, a width of 75 cm, and a height of 200 cm. There are three layers. The upper and middle layers of the planting racks were used for tea cultivation experiments of different varieties (Figure 10). Each cultivation area was equipped with an independent dimming controller, which can set the light quality, light and dark period and light quantum intensity. The target tea tree were Taicha No. 18 (commonly known as Ruby) and Assam tea seedlings provided by Songbaishan in Nantou, Taiwan. The viscous red soil was used as the cultivation medium.
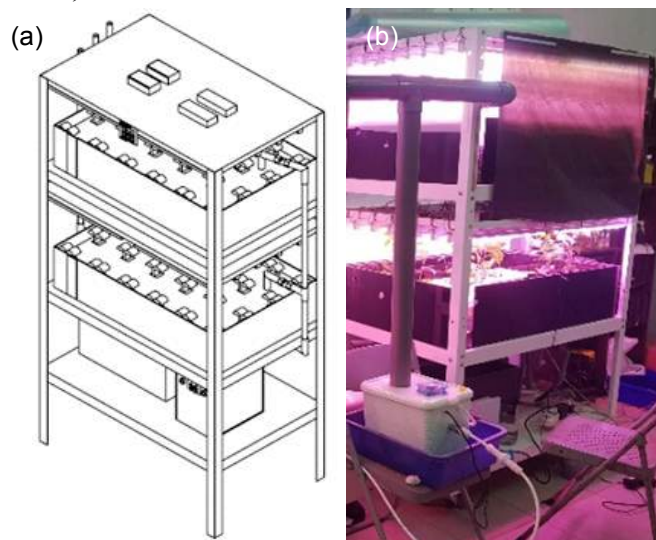
Figure 10. Planting frame for tea tree cultivation experiment; (a) rack prototype, (b) rack entity.
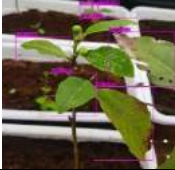
3.2. Disease identification results and accuracy performance analysis

Regarding the use of YoLov3 toolbox to detect the number of tea leaves, there are a total of 120 training samples, including 84 training samples and 36 test samples. The number of iterations was 6000, true positive (TP) was 98, false positive (FP) was 20, false negative (FN) was 16, and accuracy was 83%. Finally, take 5 test samples to evaluate the detection rate of the number of leaves, as shown in Table 1.

In terms of disease detection experiments, we used a total of 120 sample images, including 30 white scab, 30 algal leaf spot, and 60 brown blight samples for network training. We adopt the method of random sampling, and take out 84 training samples from 120 samples. The YoLov3 network had a total of 6000 iterations. The number of test samples

was 36. TP, FP, and FN were 70, 66, and 84, respectively. Figure 11 (a), (b), and (c) respectively illustrated the results of the camera with the Jenson Nano processor (Jenson Nano, NVIDIA company, CA, USA) for real-time recognition of brown blight disease, algal leaf spot, and white scab disease.

Table 1. Leaf identification result.

No.	Test sample #1	Test sample #2	Test sample #3	Test sample #4	Test sample #5
Leaves detection					
Estimated	3	7	8	8	11
Measured	3	8	9	8	12
Detection rate	100%	88%	89%	100%	92%
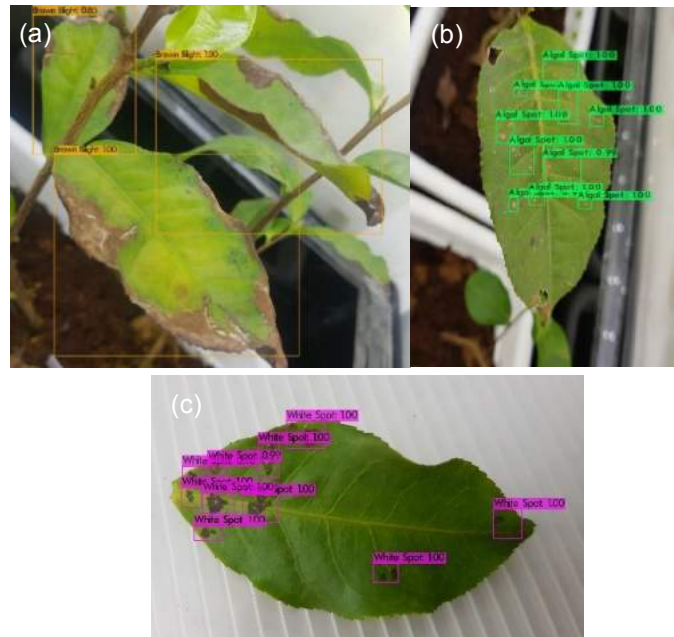
Figure 11. Results of using YoLov3 toolbox to detect tea tree diseases; (a) brown blight disease, (b)algal leaf spot, (c) and white scab disease.

3.3. Performance evaluation of environmental control

In the early period of the experiment, the experimenters frequently entered and exited the experimental site, which caused the overall temperature to be unstable. The hotter climate in July caused the compressor to run at full speed at noon, and the temperature dropped significantly after noon. In the latter part of the experiment, fan convection was added. The temperature change was small and stable (Figure 12).
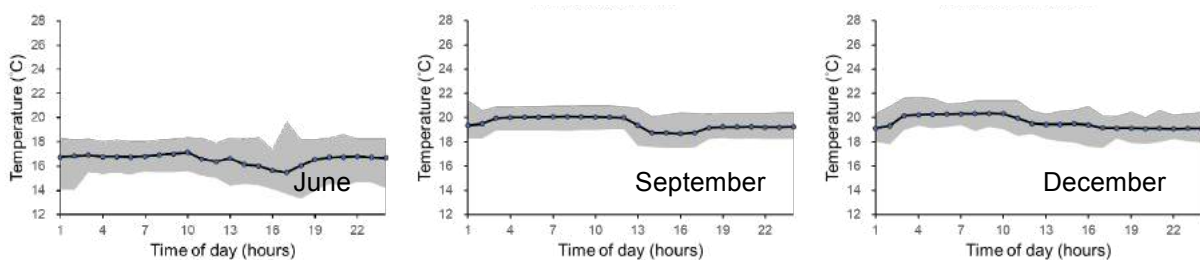
Figure 12. The temperature comparison of A1 area from June to December.

The water mist system has not been used in April, and the humidity was low. The water mist device was added in May, and the overall humidity increased a lot, often close to 100%, which caused moisture condensation and increased the number of diseased leaves. In June, shorten the opening time of fog generation to 10-12 and 16-18 to keep the humidity below 80%, and the number of diseased leaves began to decrease. A fan convection system was installed in August, the overall humidity change was significantly smaller, and the number of diseased blades dropped significantly. In September, the time was set to 16-24, during which the humidity increased significantly (Figure 13), and the number of diseased leaves rose again. In December, the actuator control rules were added to accurately control the humidity within a fixed range. Figure 14 shows the statistics of the number of diseased leaves in each month. It can be seen from this figure that the number of diseased leaves is highest from April to July, which is caused by the high light intensity and high humidity environment.
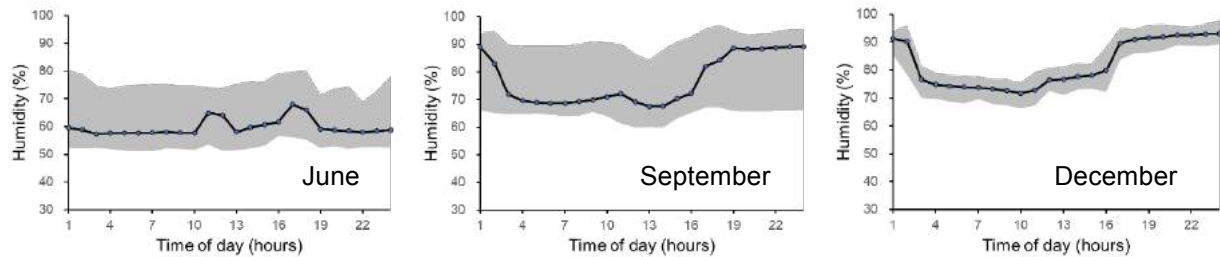
Figure 13. The humidity comparison of A1 area from June to December.
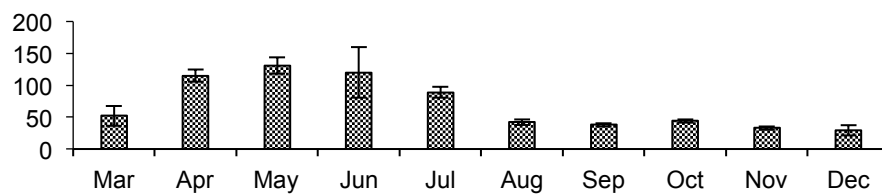
Figure 14. Statistics of diseased leaves in A1 area from March to December.

3.4. Discussion

In the process of using sensors to collect temperature and humidity data, there will be many external factors that interfere with the accuracy of the data. For example, factors such as the location or direction of the sensor and air convection. Experimental results show that the difference between the measured temperature and the temperature obtained by the sensor is within 0.5 degrees. The experimental results also show that the temperature control error is less than 1 degree. This is also because the temperature of the environment is controlled by the air conditioner, so its temperature change is relatively small. Conversely, the humidity control error can reach 20%. This also caused the tea tree leaves to be often infected by diseases during the experiment.

In terms of tea leaf disease detection, this tea leaf feature extraction experiment was divided into the use of image processing and deep learning technology to identify the number of tea leaves and the disease. First, we use image processing technology to detect three type of tea tree diseases. The image processing method was not used to identify the number of tea leaves. The reason was that when the LED plant light was turned on, there are multiple horizontal bars in the image obtained by the image capturing device, which makes it unrecognizable by this method. In the middle stage of cultivation, three types of diseases can be detected using deep learning technology. Using YoLov3 tool can distinguish different leaf diseases with only a small amount of samples, and the recognition rate was over 90%, but the problem of overfitting in the recognition of disease features still needs to be considered. Finally, the identification of different mixed diseases on the same leaf will be carried out in the future.

4. Conclusions

This research has completed the use of plant factories to cultivate tea seedlings, combined the IoT and machine learning technology to remotely monitor the growth of crops in plant factories. Planters do not have to frequently enter the factory to inspect the growth of tea trees, which helps to improve management efficiency. This platform can provide researchers with LED tea plant cultivation research. This platform has environmental and physiological data that can be collected to provide tea seedling growth modeling.

Acknowledgements

References

Ampatzidis, Y., V. Partel, L. Costa, 2020. Agroview: Cloud-based application to process, analyze and visualize UAV-collected data for precision agriculture applications utilizing artificial intelligence. Computers and Electronics in Agriculture. 174, 105457.

Bontsema, J., E. J. Henten, T. H. Gieling, G. L. A. M. Swinkels, 2011. The effect of sensor errors on production and energy consumption in greenhouse horticulture. Computers and Electronics in Agriculture. 79 (1), 63–66.

Chang, C.L., S. C. Chung, 2020. Improved deep learning-based approach for real-time plant species recognition on the farm. In *12th IEEE/IET International Symposium on Communication Systems, Networks and Digital Signal Processing*, Porto, Portugal, July 20-22. http://dx.doi.org/10.1109/CSNDSP49049.2020.9249558.

Chaudhary, P., A. Chaudhari, A. N. Cheeran, S. Godara, 2012. Color transform based approach for disease spot detection on plant leaf. International Journal of Computer Science and Telecommunications. 3 (6), 65–70.

Chen, J., Q. Liu, L. Gao, 2019. Visual tea leaf disease recognition using a convolutional neural network model. Symmetry. 11 (3), 343.

Dobrescu, R., D. Merezeanu, S. Mocanu, 2019. Context-aware control and monitoring system with IoT and cloud support. Computers and Electronics in Agriculture. 160, 91–99.

Genshenga, H., Y. Xiaoweia, Z. Yana, W. Mingzhuba, 2019. Identification of tea leaf diseases by using an improved deep convolutional neural network. Sustainable Computing: Informatics and Systems. 24, 100353.

Hajjaji, Y., W. Boulila, I. R. Farah, I. Romdhani, et al., 2021. Big data and IoT-based applications in smart environments: A systematic review. Computer Science Review. 39, 100318.

Hatou, K., T. Takeuchi, Y. Hashimoto, 2000. Image Database for the Remote Control of Plant Factories in the Internet Age. IFAC Proceedings Volumes. 33 (19), 309–314.

Kalia, P., M. A. Ansari, 2020. IOT based air quality and particulate matter concentration monitoring system. Materials Today: Proceedings. 32 (3), 468-475.

Kamilaris, A., A. Kartakoullis, F. X. Prenafeta-Boldu, 2017. A review on the practice of big data analysis in agriculture. Computers and Electronics in Agriculture. 143, 23–37.

Karmokar, B. C., L. U. Hannover, M. S. Ullah, M. K. Siddiquee, K. Md. R. Alam, 2015. Tea leaf diseases recognition using neural network ensemble. International Journal of Computer Applications. 114 (17), 27–30.

Kumar, J. P., S. Domnic, 2018. Image based leaf segmentation and counting in rosette plants. Information Processing in Agriculture. 6 (2), 233–246.

Kumara, A., V. Singh, S. Kumar, S.P. Jaiswal, V. S. Bhadoria, 2020. IoT enabled system to monitor and control greenhouse. In National Conference on Functional Materials: Emerging Technologies and Applications in Materials. Greater Noida. India, December 29.

Lee, S. Y., I. B. Lee, U. H. Yeo, R. W. Kim, J. G. Kim, 2019. Optimal sensor placement for monitoring and controlling greenhouse internal environments. Biosystems Engineering. 199, 190–206.

Lokers, R., R. Knapen, S. Janssen, Y. Randen, J. Jansen, 2016. Technoeconomic evaluation of urban plant factories: The case of basil (Ocimum basilicum). Science of The Total Environment. 554-555, 218–227.

Muangprathub, J., N. Boonnam, S. Kajornkasirat, N. Lekbangpong, et al., 2019. IoT and agriculture data analysis for smart farm. Computers and Electronics in Agriculture. 156, 467-474.

Popovic, T., N. Latinovic, A. Pesic, Z. Zecevic, et al., 2017. Architecting an IoT-enabled platform for precision agriculture and ecological monitoring: A case study. Computers and Electronics in Agriculture. 140, 255–256.

Otsu. N., 1979. A threshold selection method from gray-level histograms. IEEE Transactions on Systems, Man, and Cybernetics, 9(1), 62–66.

Quan, Q., X. Zhang, X. Z. Xue, 2018. Design and Implementation of a Closed-Loop Plant Factory. IFAC-PapersOnLine. 51 (17), 353–358.

Sahu, S. R., C. S. Panda, 2019. A review on leaves diseases segmentation and classification techniques. International Journal of Scientific Research in Science and Technology. 6 (3), 132–140.

Tzounis, A., N. Katsoulas, T. Bartzanas, C. Kittas, 2017. Internet of things in agriculture, recent advances and future challenges. Biosystems Engineering. 164, 31–48.

Wang, J. Z., M. Z. Chen, J. S. Zhou, P. P. Li, 2020. Data communication mechanism for greenhouse environment monitoring and control: An agent-based IoT system. Information Processing in Agriculture. 7 (3), 444–455.

Wang, Z. X., W. Wei. 2020. Effects of modifying industrial plant configuration on reducing air pollution-induced agricultural loss. Journal of Cleaner Production. 277 (20), 124046.

Zhang, Q. C., L. T. Yang, P. Li, 2018. A survey on deep learning for big data. Information Fusion. 42, 146–157.

Improvement of Gas Emission Models for a Naturally Ventilated Dairy Barn by Using Supervised Machine Learning

Sabrina Hempel [a,*], Julian Adolphs [a], Niels Landwehr [a,b], Dilya Willink [a], David Janke [a], Thomas Amon [a,c]

[a] Leibniz Institute for Agricultural Engineering and Bioeconomy, Potsdam, Germany

[b] Department of Mathematics, Natural Sciences, Economics and Computer Science, University of Hildesheim, Hildesheim, Germany

[c] Department of Veterinary Medicine, Institute for Animal and Environmental Hygiene, Freie Universität Berlin, Berlin, Germany

* Corresponding author. Email: shempel@atb-potsdam.de

Abstract

Agricultural emissions threaten the environment and the health of animals and humans. The design of efficient emission reduction strategies requires representative emission estimates, whose quality depends on the time and duration of measurements and the estimation approach. Regression is a common tool to derive long-term emission values from short-term measurements. Our main objective was to evaluate the potential added value of applying supervised machine learning algorithms for regression tasks (i.e. multilinear regression, ridge regression, artificial neural network and gradient boosting) given common temporal measurement strategies for ammonia and methane emissions. We based our study on a set of about 10 months of hourly emission measurements derived from a naturally ventilated dairy building in Northern Germany by CO_2 balancing. We found that in general the standard multilinear regression performed well, but was very sensitive to the selection of training data. Ridge regression and in particular gradient boosting could improve the robustness of the fit, while artificial neural networks were barely better, but much slower than the ordinary multilinear regression. For ammonia emissions best precision and accuracy were obtained when working with non-normalized data, while for methane emissions normalization with median and interquartile range resulted in the best predictions. In both cases, the gradient boosting predictions were least sensitive on the selection and normalization of the training data. In conclusion, gradient boosting can be a valuable approach to estimate long-term emission values such as annual emission factors.

Keywords: multilinear regression, regularization, artificial neural network, gradient boosting, emission factor estimation

1. Introduction

Airborne emissions from agriculture contribute considerably to the global air pollution, which impairs not only the environment, but also animal and human health (Grossi et al. 2019; Ginoux et al. 2012). On average more than half of the global air pollution caused by agriculture is associated to some degree with livestock husbandry, in particular with cattle husbandry.

Efficient emission reduction strategies in first place require representative emission estimates, but the timing of measurements used for model training as well as the selected regression and preprocessing approach can strongly affect the precision and accuracy of this emission estimate (Hempel, Adolphs, Landwehr, Janke, et al. 2020). With the increasing availability of data, machine learning is more and more used in the agricultural context, not only for classification but also for regression tasks (Arulmozhi et al. 2021; Lee et al. 2019; Hempel et al. 2019). The estimation of emission factors, however, still mainly relies a basic statistical assessment of short-term measurements (i.e., weighting and averaging) and ordinary multilinear regression (Ngwabie et al. 2014; Schrade et al. 2012).

The main objective of our study was to evaluate the potential added value of applying supervised machine learning algorithms for regression tasks based on common temporal sampling and preprocessing strategies for ammonia and methane emissions. This study focusses on similarities and differences in the projection of those two gases and is a follow-up on previously published results for the individual gases (Hempel, Adolphs, Landwehr, Willink, et al. 2020; Hempel, Adolphs, Landwehr, Janke, et al. 2020).

2. Materials and Methods

We considered long-term measurements of ammonia and methane concentrations from a naturally ventilated dairy cattle building in Northern Germany. Our dataset, which is publicly available, contains about 10 months of hourly gas concentration measurements as well as the ammonia and methane emission values derived from those concentrations by CO2 balancing. In addition, wind speed and direction measured were on the building's roof and air temperature was measured next to the building. Those additional variables were further used as features for the training of our regression models.

We considered 27 scenarios of temporal sampling which differed in the number and distribution of measurement

periods over the seasons as well as in the length of the individual measurement periods as illustrated in Table 1. In total, we considered 30 realizations of each scenario for the model evaluation, which we performed in the framework of a nested crossvalidation. Each time one period was kept for calculating the test error in the outer crossvaldiation loop and one period was kept for calculating an evaluation error in the inner crossvalidation loop, which was used for hyperparameter tuning when ever needed. The remaining part of the selected data was used for model training, while the non-selected data were used to calculate an extrapolation error.

Table 1. Temporal sampling scenarios. Given each scenarios constraint 30 training data sets were selected.

Index (duration of measurement days varies from 1 day to 7 days to 14 days)	Transition Seasons (Nov, Dec, Mar, Apr, May)	Winter Season (Jan, Feb)	Summer Season (Jun, Jul, Aug)	Total Number of measurement periods
1 – 3	1	1	1	3
4 – 6	2	1	1	4
7 – 9	2	0	2	4
10 – 12	3	0	1	4
13 – 15	2	2	2	6
16 – 18	3	1	2	6
19 – 21	4	1	1	6
22 – 24	4	0	2	6
25 – 27	5	0	1	6

We considered up to 9 input features. The first six coming from the time of day, the time of year and the wind direction as sine and cosine transformed features. The others were wind speed, air temperature and in some trials, the squared air temperature. Potential output features were the emission value or its natural logarithm.

In the following we compare the performance of 4 regression approaches: Standard Multilinear Regression with least square fitting, Ridge Regression (i.e. least square fitting with regularization), Gradient Boosting as an example of ensemble methods and an artificial neural network with backpropagation and hyperparameter tuning.

Further details on the dataset, the scenarios, the cross-validation setup and the regression approaches can be found in preceding publications (see for example (Hempel, Adolphs, Landwehr, Willink, et al. 2020)). In contrast to the analysis in those publications, here we focus on the effect of feature selection and normalization on the predictive performance of the different regression approaches. We consider the following six settings:

First, the ammonia standard case. This reflects the most common procedure in current literature on empirical ammonia modelling. This means almost no pre-processing except for some basic outlier removal. In particular, data was not normalized in this case. The output feature was the log-transformed ammonia emission value. The square of air temperature was not included as an input feature here.

Second, the normalized ammonia case. As data normalization is usually recommended to improve the quality of regression models, we used the robust scaler (i.e., remove the median and divide by the interquartile range) to normalize all features before conducting the regression. Except for the normalization the set of features was the same as in the first case.

Third, the data-driven ammonia case. Here, we tested what happens when we neglect our physio-chemical knowledge of the emission process and focus only on the scatter plots of the different variables implying a different set of features, which actually makes more sense for methane rather than for ammonia. In this setting the squared air temperature was included as an additional input feature and the untransformed ammonia emission value was considered as output feature. As in the second case all features were normalize with the robust scaler before we conducted the regression.

Fourth, the non-normalized methane case. Here the same set of input features as in case three was used, but without data normalization. The output feature was the methane emission value (also non-normalized)

Fifth, the normalized methane case. The same set of features was used as in the previous case, but with applying the robust scaler on all features.

3. Results and Discussion

3.1. Ammonia

First thing we noticed about the ammonia standard case shown in Fig. 1 was that for most scenarios multilinear regression works in principle well, but the quality of the prediction strongly depends on the selected training data. Particularly, scenarios with four measurement periods and no winter measurements (scenarios 7-11) tended to strongly

overestimate the ammonia emission. This is in line with the literature, which suggests that there is very little emission of ammonia under cold and calm environmental conditions, which are typical for winter season. A recent literature review came to the conclusion that the ammonia emissions from naturally ventilated barns increase by 1.47 g cow^{-1} d^{-1} per degree air temperature (ºC) and by 0.007 g cow^{-1} d^{-1} per 100 m^3 h^{-1} cow^{-1} (Sanchis et al. 2019). Moreover, Samer et al. reported for the same barn ten years ago ammonia emission rates of 2.9 g h^{-1} LU^{-1} derived from winter measurements and about 3.7 g h^{-1} LU^{-1} derived from summer measurements (Samer 2011b; Samer 2011a). In consequence, taking into account periods reflecting the spectrum of annual temperature and ventilation conditions can be expected to result in more accurate and robust emission estimates. We further observed that the sensitivity on the training data could be considerably reduced using the other regression approaches than ordinary multilinear linear regression. However, ridge regression tended to a systematic underestimation of the emission factor (probably because it dampens the influence of extreme conditions in the regression). ANN's quality strongly depended on the hyperparameter tuning. In order to reach a quality as shown in the figure considerably longer computation time was needed when with the other regression approaches.
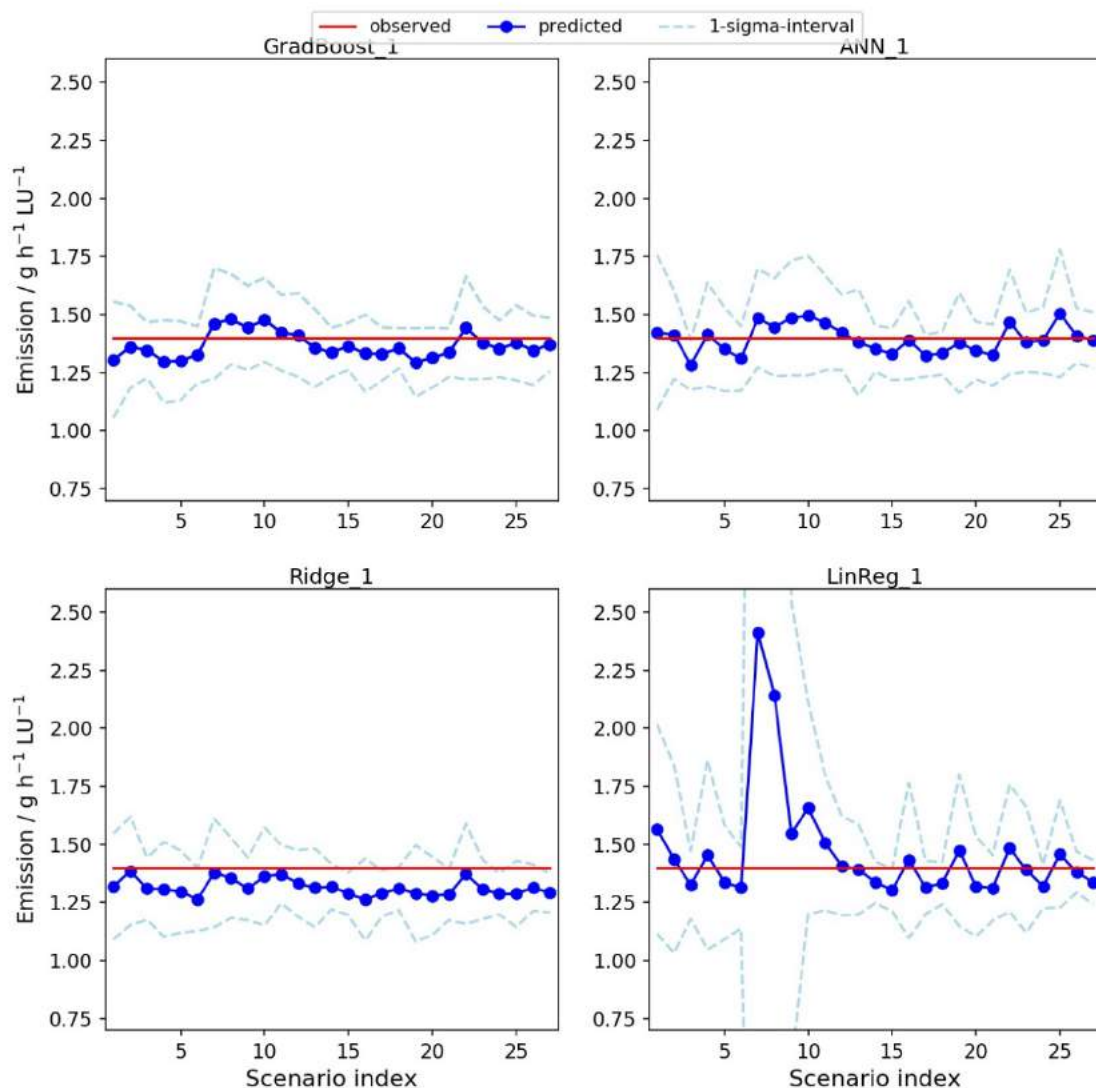
Figure 1: Estimated average ten month emission value based on 27 different scenarios for sampling training data using the ammonia standard case (i.e., no data normalization and logarithmized output feature). The dashed line indicates the variability over 30 realizations of each scenario. The red line marks the actual temporal average when considering the whole ten month dataset.

When we considered the regression results based on the normalized data we observed that for the aggregated ammonia emission value the predictive performance of the regression model was not improved in general (see Fig. 2). While the systematic bias in the rigde regression could be slightly reduced, the artificial neural network performed even worse on the normalized dataset than on the non-normalized. Multilinear regression and gradient boosting were barely

affected by the normalization procedure.
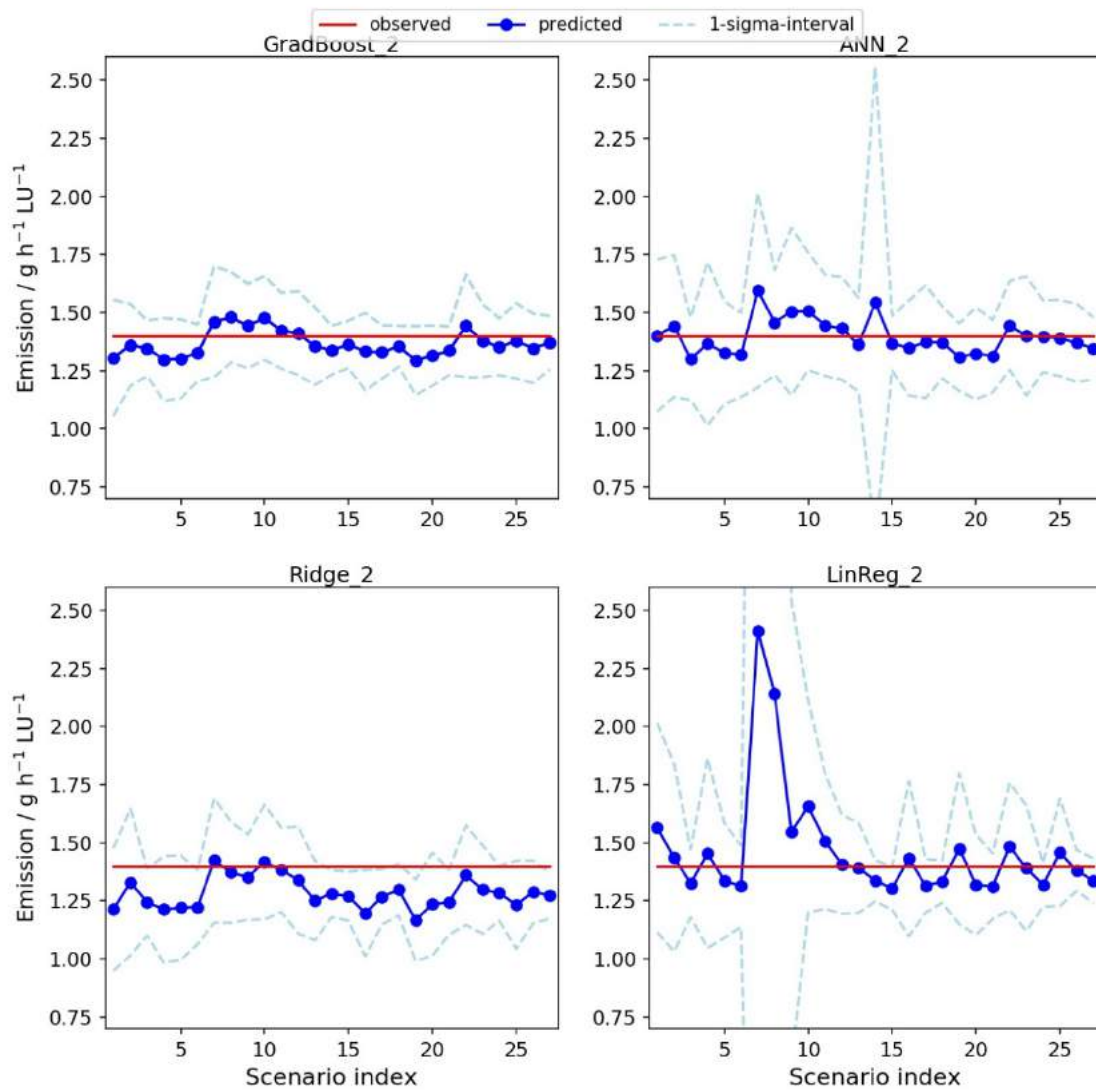
Figure 2: Estimated average ten month emission value based on 27 different scenarios for sampling training data using the normalized ammonia dataset (i.e., data normalization with median and interquartile range and logarithmized output feature). The dashed line indicates the variability over 30 realizations of each scenario. The red line marks the actual temporal average when considering the whole ten month dataset.

Using the methane analogue feature setting (again with normalized features) for ammonia brought some improvement for individual scenarios particularly with the multilinear regression and the ridge, but the overall performance for the artificial neural network (particularly for the scenarios with less training data) was still worse than with the standard feature setting (compare Fig. 1 and 3). Again the performance of gradient boosting was least affected.
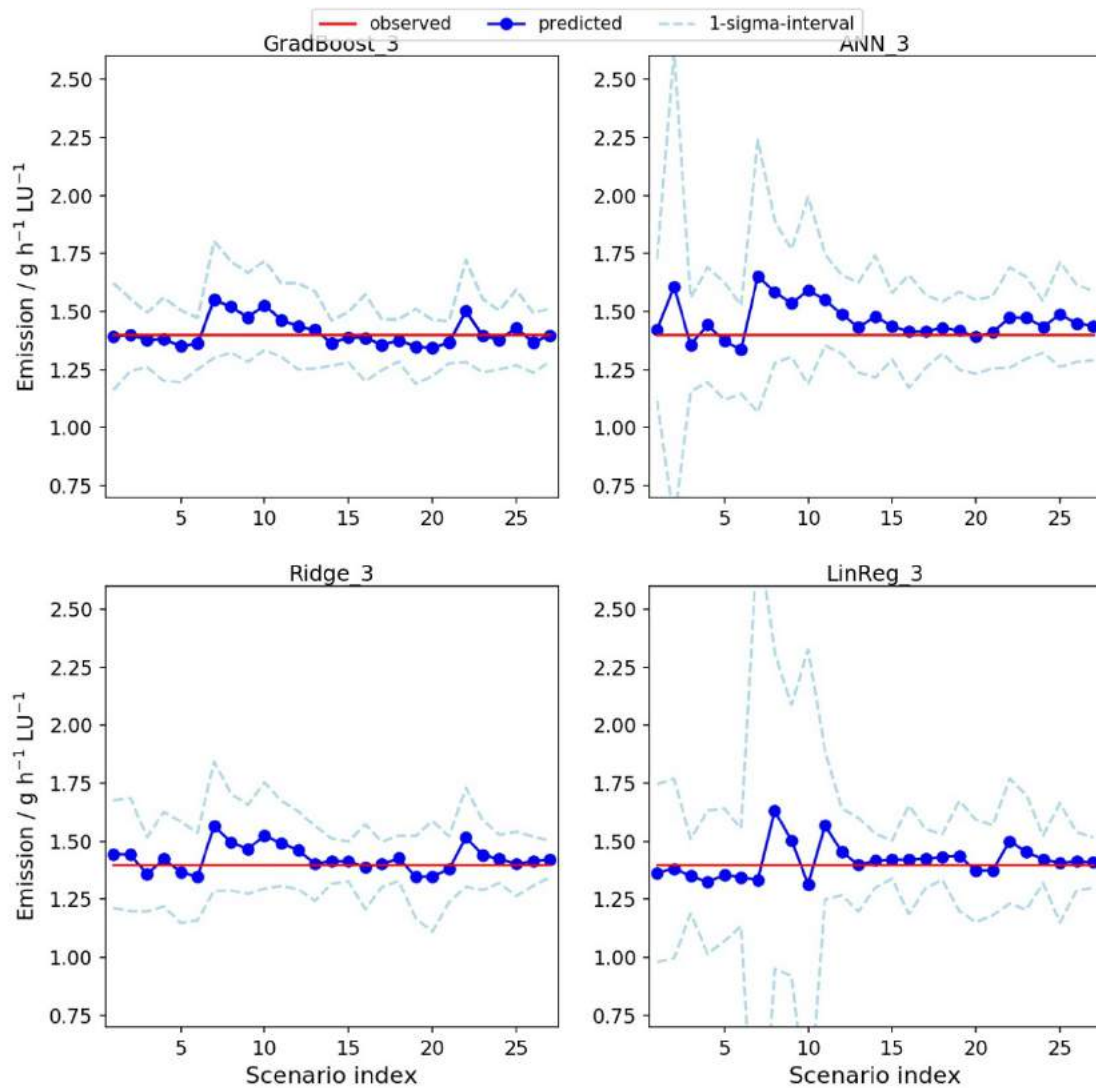
Figure 3: Estimated average ten month emission value based on 27 different scenarios for sampling training data using the methane analogue ammonia case (i.e.,data normalization with median and interquartile range, additional input feature (temperature2) and non-logarithmized output feature). The dashed line indicates the variability over 30 realizations of each scenario. The red line marks the actual temporal average when considering the whole ten month dataset.

3.2. Methane

Similar to the ammonia cases we observed less precision and accuracy with the multilinear regression in many of the scenarios 1-11 when we performed the regression for the methane dataset on the non-normalized data (see Fig. 4). Ridge regression and gradient boosting performed best in this case, while the artificial neural network considerably underestimated the emission value.

The scenarios with the worst performance were similar to the ammonia cases, but the differences between the scenarios were less (probably because of the superposition of the methane emission dynamics from manure and rumination). This is also in line with the reporting of emission factors of Samer et al. who found methane emission rates of 14.5 g h^{-1} LU^{-1} in winter measurements and about 18 g h^{-1} LU^{-1} in summer measurements for the same barn under study, which is a smaller relative difference than for the ammonia emissions (Samer 2011b; Samer 2011a).

Finally, comparing the regression on the non-normalized (Fig. 4) and the normalized (Fig. 5) methane dataset we observed that out of the regression approaches only the artificial neural network was considerably affected. The performance of the latter, however, was considerably improved for most scenarios.
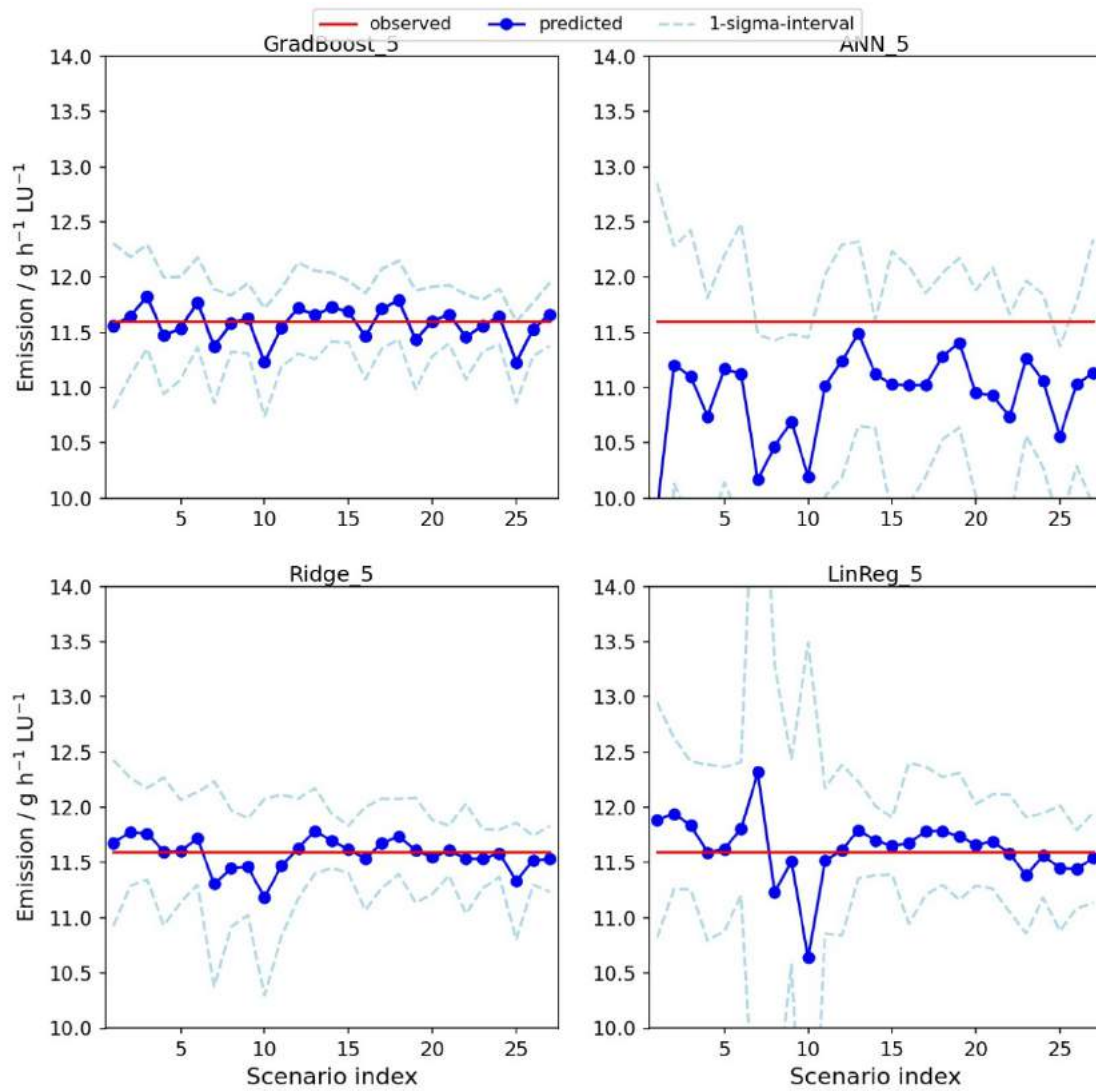
Figure 4: Estimated average ten month emission value based on 27 different scenarios for sampling training data using the non-nomalized methane case (i.e., no data normalization, additional feature (temperature2) and non-logarithmized output feature). The dashed line indicates the variability over 30 realizations of each scenario. The red line marks the actual temporal average when considering the whole ten month dataset.
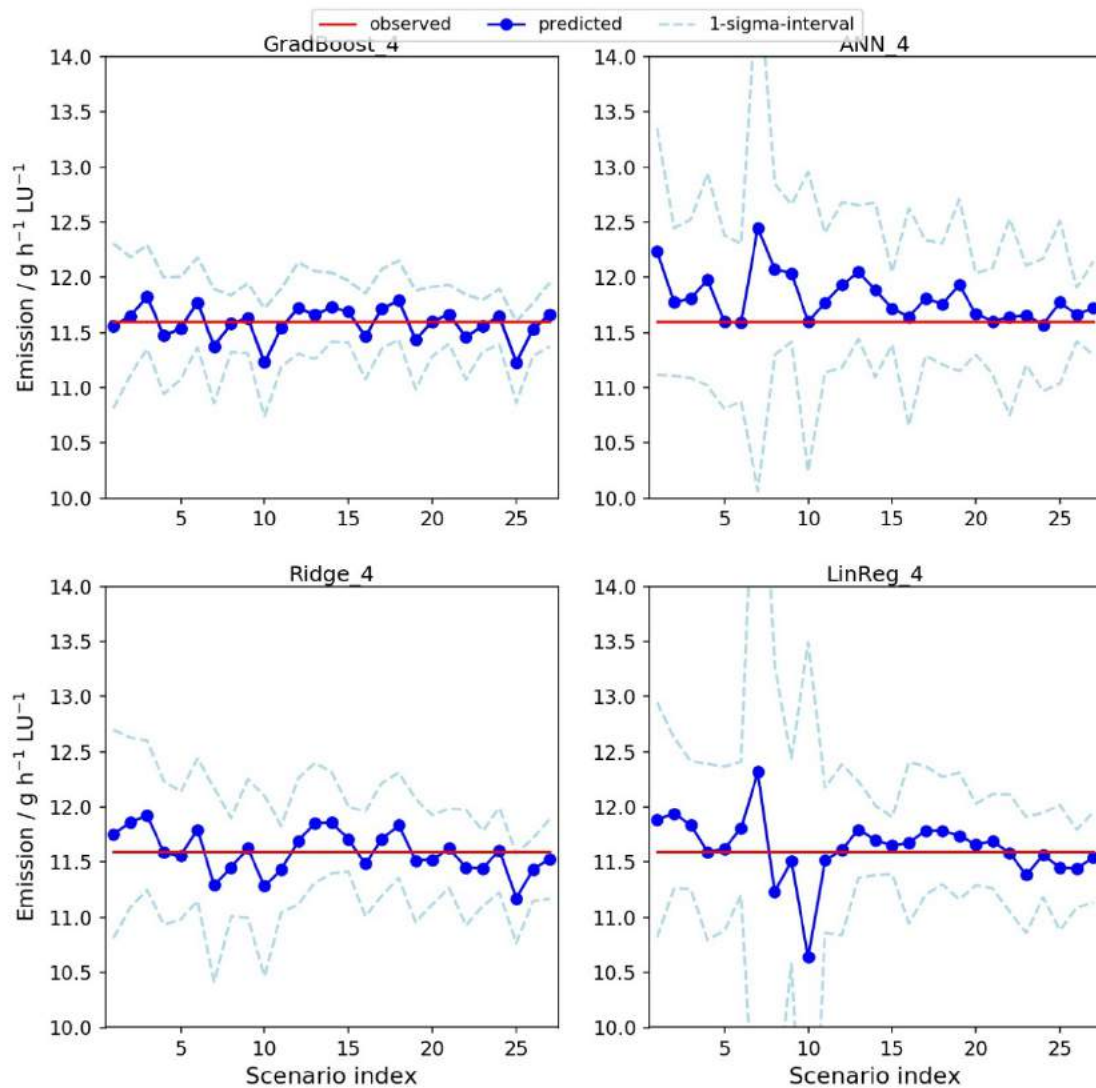
Figure 5: Estimated average ten month emission value based on 27 different scenarios for sampling training data using the nomalized methane case (i.e., data normalization with median and interquartile range, additional feature (temperature2) and non-logarithmized output feature). The dashed line indicates the variability over 30 realizations of each scenario. The red line marks the actual temporal average when considering the whole ten month dataset.

4. Conclusions

We found that while multilinear regression predicted the emission factor in many cases sufficiently well, the quality of the prediction is rather sensitive to the selection and normalization of training data. While the prediction of ammonia emission factors was in many cases better when using non-normalized training data, for methane emission factors the opposite was true. Regularization as in the case of ridge regression could improve the robustness of the fit. The usage of artificial neural networks had barely an added value as the predictions were very sensitive to the selection and normalization of the training data, while the extensive hyperparameter tuning required long computation time. Gradient boosting, however, was the most robust method with regards to the selection and normalization of training data and can thus be a valuable tool for future derivation of emission factors from short-term emission measurements in naturally ventilated livestock barns. However, we recommend further studies with data from other geographical locations, livestock species and gases to prove the generalizability of our findings.

Acknowledgements

References

Arulmozhi, Elanchezhian, Jayanta Kumar Basak, Thavisack Sihalath, Jaesung Park, Hyeon Tae Kim, and Byeong Eun Moon. 2021. 'Machine Learning-Based Microclimate Model for Indoor Air Temperature and Relative Humidity Prediction in a Swine Building', *Animals*, 11: 222.

Ginoux, Paul, Lieven Clarisse, Cathy Clerbaux, P-F Coheur, Oleg Dubovik, NC Hsu, and M Van Damme. 2012. 'Mixing of dust and NH 3 observed globally over anthropogenic dust sources', *Atmospheric Chemistry and Physics*, 12: 7351-63.

Grossi, Giampiero, Pietro Goglio, Andrea Vitali, and Adrian G Williams. 2019. 'Livestock and climate change: impact of livestock on climate and mitigation strategies', *Animal Frontiers*, 9: 69-76.

Hempel, Sabrina, Julian Adolphs, Niels Landwehr, David Janke, and Thomas Amon. 2020. 'How the selection of training data and modeling approach affects the estimation of ammonia emissions from a naturally ventilated dairy barn—Classical statistics versus machine learning', *Sustainability*, 12: 1030.

Hempel, Sabrina, Julian Adolphs, Niels Landwehr, Dilya Willink, David Janke, and Thomas Amon. 2020. 'Supervised Machine Learning to Assess Methane Emissions of a Dairy Building with Natural Ventilation', *Applied Sciences*, 10: 6938.

Hempel, Sabrina, Christoph Menz, Severino Pinto, Elena Galán, David Janke, Fernando Estellés, Theresa Müschner-Siemens, Xiaoshuai Wang, Julia Heinicke, and Guoqiang Zhang. 2019. 'Heat stress risk in European dairy cattle husbandry under different climate change scenarios–uncertainties and potential impacts', *Earth System Dynamics*, 10: 859-84.

Lee, Woongsup, Younghwa Ham, Tae-Won Ban, and Ohyun Jo. 2019. 'Analysis of growth performance in swine based on machine learning', *IEEE Access*, 7: 161716-24.

Ngwabie, Ngwa M, Andrew Vanderzaag, Susantha Jayasundara, and Claudia Wagner-Riddle. 2014. 'Measurements of emission factors from a naturally ventilated commercial barn for dairy cows in a cold climate', *Biosystems Engineering*, 127: 103-14.

Samer, M and Berg, W and M{\"u}ller, H-J and Fiedler, M and Gl{\"a}ser, M and Ammon, C and Sanftleben, P and Brunsch, R. 2011a. 'Radioactive 85Kr and CO2 balance for ventilation rate measurements and gaseous emissions quantification through naturally ventilated barns', *Transactions of the ASABE*, 54: 1137--48.

Samer, M and Fiedler, M and M{\"u}ller, H-J and Gl{\"a}ser, M and Ammon, C and Berg, W and Sanftleben, P and Brunsch, R. 2011b. 'Winter measurements of air exchange rates using tracer gas technique and quantification of gaseous emissions from a naturally ventilated dairy barn', *Applied engineering in agriculture*, 27: 1015--25.

Sanchis, Elena, Salvador Calvet, Agustín Del Prado, and Fernando Estellés. 2019. 'A meta-analysis of environmental factor effects on ammonia emissions from dairy cattle houses', *Biosystems Engineering*, 178: 176-83.

Schrade, Sabine, Kerstin Zeyer, Lorenz Gygax, Lukas Emmenegger, Eberhard Hartung, and Margret Keck. 2012. 'Ammonia emissions and emission factors of naturally ventilated dairy housing with solid floors and an outdoor exercise area in Switzerland', *Atmospheric Environment*, 47: 183-94.

Prediction of Ambient Temperature for Agricultural Applications Using ANNs: A Case Study in Castile and León, Spain

F.J. Diez [a,*], L. Chico-Santamarta [b], A. Correa-Guimaraes [a], L.M. Navas-Gracia [a], A. Martínez-Rodríguez [a], R. Andara [c]

[a] Department of Agricultural and Forestry Engineering, University of Valladolid, Campus La Yutera, 34004 Palencia, Spain

[b] International Department, Harper Adams University, Newport TF10 8NB, Shropshire, UK

[c] Antonio José de Sucre National Experimental Polytechnic University, 3001 Barquisimeto, Venezuela

* Corresponding author. Email: x5pino@yahoo.es

Abstract

This article evaluates predictive modelling of daily and hourly average ambient temperature using artificial neural networks (ANNs) for its application in agricultural sciences and technologies. For that purpose, the prediction of the daily ambient temperature the day after (maximum, T_{max}; average, T_{ave}; and minimum, T_{min}) and its hourly estimation ($T_{0h}, \ldots, T_{23h}$) is done using ANNs. The data series used (i.e., the period 2004–2010 was used for ANNs training, and validation was done in 2011) were monitored at the agrometeorological station in Mansilla Mayor (León), Castile and León, Spain, which belongs to SIAR, the irrigation advisory system.

ANNs models formulated for the daily ambient temperature prediction the day after have three neurons in the outlet layer [$T_{max}(t+1)$, $T_{ave}(t+1)$, $T_{min}(t+1)$]. Two models were evaluated: 1) ANN-1d had three inputs for the actual daily temperature data [$T_{max}(t)$, $T_{ave}(t)$, $T_{min}(t)$], and 2) ANN-2d had the day of the year [$J(t)$] as the fourth input. Including [$J(t)$] improves the model predictions, achieving a RMSE for T_{max}=2.56, T_{ave}=1.65 and T_{min}=2.09 (°C), and it achieves better estimations compared with the classical statistical methods predictions (typical year T_{ave}=3.64 °C; weighted mobile mean T_{max}=2.76, T_{ave}=1.81 and T_{min}=2.52 (°C); linear regression T_{ave}=1.85 °C; and Fourier analysis T_{max}=3.75, T_{ave}=2.67 and T_{min}=3.34 (°C)).

ANN models formulated for average hourly ambient temperature estimation have 24 neurons in the outlet layer [$T_{0h}(t), \ldots, T_{23h}(t)$] corresponding to the daily hours. Two ANNs models have been trained: First model (ANN-1h) has three inputs for the daily data of the actual daily temperature [$T_{max}(t)$, $T_{ave}(t)$, $T_{min}(t)$], and second one (ANN-2h) had the day of the year [$J(t)$] as the fourth input. In this case, including the variable [$J(t)$] does not improve significantly the estimations of the first model, which achieves RMSE=1.25 °C, but it improves those of the ASHRAE method, with which a RMSE=2.36 °C is obtained during a whole week.

Keywords: ambient temperature; evapotranspiration; agrometeorology; artificial neuronal networks; prediction.

1. Introduction

Climate is a significant factor in agricultural production, which depends on the awareness of the meteorological variables (rainfall, temperature, solar radiation, humidity, and wind speed), and these are decisive to favor growth and obtain adequate production. Specifically, ambient temperature is one of the fundamental variables for crop prediction, especially in precision agriculture. Also, selection on the transformation of raw materials, and simulation of the impact of the weather, can be accomplished thanks to efficient weather forecasts.

The availability of crop yield forecasts provides valuable information for producers and the industry. Thanks to the effectiveness of these forecasts, you can base your raw material transformation decisions. The use of global climate models provides considerable information for the simulation of agricultural impacts (Brinkhoff and Robson, 2021; Ogutu et al., 2018). Ambient temperature is used to simulate crop development and growth processes (e.g., leaf development, photosynthesis, and respiration). The models for estimating evaporation and evapotranspiration require very precise meteorological observations of the input data which will determine the quality of the estimation of evaporation and evapotranspiration (Abtew and Melesse, 2013).

The time series of the ambient temperature is studied to make their prediction from different approaches. One of these approaches is analyzed with artificial neural networks that can make full use of certain unknown and hidden information in large-scale climate data, although this information cannot be directly extracted (Zhang, 2018). (Dombayci and Gölcü, 2009) show the efficacy of using the prediction of the daily mean environmental temperature, using an artificial neural network (ANN) model. They concluded that the best-fitting ANN model was multilayer and consisted of 3 inputs (i.e., the month of the year, day of the month, and mean temperature of the previous day) and 6 hidden neurons.

In this article, we study the daily ambient temperature (maximum, average, and minimum) for the next day (that is, [$T(t+1)$]) and its estimate of the hourly mean distribution (that is, [$T_{0h}(t), \ldots, T_{23h}(t)$]), through ANN-based models and

using measured data from Mansilla Mayor, León, Castile and León, Spain. The main objective of this work is to achieve better daily and hourly predictions of ambient temperature, especially for agricultural purposes, and to obtain a better prediction of [T(t+1)] and estimate of [T_{0h}(t),…, T_{23h}(t)], using the least possible number of inputs; also, to facilitate its practical application in the processes of water needs to establish guidelines in the irrigation of crops and evaluation systems. In the same way, to predict the growth of plants and the control of diseases (developed by the presence of high temperatures and high humidity). For this, different ANNs were evaluated with temperature data (maximum, average, and minimum), resulting in a better simulation fit than that achieved with the classic models, which were slightly improved by adding the day of the year [J(t)] as a predictor, which considers the trend at the time of year.

2. Materials and Methods

This section describes: 1) the ambient temperature data, the agrometeorological station and the place, 2) the ANN models designed for the prediction of the daily and hourly ambient temperature, and 3) the classical models (i.e., CENSOLAR typical year, weighted moving mean (WMM) with partial autocorrelation, linear regression, Fourier analysis, and ASHRAE method for hourly ambient temperature) used for comparison.

2.1. Ambient temperature data

The ambient temperature data used in this study, over a period of eight years (i.e., 2004–2011), were collected at the agrometeorological station that belongs to the SIAR system (Agroclimatic Information System for Irrigation, in Spanish) located in Mansilla Mayor (León, Castile, and León, center-north of Spain), with geographical coordinates 42°30'43" N and 5°26'46" W, altitude 791 MAMsl and local time GMT-21.725555. The SIAR system is a project from the Ministry of Environment and Rural Areas and Maritime of Spain, which is managed by ITACyL (Agricultural Technological Institute in Castile and León, in Spanish), through the weather information service InfoRiego (2021), by which farmers obtain advice on irrigation water doses with the objective of its rationalization.

The ambient temperature at the reference agrometeorological station is measured with a Pt-1000 temperature sensor. The electronic circuit for the linearization and the amplification of that sensor is situated next to the Vaisala HMP45C probe (Campbell Scientific, Inc., North Logan, UT, USA), to measure temperature and ambient relative humidity, in the ranges of −40 to 60 °C, and 0 to 100%, respectively. Climate classification of the location of the agrometeorological station is Csb (Chazarra et al., 2018), according to Koppen–Geiger climate classification, with the following average yearly values (data from 1981–2010).

2.2. The prediction of ambient temperature using ANNs

The prediction of the ambient temperature (maximum, average and minimum) of the next day ([T_{max}(t+1), T_{ave}(t+1), T_{min}(t+1)], °C), was carried out with two empirical models of the black-box type, implemented with ANNs that use data corresponding to the seven years from 2004 to 2010. The automatic data preprocessing and postprocessing were done with the Graphical User Interface (GUI) of Neural Network Fitting Toolbox 'nftool' in MATLAB (Demuth et al., 2017).

To achieve the proposed objective, two models with ANN architecture (ie, ANN-1d and ANN-2d) were designed, with different combination of input data: [T_{max}(t)], the maximum daily temperature of the day, °C; [T_{ave}(t)], the average daily temperature of the day, °C; [T_{min}(t)], the minimum daily temperature of the day, °C; and [J(t)], number of the day of the year (1,..., 365), dimensionless.

In the hidden layer of the two evaluated ANNs, different number of neurons were used (i.e., 1–10, 20, 30, 40, and 50) in order to understand its influence in the simulation precision. The output layer of the two ANN models that were tried have three neurons which correspond to the predictions [T_{max}(t+1), T_{ave}(t+1), T_{min}(t+1)] during a whole year (year 2011), by calculating the root mean square error (RMSE, °C), which was obtained in those predictions regarding the measured data, with the objective of selecting a better predictive behavior ANN model. The evaluated ANNs architectures are shown in Figure 1.
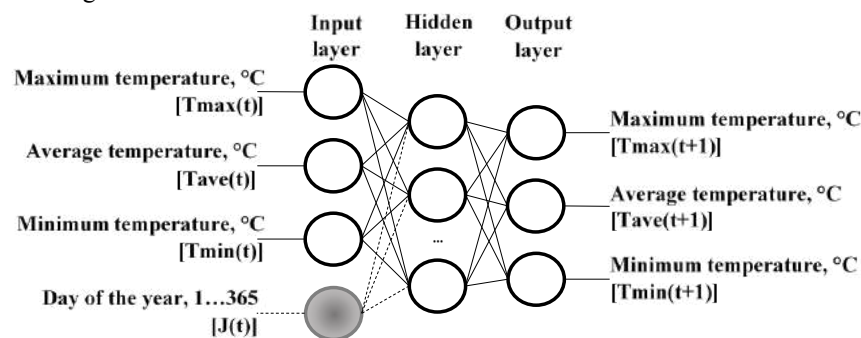
Figure 1. Evaluated ANN architectural models based on input variables for daily temperature. ANN-1d model, with 3 inputs [T_{max}(t), T_{ave}(t), T_{min}(t)]. ANN-2d model, with 4 inputs [T_{max}(t), T_{ave}(t), T_{min}(t), J(t)].

The estimation of the hourly ambient temperature during the 24 hours of the same day ([$T_{0h}(t)$, $T_{1h}(t)$,…, $T_{23h}(t)$], °C), was carried out with two empirical models of the black-box type, implemented with ANNs that use data for the seven years 2004–2010.

To achieve the proposed objective, two models with ANN architecture (i.e., ANN-1h and ANN-2h) were designed, with the same combination of input data used previously in the prediction of daily temperature values.

In the hidden layer of the two ANNs evaluated, two neuron numbers were used (i.e., 28 and 26) for the ANN-1h and ANN-2h model, respectively. The output layer in the two ANN models tested has 24 neurons that correspond to the estimates of the mean hourly ambient temperature [$T_{0h}(t)$, $T_{1h}(t)$,…, $T_{23h}(t)$] during a whole week (week 10,…, 16/05/2011), by calculating the root mean square error (RMSE, °C), which was obtained in those predictions regarding the measured data, with the objective of selecting a better predictive behavior ANN model. The evaluated ANNs architectures are shown in Figure 2.
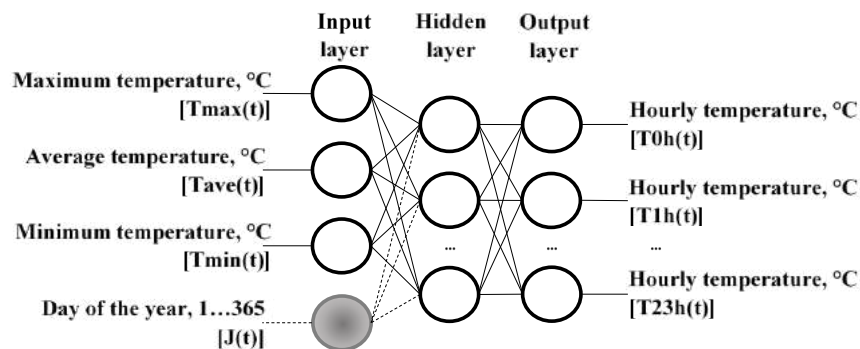
Figure 2. Evaluated ANN architectural models based on input variables for hourly temperature. ANN-1h model, with 3 inputs [$T_{max}(t)$, $T_{ave}(t)$, $T_{min}(t)$]. ANN-2h model, with 4 inputs [$T_{max}(t)$, $T_{ave}(t)$, $T_{min}(t)$, J(t)].

ANNs are created with the *feedforwardnet* function, fed with the input and output data vectors, which determines the size of the respective layers, generating a multilayer feed-forward perceptron (MLP) ANN with just one hidden layer, where the selected transference function between neurons in the hidden layer is the hyperbolic tangent sigmoid (*tansig*), whilst the selected transference function for the output layer neuron is lineal (*purelin*) (Diez et al., 2016, 2019, 2020).

The back-propagation Levenberg–Marquardt (BP-LM) algorithm is applied to achieve a quick optimization (*trainlm*), as well as the following options: bias learning function and weight moment with descendent gradient (*learngdm*); normalized function of squared error (*mse*); and functions of the processing of input matrix elements, such as data processing to recoding unknown data rows (*fixunknowns*), repeated data vectors at the inlet, which do not provide useful information (removeconstantrows), and the matrixes processing to normalized vectors with minimum and maximum values in the range of [−1, 1] (*mapminmax*) (Diez et al., 2016, 2019, 2020).

ANN training was done with the *train* function, with input and output data vector matrixes over a period of seven years (i.e., from 2004 to 2010, without the consideration of 2011, as it was the year of verification), registering the whole training period (*epoch* and *performance* functions). Finally, *sim* function was used, with previously trained ANNs, to do the prediction of [$T_{max}(t+1)$, $T_{ave}(t+1)$, $T_{min}(t+1)$], with the vector matrix of input data from 2011; and to do the estimation of [$T_{0h}(t)$, $T_{1h}(t)$,…, $T_{23h}(t)$], with the vector matrix of input data from 10,…, 16/05/2011.

2.3. The prediction of ambient temperature using classic models

2.3.1.CENSOLAR typical year

The diurnal ambient temperature values included in the tables CENSOLAR (2009) table characterize an average day of each month in a typical year. This is why this model is mainly applicable to large geographical areas and for long periods of time. The information is available for each of the Spanish provinces.

2.3.2.Weighted moving mean with partial autocorrelation

Partial autocorrelation makes reference to variable value dependency with the same variable values precedents in time. For that reason, the weighted moving mean (WMM) model with partial autocorrelation is applied, giving more weight to the values closer to the simulation day and less weight to the ones furthest, with the objective that the average value behaves more flexible than when a simple mobile mean model is used.

In this current work, partial autocorrelation coe cients obtained over a seven year period was used, which were calculated with the *parcorr* MATLAB function, defining the weighted mobile mean with 2 to 20 days' time delays, in 2011. The partial autocorrelation coe cients are applied to the ambient temperature value corresponding to its delay day, doing the summation of those products and dividing by the sum of those coe cients.

2.3.3.Linear regression

Ambient temperature prediction can be done through a lineal regression, that models the relation between a dependent variable, in this case the ambient temperature (maximum, average, and minimum) the day after (T_{max}(t+1), T_{ave}(t+1), and T_{min}(t+1)), and an independent variable, in this case the ambient tmperature (maximum, average and minimum) of the current day (T_{max}(t), T_{ave}(t), and T_{min}(t)), together with a calculated random term using MATLAB Curve Fitting Toolbox '*cftool*'.

2.3.4.Fourier analysis

Fourier analysis is applied to the variables that show significant frequencies (Zhang, 2018; Duchon and Hale, 2012), such as it occurs with the ambient temperature (maximum, average and minimum). In this case, MATLAB Curve Fitting Toolbox '*cftool*' was used to calculate the first to eight harmonic coe cients.

2.3.5.ASHRAE method for hourly ambient temperature

The cycle of daily solar irradiation conditions that the minimum ambient temperature usually takes place shortly before dawn, and that the maximum ambient temperature occurs between one and four hours after solar noon. Then, the daily hourly room temperature curve is divided into two periods, one for warming up in the morning and the other for cooling after the afternoon. The ASHRAE method provides a value for the ambient air temperature during each hour of the day (i.e, $T_{ASHRAE}=T_{max}-[f_{hour}(T_{max}-T_{min})]$), depending on the daily maximum and minimum ambient temperature, and a factor for every hour of the day (ASHRAE, 2017).

3. Results and Discussion

3.1. Results of simulations with the artificial neural networks models

First of all, the research was focused in ANN models to identify the network architecture that simulates with more precision [T_{max}(t+1), T_{ave}(t+1), T_{min}(t+1)], as a function of the neuron number (i.e., 1–10, 20, 30, 40, and 50) that forms the hidden layer. The statistic used for this validation is the RMSE of the simulated outlet based on the data measured for the same variable. Obtained results for the ANN-1d model are shown in Figure 3. The best results for the prediction done for the [T_{max}(t+1)] output variable were achieved with the (3-4-3) and (3-8-3) architectures, with RMSE=2.75 °C, whilst for [T_{ave}(t+1)] output variable the best results were achieved with the (3-5-3) architecture, with RMSE=1.75 °C. Finally, the best behavior for [T_{min}(t+1)] output variable was obtained with the (3-5-3) architecture, with a RMSE=2.11 °C. Table 1 shows the other statistics analyzed for the architecture (3-8-3). It is observed that the prediction error is much lower for the daily average temperature, than for the daily minimum temperature, and for the daily maximum temperature the worst result is achieved.

Furthermore, the results were obtained with the simulation by using ANN-2d (Figure 3). It can be seen that best results of the prediction done for the [T_{max}(t+1)] output variable were those for the (4-5-3) architecture, RMSE=2.56 °C, whilst for [T_{ave}(t+1)] output variable the best results were achieved with the (4-3-3), (4-5-3) and (4-10-3) architectures, with RMSE=1.65 °C. Finally, the best behavior for [T_{min}(t+1)] output variable was obtained with the (4-3-3) architecture, with a RMSE=2.09 °C. Table 1 shows the other statistics analyzed for the architecture (4-8-3). It is observed that the prediction error is slightly lower when the entry of the day of the year [J (t)] is added for the three temperatures, which may have to do with the greater persistence of the daily temperature, which (e.g., daily solar irradiation).

ANN-1d model, with 3 inputs [T_{max}(t), T_{ave}(t), T_{min}(t)]   ANN-2d model, with 4 inputs [T_{max}(t), T_{ave}(t), T_{min}(t), J(t)]
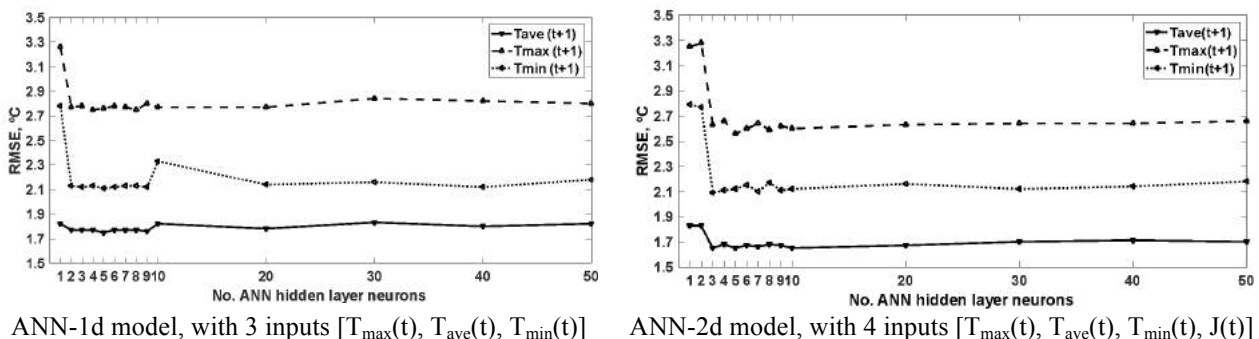
Figure 3. Daily ambient temperature effectiveness of prediction the day after (maximum, T_{max}; average, T_{ave}; and minimum, T_{min}) simulated with the ANN model, compared with the variable measured values, in 2011, as a function of the neurons number in the hidden layer. RMSE: root mean square error (°C).

Table 1. Effectiveness of the daily temperature neural prediction using the ANN-1d (3-8-3) and ANN-2d (4-8-3) models with respect to the SIAR data in Mansilla Mayor (León) for the year 2011.

ANN prediction models: Daily temperature (maximum, average and minimum)							
ANN	Outputs	RMSE	R^2	DW	MPE	FA	AIC
ANN-1d (3-8-3)	$T_{max}(t+1)$	2.75	0.8714	1.9245	-0.0390	0.8410	2.7991
	$T_{ave}(t+1)$	1.77	0.9181	1.8461	-0.0170	0.7843	1.8021
	$T_{min}(t+1)$	2.13	0.8322	1.6176	0.1010	0.6507	2.1578
ANN-2d (4-8-3)	$T_{max}(t+1)$	2.59	0.8863	1.7957	-0.0256	0.8505	2.6456
	$T_{ave}(t+1)$	1.68	0.9269	1.7168	0.0045	0.7772	1.7126
	$T_{min}(t+1)$	2.17	0.8393	1.6303	0.0390	0.6711	2.2180

The estimation of the mean hourly ambient air temperature of the same day $[T_{0h}(t), T_{1h}(t),…, T_{23h}(t)]$, which was carried out using the ANN-1h model, from the input variables: daily maximum, mean and minimum temperature of the same day $[T_{max}(t), T_{ave}(t), T_{min}(t)]$, with 28 neurons in the hidden layer of the artificial neural network. The output simulation, together with the data measured during week 10,…, 05/16/2011, obtains an RMSE=1.25 °C and other statistics analyzed in Table 2.

In addition, the result obtained with the simulation using the ANN-2h model, from the input variables: maximum, mean, and daily minimum temperature of the same day and the day of the year $[T_{max}(t), T_{ave}(t), T_{min}(t), J(t)]$, with 26 neurons in the hidden layer of the artificial neural network, obtain an RMSE=1.42 °C and other statistics analyzed in Table 2.

Table 2. Effectiveness of the hourly temperature neural prediction using the ANN-1h (3-28-3) and ANN-2h (4-26-3) models with respect to the SIAR data in Mansilla Mayor (León) for week 10,…, 16/05/2011.

ANN estimation models: Hourly average temperature							
ANN	Outputs	RMSE	R^2	DW	MPE	FA	AIC
ANN-1h	$T_{0h}(t)…T_{23h}(t)$	1.25	0.9565	0.4339	-0.0131	0.9199	0.8766
ANN-2h	$T_{0h}(t)…T_{23h}(t)$	1.42	0.9444	0.3695	-0.0008	0.9081	1.0030

The ANN-2h model, if the inclusion of the day of the year $[J(t)]$ does not provide a significant improvement in the effectiveness of the estimation of the hourly distribution, as it depends on the particular climatic conditions of the specific day and not on the trend in the time of year that is what this variable contributes.

3.2. Results of the classic models

3.2.1. CENSOLAR typical year

The values of the average daily ambient temperature during the sunny hours of a typical year in the province of León (Spain) found in the CENSOLAR tables (2009), compared to the SIAR database in Mansilla Mayor (León) during 2011, they obtained an RMSE=3.64 °C and other statistics analyzed in Table 3.

Table 3. Effectiveness of the CENSOLAR daytime ambient temperature tables with respect to the SIAR data in Mansilla Mayor (León) for the year 2011.

CENSOLAR typical year: Average daily daytime temperature							
	Outputs	RMSE	R^2	DW	MPE	FA	AIC
CENSOLAR	$T_{ave}(t)$	3.64	0.7505	0.4255	-0.1157	0.6524	3.6546

CENSOLAR typical year can be used for a first approximation, as well as being quick and easy to apply. The model does not take into account the daily variations for each day of the month (i.e., it gives similar data for all the days of the same month), and its spatial resolution is provincial (i.e., it provides the same data for all points of the same province).

3.2.2. Weighted moving mean with partial autocorrelation

The partial autocorrelation coefficients that stem when using the SIAR data in Mansilla Mayor (León) of daily ambient temperature (maximum, average, and minimum) studied during seven years (2004-2010), with delays between 1 and 20 days, are shown in Table 4. Where it is observed that the dependence of the ambient temperature $[T_{max}(t+1)]$, $[T_{ave}(t+1)]$, and $[T_{min}(t+1)]$) on a particular day is all-out (partial autocorrelation coe cients of (0.9326, 0.9579 and 0.8961) for the day after ($[T_{max}(t)]$, $[T_{ave}(t)]$, and $[T_{min}(t)]$), respectively), decreasing the dependency very quickly with the received ambient temperature the days before: (0.0817, -0.0863, 0.0331) for two days $[T(t−1), T(t)]$, (0.1006, 0.1626, 0.1239) for three days $[T(t−2), T(t−1), T(t)]$, (0.0988, 0.1057, 0.1303) for four days $[T(t−3), T(t−2), T(t−1), T(t)]$, without going above (0.0192, -0.0049, 0.0160) with any of the considered delays up to 20 days $[T(t−19), T(t−18), …, T(t)]$.

Table 4. Partial autocorrelation coefficients of the weighted moving mean model, for time delays of 1–20 days with the SIAR data of seven years (2004–2010) in Mansilla Mayor (León) of (maximum, average and minimum) daily ambient temperature.

Partial Autocorrelation Coefficients: Daily temperature (maximum, average and minimum)			
Delay Days	Maximum	Average	Minimum
1	0.9326	0.9579	0.8961
2	0.0817	-0.0863	0.0331
3	0.1006	0.1626	0.1239
4	0.0988	0.1057	0.1303
5	0.0816	0.0757	0.0994
6	0.0734	0.0855	0.0904
7	0.1014	0.0679	0.0357
8	0.0248	0.0105	0.0222
9	0.0600	0.0468	0.0459
10	0.0490	0.0689	0.0593
11	0.0462	0.0332	0.0598
12	0.0255	0.0568	0.0397
13	0.0384	0.0024	0.0637
14	0.0448	0.0254	0.0170
15	0.0225	0.0545	0.0354
16	0.0249	0.0204	0.0286
17	0.0085	0.0289	0.0578
18	0.0540	0.0320	0.0246
19	0.0406	0.0454	0.0257
20	0.0192	-0.0049	0.0160

Subsequently, the WMM model with the partial autocorrelation coefficients that corresponded to the period between 2 and 20 days delay was used for the $[T(t+1)]$ prediction during 2011, obtaining the simulation errors shown in Figure 4. The best results for the prediction done for the $[T_{max}(t+1)]$ output variable were achieved with 6 days delay, with RMSE=2.75 °C, whilst for $[T_{ave}(t+1)]$ output variable the best results were achieved with 5 days delay, with RMSE=1.81 °C. Finally, the best behavior for $[T_{min}(t+1)]$ output variable was obtained with 10 days delay, with a RMSE=2.50 °C.
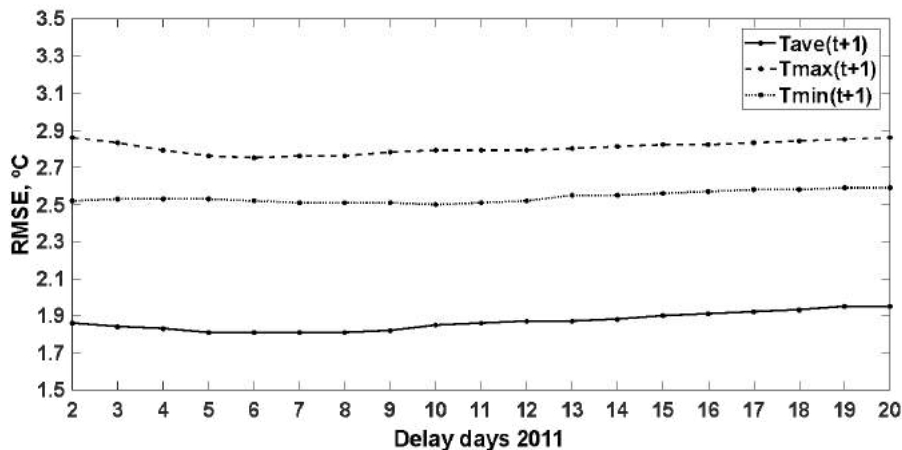
Figure 4. Effectiveness of prediction of the daily ambient temperature (maximum, T_{max}; average, T_{ave}; and minimum, T_{min}) the day after, simulated with the weighted moving mean model, together with the variable measured values in 2011, as a function of the considered number of delay (from 2 to 20 days). RMSE, root mean square error (°C).

The model of the weighted moving mean with 2 days of delay for the daily ambient temperature (maximum, average and minimum) is shown in Eq. (1abc), respectively.

$$T_{max}(t+1) = \frac{0.9326\, T_{max}(t) + 0.0817\, T_{max}(t-1)}{0.9326 + 0.0817} \tag{1a}$$

$$T_{ave}(t+1) = \frac{0.9579\, T_{ave}(t) - 0.0863\, T_{ave}(t-1)}{0.9579 - 0.0863} \tag{1b}$$

$$T_{min}(t+1) = \frac{0.8961\, T_{min}(t) + 0.0331\, T_{min}(t-1)}{0.8961 + 0.0331} \tag{1c}$$

The simulation carried out for the year 2011 with the WMM equation obtained Eq. (1abc), along with the SIAR data, result in a RMSE=(2.86, 1.86 and 2.52) °C, respectively and other statistical data analyzed in Table 5.

The model of the weighted moving mean with 5 days of delay for the daily ambient temperature (maximum, average and minimum) is shown in Eq. (2abc), respectively, that obtain an RMSE=(2.76, 1.81 and 2.53) °C and other statistics analyzed in Table 5.

$$T_{max}(t+1) = \frac{0.9326\, T_{max}(t) + 0.0817\, T_{max}(t-1) + 0.1006\, T_{max}(t-2) + 0.0988\, T_{max}(t-3) + 0.0816\, T_{max}(t-4)}{0.9326 + 0.0817 + 0.1006 + 0.0988 + 0.0816} \tag{2a}$$

$$T_{ave}(t+1) = \frac{0.9579\, T_{ave}(t) - 0.0863\, T_{ave}(t-1) + 0.1620\, T_{ave}(t-2) + 0.1057\, T_{ave}(t-3) + 0.0757\, T_{ave}(t-4)}{0.9579 - 0.0863 + 0.1620 + 0.1057 + 0.0757} \tag{2b}$$

$$T_{min}(t+1) = \frac{0.8961\, T_{min}(t) + 0.0331\, T_{min}(t-1) + 0.1239\, T_{min}(t-2) + 0.1303\, T_{min}(t-3) + 0.0994\, T_{min}(t-4)}{0.8961 + 0.0331 + 0.1239 + 0.1303 + 0.0994} \tag{2c}$$

Table 5. Effectiveness of the weighted moving mean prediction using the partial autocorrelation coefficients for 2 and 5 delay days of the maximum, average and minimum temperature with respect to the SIAR data in Mansilla Mayor (León) for the year 2011.

WMM Prediction Models: Daily temperature (maximum, average and minimum)							
Inputs	Outputs	RMSE	R^2	DW	MPE	FA	AIC
T_{max}(t-1),(t)	T_{max}(t+1)	2.86	0.8610	1.8969	-0.0316	0.8366	2.8941
T_{ave}(t-1),(t)	T_{ave}(t+1)	1.86	0.9097	1.9296	-0.0463	0.7534	1.7811
T_{min}(t-1),(t)	T_{min}(t+1)	2.52	0.7740	1.8751	0.1455	0.7016	2.5458
T_{max}(t-4)…(t)	T_{max}(t+1)	2.76	0.8711	1.6610	-0.0380	0.8391	2.8324
T_{ave}(t-4)…(t)	T_{ave}(t+1)	1.81	0.9144	1.5192	-0.0116	0.7967	1.8636
T_{min}(t-4)…(t)	T_{min}(t+1)	2.53	0.7729	1.4721	0.2502	0.7670	2.5970

WMM can be used for a good prediction, improving the results of the CENSOLAR typical year, making a daily prediction on the values recorded in the previous day, and using several days of delay slightly improves the predictions. Partial autocorrelation coefficients close to one confirm the persistence of room temperature from one day to the next. The strongest partial autocorrelation occurs one day late, decreasing dramatically for the following days. Using several days of delay slightly improves predictions.

3.2.3.Linear regression

The prediction of the daily mean temperature for the following day was executed with linear regression or linear adjustment, which is a mathematical method that models the relationship between a dependent variable, in this case, the value of the mean daily temperature for the next day [T_{ave}(t+1)], the independent variables, in this case, the value of today's mean daily temperature [T_{ave}(t)] and a random term. This model can be expressed as the equation Eq. (3), obtained from the data of the mean daily temperature for the years 2004–2010 SIAR in Mansilla Mayor (León), with a RMSE=1.96 °C.

$$T_{ave}(t+1) = 0.9576\, T_{ave}(t) + 0.4357 \tag{3}$$

The simulation performed for the year 2011 with the linear regression equation obtained Eq. (3), along with the SIAR data, results in a RMSE=1.85 °C, and other statistical results analyzed in Table 6.

Table 6. Effectiveness of the linear regression prediction of daily mean temperature with respect to the SIAR data in Mansilla Mayor (León) for the year 2011.

Linear Regression Model Eq. (3): Daily average temperature							
Inputs	Outputs	RMSE	R^2	DW	MPE	FA	AIC
T_{ave}(t)	T_{ave}(t+1)	1.85	0.9109	1.7523	-0.0685	0.7552	1.8580

The linear regression obtains a precision similar to the WMM in the prediction of the daily mean temperature, when also using the daily persistence of the ambient temperature.

3.2.4.Fourier analysis

The prediction of the daily ambient temperature (maximum, average, and minimum) was carried out by calculating the coefficients of the Fourier analysis for the data from 2004 to 2010 SIAR in Mansilla Mayor (León), obtaining the typical annual Fourier functions, which for the 1st harmonic correspond to Eq. (4abc).

$$T_{max}(t) = 17.38 - 9.237 \cos(0.01742\, t) - 3.553 \sin(0.01742\, t) \tag{4a}$$

$$T_{ave}(t) = 10.59 - 7.77 \cos(0.01791\, t) - 3.511 \sin(0.01791\, t) \tag{4b}$$

$$T_{min}(t) = 4.232 - 5.568 \cos(0.01853\, t) - 3.642 \sin(0.01853\, t) \tag{4c}$$

The simulation carried out with typical annual Fourier functions obtained for the 1st harmonic, together with the

SIAR data for the year 2011, resulting in an RMSE=(3.84, 2.67 and 3.37) °C, and other statistics analyzed in Table 7–9 for the daily ambient temperature (maximum, average and minimum) of the 1st–8th harmonics.

Table 7. Effectiveness of the typical annual Fourier function from the 1st to the 8th harmonic of maximum temperature with respect to the SIAR data in Mansilla Mayor (León) for the year 2011.

Harmonics	Outputs	RMSE	R^2	DW	MPE	FA	AIC
			Fourier analysis: Daily maximum temperature				
1	$T_{max}(t)$	3.84	0.7505	0.5492	-0.0106	0.7969	3.8555
2	$T_{max}(t)$	3.75	0.7610	0.5741	-0.0076	0.7972	<u>3.7916</u>
3	$T_{max}(t)$	<u>3.75</u>	<u>0.7620</u>	<u>0.5760</u>	<u>-0.0072</u>	0.7974	3.8061
4	$T_{max}(t)$	3.75	0.7617	0.5755	<u>-0.0072</u>	<u>0.7975</u>	3.8289
5	$T_{max}(t)$	3.75	0.7612	0.5744	-0.0110	0.7969	3.8535
6	$T_{max}(t)$	3.79	0.7563	0.5629	-0.0076	0.7959	3.9152
7	$T_{max}(t)$	3.76	0.7604	0.5717	-0.0075	0.7956	3.9042
8	$T_{max}(t)$	3.85	0.7487	0.5467	-0.0082	0.7925	4.0183

Table 8. Effectiveness of the typical annual Fourier function from the 1st to the 8th harmonic of average temperature with respect to the SIAR data in Mansilla Mayor (León) for the year 2011.

Harmonics	Outputs	RMSE	R^2	DW	MPE	FA	AIC
			Fourier analysis: Daily average temperature				
1	$T_{ave}(t)$	<u>2.67</u>	<u>0.8148</u>	<u>0.4825</u>	0.0266	<u>0.7489</u>	<u>2.6815</u>
2	$T_{ave}(t)$	2.68	0.8135	0.4794	0.0146	0.7295	2.7047
3	$T_{ave}(t)$	2.71	0.8093	0.4689	0.0163	0.7357	2.7507
4	$T_{ave}(t)$	2.70	0.8099	0.4703	0.0145	0.7324	2.7617
5	$T_{ave}(t)$	2.70	0.8105	0.4721	0.0178	0.7352	2.7712
6	$T_{ave}(t)$	2.71	0.8095	0.4696	0.0169	0.7337	2.7919
7	$T_{ave}(t)$	2.72	0.8078	0.4659	0.0190	0.7349	2.8210
8	$T_{ave}(t)$	2.83	0.7919	0.4320	<u>0.0036</u>	0.7145	2.9505

Table 9. Effectiveness of the typical annual Fourier function from the 1st to the 8th harmonic of minimum temperature with respect to the SIAR data in Mansilla Mayor (León) for the year 2011.

Harmonics	Outputs	RMSE	R^2	DW	MPE	FA	AIC
			Fourier analysis: Daily minimum temperature				
1	$T_{min}(t)$	3.37	0.5955	0.5521	0.2576	0.6710	3.3930
2	$T_{min}(t)$	<u>3.34</u>	<u>0.6035</u>	<u>0.5630</u>	0.2464	0.6733	<u>3.3782</u>
3	$T_{min}(t)$	3.37	0.5957	0.5521	0.2649	0.6910	3.4296
4	$T_{min}(t)$	3.39	0.5908	0.5460	0.2881	0.7062	3.4695
5	$T_{min}(t)$	3.37	0.5969	0.5537	0.2933	<u>0.7511</u>	3.4626
6	$T_{min}(t)$	3.37	0.5963	0.5530	0.2875	0.7441	3.4839
7	$T_{min}(t)$	3.37	0.5957	0.5522	0.2652	0.7302	3.5053
8	$T_{min}(t)$	3.40	0.5883	0.5425	<u>0.2354</u>	0.7002	3.5567

The Fourier analysis can be used for a first approximation. The precision of the typical annual Fourier functions is less than the WMM, by not taking into account daily temperature variations such as the latter.

3.2.5. ASHRAE method for hourly ambient temperature

The prediction of the hourly ambient temperature was made with the ASHRAE method, for week 10,…, 05/16/2011, which with respect to the SIAR data, obtained an RMSE=2.36 °C, and other statistics analyzed in Table 10.

Table 10. Effectiveness of the estimation of the hourly average temperature with the ASHRAE method with respect to the SIAR data in Mansilla Mayor (León) for week 10,…, 16/05/2011.

	Outputs	RMSE	R^2	DW	MPE	FA	AIC
			ASHRAE method: Hourly average temperature				
ASHRAE	$T_{0h}(t)…T_{23h}(t)$	2.36	0.8460	0.2229	0.0948	0.8622	2.4151

This hourly temperature distribution that rises during the morning until a few hours after solar noon, to continue descending until dawn, is typical on clear days, when the variability of the atmospheric components is not very pronounced (Bristow and Campbell, 1984). When clouds appear, which reduce the intensity of solar radiation received

by the surface of the ground, the effect of a more constant temperature usually happens throughout those hours, and when there are sudden storms or rains the temperature drops more suddenly.

4. Conclusions

Artificial neural networks (ANNs) can learn, as the process varies over time, which makes them interesting for the creation of models, applied in the prediction of the daily ambient temperature (maximum, average and minimum) and the estimation of its hourly distribution. In this study, ANN inputs are established as the daily ambient temperature (maximum, average and minimum) of the day on which we make the prediction and adding the day of the year, the ANN output being the future value, of the next day, predicted from the ambient temperature (maximum, average and minimum) for the daily case, and its distribution, on the same day, estimated of the mean temperature for the hourly case.

The prediction of the ambient temperature of the next day ($[T(t+1)]$) is of great interest for all types of agricultural applications, particularly to estimate the evapotranspiration of crops, which conditions irrigation, and to monitor the growth and development of plants, disease control, as well as its application to precision agriculture. In this article, a prediction of $[T_{max}(t+1), T_{ave}(t+1), T_{min}(t+1)]$ and an estimate of $[T_{0h}(t),…, T_{23h}(t)]$ were made using ANNs, trying to design the networks with the simplest architecture and the least possible number of inputs (i.e., $[T_{max}(t), T_{ave}(t), T_{min}(t)]$ and the day of year $[J(t)]$), to facilitate its practical technological application. The only requirement is to have an important and reliable set of ambient temperature data, which can be measured on site, for training the ANN models.

In the predictions made with ANNs, current temperature data were used, obtaining models with which the predictive performance is improved compared to the classic models considered (typical CENSOLAR year, weighted moving average with a delay of several days, linear regression and Fourier analysis). Except for the weighted moving average model $[T_{max}(t+1)]$ with a 6-day delay, for which a similar fit was obtained (i.e., RMSE=2.76 °C), but which is improved with the ANN-2d model for the architecture (4-5-3) that includes the predictor variable of the day of the year $[J(t)]$ (i.e., RMSE=2.56 °C). Therefore, the daily predictive improvement of the ANN models is achieved when we apply the day of the year as the input variable, thus the prediction refers to the time of year in which it occurs, not so in the case of the hourly estimate by depending its distribution of the particular climatic conditions of the concrete day.

To continue working on the predictive capacity and applicability of ambient temperature, the following lines of research are proposed:

1) Use of other ANN input variables, (e.g., humidity, atmospheric pressure, cloudiness) that help detect changes in the evolution of temperature, mainly days with sudden changes in the weather.

2) Creation of ANN models for different times/seasons of the year with similar climatological characteristics.

3) Use of forecasts from national meteorological services as input data for the ANN model, in addition to the historical data recorded in the area.

Acknowledgments

References

Abtew, W., A. Melesse, 2013. *Evaporation and Evapotranspiration: Measurements and Estimations*. Dordrecht: Springer.

ASHRAE (American Society of Heating, Refrigerating and Air-Conditioning Engineers), 2017. *Handbook of Fundamentals*. Atlanta: ASHRAE.

Brinkhoff, J., A.J. Robson, 2021. Block-level macadamia yield forecasting using spatio-temporal datasets. Agricultural and Forest Meteorology. 303, 108369. https://doi.org/10.1016/j.agrformet.2021.108369

Bristow, K., G. Campbell, 1984. On the relationship between incoming solar radiation and daily maximum and minimum temperature. Agricultural and Forest Meteorology. 31, 159–166. https://doi.org/10.1016/0168-1923(84)90017-0

CENSOLAR (Centro de Estudios de la Energía Solar), 2009. *Pliego de Condiciones Técnicas de Instalaciones de Baja Temperatura: Instalaciones de Energía Solar Térmica*. Madrid: IDAE (Instituto para la Diversificación y Ahorro de la Energía). https://www.idae.es/publicaciones/instalaciones-de-energia-solar-termica-pliego-de-condiciones-tecnicas-de-instalaciones-de-baja

Chazarra, A., E. Flórez, B. Peraza, T. Tohá, B. Lorenzo, E. Criado, J.V. Moreno, R. Romero, R. Botey, 2018. *Mapas Climáticos de España (1981–2010) y ETo (1996–2016)*. Madrid: AEMET (Agencia Estatal de Meteorología), Ministerio para la Transición Ecológica.

https//www.aemet.es/documentos/es/conocermas/recursos_en_linea/publicaciones_y_estudios/publicaciones/Mapascli maticosdeEspana19812010/MapasclimaticosdeEspana19812010.pdf

Demuth, H.B., M.H. Beale, M.T. Hagan, 2017. *Neural Network Toolbox: User's Guide MATLAB*. Natick: The MathWorks.

Diez, F.J., L.M., Navas, A. Martínez, 2016. Prediction and identification of the evolution of solar-heated hot water temperature in a stratified tank in static mode using artificial neural networks. Applied Solar Energy. 52 (3), 183-192. https://dx.doi.org/10.3103/S0003701X16030051

Diez, F.J., L.M. Navas-Gracia, A. Martínez-Rodríguez, A. Correa-Guimaraes, L. Chico-Santamarta, 2019. Modelling of a flat-plate solar collector using artificial neural networks for di erent working fluid (water) flow rates. Solar Energy, 188 (3), 1320-1331. https://dx.doi.org/10.1016/j.solener.2019.07.022

Diez, F.J., L.M. Navas-Gracia, L. Chico-Santamarta, A. Correa-Guimaraes, A. Martínez-Rodríguez, 2020. Prediction of horizontal daily global solar irradiation using artificial neural networks (ANNs) in the Castile and León Region, Spain. Agronomy. 10 (1), 96. https://dx.doi.org/10.3390/agronomy10010096

Dombayci, Ö.A., M. Gölcü, 2009. Daily means ambient temperature prediction using artificial neural network method: A case study of Turkey. Renewable Energy. 34 (4), 1158-1161. https://doi.org/10.1016/j.renene.2008.07.007

Duchon, C., R. Hale, 2012. *Time Series Analysis in Meteorology and Climatology: An Introduction*. Chichester: Wiley-Blackwell.

InfoRiego, 2020. Información Meteorológica. http://www.inforiego.org. Accessed March 1, 2020.

Ogutu, G.E.O., W.H.P. Franssen, I. Supit, P. Omondi, R.W.A. Hutjes, 2018. Probabilistic maize yield prediction over East Africa using dynamic ensemble seasonal climate forecasts. Agricultural and Forest Meteorology. 250-251, 243-261. https://doi.org/10.1016/j.agrformet.2017.12.256

Zhang, Z., 2018. *Multivariate Time Series Analysis in Climate and Environmental Research*. Cham: Springer.

Detection of Tomato Fruit from RGBD Images Using Color-Spaces and Geometry

Manya Afonso[a*], Hubert Fonteijn[a], Angelo Mencarelli[a], Dick Lensink[b], Marcel Mooij[b], Nanne Faber[b], Gerrit Polder[a], Ron Wehrens[a]

[a] Wageningen University and Research, Wageningen, The Netherlands
[b] Enza Zaden, Enkhuizen, The Netherlands
* Corresponding author. Email: manya.afonso@wur.nl

Abstract

Detection of fruits and other plant parts using computer vision is an important step in automating tasks like harvesting, phenotyping, and yield prediction. This kind of image analysis is being used increasingly in agriculture since it is quick, non-destructive, and can avoid time-consuming and labor-intensive manual measurements. Segmenting tomatoes from images taken in a production greenhouse is difficult, a.o., because of occlusions, overlap of the fruit color with other plant parts, and illumination variations. Recent approaches to detecting fruits mostly focus on supervised and deep learning methods, in which a large number of images need to be annotated to train the algorithm to be able to decide what is a fruit. While these methods have the advantage of not having to hand-craft discriminative features, annotating hundreds of images to obtain a workable training set is very labor intensive. In this work, we developed a method for the detection of tomatoes, which does not require a training dataset containing labelled fruits. We used an Intel RealSense[TM] D435 camera which provides pixel registered depth and color images, mounted on a trolley that autonomously navigates through the greenhouse and images all plants at regular intervals. First, the depth is used to extract the front row plants from the RGB image. The intensity of fruit pixels is then enhanced by grayscale transforms. The fruit pixels are then segmented by thresholding. Next, the watershed algorithm is applied to separate contiguous regions. Finally, regions above a certain size and whose perimeters approximately fit a circle are selected as individual fruit instances. Experimental results over 123 images acquired in a greenhouse show that this approach could detect tomatoes with a recall of 0.8 and a precision of 0.6. In addition to being applicable in a practical context in itself, this approach has potential for use as a tool to generate data to train supervised (deep) machine learning methods.

Keywords: computer vision, image segmentation, object detection, phenotyping.

1. Introduction

Due to their nutritional value as a source of vitamins and their economic importance as a staple food, tomatoes are the subject of research in seed development to improve yield. Plant breeding requires phenotypic information to differentiate between different varieties. For horticultural crops such as tomatoes, the number and size of fruits is an important phenotypic indicator as it directly relates to the yield. Automatic data acquisition using imaging is increasingly replacing manual phenotypic measurements due to it being quick, non-destructive, less prone to error, and cost-effective in terms of the cost of skilled labor. The detection of fruits from images is also an important step in automating other agricultural processes such as harvesting.

Before the recent research interest in deep learning, classical computer vision methods in which the features of interest that are used for detection and classification are hand-crafted were used for detecting fruits or other plant parts (Song et al., 2014). These features include, among others, fruit shape, color, and texture. Such methods are able to work in the experimental settings, such as illumination, for which they were tailored but cannot necessarily adapt to variations unlike deep learning methods trained on a sufficiently representative dataset. On the other hand, deep learning and machine learning methods require effort in data annotation, which is not required in classical segmentation. Moreover, deep learning methods are computationally intensive, thus requiring specialized hardware or stable internet connection to cloud computing facilities for deployment.

A work on post-harvest image analysis for phenotypic variation (Brewer et al., 2006) imaged tomatoes placed on a dark background, but this cannot be applied in real world greenhouse settings. An orange fruit counting method (Hannan et al., 2009), used adaptive thresholding on colorspace transforms, followed by sliding windows applied on the segmented blob perimeters to fit circles, with voting based on the fitted centroids and radii. A method for ripe sweet pepper detection and harvesting was proposed in (Bac et al., 2017), that used detection of red blobs from the normalized difference of the red and green components, followed by a threshold number of pixels per fruit. A Support Vector Machine (SVM) binary classifier followed by fusing the decisions at different parts of the image was proposed for detecting tomatoes in (Schillaci et al., 2012). In (Zhao et al., 2016a), a semantic (pixel level) segmentation method for ripe tomatoes was presented, based on fusing information from the Lab and YIQ color spaces which emphasize the color red and therefore the ripe tomatoes, followed by an adaptive threshold. This work was extended to detecting tomato fruit instances in (Zhao et al., 2016b) using Haar features and adaboost classification. In (Yamamoto et al.,

2014), a method was presented for counting individual tomato fruits from images of a plant growing in a lab setting based on decision trees on color features to obtain a pixel wise segmentation, and further blob-level processing on the pixels corresponding to fruits to obtain and count individual fruit centroids. A method for detecting tomato flowers in a greenhouse (Afonso et al., 2019) used color spaces to emphasize the color yellow and morphological operations for detection and counting. For a comprehensive description of related work, the reader is referred to (Afonso et al., 2020).

In this paper we present a method for detecting ripe as well as unripe tomatoes from images taken in practical settings in a production greenhouse, based on color spaces and assuming that the fruits are approximately spherical. A combination of color space transforms are used to select regions from the images that are of the colors of the fruits, followed by watershed segmentation to isolate the blobs corresponding to fruits, and finally circles are fitted to the contours of each object.

2. Materials and Methods

2.1. Images

A dataset of 123 images was acquired with a set of four Intel RealSense D435 depth cameras mounted on a moving trolley that moves along the heating pipes of the greenhouse. The cameras were arranged in landscape mode at different heights, and acquired pixel aligned color Red Green Blue (RGB) and depth images of size 1280 x 720. The distance between the camera and the foreground plants was roughly half a meter. The images were acquired on pre-programmed night runs, with illumination provided by a set of LED flashes.

For evaluation, the annotation tool LabelMe[1] was used to label the fruits in the dataset. The annotators marked polygons around the outlines of the fruits, with an empirical criterion used to assign the ripeness classes based on color, with red for ripe and green for unripe. The dataset is available online[2] and a detailed description can be found in (Afonso et al., 2020).

2.2. Software and Algorithm

The fruit detection method was developed using the Halcon software from MVTecSoftware GmbH, Germany on a Linux Mint 18.2 system. The segmentation results were saved in JSON files, and the evaluation with respect to the annotated ground truth was done in Matlab 2017 from The Mathworks, Natick MA, USA.

Following an approach similar to our earlier work on detecting tomato flowers (Afonso et al., 2019), we apply suitable color space transforms to the RGB image so that the ripe fruits which are red and the unripe fruits which are green stand out from the rest of the image. Red regions were observed to stand out as brighter than the rest of the image in the A color component of the CieLAB colorspace (L stands for luminance,and A and B are the color components), the differences red - green and red - blue. Similarly, the green regions stand out as darker than the rest of the image in the U component of the YUV transform (Szeliski, 2011). It must be noted that the green fruits are more difficult to segment as other plant parts such as leaves and stems are also green, thus the thresholds must be empirically chosen to minimize other plant parts being grouped with unripe fruits.

After obtaining the pixel level segmentation of the fruits from the above transforms, the individual fruits are segmented by using the morphological watershed segmentation to separate blobs corresponding to fruits based on distances of points from the blob centers. Finally, the fruit size is estimated by fitting a circle over the contour for each fruit blob and obtaining the center and radius. The thresholds and other parameters used were chosen empirically.

The processing pipeline is as follows, and is illustrated in (Figure 1):

1. Image pre-processing: The white and blue regions in the image which correspond to the greenhouse background substrate and plot marker ribbons are discarded using the chromaticity transform and discarding those pixels for which the blue component of the chromaticity exceeds the red component.

2. Colorspace transformations: The red regions stand out as brighter than the rest of the image in the color spaces CieLAB (A*) and the difference red - blue. Thus, to obtain the pixel-level segmentation of the red fruits, we apply an adaptive threshold on A* using the Otsu method (Otsu, 1979), as done in (Zhao et al., 2016a) and find its logical intersection with the pixels for which red - blue > 160. For the green fruits, the pixel-wise segmentation was obtained by thresholding the U component of the YUV colorspace, U < 105. These values were empirically chosen. These colorspace components are shown in (Figure 1B, 1C, 1D) and the pixel-wise segmentation is shown in (Figure 1E).

3. Morphological operations: In order to discard false positives and background fruits, connected components from the binary image for both the red and green pixel-wise segmentations are filtered to discard regions smaller than 500 pixels and with a circularity score of less than 0.5 (the maximum being 1). The circularity of

---

[1] https://github.com/wkentaro/labelme
[2] https://data.4tu.nl/articles/dataset/Rob2Pheno_Annotated_Tomato_Image_Dataset/13173422

a region with area F and with d being the maximum distance between the center and any point on its contour, is defined as min(1, F/(π d^2)). A watershed segmentation thresholding (Gonzalez et al., 2006) is applied on the distance transform of both binary images, to obtain blobs corresponding to fruit instances, as illustrated in (Figure 1F).

4. Circle fitting: The size of the fruits is estimated by fitting a circle around the contour of the perimeter of each blob that corresponds to a fruit. The algebraic distance between the contour and fitted circle is minimized, with a robust error statistic (standard deviation of the distances from the contour) used to discard outliers. Contours of length below 60 pixels are discarded. Finally, post-processing is applied to discard those circles completely enclosed by others, and with radii outside the range 30 to 130 pixels. This is shown in (Figure 1G).
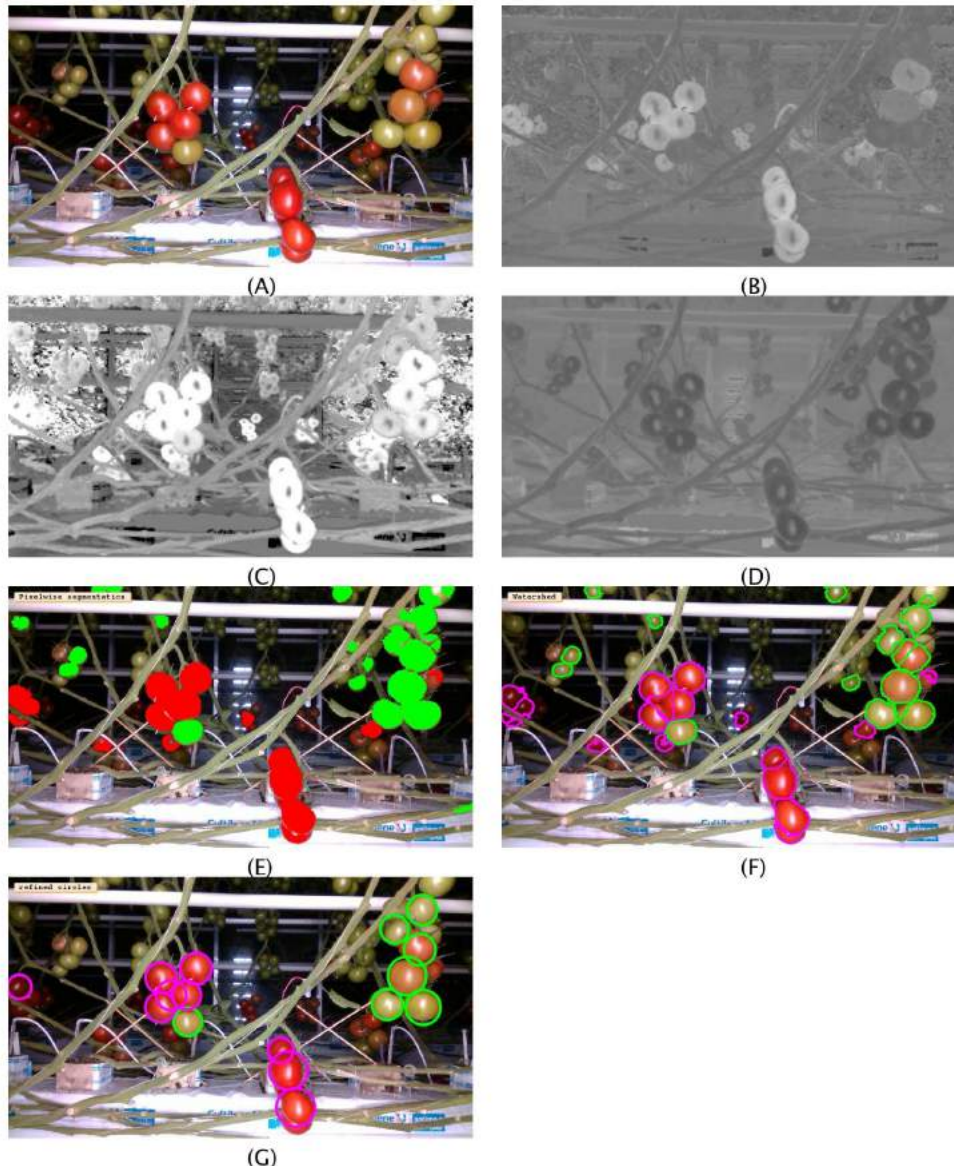
Figure 1. Proposed detection pipeline. (A) RGB image, (B) CieLAB A* component, (C) difference Red - Blue, (D) YUV colorspace U component, (E) pixel-wise segmentation of red and green fruits, (F) individual blobs separated by watershed segmentation, (G) detected fruits.

2.3. Evaluation Procedure

The performance of the fruits detected using our method is evaluated using the 123 images for which the ground truth fruit annotations are available. A detected tomato instance is considered a true positive if its binary circular mask generated using the detected center and radius has a Jaccard Index similarity coefficient also known as intersection-over-union (IOU) (He and Garcia, 2009; Csurka et al., 2013) of 0.25 or more with a ground truth instance. The IOU is defined as the ratio of the number of pixels in the intersection to the number of pixels in the union. This value which is

relatively low was chosen because the circular shape is only approximately correct and due to occlusions losing part of the circular areas. A higher value can be expected to lower the precision and recall values, necessitating further processing to recover the boundary regions.

A detected fruit which does not have sufficient overlap with any ground truth instance is considered a false positive. Those ground truth instances which did not overlap with any detected instance are considered false negatives. From these measures, the precision and recall were calculated, as Precision = TP/(TP+FP), Recall = TP/(TP+FN), where TP is the number of true positives, FP is the number of false positives, and FN is the number of false negatives.

3. Results and Discussion

The proposed detection pipeline is evaluated over a set of 123 images from the dataset from (Afonso et al., 2020). In the present paper, since there is no training phase, we run the proposed detection over the entire dataset. (Figure 2) shows a few examples with the detected fruits overlaid as circles. For visual clarity, the ripe fruits are shown as magenta circles and the unripe ones as green circles.

It can be seen from the detections in (Figure 2) that while the larger unoccluded tomatoes are getting detected accurately, the occluded ones sometimes get missed and sometimes large tomatoes and trusses in the background get counted as false positives. Also while the very ripe tomatoes which are almost ready to be harvested are clearly red and therefore getting detected as ripe fruits, there is a stage when the fruits are not fully ripe that their color may be closer to orange and therefore may not always be correctly classified as unripe.
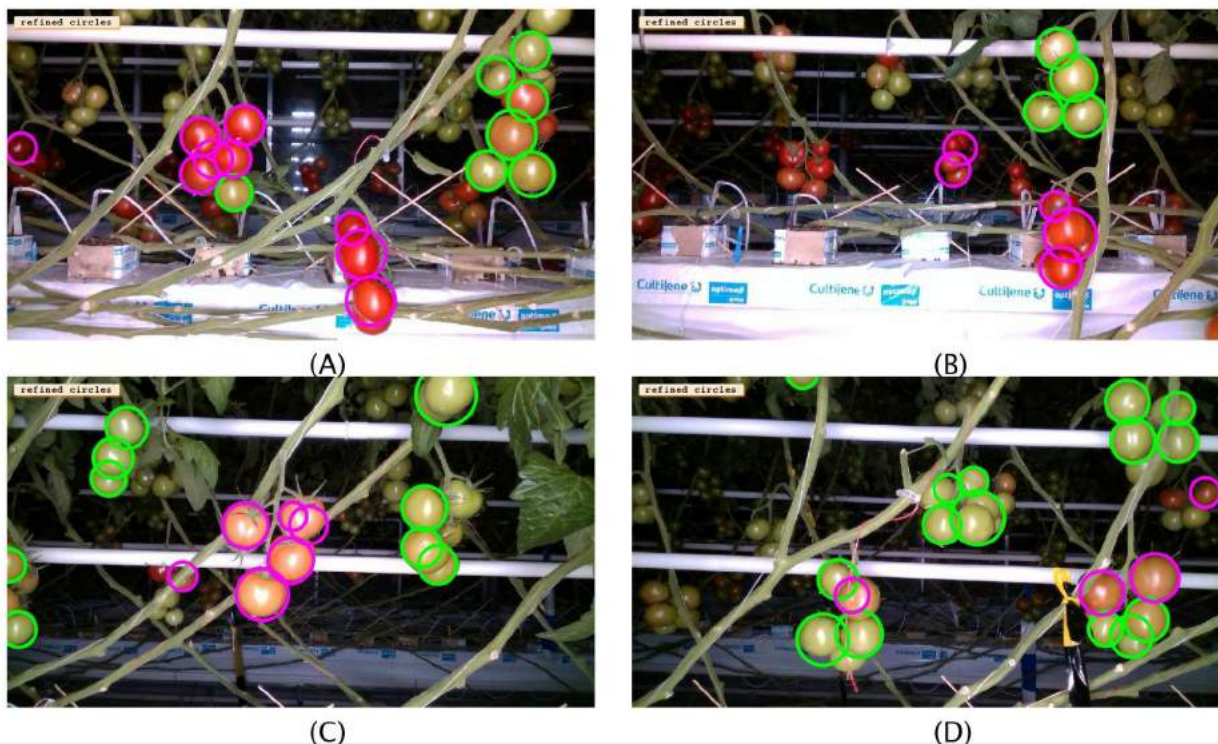
Figure 2. Results of detected fruits overlaid on four different images, magenta: ripe, green: unripe.

Table 1. Metrics of the performance of the proposed fruit detection method, wrt the annotated ground truth.

	Precision	Recall	IoU
Single fruit class	0.61	0.79	0.49
Ripe fruits	0.58	0.83	0.48
Unripe fruits	0.59	0.73	0.48

The precision and recall metrics of detection are presented in Table 1. The recall values obtained are close to or exceed 0.8, which is comparable to the recall value of 0.8 reported in (Yamamoto et al., 2014). While the precision

reported in (Yamamoto et al., 2014) is considerably higher (0.88), it must be noted that the imaging setup used was in the laboratory and therefore without background tomatoes that could appear as false positives. In (Zhao et al., 2016b), a recall value of 0.93 was reported for the ripe fruits, but this method required training an adaboost classifier on an annotated dataset.

When considering both the ripe and unripe fruits as belonging to a single fruit class leads to a better precision than either the ripe or unripe fruits alone. This indicates that while the proposed method is able to detect fruits, it may misclassify their ripeness in some cases. In terms of recall, unripe fruits expectedly have the lowest value, due to the fact that the method was optimized to avoid other plant parts, which could lead to some green fruits being missed. The overall detection performance can be expected to improve if other green plant parts such as stems and leaves were also to be segmented, for example on the basis of texture.

4. Conclusions

We have developed a segmentation method for red and green tomatoes that is able to detect as many as 80 % of the tomatoes present in images, under practical greenhouse settings, which is in line with results reported in literature obtained with classical computer vision methods or under laboratory settings. This method does not require a training phase nor data annotation, and is therefore promising for use in practical application as well as a potentially useful method for generating annotated datasets through active learning. Topics that will be addressed in future include adapting this method to different situations such as cherry tomatoes instead of regular sized ones, using different shape models to be able to deal with other crops or more accurate models such as ellipses, using texture along with color to improve the segmentation, and tracking across images to incorporate information across neighboring images to improve the fruit detection.

Acknowledgements

References

Afonso, M., Fonteijn, H., Fiorentin, F. S., Lensink, D., Mooij, M., Faber, N., Polder, G., & Wehrens, R. (2020). Tomato Fruit Detection and Counting in Greenhouses Using Deep Learning. Frontiers in plant science, 11, 1759

Afonso, M., Mencarelli, A., Polder, G., Wehrens, R., Lensink, D., & Faber, N. (2019, September). Detection of tomato flowers from greenhouse images using colorspace transformations. In EPIA Conference on Artificial Intelligence (pp. 146-155). Springer, Cham.

Bac, C. W., Hemming, J., van Tuijl, B., Barth, R., Wais, E., and van Henten, E. J. (2017). Performance evaluation of a harvesting robot for sweet pepper. J. Field Robot. 34, 1123–1139. doi: 10.1002/rob.21709

Brewer, M. T., Lang, L., Fujimura, K., Dujmovic, N., Gray, S., and van der Knaap, E. (2006). Development of a controlled vocabulary and software application to analyze fruit shape variation in tomato and other plant species. Plant Physiol. 141, 15–25. doi: 10.1104/pp.106.077867

Csurka, G., Larlus, D., and Perronnin, F. (2013). "What is a good evaluation measure for semantic segmentation?," in Proceedings of the British Machine Vision Conference (Bristol: BMVA Press).

Gonzalez, R. C., & Woods, R. E. 2006. Digital Image Processing (3rd Edition). Prentice-Hall, Inc., USA.

Hannan, M., Burks, T., and Bulanon, D. M. (2009). A machine vision algorithm combining adaptive segmentation and shape analysis for orange fruit detection. Agric. Eng. Int. CIGR J. XI(2001), 1–17. Available online at: https://cigrjournal.org/index.php/Ejounral/article/view/1281

He, H., and Garcia, E. A. (2009). Learning from imbalanced data. IEEE Trans. Knowl. Data Eng. 21, 1263–1284. doi: 10.1109/TKDE.2008.239

Otsu, N. (1979). A threshold selection method from gray-level histograms. IEEE transactions on systems, man, and cybernetics, 9(1), 62-66.

Schillaci, G., Pennisi, A., Franco, F., and Longo, D. (2012). "Detecting tomato crops in greenhouses using a vision based method," in Proceedings of International Conference on Safety, Health and Welfare in Agriculture and Agro (Ragusa), 3–6.

Song, Y., Glasbey, C., Horgan, G., Polder, G., Dieleman, J., and Van der Heijden, G. (2014). Automatic fruit recognition and counting from multiple images. Biosyst. Eng. 118, 203–215. doi: 10.1016/j.biosystemseng.2013.12.008

Szeliski, R. (2011). Computer vision algorithms and applications, Springer

Yamamoto, K., Guo, W., Yoshioka, Y., and Ninomiya, S. (2014). On plant detection of intact tomato fruits using image analysis and machine learning methods. Sensors 14, 12191–12206. doi: 10.3390/s140712191

Zhao, Y., Gong, L., Huang, Y., and Liu, C. (2016a). Robust tomato recognition for robotic harvesting using feature images fusion. Sensors 16:173. doi: 10.3390/s16020173

Zhao, Y., Gong, L., Zhou, B., Huang, Y., and Liu, C. (2016b). Detecting tomatoes in greenhouse scenes by combining adaboost classifier and colour analysis. Biosyst. Eng. 148, 127–137. doi: 10.1016/j.biosystemseng.2016.05.001

Deep Learning Technique and UAV Imagery Dataset for Paddy Rice Panicle Detection at Early Stage

Hao Wang [a,b*], Suxing Lyu[b], Yaxin Ren[c]

[a] Beijing Research Center of Intelligent Equipment for Agriculture, Beijing Academy of Agriculture and Forestry Sciences, Beijing, China

[b] Graduate School of Agriculture, Hokkaido University, Sapporo, Hokkaido, Japan

[a] Beijing Research Center for Information Technology in Agriculture, Beijing Academy of Agriculture and Forestry Sciences, Beijing, China

* Corresponding author. Email: wanghao.bit@gmail.com

Abstract

Accurate panicle segmentation is a key step in rice field phenotyping. Deep learning methods based on high spatial resolution images provide a potential solution to increase the throughput as well as the accuracy of panicle identification. The quality and volume of the dataset are crucial to training an accurate and robust deep learning model. Panicle segmentation tasks require particularly costly annotations. However, few public datasets are available for rice panicle phenotyping. We present a semi-supervised semantic segment model training process, which greatly assists the annotation and refinement of training datasets. The model learns the panicle features with limited annotations, and localizes more positive samples in the datasets without further interaction. After the dataset refinement, the number of annotations increased by 40.6%. In addition, the annotation generated by the DNN model is proved to be more precise than the manual label. Finally, we built a well-labelled dataset of rice panicle images at different growth stages. It contains 400 images with 4096×2160 resolution and 50730 pixel-level annotations. We trained and tested modern deep learning models, including EfficientDet-D7, Mask R-CNN, U-Net and DeepLab v3+, to show how the dataset is beneficial to both detection and segmentation tasks. Baseline results are analyzed using five indicators, including Precision, Recall, F1-score, mAP and mIoU.

Keywords: Image segmentation, Plant phenotyping, Semantic segmentation, Smart agriculture, Convolutional neural network

1. Introduction

Rice is one of the most cultivated cereal crops in the world, along with wheat and maize (Xiong et al., 2019). It is a staple food for feeding a large proportion of the world population. Therefore, accurate estimation of rice yield is essential for ensuring regional food security, regulating the market price of the rice grain, and addressing food shortage problems (Xiong et al., 2017; Zhang et al., 2020). The rice panicle density is one of important agronomic components for plant breeders and agronomists in understanding the grain yield and determining the growth period (Chandra et al., 2020; Ikeda et al., 2010). It also plays an important role in nutrition examination and disease detection (Xiong et al., 2017). Therefore, accurate panicle segmentation is a key step in rice field phenotyping. However, conventional panicle observation relies to a large degree on the human labour force. It is tedious and labour-intensive. Also, the results are prone to unrepresentativeness due to limited sampling areas (Madec et al., 2019; Xiong et al., 2019). Therefore, panicle detection is desired to be conducted automatically without harmful impact on the crops. For the application in the area of smart agriculture, the detection method is also required to be accurate, reliable, efficient and possibly with low cost.

Computer vision methods based on high spatial resolution images provide a potential solution to increase the throughput as well as the accuracy of counting panicle (Ikeda et al., 2010; Madec et al., 2019). With the development of deep learning methods, convolutional neural networks have been shown to outperform human beings in diverse fields including phenotyping (Xiong et al., 2019), disease recognition (Singh et al., 2018), flowering and ear counting (Madec et al., 2019; Sadeghi-Tehran et al., 2019). Even though many studies showing success in phenotyping tasks, developing robust and effective models to detect panicles from high throughput phenotypic data remains a significant challenge because of varying illumination, diversity of appearance of the panicles, shape deformation, partial occlusion, and complex background (Guo et al., 2015). In addition, requiring large training datasets limits the practical usage of deep learning models in panicle detection (Chandra et al., 2020). It is a fundamental problem of most deep learning methods to reach an expected level of accuracy and robustness. Semantic labelling and instance segmentation are two tasks that require particularly costly annotations. However, few public datasets are available for crop phenotyping. Some successful methods for panicle segmentation based on deep learning, like Panicle-SEG (Xiong et al., 2017), have generally been calibrated and validated on their own limited datasets. Therefore, annotation is still tedious and time-consuming. Data augmentation is a common strategy for handling limited datasets, such as rotation, mirror-reverse, scaling, contrast adjustment, affine transformation, and so on. However, generic data augmentation fails in some cases

and sophisticated choices have to be made for well training the neural network (Ghosal et al., 2019).

Weakly-supervised machine learning, also termed semi-supervised data labelling, has been extensively studied as it does not require too much human labour force (Vijayanarasimhan and Grauman, 2014; Wei et al., 2018). More recently, active learning approaches with weak supervision are proposed to reduce the number of labelled training images for panicle detection in cereal crops such as sorghum and wheat (Chandra et al., 2020; Ghosal et al., 2019). Most weakly supervised localization and detection approaches learn the positive features from image-level labels (Jie et al., 2017; Papadopoulos et al., 2016). Collecting a large number of pixel-level annotations for training semantic segmentation models is labour-intensive. To overcome this issue, some work has been reported in the field of semi-supervised object identification with sparsely labelled datasets. Papandreou et al. (2015) developed semi-supervised EM algorithms for semantic image segmentation model training with image-level or bounding box annotation. Wei et al. (2018) proposed a semi-supervised semantic segmentation model by equipping a standard classification network with multiple dilated convolutional blocks. Wang et al. (2016) and Lin et al. (2020) developed interactive image segmentation with simple user interaction, such as re-identification and click.

In this research, we propose a weakly supervised semantic segment model training process, which greatly assists the annotation and refinement of training datasets. This paper details the whole process of data collection, data processing and refinement. Finally, the dataset created by the semi-supervised deep learning method is used to benchmark other modern object detection and segmentation methods.

2. Materials and Methods

2.1. Data acquisition

The data collection was conducted in August 2018 at the experimental paddy field of Hokkaido University, Sapporo, Japan. The orthoimage of the paddy field is shown in Fig. 1. The white dashed line indicates the flight route. There are two rice species, Kitaake and Kokusyokuto-2. The cultivation densities are around 11.46 ~ 16.18 plants/m2. We use commercial unmanned aerial vehicles (UAV) to capture the rice field images. Deep neural network methods along with UAV based photogrammetry have been proved to be reliable alternatives to the labour-intensive field survey and crop monitoring, such as the phenotyping of wheat plant height and growth rate (Holman et al., 2016), sorghum head survey (Ghosal et al., 2019), crop species identification (Tsouros et al., 2019), and so on. It is better than a handheld data collection system in efficiency. A larger UAV can load heavier cameras and lenses for capturing higher-quality images. However, the downward wind caused by the rotors will strongly blow rice stems and degrades the image quality. Therefore, based on trade-offs between flight height, image quality, and ease-of-use, the Mavic Pro designed by the DJI Corporation was used in this study. It is a lightweight and compact UAV with an embedded 1/2.3-inch CMOS.
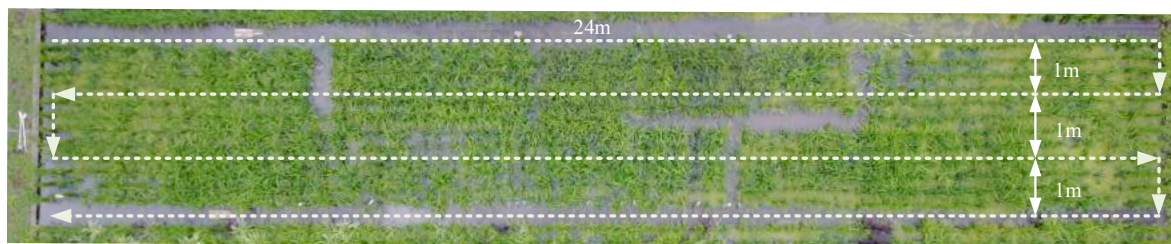
Fig. 1. Experimental paddy field and flight route

The configurations for data acquisition are listed in Table 1. We collect the data using UAV from 1.2 m attitudes. The setup leads to a 0.04 cm/px ground sampling distance (GSD). The ratio of horizontal overlap is 43% and the ratio of vertical overlap is 70%. Frames were extracted from acquired videos while ensuring no duplication and avoiding blurring and overexposure. Each frame is in the resolution of 4096×2160. It covers the phenotype of rice panicles over the entire rice reproductive stage of which, specifically, rice went through heading, flowering and ripening. Some sample images are shown in Fig. 2. The heading stage is the period that the panicle is fully visible. The flowering stage begins right after heading with the appearance of tiny white spikes on the panicles. The flowering stage lasts about 7 days. The ripening stage starts after flowering and ends before harvest. The texture, colour and shape of the panicle change a lot at this stage.

Table 1. Configurations of UAV and the camera

FOV	Aperture	Gimbal	Resolution	Velocity (m/s)	Altitude (m)	GSD (cm/px)
78.8 (26mm)	f/2.2	-90	4096×2160	0.28	1.2	0.04

(a)Heading   (b)Flowering   (c)Ripening
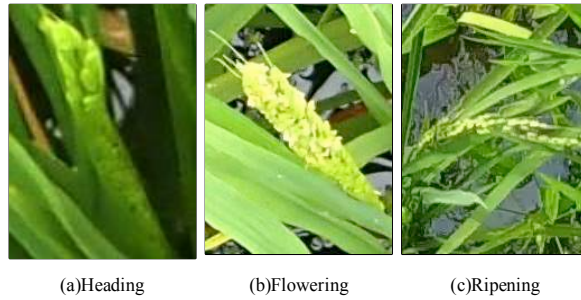
Fig. 2. Sample images at different growth stages.

2.2. Data processing

2.2.1.Basic dataset preparation

We manually annotate the panicle's boundary with a polygon using the tool called Labelme (Russell et al., 2008). The annotations of sample images at each stage are analyzed in Fig. 3. Images taken at the early stage of rice growth is not informative because few panicles are observable. As shown in the first panel, the average number of annotations per image taken on August 4 is about 40. The number of annotations in each image increases gradually as the rice grows to mature, from August 4 to August 22. For the same reason, the number of average pixels per annotation accelerates from the flowering period (August 4) to the heading period (August 12). The number of pixels per annotation at the second panel is related to the size of panicles. With the growth of the rice, the panicles cannot be fully observed because of overlapping to each other. Therefore, the average pixels per annotation drops from August 12 to August 22. According to the previous observation and analysis, the images taken on August 12 are considered to be representative and informative for panicle identification. The data collection time (UTC +9) is listed in the third panel. In all, 400 images with 36089 annotations are dedicatedly selected as a basic dataset. Fifty percent of the total images are taken after the heading period on August 12. We manually label no more than 200 panicles in each image. Labelling all panicles in one image is a labour-intensive task. The next step is to refine the dataset based on the manual annotations.
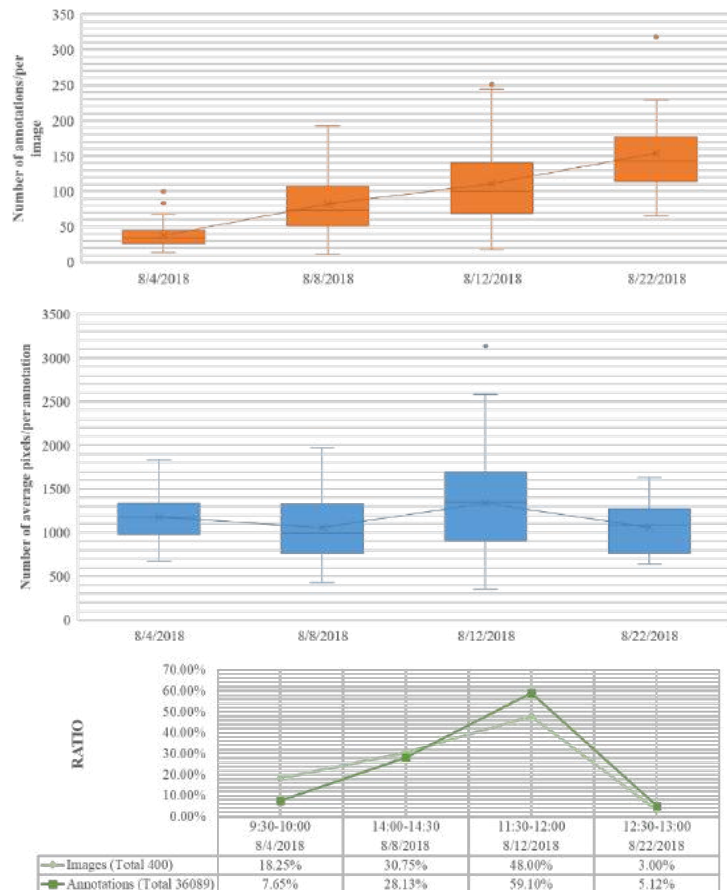
Fig. 3. Basic dataset with manual annotations.

2.2.2.Dataset refinement

The dataset refinement process has two steps as depicted in Fig. 4. The first step is to train an instance segmentation model, Mask R-CNN(He et al., 2017), using the manual annotations. Processing a full 4K image occupies too much GPU memory, which is not an economical way to training a deep neural network model. Besides, the negative labels in an image are much more than the positive ones. To balance the negative and positive samples and limit the GPU memory occupation, the image with 4096×2160 resolution is split into small tiles with 128 × 128 resolution. Tile-to-tile is non-overlapping. We further denoise the dataset by eliminating the tiles with positive labels less than 32 pixels. The dataset contains 13857 images (with resolution 128×128) and 38799 pixel-level annotations. It is divided into training set (80%) and validation set (20%) to train the Mask R-CNN model. The backbone of the model is ResNet101 (He et al., 2016).

The next step is to refine the basic dataset by implementing the trained model on it. We scan the full 4K image using a 512 × 512 sized sliding window with 75% overlapping in both vertical and horizontal directions. The model gives confidence of prediction at each pixel. After scanning the whole image, a confidence map is generated. Applying threshold and morphology filtering methods to the confidence map, we can get the refined dataset with manually labeled annotations and newly added annotations created by the model.
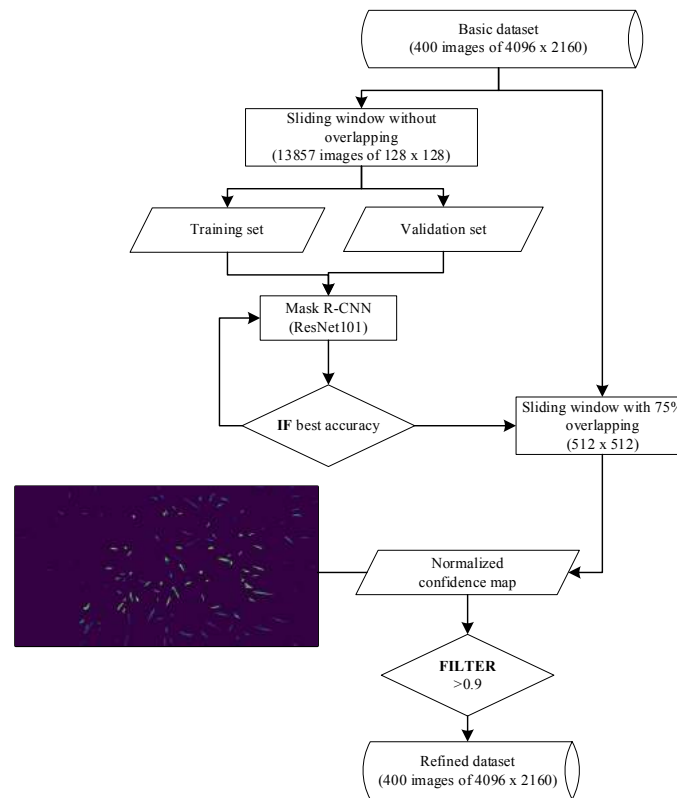
Fig. 4. Flowchart of the proposed panicle labeling method.

3. Results and Discussions

3.1. Dataset refinement

A sample image from the dataset after re-annotation is shown in Fig. 5. It was taken on August 12. The DNN model accurately identified the panicles that are missed in the manual annotations, marked in red circles. As shown in the first panel of Fig. 6, the total number of annotations in the refined dataset is 50730. The improvement of the basic dataset is about 40.6%. The distribution and variation of annotations after refinement are entirely consistent with the results before re-annotation. The number of annotations per image keeps increase from August 4 to August 22. The DNN model can detect panicles all through the growth period. In addition, the annotation generated by the DNN model is proved to be more precise than the manual label. It can be observed from the annotation enlarged in Fig. 5. The average pixel per annotation decreased after the refinement process, as shown in the third panel of Fig. 6, This tendency also proved the improvement of accuracy for each annotation.

annotated in basic dataset

annotated in refined dataset

annotated in both basic and refined datasets
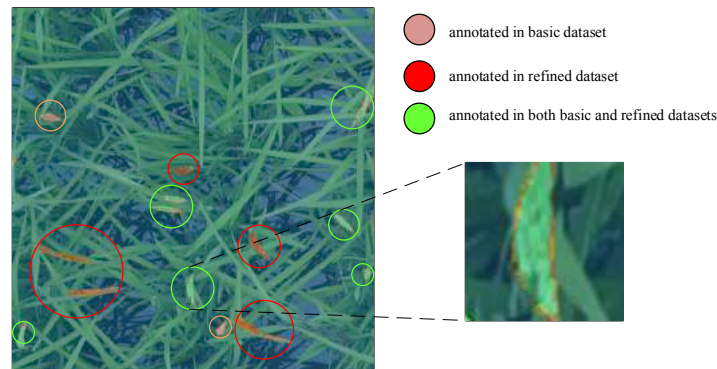
Fig. 5. Sample images after refinement.

	9:30-10:00 8/4/2018	14:00-14:30 8/8/2018	11:30-12:00 8/12/2018	12:30-13:00 8/22/2018
Images (Total 400)	18.25%	30.75%	48.00%	3.00%
Basic dataset (Total 36089)	7.65%	28.13%	59.10%	5.12%
Refined dataset (Total 50730)	8.78%	26.37%	60.21%	4.65%
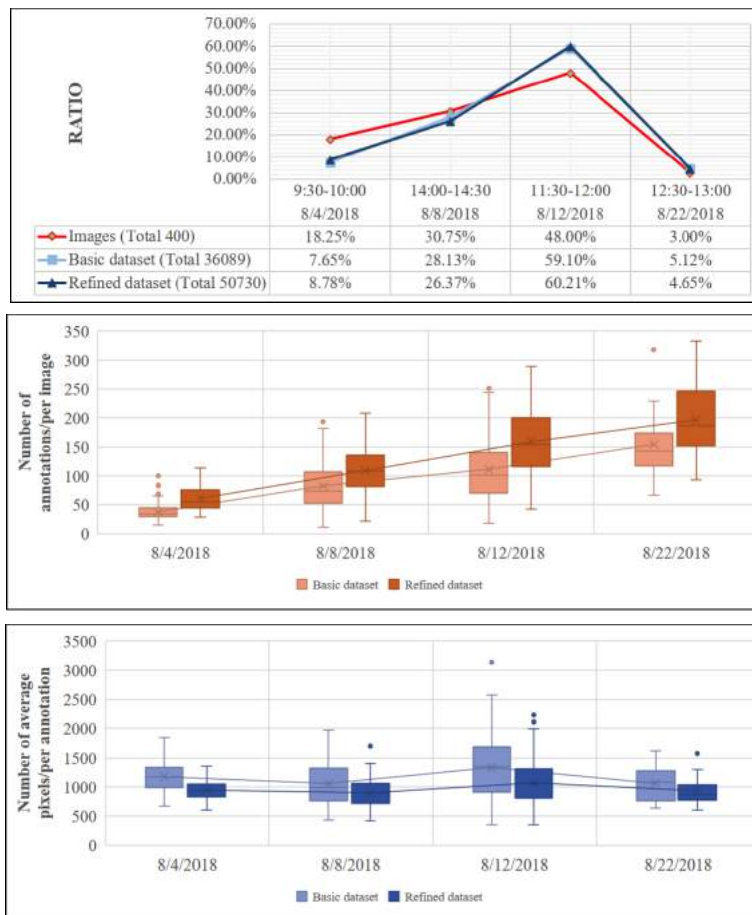
Fig. 6. Annotation analysis after refinement

3.2. Application in detection and segmentation tasks

Panicle phenotyping research can be classified as a detection task or segmentation task. The annotation in this dataset can be used for both applications. We provide results based on modern object detection and segmentation models to set a baseline identification accuracy for the dataset.

Applying the data for panicle detection tasks, we trained two object detection models, the EfficientDet-D7 (Tan et al., 2020) and the Mask R-CNN, with an Inception-ResNet v2 (Szegedy et al., 2017) as the backbone. EfficientDet is a state-of-the-art object detection family, which improves model efficiency and achieves high accuracy simultaneously based on EfficientNet (Tan and Le, 2019). Mask R-CNN evolves from Faster R-CNN (Ren et al., 2017) by adding a semantic segmentation head for pixel-level masking task. The backbone, which is the feature extraction part of Mask R-CNN, is Inception-ResNet v2. The Inception-ResNet v2 backbone consists of a deeper and wider architecture and superiority on detection accuracy, but meanwhile, it is far heavier than any other alternative backbones.

In addition, we trained two segmentation models, U-Net (Ronneberger et al., 2015) with ResNet 50 as the backbone

and DeepLab v3+ (Chen et al., 2018) with Xception as the backbone (Chollet, 2017). U-Net is a lightweight model, which is widely implemented in medical image segmentation (Siddique et al., 2020) and aerial image segmentation (Ivanovsky et al., 2019). DeepLab v3+ is an extension based on DeepLab v3 (Chen et al., 2017), and currently achieves the best accuracy within the DeepLab family.

All the results of panicle detection and segmentation are listed in Table 2 and Table 3, respectively. In the baseline results, the detection or segmentation effects of a DNN model are evaluated using four metrics. The standard metrics include Precision, Recall, and F1-score for validating all machine learning tasks. In addition, the mean Average Precision (mAP) and mean Intersection over Union (mIoU) are used for evaluating the performance of the detection model and segmentation model, respectively.

Table 2. Baseline results of panicle detection, measured on refined dataset.

Model	Image Size	mAP	Precision	Recall	F1-score
EfficientDet-D7	128×128	0.6330	0.6635	0.7608	0.7088
EfficientDet-D7	256×256	0.3980	0.4212	0.6241	0.5030
EfficientDet-D7	512×512	0.3070	0.8472	0.3315	0.4765
Mask R-CNN (Inception ResNet V2)	128×128	0.0280	0.1139	0.1956	0.1440
Mask R-CNN (Inception ResNet V2)	256×256	0.4610	0.4942	0.6426	0.5587
Mask R-CNN (Inception ResNet V2)	512×512	0.5450	0.7037	0.6374	0.6689

Table 3. Baseline results of panicle segmentation, measured on refined dataset.

Model	Train	mIoU	Precision	Recall	F1-score
DeepLab v3+	128×128	0.7944	0.8048	0.7731	0.7886
DeepLab v3+	256×256	0.7834	0.7705	0.7271	0.7481
DeepLab v3+	512×512	0.6786	0.7427	0.4701	0.5758
U-Net-ResNet50	128×128	0.6775	0.7853	0.5194	0.6253
U-Net-ResNet50	256×256	0.6532	0.7246	0.4152	0.5279
U-Net-ResNet50	512×512	0.5924	0.7288	0.2306	0.3504

4. Conclusions

Localizing and identifying panicles from RGB images are useful for rice breeders and farm managers. Panicle identification is elementary for other traits, such as yield estimation, head population density estimation, crop health and production monitoring. This research presents a cost-effective process of panicle image acquisition and refinement. Firstly, we present a solution for paddy rice panicle segmentation in RGB images using deep learning methods. It provides quick and precise panicle phenotyping. Secondly, we propose a semi-supervised semantic segment model training process, which greatly assists the annotation and refinement of training datasets. Thirdly, we provide a pixel-level labelled rice panicle dataset containing 400 images with 50730 pixel-level annotations. The main objective of the dataset is to contribute to solving the problem of rice panicle identification from RGB images. The dataset can be used for both panicle detection and segmentation tasks.

As future work, we hope to develop robust panicle identification methods and expand the variety and volume of the dataset. Users can apply this dataset or the subsets to complement their data. We also invite researchers to complement the dataset with their subsets. Data expansion should follow the Findable, Accessible, Interoperable and Reusable (FAIR) principles to keep the consistency (Pommier et al., 2019). For image acquisition, the optimal reference height at which to capture the panicle area, as well as the GSD, is yet to be defined. We observed that the receptive field of view affects the performance of DNN models. Our experience suggests that a near nadir viewing direction and a sub-millimetre resolution is required for efficient panicle identification. We also recommend acquiring panicle images at the stages, between flowering and mature, when the panicle has fully emerged but not matured. These settings can effectively limit the overlap among panicles. Besides the data quality assurance, a minimum set of metadata should be associated with newly added images or datasets. We recommend attaching all the metadata related to the camera and acquisition platform used.

Acknowledgements

References

Chandra, A.L., Desai, S.V., Balasubramanian, V.N., Ninomiya, S., Guo, W., 2020. Active learning with point supervision for cost-effective panicle detection in cereal crops. Plant Methods 16. https://doi.org/10.1186/s13007-020-00575-8

Chen, L.-C., Papandreou, G., Schroff, F., Adam, H., 2017. Rethinking Atrous Convolution for Semantic Image Segmentation. arXiv.

Chen, L.-C., Zhu, Y., Papandreou, G., Schroff, F., Adam, H., 2018. Encoder-Decoder with Atrous Separable Convolution for Semantic Image Segmentation, in: Proceedings of the European Conference on Computer Vision (ECCV). Springer Verlag, pp. 801–818. https://doi.org/10.1007/978-3-030-01234-2_49

Chollet, F., 2017. Xception: Deep Learning with Depthwise Separable Convolutions, in: 2017 IEEE Conference on Computer Vision and Pattern Recognition (CVPR). IEEE, pp. 1800–1807. https://doi.org/10.1109/CVPR.2017.195

Ghosal, S., Zheng, B., Chapman, S.C., Potgieter, A.B., Jordan, D.R., Wang, X., Singh, A.K., Singh, A., Hirafuji, M., Ninomiya, S., Ganapathysubramanian, B., Sarkar, S., Guo, W., 2019. A Weakly Supervised Deep Learning Framework for Sorghum Head Detection and Counting. Plant Phenomics 2019, 1525874. https://doi.org/10.34133/2019/1525874

Guo, W., Fukatsu, T., Ninomiya, S., 2015. Automated characterization of flowering dynamics in rice using field-acquired time-series RGB images. Plant Methods 11, 7. https://doi.org/10.1186/s13007-015-0047-9

He, K., Gkioxari, G., Dollar, P., Girshick, R., 2017. Mask R-CNN, in: 2017 IEEE International Conference on Computer Vision (ICCV). IEEE, pp. 2980–2988. https://doi.org/10.1109/ICCV.2017.322

He, K., Zhang, X., Ren, S., Sun, J., 2016. Deep Residual Learning for Image Recognition, in: 2016 IEEE Conference on Computer Vision and Pattern Recognition (CVPR). IEEE, pp. 770–778. https://doi.org/10.1109/CVPR.2016.90

Holman, F.H., Riche, A.B., Michalski, A., Castle, M., Wooster, M.J., Hawkesford, M.J., 2016. High throughput field phenotyping of wheat plant height and growth rate in field plot trials using UAV based remote sensing. Remote Sens. 8, 1031. https://doi.org/10.3390/rs8121031

Ikeda, M., Hirose, Y., Takashi, T., Shibata, Y., Yamamura, T., Komura, T., Doi, K., Ashikari, M., Matsuoka, M., Kitano, H., 2010. Analysis of rice panicle traits and detection of QTLs using an image analyzing method. Breed. Sci. 60, 55–64. https://doi.org/10.1270/jsbbs.60.55

Ivanovsky, L., Khryashchev, V., Pavlov, V., Ostrovskaya, A., 2019. Building Detection on Aerial Images Using U-NET Neural Networks, in: 2019 24th Conference of Open Innovations Association (FRUCT). IEEE, pp. 116–122. https://doi.org/10.23919/FRUCT.2019.8711930

Jie, Z., Wei, Y., Jin, X., Feng, J., Liu, W., 2017. Deep self-taught learning for weakly supervised object localization, in: Proceedings - 30th IEEE Conference on Computer Vision and Pattern Recognition, CVPR 2017. Institute of Electrical and Electronics Engineers Inc., pp. 4294–4302. https://doi.org/10.1109/CVPR.2017.457

Lin, Z., Zhang, Z., Chen, L.-Z., Cheng, M.-M., Lu, S.-P., 2020. Interactive Image Segmentation with First Click Attention, in: IEEE CVPR 2020. pp. 13339–13348.

Madec, S., Jin, X., Lu, H., De Solan, B., Liu, S., Duyme, F., Heritier, E., Baret, F., 2019. Ear density estimation from high resolution RGB imagery using deep learning technique. Agric. For. Meteorol. 264, 225–234. https://doi.org/10.1016/j.agrformet.2018.10.013

Papadopoulos, D.P., Uijlings, J.R.R., Keller, F., Ferrari, V., 2016. We don't need no bounding-boxes: Training object class detectors using only human verification, in: Proceedings of the IEEE Computer Society Conference on Computer Vision and Pattern Recognition(CVPR). IEEE Computer Society, pp. 854–863. https://doi.org/10.1109/CVPR.2016.99

Papandreou, G., Chen, L.-C., Murphy, K.P., Yuille, A.L., 2015. Weakly-and semi-supervised learning of a deep convolutional network for semantic image segmentation, in: Proceedings of the IEEE International Conference on Computer Vision. pp. 1742–1750.

Pommier, C., Michotey, C., Cornut, G., Roumet, P., Duchêne, E., Flores, R., Lebreton, A., Alaux, M., Durand, S., Kimmel, E., Letellier, T., Merceron, G., Laine, M., Guerche, C., Loaec, M., Steinbach, D., Laporte, M.A., Arnaud, E., Quesneville, H., Adam-Blondon, A.F., 2019. Applying FAIR Principles to Plant Phenotypic Data Management in GnpIS. Plant Phenomics 2019, 1–15. https://doi.org/10.34133/2019/1671403

Ren, S., He, K., Girshick, R., Sun, J., 2017. Faster R-CNN: Towards Real-Time Object Detection with Region Proposal Networks. IEEE Trans. Pattern Anal. Mach. Intell. 39, 1137–1149. https://doi.org/10.1109/TPAMI.2016.2577031

Ronneberger, O., Fischer, P., Brox, T., 2015. U-net: Convolutional networks for biomedical image segmentation, in: Lecture Notes in Computer Science (Including Subseries Lecture Notes in Artificial Intelligence and Lecture Notes in Bioinformatics). Springer Verlag, pp. 234–241. https://doi.org/10.1007/978-3-319-24574-4_28

Russell, B.C., Torralba, A., Murphy, K.P., Freeman, W.T., 2008. LabelMe: a database and web-based tool for image annotation. Int. J. Comput. Vis. 77, 157–173.

Sadeghi-Tehran, P., Virlet, N., Ampe, E.M., Reyns, P., Hawkesford, M.J., 2019. DeepCount: In-Field Automatic Quantification of Wheat Spikes Using Simple Linear Iterative Clustering and Deep Convolutional Neural Networks. Front. Plant Sci. 10, 1176. https://doi.org/10.3389/fpls.2019.01176

Siddique, N., Sidike, P., Elkin, C., Devabhaktuni, V., 2020. U-Net and its variants for medical image segmentation: theory and applications.

Singh, A.K., Ganapathysubramanian, B., Sarkar, S., Singh, A., 2018. Deep Learning for Plant Stress Phenotyping: Trends and Future Perspectives. Trends Plant Sci. https://doi.org/10.1016/j.tplants.2018.07.004

Szegedy, C., Ioffe, S., Vanhoucke, V., Alemi, A.A., 2017. Inception-v4, inception-ResNet and the impact of residual connections on learning, in: 31st AAAI Conference on Artificial Intelligence, AAAI 2017. pp. 4278–4284.

Tan, M., Le, Q. V., 2019. EfficientNet: Rethinking model scaling for convolutional neural networks, in: 36th International Conference on Machine Learning, ICML 2019. International Machine Learning Society (IMLS), pp. 10691–10700.

Tan, M., Pang, R., Le, Q. V., 2020. EfficientDet: Scalable and efficient object detection, in: Proceedings of the IEEE Computer Society Conference on Computer Vision and Pattern Recognition. IEEE Computer Society, pp. 10778–10787. https://doi.org/10.1109/CVPR42600.2020.01079

Tsouros, D.C., Bibi, S., Sarigiannidis, P.G., 2019. A Review on UAV-Based Applications for Precision Agriculture. Information 10, 349. https://doi.org/10.3390/info10110349

Vijayanarasimhan, S., Grauman, K., 2014. Large-scale live active learning: Training object detectors with crawled data and crowds. Int. J. Comput. Vis. 108, 97–114. https://doi.org/10.1007/s11263-014-0721-9

Wang, H., Gong, S., Zhu, X., Xiang, T., 2016. Human-in-the-loop person re-identification, in: ECCV 2016. Springer Verlag, pp. 405–422. https://doi.org/10.1007/978-3-319-46493-0_25

Wei, Y., Xiao, H., Shi, H., Jie, Z., Feng, J., Huang, T.S., 2018. Revisiting dilated convolution: A simple approach for weakly-and semi-supervised semantic segmentation, in: Proceedings of the IEEE Conference on Computer Vision and Pattern Recognition (CVPR). pp. 7268–7277.

Xiong, H., Cao, Z., Lu, H., Madec, S., Liu, L., Shen, C., 2019. TasselNetv2: In-field counting of wheat spikes with context-augmented local regression networks. Plant Methods 15, 150. https://doi.org/10.1186/s13007-019-0537-2

Xiong, X., Duan, L., Liu, L., Tu, H., Yang, P., Wu, D., Chen, G., Xiong, L., Yang, W., Liu, Q., 2017. Panicle-SEG: A robust image segmentation method for rice panicles in the field based on deep learning and superpixel optimization. Plant Methods 13, 104. https://doi.org/10.1186/s13007-017-0254-7

Zhang, Y., Yan, W., Yang, B., Yang, T., Liu, X., 2020. Estimation of rice yield from a C-band radar remote sensing image by integrating a physical scattering model and an optimization algorithm. Precis. Agric. 21, 245–263. https://doi.org/10.1007/s11119-019-09664-8

Implementation Techniques of Pre-trained Deep Learning Networks for Plant Disease Classification

Anil Bhujel [a,b], Woo Il Kim [c] , Hyo Jeong Jin [c] ,Hyeon Tae Kim [a,*]

[a] Department of Biosystems Engineering, Gyeongsang National University, Jinju, Republic of Korea

[b] Ministry of Communication and Information Technology, Kathmandu, Nepal

[c] Horticultural Research Division, Gyeongsangnam-do Agricultural Research and Extension Services, Jinju, Republic of Korea

* Corresponding author. Email: bioani@gnu.ac.kr

Abstract

Deep Convolutional Neural Networks (CNNs) is becoming dominant in various computer vision applications since last decade. It has also been showing a strong presence in agriculture. However, designing deep networks, training, and implementation from scratch, requires expert knowledge, high-performance hardware, and massive training datasets. Therefore, various deep learning networks, developed by an expert group and trained with a million images, are available in open-source, which can re-use in the various domain through knowledge transfer techniques. Here, different types of transfer learning techniques were applied in plant disease classification and evaluated their performances. Sixteen distinct healthy and diseased classes from 4 plant species were used to train and test the models. The training datasets (23,054 images) were further divided into five sets (5%, 25%, 50%, 75%, and 100% of training images) to assess the efficacy of each transfer learning technique according to available training datasets. Three homogeneous transfer learning techniques were implemented using InceptionV3 and MobileNetV2 pre-trained models. The output layer of the pre-trained model was changed and fine-trained the output layer only in the customized output transfer learning technique. In the feature extraction technique, new Fully-connected Classifier Networks (FCNs) were coupled and trained. However, in weight initialization, the output layer with some deeper layers of the pre-trained model was fine-tuned, freezing the weight of the initial layers. The results suggested that for a considerable amount of training data, the fine-tuning after mixed8 block of InceptionV3 model with the added output layer provides higher accuracy (98.85%) than feature extraction and customised output layer models. However, the training time did not change significantly with the size of the trainable parameter in the GPU accelerated machine. With a few epochs, models showed significant ability in plant disease classification.

Keywords: Deep learning, Transfer learning, Pre-trained network, Plant disease classification

1. Introduction

Plant disease and food security posing a severe problem due to the increase in global trading of food and climate change, there is an urgency in adopting the latest technology in phytopathology. On average, 30% of global food production was lost annually due to diseases (UNFAO, 2017). On the other hand, the continuous increase in the world population chasing the farmer and authorities in supplying enough food. Therefore, precise detection of plant disease plays a key role in phytopathology to intervene before the massive loss. Traditionally, plant diseases were estimated by visual inspection, which is very time-consuming, costly, and error-prone. Later, the computer vision technique was popularly applied, which also possessed some challenges to detect diseases precisely. With the development of high computational devices, efficient sensors, and a large number of annotated datasets, the application of deep learning networks soared exponentially. Although, CNN implementation in phytopathology started recently (Mohanty et al., 2016) deep CNNs outperformed the conventional computer vision techniques in plant disease identification providing accurate disease detection.

Although the deep learning model provides state-of-the-art performance, the main reason for implementation restraint is the requirement of high computational computers and a large number of labelled datasets with wide varieties. Also, the collection of quality image data from the field is challenging due to the complex background and uncontrolled environment, which significantly affects the performance of the models (Barbedo, 2018). However, a pre-trained model, trained with massive images, showed satisfactory results even in the limited number of datasets (Afifi et al., 2021). Therefore, implementation of the pre-trained model through transfer learning is vital in phytopathology. Several researchers have been deployed pre-trained models and assessed the performance of various networks. Rangarajan et al. (2018) used AlexNet and VGG16 networks customizing an output layer to match the desired output classes. Chen et al. (2020a) and Thangaraj et al. (2019) used pre-trained models without classifier networks as a feature extractor in the new domain, added a classifier network to the feature extractor, and finally fine-trained the model. However, some researchers added additional convolutional blocks with classifier networks to the feature extraction base networks and fine trained the added networks to the new domain (Chen et al., 2020; Jian et al., 2020b). Aravind et al. (2019) utilized the pre-trained AlexNet model. The features of diseased grape leave were extracted from the different layers, applied those features to the multiclass support vector machine and compared the classification performance.

The feature extraction from all the training images at once needs huge computational memory restricting the usage of this technique for a large number of datasets.

In this experiment, three transfer learning techniques of the pre-trained model in plant disease classification are studied. InceptionV3, an efficient model with high classification accuracy, and MobileNetV2, a lightweight architecture, are the two pre-trained models chosen to examine the different transfer learning techniques. Moreover, the impact of the number of training images on the transfer learning approaches is thoroughly studied. Furthermore, the computational efficiency versus the performance of each technique for plant disease classification is monitored. All the studies are conducted on the same hardware and software platforms to make a fair comparison. This study will provide fundamental knowledge on transfer learning of the deep learning model according to the available resources.

2. Materials and Methods

2.1. Dataset preparation

The deep learning networks' performance is highly data-sensitive. Therefore, data preparation is a very crucial step in the application of a deep learning network. A total of 23,054 images from 4 plant species (Apple, Potato, Strawberry, and Tomato) with 16 distinct classes were collected from the open-source database (PlantVillage), as shown in Table 1. In the PlantVillage datasets, the number of images of some categories was highly unbalanced. Therefore, data augmentation techniques (horizontal and vertical flip) were applied to increase the image amount. However, tomato yellow leaf curl virus images were removed massively. Figure 1 represents the example of original and created images from data augmentation. The images were pre-processed and labelled according to the class name. And the dataset was first divided randomly into training and testing datasets at a ratio of 80:20 (Mohanthy et al., 2016). Moreover, the training images were further split into four sets (Table 2) to apply the different amounts of training images to the model.

Table 1. Plant disease datasets detail.

Class label	Actual name	No. of images
0	Apple black rot	1242*
1	Apple healthy	1645
2	Apple scab	1260*
3	Potato early blight	1000
4	Potato late blight	1000
5	Strawberry healthy	1368**
6	Strawberry leaf scorch	1109
7	Tomato bacterial spot	2127
8	Tomato early blight	1000
9	Tomato healthy	1591
10	Tomato late blight	1909
11	Tomato leaf mold	952
12	Tomato septoria leaf spot	1771
13	Tomato spider mites	1676
14	Tomato target spot	1404
15	Tomato yellow leaf curl virus	2000^

Total image: 23,054

*= two-fold increment by using data augmentation (horizontal flip), **=three-fold increment (horizontal and vertical flip), and ^=reduced more than half by deleting images.

Table 2. Sub-division of training dataset and the number of images in each dataset.

Training set	No. of images	Image taken
Train_5	928	5% of training images
Train_25	4606	25% of training images
Train_50	9216	50% of training images
Train_75	13,832	75% of training images
Train_100	18,438	100% of training images
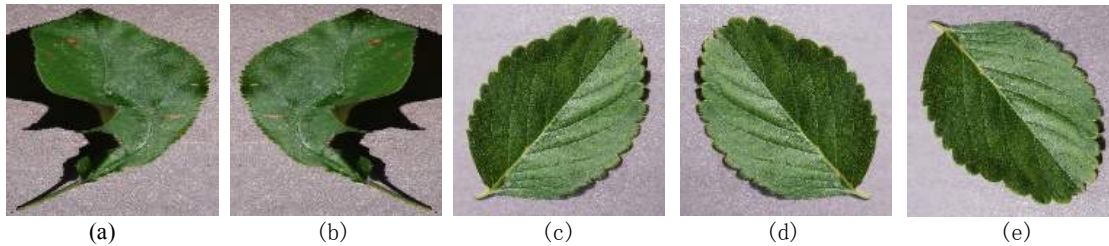
Figure 1. Samples of original and data augmented images. (a) Apple black rot original image, (b) Apple black rot horizontal flipped image, (c) Strawberry healthy original image, (d) Strawberry healthy horizontal flipped image, and (e) Strawberry healthy vertical flipped image.

2.2. Implementation of pre-trained deep models

Broadly, three different types of transfer learning strategies were implemented and evaluated in the plant disease classification domain. Based on the source and target domain, transfer learning could be a homogeneous or a heterogeneous transfer (Weiss et al., 2016). In another perspective, transfer learning strategies can be categorized into inductive, unsupervised, and transductive (Pan and Yang, 2010). However, in our study, only homogeneous inductive transfer learning was examined. Within this category, three different knowledge transfer approaches were tested, as shown in Fig. 1 (Kaya et al., 2019), and compared their performance on the different number of training images. Three different types of transfer learning strategies were implemented and evaluated in the plant disease classification domain. Based on the source and target domain, transfer learning could be a homogeneous or a heterogeneous transfer (Weiss et al., 2016). In another perspective, transfer learning strategies can be categorized into inductive, unsupervised, and transductive (Pan and Yang, 2010). However, in our study, only homogeneous inductive transfer learning were examined. Within this category, three different approaches of knowledge transfer were tested, as shown in Fig. 1 (Kaya et al., 2019), and compared their performance on different number of training images.

2.2.1. Customised output layer approach

In this method, the output layer of the pre-trained model was customised according to the required classes. Since the pre-trained model has trained in the ImageNet datasets, it has an output layer of 1000 neurons. Therefore, it was changed to 16 (as per our image classes), as shown in Fig 3a. All the network parameters except the output layer's parameter were kept constant and fine-tuned the output layer parameter only with the training dataset.

2.2.2. Feature extraction approach

There are two ways to use the pre-trained model in this approach. Firstly, the pre-trained feature extractor network was used to extract the features from all the images (train and test). And a stand-alone classifier was designed to train and test from the feature maps. Secondly, the feature extractor model was coupled with a new classifier network and fine-tuned the classifier networks (Fig. 3b), keeping the feature extractor network intact. In the first case, all the feature maps extracted from the input images need to hold in memory. However, we have applied the second strategy in our study (Fig. 3c). Classifier networks designed by stacking a global average pooling layer, a dense layer of 1024 neurons, an activation layer, and an output layer of 16 neurons were coupled with the base feature extraction model.

2.2.3. Weight initialisation approach

In the weight initialisation approach, the weight of the initial layers of the pre-trained network was frozen, fine-tuning the weight of the inner layer together with added classifier. Since the initial layers of CNN extract the common features, such as sharp edges, shapes, and distinct colours, which is universal in all domains' images, it is not essential to re-train for different domain images. However, the deeper layers are responsible for the problem specific feature extraction. In this approach, the network parameters from some deeper layers and classifier networks were fine-trained.

2.3. Pre-trained deep learning model and fine-training

Although there were several pre-trained models in the Keras library (Keras API), we chose InceptionV3 (Szegedy et al., 2015) and MobileNetV2 (Sandler et al., 2018), one due to heavy and high classification accuracy and another due to lightweight architecture. The models were chosen due to commonly applied in various classification domains. Then the modified models were trained using the same hyperparameters in all cases. The models were trained for 30 epochs with a batch size of 32 using RMSprop optimizer at default learning rate. However, the data augmentation (random zoom (0.5), width shift (0.2), height shift (0.2), and rotation (20)) were used in all the training image sets except Train_5 set, since the Train_5 was applied without data augmentation. The model checkpoints were set to save automatically on the improved validation error.
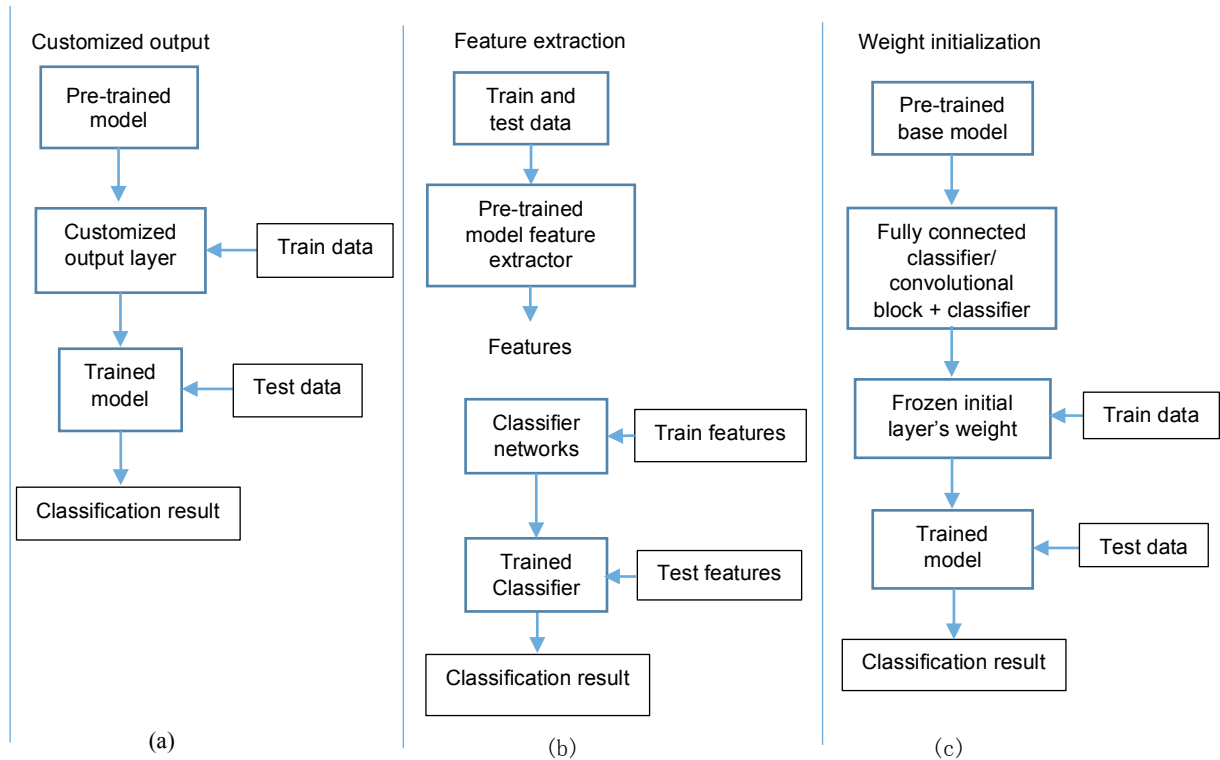
Figure 2. Different fine-tuning approaches of pre-trained model. (a) Customised output layer only, (b) Feature extraction of target images and applying feature vectors to a classifier, and (c) Weight initialisation approach
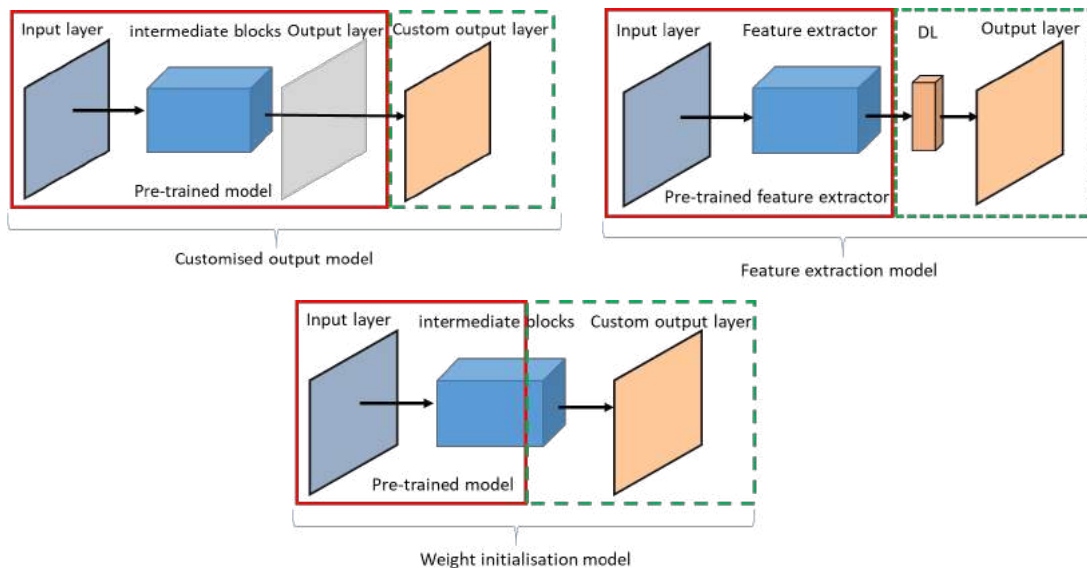
Figure 3. Transfer learning models design. (a) Customised output layer model, (b) Feature extraction model, and (c) Weight initialisation model.

3. Results and Discussion

All the models were evaluated using the same testing images (4616 images) on the same hardware and software environment. The specification of the server machine was Intel® Core™ i9-10900KF, a 3.7 GHz processor having 64 GB memory, and NVIDIA GeForce RTX 2080 with 8 GB dedicated memory GPU running on Windows 10 Pro. All the

codes, algorithms, and models were run in the Keras application, TensorFlow running at the backend, with cuDNN 11.0 and Python 3.10 environment. The network parameters (trainable and non-trainable) and the training time to converge the models in different volumes of training images are demonstrated in Table 3. The result shows no significant difference in training time with the number of trainable parameters for a particular model. However, the training time is highly affected by the number of training images as the number of steps per epoch increases. Although the network parameters of the MobileNetV2 were fewer by factors of 10 than the InceptionV3 model, MobileNetV2 took only 35~65 seconds less time to complete the given epochs. But, the testing time is significantly faster in MobileNetV2 (average 5.39 sec.) than the InceptionV3 model (average 11.46 sec.). It might be due to the fewer layers and lightweight architecture. Furthermore, the accuracy, precision, and f1-score of the models were calculated using Eqs. (1-4).

$$Accuracy = \frac{TP + TN}{Total\ test\ images} \qquad (1)$$

$$Precision = \frac{TP}{TP + FP} \qquad (2)$$

$$Recall = \frac{TP}{TP + FN} \qquad (3)$$

$$F1 - Score = \frac{2 * Precision * Recall}{Precision + Recall} \qquad (4)$$

where TP: True Positive (correctly detected), TN: True Negative (correctly not detected), FP: False Positive (wrongly detected), and FN: False Negative (wrongly not detected).

Table 3. Network trainable and non-trainable parameters and corresponding training time at different volume of training images.

Model	Parameters		Training time				
	Trainable	Non-trainable	Train_5	Train_25	Train_50	Train_75	Train_100
MobileNetV2_CO	20,496	2,257,984	0:03:40	0:18:46	0:34:36	0:50:20	1:05:58
MobileNetV2_FE	1,328,144	2,257,984	0:03:35	0:18:42	0:34:32	0:50:24	1:05:59
MobileNetV2_WI	2,214,224	1,371,904	0:03:37	0:18:55	0:34:41	0:50:33	1:06:48
InceptionV3_CO	32,784	21,802,784	0:04:21	0:19:34	0:35:15	0:50:58	1:06:51
InceptionV3_FE	2,114,576	21,802,784	0:04:19	0:19:20	0:35:10	0:50:56	1:06:56
InceptionV3_WI	13,229,456	10,687,904	0:04:38	0:19:42	0:35:33	0:51:37	1:07:32

CO: Customised output layer technique, FE: Feature extraction technique, and WI: Weight initialisation technique.

Figure 4 exhibits the average accuracies of the models trained in various training datasets. The results signify that MobileNetV2 with customised output and feature extraction transfer learning showed superior performance on a few training images (Train_5). In contrast, the weight initialisation transfer learning showed better results when the number of training images increases. However, weight initialisation transfer learning is best suited for the InceptionV3 model, showing better classification accuracies, and the accuracy is increased with the increase in training data volume. With the extremely low amount of training data, MobileNetV2 could not converge on weight initialisation training. The training and validation accuracies of the models with different transfer learning techniques in few training data (Train_5) and for a considerable amount of images (Train_100) are shown in Fig. 5. Similarly, Fig. 6 represents the confusion matrix generated by the MobileNetV2 and InceptionV3 on their best transfer learning approach (weight initialisation).

We also observed the changes in feature maps of the deeper layers with the weight initialisation transfer learning. Since the InceptionV3 model was fine-trained after the Mixed8 layer, the feature maps generated from Mixed9 and Mixed10 layers from the customised output and weight initialisation models are presented in Fig. 7. The feature maps generated from the customised output model (not trained with our images) seem some unnecessary information (Fig. 7a and b), which might be a reason to confuse the model while classifying. However, with the fine-tuning of those layers, the model able to extract only the necessary features specific to a problem, improving the classification accuracy (Fig. 7c and d).
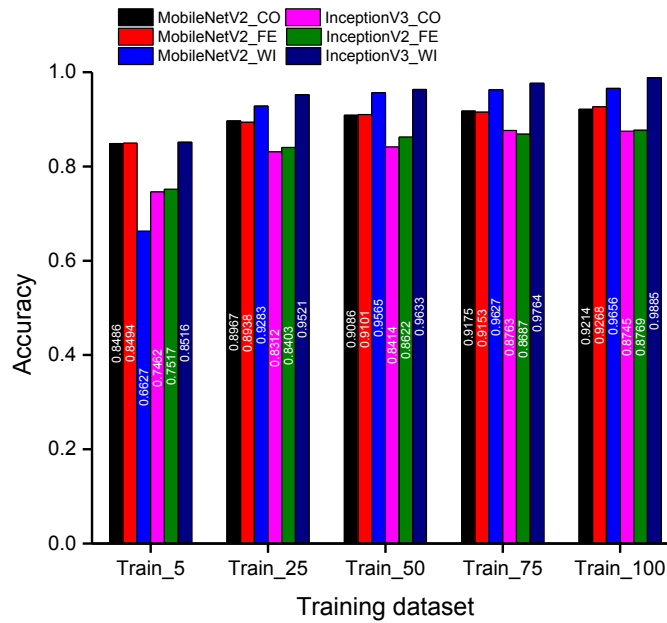
Figure 4. Testing accuracies of MobileNetV2 and InceptionV3 pre-trained model with different transfer learning techniques at different amounts of training image.

(a)

(b)
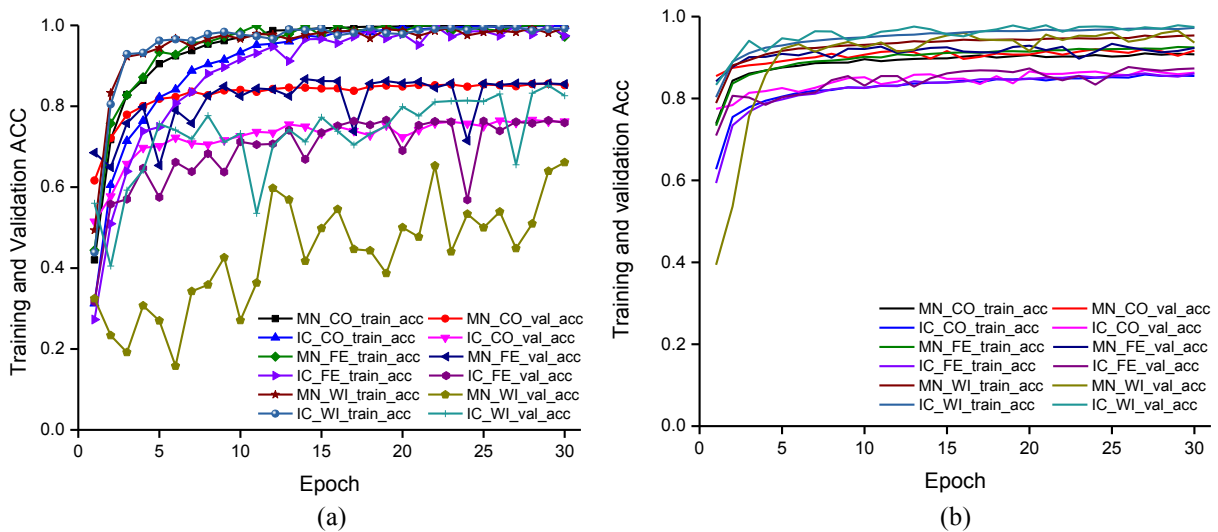
Figure 5. Training and validation accuracy plots. (a) Training and validation accuracies the models using Train_5 dataset and (b) Training and validation accuracies using Train_100 dataset. MN_CO: MobileNetV2 Customised output, MN_FE: MobileNetV2 Feature extraction, MN_WI: MobileNetV2 Weight initialisation, IC_CO: InceptionV3 Customised output, IC_FE: InceptionV3 Feature extraction, and IC_WI: InceptionV3 Weight initialisation model.

(a)　　　　　　　　　　　　　　　　　　(b)
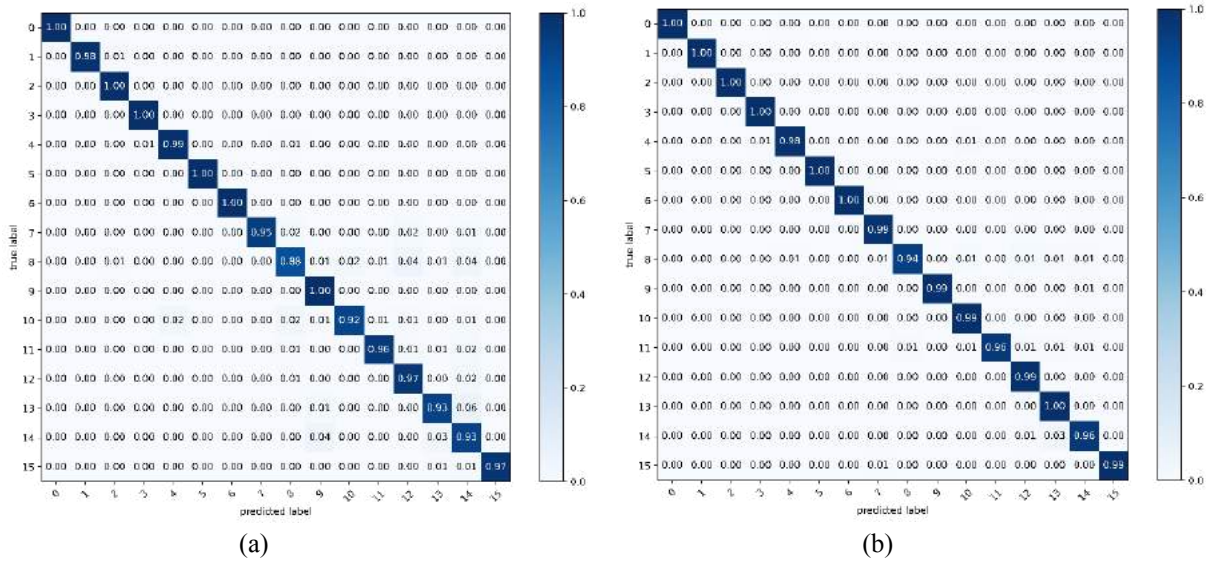
Figure 6. Confusion matrix obtained from the best models. (a) MobileNetV2 with weight initialisation transfer learning using Train_100 dataset, which provided an average accuracy of 96.56% and (b) InceptionV3 with weight initialisation transfer learning using Train_100 dataset that provided an average accuracy of 98.85%.

(a)

(b)

(c)

(d)
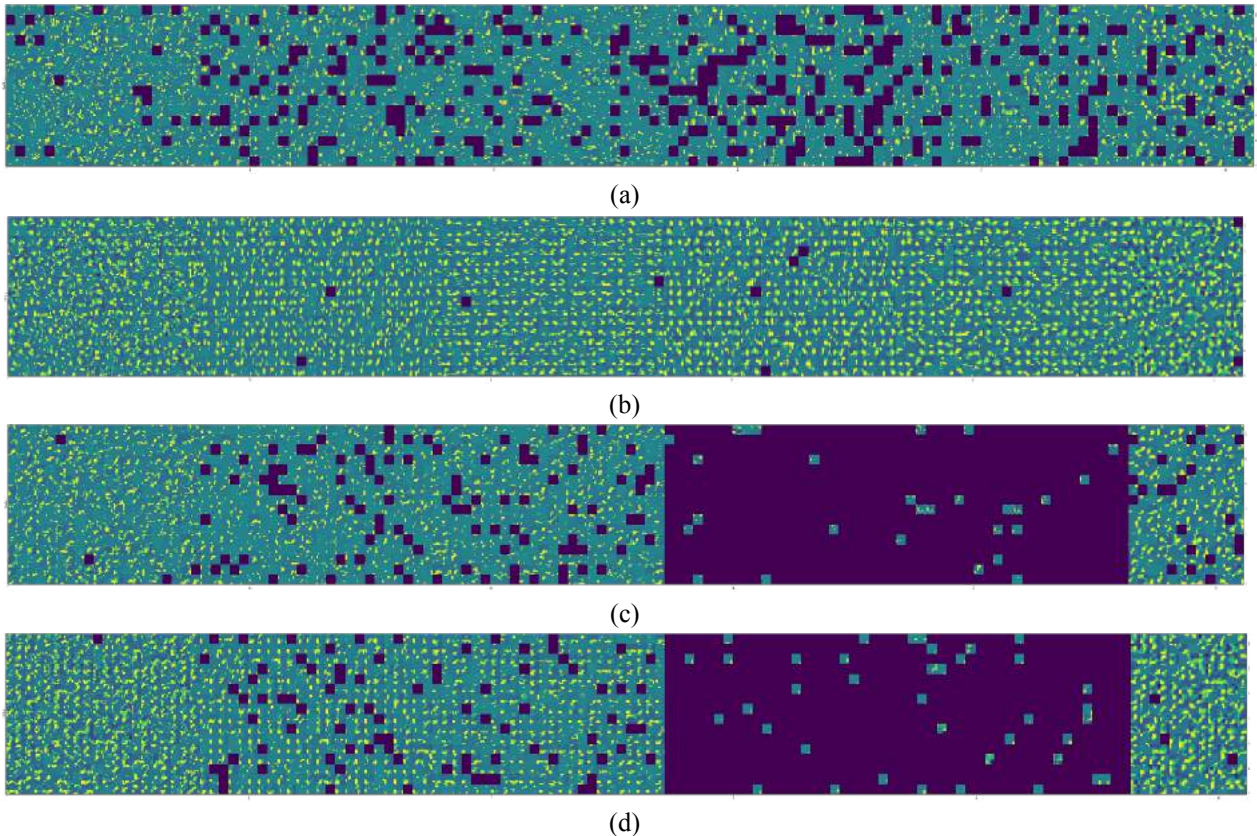
Figure 7. Feature maps visualization from intermediate layers in customised output and weight initialisation model. (a) and (b) Feature maps of customised output models' Mixed9 and Mixed10 layers, respectively and (c) and (d) Feature maps of weight initialisation models' Mixed9 and Mixed10 layers.

Hypothetically, the training time should be lower for the model having fewer trainable parameters. However, we did not observe such a phenomenon. It might be due to the GPU-enabled high computational machine. If it would train on CPU, significant differences might obtain.

With the increase in the volume of training datasets, the performance of the model improved remarkably. However, for the plant disease classification, the weight initialization approach suits the best because of the significant dissimilarity

between the ImageNet images and plant disease images. When the deeper layers of the model were fine-tuned with the new domain datasets, the model learned its parameter to identify the fine details. For instance, the tomato early blight (class: 8) shows similar characteristics to other disease classes, so that feature extraction and customized output layer approach could not differentiate it. However, fine-tuning the deeper layers made the model more specific.

4. Conclusions

From this study, following conclusion can be inferred.

- For fewer datasets, lightweight architecture with customised output or feature extraction transfer learning could prefer.
- For a medium or considerable amount of training data volume, weight initialisation transfer learning could be the best option.
- We also tried with fine-trained from some medium layers, the performance did not improve, but reduced meagrely, that means only the final few blocks of the architecture are well enough to fine-train.
- We also tested with more dense layers in classifier networks, but it also did not improve performance. Therefore, only changing the output layer of the standard architecture and fine-tune few deeper blocks could produce better result.
- Some researchers added an extra convolutional block and dense layer to the pre-trained model, but in our study, it only made the model heavy without improving the performance significantly.

Acknowledgements

References

Afifi, A., Alhumam, A., Abdelwahab, A. (2021). Convolutional Neural Network for Automatic Identification of Plant Diseases with Limited Data. Plants 10, 28.

Barbedo, J.G.A. (2018). Impact of dataset size and variety on the effectiveness of deep learning and transfer learning for plant disease classification. Computers and Electronics in Agriculture, 153(August), 46–53.

Chen, J., Zhang, D., Nanehkaran, Y., Li, D. (2020a). Detection of rice plant diseases based on deep transfer learning. Journal of Science, Food Agriculture.

Chen, J., Chen, J., Zhang, D., Sun, Y., Nanehkaran, Y.A. (2020b). Using deep transfer learning for image-based plant disease identification. Computers and Electronics in Agriculture. 173.

Food and Agriculture Organization of the United Nations. (2017). Plant health and food security. International Plant Protection Convention.

Github. PlantVillage datasets. https://github.com/spMohanty/PlantVillage-Dataset. Accessed February 1, 2021.

Kaya, A., Seydi, A., Catal, C., Yalin, H., Temucin, H. (2019). Analysis of transfer learning for deep neural network based plant classification models. Computers and Electronics in Agriculture, 158(October 2018), 20–29.

Keras API. https://keras.io/api/applications/. Accessed 31 May 2020.

Mohanty, S.P., Hughes, D.P., Salathé, M. (2016). Using deep learning for image-based plant disease detection. Frontiers in Plant Science, 7(September), 1–10.

Pan, J. P., Yang, Q. A survey on transfer learning. IEEE Transaction on Knowledge and Data Engineering. 22(10), 1345-1359.

Rangarajan, A.K., Purushothaman, R., Ramesh, A. (2018). Tomato crop disease classification using pre-trained deep learning algorithm. In: *International conference on Robotics and Smart manufacturing*. 133, 1040-1047

Sandler, M., Howard, A., Zhu, M., Zhmoginov, A., Chen, L. C. (2018). MobileNetV2: Inverted Residuals and Linear Bottlenecks. Proceedings of the IEEE Computer Society Conference on Computer Vision and Pattern Recognition, 4510–4520

Szegedy, C., Vanhoucke, V., Ioffe, S., Shlens, J. (2015). Rethinking the Inception architecture for computer vision. ArXiv:1512.00567 [cs.CV]

Tan, C., F. Sun, T. Kong, W. Zhang, C. Yang, C. Liu, 2018. A survey on deep transfer learning. In: *Artificial Neural Networks and Machine Learning – ICANN*. Kůrková V., Manolopoulos Y., Hammer B., Iliadis L., Maglogiannis I. Eds. Springer, Cham.

Thangaraj, R., Anandamurugan, S. & Kaliappan, V.K. Automated tomato leaf disease classification using transfer learning-based deep convolution neural network. Journal Plant Diseases and Protection. 128, 73–86

Early Disease Detection in Apple and Grape Using Deep Learning on a Smart-Camera

Gerrit Polder [a,*], Pieter M. Blok[a], Tim van Daalen[a], Joseph Peller[a], Nikos Mylonas[b]

[a]Agro Food Robotics, Wageningen University & Research, Wageningen, Netherlands

[b] Agricultural University of Athens, Athens, Greece

* Corresponding author. Email: gerrit.polder@wur.nl

Abstract

Downy mildew (Plasmopara viticola) and apple scab (Venturia inaequalis), are endemic diseases that affect crops worldwide. The diseases can cause severe losses in grapes, and apples, when it is not detected in an early stage. The EU Horizon 2020 OPTIMA project intends to address this problem by including early detection as part of an integrated pest management (IPM) system. In this research, we investigated the early detection of these two diseases using deep convolutional neural networks on RGB colour images. Detections serve as input to a Decision Support System (DSS), to precisely locate and quantify the infection, so that appropriate plant protection product, dose, timing, and location can be recommended.

A YOLOv5 object detection algorithm was developed that detected the apple scab and downy mildew spots on the apple and grape leaves. We specifically used the YOLOv5-small algorithm that worked on 224x224 pixel RGB images. Because the DSS and the sprayer can only work with one decision per image, we combined the detections of YOLOv5 into a single decision for each image. For real-time implementation on the sprayer a smart-camera with RGB sensor and NVIDIA Jetson TX2 edge-processing unit was used. TensorRT was used to speed-up the image analysis. The average inference time for acquiring a 1.9 MP image (1600x1200 pixels) and doing the deep-learning analysis was 0.15 seconds for YOLOv5s on TensorRT. Without TensorRT this inference times was 0.20 seconds. Results showed a false detection rate of 10% for apple scab and 8.0% for downy mildew. The accuracy of YOLOv5 was 90.0% on apple scab and 93.8% on downy mildew.

Keywords: convolutional neural networks, decision support system, integrated pest management, edge computing.

1. Introduction

Downy mildew (Plasmopara viticola) and apple scab (Venturia inaequalis) are endemic diseases that affect crops across the world. These diseases can cause severe losses in grapes and apples when not treated in an early stage. Treatment can be done by spraying either copper sulphates or fungicides onto the crop before the funguses have sporulated (Vaillancourt and Hartman, 2000, Ash, 2000). However, excessive spraying has led to a rise in disease resistance and has a negative impact on the environment (Wightwick et. al., 2012).

To reduce the amount of spraying in the field, the fungal infections should be identified so that they can be timely and precisely treated. Due to the large field sizes for each crop individually checking each leaf manually is too labour intensive, and instead machine vision could be useful. Using the advanced symptoms of apple scab on fruits, Agarwal, et. al. (2019) has been able to use traditional machine vision to correctly identify diseased fruits.

The Horizon 2020 EU project OPTIMA is working on an environmentally friendly system for integrated crop protection, which uses spectral images and predictive computer models to detect diseases, which are then controlled with biological agents that are automated. and can be applied very accurately. OPTIMA will optimize disease prediction models for downy mildew in vineyards, apple scab in apple orchards and *Alternaria* leaf blight in carrots to envisage faster the possibility of disease outspread and developing advanced early detection methods based on RGB colour imaging and spectral imaging combined with deep learning techniques to precisely localise and quantify the infection.

In this study we use deep learning techniques to detect apple scab and downy mildew under field conditions using RGB colour images.

2. Materials and Methods

2.1. Apple scab image acquisition

In the time period 2018 till 2020, hundreds of images of apple trees with and without scab were acquired in orchards of the Wageningen University & Research field station in Randwijk (The Netherlands) and an organic apple orchard near Randwijk. At the field station, trees were inoculated while at the organic farm trees suffered from natural infection. Images were taken with the IDS U3-3800SE industrial machine vision camera using a Tamron 16 mm f/1.8 lens. Additionally, cell-phone images of apple scab infected apple leaves were acquired by OPTIMA partners in Spain in two different fields in the area of Èpila. The images were annotated using the open-source program LabelImg

(https://github.com/tzutalin/labelImg) by the crop experts from the Universitat Politecnica de Catalunya (UPC) and Wageningen Research. To increase the variation in the dataset and to potentially improve the generalization of the algorithm, 20 apple scab images of the open source PlantVillage dataset (Hughes and Marcel Salathe, 2016) were added to the training data.

2.2. Vine downy mildew image acquisition

Initial trials to detect downy mildew in grapes occurred in Turin (Italy) and the Piedmont area (Italy) in 2019. The camera setup was transported to Turin and setup outside of a greenhouse compartment on the campus of the University of Turin. The greenhouse contained pots of young grapes that were inoculated with downy mildew. The plants were divided into 4 groups, 3 different fungicides were being tested, and one group of control plants. In total 146 images of infected potted plants were obtained and a control group of 5 healthy plants were also imaged. After measuring at the University, the setup was transferred to a vineyard near Frassinello Monferrato (Italy) where images were taken from the side at a distance of roughly 0.9 m from the leaves with natural infection. The camera was moved slowly down a row of grapes and areas of downy mildew were identified by the vineyard manager and in total 75 RGB images were acquired with the setup. In 2020, additional RGB images were acquired by Universita Degli Studi Ditorino (UNITO) crop experts using normal cell-phones. In 2020, the measurement setup with the high-resolution colour camera was sent to the Agricultural University of Athens (AUA) in Greece where artificial infected vines were imaged, resulting in 79 RGB images. All images were annotated by plant pathologists at AUA and UNITO using LabelImg. Every downy mildew spot was encapsulated by a rectangular bounding-box (Figure 1).
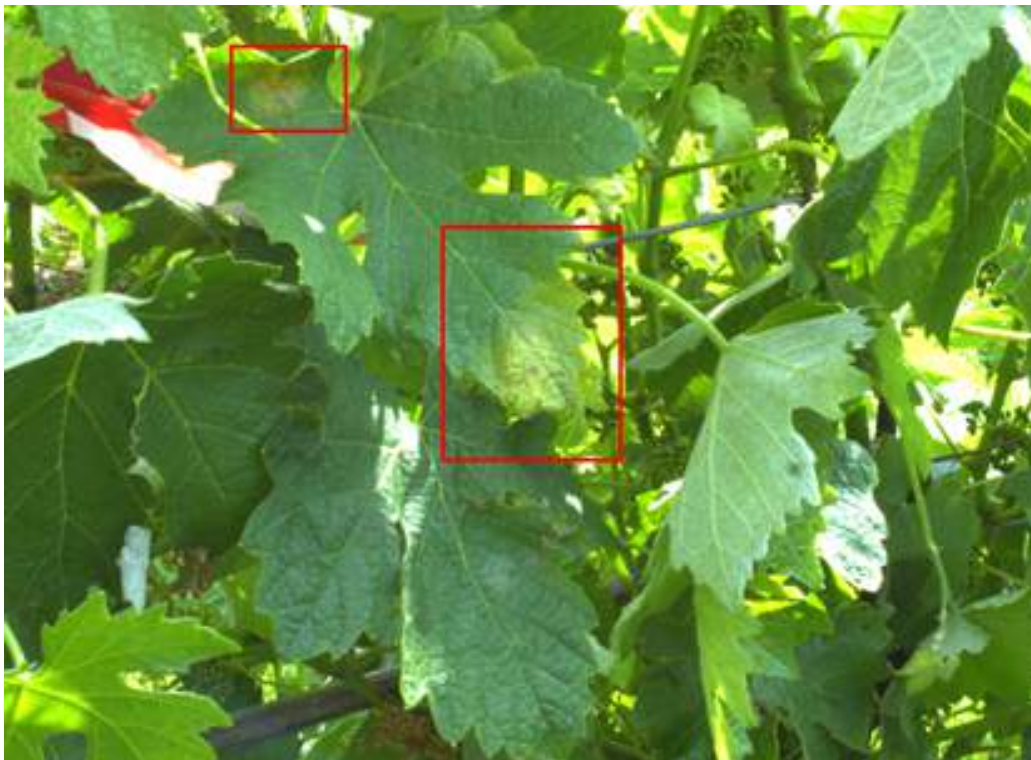
Figure 1: Example of an RGB image taken in the grape vineyard. The two red bounding-boxes encapsulate the downy mildew spots on the leaf. The bounding-boxes were annotated by crop experts and used for algorithm training and evaluation.

2.3. Disease spot detection using YOLO

The RGB images were analysed with an open-source deep learning network, called You Only Look Once (YOLO). YOLO is an algorithm that enables object detection, which is a combination of object localization and classification (Redmon, *et.al.*, 2016). As such, the relatively small diseased spots on the leaves of the two crops were classified and localized. For the initial object detection YOLO version 3 (YOLOv3) was used. The training and evaluation of YOLOv3 was done on resized RGB images of 1024x1024 pixels (this resolution was found to yield the highest performance). To improve network generalization, the network was initialized with the weights of a YOLOv3 network that was trained on the Microsoft COCO dataset (Tsung-Yi Lin, *et.al.*, 2014). This method is better known as transfer-learning. Besides transfer learning, data augmentation was used during the training to improve network generalization.

Three types of data augmentation were used: colour adjustments, image flips (right, left, up, down) and image mosaicking (merge multiple images in 1 image). Data was split in training, validation, and test dataset, making it possible to optimize the hyperparameters using the validation data and evaluate on the completely independent test data. To evaluate the performance of the algorithm, the Intersection over Union (IoU) metric was used. The IoU is a measure for the overlap between the ground truth box and the predicted box and varies between zero (no overlap) and one (full overlap). The IoU highlights the classification and localization accuracy of the algorithm. A threshold of 0.25 was chosen for the IoU, because our application can allow a less perfect localization, because the resolution of the sprayer is much lower than the resolution of the image analysis. For any diseased spot, a detection hit with marginal overlap will be sufficient. With the IoU, the total number of true positives (TP), false positives (FP) and false negatives (FN) were determined. A true positive is a diseased spot that is detected as diseased spot. A false positive is background that is detected as diseased spot. A false negative is a diseased spot that is not detected. With the total number of true positives, false positives, and false negatives, the precision (TP / (TP+FP)) and the recall (TP / (TP+FN)) were calculated. The precision is the percentage of correct detections. The recall measures how well YOLO can detect all diseased spots.

In 2020, YOLOv3 was replaced by the more advanced YOLO version 5 (YOLOv5) (https://github.com/ultralytics/yolov5). The YOLOv5-small algorithm (YOLOv5s) was used for time-efficient deployment on the smart-camera (using the Open Neural Network Exchange (ONNX) and TensorRT). For the deep learning implementation in the field, we planned to use an embedded NVIDIA Jetson TX2 GPU unit. In order to have a robust industrial platform a NEON-202B-JT2-X smart camera was chosen. This smart camera incorporates a Jetson TX2 embedded GPU and a 1.9Mpix colour camera in a IP67-certified case (Figure 2).
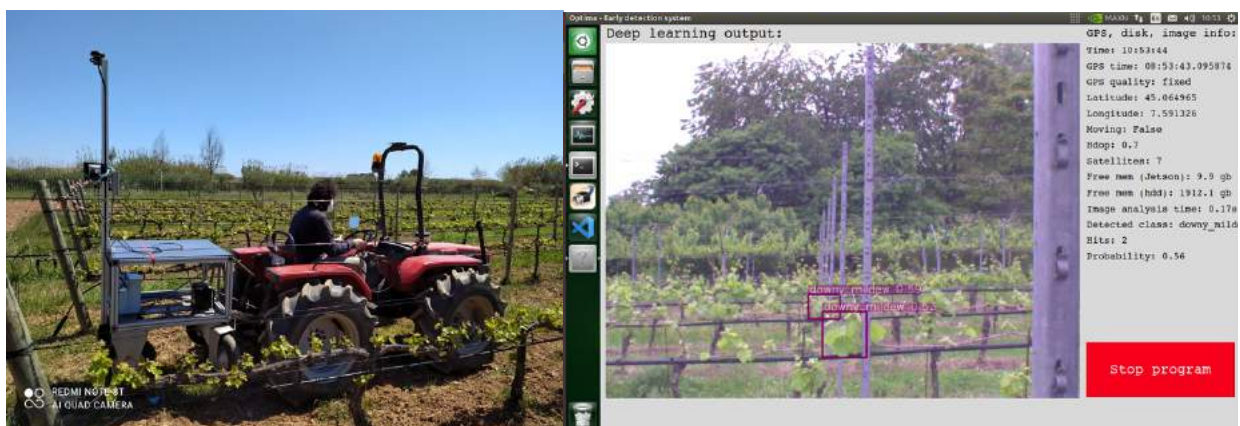
Figure 2: On the left image, the disease detection with the smart-camera in grapes. On the right image, the detection output from the YOLOv5 algorithm in the graphical user interface of the smart-camera.

3. Results and Discussion

3.1. Results scab in apple

The total number of images in the apple scab dataset was 63 and separated in 44 (70%) images for network training, 9 (14%) images for network validation and 10 (16%) as independent test dataset. The dataset consists of different cultivars from The Netherlands and Spain. The performance of the trained network is summarized in Table 1. The 10 images with apple scab had in total 163 instances of apple scab. 95 out of 163 apple scab instances were successfully detected by the network. The corresponding recall was 58.3%. 68 apple scab instances were missed (false negatives). On the 10 images, there were 12 unjustified detections (false positives). The corresponding precision was 88.8%. In Figure 3 the performance is visualized on image level in the apple orchard.

Table 1: The confusion matrix summarizes the performance metrics of YOLO on apple scab at spot level on an independent test dataset with 10 images.

	YOLO prediction		**Total**	*Recall*
Ground-truth	Apple Scab	Healthy		
Apple Scab	95	68	163	58.3%
Healthy	12	-*	-*	
Total	107	-*	-*	
Precision	88.8%			

* with a one-class object detector this comparison is not possible
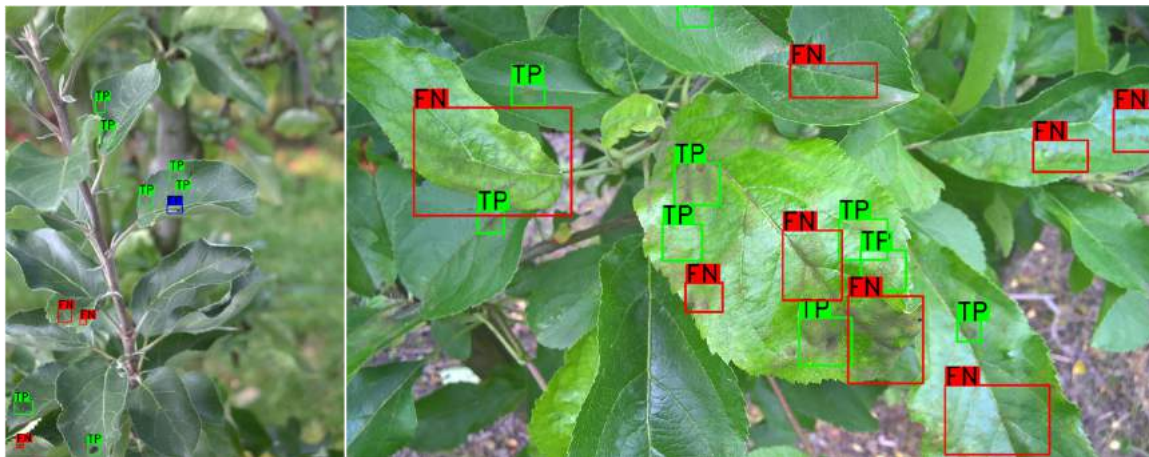
Figure 3: Two evaluation images with true positives (green), false negatives (red) and false positives (blue).

Then, the spot detections were summarised on image level. For a better comparison, we included 20 healthy images to the already existing test set of 10 images with apple-scab. The image was classified as being apple-scab when one or more spot detections were made by YOLOv5. The image was classified as being healthy, when no detections were made by YOLOv5. The results of this comparison can be found in Table 2. The overall accuracy of the algorithm was 90% with a false detection rate of 10%. For disease detection in the apple orchard, the algorithm was implemented on the NEON-202B-JT2-X smart camera. The average inference time for acquiring a 1.9 MP image (1600x1200 pixels) and doing the deep-learning analysis was 0.15 seconds for YOLOv5s on TensorRT. Without TensorRT this inference time was 0.20 seconds with YOLOv5s.

Table 2: The confusion matrix summarizes the performance metrics of YOLO on apple scab at image level on an independent test dataset with 30 images.

Ground-truth	YOLO prediction		Total	*Recall*
	Apple Scab	Healthy		
Apple Scab	9	1	10	90.0%
Healthy	2	18	20	
Total	11	19	30	
Precision	81.8%			Accuracy: 90.0%

3.2. Results downy mildew in grape

The total number of images in the grape dataset taken in 2019 and 2020 in Italy and Greece was 317. The dataset was separated in 217 (68%) images for network training, 53 (17%) images for network validation and 47 (15%) as independent test dataset. The dataset consists of three cultivars (Barbera, Moscato, Agiorgitiko). The performance of YOLO on downy mildew is summarized in Table 3. The 47 images with downy mildew contained in total 510 spot instances. 374 out of 510 downy mildew instances were successfully detected by the network. The corresponding recall was 73.3%. 136 instances were missed by the network (false negatives). On the 47 images, there were 92 unjustified detections (false positives). The corresponding precision was 80.3%. In Figure 4 and Figure 5, the performance is visualized on image level in the vineyard. Then, the spot detections were summarised on image level. For a better comparison, we included 50 healthy images to the already existing test set of 47 images with downy mildew. The image was classified as being downy mildew when one or more spot detections were made by YOLOv5. The image was classified as being healthy, when no detections were made by YOLOv5. The results of this comparison can be found in Table 4. The overall accuracy of the algorithm was 93.8% with a false detection rate of 8.0%. Inference times for acquiring the 1.9 MP image and doing the downy mildew detection was 0.15 seconds for YOLOv5s on the NEON-202B-JT2-X smart camera (using TensorRT). Without TensorRT the inference time was 0.20 seconds.

Table 3: The confusion matrix summarizes the performance metrics of YOLO on downy mildew at spot level on an independent test dataset with 47 images.

| Ground-truth | YOLO prediction | | Total | *Recall* |
	Downy Mildew	Healthy		
Downy Mildew	374	136	510	73.3%
Healthy	92	-*	-*	
Total	466	-*	-*	
Precision	80.3%			

* with a one-class object detector this comparison is not possible

Table 4: The confusion matrix summarizes the performance metrics of YOLO on downy mildew at spot level on an independent test dataset with 97 images.

| Ground-truth | YOLO prediction | | Total | *Recall* |
	Downy mildew	Healthy		
Downy mildew	45	2	47	95.7%
Healthy	4	46	50	
Total	49	48	97	
Precision	91.8%			Accuracy: 93.8%
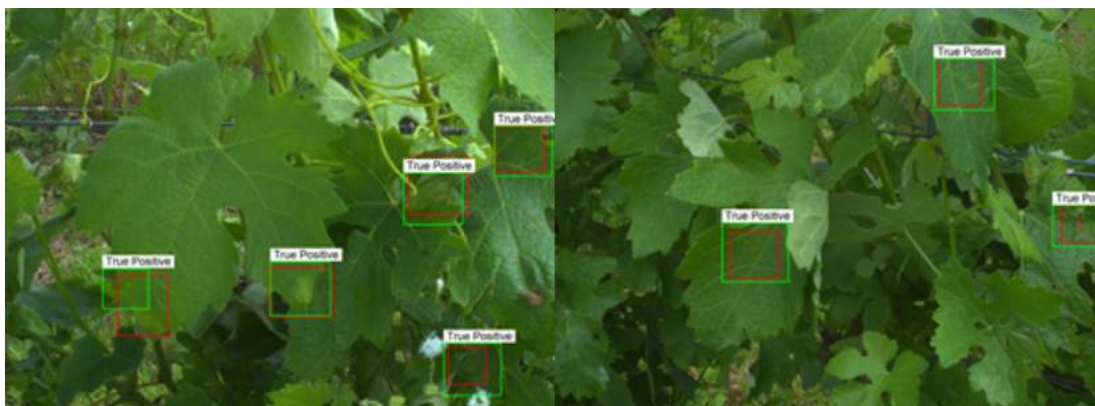
Figure 4: Two evaluation images with very early symptoms in which YOLO had a 100% true positive score. The bounding boxes in red are the annotated downy mildew instances. The bounding boxes in green are the detected instances by the network.
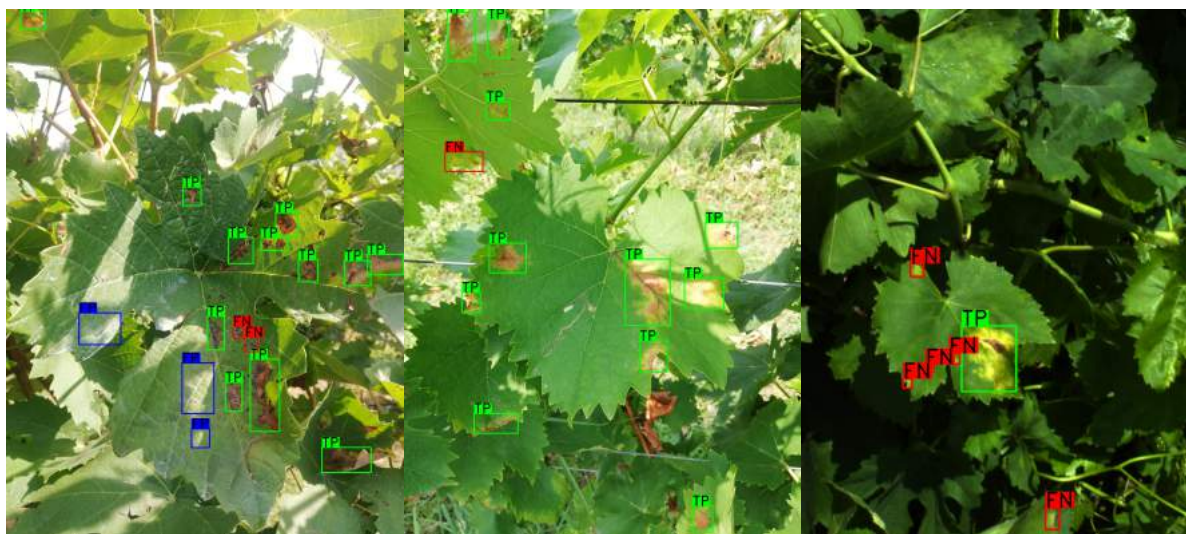
Figure 5: Three evaluation images of downy mildew in a later stage, with true positives (green), false negatives (red) and false positives (blue).

4. Discussion and conclusion

Results show good detections for disease spots, even for early and subtle symptoms. Still the network gives false positive and false negative detections. The resolution of the spot level decisions though is much higher than the resolution on which the sprayer operates in the integrated pest management approach. When translating the spot detections to the image level, which is even still a higher resolution than the sprayer, then the accuracy was 90.0% for apple scab and 93.8% for downy mildew. These values are in line with the objectives of the OPTIMA project. Main reason for false negatives (missed symptoms) when compared with the smart-camera system in the field, is that the symptoms are not visible by the camera, for instance when occluded by healthy leaves.

The initial algorithm was trained with YOLOv3 on a desktop computer with a a NVIDIA GeForce RTX 2080 Ti GPU. Switching to YOLOv5 resulted in better performance and inference time. For edge-computing in the field, the algorithm was deployed on a NEON-202B-JT2-X smart camera, using the ONNX and the TensorRT real-time implementation. The average inference time for acquiring a 1.9 MP image (1600x1200 pixels) and doing the deep-learning analysis was 0.15 seconds for YOLOv5s, which is a little faster than the 6 images/s OPTIMA objective. With an image width of 50cm, this results in a driving speed of 3 m/s (10 km/h).

Extensive field trails in Italy and Spain during the 2021 growing season will provide additional data to retrain and improve the network for apple scab and vine downy mildew. Furthermore, field trails in France will extend and improve the initial work done on the detection of *Alternaria* leaf blight in carrot.

References

Agarwal A., Sarkar A., Dubey A.K. (2019) Computer Vision-Based Fruit Disease Detection and Classification. In: *Tiwari S., Trivedi M., Mishra K., Misra A., Kumar K. (eds) Smart Innovations in Communication and Computational Sciences. Advances in Intelligent Systems and Computing*, vol 851. Springer, Singapore. https://doi.org/10.1007/978-981-13-2414-7_11

Ash, G. (2000), "Downy mildew of grape". The Plant Health Instructor. Retrieved 2021-04-02. DOI: 10.1094/PHI-I-2000-1112-01

David. P. Hughes and Marcel Salathe. (2016) An open access repository of images on plant health to enable the development of mobile disease diagnostics. arXiv:1511.08060 [cs.CV].

Tsung-Yi Lin, Michael Maire, Serge Belongie, Lubomir Bourdev, Ross Girshick, James Hays, Pietro Perona, Deva Ramanan, C. Lawrence Zitnick and Piotr Dollár. (2014) Microsoft COCO: Common Objects in Context. arXiv: 1405.0312 [cs.CV]

Joseph Redmon, Santosh Divvala, Ross Girshick and Ali Farhadi, (2016) You Only Look Once: Unified, Real-Time Object Detection. arXiv:1506.02640 [cs.CV].

Vaillancourt, L.J. and Hartman, J.R. (2000) Apple Scab. The Plant Health Instructor. https://doi.org/10.1094/PHI-I-2000-1005-01.

Wightwick, Adam M.; Salzman, Scott A.; Reichman, Suzanne M.; Allinson, Graeme; Menzies, Neal W. (2012-08-14). "Effects of copper fungicide residues on the microbial function of vineyard soils". Environmental Science and Pollution Research.

Flower Monitoring in a Hedge Almond Orchard with Image Analysis

Dias, António B.[ab*], Donno, Patrick[c], Gonçalves, Ana Cristina[ab]

[a] Departmento de Engenharia Rural, University of Évora, Évora, Portugal

[b] MED – Mediterranean Institute for Agriculture, Environment and Devlopment, Évora, Portugal

[c] Torre das Figueiras Sociedade Agrícola Lda, Monforte, Portugal

* Corresponding author. Email: adias@uevora.pt

Abstract

The hedge almond orchards is a recent technology, for which available information is scarce. In an almond orchard, variety Soleta, planted in September 2014, in Herdade da Torre das Figueiras – Monforte - Portugal (39º 04' N; 07º 29' W), a trial to evaluate different pruning treatments was established. The flowering intensity was evaluated as function of four pruning treatments, which influences the number and length of branches. The flowering was evaluated in 2019 and 2020, with image analysis. For each tree, a vertical photograph of the crown was taken perpendicularly to the tree line, using a contrasting background. A total of 360 trees were surveyed. The flowering area was quantified per tree using an image analysis software. The results show significant differences for the flowering area between years, with the largest in 2019. This is indicative of a trend towards the fluctuation of the flowering level. Significant differences were also observed between pruning treatments. In both years, the smallest flowering area was observed in manual pruning. Overall, manual pruning had lower flowers' density, which could be due to the removal of shoots of excessive development lengthwise. The results show that monitoring based on photograph image analysis might be an option to evaluate flowering and its variability between years for the hedge orchards.

Keywords: pruning, Soleta variety, variance analysis, Portugal

1. Introduction

In the Mediterranean basin, after the expansion of the super high density (SHD) or hedge olive orchards, some hedge almond orchards have also been planted. This training system could reduce harvesting costs due to the use of the same machinery as in vineyards and olive orchards (Torrents, 2015), but require the adequacy of the canopy dimensions to the over-the-row harvesting machine.

In order to control canopy dimension, Torrents (2015) suggests the use of mechanical pruning with topping and hedging since the first year of plantation. Manual pruning should only be used to eliminate dried shoots or vigorous branches (Torrents, 2015). In almond trees, the spurs, that is the very short proleptic shoots, are primordial to fruiting in mature trees (Kester *et al.,* 1996 *cit in* Valdebenito *et al.*, 2017). Thus, it is of the utmost importance to study the management practices effects, in particular pruning, on the flowering and fruiting. To attain a regular fruiting yield, it is necessary a high number of flowers annually (Kester, 1959 *cit. in* Casanova *et al.,* 2019), since almond tree yield, according to Tombesi *et al.* (2016) is primarily related to the flower number and less to the fruit set.

The image analysis has been used to study winter pruning systems in the vineyard (McFarlane *et al.*, 1997) and for the quantitative monitoring of pesticides application with hydrosensitive paper (Panneton, 2002; Marques Da Silva *et al.,* 2017). However, no references were found to the use of image analysis in the quantification of almond tree flowering as well as on the effect of pruning on flowering.

The goals of this study are twofold; the quantification of the almond tree flowering area and their interannual variability and the effect of pruning on flowering.

2. Materials and Methods

2.1. Orchard

The trial was established in a commercial hedge almond orchard. The orchard was established in September 2014 at Herdade da Torre das Figueiras-Monforte-Portalegre-Portugal (39º 04' N and 07º 29'W). The orchard was ridge planting in a 5m x 1.5m spacing with east-west orientation. The cultivars 'Soleta', 'Belona', 'Guara' and 'Lauranne' grafted on RootPac 20 or Densipac® (www.rootpac.com) rootstock (Prunus besseyi x Prunus cerasifera) were used. Plants with 6 months' nursery from Agromillora Catallana were used. Trees were tutored to ensure central axis formation, assuring that the height of the beginning of the crown was at least at 0.5 m from the ground.

2.2. Pruning treatments

The trial was established in the orchard plot of 'Soleta' cultivar. A randomized complete block design, with four pruning treatments and three replications was used (in a total of 12 plots). Each plot has 95 almond trees. The pruning treatments were (Figure 1): T0 – farmer pruning, with mechanical topping and hedging at the beginning of June in

2018, 2019 and 2020, winter manual pruning in 2018 and manual pruning complement in June 2019 and after harvest in 2020; T1 – winter manual pruning in 2018, 2019 and 2020; T2 – post-harvest mechanical pruning (topping and hedging) in September 2018, 2019 and 2020, winter manual pruning in 2018 and 2020; T3 – summer mechanical pruning (topping and hedging) at the end of July in 2018, 2019 and 2020 and winter manual pruning in 2018 and 2020.
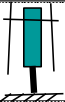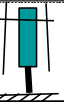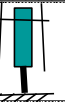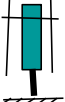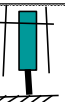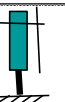
Treatment	Pruning season	2018 (Year 4)	2019 (Year 5)	2020 (Year 6)
T0	**Winter**	Manual pruning		
	Summer	Topping + Hedging	Topping + Hedging	Topping + Hedging
			Manual complement	
	Post harvest			Manual complement
T1	**Winter**	Manual pruning	Manual pruning	Manual pruning
T2	**Winter**	Manual pruning		Manual pruning
	Summer			
	Post harvest	Topping + Hedging	Topping + Hedging	Topping + Hedging
T3	**Winter**	Manual pruning		Manual pruning
	Summer	Topping + Hedging	Topping + Hedging	Topping + Hedging
	Post harvest			

Figure 1. Schematic representation of pruning interventions between 2018-2020

2.3. Methodology

For the evaluation of flowering in each pruning treatment 30 almond trees were randomly sampled. The flowering surveys were done in 2019 and 2020 when the orchard was in full bloom (February). A photograph was taken for each sampled tree (in a total of 360 trees). A photographic camera Cannon model EOS 1100D was used. The photographs were taken with the maximum aperture (position 4), without flash, focal distance of 25 mm, with a resolution of 72 ppp. Each photograph was taken perpendicularly to the tree line in the south direction at a distance to the tree of 3.5 m, at the height of the eyes of the operator (about 1.6 m), without tripod. To reduce the effect of the background (which included other almond trees and its flowering) a black canvas of 1.65 x 1.65m fixed in two wooden sticks of 2m long, was placed behind each tree, in days with uniform light.

The images were processed in two steps. In the first the images were cut by the limit of the black canvas. The second step was the identification of the flowers as function of a minimum and maximum threshold of the colour histogram. The area of flowering as calculated as a percent of the number of pixels with flowers in relation to the total number of pixels. The evaluation was done in pixels to reduce the bias deriving from the pixel conversion in metric units. The image analysis was done in Paint and SigmaScan Pro 5.0.

Data normality and homogeneity of variance were evaluated with Shapiro-Wilk normality test and Levene test. As the assumptions for normal distribution and homogeneity of variance were not met, the comparison of flowering between pruning treatment and year was carried out with non-parametric statistical tests of Kruskall-Wallis and of

Bonferroni (for multiple comparisons). The statistical analysis was done in IBM SPSS Statistics, version 24.0 (IBM Corp., 2019) with a level of significance of 0.5.

3. Results and Discussion

The results of the processing images are shown in Figure 2. The image processing was able to capture the flower level.
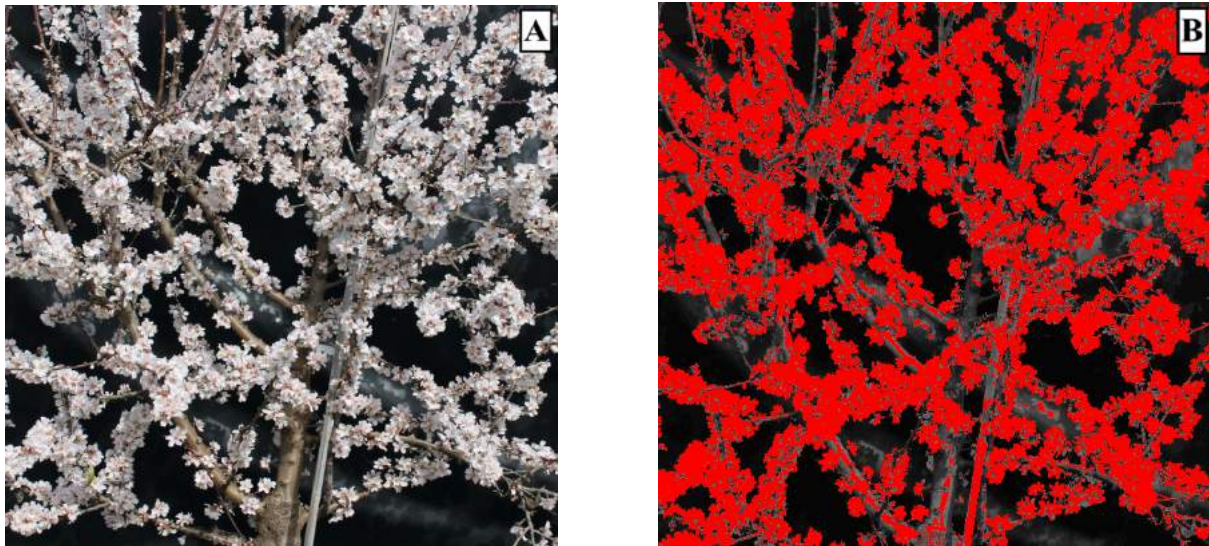
Figure 2. Photographs of the flowering of a tree (A) and the resulting area after image processing (B).

Flowering area was higher in 2019 than in 2020 (Figure 3). While in 2019 it varied between 9% and 46% with a median around 30%, in 2020 it ranged from 0% to 17%, with a median around 4%. Yet, the variability in the flowering area was higher in 2019 than in 2020. The significant differences of the flowering area between 2019 and 2020 (U = 139.000, p = 0.000), can be due to the effect of flowering in the previous year and pruning treatment.

For perennial species, and in particular for almond trees, several authors (Reidel *et al.*, 2004 *cit. in* Valdebenito *et al.*, 2017; Tombesi *et al.*, 2011) refers that flowering level is dependent on the previous year flowering and that interannual variability is large.

A similar trend was observed in this study. The higher number of flowers in 2019 may have resulted in the development of a lower number of flower buds in 2020. This is related with the crown dimension and the former year flowering level, due to the number of flower buds produced. The amount of photoassimilates used in flowering in one year with high flowering intensity results that in the following year the flowering level is lower as trees invested mostly in flowering and less in bud formation. Reidel *et al.* (2004 *cit. in* Valdebenito *et al.*, 2017) refers that the probability of death of the spurs that bear fruits when compared with those that do not is 80%. Also, flowering and fruiting needs high amounts of carbohydrates, which might result in the depletion of the trees' reserves. This will result in the reduction of the number of flowering buds and flowers and/or the death of the spurs (Tombesi *et al.*, 2011).

Pruning is a key factor in hedged orchards, because crown dimensions have to be within the thresholds of the harvesting equipment. This requires the execution of annual pruning interventions to control crown dimensions which could reduce the flowering level.

The results of this study show a trend towards the fluctuation of high and low flowering level. Yet, a longer time series is needed to confirm this trend. Also, the winter manual pruning interventions should be carefully thought so that it is carried out in the year with potentially higher flowering intensities to promote a more constant flowering in time.
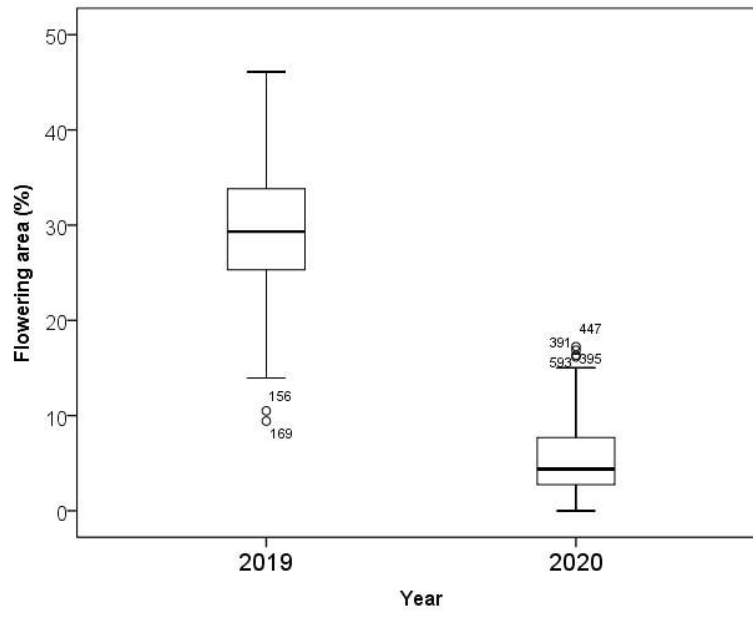
Figure 3. Flowering area per year.

The analysis per year and per pruning treatment reveals that T1 had the lowest flowering intensity and variability in 2019 (Figure 4). In spite of the interannual flowering variability, pruning determined its intensity with significant differences between the four pruning treatments in both years ($\chi^2(3) = 152.123$, $p < 0.000$ and $\chi^2(3) = 20.288$, $p < 0.000$, respectively for 2019 and 2020). Flowering of T1 differs significantly from the other three treatments for both years (*all*, $p < 0.05$). This result can be explained by the manual pruning in 2018, which resulted in larger reductions of the crown dimension than the other pruning treatments and thus on the flowering.
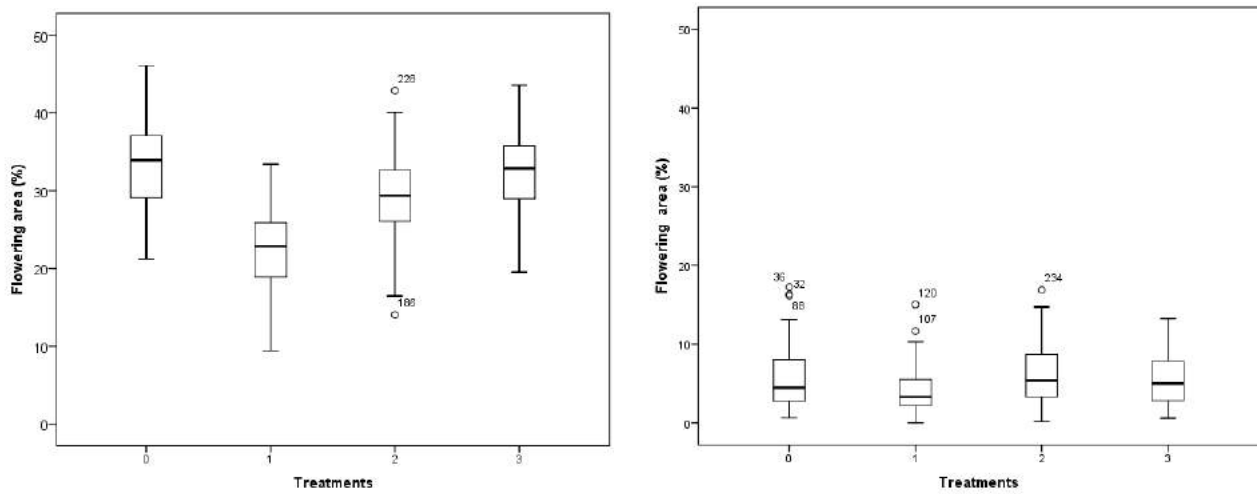
Figure 4. Flowering area per pruning treatment for 2019 (left) and 2020 (right).

No significant differences were observed between T0 and T3 (*all*, $p < 0.05$) for both years. The anticipation of the summer pruning (beginning of June for T0) or delay (final of July for T3) did not affect the flowering level in the following years (2019 and 2020). Also, the manual complement pruning (summer in T0 *versus* winter in T3) did not affect the flowering level of the following year, which was low.

Flowering in T2 had a different behavior in 2019 and 2020. In 2019 significant differences were observed between T2 and the other three treatments (*all*, $p < 0.05$). This is probably due to the higher pruning intensity in 2018, though no winter manual pruning was done. Inversely, in 2020 no significant differences were found between this and the other pruning treatments (*all*, $p > 0.05$). The lower flowering level of T2 in 2019 when compared with T0 and T3 might be explained by reserve depletion of the trees of T2, due to the higher fruit yield in 2018 (Dias *et al.*, 2019).

Overall T1 resulted for both years and most of the evaluated trees in a lower flowering level intensity. When pruners remove from the tree the longer shoots developed lengthwise, they are also reducing its density in the crown. This could explain the lower flower level found in T1.

The cuts made mechanically in the faces of the hedge (T0, T2 and T3) can contribute to higher density of branches with short length and higher density of flower buds per crown.

4. Conclusions

The image analysis used in this study to evaluate and monitor the flowering level is a cost-efficient technique. It enabled the evaluation of the interannual variability of flowering as well as the effect of pruning on flowering. It was observed a trend towards the reduction of flowering intensity from 2019 to 2020, and that mechanical pruning treatments promotes higher density of branches and shorter branches which results in higher flowering level.

The variability observed highlights the need to continue to monitor the flowering level in order to find which pruning technique optimizes flowering.

Acknowledgements

References

Casanova-Gascón, J., Figueras-Panillo, M., Iglesias-Castellarnau, I., Martín-Ramos, P. 2019. Comparison of SHD and Open-Center Training Systems in Almond Tree Orchards cv. 'Soleta'. *Agronomy*, *9*, 874. https://doi.org/10.3390/agronomy9120874

Dias, A.B., Reis, J., Rebola, J., Falcão, J., Pinheiro, P., Peça, J.O. (2019) Avaliação da influência da poda no desempenho da máquina de colheita em pomares superintensivos de amendoeiraTitle. In: García-Ramos, F.J.; Martín-Ramos, P. (Ed.). Proceedings of the 10th Iberian Agroengineering Congress. Huesca, Spain: Universidad de Zaragoza, pp. 360-372.

Marques Da Silva J.R., Correia M., Dias A., Serrano J., Nunes P. 2017. Vineyard cover spraying evaluation according to plant vigour variations. Chemical Engineering Transactions. 58, 637-642 DOI: 10.3303/CET1758107

McFarlane, N.J.B., Tisseyre, B., Sinfort, C., Tillett, R . D., Sevila, F. 1997, Image Analysis for Pruning of Long Wood Grape Vines. Journal of Agricultural Engineering Research. 66 (2), 111 – 119

Panneton, B. 2002. Image analysis of water-sensitive cards for spray coverage experiments. Applied Engineering in Agriculture. 18(2), 179-182.

Tombesi, S., Lampinen, B.D., Metcalf, S., DeJong, T. M. 2016. Yield in almond is related more to the abundance of flowers than the relative number of flowers that set fruit. California Agriculture. 71(2), 68-74. http://dx.doi.org/10.3733/ca.2016a0024.

Tombesi, S., Lampinen, B. D., Metcalf, S., DeJong, T. M. 2011. Relationships between spur- and orchard-level fruit bearing in almond (*Prunus dulcis*), *Tree Physiology*, 31(12), 1413–1421, https://doi.org/10.1093/treephys/tpr119

Torrents, J. 2015. Estado actual del cultivo superintensivo del almendro. In Simposio Nacional de Almendro y otros Frutos secos, Lérida, Espanha, 24 Set. 29-43.

Valdebenito, D. , Tombesi, S., Tixier, A., Lampinen, B., Brown, P., Saa, S. 2017. Spur behavior in Almond trees (Prunus dulcis [Mill.] DAWebb): effects of flowers, fruit, and "June drop" on leaf area, leaf nitrogen, spur survival and return bloom, Scientia Horticulturae, Volume 215, Pages 15-19, https://doi.org/10.1016/j.scienta.2016.11.050.

Automation, robotics and sensor technology

Detecting Spectral Signals in Imaging for Disease Detection in Apple and Grape

Joseph Peller [a]*, Gerrit Polder [a], Pieter M. Blok [a], Ioannis Malounas [b]

[a] Wageningen University and Research, Droevendaalsesteeg 4, 6708 PB, Netherlands
[b] Agricultural University of Athens, Iera Odos 75, 11855 Athens, Greece
* Corresponding author (Joseph.Peller@wur.nl)

Abstract

Downy mildew (*Plasmopara viticola*), and apple scab (*Venturia inaequalis*) are endemic diseases that affect crops across Europe. These diseases can respectively cause severe losses in grapes, apples in particular when not detected in an early stage. Spectral image sensing was explored to see whether it outperforms standard RGB colour imaging due to its extended wavelength range and more detailed reflection over the spectrum. Image data was acquired in apple orchards, vineyards and greenhouses of Italy and the Netherlands using a research based IMEC Snapscan spectral camera with high spectral resolution (150 bands, 470-900nm), and later a commercially available SILIOS spectral camera. We show using these datasets and a linear discriminant analysis that detection of early symptoms of both diseases is possible.

Keywords: spectral imaging, downy mildew, apple scab, linear discriminant analysis, classification

1. Introduction

Downy mildew (*Plasmopara viticola*) and apple scab (*Venturia inaequalis*) are endemic diseases that affect crops across the world. These diseases can respectively cause severe losses in grapes and apples respectively when not detected in an early stage. Both diseases can be treated by spraying of either copper sulphates or fungicides onto the crop before the funguses have sporulated.[1,2] However, excessive spraying has led to a rise in disease resistance and has many many negative environmental effects.[3]

To reduce the amount of spraying in the field, the fungal infections should be identified so that they can be timely and precisely treated. Due to the large field sizes for each crop individually checking each leaf by hand is too labour intensive, and instead machine vision could be useful. Using the advanced symptoms of downy mildew and apple scab, studies have been able to use traditional machine vision and deep learning to correctly identify fungal disease in the crop.[4] However, early detection of the disease symptoms has proven difficult.

In the last decade, much work has been done using spectral imaging (SI) for the non-destructive characterization of damages on fruit. Unlike traditional imaging, spectral imaging allows one to look simultaneously at narrow bands of light from the UV to the SWIR. These narrow bands can be used to get a deeper understanding on the biological interactions of the plant with diseases.[5,6] (Nur, 2016) has shown that it is possible to detect apple scab on apple fruits[7] and downy mildew was found to have characteristic spectral symptoms in cucumbers especially in the near infrared range.[8]

In this paper we present the results of a study conducted over 2019 and 2020. A spectral camera was taken to grape vineyards and apple orchards and images of early fungal disease symptoms on the leaves were captured. The spectral response of these early disease symptoms was analysed and a mathematical classifier was trained. Our goal was to show that early symptoms of fungal plant disease can be enhanced using spectral imaging, this could potentially lead to more robust image analysis techniques such as neural network classification on spectral images.

2. Materials and Methods

Each crop was imaged individually at two different locations. Apple trees were imaged at the experimental fruit orchards in Randwijk, Netherlands. Trees were marked and 52 branchlets leaves were inoculated with apple scab. A second group of 29 branches were inoculated with a water mixture to provide a control group. After six days the trees were imaged for 3 consecutive days in sync with the emergence of apple-scab lesions on the leaves. In total, 138 spectral images were collected over the trial.

Grape vines infected with downy mildew were imaged in a controlled greenhouse at the University of Turin and in the field in Piedmont, Italy. The grapes grown in the greenhouse trial were inoculated with downy mildew one week before imaging, and symptoms were evident to the human eye. In total 201 infected plants were imaged. The field trial was conducted on an organic vineyard that did not use pesticides. Due to these conditions, spores were present across the crop. The crop was imaged the day after a rainstorm and the fungus had just begun sporulation.

An imaging platform was deployed in the field with several cameras. The measurement rig was designed to fit on to

a standard cart to be pulled through the field or greenhouse rows. A stationary frame was used, with a camera plate that can pivot forward for field trials, and down for greenhouse pots (Figure 1). For this experiment multiple cameras were placed on a sensor platform and mounted with their field of view overlapping. A RGB camera, an IDS 10 Mpixel NXT camera, a Hyphen Airphen six band multispectral camera, and the IMEC Snapscan. The IMEC Snapscan was chosen as the spectral camera for this experiment. The camera has 150 wavelength bands from 470 - 900 nm. The camera is relatively fast for a spectral camera and has a high signal to noise ratio and an acquisition time as low as 200 ms in high light conditions. All three camera recorded an overlapping field of view, the Imec provided our spectral image, the RGB camera was used to annotate the images for fungal disease by experts after the data collection, and the hyphen camera was used to see if a standard agricultural multispectral camera could be used to detect the diseases. The data from the Airphen will be used in future studies.

Figure 1. An example of the setup in the field and all three cameras imaging downy mildew

2.1. Spectral Image analysis

2.1.1.Spectral Image analysis

RGB images were annotated by experts to mark regions of apple scab or downy mildew infection in each image. These annotations were then used to identify and mask out areas in the spectral image that correspond to the disease expression on the plant.

Raw spectral images were pre-processed by the spectral camera using an image of a white Polytetrafluoroethylene (PTFE) sheet to create a white reference and images with the shutter closed to create a dark reference using equation 1.

$$R_\lambda = \frac{I_\lambda - B}{W_\lambda - B} \tag{1}$$

Where R_λ is the reflection value at wavelength λ, I_λ is the original measured reflection value, W_λ is the spectral radiation of the white reference and B is the black reference.

All images were processed into reflectance images automatically during image capture.

Due to variance in lighting conditions across images in the open field, the images were normalized by dividing the spectrum of each pixel in the image by their max intensity value. This created a normalized intensity image with all spectral values scaled between 0 and 1.

2.1.2.Linear discriminant disease classification

Images were processed using the PerClass statistical toolbox (Version 5.4, Wageningen, The Netherlands) in MATLAB. For each disease dataset the images were annotated by hand. Using this annotation two classes were created, 'diseased' and 'healthy'. Ten images were selected with clear indications of disease to create the classes and each class region had over 5000 pixels. These classes were used to train a linear discriminant analysis (LDA) classifier[9] and tested on 5 additional labelled images. The output of the LDA training is a weight vector which when multiplied by the input spectrum, summed over the wavelengths and after applying a threshold separates the input spectrum between the two classes.

For spectral imaging in the field the effectiveness of the classifier must be balanced with speed due to the constantly changing situation in the field. It is often not practical to allow for long acquisitions of high spectral resolution images when symptomatic features are often broad. For this reason, a few discriminating wavelengths can be selected that accurately indicate the disease while increasing acquisition speed.

To select the most discriminating wavelengths for each classification the feature weight vector was examined in more depth. The LDA feature vector corresponds to each wavelength band of the image, therefore the feature weight vector shows the relative power of each wavelength band to separate the 'diseased' and 'healthy' classes. From this analysis, wavelength regions of high discriminatory power can be identified. These most important wavelength regions can be implemented in a multispectral snapshot camera, for the implementation of real-time disease detection in the field.

3. Results

3.1. Disease classification

Figure 2 shows an example of the average spectra of healthy leaf tissue, and leaf tissue infected with apple-scab. From this figure we learned that the region between 480 nm to 720 nm was shown to be highly indicative of the darkening of the leaf tissue caused by apple scab, with the secondary region from 740-880 nm showing a much wider variation in the spectrum across apple scab spots.
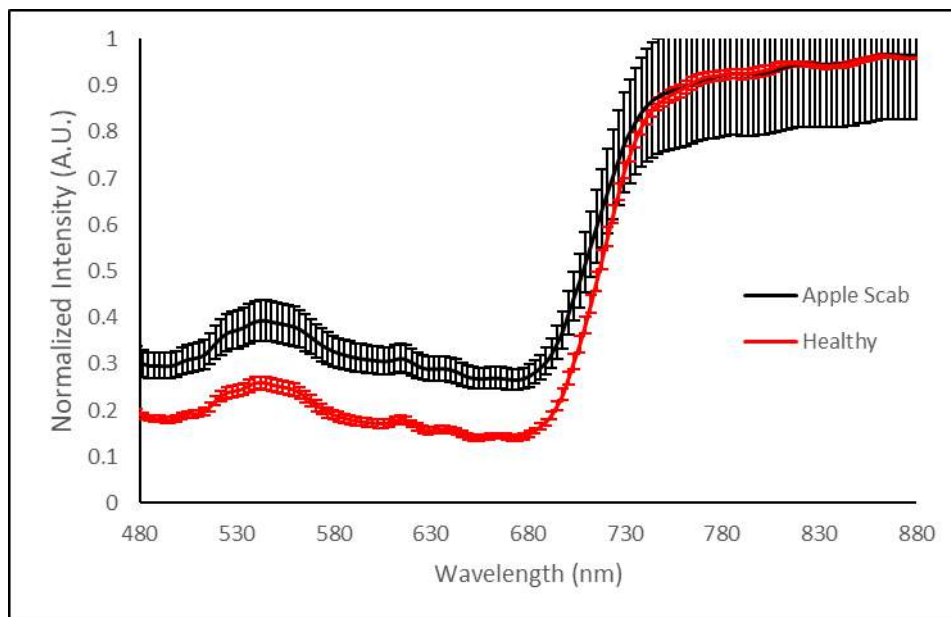
Figure 2: An example of the average spectra of healthy leaf tissue, and leaf tissue infected with apple scab.

For downy mildew, after normalizing the spectrum, a clear difference in the spectrum was observed from 535 to 680 nm (Figure 3). This seems to come from early stages of senescence in the leaf, and in this range the mildew was more reflective than the surrounding healthy leaf.
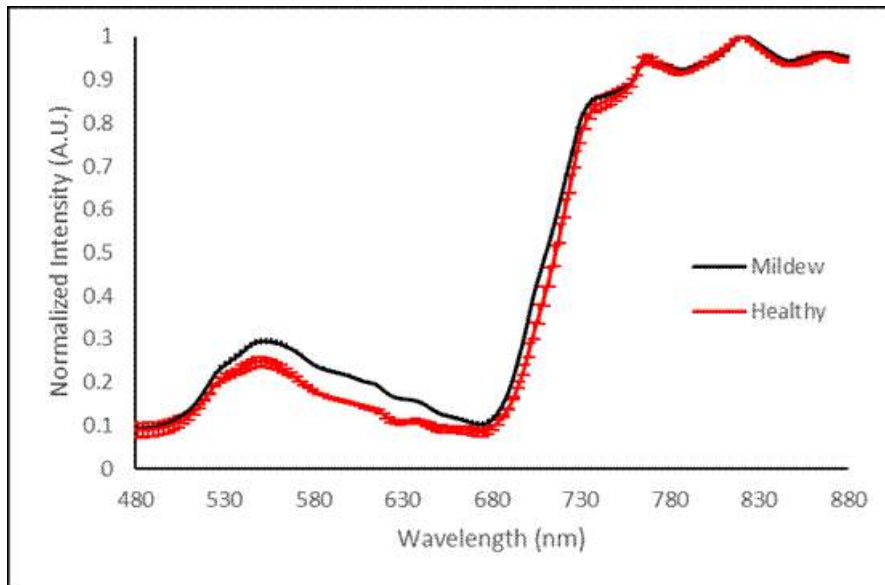
Figure 3: An example of the average spectra of healthy leaf tissue, and leaf tissue infected with downy mildew. The difference in the spectra is apparent to growers as a lightening of the leaf.

3.2. Spectral band selection
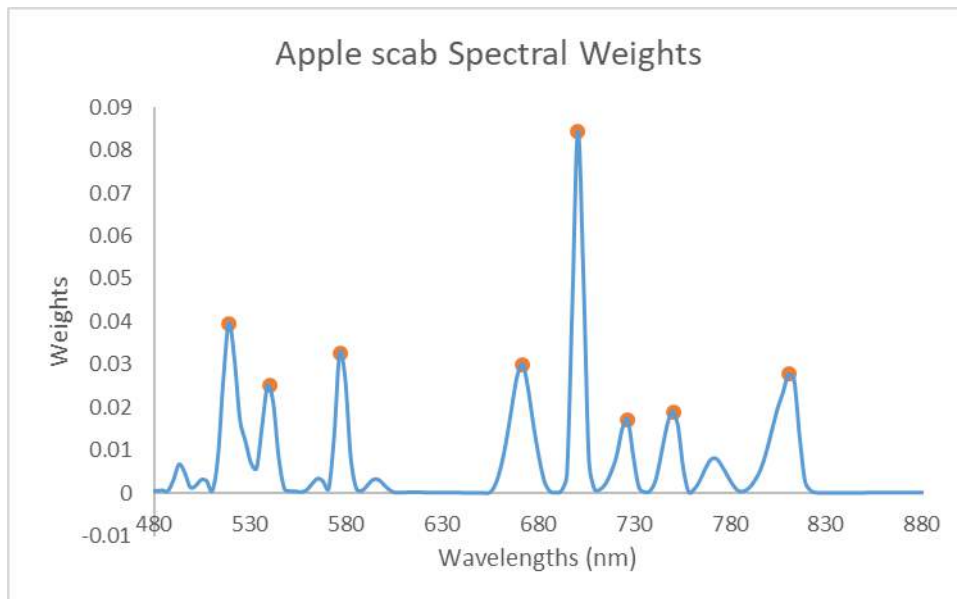
Figure 4: The spectral weights of each wavelength in determining apple scab. Higher weights denote more discriminative power in separating the classes. The most discriminatory region is shown around the peak at 690 nm.

In the case of apple-scab the weights showed that the visible region from 480- 600 nm had discriminating power corresponding to the darkening of the spectrum. Surprisingly, the infrared and specifically the red edge showed as much discriminating power as the remainder of the spectrum. This seems to indicate that the fluctuations in the infrared spectrum are a stronger indication of the disease then the more obvious darkening in the visible.
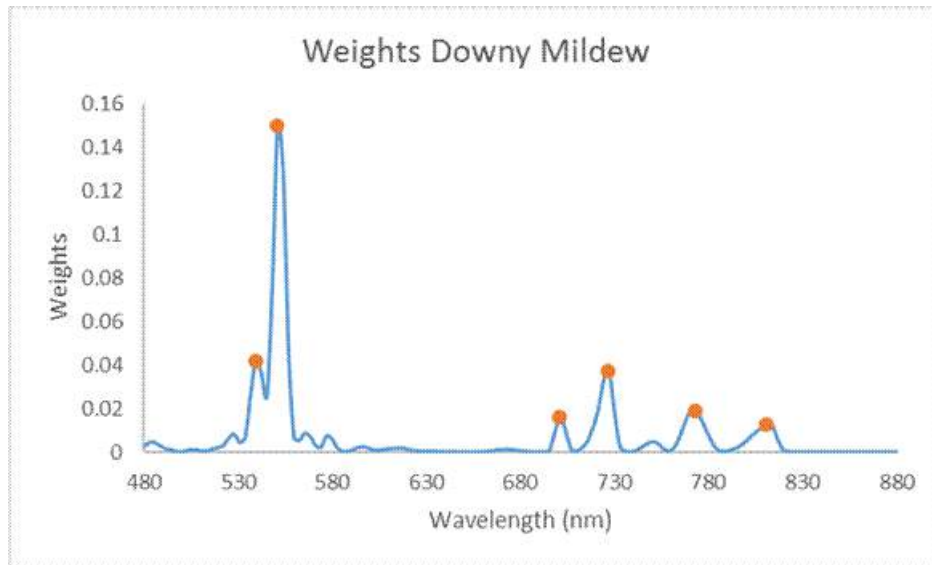
Figure 5: The spectral weights of each wavelength in determining downy mildew. Higher weights denote more discriminative power in separating the classes. The most discriminatory wavelength's by far are around 540 nm, with additional areas in the IR noted with orange dots.

For downy mildew in grapes, the most discriminatory wavelengths are around 540 nm (green) corresponding to the senescence seen in the visible spectrum. In addition, some additional areas in the infrared showed discriminatory power which was not obvious to the naked eye. (Figure 5)

3.3. Multispectral implementation

Using the results of the LDA weight vector, multispectral images were reconstructed from the hyperspectral images. These false color images were created by using the three wavelengths selected by the LDA as having the most discriminating power. We initially chose three band for each image that correspond to the two specific areas of the spectrum where we saw the highest discriminating power, the region from 500 nm - 600 nm and the second from 680 nm – 850 nm. These regions broadly relate to how chlorophyll absorbs light, and the photosynthetic rate of the leaves. For downy mildew these selected wavelengths were 542 nm, 560 nm, and 725 nm. and for apple scab they were 705 nm, and 824 nm. This method is meant to show what a snapshot multispectral camera setup could produce if using a minimum number of wavelengths. These images were assessed qualitatively for higher contrast between fungal infections and healthy leaf tissue. An example of each disease is shown below.

Figure 6: A comparison of false color spectral images on the left and true color images on the right for downy mildew (top) and apple scab (bottom).

4. Discussion

What we found in the downy mildew data was that by using multispectral imaging a false color image can be created that can enhance the image and the disease and make it much more apparent. However, the spectra of mildew is also very similar to other objects such as young leaves, so a single spectral detector continues to be difficult to train. This was also true in the apple scab images, however the spectral contrast there was higher. We hypothesize this is due to the fact that the downy mildew is a biotrophic disease and the apple scab necrotrophic. That makes the senescence in the plant easier to identify with apple scabs.

In addition lighting differences further complicate the images even after normalization. Many areas of in full sunlight had differences in spectra that confused the classifier when applied across the full image.

To solve both problems it may be possible to use a deep learning approach. The spatial distribution of early symptoms of apple scabs and downy mildew both form small lesions. If this spatial information could be paired with the higher contrast in the spectral images a better classifier could be constructed.

5. Conclusions

We have shown that with spectral imaging it is possible to differentiate between the spectrum of healthy and diseased leaf tissue in two different fungal diseases. By using spectral imaging two data sets of healthy and diseased spectra were obtained and an LDA discriminator was trained. This allowed for the separation of the two classes based on discrete wavelengths. By increasing the contrast of images, more advanced methods of machine vision may be used in the future such as a spectral deep learning network.

Acknowledgements

References

[1]   Gauthier, Nicole (2018). "Apple scab". American Phytopathological Society. Retrieved 2021-04-02.

[2]   Ash, G. (2000), "Downy mildew of grape". The Plant Health Instructor. Retrieved 2021-04-02. DOI: 10.1094/PHI-I-2000-1112-01

[3] Wightwick, Adam M.; Salzman, Scott A.; Reichman, Suzanne M.; Allinson, Graeme; Menzies, Neal W. (2012-08-14). "Effects of copper fungicide residues on the microbial function of vineyard soils". Environmental Science and Pollution Research.

[4] Agarwal A., Sarkar A., Dubey A.K. (2019) Computer Vision-Based Fruit Disease Detection and Classification. In: Tiwari S., Trivedi M., Mishra K., Misra A., Kumar K. (eds) Smart Innovations in Communication and Computational Sciences. Advances in Intelligent Systems and Computing, vol 851. Springer, Singapore. https://doi.org/10.1007/978-981-13-2414-7_11

[5] Mishra, P., Polder, G. & Vilfan, N. Close Range Spectral Imaging for Disease Detection in Plants Using Autonomous Platforms: a Review on Recent Studies. Curr Robot Rep 1, 43–48 (2020). https://doi.org/10.1007/s43154-020-00004-7

[6] A.-K. Mahlein, M.T. Kuska, J. Behmann, G. Polder, A. Walter, "Hyperspectral Sensors and Imaging Technologies in Phytopathology: State of the Art", Annual Review of Phytopathology 2018 56:1, 535-558, https://doi.org/10.1146/annurev-phyto-080417-050100

[7] Md, Nur & Ou-Bong, Gwun & Lim, Jong. (2016). APPLE SCAB DETECTION USING HYPERSPECTRAL IMAGING.

[8] Li, Guanlin & Ma, Zhanhong & Wang, Haiguang. (2011). Image Recognition of Grape Downy mildew and Grape Powdery mildew Based on Support Vector Machine. IFIP Advances in Information and Communication Technology. 370. 151-162. 10.1007/978-3-642-27275-2_17.CFD BioAgEng, 2016. International Symposium of CFD Application in Biosystems & Agricultural Engineering. http://conferences.au.dk/fileadmin/conferences/cigr/pdf/CIGR-AgEng_2016_CFD_Symposium_Final_Rev2.pdf Accessed March 1, 2016.

[9] Izenman A.J. (2013) Linear Discriminant Analysis. In: Modern Multivariate Statistical Techniques. Springer Texts in Statistics. Springer, New York, NY. https://doi.org/10.1007/978-0-387-78189-1_8

Effect of Vis-NIR Wavelength Range on the Estimation of Three Aggregate Stability Indices

Ernest Afriyie; Ann Verdoodt; Abdul M. Mouazen*[1]

Department of Environment, Ghent University, Coupure Links 653, 9000 Gent, Belgium

* Corresponding author. Abdul.Mouazen@UGent.be

Abstract

Soil aggregate stability (AS) is a principal indicator of soil erodibility. Standard laboratory procedures for determining AS are time consuming and laborious. Recently, visible and near-infrared diffuse reflectance spectroscopy (vis-NIR) has provided a rapid and inexpensive means of predicting various soil properties. Because AS is associated with soil organic carbon, clay content, and calcium carbonates, which have direct response in NIR spectroscopy, vis-NIR was identified a potential for the estimation of AS index. However, sensitivity and accuracy of vis-NIR spectrophotometers vary due to varying technical parameters (e.g., spectral range, spectra resolution, and detector type). This study compared the performance of two commercially available vis-NIR spectrophotometers [one having a diode array detector with a short wavelength range (SWR; 350 – 1700 nm) and the other having Fourier transform scanning detector with a full wavelength range (FWR; 350 – 2600 nm)] for the estimation of three AS indices, namely, mean weight diameter under fast wetting (FW), slow wetting (SW) and mechanical breakdown (MB). Partial least squares regression was used to build calibration models for the three indices. Results showed that the larger spectrum range of the FWR instrument did not provide improved accuracy in the estimation of SW and MB. In the case of FW, a superior prediction performance was recorded with the FWR model over that of the SWR. This was attributed to the significant spectral feature evident around 2200–2300 nm for the FWR spectrophotometer, which could be associated with hydrophobic-inducing organic matter constituents. Therefore, the FWR is recommended for the measurement of FW AS index, whereas the SWR or FWR spectrophotometers can both be equally successful used for measurement of the SW and MB indices, using vis-NIR spectroscopy.

Keywords: fast wetting, slow wetting, mechanical breakdown, soil erosion, spectral range.

1. Introduction

The resistant forces of soil aggregates to the disruptive forces of raindrop and runoff, termed as aggregate stability (AS), is an important soil physical property controlling soil loss as well as a surrogate for soil erosion (Xiao et al., 2018). Data on the aggregate stability status therefore has become crucial for the monitoring and better management of soils against these forms of land degradation. But this data has conventionally been obtained by field soil sampling and subsequent use of arduous physical methods in the laboratory. Also, the complexity of the breakdown process in a soil erosion event has necessitated that aggregates be subjected to at least three standardised disruptive tests [i.e. breakdown by slaking (fast wetting, FW), physico-chemical dispersion (slow wetting, SW) and mechanical impact (mechanical breakdown, MB)] in order to capture well breakdown process (Le Bissonnais, 1996). But the laborious nature of even one disruptive test, has encouraged the increasing interest for the usage of proximal soil sensing technologies, including the visible and near infrared (vis-NIR) spectroscopy as substitute of the physical laboratory methods for aggregate stability estimation.

Even though soil aggregate stability does not have direct spectral response in the vis-NIR spectral range, accurate predictions of some spectrally active soil properties [such as soil organic carbon (OC), calcium carbonates (CaCO3), and clay] that directly affect aggregate stability have positioned vis-NIR spectroscopy as a potential method for quantifying soil aggregate stability successfully (Cañasveras et al., 2010; Gomez et al., 2013). But studies have reported the negative effect of external parameters on the prediction accuracy of vis-NIR spectroscopy (Hong et al., 2018). Mannschatz and Dietrich (2017) analysed series of studies on the estimation of soil properties from spectra and reported the dependency of prediction performance of spectroscopy models on either instrument type, instrument setup or study site (material composition variation). Mouazen et al. (2005) assessed the effect of different technical specifications (i.e. detector type, spectral range, and measurement principle) of four spectrophotometers on the prediction accuracies of some agricultural materials and reported a significant effect of wavelength range on prediction accuracy. The researchers opined that the latter effect was not general but rather, material and property specific. Knadel et al. (2013) observed that the absence of the 2200 to 2500 nm wavelength region in a vis-NIR spectrometer (Veris Technologies, KS, USA, covering a wavelength range of 350–2200 nm) did not reduce clay prediction accuracy in comparison to two other full range (350 – 2500 nm) vis-NIR spectrophotometers. But Mouazen et al. (2006) observed that the prediction accuracy of a spectrophotometer with shorter spectral range (350-1700 nm) was better than that from a spectrophotometer with longer spectra range (350-2500 nm) for the prediction of soil pH, available phosphorus (P), cation exchange capacity (CEC), potassium (K) and calcium (Ca) on some field moist soils. In the case of total nitrogen (N), total carbon (C), sodium (Na) and magnesium (Mg), the longer spectra range performed better than the shorter.

But, information on the effect wavelength range has on the prediction accuracy of a critical soil property like soil aggregate stability, is yet to be published in the literature. This study was therefore evaluated the effect wavelength range could have on the vis-NIR prediction accuracies of three aggregate stability indices on some non-sieved soils of the Belgian loam belt.

2. Materials and Methods

2.1. Soil sampling

The study sites were three fields of the Hof Ten Bosch farm, located near Brussels, in Flanders, Belgium (50° 48'N, 4° 35'E). The fields being, Lange Weide (LW), Duidelbergen (DB) and Voor de Hoeve (VH), with areas of 3.2 ha, 7.4 ha and 8.6 ha, respectively and an elevation range of 65 to 97 m above sea level. The dominant slope gradient of the area is about 9%. A silty loam textural class (USDA classification) is characteristic of this area [Belgian soil map (Dudal, 1996)]. Also, the soils of the area belong to the Eutric Nudiargic Retisols (Siltic), Haplic Luvisols (Siltic, Colluvic) and Eutric Cambisols (Siltic) classes (Dondeyne et al., 2014). Due to the varying management practices within and between fields, the topsoil between fields have been reported to be heterogeneous, even though the farm is characterised by similar soil types (Afriyie et al., 2020). This wide range of variability in soil characteristics was necessary for the development of vis-NIR sub-catchment models with high levels of robustness.

A total of 111 points were randomly selected for sampling on the fields, i.e., LW (23), DB (48) and VH (40), with number of sampling points being roughly proportional to the size of the fields. Samplings were done between summer and early periods of winter, 2018 (July-November). At each sampling location, three samples were collected with a cylindrical core pushed to a depth of 5 cm. One portion of the three samples was used for the laboratory aggregate stability determination, while the other two parts were homogenised and subsequently partitioned into two parts. One part was used for the wet-chemistry analysis, while the other part was used for the spectra measurement.

2.2. Laboratory analyses

The sample set designated for the wet-chemistry laboratory analysis were air dried, sieved (<2 mm), and homogenised before transporting to the Soil Survey of Belgium (BDB). For the determination of the OC content, total inorganic carbon (TIC) compounds are in advance removed by treating the soil sample with hydrochloric acid. The extractable potassium (K) and phosphorous (P) were analysed using ammonium lactate extract with inductively coupled plasma atomic emission spectroscopy (ISO 11885; CMA 2 / I / B1). Percent clay (%c), percent silt (%z) and percent sand (%s) were analysed in the soil laboratory of Ghent University, by employing the Robinson-Kohn pipette method (ISO 11277).

Soil aggregate stability was determined on the air dried samples using the normalized international method (Le Bissonnais, 1996) in the soil laboratory of Ghent University. The method consists of three treatments that result in three aggregate stability indices of (1) fast wetting-mean weight diameter (FW-MWD), (2) slow wetting (SW) and (3) mechanical breakdown (MB), describing distinct mechanisms of aggregate breakdown in a soil erosion event. Soil aggregates were sieved through a stack of 5 mm and 3 mm sieves. Aggregates that remained on the 3 mm sieve were collected and oven dried at 40 °C for 24 h. Oven drying of the collected aggregates was necessary to ensure that all samples were at a similar matric potential before aggregates were then subjected to the various breakdown mechanisms (Afriyie et al., 2020). For each sample, two replicates under each of the three aggregate disruptive treatments were done. Therefore, the results of laboratory determined MWD presented in this study made use of the average values of these two replicates.

2.3. Visible and near infrared (vis-NIR) spectroscopy

Two vis-NIR spectrophotometers, mainly differed in the detector type and wavelength range were used for the scanning. A CompactSpec$^{®}$ fibre type, vis–NIR spectrophotometer (tec5 Technology for Spectroscopy, Germany) was used as the short wavelength range instrument and a vis-NIR spectrometer (Arcoptix, Switzerland) was also used as the full wavelength range (FWR) instrument. An overview of the technical specifications of the two spectrophotometers are provided in Table 1. A 50 W light source from tec5 Technology for Spectroscopy (Germany) was used with both spectrophotometers.

Table 1: overview of two visible and near infrared (vis-NIR) instruments used in the present study

Spectrophotometer model	Range of wavelength	Spectral resolution	Detectors
CompactSpec vis–NIR 1.7uc ETH	305-1700 nm	1 nm	A silicon array at the 306.5-968.3 nm region and an InGaAs diode array at the 971.8-1710.9 nm region
ARCoptix fibered vis-NIR	350- 2600 nm	1 nm	Multichannel grating type silicon array detector (3648 pixels) 16-bit ADC at 350-1000 nm and Fourier-Transform scanning type InGaAs photodiode, 24-bit ADC at the 900-2600 nm

The setup in both cases made use of fibre optics to transmit light between the measured soil and the instrument. The fibre optic cables used had a Y-branch at one of its ends (Analytical Spectral Devices, Inc., USA). In the case of the SWR setup, one fibre optic cable was used with a single end connected to a confocal lens that was fitted into a lens holder. One leg of the Y-branched end of the fibre cable was connected to the light source and the other leg to the spectrophotometer. In the case of the FWR setup, two fibre optics cables were deployed with two confocal lenses, fitted in a lens holder. The double end at the Y-branched was connected with the spectrophotometer [one for the Vis (350-1000 nm) detector and one for the NIR (900-2600 nm) detector]. The second fibre cable was connected with the 50 W light source to the probe.

Plant remains, debris and stones were removed from the set of soil samples, before subsequently air dried. No grinding and sieving were followed, as the intension was to simulate field conditions of samples, for which only moisture was removed by air drying. Afterwards, the dried soils were packed into Petri dishes of 1.0 cm height by 3.6 cm in diameter. The soil in a Petri dish was mixed properly and gentle pressure was applied on the surface with a stainless-steel blade to generate a levelled and smooth surface to ensure maximum diffuse reflection and thus a good signal-to-noise ratio (Kuang et al., 2012). Three replicates of each sample were prepared, after which soils were scanned in a black box in the case of both devices to better control the irradiance conditions. Before the soil samples were scanned and at intervals of 30 min, a white reference Spectralon disc was scanned to generate the baseline of a 100 % reflected spectra. Each spectrum was an average of ten successive spectra measured. The average of the three scans was used for spectra pre-treatment and model establishment.

2.4. Multivariate statistical analysis

The laboratory measured data of the three aggregate stability indices and the per sample averaged spectral data were compiled in a worksheet of MS Excel and exported to an R open source statistical software (R Core Team, Vienna, Austria) to perform the multivariate analysis. Also, to reduce noise, visual evaluation of spectra enabled identification and removal of the noisy parts at the edges of spectra. After the noise removal at the edges, spectra ranges in the SWR and FWR became 390-1660 nm and 480-2480 nm, respectively. Spectra after noise cut at edges were pre-treated so as to improve the extraction of useful information from both additive and multiplicative effects superimposed in the reflectance spectra (Adeline et al., 2017). Different pre-treatment combinations were tested from a pool of techniques such as moving average (MA), first derivative of the Savitzky Golay (SG), multiplicative scatter correction (MSC), standardisation and smoothing with SG. In all cases, the combinations of the pre-treatment techniques (Table 3) that gave the best model output in terms of the lowest RMSEP, the highest R^2, ratio of performance to interquartile range (RPIQ) and RPD was the one selected and used in producing the three prediction models.

The pre-treated spectra and measured aggregate stability indices for the three fields were partitioned into two sets of 70% (calibration set - 76 samples) and 30 % (prediction set - 33 samples) for FW and SW and 75% (calibration set - 82 samples) and 25 % (prediction set - 28 samples) for MB. This partitioning was done using the Kennard-Stone algorithm (Kennard and Stone, 1969) (with a Mahalanobis metric argument), which ensured a uniform distribution of the subset along the X data space (Nawar and Mouazen, 2018). In order to ensure that the calibration models captured all variability in each index for maximised prediction performance, the size of the calibration sets slightly differed between the aggregate breakdown indices. To ensure a fair baseline for comparison between SWR and FWR, the size of calibration and prediction sets under a single aggregate stability index was same for both the SWR and FWR models. It is worth mentioning that one spectral outlier was identified and removed from the SWR spectra data, before the partitioning into calibration and prediction sets (i.e., a total of 110 samples were used).

The partial least square regression (PLSR) with leave-one-out (LOO) cross-validation analysis was carried out on the calibration set to establish a relationship between a referenced aggregate stability index of FW, SW or MB with the pre-treated vis-NIR soil spectra. PLSR was chosen for this study due to its advantage in producing better accuracy, compared to other regression methods when number of samples is rather small in comparison to the number of variables (De Jong and Kiers, 1992). The established PLSR models were validated using the prediction sets. The prediction accuracy of both the cross-validation and the prediction sets was evaluated using the R^2, RMSEP, RPD as well as RPIQ (Bellon-Maurel et al., 2010). The RPD criteria provided by Viscarra Rossel et al. (2006) was used to grade quality of prediction on the basis of their RPD values. To test variation between the predictions means of the two vis-NIR instruments for the prediction of the three aggregate stability indices, a dependent paired sample t-test was undertaken. Before conducting the t-test, the assumption of normality for the prediction differences of the two instruments were examined.

3.   Results and Discussion

3.1. Soil characteristics

Descriptive statistics of the conventional laboratory soil analyses are summarised in Table 2. The ranges of soil physico-chemical properties as reported in this study are comparable to those previously obtained for similar soils (De Gryze et al., 2007). Also, ranges of MWD for the three different aggregate stability indices obtained in this study are

comparable to those reported by Gomez et al. (2013). On the basis of the mean weight diameter values, the studied soils could be classed as unstable with frequent crusting (Le Bissonnais, 1996), as evident from the FW method. The soils could be said to be stable (rare crusting) and very stable (no crusting) to breakdown by mechanical impact (MB) and physico-chemical dispersion (SW), respectively. This agrees with a previous study, which reported that soils in the loess belt region of Belgium are more prone to slaking (Mullan et al., 2019).

Table 2: Laboratory measurement of soil physical and chemical properties

Soil Properties	Number of samples	Minimum	Maximum	Mean	Range	SD	C.V (%)
pH-KCl	111	5.70	7.70	6.70	2.00	0.50	7.40
OC (%)	111	0.39	2.90	1.46	2.51	0.51	35.05
P (mg/100g)	111	9.00	52.00	21.92	43.00	8.87	40.44
K (mg/100g)	111	19.00	75.00	36.69	56.00	14.03	38.24
% Sand	30	8.30	12.80	10.05	4.5	1.50	14.97
% Silt	30	69.30	86.50	79.09	17.20	4.49	5.68
% Clay	30	3.50	17.90	10.87	14.40	4.24	38.99
FW-MWD (mm)	111	0.22	2.77	0.80	2.55	0.55	68.24
SW-MWD (mm)	111	0.50	4.76	2.20	4.26	1.24	56.39
MB-MWD (mm)	111	0.55	3.25	1.56	2.70	0.64	41.18

Coefficient of variation (C.V); standard deviation (SD); organic carbon (OC); extractable potassium (K) and phosphorous (P); mean weight diameter (MWD); fast wetting (FW); slow wetting (SW); mechanical breakdown (MB).

3.2. Spectral modelling of aggregate stability indices

3.2.1. *Prediction of aggregate stability indices*

Results of the cross-validation and prediction for the three aggregate stability indices obtained from the SWR-PLSR and FWR-PLSR models are summarised in Table 3. According to the accuracy criteria proposed by Viscarra Rossel et al. (2006), aggregate stability index models of SW and MB developed for both instruments provided very good (RPD = 2.30 – 2.35) and good (RPD = 1.93 – 1.99) prediction accuracies, respectively. But for the FW aggregate stability index, whiles the model developed from the FWR instrument provided good prediction accuracy (RPD = 1.97) in the prediction set, the model of the SWR instrument could only provide fair (RPD = 1.73) prediction result.

Table 3: Prediction results of the calibration (cross-validation) and prediction datasets for the three aggregate stability indices based-on the visible and infrared partial least squares regression (vis-NIR-PLSR) models produced for the two spectrophotometer.

Aggregate breakdown method	Spectrum range	Pre-processing	LV	Prediction type	R^2	RMSE (mm)	RPD	RPIQ
Fast wetting	SWR	MA+Dev	3	Cal	0.67	0.31	1.76	2.02
				val	0.66	0.33	1.73	1.96
	FWR	MA+stan+Dev	5	Cal	0.78	0.25	2.17	2.49
				Val	0.73	0.29	1.97	2.23
Slow wetting	SWR	MA+stan+ Dev	5	Cal	0.87	0.47	2.76	5.12
				val	0.81	0.49	2.35	4.15
	FWR	MV+MSC	5	Cal	0.86	0.47	2.70	5.00
				val	0.81	0.51	2.30	4.15
Mechanical breakdown	SWR	MA+stan+ MSC+Dev	4	Cal	0.80	0.28	2.24	3.81
				val	0.74	0.33	1.99	3.12
	FWR	Stan+Dev	3	Cal	0.78	0.30	2.14	3.65
				val	0.72	0.35	1.93	3.01

SWR = short wavelength range; FWR = full wavelength range; R^2 = coefficient of determination; RMSE = root mean

square error; RPD = residual prediction deviation; RPIQ= ratio of performance to interquartile range; LV = latent variable; MA = moving average; Dev = first derivative; stan = standardisation; MSC = multiplicative scatter correction.

From Table 3 it can be concluded that the FWR instrument predicted FW aggregate stability index to a comparative accuracy of previously published work by Shi et al. (2020) (R^2 = 0.72 and RPD = 0.72, achieved with spectrum range of 350 – 2500 nm) and a higher accuracy compared to that published by Cañasveras et al. (2010) (R^2p = 0.52 and standard error of validation [SEV] = 0.4 mm, for a spectral range spectrophotometer of 300 – 2500 nm). Although samples in our work have not been grinded or sieved (followed by the two cited literature), the prediction result was comparable or better than those reported in the literature. Higher predictive ability of MB models are reported in this study in comparison to previously published literature (Gomez et al., 2013). To the best of our knowledge, no vis-NIR prediction of SW aggregate stability index is yet reported in published literature and therefore the SW models in this study cannot be put into context with other studies.

3.2.2. *Wavelength range effect on aggregate stability prediction accuracies*

The estimated skewness and kurtosis for the three aggregate stability indices resulted from the t-test (Table 4), showed prediction differences conformed to the assumption of normal distribution as they were lesser than the maximum allowable values (skew < |2.0| and kurtosis < |9.0|) (Posten, 1978). The predictions provided by the SWR models did not differ significantly ($p < 0.05$) from the predictions provided by the FWR models for all three aggregate stability indices (Table 4). Similar conclusion on the insignificant effect of the wavelength range on the prediction accuracies were reported for soil moisture content (Mouazen et al., 2005), OC and clay (Knadel et al. 2013).

Table 4: Summary statistics and results of paired t-test for mean comparison of predictions generated from the two instruments.

Agg index	mean diff	sd	skew	kurt	df	T-test for quality of variance		t	std. error diff
						F	sig		
FW	0.02	0.19	0.59	0.23	109	0.39	0.05	0.86	0.02
SW	1.40	0.80	-0.34	-1.07	109	0.92	0.05	-0.09	-0.004
MB	0.01	0.25	-0.26	0.24	109	0.55	0.05	0.60	0.01

Agg = aggregate stability; diff = difference; sd = standard deviation; skew = Skewness; kurt = kurtosis; F = critical value; sig = P-value; t = t-value, FW= fast wetting, SW= slow wetting and MB= mechanical breakdown.

When the RPD criteria proposed by Viscarra Rossel et al. (2006) is used to assess the range effect, prediction accuracy difference is witnessed between the two instruments for the FW index only. The FWR provided good prediction, whilst that of SWR was fairly accurate (Table 4). This agrees with Mouazen et al. (2006), who reported superior prediction accuracy for a vis-NIR spectrometer with FWR (combined diode array and scanning monochromator detectors and range of 350-2500 nm) in comparison to that of a SWR (a diode array detector and range of 300-1700 nm) for studied soil constituents [i.e., total nitrogen (N), total carbon (C), sodium (Na) and magnesium (Mg)].

Figure 3 shows the regression coefficient plots as a function of wavelength obtained from PLSR of the two spectra models (i.e., FWR and SWR), for the three aggregate stability indices. A critical observation of the figure generally shows lesser number of spectra peaks between 800 nm and 1300 nm, in both the FWR and SWR model plots for the FW index in comparison to the other two. But the spectra signatures in the above wavelength region (i.e. between 800 and 1300 nm), have been reported to be OC associated, likewise the combination bands between 2200 and 2450 nm (Viscarra-Rossel and Behrens, 2010). OC is a known crucial aggregate stability control property due to its role as cementing agent in soil aggregation (Le Bissonnais and Singer, 1993). It can therefore be argued that, whilst the OC bands in the region between 2200 and 2450 nm could only be playing a complementary role to the OC wavelength region between 800 and 1300 nm, in the SW and MB models and therefore might have little to no impact on prediction accuracy, the case may be different in the FW model. In the FW model, OC constituents that greatly influenced the aggregation may dominantly be between the 2200 and 2450 nm region and therefore spectrophotometers (e.g., like the FWR of this work) that covers this wavelength range could tend to produce a better prediction accuracy for the FW index.
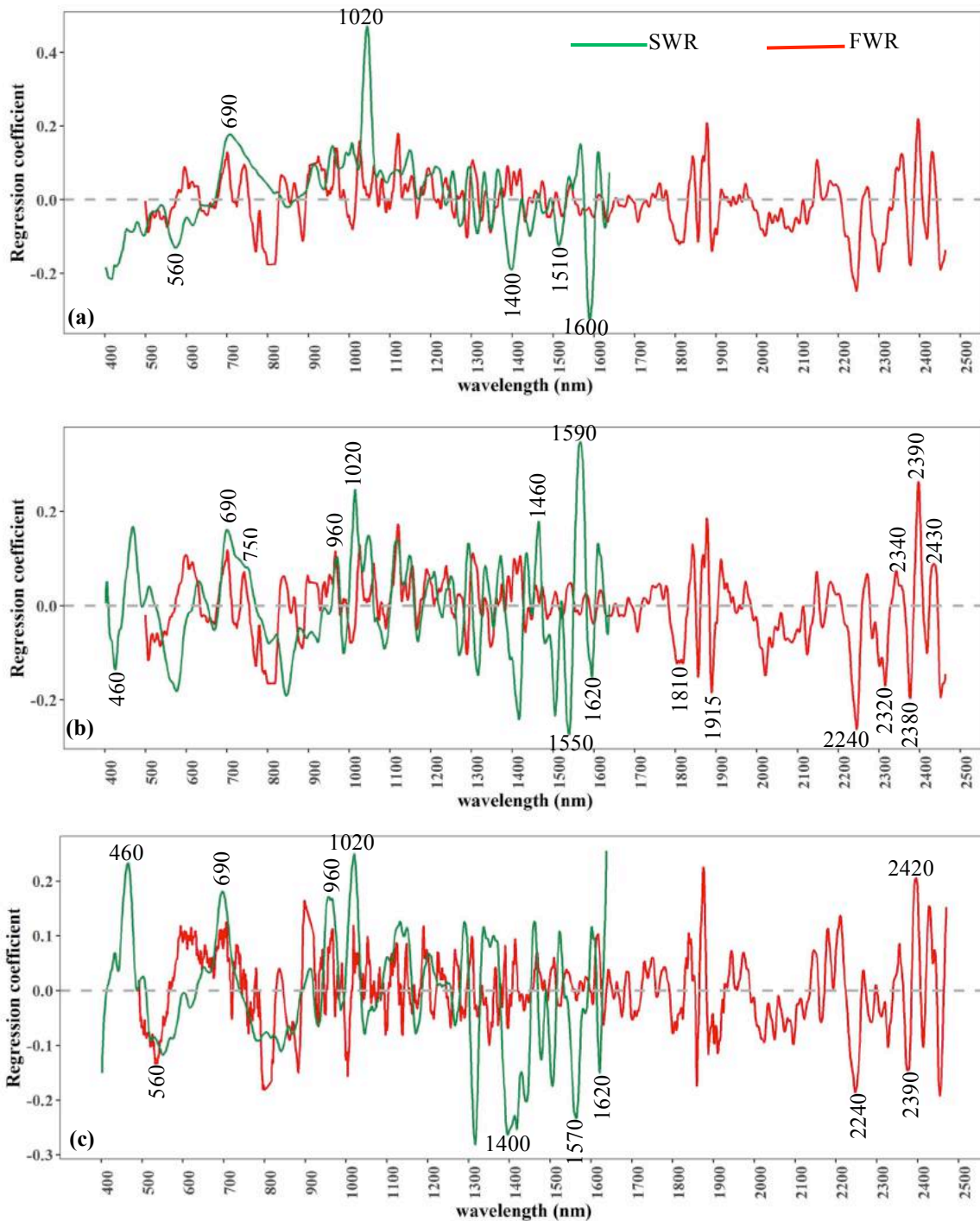
Figure 1: Regression coefficient plots for the three studied aggregate stability indices of fast wetting (a), slow wetting (b) and mechanical breakdown (c) methods, obtained from partial least squares regression (PLSR) models, using spectra scanned by full range spectrophotometer (FWR) and short range spectrophotometer (SWR).

4. Conclusions

The prediction accuracy of three soil aggregate stability indices, namely, fast wetting (FW), slow wetting (SW) and mechanical breakdown (MB) using two visible and near infrared (vis-NIR) spectroscopy coupled with partial least squares regression (PLSR) has been evaluated. The results achieved in this study allow the following conclusions to be made:

- Promising prediction accuracies achieved in this study in comparison to similar studies in published literature for the FW and MB indices.
- vis-NIR prediction for SW index have been reported for the first time in this study with promising accuracy.
- It was evident that, the technical specifications of a spectrophotometer, particularly the wavelength range, influence the prediction accuracy of the FW index only. Therefore, during the selection of a vis-NIR instrument for FW estimation, a spectrophotometer with a large wavelength range greater than 2200 nm is recommended, as this range is significant for primary soil properties (with direct spectral responses in near infrared spectroscopy) having strong correlation with the FW index.

References

Adeline, K. R. M., Gomez, C., Gorretta, N., & Roger, J. M. (2017). Predictive ability of soil properties to spectral degradation from laboratory Vis-NIR spectroscopy data. *Geoderma*. https://doi.org/10.1016/j.geoderma.2016.11.010

Afriyie, E., Verdoodt, A., & Mouazen, A. M. (2020). Estimation of aggregate stability of some soils in the loam belt of Belgium using mid-infrared spectroscopy. *Science of the Total Environment*, *744*, 140727. https://doi.org/10.1016/j.scitotenv.2020.140727

Bellon-Maurel, V., Fernandez-Ahumada, E., Palagos, B., Roger, J.-M., & McBratney, A. (2010). Critical review of chemometric indicators commonly used for assessing the quality of the prediction of soil attributes by NIR spectroscopy. *TrAC Trends in Analytical Chemistry*, *29*(9), 1073–1081. https://doi.org/10.1016/J.TRAC.2010.05.006

Cañasveras, J. C., Barrón, V., del Campillo, M. C., Torrent, J., & Gómez, J. A. (2010). Estimation of aggregate stability indices in Mediterranean soils by diffuse reflectance spectroscopy. *Geoderma*, *158*(1–2), 78–84. https://doi.org/10.1016/j.geoderma.2009.09.004

De Gryze, S., Bossuyt, H., Six, J., Van Meirvenne, M., Govers, G., & Merckx, R. (2007). Factors controlling aggregation in a minimum and a conventionally tilled undulating field. *European Journal of Soil Science*, *58*(5), 1017–1026. https://doi.org/10.1111/j.1365-2389.2006.00881.x

De Jong, S. Kiers, H. A. L. (1992). Principal covariates regression. Part I Theory. *Chemometric and Intelligent Laboratory Systems*, *14*, 155.

Dondeyne, S.; Vanierscot, L.; Langohr, R.; Van Ranst, E.; Deckers, J. (2014). The Soil Map of the Flemish Region Converted to the 3rd Edition of the World Reference Base for Soil Resources. Brussels: Departement Leefmilieu, Natuur & Energie, 2014.

Dudal, R. (1996). The assessment of soil resources of Belgium,. In *In: Soil databases to support sustainable development by C. Le Bas and M. Jamagne (eds.),:Soil databases to support sustainable development, Joint Research Centre of the European Commission EU*.

Gomez, C., Le Bissonnais, Y., Annabi, M., Bahri, H., & Raclot, D. (2013). Laboratory Vis-NIR spectroscopy as an alternative method for estimating the soil aggregate stability indexes of Mediterranean soils. *Geoderma*, *209–210*, 86–97. https://doi.org/10.1016/j.geoderma.2013.06.002

Hong, Y., Yu, L., Chen, Y., Liu, Y., Liu, Y., Liu, Y., & Cheng, H. (2018). Prediction of soil organic matter by VIS-NIR spectroscopy using normalized soil moisture index as a proxy of soil moisture. *Remote Sensing*, *10*(1), 1–17. https://doi.org/10.3390/rs10010028

Kennard, R. W. and Stone, L. A. (1969). Computer Aided Design of Experiments. *Technometrics*, *11*(1), 137–148. https://doi.org/10.1080/00401706.1969.10490666

Knadel, M., Stenberg, B., Deng, F., Thomsen, A., & Greve, M. H. (2013). Comparing predictive abilities of three visible-near infrared spectrophotometers for soil organic carbon and clay determination. *Journal of Near Infrared Spectroscopy*, *21*(1), 67–80. https://doi.org/10.1255/jnirs.1035

Kuang, B., Mahmood, H. S., Quraishi, M. Z., Hoogmoed, W. B., Mouazen, A. M., & van Henten, E. J. (2012). *Sensing soil properties in the laboratory, in situ, and on-line. A review*. *Advances in Agronomy* (Vol. 114). Elsevier Inc. https://doi.org/10.1016/B978-0-12-394275-3.00003-1

Le Bissonnais, Y. & Singer, M. J. (1993). Seal formation, runoff and interrill erosion from seventeen California soils. *Soil Science Society of America Journal*, *57*, 224–229. Retrieved from https://doi.org/10.2136/sssaj1993.03615995005700010039x

Le Bissonnais, Y. (1996). Soil aggregate stability and assessment of soil crustability and erodibility: I theory and

methodology. *European Journal of Soil Science*, *47*, 425–431. Retrieved from https://doi.org/10.1111/ejss.3_12311

Mannschatz, T., & Dietrich, P. (2017). Model Input Data Uncertainty and Its Potential Impact on Soil Properties. In *Sensitivity Analysis in Earth Observation Modelling* (pp. 25–52). Amsterdam, Netherlands: Elsevier Inc. https://doi.org/10.1016/B978-0-12-803011-0.00002-1

Mouazen, A. M., Saeys, W., Xing, J., De Baerdemaeker, J., & Ramon, H. (2005). Near infrared spectroscopy for agricultural materials: An instrument comparison. *Journal of Near Infrared Spectroscopy*, *13*(2), 87–97. https://doi.org/10.1255/jnirs.461

Mouazen, A. M., De Baerdemaeker, J., & Ramon, H. (2006). Effect of wavelength range on the measurement accuracy of some selected soil constituents using visual-near infrared spectroscopy. *Journal of Near Infrared Spectroscopy*, *14*(3), 189–199. https://doi.org/10.1255/jnirs.614

Mullan, D., Matthews, T., Vandaele, K., Barr, I. D., Swindles, G. T., Meneely, J., … Murphy, C. (2019). Climate impacts on soil erosion and muddy flooding at 1.5 versus 2°C warming. *Land Degradation and Development*, *30*(1), 94–108. https://doi.org/10.1002/ldr.3214

Nawar, S., & Mouazen, A. M. (2018). Optimal sample selection for measurement of soil organic carbon using on-line vis-NIR spectroscopy. *Computers and Electronics in Agriculture*, *151*(February), 469–477. https://doi.org/10.1016/j.compag.2018.06.042

Posten, H. O. (1978). The Robustness of the Two-Sample t-Test Over the Pearson System. *Journal of Statistical Computation and Simulation*, *6*((3-4)), 295–311. https://doi.org/DOI: 10.1080/00949657808810197

Shi, P., Castaldi, F., Wesemael, B. Van, & Oost, K. Van. (2020). Geoderma Vis-NIR spectroscopic assessment of soil aggregate stability and aggregate size distribution in the Belgian Loam Belt. *Geoderma*, *357*(September 2019), 113958. https://doi.org/10.1016/j.geoderma.2019.113958

Viscarra-Rossel, R. A., & Behrens, T. (2010). Using data mining to model and interpret soil diffuse reflectance spectra. *Geoderma*, *158*(1–2), 46–54. https://doi.org/10.1016/j.geoderma.2009.12.025

Viscarra Rossel, R. A., Walvoort, D. J. J., McBratney, A. B., & Janik, L. J., & Skjemstad, J. O. (2006). Visible, near infrared, mid infrared or combined diffuse reflectance spectroscopy for simultaneous assessment of various soil properties. *Geoderma, 131*(59e75.). Retrieved from doi:10.1016/j.geoderma.2005.03.007

Xiao, Hai, Liu, G., Zhang, Q., Fenli, Z., Zhang, X., Liu, P., … Elbasit, M. A. M. A. (2018). Quantifying contributions of slaking and mechanical breakdown of soil aggregates to splash erosion for different soils from the Loess plateau of China. *Soil and Tillage Research*, *178*(26), 150–158. https://doi.org/10.1016/j.still.2017.12.026

CityVeg: A robotic Platform for Urban Vegetable Production

Michail Moraitis[a], Konstantinos Vaiopoulos[a], Athanasios Balafoutis[a*],

[a] Centre for Research and Technology Hellas, Greece

* Corresponding author. Email: a.balafoutis@certh.gr

Abstract

Urban agriculture can be shortly defined as the growing of plants and/or the livestock husbandry in and around cities. Although it has been a common occupation for the urban population all along, recently there is a growing interest in it both from public bodies and researchers, as well as from ordinary citizens who want to engage in self-cultivation. The modern citizen, though, will hardly find the free time to grow his own vegetables as it is a process that requires, in addition to knowledge and disposition, consistency.

Given the above considerations, the purpose of this work was to develop an economic robotic system for the automatic monitoring and management of an urban garden. The robotic system was designed and built entirely from scratch. It had to have suitable dimensions so that it could be placed in a balcony or a terrace, and be able to scout vegetables from planting to harvest and primarily conduct precision irrigation based on the growth stage of each plant (fertigation and weed control will also follow). For its development, a number of technologies were combined such as Cartesian robots' motion, machine vision, deep learning for the identification and detection of plants, irrigation dosage and scheduling based on plants' growth stage and cloud storage. The complete process of software and hardware development to a robust robotic platform is described in detail in the respective sections. The experimental procedure was performed for lettuce plants, and according to the results obtained the robotic system provides precise movement of its actuator and applies precision irrigation based on the specific needs of the plants.

Keywords: agriculture, robot, vegetables, plant detection, precision irrigation

1. Introduction

Nowadays, more than 50% of the world population lives in cities and by 2030 this percentage will reach 80% (Bakker et al., 2000). The urbanization process has led food availability to extensive supply chains that in most cases end-up at super markets (ScienceDaily, 2007). Urban agriculture is defined as crop production within homes or plots in urban areas and has important broad benefits for the citizens worldwide (Dubbeling et al., 2010), such as (i) Shortened supply chains, (ii) Carbon sequestration, (iii) Potentially reduced urban heat, (iv) Improved physical and mental health, (v) Improved aesthetics, (vi) Community building, (vii) Employment opportunities, (viii) Improved local land prices, (ix) Provision of habitats for wildlife, (x) Waste recycling. In developed countries, time availability is the main problem hindering adoption of this system, as medium to high-income professionals do seek high quality homemade fresh horticultural products, but do not have the time to take care of a family garden appropriately. Therefore, development of automated solutions could solve this problem.

Different technologies and automations are already used towards this direction, from simple integrated circuits (IC) to more complex microcontrollers, sensors, microcomputers and IoT applications (Anitson et al., 2017, Olawepo et al., 2020). Under this context, the objective of this work is to assemble and test an automated robotic system for vegetable production in situ, for city dwellers. In Section 2 is provided a detailed presentation of the materials and methods used to construct the robotic system, together with the experimental apparatus and the methodology followed. Section 3 shows the results and discusses them and finally Section 4 offers our conclusions and describes some future directions for research.

2. Materials and Methods

A 3D robotic platform (CityVeg) has been developed for the automatic monitoring and management of urban gardens. The implementation is divided into (a) the hardware, presenting the design and construction of CityVeg and (b) the software, describing the system pipeline that feeds CityVeg with the commands to be executed.

2.1. Hardware – Design and Construction

For the design and construction of CityVeg, factors such as the cost and the availability of materials and tools, the ease of assembly and the maintenance costs were taken into account. Additionally, a number of prerequisites were defined early in the process, namely (i) the system as a whole has to be light and robust also in respect to external factors as weather conditions; (ii) the system should be the size of a small urban garden (e.g. for being placed in a balcony) but also easily scalable if needed; (iii) in order for vertical growth of plants to be also taken into account, the

actuator should have 3 Degrees of Freedom (DoF) to allow three-dimensional movement; (iv) the actuator should move with the utmost precision to reach accurately each of the respective plants; (v) its components should not impede plant growth and (vi) no human intervention should be necessary at any stage of the plant development.

2.1.1.Frame and moving parts

A 3D printer layout was selected to achieve precise 3-axis movement,. The aluminium frame consists of 2 parallel horizontal rails, a separate aluminium frame with a pi (Π) shape that runs on the rails and the actuation component that runs horizontally and vertically on the Π frame, thus achieving 3 DoF for the actuator at its lowest point (Figure 1).
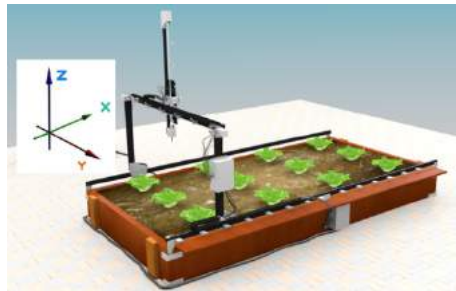
Figure 1. Plain schematic of CityVeg's layout.

The frame was assembled mainly by combining aluminium V-Slot linear rails (20mm x 40mm). V-Slot extrusions are high quality linear aluminium profiles with V-shaped internal channels on all 4 sides, which allow the linear movement of the respective V-Slot wheels (GRobotronics, 2021a). The frame's final dimensions are 1.75m x 1m x 1m.

The smooth movements of (a) the Π frame on the 2 parallel horizontal rails and (b) the vertical actuation component on the upper (horizontal) rail of the Π frame are achieved by utilizing the properly adapted V-Slot plates and wheels. The plates are made of anodized aluminium alloy 6036-T6 (127mm x 88mm x 3mm) and the wheels are made of polycarbonate plastic (outer diameter of 24.39mm, pressure limits up to 86Mpa). The stability of the frame is ensured by the respective joints between extrusions and eccentric spacers between wheels of opposite rail sides (Figure 2a).
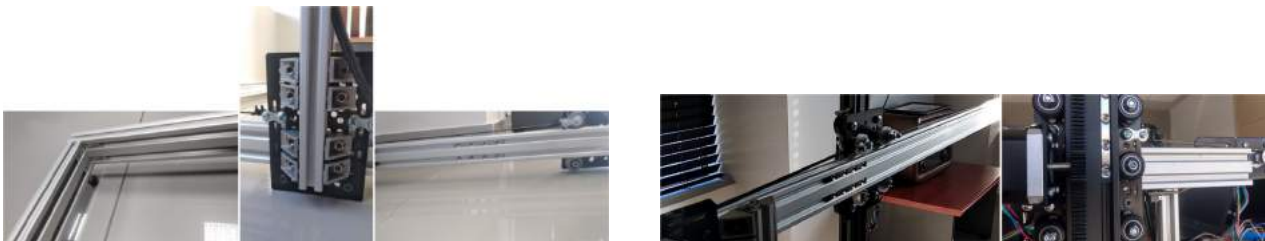
Figure 2. Details of the (a) frame joints; (b) Z axis details

2.1.2.Motors and transmission

The movement of individual parts of CityVeg is performed by 4 stepper motors (12V, 0.4A/phase, NEMA17, 200 steps/rev, T = 28N.cm). Two of these motors are utilized for the uniform movement of the Π frame onto the 2 parallel horizontal rails, also combined with 2 idler pulleys at the opposite side of the rails and 2 GT2 timing belts connected to the plates that bear the Π frame. The third plate movement along the horizontal rail of the Π frame was arranged similarly (3rd motor). The 4th motor is utilized for the vertical movement of the actuator. A rack was mounted along the vertical bar and a gear was fitted to the 4th motor. The gear and the rack (Mod.1 - 15mm x 15mm) were designed and 3D-printed together with the motor base. Figure 2b shows the final arrangement of the Z axis plate/wagon. The motors connection and control was achieved by 4 stepper drivers A4988 (GRobotronics, 2021b) coupled to the motors, Arduino and power supply.

2.1.3.Sensors and switches

For the monitoring of the urban garden, a soil humidity sensor and an RGB camera are utilized. The purpose of humidity monitoring is to evaluate soil water content before each application cycle, in case sufficient water was provided by external factors, such as rain. An economic resistive soil moisture detection module has been installed and properly calibrated. For cloud communication the NodeMCU (Lua based ESP8266) was selected, also providing scalability in case it is deemed appropriate to add more sensors of any type in the future.

The second input of the system is a camera that sends multiple images of the garden parcel to the cloud before each application. The purpose of taking multiple photos lays in the quality of the final combined image which will result by the union of the different images and will be fed into the neural network at a next step. The selected camera module is the ESP32-CAM, a compact, low-power OV2640 camera based on ESP32 that offers among else satisfactory resolution

(1600 x 1200 pixels), auto-focus and built-in Wi-Fi/Bluetooth modules on the ESP32 (Waveshare, 2020). A plastic casing was designed and 3D printed aiming to protect it from external factors and mount it on the frame. It was placed on the third plate as this position offers multiple advantages: (a) fixed height with sufficient field of view across the width of the parcel, (b) ability to move along the X axis so that it's possible to take multiple photos for a complete depiction of the garden, (c) unhindered view to the garden parcel provided that the actuation component (Z axis) rises by a few centimetres, (d) no need to install electronic parts onto the actuation component and (e) it is a protected position in general. As the stepper motors do not return feedback regarding the reached position, 8 "limit switches" were installed to fully cover the ends of all axes (4 in X axis, 2 in Y and 2 in Z axis) for safety reasons and for creating a reference point/position (Figure 3) (GRobotronics 2021c).

Figure 3. (a) ESP32-CAM, (b) Camera casing design, (c) Soil humidity sensor, (d) NodeMCU, (e) Limit switch.

2.1.4. Irrigation system

To apply irrigation, a centrifugal electric pump (12V DC, 0.67A, 3L/min maximum flow rate) was used together with a 20L water tank. A 6mm PE hose was used to channel the water up to the dripper of the actuation component. The control of the pump was achieved with a typical relay module connected to the Arduino.

2.1.5. Arduino microcontroller

In order to control the stepper motor drivers, the limit switches and the water pump relay, the Arduino Mega 2560 Rev3 was used (Arduino, 2020). Limit switches are very sensitive to noise, so to mitigate the disturbance, a 4.7K resistor and a 100nF capacitor were added in the wiring of each switch (in the 5V and the GND output respectively). A Wi-Fi connection to the cloud was established via the ESP8266 Wi-Fi module ESP-12 (Nurdspace, 2020). Finally, a 12V DC, 8.5A (102 Watt) power supply and the appropriate DC / DC voltage reducers were used to power all the components of the robotic system.

2.2. Software – System pipeline

CityVeg is programmed to "wake up" every 24 hours and perform a sequence of processes – referred to from this point forward as "application cycle". The cycle begins with the monitoring of the urban garden and ends with the application of precision irrigation. In short, the system every 24 hours (i) receives and sends the data from both sensors (humidity, images) to the cloud, (ii) processes the images before feeding them to the neural network, (iii) identifies the plants exact position and classifies them according to their size and (iv) produces and forwards to the actuator the commands for the application. Figure 4 shows the flow chart of CityVeg overall system pipeline.
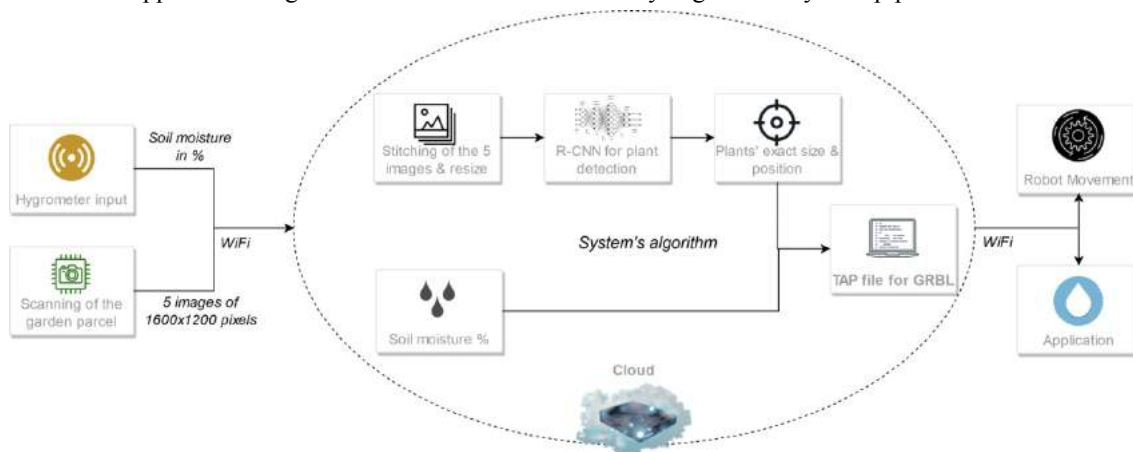
Figure 4. Flow chart of CityVeg overall system pipeline.

2.2.1. Urban garden monitoring and image acquisition

The initial process that the system must perform is the supervision of the urban garden. Regarding soil moisture, in this step it is considered adequate to send to the cloud the (%) percentage of soil moisture which will be utilized in the next step to assess the need to apply irrigation to the garden parcel.

The second input is the garden's images. The images are captured in such a way to partially overlap each other so

that during their union in the next step, they have enough common sections for the process to be carried out and the photos to be successfully combined into a single, final image – panorama. This process is called image stitching or image mosaicing and the exact methodology that was followed is described in Section 2.5.2.

As shown in Figure 5, five (5) overlapping photos are combined to one. The process of image capturing consists of: (a) partial raise of the vertical component so as not to interfere with the camera's field of view, (b) movement of the third plate/wagon (Y axis) so that the camera's lens is positioned in the middle of the Y axis and its field of view captures the full system's width and (c) movement of the Π frame along the garden, consecutively stopping at the 5 fixed points where the photos are to be captured. Before each capture the Π frame is immobilized for 1.5 sec in order to dampen any oscillations that would lead to blurred images. Due to memory limitations each photo is captured and sent to the cloud before capturing the next one. All the commands above are given for predefined coordinates. When all 5 captures are completed, all axes return to the home position (X0, Y0, Z0). Details are given in Section 2.5.3.

2.2.2. Data processing

The purpose of data processing in the current system is: (a) the identification of the exact position of the plants, (b) their classification in 5 classes according to their size, (c) the determination of the soil moisture content threshold, below which irrigation should be applied, and (d) the determination of the irrigation dose for each individual plant.

The first step towards extracting plants' position and size is the image stitching process. Algorithms for aligning images and combining them into a single image-mosaic are commonly used in Computer Vision, typical examples are the panorama mode in most commercial digital cameras and the creation of maps by combining multiple satellite or other aerial photos (Mehta and Bhirud, 2011). In the current system this process is done mainly by using the open library OpenCV 4.2 (OpenCV, 2021a) in python 3.5.6. OpenCV is an open source computer vision and machine learning software library, built to provide a common infrastructure for computer vision applications and to accelerate the use of machine perception in commercial products (OpenCV, 2021b).

The field of view in each capture in relation to the total area of the garden is shown graphically in Figure 5-a. Each photo is captured with the same resolution (1600 x 1200 pixels) and covers the same area size as the 5th. Due to overlap, sections of captures 1, 2, 3 and 4 are not shown in the figure. The image stitching process is graphically explained in Figure 5-b. In the first step, each photo is combined with the one/two next to it. In the second step the stitched images – results of the first step – are being combined in pairs and in the third step the final, single image is produced. The above methodology emerged after multiple tests that resulted in this reliable application of the algorithm, mostly due to the high degree of overlap between the images that are going to be stitched, in each step of the process.
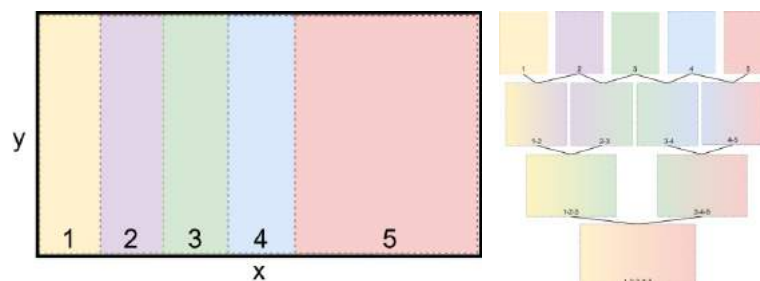
Figure 5. Image acquisition and stitching.

Having completed the stitching process, the produced single image depicts the total area of the garden parcel. The next step is its transformation so that its four sides tangent in the inner borders of the frame that surrounds the garden and its dimensions correspond to its real dimensions. The transformation is carried out with another tool from the OpenCV library *(cv2.getPerspectiveTransform)*, in predefined dimensions that resulted from the accurate measurement and matching of the final image's pixels to the real world.

Having defined its dimensions, the image is being fed into a neural network to extract the exact position and size of the plants. The open-source software library for machine learning by Google, TensorFlow (Tensorflow, 2021) (GPU-enabled version) was utilized with a NVIDIA GeForce GTX 1060 Max-Q 6GB GPU. In order to make use of the specific GPU for the training, the parallel computing platform and application programming interface model by NVIDIA, CUDA (Compute Unified Device Architecture) (NVIDIA, 2021a) was used together with the library cuDNN (CUDA Deep Neural Network library) (NVIDIA, 2021b). For compatibility reasons, specifically CUDA 10.0, cuDNN 7.4, TensorFlow-GPU 1.13.2 were used in python 3.5.6.

TensorFlow provides several pre-trained detection models with specific neural network architectures (Tensorflow1, 2021). Some models (such as the SSD-MobileNet) use an architecture that allows faster detection but with less accuracy, while other models (such as the Faster-RCNN) provide slower detection but with greater accuracy. As detection speed is not of major concern in the specific robotic system, the training was conducted on the Faster-RCNN-Inception-V2 model.

In order to create the dataset, 400 images of lettuce plants at different stages of development were captured. All shots were taken from 1m height, so that the display of each plant is similar to the top view captures of the system's camera. Training was conducted using 80% of the captured images, while the remaining 20% was used for training. The labelling process was carried out with a tool named LabelImg (LabelImg, 2021).

After the training process the model has been able to identify lettuce plants with an accuracy of up to 92%. For each detected lettuce plant the following data is extracted: (a) area of the bounding box that encloses it, (b) coordinates of the box's centre point and (c) detection score having set a threshold of 80% (anything detected with a lower score is not taken into account). The data is exported in a CSV format and as a final step the entries are sorted based on their centres' X coordinate (ascending). The sorting serves the smooth movement of the actuation component during the application, as it will be picking the plants to be irrigated in an ascending X axis order, which is not the ideal (shortest) path but it is adequately short.

As shown in the flowchart (Figure 4) the soil moisture percentage is combined with the neural network's input to produce the commands for the actions of CityVeg. In fact, there has been set a soil moisture threshold above which the irrigation of the garden is considered unnecessary. The determination of this threshold was done in a first stage empirically, taking into account parameters such as the sensor's depth, ground water availability and plant type, and was later experimentally corrected. Indicatively, most lettuce varieties as soon as they are transplanted have a root zone depth of 3 – 4 cm, while when the harvest season is approaching their roots have developed to a depth of up to 30 cm (GAIApedia 2021, Gardeningknowhow, 2021, VeggieHarvest, 2021).

The precision irrigation concept that CityVeg aims to achieve consists of 4 main aspects (Shah and Das, 2012). The first concerns the application of the irrigation on the exact plant's position and is met by the actuator's precise movement. The second and third concern the irrigation dose and method of application and are explained in the next paragraph. The fourth concerns the timing of the application (no-application in the specific 24-hour cycle, if the moisture threshold in not passed).

The water is being applied through an adjustable dripper mounted on the actuation component. Its supply is fixed at 25 L/h and the applications can be targeted as long as they are being carried out from the appropriate height. The – specific for each plant – dose is calculated based on the area of its bounding box. Five different classes and respective doses have been set (Low – Medium Low – Medium – Medium High – High) according to the literature (Gallardo et al., 1996, Gallardo et al., 1996, Both A., 2021). The irrigation dose is expressed in seconds of pump operation. Based on the same classification method, the estimation of each plant's height is derived. This estimate will serve to slightly differentiate the height from which the irrigation will be applied on each plant (lettuce can reach 15 – 30 cm height).

Having processed the input data and given that the available soil moisture is deemed insufficient; the system will proceed to generate the commands for the robot's actions.

2.2.3. Generation of the commands to be executed

This step combines all previous data and expresses it in a readable way for the GRBL software (GRBL, 2021), a modification of which is installed into the Arduino microcontroller to control the stepper motor drivers and the irrigation component. GRBL is an open-source motion control software for CNC (Computer Numerical Control) milling that reads G-code (or RS-274) (Howtomechatronics, 2021) language, which is the most widely used CNC programming language. GRBL runs the produced code sequentially, receiving feedback for the successful execution of the previous sequence before executing the next. Having expressed, therefore, the required actions for the irrigation with G-code commands, the system will initiate the communication with the GRBL software installed in the Arduino to carry out the application. It shall be noted that during the image acquisition process at an earlier stage, the movement is executed in a similar way but for a fixed G-code file with given coordinates, as the points that the 5 photos are captured are predefined.

2.2.4. Movement and application

Although there are variations between the application cycles, the general principle is the same. Initially, the system receives feedback on its position and confirms its starting position (X0, Y0, Z0 – home). Before heading to the nearest (as for the X axis) plant, the vertical component (Z axis) is raised by 35 cm (safe movement height). Then, after the movement of X and Y axes, the actuator is placed above the first plant-target to be irrigated, descending to the application height set for the specific plant. The pump is then activated and runs until the defined dose for the specific plant is applied. Then, it gets switched off and the actuation component will be raised to the safe movement height. Axes X and Y moves the actuator above the next plant and the process is repeated for all identified plants. At the end of the cycle the 3 axes will return to home and the robot will be switched off. In the next day the system will "wake up" again to follow the same processes' sequence as shown in Figure 4.

2.3. Experiments

Multiple methods for precision movement, monitoring and application have been tried, improved and/or rejected. However, the main experiments that were carried out and in particular those to extract the necessary metrics for their

evaluation concerned: (a) the success of the image stitching process, (b) the realization of the plant identification and localization and (c) the precision of the robot's movement.

2.3.1. Image stitching

For the image stitching process even after selecting the OpenCV library, many different methods were tested mostly differentiated by the overlapping rate between 2 adjacent photos. The final method as presented in Section 2.5.2 was initially tested on a set of 6 equally divided – in 5 adequately overlapping final image sections – images. Three of them were manually cropped into 5 sections while the rest were real captures of the robot camera. The resolutions of the manually cropped images were similar to the camera's captures (1600 x 1200 pixels). In Figure 7a can be seen an example of a stitched image out of 5 captures of the robot camera. A segmentation of one of the parallel rails is observed at the lower side of the image which was later overcome with the optimization of the camera's mount position in order to capture absolutely vertical photos.

Figure 6. (a) Stitched image example; (b) Plant detection and localization example.

2.3.2. Plant identification and localization

As mentioned previously, the Faster-RCNN-Inception-V2 model was trained with 400 lettuce images in various development stages. The evaluation of the model was carried out for 10 images representing 8 to 22 plants (lettuces and weeds) each. The point of view was similar to the images captured from the robot's camera (top view) and the resolution was equal to the final, combined image resulting from the stitching process. An example is given in Figure 7b. It can be seen that the model successfully detected all the lettuce plants and also detected and classified as lettuces 2 weeds, but with very low score (56% and 50%).

2.3.3. Precision of robot's movement

As mentioned before, after the detection process, the model exports data from the bounding boxes enclosing each plant. Boxes' angles are utilized to export their centres as shown in Figure 7a. These centres are the "targets" that the actuation component must navigate to in the highest precision possible, so to circularly apply irrigation around them through its dripper.

The characteristics of the robot that were measured in this experiment were its repeatability and its accuracy. Repeatability can be briefly defined as its ability to repeat the same task while accuracy is the difference (error) between the requested and the finally obtained task. Thus, in this system repeatability refers to the movement at the same point over and over, while accuracy refers to finding the correct plant/target each time.
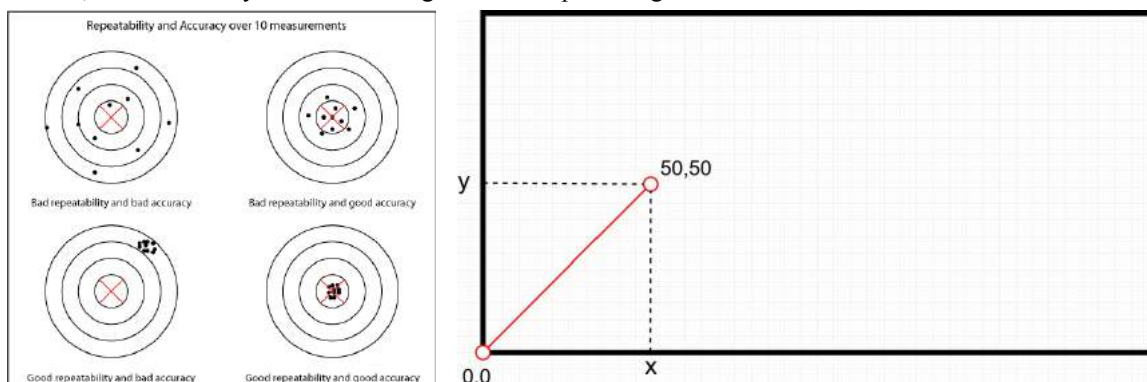
Figure 7. (a) Repeatability and precision after 10 measurements (Robotiq, 2021), (b) 2D schematic representation of the set path.

To perform the above measurements the dripper was removed and a marker was mounted at the actuation

component instead. The X50, Y50, Z0 position was then manually measured and marked on a millimetre paper on the floor (always in respect to the "home" X0, Y0, Z0). Accuracy and repeatability were measured for 10 operating cycles of moving back and forth from the "home" position to the designated spot (Figure 7b). Z-axis' movement accuracy was not evaluated in this experiment, as it was only slightly moved up and down for the experiment's purpose (marking). It shall be noted that (a) this experiment was performed before the installation of the limit switches that improve the system's movement accuracy by reducing the cumulative error since in each cycle the system "resets", and (b) it was the final of a series of experiments aiming to optimize the – absolute – movement accuracy. In all operating cycles the marker's point coincided with the manually marked one (deviation +/- 1 mm due to the diameter of the manual mark).

3. Results and Discussion

The experiments of section 2 concern fundamental functions of the system, the correct execution of which is the basis for the final stage of this implementation – precision irrigation – but also all future extensions (fertigation and weed control) briefly outlined in the conclusions.

Regarding the experiments of Section 2.6.1 for the image stitching process, it was observed that (i) the final method lacks the issues arisen in previous implementations (e.g. stitching inability or strong distortion on the final images) and works effectively, successfully combining the given images each time; (ii) the cause of a very light distortion that was observed in terms of the height of the final images could not be identified and therefore could not be addressed. It was considered a minor problem as its scale does not affect the accuracy of the detection beyond acceptable limits and (iii) Some unwanted segmentation was observed in one of the parallel rails at the images acquired by the system's camera. That segmentation was a result of the not absolutely vertical position of the camera's mount. Even though this distortion did not ultimately affect the efficient operation of the system, the camera mount was properly re-adjusted.

The detection model achieved very satisfactory accuracy.

Table 1. Confusion Matrix.

	Actually Positive	Actually Negative
Predicted Positive	148 (TP)	4 (FP)
Predicted Negative	9 (FN)	2 (TN)

The results of Section 2.6.2 experiments proved that (i) the model detects even the smaller (in size/development) lettuce plants, but with lower score. At this stage of development this is not significant but at a later stage it could become a major problem (e.g. weeding on the wrong target). The model will be further trained with more plant images and especially at earlier development stages. The low score could also occur due to the low-cost camera and its generally low resolution (max 1600 x 1200 pixels). A possible replacement is considered by the time weeding function will be added, (ii) mature plants are successfully identified as separate plants even in cases where there is overlap between the foliage of nearby plants. In a few cases where identification failed, this was most likely due to the absence of a complete view of the plant. In the demarcated garden parcel of the system no such issue arises and (iii) some weeds were sometimes identified as lettuce plants with a low score. Identifying weeds as desirable plants is a problem as the robotic system should not boost the weeds by irrigating them. As previously, it is considered advisable to further train the model with additional lettuce plants in early development stages.

The precision of the robot's movement was satisfactory from the very first experiments. The type of motors (stepper motors) but also of the specific model proved to be adequate, as it was observed in the experiments of Section 2.6.3. The actuation component moves each time precisely at the selected point. To this precision is added the extra safety factor provided by the presence of limit switches, which contribute to the correct finding of the "home" position before each cycle. There were deviations between the navigation of the actuation component to: (a) the centre of each bounding box containing a plant and (b) to the actual centre of each plant. These deviations are not attainable with the selected classifier, but in any case, the final accuracy is considered absolutely satisfactory for the purposes of applying precision irrigation to the plants. Finally, much of the precision in movement is due to the stepper motors and their driving software. However, the quality of the individual components of CityVeg also contributes to this. The selection of pulleys, the adjustment of the distance between the plates'/wagons' wheels, the securing of the belts and the addition of belt tensioners and more, all contribute to the system being able to perform many repetitions without constantly requiring adjustments due to wear. Of course, as a mechanical structure with moving parts it will require maintenance from time to time.

4. Conclusions

The experimental procedure proved that the developed robotic system adequately performs all of the aforementioned processes in lab scale. According to the system pipeline, the developed algorithm acquires the garden data as input,

processes it and exports the information needed in order for the robot to precisely irrigate the desired plants according to their specific needs. The precise spatial navigation (detection, approaching and application upon the detected plant) is a direct result of the successful operations of depiction of the garden parcel and processing them to extract the real scale, through the obtained images. As mentioned previously, all training and experiments were carried out for lettuce plants. After the system is tested in real conditions for the specific crop and the necessary adjustments are made, the next steps will prioritize in: (a) addition of fertigation (utilizing Normalized Difference Vegetation Index (NDVI)), (b) weeding capability, making the proper modifications in system's hardware and software, (c) optimization of the applied dosages for each type of application with tests in real conditions, (d) training of the whole algorithm in order to support more plants, (e) addition of more sensor types in order to holistically monitor the urban garden (air humidity/temperature, light intensity, etc.) and (f) development of a mobile App for remote monitoring and record keeping.

References

Anitson T. T., & Saji, Jaison & Dubey, Rahul & Saravanakumar, K. (2017). Food Computer Automated Gardening System. Special Issue Published in International Journal of Trend in Research and Development (IJTRD), ISSN: 2394-9333, www.ijtrd.com

Arduino Mega 2560 Rev3. https://store.arduino.cc/arduino-mega-2560-rev3, Accessed June 1, 2021.

Bakker, N., Dubbeling, M., Gündel, S., Sabel-Koschella, U., de Zeeuw, H. (2000). Growing cities, growing food. Dtsch Stift int Entw, Feldafing, p 531.

Both, A. J., Ten years of Hydroponic lettuce research, https://www.researchgate.net/publication/266453402_TEN_YEARS_OF_HYDROPONIC_LETTUCE_RESEARCH, Accessed June 8, 2021.

ESP8266 Datasheet and more: https://nurdspace.nl/ESP8266, Accessed June 6, 2020.

GAIApedia Καλλιέργεια μαρουλιού, http://www.gaiapedia.gr/gaiapedia/index.php/Καλλιέργεια_μαρουλιού , Accessed June 4, 2020.

Gallardo M., Jackson L. E., Schulbach K., Snyder R. L., Thompson R. B., Wyland L. J., "Production and water use in lettuces under variable water supply," Irrig. Sci., vol. 16, no. 3, pp. 125–137, Mar. 1996, doi: 10.1007/s002710050011.

Gallardo M., Snyder R. L., Schulbach K., Jackson L. E., "Crop Growth and Water Use Model for Lettuce," J. Irrig. Drain. Eng., vol. 122, no. 6, pp. 354–359, Nov. 1996, doi: 10.1061/(asce)0733-9437(1996)122:6(354).

Gardeningknowhow, Tips For Growing Lettuce In Containers, https://www.gardeningknowhow.com/edible/vegetables/lettuce/growing-lettuce-containers.htm, Accessed June 8, 2020.

Graphical image annotation tool LabelImg: https://github.com/tzutalin/labelImg, Accessed June 7, 2020.

GRBL g-code parcer: https://github.com/grbl/grbl, Accessed June 8, 2020.

GRobotronics, V-Slot 2020 250mm - Natural Anodized. https://grobotronics.com/v-slot-2020-250mm-natural-anodized.html, Accessed June 2, 2020.

GRobotronics stepper driver A4988. https://grobotronics.com/a4988.html, Accessed June 3, 2020.

GRobotronics E88392 Snap Action Switch. Datasheet: http://grobotronics.com/images/companies/1/ss-series.pdf, Accessed June 5, 2021

GRobotronics LRS-100 series MeanWell Datasheet: http://grobotronics.com/images/companies/1/datasheets/LRS-100-SPEC.pdf, Accessed June 4, 2020.

Howtomechatronics, G-code Explained | List of Most Important G-code Commands, https://howtomechatronics.com/tutorials/g-code-explained-list-of-most-important-g-code-commands/, Accessed June 8, 2020.

Mehta J. D. and Bhirud S. G., "Image stitching techniques," in Thinkquest~2010, Springer India, 2011, pp. 74–80.

NVIDIA Developer. CUDA Zone: https://developer.nvidia.com/cuda-zone, Accessed June 3, 2020.

NVIDIA Developer. cuDNN: https://developer.nvidia.com/CUDnn, Accessed June 4, 2020.

Olawepo, Samuel & Adebiyi, Ayodele & Adebiyi, Marion & Okesola, Olatunji. (2020). An Overview Of Smart Garden Automation. 1-6. 10.1109/ICMCECS47690.2020.240892.

OpenCV 4.2 Stitching, https://docs.opencv.org/4.2.0/d8/d19/tutorial_stitcher.html, Accessed June 3, 2020.

OpenCV: https://opencv.org/about/, Accessed June 8, 2021.

OV2640 by OmniVision. Datasheet: https://www.waveshare.com/w/upload/9/92/Ov2640_ds_1.8_.pdf, Accessed June 2, 2020.

Robotiq, https://blog.robotiq.com/bid/72766/What-are-Accuracy-and-Repeatability-in-Industrial-Robots, Accessed June 8, 2020.

ScienceDaily (2007), Mayday 23: world population becomes more urban than rural. http://www.sciencedaily.com/releases/2007/05/070525000642.htm, Accessed June 3, 2020.

Shah N. and Das I., "Precision Irrigation: Sensor Network Based Irrigation," in Problems, Perspectives and Challenges of Agricultural Water Management, 2012.

TensorFlow1DetectionModelZoo.https://github.com/tensorflow/models/blob/master/research/object_detection/g3doc/tf1_detection_zoo.md, Accessed June 8, 2020.

TensorFlow homepage: https://www.tensorflow.org/, Accessed June 2, 2020.

VeggieHarvest, Lettuce Growing and Harvest Information, https://veggieharvest.com/vegetables/lettuce-growing-and-harvest-information/, Accessed June 8, 2020.

Analysing the Behaviour of Individual Laying Hen by Using Machine Learning and Inertia Sensor

Sayed M. Derakhshani [a,b,*], M. Overduin [a] ,T.G.C.M van Niekerk [c] , P.W.G. Groot Koerkamp [a]

[a] Wageningen University, Farm Technology Group, Wageningen, the Netherlands
[b] Wageningen University, Biometris, Wageningen, the Netherlands
[c] Wageningen Research, Wageningen Livestock Research, Wageningen, the Netherlands
* Corresponding author. Email: sayed.derakhshani@wur.nl

Abstract

Welfare-oriented regulations caused farmers to shift to more welfare-friendly systems with larger groups of hens, more space per hen and a more complex environment to meet the behavioural needs of the birds. In contrast to the traditional cage housing with small groups of birds, management of these larger units demand more knowledge of the actual bird behaviour and adjustment of the management based on these behavioural observations. The main goal of this research is to design and develop a machine learning model for analysing the daily behaviour of chickens by using wearable inertia sensor technology.

In this study, a simplification was made by dividing the chicken behaviour into three separate classes: static, semi-dynamic, and highly-dynamic behaviour. Besides the inertia sensor, the activities of chickens were continuously recorded on video to synchronise the sensor signals with the recorded images. Two chickens were wearing backpacks, marked green and blue, for five days to collect the data. The collected signals and video data were used in the training (green marker) and testing (blue marker) of the machine learning (ML) model.

Applying principal component analysis (PCA) did not have a significant effect on the performance of the ML model. It indicated that the ML model can accurately classify the highly-dynamic behaviours with a one-second time window and a four-second time window is accurate for static and semi-dynamic behaviours. The bagged trees model with an overall accuracy of 89% was the best ML model with the F1-scores of 89%, 91%, and 87% for the static, semi-dynamic, and highly-dynamic behaviours, respectively. It also performed well in classifying the behaviours of the chicken with a blue marker with an overall F1-score of 0.92. Considering the results obtained during this research, machine learning can be recognized as a viable tool to analyse and classify the behaviours of laying hens in different levels of activity.

Keywords: Laying hen, daily behaviour, machine learning, inertia sensor.

1. Introduction

Welfare oriented legislation, like the European Directive (Council of the European Union 1999), imposing specific regulations for the keeping of laying hens, has caused a shift from cage housing towards more welfare-friendly systems with more possibilities for the birds to meet their behavioural needs. These housing systems typically house larger groups of hens and provide them with a litter surface and more space per bird (EFSA 2005). With increasing the complexity of these systems, the influence of bird behaviour on technical results increases, making the management for the farmer more challenging (Elson 2015).

A major source of fine dust emissions in the Netherlands is coming from the agricultural sector. Fine dust consists primarily of feed and animal matter, such as hairs, feathers and faeces (Casey et al. 2020). Fine dust is regarded as a pollutant that causes harmful effects for both the environment and the health and welfare of humans and animals (Takai et al. 1998; Cambra-López et al. 2010). A high amount of PM10 (particular matter with an aerodynamic equivalent diameter equal to and less than 10 µm (Hadlocon et al. 2015) is emitted by the poultry sector and many of these poultry farms are exceeding air quality thresholds set by the European Union (Aarnink et al. 2009).

Monitoring the daily behaviour of the chickens may provide useful insights into decreasing dust release from the litter and its emissions from poultry barns. Moreover, daily behaviour needs to be monitored to imply optimal management. Daily behaviours are not equally distributed over the day, therefore a good impression of behaviour can only be obtained if assessed throughout the entire day. This is too time consuming for farmers and for research purpose very expensive and inefficient. In order to develop an automized system to assess bird behaviour, simplification is needed because too many classes would make it impossible to analyse the information for flock management. Also, not all behaviours are equally important for management decisions. One way to simplify laying hen behaviour could be clustering in groups or classes based on the activity level. Hence, three main classes of laying hen behaviour based on their individual intensity were addresses as: low-, moderate- and high-intensity physical activities (Kozak et al. 2016). We used their list of behavioural activities of laying hens and the class that they are assigned to in our research.

In general, all animal monitoring techniques can be divided into two categories, body-worn sensor technologies and remote sensor technologies. To monitor chicken behaviour, both technologies have advantages and disadvantages. One of the advantages of body-worn sensor technologies is that the identification of individual chickens is ensured as they all have their own sensor. By using remote sensor technologies, such as computer vision, the distinction between various individual animals can be more difficult. However, in the case of body-worn sensors, one sensor is needed for each chicken, which might cause problems to upscale the system to commercial flock size (Winkel et al. 2011).

Machine learning is a technique that can be used to efficiently analyse large datasets. This technique consists of a system with multiple algorithms that enable the subtraction of hidden features and relationships from datasets. The complexity of the different algorithms varies and involves several stages of sophisticated decision making, which invites the use of machine learning algorithms into optimizing automating processes (Hepworth et al. 2012). These types of monitoring are even able to operate in real-time which potentially alleviates the task of monitoring (Hepworth et al. 2012).

Machine learning distinguishes two main types of learning: supervised and unsupervised learning. Supervised learning consists of algorithms that try to classify data based on labelled input data, while unsupervised learning models a set of inputs where labelled input is not available. One type of supervised techniques that is often applied in research is the Support Vector Machine (SVM), which is preferred because of its ability to generalize well (Oladipupo 2010). Hepworth et al. (Hepworth et al. 2012) showed that applying SVM to recognize poultry samples was able to correctly predict whether a chicken was sick or not (accuracy rate of 99.469 %). They also compared additional algorithms such as Bayesian classifier, Random Forest and an artificial neural network and all of these methods had accuracies above 95%. A model of (Oladipupo 2010) showed that a Random Forest classification algorithm was able to correctly classify the behaviour of individual laying hens into three classes of behaviour. They also investigated the use of Principle Component Analysis, but they found that it did not have a major effect on the classification performance. This shows that applying machine learning algorithms to behavioural chicken data is able to classify the behaviour of a chicken.

The literature review shows a lot of potential for improving the performance of these algorithms. Examples of these improvements include classifying more behavioural categories and improving the outcomes of machine learning models by validating the parameters. While accelerometers are widely used, there is no consistent approach to process the data that is being generated by these devices (Hepworth et al. 2012). This restricts the ability to compare results across research. Also, behavioural studies are for practical reasons often performed in smaller sized systems, and results obtained by these studies do not necessarily reflect behaviour in commercially sized systems (Hepworth et al. 2012). The main objective of this study was to investigate if machine learning can be recognized as a viable tool to analyse and classify the behaviours of laying hens in three levels of activity.

2. Materials and Methods

2.1. Experimental setup

An experiment was designed to collect data related to the daily behaviour of chickens. The experiment was performed in a section of a commercial aviary laying hen house, which was separated from the rest of the house by steel wire mesh. The experimental area was about 5x4x4 meters in size. During the experiment, 15 white laying hens were present in the experimental area. The chickens were approximately 34 weeks of age.

2.2. Inertial measurement unit (IMU)

The MTw2 Awinda wireless motion tracker of Xsens as the inertial measurement unit was used in this study. The sensor consists of an accelerometer and a gyroscope which can measure the acceleration and angular velocity, respectively. Besides the accelerometer and the gyroscope, an IMU can also consist of a magnetometer. The technical properties for the IMU's have been provided in Table 1.

Table 1 Technical properties of the MTw2 Awinda Wireless 3DOF Motion Tracker (www.xsens.com)

	Angular velocity	Acceleration	Magnetic field
Dimensions	3 axes	3 axes	3 axes
Full scale	2000 deg/s	160 m/s2	1.9 Gauss
Non-linearity	0.1 % of FS	0.5 % of FS	0.1 % of FS
Bias stability	10 deg/hr	0.1 mg	-
Noise	0.01deg/s/√Hz	0.01 μg/√Hz	0.2 mGauss/√Hz
Alignment error	0.1 deg	0.1 deg	0.1 deg
Bandwidth	180 Hz	180 Hz	10-60 Hz (var.)

2.3. Data analysis and classification algorithm

Before the experimental data could be used for the identification of the chicken behaviour, various steps had to be completed. An overview of the main steps is shown in Figure 1. Some important pre-processing steps were video annotation and linking the video data to the sensor data. After pre-processing the data, time windows containing data of several seconds were created. From the specific data in the windows it was possible to calculate important characteristics, also called features. These features could then be used for classification of the behaviour. However, before using the feature data, the data was standardized.
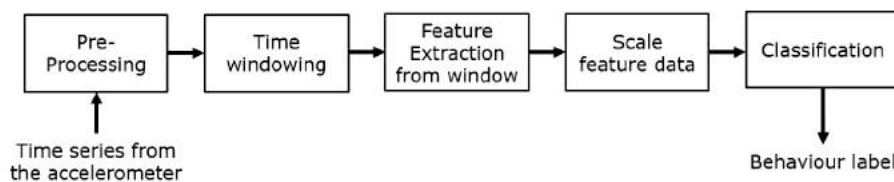
Figure 1 Overview of behaviour classification process (Adapted from Rahman et al., 2018)

Raw data from the sensors needs to be pre-processed, which requires file type changes so that it can be read by data software such as Matlab. Pre-processing also requires manual labelling of the video data. Time windowing is needed in order to generalise data points and extracting more information from the acceleration data. Feature extraction is needed to reduce dimensionality so that the data can be classified. Model creation and statistical analysis were performed using MATLAB R2020b, version 1.0.0.1. (MathWorks, Inc.) and Microsoft Office Excel 2016. The Random Forest classification model was created in Matlab2018 software. The Classification Learner application supported by Matlab was used to create a basic Random Forest classification model. The Machine Learning ToolboxTM was used to analyse and model the data by using different Machine Learning methods. It provides principal component analysis (PCA), regularisation, dimensionality reduction, and feature selection methods that allow identifying features with the best predictive power (Matlab, 2021b). It also provides supervised, semi-supervised, and unsupervised machine learning algorithms, including support vector machines, decision trees, k-means, and more clustering methods. A two-tailed paired samples t-test was used to statistically show a significant difference between results. This was implemented to show whether for example a difference of 4% in an accuracy value would be significantly different or not. This section will not discuss the statistics in detail, but a general explanation is provided in order to explain the tests.

2.4. Datasets

We used the classification of behavioural activities of laying hens based on their individual intensity (Hepworth et al. 2012): low-, moderate- and high-intensity physical activities (Table 2)

Table 2 Classification of physical activity of laying hens based on their intensity (taken from (Kozak et al. 2016))

Low-intensity	Moderate-intensity	High-intensity
• Sleep like resting (neck tucked into feathers of back, breast or wing-awake)	• Preening	• Walking (head/neck bobbing involved)
• Neck shortening resting (neck retracted in U shape)	• Foraging (ground scratching, pecking)	• Running (Neck stretched forward, no head bobbing)
• Sleeping	• Eating	• Jumping
• Quiet sitting/standing	• Drinking	• Wing flapping (With or without change in location. Can be combined with any above behavioural events)
• Small postural head/shoulder/neck movements	• Small wing adjustments	• Controlled aerial ascent/descent
• Perching	• Scratching	• Full-body shaking
• Egg laying	• Stretching	• Shaking phase of dust bathing
• Side-laying phase of dust bathing	• Head shaking	
	• Feather fluffing	
	• Pecking	
	• Searching behaviour (small steps, up and down head movement)	
	• One to two slow steps (minimal distance covered)	
	• Scratching behaviour of dust bathing	

Class 1 represents static laying hen behaviour, class 2 represents semi-dynamic behaviour and class 3 represents highly dynamic laying hen behaviour. The original dataset consists of the standardized datasets for the green chicken. Dataset A is a modified version of the original dataset, with more precise labelling for class 3. Dataset B was used to validate the classification performance of models that were of interest on data of different chickens. An overview of the different datasets and their class distributions is provided in Table 3.

Table 3 Dataset overview with the available number of data points per class and additional information. Two chickens were observed, one wearing a green backpack and one wearing a blue backpack.

	Original dataset	Dataset A	Dataset B
Number of datapoints class 1	3,023	3,017	747
Number of datapoints class 2	3,606	3,588	2,638
Number of datapoints class 3	37	61	47
Total measurements	6,666	6,666	3,432
Chicken	Green	Green	Blue
Day of recording	Wednesday	Wednesday	Friday
Total length of recording	2 hours 20 minutes	2 hours 20 minutes	29 minutes

The classes are highly imbalanced, with class 3 having significantly less data points than classes 1 and 2. By assigning higher penalties to minority classes, the ML models can equalize the weights of the classes in case of an imbalance between available data points. The penalty of misclassifying a sample of class i is calculated by:

$$penalty_i = nTotal/nClass_i \qquad (1)$$

where nTotal is the total number of samples in the dataset and nClass$_i$ is the number of samples in the dataset that is annotated as class i (Oladipupo 2010). The resulting penalty matrices are provided in Figure 2.
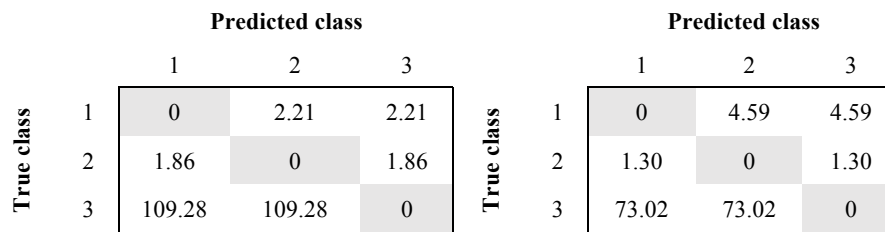
Figure 2 Penalty matrices of datasets A (left) and B (right). The rows represent the true classes, while the columns represent the predicted classes.

This data will then be exposed to feature extraction, which means to reduces the dimensionality, normalize and standardize the dataset. This dataset is then split into a training data set and a test data set, where the training data is a subset used in order to train a model and the test set is used to test the trained model. Finally, the test data is used to compute the generalization performance of the model, in other words, the ability of the model to generalize the outcome.

2.5. Model performance measures

In order to assess the model performance, cross-validation and principal component analysis were introduced. When training a model, occurrences such as overfitting and underfitting are important to keep into consideration. Cross-validation is a technique that splits the data in a certain way to find the best algorithm for the model. It is used to evaluate the performance of a machine learning model by predicting new datasets that the model has not previously been trained on. This is done by partitioning an available dataset by using a subset of the whole dataset to train the algorithm and the remaining data of the dataset to test the model to evaluate its performance. Each round involves randomly partitioning the original dataset into a training and a test set. This process is then repeated several times as can be seen in Figure 3.

Figure 3 Four-fold Cross-Validation. The original dataset is partitioned into 4 equally sized subsets, which are repeatedly used as either testing or training set. (Matlab, 2021a)

3. Results and Discussion

3.1. Correlation

The first step was to check for correlation between individual features in order to find important relationships between individual variables. The variables that are highly correlating with at least one other variable are the standard deviation, the variance, the minimum and maximum and the energy for each direction (X-, Y-, and Z-direction, Pearson Correlation Coefficient > 0.7 or < -0.7).

To check the effect of the correlating variables, some of the correlating variables were removed before the training process. This led to a selection of 24 out of the 31 available features for training the models. The remaining variables were the skewness, kurtosis, mean, covariance and entropy along with the standard deviation, variance and minimum for each direction.

For the 4 second time window, there was no statistical difference found between the accuracy values when all variables were included and when some highly correlating variables were removed (P = 0.987). However, for the 1 second time window, removing some highly correlating variables decreased the mean accuracy of all the models with 0.5% (P = 0.0008).

3.2. Principal Component Analysis

The next analysis involved Principal Component Analysis (PCA) and checking its effects on the performance of the different Machine Learning techniques. With each comparison, the classification models were trained and tested on the same datasets with the same time window, being either 4 seconds (long) or 1 second (short).

The effect of the randomization part that is introduced by cross-validation (due to randomly assigned subsets) was investigated before the PCA results were analysed. This was done by running the models multiple times with the same settings applied. When looking at the 1 second time window with dataset A, there was no significant difference in the accuracy values for both PCA and no PCA (P = 0.318 and P = 0.277 respectively). The 4 second time window also showed that the randomization due to applying cross-validation did not introduce significant differences with P-values of 0.551 and 0.341 for respectively PCA and no PCA.

3.2.1.Time window

When looking at the 4 second time window and comparing PCA vs no PCA; not applying PCA on dataset A showed a 1.3% higher accuracy value (P = 0.0004). The F1-scores of classes 1 and 2 were both equal to 0.89, which was 1% higher for both instances (P = 0.0113 and P = 0.0006). This resulted in a 3% higher overall F1-score of 0.58 (P = 0.0185). The F1-score of classes 1 and 2 were both 0.89. The F1-score of class 3 was not significantly different.

The 1 second time window showed significant differences in all measured parameter values for dataset A except for the F1-score of class 3 and the training time. Not applying PCA resulted in a 2.7% higher overall accuracy of 83.6% (P = 1.49 · 10^{-8}). There were also significant differences in the F1-scores of classes 1 and 2 and the overall F1-score. The F1-scores for classes 1 and 2 were 2% and 3% higher with no PCA, resulting in a 3% higher overall F1-score (P = 9.86 · 10^{-9}, P = 2.20 · 10^{-6}, and P = 0.0003 respectively). The F1-score of class 3 was not significantly different as the P-value was equal to 0.130.

3.3. Time windows

Dataset A shows significant differences between the accuracy values when comparing the long-time window with the short time window, which are respectively 4 seconds and 1 second. For dataset A with no PCA applied, there were differences in all measured outcomes, except for the training time. The models had an average accuracy of 88.8% for the 4 second time window and 83.6% for the 1 second time window (P = 5.48 · 10^{-5}). The F1-scores for the 4 second time window were equal to 0.89, 0.89, and 0.58 for respectively classes 1, 2, and 3, resulting in an overall F1-score of 0.79. The one second time window resulted in F1-scores equal to 0.85, 0.82, and 0.37 for respectively classes 1, 2, and 3. This resulted in an overall F1-score of 0.68. These values were statistically different with the P-values being equal to 0.013, 2.67 · 10^{-6}, 4.07 · 10^{-7}, and 9.25 · 10^{-8} for respectively the F1-score of class 1, 2, and 3, and the overall F1-score. Since the type of highly dynamic behaviour is very short and often a sharp move in the acceleration data, the time window that is being used is important. When time windows are longer, they contain more data, this should increase the classification performance of the model, as the model has more data that could be of use.

3.4. Machine Learning models

A comparison was made between an existing Random Forest model and the other available models in order to find the best model for this study. This means that the original dataset with a small-time window was selected without applying PCA. When comparing these results, the level of significance is important in order to indicate whether the results are significantly different. Therefore, two situations were investigated: one situation with the default significance level of 5% (P < 0.05) and one situation with a significance level of 10% (P < 0.1).

3.4.1.Best performing models

When looking at the default significance level, we found that there were no models significantly better than the Random Forest model. When altering the significance level to a level that allows less than 1 in 10 chance of being wrong (P-value of 0.1), two models showed significantly higher values. These models are the bagged trees and subspace KNN within the ensemble Machine Learning technique. Their P-values were respectively 0.054 and 0.097 and provided a significantly better fit on the data than the initial Random Forest model. Only the results of the bagged trees model will be considered, as this model was the best performing model in this study.

The Bagged trees model had an accuracy value of 90.0% and its F1-scores were equal to 0.89, 0.91, and 0.87 for respectively classes 1, 2, and 3. This resulted in an overall F1-score of 0.89. The accuracy was increased by 1%, but the increase in F1-scores showed a better fit on the different classes compared to the Random Forest model. The F1-scores increased by 2%, 1%, and 6% for classes 1, 2, and 3, resulting in an overall F1-score increase of 3%. The confusion matrices of the Random Forest model and the bagged trees model are provided in Figure 4.

(A)	Predicted class			Recall		(B)	Predicted class			Recall
	1	**2**	**3**				**1**	**2**	**3**	
1	2435	588	0	**0.81**		**1**	2677	346	0	**0.89**
2	162	3435	9	**0.95**		**2**	322	3281	3	**0.91**
3	1	6	31	**0.82**		**3**	0	6	31	**0.84**
Precision	**0.94**	**0.85**	**0.78**			Precision	**0.89**	**0.90**	**0.91**	
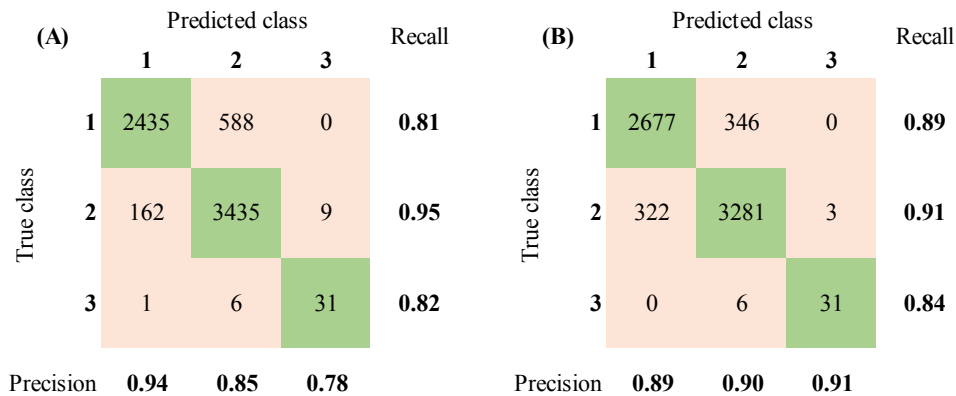
Figure 4 Confusion matrices of the Random Forest model (A) and the bagged trees model (B). (Class 1 = static behaviour, class 2 = semi-dynamic behaviour, class 3 = high-dynamic behaviour)

3.4.2.Performance on data of the blue chicken

To verify the classification performance of the bagged trees model, this model was exposed to accelerometer data and labelled data of a different chicken (blue chicken, dataset B). The same situation was used to check the classification performance (short time window and no PCA applied). The bagged trees model was able to predict the data with an accuracy of 97.1%. This resulted in F1-scores of 0.95, 0.98, and 0.82 of classes 1, 2, and 3. The overall F1-score was equal to 0.92. Comparing these results with the results of the Random Forest model showed that the F1-score of class 1 decreased by 1% when using the bagged trees model over the Random Forest model. The F1-score of class 2 remained equal. Nonetheless, the bagged trees model was able to increase the F1-score of class 3 by 13%, going from 0.69 for the Random Forest model to 0.82 by using the bagged trees model. Subsequently, the overall F1-score increased by 4% (0.88 for the Random Forest model and 0.92 for the bagged trees model). The confusion matrices of both models with dataset B as input data are given in Figure 5.

(A)	Predicted class			Recall		(B)	Predicted class			Recall
	1	**2**	**3**				**1**	**2**	**3**	
1	721	26	0	**0.97**		**1**	725	22	0	**0.97**
2	32	2577	29	**0.98**		**2**	58	2568	12	**0.97**
3	0	7	40	**0.85**		**3**	0	6	41	**0.87**
Precision	**0.96**	**0.99**	**0.58**			Precision	**0.93**	**0.99**	**0.77**	
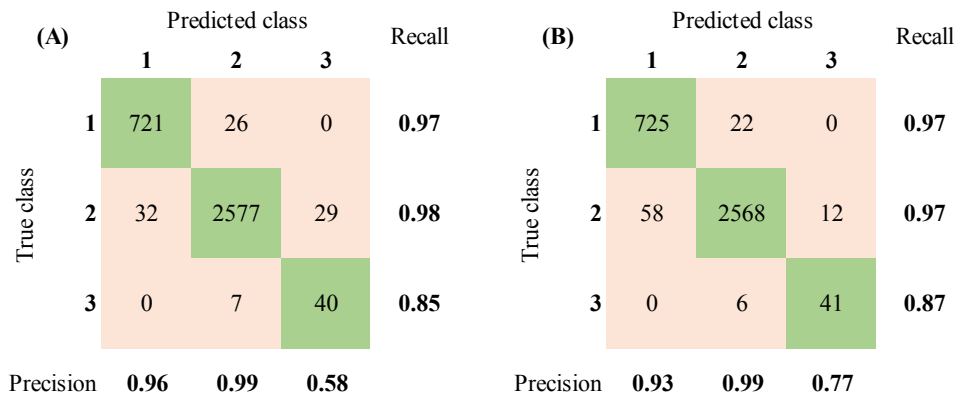
Figure 5 Confusion matrix of the Random Forest model (A) and the bagged trees model (B) with dataset B as input data and no PCA applied. (Class 1 = static behaviour, class 2 = semi-dynamic behaviour, class 3 = high-dynamic behaviour)

4. Conclusion

When considering the obtained results in this research, machine learning can be recognized as a viable tool to analyse and classify laying hen behavioural activity levels. Accelerometer data can be used to predict the activity level of laying hens, but the initial training of the models still needs manual labelling. The machine learning model of this study can predict the three activity levels that were considered during this research with overall accuracy values of over 90%.

Removing some of the highly correlating variables did not introduce significant model improvement for both the 1 second and 4 second time window with the original dataset. Also, applying PCA did not result in better model classification performance. The suggested time window for classes 1 and 2 is for all models the long-time window (4 seconds). Using a shorter time window (1 second) resulted in higher F1-scores of class 3, which improves the ability of the models to accurately predict highly dynamic behaviour. Annotating data of class 3 more precisely only increases model performance for the 4 second time window, not for the 1 second time window. The best machine learning technique to use is the ensemble technique, which uses multiple learning algorithms to obtain better prediction performance than a standalone algorithm would. The best performing machine learning model was the bagged trees with an accuracy of 90% for the original dataset. The F1-scores were equal to 0.89, 0.91, and 0.87, resulting in an overall F1-score of 0.89. This resulted in a 1% increase in model accuracy compared to the original Random Forest model. Also, the F1-scores of classes 1, 2, and 3 increased by respectively 2%, 1%, and 6% by using the bagged trees model.

There is still manual labour involved in the training process of the models by labelling video data. Most of the models that were studied are supervised learning algorithms, which need pre-labelled data to learn and be able to classify unseen data. However, the use of devices like an accelerometer enables the possibility to accurately classifying laying hen behavioural data into static, semi-dynamic, and highly-dynamic classes. In order to let a Machine Learning model classify chicken behaviour fully automatically, an unsupervised learning algorithm should be selected, which does not require manual intervention by requiring pre-labelled data.

References

Aarnink AJA, Mosquera J, Winkel A, et al (2009) Options for dust reduction from poultry houses. In: Agricultural Technologies In a Changing Climate: The 2009 CIGR International Symposium of the Australian Society for Engineering in Agriculture. pp 1–8

Cambra-López M, Aarnink AJA, Zhao Y, et al (2010) Airborne particulate matter from livestock production systems: A review of an air pollution problem. Environ. Pollut. 158:1–17

Casey K, Bicudo J, Schmidt D, et al (2020) Air Quality and Emissions from Livestock and Poultry Production/Waste Management Systems. In: Animal Agriculture and the Environment: National Center for Manure and Animal Waste Management White Papers

Council of the European Union (1999) Council Directive 99/74/EC of 19 July 1999 laying down minimum standards for the protection of laying hens. Off J Eur Communities 53–57

EFSA (2005) Opinion of the Scientific Panel on Animal Health and Welfare (AHAW) on a request from the Commission related to the welfare aspects of various systems of keeping laying hens. EFSA J 3:197. https://doi.org/10.2903/j.efsa.2005.197

Elson HA (2015) Poultry welfare in intensive and extensive production systems. Worlds Poult Sci J 71:449–460. https://doi.org/10.1017/S0043933915002172

Hadlocon LS, Zhao LY, Bohrer G, et al (2015) Modeling of particulate matter dispersion from a poultry facility using AERMOD. J Air Waste Manage Assoc 65:206–217. https://doi.org/10.1080/10962247.2014.986306

Hepworth PJ, Nefedov A V., Muchnik IB, Morgan KL (2012) Broiler chickens can benefit from machine learning: support vector machine analysis of observational epidemiological data. J R Soc Interface 9:1934–1942. https://doi.org/10.1098/rsif.2011.0852

Kozak M, Tobalske B, Springthorpe D, et al (2016) Development of physical activity levels in laying hens in three-dimensional aviaries. Appl Anim Behav Sci 185:66–72. https://doi.org/10.1016/j.applanim.2016.10.004

Oladipupo T (2010) Types of Machine Learning Algorithms. In: New Advances in Machine Learning. InTech

Takai H, Pedersen S, Johnsen JO, et al (1998) Concentrations and Emissions of Airborne Dust in Livestock Buildings in Northern Europe. J Agric Eng Res 70:59–77. https://doi.org/10.1006/jaer.1997.0280

Winkel A, Mosquera J, Huis in J, et al (2011) Maatregelen ter vermindering van fijnstofemissie uit de pluimveehouderij: validatie van een ionisatiesysteem op vleeskuikenbedrijven

Mobile Robot Weeder prototype for Cotton Production

Joe Mari Maja [a,*], Matthew Cutulle [b] , Edward Barnes [c], Jake Enloe [d], Jakob Weber [d]

[a] Department Agricultural Science, Clemson University, 247 McAdams Hall, Clemson, South Carolina, USA

[b] Plant and Environmental Science Department, Clemson University, 2700 Savannah Hwy, Charleston, South Carolina, USA

[c] Cotton Incorporated, 6399 Weston Parkway, Cary, North Carolina, USA

[d] Department of Mechanical Engineering, Clemson University, Fluor Daniel Engineering Innovation Building, Clemson, South Carolina, USA

* Corresponding author. Email: jmaja@clemson.edu

Abstract

The U.S. cotton industry provided over 190,000 jobs and more than $28 billion total economic contributions to the United States in 2012. The U.S. is the third-largest cotton producing country in the world, following India and China. The U.S. cotton producers have been able to stay competitive with countries like India and China by adopting the latest technologies. Despite the success of technology adoption, there are still many challenges, e.g., increase pest resistance, mainly glyphosate resistance weeds, and early indications of bollworm resistance to Bt cotton (genetically modified cotton that contains genes for an insecticide). Cotton producers have little options to address weeds due to; limited herbicide options, high technology fees for herbicide-resistant varieties, and labor shortage for hand weeding. This paper will first present the navigations and obstacle avoidance technique, its implementation on our mobile robot and present the weeder prototype developed for cotton and the field test results in 2019 and early 2020. The autonomous mobile platform used a Robot Operating System (ROS) version kinetic and runs in Ubuntu 16.04. Two different weeder modules were designed, built, and tested. The first design has six individual prongs on each side, where each prong measured approximately 15 cm. The prong was designed to penetrate about 3.8 cm. into the soil. Two wheels were used to ensure the prongs would be kept at a constant depth into the ground. The second design was based on a cultivator with a harrow disk. A randomized complete block with three replications was used to test the mobile robot platform's speed with the weeder prototype, where half of the test was irrigated (drip), and the other half was non-irrigated. The preliminary field test showed that the average time of the mobile robot's travel only has a minimal difference between the two irrigated rows (10% saturation and 65% saturation) but has a significant difference between irrigated and non-irrigated. Approximately, 10%~15% weed control was observed on one of the test plots and 80% weed control was observed in the second test plot.

Keywords: Unmanned Ground Vehicle (UGV), Crop Protection, Weeding, Robot Operating System (ROS)

1. Introduction

The U.S is the third largest cotton producing country in the world. It is apparent that Cotton producers must stay competitive by adopting the latest technologies. The cotton industry in the US has significant impact to the economy with 190,000 jobs and more than $25B per year. This year's yield forecast at 386 kgs. per harvested acre was slightly above the previous year (Meyer, 2020). The U.S. cotton industry has a long history of the adoption of distributive technologies starting with the invention of the cotton gin in 1790's, the adoption of mechanic harvesters in the 1950s, and development of the module builder in the 1970's (Hughs et al., 2008). Each of these technologies significantly decreased labor requirements and has allowed the labor to produce a 218-kg bale of cotton fiber to decrease from 140 hours in 1940 to less than 3 hours today (Wanjura et al., 2015). Despite the success of technology adoption, there are still many challenges faced by the U.S. cotton producer. One major challenge is competition from polyester, where overproduction in China has resulted in polyester prices that are approximately 50% less than cotton and has resulted in suppressed cotton prices (Meyer, 2016). Thus, producers must continue to increase their production efficiency as increased cotton prices on the near horizon. Other challenges now facing cotton producers are increased pest resistance, particularly glyphosate resistance weeds (Norsworthy et al., 2016), and early indications of bollworm resistance to Bt cotton (genetically modified cotton that contains genes for an insecticide).

Sistler (1987) provided a review of the different robotic applications and its future possibilities in agriculture. More robot-based technologies have been used in agriculture and have been implemented through the use of automation and with ranges of form factors, e.g., ground-based (e.g., smart tractors, unmanned ground vehicle [UGV]), crane-based systems, aerial-based (e.g., unmanned aerial vehicles [UAV]). A rapidly adopted automation in agriculture for example is an automated system for milking cows. Salfer et al. (2019) estimated over 35,000 milking systems are currently used all over the world. For row crops, weed control with the rise of herbicide resistant weeds and lack of new herbicide modes of action is a significant concern and robotic systems are one of the proposed solutions (Westwood et al., 2018). Most of the major agricultural machinery companies have announced autonomous machinery plans, have prototype

machines and/or have filed patents on autonomous robotic systems for agriculture (e.g., Murray et al., 2018).

UGVs have been used for different purposes in agriculture. BoniRob is a four-wheeled-steering robot with adjustable track width and used as a crop scout (Bangert et al., 2013). Its sensor suite includes different cameras (3D time of flight, spectral), and laser distance sensors. It was at first design as a phenotyping robot but as its development progresses, additional functionality was added as a weeder. It used a hammer type of mechanism to destroy weeds. Unfortunately, BoniRob development was discontinued for an unknown reason. Vinobot is a phenotyping UGV implemented on a popular mobile platform from clearpathrobotics. Vinobot can measure phenotypic traits of plants and used different sensors (Shafiekhani et al., 2017). TERRA-MEPP (Transportation Energy Resource from Renewable Agriculture Mobile Energy-crop Phenotyping Platform) is another UGV that was used for high-throughput phenotyping of energy sorghum. It used imaging sensors to measures plant from both sides as it traverses within rows thereby overcoming the limitations of bigger UGV (Young et al., 2019).

Robots are becoming more integrated in the manufacturing industry. Though, most of the manufacturing environment is not as complicated as the outdoors, recent advances on sensors and algorithm provide an interesting outlook on how robots will be working outdoors with humans. Commercial small Unmanned Ground Vehicle (UGV) or mobile ground robots with navigation sensing modality provides a platform to increase farm management efficiency. The platform, Husky, (clearpathrobotics) can be retrofitted with different manifolds that performs specific task, e.g., spraying, scouting (having multiple sensors), phenotyping, weeding, harvesting, etc. An autonomous map-based robot navigation was developed, and a selective harvesting proof of concept was also designed, and field tested in 2018. The robot was retrofitted with a vacuum-type system with a small storage bin. Performance evaluation for the cotton harvesting was performed in terms of how effective the harvester suctions of the cotton bolls and the effective distance (Burce et al., 2019; Maja et al., 2021). Using the same robotic platform, a new module was designed and tested in 2019. A weeding module which can be used for precision weed control, broadcast insecticide, and fungicide applications.

This work is part of a bigger project sponsored by the Cotton Incorporated to developed and designed different robotic platforms or automation for cotton field operation. The purpose of this research is to investigate the potential of UGV to be used for multiple operations. The specific objective is to i) designed and test two weeder modules, and ii) investigate the efficacy of the module in terms of the UGV speed for both irrigated and non-irrigated rows.

2. Materials and Methods

2.1. Mobile Robot Platform

The robot used in this work is the Husky A200 (Figure 1) from Clearpath Robotics. The robot is suitable for field operations as its width of 68 cm fits common cotton row spacings. It is lightweight for field traffic and thus soil compaction is not an issue as compared to huge farm machines. The robot is powerful enough to handle payloads of up to 75 kgs and, can operate at speeds of 1 meter per second. It has a 24VDC Lead-acid battery which can provide 2 hours of operation. Two new lithium polymer battery with 6 Cells each and 10Ah rating provide up to 3 hours of operation. Husky is equipped with IMU (CHR-UM7, CH Robotics, Australia), GPS (Novatel Smart6-L, Novatel, Canada), individual steering motors and encoders for each wheel for basic navigation and a laser scanner (UST-10LX, Hokuyo, Japan) for obstacle detection. The robot can be programmed to perform specific tasks like mapping, navigation, and obstacle avoidance through its onboard PC (mini-ITX) running on Ubuntu 16.04 operating system and the Robot Operating System (ROS, Kinetic version) framework. A mini-LCD screen, keyboard and pointing device was connected to the onboard PC allowing the user to easily write and test code, view and perform operations.
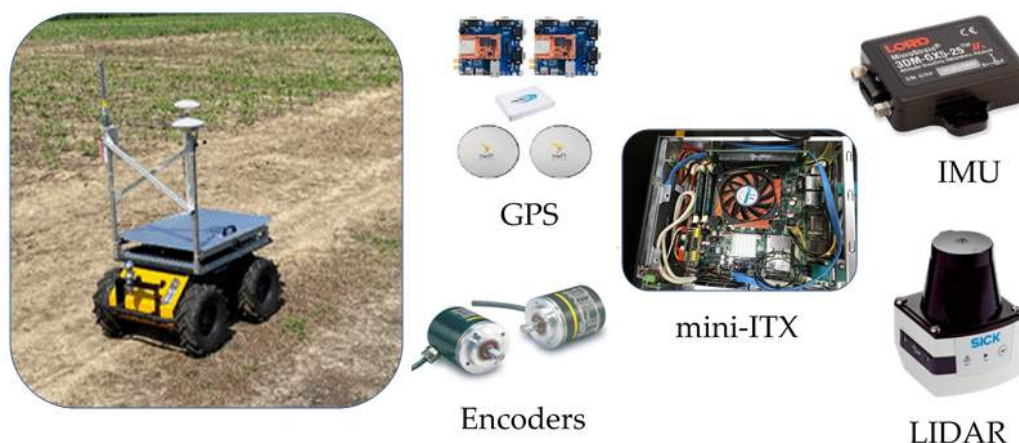
Figure 1. Mobile robot platform used in this project.

2.2. Field Navigation

Autonomous field navigation is achieved by having a digital map of the field and localizing the robot on that map. Localization involves integrating the coordinate frame of the robot with the coordinate frame of the digital map. The robot's coordinate frame, commonly referred as its odometry, estimates the robot's position and orientation over time. The accuracy of the robot's odometry may be enhanced by integrating it with other positional readings from an IMU or a GPS device. The robot's position is first determined using the kinematic model in Figure 2. The kinematic model of the four-wheeled robot used in this study was treated as a two-wheeled differential robot with virtual wheels WL and WR to simplify calculations. The robot's current position is determined by a tuple (x_c, y_c, α) and its new position (x_c, y_c, α)' after time δt, given its right and left virtual wheel linear speeds, v_R and v_L, respectively. The linear speed of each virtual wheel is shown in Equation (1) and (2).
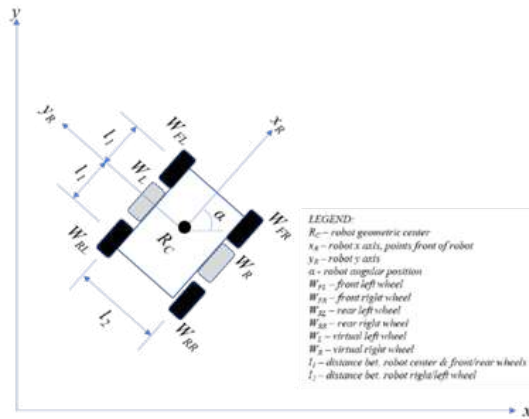
Figure 2. Robot's kinematics to determine its current position.

$$v_R = \omega_{W_R} \cdot r \qquad (1)$$

$$v_L = \omega_{W_L} \cdot r \qquad (2)$$

where ω is the angular speed and r is the wheel radius. The angular speeds ω and angular position φ of each virtual wheel is the average of its real counterparts as shown in Equations (3) to (6),

$$\varphi_{W_L} = \frac{\left(\varphi_{W_{FL}} + \varphi_{W_{RL}}\right)}{2} \qquad (3)$$

$$\varphi_{W_R} = \frac{\left(\varphi_{W_{FR}} + \varphi_{W_{RR}}\right)}{2} \qquad (4)$$

$$\omega_{W_L} = \frac{\left(\omega_{W_{FL}} + \omega_{W_{RL}}\right)}{2} \qquad (5)$$

$$\omega_{W_R} = \frac{\left(\omega_{W_{FR}} + \omega_{W_{RR}}\right)}{2} \qquad (6)$$

The robot's angular speed and position are shown in Equations (7) and (8),

$$a = \frac{\left(\varphi_{W_R} - \varphi_{W_L}\right)}{2} \cdot \left(\frac{r}{l_2}\right) \qquad (7)$$

$$\dot{\alpha} = \frac{d\alpha}{dt} \qquad (8)$$

and Equations (9) and (10) computes the robot's x and y component,

$$\dot{x}_C = \left(v_L + \dot{\alpha}\left(\frac{l_2}{2}\right)\right)\cos(\alpha) \qquad (9)$$

$$\dot{y}_C = \left(v_L + \dot{\alpha}\left(\frac{l_2}{2}\right)\right)\sin(\alpha) \qquad (10)$$

and to get the actual position we compute Equations (11) and (12),

$$x_c = \int_0^t \dot{x}_c \, dt \qquad (11)$$

$$y_c = \int_0^t \dot{y}_c \, dt \qquad (12)$$

2.3. ROS Navigation Stack

The ROS Navigation Stack is an integrated framework of individual software or algorithmic packages bundled together as nodes for steering the robot from one point to the next as shown in Figure 3. Users configure the navigation stack by either plugging-in built-in or custom-built packages in any of the nodes of the navigation stack. Estimation of the robot's odometry is therefore handled internally by the nodes in the navigation stack that automatically loads, references, and updates the configuration file during runtime execution of the robot.
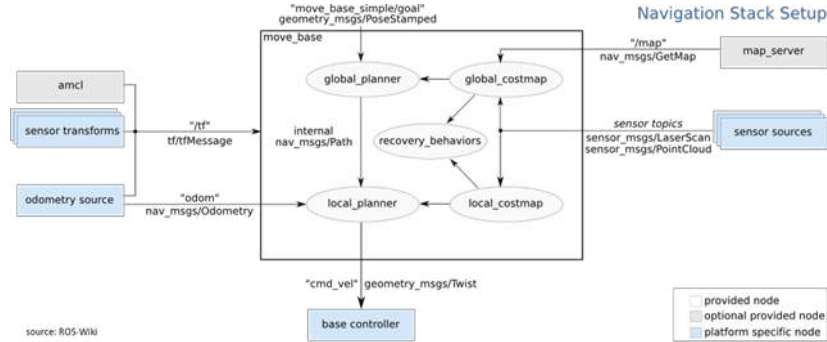
Figure 3. The ROS Navigation Stack used in our mobile robot platform.

2.4. Study Site

The field trials occurred at two separate locations, Edisto Research and Education Center [Edisto-REC] (33°21'26.6"N, 81°19'39.9"W) and Coastal Research and Education Center (32°47'27.2"N, 80°03'37.6"W) [Coastal-REC] of Clemson University in the months of July ~ August of 2018, 2019, and early 2020. Prior to the field trials, the navigation of the mobile robot was tested in the months of April ~ June. The row spacing of the cotton plants was approximately 96 cm and 10 cm in-row plant spacing. For this trials, common skip-row planting configurations was implemented with alternate rows. Seeding was done on early May and harvesting in the first week of December. Regular crop management practices were applied during the growing season.

During the field trials, the mobile robot was tested twice per month through 5,000 sq. m. without critical issues on the platform. Most of the issues during the trials were attributed to the mechanical vibrations that loosen the IMU from its holder, wheel nuts, and the ball joint holder loosening. The issue with loose IMU was not detected early on as its location was obscured. ROS has a useful command line, rosbag, which can be used both to record and replay bag files. Bag file is a file format in ROS for storing data. Examining the bag files provides a clue on why the mobile robot was acting weird on some of the prior test.

2.5. Weeder Prototype

Two different weeder modules were designed, built, and tested. The first design (Figure 4a), V-shaped, has six individual prongs on each side, where each prong measured approximately six inches. The prong was designed to penetrate about 3.8 cm (1.5 inches) into the soil. Two wheels were used to ensure the prongs would be kept at a constant depth into the ground. A slider mechanism was designed to make the width of the two-prong holder adjustable. The second weeder (Figure 4b) was an adjustable harrow disk, where the disk holder can be adjusted at certain angle with no wheels to support the disk. Since the disk used was an off the shelf and heavy, it was retrofitted with two wheels to minimize the force needed by the mobile robot to pull the weeder.

Figure 4. Two weeder designs tested for this work: (a) Weeder with V-shaped and (b) Weeder with adjustable harrow disk.

2.6. Field Trials

The mobile robot speed (with and without the weeder) was tested in two terrain types (rough and flat) and two distinct soil moisture types (irrigated and non-irrigated) using randomized block with three replications. The

preliminary test was set to 30 meters. The speed was held constant at start up to 0.5 m/s but will compensate if slippage was detected during travel. The compensation for slippage was set to a maximum of 2 seconds where if the robot will not change its displacement, the robot will increment by 0.1 m/s, until a displacement occurred. The mobile robot will stop the motors if the set speed reaches to 1 m/s. with no displacement. This will prevent the platform from either destroying the motors caused by slippage or heavy load. The travel times were recorded for both irrigated and non-irrigated.

The second trials were focus on the weed control. At the Edisto-REC trial, the speed was set to around 0.75 m/s, while in the Coastal-REC, the speed was set to 1 m/s for ground covered with mat of killed ryegrass and 0.75 m/s without the cover. Weed at the Edisto-REC comprised of goosegrass, palmer amaranth, and purslane, while at the Coastal-REC were Carpet weed and crabgrass.

3. Results and Discussion

Early field test on the mobile robot navigation showed that the GPS device accuracy is very important especially when the plants are still on the germination and emergence of shoots. The Lidar data does not provide any useful information as the height of the plants was below the Lidar height with respect to the ground. Due to the inaccuracy of using a Novatel GPS (Figure 8), a new GPS (Piksi Multi, Swift Navigation, USA) was used. A new configuration of the nodes and topics were created to integrate the new GPS with the waypoint navigation with the following tasks:

- Reconfiguration of the different GPS nodes and topics for the GPS waypoint navigation code. (Figure 5)
- Conversion of aerial view map (geotiff image) to customized map used for navigation. (Figure 6)
- Writing a python script to convert latitude and longitude points for each pixel in the geotiff image. (Figure 7a)
- Exporting latitude and longitude points and overlaying it to geotiff image pixels in QGIS. (Figure 7b)
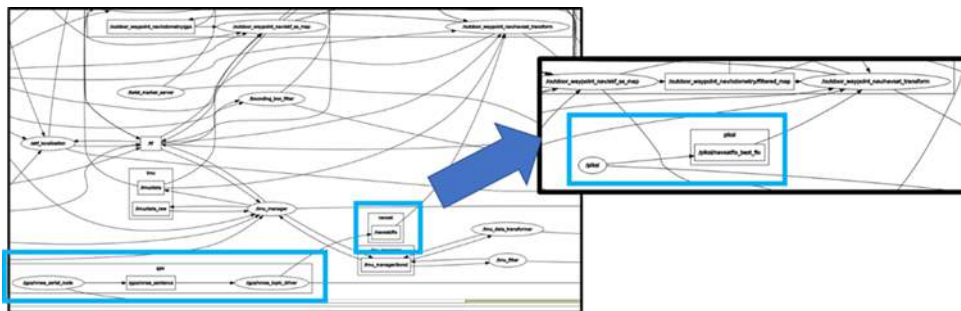
Figure 5. Reconfigured GPS nodes and topics.

Figure 6. (a) Aerial geotiff image of the field to (b) customized map.
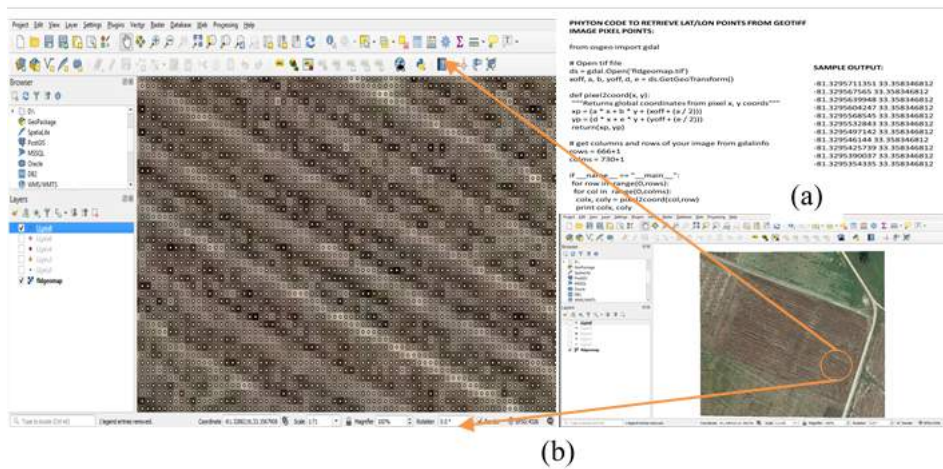
Figure 7.(a) Python code for conversion of geotiff image pixel points to latitude/longitude points. (b) Overlayed latitude and longitude points to the image.

Figure 8. GPS data from the previous GPS device.

Figure 9a shows a partial map generated using the Lidar during the flower bud and peak flowering growth stages. Figure 9b shows the robot's localization test using the generated map of the cotton field.
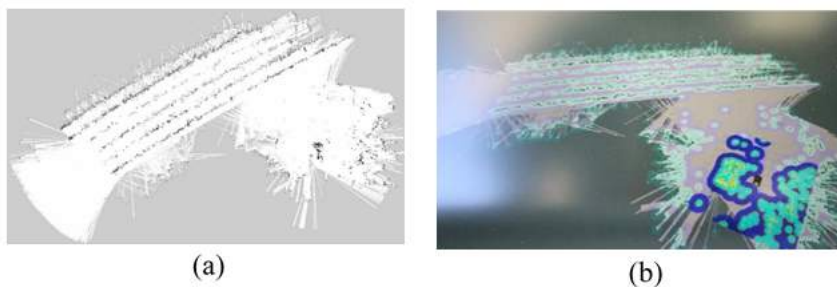
Figure 9. Map of the cotton field at Edisto-REC showing five crop rows from laser scans and (b) localization using generated map.

3.1. Weeder Field Trials

The soil moisture average on the two months trial was around 20%.The results as shown in Figure 10c indicate that the mobile robot's travel times were the same for both dry and wet soil. The same test was replicated with the weeder attached and the results (Figure 10d) showed that on average travel time with wet soil is similar to without the weeder but there was a significant travel time with the weeder on dry soil (~138 seconds). Figure 10a and 10b shows the two weeders tested during the field trial. The field test showed that the average time of the mobile robot's travel only has a minimal difference between the two irrigated rows (10% saturation and 65% saturation) but has a significant difference between irrigated and non-irrigated.
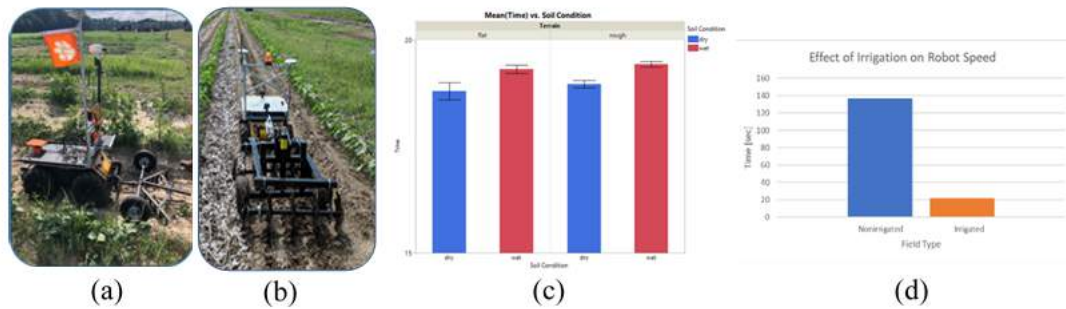
Figure 10. The two weeders being tested: (a) V-shaped and (b)Harrow-disk. Results for the travel time (c)with or without the weeder and (d) irrigated and non-irrigated.

3.2. Weed Control Trial

The V-shaped weeder was not effective in weed control (Figure 11a) during the preliminary test. A weight was added to maintain the penetration but its connection to the hitch eventually broke. Succeeding field trials on the weed control was only focused on the harrow disk. Approximately, 10%~15% weed control was observed at the Edisto-REC field trials (Figure 11b). There were three different weeds found in this area (goosegrass, palmer amaranth, and purslane). The terrain in this location is not flat and thus the lower weed control results. The Coastal-REC field trials resulted in higher weed control was observed (80%). Note that the robot was tested on two different ground cover and the terrain on this location was flat.

Figure 11. Weed control feed trials results for (a) V-shaped weeder and (b) Harrow disk weeder.

4. Conclusions

This work demonstrated the mobile platform with two different weeders for weed management for cotton. The mobile platform was successfully deployed in cotton field at two different field sites. Data collected from the trials were used to measure the efficacy of the two weeding modules and for future designs of weeding mechanism. Due to the available robot platform, the design constraint for the weeding module was that it must be a pull behind type. Although there are many mobile platforms already available but most of these systems are either large or that it can only be used for one specific operation, e.g., weeding, or spraying. The one use in this work addresses weaknesses in other designs and fills a niche as a compact and easily transportable. The mobile platform also used the popular ROS which can easily be adapted to another platform that used the same operating system. Equally important for this work was the autonomous navigation of the platform which has been field tested. Results for flat terrain was very promising and new designs were already in the works to be tested in the future. Although, the focus for this work was on cotton, the same system could be deployed for other crops as well.

References

Bangert, W., Kielhorn, A., Rahe, F., Albert, A., Biber, P., Grzonka, S., et al. 2013. Field-Robot-Based Agriculture: "RemoteFarming.1″ and "BoniRob-Apps". In AgEng, Internationale Tagung Land.Technik (pp. 439–445). Düsseldorf, Germany: VDI-Verlag.

Burce, M., J.M. Maja, E. Barnes. 2019. Adaption of Mobile Robot Platform for Cotton Harvesting. Beltwide Cotton Conferences, New Orleans, LA, January 8-10, 2019. National Cotton Council, Memphis, TN.

Clearpath Robotics Husky Unmanned Ground Vehicle. 2021. from https://www.clearpathrobotics.com/husky-unmanned-ground-vehicle-robot/ Accessed March 10, 2021

Hughs, S.E., T. D. Valco, and J. R. Williford. 2008. 100 Years of Cotton Production, Harvesting, and Ginning Systems Engineering: 1907 – 2007. Transactions of the ASABE 51(4): 1187-1198.

Maja, J.M.; Polak, M.; Burce, M.E.; Barnes, E. 2021. CHAP: Cotton-Harvesting Autonomous Platform. AgriEngineering 2021, 3, 199-217. https://doi.org/10.3390/agriengineering3020013

Meyer, L.A. 2016. The World and U.S. Cotton Outlook for 2016/17. Presented at the Interagency Commodity Estimates Committee, Agricultural Outlook Forum, USDA, Office of the Chief Economist, February 26, 2016. https://www.usda.gov/oce/forum/2016_speeches/meyer.pdf

Meyer, L.A. 2020. Cotton and Wool Outlook, CWS-20k, U.S. Department of Agriculture, Economic Research Service, December 14, 2020. https://usda.library.cornell.edu/concern/publications/n870zq801?locale=en Accessed March 12, 2021.

Murray, C.L., and M.E. Barker. 2018. Autonomous robotic agricultural machine and system thereof. United States Patent No. 9,891,629 B2. Feb. 13, 2018.

Norsworthy, J.K., L.M. Schwartz, and L.T. Barber. 2016. The incidence and ramifications of glyphosate resistance in cotton. Outlooks on Pest Management – February 2016. pp. 31-35. http://www.researchinformation.co.uk/pest/sample/S7.pdf

Salfer J., M. Endres, W. Lazarus, K. Minegishi, B. Berning. 2019. Dairy Robotic Milking Systems – What are the Economics? DAIReXNET. https://dairy-cattle.extension.org/2019/08/dairy-robotic-milking-systems-what-are-the-economics/

Shafiekhani, A., Kadam, S., Fritschi, B. F., & DeSouza, N. G. 2017. Vinobot and vinoculer: Two robotic platforms for high-throughput field phenotyping. Sensors, 17(1), 214. https://doi.org/10.3390/s17010214

Sistler, F.E. 1987. Robotics and Intelligent Machines in Agriculture. IEEE Journal of Robotics and Automation RA-3(1):3-6

Wanjura, J.D., E.M. Barnes, M.S. Kelley, and R.K. Boman. 2015. Harvesting (book chapter) in Cotton, 2nd Edition, D.D. Fang and R.G. Percy, Editors. Agronomy Monograph 57.

Westwood JH, Charudattan R, Duke SO, Fennimore SA, Marrone P, Slaughter DC, Swanton C, Zollinger R. 2018. Weed Management in 2050: Perspectives on the Future of Weed Science. Weed Sci. https://doi.org/10.1017/wsc.2017.78

Young, S., Kayacan, E., Peschel, J. 2019. Design and field evaluation of a ground robot for high-throughput phenotyping of energy sorghum. Precision Agriculture 20:697-722. https://doi.org/10.1007/s11119-018-9601-6

Robotic Cultivation of Pome Fruit: a Benchmark Study of Manipulation Tools - from Research to Industrial Standards

Gert Schouterden [a,*], Rafaël Verbiest [a], Eric Demeester [a], Karel Kellens [a]

[a] Department Mechanical Engineering, University of Leuven, Campus Diepenbeek, Belgium

* Corresponding author. Email: gert.schouterden@kuleuven.be

Abstract

During the cultivation of pome fruit, apples and pears need to be harvested, sorted and handled in various processes. Currently, the majority of these processes require a vast amount of manual labour. Combined with the structural shortage of seasonal workers, innovation in this field is crucial. Transition to automated processes could provide a solution wherein the search for an appropriate manipulation tool will be essential.

While other researchers already present a set of customized grippers for fruit harvesting, a wide variety of manipulation tools is available in robotic industry, ranging from standardized general-purpose grippers to optimized soft grippers. In this paper, nearly all relevant gripping principles are primarily tested and compared to each other based on both their gripping success as well as on their ability of not damaging the manipulated fruit. Other parameters, such as energy consumption and general feasibility, are evaluated as well. Concluding from the tests, these grippers are rated as applicable for harvesting, usable for fruit processing or not usable for fruit industry at all.

The performed benchmark study showed that the customized foam gripper scores the overall best for all test scenarios at the cost of being the least energy efficient. These test scenarios being the harvesting and other processing of both apples and pears. On the other hand, the majority of the other gripping principles and related tools excelled at certain specific tasks rather than being generally deployable. Impactive gripping tools are better suited for harvesting at low energy consumption, while astrictive suction cup grippers are more suited for sorting tasks constricted by the available space. A remarkable result was that not all commercially available soft grippers are capable of handling more sensitive fruits such as pears without causing damage.

Keywords: Manipulation, Automation, Pome Fruit, Harvesting, Benchmark Study

1. Introduction

During the cultivation of pome fruit, apples and pears need to be harvested, sorted, and handled in various processes. Currently, the majority of these processes require a vast amount of manual labour. Combined with the structural and further increasing shortage of seasonal workers, innovation in this field is crucial. Transition to automated processes could provide a solution; however, a challenging aspect of this automation is the manipulation of the fruit itself. Hence, the search for an appropriate gripping tool for this application will be essential. To deliver high-quality fruit to the consumer, both harvesting and processing pome fruit demand a considerable amount of care, as they are fragile products. However, besides this soft touch, a firm grip is still necessary to complete tasks such as harvesting. Consequently, the development of a usable gripper for fruit picking involves a delicate balance between gripping success and not harming the fruit.

Verbiest et. al. (2020) reviewed the current state of the art regarding the automation of the entire cultivation chain of pome fruit, presenting an overview of the advancements made in the last two decades. Most research focused on the development of robotic harvesting machines, whereby the gripping tool was only one element of the total development, being investigated to a lesser extent. The results considering the gripper principles used in existing research were analysed as a starting point for this study. Already in 2004, Setiawan et al. (2004) developed a gripper for apples based on an inflatable bellow principle, which first encloses the apple before it inflates to grip the fruit on multiple points. Using the same concept of total enclosure, Li et al. (2019) have recently developed an origami-inspired gripper for multi-purpose robotic soft gripping. Both Baeten et al. (2008) and the company Abundant Robotics (Abundant Robotics, USA‑CA, 2019) used a custom-made suction cup to harvest apples. In contrast to the suction cup principle, Onishi et al. (2019) used a three-fingered gripper with yaws that enclose the fruit on multiple sides. This is comparable to the three-fingered gripper of Davidson et al. (2016, 2017); however, the latter integrated an extra compliant mechanism to enclose the apple depending on its shape. Although it was for sweet peppers instead of pome fruit, Eizicovits et al. (2016) developed a soft gripper with four Finray jaws, which has a compliant mechanism as well. The last gripper taken into account in this study is the two-jaw gripper with active force control based on built-in pressure sensors developed by Zhao et al. (2011).

In contrast to the previously mentioned grippers, which are all customised gripping designs, the robotic industry offers a wide spectrum of standardised grippers that can be used for several applications. This study involves a

benchmark of nearly all relevant gripping principles, considering customised as well as standardised grippers for the application of robotic pome fruit manipulation. An overview of the tested grippers and a description of the testing protocol are further described in Section 2. Within the tests, all grippers were compared based on the following aspects: gripping success, the ability not to harm the fruits, and energy consumption. These results and the accompanying discussion can be found in Section 3. Finally, Section 4 concludes with a broad summary of the performed benchmark study and deliberates some tracks for future work.

2. Materials and Methods

2.1. Gripping principles

According to Monkman et al. (2006) and Shintake et al. (2018), the benchmarked grippers can be divided into two categories as follows: impactive based grippers and astrictive pneumatic suction-based grippers. The impactive based grippers generate a gripping force by either friction or form closure of the gripping elements (fingers) contacting the object. The astrictive based grippers generate a gripping force through the creation of a negative pressure field between the gripper and the object. Both categories can be divided further into subcategories, based on the design of the fingers and the method of vacuum generation. Figure 1 below provides an overview of the range of tested grippers. The dark blue boxes indicate the gripper category, the light blue boxes indicate the finger design or type of vacuum generation, and the grey boxes describe the basic components of the gripper.

Figure 1. Overview of tested gripper principles.

Seven impactive based grippers were evaluated in this study, which can be divided into three groups. The first group consists of three grippers with fingers, made of a soft compliant mechanism that adapts to the shape of the object through the actuation force. The FESTO and Piab based grippers are pneumatically powered using angular actuators and a vacuum ejector, respectively. On the contrary, the OnRobot gripper is electrically powered. The three previously mentioned grippers solely consist of standard industrial parts, however, the Piab piSoft being a prototype sample at the moment of the tests. Differently, the four grippers of the next two groups that are equipped with two custom-made cone shaped jaw designs with a soft and a rigid contact surface, respectively. The soft design is created by mounting two cone shaped silicone suction cups with a diameter of 50 mm on the fingers, while the rigid design has a similar 3D printed cone shape coated with a plastic layer, creating a smoother and more clutching surface. Both cone shaped finger designs are mounted on a pneumatic (FESTO), as well as an electric (Robotiq) actuator.

Besides the seven impactive based grippers, three astrictive suction-based grippers were evaluated as well. The first group of astrictive based grippers is actuated by a pneumatic two stage ejector, equipped with food grade bellow shaped suction cups. The second group is actuated by an electric blower motor using a further development of the gripper described in Baeten et al. (2008) as a large custom suction cup. This suction cup consists out of a 3D-printed mount and a thick EPDM foam, with a 100 mm diameter and 60 mm height, with a conical cut out in the centre.

While the grippers using the FESTO DHRS-40-A actuator or Piab VGS3010 are powered by pressurised air, the custom foam gripper's blower is powered by 3-phase power. All other grippers are powered on 24V DC power.

2.2. Grasping and damage assessment - Testing protocol

The primary required characteristics of the above-mentioned grippers are the ability to grasp the fruits successfully, without causing any damage to the fruits. These parameters will be evaluated through the execution of a simplified harvesting operation in a controlled environment. The used testing setup is shown in Figure 2a.

The setup consists of an industrial robot placed next to an aluminium construction at which fruits are placed by their stem using a friction fit clamp, representing the fruits attached to the branch of a tree. The robot, more specifically a KUKA iiwa 14 R820, has been equipped with the tested grippers.

The testing sequence was executed as follows: (I) The fruits are manually hung from the aluminium construction on a fixed location. (II) The robot moves into a fixed picking position diagonally below the fruit, closes the gripper and performs a slow vertical downward motion to harvest the fruit. (III) If this picking operation is executed successfully, the robot performs an acceleration test, which is defined by the movement in both directions along a path consisting of a horizontal movement of 620 mm followed by a downward vertical movement of 370 mm. The transition between these two segments is rounded off with a radius of 130mm. The velocity and acceleration of the end effector along the path are displayed in the graph below (Figure 2b).
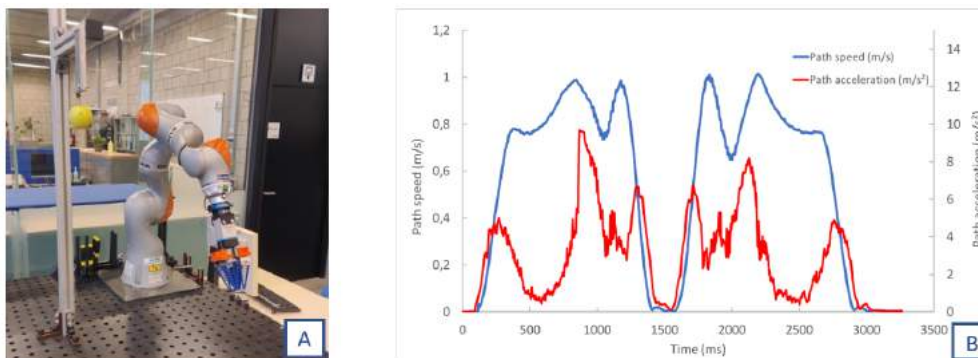
Figure 2. a) The used testing setup with the KUKA iiwa 14 R820 and b) Velocity and acceleration diagram of the end effector along the movement path during one testing sequence.

This testing sequence was performed on each gripper for both apples (Cultivar: Golden Delicious) and pears (Cultivar: Conference) on three gripping force settings and each of these tests was repeated thrice for validation (Figure 3). This resulted in nine tested apples and nine tested pears per gripper. The actuation speed of the grippers was minimised, reducing the impact force of the closing gripper. Thus, the damage caused to the fruits could be evaluated as solely influenced by the grippers' design and the gripping force. The fixed gripping position in combination with the size and shape variation of the fruit caused some planned deviation from the ideal gripping position. This deviation gave useful insights regarding the grippers' abilities to cope with similar realistic scenarios, such as moving branches or detection errors.

The gripping success was determined based on the grippers ability to successfully grasp, harvest, and hold on to the fruit during the testing sequence. The damage caused to the fruits was examined on two discrete moments in time. Initially the presence of externally visible damage was evaluated immediately after the above-mentioned testing sequence. Next, the harvested apples and pears were stored for respectively six and four days at room temperature. This storage time made smaller defects and internal damage better perceivable by the human eye through discoloration or local decay. Subsequently, the presence of damage was evaluated a second time, examining the fruits outside as well as inside through cross-sections. No further classification regarding the magnitude and type of damage was made in this evaluation. Due to the high variety of these parameters and the highly variable threshold of the allowable damage, depending on the usage of the fruits, this would only have resulted in a subjective classification.

2.3. Energy consumption

Besides the characteristics regarding the grasp quality, the power usage of each gripper was also determined for the following simulated harvesting scenario. The grippers will perform a picking operation where the movement between pick and drop location will last 5 seconds in each direction. Between these movements the gripper executes a pick and release action of which the time is determined for each of the grippers individually. These picking and release actions are performed on the settings as described in the Section 2.1.

The grippers benchmarked in the study can be divided into two different categories when determining their energy consumption based on the source of the energy. The first category is powered by electric energy, such as in the electrical motors of the OnRobot and Robotiq grippers or the blower motor of the custom foam gripper. The grippers of the second category, including the Festo actuator or the Piab ejector, are pneumatic powered.

The power consumption of the first category was measured using a DC current probe in combination with a digital oscilloscope in the case of the Robotiq and OnRobot grippers, and with a 3-phase power analyser (Chauvin Arnoux C.A 8335) in the case of the custom foam grippers' blower motor. The power consumption of the second category was calculated with equation (1), using the air consumption stated on the datasheets. Only the power used by the actuators or blower motor was taken into account, in order to exclude all inefficiencies due to transformer losses, switching power supplies, or pressurised air generation and air distribution, since their presence is depending on the construction and design of the whole automated setup.

$$\dot{E}_{gripper} = P_a \, Q \, \ln(P_u/P_a) \tag{1}$$

Where Pa is the atmospheric pressure; Pu the upstream pressure; and Q, the flow rate in the standard state. This equation thus converts the upstream pressure and flow rate into energy [W].

3. Results and Discussion

3.1. Grasping and damage assessment

The summarised results of the grasp and damage assessment are displayed for each fruit type in three graphs on Figure 3. The first graph displays the gripping success for each of the grippers and this for their three respective force settings. The other two graphs display the damage assessment results on the two discrete evaluation moments. Additionally, to these summarising graphs, some remarks, that were observed during testing and damage assessment, are given specifically for each gripper.

With regards to the damage assessment the following notes should be made. The state of the tested apples was comparable to the state during the harvest, whereby the damage results of the apples are representative to a realistic situation. On the contrary, the pears were purposely verry ripe, increasing their susceptibility to being damaged and magnifying the minor differences between the tested grippers. Consequently, these results should rather be used for a relative comparison between the grippers and not absolute for the harvesting of pears. Failed gripping attempts could also render the fruits unfit for damage assessment causing a large set of excluded pears.
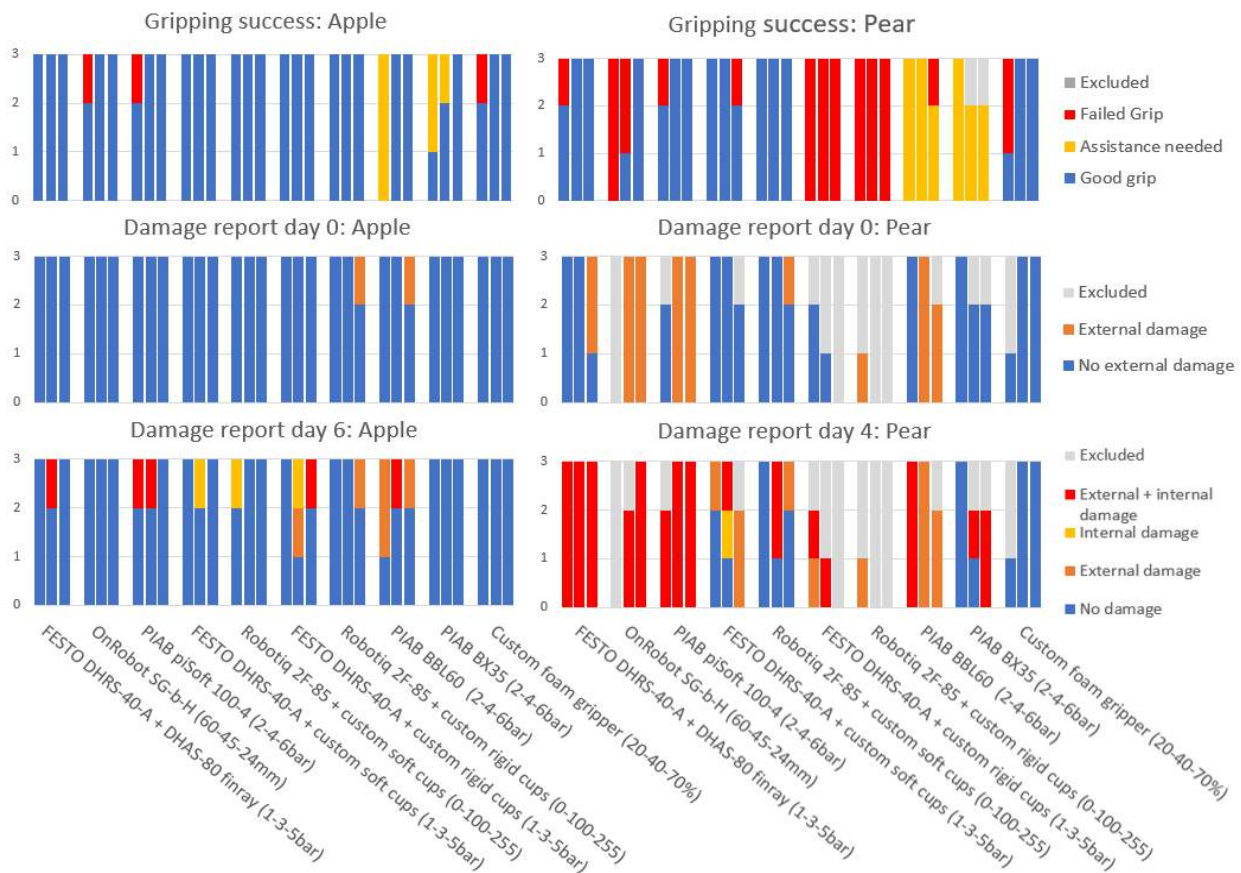
Figure 3. Synthesis of the test results: left are the results for apples, and right for pears. For each gripper tested, the three force settings, defined between brackets, are displayed in three separate columns.

3.1.1.FESTO DHRS-40-A + DHAS-80 finray

The finrays on the pneumatic actuator performed well both on gripping success and damage assessment when picking apples. In the case of gripping pears, a similar result was observed regarding the gripping success. Immediate damage was only present on the highest force setting. After the storage time of four days, extra damage on all force settings was detected, caused by the textured gripping surface of the finrays, which was imprinted on the pears (Figure 4a).

An additional trial was made using the smooth side of the finray fingers. A similar number of injuries were noticed during this trial. This could be induced by a combination of two phenomenon. The first being the less spherical shape of the picking position on the pears resulting in an uneven distribution of force between the finray fingers. The second cause could be that the finrays did not completely deform to the shape of the fruit due to the lower gripping force setting, distributing the gripping force over a smaller area. Furthermore, this also resulted in a grip that was more based on force rather than the intended form fit, which is considered less secure. At higher force settings the finrays would properly adapt to the fruits (Figure 5a), however, at this setting the sheer magnitude of the force became the damaging factor.

3.1.2.OnRobot Sg-b-H

The OnRobot soft gripper achieved satisfactory results handling the apples. However, for the larger specimens, the gripper's soft mechanisms were observed to be too shallow, turning the intended form fit grip into a less secure friction fit. In contrast to apples, a range of issues were observed with the pears. The OnRobot soft gripper is not inherently force but position controlled. The force is generated by the deformation of the compliant soft mechanism. This causes the actual gripping force to be equally influenced by the setting as well as the size object itself, resulting in a range of bad gripping attempts on the smaller pears at the lower force settings. Hence, these bad results could partially be assigned to user errors.

When gripping any other object, with non-ideal dimensions for the grippers design, the gripper's fingers often curled up putting all their clamping force on a small area as shown in Figure 4b. Additionally, the non-spherical shape in the gripping location of the pears caused an uneven force distribution between the gripper's fingers, which even enlarged the previous point contact issue. Better results could be achieved if the fruit could be approached from directly below, however, this gripping pose is in reality unachievable for both harvesting and sorting operations.

For creating an ideal grasp with this gripper, a simultaneous movement towards the object, while closing the gripper, could be executed to compensate the movement of the soft mechanism. Additional tests indicated this could partially compensate the previously mentioned bad grasps caused by the gripper's shallowness.

3.1.3.Piab piSoft 100-4

The tests with the Piab piSoft gripper resulted in decent gripping success for both apples and pears. However, the ribbed design of the gripper tips (Figure 4c) was observed to be detrimental for handling both pome fruits, creating small areas of high contact force and thus causing damage. This effect was especially noticeable on the more sensitive pears.

Similar to the symmetrical four-fingered design of the tested OnRobot gripper, this design was observed to be disadvantageous when gripping the non-spherical shape of the pear from diagonally below, causing extra injuries due to not ideal gripping point placement and force distribution.

3.1.4.Custom soft cups (FESTO DHRS-40-A and Robotiq 2F-85)

This grippers' design performed well on both the gripping success and the immediate damage assessment through good adaptation to the fruit's shape (Figure 5b). Despite the soft contact interface of the suction cups, injuries due to a too high contact force were observed for the pears after the four-day storage at room temperature. The implementation of a more deformable suction cup could reduce the damage these fingers cause to the more sensitive fruit, by better distributing the contact force.

The gripper's design could also facilitate a combined gripping principle by turning on the suction cups for extra gripping force. This feature was not implemented as the impactive grip was already adequate and the extra upgrade would only create extra energy consumption and an extra source of potential damage (suction spots).

3.1.5.Custom rigid cups (FESTO DHRS-40-A and Robotiq 2F-85)

The gripping success of the apples was comparable to the above mentioned custom soft cups alternative. In contrary, none of the pears were gripped successfully, because the grippers could not close far enough to completely fixate the pears. This was caused by heat deformation of the cups during the application of the soft substrate. As the cups were rigid, the lacking ability to adapt in case of non-ideal gripping position resulted in an increased number of damaged fruits compared to the custom soft cups.

3.1.6. Piab BBL60 and Piab BX35

Whereas both industrial suction cups have a similar design, their gripping success was also similar. When approaching for the grip, these suction cups need to be pushed against the fruit to deform themselves and create a successful seal, since, due to the rather low suction rate, no large gaps can be bridged to attract the fruits. However, the force needed for this deformation is in the majority of cases too high, resulting in no more than pushing away the fruit without completely sealing the vacuum. When this occurred during testing an intervention was made by applying a manual counter force preventing the fruits from being pushed away. These scenarios are displayed in Figure 3 with the specific designation "assistance needed". Therefore, these grippers are not advised to be used for harvesting operations but rather for sorting or packaging activities. In these applications their ability to grip fruits surrounded by other fruits or other machine elements close to them becomes an advantage. A slight edge could be given to the BX35 cup that has a better chance of finding a good gripping spot due to its smaller size and thinner and more flexible sealing lip, adapting better to the fruits' irregularities (Figure 5c). This advantage however comes at the cost of lower stability during movement and a higher change of a collapsing suction lip during gripping.

Both suction cups created suction spots on the pears that became especially observable after the storage time. Additionally, the BBL60's connector design could leave an impression on both fruit types when they got sucked up against it. Modifications made to the suction cups connector, shown in Figure 4d slightly alleviated this. Similar impressions were not observed with the BX35 since the fruits are only sucked into the soft bellow and will never make contact with the suction cups connector.

3.1.7. Custom Foam suction cup

The custom foam gripper was able to nearly grip all apples and pears, and of these successful grips, no fruits were damaged. Unsuccessful grips only occurred on the lower power setting where the suction force was not high enough the suck in the fruits and deform the foam to ensure a good seal (Figure 5d). Still, the higher suction rate gave this gripper the ability to overcome larger gaps between the fruits and seal thus eliminating the assistance the other astrictive based designs needed. Moreover, no suction spots could be observed due to the lower vacuum level.
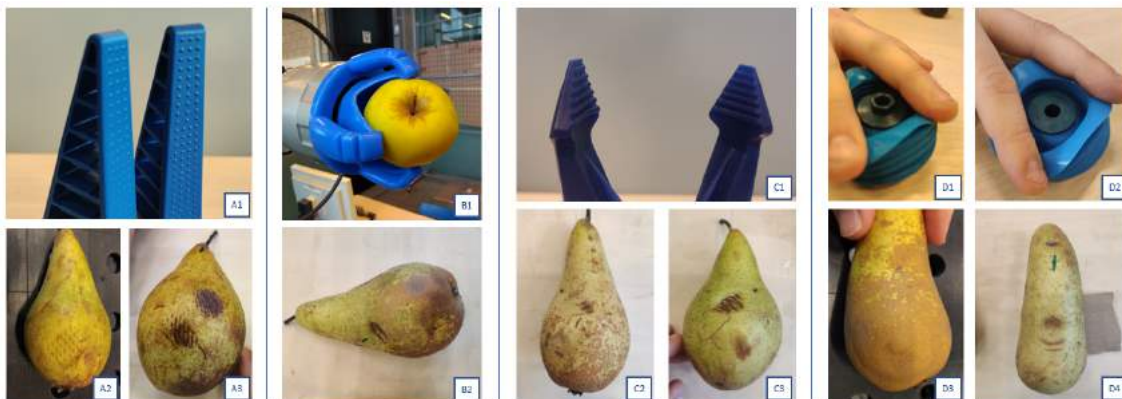
Figure 4. Overview of damage results. a1) FESTO finray with textured gripping surface; a2) damage caused by finray on day 0; a3) damage caused by finray on day 4; b1) the fingertips of the OnRobot gripper curling up into point contacts; b2) damage caused by OnRobot point contact on day 4; c1) piSoft with ribbed gripping surface; c2) damage caused by piSoft on day 0; c3) damage caused by piSoft on day 4; d1) original BBL60 fitting; d2) Customised BBL60 fitting; d3) customised BBL60 indentation on day 0; d4) suction spot caused by suction cups on day 4.
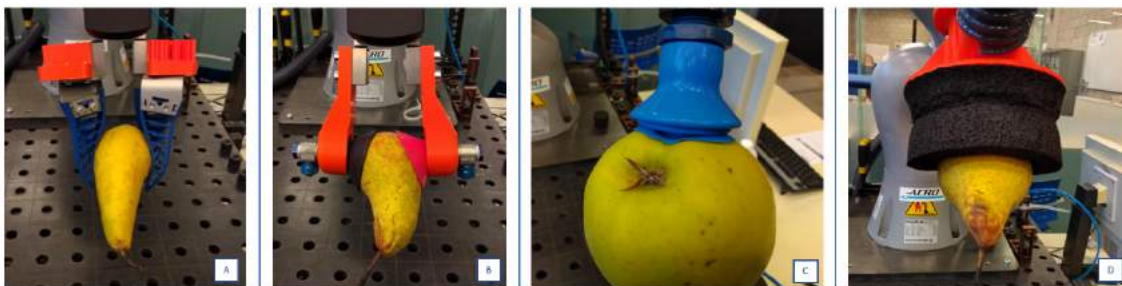
Figure 5. Overview of advantages of soft gripping principles, due to the adaptivity of: a) the compliant structure of the finray fingers; b) the soft cups; c) the flexible sealing lip; d) the compliant structure of the finray fingers; and d) the adaptivity after sealing the foam gripper.

3.2. Electrical vs pneumatic force control

When comparing the pneumatic FESTO actuator to the electrical Robotiq actuator, both equipped with the same fingers (the custom soft cups or the rigid cups), their gripping force setting should not be compared directly, since the force ranges of both grippers do not match. Adjusting for this mismatch, a slight advantage could be given to the electric Robotiq, based on the lower number of damaged fruits.

The scaling of this advantage with regards to the gripping speed will depend on the used gripper fingers. The gripping force measurement curves of the gripper's datasheet (Robotiq, 2020, p.60) indicate that the lower forces will not be sustained at the higher speed settings when gripping a rigid object with rigid gripper fingers. This is probably caused by the absence of reaction time for the force control system when two rigid objects contact each other. The addition of the soft deformable custom suction cup fingers will result in a better control over lower gripping forces on higher speeds at the cost of an overall lower achievable gripping (Robotiq, 2020, pp. 61-62). This could even be improved upon through the use of even softer contact elements ref PU graph. In contrary, the clamping force of pneumatic actuators is mostly dependant on the supplied air pressure. All achievable speeds with this supplied air pressure will theoretically result in the same gripping force. Besides the effect of the grasping speed on the controllability of the grasping force, the impact force will increase for both drive mechanisms. As indicated in Section 2, this impact force has been excluded in this study.

The gripping force of the pneumatic actuators might be less influenced by the actuation speed but depends in the case of the radial actuator design of the FESTO DHRS on the size of the gripped object. In the current finger design this results in a higher clamping force the smaller the gripped fruit is. This effect could be reversed through the adaption of the gripper's fingers so the working area of the actuator is between 50° and fully open. The effect could also be eliminated using a parallel actuator at the cost of a substantial reduction of grippable object sizes. The electrical actuation of the similar radial base actuator of the tested Robotiq gripper is not affected by the object's size.

3.3. Power consumption results

Table 1 shows the results of the power consumption measurements for each of the actuators. The vacuum blower used for the custom foam cup was observed to be the main outlier having an energy consumption of a factor 10 to 350 larger than the other actuators. As expected, the large suction rate of the vacuum blower that resulted in good gripping results, forms also its main disadvantage when determining the energy consumption. Besides the high amount of energy needed to generate the required high flow rate, the need for the blower to be continuously active, due to its too slow ramp up and down rate, also contributed to this high energy demand. The second highest energy consuming actuator was the Piab pneumatic ejector. Similar as with the blower, the ejectors need to run continuously during the gripping process, which consumes a large volume of compressed air. The OnRobot gripper used substantially less power than the previous actuators. However, its consumption was notably higher than the other electric actuator. Both using more power during the actual actuation, and a higher than idle power to hold the object during transport. The last two actuators FESTO DHRS-40-A and Robotiq 2F-85 consumed nearly the same amount of power. The FESTO actuator only consuming compressed air during the actual actuation of the fingers. The Robotiq mainly using power during actuation, supplemented by a small idle consumption of the electronics.

Since the energy consumption was determined for a simulated scenario, the ratio between the grippers might shift due to a related shift in the ratio of gripping, transport and idle time. An increase in transport or idle time would benefit the pneumatic FESTO DHRS-40-A actuator and in a lesser degree the Robotiq 2F-85.

These results need to be evaluated in perspective to the rest of the automation setup. The low power consumption of the DC powered electrical actuators will be beneficial for the use on smaller battery powered autonomous platforms. Additionally, no other energy conversions would be required in these setups. Otherwise, for off-orchard processing processes or larger fossil fuel powered autonomous platforms, the availability of power becomes a minor issue and the extra cost could be justified by an increase in the performance of the gripping principal as for the custom foam gripper.

Table 1. Results of the Power consumption test

Actuator	Wh/100,000 picks	Cost/ 100,000 picks [€] (at €0.15/kW)
Festo DHRS-40-A	840	0.13
OnRobot SG-b-H	2239	0.34
Robotiq 2F-85	576	0.09
Piab VGS 3010 SI08-2	13140	1.97
Becker blower SV 201/2	177083	26.56

4. Conclusions

Based on the performed benchmark it can be concluded that all gripping principles are to a certain degree usable for

handling apples. The damage caused to apples, however, clearly indicated the beneficial effect of a soft and smooth gripper interface. Unlike the impactive grippers, the industrial ejector driven suction cups proved to be less suited for harvesting operations, but rather for other handling operations, such as sorting or packaging. In this case, these grippers have a substantial advantage over all impactive based gripping principles, due to their ability to pick fruits surrounded by other fruits close to them, on for example a conveyor.

In contrast to apples, the tests with the ripe and oversensitive pears provided better insights in the relative differences in performance between the grippers. All three commercial impactive soft grippers were able to successfully grab the pears, when set correctly. A slight disadvantage could be given to the two symmetrical four-fingered designs, the OnRobot and the Piab piSoft, which were not able to adapt properly to the non-spherical shape of the pears in the current gripping pose. Moreover, despite their soft design, none of the industrial soft grippers were able to handle the pears without damaging them. However, minor adaptions to these grippers could make them viable for the handling of the more fragile fruits. By making the substrates of the compliant mechanisms softer, and by removing textures and other rough features, the presence of force concentrations could be reduced. Neither the rigid custom cups were able to successfully grip any pears without damaging them. The custom soft cup fingers and industrial suction cups performed better to some degree; however, still causing many injuries due to force concentrations or high vacuum level respectively.

The soft EPDM foam interface combined with the low vacuum level of the custom foam suction cups proved to be the best approach of the tested grippers to handle the more delicate pears. This success comes with a large drawback, a substantially higher energy consumption of the blower motor. The higher energy consumption turned out to be a disadvantage for the astrictive gripping principals in general, being on average a factor 75 higher than their impactive counterparts, the exception being the Piab piSoft. Within the impactive grippers, the results did not indicate a substantial difference in gripping success or quality between the more conventional pneumatic actuators (FESTO) and similar but newer electrical actuators (Robotiq) on the tested parameters.

Second to the grippers evaluated ability to complete the needed manipulations for a certain task without causing damage, the differentiation parameters currently are the available energy supply and control structure of the automation setup.

Not all applicable gripping principles were able to be tested in the current benchmark. Future testing might include grippers such as origami grippers (Li et al. 2019) that are still in research or readily commercially available Fluidic elastomeric actuators (FEA). The influence of additional parameters such as variation in gripping speed on the scaling of the current results might also be evaluated.

Acknowledgements

References

Abundant Robotics, USA CA. 2019. https://www.abundantrobotics.com/ Accessed April 26, 2021.

Baeten J., K. Donné, S. Boedrij, W. Beckers, and E. Claesen. 2008. Autonomous fruit picking machine: A robotic apple harvester. Field and Service Robotics. 42, 531–539. https://doi.org/10.1007/978-3- 540-75404-6_51.

Davidson, J. R., Silwal, A., Hohimer, C. J., Karkee, M., Mo, C., & Zhang, Q. 2016. Proof of concept of a robotic apple harvester. In *IEEE International Conference on Intelligent Robots and Systems.* Daejeon, Korea, October 9-14. 634–639. https://doi.org/10.1109/IROS.2016.7759119.

Davidson, J. R., Hohimer, C. J., Mo, C., & Karkee, M. 2017. Dual robot coordination for apple harvesting. In *2017 ASABE annual international meeting.* Spokane, Washington, United States of America, July 16-19. 1–10. https://doi.org/10.13031/aim.201700567.

Eizicovits D., B. van Tuijl, S. Berman, and Y. Edan. 2016. Integration of perception capabilities in gripper design using graspability maps. Biosystems Engineering, 146, 98–113. https://doi.org/10.1016/j.biosystemseng.2015.12.016.

Li S., J. Stampfli, H. Xu, E. Malkin, E. V. Diaz, D. Rus, and R. J. Wood, 2019. A Vacuum-driven Origami "Magic-ball" Soft Gripper. In *Proceedings—IEEE International Conference on Robotics and Automation (ICRA).* Montreal, Canada, May 20-24. 7401-7408. https://doi.org/10.1109/ICRA.2019.8794068

Monkman G. J., S. Hesse, R. Steinmann, and H. Schunk. 2006. *Robot Grippers.* John Wiley & Sons, Ltd. 453 p. https://doi.org/10.1002/9783527610280.

Onishi Y., T. Yoshida, H. Kurita, T. Fukao, H. Arihara, and A. Iwai. 201. An automated fruit harvesting robot by using deep learning. Robomech Journal, 6 (13), 1–8. https://doi.org/10.1186/s40648-019-0141-2.

Setiawan A. I., T. Furukawa, and A. Preston. 2004. A low   cost gripper for an apple picking robot. *Proceedings—IEEE International Conference on Robotics and Automation*, New Orleans, LA, United States of America, April 26 – May 1, 2004 (5), 4448–4453. https://doi.org/10.1109/ROBOT.2004.1302418.

Shintake J., V. Cacucciolo, D. Floreano, and H. Shea. 2018. Soft Robotic Grippers. Advanced Materials. 30 (29). 1-33. http://dx.doi.org/10.1002/adma.201707035.

Verbiest R., K. Ruysen, T. Vanwalleghem, E. Demeester, and K. Kellens. 2021. Automation and robotics in the cultivation of pome fruit: Where do we stand today? Journal of Field Robotics, 38. 513–531. https://doi.org/10.1002/rob.22000.

Zhao D., J. Lu, W. Ji, Y. Zhang, and Y. Chen. 2011. Design and control of an apple harvesting robot. Biosystems Engineering. 110 (2). 112-122. https://doi.org/10.1016/j.biosystemseng.2011.07.005.

Robotiq, 2020. Robotiq 2F-85 & 2F-140 Instruction Manual. https://assets.robotiq.com/website-assets/support_documents/document/2F-85_2F-140_UR_PDF_20200211.pdf Accessed April 26, 2021.

Remote Sensing Applications to Improve Pomegranate Irrigation in Vega Baja del Segura Area (Alicante, Spain)

Joaquín Solano, Herminia Puerto, Carmen Rocamora, Sergio Rodríguez, José María Cámara-Zapata

Grupo de investigación Agua y energía para una agricultura sostenible, Universidad Miguel Hernández, Alicante, Spain

Corresponding author. Email: jm.camara@umh.es

Abstract

Enabling digital technologies have great potential to improve crop management. In this regard, remote sensing is a tool that can provide with certain vegetation indices values, such as NDVI and MSAVI, that help ameliorate irrigation management. Currently there are commercial platforms that generate this information using satellite images from different sources, endorsed with weather station data. Furthermore, open access satellites, like SENTINEL-2, provide images that can be processed with open access applications such as QGIS. Using these two methods, it is possible to improve irrigation management in certain herbaceous crops, that show high homogeneity and are stablished in large plots. However, in the case of fruit trees stablished in small plots, remote sensing information based on satellite images may prove to be insufficient due to interferences such as soil not covered by the crop, adventitious plants, or due to image resolution. This paper aims to suggest improvements in pomegranate irrigation based on low-cost remote sensing tools. For this purpose, the trend of five commonly used vegetation indices during one crop cycle is analysed. The plots studied were irrigated using drip irrigation, and were situated in Vega Baja del Segura area (Alicante, Spain). The values of these vegetation indices were determined making use of a commercial platform and open access software QGIS, using SENTINEL-2 images. The results indicate a significant linear correlation between the values of the vegetation indices and those of the irrigation water distribution throughout the annual crop cycle, although this is not the case when comparing the indices with the water needs of the crop. The significant correlation tends to improve when the indices values are calculated from the free QGIS application. Vegetation indices together with edaphoclimatic and irrigation information determined directly in the field can contribute to the prediction of crop behavior and to the optimization of pomegranate irrigation, in order to improve the sustainability of the crop and the resilience of producers against climate change.

Keywords: Enabling digital technologies, SENTINEL-2, QGIS, NDVI, MSAVI.

1. Introduction

The arid and semi-arid areas of the Mediterranean, such as Vega Baja del Segura in the south of the Valencian Community, Spain, are characterized by their low rainfall (between 200 and 300 mm per year), irregularly distributed precipitation, high temperatures throughout the year, a great daily temperature range, mild winters and very hot summers. In addition, the region presents saline soils, being the electrical conductivity of the saturation extract (CEES) higher than 2.0 dS m-1 in many cases, resulting in a yield loss of more than 10% in 80% of the irrigated surface, approximately (De Paz *et al*., 2011). As the pomegranate has a high salinity tolerance, it is one of the few species that can be grown in areas especially affected by this problem (Grieve *et al*., 2012). It is a fruit tree that prefers high temperatures and low environmental humidity for growth, thriving perfectly in arid and semi-arid environments, being able to withstand periodic droughts without permanent damage (Rodríguez *et al*., 2012). Despite the fact it is a very resistant crop, irrigation is needed to satisfy the demand of the harvest, being drip irrigation the one that best allows controlling the needs of the crop.

Precision farming includes all the applications of digital enabling technologies aimed to optimize of the management of the agri-food sector (Van Woensel *et al*., 2016). Data collection, communication networks, information management, modeling, simulation and/or prediction of the behaviour of systems, performance and/or robotics have great potential to improve the efficiency and sustainability of production (Coble *et al*., 2018). Among these technologies, remote sensing can play an important role as a source of complementary information. Satellite Earth observation systems, such as LANDSAT, SPOT and Sentinel 2, among others, offer images that are widely used to assess and monitor the state of vegetation. These satellite platforms provide information on a series of spectral bands that can be used to determine the conditions of vegetation and are able to emphasize properties of crop related objects, minimizing the influence of distorting factors, such as bare ground, solar radiation, the angle of the Sun and the atmosphere itself (Ruíz, 2011). These advantages of remote sensing are reinforced by the existence of numerous free applications, such as QGIS, which promote the development of precision farming.

The optimization of the irrigation of crops is a priority in arid and semi-arid areas, such as Vega Baja del Segura in the south of the Valencian Community, Spain, especially with the current perspectives of climate change. There are numerous studies in which remote sensing has successfully contributed to the estimation of the irrigation needs of

herbaceous crops in large plantations. However, this technology has hardly been used in woody crops in small plots. In order to evaluate the technical feasibility of this technology in this type of applications, in this work, the vegetation indices are determined by remote sensing and are then correlated with irrigation needs and with the distribution of irrigation supplies in a pomegranate plot. To do so, commercial information obtained from a private on-line platform is used, as well as processed data from free applications such as QGIS.

2. Materials and Methods

The pomegranate plot has an area of 18,450 m^2 and is located in the municipality of Albatera (Alicante, Spain). It is an adult pomegranate plantation, Mollar de Elche cultivar, distributed in a planting of 4.5 x 3.0 m^2. The digital determination of the plot was carried out using the Google Earth platform in the first place and a subsequent verification with the "Street View" application, being the images updated to 2020 in both cases. Furthermore, through an interview with personnel from the Community of Irrigators of Albatera, it was deduced that it was an adult plantation of Mollar de Elche pomegranate and, afterwards, a visit to the plot and an interview with the producer was carried out to determine the main indicators that characterized the irrigation management (Figure 1).
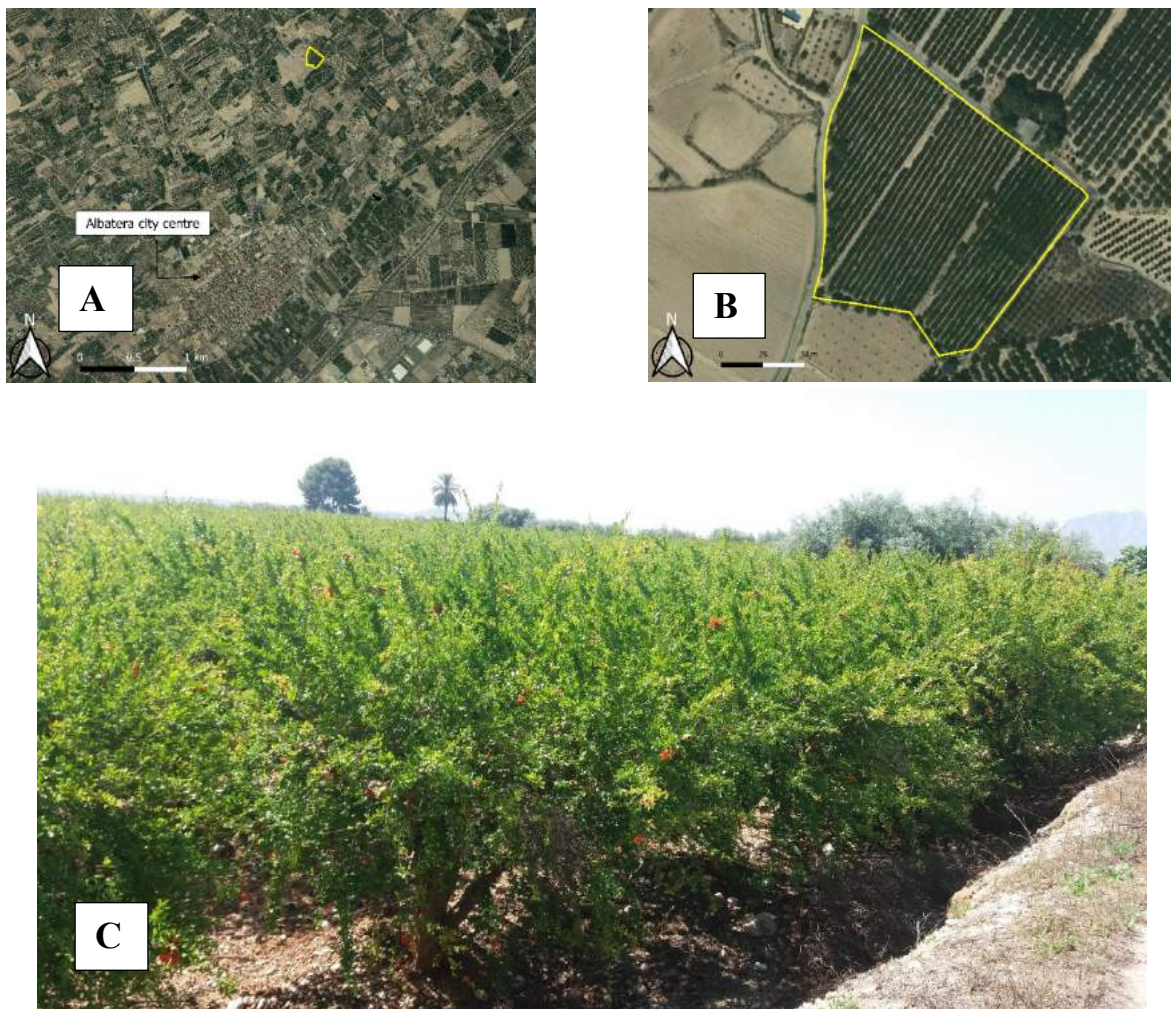
Figure 1. Pomegranate plot with localized irrigation (A: Location image; B: Plot image; C: Crop photograph from the North corner of the plot).

Based on the climatic data recorded in the closest meteorological station which was part of the National Meteorological Agency of Spain, the reference evapotranspiration (Howell and Evett, 2004) and crop needs (Introgliolo *et al.* 2011a) were determined.

2.1. Índices de vegetación

Determination of the vegetation indices was carried out in two different ways. On the one hand, it was accomplished using the information provided by a commercial platform after subscribing. In this regard, the shape file containing the

plot under study was introduced into the platform. This platform uses the images of Sentinel 2, a satellite of the Copernicus program, that offers hyperspectral images with a frequency of 5 days and a pixel size of 10x10 m^2. Besides, it discards those corresponding to days with a percentage of clouds greater than 15%. In order to calculate the vegetation indices, when selecting the plot, the software downloads the image that corresponds to the area and day of interest and performs the mathematical operations. The result provided by the platform is the average value of the index in the plot. Subsequently, the values throughout the year of study were downloaded into an Excel sheet.

On the other hand, the index values were also determined using QGIS and Sentinel 2 satellite images. In this sense, the shape file containing the delimited plot was the same as in the case of the online platform. QGIS raster calculator was used to calculate the indices. For this, the expression of each index was entered using the corresponding bands. Unlike the online platform, an Excel sheet was obtained with the daily maximum and daily minimum data of the plot throughout the year, and the mean value was determined from them. In a similar way to the previous case, the cloudy satellite images were discarded.

The vegetation indices used in this work are as follow.

2.1.1. Normalized Difference Vegetation Index (NDVI)

It was proposed by Rouse *et al*. (1974) and it is the most widely used index throughout the short history of Remote Sensing. It considers the amount of red energy (R) that is absorbed by chlorophyll and the amount of near infrared energy (NIR) that is reflected by the cellular structure of the leaf (Rubio *et al*., 2020). It is used to measure the vegetation cover present in each pixel. Its expression is the following:

$$NDVI = \frac{NIR - R}{NIR + R}$$

2.1.2. Normalized Difference Red Edge (NDRE)

According to Boiarskii and Hasegawa (2019), the NDRE reveals crops with a low chlorophyll content, which indicates a limitation in foliar nitrogen. The energy in the near infrared (NIR) and the energy in the red edge (Red Edge, RE) are used. Its expression is the following:

$$NDRE = \frac{NIR - RE}{NIR + RE}$$

2.1.3. Soil Adjusted Vegetation Index (SAVI)

It is a variation of the NDVI that considers the influence of the soil and minimizes its effects through a parameter, L, which is a function of the density of the vegetation and takes the value of 0.5 for intermediate densities (Huete, 1988). This index is very useful when used on land with a high percentage of bare soil. Its expression is the following:

$$SAVI = \frac{(NIR - R)(1 + L)}{(NIR + R + L)}$$

2.1.4. Red Edge Chlorophyll Index (RECI)

The Red Edge Chlorophyll Index is an index related to the photosynthetic activity of the plant cover, due to its sensitive to the chlorophyll content in the leaves. Since the chlorophyll level is directly related to the nitrogen level in the crop, this index allows identifying the areas of the field with this type of deficiency. Its expression is the following:

$$RECI = \frac{NIR}{RE} - 1$$

2.1.5. Normalized Difference Moisture Index (NDMI)

This index shows the level of water stress present in the crop. Its values vary from -1 to 1. In its calculation, the SWIR variable is used, which refers to the Short Wave Infrared band. The expression is the following:

$$NDMI = \frac{NIR - SWIR}{NIR + SWIR}$$

3. Results and Discussion

3.1. Edaphoclimatic characteristics of the plot and water needs of the crop.

Table 1 shows the monthly mean values (year 2020) for temperature, relative humidity (in both cases, maximum, average and minimum), solar radiation, wind speed and precipitation recorded in the meteorological station of Catral, Alicante, Spain, located less than 2 km away from the analyzed plot. Maximum temperature values reached practically 40.0 ºC, exceeding 30.0 ºC every day during the months of July and August. On the other hand, the minimum temperatures reached values lower than 0.0 ºC, although without affecting the crop, as this occurs during the months of December and January, when the tree has not started its vegetative development. There was a thermal amplitude of 10.0 ºC or more in approximately 85% of the days. Solar radiation exceeded 25.0 MJ m^{-2} throughout the months of May to August, both included. The area did not experience strong winds throughout the year, being the maximum wind speeds greater than 40 km h-1 during four months and 30% of the days with maximum values of speed greater than 20 km h^{-1}. Rainfall in 2020 was slightly higher than the average value in the area (between 200 and 300 mm), with a total accumulated value of 320.0 mm.

Table 1. Monthly mean values of climatic properties in the study area.

2020	Temperature (ºC)			Relative Humidity (%)			Solar radiation (MJ m^{-2})	Wind speed (km h^{-1})		Precipitation (mm)
	Max.	Average	Min.	Max.	Average	Min.		Max.	Average	
January	22.6	9.8	-0.9	91	80	62	8.5	48.7	3.3	57.1
February	29.1	13.9	2.0	91	76	49	13.0	41.9	3.8	3.4
March	29.1	14.4	4.5	92	70	38	13.3	41.9	4.6	125.1
April	28.3	15.9	7.2	89	76	55	18.3	28.7	2.9	32.4
May	33.0	20.6	10.3	79	66	51	25.1	31.2	3.4	12.9
June	33.2	23.4	13.9	84	66	41	26.8	35.4	3.2	23.9
July	39.7	26.3	17.4	75	67	57	26.5	26.1	3.0	0.2
August	37.4	26.5	15.1	78	69	48	23.6	27.0	2.6	32.9
September	34.0	23.0	10.5	85	67	35	17.8	28.0	2.8	5.5
October	33.8	17.9	6.8	87	64	43	13.9	42.2	3.3	2.0
November	27.1	15.3	3.7	91	82	73	8.9	34.5	2.7	20.4
December	25.3	11.3	-1.6	86	65	44	8.2	37.1	4.1	4.2

Figure 2 illustrates the annual evolution of the mean value for the reference evapotranspiration in the study area and the water needs of the crop. The reference evapotranspiration shows a very similar evolution to that of the ambient temperature (data not shown), with maximum values higher than 6.0 mm in June and July. On the other hand, the water needs clearly show the effect of the winter dormancy of the pomegranate, according to the results found by Intrigliolo *et al*. (2011b).
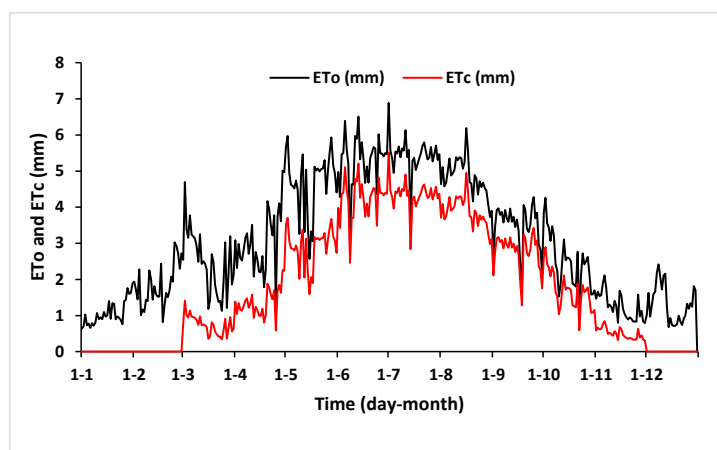
Figure 2. Reference evapotranspiration and pomegranate evapotranspiration trends

The arable areas of the municipality of Albatera present mean values of EC of the saturation extract between 0 and 50 cm that range from 4.0 to 6.0 dS m^{-1} (De Paz *et al*. 2011). The irrigation water comes from the Tajo-Segura transfer, with an EC that oscillates around 1.0 dS m^{-1}, which makes it very suitable for the irrigation of fruit trees (Intrigliolo *et al*., 2013). In some cases throughout the year, it is necessary to resort to water from desalination plants in the area. Figure 3 shows the endowments and the monthly needs for irrigation water. The endowment is 380 m^3 ha-1 for March and November, 510 m^3 ha^{-1} for April and October, 630 m^3 ha^{-1} for May, June and September and 760 m^3 ha^{-1} for July and August, which represents approximately an annual consumption of 5,200 m^3 ha^{-1}, that is, 75% of the cultivation needs (6,870 m^3 ha^{-1}). Furthermore, the distribution of the irrigation in the plot differs from the irrigation needs, being higher than the needs in March, April and November and lower in the rest of spring, summer and autumn. To explain this irrigation management, it must be considered that an early irrigation can protect the tree from frost damage, although the risk is low, and can also favor the beginning of the vegetative cycle. This is a common practice in the area, as it accelerates the entry into production. Irrigation is likewise increased at the end of the cycle, probably to ensure production and maintain crop quality.
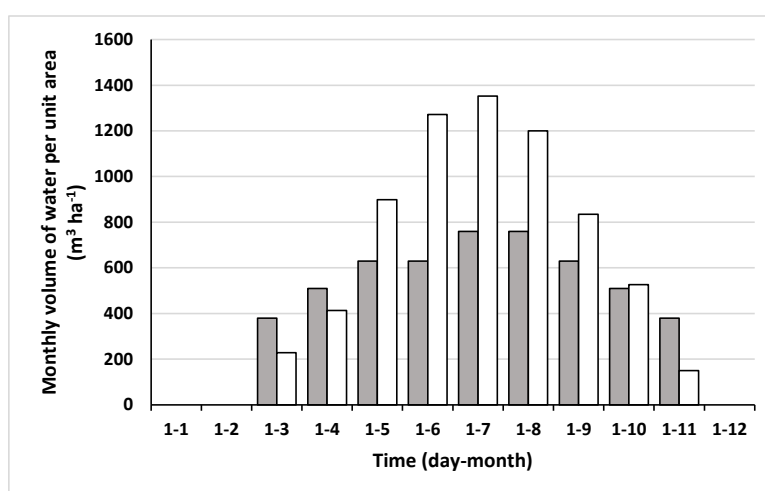
Figure 3. Year 2020 trends for monthly endowments (gray) and irrigation water needs (white) (m^3 ha^{-1})

3.2. Vegetation indices values

The mean value of the NDVI is low when compared to those found in other studies with the same crop (Niu *et al*., 2020) (Table 2), probably due to the moderate salinity of the plot soil and an insufficient water endowment. Like the NDVI, the NDRE is sensitive to the biomass and the structure of the aerial part of the crop, and it is correlated with the foliar nitrogen level (García, 2019). The mean value found is lower than the NDVI value, in a similar manner to other studies with comparable crops (Tsouros *et al*., 2019). The SAVI value slightly exceeds the NDVI value, since it reduces the effect of the fraction of soil not covered by the crop. Meanwhile, the mean value for RECl is high, indicating an adequate level of nitrogen in the crop. Lastly, the practically mean value of zero for the NDMI could indicate deficient water content, as a consequence of the annual supply of irrigation being lower than the needs of the crop.

Table 2. Annual mean values for the vegetation indices in the pomegranate plot

NDVI	0.49
NDRE	0.29
SAVI	0.64
RECl	2.38
NDMI	0.07

The analysis of the NDVI values (Figure 3A) indicates that pomegranate trees initiate their growth at the beginning of spring, coinciding with irrigation water supplies higher than the needs of the crop. Index values increase approximately from March 10, remain constant throughout spring and summer, and decrease from October 17. Its average value during the vegetative interval is 0.56. The trends for the rest of the vegetation indices are very similar. The mean value during the approximately constant phase of evolution is 0.33 for the NDRE, 0.71 for the SAVI, 2.98 for the RECI and 0.13 for the NDMI.
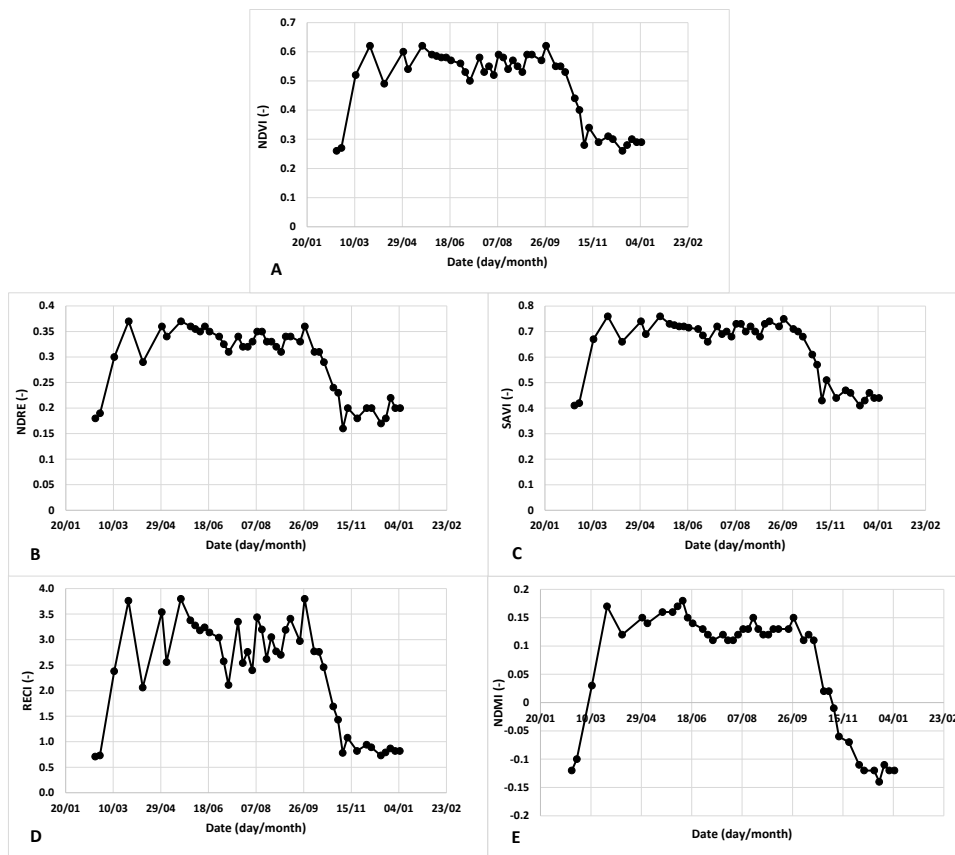
Figure 3. Time trends of the vegetation indices values (A: NDVI; B: NDRE; C: SAVI; D: RECI; E: NDMI) during the 2020 crop cycle in a pomegranate plot with localized irrigation system

3.3. NDVI estimation using low-cost applications.

QGIS program is used to obtain the maximum, minimum and average values of the vegetation indices. In general, a highly significant linear correlation (P-values <0.001) has been found between the values provided by the commercial platform and the mean values obtained from QGIS. Figure 4 shows the linear correlation between both types of values for the vegetation indices NDVI and SAVI.
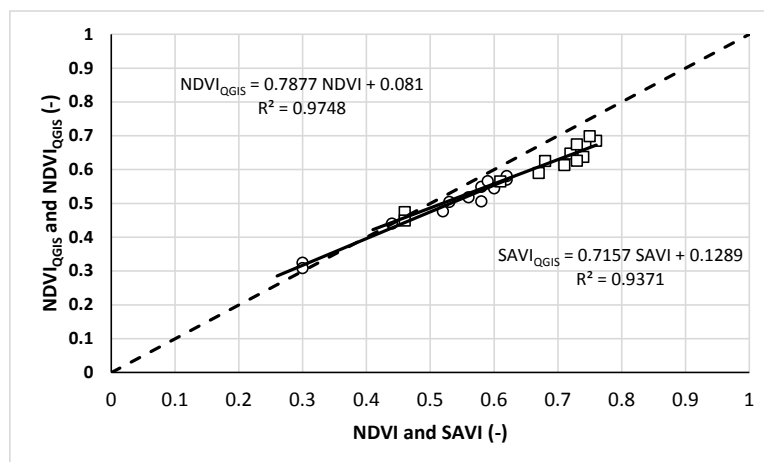
Figure 4. Correlation between values of the vegetation indices NDVI (circles) and SAVI (squares) provided by a commercial platform and those determined using QGIS as the mean value of the maximums and minimums of the plot.

3.4. Applications in irrigation scheduling

The values of the vegetation indices show a significant linear correlation with those corresponding to the irrigation endowment. However, they barely show a correlation with the irrigation needs of the crop. Table 3 shows the coefficient of determination between the values of the vegetation indices provided by a commercial platform and the monthly water supply and irrigation needs. The values of these coefficients of determination tend to increase when the values of the indices obtained through the QGIS application are used. Thus, for example, the coefficient of determination between the NDVI values obtained by QGIS and the water supply was 0.79, and 0.61 when working with irrigation needs (compared to 0.76 and 0.54 obtained with the values provided by the trading platform; Table 3).

Table 3. Coefficients of determination of the values of the vegetation indices compared to the irrigation endowment and the irrigation needs of the crop

	Dotación de riego	Necesidades de riego
NDVI	0.76	0.54
NDRE	0.75	0.54
SAVI	0.73	0.49
RECI	0.70	0.54
NDMI	0.57	0.52

4. Conclusions

In this study, remote sensing techniques are used for the analysis of irrigation scheduling in a pomegranate plot located in Vega Baja del Segura, in the south of the Valencian Community, Spain. The results indicate a significant linear correlation between the values of the vegetation indices and those of the irrigation water distribution throughout the annual crop cycle. Nevertheless, these indicators do not correlate with the water needs of the crop. The significant correlation tends to improve when index values are calculated using QGIS, which is a free software.

The determination of the trend of the values of the vegetation indices, together with edaphoclimatic and irrigation information determined directly in the field can help with the crop modeling and the simulation of its tendency with the aim of predicting its behavior when changing the growing conditions. It is necessary to continue carrying out this type of determinations in order to contribute to the optimization of the irrigation of the pomegranate, thus, improving the sustainability of the crop and the resilience of the producers against climate change.

Acknowledgements

References

Boiarskii, B., H. Hasegawa, 2019. Comparison of NDVI and NDRE indices to detect differences in vegetation and chlorophyll content. Journal of Mechanics of Continua and Mathematical Sciences, (4), 20.

Coble, K.H., A.K. Mishra, S. Ferrell, T. Griffin, 2018. Big data in agriculture: A challenge for the future. Applied Economic Perspectives and Policy, 40 (1), 79-96. http://dx.doi/10.1093/aepp/ppx056.

De Paz, J.M., F. Visconti, J.L. Rubio, 2011. Spatial evaluation of soil salinity using the WET sensor in the irrigated area of the Segura river lowland. Journal of Plant Nutrition and Soil Science, 174, 103-112. http://dx.doi.org/10.1002/jpln.200900221.

García, J. 2019. A Review on the Use of Unmanned Aerial Vehicles and Imaging Sensors for Monitoring and Assessing Plant Stresses. Drones, 3, 40. http://dx.doi.org/10.3390/drones3020040.

Grieve, C.M., S.R. Grattan, E.V. Maas, 2012. Plant salt tolerance. In ASCE Manual and Reports on Engineering Practice.

Howell, T.A., S.R. Evett. 2004. The Penman-Monteith method. Section 3 in Evapotranspiration: Determination of Consumptive Use in Water Rights Proceedings. Continuing Legal Education in Colorado, Inc. Denver, CO.

Huete, A. A soil-adjusted vegetation index (SAVI). Remote Sens. Environ. 1988, 25, 295-309.

Intrigliolo D.S., E. Nicolas, L. Bonet, P. Ferrer, J.J. Alarcón, J. Bartual, 2011a. Water relations of field grown Pomegranate trees (*Punica granatum*) under different drip irrigation regimes. Agric Water Manag 98:1462–1468

Intrigliolo, D.S., H. Puerto, L. Bonet, J.J. Alarcón, E. Nicolas, J. Bartual. 2011b. Usefulness of Trunk Diameter Variations as Continuous Water Stress Indicators of Pomegranate (*Punica Granatum*) Trees. Agricultural Water Management, 98, http://dx.doi.org/10.1016/j.agwat.2011.05.001.

Intrigliolo, D.S., L. Bonet, P.A. Nortes, H. Puerto, E. Nicolas, J. Bartual. 2013. Pomegranate Trees Performance under Sustained and Regulated Deficit Irrigation. Irrigation Science, 31. http://dx.doi.org/10.1007/s00271-012-0372-y.

Niu H., D. Wang, Y. Chen, 2020. Estimating actual crop evapotranspiration using Deep Stochastic Configuration Networks model and UAV-based crop coefficients in a pomegranate orchard Proc. SPIE 11414, In *Autonomous Air and Ground Sensing Systems for Agricultural Optimization and Phenotyping V*, 114140C. http://dx.doi.org/10.1117/12.2558221.

Rodríguez, P., C.D. Mellisho, W. Conejero, Z.N. Cruz, M.F. Ortuño, A. Galindo, A. Torrecillas, 2012. Plant water relations of leaves of pomegranate trees under different irrigation conditions. Environmental and Experimental Botany, 77, 19-24. http://dx.doi.org/10.1016/j.envexpbot.2011.08.018.

Rouse, J.W., R.H. Haas, J.A. Schell, D.W. Deering, J.C. Harlan, 1974. Monitoring the vernal advancement and retrogradation (green wave effect) of natural vegetation. NASA/GSFC Type III Final eport, 371.

Ruíz, A., 2011. Comportamiento y análisis de Descriptores de texturas en imágenes Modis (Trabajo final de máster). Universidad Complutense de Madrid, Madrid.

Tsouros, D.C., B. Stamatia, P.G. Sarigiannidis, 2019. A Review on UAV-Based Applications for Precision Agriculture. Information. 10 (11), 349. https://dx.doi.org/10.3390/info10110349.

Van Woensel, L., C. Kurrer, J. Tarlton, K. Pope, C. Daheim, E. Bol, S. den Hartog-de Wilde, 2016. Precision agriculture and the future of farming in Europe. Scientific Foresight Unit. European Parliamentary Research Service. December.

Single Plant Fertilization using a Robotic Platform in an Organic Cropping Environment

Constantino Valero [1,*] **, Anne Krus** [1] **, Christyan Cruz Ulloa** [2] **, Antonio Barrientos** [2] **, Jaime del Cerro** [2] **, Juan José Ramírez** [1]

[1]   GI LPF_Tagralia, Departamento de Ingeniería Agroforestal, ETSI Agronómica, Alimentaria y de Biosistemas, Universidad Politécnica de Madrid, 28040 Madrid, Spain

[2]   Centre for Automation and Robotics (UPM-CSIC), José Gutiérrez Abascal, 2, Madrid 28006, Spain

*Correspondence: constantino.valero@upm.es ; ORCID: 0000-0003-4473-3209

Abstract

The increasing demand of organic vegetables has driven conventional farmers to change their businesses in order to develop organic methods for cultivation and the use of alternative techniques to avoid damaging the soil and the quality of the products. In some cases, to enhance biodiversity and soil fertility, crops are established in a mixed pattern called 'strip cropping' where single or dual lines of a given species are alternated with a second compatible species, with the aim to enhance resilience, system sustainability, local nutrient recycling, and soil carbon storage. However, this husbandry of crops grown and mixed in a strip design pose new challenges regarding mechanisation, which in many cases can only be overcome by increasing human tasks. To counteract the additional labour of a multi-crop system, one of the main objectives of the 'Sureveg' CORE Organic Cofund ERA-Net European project is to evaluate the benefits of growing in alternate rows for the production of organic vegetables and includes the use of robots as a tool to facilitate the automation of the process, allowing the individual treatment of organic fertilization at plant level. Within the project framework a modular proof-of-concept version has been produced, combining several sensing technologies (3x LiDAR, plus a multispectral RGB-NIR camera) with actuation in the form of a robotic arm operating upside down. The present work describes a method to develop fertilization tasks with recycled organic waste in strip-cropping farms, based on detection of plant species (cabbage) using and liquid fertilizer application with a robot. For that, it is necessary to identify the crop (variable in the rows) and place the robot with respect to the plants to apply the product. Test fields were located at ETSIAAB - UPM (40°26'33.1"N, 3°43'41.9"W) where stripped crops were established and monitored along the growing season. In order to detect autonomously each single plant, point clouds of the three LiDAR units were combined, soil was removed applying a weighted threshold, and plants were identified using clustering and convolutional neural network methodologies. To trigger the actuation system, the decision on which plant had to be sprayed with the liquid fertilizer was taken according to two factors: 1) the estimated volume of every single plant, and 2) the multispectral indexes calculated using the RGB-NIR camera. The prototype is fully functional, and further test are needed to quantify its performance.

Keywords: organic farming, robot, actuation system, fertilization, LiDAR, multispectral camera.

1. Introduction

The increase in food consumption worldwide needs to be tackled by producers and technicians (Ritson 2020; Pachapur et al., 2020). However, due to conventional agricultural practices, the environmental effect associated to the use of fertilisers and herbicides has grown (Srivasta et al., 2020). Fortunately, precision agriculture allows to produce higher quality products, through sustainable development (Loures et al., 2020), the use of technological tools, sensory systems (Poblete-Echeverría et al., 2020; Singh et al., 2020), and modern actuation systems (Cubero et al., 2020; Moysiadis et al., 2020; Fue et al., 2020; Hussain et al., 2020). The Sureveg project (CORE Organic Cofund, 2019) focuses on the application of diversified strip-cropping systems to intensive organic vegetable cultivation, the reuse of biodegradable waste, as well as development of 31 automated machinery for the management of strip-cropping systems. For this purpose, a proof of concept was proposed in the form of a manually operated robotic prototype, containing 3 lidar sensors, a multi-spectral camera, and a 5 degrees-of-freedom (DOF) manipulator. A nozzle connected to a tank of organic fertiliser is used as the end-effector of the actuator.

2. Materials and Methods

The mobile platform implemented to the proof of concept of this work consists of different subsystems: the mobile structure with wheels, the robotic arm, the sensory system, the actuation system for the application of fertiliser, and the storage tank of liquid fertiliser.

2.1. Mobile Structure

The mobile structure that supports the robot and sensory systems - actuation, was built with aluminium bars (Bosch Rexroth 45 x 45) and four wheels, according to previously established requirements in the framework of an organic stripped crop. The frame supports the different elements and does not rely on an autonomous traction system. Figure 1 shows the implemented structure. In Figure 1, the robot is replaced by a dummy volume shown hanging down from the middle of the structure. This location and orientation allow it to reach the ground to acquire data and apply treatments.

Figure 1. Structure implemented with aluminium profiles (45x45) and wheels.

2.2. Robotic Arm

The robotic arm acquired for the prototype (Robolink Igus CPR RL-DC-5 STEP RL-D-RBT-5532S-BF) has the following characteristics: a load capacity of 1.5 kg, 5 degrees of freedom, IP54 protection, and able to follow point to point trajectories. The robot has a reach of 790 millimetres with a precision of 1 mm. Additionally, the robot weighs around 20 kg, including the electromechanical components and excluding the control and power elements. Its load capacity is 2.5 kg.

2.3. Sensory System

The sensory system mainly relies on two types of sensors: a multi-spectral camera and 3 lidars. Both provide information on vegetational health status and development. The multispectral camera is used to obtain multispectral images and compute vegetation indices of plants. This camera was installed on the centre of the frame of the cart, to take pictures of the target plants from the desired perspective. Additionally, 3 lidars provide 3D models of the soil and plants from multiple perspectives. Besides information on crop architecture, the combined 3D world model facilitates the motion planning of the robotic arm and the application of treatments in the adequate locations. Figure 2 specifies the sensor locations on the mobile structure.

Figure 2. Frontal view (right) and rear of the platform (left), the yellow circles show the 3 lidar sensors and the red circle indicates the multispectral camera.

2.4. Sensing Algorithms

The sensing algorithms can be divided into two sub-categories: multi-spectral sensing using the multispectral camera (aimed at searching for differences in plant health) and 3D sensing using the LiDAR (focused on detecting growth volume differences). At the beginning of the crop season, the newly transplanted crops provide very little altitude difference when compared to the coarseness of the soil, which is why at the beginning of the season, only the use of the multi-spectral algorithms is recommended.

2.5. Fertilization System

The implemented actuation system consists of a tank containing a liquid treatment (Figure 3, highlighted in red), a hose from the tank to the robot tooltip, and a nozzle to spray the liquid (Figure 3, Indicated in yellow). In this way, the robotic arm can apply the liquid treatment in the desired position and orientation, as shown in Figure 4. The drive of the nozzle is carried out by means of the electronic control of a hydraulic motor.
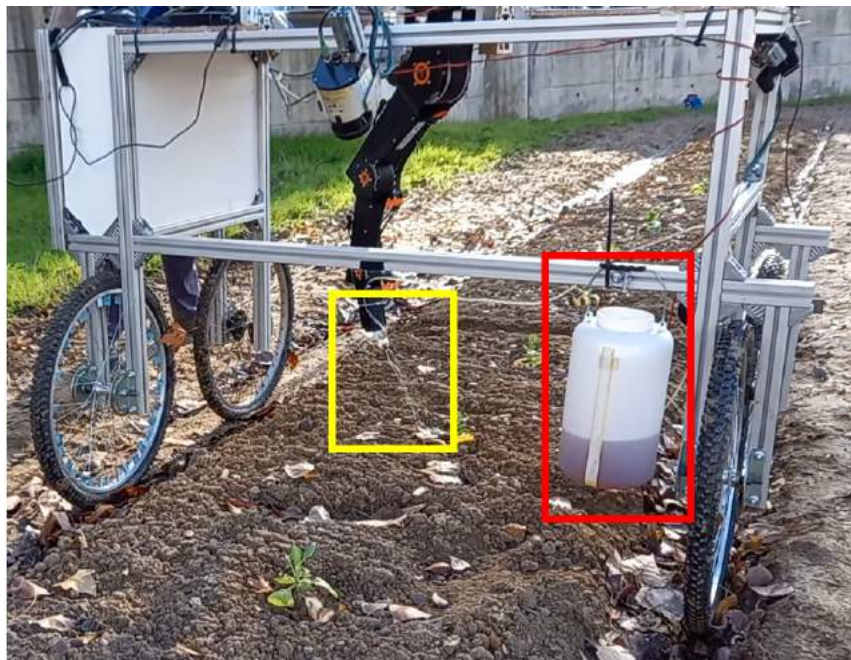
Figure 3. Robotic fertilization prototype in the cultivation row. Red: the tank with liquid treatment, yellow: the nozzle.

Test fields were located at ETSIAAB - UPM (40°26'33.1"N, 3°43'41.9"W) where stripped crops of cabbages and leaks were established and monitored along the growing season.

3. Results and Discussion

3.1. Multi-Spectral Sensing

The Parrot Sequoia camera produces each image in fivefold: green, red, red-edge, near-infrared, and (high resolution) RGB. The time-lapse setting in combination with a forward speed generates a series of partly overlapping images that were be stitched together using Hugin Panorama, as it is open-source and allows for manual manipulation of automatically extracted features such that the exact same mosaicking operations can subsequently be applied to the other spectral bands.

Each of the spectral images is obtained through a different lens, as can be seen on the bottom of the sensor shown on the left in. As a result, the images themselves show a slight translation with respect to one another, something that was assessed and corrected for automatically using e.g. `imgregtform` in Matlab.

With the corrected mosaicked images, a series of vegetation indexes were calculated for the entire field. The most optimal vegetation index can depend on the crop type and variant, and can be optimised regarding the specific characteristics of the crops and soil spectra present in a certain field. In this work, results using NDVI are presented.

The vegetation index was used to separate plant matter from soil, as well as assess the health of the plant. In Figure 4, the distribution of the vegetation index values in the entire row is shown in the form of a histogram, clearly revealing the three types of areas present in the image. In the distribution of NDVI values three gaussian distributions can be recognised: a wide one around low (negative) values for soil; a narrow one around 0 describing the stark shadows, i.,e. areas where all spectral reflectance values were very small; and a wide one of positive NDVI values describing the plant

matter. The relative heights of these three peaks depends on the number of plants with regard to the amount of visible soil, as well as the lighting conditions.

To facilitate the identification of the optimal cut-off value to define plant matter, the vegetation index values were passed through a filter, further separating the peaks in the histogram, revealing a minimum between the plant matter pixels and the remaining pixels that was not present in the original distribution, as shown in Figure 5. Using Otsu's method, the cut-off value that minimizes the variance in each of the pixel populations (plant matter vs. non plant matter) was identified.
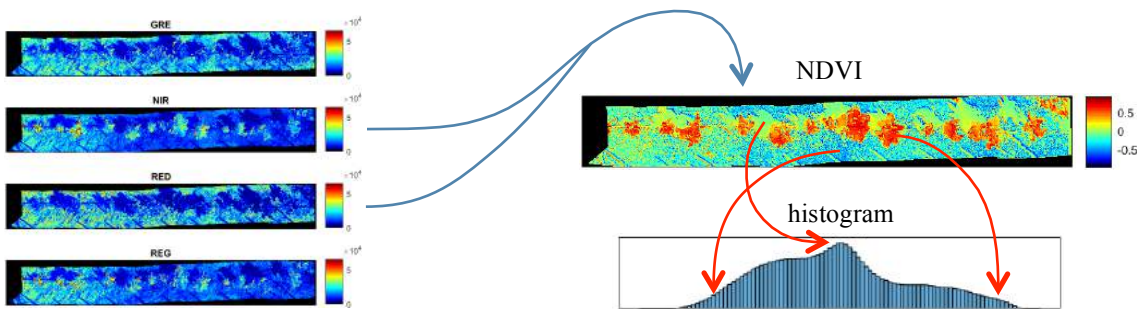
Figure 4 Process of calculation of the vegetation index from spectral data, and its correspondence with histogram information.
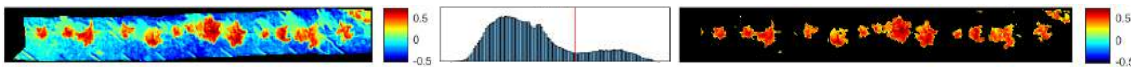
Figure 5. The same NDVI map from Figure 4 after passing through a Gaussian filter, yielding the histogram shown in the middle. On the right the final result is included.

After applying the Otsu procedure, the range of the filtered image no longer corresponds to the [-1,1] range of the original NDVI index. The altered values reveal a minimum between the plant matter and the non-plant matter, as obtained through Otsu's method, indicated in the histogram with a red vertical line in Figure 5. For each resulting cluster in the new image, a range of characteristics can be considered: e.g. vegetation index mean value, vegetation index distribution, cluster area, or perimeter. In this proof of concept, the mean value within a cluster was used. This value is then compared to the mean NDVI values of the other clusters within the same row to identify fertilisation necessities on a single crop scale.

3.2. 3D Sensing

The 3D data was gathered using multiple SICK A.G. lidars. Each lidar uses an infrared rotating laser pulse, where the time of flight between emission and reflection in each rotational increment is used to calculate the distance of the sensor to any object. The reflectance intensity of the beam was found to not provide any additional information in this setting and was therefore disregarded. From the cylindrical coordinates, each distance was converted to a Cartesian coordinate system, where the inclination of the sensor and the odometry data of the cart's wheels were combined to provide the dimension perpendicular to the plane of rotation of the laser. This results in a 3D point cloud per lidar, that all describe a single crop row. They point clouds provide complementary information inherent to their varying angles and installation heights, while the majority of the surfaces is picked up by all lidars. This overlap was used to merge the point clouds into a high-resolution single point cloud, describing all surfaces within a crop row, i.e. both plant matter and non-plant matter such as soil.

As three-dimensional information is the only information present in this type of point cloud, i.e. no colour or reflectance information is retained, the points needed to be identified as crop or non-crop purely based on their location and height. Especially for smaller plants, the coarseness of the terrain yields height data that is comparable to the height data of lower hanging leaves. This means an identification based on only height data was not possible.

To overcome this, each point was assigned a value J based on the heights of all points in within a 150 mm radius, where the points that are closest are taken into account more heavily than those at the border of this sphere, i.e., J is a weighted sum of height squared over distance. The number of points that are present in this vicinity also contributes to this value, as higher surfaces such as plant leaves are closer to the sensor and are therefore sampled at a higher frequency than any points further away.

The resulting values J for all points within a point cloud can be sorted in ascending order. The texture predictability and constant distance of the soil assures that the values of J of the soil points yield a nice linear distribution. This linearity wa used to identify the value of J for a given point cloud where the sorted distribution deviates from this expectation. The points with a value of J higher than this threshold were considered plant points, and lower values were considered to describe non-plant matter. This algorithm allows for low plant leaves and protruding surfaces like rocks to be identified correctly, despite the rock points possibly having higher altitude values than those of the low leaf, as shown in Figure 6.
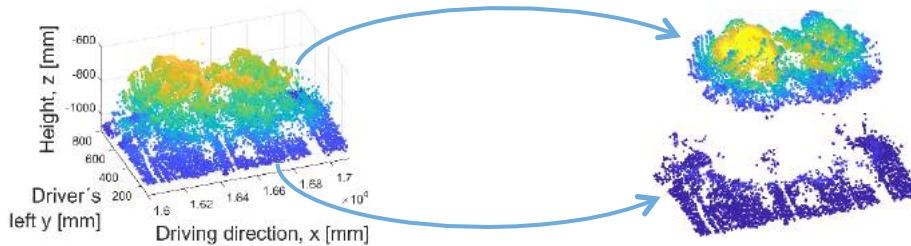
Figure 6. The point cloud with colour denoting height data (left) alongside the same cloud coloured by the values of J.

The resulting 3D point cloud containing only plant points can subsequently be cleaned, where any singular noise points were removed, yielding only clusters of a certain size and up. For each of these clusters, a range of characteristics were calculated, e.g. covered soil surface area, cluster volume, cluster surface to volume ratio, or distribution of J values. These were compared to the other clusters within the same row to identify anomalies.

3.3. Combination
The multi-spectral sensing algorithm is able to detect any individual crops with either delayed size in terms of covered soil or altered vegetation index values. The 3D sensing algorithm identifies delayed development in terms of volume or height as well. This means a combination of both sensors was preferred to determine the fertilisation necessity of individual plants.

Besides the prescription map, the data of the 3D algorithm was used as a reference world model for the actuation algorithms, which serves both to locate the cart in the field as well as to plan the movements of the robotic arm as discussed below.

Drawbacks and potential pitfalls of these algorithms are the detectability of newly transplanted crops, as they might be missed by both sensors and therefore wouldn't get any treatment. As the field is prepared before transplantation and all individuals will need fertiliser this is not assumed to pose a big problem. The distance between plants is another aspect that needs to be considered, as plants that reach overlap or physically touch each other cannot be separated by either of the proposed sensing algorithms. This should be taken into account when assessing the results once the plants reach a certain growth stage where this starts to occur. Finally, the algorithms now assume all plant matter to belong to desired crops, i.e. weeds could mistakenly be identified as individuals with a delayed development when compared to the plants of the desired crop in that row. Crop type identification can be added to these algorithms in the future, but was not yet considered in this proof of concept.

3.4. Actuation

3.4.1.Geometrical Characterisation
The clusters extracted in the previous section served as a reference to establish a path for the movements of the robotic arm to apply the liquid treatment. The extracted parameters are shown in Figure 7: in the form of centres and defined edges. Colours indicate each identified group. For the processing of the clusters, the unsupervised learning process K-means has been used, where the clusters are grouped with labels "cluster 1-10".

Figure 7. K-means classification and geometrical parameters extraction from a row crop.

3.4.2. *Localisation*

One of the essential aspects during the application of fertiliser with the robotic arm was to locate the robotic platform within the crop at all times without using an external positioning device (such a GPS). The developed method takes the previously developed point cloud, captured with 3 lidars, creating a G-PC (Global Point Cloud) as well as a second real-time cloud L-PC (Local Point Cloud) of only 1 lidar, concerning the sections of G-PC that the platform reads while moving forward (being initially small).

In Figure 8 the correspondence of L-PC points with G-PC points are indicated with red lines for two examples of L-PC's of different sizes. This establishes the position of the local cloud within the known environment, and thus the position of the robotic platform within the crop row.
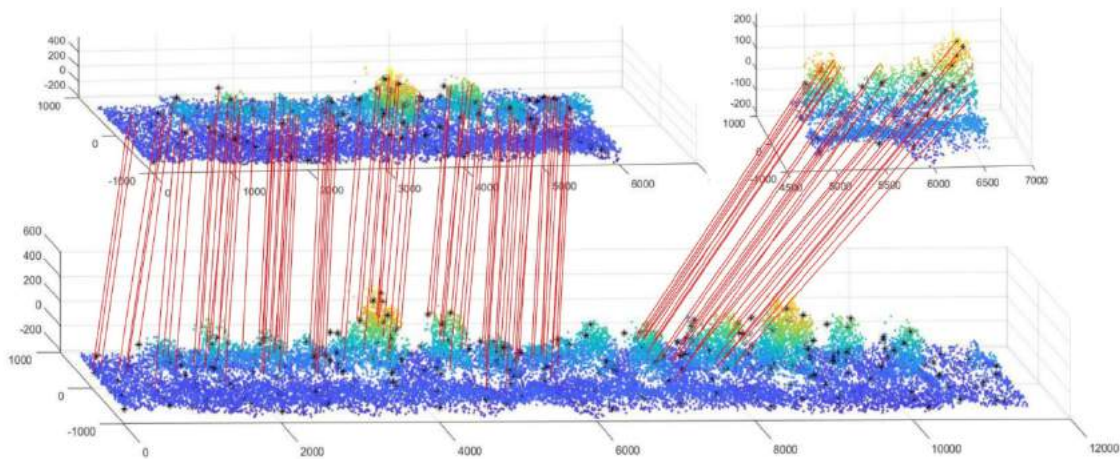
Figure 8. Matching key points from the L-PC (upper—two captured partial sections) to the G-PC (lower).

Figure 9 shows the perception system (G-PC and robot visualisation), where the point cloud and the estimated position of the platform are shown for each instance. As the robotic platform advances from point 1 through 7, the L-PC accumulates earlier values, which continuously improves the location estimation.
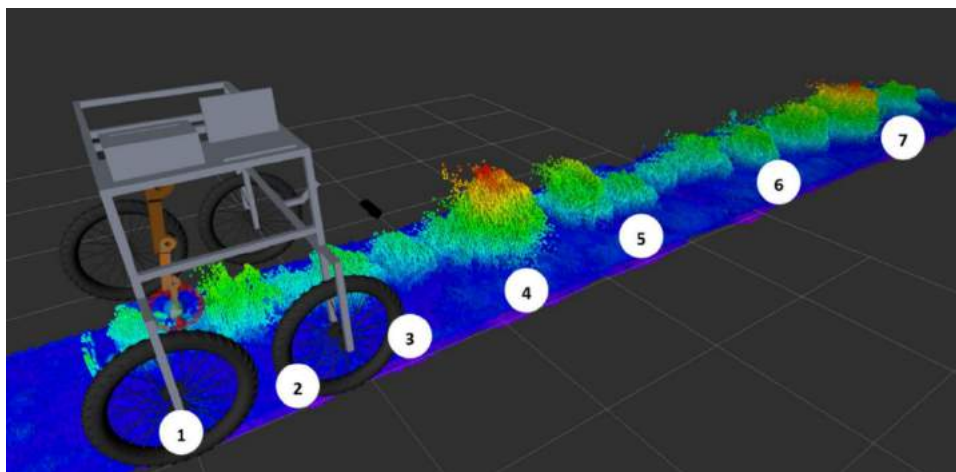
Figure 9. Mobile robotics platform position and data visualisation in rviz.

In Figure 10, a box plot shows the declining localisation error found at each of the positions indicated in Figure 9. Initially, the average error was around 12 mm; which reduces to approximately 0.1% at the end of a row.

This initial positioning error did not affect fertilisation, because a margin of 5 cm was added to the radius defined in the geometrical parameters extraction to encompass the plant and define the passage zone of the arm's trajectory, thus avoiding the fertiliser being applied directly on the plant and damaging it. As the platform progresses, new points are added to the L-PC, allowing for more key points and improved localisation, resulting in errors with an average of 5 mm.
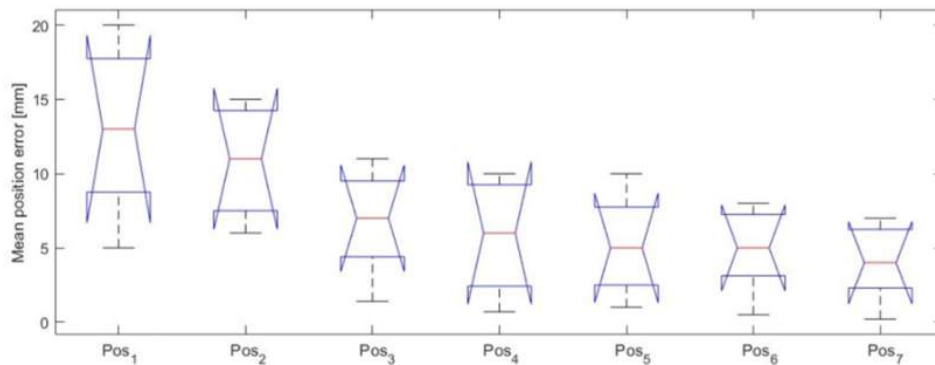
Figure 10. Box diagram of mean localisation errors at each of the positions indicated in Figure 9.

4. Conclusions

A proof-of-concept prototype has been built, based on a mobile platform, a sensing system composed of lidar sensors, a multispectral camera and odometry, and an actuation system based on a robotic arm and a pumping system for liquid fertiliser. The system gathers information from the plants in the row about crop volume (lidar), crop health (multispectral images) and plant position (point cloud for navigation). Then a decision about fertilisation need (yes/no) is made and the actuation system applies liquid fertiliser to the soil around the plant avoiding contacting the crop. The prototype can be enhanced with more sensors, and it can be also adapted to perform other types of field work.

References

Cofund, CORE Organic. Sureveg Project. 2019 Available online: https://projects.au.dk/coreorganiccofund/core-organic-cofund-projects/sureveg/ (accessed on 2 June 2021).

Cubero, S.; Marco-Noales, E.; Aleixos, N.; Barbé, S.; Blasco, J. RobHortic: A Field Robot to Detect Pests and Diseases in Horticultural Crops by Proximal Sensing. Agriculture 2020, 10, 276.

Fue, K.G.; Porter,W.M.; Barnes, E.M.; Rains, G.C. An Extensive Review of Mobile Agricultural Robotics for Field Operations: Focus on Cotton Harvesting. AgriEngineering 2020, 2, 150–174.

Hussain,M.; Naqvi, S.H.A.; Khan, S.H.; Farhan,M. An Intelligent Autonomous Robotic Systemfor Precision Farming. In Proceedings of the 2020 3rd International Conference on Intelligent Autonomous Systems (ICoIAS), Singapore, 26–29 February 2020; pp. 133–139.

Loures, L.; Chamizo, A.; Ferreira, P.; Loures, A.; Castanho, R.; Panagopoulos, T. Assessing the Effectiveness of Precision Agriculture Management Systems inMediterranean Small Farms. Sustainability 2020, 12, 3765.

Moysiadis, V.; Tsolakis, N.; Katikaridis, D.; Sørensen, C.G.; Pearson, S.; Bochtis, D. Mobile Robotics in Agricultural Operations: A Narrative Review on Planning Aspects. Appl. Sci. 2020, 10, 3453.

Pachapur, P.K.; Pachapur, V.L.; Brar, S.K.; Galvez, R.; Le Bihan, Y.; Surampalli, R.Y. Food Security and Sustainability. In Sustainability; John Wiley & Sons, Ltd.: Hoboken, NJ, USA, 2020; Chapter 17, pp. 357–374.

Poblete-Echeverría, C.; Fuentes, S. Editorial: Special Issue "Emerging Sensor Technology in Agriculture". Sensors 2020, 20, 3827.

Ritson, C. Population Growth and Global Food Supplies. In Food Education and Food Technology in School Curricula: International Perspectives; Springer International Publishing: Cham, Switzerland, 2020; pp. 261–271.

Singh, R.K.; Aernouts, M.; De Meyer, M.; Weyn, M.; Berkvens, R. Leveraging LoRaWAN Technology for Precision Agriculture in Greenhouses. Sensors 2020, 20, 1827.

Srivasta, R.K. Influence of Sustainable Agricultural Practices on Healthy Food Cultivation. In Environmental Biotechnology Vol. 2; Springer International Publishing: Cham, Switzerland, 2020; pp. 95–124.

Towards a Phenotype Classification of Agricultural Robots

Giuseppe Anacoreta [a], Marco Medici [a,*], Maurizio Canavari [a]

[a] Department of Agricultural and Food Sciences, University of Bologna, Bologna, Italy

* Corresponding author. Email: m.medici@unibo.it

Abstract

The use of robot systems in agriculture has heavily increased in recent years. Together with the Internet of Things and Big Data, these technologies can represent an opportunity to make food production more sustainable. Being able to carry out hard physical tasks hitherto covered by operators and potentially ensuring night work cycles, these technologies accompany many advantages related to reducing work-related accidents and the autonomous conduction of operations. Despite these opportunities, their large-scale diffusion is limited today by a lack of clarity and exhaustiveness in the regulatory framework that is intrinsically tied with ethical and legal issues concerning the management of robots. Existing legislation places obligations related to machine registration and human supervision in operations, but several issues concerning the use of such technologies still have to be addressed, such as legal responsibility, privacy issues, and data management.

To date, a clear and agreed classification of the various types of agricultural robots is missing. The main goal of this study is to classify the many types of robots available (i.e., phenotyping) to obtain an exhaustive and efficient information framework able to facilitate the production of ad-hoc legislative supports and promote primary market segmentation practices. We used an observational survey method that involved a web search of robots and systems, which were described with qualitative variables based on specific criteria describing their usage in farms. Collected data was hence used to picture homogeneous groups of robots. The classification was performed with a double step cluster analysis based on the nominal descriptive variables and a factor analysis used to reduce classification redundancy. Five clusters of robots have been identified, opening up the possibility to set specific regulatory policies and market strategies based on recurring characteristics within the identified clusters.

Keywords: agrobots, unmanned vehicles, robotics, agricultural machinery, classification, clustering.

1. Introduction

The use of robots in agriculture heavily increased in recent years and represents an opportunity to make food production more sustainable (Reis et al., 2013; Benke & Tomkins, 2017; Rose et al., 2021; NFU, 2019). Among the various functions, agricultural robots can carry out operations like weeding, fertilisation, harvest, and other agricultural inputs more effectively and efficiently, allowing economic and environmental benefits to be achieved (Medici et al. 2019). The growing trend also involved the use of automatic technologies for livestock, with robotic milking technologies and robots for feeding and manure management became key success factors in many farms (Pezzuolo et al. 2017; Salfer et al. 2017; Sharipov et al. 2021).

Agricultural robots, automatic tractors, drones, robotic arms can automate a large piece of agricultural production, especially those slow and repetitive tasks for farmers, allowing them to focus more on other core activities (Martinelli 2002). Being able to carry out hard physical tasks too hitherto covered by agricultural operators and potentially ensuring night work cycles, these technologies accompany many advantages, such as reducing work-related accidents and the autonomous conduction of potentially dangerous operations for human health like pesticide application.

However, it should be noted that there is no formal definition for the term "agricultural robot" or "agrobot" nor any formal recognition of the features of robots performing agricultural operations. Recently, it was proposed to define the field crop robot as "*a mobile, autonomous, decision making, mechatronic device that accomplishes crop production tasks [...] under human supervision, but without direct human labour*" (Lowenberg-DeBoer et al., 2019, p.279). Other authors have defined agricultural robots as programmable perceptual machines that perform various agricultural tasks, such as cultivation, transplanting, spraying and selective harvesting (Bechar and Vigneault 2016). These definitions indicate that agricultural robots are a collection of heterogeneous machines composed of various technologies designed for a variety of uses in the broad domains of the agri-food sector.

To date, only a limited number of these machines are available on the market, but a wider distribution is expected in the coming years. To give an example, in 2019, over 60 projects on agrobot development were presented at the International Forum of Agricultural Robotics (FIRA, 2018).

Despite their features and opportunities, the large-scale diffusion of robots is also limited today by a lack of clarity and exhaustiveness in the regulatory framework that is intrinsically tied with ethical and legal issues concerning the use and management of many types of robots (Basu et al. 2020; Lattanzi 2018), with the development of autonomous

equipment depending on the legal and regulatory framework (Lowenberg-DeBoer et al. 2021). Existing legislation places obligations related to machine registration and human supervision in operations, but several issues concerning the use of novel technologies still have to be comprehensively addressed, both directly, in terms of civil responsibility, privacy issues, and data management, and indirectly, claiming regulations on water, soil, nitrates, plant protection products, animal welfare, to name but a few (Fabiano 2019; Thompson 2019). In this regard, it would be useful to precisely narrow the different types of technologies to provide a precise and defined framework for technology users and developers and better define the regulatory aspects within which to move. The areas of law touched by the diffusion and the use of digitisation in agriculture are several: legislation on drones, GPS, driverless driving systems, operator safety, civil liability; secondly, all agri-food purposes for which these technologies are used claim regulations on water, nitrates, plant protection products, animal welfare, soil degradation, to name but a few. Last, a special focus deserves the emerging field of data protection and exchange (Lattanzi 2018).

To date, a clear and agreed classification of the various types of agricultural robots is missing. Aimed at reducing fragmentation, the main objective of this study is to obtain a robot classification based on observable features (i.e., phenotyping) to facilitate the production of ad-hoc legislative instruments and allow market segmentation practices.

2. Materials and Methods

The survey method has involved a web search of robots and systems, which were described with qualitative variables based on specific criteria describing their usage in farms. The web search was performed by using the search tags "agricultural robots", "agrobot", "agricultural robot companies", as well as queries including the various agricultural activities, such as "weeding robot" and "harvest robot". Three inclusion criteria were considered to guarantee an acceptable level of information quality. In total, three inclusion criteria were considered to guarantee a minimum threshold level of information quality (Table 1).

Table 1. Inclusion criteria of sources.

Inclusion criteria	Rationale
The source reported exhaustive textual or numerical description.	Quantitative or qualitative information are necessary to make comparisons between technologies.
The source provided information not conditioned by site subscription.	Most of the companies avoided to spread information for non-commercial purposes.
The source reported information concerning existing and working technology at least at TRL 7.	Products not available are considered less relevant to produce insights on current state-of-the-art technology.

Following this procedure, 227 robots were assessed for eligibility. Data were input in an Excel file in terms of descriptive variables and information concerning the manufacturing company, company location, brand(s), website, and robot name. Thus, robots were classified based on 45 binary variables:

- Based on the production domain: agriculture "AGR", livestock "LIV";
- Based on the activity environment: outdoor "OUT", indoor, "IN";
- Based on the place of activity: open field "FIELD", industrial setting "IND", stable "STA";
- Based on the type of machine: single-purpose robot "ROB", drone "DRO", multi-task robot "MULTIT", technologies packages for tractors "TRACT", autonomous driving systems "DRIVLE";
- Based on the type of moving: fixed "FIXED", self-propelled "SELFP", pulled "PULLED", on-track "TRACK";
- Based on the type of activity carried out: crop monitoring "CROP_M", mapping "MAP", animal monitoring "ANIM_M", logistic operations "LOGI", irrigation "WATER", hoeing "HOE", chemical weeding "WEED_C", mechanical weeding "WEED_M", crop defence "DEF", fertilisation "FERT", harvesting "HARV", pruning "PRUN", sowing "SOW", harrowing "HARROW", animal washing "ANIM_WASH", animal feed "ANIM_FEED", milking "MILK", cutting "CUT", grafting "GRAFT", soil mixing "SOIL_MIX", tray filling "TRAY_FIL", tray washing "TRAY_WASH", DNA samples "DNA_SAM";
- Based on the type of energy supply: diesel fuel "D", petrol fuel "P", rechargeable battery "B", direct electrical supply "EL", attached to tractor "ATT", hybrid engine "H".

After removing items characterised by diffused missing values, 171 agrobots were finally identified and included in the analysis. The sample dataset containing 171 pieces of equipment described by the 45 binary variables aforementioned was analysed using the software R (R Core Team 2020).

Tetrachoric correlation was used to measure correlation between binary variables: a latent bivariate normal distribution for each pair of binary variables was assumed, and the correlation coefficient rho (i.e., the tetrachoric

correlation coefficient) was estimated. Then, the returned correlation matrix was used to perform a factor analysis, with the aim to express data variability with the least but significant number of factors. To determine the number of factors, the criterion of keeping enough factors to account for 75% of the variance was assumed. Finally, the varimax rotation algorithm was used to simplify and better interpret the results.

Then, cluster analysis was performed based on the set of extracted factors and the resulting factor scores. Final groups characteristics have been tested with ANOVA and Tukey's HSD tests.

3. Results and Discussion

The distribution of the 45 binary variables describing the 171 agrobots is shown in Table 2. In total, five clusters of robots have been identified (Figure 1) based on the scores of 7 factors accounting for the most significant robot features identified (Figure 2). These factors are described as follows:

- Factor a, accounting for the activity environment (indoor or outdoor);
- Factor b, representing the type of activity carried out, particularly processing and agronomic operations;
- Factor c, describing animal welfare and greenhouse-nursery production;
- Factor d, accounting for monitoring technologies and operations for data collection;
- Factor e, including features for fixed robots and rail movement;
- Factor f, describing cultivation systems using water for irrigation and application of agrochemicals;
- Factor g, accounting for any items showing a physical connection to the tractor.

The most significant differences across clusters were clearly observed for factors a, b, d, e, and f, for which a single cluster emerged among the others (Figure 2). Regarding factor c, only Clusters #1, #4, and #5 were considered, while for factor g all clusters were considered except for Cluster #4. Clusters are following described.

<u>Cluster #1 - Robots and drones for crop monitoring</u>. The set, consisting of 38 robots, includes unmanned aerial vehicles (UAVs) and unmanned ground vehicles (UGVs) performing crop monitoring in the open field with sensors and cameras.

<u>Cluster #2 - Self-propelled robots for agricultural operations</u>. This group is populated by 28 robots featuring self-propelled machines performing a broad range of tasks in the field and indoor, from weed control to logistic operations. Drones are absent.

<u>Cluster #3 - Indoor livestock robotics</u>. The third cluster consists of 42 robots for livestock rearing, operating indoor. They include technologies used for feeding animals and washing and sanitising environments and kennels.

<u>Cluster #4 - Fixed robots</u>. The set includes 56 items carrying out various operations, from sowing to transplanting in garden centres to milking robots serving indoor livestock.

<u>Cluster #5: Multi-purpose robots</u>. This small group include seven robots able to perform more than a single operation.
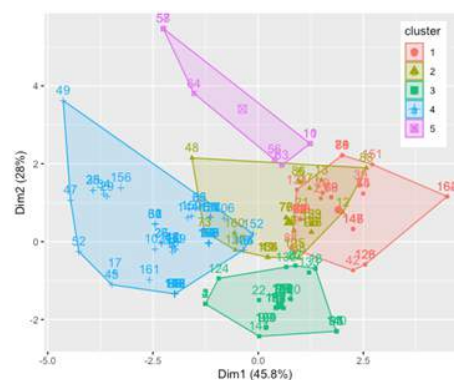
Figure 1. Cluster plot (n=5, 7 factors).

Overall, the factor and cluster analysis performed gave reasonable results, providing food for thought and opening up the possibility to set specific regulatory policies and market strategies based on recurring characteristics within the identified clusters. Cluster #1 included mainly UGVs and UAVs mostly performing crop monitoring. Although the same technology can be used for pesticide application and fertilisation, its use in this domain is restricted in several countries because aerial application of pesticides is not allowed. Another set of machines, summarised by Cluster #3, includes technologies used in livestock and animal rearing, such as robots that autonomously manage feedings and also systems for the sanitation of environments. These technologies constitute relevant support for farmers in terms of time savings and health safeguard. The large family of fixed robots needing direct electrical supply is represented by Cluster

#4. In fact, they are mostly fixed indoor products, used, for example, in technological nurseries or to automate sowing or transplanting in an indoor environment. Last, a general set of multi-purpose robots used for agricultural operations, identified by Cluster #2, includes robots operating in the open field and protected environment, able to carry out weeding
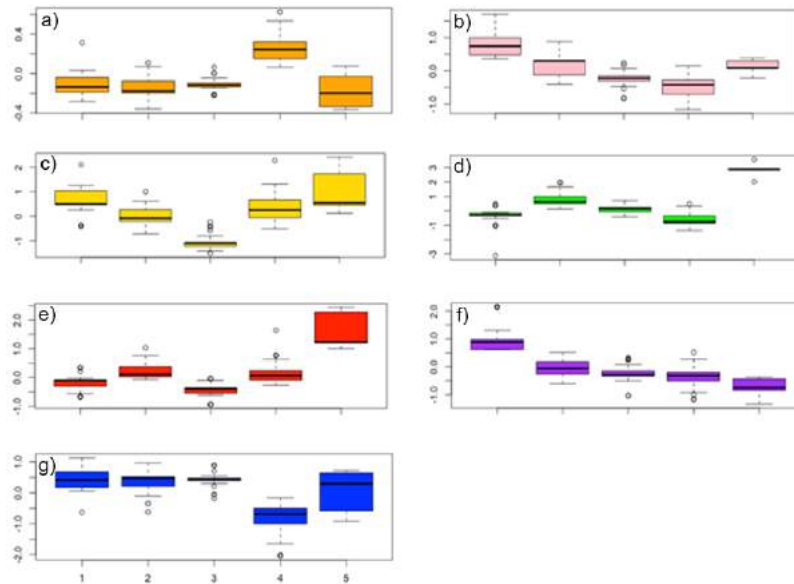
Figure 2. Tested factors across clusters.

Table 2. The 45 binary variables

Domain	Variable	Label	Distribution
Production	Agriculture	AGR	70.7%
	Livestock	LIV	29.3%
Working environment	Indoor	IN	65.4%
	Outdoor	OUT	36.3%
Place of activity	Open field	FIELD	34.5%
	Industry	IND	36.2%
	Stable	STA	29.2%
Type of machine	Single-purpose robot	ROB	76.0%
	Drone	DRO	14.6%
	Multi-purpose systems	MULTIT	8.1%
	Technological packages for tractors	TRACT	0.5%
	Autonomous driving systems	DRIVLE	0.5%
Type of moving	Fixed	FIXED	35.0%
	Self-propelled	SELFP	48.5%
	Pulled	PULLED	4.6%
	On-Track	TRACK	9.3%
Type of activity	Crop monitoring	CROP_M	18.1%
	Mapping	MAP	11.6%
	Animal monitoring	ANIM_M	0.5%
	Logistic operations	LOGI	12.8%
	Irrigation	WATER	7.0%
	Hoeing	HOE	1.7%
	Chemical weeding	WEED_C	16.3%
	Mechanical weeding	WEED_M	11.6%
	Crop defence	DEF	3.5%
	Fertilisation	FERT	0.5%
	Harvesting	HARV	4.6%
	Pruning	PRUN	0.5%
	Sowing	SOW	12.8%

	Harrowing	HARROW	1.7%
	Animal washing	ANIM_WASH	7.6%
	Animal feed	ANIM_FEED	14.0%
	Milking	MILK	6.4%
	Cutting	CUT	2.3%
	Grafting	GRAFT	1.7%
	Soil mixing	SOIL_MIX	2.9%
	Tray filling	TRAY_FIL	2.3%
	Tray washing	TRAY_WASH	0.5%
	DNA samples	DNA_SAM	0.5%
Type of energy supply	Diesel fuel	D	3.5%
	Petrol fuel	P	0.5%
	Rechargeable battery	B	45.0%
	Direct electrical supply	EL	43.2%
	Attached to tractor	ATT	4.0%
	Hybrid engine	H	3.5%

operations or support humans in moving collection boxes. Cluster #5 includes multi-purpose machines too, but in this case, robots are able to perform more than one operation.

In the context of cluster analysis, a total of 11 outliers (6.4%) representing robots that do not meet group requirements were identified. This outcome calls for a more refined methodology in terms of the search query, eligibility criteria and, mostly, filling out the missing information. Nevertheless, this issue proved to be relevant only for Clusters #3 and #4, showing 4 and 5 outliers, respectively. Other authors attempted to classify robots, and the problem of exhaustiveness recurred (Santos Valle and Kienzle 2020). In any case, the issue of including as much as available items as possible remains.

4. Conclusions

Robots can ensure more efficient use of production inputs, with the new frontiers of deep learning and machine learning approaches paving the way for an even more reduced human support thanks to current signs of progress in autonomous decision-making and performance improvement.

This study provides useful information for the classification of robots taking into account a large dataset of relevant equipment. The research presented in this study can be improved considering other information, such as the working capacity that these robots can serve and the technological readiness level (TRL). Other limits regard scarce information obtainable by screening websites, whilst direct contact with manufacturers could reduce missing data. The classification based on several binary variables covering various domains proposed in this study can guide more precise technology classification based on phenotypisation in the field of ontology design. In this context, robot attributes can be defined by properties and entities describing, e.g., the types of production, the working environment, the type of activity carried out.

References

Basu, Subhajit, Adekemi Omotubora, Matt Beeson, and Charles Fox. 2020. "Legal Framework for Small Autonomous Agricultural Robots." AI and Society 35(1):113–34.

Bechar, Avital, and Clément Vigneault. 2016. "Agricultural Robots for Field Operations: Concepts and Components." Biosystems Engineering 149:94–111.

Benke, Kurt, and Bruce Tomkins. 2017. "Future Food-Production Systems: Vertical Farming and Controlled-Environment Agriculture." Sustainability: Science, Practice, and Policy 13(1):13–26.

Fabiano, Nicola. 2019. "Robotics, Big Data, Ethics and Data Protection: A Matter of Approach." Pp. 79–87 in Intelligent Systems, Control and Automation: Science and Engineering. Vol. 95. Springer Netherlands.

FIRA (2018). International Forum of Agricultural Robotics. https://www.fira-agtech.com/en/exhibitors/

Lattanzi, Pamela. 2018. "L'agricoltura Di Precisione, Una Sfida Anche per Il Diritto." AGRIREGIONIEUROPA 53:5.

Lowenberg-DeBoer, J., K. Behrendt, M. Canavari, M. H. Ehlers, A. Gabriel, I. Huang, S. Kopfinger, R. Lenain, A. Meyer-Aurich, G. Milics, K. Oluseyi Olagunju, S. M. Pedersen, D. Rose, O. Spykman, B. Tisseyre, and I. Zdráhal. 2021. "85. The Impact of Regulation on Autonomous Crop Equipment in Europe." *Precision Agriculture '21* 711–717.

Lowenberg-DeBoer, James, Iona Yuelu Huang, Vasileios Grigoriadis, and Simon Blackmore. 2019. "Economics of Robots and Automation in Field Crop Production." Precision Agriculture 2019 21:2 21(2):278–99.

Martinelli, Agostino. 2002. "The Odometry Error of a Mobile Robot with a Synchronous Drive System." IEEE Transactions on Robotics and Automation 18(3):399–405.

Medici, Marco, Søren Marcus Pedersen, Giacomo Carli, and Maria Rita Tagliaventi. 2019. "Environmental Benefits of Precision Agriculture Adoption." Economia Agro-Alimentare / Food Economy 21(3):637–565.

NFU (2019). The Future of Food 2040. www.nfuonline.com/nfu-online/news/the-future-of-food-2040

Pezzuolo, Andrea, Donato Cillis, Francesco Marinello, and Luigi Sartori. 2017. "Estimating Efficiency in Automatic Milking Systems." Engineering for Rural Development 16:736–41.

Reis, Luís Paulo, Fernando Almeida, Luís Mota, and Nuno Lau. 2013. "Coordination in Multi-Robot Systems: Applications in Robotic Soccer." Pp. 3–21 in Communications in Computer and Information Science. Vol. 358. Springer Verlag.

Rose, David Christian, Rebecca Wheeler, Michael Winter, Matt Lobley, and Charlotte Anne Chivers. 2021. "Agriculture 4.0: Making It Work for People, Production, and the Planet." Land Use Policy 100:104933.

R Core Team (2020). R: A language and environment for statistical computing, version 3.6.3. R Foundation for Statistical Computing, Vienna, Austria. https://www.R-project.org/.

Salfer, J. A., K. Minegishi, W. Lazarus, E. Berning, and M. I. Endres. 2017. "Finances and Returns for Robotic Dairies." Journal of Dairy Science 100(9):7739–49.

Santos Valle, S., and J. Kienzle. 2020. "Agriculture 4.0 – Agricultural Robotics and Automated Equipment for Sustainable Crop Production." Integrated Crop Management, 24, 40.

Sharipov, D. R., O. A. Yakimov, M. K. Gainullina, A. R. Kashaeva, and I. N. Kamaldinov. 2021. "Development of Automatic Milking Systems and Their Classification." IOP Conference Series: Earth and Environmental Science 659(1):012080.

Thompson, Felix. 2019. "Next Generation Farming: How Drones Are Changing the Face of British Agriculture." Dw.Com. Retrieved June 18, 2021 (https://p.dw.com/p/3KcTG).

Circular Economy

Effect of pH on *Schizochytrium limacinum* Production grown using Crude Glycerol and Biogas Digestate Effluent

Sofoklis Bouras[a], Dimitrios Antoniadis[a], George Kountrias[a], Ioannis T. Karapanagiotidis[b], Nikolaos Katsoulas[a]*

[a]Laboratory of Agricultural Constructions and Environmental Control; Department of Agriculture Crop Production and Rural Environment; University of Thessaly; Fytokou Street; 38446; Volos; Greece

[b]Aquaculture Laboratory; Department of Ichthyology and Aquatic Environment; University of Thessaly; Fytokou Street; 38446; Volos; Greece

* Corresponding author. Email: nkatsoul@uth.gr

Abstract

Fish oil is a vital component in aqua feeds due to its rich content in n-3 polyunsaturated fatty acids (PUFA). However, the expensive price and conventional extraction practices have led the aquaculture industry to seek alternative sources of PUFA other than wild fish stocks, encompassing environmentally friendly and sustainable production practices. Marine microorganisms such as microalgae serve as a promising alternative component of aqua feeds due to their high content of proteins, lipids and PUFA. Also, their ability to utilize nutrients in their culture media derived from low-cost nutrient sources such as liquid wastes of food or biofuel industry, make them a promising low-cost alternative source for the production of useful substances. In this study, we assessed the potential cultivation of the rich in the PUFA docosahexaenoic acid (DHA) heterotrophic marine microalgae *Schizochytrium limacinum* SR21, in a growth media containing two different alternative nutrient sources, crude glycerol derived from biofuel industry as carbon source and effluent digestate from biogas production of livestock decomposition, as a source of nutrients and trace elements and the effect of varying levels of pH (6,7,8,9) of the growth media on biomass productivity, lipid accumulation, proximate composition, carbon assimilation and DHA content. It was shown that *Schizochytrium limacinum* SR21 can be used to heterotrophically remediate waste streams from the biofuel industry as alternative nutrient sources in a sustainable and environmental friendly way, and that a neutral pH (7) is the optimum ion concentration in order to enhance biomass productivity and DHA content, 44.9 g L^{-1} and 7.5% of their total lipid content respectively. Although this study did not achieve to reach industrial production standards with regards to the DHA content (0.58 g L^{-1}), a further assessment of other culture parameters (nitrogen concentration, oxygen dilution, temperature) is needed to optimize DHA production.

Keywords: microalgae; docosahexaenoic acid; greenhouse production; aqua feed; sustainability; waste management

1. Introduction

Heavy industrialization has an impact on natural ecosystems, leading to depletion of energy resources and environmental pollution. An innovative modern approach to offset global dependence on fossil fuel consumption in a sustainable and environmentally friendly way, is the emergence of the biofuel industry. Since 1992, countries of the European union are producing biodiesel at an industrial scale, with an annual production of 11.8 billion litters in 2015 (Eryilmaz et al., 2016). One of the by-products of the production process is crude glycerol. For each ton of biodiesel produced 100 kg of crude glycerol is generated. Crude glycerol has low economic value while its purification has a cost that may be significant especially for small scale refineries (Thompson and He, 2006). Regardless to say land disposal of crude glycerol can be harmful for the environment, consequently alternative methods of valorisation have been explored with a high interest shifting towards the utilization of this waste stream as an organic carbon source for microbial and microalgae fermentation (McNutt and Yang, 2007).

Europe generates annually approximately 1500 million tons of animal manure with pig manure management alone, being responsible for 18 % of the total greenhouse gas emissions derived from global livestock farming (Holm-Nielsen et al., 2009). A potential solution in order to alleviate these environmental threats is the implementation of remediation practices. Anaerobic digestion or co–digestion of livestock manure with agriculture crop residues is a process where microbial decomposition of organic matter produces biogas in order to generate electricity. By-product from this process is the digestate which can be further utilized in agriculture crop fertilization due to its high nutritional value, since it's a rich source of nitrogen, phosphorous, potassium and trace elements (Campel et al., 2019). However uncontrolled land applications can induce eutrophication due to excess nutrient leeching (Zhu et al., 2016). Both waste streams have been successfully implemented as alternative nutrients sources in microalgae production systems either as a remediation tool or substitution of expensive nutrient components in order to produce high cash yield health compounds (Phang et al., 2015) with an increasing interest on n-3 polyunsaturated fatty acids (PUFA) such as docosahexaenoic acid (DHA). Since DHA is only available in fish oil and considering its importance as a critical component in aqua feeds the aquaculture industry is seeking alternative and sustainable sources.

Schizochytrium sp., is a genus of non-photosynthetic unicellular eukaryotes in the family *Thraustochytriaceae* (Leyland et al., 2017), that synthesizes the highest yield of DHA. The strain *Schizochytrium limacinum* SR21, accumulates up to 50 % of its dry weight in lipids yielding a 35% DHA of its total lipid content in short production cycles (Sun et al., 2014). The toxicological evaluation has shown its safety for proposed uses in food (Lewis et al., 2016). *Schizochytrium* sp. is now considered to be a good DHA resource for replacing of sea fish (Zhao et al., 2018).

In our previous research, we successfully cultivated the strain *Schizochytrium limacinum* utilizing waste streams from the biofuel industry, crude glycerol derived from biofuel industry as an alternative carbon source and effluent digestate from biogas production of livestock decomposition, as a source of nutrients and trace elements (Bouras et al., 2020). The DHA yield is closely related to the cell morphology and pH value during fermentation period (Zhao et al., 2017). Therefore, optimising abiotic factors of the fermentation process, such as the pH, is important since it affects growth development and metabolic pathways of microalgae (Zhang et al., 2018). In this study we evaluate the effect of varying pH levels of the growth media on biomass productivity, lipid accumulation, proximate composition, carbon assimilation and DHA content of *Schizochytrium limacinum* SR21 cultivated heterotrophically utilizing crude glycerol as an organic carbon source and effluent digestate as an alternative source of nutrients and trace elements.

2. Materials and Methods

The microalgae strain *Schizochytrium limacinum* SR21 (*Aurantiochytrium limacinum* SR21, ATCC ® MYA-1381 ™) was obtained from the American Type Culture Collection (ATCC). Activation of cells in order to develop the seed inoculum was performed according to the ATCC protocol. The elemental composition and the optimal concentration of anaerobic digestate 48% (v/v) and crude glycerol (120 g L^{-1}) which promoted growth, development and maximized DHA content, was evidenced in a previous study (Bouras et al., 2020). In order to investigate the effect of ionic concentration on growth, development and DHA, the microorganisms were cultivated in 4 different initial pH levels of the growth medium: 6, 7, 8 and 9. The experiment was carried out in 500 mL shake flasks (DURAN ® GLS 80 ® Laboratory Bottle Wide Mouth) with 400 mL working volume containing 10% (v/v) inoculum of the seed culture of the microorganisms. Cultures were incubated in a growth chamber at 25 ^{o}C for 7 days on an orbital shaker set at 120 rpm. Ionic concertation was constantly corrected with 2M KOH. Oxygen was sparged into the medium with compressed air at a rate of 150L h^{-1}. During the experiment, dissolved oxygen (DO) level was maintained at 50% of saturation by regulating the oxygen supply. Prior to inoculation, the pH of the medium was adjusted to designated target values with 2M KOH or 1N HCL and autoclaved at 121∘ C for 15 min. The experiment was carried out for 7 days.

Biomass was determined daily gravimetrically by cell dry weight and total lipids were extracted according to Folch et al. (2016) with a solution of Chloroform/Methanol (C:M- 2:1 v/v). The analysis of the fatty acids of lipids was done by preparing fatty acid methyl esters (FAME) by acid catalysed transesterification according to Christie and Han (2003) and their quantification was done by gas-liquid chromatography (Perkin Elmer Clarus 680) coupled with a Col-Elite FAME Wax capillary column (30 m × 0.25 mm id, film thickness 0.25 µ m).The crude protein content was determined with Kjeldahl analysis, ash content was measured by dry ashing the samples at 600 ∘ C for 5 h, the calorific value was determined with an IKA calorimeter and crude carbohydrate content was quantified by subtracting the sum of the percentages of crude protein, total lipid, moisture and ash from 100. Finally, total organic carbon was quantified with a total organic carbon analyser (TOC-L, Shimadzu Corp, Kyoto, Japan). Further details on the methods used can be found at Bouras et al. (2020).

3. Results and Discussion

The initial pH of medium alters the DHA yield and total lipid accumulation by affecting cell membrane function and the uptake of nutrients (Sahin et al., 2018). Different pH levels of the enriched growth medium with pre-treated effluent had a pronounced effect on biomass productivity of *S. limacinum*. As shown in Table 1, highest biomass productivity (44.9 ± 2.7 g L^{-1}) was achieved when the cells were cultivated at a pH level of 7, while higher pH levels inhibited growth significantly with an average biomass productivity of 11.5 g L^{-1}. This trend comes in accordance with Wu et al. (2005) who found that the maximum biomass and DHA yield were obtained at pH 7.0 when cultivating *Schizochytrium* sp. S31 in conventional culture media, while Zhu et al., (2008) found that the maximum DHA yield (1.77 g L^{-1}) was obtained at a pH of 7.0, while higher pH reduced biomass productivity and lipid accumulation, when cultivating *S. limacinum* at GSM medium culture at a wide range of initial pH growth medium values. The sharp decrease of biomass productivity at elevated pH levels could also be explained by the vaporization of nitrogen as ammonia, as while increasing the pH there is a shift in the equilibrium state of nitrogen from aqueous to a gaseous phase (Wu et al., 2019). This process is enhanced with increasing pH levels above 7 leading to an ammonia removal efficiency approximately of 10-25% in 60 minutes.

With regards to the target compound DHA, the production of DHA at optimal pH of 7 reached 0.58 g L^{-1}. At lower or higher pH values resulted in lower DHA levels, ranging from 18-80% respectively. This comes in accordance with

previous research where increasing levels of pH decreased the amount of DHA (Zhao et al., 2017). According to their findings, high pH values immobilise in the nutrient media several micronutrients such as Mg^{+2}, Fe^{+2}, and Ca^{+2}, which are closely related to proper enzyme activity related to DHA synthesis.

The residual of total organic carbon after seven days of cultivation was lower at pH 7 (Table 1), meaning higher total organic carbon assimilation observed at pH 7, while the increasing concertation of pH inhibited utilization of crude glycerol for growth and the relative assimilation of organic carbon. Thus, heterotrophic cultivation of *S. limacinum* can effectively remediate crude glycerol and effluent digestate from the biofuel industry and can enhance biomass production.

Table 1. Biomass productivity, lipid production as % of dry weight biomass, DHA content as % of total lipids, residual of organic carbon after 7 days of cultivation and proximate composition of dried algal biomass of *S. limacinum* grown on medium containing 48 % (v/v*)* effluent digestate and crude glycerol at varying pH levels (6, 7, 8 and 9).

pH Level	Dry Weight (g L^{-1})	Crude lipid (%)	DHA (%)	Residual of organic carbon (g L^{-1})	Crude Protein (%)	Ash (%)	Moisture (%)
6	22.9 ± 3.6[a]	16.8 ± 0.6[a]	6.1 ± 2.7[a]	27.8 ±0.7	44.0 ± 3.70[a]	8.0 ± 0.3[a]	0.37 ± 0.03[a]
7	44.9 ± 2.7[b]	17.3 ± 3.5[a]	7.5 ± 1.2[b]	22.3 ±0.4	25.0 ± 0.08[b]	30.4 ± 8.1[b]	0.34 ± 0.04[a]
8	11.6 ± 1.5[c]	28.0 ± 5.3[c]	1.3 ± 0.2[c]	32.4 ±0.5	36.5 ± 0.78[c]	26.5 ± 0.2[c]	0.27 ± 0.01[a]
9	11.7 ± 0.7[c]	31.5 ± 2.0[c]	N.D	31.4 ±0.2	36.0 ± 0.19[c]	29.0 ± 1.0[d]	0.51 ± 0.05[a]

[1]Values (percentages) are represented as the mean ± standard deviation of triplicates, whereas letters (a, b and c) indicate statistical differences analysed at a level of $p < 0.05$.
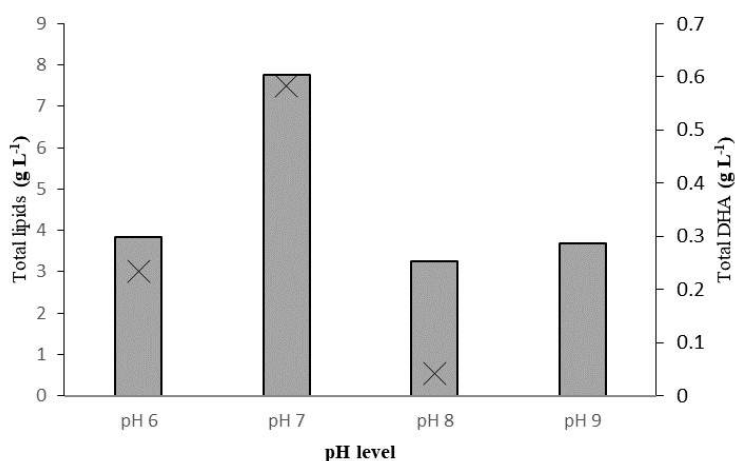
Figure 1. Total lipids (columns) and total DHA (x) in g per L of microalgae culture under different pH levels.

4. Conclusion

The marine microalgae *S. limacinum* SR21 is an effective tool to process waste streams from the biofuel industry, in an optimal pH level of growth medium at 7, enhancing biomass and DHA production. Although this study did not achieve to reach industrial production standards with regards to the DHA content (0.58 g L^{-1}), a further assessment of other culture parameters (nitrogen concentration, oxygen dilution, temperature) is needed to optimize DHA production and to produce supplements for aquaculture feeds using as growth medium alternative and low cost nutrient sources such as crude glycerol and effluent digestate from biofuel industry, contributing to the sustainable food production rules of cyclic economy.

References

Bouras, S., Katsoulas, N., Antoniadis, D., and Karapanagiotidis, I. T. (2020). Use of Biofuel Industry Wastes as Alternative Nutrient Sources for DHA-Yielding *Schizochytrium limacinum* Production. *Applied Sciences* **10**, 4398.

Campbell, J. E., Lobell, D. B., and Field, C. B. (2009). Greater transportation energy and GHG offsets from bioelectricity than ethanol. *Science* **324**, 1055-1057.

Christie, W., and Han, X. (2003). Lipid analysis-isolation, separation, identification and lipidomic analysis (Fourth). Woodhead Publishing USA.

Eryilmaz, T., Yesilyurt, M. K., Cesur, C., and Gokdogan, O. (2016). Biodiesel production potential from oil seeds in Turkey. *Renewable and Sustainable Energy Reviews* **58**, 842-851.

Folch, J., Lees, M., and Stanley, G. S. (1957). A simple method for the isolation and purification of total lipides from animal tissues. *Journal of biological chemistry* **226**, 497-509.

Holm-Nielsen, J. B., Al Seadi, T., and Oleskowicz-Popiel, P. (2009). The future of anaerobic digestion and biogas utilization. *Bioresource technology* **100**, 5478-5484.

Lewis, K.D., Huang, W.F., Zheng, X.H., Jiang, Y., Feldman, R.S, Falk, M.C. (2016) Toxicological evaluation of arachidonic acid (ARA)-rich oil and dcosahexaenoic acid (DHA)-rich oil. *Food and Chemical Toxicology* **96**,133–144.

Leyland B, Leu S, Boussiba S (2017) Are Thraustochytrids algae? Fungal Biol 121(10):835–840 McNutt, J., and Yang, J. (2017). Utilization of the residual glycerol from biodiesel production for renewable energy generation. *Renewable and Sustainable Energy Reviews* **71**, 63-76.

Phang, S.-M., Chu, W.-L., and Rabiei, R. (2015). Phycoremediation. *In* "The Algae World", pp. 357-389. Springer.

Sahin, D., Tas, E., and Altindag, U.H. (2018). Enhancement of docosahexaenoic acid (DHA) production from *Schizochytrium* sp. S31 using different growth medium conditions. *AMB Express*, **8**, 7.

Sun, L., Ren, L., Zhuang, X., Ji, X., Yan, J., and Huang, H. (2014). Differential effects of nutrient limitations on biochemical constituents and docosahexaenoic acid production of *Schizochytrium* sp. *Bioresource technology* **159**, 199-206.

Thompson, J. C., and He, B. B. (2006). Characterization of crude glycerol from biodiesel production from multiple feedstocks. *Applied engineering in agriculture* **22**, 261-265.

Wu, S.T., Yu, S. T., and Lin L.P. (2005). Effect of culture conditions on docosahexaenoic acid production by *Schizochytrium* sp. S31. *Proc. Biochem*., 40: 3103-3108.

Wu, C., Zhang, Y., and Chen, X. (2019). Ammonia removal mechanism by the combination of air stripping and ultrasound as the function of pH. *In* "IOP Conference Series: Earth and Environmental Science", **344**, 012051. IOP Publishing.

Zhang, L., Zhang, J., Zeng, G., Dong, H., Chen, Y., Huang, C., Zhu, Y., Xu, R., Cheng, Y., and Hou, K. (2018). Multivariate relationships between microbial communities and environmental variables during co-composting of sewage sludge and agricultural waste in the presence of PVP-AgNPs. *Bioresource technology* **261**, 10-18.

Zhao, B., Li, Y., Li, C., Yang, H., and Wang W. (2018). Enhancement of Schizochytrium DHA synthesis by plasma mutagenesis aided with malonic acid and zeocin screening. *Applied Microbiological Biotechnology,* **102**, 2351–2361.

Zhao, B, Li, Y., Mbifile, M.D., Li, C., Yang, H., Wang, W. (2017). Improvement of docosahexaenoic acid fermentation from *Schizochytrium* sp. AB610 by staged pH control based on cell morphological changes. *Engineering in Life Sciences*, **17**, 981–988.

Zhu, L., Yan, C., and Li, Z. (2016). Microalgal cultivation with biogas slurry for biofuel production. *Bioresource technology* **220**, 629-636.

Zhu, L., Zhang, L., Ren X., and Zhu Q. (2008). Effects of culture conditions on growth and DHA production from *S. limacinum*. *Journal of Oceanic and Coastal Sea Research* **7**, 83-88.

Planning the Integrated Management of Organic Waste Flows and Agricultural Residues for a Circular Economy

Canio Manniello [a,*], Dina Statuto [a], Andrea Di Pasquale [b], Pietro Picuno [a]

[a] SAFE School of Agriculture, Forest, Food and Environmental Sciences, University of Basilicata, Potenza, Italy
[b] INNOVA Consorzio per l'Informatica e la Telematica srl, Matera, Italy

* Corresponding author. E-mail: canio.manniello@unibas.it

Abstract

In the recent years, the production, management and disposal of both organic waste and agricultural residues has become significantly difficult in Italy, due to the lack of suitable facilities. Very often, indeed, within the different regions, there are no treatment plants for the organic fraction of municipal solid waste or agricultural residues treatment centres, so as to give them a second life in the perspective of a circular economy. The lack of proximity treatment centres, forces local administrations to send these flows to plants outside their territorial area, with a consequent increase for transport and treatment costs.

This paper, with reference to the study area of the Matera municipality (Basilicata region - Southern Italy), taking into consideration the organic waste flows of non-domestic users from separate collection and agricultural residues - especially those coming from the wine production chain - provides a state-of-the-art analysis of the problems related to their collection, management and disposal. Subsequently, an alternative model feasibility study - called "*proximity composting*", aimed at a more sustainable management of these flows based on their "zero-kilometers treatment" – has been implemented.

The results obtained have demonstrated that the proposed scenario is much more sustainable when compared to the current situation, both from an economic and environmental point of view. Indeed, thanks to the use of calculation tools, the economic (€/year) and environmental (Kg CO_2 avoided/year) advantages, due to the save of transport and disposal of flows outside the region, have been quantified, with consequent reduction of waste tax for citizens (€/year). In addition, the implementation of maps using a Geographical Information System (GIS) has demonstrated a better optimization of the system. Finally, it was highlighted the social utility of the proposed model, because citizens become an active part in the process and self-produce soil fertilisers.

Keywords: Wine production chain, Proximity composting, CO_2, Waste tax, Geographical Information Systems.

.

1. Introduction

The concept of *circular economy* is based on the idea that the value of materials and products is kept as high as possible for as long as possible, in order to minimize the need to introduce new materials and energy, thus reducing the environmental pressure related to their use (European Environment Agency, 2017).

The urgent need to transform the linear model into a circular one is particularly important in the case of agriculture by-products and urban waste.

The improvement of agricultural *co-products*, *by-products* and *waste* is indeed fundamental for the production of renewable biological resources and the conversion of these resources and waste streams into added-value products, such as food, feed, bio-based products and bioenergy (Carus and Dammer, 2018).

Agricultural and agro-industrial activities generate significant quantities of product residuals and organic waste of different types, potentially usable not only as an alternative fuel in energy plants for the production of energy (Statuto et al., 2018), but also for the restoration of soil fertility, as added-value components in other industrial sectors (nutraceutical, cosmetic, etc.), or in the building sector - as a natural additive that could be incorporated into clay bricks to increase their technical performance (Statuto et al.,2018/a).

Subsequently, there are other secondary options that could be exploited, offered in same the agricultural sector, which can contribute to its sustainable development (Statuto and Picuno, 2016). Indeed, mostly in case of residual biomass coming from the wine production chain, there are currently different possibilities of reuse of residues which, depending on the relevant industrial process, may have a very different environmental impact. So, they could find a second life in different areas, e.g.: the pomace as a substrate for plants growth (Diaz et al., 2002; Nogales et al., 2005; Bustamante et al., 2009; Paradelo et al., 2010) or as dyes for the food industry and as antioxidants due to its high percentage of polyphenols (Ping. et al., 2011; Thorngate and Singleton, 1994; Karleskind, 1992); as a raw material for the production of tartaric acid (vinification dregs) (Versari et al., 2001; Braga et al., 2002); stalks as fuel for the electricity and the production of heat (Università Politecnica delle Marche, 2013) or as potent adsorbents for heavy

metal removal (Tripathi and Ranjan, 2015); finally, as a raw material for the production of oil and flour (grape seeds) (Bail et al., 2008).

Considering, instead, the activity of management and recovery of *municipal solid waste*, through separate collection, it is possible to obtain interesting by-products to be reused in the circular economy. From the process of aerobic or anaerobic transformation of the organic fraction of municipal solid waste, two products of particular interest can be obtained: biogas, further transformed into biomethane; and quality compost, that is reusable in agriculture.

The organic fraction of municipal solid waste, or bio-waste, is composed mainly of food waste of plant or animal origin and green waste, in an amount that depends on the area under consideration (Eurostat, 2013). According to European recommendations and environmental considerations, this waste must be collected separately at home, to be then biologically treated by composting or anaerobic digestion to ensure the production of high-quality compost, in accordance with new European regulations (European Union, 2008).

The current organizational model of management, treatment and valorisation of organic waste is very complicated and expensive due to the lack of proximity treatment plants. This problem forces local administrations to send these flows to plants outside their territorial area, with a consequent increase for treatment and transport costs.

The imbalance between the various areas of the country, indeed, forces the centre and south of Italy to transfer their organic waste (from separate collection) in other regions, with great economic disadvantages and air pollution for emissions due to the frequent and constant movement of vehicles.

The flows that are not treated but are transferred to landfill, instead, have a high disposal cost, due to the difficulty of finding suitable landfills, with an increase in expenditure on citizens. Even the separate collection itself and in particular the "door to door" model (more widely used) has significant criticalities, such as traffic due to vehicles (especially in narrow streets or, on the contrary, in very crowded and busy streets) with consequent excessive consumption of the road surface as well as emission of CO_2 into the atmosphere; the exposure of the bins on the street subject to bad weather, or the presence of animals; the withdrawal concentrated in narrow time slots; etc.

The same problems concern the management and valorisation of *wine by-products*, currently also complicated by strict regulations and bad practices. They represent a real problem for producers, because they are produced in considerable quantities but concentrated in short periods of the year (September-October, generally).

Indeed, very often they are disposed without respecting the law, reused without relevant results or sent to distilleries, also outside the region, with considerable economic and environmental disadvantages. Therefore, in both cases, at present, both for organic waste and wine by-products, there are problems that weigh on the strategies of the various municipalities and are complicated to manage.

Table 1 shows the main residual materials classifiable as by-products and the processing yields of grapes (Università Politecnica delle Marche, 2013).

Table 1. Wine production and relevant by-products from the transformation of 100 kg of grape.

Entrance (kg)	Exit (kg)	Residues Classifiable as by-Products (%)	
Grapes (100 Kg)	Wine (77 Kg)	Virgin (5.4) and exhausted pomace (4.6)	10
		Grapeseeds	5
		Stalks	3
		Dregs	5

From each one of the winemaking phases, different types of by-products are generated. The stalks are the first to be released. They correspond to the woody part of the bunch and are eliminated during de-stemming. The vinification dreg is the muddy residue that is deposited in the containers, after fermentation, during storage or after authorized treatments, as well as the residues obtained by filtration or centrifugation of this product. This consists mainly of yeast cells produced during alcoholic fermentation, bacteria, tartaric salts, plant cell residues and ethanol (Bai et al.,2008; Naziri et al.,2012).

The main by-product of the supply chain is the pomace, which represents about 10%–30% of the mass of grapes crushed. It is composed of grape seeds, grape skins and stems residues and it consists mainly of unfermented sugars, alcohol, polyphenols, tannins, pigments and other valuable products. The size of the winery and the winemaking methods used directly influence its quantity and quality (Muhlack et al.,2018). Together with the residual sugars, it has other physical (e.g., pH, moisture, etc.) and chemical (e.g., lignocellulose, polyphenols, ash, etc.) characteristics, which are important to consider when pomace is used as raw material (Table 2).

Table 2. Physical and chemical properties of grape pomace and other by-products.

Parameter	Stalks	Pomace	Dregs	Reference
pH	4.4	3.8	4	
Organic Substance (g/kg)	920	915	759	
Oxidizable organic carbon (g/kg)	316	280	300	
Water soluble carbon (g/kg)	74.5	37.4	87.8	
Total nitrogen (g/kg)	12.4	20.3	35.2	(Bustamante et al.,2008)
P (g/kg)	0.94	1.15	4.94	
K (g/kg)	30	24.2	72.8	
Ca (g/kg)	9.5	9.4	9.2	
Mg (g/kg)	2.1	1.2	1.6	
Fe (mg/kg)	128	136	357	
Mn (mg/kg)	25	12	12	
Cu (mg/kg)	22	28	189	
Zn (mg/kg)	26	24	46	

2.   Materials and Methods

The study area is the total territory of the municipality of Matera (Basilicata region - Southern Italy) (Figure 1). It has a population of 60,341 inhabitants (Istat, 2019). With a total geographical area of 392,09 Km^2 (Urbistat, 2019) it is the second largest municipality of Basilicata region *(*after Potenza*)* and it is predominantly covered by rural land, with a quite low regional population medium density, equal to 153,9 inhabitants/km^2 (RSDI, 2019). The territory of Matera (403 meters a.s.l.) is characterised by a warm and temperate climate, with an average temperature of 15.4 °C and an average annual rainfall of 593 mm (climate-data.org, 2020). The total agricultural area is 195,596.14 ha (accounting for 19.56% of the regional surface area); 164,300.75 ha are actually used for agricultural production (RSDI,2019).
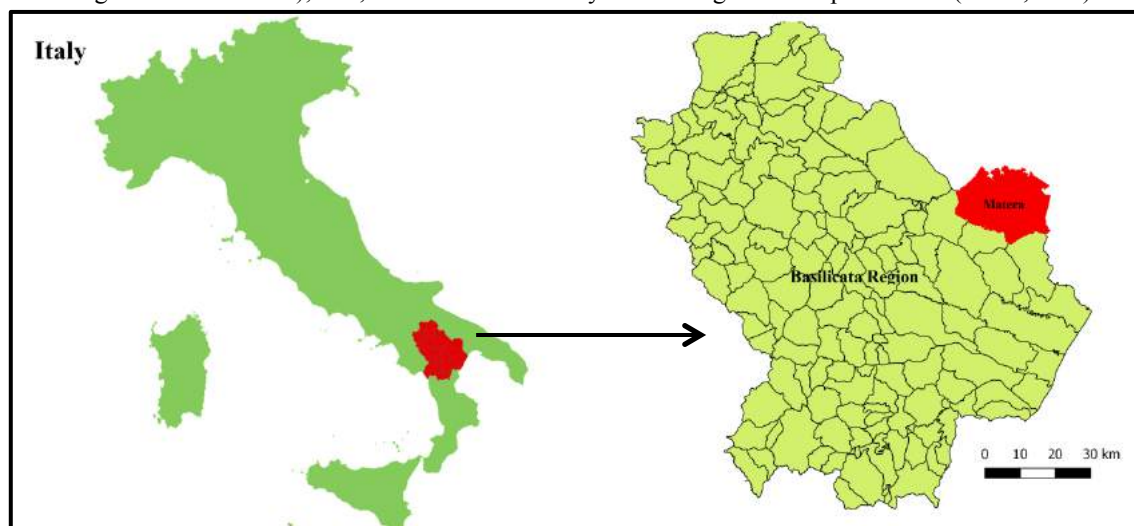
Figure 1. Location of the study area.

Considering the area of the municipality of Matera potentially producing D.O.C. (Denominazione di Origine Controllata – Product of a Controlled Origin) wines, equal to 32% of the total area covered with grapes (25.08 hectares), assuming an annual production of 8 tons/ha of grapes, and calculating the territory dedicated to the whole amount of wine grapes production, the amount of the pomace usable, equal to 200.64 tons, has been determined (Statuto et al., 2018). Moreover, the percentage of the total amount of the ***pomace*** considered in this case is the 10% of wine grapes production, which means a production of about 20.06 tons/year.

Regarding the **organic waste**, with reference to the study area, considering the main non-domestic users most relevant to waste production such as refectories, hospitals, restaurants etc., their urban waste production (t/year) which depends on surface area and on the relative production coefficient (Dipartimento delle Finanze,2018), and taking into account the waste composition in Basilicata region according to which the organic fraction corresponds to 40% of the total production, the total amount of organic waste has been also determined (Table 3).

Table 3. Organic waste production for non domestic users considered.

Category	Urban waste production (t/year)	Organic fraction (%)
Museums, libraries, schools, associations, worship places	313.06	
Hotels with restaurant	8.64	
Nursing and retirement home	186.40	
Hospital	525.91	
Offices, agencies and professional offices	2,108.6	40
Restaurants, inns, taverns, pubs	444.49	
Refectories, breweries	13.21	
Bar, coffee shop, bakeries	120.26	
Fruit and vegetables, fishmongers, flowers and plants	80.93	
Bed and Breakfast	22.27	
Agritourisms	14.21	
Total Organic waste production 1,535.19 t/year		

2.1 Economic and environmental feasibility study of the proposed model

In order to prevent some of the main problems, previously described, regarding the current organizational model of collection, management and disposal of organic waste (from separate collection) and wine by-products, a new integrated model of collection and management of both organic waste of non-domestic users (from separate collection), and wine by-products has been hypothesized, studied and proposed called "*proximity composting*".

This last model, based on "zero-kilometres treatment" of the considered flows, different from the current one (composting in very distant industrial plants), not very sustainable, very expensive and disadvantageous, on the one hand aims to improve the separate collection in individual municipalities, and consequently reduce the amount of organic waste to be treated, on the other hand to give a second life, more sustainable, to wine by-products in the perspective of the circular economy.

The basic organizational idea includes the deposit of organic waste produced by non-domestic users and by-products coming from the wine supply-chain, at a temporary collection centre, located within the municipality itself, that host mini-composting plants (composter) for the production of biological fertilizer, that each user or producer will be able to reuse in their own land, to close the circle of circular economy and restore the level of soil fertility.

In recent decades, indeed, a persisting inadequate substitution of soil nutrients has led to the lack of organic matter (Manniello et al., 2020) and consequent low level of soil fertility (Manniello et al., 2020/a), only partly balanced by the reuse of agricultural residues (Manniello et al., 2020/b).

After analysing the costs referred to the current scenario (Table 4), the area for the processing of such flows has been localised (Figure 2). The geographical localisation of the area has been performed using a GIS (QGIS - v. 3.4) in which the municipality has been considered as reference unit and it has been carried out taking into account particular constraints such as areas at landslides risk, or proximity to polluted sites (and therefore sites reported and to be reclaimed) or to industrial areas, nature reserves or areas with landscape and archaeological constraints, sites of community interest (Sci) and Special protection areas (Spa).

Preferential factors such as, for example, the multiplicity of access roads, accessibility not conditioned by atmospheric events (snow, ice), barycentrality to waste production, the financial cost of the areas and the absence of industrial plants with a strong environmental impact in the proximity have been also considered.

Thanks to the direct interviews with experts in the sector, all the initial costs of the proposed model, supported by the municipality, such as the investment cost of the composter (about 600 euros for each ton of organic waste to be treated), the various costs for the purchase and video surveillance of the area, staff training, informatisation of the collection center and the entire process, have been also estimated. Moreover, the annual fixed costs including cost of personnel, the electricity consumption of the machinery and the related maintenance costs (obtained directly from the technical data sheet of the machinery) have been also added (Table 5).

Table 4. State of the art data for the collection and disposal of organic waste and winery-by products.

Current scenario		Reference
Organic waste collection cost (€/tons)	200	Direct interviews with operators
Organic waste disposal cost (€/tons)	150	Direct interviews with operators
Distance from the nearest composting plant (Laterza-Taranto) (Km)	22	
Fuel yield (Km/l)	2,8	Ministero dello Sviluppo Economico, 2018 (vehicles with a mass greater than 26 tons)
Fuel cost (€/l)	1,5	Ministero della Transizione Ecologica, 2020
Average transportable quantity (tons)	30	Direct interviews with operators
Winery by-products disposal cost (€/tons)	0.22	Novello, 2015
Distance from the nearest distillery (Km)	500	Direct interviews with operators
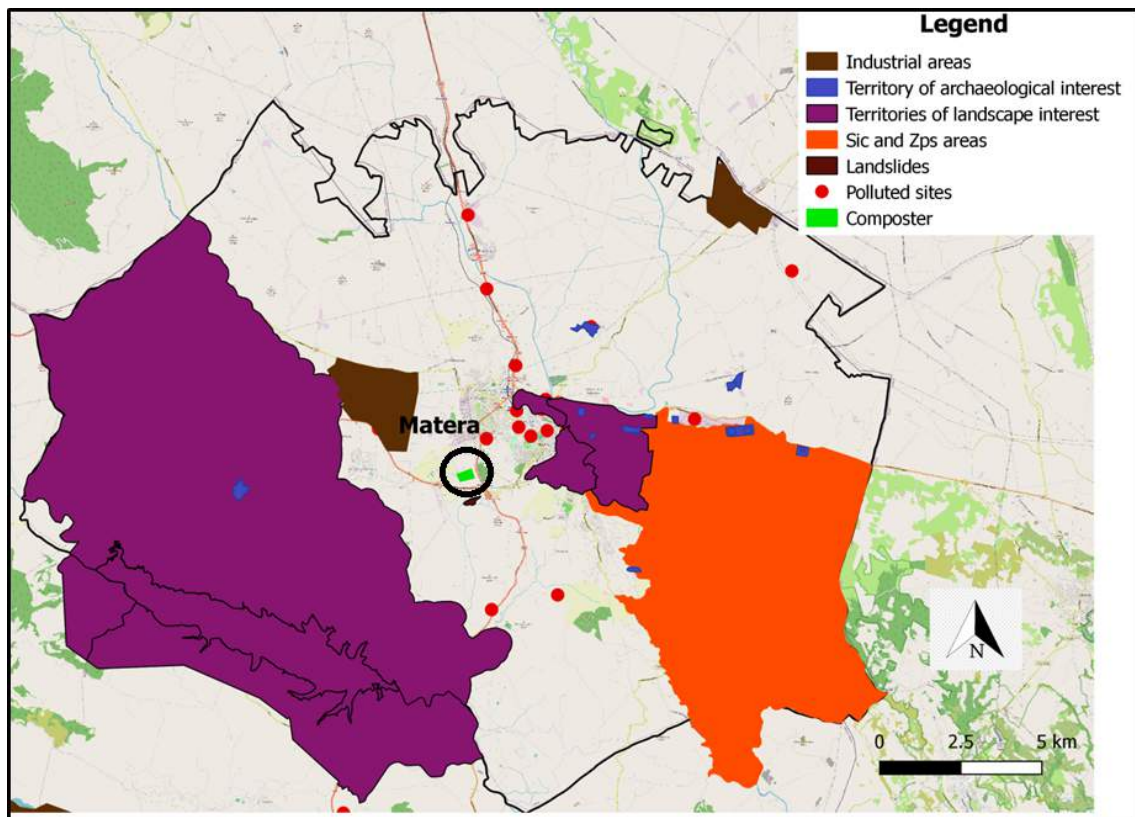
Figure 2. Geographical localisation of the area for "proximity composting".

Table 5. Initial and annual fixed costs for the electro-mechanical composter

Composter Investment Cost (€)	900,000
Various costs (Videos, Bureaucracy, Area) (€)	10,000
Staff Training (€)	1,500
Collection Center and Processing Informatisation (€)	25,000
Municipal Initial Costs (€)	**936,500**
Personnel costs (€/year)	50,000
Electricity consumption (€/year)	500
Composter maintenance (€/year)	3,500
Municipality Fixed Costs (€/year)	**54,000**

Finally, the avoided costs related to the transport (equation 1) and disposal (equation 2) of organic waste, and disposal of winery by-products (equation 3) has been calculated.

$$\textbf{Organic Waste} - \textbf{ Avoided Transport Cost } \left(\frac{€}{\textbf{year}}\right) = \frac{D}{R} * 2 * C * \left(\frac{Qt}{Qm}\right) \qquad (1)$$

where "D" is the distance from the nearest composting plant considered (Puglia region – Southern Italy); "R" is the average fuel yield for vehicles transporting waste (Table 4); "C" is the fuel cost calculated in table 4; "Factor 2", because the round trip has been considered; "Q_m" is the average transportable quantity (Table 4); "Q_t" is the total organic waste production (Table 3).

$$\textbf{Organic Waste} - \textbf{ Avoided Disposal Cost } \left(\frac{€}{\textbf{year}}\right) = \text{Disposal cost} \left(\frac{€}{t}\right) * Qt \text{ (t)} \qquad (2)$$

where "Disposal cost" represents the disposal cost per ton of waste (Table 4); "Q_t" is the total organic waste production (Table 3).

$$\textbf{Winery By} - \textbf{products Avoided Disposal Cost } \left(\frac{€}{\textbf{year}}\right) = \text{Disposal cost} \left(\frac{€}{t}\right) * Qt \text{ (t)} \quad (3)$$

where "Disposal cost" represents the disposal cost for wine by-products in distillery (Table 4); "Qt" is the total winery by-products production, previously calculated.

2.2 Calculation of economic and environmental saving

Following the adoption of the hypothesized model, the economic and environmental savings, compared to the current scenario, both for organic waste and wine by-products has been calculated as follows:

$$\textbf{\textit{Organic Waste Economic saving}} \left(\frac{€}{year}\right)$$
$$= \left[\left(\frac{Ci}{5}\right) + Cf\right]\left(\frac{€}{year}\right) - [Avoided\ Transport\ Cost + Avoided\ Disposal\ Cost]\left(\frac{€}{year}\right) \quad (4)$$

where "Ci" are initial costs of the municipality (spread over 5 years); "C_f" are the fixed costs of the municipality; "Avoided Transport Cost + Avoided Disposal Cost" are the economic savings due to the lack of movement of flows to the composting plant, because in the hypothesised model they remain within the municipality of production (so-called, "proximity" composting).

$$\textbf{\textit{Wine By}} - \textbf{\textit{products Economic saving}} \left(\frac{€}{year}\right) = Avoided\ disposal\ cost\ in\ distillery \left(\frac{€}{year}\right) \quad (5)$$

For wine by-products, the economic saving is essentially due to the failed disposal to distillery, because in the hypothesized model they are valued within the municipality itself.

The related environmental savings are essentially due to CO_2 avoided due to non-movement vehicles to the composting plant (equation 6) or to the distillery (equation 7), since in the proposed model the flows are valorised within the municipality itself:

$$\textbf{\textit{Avoided CO2 emissions composting plant}} \left(\frac{Kg}{year}\right) = CO2\ consumption \left(\frac{g}{Km}\right) * No\ of\ trips \left(\frac{Km}{year}\right) \quad (6)$$

$$\textbf{\textit{Avoided CO2 emissions distillery}} \left(\frac{Kg}{year}\right) = CO2\ consumption \left(\frac{g}{Km}\right) * No\ of\ trips \left(\frac{Km}{year}\right) \quad (7)$$

The calculation, in addition to considering the number of trips per year, which is a function of the distance (round trip) to the composting plant or to the distillery (Table 4), of the average quantity transported by each vehicle and of the quantity of flows moved, also takes into consideration the parameter of CO_2 consumption (800 g/Km), obtained from personal processing by studying the registration books of the vehicles, their relative CO_2 consumption and considering an average value that is representative of the regional parameters.

3. Results and Discussion

Following the feasibility study conducted, table 6 shows the annual economic savings (€/year) with the relative payback period, due to the non-transfer of organic waste out of the region, while similarly the following table (Table 7) shows the economic savings associated with the non-transfer of wine by-products to the distillery. The environmental savings (CO_2 avoided) associated with the two processes is reported in table 8.

Table 6. Annual economic savings associated with "proximity composting model" regarding organic waste.

Organic Waste Economic saving	Costs (€)	Saving (€)	Final saving (€)
First Year	241,300	227,559.62	-13,740.38
Second Year	241,300	227,559.62	-27,480.76
Third Year	241,300	227,559.62	-41,221.15
Fourth Year	241,300	227,559.62	-54,961.53
Fifth Year	241,300	227,559.62	-68,701.91
Sixth Year	54,000	227,559.62	104,857.71
Investment return 6⁰ YEAR			

Table 7. Annual economic savings associated with "proximity composting model" regarding winery by-products.

Winery By-products Economic saving (€/year)
458.48

Table 8. Annual environmental savings associated with "proximity composting model".

Avoided CO_2 emissions (Kg/year) – composting plant	Avoided CO_2 emissions (Kg/year) - distillery
1,770.75	555.73

The obtained results shows that the proposed model is feasible above all from the economic point of view, most important aspect of both the municipality's management and planning strategies and the model's key players. The valorisation of the organic waste inside the municipality of Matera produces an economic benefit starting from the sixth year. Taking into account the useful life of the industrial plant used (20 years) the result appears satisfying. For wine by-products, on the other hand, the annual economic benefit is much lower, even if however interesting, because we are obviously dealing with a smaller flow than for organic waste, because they are not produced continuously, but only in certain months of the year.

There are also considerable quantities of CO_2 avoided due to the lack of movement of vehicles outside the region.

The results obtained are very interesting already at the municipal level but they obviously assume greater relevance in planning strategies at the regional level.

4. Conclusions

The current model of waste production and management and wine by-products represents an unsustainable model, both from an environmental and economic point of view. This type of organization is part of the so-called linear economy, based on the production of a good, its consumption and its subsequent disposal. It is essential to contrast this model with a new model, based on a circular economy concept. To achieve this objective, the collaboration of various players is fundamental: from legislators to producers, from environmental protection agencies to the infrastructures for the management of materials, from the personnel responsible for collection and disposal to the citizen, who must commit to a model of eco-sustainable living model.

The entire world is moving towards this new approach, facing numerous challenges and critical issues. One of these, perhaps the most serious, with regard to the management and disposal of organic waste and wine by-products is represented by the chronic lack of facilities: there are many municipalities that do not make (or make little) collection of these flows because there are no plants "on site" for their treatment and therefore high transportation costs must be sustained.

Currently, the most modern approaches to the issue suggest the treatment and recovery of waste and wine by-products near to the places of production, through small plants of negligible impact, responding to the targeted needs of many local realities contributing to use the compost on site produced.

References

Bai, Z., Jin, B., Li. Y., Chen. J., Li. Z., 2008. Utilization of winery wastes for Trichoderma viride biocontrol agent production by solid state fermentation. Journal of Environmental Sciences. 20, 353–358. https://doi.org/10.1016/S1001-0742(08)60055-8

Bail, S., Stuebiger, G., Krist, S., Unterweger, H., Buchbauer, G., 2008. Characterisation of various grape seed oils by volatile compounds, triacylglycerol composition, total phenols and antioxidant capacity. Food Chemistry. 108, 1122–32. https://doi.org/10.1016/j.foodchem.2007.11.063.

Braga, FG., Lencart and Silva, F.A., Alves, A., 2002. Recovery of winery by-products in the Douro demarcated region: Production of calcium tartrate and grape pigments. American Journal of Enology and Viticulture. 53, 42-45.

Bustamante, M.A., Moral, R., Paredes, C., Pérez-Espinosa, A., Moreno-Caselles, J., Pérez Murcia, M.D., 2008. Agrochemical characterisation of the solid by-products and residues from the winery and distillery industry. Waste Management. 28, 372-380. https://doi.org/10.1016/j.wasman.2007.01.013.

Bustamante, M.A., Paredes, C., Morales, J., Mayoral, A.M., Moral, R., 2009. Study of the composting process of winery and distillery wastes using multivariate techniques. Bioresource Technology. 100(20), 4766-4772. https://doi.org/10.1016/j.biortech.2009.04.033.

Carus, M., Dammer, L., 2018. The Circular Bioeconomy — Concepts, Opportunities, and Limitations. Industrial Biotechnology. 14, 83–91. https://doi.org/10.1089/ind.2018.29121.mca.

Dipartimento delle Finanze: Comune di Matera – Regolamento TARI, 2018. https://www1.finanze.gov.it/finanze2/dipartimentopolitichefiscali/fiscalitalocale. Accessed on February 28, 2020.

Dati climatici sulle città del mondo. 2020. https://it.climate-data.org. Accessed April 18, 2021.

Díaz, M.J., Madejón, E., López, F., López, R., Cabrera, F., 2002. Optimization of the rate vinasse/grape marc for co-composting process. Process Biochemistry. 37(10), 1143-1145. http://dx.doi.org/10.1016/S0032-9592(01)00327-2.

European Environment Agency. Circular by Design: Products in the Circular Economy. 2017. Copenhagen, Denmark.

European Union, 2008. Green paper on Management of Bio-waste in the European Union.

Eurostat - Waste Statistics. 2013. https://ec.europa.eu/eurostat. Accessed February 28, 2021.

ISTAT (Italian National Institute for Statistic). 2019. http://istat.it. Accessed October 10, 2019.

Karleskind, A., 1992. Association française pour l'étude des corps gras. In Manuel des corps gras; Technique et Documentation–Lavoisier: Paris, France; London, UK; New York, NY, USA. Volume 1.

Manniello, C., Statuto, D., Di Pasquale, A., Cillis, G., Picuno, P. 2020. The impact of soil fertility on the characteristics of the rural landscape for its protection. *Public Recreation and Landscape Protection - With Sense Hand in hand? Conference Proceedings* . 484-488.

Manniello, C., Statuto, D., Di Pasquale, A., Picuno, P., 2020/a. Planning the Flows of Residual Biomass Produced by Wineries for Their Valorization in the Framework of a Circular Bioeconomy. Springer. 67, 295-303. https://doi.org/10.1007/978-3-030-39299-4

Manniello, C., Statuto, D., Di Pasquale, A., Giuratrabocchetti, G., Picuno, P., 2020/b. Planning the Flows of Residual Biomass Produced by Wineries for the Preservation of the Rural Landscape. Sustainability. 12, 847. https://doi.org/10.3390/su12030847.

Ministero della Transizione Ecologica – Analisi e Statistiche Energetiche e Minerarie 2020. https://www.minambiente.it. Accessed February 28, 2021.

Ministero dello Sviluppo Economico (MISE) – Osservatorio sui Prezzi. 2018. https://www.mise.gov.it/index.php/it. Accessed February 28, 2021.

Muhlack, R.A., Potumarthi, R., Jeffery, D.W., 2018. Sustainable wineries through waste valorization: A review of grape marc utilization for value-added products. Waste Management. 72, 99–118. https://doi.org/10.1016/j.wasman.2017.11.011.

Naziri, E., Mantzouridou, F., Tsimidou, M.Z., 2012. Recovery of Squalene from Wine Lees Using Ultrasound Assisted Extraction—A Feasibility Study. Journal of Agricultural and Food Chemistry. 60, 9195–9201. https://doi.org/10.1021/jf301059y.

Nogales, R., Cifuentes, C., Benítez, E., 2005. Vermicomposting of winery wastes: a laboratory study. Journal of Environmental Science Health. 40(4), 659-667. https://doi.org/10.1081/PFC-200061595.

Novello,V., 2015. Filiera vitivinicola: valorizzare residui e sottoprodotti. Disafa – Università di Torino.

Paradelo, R., Moldes, A.B., Barral, M.T., 2010. Utilisation of a factorial design to study the composting of hydrolyzed grape marc and vinification lees. Journal of Agriculture and Food Chemistry. 58(5), 3085-3089. https://doi.org/10.1021/jf9037584.

Ping, L., Brosse, N., Chrusciel, L., Navarrete, P., Pizzi, A., 2011. Extraction of condensed tannins from grape pomace for use as wood adhesives. Industrial Crop Production. 33(1), 253-257. http://dx.doi.org/10.1016/j.indcrop.2010.10.007.

RSDI—Regional Spatial Data Infracstructure—2019. Map of Land use. https://rsdi.regione.basilicata.it. Accessed October 11, 2019.

Statuto, D., and Picuno, P., 2016. Analysis of renewable energy and agro-food by-products in a rural landscape: the Energyscapes. *CIGR-AgEng conference.* Aarhus, Denmark. June 26–29.

Statuto, D., Frederiksen, P., Picuno, P., 2018. Valorization of agricultural by-products whithin the "Energyscapes": Renewable energy as driving force in modeling rural landscape. Natural Resources Research. https://doi.org/10.1007/s11053-018-9408-1.

Statuto, D., Bochicchio, M., Sica, C., and Picuno, P., 2018/a. Experimental development of clay bricks reinforced with agricultural by-products. *Symposium "Actual Tasks on Agricultural Engineering."* Opatija, Croatia.

Thorngate, J.H., Singleton, V.L., 1994. Localisation of procyanidins in grape seeds. American Journal Enology Viticolture. 45, 259-262.

Tripathi, A., Ranjan, M.R., 2015. Heavy metal removal from wastewater using low cost adsorbents. Journal Bioremediation Biodegredation. 6(6):1. http://dx.doi.org/10.4172/2155-6199.1000315.

Università Politecnica delle Marche, 2013. *I sottoprodotti agroforestali e industriali a base rinnovabile*. Extravalore - Progetto MiPAAF Bando Settore Bioenergetico DM246/07.

Urbistat-Geomarketing and Market Research. 2019. http://ugeo.urbistat.com. Accessed October 10, 2019.

Versari, A., Castellari, M., Spinabelli, U., Galassi, S., 2001. Recovery of tartaric acid from industrial enological wastes. Journal of Chemical Technology and Biotechnology. 76, 485-488. https://doi.org/10.1002/jctb.412.

Development of a Simulation Model for Macronutrients Concentration Estimation in a Lab-scale Aquaponic System

Maria Aslanidou[a], Evagelia Tsoumalakou[a], Angeliki Elvalidi[a], Efthimia Levizou[a], Elena Mente[b], Nikolaos Katsoulas[a*]

[a] University of Thessaly, Dept. of Agriculture Crop Production and Rural Environment, Fytokou Str., 38446, 8 Volos, Greece
[b] University of Thessaly, Dept. of Ichthyology and Aquatic Environment, Fytokou Str., 38446, 8 Volos, Greece
* Corresponding author. Email: nkatsoul@uth.gr

Abstract

Aquaponics is an innovative, sustainable food production system that integrates fish culture with hydroponic crops cultivation in a closed loop system. Aquaponics has a key role to play in food production since it tackles global challenges such as reduction of energy use, food security and water scarcity. The fluctuation of nutrients in closed loop aquaponic systems depends mainly on fish effluents and plant absorption. In this work, a model to assess nutrient concentrations into a laboratory-scale aquaponic system was developed and validated. The model estimates the concentration of NO_3^-, PO_4^{-2}, NH_4^+, K^+, Ca^{+2} in the different parts of the system (fish tank, plant grow bed). To evaluate the model efficiency, a lab scale aquaponic system was used with a combination of lettuce and tilapia. The water of the fish tank was recirculated constantly from the fish tank to the grow bed and back to the fish tank. Measurements were performed during a cultivation 40 days crop cycle. The model predicted with fair accuracy the nutrient concentrations in the two main parts of the system: before and after the grow bed. The model will be further used as a part of a designing tool for aquaponic systems dimensioning.

Keywords: Decision Support System; model; tilapia; lettuce; circularity

1. Introduction

Aquaponics is an emerging system applied nowadays in the framework of circular economy representing a food production technology that combines aquaculture and hydroponic in an integrated recirculating system without soil (Rakocy et al., 2006). Aquaponics involves a dynamic interaction between fish, plants, bacteria and their aquatic environment (Klinger & Naylor, 2012). Fish feed is inserted in fish tanks, fish waste is filtered, and organic waste metabolites are converted by microbial breakdown into inorganic nutrient elements-food for the plant roots.

In a closed aquaponic system (coupled), the aquaculture effluent flows through the filters, inserts the hydroponic troughs, and the resulted drainage solution is sent back to the fish-rearing tanks for the completely recirculation of the water (Vermeulen & Kamstra, 2013). One of the key drawbacks of such systems, however, is that the improvement of the solution is not possible in terms of the pH, temperature, and nutrient concentrations for the subsystems separately. On the contrary, in a coupled aquaponic set-up, it is feasible to illustrate the level of nutrients in the whole system on any time of the day. There is no more complex set-up that requires greater technical expertise in the management process as the nutrient solution is continuously recirculating between the two components always providing water adequacy to plants and diminishing concerns about water stress.

The integration of a decision support model in aquaponics is the key to maintain a harmonious nutrient exchange cycle for growing plants and fish together. Up to now in most researches in the aquaponic field, the models developed to predict the nutrient accumulation in the aquaponic water, were concerned mostly the nitrogen and phosphorous concentration and how these elements affect eutrophication in the water solution (Adler et al., 2003; Boxman, 2015). The aim of this research was to study the accuracy of a simulation model that was developed in the frame of the FoodOASIS project to predict the concentrations of all the main macronutrients required for plants to grow at a coupled aquaponic system. In the current research is presented the evaluation of the nitrate (NO_3^-), ammonium (NH_4^+), phosphorous (PO_4^{-2}), potassium (K^+) and calcium (Ca^{+2}) elements in the solution imposed and drained from the plants.

2. Materials and Methods

2.1. Experimental set-up and measurements

An experiment was carried out during March and April of 2019 in the laboratory scale aquaponic system of the University of Thessaly located in Volos (Thessaly, Greece). Air temperature and relative humidity were pointed at an average set-point of $20.26 \pm 0.92 \circ C$ and 60.69 ± 3.52 % respectively. The coupled aquaponic system was consisted of the hydroponic and aqua set-up of a ground area equal to 1 m^2 and 400 L respectively.

In the aqua system, a total of 30 Nile tilapia fingerlings were grown in the tank interconnected by polyvinyl chloride (PVC) tubing with the mechanical (barrel filled with glass wool and filter EHEIM) and biological filters (ceramic rings,

15 mm) and finally to the plant grow bed clean and purified. The flow rate of the aqua solution emerged by the clean tank to the grow bed was 264 L h^{-1}, while the entire system contained 625 L of water. An air blower of 70 L h^{-1} capacity (Compressor Hailea, ACO-328) provided air to each rearing tank with eight air diffusers (KW Airstone, 4 inch). Fish were fed with fish feed of crude protein 47.5%, crude ash 10.5%, crude fibres 2%, crude fat 6.5%, moisture 6% (Tetra Tetrabits Complete). About 2% of the total volume of the water was replenished daily by using tap water stored in a 400 L tank. The aquaponic solution was treated with 40 ml of phosphoric acid (H$_3$PO$_4$) 85%, 4 days before the transplantation of plants. The initial set point value of pH was 7.5.

The grow bed was filled with expanded clay. Lettuce plants (*Lactuca sativa* var. Romana) of 15 days-old were transplanted at density of 8 plants m^{-2}. The crop cultivation period lasted 45 days after transplanting (45 DAT). The drainage solution was returned to the fish tank via ebb and flow system. The average values of electrical conductivity pointed at 0.6 ds m^{-1} (SD± 0.09) and pH at 7.04 (SD± 0.2). To evaluate the model, the macronutrients concentration was measured in the lab and the measured values were correlated with the same set of values predicted by the model. The sampling of the solution in the two parts of the system was performed in triplicate once a week (for nitrate, ammonium and phosphorous) and three times per week in triplicate (for potassium and calcium). Samples were filtered (filter net, 7 µm) and analysed with a Flame Photometer (Jenway, model PFP7) [method according to Vainshtein & Lebedev (1961)] in order to estimate their concentration in potassium and calcium. For the concentration in nitrate (NO$_3$$^-$), ammonium (NH$_4$$^+$) and phosphorous (PO$_4$$^{-2}$), a Spectrophotometer (Hach DR3900) (method according to A.P.H.A 2005) was used. A similar protocol was used to estimate the elements content of the tap water in the laboratory in order to define the validation data that correspond to the nutrients inserted in the aquaponic system. For the current simulation, the percentage of feed consumption from fish was defined at 88% and the quantity of the metabolized product at 17%. Additionally, the measured nitrate, ammonium, potassium, and calcium concentration values of the tap water that were estimated around 30.8 mg L^{-1}, 0.09 mg L^{-1}, 3 mg L^{-1} and 32 mg L^{-1} respectively, were added as a constant value in the model (see Cw in the model set-up).

The comparison between the experimental values and the simulated by the model was performed by the one-way ANOVA method with 95% confidence level (p ≤ 0.05) using SPSS Statistical Package for the Social Sciences, IBM, Armonk, NY , USA). In addition, a linear correlation was applied between the model values and those obtained from the laboratory analysis to define the significance of the determination coefficient.

2.2. Model set-up

A series of algorithms simulating the concentration of nutrients in the main parts of the system were used to compose the model. Firstly, the model considers the main sources of nutrients in the system which are fish feed, tap water and the metabolized products in the fish tank. The quantity of metabolized product and the percentage of feed consumption were inserted according to Montanhini Neto & Ostrensky (2015). Nitrate and ammonium are elements directly connected with the presence of biological filter. The equation developed to estimate their concentration in the fish tank is presented in Eq. (1):

$$C_{input\ NO_3} = \frac{EsC \times PW \times CF \times Pc \times C \times (1-a) \times 1.21589 \times b \times c}{Vst + CW + Cdr} \qquad (1)$$

where EsC represents the quantity of the metabolized product (%) in the fish tanks, CF the quantity of fish feed (g), PW the percentage of feed consumption (%), Pc the content of fish feed in the studied nutrient (mg g^{-1}), C the coefficient for the conversion of protein to nitrogen, a the molar fraction of ammonia, b the ratio of the molecular weight of ammonia to nitrate's resulting from the oxidative reaction, c the efficiency of the filter (%), Cw the concentration of the element resulting from the addition of tap water to the system (mg L^{-1}), Vst the total volume of aquaculture solution (L) and Cdr the concentration of the element in the drainage solution (mg L^{-1}).

Phosphorous, potassium and calcium are macronutrients that their concentration is not affected by the presence of the biological filter. The equation that expresses their concentration in the fish tank and at the same time their concentration at the entrance of the grow bed is described in the Eq. (2):

$$C_{input} = \frac{EsC \times PW \times CF \times PS}{Vst + CW + Cdr} \qquad (2)$$

To start the simulation process, the initial values of the concentrations were given. The model used the first input to run the algorithms in order to predict the evolution of the nutrient's concentration on time. Then the concentration of the nutrients in the drainage solution was calculated by Eq. (3):

$$C_{dr} = \frac{A_{input} \times V_{st} - (d \times C_{dr}{}^{\wedge e})}{V_{dr}} \tag{3}$$

where d and e are the coefficients related to the vegetative stage of the crop and are calculated through the analysis of linear regression, Vdr is the volume of drainage solution (L), Ainput is the quantity of nutrient in the irrigation solution (mg) and Vbr is the volume of water absorbed by the plants. The crop coefficients (d, e) as calculated from the current experiment through the analysis of linear regression refers to 1.83 and 0.037 for nitrate, ammonium and phosphorous absorption -19.96 and 294.65 for potassium and 18.83 and -3.31 respectively. The coefficients for nitrate, ammonium and phosphorous, were similar to those mentioned in the literature (Savvas et al., 2005). For the coefficients that corresponds to potassium and calcium, the concentrations of nutrients in the grow bed and drainage solution were analysed weekly and correlated with the volume of water imposed and drained respectively to define the absorbed nutrient concentration (mg L^{-1}). The coefficients d and e were estimated by the linear regression between the concentration of the nutrient in the irrigation solution and the absorption concentration.

3. Results and Discussion

Potassium presented a decreasing trend in the entrance of the grow bed and in the drainage solution during the experimental period. The initial concentration of the potassium inserted in the model was 10.43 mg L^{-1} and reached 6.3 mg L^{-1} at the end of the experiment. Similarly, the potassium was reduced from 11 mg L^{-1} to 6.42 mg L^{-1} in the drainage solution. The simulated values of the element's concentration demonstrated a similar pattern to the measured one with some discrepancies. The evolution of the simulated and measured data of the aquaculture and drainage solution is presented in Figure 1 (a). The prediction accuracy of the potassium concentration values in the drainage solution was also high since the data followed the same trend. When plotting the predicted vs. actual values, a strong linear relationship was found while the determination coefficient (R^2) of the mentioned regression was found to be equal to 0.92 in both aquaculture and drainage solution, respectively (p<0.05). As confirmed by many researchers (Graber & Junge, 2009; Seawright et al., 1998), fish food does not obtain the appropriate content of potassium and calcium to contribute to abundant values for plant nutrition. For this reason, the main parameter determining the course of these elements is the concentration in the tap water and the absorption of plants. Tap water contains higher concentration of calcium than potassium according to laboratory analysis. Furthermore, lettuce plants absorb high quantity of potassium especially in the end of their biological cycle. The high decrease rate of potassium from lettuce plants is in agreement with Goddek et al. (2016), where the initial concentration of the element was 5 mg L^{-1} and the final (after 35 days) 0.5 mg L^{-1}. As far as the calcium trend is concerned, it is in common the accumulation of the element in aquaponic systems (Delaide, 2017).
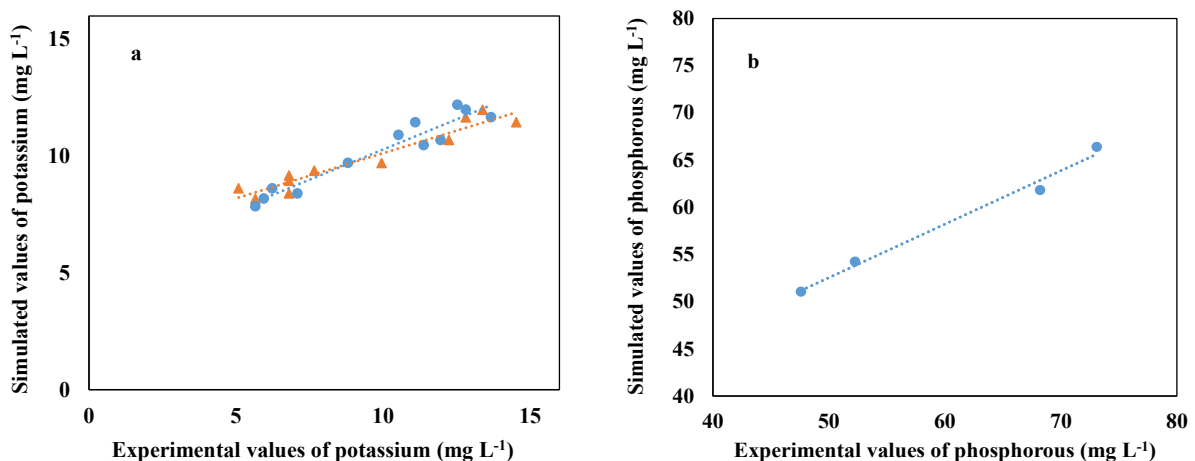
Figure 1. Linear regression between (a) the measured and simulated potassium concentration values in grow bed solution (blue circle) (y = 0.386 x – 6.27) and in the drainage solution (orange triangle) (y = 0.518 x + 5.10), (b) the measured phosphorous concentration values and the simulated in grow bed solution (y = -0.49 x + 84.84).

Similar to the potassium, the phosphorous element performed a decreasing trend in the recirculating system during the experimental period in the drainage solution. The initial concentration of phosphorous measured in the grow bed solution was 66.23 mg L^{-1} and reached 73.97 mg L^{-1} at the end of the experiment. In the drainage solution, the

concentration fluctuated from initial value of 73.11 mg L^{-1}, reduced to 54.24 mg L^{-1} (DAT 21) and finally decreased to 48.17 mg L^{-1} (DAT 35). The results of the linear correlation between the simulated and the measured values demonstrated R^2 of 0.99 for the drainage solution. The evolution of the simulated and measured data of the drainage solution is presented in Figure 1 (b). The prediction accuracy of phosphorous concentration values in the drainage solution was higher than in the grow bed solution. That is highlighted by the distinct difference between the actual and the predicted values occurred from DAT 21 until DAT 35, with the measured value being raised up to 73.97 mg L^{-1} and the simulated value decreased to 48.17 mg L^{-1}. The results of the linear correlation between the simulated and the measured values of the grow bed solution was low R^2 of 0.24 and therefore is not presented in the current research. Mainly, phosphorous presents many fluctuations in an aquaponic system. It is known that in an aqueous solution the presence of calcium (Ca^{+2}) macronutrient and dihydrogen phosphate (H$_2$PO$_4$) can lead to the precipitation reaction with the creation of tricalcium diphosphate (Ca$_3$(PO$_4$)$_2$) and tetracalcium hydrogen triphosphate (Ca$_4$H(PO$_4$)^3) (De Rijck & Schrevens, 2001). Deun and Dyck (2008) noticed the exchanging capacity of the expanded clay in a research on nitrate, ammonium and phosphorous by three different species of expanded clay. Nevertheless, there are other physicochemical parameters as well, determining the course of nutrients in the aquaculture system. Barak et al. (2003) refers that 60–83% of phosphorous not remained in fish tissue will be lost in fish faces. The more increasing course of the element in the grow bed solution may is related with its presence in the mechanical filter by the mineralization of the fish faces. Consequently, to improve the prediction accuracy of the simulation model, the above activities should be adjusted.

Nitrate followed increasing trend in both grow bed and drainage solution. The initial values were 35.94 mg L^{-1} and 46.87 mg L^{-1} while the final 198.02 mg L^{-1} and 165.99 mg L^{-1} respectively. The correlation between the simulated and measured data of the aquaculture and drainage solution is presented in Figure 2 (a). The mean increase rate of the actual values in the grow bed solution was 5 mg L^{-1} day^{-1}. Nitrate and ammonium are closely affected by the bacteria colony in the aquaponic system. The smaller increase rate of nitrate may be due to the inaccurate simulation of the oxidation ability of the biological filter or to the higher prediction of nitrate absorption from plants. Boxman et al. (2018) highlighted that the presence of plants (Halophytes species) contribute to removal rate of 9.4 ± 11 g N day^{-1}, quantity much higher from the simulated one referring to 0.09 g N day^{-1}.

The measured concentration of calcium in the aquaponic solution was 10.97 mg L^{-1} during the first experimental day raising to 26.54 mg L^{-1} at the end. The same trend followed the element in the drainage solution increasing from 11.96 mg L^{-1} to 26.54 mg L^{-1}. The correlation between measured and simulated values of calcium concentration are presented in Figure 2 (b). The results of the linear correlation between the simulated and the measured values demonstrated R^2 of 0.93 for the grow bed solution and R^2 of 0.91 for the drainage solution.
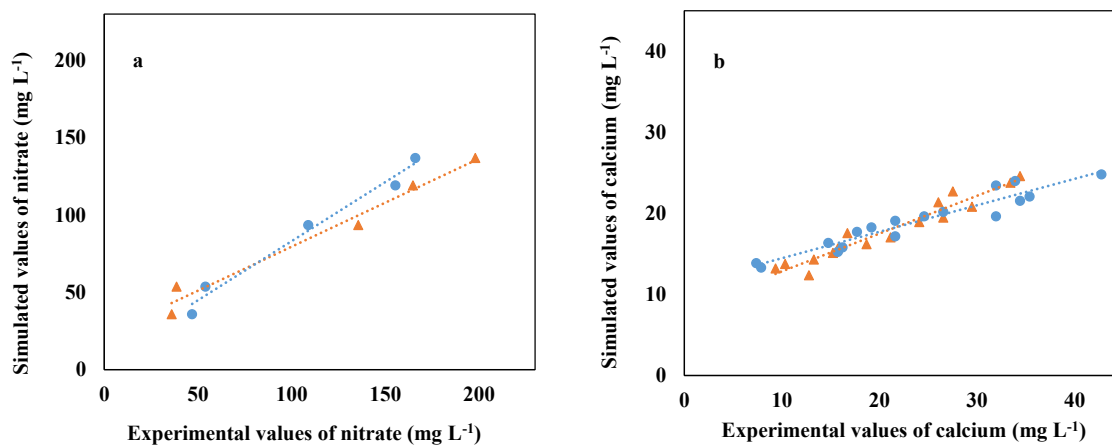
Figure 2. Correlation between (a) the measured and the simulated nitrate concentration values in the grow bed solution (blue circle) (y = 0.569 x + 22.56, R^2= 0.97) and in the drainage solution (orange triangle) (y = 0.763 x + 6.69, R^2= 0.98), (b) the measurable calcium concentration values and the simulated in grow bed solution (blue circle) (y = 0.465 x + 8.19, R^2= 0.93) and in the drainage solution (orange triangle) (y = 0.326 x + 11.19, R^2=0.91).

Ammonium had mainly an increasing trend but there were fluctuations during the experimental period. Nevertheless, the model estimated the increasing rhythm with high accuracy at 0.0045 mg L^{-1} day^{-1}. The initial concentration of ammonium measured in grow bed solution was 0.075 mg L^{-1} and reached 0.125 mg L^{-1} at the end of the experiment. The results of the linear correlation between the simulated and the measured values demonstrated R^2 of 0.98 for the grow bed solution. The corelation between the simulated and measured data in the grow bed solution is presented in Figure 3.
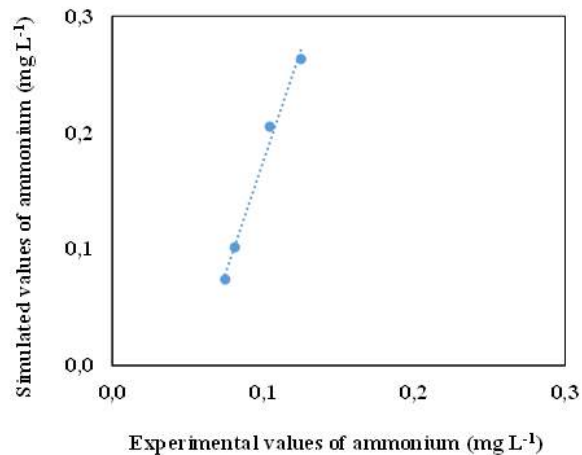
Figure 3. Correlation between measured and simulated ammonium concentration values in grow bed solution (y = 3.067 x – 0.12, R^2 = 0.98).

The model, however, performed a great ability to predict the increasing or decreasing trends of the macronutrients in the recirculating aquaponic system in the grow bed and the drainage solution as well. This result comes from the accurate input of constants and variable values during the experimental period illustrating the main parameters concerning the water and nutrient balances. The upward trend of some elements such as nitrate and calcium indicate the ability of the system to grow more plants until the completely removal of the elements as resulted in the case of potassium (Goddek, 2017). On the contrary the decreasing trend of potassium and phosphorous consists of a restrictive factor for the implementation of more plants in the system.

4. Conclusions

The simulation model tested in this study was efficient in estimating the concentration of nitrate, ammonium, phosphorous, potassium and calcium in the grow bed and the drainage solution. The oxidation ability of the biological filter, the precipitation of phosphorous and the exchangeable ability of expanded clay are parameters that can be improved or inserted in the simulation model, respectively. The model has the flexibility to run for other macronutrients (e.g. magnesium) and scales (e.g. pilot) or types (e.g. decoupled) of aquaponic systems, raising the expectations for the development of a multi-applied simulation model for the best design and management of aquaponic systems.

References

Adler, P. R., Summerfelt, S. T., Glenn, D. M., & Takeda, F. (2003). Mechanistic approach to phytoremediation of water. *Ecological Engineering*, *20*(3), 251–264. https://doi.org/10.1016/S0925-8574(03)00044-2

Barak, Y., Cytryn, E., Gelfand, I., Krom, M., & Van Rijn, J. (2003). Phosphorus removal in a marine prototype, recirculating aquaculture system. *Aquaculture*, *220*(1–4), 313–326. https://doi.org/10.1016/S0044-8486(02)00342-3

Boxman, S E. (2015). Resource Recovery through Halophyte Production in Marine Aquaponics: an Evaluation of the Nutrient Cycling and the Environmental Sustainability of Aquaponics. *Resource Recovery through Halophyte Production in Marine Aquaponics: An Evaluation of the Nutrient Cycling and the Environmental Sustainability of Aquaponics*, *November*, 234 pp-234 pp. http://scholarcommons.usf.edu/etd%5Cnhttp://scholarcommons.usf.edu/etd/5915

Boxman, Suzanne E., Nystrom, M., Ergas, S. J., Main, K. L., & Trotz, M. A. (2018). Evaluation of water treatment capacity, nutrient cycling, and biomass production in a marine aquaponic system. *Ecological Engineering*, *120*(June 2017), 299–310. https://doi.org/10.1016/j.ecoleng.2018.06.003

De Rijck, G., & Schrevens, E. (2001). Methodology to simultaneously optimize the macrocation and the macroanion composition of nutrient solutions, using mixture theory. *Journal of Agricultural and Engineering Research*, *78*(1), 89–

97. https://doi.org/10.1006/jaer.2000.0627

Delaide, B. (2017). *A study on the mineral elements available in aquaponics, their impact on lettuce productivity and the potential improvement of their availability*. UNIVERSITÉ DE LIÈGE – GEMBLOUX AGRO-BIO TECH.

Deun, R. Van, Dyck, M. Van, & Kempen, K. H. (2008). *Expanded clay and lava rock as potential filter media for nutrient removal in vertical subsurface flow constructed wetlands Introduction Lightweight Expanded Clay Aggregates : Literature Æ possible P-removal*. July.

Goddek, S. (2017). *Opportunities and Challenges of Multi-Loop Aquaponic Systems* (Issue November). https://doi.org/10.18174/412236

Goddek, S., Schmautz, Z., Scott, B., Delaide, B., Keesman, K. J., Wuertz, S., & Junge, R. (2016). The effect of anaerobic and aerobic fish sludge supernatant on hydroponic lettuce. *Agronomy*, *6*(2), 1–12. https://doi.org/10.3390/agronomy6020037

Graber, A., & Junge, R. (2009). Aquaponic Systems: Nutrient recycling from fish wastewater by vegetable production. *Desalination*, *246*(1–3), 147–156. https://doi.org/10.1016/j.desal.2008.03.048

Klinger, D., & Naylor, R. (2012). Searching for Solutions in Aquaculture: Charting a Sustainable Course. *Annual Review of Environment and Resources*, *37*(1), 247–276. https://doi.org/10.1146/annurev-environ-021111-161531

Montanhini Neto, R., & Ostrensky, A. (2015). Nutrient load estimation in the waste of Nile tilapia Oreochromis niloticus (L.) reared in cages in tropical climate conditions. *Aquaculture Research*, *46*(6), 1309–1322. https://doi.org/10.1111/are.12280

Rakocy, J. E., Masser, M. P., & Losordo, T. M. (2006). Aquaculture tank production systems. *SRAC No. 454*, *451*(452), 18–31. https://doi.org/10.1080/1025386032000168294

Savvas, D., Meletiou, G., Margariti, S., Tsirogiannis, I., & Kotsiras, A. (2005). Modeling the relationship between water uptake by cucumber and NaCl accumulation in a closed hydroponic system. *HortScience*, *40*(3), 802–807. https://doi.org/10.21273/hortsci.40.3.802

Vainshtein, E. E., & Lebedev, V. I. (1961). New determinations of Li, Na, K, Rb, Cs, Ca, and Sr in standards W-1 and G-1 by flame photometry. Geochemistry, 386-388.

Vermeulen, T., & Kamstra, A. (2013). The need for systems design for robust aquaponic systems in the urban environment. *Acta Horticulturae*, *1004*, 71–78. https://doi.org/10.17660/actahortic.2013.1004.6

Potential of Slurry from Intensive Dairy Cattle Farms for *Paulownia* and *Populus* Trees, as Organic Fertilizer: I. Effect on Production

Menino, R.[a],*, Pereira, S.I.A.[b], Moreira, H.[b], Castelo-Branco, A.[a], Gomes, A.A.[a], Rodrigues, A.[a], Cunha, J.[b], Castro, P.M.L.[b], Vega, A.[b], Cardoso, E.[b], Machado, M.J.[c], Alves, R.[d], Cardoso, F.[e], Lopes, F.[e], Guedes, R.[c]

[a] UEIS Sistemas Agrários e Florestais e Sanidade Vegetal-Laboratório de Solos, Plantas e Águas, Instituto Nacional de Investigação Agrária e Veterinária, I.P. (INIAV), Av. da República, Quinta do Marquês, 2780-159 Oeiras, Portugal

[b] Universidade Católica Portuguesa, Centro de Biotecnologia e Química Fina – Laboratório Associado, Esc. Sup. de Biotecnologia

[c] Aveleda S.A.

[d] Forestis – Associação Florestal de Portugal

[e] Fenalac - Federação Nacional das Cooperativas de Produtores de Leite

*Corresponding author. Email: regina.menino@iniav.pt

Abstract

Intensive dairy cattle breeding have a relevant social and economic impact in Portugal, particularly in the northern region. This activity generates a high flow of livestock effluents (slurry), rich in important nutrients for plant growth, which can be introduced into forest production systems. These effluents can provide a good alternative to mineral fertilizers, not only from an economic perspective, but also from the point of view of soil fertility resilience. In the present study, the effect of increasing doses of slurry on tree growth was evaluated in clones of *Paulownia* and *Populus*, as they are genotypes that have a high efficiency in the mobilization of soil nutrients and in the capture of CO_2 from the atmosphere, as well as high biomass calorific value. To this end, a demonstration field was installed, where the trees were planted with the compasses of: 2.5 x 1.5 m and 2.5 x 0.75 m, respectively for *Paulownia* and for *Populus*. In the field, the following treatments were performed: T0 - no fertilization, either mineral or organic; T1 - amount of slurry equivalent to 85 kg of N ha^{-1}; T2 - amount of slurry equivalent to 170 kg of N ha^{-1}; T3 - amount of slurry equivalent to 340 kg of N ha^{-1}, either with or without inoculation prior to transplantation, with mycorrhizal arbuscular fungi and plant growth-promoting bacteria. Results evidenced a positive effect of the slurry application, both in the diameter at breast height and in total stand height, showing its fertilizing potential which should later be assessed on the ability to constitute an alternative or, simply, a complement to mineral fertilization.

Keywords: bovine slurry, organic fertilization, *Paulownia* CoT2, *Populus* i214

1. Introduction

Intensive dairy cattle breeding have a relevant social and economic impact in Portugal, particularly in the northern region. This activity generates a high flow of livestock effluents (slurry), rich in important nutrients for plant growth, which can be introduced into forest production systems. These effluents can provide a good alternative to mineral fertilizers, not only from an economic perspective, but also from the point of view of soil fertility resilience.

In fact, these effluents have high levels of macronutrients, such as nitrogen (N), phosphorus (P) and potassium (K), and micronutrients, such as copper (Cu) and zinc (Zn), constituting a valuable resource as an organic fertilizer for soils, increasing its content in organic matter (OM) and available nutrients, while improving its structure. Therefore, the use of slurry as an alternative (or even just as a complement) to mineral fertilization, in agroforestry exploration systems, could be an adequate means of recycling a free polluting product, and avoid, or at least reduce, the use of expensive mineral fertilizers.

However uncontrolled deposition of high amounts of slurry in the soil, as with mineral fertilizers, increases the risk of contamination of surface and groundwater with nitrates, and the ammoniacal formulation of N may also represent a significant environmental risk, due to the volatilisation of ammonia and other compounds that contribute to the aggravation of the greenhouse effect.

All these drawbacks may be true for most organic fertilizers, when managed incorrectly, but it is much more likely for mineral fertilizers, as the N in the former is mostly in the organic formulation and the remaining formulations are slowly leached out by the mineralization process in the soils, as the roots will progressively absorb them physiologically, thus reducing the opportunity for leaching to the ground waters of the more soluble nitric formulations and, likewise, reducing the possibility of ammonia volatilisation to the atmosphere.

Thus, it is of utmost relevance to optimise the fertilizer dosage. To solve this conundrum, the adequate selection of the genotypes of forest species to be used and the adequate fertilizer inputs are the most crucial factors.

As stated by Evangelou *et al*. (2012), "from the environmental point of view, fast-growing tree biomass production

replaces non-renewable carbon materials and promotes carbon sequestration and other ecosystem services, such as improvement of soil and water quality, reduction of erosion and increase of biodiversity".

Species like *Paulownia* and *Populus*, are known as fast growing species, suitable for phytoremediation and for the recovery of polluted soils (Macci *et al*., 2013; Macci *et al*., 2016). In a study, carried out by Madejón *et al*. (2016), also working with *Paulownia* and *Populus*, using organic compost to avoid soil fertility loss and to increase biomass production, the researchers concluded that the addition of organic composts to this type of "intensive crops" could be part of the solution of the "waste" disposal, solving the problem of loss of soil fertility as well as production of relevant biomass in marginal soils.

Particularly, with regard to *Paulownia*, the high forage potential of its leaves, which can be used as a source of nutrient-rich food for cattle, allows to complete a cycle of remarkable interest, in a perspective of "circular economy" and, in this way, contribute to a better economic performance of dairy companies.

As far as the poplar is concerned, as it is a silvicultural species of rapid growth that has long been cultivated in Portugal, its choice provides the appropriate reference for measuring the capacity of interaction with organic fertilizers.

In the present report, the effect on tree growth of increasing doses of slurry, either with or without mycorrhizal arbuscular fungi and plant growth-promoting bacteria inoculation, was observed over the first two years (2020 and 2021) after transplanting from nursery to field, of an experimental demonstration forest field, in clones of *Paulownia* and *Populus*.

2. Materials and Methods

The experimental demonstration forest field, occupying an area of 14,607 m^2, was installed in 2019 in the region of Penafiel (North of Portugal) in a compact soil, derived from granites, which are prone to waterlogging during the autumn and winter periods and characterized by a low internal drainage capacity. For this reason, it was necessary to remove the top layer (to a depth of about 50 cm), install a drainage pipe system, cover with a gravel layer of about 20 cm, and top with the previously removed soil.

A sample of the resulting Anthrosol - according with FAO classification (IUSS-FAO, 2006) - was analysed for selected properties, according to the methods used routinely in the laboratories of the "National Research Institute of Agriculture and Veterinary", in Oeiras (Portugal), presenting the following physicochemical characteristics:

- Texture sandy-loam;
- pH (H_2O) 6.4 slightly acid
- organic matter 17.6 $g\ kg^{-1}$ medium level;
- N Kjeldhal 0.9 $g\ kg^{-1}$ medium level;
- P_2O_5 (extractable) 54.1 $mg\ kg^{-1}$ medium level;
- K_2O (extractable) 131 $mg\ kg^{-1}$ high level.

The trees were planted with the compasses of: 2.5 x 1.5 m and 2.5 x 0.75 m, respectively, for *Paulownia* CoT2 (*Paulownia elongata* x *Paulownia fortunei*), and for poplar i214 clones (*Populus deltoides* x *Populus nigra* [*Populus* x *euramericana* (Dode) Guinier]).

Prior to transplantation to the field, and as a complement to the main purpose of this demonstration display, some plants were inoculated with mycorrhizal arbuscular fungi (MAF) and plant growth-promoting bacteria (PGPB), which, associated with trees, are supposed to enhance a greater supply of nutrients and a greater resistance to diseases, preparing them for transplantation and healthier establishment.

The cattle slurry used on the experimental display was chemically analysed, each year after transplantation (2020 and 2021), for N (for the calculation of the quantities to be applied in each treatment) as well as for the main characteristics considered in the EU legislation, and the results were the following:

- Moisture 97% 96% EN 13040:2007
- Dry matter 3.3% 4.0% Calculation by weight difference
- pH(H_2O) (25°C) 7.7 7.2 EN 13037:2011
- Electric conductivity (25°C) 17.5 mS/cm 16.6mS/cm EN 13038:2011
- Total nitrogen (N) 3260 $mg\ L^{-1}$ 3124 $mg\ L^{-1}$ Bremner & Mulvaney, 1982
- Organic matter 2% 3% EN 13039:2011
- Total phosphorus (P_2O_5) 0.07% 0.09% EN 13650:2001
- Total potassium (K_2O) 0.17% 0.16% EN 13650:2001
- Total calcium (CaO) 0.20% 0.17% EN 13650:2001

- Total magnesium (MgO)   0.08%   0.07%   EN 13650:2001
- Total boron (B   0.93 mg kg^{-1} 0.85 mg kg^{-1} EN 13650:2001
- Total sodium (Na)   0.09%   0.05%   EN 13650:2001
- Chlorine (Cl^{-})   0.20%   0.07%   PE-117-LQARS/LAF (Ed. nº1)
- Total copper (Cu)   2.33 mg kg^{-1} 2.86 mg kg^{-1} EN 13650:2001
- Total zinc (Zn)   12.1 mg kg^{-1} 16.7 mg kg^{-1} EN 13650:2001
- Total nickel (Ni)   <33.3 mg kg^{-1} <33.3 mg kg^{-1} EN 13650:2001
- Total chromium (Cr)   <16.6 mg kg^{-1} <16.6 mg kg^{-1} EN 13650:2001
- Total lead (Pb)   <33.3 mg kg^{-1} <33.3 mg kg^{-1} EN 13650:2001

In the field, the following treatments were performed: T0 - without slurry application; T1 - quantity of slurry in order to supply 85 kg of N ha^{-1}; T2 - quantity of slurry in order to supply 170 kg of N ha^{-1}; T3 - quantity of slurry in order to supply 340 kg of N ha^{-1}; all of them with and without inoculation. Slurry application was done, in continuous bands, three times throughout the year, namely in spring, summer and autumn.

The treatments without inoculation were included in blocks with eight plots with nine trees each. The treatments with inoculation were included in blocks with eight plots with six trees each.

Biometric data for diameter at breast height (DBH) and trees total height (TH) were recorded for all trees in all plots, in order to assess the Growth Increase (GI) for each treatment. For that purpose, the measures registered in 2021 were subtracted from the measures registered in the previous year to evaluate the increments that resulted for each treatment.

The experimental data were analyzed for variance by the General Linear Model and means separation was performed using Tukey's Honestly Significant Difference test at $p \leq 0.05$.

3. Results and Discussion

The average GI recorded for both species in the treatments without inoculation were as shown in Table 1, with values that can justify the following considerations:

With regard to DBH, the treatments with slurry, in both species, always showed a higher value than those recorded for the treatments without slurry, although only by a statistically significant margin for treatment T1, in the case of *Paulownia*, and for treatments T2 and T3, in the case of poplar.

This is also true for the data recorded for TH in the case of *Paulownia*. In the case of poplar, the effect of fertilizer only becomes significant in the T3 treatment, although here in an exuberant way.

Although not significant, the pattern of response to fertilizer for the two species under consideration was the opposite, being decreasing in the case of *Paulownia* and increasing in the case of poplar.

Table 1. Mean values for *Paulownia* and *Populus* GI, from 2020 to 2021, with respect to DBH and TH of trees, for each treatment without mycorrhizal inoculation

Treatment	DBH (cm)	TH (m)
Paulownia T0	1.79 c	1.47 d
Paulownia T1	2.79 ab	2.47 c
Paulownia T2	2.50 abc	1.83 cd
Paulownia T3	2.23 abc	1.28 d
Populus T0	2.07 bc	2.50 bc
Populus T1	2.23 bc	2.46 c
Populus T2	2.59 ab	2.70 c
Populus T3	2.91 a	3.52 a

Means in the same column with the same small letter do not differ significantly (p≤0.05), as judged by the Tukey test.

It seems, therefore, legitimate to conclude that, under the present experimental conditions, while *Pawlownia* reacts to slurry fertilization at lower doses and does not benefit from higher doses of the fertilizer, the poplar needs successively higher doses, which is not fully in agreement with what has been verified by Ceotto *et al.* (2016) who, in their research on the effects of cattle slurry on poplar, conclude that this species had a poor nitrogen (N) use efficiency.

Despite only evidenced in the significance of the data recorded in the TH for the T0 treatment of both species, there

was a significantly more positive performance of the poplar. This fact is in line with what is generally recognized. Nevertheless, Macci *et al*. (2016) found lowest growth for *Paulownia*, when compared to *Populus*, although these authors recognise that in their study the "environmental conditions" were not adequate, or the best, for this species, as it is the case in the present study.

Even though the land had been worked to increase its internal drainage, this proved insufficient, as the climatic conditions during the experimental period were not the most favourable for Paulownia. As Berdón *et al*. (2017) concluded, after studying several clones of *Paulownia*, this species demands conditions of well drained soils, with good aeration, not clayey. This is particularly noticeable in the results verified in the experimental set-up for evaluating the effect of inoculation in GI, since its location was much more unfavourable as far as waterlogging was concerned.

On the contrary the poplar, being a riparian species, is better equipped to face situations of excess water, which can be seen in the data for both parameters recorded in table 2.

Table 2. Mean values for *Paulownia* and *Populus* GI, from 2020 to 2021, with respect to the DBH and TH of trees, for each treatment of increasing rates of slurry land use, with mycorrhizal inoculation

Treatment	DBH (cm)	TH (m)
Paulownia mycorrhized T0	1.14 bc	0.68 b
Paulownia mycorrhized T1	0.76 c	0.50 b
Paulownia mycorrhized T2	1.78 ab	2.86 a
Paulownia mycorrhized T3	1.88 ab	2.87 a
Populus mycorrhized T0	2.40 a	2.82 a
Populus mycorrhized T1	2.22 a	3.00 a
Populus mycorrhized T2	2.41 a	2.73 a
Populus mycorrhized T3	2.48 a	3.10 a

Means in the same column with the same small letter do not differ significantly ($p \leq 0.05$), as judged by the Tukey test.

As can be seen in this last table, no significant differences were recorded for both parameters measured for the poplar. This was not the case for *Paulownia* where significant differences, with regard to the data recorded for both parameters, showed significant differences. Here the DBH recorded for T1, although by a non-significant margin, was lower than that for T0 itself, differing from the other treatments by a significant margin. As far as trees TH is concerned, in addition to a relationship between T1 and T0 identical to that for DBH, the differentiation for the more generous slurry endowment treatments was significant; in this case the pattern of response to slurry application was opposite to that seen in the treatments without inoculation, with conspicuously and significantly higher values for treatments T2 and T3.

Given the soil and climatic conditions prevailing during the two years of the trial, the data verified for the trial with inoculation of MAF and PGPB are inconclusive.

4. Conclusions

Concerning the main hypothesis that justified the present study, the results revealed a significant and positive effect of the slurry application, either in the diameter at breast height (DBH) or in the total stand height, showing the high fertilizing potential of this organic compost and, thus, providing an alternative to chemical fertilization and to uncontrolled disposal of highly polluting waste.

Under the present experimental conditions, while *Pawlownia* reacted to slurry fertilization at lower doses and does not benefit from higher doses of the fertilizer, poplar showed an opposite pattern, with a positive response to increasing slurry inputs.

Acknowledgements

References

Berdón J.B., A.J.M. Calvo, L.R. Barroso, P.A.I. Alcobendas, J.G. Cortés, 2017. Study of Paulownia's Biomass Production in Mérida (Badajoz), Southwestern Spain. Environment and Ecology Research. 5 (7), 521-527. DOI: 10.13189/eer.2017.050709.

Bremner, J.M., and C.S. Mulvaney, 1982. Nitrogen-Total. In Methods of soil analysis. Part 2. Chemical and microbiological properties. 2nd ed. (Agronomy 9). American Society of Agronomy, Soil Science Society of America, Madison, Wisconsin. Eds., Page A.L., R.H. Miller and D.R. Keeney. 595-624.

Ceotto, E., F. Castelli, A. Moschella, M. Diozzi, M. Di Candilo, 2016. Poplar short rotation coppice is not a first choice crop for cattle slurry fertilization: Biomass yield and nitrogen-use efficiency. Industrial Crops and Products. 85, 167-173. https://doi.org/10.1016/j.indcrop.2016.02.042.

Evangelou, M.W.H., H.M. Conesa, B.H. Robinson, R. Schulin, 2012. Biomass production on trace elemente contaminated land: a review. Environ. Eng. Sci. 29 (9), 823-839. https://doi.org/10.1089/ees.2011.0428.

IUSS Working Group WRB, (2006): World reference base for soil resources 2006 - A framework for international classification, correlation and communication, Rome, Food and Agriculture Organization of the United Nations. 10013/epic.43321.d001

Macci, C., E. Peruzzi, S. Doni, G. Poggio, G. Masciandaro, 2016. The phytoremediation of an organic and inorganic polluted soil: A real scale experience. International Journal of Phytoremediation. 18 (4), 378-386, DOI: 10.1080/15226514.2015.1109595. http://dx.doi.org/10.1080/15226514.2015.1109595.

Macci, C., S. Doni, E. Peruzzi, S. Bardella, G. Filippis, B. Ceccanti, G. Masciandaro, 2013. A real-scale soil phytoremediation. Biodegradation. 24 (4), 521–538. doi:10.1007/s10532-012-9608-z.

Madejón, P., J. Alaejos, J. García-Álbala, M. Fernández, E. Madejón, 2016. Three-year study of fast-growing trees in degraded soils amended with composts: Effects on soil fertility and productivity. Journal of Environmental Management. 169, 18-26. https://doi.org/10.1016/j.jenvman.2015.11.050.

Quaye, A.K., T.A. Volk, S. Hafner, D.J. Leopold, C. Schirmer, 2011. Impacts of paper sludge and manure on soil and biomass production of willow. Biomass and Bioenergy. 35 (7), 2796-2806. https://doi.org/10.1016/j.biombioe.2011.03.008.

Plastics in Agriculture - the Problem and One Potential Solution

Barbara Tita [a], Ana Ilhéu [a], Teresa Batista [b,c], Luis Metrogos [c], Isabel Pestana da Paixão Cansado *[,b,d], Paulo Alexandre Mira Mourão [b], João Manuel Valente Nabais [e], José Castanheiro [b], Cátia Borges [f], Gilda Matos [f]

[a] Empresa de Desenvolvimento e Infraestruturas de Alqueva (EDIA, SA), Departamento de Ambiente e Ordenamento do Território – Rua Zeca Afonso, n.º 2, 7800-522, Beja, Portugal

[b] MED - Instituto Mediterrâneo para a Agricultura, Ambiente e Desenvolvimento, IIFA, Universidade de Évora, Pólo da Mitra, Apartado 94,7006-554 Évora – Portugal

[c] Comunidade Intermunicipal do Alentejo Central, rua 24 de Julho, nº1 7000-673, Évora, Portugal

[d] LAQV-REQUIMTE, Instituto de Investigação e Formação Avançada, and Departamento de Química, Escola de Ciências e Tecnologia, Universidade de Évora, Colégio Luís António Verney, 7000-671, Évora, Portugal

[e] Comprehensive Health Research Center (CHRC), Departamento de Ciências Médicas e da Saúde, Escola da Saúde e Desenvolvimento Humano, Universidade de Évora, Rua Romão Ramalho, 56, 7000-671, Évora, Portugal

[f] Gesamb – Gestão Ambiental e de Resíduos, EIM, Estrada das Alcáçovas, EN 380, 7000-175, Évora, Portugal

* Corresponding author. Email: ippc@uevora.pt

Abstract

For years, increased agricultural production and food quality has forced the increasing use of plastics in various activities. Currently, the plastic waste that results from the agricultural activity is recycled outside Portugal which increases the ecological footprint associated with the life cycle of these materials. It is crucial to consider new models for their valorisation at a local and regional level and in a circular economy perspective.

In the scope of the Placarvões project (from plastic waste to activated carbons) it was elaborate the study of the types and quantities of plastics used in one of the biggest irrigated areas in Portugal, the Alqueva dam irrigation area. The methodology establishes a reference plot of 700 x 700 meters (49 ha) with is 90% irrigated land and details, for each crop, the types of plastic used throughout the culture cycle. Currently, the agricultural plastic volume in the Alqueva irrigation area is 1.880 tons per year, and with the expected growth of the irrigated area, it can reach 3.500 tons per year. Plastic are the plant protectors with the greatest influence, 56% in the total, followed by the plastic film. These 2 types of plastic represent about 85%. The crops that use most plastic are intensive olive groves, almond (plant protectors) and table grapes (plastic film) and represents more than 91% of the total plastic wastes of the area agricultural. Alentejo cannot afford not to value some waste, thus transforming it into valuable materials that allow increasing regional yields.

The Placarvões solution involves the production of activated carbons from plastic wastes derived from agriculture, disposable plastics and the fraction rest that results from the mechanical/biological treatment of municipal solid wastes (CDR). The activated carbons were produced by physical and chemical activation. The activated carbons were tested as adsorbents for the removal of 2,4-D and MCPA from a liquid phase. This solution may be applicable in the water waste treatment in the region, contributing to the circular economy in the territory.

Keywords: Placarvões, circular economy, agriculture by-products, Alentejo, Alqueva

1. Introduction

The increase in the world's population has led man to improve farming practices to increase agriculture productivity. This was firstly achieved through the exploitation of natural resources such as water and plant resources and the excessive use of fertilizers and pesticides. On the other way, for crops protection and yield increase, the use of containers, screens, sticks and plastic greenhouses has become a routine.

The excessive use of plastics in the various stages of cultivation threatens the overall sustainability of our agricultural soils and aquatic environments, due to the plastic waste that persists thereafter the harvest seasons. Around the world, the global use of plastics in agriculture was around 4.4 million tons in 2012 and reach 7.4 million tons in 2019 (Gao et al., 2019).

The management of large-sized plastics can produce micro pollution through the accumulation of plastic debris and potentially fragmenting into smaller pieces, classified as particulate plastics, which can be divided as microplastics (fragments <5 mm) and nanoplastics (fragments <0.1 μm) (Li et al., 2021). A literature revision allows to state that, the majority of microplastics research reported the presence of plastics or microplastics in the aquatic environments, especially the marine ones. Works reporting the contamination of soils by large-size plastics, microplastics and nanoplastics from the agricultural practices are highly lacking. Wang et al., 2020 presented a work concerning the

ecotoxicological consequences of microplastics contamination on soil ecosystems, including the effects on soil physical and chemical properties, terrestrial plants, soil fauna, and soil microbes.

The plastics degradation take place very solely and produce a host of secondary pollutants, which include a diversity of volatile organic representing a risk of groundwater contamination (Rhodes, 2018, Gi et al., 2020). The presence of microplastics is especially relevant in soils used for human food production and to better manage and control the plastic residues from agricultural use, the identification of the sources of their inputs into the environment becomes imperative (Bao-qing et al., 2021).

The amount of agricultural plastic used in the Alqueva Dam irrigation area, in the Alentejo region, in the south of Portugal, in a diversity of applications, is now estimated as 1880 tons per year and with the growth of the irrigated area could reach 3500 tons per year over the next few years (EDIA, 2018). The Alqueva Dam irrigation Area is shown in Figure 1, the cultures occupying a greater extent of land are presented in Table 1 and examples of wastes plastic produced are illustrated in Figure 2. In Table, ha = 10 000 m^2.
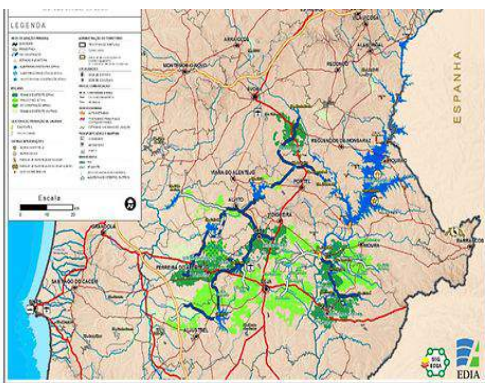
Figure 1 - Map of Alqueva Dam irrigation area

Culture	Area (ha) 2020	Mean productivity (ton/ha)	Plastic used (ton/ha/year)	Plastic wastes (ton/Year)
Intensive Olive Groves	68 346	10	0.03	2 050
Almond	15 241	3	0.03	457
Wine grape	5 755	10	0.003	17
Table grape	414	30	1.34	555

Table 1 - Main cultures practice in the Alqueva Dam irrigation area

Figure 2 – Photos from the culture more present in Alqueva Dam irrigation region and examples of waste plastics produced

Agriculture uses a large amount of conventional polyethylene film on diverse activities. The degradation of polyethylene film can be separated as an abiotic or biotic process. The abiotic being defined as a process caused by

environmental factors and the biotic is defined as biodegradation caused by the action of microorganisms present on the soil. However, the degradation process is too long. It could stay in the environment for more than one hundred years, it could be considered inert. Hadad et al., in 2005 presented a work concerning the biodegradation of PE. They stated that the polyethylene film could be biodegraded if the right microbial strain is isolated. However, they reported that, after 10 years of a PE sheet incubation in soil, submitted to a UV-irradiation, less than 0.5% of the PE sheet was degraded. After incubation in the moist soil of 12 years, no degradation signals were identified and only partial degradation was observed in a polyethylene film buried in soil for 32 years (Hadad et al., 2005).

The development of bioplastics emerges as an extraordinary alternative, but their high price and lower reliability of consumers associated avoid its widespread use. The major part of plastics from agricultural activities are not biodegraded and is treated mostly by incineration and mechanical recycling, but the increase in the ecological footprint intrinsic due to this treatment and the presence of dirty and agrochemicals in these plastics requires the use of new and more eco-friendly methods (Ragaert et al., 2017, Cowan et al., 2021). In this perspective, the wastes valorization through their transformation in activated carbons (ACs), presents itself as a viable solution.

ACs are materials adsorbents that present exceptional physical and chemical properties, such as high surface area, well-developed pore structure (micro, meso and macro), and a high degree of surface reactivity. ACs are economical adsorbents for a diversity of industrial applications (Belo et al. 2017, Cabrita et al., 2010, Cansado et al., 2018) They are used to eliminate, from the liquid or gaseous phases, unwanted odour, pollutants, taste, colouration metal ions, organic chemicals such as paint thinners, pesticides, pharmaceutical compounds, masks for individual protection, among others. With the implementation of new regulations for the wastes discharge and novel applications, an increase in the global activated carbon market is expected in the coming years.

In another perspective, the continued use of agrochemicals contributes to the contamination of soils and water streams. A study was done, in the Alqueva region, reported the presence of 25 pesticides. Among the most abundant were bentazone, metolachlor, terbuthylazine, 2,4-dichlorophenoxyacetic acid (2,4-D) and 4-chloro-2-methyl-phenoxyacetic acid (MCPA). At some sampling points, the MCPA showed an individual concentration reaching 580 ng/L (Palma et al., 2014).

This work uses the concept of circular economy to better manage and control the plastic residues from agricultural use, in particular the area of influence of Alqueva and its adjacent irrigated perimeters by the valorization of dirty waste plastics used in an agricultural environment through their transformation into activated carbons, which were subsequently tested for the removal of pesticides from the liquid phase.

2. Materials and Methods

The qualitative and quantitative characterization and identification of the plastics used in irrigated crops, covering the area of influence of Alqueva and its adjacent irrigated perimeters was made within the scope of the PLACarvões Project. In particular, the plastics used throughout the agriculture cycle, either in the installation or exploitation phases, were identified for each culture (EDIA, 2018).

The dirty plastics were collected from the field and cut into small pieces (around 2.5 cm*2.5 cm). These pieces were put into a steel container and placed into the semi-industrial rotative horizontal tubular furnace use for this propose. The physical activation was done using carbon dioxide or air as activating agents, at 973 or 1073 K, for different activating times. The chemical activation was done with potassium hydroxide or potassium carbonate, under a nitrogen flow, at 973 K. The excess of activating agent used was removed by successive washing cycles. ACs were full characterised by nitrogen adsorption at 77 K, elemental analysis (EA-CHNS), SEM and determination of the pH at the point of zero charge (pHpzc) by mass titration. Further details can be seen elsewhere (Cansado et al., 2019).

Selected ACs were tested for MCPA and 2,4-D removal from the liquid phase. The equilibrium time was evaluated by placing suspensions, containing 10 mg of ACs on 25 mL of pesticides solutions in a thermostat bath, under agitation, for 24 h. At different times intervals, aliquots were collected and the absorbance was measured, at a wavelength of 228 and 279 nm for MCPA and 230 and 284 nm for 2,4-D, using a UV-Vis Spectrophotometer equipment.

3. Results and Discussion

The plastics used throughout the agriculture cycle, either in the installation or exploitation phases, were identified for each culture. Detailed data can be found on EDIA, 2018, but in a nutshell Figure 3 and 4 show the total amount of plastic, expressed in percentage, by culture type and the typology of plastic used by culture type, respectively.
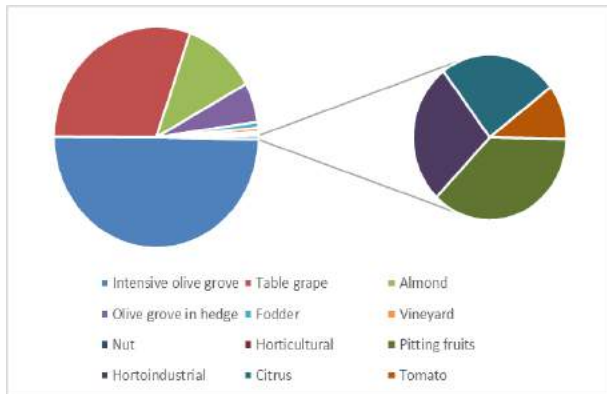
Figure 3 - Percentage of the plastic amounts used by culture type, in the Alqueva irrigation area.
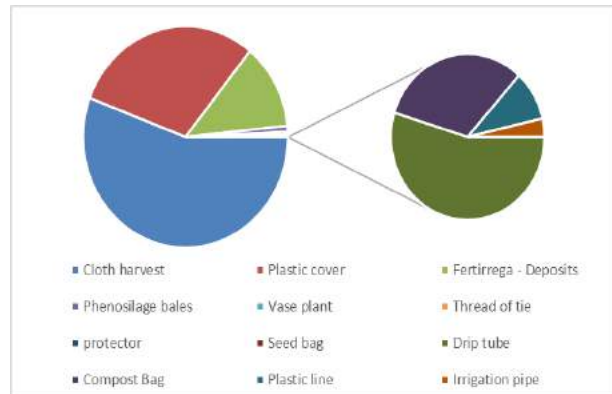
Figure 4 – Percentage of kind of plastic used by culture type, in the Alqueva irrigation area.

The data obtained in this study was the starting point of this work, which mobilized the scientific community and entrepreneurs of the region, for the wastes plastic valorization as precursors for the production of adsorbent materials that were later used in the removal of pesticides from the aqueous medium.

The ACs produced exhibited a microporous volume varying from 0.01 to 0.32 cm3 g-1 and an apparent superficial area varying from 12 to 623 m2 g-1. The better results were obtained from plastic sheeting activated with KOH (area – 542 m2 g-1 and volume – 0.24 cm3 g-1) and K2CO3 (area – 632 m2 g-1 and volume – 0.25 cm3 g-1), at 973 K. These values are comparable with data found in in the literature, concerning the ACs prepared from different precursors. As an example, Kacan, in 2016, prepared ACS from textile sewage sludge by chemical activation with potassium hydroxide, at 973 K, which presented an apparent surface area of 330 m2 g-1 (Kacan, 2016).

The major elements present on the ACs are carbon, oxygen and other heteroatoms. The surface of the ACs was evaluated by SEM, a representative example is shown in figure 5. The ACs presented a slightly basic surface character, which anticipates their good performance in adsorption of pesticides with predominantly acid character, such as MCPA and 2,4-D. Selected ACs were tested on the MCPA and 2,4-D removals from the aqueous phase. The equilibrium of the removal process was achieved after a contact time of less than 24 h, interestingly we can higligth that for a contact time of 120 min., 60% of the total amount adsorbed of both pesticides was removed from the solution, as illustrated in Figure 6.
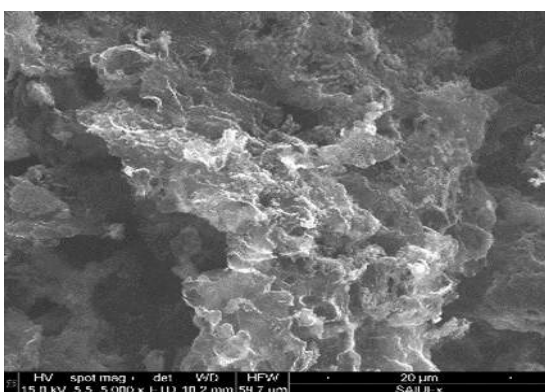
Figure 5 – SEM image obtained on the AC prepared from plastic sheeting with K_2CO_3.
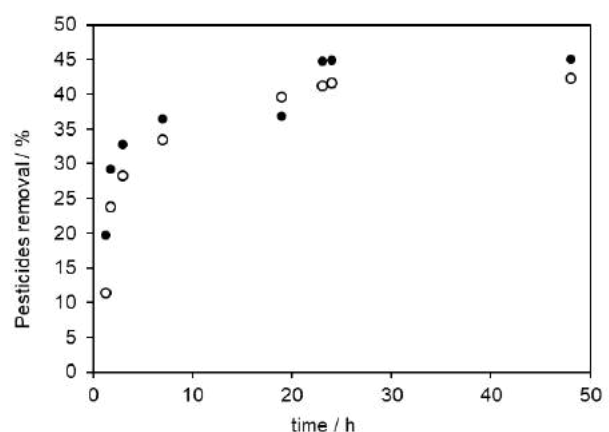
Figure 6 – Adsorption kinetics of 2,4-D and MCPA at 298 K. Open data points relate to adsorption of 2,4-D; filled data points relate to adsorption of MCPA.

4. Conclusions

In a short term, there is no doubt that the use of plastic sheeting in different agriculture activities increases crops yields. However, the contamination of soils and aquifers environments by their one's debris drew attention to scientists and the general population. During this work, the identification of the quantities and types of plastics used in the different cultures will allow the delineation of strategies for the disposal of their wastes. A way to treat these wastes was evaluated through their transformation into ACs.

The ACs produced exhibited textural and chemical characteristics similar to a variety of ACs found in the literature prepared from clean precursors. A large amount of low-cost ACs was produced from dirty plastic wastes, collected directly from the field, by physical and chemical activation, with KOH or K2CO3, at 973 K. The ACs produced through chemical activation were successfully used on pesticides removals, such as MCPA and 2,4-D, from aqueous media, presenting a maximum adsorption capacity of 169 and 245 mg g-1, respectively.

The wastes plastic from agricultural use were valorized through their transformation into ACs. These were successful used on pesticides removal from the aqueous medium. The ACs can be regenerated and reused which goes again to the circular economy.

Acknowledgements

References

Bao-qing, C., S. Baram, D.Wen-yi, H. Wen-qing, L. En-Ke, Y. Chang-rong. 2021. Response of carbon footprint to plastic film mulch application in maize production and mitigation strategy. Journal of integrative agriculture, 20 (7), 1933-1943.

Belo, C.R., I.P.P. Cansado, P.A.M. Mourão, 2017. Synthetic polymers blend used in the production of high activated carbon for pesticides removals from the liquid phase, Environ. Technol., 38:3, 285-296.

Cabrita, I., B. Ruiz, A.S., Mestre, I.M. Fonseca, A.P. Carvalho, C.O. Ania, 2010. Removal of an analgesic using activated carbons prepared from urban and industrial residues. Chemical Engineering Journal, 163, 249–255.

Cansado, I.P.P., C.R. Belo, P.A.M. Mourão, 2019. Pesticides abatement using activated carbon produced from a mixture of synthetic polymers by chemical activation with KOH and K2CO3. Environmental Nanotechnology, Monitoring & Management, 12, 100261.

Cansado, I.P.P., C.R. Belo, P.A.M. Mourão, 2018. Valorisation of Tectona Grandis tree sawdust through the production of high activated carbon for environmental applications. Bioresour. Technol., 249, 28–333.

Cowan, A.R., C.M. Costanzo, R. Benham, E.J. Loveridge, S.C. Moody, 2021. Fungal bioremediation of polyethylene: challenges and perspectives. Journal of Applied microbiology. https://doi.org/10.1111/jam.15203

EDIA, 2018; Avaliação do Ciclo de Vida dos Plásticos Agrícolas e Enquadramento Regulatório – Relatório Final; Consulai para EDIA; financiado pelo Fundo Ambiental, Portugal. (Início - EDIA, S.A.)

Gao, H., C. Yan, Q., Liu, W. Ding, B., Chen, Z. Li, 2019. Effects os plastic mulching an plastic residue on agricultural production: a meta-analysis. Sci. total Environ, 651, 484-492. Doi.org/10.1016/j.Scitotenc.2018.09.15.

Hadad, D, S. Geresh, A. Sivan, 2005. Biodegradation of polyethylene by thermophilic bacterium Brevibacillus borstelensis. Journal of Applied Microbiology, 98, 1093-1100.

Kacan, E., 2016. Optimum BET surface areas for activated carbon produced from textile sewage sludges and its application as dye removal. J Environ Management, 15 (166) 116-123. doi: 10.1016/j.jenvman.2015.09.044. Epub 2015 Oct 24.

Li, B., S. Huang, H.Wang, m. Liu, S. Xue, D. Tang, W. Cheng, T. Fan, F. Yang, 2021. Effects of plastic particles on germination and growth of soybean (Glycine max): A pot experiment under field condition. Environmental Pollution, 272, 116418.

Qi, Y., N. Beriot, G. gort, E.H. Lwanga, H. Gooren, X. Yang, V. Geissen, 2020. Impact of plastic mulch film debris on soil physicochemical and hydrological properties. Environmental Pollution, 266, 115097.

Ragaert, K., L. Delva, K. Van Geem, 2017. Mechanical and Chemical Recycling of Solid Plastic Waste. Waste Management, 69, 24–58.

Rhodes, C.J., 2018. Plastic pollution and potential solutions. Science Progress 101(3), 207-260. doi.org/10.3184 /003685018Xl5294876706211

Wang, W., J. Ge, X. Yu, H. Li, 2020. Environmental fate and impacts of microplastics in soil ecosystems: Progress and perspective. Sci Total Environ. 15 (708) 134841. doi: 10.1016/j.scitotenv.2019.134841.

Livestock Effluents: Strategic Approach Towards Agronomic and Energetic Valorization of Flows in the Farming Activity

Olga Moreira [a], Vasco Fitas da Cruz [b*], Daniel Murta [c] , Henrique Trindade [d], Rita Fragoso [e] , Elizabeth Duarte [e]

[a] INIAV, Oeiras, Portugal

[b] University of Évora, Évora, Portugal

[c] Entogreen®, Santarém, Portugal

[d] University of Trás-os-Montes and Alto Douro, Vila Real, Portugal

[e] Agronomy High Institute, University of Lisbon, Lisboa, Portugal

* Vasco Fitas da Cruz. Email: vfc@uevora.pt

Abstract

Livestock production is concentrated in specific regions, some without enough area for land spreading valorisation of effluents. Therefore, in order to be competitive and comply with legal requirements, the sector should promote a circular economy, pursuing new alternatives for effluents management. This project aims to valorise the livestock effluents as a resource, focusing on the production and integrated management of the different flows generated as well as to optimise effluents use as secondary raw materials, recovering energy and nutrients, improving farm nutrient balances and promoting sustainable management. The core activities to achieve these objectives relate with the four main routes: manure processing/composting, bioenergy production in a livestock farm, biodegradation by Black Soldier Fly (BSF) larvae and agronomic efficacy studies. Preliminary results of some of the activities developed within the project will be presented: characterization of the Portuguese intensive livestock sector (poultry, pigs and dairy cows), biochar valorisation, anaerobic digestion and biodegradation by BSF larvae of manure. The main goal of the project is the application of an established roadmap, including technology portfolio, for effluents management and testing the weak and strong points to promote common advances in the nexus biowaste/bioenergy/bio-fertilizer, closing the nutrients' cycle towards a sustainable bioenergy economy, creating a positive balance between manure production and manure valorisation due to its add-value use. Besides the results will support decision-making on centralized/decentralized solutions and also contribute to sustainable livestock intensification and landscape planning, to face climate change and resources scarcity.

Keywords: Circular economy, Animal waste, Integrated management.

1. Introduction

Animal production is crucial for the sustainability of traditional agricultural systems. This is primarily due to the fact that they provide soil improvers (manure) which still hold around 70% of the food's original nutrients and which would otherwise be lost. However, the intensification of these systems results in a global loss of nutrients at various levels. Nutrients related issues include competition for the use of cereals that would otherwise be intended for human consumption; low animal digestive efficiency; excess excreta and negative environmental impacts when manure handling is inadequate (such as improper or accidental effluent discharges). Another problem relates to the high concentrations of holdings in certain regions, which limits their capacity to handle the waste they produce (Teenstra et al., 2014; Teenstra et al., 2015).

The concepts of "circular economy" and "zero residues" are becoming part of the broader policy agenda and are of greater importance in Mediterranean countries due to their climatic and geographical characteristics: high temperatures during the summer, with an average increase per decade of 0,5ºC; a decrease of about 30% in precipitation and an increase in the frequency and intensity of droughts; erosion and leaching of soil nutrients. Soils in southern Europe have low organic matter and poor soil quality. In order to address these issues, the EU has introduced the current extensive legislation including the Nitrates Directive, Water, Ceiling of Emissions, etc. (UNEP/MAP and Plan Bleu, 2020).

In Portugal, adaptation policies promote the increased resilience of the territory and the economy to climate change. These include the Green Growth Commitment; the Strategic Framework for Climate Policy adopted by Portugal that includes the National Programme for Climate Change 2020/2030 (PNAAC) and the second phase of ENAAC 2020; as well as, the SNIERPA (the Portuguese National System for the Estimation of Emissions by Sources and Removals by Sinks of Air Pollutants, RCM 20/2015) for monitoring and reporting on GHG emissions (QEPic, 2015).

SNIERPA proposes that the agricultural sector reduce emissions through the structural adjustment of farms and their improved resource and energy efficiency. As objectives for manure management, SNIERPA encourages the reduction of carbon intensity through manure treatment: i) through more efficient effluent treatment systems (anaerobic digestion with biogas energy recovery, combined with complementary treatment systems e.g. composting; application of the

Code of Good Agricultural Practices, etc.); ii) by reinforcing the implementation of the REAP approach, which gives priority to the agricultural valorization of livestock residues, incorporating organic matter in the soil; iii) GHG monitoring in order to improve the environmental performance of the livestock sector, using methods that are compatible with the Portuguese emissions inventory and the REAP approach (SNIERPA, 2015).

Considering the economic and environmental importance of the agricultural sector, and the challenges it faces, an Operational Group for livestock effluents was created. The GoEfluentes Project (PDR2020-101-031831) emerged with the main goal of creating concrete solutions in order to increase the efficiency of water and nutrient utilization, reduce the environmental impact of farming and add value to what was, until recently, considered as waste.

2. Project Details

The objectives of this operational group are valorise livestock effluents as a resource, focusing on the sustainability.

In order to operate this project, a consortium led by INIAV was create. This consortium integrates institutions of R&D, and Associations and Companies from the Agrifood sector. The scope of this operational group covered 3 livestock production systems (dairy, poultry and pigs).

The Action Plan consists of the following main activities:
• ACTION 1: characterization of the Portuguese intensive livestock sector (poultry, pigs and dairy cows)
• ACTION 2: Mitigation measures for gaseous emissions and primary livestock effluent treatment
• ACTION 3: Valorisation of livestock effluents as a resource
       3.1. Composting of dairy cattle manure
       3.2. Anaerobic digestion of livestock effluents
       3.3. Biodegradation of livestock effluents by BSF larvae
       3.4. Agronomic valorisation
       3.5. Bioenergy production
• ACTION 4: Socioeconomic impact studies
• ACTION 5: Demonstration and Dissemination

3. Activities and Preliminary Results

In this chapter will be explained some details and preliminary results of some activities of the project related with the production and valorisation of livestock effluents.

3.1. Action 1

In order to characterize the Portuguese intensive livestock sector and understand better the animal waste production were developed a state of arte and elaborated questionnaires. These questionnaires include questions about farm details, water and energy use, feeding system, animal housing conditions and waste management system.

The questionnaires were distributed to selected poultry, pigs and dairy cows' farms located around Portugal. In total, were applied more than 50 questionnaires. This work still in process and at this moment were received and validated 21 questionnaires from poultry production, 25 from dairy cow production and 10 from pig production.

These data, compiled with the state of the art, will allow the development of a document with information on the typology of farms, production systems, waste management systems, geographic distributions, etc. which will be an important support tool in the other activities of the project and will be integrated into the digital platform developed within the scope of the project.

3.2. Action 3

In this action the main goal was to study techniques framed in the Portuguese reality that allow to value livestock effluents as a resource, focusing on the production and integrated management of the different flows generated. The studied techniques were composting, anaerobic digestion, bioenergy production, biodegradation by BSF larvae and agronomic valorisation.

3.2.1. Composting of dairy cattle manure

In this task two different types of dairy cattle manure were used to test the composting process. The type 1 was supplied by a farm that feeds the animals with silage and commercial dairy feed and used sawdust as bedding material. In type 2, the cows were fed with a total mixed ration system and the material used in the animal bedding was a reused sawdust (2 or 3 times). In both types the manure was subjected to a solid-liquid separation process.

The composting process occurred according the expectations and at the moment the compost is being analysed in the laboratory in order to evaluate the qualitative and quantitative parameters.

3.2.2.Anaerobic digestion of livestock effluents and Bioenergy production

In this task were characterized and compared two different samples of pig's slurry according the type of production: (1) closed cycle and (2) growing-finishing phase. This characterization (physical and chemical) allows evaluate the bioenergetics potential of pig slurry.

The anaerobic digestion trials occurred in lab scale using a continuous stirring tank reactor (CSTR) to define the best operational parameters and performance for anaerobic digestion process. According to the experimental work developed the sample with the best potential for energy recovery is the slurry from growing/finishing pigs.

3.2.3.Biodegradation of livestock effluents by BSF larvae

In this task, an experimental work is ongoing related to the use of chicken, swine and cattle manure, as a food source for BSF larvae.

Replica incubations were carried out for each type of manure: control, manure from chicken, swine and cattle with larvae and manure from chicken, swine and cattle without larvae.

BSF eggs were inoculated in commercial feed (EntoGreen®) until five days of age, being then inoculated in different experimental substrates (manure). In the control trial the single substrate used was the EntoGreen® feed. At different times after incubation of the larvae in the substrate, temperatures were recorded and collected/weighed larvae samples.

At the end of incubation, the larvae presented in each subtracts were weighed. A sample of larvae and frass (product of biodigestion for agronomic valorisation) was collected for further chemical characterization and valorisation.

The results of this analysis are being processed, however at the end of the experimental work the larvae demonstrated a better body development in the substrate with animal manure.

3.2.4.Agronomic valorisation

In this task, some experimental trials in a lab scale are in process. Once some experimental work of action 3 still in process, this work is dependent of some results to study and evaluate the agronomic and environmental potential of some of this techniques studied in the frame of GoEfluentes Project.

4. Conclusions

The pandemic situation compromised the normal development of the GoEfluentes Project, mainly in actions that involve personal contact between the operational group and the agricultural entrepreneurs. However, some adjustments are being made in order to achieve the main goals of the Project.

At this moment, the Project team are in the development of the digital platform "Land and Effluents". With this platform, the operation group expect to contribute for an Integration of livestock production data at local/regional/national scale and for a Landscape planning for livestock production towards environmental sustainability, sector competitiveness and rural development.

The expected impacts of the operational group are:
- To Provide an effluent management Roadmap that includes a technology portfolio linked to farm characteristics and regional conditions/limitations;
- To Support decision-making on centralized/decentralized solutions;
- To Contribute to a sustainable intensification and landscape planning facing climate changes and resource scarcity contexts
- To Contribute to environmental sustainability, competitiveness of the intensive livestock sector and rural development.

References

QEPiC. Quadro Estratégico para a Política Climática. Resolução do Conselho de Ministros No. 56/2015. Diário da República, 1ª série, No. 147, 30 de Julho de 2015. https://dre.pt/

SNIERPA, Sistema Nacional de Inventário de Emissões por Fontes e Remoção por Sumidouros de Poluentes Atmosféricos. Resolução do Conselho de Ministros No. 20/2015. Diário da República, 1ª série, No. 72, 14 de Abril de 2015. https://dre.pt/home

Teenstra E, Vellinga T, Aektasaeng N, Amatayakul W, Ndambi A, Pelster D, Germer L, Jenet A, Opio C, Andeweg K. 2014. Global Assessment of Manure Management Policies and Practices. Livestock Research Report 844. Wageningen, The Netherlands: Wageningen UR Livestock Research. http://edepot.wur.nl/335445

Teenstra E, De Buisonjé F, Ndambi A, Pelster D. 2015. Manure Management in the (Sub-) Tropics; Training Manual for Extension Workers. Livestock Research Report 919. The Netherlands: Wageningen UR Livestock Research. http://edepot.wur.nl/362491

United Nations Environment Programme/Mediterranean Action Plan and Plan Bleu (2020). State of the Environment and Development in the Mediterranean. Nairobi.

Traditional Compost and BSF-biodigested Compost in the Organic Fertilization of Ryegrass

Regina Menino[a,*], José N. Semedo[b], Paula Scotti-Campos[b], Amélia Castelo-Branco[a], Daniel Murta[c,d], Cecília Nestle[e], Vasco Fitas da Cruz[f], Olga Moreira[g]

[a] UEIS Sistemas Agrários e Florestais e Sanidade Vegetal-Laboratório de Solos, Plantas e Águas, Instituto Nacional de Investigação Agrária e Veterinária, I.P. (INIAV), Av. da República, Quinta do Marquês, 2780-159 Oeiras, Portugal

[b] UEIS Biotecnologia e Recursos Genéticos, INIAV, Oeiras, Portugal

[c] EntoGreen - Ingredient Odyssey, Santarém, Portugal; [d]CiiEM-Centro de investigação interdisciplinar Egas Moniz, Campus Universitário, Quinta da Granja Monte de Caparica, 2829-511 Caparica, Portugal

[e] Leal & Soares, S.A., Zona Industrial Mira | Polo I – Lote 39 | 3070-337 Mira, Portugal

[f] MED-Universidade de Évora

[g] Unidade Estratégica de Produção e Saúde Animal, INIAV, I.P., Pólo de Investigação da Fonte Boa, Santarém, Portugal.

* Corresponding author. Email: regina.menino@iniav.pt

Abstract

The present study is a contribution to evaluate the agronomic potential of two different organic products (cattle effluents, either composted or digested by Black Soldier Fly larvae) as organic fertilizers, through the measurement of production and the photosynthetic activity of ryegrass (*Lolium multiflorum* L.), growing in a sandy soil, treated with different doses of those products. Within this aim, an experiment was conducted in a semi-controlled greenhouse with ryegrass plants cultivated in pots, with ten treatments: four different treatments of traditionally composted material, four different treatments of biodigested material, a mineral control (using the recommended rate of mineral fertilizer for ryegrass), and a zero control (without any type of fertilization). Under the experimental conditions, the results showed a significant effect of both organic composts over mineral fertilization, with a better performance of the biodigested by black soldier fly larvae. As for the informative capacity of photosynthetic activity data, in assessing the vegetative development of crops, "net assimilation rate" and "water use efficiency" proved to be the most suitable parameters.

Keywords: Biodegraded effluent, composted effluent, photosynthetic performance, ryegrass yield pot trial.

1. Introduction

The promise of the so-called "green revolution" (of the 1960s), based on the ability to create new highly productive varieties at the expense of high chemical inputs (fertilizers, phytopharmaceuticals, and fuels), was then praised for the resounding success in several countries where it was implemented, but it has been progressively revealing its perverse side, namely: in the exhaustion of fertility and in the pollution of soils and groundwater, in the reduction of water resources (by the proliferation of irrigated areas); and in climate change due to the intensive use of agricultural machinery burning fossil fuels.

In order to counteract all these inconveniences, various alternatives have been tested, either at the general level of the entire production philosophy, or at the specific level of the various factors that contribute to saving production and protecting the environment, without losing a scale of production compatible with the planet's needs.

The resurgence of organic fertilizers, which are more robust than mineral fertilizers, in improving soil fertility and reduce groundwater contamination, has been successfully tested in several situations. Among these, livestock manure, which is one of the traditional organic fertilizers discarded by the intensivist option that informed the "green revolution", is undoubtedly one of the obvious candidates.

Moreover, the progressive high concentration of intensive livestock farming in some regions, and the limited area for the disposal of the slurry produced, is a reality, causing difficult issues that need to be urgently solved. The direct disposal brings a sanitary problem, if not adequately managed, and one of the ways to overcome it is to submit the slurry to a composting process to use in crop fertilization. The organic products generated through these processes have to be used cautiously, because their composition is not standard and has to be adequate to each culture, in terms of quality and quantity. However, these organic composts are usually rich in plant nutrients, especially nitrogen (N), which is one of the most important nutrients for plant growth.

The problem with the organic "fertilizers" is that the N content is mainly in organic form and it needs to be mineralized for plant absorption. Nevertheless, this mineralization process does not always go along with the plant needs and, so, the fertilising potential of different types of composts depends, to a large extent, on the reconciliation of these processes in the relationship of the different plant genotypes with the different composts.

The photosynthetic activity reflects the response of the plants to changes in the environment, being a sensitive physiological parameter of plant metabolism and development (Liu *et al*., 2013) and is closely linked to N availability, since N is a major constituent of light-harvesting complexes and reaction center systems, in which chlorophyll and other

pigments are associated with proteins to form chlorophyll proteins, and there is a positive correlation between these pigments and leaf N concentration (Bredemeier and Schmidhalter, 2001).

In the present study, the effect of traditional bovine slurry compost and a compost of the same origin biodigested by Black Soldier Fly larvae (BSFL) are evaluated on ryegrass plants, through production and photosynthetic rate, between each other and with a mineral fertilization, all with equal N endowments.

2. Materials and Methods

The trial was conducted in a greenhouse, located in Oeiras (Portugal), belonging to the National Institute for Agrarian and Veterinarian Research (INIAV I.P.).

The soil used for the experiment was classified as a Gleyic Podzol (IUSS-FAO, 2006). A sample of the soil was analysed for selected physicochemical properties, according to the methods used routinely in INIAV laboratories. The results for soil surface layer (0-25 cm) analysis revealed a coarse texture (96% sand), a pH around 6, a cation exchange capacity of 3.8 cmol.kg^{-1}, poor in nutrients and with 5.1 g of organic matter per kg.

The soil collected to be used for the pot trial was air-dried, at room temperature, and sieved to pass a 2mm mesh, using a total weight of 3 Kg per pot.

The organic composts used in the experiment were analyzed for N content, by the Kjeldahl method (Bremner and Mulvaney, 1982), and the results obtained for the bovine slurry composted (designated by the C letter – for **C**omposted) was 12.3 g N kg^{-1}, and for the Black Soldier Fly larvae (BSFL) biodigested bovine slurry (designated by the F letter – for **F**rass) the result was 14g N kg^{-1}.

A greenhouse pot experiment, using ryegrass (*Lolium multiflorum* Lam.), was set up in order to evaluate the agronomic potential of a composted bovine slurry (**C**) and a BSFL biodigested slurry (**F**) of the same origin, and was carried out in cylindrical plastic pots (with 15 cm height, 12.5 cm in diameter at the bottom, and 17 cm in diameter at the top) with a surface area of 226.9 cm^2, filled with 3 Kg of sandy soil.

During the plant growth cycle, the greenhouse temperature was kept between 18 and 25 ºC, and the pots were daily watered, with deionized water, to maintain the soil moisture near to 80% of water holding capacity, estimated by weight difference. The pots were disposed in different places every day, in a randomized way, after watering, to eliminate any influence of the day light.

The experiment, in a randomized plot design, consisted of 10 treatments (1 control, 1 mineral, 4 **C** and 4 **F,** these last 8 with a complement of 10% nitro ammoniacal N) with five replicates, totalizing fifty cylindrical plastic pots. The rates of compost were calculated based on the N demand by the crop (estimated in 140 kg N per hectare), considering a mineralization rate of 50%, and a ryegrass N use efficiency of 50%. Based on these assumptions, the treatments were the following: T0, corresponding to the negative control, without fertilization; TM, with 1.2 g of mineral fertilizer per pot (equivalent to 140 kg N per hectare); TC1, TC2, TC3, and TC4, using, respectively, 83 g, 166 g, 248 g, and 331 g of compost, per pot; TF1, TF2, TF3, and TF4, using, respectively, 22.7 g, 45.4 g, 90.8 g, and 113.5 g, of biodigested compost per pot.

Before sowing, the material to be tested was mixed with soil. The seeds were surface sown in each pot, using a seed density equivalent to 40 kg per hectare.

Gas exchanges were measured in adult expanded leaves of 6 weeks old plants, prior to the first plant cut. Net photosynthesis rate (P$_n$), stomatal conductance (g$_s$) and transpiration rate (E) were determined using a portable infra-red gas analyzer (LI6400, LI-COR, Lincoln, U.S.A.), under 20-25 ºC, with a light supply of 700 µmol m^{-2} s^{-1}, as described in Semedo *et al*. (2021) Water use efficiency (WUE) was calculated as P$_n$/E.

After measurements of leaf exchange evaluation, the plants were harvested, at about 2 cm above the soil surface, for yield evaluation (for fresh and dry weight). After weighted, the samples of fresh material were washed with deionized water, dried at 60ºC, till constant weight, and, after dry weighted, grounded for N chemical analyses, by the Kjeldahl method (Bremner and Mulvaney, 1982).

The data were analyzed statistically using a one-way AOV with a significance level of $P < 0.05$, which was applied to test for differences between treatments in respect to weight, N tissues concentration, and gas exchange parameters. Tukey HSD test for mean comparison was performed (for a 95% confidence level). Results were statistically analyzed by Statistix 9.0, Analytical Software.

3. Results and Discussion

The results obtained for ryegrass production and N concentration in leaf tissues are presented in Table 1. From the data, and as registered both for fresh and dry weight, it is possible to observe that the higher yield was obtained in the treatment TF4, by a significant difference compared to all the other treatments and the second highest yield was

observed for treatments TC4 and TF3, by a significant margin over the remaining treatments, which means that the biodigested was more efficient than the traditional compost and the biological fertilisers gave a higher yield than the mineral fertiliser treatment. In fact, the TM treatment only led to a higher yield than that recorded for organic fertilizers for treatments TC1 and TF1, which proves that the allocation to these treatments is insufficient.

Table 1. Mean values (n=5) for ryegrass production, expressed as fresh and dry weight (g) per pot, and total N concentration in plant tissues, in each treatment

Treatment	Fresh weight (g)	Dry weight (g)	Total N (g kg^{-1})
T0	9 f	1.7 g	10.2 g
TM	42 d	5.3 de	34.2 a
TC1	28 e	4.7 ef	11.1 fg
TC2	61 c	8.4 c	15.7 de
TC3	64 c	8.6 bc	16.2 de
TC4	76 b	9.7 b	17.6 cd
TF1	26 e	4.2 f	12.5 f
TF2	41 d	6.2 d	14.8 e
TF3	76 b	9.5 b	19.0 bc
TF4	89 a	10.9 a	20.5 b

Means in the same column with the same small letter do not differ significantly (p≤0.05), as assessed by the Tukey test

As expected for a sandy soil, the lowest production was recorded for treatment T0, by a significant difference compared to the others.

Compared to the results obtained by Menino *et al*. (2021), also working in similar conditions (but in a different soil, with another organic compost and no mineral fertilizer complement) the yield values obtained in the present experiment are much higher, maybe due to the higher rates of the composts but undoubtedly also due to the complementary mineral fertilizer for the start of the ryegrass crop, as it was hypothesised in the referred work.

With regard to the concentration of N in the plant tissue, the highest values, and significantly different from the other treatments, were recorded for TM, since the directly assimilable formulation of N is here much more adapted to the needs of the plant. On the other hand, again as expected for a sandy soil, the lowest N concentration was recorded for treatment T0, by a significant difference compared to the others. The remaining data for N concentration followed the same pattern recorded for the production of biomass.

The results obtained for the gas exchange measurements are presented in Table 2, and suggest the following comments:

Table 2. Mean values (n=9) for net assimilation rate (Pn), stomatal conductance (gs), transpiration (E), and water use efficiency (WUE), calculated as Pn/E, for ryegrass grown under different fertilization treatments

Treatment	P_n (μmol m^{-2}s^{-1})	g_s (mmol m^{-2}s^{-1})	E (mmol m^{-2}s^{-1})	WUE [μmol (CO$_2$) mol^{-1} (H$_2$O)]
T0	3.0 f	106 b	2.3 c	1.3 c
TM	10.3 bc	332 a	5.6 a	1.9 bc
TC1	5.4 e	196 b	3.5 bc	1.5 bc
TC2	6.4 de	331 a	4.7 ab	1.4 c
TC3	8.3 cd	239 ab	4.2 ab	2.0 bc
TC4	10.4 abc	244 ab	4.0 abc	2.8 ab
TF1	5.9 e	194 b	3.3 bc	1.8 bc
TF2	8.2 d	318 a	4.4 ab	2.1 bc
TF3	11.1 ab	312 a	4.6 ab	2.9 ab
TF4	12.5 a	291 a	4.1 ab	4.0 a

Means in the same column with the same small letter do not differ significantly (p≤0.05), as assessed by the Tukey test

The pattern of the values recorded for P_n and WUE is consistent with that observed for biomass production, confirming their informative value with respect to the vegetative state of the plants. However here, the higher net assimilation rate recorded for the TF4 treatment, relative to TF3 and TC4, although by a wide margin did not reveal statistical significance. On the other hand, regarding g_s and E, the values registered do not suggest relevant conclusions regarding their relationship with the production.

The results from a work developed by Jia *et al*. (2010), on physiological characteristics of ryegrass, found values of P_n varying between 10.8 and 16.5 μmol m^{-2}s^{-1}, respectively with low and high atmospheric CO$_2$, which are higher than

the values obtained in the present experiment, except for the treatments TM, TC4, TF3 and TF4, that were within the low values obtained in that experiment. Given the systematically increasing pattern of results for both organic fertilizers, we can therefore assume that the maximum amounts tested were sub-optimal.

4. Conclusions

The main hypothesis that informed the present study is confirmed in the results that show, in a statistically demonstrated manner, the better performance, in ryegrass production, of cattle slurry biodigested by the black soldier fly larvae, in comparison with traditional compost with the same raw material (both with a complement of readily available N). Both organic fertilizers gave a higher yield than the mineral fertilizer treatment, very clearly, due to the addition of directly available N, which again proved to be paramount to accelerate initial plant growth under any organic fertilization.

As for the informative capacity of photosynthetic activity data, in assessing the vegetative development of crops, "net assimilation rate" and "water use efficiency" proved to be suitable parameters. As a matter of fact, significant effect of both organic composts was also perceived through overall photosynthetic activity of ryegrass plants and biomass production, showing the potential of these organic products as fertilizers.

The pattern of the values recorded for P_n and WUE is consistent with that observed for biomass production, confirming their informative value with respect to the vegetative state of the plants.

With regard to the concentration of N in the plant tissue, the highest values, and significantly different from the other treatments, were recorded for TM, which suggests the possibility that the additional 10% N added to the organic fertilizer may have been insufficient.

Given the systematically increasing pattern of results for both organic fertilizers, we can therefore assume that the maximum amounts tested were sub-optimal.

Acknowledgements

References

Bredemeier. C., and U. Schmidhalter, 2001. Laser-induced chlorophyll fluorescence to determine the nitrogen status of plants. In *Plant nutrition - Food security and sustainability of agro-ecosystems*. Dordrecht. The Netherlands: Kluwer Academic Publishers. Eds., W.J. Horst *et al*. 92, 726-727. https://doi.org/10.1007/0-306-47624-X_352

Bremner, J.M., and C.S. Mulvaney, 1982. Nitrogen-Total. In Methods of soil analysis. Part 2. Chemical and microbiological properties. 2nd ed. (Agronomy 9). American Society of Agronomy, Soil Science Society of America, Madison, Wisconsin. Eds., Page A.L., R.H. Miller and D.R. Keeney. 595-624.

Concenço. G., E.A. Ferreira, A.A. Silva, F.A. Ferreira, L. Galon, M.R. Reis, L. d'Antonino, L. Vargas, L.V.B.D. Silva, 2008. Fotossíntese de biótipos de azevém sob condição de competição. Planta Daninha. 26 (3), 595-600. https://doi.org/10.1590/S0100-83582008000300015

IUSS-FAO Working Group WRB, (2006): World reference base for soil resources 2006 - A framework for international classification, correlation and communication, Rome, Food and Agriculture Organization of the United Nations. 10013/epic.43321.d001

Jia, Y., S. Tang, R. Wang, X. Ju, Y. Ding, S. Tu, D.L. Smith, 2010. Effects of elevated CO_2 on growth. Photosynthesis, elemental composition, antioxidant level, and phytochelatin concentration in *Lolium mutiflorum* and *Lolium perenne* under Cd stress. Journal of Hazardous Materials. 180 (1-3), 384-394. https://doi.org/10.1016/j.jhazmat.2010.04.043.

Liu, X., Y.Fan, J.Long, R. Wei, R. Kjelgren, C. Gong, J. Zhao, 2013. Effects of soil water and nitrogen availability on photosynthesis and water use efficiency of *Robinia pseudoacacia* seedlings. Journal of Environmental Sciences, 25 (3), 585–595. doi:10.1016/s1001-0742(12)60081-3

Menino R., F. Felizes, M.A. Castelo-Branco, P. Fareleira, O. Moreira, R. Nunes, D.Murta, 2021. Agricultural value of Black Soldier Fly larvae frass as organic fertilizer on ryegrass. Heliyon, Jan 2, 7 (1), e05855. doi: 10.1016/j.heliyon.2020.e05855. PMID: 33426352, PMCID: PMC7785954.

Education and Rural development

Attitude of Spanish Agriculture Students towards Education in Sustainable Precision Agriculture

Anne Krus [a,*], Jeremy Karouta [b], Juan José Ramirez [a], Dionisio Andújar [b], Constantino Valero [a], Anastasios Michailidis [c]

[a] Universidad Politécnica de Madrid (UPM), Spain

[b] Centre for Automation and Robotics (CAR), CSIC-UPM, Spain

[c] Aristotle University of Thessaloniki, Greece

* Corresponding author. Email: a.m.krus@upm.es ORCID: 0003-3606-4826

Abstract

The principles of Sustainable Precision Agriculture (SPA) have been around for decades, and due to technological advancements in recent years, the commercial market for SPA has expanded substantially. Adoption rates by farmers have however been lacking behind their prediction since the beginning. These days, a farmer has to possess a wide variety of skills, which aren't all covered in common agronomy curricula. The Erasmus+ Project "Sparkle" aims to complement traditional agronomist education with entrepreneurial skills and SPA knowledge, through a mixed format of online courses and face-to-face learning. To develop the contents of this proposed course the perception of agronomy students first had to be assessed, to pinpoint their interests and their perceived knowledge gaps. This paper presents survey results of 192 students at the agronomy faculties of 4 universities across Spain, 48% bachelor and 52% master students. Students perceive a lack in knowledge in all skill types included in the questionnaire. They are consistent in rating their own knowledge and are interested in learning more on all proposed topics, regardless of age or study level. Generally, they prefer on-site or face-to-face teaching, and interactive teaching methods over passive communication. When combined with other studies that are being carried out within the project, the results of these questionnaires will provide the basis for the agri-entrepreneurial Sparkle course.

Keywords: precision farming, education, knowledge gap, survey research.

1. Introduction

The field of Sustainable Precision Agriculture (SPA) has been around since the 1980's and is defined as a holistic approach to crop management, taking into account spatial and temporal variations as well as reducing the environmental impact. The application of these techniques results in a reduction of costs, but also in an increase of yield quantity and quality (Bramley and Ouzman, 2019). First commercial devices were released at the end of the last century but, despite its long-lasting existence and its current expansion in commercial market applications, the adoption of SPA seems to lack behind (Lowenberg-DeBoer and Erickson, 2019). An important factor is that SPA requires a large skill set and knowledge of multi-disciplinary techniques. Several studies stress the necessity of providing education on these new skills to farmers and field technicians, in order to master such innovative tools (Eastwood et al., 2017; Erickson et al., 2018). Common agronomy curricula currently have a knowledge gap towards the necessary technologies, whereas other specific technological curricula miss the biological aspects (Fausti et al., 2018).

Some aspects are reported to influence the adoption rate of SPA, such as communication (Kutter et al., 2011) and trust (Kester et al., 2013). Nevertheless, many studies aim to identify the areas lacking in current curricula (Kitchen et al., 2002; Erickson et al., 2018; Eastwood et al. 2017) to be able to reduce the knowledge gap.

The Erasmus+ project "SPARKLE" –*Sustainable Precision Agriculture: Research and Knowledge for Learning how to be an agri-Entrepreneur*– aims to complement these curricula with entrepreneurial skills as well as specific SPA knowledge, by producing a mixed format of online and face-to-face contents. To this end, the perception of current agronomy students is analysed, with the aim to pinpoint both interests and self-assessed knowledge gaps. An in-depth analysis of educational needs by students and agricultural technicians was done in the framework of this project, and it is freely available at its web page (Sparkle consortium, 2018).

This paper intends to show and discuss the preliminary results of the analysis of the Spanish respondents to a Likert-scale survey, in which their opinions, needs and interests are gathered to use as a set-up for the development of new precision agriculture (PA) teaching materials. Specifically, the following research questions are proposed:

Q1: Do students feel well-informed on these topics?

Q2: Do students feel like they need more information on these topics?

Q3: How do interests in technologies compare to interests in business skills?

Q4: How would students prefer to acquire these proposed new skills?

Q5: Is there a difference between the surveyed universities?

Q6: Do master's students feel better prepared in these topics than bachelor's?

Q7: Is there a correlation with gender or age?

In this work, the materials and methods employed, both for the surveying as well as for the results analysis, are explained first. Then, the results are presented, after which they are discussed and compared to other studies. Lastly, the most important findings are summarized in the conclusion.

2. Materials and Methods

The questionnaire has been developed by the University of Thessaloniki, a partner in the "Sparkle" Erasmus+ Project. The entire survey has been translated into the native language of each of the four participating countries. This study only focuses on the respondents of the Spanish version. The questionnaire was administered physically between May 3rd and June 5th 2018 during classes within four agronomy faculties in Spain, namely Universidad Politécnica de Madrid (UPM), Universidad de Zaragoza (UZ), Universidad Sevilla (US), and Universitat Politécnica de Valencia (UPV). The number of respondents is distributed amongst the universities as shown in Table 1. The questionnaire contains 18 questions, of which 14 contain multiple sub-questions to be rated using a Likert-scale from 1 to 5, totalling 116 responses per entry, and taking about 25 minutes on average to fill out. The questions were presented to each respondent in the same order.

Table 1. Geographical distribution of respondents.

University	Number of Classes	Number of Students
UPM	9	126
UZ	1	7
US	2	31
UPV	1	28
Total	**12**	**192**

2.1. Questionnaire Contents

The employed questionnaire consists of 18 subjects, that are divided into three parts. In the first part the students are asked to assess their own knowledge and skills. The second part of the questionnaire asks them what they expect to be the most important and useful to learn should they want to practice PA, as well as their preferences on how and when this education should take place. The questionnaire finishes with some inquiries for demographics purposes. Moreover, based on their contents, the questions can also be divided into 6 categories. Table 2 shows the structure of the survey and specifies the contents of each of these topics, as well as the way the questions are presented. In the knowledge assessment section at the beginning of the questionnaire, the following three definitions were included, in order to serve as an introduction for students with less knowledge about PA:

- "Precision Agriculture (PA)" is a method of agricultural practice based on information and technology which aims to improve efficiency, productivity and profitability while minimizing environmental impacts.
- "Soft PA" relies more on traditional means of obtaining information and they are less automated (for example, drip irrigation, moisture sensors).
- "Hard PA" depends on information-management technologies such as remote sensing, geographic information systems (GIS), global positioning systems (GPS).

Table 2: Structure of the questionnaire. MC stands for Multiple Choice, LS for Likert scale.

Parts and categories	Question Nr	Sub-Questions	Type
PART 1: Knowledge	**1-4, 6**	**17x**	**5 point LS**
	Self-assessment of PA knowledge and skills on a variety of subtopics, with options ranging from 'none' to 'very high'. This section also includes definitions of PA, soft PA and hard PA.		
PART 1: Interests	**5**	**2x**	**5 point LS**
	Assessment of interest in both hard and soft PA, with options ranging from 'none' to 'very high'. Both definitions are given as a part of the questions belonging to the knowledge assessment topic.		

Parts and categories	Question Nr	Sub-Questions	Type
PART 2: Topics	**7-9**	**38x**	**5 point LS**
	These questions are about respondents' opinion on the importance of several topics within PA. The attitude towards training needs of certain areas of PA is asked first, after which respondents need to rate their level of agreement with statements regarding their relative importance. Lastly, the respondents are asked to rate the importance of several subtopics within some of the areas.		
PART 2: Methods	**10-11**	**24x**	**5 point LS**
	Questions 10 and 11 cover the applicability of several new and hybrid teaching methods, and the efficiency of certain teaching media, respectively.		
PART 2: Statements	**12-13, 15**	**29x**	**5 point LS**
	These questions are collections of statements where the respondents rate their level of agreement. Question 13 is about the willingness to pay for a massive open online course (MOOC), and question 15 challenges the respondent to rate how important certain benefits of PA are for the future.		
PART 2: Timing of a Course	**14**	**1x**	**3 options MC**
	This question asks the opinion of the respondents as to when a specific PA		

2.2. Data Cleaning

In the obtained data set not all respondents produced usable data. The following types of faulty data have been removed from the set:

- Incomplete surveys: 3 respondents skipped large parts (>25 questions) of the questionnaire. All other respondents only left 5 or less blanks, which did not show any bias or pattern towards specific questions.
- Straight-line respondents: 13 respondents entered the same response for an abnormal part of the questionnaire and were deemed inadmissible. Furthermore, 8 other respondents who also entered the same response for an abnormal part of the questionnaire, were manually reviewed and were deemed plausible responses.

After removal of the 3 entries with many blanks, and 13 straight-line respondents, the survey data set contains 176 entries with higher reliability. The remaining blank, or missing values (41, spread over 35 questions and 28 respondents) are then substituted with the question median. As the maximum number of missing entries per question is 2, it is assumed to have a small enough effect on the statistical soundness of the data set, such to not interfere with the regression techniques. Visually, the data cleaning effects are included in Figure 1.
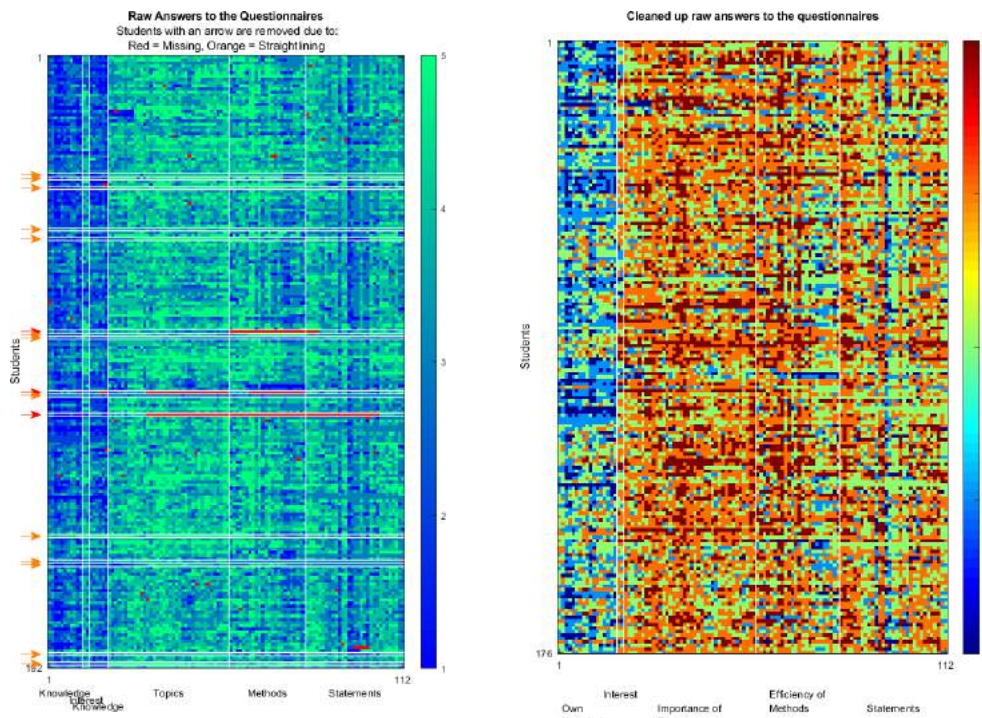
Figure 1. Survey results before (left) and after (right) data cleaning

2.3. Audience Reached

As shown in Table 1, the survey was administered in 4 universities in a variety of lectures. After cleaning up the data, the remaining audience's demographics can be visually summarized as shown in Figure 2. The age distribution follows the typical distribution of a university student body, confirming that a representative cross section of the Spanish students was reached with this method. The geographical distribution, as mentioned in Table 1, unfortunately is biased towards Madrid, which is addressed in one of the hypotheses.

(a)   (b)
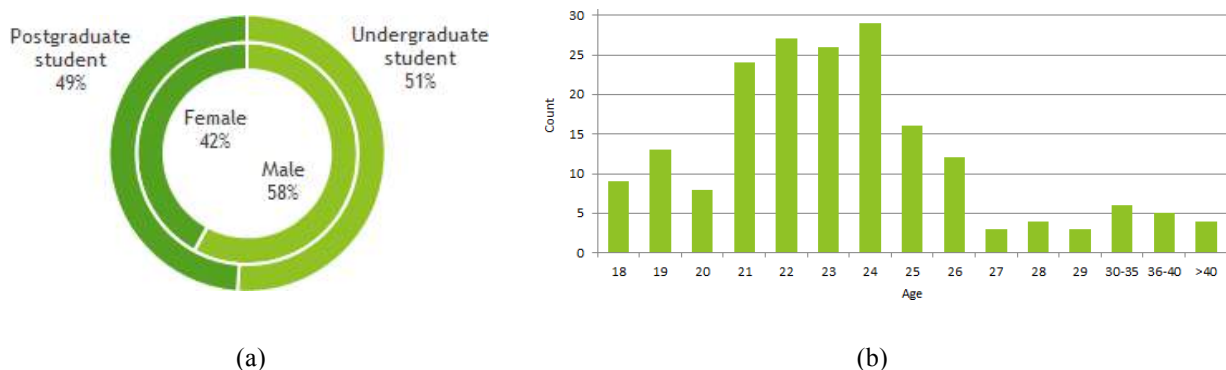
Figure 2. Demographics (a) and ages (b)

3. Results and Discussion

The hypotheses outlined in the introduction dictate the structure of this section, in the form of the main questions addressed with the questionnaire design:

Q1: Do students feel well-informed on these topics?

The self-evaluated knowledge level of the students was generally evaluated small to medium. Noticeably, only 5% responded to the most global question regarding their knowledge level on PA that their level was *None*. When distinguishing between soft and hard PA, however, 34% and 22% respectively evaluated their knowledge as *None*. As the

definition of what we considered to be soft or hard PA was included in the questionnaire, it can be concluded that a large portion of students thought to be informed on PA topics while they were thinking of technologies that do not meet the given descriptions. When regarding both the general and more specified questions, i.e. question 1-3, less than 1 in 10 students marked their knowledge level as high or very high. In question 6 the students got to rate their knowledge on 6 specific subsets of PA topics, with included examples of exactly which technologies were meant. On average, around half indicated to have little to no knowledge in each of these categories as well.

Q2: Do students feel like they need more information on these topics?

Based on the same definitions provided for the knowledge assessment on soft and hard PA, the students are also asked about their interest in each of these respective fields. A total of 82% and 90% indicated medium to very high interest in soft and hard PA respectively. Hard PA was deemed to be more interesting than soft PA, with more votes in the (*Very*) *High* categories as well as less votes in the *Small* to *None* categories. In other words, students indicated to be more interested in more advanced and automated technologies, than in the more traditional means of addressing site-specific variations.

Q3: How do interests in technologies compare to interests in business skills?

In order to apply PA successfully, 92% of students believed learning new skills are a necessity. To the statement "technological skills are most needed", 8 out of 10 respondents agreed or agreed strongly. To the statement "business skills are most needed", however, only 55% agreed (strongly). This demonstrates a clear preference for technological training, while also showing that the business side of a PA enterprise should not be overlooked. In another question, the students were asked to rate their needs on 8 proposed training topics. The results are shown in descending order of necessity in Figure 3, where the sum of *High* and *Very High* is used as the sorting value. From the sorted list, the conclusion can be drawn that whereas trainings focused on technological advancements (A&B in the figure) are overall seen as most important, the agricultural topics (C&D in the figure) both got the most *Very High* classifications. This might have its origin in the focus of the respondents pool, i.e. the fact that all students questioned were currently enrolled in an agricultural degree. The remaining (business) topics are once again rated as necessary by about half of the respondents.

Q4: How would students prefer to acquire these proposed new skills?

The teaching forms deemed most applicable or important for these types of trainings were considered to be knowledge sharing mechanisms and experienced farmers as mentors. The third-most favorite both in amount of *Very High* votes as well as combined votes for (*Very*) *High* are MOOCs. Interestingly enough, the option "Apps for learning via smartphone" was not popular among the students, despite them forming a relatively young demographic. When presented with 18 more detailed forms of training, as shown in Figure 4, some general tendencies become clear: students prefer interactive methods over passive ones, as well as on-site education over distance-learning.

Q5: Is there a difference between the surveyed universities?

In general, all universities responded to the questionnaire in a similar trend, and no significant comparison can be made. Nevertheless, some slight differences can be observed. In general students from UNIZAR gave higher scores to some questions, whereas the UPV scores the lowest. This is interesting as the UNIZAR students on average have the lowest level of education in years, all the while they rate both their current knowledge as well as the importance of all topics higher than the other students. This might be caused by a cognitive bias, as well as the difference in curriculum. The largest differences in answers were found scattered through the questionnaire, but an interesting one lies in the rating of efficiency of training methods, where UNIZAR students rated radio broadcasts and helpline instructions as efficient, whereas the other universities tend to disagree. Areas all students agreed on were also scattered, but one important agreement is found in the rating of training needs. Here technological, innovation, sustainability, and local ecosystem training were all consequently rated higher than the rest. Another area on which the students agreed, is that MOOCs are an important form of learning training, albeit that it did not receive the highest rating overall, but a consistent one.

Q6: Do master's students feel better prepared in these topics than bachelor's?

A small shift can be detected when comparing the self-assessed skill level of bachelor's students and master's students, as shown in Figure 5. In general master's assess their knowledge less often as *None* in nearly all of the proposed topics, and slow slightly more confidence in the *High* and *Very High* categories. In total, 90 bachelor's students and 86 master's students responded, which is why these results could be represented directly without scaling. Note that the categories as presented in the legend are shown in the graph in the same order, causing the uppermost line of this cumulative graph, corresponding to local ecosystems, to double as a totals line when summing up the votes in all 8 categories per education level. To deduce the number of votes each option got from either of the two student pools within each separate category, one would have to look at the difference between that category and the following category in the legend.

LEVEL OF TRAINING NEEDS
(in %)

■ None ■ Small ■ Medium ■ High ■ Very High

A: Innovation theory and -management
B: New technology and equipment
C: Sustainability issues and circular agriculture
D: Local ecosystems
E: Business management
F: Laws, regulations, and provisions
G: Marketing
H: Opinion leadership / detection of local community influencers
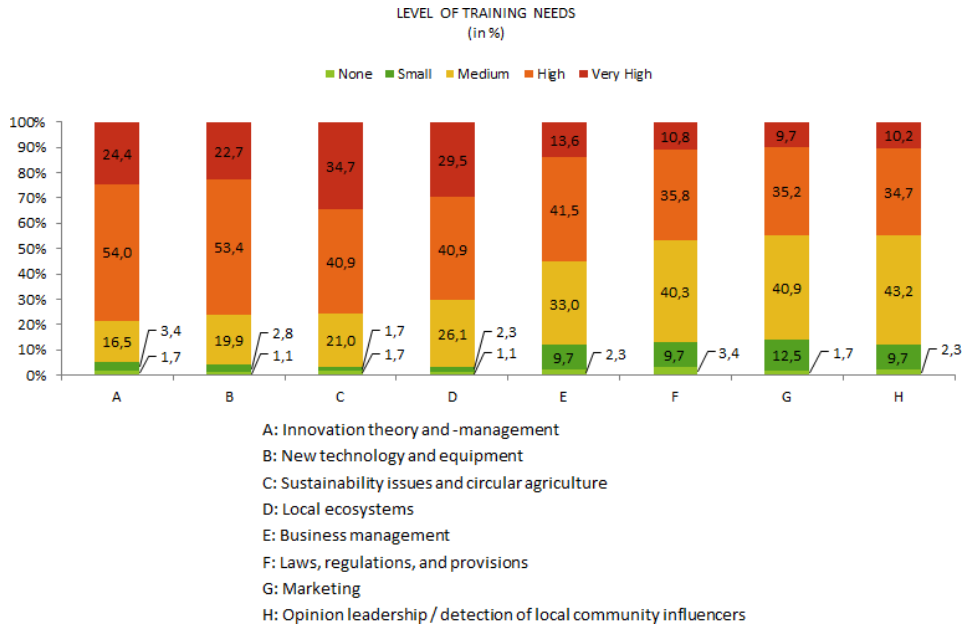
Figure 3. Training needs of Spanish agricultural engineering students, sorted by declining combined percentage of *High* and *Very High*

TRAINING METHODS EFFICIENCY
(grouped in average % per type)

■ 5 (Extremely important) ■ 4 ■ 3 ■ 2 ■ 1 (Not important)

Interactive On-site	Interactive Off-site	Passive Face-to-face	Passive Remotely
- Educational excursions / visits	- Practical courses / exercises	- Short-term seminars	- Creating news groups
- Field demonstrations	- Online courses / e-learning	- Lectures at meetings	- Broadcasts on radio
- Agriculturalist's visits in farms	- Individual education		- Brochures
	- Online communication with agriculturalist		- Television broadcasts
	- Visits to the agriculturalist's office		- Articles in newspapers
	- Helpline instructions		- Agricultural journals
			- DVD's / videos

Figure 4. Preferred training methods
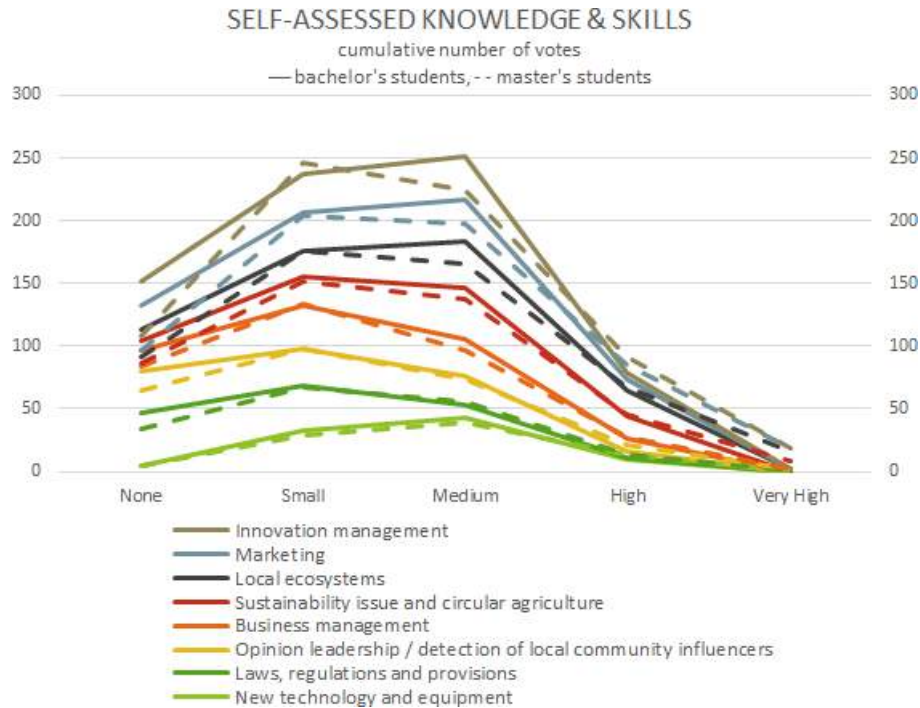
Figure 5. Perception of the self-assessed skills between bachelor and master students

Q7: Is there a correlation with gender or age?

Regarding gender, answers show hardly any difference or significate trend. Male students consistently rate themselves higher when assessing their own knowledge, but not enough to be statistically sound.

Regarding the age of the respondents, bachelor's thought they have more business skills, and showed higher interest in both soft and hard PA. Master's students appreciation of teaching methods that are passive and distant drops more than for bachelor's students. However, none of these considerations are statistically sound.

Regarding the questionnaire and data acquisition, some shortcomings have been identified. First of all, although the sample is representative with respect to demographics, the sample size is limited, especially outside the UPM, which may skew the results. Furthermore, the questionnaire was presented to students on paper and in a fixed format where all students were presented the questions in the same order. This may generate certain biases in the responses, e.g. with respect to positioning relative to page breaks. Finally, the authors are aware of the inherent bias in self-assessment questionnaires, as opposed to objective testing. All in all, further research is needed to extend the validity of the conclusions made in this paper to larger samples that may include other institutions.

4. Conclusions

Results of a survey completed by 192 students of different Spanish universities revealed useful information to outline respondents perception of their own knowledge about PA and about their thoughts on educational needs. For most of them PA was something they had heard about, although almost none declared to have high levels of knowledge. Nevertheless, curiosity was high across all students, and they indicated to be more interested in the more advanced and automated technologies, than in the more traditional means of addressing site-specific variations. Educational gaps are clearly raised by students, whose replies show a clear preference for technological training, while also showing that the business side of a PA enterprise should not be overlooked. Students prefer interactive methods (such as practical sessions with experienced farmers) over passive ones, as well as on-site education over distance-learning; however, MOOCs are also appreciated.

Acknowledgements

References

Bramley R. G.V. and J. Ouzman. Farmer attitudes to the use of sen- sors and automation in fertilizer decision-making: nitrogen fertilization in the Australian grains sector. 2019. In: *Precision Agriculture 2019* , pp. 157–175. issn: 15731618. doi: 10.1007/s11119-018-9589- y.

Eastwood, C., L. Klerkx, , R. Nettle. 2017. Dynamics and distribution of public and private research and extension roles for technological innovation and diffusion: Case studies of the implementation and adaptation of precision farming technologies. Journal of Rural Studies, 49, 1-12.

Erickson, B., S. Fausti, , D.Clay, , S.Clay. 2018. Knowledge, skills, and abilities in the precision agriculture workforce: an industry survey. Natural Sciences Education, 47(1), 1-11. doi: 10.4195/nse2018.04. 0010

Fausti, S, Erickson, B, Clay, S, Schumacher, L, Clay, D and Skouby, D, 2018. Educator Survey: Do Institutions Provide the Precision Agriculture Education Needed by Agribusiness?, Journal of Agribusiness, 36, issue 1, number 302474, https://EconPapers.repec.org/RePEc:ags:jloagb:302474.

Kester C. HW Griepentrog, R Hörner, Z Tuncer 2013 A survey of future farm automation - A descrip-   tive analysis of survey responses. In: Precision Agriculture 2013 - Papers Presented at the 9th European Conference on Precision Agri- culture, ECPA 2013. Wageningen Academic Publishers, Wageningen, , pp. 785–792. isbn: 9789086862245. doi: 10.3920/978-90-8686- 778-3_97.

Kitchen N. R., C. J. Snyder, D. W. Franzen, W. J. Wiebold. 2002. Educational needs of precision agriculture. In: *Precision Agriculture. Vol. 3*. 4. Dec. 2002, pp. 341–351. doi: 10.1023/A:1021588721188.

Lowenberg-DeBoer, J. B. Erickson. 2019. Setting the Record Straight on Precision Agriculture Adoption. Agron. J., 111: 1552-1569. https://doi.org/10.2134/agronj2018.12.077

Sparkle Consortium. Training needs assessment in the field of SPA. 2018. Available at: http://sparkle-project.eu/wp-content/uploads/2019/09/Training-Needs-Assessment-in-the-field-of-SPA.pdf (Accessed June 1st 2021)

Acquisition of Knowledge Through Creativity and Leadership in A Multidisciplinary Environment

Miguel-Ángel Muñoz-García[a,*], Leidy-Oliva Guananga Arrieta[a] , Sonia Benito Hernández[b] , Guillermo Moreda Cantero[a], Adolfo Moya González[a]

[a] Department of Agroforestry Engineering, Universidad Politécnica de Madrid, Madrid, Spain

[b] Department of Agronomic Economy, Statistics and Business Management, Universidad Politécnica de Madrid, Madrid, Spain

* Corresponding author. Email: miguelangel.munoz@upm.es

Abstract

Involving students in collaborative projects and experiential learning helps develop transversal skills that, with passive learning, do not usually have specific training or reinforcement. Additionally, certain transversal skills such as the ability to communicate and coordinate in interdisciplinary work groups are essential for our graduates in their professional activity.

The project consisted of a simulation of a real work environment in which a multidisciplinary team, made up of students from two different subjects of different degrees, must coordinate their efforts to propose a coherent solution to a problem. This project aims to reinforce the skills and competencies necessary both for the development of the rest of the subjects and for the subsequent exercise of the profession. These skills require reinforcement not only from the teacher but also from the classmates themselves, who would be competitors, students and the jury at the same time when assessing the results of the rest of the students.

The problem to be solved focused on a proposal related to the supply of energy for a hypothetical agricultural industry, where agricultural engineering students carried out a design project for an electrical installation and the building students participated in the project by conducting an energy audit.

Through collaborative work, it has been seen that students show a total willingness to work with students of other degrees and that the learning process improves since there is a greater interaction of skills and knowledge, which gives them an interdisciplinary vision of what it would perform a real job.

Despite the difficult situation motivated by COVID pandemic, the project was successful and in total 25 students participated demonstrating that cooperative learning improves transversal skills.

Keywords: Active Learning, Cooperative Learning, Teamwork, Interdisciplinary environment, Transversal competences

1. Introduction

In an increasingly interdependent world, teamwork skills are especially important. These skills allow them to collaborate with professionals from different disciplines (Navarro Soria, I. et al., 2015). With traditional teaching methods, students often do not achieve satisfactory results in their subjects due to deficiencies in transversal skills. Although the latter in theory are present within each subject, they generally do not have specific reinforcement. The training of the agricultural engineer requires more and more multidisciplinary and the acquisition of transversal competences that help them in their working life and in the interaction with the rural environment. This work addresses the acquisition of knowledge by working in multidisciplinary teams in which the student is an active part of learning.

The Project has been carried out by forming small interdisciplinary groups of four or five people and taking into account different active learning methods, such as the cooperative and collaborative learning method and project-based learning, in order to enhance the transversal competences of the students.

1.1. Cooperative Learning

Cooperative learning is a learning method based on student teamwork, according to the definition provided by the UPM Educational Innovation Service (2008), in which students work at the same time to achieve certain common learning objectives those responsible for all members of the group.

In this sense, there are two learning methods that are often used synonymously: cooperative learning and collaborative learning. Although authors like Zañartu (2000) o Panitz (1999), make a difference between the two terms in the degree of structure of the task and of the interactions between the students. Thus, cooperative learning needs more structuring and control by the teacher, while collaborative learning requires more autonomy from the work group, and they maintain almost complete control over the structure of interactions and the results to be obtained.

The meta-analysis carried out on the effects of Cooperative Learning (Goikoetxea, Pascual 2002), concludes that cooperative learning methods have positive effects on academic performance and on other variables such as

productivity and attitudes towards learning compared to other traditional methods. Likewise, it allows the teacher to raise the performance of all his students, both those who are especially gifted and those who have learning difficulties. It also helps to establish positive relationships among students, thus laying the foundations of a learning community in which diversity is valued and, in addition, it provides students with experiences for better social, psychological and cognitive development (Johnson, Johnson et al., 1999).

When students cooperate, they work toward shared goals (Deutsch, 1962; Johnson & Johnson, 1989). For the application of these methods in which they work as a team, the number of members is a very relevant aspect, since the smaller the groups, the greater the effort and involvement. David W. Johnson et al., (1997), state that students work together in small groups to ensure that all members of the group meet the pre-established criteria. In this way, positive interdependence is worked on, in which students encourage and facilitate each one's efforts to learn. In addition, it improves interpersonal relationships and social skills, individual responsibility and group processing (Johnson & Johnson, 1989). However, in many universities traditional teaching still dominates, combining competitive and individualistic practices such as class dictation and assessment based on the learning curve. Therefore, understanding cooperative learning requires differentiating it from competitive and individual learning (David W. Johnson et al., 1997). According to Johnson, Johnson, & Smith, 1991, any activity in any subject, in any type of curriculum, can be structured competitively or individually, or cooperatively.

Previous studies (David W. Johnson et al., 1997) establish that cooperative groups are perhaps the most effective tool that universities have to instill the desired attitudes in students. Numerous studies have found that students strive to maximize their learning and that of their peers in the group and achieve the goals of the project or activity they undertake.

1.2. Challenge Based Learning (CBL)

According to the Challenge-Based Learning Guide, published by the UPM Educational Innovation Service (July 2020), the main precursors of CBL are Problem-Based Learning and Project-Oriented Learning, active methodologies in which Student teams participate to develop a project or solve a diagnostic, design or research problem. In this way, they define Challenge-Based Learning as an active learning approach that seeks the comprehensive development of specific competencies and transversal skills, through a collaborative process in which applied and multidisciplinary knowledge is generated among equals (Educational Innovation Service of the UPM (July 2020)).

In the Guide, they continue to say that the successful development of this method will depend on the instructional design, which will be more complex if the CBL experience covers more than one subject and more when it comes to a coordinated action that affects several departments, degrees or centers.

1.3. Project Based Learning (PBL)

Project-based learning is a learning model in which students plan, implement, and evaluate projects that have real-world application beyond the classroom (Blank, 1997; Dickinson, et al, 1998; Harwell, 1997). According to (Alptekin, DeTurris et al. 2005), Project Based Learning has become a favorable pedagogical model for teaching in engineering programs, in which students work in groups to solve open problems. The pedagogical strategy is complemented by bringing industrial projects to the classroom to offer the most authentic experience possible. The tendency is also to carry out these projects in an interdisciplinary way, with the collaboration of other engineering departments or departments.

For the application of the PBL, learning activities of different disciplines are carried out, which involve the situation to be solved, the formulation of the desired learning objective, the planning of activities to achieve the objective and the analysis and presentation of the results obtained (M. Orozco and A. Tovar 2015).

1.4. Transversal competences

The transversal competences are those aptitudes and abilities that are used for all professions and that make us effective in the development of professional activities, since for a good performance it is necessary to find the balance and put into practice knowledge, experience, values and personality. The role of teachers is to accompany students towards autonomous learning, motivating them to work autonomously. Students take an active role, work as a team, seek information and plan work, making their own decisions, integrating knowledge and developing diverse skills (Vilà Baños, Rubio Hurtado et al. 2014).

The aim of the project is to reinforce the skills and competencies necessary for learning such useful subjects in the subsequent exercise of the profession. The worked skills are:

CT1: Oral and written communication

CT2: Analysis / synthesis and critical reasoning

CT5: Respect for the environment: Promotion of the inclusion of the SDGs

CT6: Organization and planning

CT8: Teamwork

CT10: Leadership and decision making

CT12: Creativity

2. Materials and Methods

2.1. Subjects and students

The proposal includes carrying out of projects in groups of students from different subjects and degrees taught at the Technical School for Agriculture, Food and Biosystems (ETSIAAB) and the Technical School for Building (ETSIE) at the UPM. The project integrated teams of two subjects, which carried out the analysis of a problem and the proposal of a solution, understanding the knowledge of the two subjects involved. One of the subjects, related to the calculation of low voltage electrical installations, belonging to the Degree in Agricultural Engineering of the ETSIAAB (6 students) and the other, related to auditing issues, belonging to the double degree in Building and Business Administration at ETSIE (19 students), which gives it an interdisciplinary character. The approach consisted of a real simulation that involved several disciplines and was carried out in small groups of 3 and 4 students.

To perform the project, the syllabi of each of the subjects were analyzed looking for common points of interest that could be developed in group projects. The "Low Voltage Installations" course seeks for the student to acquire the skills and knowledge necessary to develop and carry out the design of electrical installation projects in rural areas. On its behalf, the syllabus of the subject "Introduction to auditing" covers the typologies, auditing objectives and their application in the financial field, especially. Therefore, focusing on the different types of audits and energy saving and efficiency, it was proposed to carry out an energy audit of an industry in the agricultural sector, thus combining the knowledge of the two subjects involved in the study.

In this way, the projects integrated teams of students from the two subjects, where the agricultural engineering students carried out a design project for an electrical installation and, on the other hand, the building students participated in the project by conducting an energy audit. Finally, the students' evaluation was based on the structure of the energy audit and on the design of the electrical project and the degree of integration between them.

It should be noted that the project has been developed in the midst of a health crisis caused by COVID-19, which has caused some changes in the initially proposed methodology and in the implementation of the project, limiting its development to the online modality and the use of ICT.

2.2. Methodology

First, students were asked to carry out a collaborative project that they must develop throughout the semester, in which they applied the knowledge acquired in the subject. Subsequently, a survey was carried out to find out their opinion about the innovation projects and the degree of implementation in their degrees. Next, interdisciplinary groups were formed and they get in touch so that they could work as a team and solve the problem posed. Each working group planned, searched for information, organized and prepared the report with the solution adopted and presented the results in writing to be evaluated.

The evaluation of the impact of the project was carried out through anonymous surveys, in which the influence and degree of usefulness that innovation projects have on students and in the respective grades is verified. The first was done before the students began to interact. The second and third were carried out during the project, once they began to work together, with the aim of knowing their experience when carrying out the project. Finally, once the project was completed, the initial survey was repeated to contrast and compare the results at the beginning and at the end of the experience and thus be able to determine if the active work method has helped the students' learning. The survey was answered by evaluating from 0 to 10, where 0 does not agree at all or very little and 10 is totally in agreement or very much. In addition, a question was freely answered in which the students were able to express their comments about their satisfaction with the experience.

Table 1. Initial survey to know the students' expectations.

INITIAL SURVEY QUESTIONS	ANSWERS
1. Do you have a precise idea of what educational innovation projects are?	_____ (0-10)
2. Do you think that the educational innovation that is applied improves the teaching process?	_____ (0-10)
3. How do you value the elements of innovation applied to your degree program?	_____ (0-10)
4. In how many innovation projects have you participated in some way?	_____ (0-10)
5. In relation to your degree program, do you know many students from other degree programs?	_____ (0-10)
6. Do you think that the interaction with other degrees is useful to your training?	_____ (0-10)
7. Being the subject of the last courses, how do you value the multidisciplinary in it?	_____ (0-10)
8. Indicate how do you think that the diversity of profiles in a group affects the formation of the students?	_____ (0-10)

9. Indicate the grade of interest in the subject within your degree.	_____ (0-10)
10. Evaluate the expectations that generate the implementation of an innovation project in the subject.	_____ (0-10)
11. Value the team working as part of the learning process.	_____ (0-10)
12. Values the magisterial classes as part of the training.	_____ (0-10)

Table 2. Final survey of the educational innovation project.

FINAL SURVEY QUESTIONS	ANSWERS
1. How much has your knowledge of what educational innovation projects are improved?	_____ (0-10)
2. Taking into account the limitations of the situation, do you think that educational innovation improves the teaching process?	_____ (0-10)
3. How do you value the elements of innovation used in your degree program?	_____ (0-10)
4. Do you feel motivated to participate in other innovation projects?	_____ (0-10)
5. Has your participation in the project allowed you to meet students from other degrees?	_____ (0-10)
6. Do you think that the interaction with other degrees is useful to your training?	_____ (0-10)
7. After the experience of the project, how do you value the pluridisciplinarity?	_____ (0-10)
8. Indicate how you think the diversity of profiles in a group affects the training.	_____ (0-10)
9. Indicate the grade of interest in the subject within your degree.	_____ (0-10)
10. Rate the degree of positive experiences that the project has given you.	_____ (0-10)
11. Value the team work as part of the learning process.	_____ (0-10)
12. Value the magisterial classes as part of the training.	_____ (0-10)

Table 3. Intermediate survey to evaluate the motivation of the students throughout the experience, before the teams were created.

PRE-GROUP SURVEY QUESTIONS	ANSWERS
1. What is your assessment of the degree with which you will have to collaborate?	_____ (0-10)
2. Do you know the field of work of the other degree?	_____ (0-10)
3. How likely are you to collaborate with someone from the other degree program in a future job?	_____ (0-10)
4. What are your expectations regarding the job, what do you expect from this interaction?	

Table 4. Intermediate survey to evaluate the motivation of the students throughout the experience, after the interaction by teams

POST-GROUP SURVEY QUESTIONS	ANSWERS
1. What is your assessment of the degree with which you have collaborated?	_____ (0-10)
2. What did you think of the other degree's scope of work?	_____ (0-10)
3. Once you have finished the cooperative work, assess the probability of collaboration with someone from the other degree in a future job.	_____ (0-10)
4. Were your expectations for the job met?	_____ (0-10)
5. Has the interaction with students from the other degree program been as you expected?	_____ (0-10)

The project seeks that students get involved in their own learning and expand the range of possibilities of what can be found in a future job. For the development of the project, the use of ICT has been essential for the search for information, the preparation of documents and communication between the members of the groups, since it was not possible to hold face-to-face meetings.

3. Results and Discussion

The questions of the first and final surveys, were formulated in such a way that results can be obtained in terms of students' knowledge about educational innovation projects and their participation in them (question 1 to question 4). With questions 5 and 6 we seek to know the opinion about the usefulness when interacting with other degrees students. With question 10 it is intended to know what expectations the application of an innovation project generates in the

subjects. It also asked how they value group work (question 11) and lectures (question 12) and, finally, the importance that students give to multidisciplinary (question 7) and the diversity of profiles (question 8) in their training professional. The average of the answers given to the questions at the beginning and at the end of the experience is shown in Figure 1.
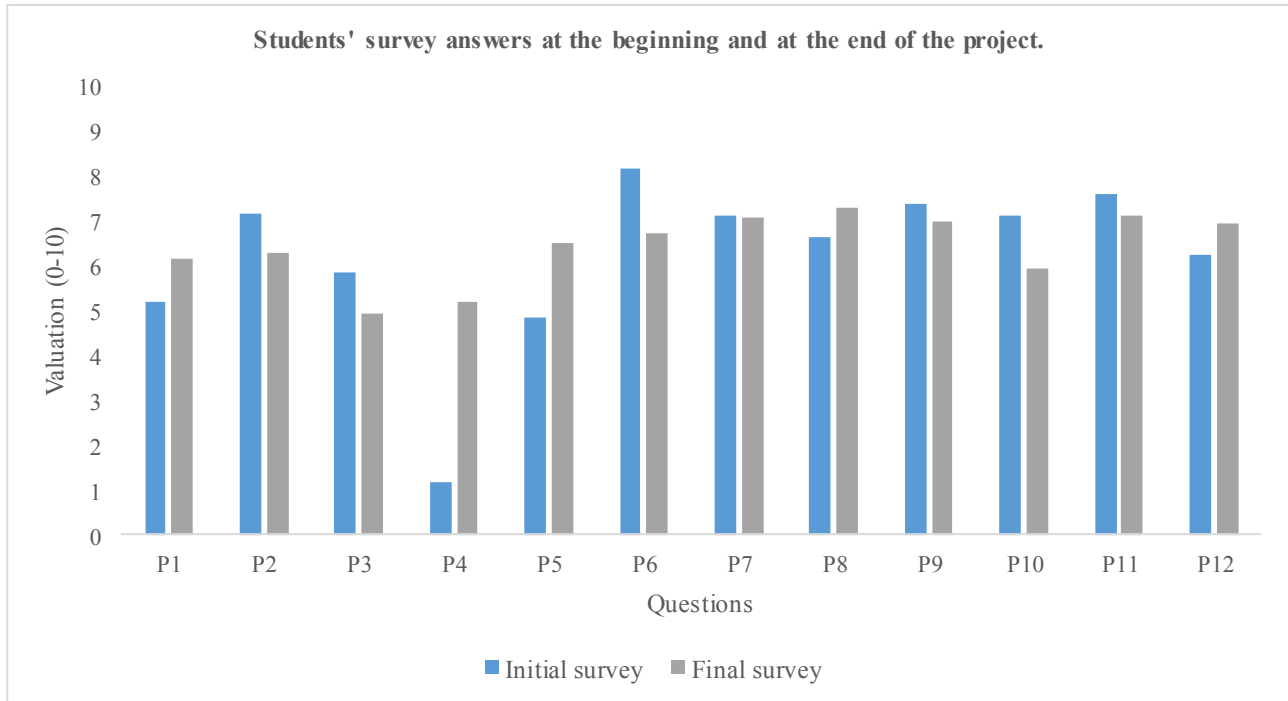
Figure 1. Average of students' survey answers at the beginning and at the end of the project.

About 58% of the questions had a lower rating at the end of the experience. This is mainly due to the circumstances in which the project was developed due to the health crisis that we are going through due to COVID-19, to the workload of the students, which did not allow them to dedicate much time to the development of the project and especially the difficulties for the interaction between the groups. However, after the end of the project, aspects such as knowledge of what are the innovation projects and cooperative groups (question 1) and the motivation to participate in other projects (question 4) had a better evaluation. The opportunity to meet and collaborate with students of other degrees was also valued positively (question 5).
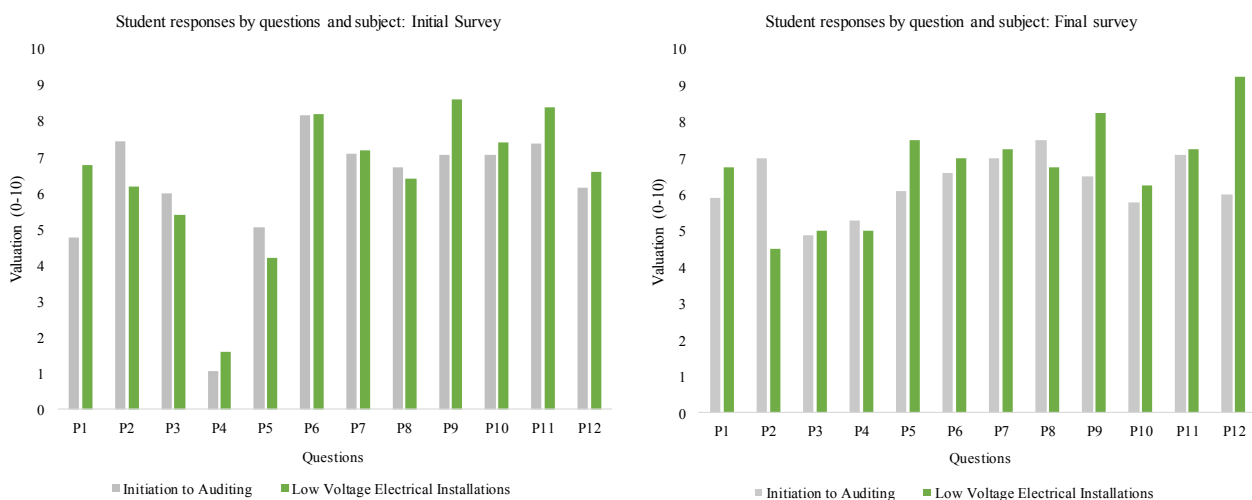
Figure 2. Average of student responses per question and subject, from the initial and final surveys of the project.
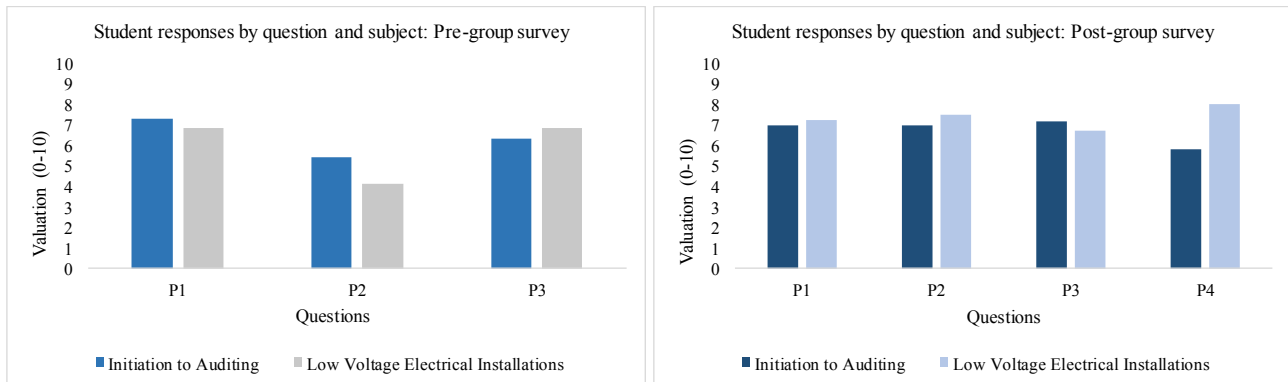
Figure 3. Average of student responses per question and subject from the project's intermediate surveys.

Analyzing the students' answers of the two subjects separately, it should be noted that in both the assessment regarding participation in an innovation project has been low, at least 40% of the students have not participated in any project of this type. This, linked to the responses obtained regarding the students' assessment of the innovation elements applied to their degree, which have an average that varies between 5 and 6 points out of 10, indicates that active learning methods are not integrated into largely in universities.

Comparing the assessment of the students of the master classes as part of the training with the group work, in the first survey group work received a higher score compared to the master classes, but in the second survey, although this was maintained trend, the score was lower than at the beginning. This may be due to the limitations set by the pandemic and the lack of knowledge between the degrees. Since, although the contents of the subjects had points in common, it was difficult for the students to channel the objectives of the project.

In the intermediate questionnaires, open questions were asked, which were analyzed in order to provide additional qualitative information to complement the numerical results obtained. Thanks to this, it is possible to understand the reason for the negative variation of the expectations that the students had at the beginning and at the end of the project. In most cases, the initial expectations were not met due to the lack of time to prepare the work well and the incompatibility of schedules, since they were expected that the problem to be solved had a direct application of the concepts studied and the project went further , since the objective was to work in a multidisciplinary environment in which it was necessary to adapt to the circumstances of a possible job, where you have to collaborate with different profiles of professionals and work in a group, to find an optimal solution to a problem real .

Upon completion of the collaborative project, most students believe that collaboration in future work is highly likely, based on the results of question 3 of Figure 3. In question 4 (Figure 4), knowledge of the scope of the work between degrees, the average rose almost two points compared to the beginning of the project.

4. Conclusions

The interdisciplinary nature of the project outstands since it has involved students from two rather different subjects and degrees. Developing this project helped students to learn more about other degrees, broaden their points of view for a future job, and be aware of the multidisciplinary nature that they will found in their professional career. In addition, starting from a real approach, helped the students to increase their motivation to collaborate in the Project and also allowed them see the practical application of what they had studied in the subjects.

The study has been developed in an exceptional situation, so it is worth noting the additional effort that the students had to make to carry out the project. There have been several limitations, on the one hand, pandemic fatigue and, on the other, lack of knowledge between degrees, which has made the relationship between the different groups of students somewhat difficult. Organization, teamwork, oral and written communication and the use of ICT have been fundamental since the project could not be developed face-to-face.

Despite the number of students who participated in the study is not very large and that the analysis of the results is solely based on their perception, the results of the project coincide with previous research that maintains that active teaching methodologies imply more demand activity and autonomy to students.

The project also allowed students to have a better understanding of how other faculties work and what is the scope of professional development of the different engineering degrees. In addition, distance interaction with other students who did not know, participation, the ability to form and debate opinions, oral expression, critical spirit and teamwork were encouraged. In short, the application of this type of projects exercises social skills, gives them autonomy and

prepares them so that they are capable of solving any challenge or problem that may be encountered in a future professional position. Collaborative Learning, Challenge-Based Learning and Project-Oriented Learning are the ones that have the greatest effectiveness in the formation of competencies.

Due to the limitations, some lines of study arise, repeating this experience in successive academic courses and interacting with degrees that can complement the knowledge acquired in the different subjects, with the aim of obtaining data that provide greater solidity to the results. In addition, it would be convenient to open fronts for joint collaboration with other research groups and other areas of knowledge, in order to ratify the transferability of the teaching experience to other subjects and disciplines.

Acknowledgements

References

Journal articles:

Alptekin, S.E., Deturris, D., Macy, D.J. and Ervin, J.E., 2005. Development of a flying eye: A project-based learning experience. Journal of Manufacturing Systems, 24(3), pp. 226-236. https://doi.org/10.1016/S0278-6125(06)80012-9

Blank, W. (1997). Authentic instruction. In W.E. Blank y S. Harwell (Eds.), Promising practices for connecting high school to the real world (pp. 15–21). Tampa, FL: University of South Florida. (ERIC Document Reproduction Service No. ED407586).

David W. Johnson, Roger T. Johnson, and Karl A. Smith, 1997. Universidad de Minesota. 60 Peik Hall. 159 Pillsbury Drive, S.E. Minneapolis, Minnesota 55455. Mayo de 1997; revisado en septiembre de 1997. https://studylib.es/doc/6435716/el-aprendizaje-cooperativo-regresa-a-la-universidad

Deutsch, M. (1962). Cooperation and trust: Some theoretical notes. In M. R. Jones (Ed.), Nebraska symposium on motivation (pp. 275-319). Lincoln, NE: University of Nebraska Press.

Goikoetxea, E. and Pascual, G., 2002. Aprendizaje Cooperativo: Bases teóricas y hallazgos empíricos que explican su eficacia. Educación XX1, 5(1), pp. 227-247. http://hdl.handle.net/11162/24046

Johnson, D. W., & Johnson, R., 1989. Cooperation and competition: Theory and research. Edina, MN: Interaction Book Company.

Johnson, D.W., Johnson, R.T., & Smith, K.A. ,1991. Active learning: Cooperation in the college classroom. Edina, MN: Interaction. DOI:10.5926/arepj1962.47.0_29

Johnson, D.W., Johnson, R.T. and Holubec, E.J., 1999. El aprendizaje cooperativo en el aula. https://www.researchgate.net/publication/265567256_El_aprendizaje_cooperativo_en_el_aula

M.Orozco and A.Tovar, 2015. Universidad Autónoma de Nayarit Ciudad de la Cultura Amado Nervo Boulevard Tepic-Xalisco S/N C.P. 63190 Tepic, Nayarit. México. J. Peña, M. Moctezuma, (eds.). Ciencias de la Docencia Universitaria.Proceedings-©ECORFAN-México, Nayarit, 2015.

Navarro Soria, Ignasi; González Gómez, Carlota; López Monsalve, Begoña; Botella Pérez, Paula, 2015. Aprendizaje de contenidos académicos y desarrollo de competencias profesionales mediante prácticas didácticas centradas en el trabajo cooperativo y relaciones multidisciplinares. Revista de Investigación Educativa, 33(1), 99-117. DOI: https://doi.org/10.6018/rie.33.1.183971

Panitz, T., 1999. Collaborative versus Cooperative Learning: A Comparison of the Two Concepts Which Will Help Us Understand the Underlying Nature of Interactive Learning. For full text: http://www.capecod.net/~TPanitz/Tedspage.

Vilà Baños, R., Rubio Hurtado, M.J. and Berlanga, V., 2014. La investigación formativa a través del aprendizaje orientado a proyectos: una propuesta de innovación en el grado de pedagogía. RECERCAT (Dipòsit de la Recerca de Catalunya). http://hdl.handle.net/2072/330936

Zañartu Correa, M. L. (2000): "Aprendizaje colaborativo: una nueva forma de diálogo interpersonal en red", en Revista digital de educación y nuevas tecnologías. Contexto Educativo, V-28.

Web pages:

Servicio de Innovación Educativa de la UPM (2008). Aprendizaje Orientado a Proyectos. Madrid: Universidad Politécnica de Madrid. Recuperado en: https://innovacioneducativa.upm.es/sites/default/files/guias/AP_PROYECTOS.pdf

Servicio de Innovación Educativa de la UPM (2008). Aprendizaje Cooperativo. Madrid: Universidad Politécnica de Madrid. Recuperado en: https://innovacioneducativa.upm.es/sites/default/files/guias/Aprendizaje_cooperativo.pdf

Servicio de Innovación Educativa de la UPM (Julio 2020). Guía de Design Thinking. Madrid: Universidad Politécnica de Madrid. Recuperado en: https://innovacioneducativa.upm.es/sites/default/files/guias/Guia-DesignThinKing.pdf

Servicio de Innovación Educativa de la UPM (Julio 2020). Guía de Aprendizaje Basado en Retos. Madrid: Universidad Politécnica de Madrid. Recuperado en: https://innovacioneducativa.upm.es/sites/default/files/guias/GUIA-ABR.pdf

State of the Art on Degree Study Programs in Agricultural/Biosystems Engineering in EU

Antonio Comparetti[a,*], Pierluigi Febo

[a] Department of Agricultural, Food and Forest Sciences, University of Palermo, Palermo, Italy

* Corresponding author. Email: antonio.comparetti@unipa.it

Abstract

The process of international harmonisation of the degree study programs in Agricultural/Biosystems Engineering (ABE) was started by Prof. Giuseppe Pellizzi during CIGR 1989 Conference and was continued by Prof. Pierluigi Febo in EU, within EurAgEng SIG RD12 - Education and Communication, and also within CIGR WG1 - Agricultural Engineering University Curricula Harmonization.

Then, four thematic networks were effective:

1) USAEE-TN (University Studies of Agricultural Engineering in Europe - A Thematic Network), comprising 31 HEIs (Higher Education Institutions) from 27 countries, from 2002 to 2006;

2) Consortium POMSEBES (Policy Oriented Measures in Support of the Evolving Biosystems Engineering Studies in USA - EU), comprising eight EU and four USA HEIs, from 2006 to 2008;

3) ERABEE-TN (Education and Research in Biosystems Engineering in Europe - A Thematic Network), comprising 35 HEIs from 27 countries, from 2007 to 2010;

4) Consortium TABE.NET (Trans-Atlantic Biosystems Engineering Curriculum and Mobility), comprising four EU and two USA HEIs, from 2009 to 2013.

Some examples of significant changes relevant to ABE degree study programs occurred in EU after the end of ERABEE-TN project: they were the curricula established by the HEIs of seven countries (Czech Republic, France, Germany, Lithuania, Netherlands, Norway and Portugal).

The aim of this work is to show the state of the art on ABE degree study programs in EU 21 years after the last overview, presented during AgEng2000 Conference ("The University Structure and Curricula on Agricultural Engineering - An Overview of 36 Countries", Editors Pierluigi Febo and Da-Wen Sun).

The Universities of the above seven countries offer BSc. and MSc. curricula in ABE area, while the HEIs of other countries (e.g. Austria, Denmark, Finland and Italy) offer BSc. and MSc. curricula including subjects related to Agricultural Engineering and Applied Agricultural Engineering as at least 30% of the total ECTS (European Credit Transfer System) study load.

Keywords: Higher Education, Agricultural Engineering, Biosystems Engineering, harmonisation, ECTS.

1. Introduction

The process of international harmonisation of the degree study programs in Agricultural/Biosystems Engineering (ABE) was started by Prof. Giuseppe Pellizzi during CIGR 1989 Conference and was continued by Prof. Pierluigi Febo in EU, within EurAgEng SIG RD12 - Education and Communication, and also within CIGR WG1 - Agricultural Engineering University Curricula Harmonization (Comparetti and Febo, 2018 a, b).

Then, four thematic networks were effective:

1) USAEE-TN (University Studies of Agricultural Engineering in Europe - A Thematic Network), comprising 31 HEIs (Higher Education Institutions) from 27 countries, from 2002 to 2006;

2) Consortium POMSEBES (Policy Oriented Measures in Support of the Evolving Biosystems Engineering Studies in USA - EU), comprising eight EU and four USA HEIs, from 2006 to 2008 (http://www.pomsebes.aua.gr/);

3) ERABEE-TN (Education and Research in Biosystems Engineering in Europe - A Thematic Network), comprising 35 HEIs from 27 countries, from 2007 to 2010 (http://www.erabee.aua.gr/);

4) Consortium TABE.NET (Trans-Atlantic Biosystems Engineering Curriculum and Mobility), comprising four EU and two USA HEIs, from 2009 to 2013.

The authors of this work were partners of the above thematic networks 1, 2 and 3.

Some examples of significant changes relevant to ABE degree study programs occurred in EU after the end of ERABEE-TN project: they were the curricula established by the HEIs of seven countries (Czech Republic, France, Germany, Lithuania, Netherlands, Norway and Portugal).

The aim of this work is to show the state of the art on ABE degree study programs in EU 21 years after the last overview, presented during AgEng2000 Conference, i.e. "The University Structure and Curricula on Agricultural

Engineering - An Overview of 36 Countries", Editors Pierluigi Febo and Da-Wen Sun (Febo and Sun, 2000).

2. Materials and Methods

Upon request to at least one University delegate per each EU country, some of them provided the authors of this work with the data used for this survey.

Moreover, an updated survey was carried out at the web-sites of the EU Universities of the above seven countries (Czech Republic, France, Germany, Lithuania, Netherlands, Norway and Portugal), in order to measure, within the BSc. and MSc. degree study programs, the study load of the subjects related to Agricultural Engineering and Applied Agricultural Engineering.

3. Results and Discussion

The updated survey results (2021) related to three of the seven EU countries (Czech Republic, France, Germany, Lithuania, Netherlands, Norway and Portugal) where Agricultural/Biosystems Engineering curricula were established after the end of ERABEE-TN project are summarised in Table 1.

Table 1. Updated survey results (2021) related to three of the seven EU countries where ABE curricula were established after the end of ERABEE-TN project.

Country	Study cycle	Degree study program	Total ECTS	Agricultural Engineering and Applied Agricultural Engineering ECTS (%)
Czech Republic	BSc.	Agricultural Engineering	180	51
	MSc.	Technology and Environmental Engineering	120	60
Lithuania	BSc.	Smart Engineering	240	41
	MSc.	Hydraulic Engineering	120	45
Portugal	MSc.	Agricultural (Agronomical) Engineering	120	35
	MSc.	Precision Agriculture Technologies	120	32

The Universities of the above seven countries (Czech Republic, France, Germany, Lithuania, Netherlands, Norway and Portugal) offer BSc. and MSc. curricula in ABE area. Some of them are reported in the following sub-paragraphs.

Instead, the HEIs of other countries (e.g. Austria, Denmark, Finland and Italy) offer BSc. and MSc. curricula including subjects related to Agricultural Engineering and Applied Agricultural Engineering as at least 30% of the total ECTS (European Credit Transfer System) study load.

3.1. Czech Republic

The Czech University of Life Sciences Prague (CZU) (https://www.czu.cz/en/) is a public University, having more than 18,000 students (10% are international students), six Faculties and one Institute, offers over 170 accredited degree study programs at BSc., MSc. and PhD levels (in nine BSc., 20 MSc. and 18 PhD programs the language of instruction is English), is member of the Euroleague for Life Sciences (www.euroleague-study.org) and has implemented the ECTS, which highly facilitates the mobility of students.

Within CZU, the Faculty of Engineering (https://www.tf.czu.cz/en/) consists of 10 departments, one Laboratory of Information Technologies, one Technology Certification Centre and one Department of Expert Activities (Expert Institute), as well as it is equipped with a research and development mini-brewery, which has especially made a great contribution to the practical instruction of the degree study program in Technological Equipment of Buildings.

The academic year begins in October and is divided into two semesters.

The Faculty of Engineering offers the following nine 3-year BSc. degree study programs and one 2-year follow-up MSc. degree study programs in Agricultural/Biosystems Engineering:
1) Agriculture Machinery (ZT);
2) Road and City Automobile Transport (SMAD);
3) Technique and Technology of Waste Treatment (TTZO);
4) Technological Equipment of Buildings (TZS);
5) Trade and Business with Technology (OPT);
6) Information and Control Technology in the Agro-Food Complex (IŘT);
7) Technology and Environmental Engineering (TEE);
8) Maintenance Engineering (IU);

9) Agricultural Engineering (AE) (taught in English and including the first two years dealing with theoretical basis in agricultural technology and the third year focused on the practical application of the theoretical knowledge in technical and biological sciences).

After BSc. graduation, it is possible to attend a 2-year MSc. degree study program, also taught in English. The graduates will achieve theoretical knowledge on the application of exact procedures in agricultural technology, as well as deep technical knowledge on the theory of technical disciplines that enable them to work in the areas of machine development, technological use and maintenance of technology.

3.2. The Netherlands

In the Netherlands, higher education is provided by both Universities and Applied Universities (http://info.studielink.nl/en/studenten/Pages/Default.aspx).

The academic year begins on the 1st of September and ends in early July, consists of 40 weeks, each of 42 hours. One ECTS equals a study load of 28 hours, so that one year consists of 60 ECTS.

Universities offer higher scientific and artistic education and award 3-year BSc. and 2-year MSc. degrees, as well as PhD degrees.

Universities of Applied Sciences (UAS) provide more practical education, aiming at satisfying the needs of the labour market, as well as they award UAS BSc. degrees and UAS MSc. degrees, for a total of four years.

The University of Wageningen has one faculty, 19 BSc. degree study programs and 30 MSc. degree study programs, e.g. the BSc. in Agrotechnology and the MSc. in Biosystems Engineering.

The above BSc. degree study program is taught in Dutch language in the first year, partly in Dutch and partly in English in the second year, in English in the third year (https://ssc.wur.nl/Handbook/Programme/BAT).

The MSc. degree study program in Biosystems Engineering is taught in English language (https://ssc.wur.nl/Handbook/Programme/MBESome).

HAS University of Applied Sciences offers the following four agricultural related BSc. degree study programs:
1) Business Management in Agriculture & Food (in English language) (https://hasuniversity.nl/study-programmes/business-management-in-agriculture-food);
2) Horticulture and Business Management (in English language) (https://hasuniversity.nl/study-programmes/horticulture-business-management-den-bosch);
3) International Food and Agrobusiness (in English language) (https://hasuniversity.nl/study-programmes/international-food-agribusiness-den-bosch);
4) Animal Husbandry (in Dutch language) (https://hasuniversity.nl/study-programmes/animal-husbandry-den-bosch).
Van Hall Larenstein University of Applied Sciences offers the following four agricultural related degree study programs:
1) Animal Husbandry (4-year BSc. in English language) (https://www.vhluniversity.com/study/programmes/bachelor/animal-husbandry);
2) International Business in Food and Flowers (4-year BSc. in English language) (https://www.vhluniversity.com/study/programmes/bachelor/internationalbusiness-in-food-and-flowers);
3) Agricultural Production Chain Management (1-year MSc. in English language) (https://www.vhluniversity.com/study/programmes/master/agricultural-production-chain-management);
4) Innovative Dairy Chain Management (1-year MSc. in English language) (https://www.vhluniversity.com/study/programmes/master/innovative-dairy-chain-management).
AERES University of Applied Sciences offers the following agricultural related degree study programs:
1) several 1 and 2-year degree study programs (https://www.aeresuas.com/programmes?facetIds=00000000-0000-0000-0000-000000000000&page=1);
2) European Food Business (BSc. in English language) (https://www.aeresuas.com/programmes/bachelor-programmes/european-food-business);
3) Agribusiness Development (1-year MSc. in English language) (https://www.aeresuas.com/programmes/master-programmes/agribusiness-development).

3.3. Norway

Inland Norway University of Applied Sciences (INN) offers BSc. degree study programs in Agronomy and Agricultural Engineering (https://eng.inn.no/).

Norwegian University of Life Sciences (NMBU) offers several degree study programs (https://www.nmbu.no/en), e.g. a 5-year MSc. degree study program in Engineering.

However, from 2019, this HEI offers a 5-year MSc. degree study program in Applied Field Robotics, based on Thorvald robot developed by the University itself (https://sagarobotics.com/).

At the moment starting a MSc. or BSc. degree study program in precision agriculture is being discussed at NMBU,

because a need for such a study program is seen.

3.4. Portugal

In Portugal, in 2019, there were 287 HEIs, of which 123 were Universities and 164 were polytechnic education institutions.

The academic year begins in September and ends in July, as well as it is divided in two semesters, i.e. two per academic year.

In 2005, following the Bologna Process, higher education began to have a new structure of three cycles of studies, leading to the academic degrees of "licenciado" (BSc.), "mestre" (MSc.) and "doutor" (PhD). This structure was introduced in 2006 and fully implemented from the academic year 2009-2010.

In 2014, in order to implement the short 1st cycle degree study program provided in the Qualifications Framework of the European Higher Education Area, a non-academic higher education cycle, called professional higher technical degree study program, was established.

There are 17 Universities and polytechnic education institutions offering BSc. degree study programs in the area of Agricultural/Biosystems Engineering, e.g. Agricultural Engineering (4), Food Engineering (4), Agricultural and Animal Engineering (1), Agronomy (6) and Organic Agriculture (1).

Moreover, there are 18 Universities and polytechnic education institutions offering MSc. degree study programs similar to Agricultural/Biosystems Engineering, e.g. Agricultural (Agronomical) Engineering (7), Animal Production Engineering (1), Mediterranean Agro-Forestry Systems (1), Precision Agriculture Technologies (1), Tropical Agronomy and Sustainable Development (1), Agroecology (1), Agronomy (1), Sustainable Agriculture (2), Mediterranean Agro-Forestry Systems (1), Organic Farming (1) and Agricultural and Animal Production Engineering (1).

In the MSc. degree study program in Agricultural (Agronomical) Engineering, sustainable production is a concern and a discipline that is included in the majority of the subjects.

The BSc. degree study program in Agronomy offered by the University of Évora is taught in Portuguese language, has 3-year duration and includes 180 ECTS (60 ECTS per year) (https://www.en.mobilidade.uevora.pt/course_catalog/Curricular-Units-offered-by-Course/bachelor_degree-1st-Cycle/(curso)/2504).

The MSc. degree study program in Agricultural (Agronomical) Engineering offered by the University of Évora is taught in Portuguese language, has a 2-year duration and includes 120 ECTS (60 ECTS per year, of which 42 ECTS are for the thesis) (https://www.en.mobilidade.uevora.pt/course_catalog/2nd_cycle/curso/(codigo)/448/(view)/plano_estudos).

As examples, the outlines of the BSc. and MSc. degree study programs offered by the University of Évora are shown in Figures 1 and 2, respectively.

PORTUGAL

7.2A

University of Évora

School of Sciences and Technology

```
Degree Title: BSc
Duration: 3 years (6 semesters)
180 ECTS (150 required in compulsory subjects and 30 in optional subjects)
```

Agronomy (academic year 2019/2020)

COMPULSORY SUBJECTS RELATED TO AGRICULTURAL ENGINEERING

Mathematics (6 ECTS)
General Physics (6 ECTS)
Water Resources and Irrigation (6 ECTS)

OPTIONAL SUBJECTS RELATED TO AGRICULTURAL ENGINEERING

Post-harvest Technology (5 ECTS)
Wine and Olive Oil Technology (5 ECTS)
Greenhouse Technology (5 ECTS)
Farm Tractors and Self-propelled Equipment (5 ECTS)
Drainage and Soil and Water Conservation (5 ECTS)
Training with Farm Equipment (5 ECTS)

SUBJECTS RELATED TO AGRICULTURAL ENGINEERING TAKE UP:

27 %

OF THE HOURS FOR THE DEGREE (lectures + practical training).

Figure 1. Outline of the BSc. degree study program in Agronomy offered by the University of Évora (Portugal).

PORTUGAL

7.2B

University of Évora

School of Sciences and Technology

```
Degree Title: MSc
Duration: 2 years (4 semesters)
120 ECTS (72 required in compulsory subjects and 6 in optional subjects)
```

Agronomical Engineering (academic year 2019/2020)

```
COMPULSORY SUBJECTS RELATED TO AGRICULTURAL ENGINEERING
```

Experimental Design (6 ECTS)
Applied Hydraulics (6 ECTS)
Analysis and Technology of Irrigation Systems (6 ECTS)
Project in Agronomical Engineering (9 ECTS)

```
OPTIONAL SUBJECTS RELATED TO AGRICULTURAL ENGINEERING
```

Conservation Agriculture (6 ECTS)
Post-harvest and Quality Instrumentation of Horticultural Products (6 ECTS)
Irrigation and Drainage Systems Design (6 ECTS)
Precision Agriculture (6 ECTS)
Planning of Rural Facilities and Equipment (6 ECTS)
Farm Mechanisation Projects (6 ECTS)

```
SUBJECTS RELATED TO AGRICULTURAL ENGINEERING TAKE UP:

                        52 %

OF THE HOURS FOR THE DEGREE (lectures + practical training).
```

Figure 2. Outline of the MSc. degree study program in Agricultural (Agronomical) Engineering offered by the University of Évora (Portugal).

4. Conclusions

From the results of this work it is possible to deduce that the harmonisation, the simplification and the increase of the transparency of the degree study programs in Agricultural/Biosystems Engineering occurred during the last 21 years.

The harmonisation, as implementation of Bologna process, i.e. the education system 3 + 2, occurred in the whole EU. Yet, firstly the 1st cycle (BSc.) was more specialised than the 2nd cycle (MSc.) in some countries (e.g. Italy), while currently this situation occurs in other countries (e.g. Spain).

Instead, the harmonisation of ABE degree study programs occurred only in some countries, while this was inhibited by the poor or absent relationship between Universities and the national Ministry of Education in the majority of them (e.g. Italy) and, sometimes, also by a weak influence of Agricultural Engineers within each University (e.g. Palermo University).

The simplification of the degree study programs in this area was obtained through the establishment of new curricula, as those offered by the above seven EU countries after the end of ERABEE-TN project.

Finally, the increase of transparency was made easier by the updating of the web-sites of EU Universities and also by the database on the degree study programs in Agricultural/Biosystems Engineering developed under USAEE-TN and ERABEE-TN projects.

Another result of ERABEE-TN project was the establishment of new Erasmus+ inter-institutional agreements, e.g. between Palermo University (Italy) and Vytautas Magnus University (Lithuania), Agricultural University of Athens (Greece) and Ruse University (Bulgaria), respectively. This contributed to increase the student and teaching staff

mobility between these Universities, that was one of the objectives of ERABEE-TN project.

Even if it is not funded anymore, the ERABEE thematic network is going on implementing the objectives of the related project (http://www.erabee.aua.gr/OBJECTIVES.htm).

References

Febo, P., D.-W. Sun, 2000. *The University Structure and Curricula on Agricultural Engineering - An Overview of 36 Countries*. FAO, CIGR, EurAgEng. 236 p.

Comparetti, A., P. Febo, 2018. Harmonisation of Higher Education in Agricultural/Biosystems Engineering. In *EurAgEng 2018 Conference*. Wageningen, The Netherlands, July 8-11.

Comparetti, A., P. Febo, 2018. Harmonization of Higher Education in Agricultural/Biosystems Engineering. CIGR (International Commission of Agricultural and Biosystems Engineering) Newsletter December 2018. 115, 4-6. https://cigr.org/sites/default/files/newsletters/CIGR_NL115.pdf.

Diagnosis and Assessment of Visual Impacts for Aesthetics Improvement of Jerte Valley Municipalities (Spain)

Julio Hernández Blanco[1], M. Montserrat Jiménez Martín[2], Jacinto Garrido Velarde[3], María Jesús Montero Parejo[1]

[1] Department of Graphics Design and Research Group of Desing, Sustainability and Added Value (INNOVA), University of Extremadura, 10600 Plasencia (Cáceres), (SPAIN); juliohb@unex.es ; cmontero@unex.ex

[2] Graduate in Forestry and Natural Environment Engineering by University of Extremadura (SPAIN); marratjm@gmail.com

[3] Department of Social Sciences, Languages and Literatures, and University Research Institute for Sustainable Territorial Development (INTERRA), University of Extremadura, 06071 Badajoz, (SPAIN). jgarridoif@gmail.com ; jgvelarde@unex.es

Abstract

The achievement of an inventory of the different visual impacts on each municipality of the Region "Valle del Jerte" has been proposed in this work. The analysis of each case, the diagnosis and the proposals of corrective actions and the enhancing actions of the resources of the area in an integral way, taking full advantage of the synergies that take place in the territory, have completed the work. The main aim of this work is to turn the "Valle del Jerte" into an innovative space that works for the sustainability of its natural, economic and cultural heritage.

The project was approached in two phases:

1st phase: where a methodology and work plan to generate an inventory of urban and landscape visual damage of each municipality was developed. Then, an analysis and diagnosis of urban and landscape impacts and the correct and empowering action proposals of each municipality was identified, given that the objective is to create a plan or guide to improve and strengthen each municipality.

2nd phase: where a proposal for budgeted action agreed with the municipal corporations of each municipality has been made, to reach villages aesthetically more attractive.

Keywords: Rural Development, Visual Impact, Landscape Planning, Cultural Heritage.

1. Introduction

1.1. Introduction to traditional architecture in the Jerte Valley

The Jerte Valley is characterized by having a very typical architecture in the mountainous areas of northern Cáceres. In general, construction models characteristic of mountain areas are followed, where masonry and seating walls, overhangs, javelins, balconies, arcades, crossbars, lintels, laps, hallways and other characteristic elements come together to make structures stronger and protect their inhabitants from the cold, rain and wind of harsh winters.

The different municipalities have various architectural typologies, modern and traditional, being able to classify the latter into three main ones: the mountain range, the half-timbered and the mixed.

The mountain architecture uses stone as a main building element, either in its uncoated form (masonry) or carved (seating). This makes constructions especially strong and durable, at the expense, certainly of a greater cost and difficulty in their construction.

The half-timbered architecture consists of masonry on the ground floor, but on the following floors it uses a wooden fabric filled with sun-cooked mud and straw adobes. Then, on the facades, it is revoked with lime mortar. These constructions are also strong and resistant, but not as durable over time as the previous ones.

The mixed typology is the one that appear elements of the mountain and half-timbered typologies at the same time.

Of course, all typologies can be given in the same municipality. And all three styles are complemented by wooden structures on floors, eaves, struts, balconies, etc.

1.2. Justification of research activities

Within the Action Plan (2014-2020) of the Participatory Local Development Strategy of the Jerte Valley (PLDS) is defined the line of action of RENEWAL OF POPULATIONS that has a program of beautification of peoples whose objective is the aesthetic improvement of urban spaces, creating an urban identity collectively. Among others, the following improvement actions stand out:

- cover urban solid waste containers (SUR)
- homogenize urban furniture and street lighting
- employ urban art
- improve the entry and exit of villages

- create recreation and parking areas
- eliminate the main black dots
- recover from iconic spaces
- landscaping of indoor areas
- eliminate wiring
- green areas and playgrounds
- recover and improve squares, fountains, viewpoints, rest areas, bridges, etc.

Figure 1. Half-timbered architecture

Figure 2. Mountain architecture

Figure 3. Mixed architecture

The proposal for action that has been carried out for each municipality is intended to implement with the Public Call for 6/18 aid under the LEADER methodology, thus contributing to the long-term sustainable development of rural territories, as well as contributing to the improvement of governance and mobilization of the endogenous development potential of rural areas in the Jerte Valley Shire.

This call frames sub-measures 19.2 Support for the implementation of operations in accordance with the Participatory Local Development Strategy

1.3. Objectives

The objectives pursued by this work are the inventory, analysis and diagnosis of the main urban and landscape visual impacts detected in each municipality of the Jerte Valley that decrease the aesthetics of the population core and adjacent areas, as well as the approach of possible actions to mitigate these impacts with actions of recovery, rehabilitation, renovation, reforms and modernization of the inventoried areas.

Proposals for action will be made from two points of view. The first, homogenization proposals for the eleven municipalities and the second, actions aimed at maintaining the idiosyncrasies of each municipality.

The power-up proposals aim to strengthen the landscape resources possessed by each municipality and contribute to the enrichment of the Jerte Valley as a whole.

2. Materials and Methods

2.1. Study area

The region of Jerte Valley is a mountain area located on the northwestern border of the province of Cáceres, located

on the Central System between the Sierra de Gredos (Sierra de Tormantos to the southeast and the Traslasierra mountains) and Sierra de Béjar to the northwest (in the western massif of Gredos) that constitute its natural boundaries. Limited to the north with the province of Avila and Salamanca, to the west with the region of Ambroz, to the south with the municipality of Plasencia and to the east with the Vera Shire. It is a natural passage between the highlands of Castilla and the Cáceres peneplain through the port of Tornavacas (1,283 m).
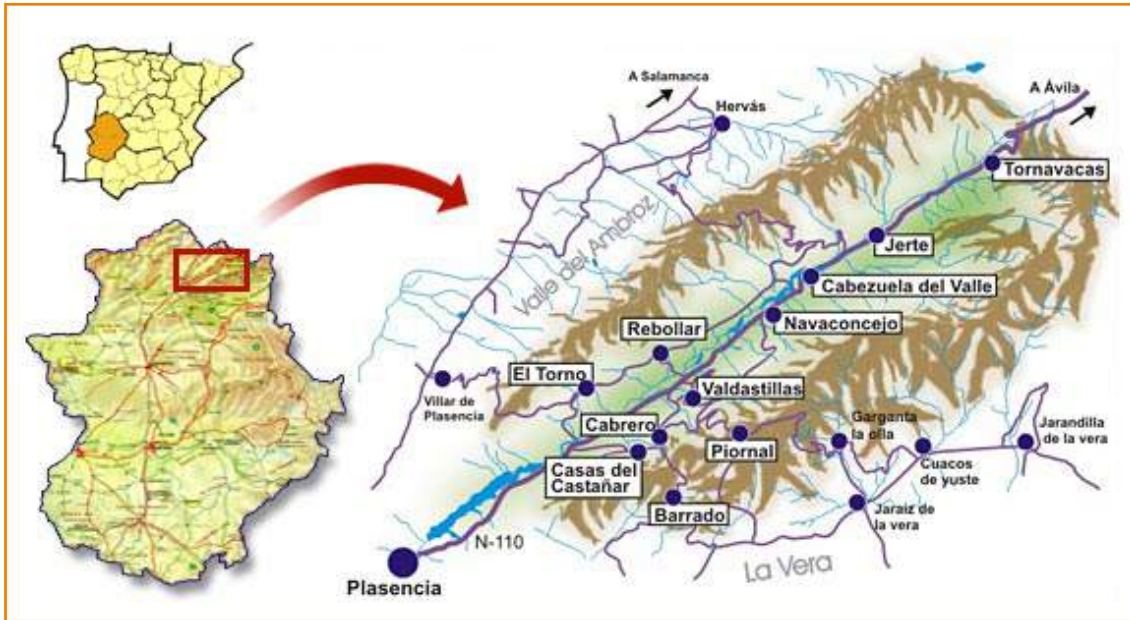
Figure 4. Location of Jerte Valley Shire.

It is geographically defined by the Jerte River and its valley, hence its name. It is a geographical unit perfectly delimited, with a remarkable landscape and natural richness, which has the majority of the protected area of Extremadura (90.96%)

The region has an area of 374.33 km2 and is composed of eleven municipalities: Barrado, Cabezuela del Valle, Cabrero, Casas del Castañar, Jerte, Navaconcejo, Piornal, Rebollar, Tornavacas, El Torno and Valdastillas.

The region has been declared of cultural interest since 1973

Table 1. Municipalities of Jerte Valley Shire

MUNICIPALITY	POPULATION (2017)	AREA (km2)	DENSITY (/km2)
Barrado	424	21,29	19,92
Cabezuela del Valle	2.250	56,57	39,77
Cabrero	361	6,63	54,45
Casas del Castañar	594	24,63	24,12
Jerte	1.276	58,95	21,65
Navaconcejo	2.007	51,40	39,05
Piornal	1.536	36,39	42,21
Rebollar	210	11,51	18,25
Tornavacas	1.126	76,60	14,70
El Torno	897	22,26	40,30
Valdastillas	327	8,10	40,37

The Jerte river runs about 70 km and flows into the Alagón River, which is in turn tributary of Tajo river. Its birth occurs in the vicinity of Tornavacas, at the foot of the Torreón peak (2,401 m.) and, as it passed through Plasencia, it does so at about 345 m., which gives us an idea of its rugged basin in this stretch of only about 50 km.

The average annual rainfall ranges from 800 to 1,500 mm, taking as reference the weather station of Barrado, at 800 m altitude. In the month of November, it is common to see the first snows on the summits, varying the level during the winter.

2.2. Definition of the impacts caused in the environment

Visual impacts managed for the realization of this work are the effects produced by human activities on the urban and peri-urban environment of the rural environment that negatively influence the environmental quality of the environment (Van de Berg and Vlek, 1998; Schmid, 2001; Tassinari et al., 2013; Garrido et al., 2019)

The environment is defined as all that vital environment that surrounds the human being both from a physical point of view and from a biological, cultural and social point of view. All these components interact directly or indirectly with the human being and the society in which lives and condition her or his relationship with the environment and lifestyle. Environmental quality represents the quantitative and qualitative characteristics of the environment and the perception of humans about these characteristics to meet their personal needs. Quality is formed by the physical goods of the environment and the perception that human beings have about this environment (their beauty, their history, their perception).

The environmental impact refers to any alteration that the execution of a project originates, directly or indirectly, in the environment, expressed as a difference between the evolution of this "without" project and "with" project (Deffontaines et al., 1995; Kaplan et al., 2006; Howley et al., 2012; Ryan, 1998; Hernandez et al., 2004; Garrido et al., 2017; Garrido et al., 2018). The environment includes a variety of elements and the relationships that occur between them, and is not limited to natural activities (fauna, vegetation, landscape), but encompasses the human environment, the living conditions of people, their economic, social activities and their cultural assets.

The landscape impact is related to the changes that the landscape undergoes. Its assessment depends on three key factors:

- Direct impacts on landscape elements.
- Subtle effects on elements that give the landscape its local or regional character or differentiation.
- Impacts on elements of special interest or value, such as protected or designated places of cultural interest.

The urban impact is related to the buildings or those elements of it that represent a distortion, deformation or alteration of the environment where they are located, and the effects that these changes have on people.

2.3. Methodology for inventory and diagnosis of visual urban impacts of Valley Jerte municipalities

It has been taking into consideration the busiest main roads when accessing to each urban nucleus, and those stopping points which had an important focal attention for visual urban impacts evaluation.

The main roads are catalogued as national, regional and/or provincial highways.

Normally, these roads cross the whole municipality having a structuring and distributing character of space, activities and buildings. They have the most vehicle and human traffic, giving rise to a greater number of visual impacts. In particular, the entrances of the municipality following these roads are considered focal points of attraction for the gaze of visitors. Therefore, a very detailed study of entrances points has been developed for each municipality due to their importance for the inventory of visual urban impacts. Additionally, and in a complementary way, other very crowded streets and promenades have been incorporated into the inventory of points, to make a more complete diagnosis of the urban impacts of each municipality.

The designation of visual impact by municipality, called "cases", has been carried out with the first initial of the name of the municipality. If there is a match, a second distinguishing letter is added (table 2).

The criteria used to carry out the diagnosis of cases has been the identification of urban elements with high landscape, tourist and urban impact, based on data obtained during the inventory phase by visiting each municipality. For this, potential impacts due to deterioration and / or aesthetics of the façade, lack of accessibility, conservation and improvement of gardens, improvement of urban furniture, signage, etc. have been considered, among others. Subsequently, the methodology used has consisted of ranking the impacts detected according to their importance or abundance in the entire region.

Once the inventory has been completed, an analysis and diagnosis of each case has been carried out and subsequently the correct and empowering proposals for action have been drawn up that will serve as a guide over time in each municipality.

Table 2. Designation of Visual Impacts

MUNICIPALITY	LETTER OF CASE	MUNICIPALITY	LETTER OF CASE
Barrado	B	Piornal	P
Cabezuela del Valle	Cz	Rebollar	R
Cabrero	Cr	Tornavacas	Tv
Casas del Castañar	Cc	El Torno	T
Jerte	J	Valdastillas	V
Navaconcejo	N		

The corrective actions are mainly ideas and proposals related to some regulatory breach, while the enhancers are proposals, ideas, a concept that contribute to a strengthening of the resources that each municipality has, with the intention of promoting the environmental quality of the environment.

3. Results and Discussion

3.1. Inventoried impacts

The visual impacts inventoried have been 373 in the eleven municipalities of Jerte Valley, with the criteria described in point 2.3 and distributed according to table 3 and figure 5.

Table 3. Number of visual impacts or cases per municipality

REGION OF JERTE VALLEY		
MUNICIPALITY	CASES	PERCENTAGE (%)
Barrado	21	5,63
Cabezuela del Valle	21	5,63
Cabrero	51	13,67
Casas del Castañar	29	7,77
Jerte	27	7,24
Navaconcejo	30	8,04
Piornal	58	15,55
Rebollar	25	6,70
Tornavacas	29	7,77
El Torno	42	11,26
Valdastillas	40	10,72
	373	100,00
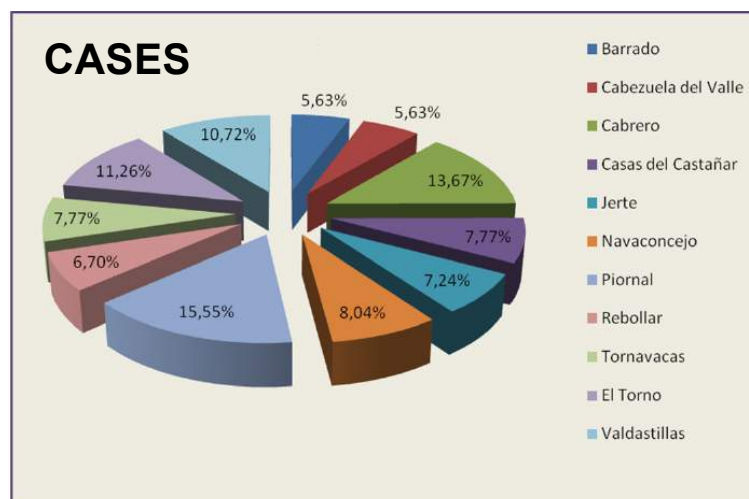
Figure 5. Percentage of visual impacts by municipalities

3.2. Typology of inventoried impacts

The results of inventoried impacts are summarized in 19 types:

1. Deteriorated pavements: pavements with broken or sunken tiles, which make it difficult for pedestrians to pass through them.

2. Storage of construction materials: stacking of construction materials or boxes of fruit which decreases visual quality of the scene.

3. Advertising: existence of too many announcements of economic activities in the same post or space generating disorder and confusion for the reader.

4. Urban solid waste containers: group of different waste containers in areas that cause great visual impact due to the environment where they are located.

5. Need of clearing: uncontrolled growth of spontaneous herbaceous and shrub species, mainly in privately owned areas.

6. Building elements: building elements discordant with the rest of the building and its surroundings, such as: darkening elements (blinds), satellite dishes, outdoor air conditioning units (air conditioning), façade carpentry, etc.

7. Undeveloped public spaces: lack of paving with concrete slabs, lack of pavements, degraded spaces, etc.

8. Lateral and gable facades: lined with corrugated metal plates that cut the view of the mountains.

9. Facades without coatings: buildings or parts of buildings made of brick without coating of mortars or paints; buildings in structure without façade enclosures.

10. Lack of accessibility: urban areas with architectural barriers that prevent access to people with reduced mobility or baby carriages.

11. Lack of conservation and maintenance of the existing garden areas.

12. Improvable spaces around protected areas: spaces located around protected areas that are without urban treatment, such as: hermitage of Christ in Navaconcejo, or hermitage of Humilladero in Tornavacas, etc.

13. Furniture of economic activities on public roads: furniture of bars and restaurants which is out of tune with the environment, among others.

14. Obsolete urban furniture or lack of maintenance of it in public spaces: benches, wastebaskets, children's games, etc. that are obsolete, neglected and / or without maintenance; lack of urban furniture.

15. Signalling of the beginning and end of the urban area: the signposting of the start and end totems of the urban section of the municipality is in an incorrect current location, generally because the urban section has been developed after its location.

16. Deteriorated and/or obsolete signage: signs of urban areas and/or economic activities with great deterioration of the material from which they are made of, with damage or broken. Even in some cases no longer exist the activities they advertise so they are now obsolete signage.

17. Treatment of facade finishing and maintenance: lack of maintenance of privately owned buildings that give the impression of neglect, abandonment and even ruin.

18. Billboard: Existence of a large-format billboard in the urban area of the municipality generating visual impact on the environment.

19. Public areas without maintenance: These are municipal spaces that are currently degraded and without maintenance with a strong visual impact

Of the inventoried cases, it should be noted that the visual impacts of buildings without cladding represent 21.98%, buildings with a lack of finishing treatment and without maintenance are 18.77%, the impacts from side facades and gables covered with sheets are 13.14%, public areas without maintenance represent 12.87%, the impact of urban solid waste containers is 9.38%, the improvement, conservation and maintenance of existing gardens 4.29%, Discordant elements of the buildings represent 3.49%, the undeveloped public spaces are 3.22%, the signage of the accesses to the urban area of the municipality are 2.68%, the deteriorated sidewalks represent 2.41 %, the improvement of the spaces around protected areas is 1.34%, with 1.07% highlighting the impacts of material storage, signage, signs and advertising, the lack of clearing and the lack of accessibility, with 0.80% is the sign Obsolete and deteriorated utilization, with 0.54% are the impacts of obsolete urban furniture and without maintenance and the furniture of economic activities on public roads and with 0.27% are the impacts of billboards.

Taking into account the public or private ownership of the space where the visual impact occurs, it is found that 40% of the impacts occur in publicly owned spaces and 60% in privately owned areas, as indicated in Table 4. The relationship of visual impacts in areas of public and private ownership indicates that the Local Administration must have greater control over these impacts, which in most cases, are regulatory breaches of the urban regulations of the

Plans Municipal Generals.
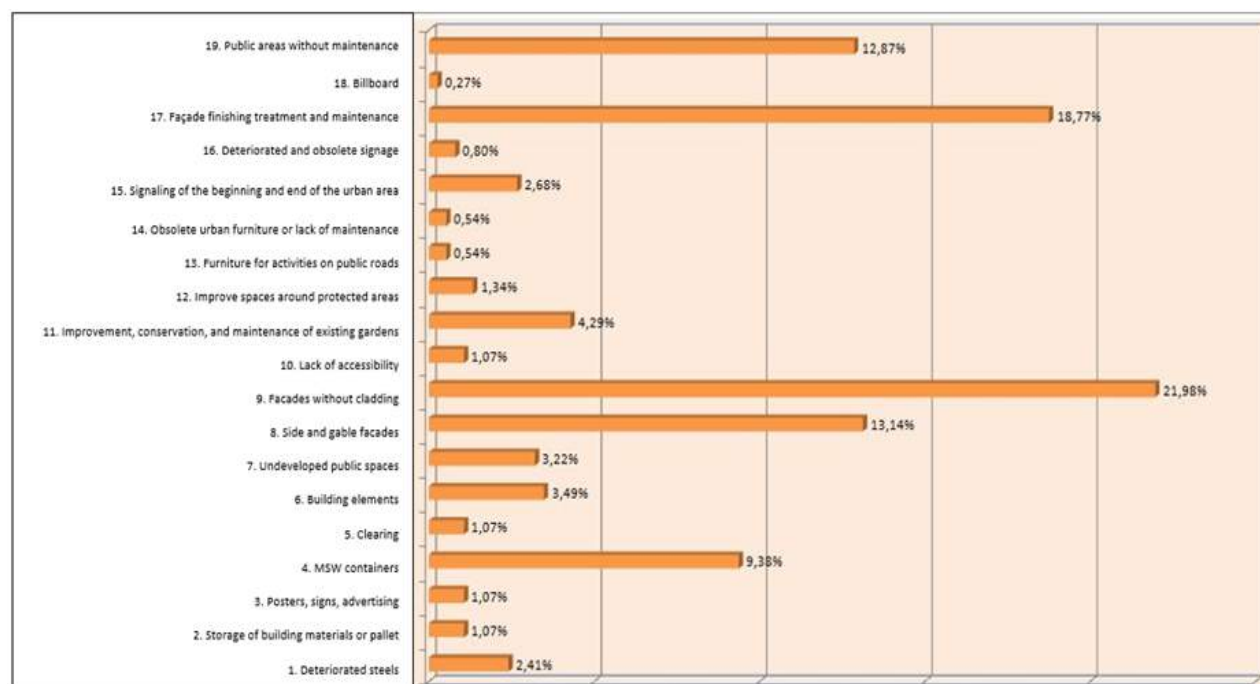
Figure 6. Percentage of the different visual impacts according to their typology

Table 4. List of visual impacts in areas of public and private ownership

CASES	OWNERSHIP	
	PUBLIC	PRIVATE
1. Deteriorated steels	9	
2. Storage of building materials or pallet		4
3. Posters, signs, advertising	4	
4. RSU containers	35	
5. Clearing		4
6. Building elements		13
7. Undeveloped public spaces	12	
8. Side and gable facades		49
9. Facades without cladding		82
10. Lack of accessibility	4	
11. Improvement, conservation, and maintenance of existing gardens	16	
12. Improve spaces around protected areas	5	
13. Furniture for activities on public roads	2	
14. Obsolete urban furniture or lack of maintenance	2	
15. Signalling of the beginning and end of the urban area	10	
16. deteriorated and obsolete signage	3	
17. Façade finishing treatment and maintenance		70

18. Billboard	1	
19. Public areas without maintenance	48	
TOTAL	151	222

4. Conclusions

The conclusions of the analysis and diagnosis of the main urban and landscape visual impacts detected in each municipality, and the proposal of possible actions to eliminate or mitigate them, offers the following result:

1. Barrado: The proposed action is aimed at covering the MSW containers on "Avenida de Plasencia" (EX - 213), specifically in the North and South entrances of the municipality (impact: B2, 10 and 15), the installation of planters, in the railings of the viewpoint of the town towards the "Garganta del Obispo" (impact: B8) and putting in value the elements of the rural heritage existing in this avenue: a mechanical engine (impact: B12) and a pavilion or canopy (impact: B14).

2. Cabezuela del Valle: The proposed action aims to aesthetically improve the appearance of the slope of the right bank of the Jerte river upstream from the Cabezuela Bridge (N-110) and create or strengthen the habitat of the different animal species that inhabit this space declared a Site of Community Importance (SCI) of the NATURA 2000 NETWORK (corresponds to the first point of action indicated in the first meeting held with the Consistory).

3. Cabrero: The proposed action plans to cover the groups of MSW containers No. 2 and 6 located in "Paseo del Canchal" (impacts: Cr11 and Cr31) and group 3, located in "Cervantes" street" will be relocated, landscaping of the roundabout in "Paseo del Canchal" and Barrado road (impact Cr7) and mural painting on the facade of the cooperative "San Miguel" with a theme related to the conservation of the traditional culture of transporting cherries from the cherry tree to the cooperative (impact Cr9).

4. Casas de Castañar: The proposed action is aimed at recovering and enhancing the "Barbajones" Stream Fountain and its surroundings, as a natural water resource and element of the natural heritage, with landscaping that integrates with the environment (impact: Cc28).

5. Jerte: The proposed action plans to enhance the popular architecture of the "Plaza de la Independencia" de Jerte with an efficient lighting system that meets visual needs and creates healthy environments that allow users to enjoy a pleasant environment, eliminating parking throughout the square and installation of gardens in front of the Church and placement of loose letters with the name of the municipality that can serve as a seat for users.

6. Navaconcejo: The proposed action is aimed at promoting the natural heritage of the waterfalls of the Garganta de las Nogaledas as a landscape element of singular value in this municipality through the installation of a monument - a fountain with lighting and the placement of 6 planters with double function, because apart from contributing to the beautification of this public space, it would serve to organize road traffic in the area and avoid vehicle parking

7. Piornal: The proposed action seeks to renew and enhance the existing garden on "Avenida de La Vera" (CC-139) with new plantings of plant species and the creation of a children's play area for the enjoyment of residents and visitors (impact: P5).

8. Rebollar: The proposed action seeks to improve the appearance of "Plaza Calvo Sotelo" by embellishing it with garden elements and eliminating the landscaping impact produced by the facades: rear of the Social Centre and right side of the Public School due to lack of maintenance of the cladding.

9. Tornavacas: The proposed action aims to reduce or eliminate the landscape impact of the northern access to the municipality by landscaping space to enhance the beautification of this access and, on the other hand, to clean up the façade of the municipal building destined for the House of Culture (corresponds to the first point of action indicated in the first meeting held with the Consistory).

10. El Torno: The proposed action would meet two objectives, on the one hand, renovating and enhancing the existing garden for the use and enjoyment of the town's inhabitants and, on the other, attracting visitors to the town by placing a typical monument Sculptural with argumentation links to that of the memory viewpoint (memory of the forgotten in the Civil War and the dictatorship), as a phase II (Impact: T.7).

11. Valdastillas: The proposed action plans to reduce or eliminate the landscape impact that has been created in the access to "Colón" Street from "Costanillas" Street through the retaining wall of granite masonry (impact V22) crowned with balustrades painted white as elements. For protection, it is proposed to replace the railing with a metal one with bars with rectangular planters for the exterior and with the shape of a tetrahedron for the interior with flowering

herbaceous species and a small garden area in the corner of the public staircase. The identification totems of Valdastillas located in the North and South entrances of the town with lighting have been strengthened.

Acknowledgements

References

Deffontaines, J.P.; Thenail, C.; Baudry, J. Agricultural systems and landscapes patterns: how can we build a relationship? Landsc Urban Plan. 1995, 31, 3-10.

Garrido-Velarde, J.; Montero-Parejo, M.J.; Hernández-Blanco, J.; García-Moruno, L. Use of video and 3D scenario visualisation to rate vegetation screens for integrating buildings into the landscape. Sustainability 2017, 9, 1102.

Garrido-Velarde, J.; Montero-Parejo, M.J.; Hernández-Blanco, J.; García-Moruno, L. Using Native Vegetation Screens to Lessen the Visual Impact of Rural Buildings in the Sierras de Béjar and Francia Biosphere Reserve: Case Studies and Public Survey. Sustainability 2019, 11, 2595.

Garrido-Velarde, J.; Montero-Parejo, M.J.; Hernández-Blanco, J.; García-Moruno, L. Visual analysis of the height ratio between building and background vegetation. Two rural cases of study: Spain and Sweden. Sustainability 2018, 10, 2593.

Hernández, J.; García, L.; Ayuga, F. Integration Methodologies for Visual Impact Assessment of Rural Buildings by Geographic Information Systems. Biosyst Eng. 2004, 88 (2), 255-263.

Howley, P.; Donoghue, C.O.; Hynes, S. Exploring public preferences for traditional farming landscapes. Landsc Urban Plan. 2012, 104 (1), 66–74.

Kaplan, A.; Taşkin, T.; Önenç, A. Assessing the Visual Quality of Rural and Urban-fringed Landscapes surrounding Livestock Farms. Biosyst Eng. 2006, 95 (3), 437–448.

Ryan, R.L. Local perceptions and values for a midwestern river corridor. Landsc Urban Plan. 1998, 42, 225-237.

Schmid, W.A. The emerging role of visual resource assessment and visualisation in landscape planning in Switzerland. Landsc Urban Plan. 2001, 54 (1–4), 213–221.

Tassinari, P.; Torreggiani, D.; Benni, S. Dealing with agriculture, environment and landscape in spatial planning, A discussion about the Italian case study. Land Use Policy. 2013, 30 (1), 739–747.

Van den Berg, A.; Vlek, C. The influence of planned-change context on the evaluation of natural landscapes. Landsc Urban Plan. 1998, 43, 1-10.

Curricula on Smart Greenhouses in the Framework of the NEGHTRA Project

José María Cámara-Zapata [a]*, Carmen Rocamora [b], Herminia Puerto [b], Jorge Antonio Sánchez-Molina [c], Francisco Rodríguez [c], Francisco García [d], Evelia Schettini [e], Giuliano Vox [e], Tomaz Zadravec [f], Yiannis Troulis [g], Angeliki Kavga [h], Fátima Baptista [i]

[a] Department of Applied Physic, University Miguel Hernández, Elche, Spain

[b] Department of Engineering, University Miguel Hernández, Elche, Spain

[c] Department of Informatics, University of Almería, Almería, Spain

[d] Department of Plant Nutrition, Center for Edaphology and Applied Biology of the Segura, Spain

[e] Department of Agricultural and Environmental Science, University of Bari, Bari, Italy

[f] Innovation Technology Cluster Murska Sobota, Slovenia

[g] Technology Transfer Marketing Innovation Consulting LTD, Greece

[h] Department of Agriculture, University of Patras, Patras, Greece

[i] Department of Agricultural Engineering, University of Evora, Evora, Portugal

* Corresponding author. Email: jm.camara@umh.es

Abstract

Next Generation Training on Intelligent Greenhouses (NEGHTRA) is a specialized training project that addresses knowledge transfer in precision agriculture based on specific needs and challenges. However, competition with new production areas threatens the profitability of farms and forces the rethinking of production strategies. This situation may be aggravated by the growing uncertainty in the markets. In addition, the intensive agriculture sector is considered by society as one of the main causes of, as well as the most affected by, climate change. Specifically, greenhouse growers must rethink their production strategy to promote sustainable production, with special emphasis on the use of new materials and technologies to improve the climate, irrigation, and fertigation, and reduce inputs and waste, the use of renewable energies, and the circular economy. The digitization of agriculture aims to improve and / or simplify all the processes included in the productive activity (data collection, communication and storage of information, analysis and interpretation of data, evaluation or diagnosis of the state of the crop, preparation of recommendations, decision-making and action). Finally, it is necessary to develop capacities that favour innovation and entrepreneurship to strengthen the sector and promote the resilience of this farms.

NEGHTRA has the following target groups a) Higher Education Institutions and Research Institutions, which will update the training *curricula* portfolio, b) agricultural intermediaries that provide counselling and training to the farming communities, and c) the farming community. In this work, we present the *curricula* that can be used to provide the necessary capacities to improve the sustainability of production, promote the resilience of farms, increase the efficiency of crops, and contribute to improving the social recognition of growers.

Keywords: training, knowledge transfer, precision agriculture, sustainability, climate change.

1. Introduction

The European Union considers education, training, and youth, among its key areas for supporting citizens in their personal and professional development. The Erasmus+ program is a key component for achieving the objectives of the European Education Area, the Digital Education Action Plan 2021-2027, and the European Youth Strategy. European citizens must improve their knowledge, skills, and competences to be part of an increasingly changing, multicultural and digital society. The Erasmus+ program supports opportunities for personal, socio-educational, and professional development. To increase the qualitative impact of its actions and guarantee equal opportunities, the Program must more successfully reach people of different ages and of diverse cultural, social, and economic origins. It is therefore essential for the program to reach out to individuals with fewer opportunities, including people with disabilities and immigrants, as well as citizens of the European Union living in remote areas or facing socio-economic difficulties. In doing so, the Program should also encourage its participants, particularly young people, to become involved and learn to participate in civil society, raising awareness about the common values of the European Union. In addition, developing digital skills, and competencies and skills in forward-thinking fields such as combating climate change, clean energy, artificial intelligence, robotics, analysis of large amounts of data, etc., is essential for the sustainable growth and cohesion in Europe in the short and medium term. The program can make a significant contribution by stimulating innovation and reducing Europe's knowledge, skills, and competences gap. Within the Program, Knowledge Alliances are transnational projects between higher education institutions and companies to work on common issues with the general objective of consolidating Europe's innovative capacity and promoting the modernization of European higher education systems. They focus on one or more of the following: developing new, innovative, and

multidisciplinary approaches to teaching and learning; stimulate entrepreneurship and business skills of university teaching staff and company personnel; exchange knowledge and collaborate on finding new solutions (European Commission, 2020).

The proposals of the European Commission on the Common Agricultural Policy during the 2021-2027 interval aim to boost the sustainability and competitiveness of the agricultural sector to significantly contribute to the European Green Deal, especially within the framework of the "Farm to Fork" and the Biodiversity Strategy. In particular, the proposals focus on ensuring fair treatment and economic stability of farmers, setting more ambitious goals for the environment and climate action, and maintaining the primary place of agriculture in European society (European Commission, 2021). To achieve these general goals, the European Commission has established the following specific objectives:

- To guarantee a fair income to farmers. In 2018, farmers earned on average just under half of what could be earned in other jobs, while it was 37% a decade ago in 2008. The agricultural income per worker steadily increased over time to 18,200 EUR in 2019. Direct payments provide a safety net to farmers, which account for about 1/4 of the agricultural income.
- To increase competitiveness. The trade balance in the EU-27 is positive, and followed a positive trend in which both imports and exports increased over time. 2019 was a record year for both imports and exports of EU agrifood products.
- Rebalancing power in the food chain. Agriculture is characterised by a stagnant and low share of value added in the value chain (around 25% of the total value added), due to high input costs, variation in production and incorporation of new services.
- To take action against climate change. Greenhouse gas emissions (GHG) from agriculture have declined substantially between 1990 and 2010. Since then, emission levels appear to be relatively stable. Emissions from agriculture (including croplands and grasslands), accounted for roughly 13% of total EU GHG emissions in 2017.
- To protect the environment. The nitrogen surplus in the EU-27 remained stable in the last decade (2005-2015) at around 50 kg N per hectare per year. The target under the Farm to Fork strategy aims to reduce the nutrient losses on agricultural land by 50% by 2030. An important area of focus in the greenhouse sector is the exploration of optimal energy management.
- To preserve landscapes and biodiversity. Landscape features are providing many benefits to agro-ecosystems and the wider environment. Currently, about 0.5% of the agricultural area is covered by landscape features. In addition, 4% is land lying fallow.
- Support generational renewal. In the EU-27, the share of farmers younger than 35 years of age, in the total number of farm managers, decreased between 2010 and 2016 to 5%.
- Maintain dynamic rural areas. The employment rate in rural areas has increased, and the gap with urban areas almost disappeared in 2018, when 72% of the working-age population (aged 20 to 64) was employed in rural areas. In addition, the rural poverty rate in the EU-27 decreased over time from 30% in 2010 to 24% in 2018. It showed a continuous downward trend between 2010 and 2018. At the end of 2018, 52% of rural households were served by a Next Generation Access network, compared to 81% of total EU rural households. There was a clear improvement on the situation over time in rural areas, but closing the connectivity gap of rural areas with regard to Next Generation Access remains a challenge.
- To protect quality and safety. The overall sales of veterinary antimicrobials across the EU-27 decreased by more than one third between 2010 and 2017, weighted for those MS that provided data each year. The total area under organic farming is increasing in the EU-27, covering almost 13 million hectares in 2018. With 8% of the total utilized agricultural area under organic farming in 2018, the EU-27 area follows a positive trend. Finally, it should be noted that in the EU-27, the share of managers with basic agricultural training equals 23%, whereas 9% attained a full agricultural training in 2016. This share rather slowly increased between 2010 and 2016. Full agricultural training means any training course equivalent to at least two years full time training after the end of compulsory education and completed at an agricultural college, university, or other institute of higher education in agriculture (European Commission, 2021).

The Executive Agency for Small and Medium-sized Enterprises of the European Commission, in its report on the Technological Trends in the Agri-food Industry, sets out key messages to understand the situation and perspectives of the sector (Van de Velde, 2020):

- The agri-food sector is composed of both agriculture & farming and food processing activities. In the face of global change, including demographic change and climate change, the challenge remains to deliver a sustainable food and agricultural production system (FAO, 2017). Advanced technologies are essential for enabling the agri-food industry to increase efficiency in production, while limiting the global impact of food production on the environment. Through developments in precision agriculture and farming, as well as smart food processing, the agri-food industry is responding to these challenges with increased digitalisation and the uptake of advanced

technologies (Van Woensel et al., 2016). Changes in the agri-food industries are also driven by consumer demand for food safety, security, traceability and higher quality, and the value of food products. The EU is an agricultural production leader and exporter of products, creating over 44 million jobs in the EU in the wider agri-food industry (European Commission, 2017).

- Technology shifts in agri-food are occurring in line with the shift to Industry 4.0. As industrial processes are becoming increasingly digital, automated, and connected, an agri-food 4.0 is coming into place. Advanced technologies across the agri-food industry include Internet of Things, Advanced Manufacturing, and Photonics - together with sensors, and include the use of robotics and especially co-bots. Overall, the value chain is becoming increasingly digital, supported by farm management systems and tools to manage and oversee activities at the farm and production levels. Sensors are utilized in farm and animal sensing, as well as in the form of smart sensors for food packaging. Consumers are increasingly interested in high quality food, but also in information flows associated to the origins and impacts of food products and consumer products.

- Transformations and fundamental shifts in agri-food require diverse advanced skills. According to agri-food company websites that reference specific terms associated with advanced technologies, Industrial Biotechnology is the term most associated with the agri-food sector company websites, followed by Robotics and Big Data. Further prominent categories include Advanced Manufacturing and Cloud technologies. It can be observed that France, Spain, and Italy are leading in terms of absolute number of professionals with advanced technology skills employed in the agri-food sector. The results emphasise the growing importance of digital technologies and digital skills in the agri-food industry. The five technological skills with the highest growth within the previous year (from 2018 to 2019) included AI followed by Security, Blockchain, IoT, and Big Data.

Next Generation Training on Intelligent Greenhouses (NEGHTRA) is a specialized Erasmus+ Knowledge Alliances training project, which begun in November 2020, and is expected to last three years. It addresses knowledge transfer in precision agriculture based on specific needs and challenges, identified from a comprehensive need analysis. The project aims at the development of an adaptable and flexible lifelong learning system, for its application in theoretical and practical training on intelligent greenhouses. This will be achieved by:

- Utilizing a training system that will be flexible, responsive, and adaptable enough to accommodate the fast evolution of the economic and environmental sectors, as well as the new technologies.
- Creating national/regional Reference Contact Centers (RCCs) organized by intermediate beneficiaries to remotely assist end-users.
- Including farmers' unions and agricultural associations, which facilitates the acquisition and dissemination of knowledge.

NEGHTRA ensures high quality and efficient teaching: - the teaching material will be available in 7 languages; - the lifelong learning system will incorporate theoretical and practical components, assisted by instructional videos and demonstrations of good practices; - the reference capacity of the national/regional RCC's provision of adequate initial education; and - the continuous improvement of the system by incorporating new teaching material and technologies. This project supports the equal opportunity and accessibility to education and learning, irrespective of any personal, social, or economic background. The training targets the supply of job-specific knowledge, skills, and key competencies to young farmers for the use of new technologies in their profession, and invokes their increased employability and active citizenship. It also provides for a HEI level of knowledge, albeit in laymen's form, to comply with farmers' needs without any formal education, and to effectively provide them with the opportunity to use new technologies. NEGHTRA aspires to deliver young farmers the knowledge of how innovation, entrepreneurship, and technology utilization can benefit their businesses, personal skills, and competence development. The multi-disciplinary scope of this project and conjunctions with various partners maximizes the dissemination of knowledge in all productive aspects of the industry. Throughout the project, emphasis is given to the reinforcement of the quadruple helix concept by infusing its mindset and practices into all related activities, facilitating stakeholder collaborations for economic and societal development, as well as for building the Reference Contact Centres for user support and enhancement of exploitation and sustainability of the project (Figure 1).
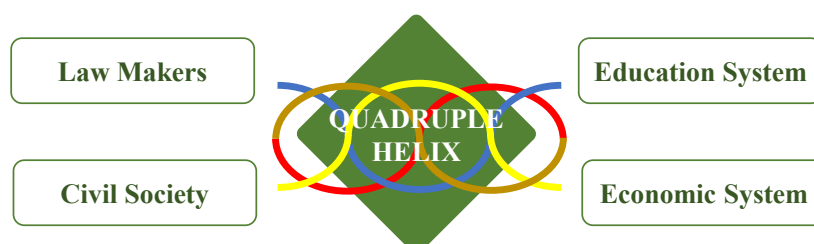
Figure 1. Schematic of the quadruple helix reached by NEGHTRA.

The target groups are: - HEIs and RIs which will update the training *curricula* portfolio; - agricultural intermediaries, which provide counselling and training to the farming communities, and: - the farming community of the participating countries and beyond. The training will be delivered to two distinct groups:

- 1st tier learners including HEIs/RIs staff/researchers, intermediary staff and trainers, local stakeholders, and regional authorities engaged in agricultural development.
- 2nd tier learners including farmers of any size and type of cultivation and students.

All the educational material will be free and available through the e-training platform, where users assess a specific learning process. It will also help in administration, documentation, tracking, and recording of the learning process. The website will facilitate the link between the users and the e-training platform. The educational materials offered therein could be used for distance education and professional training.

The objective of this work is to present a description of the modules included in the NEGHTRA project *curricula* aimed at 1st tier learners. In all cases, the scope, description and learning topics are included. The following sections will briefly present the components of the consortium and the partners associated with the project. In addition, a description of the study on the analysis of training needs will be made. The results of the preliminary training needs analysis and the *curriculum* proposals will also be presented, and finally some conclusions supported by these preliminary results will be described.

2. Materials and Methods

Below is a description of how a previous analysis of training needs was carried out and how the material for the design of *curricula* was prepared.

2.1. Training needs

A needs analysis research was conducted by the partners using an open-ended questionnaire and covering all relevant parameters of training for greenhouse farmers. The partners reached their key stakeholders within their domain including staff, members, trainers, farmers, innovative initiatives, farming schools, VET organizations etc. so that they captured the main issues of training in this sector.

2.2. *Curriculum* Design

The training material will be developed by a consortium made up of 5 Higher Training Centres, 4 specialized SMEs, and 6 groups of intermediaries (1 agro-ICT group, 1 research institute, 1 farmer's federation, 1 farmer's association, 1 specialist in FP, 1 agricultural school), each contributing with their experience and dissemination capacity, in seven languages. The consortium is composed by:

- University of Patras (Greece)
- Geotechnical Chamber of Greece (Greece)
- TTMI Consulting Ltd. (Greece)
- Università degli Studi di Bari Aldo Moro (Italy)
- Confagricoltura Puglia (Italy)
- Istituto Formazione Operatori Aziendali (Italy)
- Leaf Net LTD (Cyprus)
- Cloudpharm Private Company (Greece)
- Institut National de Recherce pour l'Agriculture, l'Alimentat (France)
- GIP Formation et Insertion Professinnelle de l'Academie de Nic (France)
- Universidad Miguel Hernández de Elche (Spain)
- Universidad de Almería (Spain)
- Consejo Superior de Investigaciones Científicas (Spain)
- Grupo HISPATEC Informática Empresarial SA (Spain)
- Universidade de Evora (Portugal)
- ITC Murska Sobota (Slovenia)

The training material will be completed by 5 associated partners with direct access to existing and potential agricultural communities: (i) Formations Vert D'Azur Antibes, Agriculture high school, France; (ii) Surinver El Grupo, Agrarian Producer Cooperative, Spain; (iii) Cooperatives Agro-Alimentaries, Farming and Agrifood Cooperative, Spain; (iv) Coexphal, Association of Fruit and Vegetable Producer's Organizations of Almería, Spain; (v) SLOVCHAGR, Institute for agriculture and forestry Murska Sobota, Slovenia.

3. Results and Discussions

3.1. Training needs

The three top concerns in greenhouse farming were: Knowledge, technology, and crops. Use of energy, fertigation, costs, and selling prices were also common findings. Regarding technological knowledge, it was found that farmers were aware of them, but were limited to fertigation systems, the reason being the lack of their available time and skills to learn, evaluate and use them. Also, there was lack of qualified personnel to assist in implementing these new technologies. The relevant technological parameters in greenhouse cultivations were: - environmental control, fertigation, and smart farming; - market, available resources, and management of production process; and - management of climate control (Table 1). Energy consumption related concerns were found to be: - Irrigation systems & indirect energy use for fertilizers & materials & efficient use of resources, and use of solar energy; - Cooling systems in the summer or heating systems in the winter; and - Climate control.

Table 1. Results of the training needs analysis.

Top concerns in greenhouse farming	Knowledge
	Technology
	Crop
Relevant technological parameters in greenhouse cultivations	Environmental control, Fertigation and Smart farming
	Market, available resources, and management of production process
	Management of climate control
Main issues in innovation uptake	Lack of knowledge, digital/environment management skills and qualified personnel/skills
	Small farm size
	Economic and Financial issues
	Need for Demonstration of Innovation Advantages
	Sensors, wireless connection remote management for climate and fertigation
	Information uncertainty, market information, survival farming
	Useful to integrate consultants and agriculturalists
Training issues in greenhouse farming	Small farms/all day work by owners, thus no free time for training
	Old age farmers with low academic education
	Recent younger farmers open to training
	Short course duration, difficult to understand new technologies
	Few available offers for specific greenhouse training
	Need for specific training on sustainable and precision agriculture
	Various types of training course according to education/skill levels

As for the attitudes regarding smart farming, greenhouse farmers and young farmers were more open to innovation than open field and old farmers. There was more interest in fertigation, and there was a lack of knowledge/interest from small size farmers. The main issue in technological adaptability were: - knowledge or lack of it; - lack of skills and understanding new technologies; - lack of technical training and distrust, and; - lack of qualified personnel.

Most importantly, regarding the training issues in greenhouse farming, the key outputs are: - small farms/all day work by owners, thus no free time for training; - old age farmers with low academic education; - recent younger farmers open to training; - short course duration, difficult to understand new technologies; - few available offers for specific greenhouse training; - need for specific training on sustainable and precision agriculture; and - various types of training course according to education/skill levels.

To summarise the Needs Analysis findings, the greenhouse cultivation lacks updated technological knowledge due to time, skills, and attitude constraints. There is an awareness of available solutions, but not of their relevancy and usefulness in their particular cases. Larger farm units and younger farmers are more prone to uptake innovation, and this process can be accelerated for all farmers using training and consulting services.

3.2. *Curriculum* design

The project *curriculum* for 1st tier learners is comprised of 14 modules, 10 on technologies and crop, and 4 on knowledge and entrepreneurship. Below is an overview of all the included modules.

3.2.1. Coverage & PV

The aim of this module is the acquisition of knowledge for the identification of suitable greenhouse covering materials. These must guarantee a protected environment inside that provides an adequate microclimate for the plants, in relation with the climate of the geographical area, the growing season, and the crop species. The learning topics are: (i) notions on concepts and principles on radiometric properties of greenhouse covering material to define its radiation

behaviour; (ii) notions on concepts on the physical and mechanical properties of the most-utilized covering materials in the Mediterranean area; (iii) notions on concepts and principles applied to Photovoltaic textiles for PV shade screens; (iv) notions on best practices for greenhouse covering material; and (v) skills for choosing greenhouse covering material.

3.2.2. Irrigation & Fertigation

The main objective of this course is to train students on irrigation, fertigation, biostimulants, indigenous arbuscular mycorrhizal fungi (AMFs), and nutrient analysis. All of this is needed for students to achieve their educational goals and to be able to understand the different forms, techniques, use, and application of these elements in agriculture. All this, under the premise that a correct use of these techniques can be very useful. The learning issues are: (i) to know different forms and applications of irrigation, products that can improve the quality of the crops, different forms of cultivation, and diagnostic methods to assess the quality of plants; (ii) show students the evolution of the sector, adapting to new technologies to make students aware of the importance of being up-to-date in the sector, interest in new technologies and method of use, and focus new knowledge to obtain higher quality products in a manner that is more sustainable with the environment; (iii) offer a perspective on the current state of the sector. All of this will allow the application of the techniques learned in a concisely and appropriately manner, depending on the needs.

3.2.3. Climate Technologies / Equipment

The aim of the module is to present, inform, and educate students on climate technologies and greenhouse techniques, and to design and manage the main greenhouse climate control systems to make production economically, socially, and environmentally profitable. The training topics are: (i) notions on concepts and principles applied to greenhouse climate control; (ii) notions on greenhouse climate control techniques; (iii) notions on best practices for greenhouse climate control; and (iv) skills to implement and/or use greenhouse climate control technologies.

3.2.4. Energy management

The aim is to understand the importance of the sustainable use of energy. Identify and analyse measures of energy savings, and energy efficiency improvement towards a sustainable production (reduce environmental impacts and costs). The training issues are: (i) overview of energy use/demand; (ii) energy audits; (iii) energy measurement; (iv) energy saving / energy efficiency; and (v) renewable energies.

3.2.5. Climate management

In this activity, two problems related to the control of greenhouse production processes are presented, specifically the analysis of a computer tool for the control of climatic variables inside greenhouses, and the analysis of a real system for the control. The learning topics are: (i) to explain the advantages and the need for the application of automatic control techniques in the fundamental processes of greenhouse crop production, specifically the control of climatic variables, irrigation and fertilizer injection; (ii) to describe the necessary elements (sensors, controllers and actuators), that compose this particular type of control systems; (iii) to show the necessity of using advanced control techniques such as table set control or parallel feedforward control to improve disturbance rejection, as well as to describe the principles of operation of these techniques; (iv) describe the cascade control technique due to the operation of the actuation systems required for night time control of the greenhouse's indoor air temperature, by using a hot water pipe heating system; and (v) show the need to use a supervisory system for extreme situations that operates with priority over the designed control system.

3.2.6. Automation

This course aims to introduce students to the new technologies related to Automation and Robotics used in the agricultural field, and the specific control techniques that allow the correct performance of the different systems that constitute an automated environment, as they are often not properly implemented in a specific productive environment. The learning issues are: (i) to acquire a solid base of knowledge about automatic control that allows them to analyse low and medium level control systems, recognizing their fundamental modules, and the techniques used for their design and adaptation to the evolution which these types of technologies will undergo, as they have a great future perspective; (ii) to show the student the industrial tasks in which the computer, programmable logic controllers, artificial vision, and robots can be used as basic automation tools. This allows students to become aware of the need for automation in the industrial sector, and focus their basic knowledge of industrial engineering from a process automation point of view; (iii) to offer a view of the systems that can currently be found already automated in the industrial sector. This will allow the application of the concepts and techniques learned in real systems that already exist on the market, the comparison of the different systems to study their advantages and disadvantages, namely, it will be possible to select the appropriate system according to the characteristics of the environment, and to introduce a series of basic engineering tools to perform mathematical calculations, simulation, and programming tools, elementary in process automation.

3.2.7. Greenhouse Digitalization

At present, new technological tools such as IoT, Big Data, Machine Learning and others are available that can help

build more efficient, sustainable, and competitive systems. Digitization allows the processing of large volumes of data from different sources, providing knowledge to tools which advise the farmer on making decisions in real time about the crop. This module will describe digital and information technologies, a broad term that includes all aspects of the uses of information technology, not including only hardware and software, but also communication technology, software engineering, and administration of the infrastructure for managing and delivering information. The training objective are: (i) to teach students the need to understand the importance of digitization in agriculture and help them acquire the necessary knowledge for the digitization process of the sector; (ii) to show the different systems and communication protocols available on the market, providing improved knowledge for the interconnection of devices through the different communication networks (Sigfox, Lora, GPRS,…); (iii) to know the main concepts of the Internet of Things (IoT) ecosystem; (iv) to know the importance of the data, and the correct manner to analyse data; (v) to introduce tools in charge of acquiring added value to data such as DSS, Big Data and Machine Learning, and Deep Learning; (vi) to acquire basic knowledge on the different cloud systems available on the market: Infrastructure as a Service (IaaS), Software as a Service (SaaS), Platform as a Service (PaaS), Model as a Service (MaaS); and to meet different IoT applications and current commercial solutions applied to agriculture.

3.2.8. Best farming practices in greenhouse cultivation

This present module focuses on introducing the students to the concepts of integrated management in agricultural production with best farming practices in greenhouse cultivation. Emphasis is given to the specifications for the integrated management of horticultural crops. The training issues are: (i) Standards, and requirements of Integrated Management in Agricultural Production; (ii) International, European, and national standards for Agricultural greenhouse Products; (iii) Integrated Management System Certification; (iv) harvesting and post-harvesting of greenhouse vegetables; (v) pollution management, environment, biodiversity; and (vi) best management practices for sustainable cultivation of greenhouse vegetables (FAO, 2013).

3.2.9. Circular economy

The aim of this module is the acquisition of knowledge on the circular economy with the objective of 'closing the loop' by greater re-use and recycling of materials used for protected cultivation. The learning topics are: (i) principles of circular economy; (ii) notions on the use of plastic materials in protected cultivation; (iii) notions of management of agricultural plastic waste; (iv) notions on practices to reduce and recycle agricultural plastic waste; (v) sustainable use of water and energy; and (vi) water & energy management.

3.2.10. High added value greenhouse cultivations

The present module focuses on how intelligent greenhouses can assist with producing consistent and high-quality raw materials for industrial high added value products (functional foods, dietary supplements, and cosmetics). Emphasis is given to peculiar species (i.e., aromatic plants and herbs). The learning issues are: (i) Aromatic and medicinal plants. Applications in Food, Drug and Cosmetic Industries. General introduction to Aromatic and Medicinal Plants and their applications to Health. Provide information regarding herbal raw materials in Food, Drug and Cosmetic Industries. Current status and future trends. Brief market description for these sectors; and (ii) Technical processes, skills, and know how. Describe the current technologies available to cultivate aromatic and medicinal plants in a greenhouse environment. Explain the advantages, their limitations, and the required technical skillset.

3.2.11. Business basics

The aim of this module is to understand the various requirements and dimensions of business, particularly in terms of responsiveness to problems and decision-making, as well as the tools and management techniques. The training topics are: (i) Strategic Management (creating a business and strategic plan for business); (ii) Marketing (to know how to market business through different channels (traditional, web, and social media); (iii) Accounting and Finance (which records to keep, how to keep them and how to file them, and where to find financing and how to manage it); (iv) Operations Management (choosing and managing suppliers, logistics, and supply chain management); and (v) People Management (hiring employees and how to manage them).

3.2.12. Owning / Managing a fresh produce business

This module analyses the basic economic concepts used for the theoretical and empirical economic analysis of how farms choose to use the available production parameters and study price setting through the interaction of supply and demand in the agricultural product markets. The training issues are: (i) Production theory: function of production, relations of production inputs, the optimal combination of production inputs and products, the productivity of production inputs; (ii) Cost theory: the concept of production costs, the distinction of cost forms; (iii) Greenhouse operation, production costs, revenues, and incomes; (iv) Theory of agricultural products demand, demand elasticities; and (v) Theory of supply of agricultural products, supply elasticity.

3.2.13. Quality & Safety

This module aims to help personnel to plan and prepare for food safety and quality audits, and to effectively engage

with auditors. The learning topics are: (i) requirements of food safety and quality audits; (ii) expectations of the external food safety auditor; (iii) audit preparation and priorities in the months before the audit; (iv) critical food safety documentation; (v) critical food safety practices; (vi) internal audits and system reviews; (vii) what to do in the weeks leading up to the audit; (viii) what to do on the day of the audit; and (ix) how to follow up on the audit and manage the outcome.

3.2.14. *Entrepreneurship in agro-food sector and new agri-business models*

The present module introduces the basics. The learning issues are: (i) innovation and entrepreneurship in the agricultural businesses. Introductory notes; (ii) bringing an idea into the market. Initial steps and decisions; (iii) building networks with Universities, SMEs, Investor schemes. Access to research infrastructures; (iv) technology transfer applications to provide Ad hoc solutions in cultivation/production; (v) intellectual property protection and management. Building assets from the farm; (vi) new business models. The case of regional innovation structures in the agri-food sector (innovation valleys, incubator & accelerators for supporting start-ups, spinoffs, and existing enterprises.

3.3. Training characteristics

The training material includes innovative solutions that strengthen green and efficient agricultural production. In addition, the *curriculum* will present guidelines on how to use innovation and technology for agribusiness development. This also enhances creativity and entrepreneurship at all levels of education and training. The project specifically targets young farmers and provides them with the knowledge, skills, and competencies to adopt new technologies for existing crops or to develop new crops with the use of new technologies. An electronic training platform (system) will be used to communicate the training material in 7 different languages, allowing interactive education and training between students and teachers. An e-learning platform will also facilitate learning using virtual technology with embedded information from 3 pilot greenhouses. E-learning techniques not only promote adult learning, but also make learning more engaging and increase the quality of guidance systems, as well as their potential to reach broader farmer populations across Europe. NEGHTRA aims to develop a quality assurance system, which will not only ensure the effective use of resources to provide the highest quality teaching, but will also contribute to the improvement of the governance and leadership of higher education institutions.

The methodologies and approaches that will be adopted and applied to learning and training systems, clearly showcase its innovative character. NEGHTRA will develop and deliver customized training material accompanied by an innovative e-training platform with embedded features from pilot intelligent greenhouses, which will enable interactive education and training, and mobile access. This platform will also represent the means for providing the beneficiaries with intense conventional training, including workshops, seminars and virtual classroom meetings.

The implemented training modules will remove the barriers which impede the fluent diffusion and application of knowledge and available technologies and know-how in the field. Researchers and experts will be able to exploit their already-conducted studies, achieving their spatial dissemination while assisting decision makers. This will contribute to spread the knowledge, techniques, and models, and plan their future strategies towards the sustainable management of agricultural air and water quality of the different growing systems.

Finally, within the content of the quadruple helix, the project empowers the collaboration and strengthens the relationships between agro-related industry, intermediate organizations/regional authorities, academia, and civil society. Accordingly, the project seeks the involvement of the agro-related industry in teaching practical entrepreneurial experience and research, for example.

4. Conclusions

Next Generation Training on Intelligent Greenhouses began in November 2020, and is expected to last three years. Its aim is to design, develop, and deliver training on sustainable and profitable smart greenhouses, suitable for individual farmers / agricultural schools and especially useful for remote and vulnerable communities. The present work presents an overview of its main characteristics, and describes the learning objectives and competencies of the modules that comprise its *curriculum*, both its technical nature and the business and entrepreneurship model. The project is expected to help advance the achievement of the sustainable development goals by developing innovative approaches to improve the quality of teaching and learning, stimulating entrepreneurial skills, and co-creating knowledge between the university and the company.

Acknowledgements

References

European Commission. 2017. The future of food and farming. https://eur-lex.europa.eu/legal-content/EN/TXT/HTML/?uri=CELEX:52017DC0713&from=EN. Accessed June 3, 2021.

European Commission. Knowledge alliances. Erasmus+, 2020. Knowledge alliances. Erasmus+. European Commission, 2020. https://ec.europa.eu/programmes/erasmus-plus/opportunities/knowledge-alliances_en. Accessed June 1, 2021

European Commission. Future of the common agricultural policy, 2021. https://ec.europa.eu/info/food-farming-fisheries/key-policies/common-agricultural-policy/future-cap_en. Accessed June 1, 2021.

Food and Agriculture Organization of The United Nations, 2013. Good Agricultural Practices for greenhouse vegetable crops Principles for Mediterranean climate areas. Fao Plant Production And Protection Paper 217

Food and Agriculture Organization of The United Nations, 2017. The future of food and agriculture: Trends and challenges, http://www.fao.org/3/a-i6583e.pdf

Van Woensel, L., C. Kurrer, J. Tarlton, K. Pope, C. Daheim, E. Bol, S. den Hartog-de Wilde. 2016. Precision agriculture and the future of farming in Europe. Scientific Foresight Unit. European Parliamentary Research Service. December.

Van de Velde, E., Kretz, D., Izsak, K. 2020. Executive Agency for Small and Medium-sized Enterprises. European Commission. Advanced Technologies for Industry-Sectorial Watch. Technological trends in the agri-food industry. August.

Training and Learning Needs for MSc Programs in Sustainable Agriculture

Patrícia Lourenço[a,b*], Fátima Baptista[a], Pietro Picuno[c], Vasco Fitas da Cruz[a], Luís Leopoldo Silva[a], José Rafael Silva[a], Adélia Sousa[a], Evangelos Dimitriou[d], Georgios Papadakis[d]

[a] MED - Mediterranean Institute for Agriculture, Environment and Development & Departamento de Engenharia Rural, Escola Ciências e Tecnologia, Universidade de Évora, Pólo da Mitra, Ap. 94, 7006-554 Évora, Portugal

[b] AgroInsider Lda., Rua Circular Norte PITE, Edf. NERE, 7005-841 Évora, Portugal

[c] University of Basilicata, Via Nazario Sauro, 85, 85100 Potenza PZ, Italy

[d] Agricultural University of Athens, Iera Odos 75, Athina 118 55, Greece

* Patrícia Lourenço. Email: pmrlourenco@gmail.com

Abstract

Sustainable agriculture is urgently needed to promote conservation and sustainable resources use in an equitable manner through integrated management of land, water, energy and biodiversity. In this way, education in agriculture emerges as a crucial tool for preparing agricultural technicians, researchers and farmers for productive contributions. Higher education institutions arise with an important mission of education in the context of social transformation and to integrate sustainable development into the educational system as a scientific subject. The aim of this study was to identify the training and learning needs to be included in a MSc program in sustainable agriculture. It was based on a questionnaire prepared and distributed to academics' experts in Agrarian Sciences in Greece, Italy and Portugal. Technologies, legislation, management and business, local community leadership and marketing were the training needs considered very important expertise's in sustainable agriculture. Traditional face-to-face learning, experienced farmers as mentors and knowledge sharing mechanisms were rated as very applicable and important. Due to COVID-19 pandemic, online learning methods, which were not considered suitable for a MSc program in sustainable agriculture, became important by providing online education. Information and communication technology and technological tools showed to be important skills for sustainable agricultural practices to effectively implement online learning and to improve the efficient access, exposure and use of up-to-date information of the agricultural sector and awareness of sustainable agricultural practices.

Keywords: Questionnaires, High education, Sustainable agricultural practices, Agrarian sciences.

1. Introduction

Nowadays, world faces huge challenges such as reducing poverty and ensuring food security. There are approximately one billion people living in hunger today. This is an undoubted worldwide concern because by 2050, there will be 2 billion more people who need to be fed and it is necessary to consider the climate changes that are negatively affecting the availability of fertile soil and water for agriculture production (EU 2012). The sustainable agriculture concept emerges on growth in sustainable productivity to ensure the continued existence of our production base to feed a growing population, also thanks to innovation, while enhancing rural livelihoods (EU 2012). The important role played by sustainable agriculture is in preservation of natural resources, reducing greenhouse gas emissions, halting biodiversity loss and caring for valued landscapes. Sustainable agriculture can help to make farming cleaner, less exposed to volatility in the prices of inputs and more resistant to disasters. Thus, the aims of sustainable agriculture are to increase the productivity without affecting the quality of soil and water, preserve the ecosystems, safeguard animal welfare, generate income for farms and improve quality of life in rural areas, support territorial development and contribute to economy (Cioloş 2012).

Therefore, it is clear that issues related with economic, social and environment aspects are key factors for a sustainable agriculture, as a practice of farming using principles which respect ecology and save natural resources. In the last few decades, the core issue of the sustainable agriculture is focused on the interaction between agriculture and the environment to the detriment of food issues (Lamine 2015). Currently, there is a conscious need to relate agriculture, food and environmental policies and issues from a perspective that takes account of the diversity of sustainable agriculture and the complexity of their interdependencies (Lamine 2015). One of the key features of extensive reforms of the Common Agricultural Policy (CAP) is to support producers rather than products. In a brochure untitled "Sustainable agriculture for the future we want" (EU 2012) some success stories are presented, such as organic farming, on-farm biogas production, extensive grazing practices, renewable energy, precision farming and agro-forestry systems. Moreover, the COVID-19 pandemic showed that it is necessary to have food systems without interruptions in the supply chains, to guarantee agricultural resources and food availability and to mitigate the socioeconomic impacts of crises (UN-FAO 2020).

In order to practice a sustainable agriculture, farmers responsible for the management of farmland must adopt correct and environmentally friendly practices, using appropriate technology and complying with regulations for a sustainable agriculture. Hence, farmers will need know-how and techniques to implement the changes, as well as, a smart governance system, fully set up, linking research, support services, farmers and their organizations and markets. These approaches require increased investments, sharing knowledge, innovation and technologies and courses dedicated to these subjects. Also, the communication gap between academics, researchers and agricultural workers will be promoting. One way to implement the know-how in sustainable agriculture is through MSc programmes since the public is more aware of environmental problems and the offer of educational courses in the universities is increasing in this area (Azeiteiro et al. 2015). For instance, the project - SFARM - Sustainable Farming (www.sfarm-project.eu) of the Erasmus+ program (Capacity Building in the Field of Higher Education) has the goal to provide agricultural workers and agricultural stakeholders with knowledge, skills and competencies in the field of agro-environmental technology for sustainable agriculture in Asian countries (China, Laos, Vietnam and Indonesia). Higher Education Institutions (HEIs) from these countries are partners in SFARM and will develop new curricula and a MSc programme that integrate in a practical way the latest developments in agricultural applied research.

This study aims to identify the training and learning needs to develop a MSc program in sustainable agriculture through a questionnaire prepared and distributed to academics' expert in agrarian sciences in Greece, Italy and Portugal. The questionnaires were developed in order to define the fundamental competences/expertise, to identify the sustainable agricultural practices and the methods of training and learning that should be taken in consideration in a MSc programme in sustainable farming. A long-term impact in securing the sufficient, safe, as well as environmentally, socially and economically sustainable production of agricultural products is expected to be developed.

2. Materials and Methods

In order to identify the training and learning needs for a MSc programme in Sustainable Farming, a questionnaire was prepared by the University of Evora (UEVORA) with the contribution of Agricultural University of Athens (AUA) and University of Basilicata (UNIBAS). This questionnaire was distributed to academics' expert in agrarian sciences in Greece, Italy and Portugal. The main objective was to identify the most important training subjects and the most adequate methods of training and learning: Theoretical, practical classes? Presential, e-learning, b-learning?

The questionnaire results were analysed by country and were presented in percentages to allow the comparison of the results between the countries. The methodology defined for the analysis of the training needs and training methods is shown in Table 1.

Table 1. Methodology defined for the analysis of the best practices of sustainable farming in Greece, Italy and Portugal, based on the percentage of the respondents.

Training and learning needs		Percentage of the respondents (%)
Training needs	Extremely important expertise	Value 5 > 60
	Very important expertise	Sum of values 4 and 5 > 80
	Not important expertise	Sum of values 1 and 2 > 10
Skills with future training needs	Strongly agree	Sum of strongly agree and agree > 80
	Not required	Sum of neither agree nor disagree, disagree and strongly disagree > 20
Forms of learning/training	Very applicable/important	Sum of values 4 and 5 > 75
	Not very applicable/not important	Sum of values 1, 2 and don't know > 10
Training methods efficiency	Extremely efficient	Sum of values 4 and 5 > 75
	Not efficient	Sum of values 1, 2, 3 and don't know > 60

3. Results and Discussion

3.1. Training needs on sustainable farming

The Greek, Italian and Portuguese academics considered very important expertise the majority of the technological, legislative, management and business, local community leadership and marketing (Figure 1). The technological was the most important expertise, while the legislative was the least. However, it must be stated that legislative expertise was considered important only in a relative comparison less important than other competences, such as technology, management or marketing. To train properly the farmers in sustainable agriculture, it is important to provide critical

knowledge and skills to enhance the agricultural productivity and become economically self-reliant through gainful employment (Patil and Kokate 2011). Also, it is necessary to have an appropriate technology which may be economically profitable, ecologically sustainable, technically feasible and culturally compatible (Patil and Kokate 2011). As in other industries, capital investment in intelligent technologies, which supports decision making that optimizes the use agricultural inputs within a sustainable framework and reduce output waste, are the key to high labor productivity (Carson 2018). Additionally, farming training needs to provide new entrants to the industry, whatever their age, with the skills to use performance data for operations and performance management as well as to deliver technical excellence (Carson 2018). Recent developments in science and technology, that could be an added value for farmers' crop and land management, are still unutilized in many situations because farmers have not been introduced to them or have not been trained to use it. Consequently, education in agriculture plays an important role in preparing agricultural workers, researchers and extension staff for the changes and adaptations required in agriculture in the 21st century to contribute more effectively to the improvement of sustainable agricultural production and rural development.
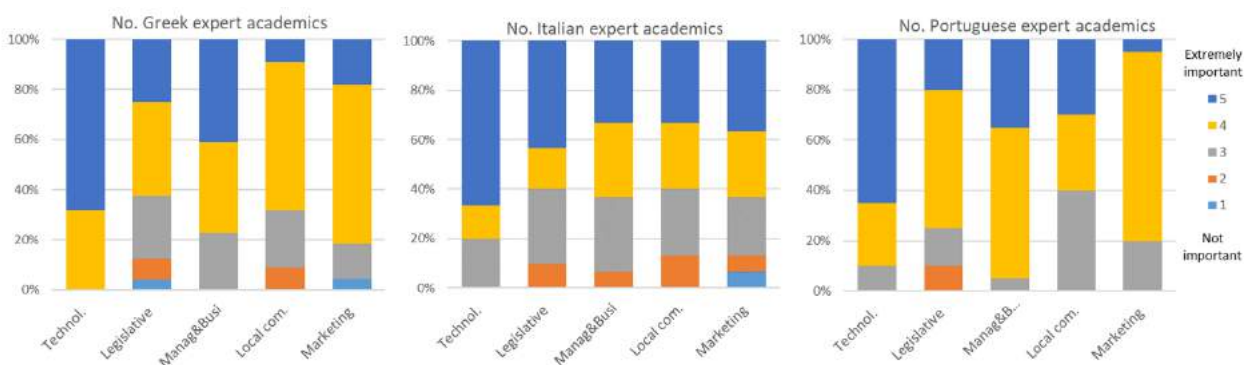
Figure 1. Expertise important rate for the future of sustainable agriculture in Greece, Italy and Portugal: technological, Legislative, Management and business, Local community leadership and Marketing expertises.

3.2. Training methods

The analysis of future training methods allows us to identify that Greek, Italian and Portuguese academics strongly agree with the required learning of new agronomical and environmental issues. Management, and information and communication technology (ICT) skills as future training needs were only considered by Greeks and Portuguese respondents. However, ICT and technological tools showed to play an important role in the online learning during the COVID-19 pandemic (Hodges et al. 2020). Skilled farmers will need to be able to understand and apply new technologies related to primary production for both food and non-food uses, soil science, crop and livestock genetics, agri-chemicals and general-purpose technologies such as remote sensors, satellites and robotics. For instance, communication technology gives farmers greater control over their access and exposure to information. It enables to take initiative as information seekers, rather than adopting a passive role as information recipients (Meera et al. 2004). Text messaging is one of the most widely used mobile data service worldwide, and many services or equipment can use this tool to interact with the farmer providing him with real time information. This can be very useful for farm management. The use of common word processors and spreadsheets are essential for data management and are becoming an important skill in farming practice, allowing workers to process information collected from different sensors and mapping systems (European Commission 2014). Software can also store digital evidence to be presented to national and EU agricultural regulators on the fulfilment of subsidy conditions. Furthermore, we found that traditional face-to-face learning, experienced farmers as mentors and knowledge sharing mechanisms were rated as very applicable/important by the academics. On the other hand, massive open online courses and apps for learning via a smartphone was considered not very applicable/not important forms for learning/training in sustainable farming. However, Shanley et al. (2004) considered that online education provides the trainees/students/farmers with an educational alternative to the traditional face-to-face learning, allowing them to proceed at their own pace. Parr et al. (2007) already considers that students should learn through experiences that link the classroom to field work, engaging a broad range of actors within applied settings. Their study also supports the argument that sustainable agricultural education requires progressive, integrated, experiential, interdisciplinary, systems-based curricula where learning grounds theory to practice in relevant and purposeful social and environmental contexts. Although traditional face-to-face learning is the most suitable training methods for a Master program in Sustainable Agriculture, online training

methods should be seen as complementary tools in agriculture programs for situations like the COVID-19 pandemic. In this way, there is no interruption in the studies and teaching of academic staff, students and agricultural extension staff.

The training methods educational excursions/visits, field demonstrations, short-term seminars, practical courses/exercises and agriculturalist's visits in farms were considered to be extremely efficient by the academics of the three European countries. On the other hand, these academics considered not efficient the training methods broadcasts on radio, information in the form of forms-brochures, television broadcasts and articles in newspaper.

4. Conclusions

Relevant training and learning needs in sustainable agriculture that can be taken into account when developing a MSc programme, were identified based on questionnaires. In summary, the technologies, legislation, management and business, local community leadership and marketing were the training needs considered very important expertise's in sustainable agriculture and the more adequate forms of training/learning considered were: 1) Traditional face-to-face learning; 2) Experience farmers as mentors 3) Knowledge sharing mechanisms. The more efficient training methods considered were: a) Educational study visits; b) Field demonstration; c) Short-term seminars; d) Practical courses/exercises; e) Agriculturalist's visits in farms. COVID-19 pandemic exposed the importance of ICT and technological tools as a basic need for online learning.

Acknowledgements

References

Azeiteiro, Ulisses Miranda, Paula Bacelar-Nicolau, Fernando JP Caetano, and Sandra Caeiro. 2015. "Education for Sustainable Development through E-Learning in Higher Education: Experiences from Portugal." *Journal of Cleaner Production* 106: 308–319.

Carson, Kay I. 2018. "Agricultural Training and the Labour Productivity Challenge." *International Journal of Agricultural Management* 6 (3–4): 131–133.

Cioloş, D. 2012. "Agriculture the Way towards Sustainability and Inclusiveness G20/Rio de Janeiro 21 June 2012. DG AGRI/DG DEVCO Side Event / SPEECH/12/480, 21/6/2012.," 2012.

EU. 2012. "Sustainable Agriculture for the Future We Want. European Union, DG AGRI/ DG Development and Cooperation (EuropeAid).," 2012.

European Commission, P. 2014. "Precision Agriculture: An Opportunity for EU Farmers—Potential Support with the CAP 2014-2020."

Hodges, Charles, Stephanie Moore, Barb Lockee, Torrey Trust, and Aaron Bond. 2020. "The Difference between Emergency Remote Teaching and Online Learning." Educause Review 27.

Lamine, Claire. 2015. "Sustainability and Resilience in Agrifood Systems: Reconnecting Agriculture, Food and the Environment." *Sociologia Ruralis* 55 (1): 41–61. https://doi.org/10.1111/soru.12061.

Meera, Shaik N., Anita Jhamtani, and D. U. M. Rao. 2004. "Information and Communication Technology in Agricultural Development: A Comparative Analysis of Three Projects from India." *Network Paper No* 135.

Parr, Damian M., Cary J. Trexler, Navina R. Khanna, and Bryce T. Battisti. 2007. "Designing Sustainable Agriculture Education: Academics' Suggestions for an Undergraduate Curriculum at a Land Grant University." *Agriculture and Human Values* 24 (4): 523–33. https://doi.org/10.1007/s10460-007-9084-y.

Patil, S. S., and K. D. Kokate. 2011. "Training Need Assessment of Subject Matter Specialists of Krishi Vigyan Kendras." *Indian Research Journal of Extension Education* 11 (21): 18–22.

Shanley, Ellen L., Colleen A. Thompson, Lisa A. Leuchner, and Yanyun Zhao. 2004. "Distance Education Is as Effective as Traditional Education When Teaching Food Safety§." *Food Service Technology* 4 (1): 1–8. https://doi.org/10.1111/j.1471-5740.2003.00071.x.

UN-FAO. 2020. "Urban Food Systems and COVID-19: The Role of Cities and Local Governments in Responding to the Emergency. Https ://Www.Fao.Org/3/Ca860 0en/ CA860 0EN.Pdf. Accessed 9 June 2020."

Energy and bioenergy

Description of a Pilot Scale Test Station for Measurement of Static and Dynamic Loads in Silos Under Different Conditions

Rômulo Marçal Gandia[a,b*], Wisner Coimbra de Paula[a], Francisco Carlos Gomes[a], Pedro José Aguado Rodriguez[b]

[a] Department of Agricultural Engineering, Federal University of Lavras, Lavras, Brazil

[b] Department of Engineering and Agricultural Sciences, University of León, León, Spain

* Corresponding author. Email: romagandia@gmail.com

Abstract

There are few full-scale experimental stations to study the mechanical behavior of the stored materials in silos, therefore there are few data to validate the theoretical models, what are essential to design these structures. The work aims to describe the experimental station built at the Federal University of Lavras (Brazil) according to the methodology described in the project of Pieper & Schütz (Pieper & Schütz, 1980). This model contributed to support DIN 1055-6 (DIN, 2005).

The station consists of two silos, one fully instrumented to perform the tests (pilot silo) and the other to store the test product (storage silo). These silos are connected by a bucket elevator to transport the product, enabling filling and discharging. The pilot silo is metallic and 6 meters high with a diameter between 0.69 and 0.71 depending on the wall to be used. The pilot silo is instrumented with a total of 59 measurement cells to obtain lateral pressures and friction forces on the wall. With these test facilities is possible to obtain different configurations such as: 12 height / diameter ratios, 8 hoppers (changing concentricity, eccentricity and angles), 3 different silo wall roughness, consolidation time, discharge flow and different materials.

The experimental station design by the authors is capable of obtaining horizontal and friction pressures in the silo, vertical pressures, normal hopper pressures, as well as contributing experimentally in the silo action field due to the stored product and in the future also contributing to the validation of finite element models. In addition, it can be obtained different parameters at a real scale, which have been demonstrated are different to those obtained in laboratory tests, for example the lateral to vertical pressures ratio (K), friction coefficients and the Poisson ratio.

Keywords: test silo validation, full scale experimental station, flat bottom, hydrostatic pressure, experimental study in silos.

1. Introduction

The study of the behavior of stored product in silos has been dated since 1895 by Janssen (Janssen, 1895). Since then, other theories and researches were developed (Butterfield, 1969; Deutsh & Schmidt, 1985; Fank et al., 2018; Gallego et al., 2011; JA. B LVIN, 1971; Jenike, 1964; Sadowski et al., 2020; Walker, 1967; Wenzel, 1973), however, there are still uncertainties, gaps and design flaws in the study in silos (Ayuga, 2008; Bywalski & Kamiński, 2019; Dogangun et al., 2009; Piskoty et al., 2005).

Despite the experimental study having its certainties and approximations with the real conditions, the scale factor (Nielsen & Askegaard, 1977) it is a limiting factor for this model, increasing the cost and limiting the number of full scale experimental stations in the world (Brown et al., 2000; Couto et al., 2012; Gandia et al., 2021; Härtl et al., 2008; Ramírez et al., 2010; Schuricht et al., 2001; Sun et al., 2020; Teng et al., 2001; Teng & Lin, 2005; Zhao & Teng, 2004; Zhong et al., 2001).

The storage of agricultural products is of global importance due to several factors (future market, logistics, safety, drying, processing). Only in Brazil, the agricultural production have a grain production estimation of 268.7 million tons for 2020 (CONAB, 2020). The storage capacity of Brazil reached 177.7 million tons in the second half of 2019, and of this total, 86.6 million tons are stored in tower silos (IBGE, 2020).

However, despite these data, Brazil still does not have a specific standard for projects in silos. Therefore, this work aims to describe and show the research capacity of the experimental station built at the Federal University of Lavras to study pressures, loads and flow in cylindrical silos.

2. Materials and Methods

Description

The test station was previously designed by Pieper & Schütz (Pieper and Schütz, 1980) at the Technical University of Braunschweig in Germany. The model helped to support the DIN 1055-6: Basis of design and actions on structures - Part 6: design loads for buildings and loads in silo bins (DIN, 2005). The model was subsequently studied by professors

and researchers at the University of São Paulo (C. Calil et al., 2009; J. C. Calil & Cheung, 2007) and the Federal University of Lavras (Gandia et al., 2021).

Manufacturing and construction were supported by the Kepler Weber company. The experimental station consists of a slender silo, as it is the most used geometry in the industry, although the configurations of the experimental station allow the study of different height/diameter ratio.

The term "pilot scale" (Brown & Nielsen, 1998) designates a type of scale in which if the size of the structure compared to the stored product shows a certain relation between the diameter of the silo and the diameter of the product. Therefore, the results obtained can be used in the study of real structures, with the behaviour of the pilot silo being quantitatively and qualitatively identical to the behaviour on a 1: 1 scale (real scale) (Pieper & Schütz, 1980). The pilot silo has a scale between 1: 4 to 1: 7 and considering the dimensions of all the instrumentation, the limit of the diameter of the product to be stored would be 1.8 centimetres (product diameter 40 times smaller than the internal diameter of the silo) (J. C. Calil & Cheung, 2007).

General description of the test station

The test station consists of two silos, one to perform the tests (pilot silo) and the other to store the product used in the tests (storage silo). The silo is connected by a bucket elevator to transport the product from one silo to another, facilitating filling and discharge between the silos.

The test station was instrumented using a data acquisition system and a portable computer. To measure the pressures on the wall, bottom and base of the silo under different conditions, pressure cells and load cells were positioned along the pilot silo.

The geometry of the pilot silo is cylindrical. The structure of the pilot silo is metallic, the walls and exits (flat bottom and hopper) are made of galvanized steel with a minimum thickness of 5 mm, showing a rigid behaviour in relation to the stored material. The silo structure and the location of the cells for measuring the load can be divided into the silo wall (cylinder) and the bottom of the silo (flat or hopper).

The silo cylinder measures 6 meters high and is segmented into 12 independent rings of 0.495 meters each and spaced precisely 5 millimetres (restricting the vertical influence between the rings). Each ring was cut vertically (with an opening of 5 mm). The cut was joined by two clamps pre-pulled by a set of three coil springs. In each independent ring, two tension load cells were placed, joining the clamps (lower and upper cell in the horizontal position). Each ring is supported by two tension cells connected to the two pillars. The cells are positioned vertically in the middle of the two ends of each ring (right and left cell in the vertical position).

To seal the gaps between the rings, rubbers were used between all the rings, which are changed periodically. It is worth mentioning that the connections of the tension load cells are articulated on the supports by stainless steel pins.

The pilot silo allows changing the bottoms: flat bottom and hopper bottom. The cylinder and the bottoms (flat and hopper) have internal diameters that vary between 0.69 to 0.71 m, depending on the wall to be used. All the silo bottoms have the same outlet diameter, 0.20 m.

The silo is supported and structured by two pillars arranged at 180 °, with a third pillar located at 90 ° of both pillars for lateral support, without receiving a vertical load. The set of 12 rings that represent the silo cylinder is supported by the two structural pillars on the extreme sides (180 °).

Therefore, the pilot silo can be considered slender silo or intermediate slenderness silo, depending on the material storage height. When the silo is filled with three or more rings (50 cm each) according to the Eurocode classification (CEN, 2006), it corresponds to a slender silo (H = 1.5 m and D = 0.69 m), since the height / diameter ratio is greater than or equal to 2.

Components of Pilot-Silo

The pilot silo was designed to perform tests with several variables. Therefore, it is possible to physically change the pilot silo settings. Among the configurations, the most important are changing the bottoms and changing the walls.

The bottom of the silo consists of eight interchangeable bottoms. All parts are connected vertically by a pair of tension load cells (also used in the cylinder wall rings). In addition, each bottom has 4 to 7 openings where the pressure cells are strategically positioned.

The set of bottoms consists of a flat bottom with a concentric outlet; four hopper bottoms with concentric outlet and inclinations (β) of 15, 30, 45 and 60 ° and three hopper bottoms with 100% eccentric outlet and inclinations (β) of 15, 30 and 45 °.

The silo walls can also be changed, changing the coefficient of wall friction (μ). Therefore, the pilot silo allows the exchange for three different walls: Smooth mild carbon steel, horizontally corrugated and Profiled sheeting with horizontal ribs. The basic structure of the silo wall is the smooth mild carbon steel, so the other walls are superimposed on it.

Among the parts of the pilot silo and the possible test variables, it is still possible to evaluate concentric and

eccentric fillings with twelve height/diameter ratios (the pilot silo has twelve structurally independent rings).

Storage silo

The silo wall was constructed with 1.5 mm thick horizontally corrugated steel sheets. The upper part and the hopper with 1.5 mm flat steel plates. The silo is supported by four pillars spaced at 90 °. The storage silo is classified as intermediate slenderness silo, with a H / D ratio = 1.05 (height of 1.88 and diameter 1.78 m).

The storage silo has a total volume of 5.6 m^3. The reason why the volume of the storage silo is twice as large as the pilot silo (2.55 m^3, when the hopper with the largest volume is used) is to supply the material loss material due to transport and mainly to decrease the transport of the same stored material, avoiding the variation of the granulometry in the tests.

Transport system

The transport is performed in a simple way. The bucket elevator is manually operated with a constant speed. To fill the pilot silo, it is necessary to manually open the flow change system so that the stored material is transported from the stored silo, bucket elevator and pilot silo. To discharge the pilot silo, the process is reversed, manually close the flow change system and so that the stored material is transported from the pilot silo, transition box, bucket elevator and stored silo.

Between the storage silo and the bucket elevator there is a transition tube that can be changed. The inclination of this tube is changed according to the type of material used and the maximum flow of the bucket elevator. Therefore, the objective is always to perform the tests using the maximum filling flow in the pilot silo.
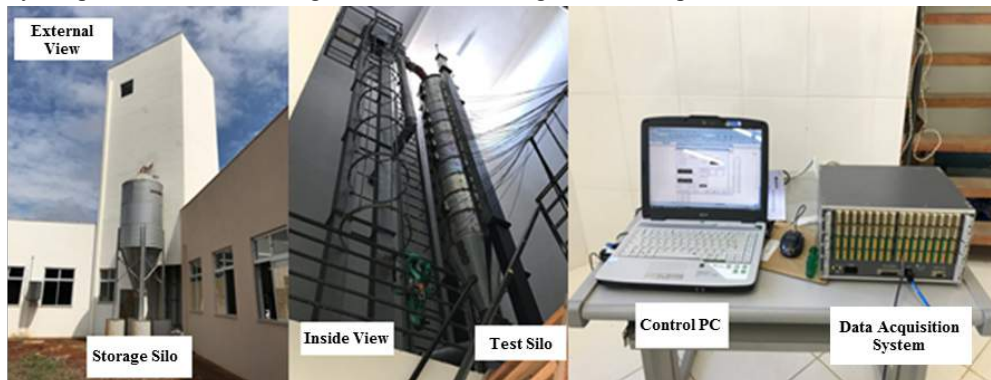
Figure 1. Test Silo Station and instrumentation.

Instrumentation

In general, the instrumentation of the pilot silo was made by a set of 59 measuring cells distributed in the pilot silo and connected in the data acquisition system controlled by a portable computer. The measuring cells can be divided into three different types: pressure cells, shear beam load cells and tension load cells (Figure 2).

Figure 2. Types of measuring cells in the pilot silo.
Pressure cell (a), shear beam load cell (b), tension load cell (c).

Regarding the loads measured in the pilot silo, we can divide it into vertical loads and normal loads. Vertical loads are measured along the silo (cylinder, bottom and supporting pillars). Normal loads are measured on the cylinder wall and the hopper wall.

Measurement cells.

As mentioned, the pilot silo was fully instrumented, presenting 59 measurement cells, where:

- Two shear beam load cells with a nominal capacity of 50 kN, located at the base of each pillar;
- Seven pressure cells with nominal capacity of 70 kPa, strategically positioned in the hoppers;
- Fifty tension load cells with a nominal capacity of 8 kN, being:
- Cinquenta células de carga de tração com capacidade de carga normal de 8kN, sendo:
o Twenty-six in an upright position supporting both ends of each ring and the bottom of the silo.

    o   Twenty-four in the horizontal position, joining the clamps that open each ring. The load cell pairs are pre-pulled by a set of three springs.

All pressure and load cells were made of aluminum with special alloy by MSI (Micro Sensores Industriais). All cables are double to avoid noise, protecting the system vibration against moisture.

Measuring vertical forces

The vertical forces in the pilot silo are measured in four ways: tension load cell located between the cylinder ring and the support pillar; tension load cell located between the bottom of the silo and the supporting pillar; shear beam load cell located at the base of the support pillars and, when using the flat bottom, pressure cell located on the flat bottom.

The vertical forces on the segmented cylinder wall (each independent ring) are measured by pairs of tension load cells located between the cylinder wall and support pillar, this is the frictional force, resulting from the vertical stress of the cylinder wall. Due to segmentation of the ring and because they have gaps (structurally independent) it is possible to obtain, and friction force distributed along each ring.

The pair of tension load cells located between the bottom of the silo (flat bottom or hopper) and the column measure the vertical force at this point, vertical stress in the stored material at the silo-hopper transition.

All tension load cells (cylinder and silo bottom) are connected to the two support pillars, so it is possible to obtain the weight of the stored material from the values of the shear beam type load cells located at the base of the two pillars.

When using the flat bottom, the four pressure cells located on this bottom will measure the vertical pressure at the bottom of the silo, this pressure is calculated directly by the pressure cells.

Measuring horizontal forces

Horizontal stresses on the cylinder wall are measured using a clamp system joined by two pre-tensioned load cells. Between the two cells are positioned three springs of the same material and dimensions to pre-pull the system. Each cell pair is located in parallel (one above and one below) and centred vertically at the union of the ring opening. The union between tension load cell / clamp was made by stainless steel pins that allows the rotation of the system caused by the pressure in the ring walls that tend to disengage the semi cylinder. With this system it is possible to obtain the horizontal force due to the pressure of the stored material.

Measuring normal pressures

Normal efforts are directly measured by pressure cells, exerted on the hopper wall. The cells are located immediately below the transition and until the outlet, each hopper has other strategically located points. The eccentric hoppers have pairs of pressure cells (on the same level) on both sides to check the pressure distribution according to the eccentricity of the outlet.

Data acquisition system

The pilot silo has a total of 59 measurement cells. This required a data acquisition system with many channels. Therefore, the acquisition of signals was performed through the LYNX data acquisition system, model DS2000, with 4 acquisition cards, being 2 (AI2160) and 2 (AI2161), making a total of 64 channels. This model allows a maximum sampling frequency of 65.5 kHz. The analogy signal sent by each cell (load and pressure) (mV / V) is processed by the A / D converter in a digital reading that is transmitted over the network (Figure 1).

A lot of preliminary tests were done before reaching the sampling frequency. The frequency used in the tests was 2Hz, that is, two points per second. This sampling was chosen because it does not have data leakage and relatively good data processing time, the same frequency was used by Couto et al., (2012) e Ruiz et al., (2012).

Calculation

- Normal wall pressures: The calculation of normal pressures on the silo wall is obtained by applying the Principle of Virtual Works (P.T.V.). It is possible to calculate the normal pressure on the silo wall at 12 different heights, relative to each independent ring.

- Frictional wall pressures: The friction pressure on the silo wall is measured indirectly by the pairs of traction load cells located on the vertical support (positioned at 180°) of each ring. It is possible to calculate the friction pressure on the silo wall at 12 different heights, relative to each independent ring.

- Weight of stored material: The weight of the material stored in a given time is obtained by the sum of the forces obtained in the beam load cells positioned at the base of the right and left columns.

- Vertical stress in the stored material at the transition: this stress begins to be measured when the hopper is filled with the stored material, from this moment, Vertical stress in the stored material at the transition exerted in this area can be obtained.

- Wall friction coefficient: The coefficient of wall friction can be obtained in the entire cylinder dividing friction pressure by normal pressure.

- Lateral pressure ratio K: The relation between horizontal and vertical pressure in the cylinder wall can be obtained at any time of interest by equation dividing normal pressure by vertical pressure.

- Specific weight of stored material: The specific weight of the stored material is obtained from the internal volume of the hopper, internal volume of the cylinder and the weight of the material stored at any time.

3. Results and Discussion

Calibration of measurement cells

Description of calibrations

As the instrumentation of the pilot silo was made by three different cell types (pressure cells, shear beam load cell and tensile load cell) different methods were used for calibration. Basically, two ways of calibrating the cells were used: Tube to measure pressure and Universal Testing Machine.

To avoid excess data (due to the large number of cells and the repetitions of the calibrations), as the calibration values were very approximate, only one curve for each cell type was presented.

Tube to measure pressure

A simple and efficient device for calibrating the pressure cells, called the "tube to measure pressure", was built. The device is illustrated in Figure 3. The pressure cell is positioned at the bottom of the tube, supported by the MDF board. Above the pressure cell, a seal is made (between the cell and the tube wall) for subsequent filling of the tube with water. The height control and reading of the water was done by a transparent hose (communicating vessels). The calibration curve (Figure 4) shows maximum correlation, 100% ($R^2 = 1$).

Figure 3. Tube to measure pressure - pressure cell calibration system.
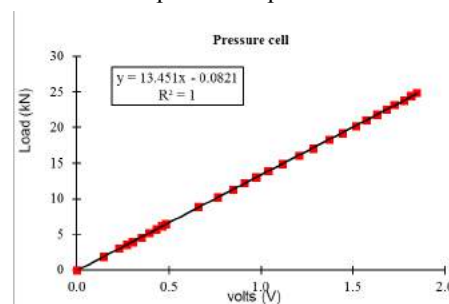
Figure 4. Calibration curve of pressure cell.

Universal Testing Machine

The calibration of the tension load cells, and the shear beam load cells were performed using the Universal Testing Machine with load capacity of 300 kN (Figure 5a).

The tension load cell was fixed by two double welded rods and fastened to the machine's claws. The cell was fixed in the rods using pins. The test was traction (Figure 5b).

The shear beam load cell was calibrated with the base of the pillar. The calibration was performed by applying a

compressive force, simulating the force exerted by the pilot silo (Figure 5c).
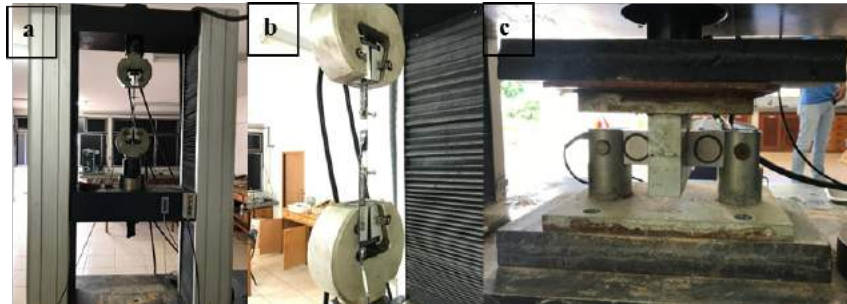
Figure 5. Universal Testing Machine - shear beam load cell and tensile load cell calibration.

Universal Testing Machine (a), tensile load cell calibration (b), shear beam load cell calibration (c).

The calibration curves (Figure 6 and Figure 7) for the two load cells: shear beam and tension showed excellent 99.99% and 99.98% correlation, respectively.
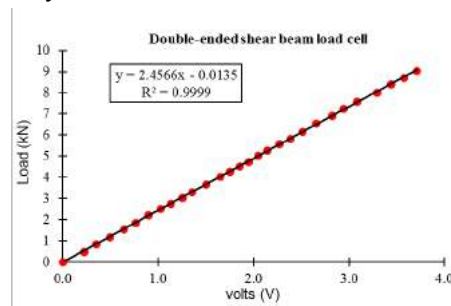
Figure 6. Calibration curve of shear beam load cell
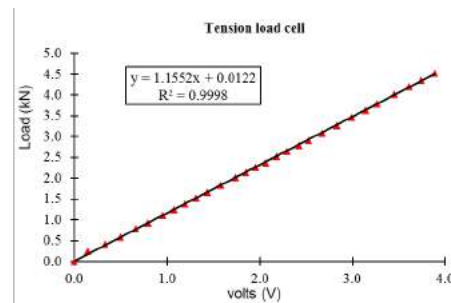
Figure 7. Calibration curve of tension load cells.

4. Conclusions

In this article, the experimental station for obtaining static and dynamic pressures in cylindrical silos under different conditions was described. In addition, the model clearly and visually showed that calibration and instrumentation generate reliable data. Therefore, in the described model it is possible to obtain the parameters:

- Horizontal pressure on the silo wall at different heights, at time t.
- Friction pressure on the silo wall at different heights, at time t.
- Normal hopper wall pressure for hopper bottom silo, at time t.
- Vertical pressure at the bottom of the silo for a flat bottom silo, at time t.
- Lateral pressure ratio (K), at time t

In addition to the parameters, it is possible to perform tests under different conditions:

- Flat bottom silo or hopper bottom silo.
- Concentric and eccentric discharges, both with angular variations.
- Roughness of the silo wall.
- Height/diameter (H / D) ratio of the silo.
- Materials (powdered or granular) with a larger diameter less than 18 mm

- Concentric or eccentric filling.
- Storage time for consolidation and segregation analysis of stored material.

Therefore, it is possible to analyse numerous boundary conditions obtaining a considerable amount of data for the analysis of pressures in full-scale silos. The boundary conditions also allow a greater understanding of numerical studies, since there are few experimental stations in the world. Therefore, the experimental station in the present study will also assist the study in the validation of numerical models.

The great possibility of research and future contributions to silo structures are high due to the interchange of the station's components. Enabling the replacement of the walls (changing the roughness of the material), the bottom of the silo (changing the type of flow and pressure configuration), as well as the use of various agricultural or industrial materials, analysing H / D ratios and also changing the storage time of the materials (analysing the consolidation and segregation of the materials).

Acknowledgements

References

Ayuga, F., 2008. Some unresolved problems in the design of steel cylindrical silos. In J. G. Chen, J.F., Teng (Ed.), *Structures and Granular Solids: From Scientific Principles to Engineering Applications* (pp. 123–133). CRC Press-Taylor & Francis Group.

Brown, C. J., Lahlouh, E. H., & Rotter, J. M., 2000. Experiments on a square planform steel silo. *Chemical Engineering Science*, *55*(20), 4399–4413. https://doi.org/10.1016/S0009-2509(99)00574-6

Brown, C. J., & Nielsen, J., 1998. *Silos: Fundamentals of theory, behaviour and design* (E & FN Spon (ed.)).

Butterfield, R., 1969. A theoretical study of the pressures developed in a silo containing single-size particles in a regular packing. *International Journal of Rock Mechanics and Mining Sciences And*, *6*(2), 227–238. https://doi.org/10.1016/0148-9062(69)90037-0

Bywalski, C., & Kamiński, M., 2019. A case study of the collapse of the over-chamber reinforced concrete ceiling of a meal silo. *Engineering Structures*, *192*(March), 103–112. https://doi.org/10.1016/j.engstruct.2019.04.100

Calil, C., Palma, G., & Cheung, A. B., 2009. Failure Modes of Cylindrical Corrugated Steel Silos in Brazil. *Bulk Solids Handling*, *29*(6), 346.

Calil, J. C., & Cheung, A. B., 2007. *Silos: pressões, fluxo, recomendações para o projeto e exemplo de cálculo* (SET/EESC-USP (ed.)).

CEN, 2006. *EN 1991-4:2006. Eurocode 1: Actions on Structures. Part 4: Silos and Tanks*.

CONAB, 2020. Acompanhamento da safra brasileira 2019/2020. In *Acompanhamento da Safra Brasileira de Grãos 2019/2020* (Vol. 7). https://www.conab.gov.br/info-agro/safras

Couto, A., Ruiz, A., & Aguado, P. J., 2012. Design and instrumentation of a mid-size test station for measuring static and dynamic pressures in silos under different conditions - Part I: Description. *Computers and Electronics in Agriculture*, *85*, 164–173. https://doi.org/10.1016/j.compag.2012.04.009

Deutsh, G. P., & Schmidt, L. C., 1985. Pressures on Silo Walls. *Developments in Geotechnical Engineering*, *39*(C), 125–138. https://doi.org/10.1016/B978-0-444-42470-9.50016-7

DIN., 2005. *DIN 1055-6: Basis of design and actions on structures – Part 6: design 623 loads for buildings and loads in silo bins*.

Dogangun, A., Karaca, Z., Durmus, A., & Sezen, H., 2009. Cause of damage and failures in silo structures. *Journal of Performance of Constructed Facilities*, *23*(2), 65–71. https://doi.org/10.1061/(ASCE)0887-3828(2009)23:2(65)

Fank, M. Z., do Nascimento, J. W. B., Cardoso, D. L., Meira, A. S., & Willrich, F. L., 2018. Vertical pressures and compressive friction force in a large silo. *Engenharia Agricola*, *38*(4), 498–503. https://doi.org/10.1590/1809-4430-Eng.Agric.v38n4p498-503/2018

Gallego, E., González-Montellano, C., Ramírez, A., & Ayuga, F., 2011. A simplified analytical procedure for assessing the worst patch load location on circular steel silos with corrugated walls. *Engineering Structures*, *33*(6), 1940–1954. https://doi.org/10.1016/j.engstruct.2011.02.032

Gandia, R. M., Gomes, F. C., Paula, W. C. de, Junior, E. A. de O., & Aguado Rodriguez, P. J., 2021. Static and dynamic pressure measurements of maize grain in silos under different conditions. *Biosystems Engineering*, *209*, 180–199. https://doi.org/10.1016/j.biosystemseng.2021.07.001

Härtl, J., Ooi, J. Y., Rotter, J. M., Wojcik, M., Ding, S., & Enstad, G. G., 2008. The influence of a cone-in-cone insert on flow pattern and wall pressure in a full-scale silo. *Chemical Engineering Research and Design*, *86*(4), 370–378. https://doi.org/10.1016/j.cherd.2007.07.001

IBGE., 2020. *Levantamento Sistemático da Produção Agrícola - Estatística da Produção Agrícola*.

JA. B LVIN., 1971. Analytical Evaluation of Pressures of Granular Materials on Silo Walls. *Powder Technology*, *4*(5), 280. https://doi.org/10.1016/0032-5910(71)80050-5

Jenike, A. ., 1964. *Storage and Flow of Bulk Solids Bull. 123*. University of Utah.

Nielsen, J., & Askegaard, V., 1977. Scale errors in model tests on granular media with special reference to silo models. *Powder Technology*, *16*(1), 123–130. https://doi.org/10.1016/0032-5910(77)85029-8

Pieper, K., & Schütz, M., 1980. *Bericht über das Forschungsvorhaben Norm-Mess-Silo für Schüttguteigenschaften*. Hochbaustatik, Technische Universität.

Piskoty, G., Michel, S. A., & Zgraggen, M., 2005. Bursting of a corn silo - An interdisciplinary failure analysis. *Engineering Failure Analysis*, *12*(6 SPEC. ISS.), 915–929. https://doi.org/10.1016/j.engfailanal.2005.02.002

Ramírez, A., Nielsen, J., & Ayuga, F., 2010. On the use of plate-type normal pressure cells in silos. Part 1: Calibration and evaluation. *Computers and Electronics in Agriculture*, *71*(1), 71–76. https://doi.org/10.1016/j.compag.2009.12.004

Sadowski, A. J., Michael Rotter, J., & Nielsen, J., 2020. A theory for pressures in cylindrical silos under concentric mixed flow. *Chemical Engineering Science*, *223*, 115748. https://doi.org/10.1016/j.ces.2020.115748

Schuricht, T., Furll, C., & Eenstad, G. G., 2001. Full scale silo tests and numerical simulations of the „cone in cone" concept for mass flow. In *Handbook of Powder Technology* (Vol. 10, pp. 175–180). Elsevier Science BV.

Sun, W., Zhu, J., Zhang, X., Wang, C., Wang, L., & Feng, J., 2020. Multi-scale experimental study on filling and discharge of squat silos with aboveground conveying channels. *Journal of Stored Products Research*, *88*, 101679. https://doi.org/10.1016/j.jspr.2020.101679

Teng, J. G., & Lin, X., 2005. Fabrication of small models of large cylinders with extensive welding for buckling experiments. *Thin-Walled Structures*, *43*(7), 1091–1114. https://doi.org/10.1016/j.tws.2004.11.006

Teng, J. G., Zhao, Y., & Lam, L., 2001. Techniques for buckling experiments on steel silo transition junctions. *Thin-Walled Structures*, *39*(8), 685–707. https://doi.org/10.1016/S0263-8231(01)00030-1

Walker, D., 1967. An approximate theory for pressures and arching in hoppers. *Chemical Engineering Science*, *22*(3), 486. https://doi.org/10.1016/0009-2509(67)80145-3

Wenzel, F., 1973. Pressure behavior in double cylindrical silos. *Journal of Manufacturing Science and Engineering, Transactions of the ASME*, *95*(1), 97–100. https://doi.org/10.1115/1.3438170

Zhao, Y., & Teng, J. G., 2004. Buckling experiments on steel silo transition junctions. II: Finite element modeling. *Journal of Constructional Steel Research*, *60*(12), 1803–1823. https://doi.org/10.1016/j.jcsr.2004.05.001

Zhong, Z., Ooi, J. Y., & Rotter, J. M., 2001. The sensitivity of silo flow and wall stresses to filling method. *Engineering Structures*, *23*(7), 756–767. https://doi.org/10.1016/S0141-0296(00)00099-7

Experimental and Numerical Study of Silo Filling Using Pellets

Rômulo Marçal Gandia[a,b*], Angel Ruiz Padin[b], Gerardo Hernández Rodrigo[b], Luiz Herráez Ortega[b], Alberto Tascón Vegas[c], Pedro José Aguado Rodriguez[b]

[a] Department of Agricultural Engineering, Federal University of Lavras, Lavras, Brazil

[b] Department of Engineering and Agricultural Sciences, University of León, León, Spain

[c] Department of Agriculture and Food, University of Rioja, Logroño, Spain

* Corresponding author. Email: romagandia@gmail.com

Abstract

At present, different biological materials, agricultural crops or forest products are susceptible to be industrially transformed to be used as solid biofuels. The most common presentation for these materials is in the form of pellets, whose storage is carried out mainly in hoppers, silos or bunkers. However, there is an important lack of knowledge about the mechanical behaviour of these stored materials, what causes difficulties in the structural silo design. Numerical models have proved to be a useful tool to analyse this phenomenon and even for the design of silos. However, numerical models need parameters that must be experimentally obtained and finally they must be validated by experimental assays.

The objective of this work is to present a finite element model developed by the authors to simulate the mechanical behaviour of pellets that have been stored in a silo. This model has been compared with the experimental results obtained using a real scale silo test.

The experimental analysis was performed at the experimental station located at the University of León, designed and built by Couto, Ruiz & Aguado (Couto et al., 2012; Ruiz et al., 2012). The parameters such: specific weight, modulus of elasticity, internal friction angle, wall friction coefficient, angle of repose and Poisson's ratio were determined experimentally.

The numerical model was made in 3D, using Ansys 2021R1 software. For simulate the filling stage all nodes placed at the hopper shell of the silo were totally restricted. The behaviour of the pressures in the silo and hopper were verified, as well as the displacement of the grains and the directions of the main stresses.

Keywords: solid biofuels, static condition, finite element method, silo pressures, stored product.

1. Introduction

Since the appearance of the first tower silos at the end of the 19th century, many structural failures have been recorded (Bywalski & Kamiński, 2019; Dogangun et al., 2009; Gutiérrez et al., 2015; Y. Sun & Wang, 2012; Teng, 1998; Teng & Rotter, 1989) and many studies have been developed on these structures (Jenike et al., 1973a, 1973b; Walker, 1967; Walters, 1973a, 1973b). However, many uncertainties still remain since the behaviour of the materials stored in silos is very complex is not totally understood (Ayuga, 2008; Dogangun et al., 2009; Nielsen, 2008).

Due to the advancement of engineering combined with computational development, modelling is supported by a tripod: theoretical model, experimental model, and numerical model. These three models (working together) optimize and advance studies in most areas of engineering. For example, the finite element method (FEM) is a numerical procedure to determine approximate solutions of value problems on the contour of differential equations. The FEM subdivides the problem domain into smaller parts, denominated finite elements. Therefore, in recent years, studies using the FEM in silos have significantly increased (E Gallego et al., 2010; Eutiquio Gallego et al., 2015; Holst et al., 1999; Pardikar et al., 2020; Ramírez et al., 2010b), mainly for the quality of the answers and for the relative time and cost-saving in comparison to the experimental models in real scale.

Worldwide, the number of full-scale experimental silo stations is relatively small (Brown et al., 2000; Couto et al., 2012; Gandia et al., 2021; Härtl et al., 2008; Ramírez et al., 2010a; Schuricht et al., 2001; Schwab et al., 1994; W. Sun et al., 2020; Teng & Lin, 2005) due to the cost of construction, instrumentation and operations. Experimental models of full-scale silos provide proximity to real values, enabling confidence in the data and enhancing our understanding of pressures in silos (Chen et al., 2007).

The numerical methods are very useful for the understanding of these complex structures because silos of different geometries can be simulated with different materials at no cost, obtaining a large number of parameters at any point in the silo, which allows to analyse these phenomena more in depth. There is a great lack of knowledge and there is hardly any data in the bibliography on simulations with numerical methods and experimental tests of silos storing pellets.

Therefore, the objective of this paper was developing a Finite Element Model (FEM) to simulate the mechanical behavior of pellets stored in silo in static condition. The values obtained by the FEM were compared with the

experimental data.

2. Materials and Methods

The numerical simulation was performed using elements and the software Ansys 2020R2 student version. The model was developed by simulating the static condition. The dimensions of the silo, hopper inclination were based on the experimental silo at the University of León (Spain) designed and built by the research group of the Department of Agricultural Engineering and Sciences (Couto et al., 2012; Ruiz et al., 2012).

The silo was 2.00 meters high and had one meter in diameter with a concentric hopper angle of 34.3 and 0.48 meters in height. The silo is made of polished steel metal. According to Eurocode 1, part 4 (CEN, 2006), this silo is classified as slender (height/diameter ratio = 2) and can be seen in Figure 1.

Figure 1: Silo geometry (Couto et al., 2012).

The parameters of the stored product (pellets) and the steel sheet of the silo were obtained in the literature (Eutiquio Gallego et al., 2015; Moya et al., 2002, 2006), presented in Table 1.

Table 1. Stored product and steel parameters.

Material parameter	Value
stored material	
Specific weight, γ (kN/m^3)	7.11
Modulus of elasticity, E (kPa)	6000
Poisson's ratio, ν	0.3
Wall friction coefficient, μ	0.23
Cohesion, c (kPa)	1.60
Angle of repouse (°)	40
Angle of dilatancy of bulk material, ψi	2.5
Effective angle of internal friction of bulk material, ϕi	25
Humidity (%)	7.22
steel sheet	
Modulus of elasticity, E (kPa)	210000000
Poisson's ratio, ν	0.3
Thickness (m)	0.02

The proposed model was performed using elastoplastic material (Drucker & Prager, 1952) to simulate the pressure of the stored product (solid, pellets) inside the silo. The standard isotropic and linear model was used to represent the elastic behaviour of the silo, while Drucker and Prager's perfect plasticity criterion was used to define the plastic part.

The model was created in 3D geometry. The modelling was done initially using a small number of elements (mesh simplification). After the model was defined and generated, the mesh was refined, mainly in the areas of most significant interest (silo-hopper transition) (Figure 2). The size of the elements was 0.15 m for the solid and 0.075 m for the silo, totalling 14688 elements. The generated mesh was composed of prismatic elements with 8 and 4 knots, as shown in Figure 2. This type of mesh is stable and, when possible, allows analysis with better results. For the stored product (solid), an element with eight nodes (Solid 45, Lagrangian type) was used, which is an element that supports large deformations (Eutiquio Gallego et al., 2015). The silo (shell) wall was modelled using the 8-node shell element (Shell 63), ideal for analysing non-linear applications. For the contact (friction) between the stored product (solid) and the silo wall (shell), 4-node elements were used (Conta 173 and Target 170) (E Gallego et al., 2010). The model was vertically (z-axis) constrained in the contour of the silo-hopper transition. The gravitational force was inserted towards the z-axis.
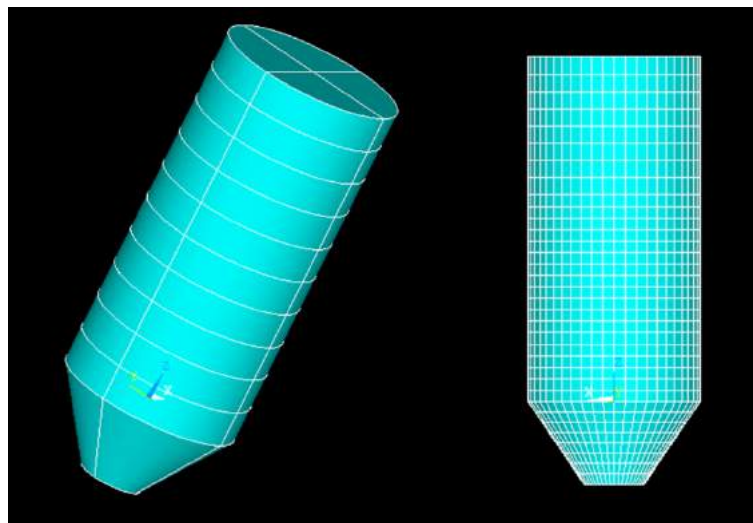
Figure 2: Geometry and mesh of the developed model.

The model were subsequently compared with Eurocode 1, part 4(CEN, 2006). The normal static pressure curves were calculated using the same parameters proposed in the development of the model using FEM: silo dimensions (height: 2 meters; internal diameter: 1 meter; β: 34.3 °); work variables (wall friction coefficient: 0.23); specific weight: 7.11 kN / m^3); other values extracted from Table E.1 - Properties of Disaggregated Solids used for the product (CEN, 2006).

Displacement in z direction, stress in z direction, horizontal and vertical pressures along the silo height and diameter were evaluated. The horizontal pressures in the silo were compared with experimental values.

3. Results and Discussion

The tension between the solid and the wall in the z direction shows that the silo-hopper transition is a region with greater tension (Figure 3 a), which is already known theoretically (CEN, 2006; Jenike et al., 1973a). As it is already known that the regions with lower tensions are those at the top of the silo and those close to the exit, due to the formation of mechanical arcs, also seen in Figure 3 a.

The displacement in z (Figure 3 b) indicates the segmented displacement up to 2/3 of the silo height due to the specific weight of the stored product and in the region close to the exit, the displacement also follows the trend of the tension arcs. Values for normal wall pressures are seen in Figure 4.

It is observed (Figure 4) that the maximum normal pressure occurs slightly below the transition. Yet it is possible to see that the maximum modular value is approximately 10.5 kN/m^2 (SMN-SMX). Observing the experimental values in Figure 5 for the same position of the measuring cell located just below the silo hopper transition (GA0) the maximum value was just above 11 kN/m^2.
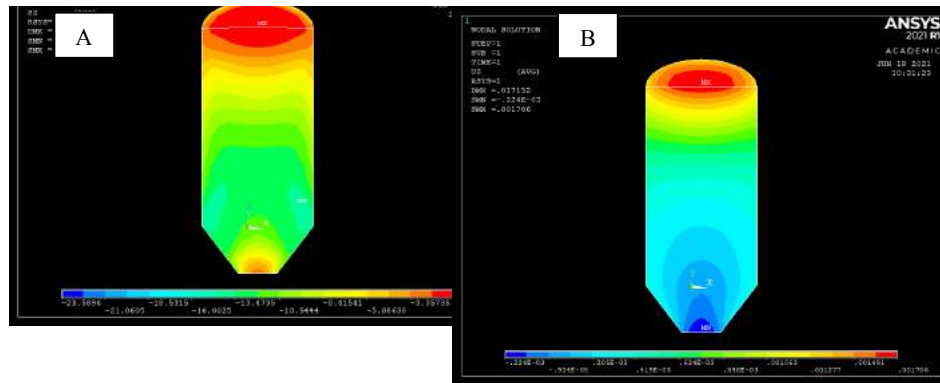
Figure 1. Stress in Z (a) and displacement in Z (b).
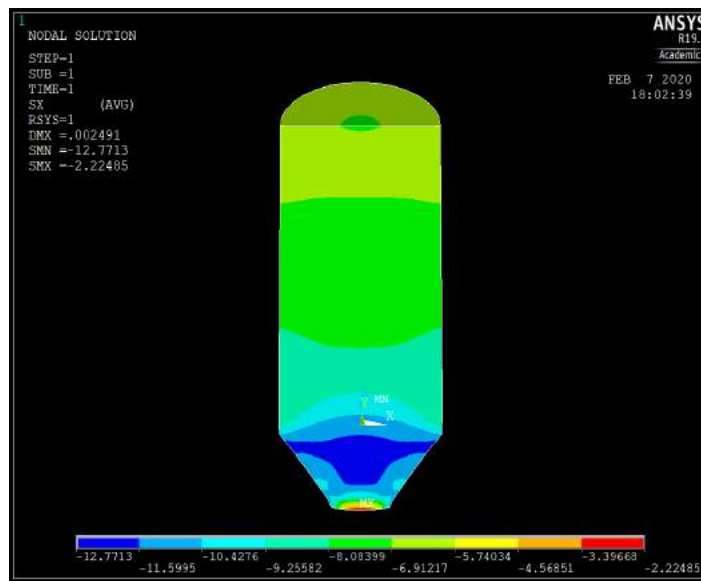
Figure 4. Horizontal pressures obtained by the finite element method.
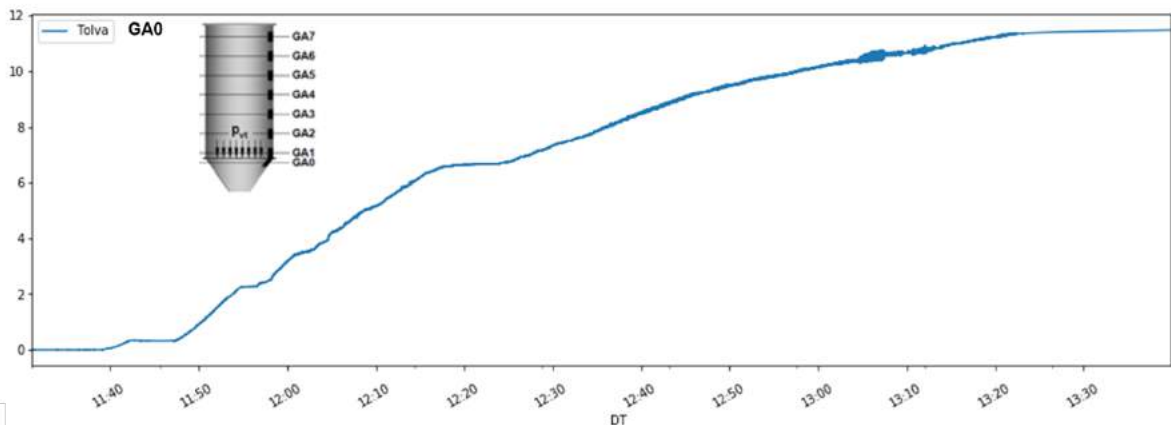
Figure 5. Horizontal pressures obtained experimentally at transition.

The experimental pressures along the silo wall are also observed (Figure 6). A great similarity in the pressures obtained by FEM (Figure 4) are the bands separated by the 3 colours visually observed in the figure. Experimental pressures tend to form 3 ranges of values when filling the silo. An exception occurs for the normal pressure (GA2) that followed an atypical behaviour and will be explained in future works.
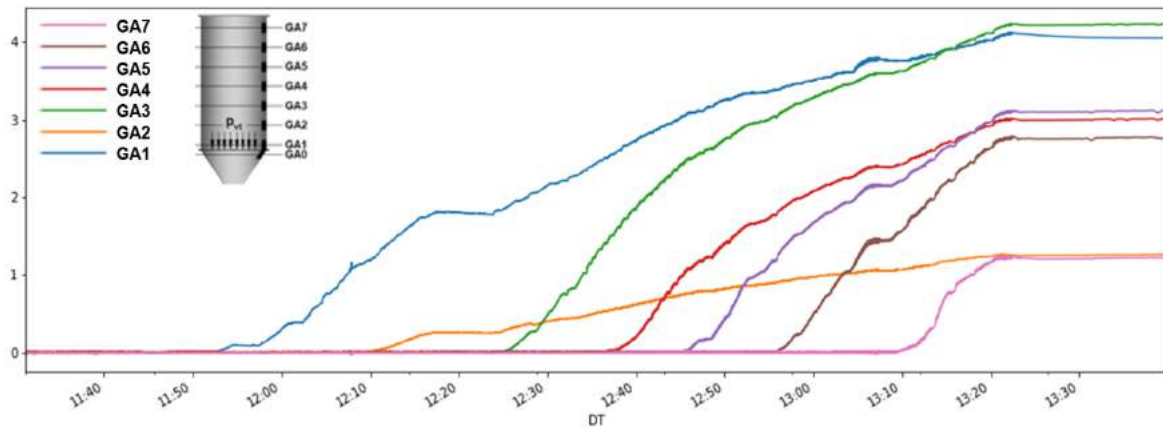
Figure 6. Horizontal pressures obtained experimentally on the silo wall.

The horizontal and vertical pressures obtained by the FEM in the transverse plane exactly in the silo-hopper transition are shown in Figure 7. The values show that with increasing horizontal pressure, vertical pressure decreases and vice versa, which was to be expected.
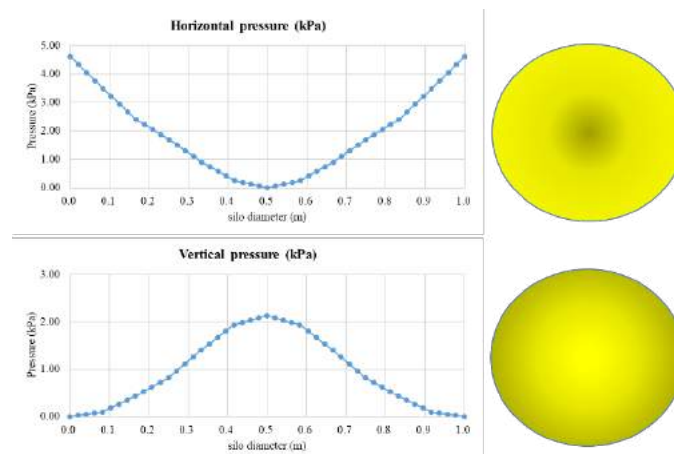
Figure 7. Horizontal and vertical pressures performed in the cross section of the silo-hopper transition.

In addition, this Figure, in addition to demonstrating that the simulation was well done, following the theories of pressure in silos already known, also makes it possible to obtain the K factor at any point in the silo.

Both pressures (horizontal and vertical) follow what was expected due to the friction of the stored product, in other words, horizontal pressures are greater near the silo wall and vertical pressures are maximum in the central region of the silo. Both are null in the central region of the silo (normal pressure) and in the silo wall (vertical pressure).

4. Conclusions

- Results of the finite element model and the experimental test are very similar; therefore, the model is suitable to simulate this type of physical phenomena.
- The lateral pressure curves are not parallel during filling in the experimental test. This had been observed in previous test developed by the authors.
- In the finite element model the lateral pressures on the wall increase with depth, but if it is observed that these pressures at a certain height become greater than in the centre of the silo, reversing the trend maintained below.
- The value of the lateral pressure below the transition from vertical wall to the hopper is very similar both the Finite Element Model and the Experimental data. However, these vertical wall values are higher in the finite element model, probably because in the finite element model the material is considered as a continuous material and not as a material with independent particles.

Acknowledgements

References

Ayuga, F., 2008. Some unresolved problems in the design of steel cylindrical silos. In J. G. Chen, J.F., Teng (Ed.), *Structures and Granular Solids: From Scientific Principles to Engineering Applications* (pp. 123–133). CRC Press-Taylor & Francis Group.

Brown, C. J., Lahlouh, E. H., & Rotter, J. M., 2000. Experiments on a square planform steel silo. *Chemical Engineering Science*, *55*(20), 4399–4413. https://doi.org/10.1016/S0009-2509(99)00574-6

Bywalski, C., & Kamiński, M., 2019. A case study of the collapse of the over-chamber reinforced concrete ceiling of a meal silo. *Engineering Structures*, *192*(March), 103–112. https://doi.org/10.1016/j.engstruct.2019.04.100

CEN. (2006). *EN 1991-4:2006. Eurocode 1: Actions on Structures. Part 4: Silos and Tanks*.

Chen, J. F., Rotter, J. M., Ooi, J. Y., & Zhong, Z., 2007. Correlation between the flow pattern and wall pressures in a full scale experimental silo. *Engineering Structures*, *29*(9), 2308–2320. https://doi.org/10.1016/j.engstruct.2006.11.011

Couto, A., Ruiz, A., & Aguado, P. J., 2012. Design and instrumentation of a mid-size test station for measuring static and dynamic pressures in silos under different conditions - Part I: Description. *Computers and Electronics in Agriculture*, *85*, 164–173. https://doi.org/10.1016/j.compag.2012.04.009

Dogangun, A., Karaca, Z., Durmus, A., & Sezen, H., 2009. Cause of damage and failures in silo structures. *Journal of Performance of Constructed Facilities*, *23*(2), 65–71. https://doi.org/10.1061/(ASCE)0887-3828(2009)23:2(65)

Drucker, D. C., & Prager, W., 1952. Soil mechanics and plastic analysis or limit design. *Quart. Appl. Math*, *10*(2), 157–165.

Gallego, E, Rombach, G. A., Neumann, F., & Ayuga, F., 2010. SIMULATIONS OF GRANULAR FLOW IN SILOS WITH DIFFERENT FINITE ELEMENT PROGRAMS: ANSYS VS. SILO. *Transactions of the ASABE*, *53*(3), 819–829.

Gallego, Eutiquio, Ruiz, A., & Aguado, P. J., 2015. Simulation of silo filling and discharge using ANSYS and comparison with experimental data. *Computers and Electronics in Agriculture*, *118*, 281–289. https://doi.org/10.1016/j.compag.2015.09.014

Gandia, R. M., Gomes, F. C., Paula, W. C. de, Junior, E. A. de O., & Rodriguez, P. J. A., 2021. Static and dynamic pressure measurements of maize grain in silos under different conditions. *Biosystems Engineering*, *209*, 180–199. https://doi.org/10.1016/j.biosystemseng.2021.07.001

Gutiérrez, G., Colonnello, C., Boltenhagen, P., Darias, J. R., Peralta-Fabi, R., Brau, F., & Clément, E., 2015. Silo collapse under granular discharge. *Physical Review Letters*, *114*(1), 5–9. https://doi.org/10.1103/PhysRevLett.114.018001

Härtl, J., Ooi, J. Y., Rotter, J. M., Wojcik, M., Ding, S., & Enstad, G. G., 2008. The influence of a cone-in-cone insert on flow pattern and wall pressure in a full-scale silo. *Chemical Engineering Research and Design*, *86*(4), 370–378. https://doi.org/10.1016/j.cherd.2007.07.001

Holst, J. M. F. G., Ooi, J. Y., Rotter, J. M., & Rong, G. H., 1999. Numerical Modeling of Silo Filling. I: Continuum Analyses. *Journal of Engineering Mechanics*, *125*(1), 94–103. https://doi.org/10.1061/(asce)0733-9399(1999)125:1(94)

Jenike, A. W., Johanson, J. R., & Carson, J. W., 1973a. Bin loads—part 3: mass-flow bins. *Journal of Manufacturing Science and Engineering, Transactions of the ASME*, *95*(1), 6–12. https://doi.org/10.1115/1.3438163

Jenike, A. W., Johanson, J. R., & Carson, J. W., 1973b. Bin Loads—Part 4: Funnel-Flow Bins. *Journal of Engineering for Industry*, *95*, 13–20.

Moya, M., Ayuga, F., Guaita, M., & Aguado, P., 2002. MECHANICAL PROPERTIES OF GRANULAR AGRICULTURAL MATERIALS. *Transactions of the ASABE*, *45*(5), 1569–1577.

Moya, M., Guaita, M., Aguado, P., & Ayuga, F., 2006. MECHANICAL PROPERTIES OF GRANULAR AGRICULTURAL MATERIALS, PART 2. *Transactions of the ASABE*, *49*(1998), 479–490.

Nielsen, J., 2008. From silo phenomena to load models. In J. F. Chen & J. G. Teng (Eds.), *Structures and Granular Solids: From Scientific Principles to Engineering Applications* (pp. 49–57). CRC Press-Taylor & Francis Group.

https://doi.org/10.1201/9780203884447

Pardikar, K., Zahid, S., & Wassgren, C., 2020. Quantitative comparison of experimental and Mohr-Coulomb finite element method simulation flow characteristics from quasi two-dimensional flat-bottomed bins. *Powder Technology*, *367*, 689–702. https://doi.org/10.1016/j.powtec.2020.04.036

Ramírez, A., Nielsen, J., & Ayuga, F., 2010a. On the use of plate-type normal pressure cells in silos. Part 1: Calibration and evaluation. *Computers and Electronics in Agriculture*, *71*(1), 71–76. https://doi.org/10.1016/j.compag.2009.12.004

Ramírez, A., Nielsen, J., & Ayuga, F., 2010b. Pressure measurements in steel silos with eccentric hoppers. *Powder Technology*, *201*(1), 7–20. https://doi.org/10.1016/j.powtec.2010.02.027

Ruiz, A., Couto, A., & Aguado, P. J., 2012. Design and instrumentation of a mid-size test station for measuring static and dynamic pressures in silos under different conditions - Part II: Construction and validation. *Computers and Electronics in Agriculture*, *85*, 174–187. https://doi.org/10.1016/j.compag.2012.04.008

Schuricht, T., Furll, C., & Eenstad, G. G., 2001. Full scale silo tests and numerical simulations of the „cone in cone" concept for mass flow. In *Handbook of Powder Technology* (Vol. 10, pp. 175–180). Elsevier Science BV.

Schwab, C. V, Ross, I. J., White, G. M., & Colliver, D. G., 1994. *WHEAT LOADS AND VERTICAL PRESSURE*. *37*(5), 1613–1619.

Sun, W., Zhu, J., Zhang, X., Wang, C., Wang, L., & Feng, J., 2020. Multi-scale experimental study on filling and discharge of squat silos with aboveground conveying channels. *Journal of Stored Products Research*, *88*, 101679. https://doi.org/10.1016/j.jspr.2020.101679

Sun, Y., & Wang, Y., 2012. Collapse reasons analysis of a large steel silo. *Advanced Materials Research*, *368–373*, 647–650. https://doi.org/10.4028/www.scientific.net/AMR.368-373.647

Teng, J. G., 1998. Collapse strength of complex metal shell intersections by the effective area method. *Journal of Pressure Vessel Technology, Transactions of the ASME*, *120*(3), 217–222. https://doi.org/10.1115/1.2842048

Teng, J. G., & Lin, X., 2005. Fabrication of small models of large cylinders with extensive welding for buckling experiments. *Thin-Walled Structures*, *43*(7), 1091–1114. https://doi.org/10.1016/j.tws.2004.11.006

Teng, J. G., & Rotter, J. M., 1989. Plastic collapse of restrained steel silo hoppers. *Journal of Constructional Steel Research*, *14*(2), 139–158. https://doi.org/10.1016/0143-974X(89)90020-5

Walker, D., 1967. An approximate theory for pressures and arching in hoppers. *Chemical Engineering Science*, *22*(3), 486. https://doi.org/10.1016/0009-2509(67)80145-3

Walters, J. K., 1973a. A theoretical analysis of stresses in axially-symmetric hoppers and bunkers. *Chemical Engineering Science*, *28*(3), 779–789. https://doi.org/10.1016/0009-2509(77)80012-2

Walters, J. K., 1973b. A theoretical analysis of stresses in silos with vertical walls. *ChemicalEngineering Science*, *28*, 13–21.

Electricity Production Based on an Agrivoltaic System. A Study Case for ETSIAAB in UPM

Guillermo P. Moreda[1], Irene Molina López[1], Miguel-Ángel Muñoz-García[1]*

[1]Department of Agroforestry Engineering. LPF – TAGRALIA. ETSIAAB. Universidad Politécnica de Madrid, Spain.

*Email: miguelangel.munoz@upm.es

Abstract

Crops lands could eventually be menaced by rapid increase in photovoltaic solar plants (PVSP) installed capacity. PVSP need large space for its operation what competes with the agricultural use of land. The so-called agrivoltaic systems can alleviate this problem with the combination of both activities, food and energy production.

Several scientific works confirm the benefits that a combined system of photovoltaic panels and crop provide. For the crops, decreased evapotranspiration and increased water use efficiency are claimed.

In the Technical School for Agriculture Engineering, Food and Biosystems (ETSIAAB), of Universidad Politécnica de Madrid (UPM), there are 16.5 ha devoted to research whereform 6.7 ha are experimental crops. The annual electricity consumption of the Experimental facilities is very high (1100 MWh/year). An agrivoltaic system is proposed to reduce electricity bill and the carbon footprint.

A simulation was conducted on a trellised vineyard to determine shading fraction under different geometries of PV module configuration and row spacing. The installation of 50 kWp of photovoltaic power panels would produce 83.90 MWh/year. This will supply 6.18% of the current electricity demand.

The annual saving would be 16,780 €, since the price of energy is 0.20 €/kWh after taxes. With a cost for the installation of 80,000 €, the payback time would be between 5 and 6 years.

Keywords: Photovoltaics, Agrivoltaic, Carbon Footprint, Energy efficiency.

1. Introduction

Solar photovoltaic (PV) energy is positioned to play a major role in the electricity generation Mix of Mediterranean countries. However, substantial increase in ground-mounted PV installed capacity could lead to competition with the agricultural use of land. A way to avert the peril is the so-called solar-sharing, agrophotovoltaic or agrivoltaic (AV). AV systems are a way of combining PV and food production on the same land area (Weselek et al., 2019).

It is demonstrated that agrivoltaic systems are beneficial to plants cultivated under photovoltaic panels (PVP) so much as to themselves. According to Marrou, Dufour et al. (2013), crops increase their yield under the shade of photovoltaic panels, since evapotranspiration is reduced by 10-30% when available sunlight is 50-70%. Therefore, agrivoltaic systems could be suitable for dry regions or drought periods because of the fact that water demand is reduced (Marrou et al., 2013; Adeh et al., 2018). Moreover, PVP offer protection against solar radiation avoiding sunburn, against frost and hail. PVP efficiency is lower because of high temperatures. However, in agrivoltaic systems, ambient temperature is diminished thanks to the location of the crop, so electric production is not reduced (Barron-Gafford et al., 2019). Dupraz et al. (2011) supported that the productivity of fields in these systems increases in a 60% - 70%.

In addition, AV systems can be a solution face to weather conditions that crops hold due to climate change. In a vineyard, high temperatures accelerate ripening. It produces a disequilibrium in grape composition, such as sugar increase giving rise to high alcohol levels (van Leeuwen y Darriet, 2016). Also, excessive radiation harms vine, sometimes grapevines become sunburned.

There are companies that have reported on the installation of vineyard AV systems, using semi-transparent bifacial PV modules. Being semi-transparent, these PV modules decrease the ratio of crop shading, and being bifacial, they harness albedo radiation, thereby featuring increased yield compared to mono-facial counterpart. Further, their PV modules are not fix-tilt, but single-axis mechanical mobile, which enables controlling tilt angle according to the phenological state of the crop. Ultimately, their PV modules are claimed to be corrosion-resistant, which is of paramount importance for vineyard-AV systems, given the chemical pesticides used to protect the grapevine.

The design proposed in this work uses monofacial opaque PV modules. To achieve tolerable shading, they are installed at a height of 5-m (measured at centerline) over the ground. This height value allows for mechanized harvesting with standard grapevine harvesters. For the sake of comparison with other works, shading calculations are extended to a hypothetical 7-m height.

A major objective of the present study was to compare the degree of shading of eight combinations, namely, landscape and portrait PV module layout with skipping of one or two grapevine crop-rows, and for PV module height of 5-m or 7-m, on the understorey trellised vineyard.

2. Materials and Methods

The agricultural plot that served as a reference for the study is a trellised vineyard located in the experimental fields of UPM-ETSIAAB in Ciudad Universitaria (Madrid, Spain). The geographical latitude and longitude of the site are, respectively, 40.443077 °N and 3.738562 °W. The aerial photograph of the grapevine orchard is included in Fig. 1. From the total crop rows shown in the satellite image, only the 13 southern gravepine rows are examined, which correspond to a denser orchard i.e. closer distance between the crop lines (as shown in Fig. 1 the northern crop rows spacing is greater).

Figure 1. Trellised vineyard in Ciudad Universitaria (Madrid, Spain). Distance interval between crop rows or alley width is wa = 2 m.

The crop rows are not exactly aligned with the East-West direction, but they make an angle of 4.3°. Notwithstanding and for the sake of universality, the analysis we have considered as if the foregoing angle was zero, i.e. vine canopy 'walls/racks' facing due-South.

To perform the shading analysis, we used the software SAM version 2020.11.29 [NREL]; in particular the software feature of *3D shade calculator*. The PV module used for the simulations is a crystalline Silicon 340 Wp opaque monofacial module, with dimensions of 1.7 m × 1 m.

The trellised vineyard height reaches 1.5 m from the ground. Since the bottom leaves start at 0.3 m over the ground, the grapevine canopy height is of 1.2 m. These values were introduced in the *3D shade calculator*.

Fig. 2 shows a perspective of the vertical trellised vineyard crop rows and the 30° tilted PV module rows, at 5-m center-height over the ground. Only skip factor (f_s) of 1 and 2 were studied. A hypothetical design with $f_s = 0$, i.e. PV module row over every crop line was disregarded, as it would cast too much shadow.

From a pure agronomical point of view, the landscape PV module geometrical layout would be preferable, as less crop shading is envisaged compared to portrait configuration. Nevertheless, the latter is preferable to maximize the installed power in the given crop line length of 44 m. Thus, while roughly 44 modules could be installed in portrait, only approximately 26 would fit with the landscape layout.
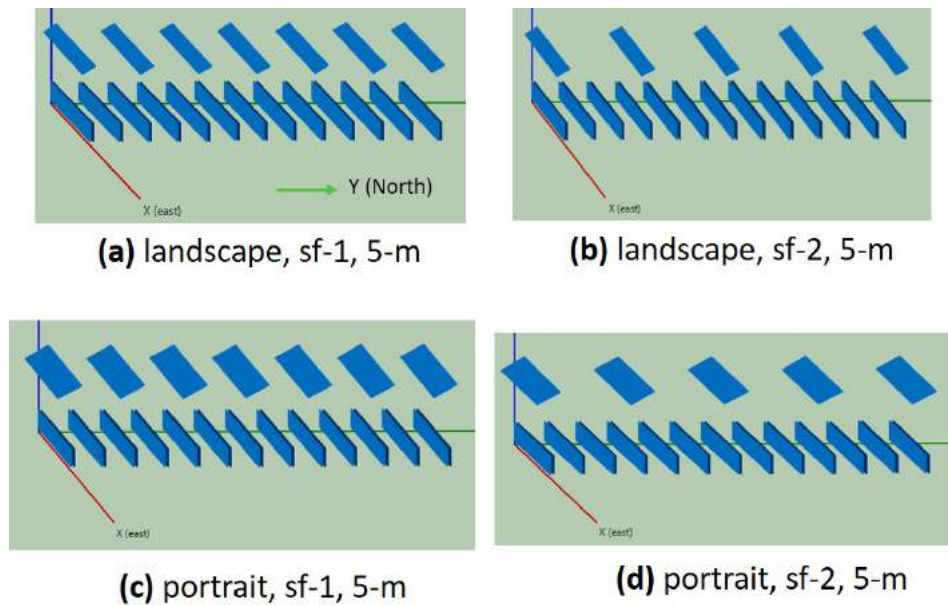
Figure 2. Factorial design combining PV module geometrical layout (landscape; portrait) and crop row skip factor of PV module rows ($f_s = 1$; $f_s = 2$), for a 5-m centerline height PV module rows.

Average annual electric consumption in experimental fields of ETSIAAB is 1100 MWh year^{-1}. It makes difficult to cover the whole consumption but a relevant part of it, reaching with this proposal 6 to 7%. Because of the fact that it is a high consumption, it has been decided to supply only a part with photovoltaic solar energy.

Rated power inverted (P_N) is 50 kW, therefore the photovoltaic system provide 6.18% of electricity to experimental fields.

The chosen inverter and photovoltaic panel characteristics are on the next tables.

Table 1. Inverter datasheet.

Inverter datasheet	
Input	
Max. PV power	75,000 Wp
Max. DC voltage, $V_{oc\ max}$	1,000 V
MPP voltage range, $V_{min\ inv} - V_{max\ inv}$	500 - 800 V
Min. DC voltage / start voltage	150 V / 188 V
Max. current / per MPP tracker	120 A / 20 A
Max. short-circuit current per MPP tracker / per string	30 A / 30 A
No. of MPP trackers / No. of PV strings per MPP tracker	6 / 2
Output	
AC nominal power (230 V, 50 Hz), P_N	50,000 W
Nominal AC voltage range	230 V/ 400 V

Table 2. Photovoltaic panel datasheet.

Photovoltaic panel datasheet	
Maximum power, P_{max}	340 W
Open-circuit voltage, V_{oc}	41.1 V
Voltage at point of maximum power, V_{mpp}	34.5 V
Short-circuit current, I_{sc}	10.53 A
Current at point of maximum power, I_{mpp}	9.86 A
Temperature coefficient-open-circuit current, α	0.03 %/K
Temperature coefficient-open-circuit voltage, β	-0.27 %/K
Operating temperature	-40ºC a 90ºC
Cell type	Monocrystalline
No. of cells	60
Module efficiency	19.8%

The agrivoltaic system design has been developed helped by PVSyst software. Taking into account inverter, panels and consumption data, as well as HSP (between 1600 – 1700 HSP annual), latitude and climatology in the location where photovoltaic panels would be placed, it would be necessaries 153 panels to supply 6.18% of electric demand. Thus, peak power of PV generator would be 52 kWp.

$$P_G = P_{max} \cdot no.panels \tag{1}$$

where P_G is peak power of PV generator, W, y P_{max} is maximum power of panel, W.

Inverter has six MPP trackers, where two strings could be connected in each one. It is established that a single string of 17 panels will be connected only in three of them, the rest of entries will have two strings of 17 panels each one.

To sizing of inverter, there are some parameters to verify that inverter is appropriate for photovoltaic generator characteristics:

1. Input MPP voltage range.
   - Minimum voltage of inverter ($V_{min\ inv}$) have to be lower than voltage at point of maximum power of PV generator at 70ºC ($V_{mpp\ G\ (70ºC)}$). Using eq. (2), $V_{mpp\ G\ (70ºC)}$ is 515.24 V against 500 V of $V_{min\ inv.}$

$$V_{mppG(70ºC)} = (V_{mppM} x N_s) + \beta_{mppG} x (T - 25) \tag{2}$$

where $V_{mpp\ M}$ is the voltage at point of maximum power of module, V, N_s is the no. of panels connected in series, $\beta_{mpp\ G}$ is the temperature coefficient at point of maximum power of PV generator, V/ºC and T is the temperature, ºC. The value of T is 70ºC.

   - Maximum voltage of inverter ($V_{max\ inv}$) ought to be bigger than voltage at point maximum power of PV generator at -10ºC ($V_{mpp\ G\ (-10ºC)}$). Using eq. (3), $V_{mpp\ G\ (-10ºC)}$ is 641.92 V against 800 V of $V_{max\ inv.}$

$$V_{mppG(-10ºC)} = (V_{mppM} x N_s) + \beta_{mppG} x (T - 25) \tag{3}$$

where the value of T in this equation is -10ºC.

2. Maximum open-circuit voltage ($V_{oc\ max}$) have to be more than open-circuit voltage of PV generator at -10ºC ($V_{oc\ G\ (-10ºC)}$). With eq. (4) $V_{oc\ G\ (-10ºC)}$ it results 764.73 V that is less than $V_{oc\ max}$ (1000 V).

$$V_{ocG(-10ºC)} = (V_{ocM} x N_s) + \beta_{ocG} x (T - 25) \tag{4}$$

where $V_{oc\ M}$ is the open-circuit voltage of module, V, $\beta_{oc\ G}$ is the temperature coefficient-open-circuit voltage of PV generator, V/ºC, and T is -10ºC.

3. Maximum inverter current ($I_{max\ inv}$) have to be bigger than short-circuit current of PV generator at 70ºC ($I_{sc\ G\ (70ºC)}$).

$$I_{scG(70^{\circ}C)} = (I_{scM} \, x \, N_p) + \alpha_{scG} \, x \, (T - 25) \qquad (5)$$

where $I_{sc\,M}$ is the short-circuit current of module, V, N_p is the no. of panels connected in parallel, $\alpha_{oc\,G}$ is the temperature coefficient-open-circuit current of PV generator, V/ºC, and T is 70ºC.

Using eq. (5), $I_{sc\,G\,(70^{\circ}C)}$ is 10.67 A in case of $N_p = 1$ (connected to three entries of inverter) and 21.34 A in case of $N_p = 2$ (connected to rest three entries of inverter). In both, $I_{sc\,G\,(70^{\circ}C)}$ is fewer than $I_{max\,inv}$ (30 A).

3. Results

Table 3 is a compilation of canopy mean shaded fraction (SF) for each combination of PV module layout (landscape, portrait) and PV module row interval (i_{rm}), for 5-m PV module height. Analogously, Table 4 compiles the results obtained for 7-m PV module height. i_{rm} can be 4 m if the number of crop rows skipped is of 1, or 6 m if the number of crop rows skipped is of 2.

Overall, the highest SF (47.9%) is for portrait layout combined with small i_{rm} and low PV-module row height. Fig. 3 and Fig. 4 show interval distribution of shade fraction for 5-m PV module height in the case of landscape-f_s2-24.9% (Table 1) and portrait-f_s1-47.9%, respectively.

Table 3. Trellised vineyard canopy mean shaded fractions (%), for 5-m high PV module rows. Skipping 1 crop row (fs =1) implies a PV module row interval (imr) of 4 m, while fs= 2 corresponds to imr = 6 m.

PV module configuration	Crop lines skip factor (f_s)	
	1	2
Landscape	34.2	24.9
Portrait	47.9	33.7

Table 4. Trellised vineyard canopy mean shaded fractions (%), for 7-m high PV module rows. Skipping 1 crop row (fs =1) implies a PV module row interval (imr) of 4 m, while fs= 2 corresponds to imr = 6 m.

PV module configuration	Crop lines skip factor (f_s)	
	1	2
Landscape	31.1	24
Portrait	42.1	30.7
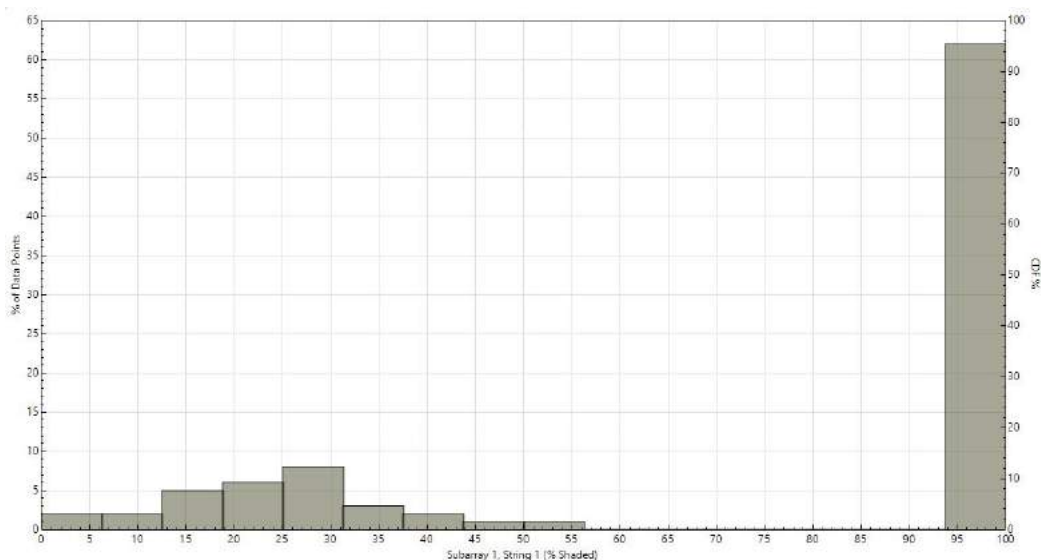
Figure 3. Shaded fraction (SF) for landscape configuration with skipping of two crop rows (fs =2) and 5-m high PV modules.
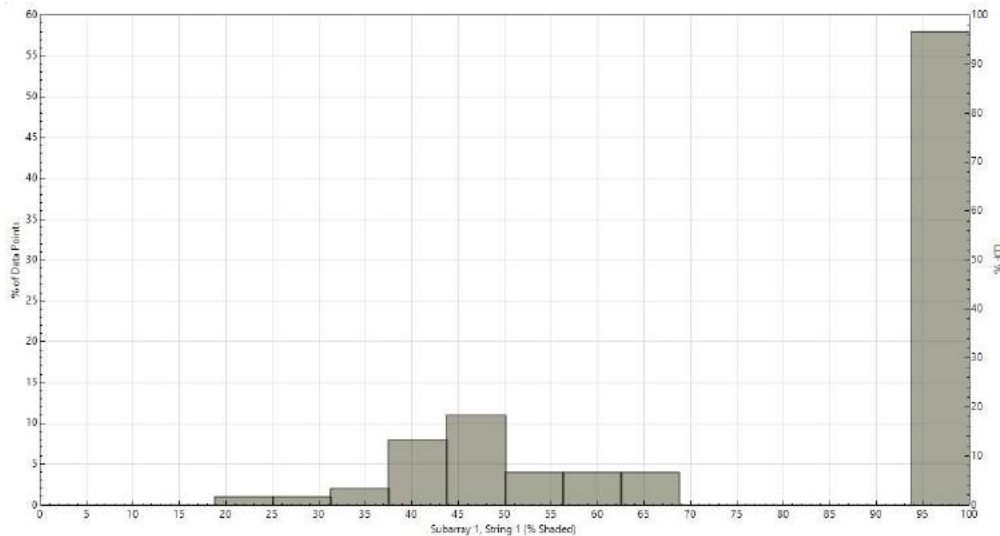
Figure 4. Shaded fraction (SF) for portrait configuration with skipping of one crop row (fs =1) and 5-m high PV modules.

Independent of high and configuration of photovoltaic panels, agrivoltaic system will be able to produce an approximate quantity of 83.90 MWh year[-1] of power, according to PVSyst software. It means around 1,600 kWh kWp[-1] per year. The rest of required electricity would be provided with electricity grid, about 1016.10 MWh year[-1]. The yield ratio (YR) of system is 85.43%.

Table 5 shows values of solar energy produced and grid energy required during months and per year.

Table 5. Incident global radiation (GlobInc), solar energy (E_Solar) and grid energy (EFrGrid) calculate by PVSyst software.

	GlobInc (kWh/m2)	E_Solar (MWh)	EFrGrid (MWh)
January	104.5	5.000	88.42
February	114.5	5.325	79.06
March	170.3	7.777	85.65
April	175.2	7.889	82.52
May	191.6	8.441	84.98
June	206.8	8.854	81.56
July	223.3	9.387	84.04
August	216.6	9.168	84.26
September	176.1	7.704	82.71
October	128.1	5.809	87.62
November	104.9	4.931	85.48
December	75.8	3.614	89.81
Year	1887.9	83.900	1016.10

The cost of the photovoltaic installation is 80,000 € approximately, because vineyards are in land before installation.

The annual saving obtained thanks to 83.90 MWh year[-1] production would be 16,780 €, since the price of energy is 0.20 € kWh[-1] after taxes.

4. Discussion

Matching 'crossings' of Table 3 and Table 4 show that SF is always lower for 7-m height compared to 5-m height (e.g. 31.1% vs. 34.2% for the combination of landscape and f_s = 1). This would play in favor of adoption of 7-m height. However, the 2 m height differential entails an important disbursement. Previous studies have determined that the supporting structure is a major cost component of AV systems.

Overall, a SF of 40% is considered as the higher limit of acceptable AV system design (e.g., the Massachusetts commonwealth SMART program). The rationale behind this is that although AV shed protects the crop from excessive radiation and the yield losses thereof (Oliveira et al. 2014), excessive shading can decrease grape berries desirable content of phytochemicals like anthocyanins (Koyama & Goto-Yamamoto, 2008).

5. Conclusions

Among the eight shading generation combinations analyzed, the one that carries the lesser shading fraction is landscape geometrical layout of PV modules spaced 6-m (skip of two grapevine rows), for 7-m PV module center-height.

Based on the slight difference with the corresponding value for 5-m height (24.9%), the latter would be recommended for cost-effectiveness. In this case, is not enough 13 southern grapevine rows (Fig. 1), so it would need necessary first northern crop row to install 153 panels.

The payback time would be between 5 and 6 years approximately.

References

Adeh, E.H., Selker, J.S. and Higgins, C.W., 2018. Remarkable agrivoltaic influence on soil moisture, micrometeorology and water-use efficiency. Plos One, 13 (11), pp. e0203256. https://doi.org/10.1371/journal.pone.0203256

Barron-Gafford, G., Pavao-Zuckerman, M., Minor, R.L., Sutter, L.F., Barnett-Moreno, I., Blackett, D.T., Thompson, M., Dimond, K., Gerlak, A.K., Nabhan, G.P. and Macknick, J.E., 2019. Agrivoltaics provide mutual benefits across the food–energy–water nexus in drylands. *Nature Sustainability,* 2 (9), pp. 848-855. https://doi.org/10.1038/s41893-019-0364-5

Dupraz, C., Marrou, H., Talbot, G., Dufour, L., Nogier, A. and Ferard, Y., 2011. Combining solar photovoltaic panels and food crops for optimising land use: Towards new agrivoltaic schemes. *Renewable Energy,* 36 (10), pp. 2725-2732. https://doi.org/10.1016/j.renene.2011.03.005

Koyama, K.; Goto-Yamamoto, N., 2008. Bunch shading during different developmental stages affects the phenolic biosynthesis in berry skins of 'Cabernet Sauvignon' grapes. *J. Amer. Soc. Hort. Sci.*, 133(6): 743-753. https://doi.org/10.21273/JASHS.133.6.743

Marrou, H., Dufour, L. and Wery, J., 2013. How does a shelter of solar panels influence water flows in a soil-crop system? *European Journal of Agronomy,* 50, pp. 38-51. https://doi.org/10.1016/j.eja.2013.05.004

Oliveira, M.; Teles, J.; Barbosa, P.; Olazábal, F.; Queiroz, J., 2014. Shading of the fruit zone to reduce grape yield and quality losses caused by sunburn. *J. Int. Sci. Vigne Vin*, 48: 179-187. https://doi.org/10.20870/oeno-one.2014.48.3.1579

Van Leeuwen, C. and Darriet, P., 2016. The Impact of Climate Change on Viticulture and Wine Quality. *Journal of Wine Economics,* 11, pp. 150-167. https://doi.org/10.1017/jwe.2015.21

Weselek, A.; Ehmann, A.; Zikeli, S.; Lewandowski, I.; Schindele, S.; Högy, P., 2019. Agrophotovoltaic systems: applications, challenges, and opportunities. A review. *Agron. Sustain. Dev.* 39:35. https://doi.org/10.1007/s13593-019-0581-3

NREL. System Advisor Model, SAM version 2020.11.29

Datasheet Inverter. Available at: https://www.bornay.com/es/productos/inversores-conexion-a-red-sma/sunny-tripower-core1-stp-50-40.pdf. Accessed on 03/06/2021.

Datasheet Photovoltaic panel. Available at: https://autosolar.es/paneles-de-conexion-a-red/panel-solar-340w-lg-neon-2-n1c. Accessed on 03/06/2021.

A Simplified Algorithm for the Optimal Setting of the Factors Affecting Agricultural Tractor Fuel Consumption During Heavy Drawbar Tasks

M. Cutini[a*], M. Brambilla[a], C. Bisaglia[a], D. Pochi[b], R. Fanigliulo[b]

[a]CREA Consiglio per la ricerca in agricoltura e l'analisi dell'economia agraria (Research Centre for Engineering and Agro-Food Processing), Via Milano, 43 -24047 Treviglio (BG), Italy

[b]CREA Consiglio per la ricerca in agricoltura e l'analisi dell'economia agraria (Research Centre for Engineering and Agro-Food Processing), Via della Pascolare, 16 – 00015 Monterotondo (Rome), Italy

*Corresponding author. Email: maurizio.cutini@crea.gov.it

Abstract

Optimising energy input in an agricultural farm, like fuel consumption, is an actual topic for research in agricultural mechanisation in order to achieve economic and environmental goals. With this purpose, CREA of Treviglio, Italy, developed a simplified algorithm focused on the finest combination set of tractor and implement. The algorithm aims to optimise the tractor's fuel consumption, taking into account the factors that mostly influence this aspect (i.e., the engine speed and power, the driveline management, the wheel slip, the mass of the tractor, and tire tractive properties).

The data of 100 tractors of different engine power (range 80-200 kW) and weight (range 3000-8000 kg) were processed to obtain a regression equation as the starting point to analyse driveline efficiency, power loss due to rolling resistance, and wheel slippage.

The ASABE equation for calculating drawbar pull force was adopted to fit the results to soil conditions. Testing agricultural tires of different sizes at different pressure settings in field conditions allowed the establishment of differences in the drawbar force required for ploughing thanks to the ASABE equation. The resulting algorithms underwent linear regression analysis to achieve a simplified algorithm for assessing the optimal wheel-slip, mass, engine power, and tires pull force properties during drawbar works that result in optimal fuel consumption with minimum tractor efficiency impairment.

The Monte Carlo Simulation method introduced randomness in the input (according to a specific probability density function) to run a sufficiently large number of trials to point out the most probable algorithm output. The result is a simplified algorithm that has been used for investigating the effect of main parameters on fuel consumption, but that can be adapted for evaluating the effect of different implements, tires, engine setting or also fleet management on fuel consumption.

Keywords: Fuel consumption, traction, agricultural tire, dynamometric vehicle.

1. Introduction

Optimizing the energy inputs of agricultural activities is increasingly important, even more so for non-renewable energy sources and emission mitigation. Concerning tractors, from the energetic perspective, heavy drawbar work (e.g., ploughing) is one the most key tasks because of the engine power requirement and the number of factors affecting the tractive efficiency of the machine. Standard methods of measurement (i.e., OECD Code 2, 2018) make it possible to obtain comparable data and develop algorithms on tractor dynamics and efficiency; however, such standards recommend running the machine on either asphalt or concrete test tracks that do not represent the ordinariness of the agricultural working conditions.

Many studies on tractor efficiency focused on the power efficiency at varying the engine, the driveline and the tires (Molari and Sedoni, 2008; Harris and Rethmel, 2011; Smerda and Cupera, 2010; Monteiro et al., 2013). However, traction performance optimisation, not only in terms of material engineering but, above all, concerning labour and energy efficiency, remains of primary importance (Gil-Sierra et al., 2007; Turker et al., 2012; Grisso and Kocher, 2004; Zoz and Grisso, 2003; Lacour et al., 2014; Tiwari et al., 2010, Pochi et al., 2013), in particular in light of the investigations that deepened the effect that soil properties have on traction efficiency and performance (Lyasko, 2010; Filho et al., 2010).

Cutini et al. (2018) investigated the fuel consumption of 100 tractors of different weight and engine power while performing tasks on cultivated soils and achieved a regression equation that served as the starting point to analyse driveline efficiency, the power lost as rolling resistance and the power lost due to slippage. The extension of such an equation to soil conditions foresaw applying a horizontal force to the agricultural tractor drawbar while running it on a test track or a field (Cutini and Bisaglia, 2016; PAMI, 1996). The measurement of the primary tractor performance outputs (i.e., drawbar force, forward speed, wheel slip and fuel consumption) highlighted how much the drawbar force relates to the wheel slippage (Cutini et al. 2020).

The Monte Carlo Simulation (MCS) method is a numerical-based probabilistic uncertainty modelling technique that uses randomness to solve deterministic problems (Metropolis, 1987). MCS provides probabilistic uncertainty analysis of highly complex engineering systems with uncertain variables (Buc et al., 2013; Osaki et al., 2017; Colantoni et al., 2021). The method relies on performing a sufficiently large number of trials differing the input variables according to a specific probability density function (PDF). Counting the outcome of each trial provides the answer to the original question describing the expected model output and its probability of occurrence (Briggs et al., 2001; Qin et al., 2016). In the present work the MCS has been used to analyse the effect of the tractor's engine in terms of engine load and speed (Grisso, 2001), of the tractor's mass, wheel slip, and the traction properties of the tires on the fuel consumption, also evaluating the impact of each of these variables. The algorithm defines the correct use or ideal setting of the selected parameters and can also be used without detailed information on the tractor and implement.

2. Materials and Methods

The equations and parameters used are reported.

2.1. The equations

The power at the drawbar (Equation 1) results from the assessment of the driveline efficiency (Cutini et al., 2018):

$$P_{db} = \alpha \cdot P_{PTO} - P_{vd} - P_s \qquad (1)$$

Where:

- P_{db} is the power at the drawbar;
- P_{PTO} is the maximum power at the engine measured at the power take off (PTO);
- P_{vd} is the power used for the vehicle's displacement;
- P_s is the power lost due to slip;
- α is the efficiency of the driveline (dimensionless).

Equation 2 shows the coefficients of the equation from the linear regression analysis in the study of Cutini et al. (2020):

$$P_{db} = 0.92 \cdot P_{PTO} - 0.07 \cdot M \cdot \vec{v} - 0.009 \cdot P_{PTO} \cdot s \qquad (2)$$

Here:

- P_{db} is the power at the drawbar
- P_{PTO} is the power measured at the power take off;
- M is the dynamic wheel load, in force units, normal to the soil surface;
- $\vec{v}$ is the forward speed;
- s is the wheel slip.

0.92 and 0.07 are, respectively, the driveline efficiency coefficient (α of Eq. 1) and the motion resistance ratio coefficient on terrain soil that affects the P_{vd}: they both are in line with the recommendations of the ASAE standard (ASAE, 2011).

The target of this study is the tractor specific fuel consumption per hectare of tilled soil (SFC$_{ha}$, kg ha^{-1}). It results from Equation 3:

$$SFC_{ha} = h_{ha} \cdot SFC_{kW} \cdot P_{kW} \cdot 10^{-3} \qquad (3)$$

where:

- h_{ha} are the worked hours one hectare requires;
- SFC_{kW} is the specific fuel consumption of the engine;
- P_{kW} is the power the vehicle's engine provides.

The h_{ha} calculation (eq. 4) occurs in the hypothesis that there are not turns of the tractor, and the operator runs it at a constant speed:

$$h_{ha} = W^{-1} \cdot \vec{v}^{-1} \cdot 10^4 \qquad (4)$$

where:

- W is the implement working width.

The development of equation 2 allows obtaining the power required at the engine (P_{kw}, eq. 5):

$$P_{kw} = (P_{db} + P_{vd}) \cdot (0.92 - 0.009 \cdot s)^{-1} \qquad (5)$$

where:

- P_{db} is the power at the drawbar that the implement requires, and it results from the required net drawbar pull force (F, from the ASAE 2003 standard, where is indicated as P) and the forward speed.

Defined F and assigned s, ASAE standard (ASAE, 2003) allows obtaining M (dynamic wheel load).

Therefore, it is possible to calculate the dynamic traction ratio (T_r; ASAE 2003), which is the ratio of drawbar pull (F) to the dynamic load on the vehicle (Eq. 6).

$$T_r = F \cdot M^{-1} \tag{6}$$

However, the dynamic traction ratio alone does not account for the tractive properties of the tires. Therefore, a new index (specific dynamic traction ratio - T_r' - Eq. 7) that includes the features of the tires, results from its multiplication with the grip coefficient (*Grip*, dimensionless), which ranges from 0.86 to 1.14 (paragraph 2.2).

$$T_r' = F \cdot M^{-1} \cdot Grip \tag{7}$$

Of course, such change affects the calculation of the M coefficient and, consequently, the parameters of eq. 5 that changes as follows (Eq. 8):

$$P_{kw} = (F \cdot \vec{v} + 0.07 \cdot F \cdot T_r^{-1} \cdot Grip \cdot \vec{v}) \cdot (\alpha - 0.009 \cdot s)^{-1} \tag{8}$$

Finally, substituting the value of P_{kw} in eq. 3, the algorithm that underwent the Montecarlo analysis is:

$$SFC_{ha} = h_{ha} \cdot SFC_{kW} \cdot (F \cdot \vec{v} + 0.07 \cdot F \cdot T_r^{-1} \cdot Grip \cdot \vec{v}) \cdot (\alpha - 0.009 \cdot s)^{-1} \cdot 10^{-3} \tag{9}$$

it requires the following inputs that, in the present work, have fixed and variable values:

- F: from the ASAE standard (fixed as it refers to a given plough);
- T_r: from ASAE standard (Bn=55);
- $\vec{v}$: forward speed(fixed, 7 km h^{-1});
- s: is the wheel slip (variable);
- SFC_{kW} (variable);
- α: fixed (0.92);
- motion resistance ratio coefficient (0.07);
- Grip (variable)

In this study the analysed agricultural task is an heavy work as ploughing, based on drawbar pull only and not on contemporary PTO use. The required implement draft and drawbar power were calculated following ASAE S296.5, 2003. In detail, it was taken into account a mouldboard plough, 1.8 m width, 0.3 m tillage depth and 7 km h^{-1} set speed (without considering slip). In this case, after having calculated the drawbar pull force required from the plough and set the desired forward speed, a level of slip to define the tractor's mass and the real forward speed was set. This allows to calculate the P_{db}. Equation 5 allows calculating the P_{kW}. At this point the tractor is defined as mass and power required at the engine.

2.2. The random independent variables

All the variables that varied randomly resulted from specific experimental activities to assess the extent and the modality of such variation.

2.2.1 Tire grip

The hypothesis is that adopting or setting a tractor with high tractive tires could optimise fuel consumption. With this aim, 18 sets of tires with different sizes and inflation pressures were tested in field conditions (Fig. 1) to define the dynamic traction ratio (T_r). Soil features were: mean resistance to penetration of 1-1.3 MPa, 14% moisture, 68% sand, 24% loam and 8% clay (the skeleton was 30%).

Figure 1. Layout of a drawbar power test on the field by boosted dynamometer application.

The experience foresaw running the tractor with specific wheel slip values between 15 and 35%. For this work the attention is focused on the traction variations occurring at the lowest slip values (i.e. 15%).

The average T_r resulted in 0.46 that fully complied with the output of the ASAE standard for the same conditions. However, the associated standard deviation was 0.07, meaning a coefficient of variation of 14%. Such variation is therefore ascribable to the *Grip* coefficient of the wheels that subsequently ranged from 0.86 to 1.14.

2.2.2 The specific fuel consumption of the engine (SFC_{kW})

The definition of the range of variation of the SFC_{kW} resulted from the consideration of the use of the tractor engine in terms of load (throttle) and speed (min^{-1}). An example is reported considering the power at the engine required for ploughing at given conditions is 57 kW. If we consider using an 87 kW tractor, based on the curves displayed in figure 2, the required power is available from 1200 to 2200 min^{-1}, managing the engine working conditions by means of the gearbox, while for a 71 kW power tractor, the speed interval reduces at 1400 to 2200 min^{-1}. Therefore, the resulting specific fuel consumption (at full engine throttle) ranges from 242 to 293 g kWh^{-1}. If the farm machinery fleet consists of a tractor of maximum power at the engine of 57 kW, it could provide the necessary power at 2200 min^{-1} only. If the available tractor has maximum power at the engine of 150 kW, performing the task with partial fuel load would be feasible as well (Figure 2). In both cases, the engine would run far from the 242 g kWh^{-1}.
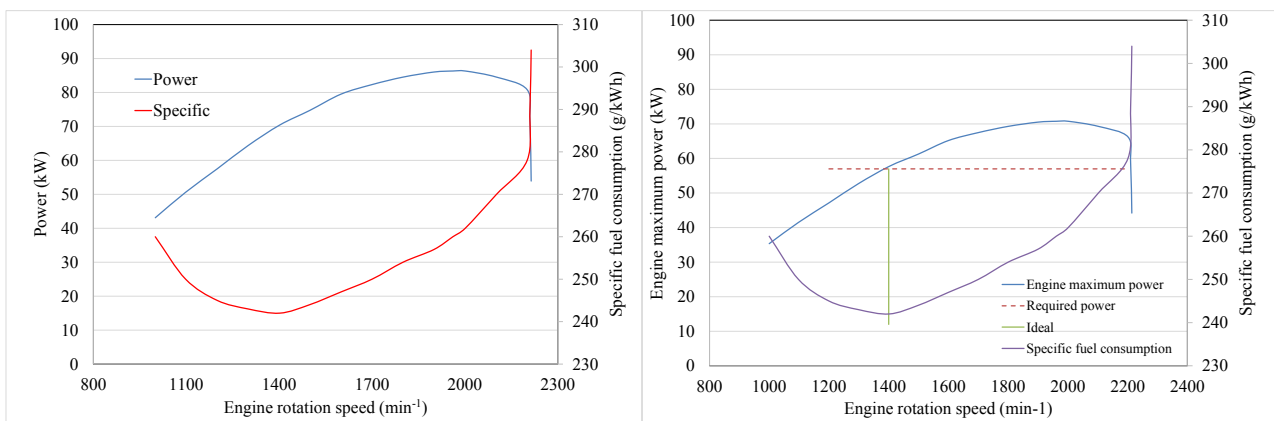
Figure 2. Examples of the shapes of maximum P_{kW} and the relative SFC_{kW} of an 87 kW agricultural tractor (on the left) and an 71 kW tractor (on the right). For this last, a representation of the required power and the ideal working point as efficiency is given.

Conceptually, it is fundamental to adopt a tractor with the required power available at 1400-1700 min^{-1} (fig. 2). Moreover, with the correct tractor's power choice, using the tractor's engine is decisive on fuel consumption (Grisso, 2001). For this reason, we simulated the correct choice of the tractor engine power and the correct use of the driveline operating on the value of the specific fuel consumption ranging from 245 (minimum) to 293 (maximum power at 2210 min^{-1}) g kWh^{-1}.

As a reference, it is possible to consider a specific fuel consumption of 262 g kWh^{-1} at maximum engine power at 2000 min^{-1}.

2.2.3 The wheel slip (s)

The wheel slip has been always retained a source of power lost only necessary to develop drawbar force. In order to understand the importance of this factor on efficiency, the considered slip variation interval was 3 to 30%.

The independent variables resulted:
- slip: 3-30%
- tire grip: ±14%
- specific fuel consumption: 245-293 g kWh^{-1}

2.3. Monte Carlo analysis

The stochastic model construction was based on the defined specific input parameters from experimental activities, i.e., tire grip (Grip), wheel slip (s), and tractor specific fuel consumption (SFC_{kW}), to predict the tractor specific consumption per unit of surface (SFC_{ha}, kg ha^{-1}) during ploughing according to eq 9.

The creation of a representative model output foresaw running the model with the input variables Grip (% of traction ratio), s (%) and SFC_{kW} (g kWh^{-1}) varying within a range of values following the PERT distribution (Clark, 1962): a continuous probability distributions defined by the minimum (a), most likely (b) and maximum (c) values that such

variables can take (Table 1) and that define the parameters of the distribution (α, β):

$$\alpha = \frac{4b+c-5a}{c-a} \qquad \beta = \frac{5c-a-4b}{c-a} \qquad\qquad (10)$$

Table 1: The independent variables distribution

Value	Grip (% net traction)	Slip (%)	SFC_{kW} (g_{fuel} kWh^{-1})
Minimum (a)	0.86	5	245
Most likely (b)	1.00	15	269
Maximum (c)	1.14	29	293

For each input variable 1000 values fed the model equation to obtain and analogous number of SFC_{ha} (kg ha^{-1}) that underwent data processing.

To assess the effect that individual components of the variables have on the outcome of the model the scatterplots representing the relation between model output and each considered variable were considered and, with these, the Pearson correlation coefficients (r) between any input value and the model output.

Following this, further investigation foresaw the adoption of stepwise linear regression analysis (LRA) with backward elimination carried out on sstandardised data. The approach of this more formal analysis is based on the linear regression model Eq. (11)

$$y_i = b_0 + \sum_{j=1} b_j x_{ij} + \varepsilon_i \qquad\qquad (11)$$

where b_j are the regression coefficients and ε_i is the error (residual of the approximation).

The computing of the coefficients allows to use them as way to indicate the importance of each variable with respect to the uncertainty of the output y. In accordance with Campolongo *et al.* (2000), the standardised regression coefficients (SRC), calculated according to Eq. (12) were used:

$$SRC = \frac{b_j \sqrt{\frac{\sum (x_{ij}-\bar{x}_j)^2}{N-1}}}{\sqrt{\frac{\sum (y_i-\bar{y})^2}{N-1}}} = b_j \frac{\sigma_x}{\sigma_y} \qquad\qquad (12)$$

These coefficients have the advantage of quantifying the effect of varying each input variable away from its mean by a fixed fraction of its variance while all the other variables remain at their expected value.

Statistical processing was performed using the MINITAB 17.0 ™ software (Minitab, 2010). Model output underwent graphical summarisation with histogram of data with an overlaid normal curve, boxplot, 95% confidence intervals for both average and median values. Linear Regression Analysis (LRA) allowed to obtain the regression coefficients
($p < 0.05$) whose standardisation to obtain the various SRCs was carried out with Excel spreadsheet.

3. Results and Discussion

The analysis carried out showed that in the frame of the reported range of the variables the lowest fuel consumption that can be obtained is 12.05 kg ha^{-1}. The highest would result in 17.02 kg ha^{-1} considering high values of slip (30%), but it's possible to obtain also 17.30 kg ha^{-1} with very low values of slip (3%).

The value of slip that allow to obtain 12 kg ha^{-1} are 9-10%; this is related to the tractor weight. Following the ASAE standard, it results 2.4 times the drawbar force of the plough. Increasing the weight of the tractor decreases the power lost as slip but increases the power lost in rolling resistance. The efficiency remains relatively stable at values of slip of 7-9% but starts decreasing exponentially under the 5%.

Practically, a correct management of the slip, that depends on the correct mass of the tractor, could have an influence of almost 20% on fuel consumption.

Regarding the specific fuel consumption the best efficiency is obtained from the lowest value found at the PTO test bench, in this case assumed as 245 g kWh^{-1}. This means adopting a tractor whose power, both required from the implement and losses, is close to the maximum power of the engine at about 1.400-1.600 min^{-1}.

In this case, the power required from the plough resulted 43 kW and the power required at the engine resulted 57.5 kW. In practice, this is an ideal condition, because it could not be possible to avoid an uneven behaviour of the engine or to avoid to overload or lug the tractor's engine (Grisso, 2001). Therefore it's necessary to adopt a tractor with a reserve of power or torque, but, above all, with a management system of the power. In fact with tractor with manual

gearbox it could be very difficult to keep the engine at reduced speed. With power-shift gearbox it is already possible to obtain the desired point on the engine power but the ideal technical solution would result a system that could adapt continuously the engine load and speed. This is actually obtained in two ways or their combination. The first is adopting a continuously variable transmission: the operator sets the forward speed and the tractor seek tries to maintain it. The second is the possibility of managing the engine curve deciding the unloaded engine rotation and then having a system able to maintain the desired engine speed changing the fuel admission system. A combination of the two systems is available also in automatic mode.

Consequently, in this case, the 87 kW power tractor, would result a correct choice: it presents 75 kW at 1.500 min^{-1} that would allow working with a specific fuel consumption between 245 and 262 g kWh[-1] and a tractor mass of 5810 kg.

It's important to notice that a not correct setting of the analysed conditions has an influence also on the tractor size.

The LRA provided a more formal investigation of the mapping of variable's importance to lower the model uncertainty. How well the considered variables are related to the output they give rise is represented by the correlation coefficient they have with fuel consumption for the performed task (Table 2). The resulting equation, whose R^2 is 0.89, is (Eq. 13):

$$SFC_{ha} = 0.538 - 1.739 \cdot Grip + 0.052 \cdot SFC_{kW} + 0.085 \cdot s \tag{13}$$

However, the coefficients describing the role of the variables need to be taken with extreme attention as they are not standardized. Therefore they suffer from the effects resulting from their distribution assumption. Therefore a better interpretation of their role cannot help using the SRCs hereafter reported in Table 2

Table 2: Pearson correlation coefficients of model inputs with model output and the standardized regression coefficients resulting from the LRA.

Input Variable	Corr. Coeff (r)	SRC
Grip (% net traction)	-0.15	-0.14
Slip (%)	0.73	0.74
SFC_{kW} (g$_{fuel}$ kWh^{-1})	0.57	0.60

Based on the simulation, the slippage value that identifies the higher efficiency is 9%: the effect of the rolling resistance of the wheels on the soil affects this proportion so that lower slip values would result in higher power required for vehicle displacement.

This consideration appears valid both for heavy works (such as ploughing) and light ones. The mass of the tractor (in kg) to be adopted shall be 2.4 times the drawbar force (in N) required because the higher the tractor mass, the higher the rolling resistance. However, any decrease in the tractor mass would result in higher losses due to wheel slippage: it is essential to point out that decreasing the slippage under the optimal value of 9% has a low impact on fuel consumption.

The meaning of these results could also be summarised with the following considerations: the studied variables are in strict connection with the proper choice of the tractor-implement combination that the farmer operates at the very beginning. Figure 3 reports the criteria for the choice of tractor mass and engine power; then, the operator will have to set only the correct forward speed. In the case of adopting a tractor of mass and engine power slightly higher than the ideal calculated, the difference in efficiency is negligible and could be easier for the operator managing the engine load and rpm (min^{-1}). If the required engine power allows managing the task, it could be correct to adopt a higher working width.
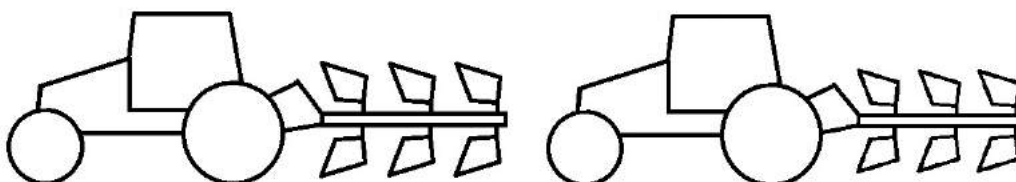
Figure 3. The correct tractor mass and engine power are the most important parameters for drawbar works (left). A slightly oversized tractor allows to maintain an high level of the efficiency of the operation (right).

In two main cases the efficiency could decrease dramatically. The first is adopting a smaller tractor than the ideal (fig. 4, left), the consequences regard all the analysed parameters. Small mass means high slip; the engine has to work

close to the maximum engine power with low efficiency of the specific fuel consumption; the small tire diameter will not allow an high traction efficiency. Also in case of a tractor of much higher mass and power than required (fig. 4, right), the efficiency will be low, above all for the high level of power lost in rolling resistance but also for the impossibility of working with the correct engine speed and load.
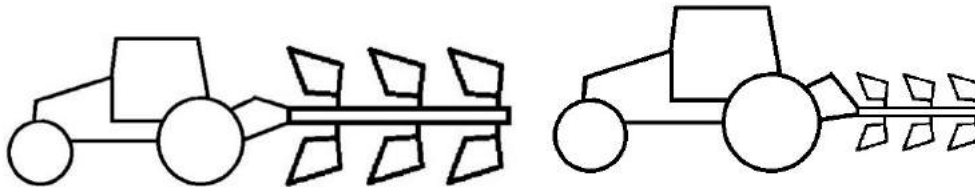
Figure 4. Incorrect coupling of the implement and of the tractor size result in both cases affecting the impossibility of managing the described parameters in an efficient way

4. Conclusions

This study presents the development of a simplified model to assess the influence of key parameters on the fuel consumption of agricultural tractors during agricultural drawbar works. The study underline and quantify the importance on the use of tractor's engine and of the relationship of the tractor's mass with the wheel slip. Less influence on fuel efficiency resulted from the tractive properties of the tires. Also considering a correct use of the tractor, differences (±15% range) could be obtained paying attention to few parameters of tractor setting and use. The study confirms the importance of keeping the slip under the value of 10%. This means that the traction tests of the agricultural tires have to be carried out also at low values of slip (7-10%). Moreover, great attention is required while measuring fuel consumption during implements test or tire test. The settings with which the engine is used - as speed and load – are fundamental to obtain comparable results. Tractors without the possibility to control the engine in economy mode could be very difficult to compare in fuel consumption during agricultural tasks.

Acknowledgements

References

ASAE D497.7, Mar 2011. Agricultural Machinery Management Data.

ASAE S296.5 Dec 2003. General Terminology for Traction of Agricultural Traction and Transport Devices and Vehicles.

Briggs A., R. Goeree, G. Blackhouse, B. O'Brien, 2001. Probabilistic Analysis of Cost-effectiveness Models: Choosing Between Treatment Strategies for Gastro-Esophogeal Reflux Disease, McMaster University Centre for Health Economics and Policy Analysis Research Working Paper 01-01, February, 2001

Buc, D., G. Màsàrova, 2013. Application of Monte Carlo simulation in the field of mechanical engineering. AD ALTA: Journal of Interdisciplinary Research, 3(2): 31-34

Campolongo F., A. Saltelli, T. Sørensen, S. Tarantola, 2000. Hitchhiker's guide to Sensitivity Analysis. In Sensitivity Analysis. Eds. A. Saltelli, K. Chan, E.M. Scott. John Wiley & Sons Ltd. (UK). 16-45.

Clark, C.E., 1962. The PERT Model for the Distribution of an Activity Time. Operations Research, 10, 405-406. https://doi.org/10.1287/opre.10.3.405

Colantoni, A., M. Villarini, D. Monarca, M. Carlini, E.M. Mosconi, E. Bocci, S. Rajabi Hamedani 2021. Economic analysis and risk assessment of biomass gasification CHP systems of different sizes through Monte Carlo simulation. Energy Reports, 7: 1954–1961. https://doi.org/10.1016/j.egyr.2021.03.028

Cutini, M., C. Bisaglia, 2016. Development of a dynamometric vehicle to assess the drawbar performances of high-powered agricultural tractors. J. of Terramechanics 65 (2016) 73-84, http://dx.doi.org/10.1016/j.jterra.2016.03.005

Cutini, M., M. Brambilla, C. Bisaglia, 2018. Tractor Drive Line Efficiency Evaluation taking into account Power Lost in Slippage, Proceedings of the "New Engineering Concepts for Valued Agriculture", 8-12 July 2018, Wageningen, The Nederlands. pp 533-538.

Cutini, M., M. Brambilla, C. Bisaglia, D. Pochi, R. Fanigliulo, 2020. Efficiency of Tractor Drawbar Power Taking into account Soil-Tire Slippage. Lecture Notes in Civil Engineering. Vol. 67, 409-417. https://doi.org/10.1007/978-3-030-39299-4

Filho, A.G., K.P. Lancas, F. Leite, J.J.B. Acosta, P.R. Jesuino, 2010. Performance of agricultural tractor on three different soil surfaces and four forward speeds. Revista Brasileira de Engenharia Agricola e Ambiental, 2010, 14 (3), pp. 333-339.

Gil-Sierra, J., J. Ortiz-Canavate, V. Gil-Quiros, J. Casanova-Kindelan, 2007. Energy efficiency in agricultural tractors: A methodology for their classification. Applied Engineering in Agriculture, 2007, 23 (2), pp. 145-150.

Grisso R.D., 2001. Gear up and throttle down, Virginia Cooperative Extension, Virginia Tech, 442-450 (BSE-326P)

Grisso, R.D., M.F. Kocher, D.H. Vaughan, (2004). Predicting tractor fuel consumption. Applied Engineering in Agriculture, 2004, 20 (5), pp. 553-561.

Harris, B.J., B.R. Rethmel, 2011. Comparison of IF and standard marked metric radial ply tires; American Society of Agricultural and Biological Engineers Annual International Meeting 2011, ASABE 2011, 7, pp. 5461-5472

Lacour, S., C. Burgun, C. Perilhon, G. Descombes, V. Doyen, 2014. A model to assess tractor operational efficiency from bench test data. Journal of Terramechanics, 2014, 54, pp. 1-18.

Lyasko, M.I., 2010. How to calculate the effect of soil conditions on tractive performance. Journal of Terramechanics, 2010, 47 (6), pp. 423-445.

Metropolis, N., 1987. The beginning of Monte Carlo methods, Los Alamos Science, 15: 125–130.

Minitab, 2010. Minitab 17 statistical software. State college, PA: Minitab.

Molari, G., E. Sedoni, 2008. Experimental evaluation of power losses in a power-shift agricultural tractor transmission. Biosystem Engineering, 2008, 100 (2), pp. 177-183.

Monteiro, L.A., D. Albiero, F.H. De Souza, R.P. Melo, I.M. Cordeiro, 2013. Tractor efficiency at different weight and power ratios. Revista Ciencie Agronomica, 2013, 44 (1), pp.70-75.

OECD Code 2, Feb. 2018 OECD Standard Codes for the official testing of agricultural and forestry tractors performance.

Osaki, M., L.R. Aparecido Alves, F.F. Lima, R. Garcia Ribeiro, G. Sant'Ana de Camargo Barros, 2017. Risks associated with a double-cropping production system – a case study in southern Brazil. Scientia Agricola, 76(2): 130-138. https://doi.org/10.1590/1678-992x-2017-0191

Pochi, D., Fanigliulo R., Pagano M., Grilli R., Fedrizzi M., Fornaciari L., 2013. Dynamic-energetic balance of agricultural tractors: active systems for the measurement of the power requirements in static tests and under field conditions, Journal of Agricultural Engineering, 44, e84: 415-420.

Prairie Agricultural Machinery Institute (PAMI), Research Update, Standardised Tractor Performance Testing. What it is – and isn't; July, 1996.

Qin F., Y. Zhao, X. Shi, S. Xu, D. Yu, 2016. Sensitivity and uncertainty analysis for the DeNitrification–DeComposition model, a case study of modeling soil organic carbon dynamics at a long-term observation site with a rice–bean rotation. Computers and Electronics in Agriculture. 124, 263-272. http://dx.doi.org/10.1016/j.compag.2016.04.017

Smerda, T., J. Cupera, 2010. Tire inflation and its influence on drawbar characteristics and performance – Energetic indicators of a tractor set. Journal of Terramechanics, 2010, 47 (6),pp. 395-400.

Tiwari, V.K., K.P. Pandey, P.K. Pranav, 2010. A review on traction prediction equations. Journal of Terramechanics, 2010, 47 (3), pp.191-199.

Turker, U., I. Ergul, M.C. Eroglu, 2012. Energy efficiency classification of agricultural tractors in Turkey based on OECD tests. Energy Education Science and Tecnology Part A: Energy Science and Research, 2012, 28 (2), pp. 917-924.

Zoz, F.M., D.R. Grisso, 2003. Tractor and Traction Performance. ASAE Publication Number 913C0403. 2003.

Integrated and sustainable Farming systems

On-Farm Dry Matter Monitoring System - Silage Sampler, Dry Matter Measurement and Mobile App for Feeding Adjustment

Tuija Kallio [a,*], Matti Härkönen [a†], Jari Komulainen [a], Minna Tanner [b], Veijo Sutinen [a], Pekka Kilpeläinen [a] and Vesa Virtanen [a]

[a] University of Oulu, Kajaani University Consortium, Unit of Measurement Technology, Kajaani, Finland

[b] ProAgria Rural Advisory Services of Eastern Finland, Kajaani, Finland

[†] Current affiliation: Bittium Wireless Ltd, Kajaani, Finland

* Corresponding author. Email: tuija.kallio@oulu.fi

Abstract

Proper feeding is important for cattle wellbeing and productivity of dairy farms. Maximizing milk yield requires regular monitoring of silage quality. The amount of concentrated feed fed depends on the dry matter content of silage. Economic impact can be significant if too dilute or concentrated total mixed ration (TMR) is fed resulting in milk yield reduction or extra bought-in feed costs. Still, in general, the process of adjusting TMR recipes requires several steps and operators and cannot be done on a daily or a lot-by-lot basis.

Smartfeed EIP-AGRI project developed silage quality monitoring enhancing time management by combining work tasks and providing tools to measure dry matter and edit feeding on site. The developed system was piloted at farms and user feedback was collected.

In the project, a new silage sampler attached to a bale gripper was designed. The sampler consists of a sampling tube and a support spike attached to a pivotable framework allowing the probe to be folded down for other work tasks. A sampling bag can be fastened to the end of the sampling tube to collect the samples.

A moisture analyser was tested for on-farm dry matter (DM) measurement of silage (n=84) and TMR (n=36) samples. Suitable methods were selected and compared to oven drying. The methods showed good correlation to the reference method. The method for silage samples gave systematically slightly lower values compared to oven drying (average deviation -4.8 %). The difference can be corrected by a coefficient (1.05x) that is valid at least for timothy-fescue grass, clover grass and whole crop silage.

An Android application was designed to adjust TMR recipes. The application calculates the changes in the amounts of different components of a TMR recipe in situations where the DM% of silage changes or the amount of component is changed. Thus, farmers are able to react to changes in dry matter as quickly as possible.

Keywords: silage, total mixed ration, dry matter, sampling, mobile application

1. Introduction

Silage is the most important source of energy and dry matter (DM) in total mixed ration, in which DM source (silage), minerals and concentrated feed are mixed in exactly optimised amounts to maximise milk production (Schingoethe, 2017; Sova et al., 2014). The total mixed ration (TMR) feed is mixed to relative homogeneity to facilitate consistent supply of nutrients to rumen microbes to optimize rumen function, and to prevent cattle from selecting themselves which components they eat. However, the dry matter content of silage may vary considerably in a silage stack or even between individual bales of a same field. In addition, heavy rain falls may soak the stack face and greatly affect the DM%. In Finland, ProAgria Rural Advisory Services have calculated that an increase or a decrease by five percentage points in silage DM% can lead to a loss of 400-500 € in profit per month in a 100-cow cattle if the change in DM has not been considered in feeding planning. The costs result from use of unnecessary bought-in feeds or from loss in milk yield.

Despite the importance of knowing the exact DM% of silage, even today it is typically determined only in few samples per stack or in few bales representing a large lot of bales (Geary, 2020). Silage sampling can be done completely manually, although there are also core samplers that are attached to handheld electric drills available at the market by various manufacturers (e.g. Gibson Engineering, Semes, Wile, Star Quality Samplers). But still, taking samples with the core sampler is a work task of its own. The DM% analysis is often done by an external laboratory, and results may arrive within 1-2 weeks. Farmers can determine DM% also themselves, but methods or devices such as microwave drying, Koster Moisture Tester and Food Dehydrator either require much time or effort or results are not fully comparable to standard laboratory methods (Donnelly et al., 2018; Pino and Heinrichs, 2014). The Koster Moisture Tester is accurate enough when sampling is representative, and able to dry silage sample at best in 30-40 minutes. Microwave drying is even quicker but requires careful sample preparation and is labour-intensive. There are

also the first handheld near-infrared spectroscopy (NIRS) instruments at the market that are able to monitor DM of silage or TMR feed (e.g. devices of Dinamica Generale; Moisture Tracker; NIR4 Farm) and intensive research is done to develop technology further (Artavia et al., 2021; Mostafa et al., 2021). Currently, some silage harvesters contain NIR analysers measuring the quality of silage (e.g. Claas harvester, EVO NIR device), and the NIR technology can be utilized also with automatic feeding systems. The NIR methods require careful calibration, and it is apparent that for the accurate results a separate calibration is required for silage types made of different raw materials or harvested at different weather conditions.

In general, the optimized TMR recipes are calculated by a feeding adviser or a representative of a concentrated feed company and the recipes are recalculated when a component changes for example when starting a new silage stack or a bale lot. For farmers the adjustment of TMR recipe on site during preparation can be quite manual if no compatible software and TMR mixers are in use and therefore, daily or lot-by-lot adjustment may be demanding. When it comes to mobile applications for feeding, there are applications for designing and saving feeding recipes such as Cattle Feed Organiser Lite (Celeber Solutions, India) and TMR Feeding Module of Cattle Compass (Mtech Digital Solutions Ltd, Finland), latter of which is connected to a commercial service including also wider feeding advice and cattle data. InTouch Forage Budgeting application (Jack Yu/Alltech, United States) is used to support feed storage monitoring either according to fresh weight or DM. However, we have not found at market or in research literature any mobile application designed for the editing of TMR recipes according to regularly performed DM measurements. Such a tool is one of the aims in European AFarCloud project (http://www.afarcloud.eu/), and the work has so far resulted in above mentioned TMR Feeding Module of Cattle Compass without DM measurement method.

Smartfeed EIP-AGRI project aimed to develop on-farm applicable silage dry matter monitoring system that enhances time management at the farm by combining silage sampling to other work tasks and providing tools to measure dry matter and edit the total mixed ration recipe on site (Figure 1). The mobile app and sampling tool are the first published ones for their purposes and are well applicable also to small family farms.

Figure 1. In the study, a system for regular monitoring of silage dry matter was developed and piloted at farms. It consisted of silage sampler attached to a bale gripper, on-farm dry matter measurement by a moisture analyser and a mobile application for TMR feeding adjustment.

2. Materials and Methods

2.1. Silage Sampler

The sampler consists of a steel sampling tube, a support spike, a pivotable framework and a sampling bag fastener at the back end of the sampling tube. The framework is either welded or bolt-fastened to the frame of a bale gripper. The pivotable framework allows the probe (sampling tube and support spike) to be folded down during other work tasks. At the sampling position a spring screw locks the probe at its position. The sampling tube has length of 435 mm reaching the centre of bale and allowing representative sampling. The conical cutting tip of the tube is 28 mm in diameter and the sampling tube has a larger inner diameter (35 mm) to allow easy removal of the sample. The support spike acts as a reinforcement preventing the probe from bending. To collect samples, a sampling bag is fastened by an elastic band to a notch at the back end of the sampling tube. Then, the probe is pressed into a silage bale and withdrawn (Figure 2). Samples can be taken by pressing horizontally or vertically. Several samples can be taken from the bale or a bale lot to obtain a representative sample. After sampling, the sampling tube is emptied with a push-out rod (Figure 3) and the sampling bag is released. After use, the probe can be folded down and secured by an elastic band.

For piloting the sampler was bolt-fastened to a bale gripper (MP-Lift, PP-2) and tested at five farms of which three tested it on a front loader of a tractor and two of them by agricultural telehandler. The tested bales included plastic-wrapped straw bales and grass silage bales.

Figure 2. Silage sampling with the designed sampler.   Figure 3. The sampling tube is emptied with a push-out rod.

2.2. Dry Matter Measurement

A halogen moisture analyser (Adam Equipment, PMB53) was tested for silage and total mixed ration (TMR) samples. The moisture analyser dries the sample on a balance and weight monitoring is done simultaneously. Based on initial screening with fresh grass, grass silage, and TMR samples, two methods were selected: 1) for grass silage samples 60 °C 5 min + 135 °C with end point determination at weight change of <0.003 g in 15 sec and 2) for fresh grass and TMR samples 60 °C 5 min + 100 °C with end point determination at weight change of <0.003 g in 15 sec.

For method validation, a larger sample set was collected and analysed with moisture analyser and a reference method. Total of 84 silage samples (40 timothy-fescue grass silage, 28 clover grass silage, and 16 whole grain silage) and 36 TMR samples were collected from Kainuu, Northern and Middle Ostrobothnia during November 2019 – November 2020. The collected samples were divided into two subsamples. One subsample was sent to SeiLab Ltd laboratory services for reference analysis (oven drying at 80 °C, 24 h). The second subsample was analysed by the moisture analyser in triplicates. 3-8 g of well-mixed sample was used for single measurement. Intra-method variation was calculated from triplicates of all samples analysed and it was calculated separately for different silage types and for TMR samples. Reproducibility was calculated from 10 samples that were analysed triplicates on 2-4 separate days.

To pilot the use of moisture analyser at on-farm setup, the device was piloted at 5 on-farm dissemination events as well as in regular use by farmers (on average one-month testing period/farm, 8 farms participating).

2.3. Mobile Application for TMR Feeding Adjustment

A mobile application was designed to recalculate and adjust TMR recipe on site. The application consists of 1) a graphical user interface with built-in calculation functions in Android OS (compatible with SDK versions 26-29) and 2) data management and storage system at a server (Apache as the web server software, PHP as a server side scripting language, and MySQL as a database management system). The data is transferred as URL-encoded JSON data format between the Android OS and the server. The user devices are smartphones and tablets with Android OS. The user control and data storage are maintained by the server thus, requiring internet connection to operate. The privacy and security of the data stored and transferred is confirmed via the best Apache and MySQL standard security protocol. The

user login information is saved on the device hence, for regular use, the login details do not have to be applied every time.

3. Results and Discussion

3.1. Silage Sampler

The aim of the study was to identify and develop new on-farm applicable tools to enable better dry matter monitoring of silage. The aims for silage sampling were the ease of use and to decrease the time and labour needed. Therefore, the silage sampler was designed and developed as a pivotable probe attached to a bale gripper allowing also other work tasks (relocation and transfer of bales). To our knowledge, there are no previous examples of silage sampling tools connected to a farm equipment. However, there are silage samplers powered by handheld electric drills and used by a person taking samples (Kaiser and Piltz, 2004).

The designed and developed silage sampler was piloted at five farms. Based on the feedback from the pilots, the fastening of sampling bag was adjusted. The overall feedback was mainly positive, and the benefits of the tool were recognized. The sampler can be used for silage sampling prior to TMR preparation or for pre-sampling when feeding planning is started for the next feeding season or silage lot. However, some future development points were arisen such as the locking of sampler when it is not in use. If the elastic band is misplaced while handling bales, the sampling tube can be released, and the cutting tip may injure the plastic wrapping. It was considered that a spring screw similar to the one locking sampling position could resolve the observed problem.

3.2. Dry Matter Measurement

To facilitate regular dry matter measurement on-farm, a moisture analyser used routinely in the food industry was tested for silage and TMR samples at laboratory and on-farm setup. Silage and TMR samples were analysed with moisture analyser, refence analysis were carried out by an external laboratory and the comparison between the methods were performed (Table 1.). The intra-method variation of moisture analyser for silage samples was 3.1 % and 3.4 % for TMR samples and the reproducibility was 3.6 %.

Table 1. Performance of moisture analyser in DM measurements.

Sample type	R^2 of correlation curve	Average difference to oven drying	Intra-method variation
Grass silage	0.9923	-4.72 %	3.23 %
Clover grass silage	0.9986	-4.34 %	3.12 %
Whole crop silage	0.9811	-5.92 %	3.00 %
All silage samples	0.9925	-4.82 %	3.10 %
TMR samples	0.9985	2.59 %	3.36 %

The comparison of moisture analyser to oven drying showed good correlation, 0.9925 and 0.9985 respectively for silage and TMR samples (Figure 4). However, the method for silage samples gave systematically slightly lower values compared to oven drying (average difference -4.8 %). The difference can be taken into account with a correction coefficient of 1.05 that is valid at least for timothy-fescue grass, clover grass and whole crop silage.

The method for TMR samples showed in average 2.6 % higher values than oven drying. Nevertheless, the difference is smaller than the intra-method variation of TMR samples. Some initial testing was also done for fresh grass, separated cow manure as well as crushed grain. The results were promising, but no larger studies have been performed yet. Furthermore, the device could have several applications in farm environment.

A)

Silage samples, n=84

B)

Total mixed ration, n=36
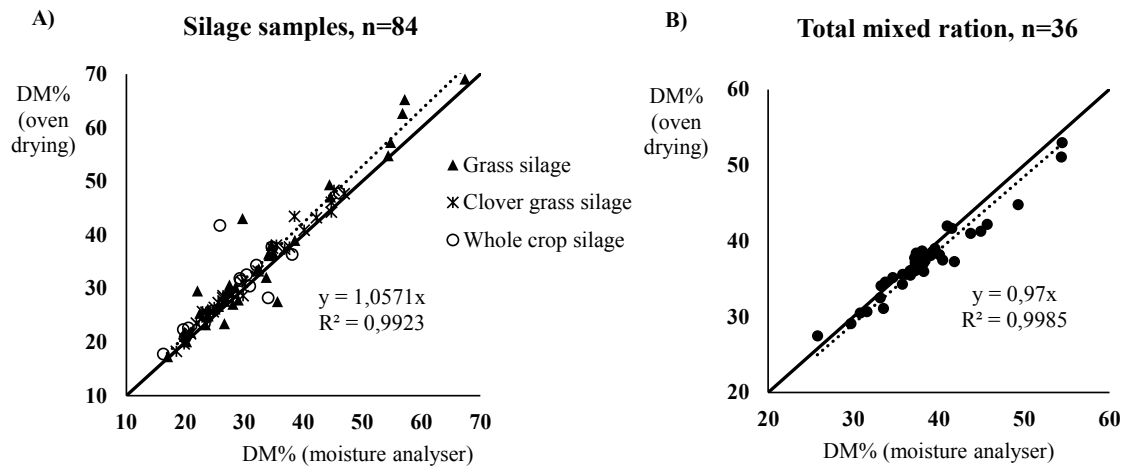
Figure 4. Correlation curves of moisture analyser and reference method (oven drying) for A) silage samples and B) TMR samples. Three different silage types, timothy-fescue grass, clover grass and whole crop were analysed, and they are represented by different markers in A).

The feedback from piloting the device was satisfied. Some had initial doubts for the relatively small sample size compared to normal silage analysis that have sample size of 2 litres. However, the farmers also sent reference samples to an external laboratory and indicated that results have been comparable. All in all, taking representative samples has been emphasized throughout the piloting in addition to duplicating measurements if the results seemed inaccurate. Some technical difficulties were faced when measuring outdoors at windy conditions and if the electrical input was unstable (when aggregate was used as a power supply, low voltage was sometimes observed). The measurement time varied from 6 minutes to 45 minutes depending on the sample type, the moisture content, and the sample amount in the measurement. However, when the sample size was set to 5-8 g the measurement time was typically between 10-20 minutes for both silage and TMR samples.

3.3. Mobile Application for TMR Feeding Adjustment

An Android application was designed to utilize dry matter (DM) measurement results to adjust total mixed ration (TMR) recipe on-site during TMR preparation (Figure 5). In the app, first the used TMR components (feeds, silage batches) and recipes are added, and they are stored to a server. Then, the app allows to calculate the changes in the amounts of different components of a TMR recipe in situations where the DM% of silage changes or the amount of a component is changed. In addition, using the bale calculator the actual weights and DM% of the individual bales added to the TMR feed lot can be taken into account for calculating the optimal amounts of other components. Finally, the app allows easy and rapid modification of total DM% of the TMR feed lot by modifying the amount of water added. The app has user-specific control and data storage that are managed via the server. Therefore, the DM% history of different silage lots can be followed and assessed.

During application development there were several iterative processes based on the feedback from user piloting. During the project, 40 user accounts were created and distributed, however, the regular use of the app has been limited due to lack of dry matter measurements and/or measurement devices at piloting farms. Without the DM measurement results, the use of app is limited to recalculation of the amounts of components. In addition to piloting at farms, there were three bigger user piloting events at vocational schools of agriculture. Based on the feedback some further development was carried out in addition to recognizing new features that yet have not been included in the app.
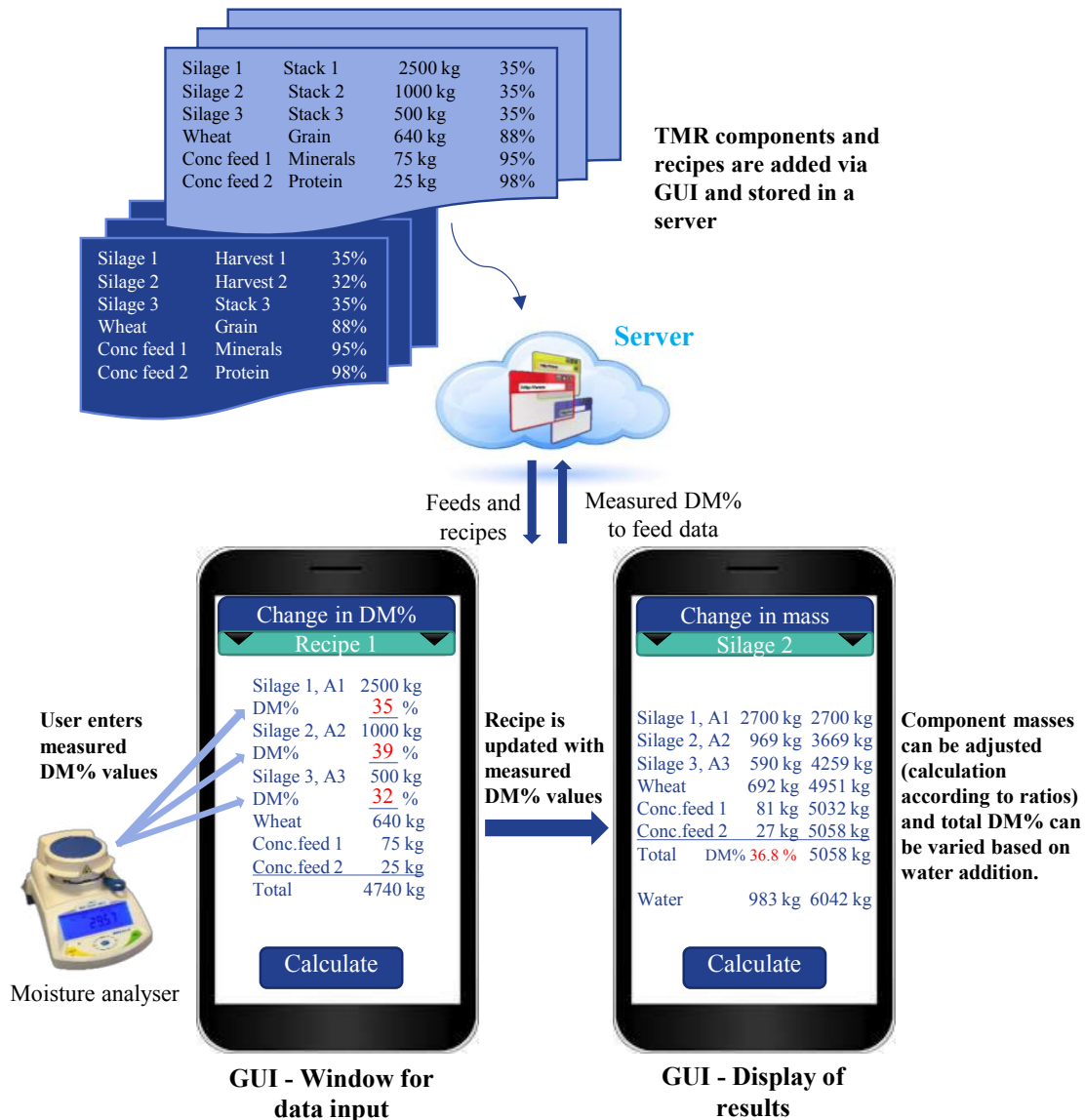
Figure 5. The mobile application for adjustment of TMR recipe was designed and constructed. First, the TMR components and recipes are added via graphical user interface (GUI). Then, measured DM% values are entered, and amounts of TMR components are recalculated. Total DM% of the TMR can be optimised by water addition.

4. Conclusions

A system for regular monitoring of silage dry matter on farm and adjusting TMR feed composition accordingly was introduced. A newly designed silage sampler facilitates easy sampling of silage bales during other work tasks. The presented moisture analyser can be used at farm level to monitor dry matter changes of silage and total mixed ration lots. The designed mobile application allows TMR recipe adjustment on site during TMR preparation. Thus, farmers can react to changes in silage dry matter even daily. The bale calculator of the mobile application secures optimisation of silage bale feeding.

Overall, the regular monitoring of silage dry matter has economic impacts on dairy production by ensuring the most economical feeding to milk yield ratio. It also secures consistent feeding and prevents waste of both silage and concentrated feed resulting in the end in increase in efficiency, productivity, and competitiveness of the farms. Rapid, semi-automated measurement systems also reduce the working time needed.

Acknowledgements

References

Artavia, G., C. Cortes-Herrera, F. Granados-Chinchilla, 2021. Selected instrumental techniques applied in food and feed quality, sagety and adulteration analysis. Foods. 10(5): 1081. oi.org/10.3390/foods10051081.

Donnelly, D.M., J.R.R. Dorea, H. Yang, and D.K. Combs, 2018. Technical note: Comparison of dry matter measurements from handheld near-infrared units with oven drying at 60 °C for 48 hours and other on-farm methods. Journal of Dairy Science. 101(11):9971-9977. Doi.org/10.3168/jds.2017-14027

Gear, M., 2020. Testing silage quality: The importance of it and how you can go about doing it. Agriland. https://www.agriland.ie/farming-news/testing-silage-quality-the-importance-of-it-and-how-you-can-go-about-doing-it/. Accessed June 9, 2021.

Kaiser, A.G., and J.W. Piltz, 2004. Feed testing: assessing silage guality, In *TopFodder Successful Silage* (Eds. Kaiser, A.G., J.W. Piltz, H.M. Burns, and N.W. Griffiths. 2nd edition, Dairy Australia and New South Wales Department of Primary Industries. 312-334. https://www.dpi.nsw.gov.au/__data/assets/pdf_file/0005/294053/successful-silage-topfodder.pdf

Mostafa, E., P. Twickler, A. Schmithausen, C. Maack, A. Ghaly, and W. Buescher, 2021. Optimisation of dry matter and nutrients in feed rations through use of a near-infrared spectroscopy system mounted on a self-propelled feed mixer. Animal Production Science, 61(5): 514-524. Doi.org/10.1071/AN19306

Pino, F.H., and A.J. Heinrichs, 2014. Comparison of on-farm forage-dry-matter methods to forced-air oven for determining forage dry matter. The professional Animal Scientist. 30(1): 33-36. Doi.org/10.15232/S1080-7446(15)30079-6.

Schingoethe, D.J, 2017. A 100-year review: Total mixed ration feeding of dairy cows. Journal of Dairy Science. 100 (12): 10143-10150. Doi: 10.3168/jds.2017-12967

Sova, A.D., S.J. LeBlanc, B.W. McBride, and T.J. DeVriesm, 2014. Accuracy and precision of total mixed ration fed on commercial farms. Journal of Dairy Science. 97(1): 562-571. Doi.org/10.316

Damages Produced to Citrus Fruits During Detachment Using a High Amplitude and Low Frequency Shaker

Coral Ortiz[a]*, Antonio Torregrosa[a]

[a]Departamento de Ingeniería Rural y Agroalimentaria, Universitat Politècnica de València, Camino de Vera s/n, 46022, Valencia
*Corresponding author: Email cortiz@dmta.upv.es

Abstract

The crucial problem of the high costs of the manual harvesting of fresh citrus in Spain could be solved using mechanical systems. Previous results have shown that long amplitudes, 60 mm or more, combined with low frequencies, 3 to 6 Hz, are highly efficient in citrus fruit detachment and produce low defoliation. Low frequency commercially available canopy shakers are too large to be used in the citrus orchards cultivated in Valencia (Spain) and produce excessive damage to the fresh market fruit. A light shaker, that can be hitched to the three-point hitch of an orchard tractor or to the arms of a compact track loader was developed, it is a linear shaker, based in a slider and crank mechanism, that allows the amplitude regulation, and a rigid arm that grips the tree branch.

Previous results have demonstrated good removal efficiency (between 62 % and 97 %) when shaking with frequencies from 3 to 6 Hz and amplitudes from 100 to 180 mm. However, fruit damages during detachment and falling through the canopy have not been tested. Video image analysis and accelerometers were used to measure rubbing of the fruit against branches and fruit striking against other fruits or branches. A methodology to assess fruit damage during detachment has been proposed. Further research should be carried out to study other factors involved in fruit injuries previous to the collecting systems during mechanical harvesting.

Keywords: citrus, mechanical harvest, shaker, low frequency

1. Introduction

In Spain citrus fruit are destined to the fresh fruits market. Mechanical harvesting systems have been studied to reduce the costs of manual harvesting but the damages produced to the fruit are crucial. Previous studies showed the effectiveness of vibration systems for mechanical citrus harvesting (Ortiz and Torregrosa, 2013; Castro-García et al., 2019). Trunk shakers can be used to harvest citrus fruits using, frequencies around 15 Hz to 25 Hz have shown promising results.

Previous laboratory studies have shown the possibility of detaching citrus fruit using lower frequencies and higher strokes to reduce leaf losses (Torregrosa et al., 2014). And cushioned and elevated canvas on the ground have proven to reduce the collecting damages (Ortiz et al., 2011)

A light-weight experimental shaker was developed and successfully tested to harvest ornamental citrus trees (Torregrosa et al., 2019). The frequency used was between 4 Hz to 6 Hz and the stroke was 0.06 m. The gripper was capable to grasp the low diameter trunk to be shaken.

The light-weight experimental shaker was improved to harvest fresh citrus orchards, gripping the main branches. However, fruit damages on the tree during the high amplitude vibration have not been previously studied.

The objective of this work was to evaluate the fruit quality and damages during detachment and falling using the experimental light-weight shaker compared to an orchard tractor mounted trunk shaker.

2. Materials and Methods

2.1. Materials

Healthy and well-managed trees from the variety 'Caracara' from an ANECOOP experimental orchard in Museros (Valencia) were tested at end of the harvesting period, February 2021 (harvesting period December 15th to February 15th).

The trees were planted in a grid with in-row spacing of 4 m and 5 m between rows. Rows were on trapezoidal ridges (0.3 m in height and 2 m wide at the top). The trunk height was (mean ± SD) 0.41 ± 0.03 m and the trunk diameter was 0.11 ± 0.01 m. The trees had three to five main branches. The canopy height of the aboveground level was 2 ± 0.2 m. The height from the ground to the canopy skirt was 0.35 ± 0.2 m. The canopy diameter perpendicular to the row was 2.9 ± 0.2 m. The canopy diameter parallel to the row was 3.6 ± 0.2 m.

2.2. Methodology

Two different harvesting systems were tested (experimental light-weight shaker and orchard tractor mounted trunk shaker).

The tractor mounted trunk shaker was arranged in two parts: one part (with a mass of 640 kg) was attached at the tractor's rear three-point hitch and included the oil tank and the pumps operated by the tractor's power take-off; the other part (with a mass of 730 kg) was coupled to the front three-point hitch and included an extendable arm and a clamp with two moving fingers. Also included was the hydraulic motor that drives an eccentric mass of 16 kg with an eccentric radius of 0.13 m that produces an orbital vibration (Topavi light shaker, Maquinaria Agrícola Garrido s.l. (Topavi), Autol, Spain, www.topavi.es). In all cases, the tree trunk was clamped at around 0.2 m above the ground. The tractor was a 66 kW four-wheel-drive model.

The experimental light-weight shaker (Figure 1) was a light weight, linear and low cost, experimental shaker. The clamp is made of two steel fingers covered with 60 mm thick rubber pads. The fingers were moved by a hydraulic cylinder. The shaker was hitched to the forks of a pedestrian hydraulic tractor (Hinowa, Nogara, VR, Italy; Hinowa.com) 'Hinowa' model 'HS 11000 provided with a fork elevator. The shaker was powered by a hydraulic motor, that received the oil from the external supplies of a tractor Lamborghini Plus 990-F that gave a flow of 21 L min^{-1} at 100 bar. The vibration amplitude used was 0.60 m.

To evaluate the fruit movement during the vibration, high-speed video recordings were analyzed.

Fifty fruits from each harvesting system (experimental shaker and trunk shaker) and collecting system (ground, ground covered with canvases, elevated canvases and manually collected, Figure 1) were carefully taken to the laboratory after harvesting, and were stored at room temperature with high relative humidity (24 and 90%) for fourteen days in order to increase bruise visualization. In the case of the elevated canvases the number of samples was duplicated. Besides, sixty fruits were manually collected, thirty to analyze fruit damages and thirty to measure fruit weight and maturity index. Fruit damage was evaluated measuring the percentage of slightly damaged fruits (small cuts, rubbing and very small bruises) and the percentage of considerable damaged fruits (bruises and cut wounds).

Figure 1. Collecting canvases (ground covered with canvases (left) and elevated canvases (right)).

3.   Results and Discussion

3.1. Detachment point

When citrus fruits are destined for the fresh market, they are usually refrigerated for weeks. In the cold storage conditions with high humidity, fungus can infect fruit if damaged or without calyx (Torregrosa et al., 2009).

Most of the fruits were detached with calyx (around 60% of the fruits). Considering that the fruit was a little overripe (maturity index of 11.8 and 14.2 Brix) only 23% of the fruits were detached without calyx (17 % were detached with peduncle). A two ways ANOVA analysis showed that no significant differences were found between the experimental shaker and the trunk shaker in the detachment point (Figure2). It seems that the high amplitude vibration does not produce a significant increase of the fruits detached without calyx.
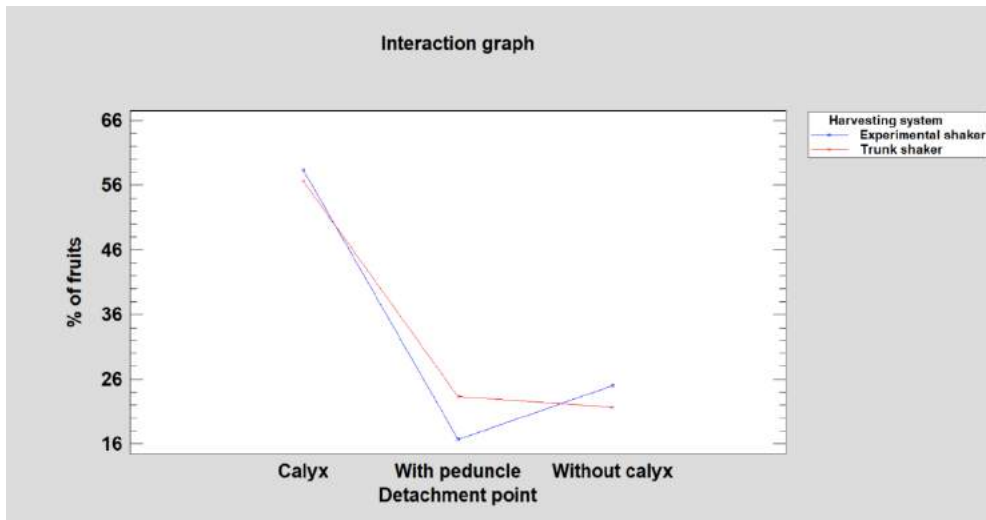
Figure 2. Percentage of fruits detached with calyx, without calyx and with peduncle using the two harvesting systems (experimental shaker and trunk shaker)

3.2. Fruit damage

As it was expected the higher percentage of damaged fruits was obtained when the fruits were collected without a protection canvas (Figure 3). The elevated canvas reception produced lower severe damage than the fruits manually harvested and a little higher percentage of slightly damaged fruits. However, the canvases on the ground protected against severe damage but produced a higher percentage of slightly damaged fruits (similar to the fruit collected directly on the ground).
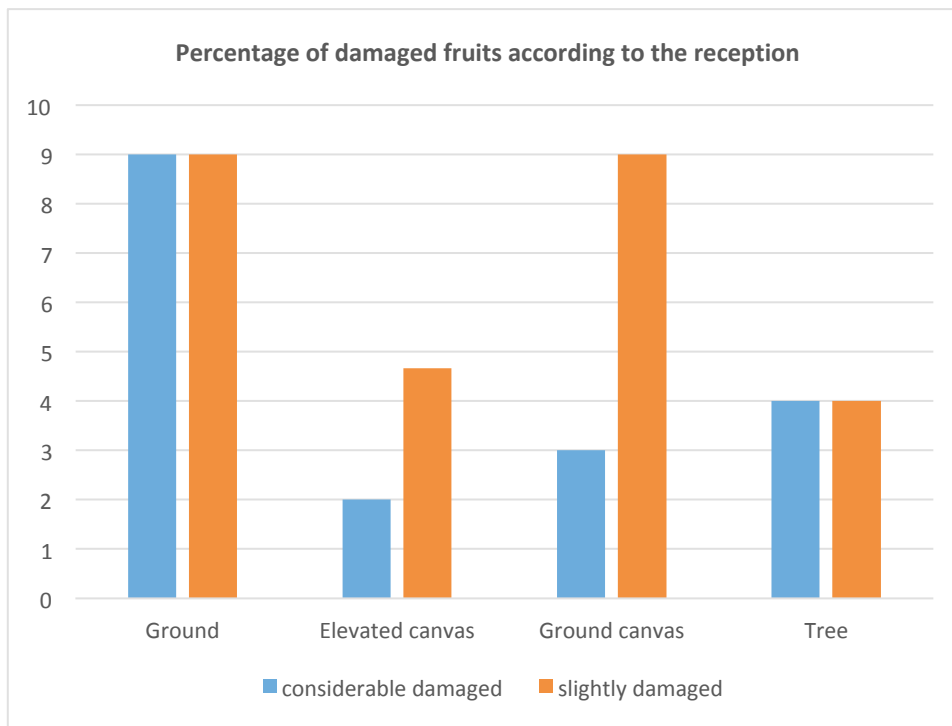
Figure 3. Percentage of damaged fruits (considerable damaged and slightly damaged) according to the reception system.

In order to analyze the citrus damage produced during the vibrating time, before collecting, only the fruits collected with the elevated canvases were studied. When comparing the considerable damaged fruits using both harvesting systems no significant differences were found. However, the percentage of slightly damaged fruits was substantially higher when using the experimental shaker with high amplitude compared to the traditional trunk shaker (p-value=0.0735 in the ANOVA analysis studying the effect of the harvesting system on the slightly damaged fruit percentage), Figure 4. In this line, 74% of the slight damages in fruits detached with the experimental shaker were small

cuts and rubbings compared to the 14% in the fruits detached with the trunk shaker. When analyzing the videos recorded during the shaking time, a high amplitude movement of the fruits related to the high amplitude of the branch vibration is confirmed. Some of the fruits, during the vibration, are rubbed against the branches and other fruits.
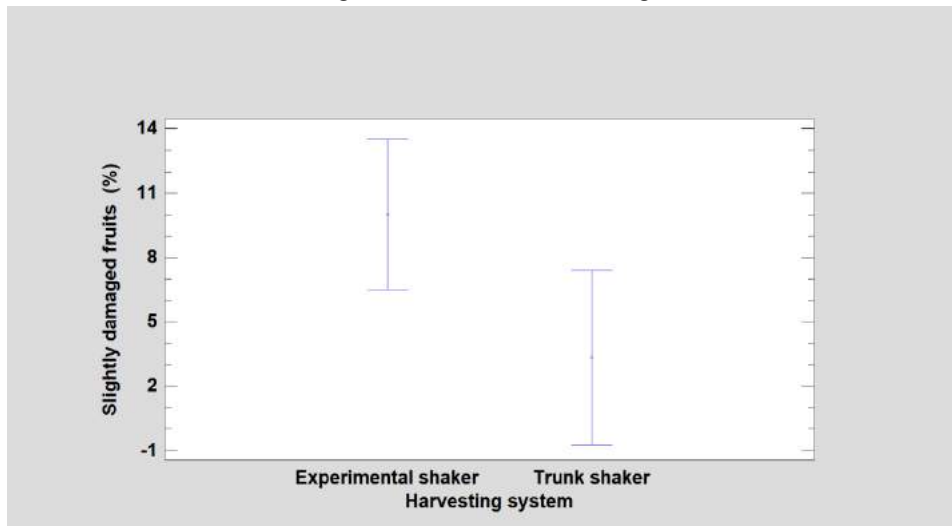
Figure 4. Slightly damaged fruits (%) related to the harvesting system (average value and Fisher LSD interval), only the ones collected on the elevated canvases.

4. Conclusions

A high amplitude-low frequency experimental citrus branch shaker was tested in field conditions. Under the experimental conditions, only 23% of the fruits were detached without calyx and most of the fruits were detached with calyx.

The canvases on the ground used to collect the oranges reduced the severe damages but were not useful to protect against light damages. However, the capability of the elevated canvases to reduced damages was verified.

It seems that the high amplitude vibration of the experimental shaker produced a higher percentage of slightly damaged oranges. The high amplitude movement of the fruits related to the high amplitude of the branch vibration was confirmed. The higher damage percentage could be due to the fact that some of the fruits are being rubbed against the branches and other fruits during the vibration. However, further research should be carried out to study other factors involved in fruit injuries previous to the collecting systems during mechanical harvesting.

Acknowledgements

References

Castro-Garcia, S., Aragon-Rodriguez, F., Sola-Guirado, R.R., Serrano, A.J., Soria-Olivas, E., Gil-Ribes, J.A. 2019.Vibration Monitoring of the Mechanical Harvesting of Citrus to Improve Fruit Detachment Efficiency. *Sensors*, *19*, 1760. https://doi.org/10.3390/s19081760

Ortiz, C., Blasco, J., Balasch, S., Torregrosa, A. 2011. Shock absorbing surfaces for collecting fruit during the mechanical harvesting of citrus. Biosystems Engineering, 110(1), 2-9. https://doi.org/10.1016/j.biosystemseng.2011.05.006

Ortiz, C., Torregrosa, A. 2013. Determining adequate vibration frequency, amplitude, and time for mechanical harvesting of fresh mandarins. Transactions of the ASABE, 56(1), 15-22. http://doi: 10.13031/2013.42581

Torregrosa, A., Ortí, E., Martín, B., Gil, J., Ortiz, c. 2009. Mechanical harvesting of oranges and mandarins in Spain, Biosystems Engineering, 104 (1), 18-24. https://doi.org/10.1016/j.biosystemseng.2009.06.005.

Torregrosa, A., Albert, F., Aleixos, N., Ortiz, C., Blasco, J. 2014.Analysis of the detachment of citrus fruits by vibration using artificial vision. Biosystems Engineering, 119,1-12. https://doi.org/10.1016/j.biosystemseng.2013.12.010

Torregrosa, A., Molina, J.M., Pérez, M., Ortí, E., Xamani, P., Ortiz, C. 2019. Mechanical Harvesting of Ornamental Citrus Trees in Valencia, Spain. *Agronomy*, *9*, 827. https://doi.org/10.3390/agronomy9120827

Effects of Planter Attachments on Corn Emergence and Corn Yield

Demmel Markus [a*], Kirchmeier Hans [a]

[a] Institute for Agricultural Engineering and Animal Husbandry, Bavarian State Research Center for Agriculture, Freising, Germany

* Corresponding author. Email: markus.demmel@lfl.bayern.de

Abstract

Conservation tillage and no till practices to sustain residue cover and soil structure, to avoid erosion and to optimize soil functions put high requirements on seeding and planting technologies. Today single-seed drills are designed and optimized to cope with the specific conditions of these practices. But there are still situations where the seeds are not well placed and covered with soil causing bad emergence and yield losses. To avoid these problems different planter attachments like row cleaners, leading coulters, combinations of both and different types of closing wheels are offered.

Although planter attachments are very popular in the USA and more than 10 manufacturers are producing them, publications or reports on scientific investigations about their effects on plant emergence and crop yield of corn could not be found. Therefor own investigations have been conducted.

To investigate the effects of selected planter attachments on corn emergence and corn yield, randomized field experiments with large plots (40 x 3 m) have been carried out over 4 years and on 3 locations in Bavaria. The 3 factors of the trials have been type of tillage strategy (conservation tillage with and without seedbed preparation), type of leading planter attachment (no additional attachment, waved coulter, fixed row cleaner, combination of waved coulter and floating row cleaner) and closing wheel combinations (two standard closing wheels, one standard closing wheel plus a structured closing wheel). All 16 variants have been repeated 4 times at each location.

The tillage strategies showed a significant influence on the emergence rate and the yield of corn (conservation tillage with seed bed preparation higher than direct seeding). Only a few attachments had significantly positive effects on the germination (waved coulter + floating row cleaner) or the yield (waved coulter). The different closing wheel combinations showed no influence.

Keywords: Planter attachments, conservation tillage, mulch tillage, direct seeding, single seed drill.

1. Introduction

Conservation tillage and no till practices to sustain residue cover and soil structure, to avoid erosion and to optimize soil functions put high requirements on seeding and planting technologies. Today single-seed drills are designed and optimized to cope with the specific conditions of these practices. But there are still situations where the seeds are not well placed and covered with soil causing bad emergence and yield losses. To avoid these problems different planter attachments like row cleaners, leading coulters, combinations of both and different types of closing wheels are offered.

Publications about conservation tillage practices highlight positive effects of additional attachments at single seed drill for plant emergence and yield, although they did not quantify these effects (Dickey and Jasa, 1989; Reader, 2001; Grisso et al., 2009). Kornecki et al. (2005) and Way et al. (2018) reported on positive effects of row cleaners and structured closing wheels in specific conditions on the emergence and yield of cotton in the US.

Although planter attachments are very popular in the USA and more than 10 manufacturers are producing more than 50 different types, publications or reports on scientific investigations about their effects on plant emergence and crop yield of corn could not be found in literature until 2020. Therefor own investigations have been conducted.

2. Materials and Methods

To quantify the effects of planter attachments on the emergence rate and yield of corn under Bavarian resp. German conditions the Institute for Agricultural Engineering and Animal Husbandry of the Bavarian State Research Center for Agriculture conducted field trials on three locations in the years 2015-2018.

The field trials had 3 factors with 2, resp. 4 variants each (table 1). The first factor was the type of conservation tillage. After establishing a cover crop mixture (GeoVital MS100A by BSV Saaten resp. humuspro by Andrea Saaten) or winter rye after grain harvest in the preceding summer, corn has been planted after a shallow seedbed preparation with a rotary harrow into the cover crops terminated by frost ("mulch tillage with seedbed preparation") or directly drilled into the cover crops terminated by frost ("mulch tillage without seedbed preparation"). The aim was to sustain a cover of the soil with residues / organic material > 30% to fulfil the requirements of conservation tillage systems.

The second factor was the type of leading planter attachments. Out of the high number of different leading planter attachments (coulters, row cleaners, coulter-row cleaner combinations, fixed or floating mounted, partly with hydraulic,

pneumatic or hydropneumatics downforce control, >50 types of more than 10 manufactures worldwide) four variants have been selected. A waved coulter (diameter 400 mm, 50 waves, wave depth 16 mm), a fixed mounted row cleaner with two spike wheels (YETTER 2967 Rigid Row Cleaner©), a combination of the waved coulter and a floating row cleaner with two spike wheels (MARTIN TILL John Deere Mounts BDC 1360©) and the variant without leading attachment.

At least two closing wheel variants have been investigated. The standard configuration with two and the combination of a standard closing wheel on one side combined with a structured closing wheel (DAWN Curvetine M Series©) on the other side.

Table 1. Factors and variants of the field trial

Factor	Variants
Type of conservation tillage	Mulch tillage with seedbed preparation (rotary harrow)
	Mulch tillage without seedbed preparation
Type of leading attachment	Without leading attachment
	Waved coulter
	Fixed mounted row cleaner
	Combination of waved coulter + floating row cleaner
Type of closing wheels	Standard closing wheels
	Standard + structured closing wheel

The combination of the factors resulted in 16 variants. All variants have been repeated four times and all plots have been randomized.

It was decided to use a large plot design. The plots had the width of 3 m (4 rows) and the length of 40 m. To avoid errors caused by boundary effects and by speeding up and slowing down the tractor only the central two rows on a length of 10 meters in the centre of the plot have been observed and harvested.

Directly after harvest the relative cover with residues / organic material has been determined applying the line-transect method (Laflen et al. 1981, Shelton et al. 1993). The emerging rate was determined by counting the plants in the 1.5 x 10 m harvesting area of the plot and comparison with the seeded grains (seed rate in all years and at all places 8 seeds/m^2).

The tractor used for establishing the cover crops, for seedbed preparation (variants mulch tillage with seedbed preparation) and running the precision seed drill was equipped with a RTK DGPS based automatic steering system. Väderstad provided a four row Tempo© single-seed drill. Its row units have a universal mounting plate at the front end which allows the mounting of the different leading attachments.

Figures 1-4 show the investigated combinations of leading planter attachments and closing wheel variants.

Figure 1. Variants without leading planter attachments with standard closing wheels (left) and standard + structured closing wheels (right)

Figure 2. Variants without fixed row cleaner with standard closing wheels (left) and
standard + structured closing wheels (right)

Figure 3. Variants without waved coulter with standard closing wheels (left) and
standard + structured closing wheels (right)

Figure 4. Variants without waved coulter plus floating row cleaners with standard closing wheels (left) and
standard + structured closing wheels (right)

3. Results and Discussion

Consecutively results of the summarizing analyses of data of all years and all locations are presented. Detailed results of every single year and every single location can be found in the full report which is only available in German language https://www.lfl.bayern.de/mam/cms07/ilt/dateien/endbericht_optimierung_mulchsaat.pdf

3.1. Effects on residue cover

The summarizing analysis showed significant differences only between the two types of tillage (table 2).

Table 2. Relative residue cover after seeding (all years, all locations)

Variant	Relative residue cover [%]	SNK test α=0.05
Mulch tillage with seedbed preparation	24.3	A
Mulch tillage without seedbed preparation	36.7	B

The low level of the residue cover is caused by very low levels of cover at one of the three locations over all four years (mulch tillage with seedbed preparation 8% coverage, mulch tillage without seedbed preparation 21% coverage). Skipping this location, which faced draught in the autumns of all four years, the following residue cover was reached (table 3).

Table 3. Relative residue cover after seeding (all years, two locations)

Variant	Relative residue cover [%]	SNK test α=0.05
Mulch tillage with seedbed preparation	32.5	A
Mulch tillage without seedbed preparation	45.5	B

At two of three locations the residue cover of both tillage types has been above the threshold value for conservation tillage (>30%). No differences between the different planter attachment variants could be detected.

3.2. Effects on emergence rates

With values between 87-93% the determined emergence rates laid on a high level and showed very little significant differences.

Although the relative difference is very small (101% resp. 99%) the average emergence rate of all variants of the factor mulch tillage with seedbed preparation has been significantly higher than of all variants of mulch tillage without seedbed preparation (table 4).

Table 4. Effects of tillage types on relative emergency rates (all years, all locations)

Variant	Relative emergence rates [%]	SNK test α=0.05
Mulch tillage with seedbed preparation	101	A
Mulch tillage without seedbed preparation	99	B

Regarding the leading planter attachments, the differences of the relative emergence rates have also been very little. Only the waved coulter + floating row cleaner showed a significant difference / advantage (table 5).

Table 5. Effects of leading planter attachments on relative emergency rates (all years, all locations)

Variant	Relative emergence rates [%]	SNK test α=0.05
Without leading planter attachment	100	B
Waved coulter	100	B
Fixed row cleaner	99	B
waved coulter + floating row cleaner	101	A

The reason for the advantage of the variant waved coulter + floating row cleaners might be the combination of the specific advantages of both tools. The waved coulter typically produces fine soil that optimizes the embedding of the seed and the floating row cleaner better follows the soil surface without digging too deep in the soil or "flying" over residues.

There could be no differences determined between the two configurations of closing wheels!

Figure 5 shows the differences in the emergency rates of alle variants.

type of mulch tillage	type of leading planter attachment	type of closing wheel combination	emergence rate [%]	relative emergence rate [%]	SNK test α=0,05
with seedbed preparation	coulter + floating row cleaner	standard closing wheels	92.65	103	A
with seedbed preparation	without attachments	standard closing wheels	91.69	102	AB
with seedbed preparation	coulter + floating row cleaner	standard + curvetine	91.36	101	ABC
with seedbed preparation	waved coulter	standard closing wheels	90.99	101	ABCD
with seedbed preparation	waved coulter	standard + curvetine	90.77	101	ABCDE
with seedbed preparation	without attachments	standard + curvetine	90.76	101	ABCDE
without seedbed preparation	coulter + floating row cleaner	standard closing wheels	90.72	101	ABCDE
with seedbed preparation	fixed row cleaner	Standardandruckrolle	90.31	100	FBCDE
with seedbed preparation	fixed row cleaner	standard + curvetine	89.92	100	FBCDE
without seedbed preparation	without attachments	standard + curvetine	89.90	100	FBCDE
without seedbed preparation	coulter + floating row cleaner	standard + curvetine	89.33	99	FGCDE
without seedbed preparation	waved coulter	standard + curvetine	89.11	99	FGCDE
without seedbed preparation	waved coulter	standard closing wheels	88.91	99	FGDE
without seedbed preparation	fixed row cleaner	standard closing wheels	88.58	98	FGE
without seedbed preparation	fixed row cleaner	standard + curvetine	88.18	98	FG
without seedbed preparation	without attachments	standard closing wheels	87.30	97	G

Figure 5. Emerging rates of all variants (all years and all places)

3.3. Effects on corn yield

With values of the absolute corn yield (86% DM) between 9.6 and 13.7 mgha^{-1} the determined yield showed a high variability depending on the year and on the location but showed very little significant differences between the variants.

The average relative yield of all variants of the factor mulch tillage with seedbed preparation have been significantly higher than the variants of mulch tillage without seedbed preparation (table 4).

Table 6. Effects of tillage types on relative corn yield (all years, all locations)

Variant	Relative yield [%]	SNK test α=0.05
Mulch tillage with seedbed preparation	103	A
Mulch tillage without seedbed preparation	97	B

These advantages in yield are combined with disadvantages in erosion control which are based on the significantly lower relative residue cover of the variants with seedbed preparation (see 3.1 Effects on residue cover) and show the conflict of objectives between the maximization of yield and the optimization of erosion control.

Regarding the leading planter attachments again only small differences could be determined (table 7).

Table 7. Effects of leading planter attachments on relative emergency rates (all years, all locations)

Variant	Relative yield [%]	SNK test α=0.05
Without leading planter attachment	100	AB
Waved coulter	102	A
Fixed row cleaner	99	B
waved coulter + floating row cleaner	99	B

Some aspects of these results are interesting and should be highlighted. The average differences between the variants are very small (between 99 und 102%)! Although the variants using the waved coulter + floating row cleaner showed the significant highest emergence rate (101%) also show the lowest relative yield (99%)! The variants using only the waved coulter showed the highest relative yield! The variants without any leading planter attachment showed no significant difference in yield with any other variant!

Again, no differences could be determined between the average yields of the variants of the two configurations of closing wheels!

Finally figure 6 shows the differences between the absolute and relative yields of all variants.

type of mulch tillage	type of leading planter attachment	type of closing wheel combination	absolute yield [mg/ha]	relative yield [%]	SNK test, α=0,05
with seedbed preparation	waved coulter	standard closing wheels	12.07	105	A
with seedbed preparation	without attachment	standard closing wheels	12.01	105	A
with seedbed preparation	fixed row cleaner	standard closing wheels	11.88	103	AB
with seedbed preparation	waved coulter	standard + curvetine	11.83	103	AB
with seedbed preparation	without attachment	standard + curvetine	11.80	103	ABC
with seedbed preparation	coulter + floating row cleaner	standard closing wheels	11.78	103	ABC
with seedbed preparation	fixed row cleaner	standard + curvetine	11.71	102	ABCD
with seedbed preparation	coulter + floating row cleaner	standard + curvetine	11.52	100	ABCDE
without seedbed preparation	waved coulter	standard + curvetine	11.38	99	ABCDE
without seedbed preparation	waved coulter	standard closing wheels	11.37	99	ABCDE
without seedbed preparation	without attachment	standard closing wheels	11.25	98	BCDE
without seedbed preparation	without attachment	standard + curvetine	11.12	97	CDE
without seedbed preparation	fixed row cleaner	standard closing wheels	11.09	97	DE
without seedbed preparation	coulter + floating row cleaner	standard + curvetine	11.05	96	DE
without seedbed preparation	coulter + floating row cleaner	standard closing wheels	11.02	96	DE
without seedbed preparation	fixed row cleaner	standard + curvetine	10.91	95	E

Figure 6. Relative an absolute of all variants (all years and all places)

Again, the difference between the variants with and without seedbed preparation becomes evident. The average yield difference was 6 %. On the other hand, the difference between the best variant without seedbed preparation and the worst variant with seedbed preparation was only 1%!

Recently Drewry et al. (2020) have reported similar results of their investigations on the "Impact of Planter Closing Wheels on Corn Emergence in No-Till Systems". Aftermarket closing wheels increased corn emergence by 2% over standard rubber wheels. But yield was not significantly affected by closing wheel type.

4. Conclusions

Modern single-seed drills for corn are optimized and able to cope with the specific conditions of mulch tillage or direct seeding also without planter attachments. In the own investigations only a few attachment combinations showed significantly positive effects on the emergence rate (waved coulter + floating row cleaner) or the yield (waved coulter). Floating row cleaners trended to result in higher emergency rates and yields than fixed ones based of a better adaption to the soil surface. The use of waved coulters also trended to result in higher emergency rates and yields due to the production of additional fine soil.

Although the soil at one location had a high content of stones all planter attachments worked without any trouble

during the whole investigation.

In the investigation, no difference in corn emergence and corn yield between the different closing wheel combinations could be detected.

All variants of mulch tillage with seedbed preparation resulted in higher emergence rates and corn yields than the variants with mulch tillage without seedbed preparation although the soil coverage with organic material of the variants with seedbed preparation was significantly lower than of the variants without seedbed preparation. That resulted in lower erosion control in the variants with seedbed preparation.

Based on the results and observations of the investigation the following additional recommendations can be made:

- If farmers expect difficult and challenging conditions for planting corn especially in conservation tillage systems, the use of planter attachments should be considered.
- If a new single-seed drill should be purchased, the possibility to mount planter attachments should be considered.
- Floating row cleaners should be preferred to fixed row cleaners.
- Waved coulters provide additional fine soil to optimize seed embedment.
- Structured clothing wheel might be favourable in very difficult situations.

References

Dickey, E. C., P. Jasa, 1989. Row Crop Planters: Equipment Adjustments and Performance in Conservation Tillage. NebGuide G83-684. https://digitalcommons.unl.edu/cgi/viewcontent.cgi?article=1692&context=extensionhist University of Nebraska Cooperative Extension, Lincoln.

Drewry, J.L., B. D. Luck, F. J. Arriaga, 2020. Impact of Planter Closing Wheels on Corn Emergence in No-Till Systems. Applied Engineering in Agriculture Vol. 36(5): 727-732, American Society of Agricultural and Biological Engineers.

Grisso, R., D. Holshouser, R. Pitman, 2009. Planter/Drill Considerations for Conservation Tillage Systems. Publication 442-457. Virginia Tech Cooperative Extension. Richmond, Virginia.

Iowa State University. 2000. Conservation Tillage Systems and Management: Crop Residue Management with No-till, Ridge-till, Mulch-till, and Strip-till, 2nd ed. Publication No. MWPS-45. Ames, Iowa: MidWest Plan Service.

Kornecki, T. S., Raper, R. L., Arriaga, F. J., Balkcom, K. S., Price, A. J., 2005. Effects of rolling/crimping rye direction and different row-cleaning attachments on cotton emergence and yield. Proc. 27th Southern Conservation Tillage Conf., 169-177.

Laflen, J.M., M. Amemya, E.A. Hinz, 1981. Measuring Crop Residue Cover. In: Journal Soil and Water Conservation 36, 341-343.

Reeder, R., 2001. Maximizing Performance in Conservation Tillage Systems – an Overview. ASAE Meeting Paper No. 021134. St. Joseph, Mich. ASAE.

Shelton, D., R. Kanable, P. Jasa, 1993. Estimating Percent Residue Cover Using the Line-Transect Method. NebGuide G93-1133, https://digitalcommons.unl.edu/cgi/viewcontent.cgi?article=1779&context=extensionhist University of Nebraska Cooperative Extension, Lincoln.

Way, T. R., T. S. Kornecki, H. Tewolde, 2018. Planter Closing Wheel Effects on Cotton Emergence in a Conservation Tillage System. Applied Engineering in Agriculture Vol. 34(1): 177-186 , American Society of Agricultural and Biological Engineers.

A New Paradigm in Biosystems Engineering: Technology-4-Ecology Based Agriculture

Fatima-Zahra Abou Eddahab Burke [a,*], Marjolein Derks[·], Niels Anten[·], Bram Bos[·], Yvette de Haas [·], Jan de Jong[·], Anja Dieleman[·], Arnout Fischer[·], Jan Kamp[·], Tamas Keviczky[·], Haris Khan[·], Eldert van Henten[·], Dook van Mechelen[·], Wouter-Jan Schouten[b], and Peter Groot Koerkamp[·]

[a] Wageningen University and Research, Wageningen, The Netherlands
[b] TiFN Food & Nutrition, Wageningen, The Netherlands
[c] Eindhoven University of Technology, Eindhoven, The Netherlands
[c] Delft University of Technology, Delft, The Netherlands
[d] University of Twente, The Netherlands
* Corresponding author. Email: Fatima-zahra.aboueddahab-burke@wur.nl

Abstract

Agricultural production worldwide is facing many challenges to be able to achieve the UN Sustainability Development Goals and international agreements with respect to environment, labour, and society. Our investigation revealed that further optimization of current farming practices with precision agriculture (PA) and precision livestock farming (PLF) technologies is insufficient to meet these challenges. Therefore, a paradigm shift is required for building the next-generation agricultural production systems that are (i) sustainable, (ii) circular, and (iii) regenerative. The Synergia research program, where this study takes place, addresses this transition through our new concept of 'Technology-4-Ecology-based Agriculture' (T4E-Agriculture) in the Netherlands. This concept implies that future agricultural systems have to (i) rely on natural processes as driver for agricultural ecosystems and primary productivity; (ii) be able to sense traits by focusing on following biological production processes instead of momentary states, and on biological and ecological traits in the systems instead of production traits and problem indicators only; (iii) build models based on the understanding of the underlying biological & ecological processes; and (iv) include control and management functions that focus on prevention of problems, and make smart use of biological diversity and ecological complexity. With this novel approach we are not opposing high tech to nature-based production, in the opposite, we are exploring how current and future farming technologies can enable and support truly ecology-based farming systems. This approach will be developed and validated within the Synergia research program in building next-generation (i) horticulture, (ii) dairy and (iii) arable farming systems.

Keywords: Agricultural production, Sustainability, Next-generation farming, Ecology-based agriculture, Biological process.

1. Introduction

The ultimate goal of agricultural production is not only to produce food but also to increase the economic output of farming systems and the sustainable development of agriculture, and to keep a win-win balance between the economic and the environmental aspects of ecosystems (Gao et al., 2019). For it to be successful, agriculture nowadays has to be sustainable in order to protect the environment, to expand the Earth's natural resource base, as well as to maintain and improve soil fertility. Combining agriculture and sustainability is challenging, as it requires balancing between economic, environmental, and social goals. Also, it requires the support of major institutions and all relevant stakeholders in the economy and society and the consideration of the present generations' needs without compromising the capacity of future ones to meet their own needs (Ristić et al., 2017). Over the last decades, a lot of attention has been given to find solutions and to build systems and societies that meet the UN Sustainability Development Goals. Unfortunately, agriculture is struggling in the process of achieving these goals. The challenges are divided into three overlapping categories: (i) environmental, (ii) labour, and (iii) societal challenges. The first one includes mainly depletion of scarce resources, global warming, acidification and eutrophication caused by nutrients losses, and biodiversity loss. The second category includes the (un)availability of skilled workers. Finally, the third one is about consumer and societal acceptance of novel technologies and production methods. Even though the Dutch agricultural sector is often seen as successful, due to its worldwide leading position in arable, animal and horticultural production, it is also facing these challenges. The high level of inputs and intensive management practices lead to depletion of resources, environmental pollution and biodiversity loss, deterioration of soil quality, and risk for food quality and safety. The sector also lacks entrepreneurs in agriculture (Simamora, 2015). To maintain its position, the Dutch agricultural production sector needs to balance sustainable development goals and economic goals like farmers' income. The Netherlands as well as the countries following the same path, need to transition towards environmentally benign, circular production systems with strongly reduced dependency on inputs and low environmental impacts, which are resilient to biotic and abiotic stresses, and that promote rather than endanger soil and water quality, carbon sequestration

and biodiversity (Dagevos & Lauwere, 2021). At the same time, such agricultural systems must be technically feasible, and provide sufficient income to farmers, while ensuring affordable healthy food. A gradual adaptation of the current systems generally only marginally improves the environmental performance, and often introduces trade-offs, e.g. higher costs, reduced animal welfare, and shifts of environmental impacts. This calls for a more radical system change (Zuev & Nitschke, 2020).

2. Setting the stage:

Organic farming and regenerative farming are considered ecological alternatives to the current traditional or conventional agriculture. These systems involve the use of biological diversity (intercropping, genetically diverse cattle herds, etc.), the use of natural ecosystem functions (natural enemies of pests, etc.), and precision farming (improved process control, milking robots, etc.). On the one hand, regenerative farming aims at capturing carbon in soil and aboveground biomass and altering atmospheric accumulation. It offers increased yields, resilience to climate instability, and higher health and vitality for farming and ranching communities (Schreefel et al., 2020). It focuses on the soil and land, its health and water, rather than on the methods and inputs (Burns, 2021). On the other hand, the essential concept of organic farming is "give back to nature" (Nagar et al., 2020). It depends on crop rotations, use of crop residues, animal manures, legumes, green manures and biofertilizers, and avoids using synthetically compounded fertilizers, pesticides and growth regulators. Research reports that both types of systems have great promise, since they demonstrated a decrease in resources use and diseases (Zhang et al., 2019). However, adoption of such systems causes an increase in biological and farming complexity (Brzozowski & Mazourek, 2018). Their implementation is hampered because (i) the biological and ecological processes and factors that determine high system performance and the role of biodiversity with reduced external inputs are still poorly understood, (ii) the required (agricultural) technology is absent or existing technology is poorly adapted to future systems, (iii) current farming systems, practices and elements (plants, crops and animals) have been developed for maximum yields, and not for an inclusive environmental performance, (iv) the current innovation capacity is fully deployed for optimising current systems and their configuration (e.g. monoculture, farm specialisation and economic scale effects), and (v) the financial (for farmers and tech suppliers) and transformational risks (e.g. acceptance by various parties) for radical new systems are too high. Accordingly, a lock-in is created leading to a non-development of high-yielding and ecology-based alternatives. This phenomenon as well as the challenges previously listed are a wake-up call to urgently develop a new farming approach or concept to overcome the lock-in. In this study we focus on building an innovative farming approach needed for the successful realization of the next-generation ecology-based farming systems. This work is part of a broad project "Synergia" that aims at building the fundamental knowledge base, and to provide the technological methods and tools, and human capacities to create opportunities and breakthroughs needed to evolve to a new generation of ecology-based sustainable production systems that are supported and enhanced by smart tailored technology. To achieve these goals, the project is composed of interdisciplinary and multidisciplinary academic and industrial partners from natural, technological and social sciences, working together to achieve promising solutions that will create a revolution in farming practices.

3. Organisation of the paper:

In the rest of the paper, we provide the reasoning model for the literature study as well as details about the state of the art in the broad field of sustainable farming approaches and outline our critical thinking which supports the development of a novel farming concept called 'Technology-4-Ecology-based agriculture' (T4E-agriculture). In Section 4, organisation of the research, we explain our reasoning and our methodological framing needed to determine our domains of interests and conducting the literature study. In Section 5, major findings, we provide the outcomes of the literature study, namely the challenges of current agricultural systems and the elements needed to be considered in the transition towards ecology-based farming systems. In Section 6, discussion and conclusions, based on critically analysing the outcomes, we introduce our T4E-agriculture concept. We list the principles of the novel concept, and we present the implications of the findings. In this section, we present our conclusions regarding what needs to be done to find solutions for the issues and deficiencies in agricultural systems, and provide a short description of our project, Synergia, as well as our long-term goals.

4. Organisation of the research

The applied methodological framework for the literature study is the research in design context (RDC) (Horváth, 2007). The goal of RDC is to explore, describe, understand, and explain design related phenomena, which occur naturally related to, or are partly or entirely created by design. Through analysis of monodisciplinary literature and finding similarities, it aims at creating insights, understanding, and predictions. It relies mainly on the knowledge of background disciplines. RDC concentrates on building and providing theories, which add to the disciplinary knowledge of design. The application of RDC is done in 4 steps: (i) divide the research topic into several interconnected domains of interest, (ii) aggregate the knowledge of each domain, (iii) discuss the findings of the aggregation, and (iv) synthesize the findings to generate knowledge. The first two steps are of an explorative nature and the last two steps are of a confirmative one (Horváth, 2007).

Based on the principles of the RDC methodology, both the explorative and confirmative steps are applied to the literature around sustainable agriculture. In the explorative phase, we organised the literature study into sequential but interrelated activities. The first activity of this phase is a shallow exploration that identifies the most relevant domains of knowledge for the study. Based on a wide range of keywords (Sustainable farming, sustainable agriculture, farming practices), a topographic landscape of related publications is developed. The second step of the exploration is a deep exploration in which we collected several hundred of relevant publications and intensively analysed various sources of knowledge. In the confirmative stage, we analysed the synthesized findings in the context of ecology-based farming systems. This analysis identified limitations and opportunities of existing farming systems. Based on the limitations, we identified the concepts needed to be followed to develop next-generation ecology-based farming systems.

The first part of the literature study was referred to as shallow exploration. It is conducted to identify the most relevant domains of knowledge for the study. Based on a wide range of keywords we developed a topographic landscape of the related publications. The objective is not only to show the distribution of the clusters of keyword-related publications but also the peaks and the plains of these clusters. Figure 1 shows the clustering resulting from keyword-based mapping of the relevant literature. The graphical mosaic of images is built using VOSviewer. Figure 1 shows not only the neighbouring (semantically related) keywords but also the distance between them as they appear in the literature. The colours indicate the frequency of the occurrence of keywords (i.e. the formation of peaks). The most frequently occurring keywords are shown in red and dark orange, and the less frequent ones are shown in green and light blue. The visual representation generated by the software application made us recognize six major clusters of papers. In a kind of transitive ordering, these were formulated as follows: (i) biological aspects, (ii) development (iii) control, (iv) ecological processes, (v) concept, and (vi) farming systems. (see Figure 1). These clusters were used as descriptors of the main domains of interest in the detailed literature study (deep exploration).
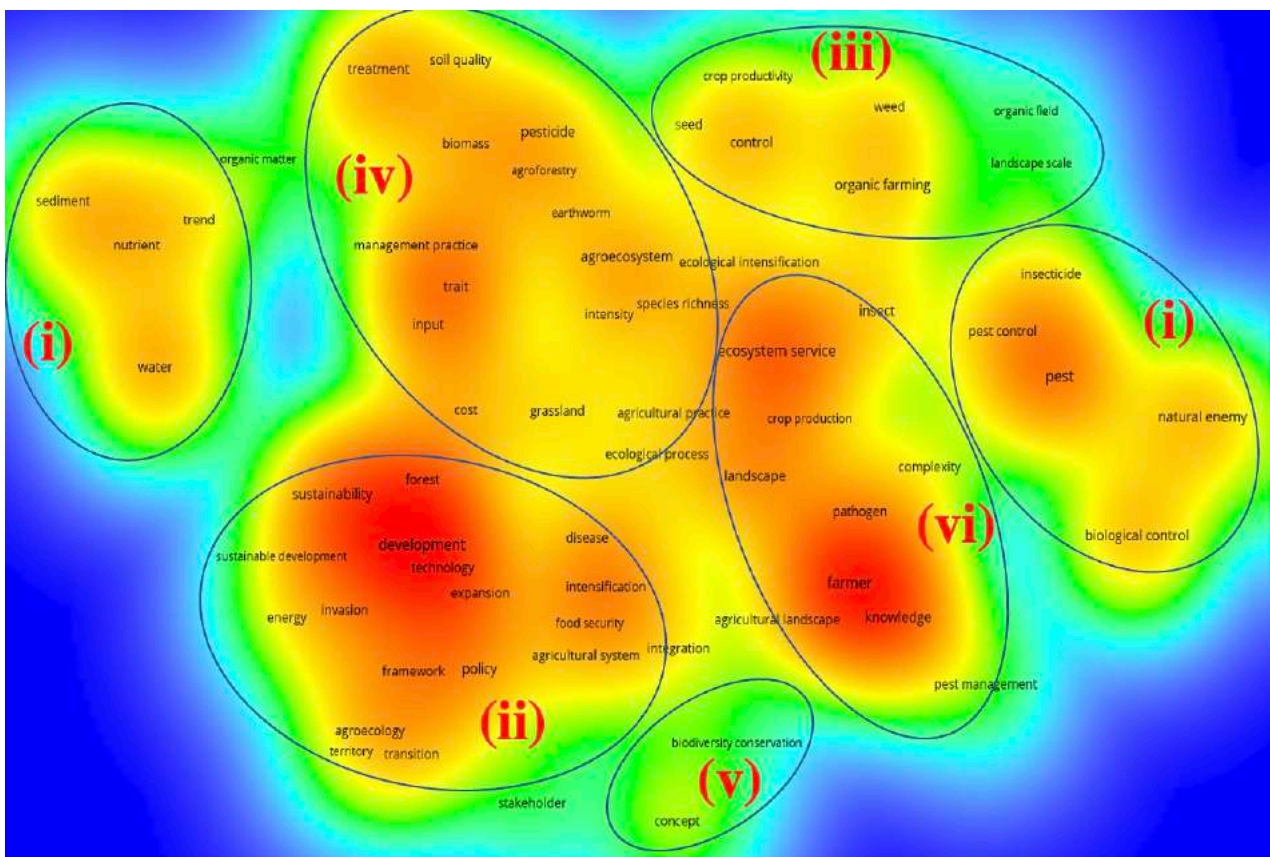
Figure 1: Occurrence of keywords in the literature – result from the sallow exploration

In the second phase of the literature study, called deep exploration, various sources such as subscription-based and open access journals, conference proceedings, web repositories, and professional publications were searched, and several hundred relevant publications were collected. The findings made it possible to define further relevant key terms on a deeper level (not presented in Figure 1). The second phase was also used to quantitatively characterize the

interrelationships found. If two terms were used in the same document, then there is a line between them, and the thickness of the line indicates how frequently they occur. In other words, the thick lines refer to combinations of terms that appear in multiple papers, whereas the thin lines refer to combinations that rarely appear in the studied publications. The connectivity diagram in Figure 2 shows that some domains that different independent topics are interconnected which reveals the multicollinearity aspect of the study. In addition, the diagram not only casts light on the complexity of the completed study but also indicates which key terms cannot be studied separately because tightly interconnectedness in the publications.
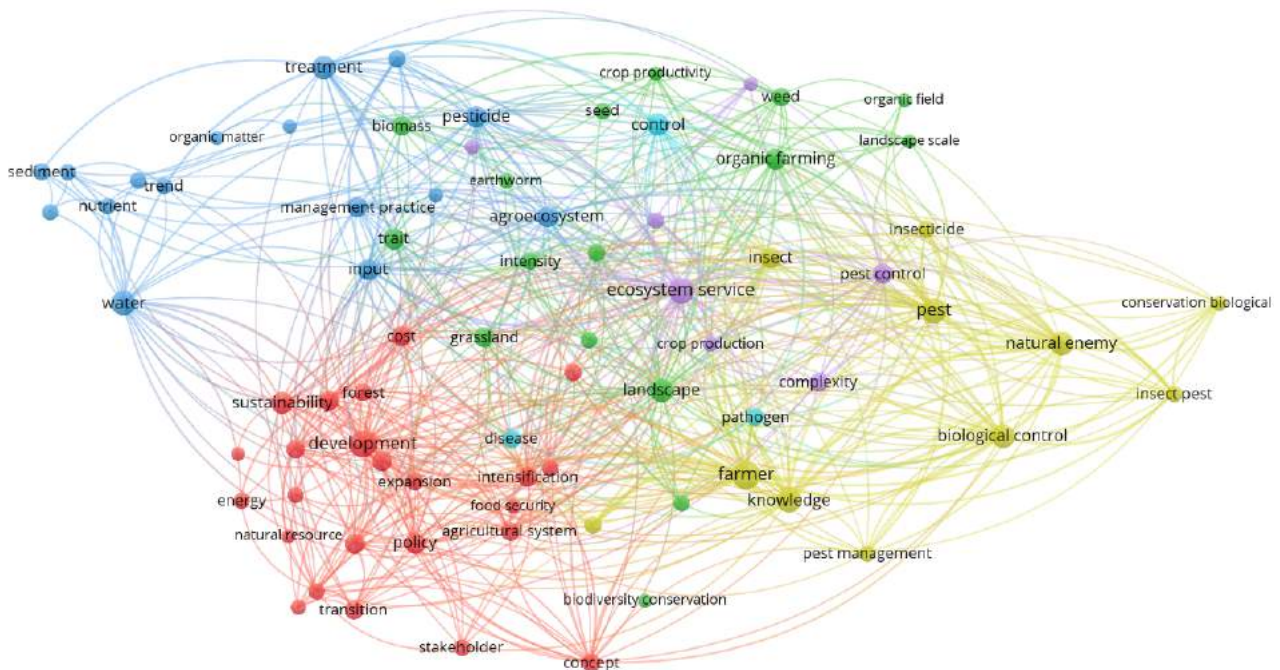
Figure 2: Connectivity graph of keywords

The set of information gained from the qualitative part of the literature study is used to develop a reasoning model for the quantitative part of the study. This part is the confirmative phase of the study. It focuses on interpreting the findings and the disclosed semantic relationships. The reasoning model is shown in Figure 3. Only the first-level key terms are indicated, whereas, the study was actually done with keywords of the second decomposition level such as farming practices (horticulture, dairy and arable farming), sensing, technological enablers, learning, disease control, weed management, biodiversity, soil protection, ecosystem etc. All the keywords were investigated in the context of sustainability. The considered papers were published at different times, ranging from 2010 until 2021. An important observation was that the domains of interest that were identified by the first level of key terms are in implicative =? relationships with each other.

The next section of this paper reviews the state of the art in the broad field of sustainable farming approaches and concepts. The reasoning model presented in Figure 3 is used to investigate the domains of interest, there connections and to what extend they influence each other.
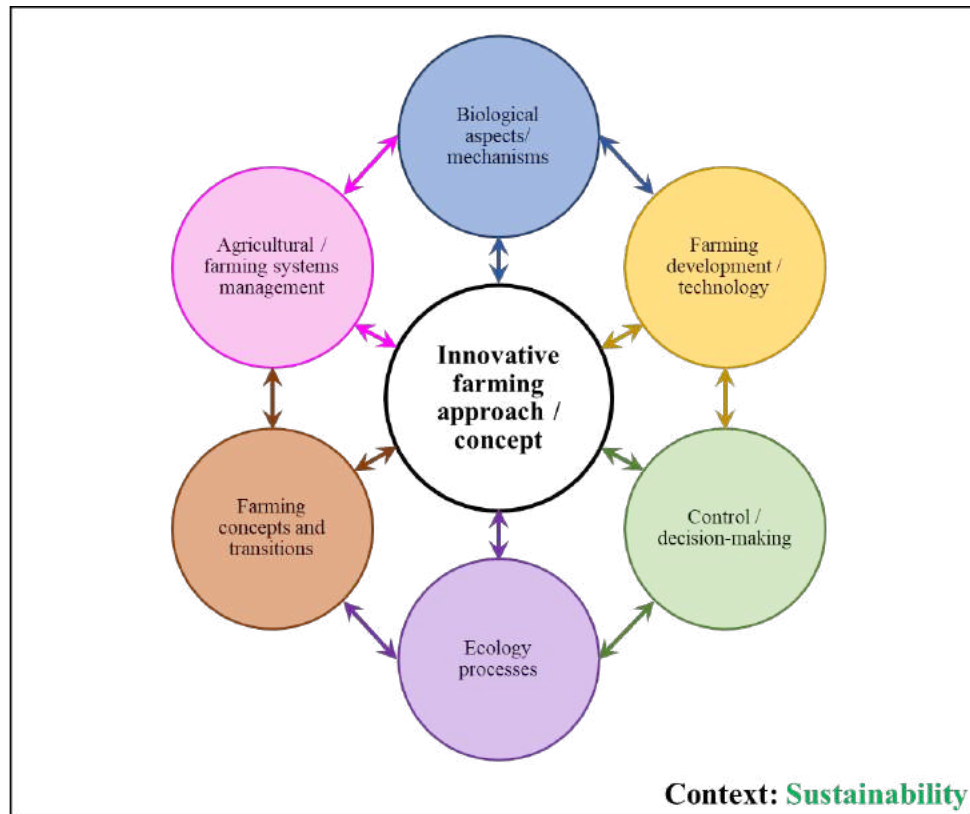
Figure 3: Reasoning model of the literature study

5. Major findings

The interconnectedness presented in our reasoning model was also found in the literature. Understanding the biological and the ecological processes that drive agricultural production systems and how these link to technological innovation, is crucial to the transition to more sustainable farming systems (Oberč & Arroyo Schnell, 2020) (David & Cofini, 2020). The literature revealed the connectedness within the topic but also its complexity, since various challenges were identified and need to be answered in the future. The major ones reported out there are crop productivity, soil nutrient levels, smart irrigation systems and crop monitoring (Tapakire & Patil, 2019). Other challenges are caused by climate change, such as droughts, floods, pests and pathogens that access new climatic regions, while others are related to the lack of labour force (Robaey & Sandin, 2021).

In agriculture, biological research (e.g. crop/animal science) focuses mainly on increasing productivity of conventional homogeneous systems through optimising external inputs (Xie et al., 2019). However, the sustainable functioning of novel low input systems will critically depend on understanding biological processes that autonomously drive performance and stability (Matlob et al., 2019) (Fateh et al., 2021). These processes and their underlying mechanisms are poorly understood (Weijers et al., 2001). The way these processes drive performance of crop and animal systems at a relevant scale is also challenging, because of (i) the spatial and temporal variation in e.g. climatic or biotic conditions (Weltzin, 2020), (ii) the high level of non-uniformity in agricultural systems (Hebrinck & Oostindie, 2018) (Oltenacu & Allen, 2019), and (iii) the complex interactions that exist between different processes at such higher integration levels (Hazard et al., 2018). Addressing these 3 challenges requires the study and development of ecology-based farming systems that has not been adequately set up (Vargas-Hernández & Domené-Painenao, 2021).

The literature investigation revealed that the adoption of ecology-based systems is very much needed but, in the meantime, hampered by the fact that their complexity makes their management and control difficult, labour intensive, and costly, let alone that appropriate technology is currently mostly lacking (Scholberg et al., 2010). Firstly, the key for the next generation of novel ecology-based agricultural systems is the use of high-tech sensors and Artificial Intelligence to monitor, quantify and understand individual plants and animals and their variability, and deal with the complexity of integrating drivers for system operation (Bogomolov, 2021). While sensing and monitoring technology is readily evolving, adapting such technology to the unpredictability and variation of living systems poses major challenges (Rogachev & Melikhova, 2020). Secondly, the management and control of the bio-physical processes (e.g.

growing conditions), identifying and understanding the biological environment (with plants and animals) and ecology-based robotic manipulation of operations, is a huge challenge in environments that are modestly defined and structured (Anglade et al., 2018). Another major scientific challenge that we determined internally based on discussion between project partners from different domains of expertise, consists of the understanding of how to organise and manage a transition process from current to future systems that are more sustainable and overcome the lock-in resulting from limited (economic) innovation capacity (restrictions to equipment and production costs) and corresponding social aspects: acceptance by farmers, business models, appreciation by other stakeholders in the chain and system transition as a whole.

It might seem a bit surprising, but worldwide trends show that conventional agriculture is still preferred, regardless of the considerable growth of ecology-based agriculture in the last few years (Siegel & Lima, 2020). The ongoing development of ecology-based agriculture, also called ecological agriculture, relies on (i) the rise of demand for organic products, (ii) the restructuring commercialization and the organization of family farmers, as well as on (iii) creating public policies with this objective (Karnopp & Weber, 2020). A successful ecological agriculture requires efforts from technical and managerial stakeholders to ensure that the concept is understood and that their corresponding duties work together towards the same objective (He, 2019). In addition, an effective development of sustainable development depends on adequate and combined development of production, industrialization and commercialization of products, as well as the development of forms of organization, the engagement of social actors and especially society planning regarding its future (Karnopp & Weber, 2020).

The concept of ecology-based agriculture is mainly based on philosophical principles about nature instead of biological aspects (Stanciu et al., 2019). This means that the concept is on a high level of abstraction and cannot yet be reproduced in a concrete farming application. It focuses on the description of the perfect agricultural system rather than on the specification of the biological aspects to be taken into consideration and how to achieve a more ecological agriculture system. No scientific evidence supports the abandonment use of synthetic mineral fertilizers as nutrients for crops, and the scientific community is bound to follow rigorous scientific criteria in the analysis of ecological agricultural production (Kirchmann, 2019). Accordingly, a successful sustainable farming need to consider concrete biological aspects rather than philosophical ones that are ideal but lack of concreteness and applicability. In order to keep up with the advances in technology, and to allow effective detection (e.g. crops images) and output identification information in real time that have a significant input on the whole production system, the ecological agricultural technologies need to be smart, including some deep learning mechanisms (Tian et al., 2019). These new technologies need to integrate sensing technologies, and data collection and monitoring capabilities in order to provide decision makers with effective management options at useful spatial and temporal scales for allowing more informed decisions about productivity while reducing environmental burdens (Zaks & Kucharik, 2011).

6. Discussion and conclusions

By putting together all the pieces of the puzzle elaborated on above, we can state that a next-generation farming systems need to be established based on a novel concept. This concept stands on two main pillars: the understanding of biological and ecological processes and the development of / technological learning technologies /. This implies an ecology-based approach to agriculture and agrotechnological development. In this approach technology is developed around ecological and biological functions and sustains these in a production context. This entails that agricultural systems are designed and operated in such a way that ecological processes are used, and their favourable and resilient functioning derives from ecological processes rather than from high levels of (chemical) inputs and control in homogenized systems. This new and unique approach is enabled by recent developments in biological and farming research, as well as in the technological domain and the management and control of complex farming systems. This approach reverses the dominant paradigm of technology over biology in current conventional farming systems. Technology is not the target anymore; it is a means to support and enable biological and ecological processes and farming. The target is to move towards ecology-based sustainable production systems. Therefore, we name it 'Technology-4-Ecology-based Agriculture'. Based on the outcomes of the literature and our critical exploration of the results, we characterize the innovative multidisciplinary T4E-agriculture concept as follow:

1. a basic reliance on natural ecological processes that inherently drive the functioning of agricultural ecosystems;
2. an adequate understanding of the biological mechanisms that determine these processes at the fundamental level;
3. sensing systems and data/signal interpretation are adapted to the monitoring of biological processes and help the understanding of these processes and associated ecosystem functioning;
4. management and human control actions and machines are attuned to the natural functioning of these systems;
5. technological systems that are adapted to natural processes or can adapt to them through self-learning;
6. a systems approach;

7. engineering design that starts and works with biological functionalities, rather than taming complexity, diversity and unpredictability with technical controls.

The T4E-agriculture concept is the base of the Synergia research program. The overall approach of this research program is based on an interdisciplinary cooperation between natural sciences and social sciences to develop high-tech and socially acceptable systems and materials along with new ICT applications, making the agricultural and food sector better adapted to future societal challenges. To this end, we take a multi-disciplinary approach, T4E-agriculture concept, that integrates knowledge and methods from the life sciences, technological sciences and social sciences. We provide novel basic knowledge, methods and tools that form the base for both integrated solutions for production systems, as well as sociotechnical scenarios for the transition towards these systems. We will do this for three use-cases representing the variety of agricultural systems in the Netherlands: greenhouse horticulture, dairy production and field crops. The fundamental research of this program will bring technological, ecological and social knowledge and principles in the agricultural domain, and solutions and systems will be developed in the three applied use-cases. As mentioned previously, the approach and set-up of this project are to organise the generation and integration of fundamental knowledge from both life sciences and social sciences, and key engineering technologies for a sustainable and ecology-based agriculture. We aim for: (i) Ecology-based solutions and sustainability strategies that are supported by technological solutions. This means reversing the dominant paradigm of technology over biology in farming systems; (ii) The next big step in the processes of precision farming (sensing, decision making and actuation) from field/plot and herd level to individual plant and animal level; and (iii) System integration and co-evolution of knowledge and insights from life sciences with social sciences and technological innovation (co-design).

Acknowledgements

References

Anglade, J., Godfroy, M., & Coquil, X. (2018). A device for sharing knowledge and experiences on experimental farm station to sustain the agroecological transition. In *Thirteen European Farming Systems Conference*, 1-5.

Bogomolov, A. (2021). Monitoring and diagnostics of forest condition using sound sensors and artificial intelligence technologies. In *IOP Conference Series: Earth and Environmental Science*. IOP Publishing. 678 (1), 012005.

Brzozowski, L., & Mazourek, M. (2018). A sustainable agricultural future relies on the transition to organic agroecological pest management. Sustainability, 10(6), 2023.

Burns, E. A. (2021). Placing regenerative farming on environmental educators' horizons. Australian Journal of Environmental Education, 37(1), 29-39.

Dagevos, H., & Lauwere, C. C. B. M. (2021). Circular agriculture: perceptions and practices of Dutch farmers. Sustainability 2021, 13, 1282.

David, S., & Cofini, F. (2020). MODULE 10: Extension and advisory approaches and methods. Agricultural extension in transition worldwide: Policies and strategies for reform, 177.

Fateh, H., Toube, A., & Gholipuri, A. Q. (2021). Wheat physiological traits response in standard and ecological agricultural systems. Earth Sciences Research Journal, 25(1), 131-136.

Gao, F., Li, B., Ren, B., Zhao, B., Liu, P., & Zhang, J. (2019). Effects of residue management strategies on greenhouse gases and yield under double cropping of winter wheat and summer maize. Science of the Total Environment, 687, 1138-1146.

Hazard, L., Steyaert, P., Martin, G., Couix, N., Navas, M. L., Duru, M., ... & Labatut, J. (2018). Mutual learning between researchers and farmers during implementation of scientific principles for sustainable development: the case of biodiversity-based agriculture. Sustainability Science, 13(2), 517-530.

He, X. (2019). *Analysis on the Development Path of Ecological Agriculture Economy from the Perspective of Sustainable Development*.

Hebinck, P., & Oostindie, H. (2018). Performing food and nutritional security in Europe: claims, promises and limitations. Food Security, 10(6), 1311-1324.

Horváth, I. (2007). Comparison of three methodological approaches of design research. In *Sixteenth International Conference on Engineering Design,* Paris, France, 361-362.

Karnopp, E., & Weber, J. M. (2020). Agroecologia: experiência em construção no contexto do Desenvolvimento Regional. Ágora, 22(1), 4-21.

Kirchmann, H. (2019). Why organic farming is not the way forward. Outlook on Agriculture, 48(1), 22-27.

Matloob, A., Safdar, M. E., Abbas, T., Aslam, F., Khaliq, A., Tanveer, A., ... & Chadhar, A. R. (2019). Challenges and prospects for weed management in Pakistan: A review. Crop Protection, 104724.

Nagar, R., Trivedi, S. K., Nagar, D., & Karnawat, M. (2020). Organic farming and its future. Biotica Research Today, 2(5 Spl.), 177-179.

Oberč, B. P., & Arroyo Schnell, A. (2020). Approaches to sustainable agriculture. Exploring the pathways.

Oltenacu, P. A., & Allen, M. S. (2019). Resource-cultural energy requirements of the dairy. Handbook of Energy Utilization in Agriculture, 363.

Ristić, L., Milijić, N., & Durkalić, D. (2017). Sustainable agricultural development in modern conditions. In *Seventh International Symposium on Environmental and Material Flow Management-EMFM*, 83-98.

Robaey, Z. H., & Sandin, P. (2021). An agent-centred approach to innovation for 21st century challenges of agriculture. Justice and Food Security in a Changing Climate. Wageningen Academic Publishers, 105-120.

Rogachev, A., & Melikhova, E. (2020). *Remote Sensing, Monitoring and Classification of Agricultural Land Using Artificial Neural Networks*. EasyChair.

Siegel, K. M., & Lima, M. G. B. (2020). When international sustainability frameworks encounter domestic politics: The sustainable development goals and agri-food governance in South America. World Development, 135, 105053.

Simamora, L. (2015). The role of agriculture based on entrepreneurship: contributes to economic development. In *Ninth International Conferences, Bulletin of Monetary Economics and Banking*, 1-5.

Schreefel, L., Schulte, R. P. O., de Boer, I. J. M., Schrijver, A. P., & van Zanten, H. H. E. (2020). Regenerative agriculture–the soil is the base. Global Food Security, *26*, 100404.

Scholberg, J. M., Dogliotti, S., Zotarelli, L., Cherr, C. M., Leoni, C., & Rossing, W. A. (2010). Cover crops in agrosystems: innovations and applications. Genetic Engineering, Biofertilisation, Soil Quality and Organic Farming, Springer, Dordrecht, 59-97.

Stanciu, S., Sârbu, R., Bichescu, C. I., & Züngün, D. (2019). Organic production in Romania: Perspectives in European context. New Trends in Sustainable Business and Consumption, 813.

Tapakire, B. A., & Patil, M. M. (2019). IoT Based Smart Agriculture Using Thingspeak. International Journal Of Engineering Research & Technology (IJERT), 8(12), 270-274.

Tian, M., Chen, H., & Wang, Q. (2019). Detection and recognition of flower image based on ssd network in video stream. Journal of Physics: Conference Series, 1237 (3), 032045.

Vargas-Hernández, J. G., & Domené-Painenao, O. E. (2021). The implications of the new geography framework of urban agro-ecology on urban planning. International Journal of Environmental Sustainability and Green Technologies, 12(1), 1-25.

Weijers, E. P., Even, A., Kos, G. P. A., Groot, A. T. J., Erisman, J. W., ten Brink, H. M., ... & van der Klein, C. A. M. (2001). *Particulate Matter in Urban Air: Health Risks, Instrumentation and Measurements and Political Awareness*. ECN-Clean Fossil Fuels Air Quality.

Weltzin, J. F., Betancourt, J. L., Cook, B. I., Crimmins, T. M., Enquist, C. A., Gerst, M. D., ... & Running, S. W. (2020). Seasonality of biological and physical systems as indicators of climatic variation and change. Climatic Change, 163(4), 1755-1771.

Xie, H., Huang, Y., Chen, Q., Zhang, Y., & Wu, Q. (2019). Prospects for agricultural sustainable intensification: A review of research. Land, 8(11), 157.

Zaks, D. P., & Kucharik, C. J. (2011). Data and monitoring needs for a more ecological agriculture. Environmental Research Letters, 6(1), 014017.

Zhang, C., Dong, Y., Tang, L., Zheng, Y., Makowski, D., Yu, Y., ... & van der Werf, W. (2019). Intercropping cereals with faba bean reduces plant disease incidence regardless of fertilizer input; a meta-analysis. European Journal of Plant Pathology, 154(4), 931-942.

Zuev, D., & Nitschke, L. (2020). Mobilities and (un) sustainability. IHandbook of Research Methods and Applications for Mobilities. Edward Elgar Publishing.

Towards Integrated Mechanised Management of Olive Farms

Sergio Bayano-Tejero[a], Fernando Aragon-Rodriguez[a], Jesus Gil-Ribes[a], Gregorio L. Blanco-Roldán[a], Sergio Castro-Garcia[a], Rafael R. Sola-Guirado[a*]

[a] Research Group AGR126. Mechanization and Rural Techology. University of Cordoba, Cordoba, 14071, Spain

* Corresponding author. Email: ir2sogur@uco.es

1. Introduction

The olive grove is currently undergoing a transition towards greater technification with a higher degree of mechanisation. Olive growing has spread outside the Mediterranean basin to other areas of the world with similar weather (Fernández-Escobar et al., 2013) and competes in a more global environment. The traditional cultivation system, with one or more trees, large tree size and low density (less than 200 trees ha-1) is being replaced by other more intensive systems, but at present, the majority of the world's olive groves (70% of the total) continue to have a configuration that is very difficult to mechanise, being relegated to market entry through differentiation. Although the choice of the planting system depends on many factors (Tous et al., 2014), the most important factor is economic, and in this sense, harvesting operations are the higher-cost (AEMO, 2020), so the trend is to an integrated management of mechanisation to increase competitiveness.

The intensification of traditional grove systems in the 1970s began to spread with the appearance of the trunk shaker, the first mass mechanized harvesting system, whose principle is based on the application of a vibration force to the trunk that is transmitted to the branches and then to the fruit, causing it is detachment (Sola-Guirado et al., 2014). This defined the morphology of the trees, with olive trees with a formation and architecture favourable to the operation, and the design of the plantation, increasing the tree density up to 400 trees ha^{-1}. However, as tree density increases, the weaknesses of these systems appear due to their operation is discontinuous and requires a lot of manual labour for the logistics of the operation, reducing their efficiency, being viable for small farms and without a very high density of trees (Ravetti, 2014). In this respect, new improvements are being introduced for the automation of the operation (Colmenero-Martinez et al., 2018), which continue to advance and improve their technology. Table olive plantations are more difficult to mechanise, as they are more traditional than olive oil plantations. They are usually harvested by hand (Rejano et al., 2010), mainly due to the damage caused by mechanised harvesting systems to the fruit. As they are at a more immature stage than fruits destined for oil, they are more susceptible to damage (Segovia-Bravo et al., 2011) and more difficult to detach, decreasing the efficiency in the use of mechanised harvesting (Kouraba et al., 2004).

Another type of intensification on a larger scale was encouraged by the implementation of continuous systems based on straddle harvesters for narrow hedgerows coming from the vineyard. This machinery advances over the row of trees that are introduced through a tunnel that compresses the canopy and in which a forced vibration is applied through the oscillatory movement of two rows of opposing rods (Sola-Guirado et al., 2019). To adopt this mechanised harvesting system, it has been necessary to redesign the plantations, changing the density (1200-2000 trees ha-1) and tree formation with the aim of closing the canopy to form a continuous hedge. This system allows a significant reduction in the labour required for harvesting and a rapid entry into production; however, it is limited by the crop vigour, the size of the farms and the slope of the plot (Fernández-Escobar et al., 2013) and, in addition, the cost of implementation is much higher than other systems, with these restrictions being compensated in certain situations by lower production costs (AEMO, 2020).

An intermediate solution for mechanisation is the lateral canopy shaker for wide hedgerow, which has a head with rods that generate an oscillating movement in the canopy of the tree. This vibration is transmitted by the contact of the rods with the branches, causing the fruit detachment. Some of these canopy shaking systems only cause the fruit detchament, so they cannot be called harvesters. However, canopy shakers can be designed, in addition to detaching the fruit, can intercept it and manage it carrying out the cleaning, storage and transport. These systems have great potential to be implemented in an intensive olive grove with large canopies, which would allow a higher planting density than a normal intensive grove and more vigorous canopies than a super-intensive grove (Sola-Guirado et al., 2017). Canopy shaker offer greater flexibility in their use in different olive orchards compared to straddle harvesters and can be used in a wide variety of crops and different plot conditions; however, efficiency decreases compared to straddle harvesters (Ravetti, 2014).

When the fruit arrives at the industry, batches from different locations converge and are mixed during the sorting process, mainly in the table olive industry. This can lead to traceability problems and loss of information in the value chain. To connect mechanised harvesting with the industry, the fruit must be sorted according to the qualities demanded in the field. The use of sorting prototypes in the field allows us to homogenise and discard those fruits that are not suitable for further industrial processing, either in the processing factory or in the oil mills, depending on the destination of the fruit, increasing the efficiency of the system. In this way, an integrated approach can be used to obtain high levels

of efficiency in the production chain, while maintaining product traceability.

To achieve this integrated management, it is also necessary to coordinate all the operations involved in olive growing. However, in the olive grove, the processes are not usually connected, but are carried out individually as independent or discontinuous tasks. The data generated in the operations are not registered or are isolated without exchange data with other operations. Harvesting machines can generate data when carrying out their operation by recording information at a critical stage for the fruit such as harvesting, providing great value and facilitating interconnection with other systems. This requires the acceptance of technologies already implemented outside the agricultural sector, but that will provide many benefits. The implementation of sensors and monitoring systems allows for a more exhaustive control of the machinery and more adequate maintenance, minimising breakdowns and, consequently, idle time. In addition, they allow relevant information to be obtained on the process being carried out. Among the most demanded systems in harvester machines for any crop are yield monitors. These systems consist of a sensor to measure continuous production, either by weight, volume, mass flow or grain impact (Qi Jiangtao et al., 2010), generating maps of spatial variability thanks to the georeferencing of the measurements. This provides information on areas with higher or lower yields and makes it possible to act accordingly by applying precision agriculture techniques in irrigation, fertilisation or phytosanitary (Suprem et al., 2013), among others. On the other hand, during harvesting, the fruit is unloaded into storage systems, generating batches that must be transported to the next management point. In order to keep track of each batch harvested during the management of the fruit, it is important to use some technology for its identification.

The information generated in the harvesting, as well as in the previous and subsequent operations, either in the field or in the industry facilities, build up the traceability or production history of the product. Nowadays, traceability is increasingly demanded by consumers and legislation to guarantee product quality and food safety. As regard quality, it is becoming increasingly common for machinery to sort the fruit by surface parameters (bruising, size and ripeness) (Dumanay et al., 2016), as this factor determines its economic value (Riquelme et al., 2008). Artificial intelligence allows these operations to be carried out easily and helps to separate and generate batches of high-quality fruit for sale at a better price, as well as to use the discarded fruit for other purposes or to sell second quality fruit at lower prices. All this information can be recorded, analysed and visualised. For this, Cloud Computing technology has proven to be able to adapt to the agricultural sector (Choudhary et al., 2016) and bring numerous advantages to the producer, industry and consumer, such as task efficiency, cost reduction, improved product quality and food safety (Bo & Wang, 2011).

In the Innolivar -Public Purchase of Innovation in its modality of Pre-commercial-, prototypes are being developed to detach the fruit, intercepting and storing it minimising olive bruising through a prototype based on a lateral canopy shaker. Later, is carried out a cleaning and sorting the fruit by morphology and/or quality in the field using adapted mobile sorters based on artificial vision systems. This work presents a methodology that allows the integral management of the mechanisation of an olive grove supported by the developments of the project. From harvesting to the arrival to the industry, a control of the batches of fruit and the information generated in each phase (harvesting - cleaning - sorting - transporting) is maintained by means of an application to interconnect field and industry.

2. Pilot proposal to implement integrated management.

The integrated management of mechanisation requires the use of different technologies to satisfy the requirements of each operation and ensure the recording of the relevant information throughout the production cycle. Among the necessary elements highlight the ECU (Electronic Control Unit) incorporated into the machinery used for field operations, for which a tractor is usually used. The ECU is responsible for centralising the information produced by the different elements installed, such as the implements, their sensors or the GPS (Global Positioning System). All this information flows through several communication protocols such as ISOBUS (International Standards Organization Binary Unit System), a standard communication protocol used to exchange information in a universal format between equipment from different manufacturers.

This information are interest variables measured by sensors in each operation carried out on the crop and which, thanks to their connection to the ECU, can be linked to the geographical coordinates. For example, it is important to record the product applied and the dose of a phytosanitary applications, or to record the weight of the batches of fruit in the case of harvesting, or the working times of the machinery used. Another interesting device are the display connected to the ECU which allow the farmer to interact and control the status of operations. To all this, it is necessary to add the data collection systems such as weather stations, sensors for irrigation, soil condition, etc. The information captured through these several sources can be recorded in a database hosted located on an on-premise server or in the cloud via a GPRS modem connected to the ECU. All this information volume is displayed to the farmer in real time via a web application where the representation of the information and its association to the spatial location has a great relevance for decision making. The cloud, shared with the other actors in the chain (fruit processing industry and the consumer) allows the entire supply chain to be managed. The spatial and temporal registration of the different operations carried

out on the crop provides great benefits in terms of work organisation and task optimisation, as well as the improvement in traceability, quality and food safety of the product.

A diagram of the interconnection between field and industry and the flow of information and fruit through the prototypes described can be checked in figure 1.
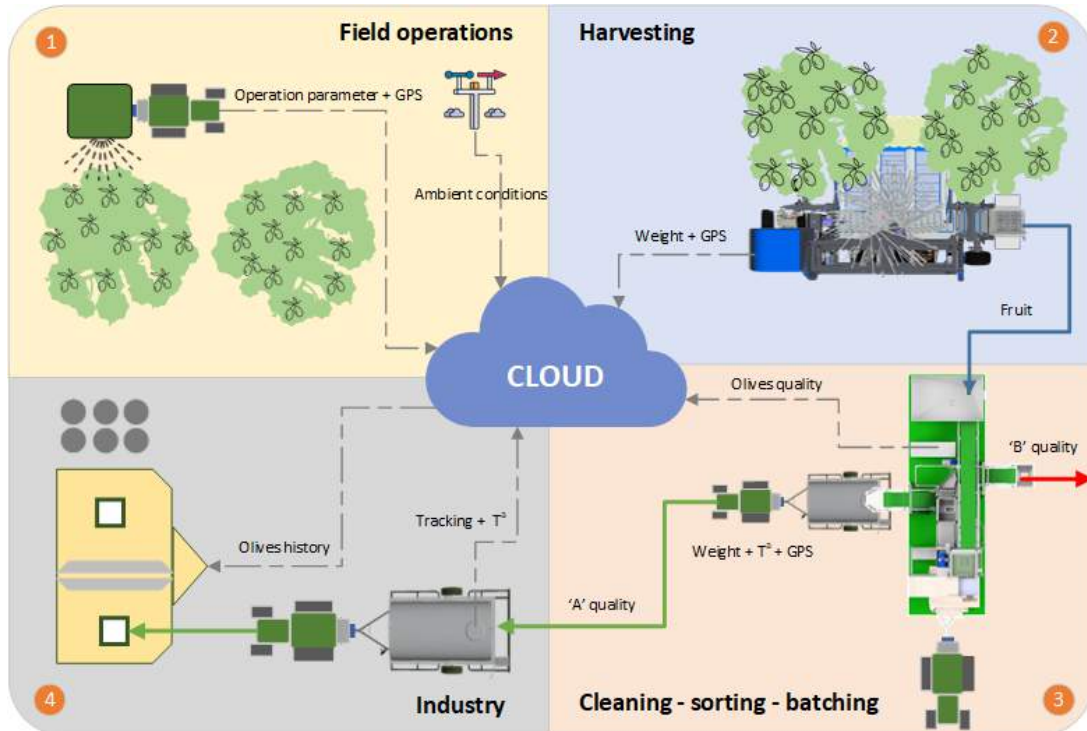
Figure 1. Olive grove, harvesting and industrial processing and information flow generated.

2.1. Field operations involved in olive grove.

Field operations are usually carried out with the help of a tractor to drive the machinery or to attach one implement to the power take-off. Among the most common operations are pruning, phytosanitary applications or fertiliser applications. The pruning is performed to control and improve olive grove yield and keep it healthy by removing unproductive or old branches or to adapt it to mechanisation (Castillo-Ruiz et al. 2016). Phytosanitary applications aim to control or eliminate pests and diseases to maintain the vitality and productivity of the olive tree. Fertilisers, on the other hand, help to improve yields and their quality. Currently, all these operations are neither digitalised nor properly recorded, beyond the field notebook that the farmer must complete according with current regulations, but which does not contain all the operations and inputs involved in the production cycle. There are applications available on the market for PC or smartphones to keeping a record of the operations carried out and some of their parameters. However, the information must be entered manually and their use is not usually adopted among producers.

The Innolivar project has developed an electronic kit consisting of an ECU and a display connected to a web application (iOlivetrack) for recording field operations (Bayano-Tejero et al., 2019). The kit is installed on board a tractor, normally used for field operations, and allows recording information from the sensors installed on it and on the implements. By means of the display, the farmer can interact with the operations being carried out, controlling the parameters and recording the relevant information. All the information is geo-referenced by GPS, sent to the web application via a modem and can be queried in real time. Some interesting parameters, for the farmer and the traceability are the date and time of the operation, the GPS coordinates and the inputs used, such as products, doses applied, pressures, flow rates, consumption, etc., which can be very diverse depending on the operation to be carried out. Greater digitalisation of field operations will enable better results and conclusions to be obtained, which will lead to better farm management.

2.2. Harvesting

Olive harvesting is mostly carried out manually, using harvesting aids, trunk shakers or a combination of these, applied in orchads with a discontinuous canopy. These orchards involve most of the olive grove, as mentioned above. The most common solution is used the trunk shaker accompanied by shaker combs (Barranco et al., 2008). The olives are detached by this system and intercepted by means of shawls or bundles that are spread under the olive tree canopy and can be dragged manually or with bundle-picking machinery. Later shawls or bundles are dumped in boxes or on

palletizable bins. Another system that can be highlighted is the one that allows the detachment and interception to be carried out jointly, using a trunk shaker with an inverted conical surface known as a reversed umbrella. Once the fruit is detached, it is intercepted by this surface and stored in a small hopper. The disadvantage of this system is that it requires large planting frames to carry out the operation and, like the previous solution, the work methodology is discontinuous. To be able to carry out an integrated management, it is necessary to combine the different tasks involved in the harvesting in a continuous manner, facilitating the register of information in the process. In this work, it is proposed that harvesting should be carried out using lateral canopy shakers due to their flexibility and greater adaptation to different olive groves. Figure 2 shows one of the prototypes developed in the project for this purpose.

Figure 2. Olive harvester prototype developed in CPP Innolivar based on lateral canopy shaker.

The possibility of integrating all the tasks of harvesting, detaching, interception, cleaning and storage improves the efficiency of the process, also enabling it to capture the information generated by the machine. The prototype has a GPS location system that determines the coordinates of the position of the harvester and a hopper with load cells that allow the fruit to be weighed continuously. This data recording allows the speed of the machine, the time used and the continuous production of the trees to be known, and the information can be further processed. Useful knowledge can be generated such as idle times in turns and stops, machine working capacity and harvesting yield maps. Once each batch is harvested, the ID (IDentification number) assigned to the harvester is incorporated with the ID assigned to the batch and the batch data by means of a system composed of a reader/writer and an RFID tag.

Once the hopper has been filled, it can be lifted and it is the fruit is dumped into the hopper of the cleaning and sorting system, which captures the information stored on the RFID tag. Another alternative is the register of the dumped batch of fruit by a tractor with a pallet-holder system in palletizable bins or big-bag and transport to the cleaning and sorting system (Figure 3). In order not to lose the traceability of the harvested product, the tractor can be equipped with a geo-referencing system that registers the tracking of the harvested product as it travels through the field and an RFID reader for the transfer of information to the sorting and cleaning system. The geo-referencing system makes it possible to analyse logistics times, alternative routes and record breakdowns or anomalies.

Figure 3. Tractor transporting pallets.

2.3. Cleaning and sorting system

Currently, the cleaning and sorting of batches of fruit is not carried out in the field, but these operations are transferred to the industry, with the consequent loss of traceability. Only in some table olive farms there is a system of cleaning used previously to immersion of the olives in transport liquid, but without discarding the fruit with an advanced degree of ripeness or of small size. This reduces the efficiency of the process as some fruit is transported in liquid unnecessarily.

In the Innolivar project, a prototype has been developed to carry out cleaning and sorting at the field while maintaining product traceability from harvesting. When the tractor that transport the pallet or harvester arrives at the

unloading area, the batch of fruit is identified by means of an RFID reader installed on board the prototype (Figure 4). The fruit is then unloaded into the receiving hopper of the cleaning system. The hopper opens and a second cleaning process begins to remove the branches and leaves that have not been removed in the first cleaning carried out in the harvester, using a destemmer and blower for this purpose. The fruits with small size that cannot be used as table olives are separated by means of a row of rollers with sufficient opening for these fruits fall onto a conveyor belt with discarded or shredded product. The remaining fruits are deposited on the sorting belt. On entering the sorting belt, the fruit is distributed into 16 inspection lines where each one is analysed by artificial vision to determine its quality by bruising and ripeness. Each row has its corresponding vision system consisting of a controller, an RGB camera and a fruit presence sensor to capture the image. The image is analysed to sorting the fruit in two possible categories depending on the quality, usually first category or maximum quality and second category or medium quality, although this can be parameterised. Depending on the result of the analysis, the order is given to the compressed air valves, located at the end of the inspection lines, to allow the fruit to pass to a first category belt or to divert it to the second category where it joins the previously separated small size olives. Once the processing of the original batch is finished, the result is the division into two batches of two different qualities, from which information such as average ripeness, average size or average bruising has been extracted and registered in the web application using the modem incorporated in the prototype. The second category batch can be transported directly to the mill for oil, in the case of table olives, or for second category oils, in the case of olives destined for the mill. The first category batch is ready to be sent either to the processing industry for fresh consumption or to the oil industry for high quality oils. Both batches are identified in their respective transports by means of an RFID tag that allows the product to be traced from its origin and the information associated with it to be queried.

Figure 4. Prototype for batches cleaning and sorting.

2.4. Transport and unloading at industry.

At present, the fruit is normally transported in conventional trailers, pallets or bins that are unloaded at the industry's facilities. In some table olive farms, food tanks are used to transport the fruit immersed in refrigerated liquid. For the unloading of the fruit in the industry, it is compulsory to indicate from which plot the fruit comes, as well as to confirm that authorised products have been used and that the established safety periods have been complied with. However, no justification or certification of any kind is required, and there is reliance on the good practice carried out by the farmer.

In the Innolivar project, the methodology followed is different. The batches of fruit destined for the mill are transported to the industry in trailers in a conventional manner, as the external appearance is not relevant to the price of the product and later will be milled. However, table olives, because they are harvested at an earlier stage of ripening, are more susceptible to damage and this is manifested in the appearance of brownish spots on the skin, known as bruising, which substantially devalues the product, occurring more frequently with mechanised harvesting (Jiménez-Jiménez et al., 2013). To stop the advance of bruising, the fruit is immersed in a refrigerated bleach liquid with 0.3% NaOH (Rejano Navarro et al., 2008). Therefore, the cleaning and sorting prototype is accompanied by a transport trailer consisting of a thermally insulated drum filled with refrigerated liquid. The first category batches are dumped in it, transported and kept in optimal conditions until their arrival at the industry (Figure 5). The trailer is equipped with an electronic system consisting of a temperature sensor, a GPS, a modem and an RFID tag. The temperature sensor allows the temperature of the refrigerated liquid to be always monitored so that the maximum time the olives can remain in the liquid is not exceeded. The GPS is used for the georeferencing of the batch during the transport route. The RFID tag helps the industry to access the information associated with the batch. Finally, the modem allows all the information to be sent to a web application for registration. The batches of fruit are received in the industry, the associated information is checked by reading the respective RFID tag and the web application is accessed to obtain the history.

Figure 5. First category batch transport trailer

2.5. Operations in industry, transport, distribution and sales.

Once the batches have been received at industry, the product is prepared and marketed. These operations include, in the case of oil mills are, for example, milling and beating, and, in the case of processing industries, cooking and fermentation. Other common operations may be washing, sorting by size or packaging. During these operations it is easier to record the traceability of the product and processes as they are carried out in a more controlled environment than in the field. Through the Innolivar project, the information generated at this stage can be added to that provided in the previous field stage to provide the consumer with the traceability of the fruit from production to processing. To do this, the industry can incorporate a QR code (Quick Response code) for querying a history of all the operations carried out to, obtaining information of the product purchased by the consumer. Subsequently, during distribution and by means of fleet management systems, it is possible to incorporate traceability until arrival at the point of sale in such a way that complete traceability is obtained from the "farm to fork".

2.6. Web application

During the Innolivar project, a web application (iOlivetrack) has been developed for the integrated management of the production chain (Bayano-Tejero et al., 2019). This requires the sharing of relevant information for each of the actors in the chain. On the one hand, the farmer will collect information from all the machines and sensors he uses (weather variables, products applied to the crop, weights of fruit batches, tracking of the harvesting operation, etc.). On the other hand, the industry will record the operations carried out (phases of the process, variables measured, products added, packaging, orders leaving the facilities, etc.). Among all information registered in each phase, production and industry, the information relevant to the consumer will be provided on to the consumer, and the remaining will be conserved and used to improve the efficiency of the respective processes. This information can also be relevant for public administrations and institutions to contrast the information published by producers and industries and to verify compliance with current legislation. This is the case, for example, of the European Directive 2009/128/EC on the sustainable use of pesticide products or Regulation (EC) No 178/2002 of 28 January 2002 laying down procedures in food safety. Furthermore, food traceability recorded by the proposed methodology is a very useful tool for quality certifying companies or for implementing designations of origin of a product. The flow of information and the technology used is shown in figure 6.
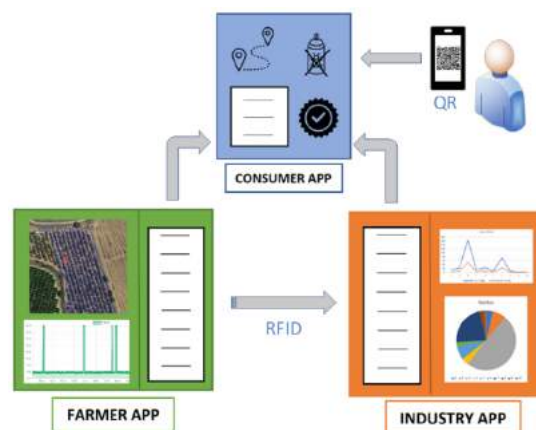
Figure 6. Information flow structure.

3. Implications of the proposed methodology

Methodological tools can be used to assess the feasibility of a project or the suitability of a solution. One of the most used methods is SWOT (Strengths, Weaknesses, Opportunities, Threats) analysis. This tool tries to find the internal and external elements that increase or decrease the performance or benefit, analyse these elements and how they contribute to the result of the solution and, finally, decide or plan future actions or strategies (Leigh, 2009). This tool focuses on conducting an internal and external analysis, with Strengths and Weaknesses corresponding to the former and Opportunities, Threats to the latter. The internal analysis focuses on aspects related to the solution or methodology itself, while the external analysis focuses on factors that affect the suitability of the solution but are not controlled by it. A table setting out the SWOT matrix of the proposed methodology is shown below (Table 1).

Table 1. SWOT matrix of the proposed methodology based on integrated mechanised management of olive farms.

	Strengths	Weaknesses
Internal	1. Traceability and collection of product and operational information. 2. Improved efficiency of processes, both in the field and in the industry, resulting in increased profitability. 3. Flexibility of the methodology in its application to different types of plantations and both olive aptitudes. 4. Interoperability of the solution between the hardware/software of different manufacturers.	1. High acquisition cost of machinery (harvester and sorter). 2. High cost of the RFID system if we need a long read/write range or a high protection of the working environment (dust, humidity, etc.). 3. The low availability of coverage can be detrimental to the transmission of streaming data, having to be transmitted in batches in a discontinuous manner.
	Opportunities	Threats
External	1. Encourage the information generated to be used by government health control bodies and certification bodies (quality, organic, PGI, PDO, etc.) to find out about the management and practices carried out by the farmer, as well as the state of the product. 2. Improved coverage through the new 5G networks that enable the transmission and analysis of streaming data. 3. Use of decentralised databases such as Blockchain to ensure the veracity of digital information.	1. Resistance to change in the execution of processes and lack of training in the management of the information generated by the sector. 2. Future obsolescence of the solution due to technological replacement of other information exchange systems.
	Enhancer	Inhibitor

Next, the different factors that have been involved in the SWOT (table 1) and how they affect the proposed methodology are presented. On the one hand, the negative factors are presented, based on weaknesses and threats. The weakness related to the high cost of machinery can be overcome by using service companies that charge a fixed or variable cost depending on the area or production harvested. Cases are established in which this alternative is widely accepted, such as in the harvesting of cereals in which the product has little economic value and yet the technology and acquisition cost of the harvesters is high (MAPA, 2015). In relation to coverage, it is estimated that coverage will improve in rural areas in the coming years. To this end, directives have been proposed to increase the density of coverage in less populated and hard-to-reach rural areas (European Commission, 2021). Also, in some processes, uninterrupted coverage is not a critical factor. If we look at the threats, these are common to other areas or sectors, being the result of the digital transformation and the rapid technological advances that are taking place in today's society. On the other hand, there are positive factors, based on strengths and opportunities. RFID is being widely used for food traceability and, together with technology that complements this data collection, improves the efficiency of processes and reduces costs, allowing rapid intervention in the event of health alerts (Costa et al., 2012). In addition, readers can be installed on machinery hoppers (Ruiz-Garcia & Lunadei, 2011) and on fruit container surfaces (Ampatzidis et al., 2008) to collect and associate information between different mobile machinery or various static elements (Sjolander et al., 2011). RFID technology has some advantages over other technologies such as Bluetooth Beacons, featuring higher encryption and data security and lacking batteries if the tags are passive (Bothe et al., 2019). Compared to other wireless technologies such as NFC, RFID has a longer range, requiring almost no physical contact, which facilitates the exchange of information in field conditions (Pigini & Conti, 2017). A major advantage of this system is the interoperability between different machinery and equipment, which is an important issue for the digitisation of agriculture (Kalatzis et al., 2019). Moreover, this methodology can be implemented in a large part of the olive orchard due to a high adaptability of the canopy shaker-based harvesting systems to the design and typology of the plantation. Furthermore, there are a number of opportunities that can promote and boost the adoption of this

methodology. 5G is identified as a technology that can facilitate the actuation or automation of machines and equipment, data exchange and monitoring of operations in real time, providing high coverage with low latency at a low cost (Tang et al., 2021). Another important aspect of fruit data collection and traceability is the possibility to aggregate this information through a platform that can be shared between different actors in the production chain. This makes the information more transparent and auditable by certification bodies for organic products, PDO, PGI, TSG, among others, as well as by competent bodies for food safety and security. To increase the veracity of information, blockchain can be used to avoid manipulation of information, whether intentional or unintentional. Several authors have used this technology to increase the incorruptibility of information, however, there are still problems with reliability in the automation of data capture and technical problems, such as transaction capacity and synchronisation, due to the immaturity of the technology itself (Feng Tian, 2016). It is therefore concluded that the net contribution between the comparison of positive factors (Strengths and Opportunities) and negative factors (Weaknesses and Threats) is favourable and the methodology may be viable.

The proposed methodology, based on the equipment and machinery developed during the Innolivar CPP, is currently in the testing phase for its subsequent pre-commercial implementation. The tests carried out and preliminary results obtained have been satisfactory and it is hoped to consolidate these results in future campaigns. The success of the methodology and its implementation will depend on the final results obtained, the acceptance by the olive sector and future legislative regulation in terms of efficiency in the use of inputs, food safety and traceability of food products.

References

AEMO (2020). Aproximación a los costes del cultivo del olivo. Acceso online: https://www.aemo.es/slides/slide/estudio-de-costes-aemo-2020-241/download. Revisado 25 de marzo de 2021

Ampatzidis, Y. G., Vougioukas, S. G., Bochtis, D. D., & Tsatsarelis, C. A. (2008). A yield mapping system for hand-harvested fruits based on RFID and GPS location technologies: field testing. *Precision Agriculture*, *10*(1), 63–72. https://doi.org/10.1007/s11119-008-9095-8

Barranco, D., Escobar, R. F., Rallo, L., Pesca, A. D. C. A. Y., Navero, D. B., & Romero, L. R. Consejería de Agricultura y Pesca. (2008). El Cultivo del olivo. Mundi-Prensa.

Bayano-Tejero, S., Sola-Guirado, R. R., Gil-Ribes, J. A., & Blanco-Roldán, G. L. (2019). Machine to machine connections for integral management of the olive production. Computers and Electronics in Agriculture, 166. https://doi.org/10.1016/j.compag.2019.104980

Bo, Y., & Wang, H. (2011). The application of cloud computing and the internet of things in agriculture and forestry. Proceedings - 2011 International Joint Conference on Service Sciences, IJCSS 2011, 168–172. https://doi.org/10.1109/IJCSS.2011.40

Bothe, A., Bauer, J., & Aschenbruck, N. (2019). RFID-assisted Continuous User Authentication for IoT-based Smart Farming. 2019 IEEE International Conference on RFID Technology and Applications (RFID-TA). Published. https://doi.org/10.1109/rfid-ta.2019.8892140

Castillo-Ruiz, F. J., Castro-Garcia, S., Blanco-Roldan, G. L., Sola-Guirado, R. R., & Gil-Ribes, J. A. (2016). Olive crown porosity measurement based on radiation transmittance: An assessment of pruning effect. Sensors (Switzerland), 16(5). https://doi.org/10.3390/s16050723

Choudhary, S. K., Jadoun, R. S., & Mandoriya, H. L. (2016). Role of Cloud Computing Technology in Agriculture Fields. Issn, 7(3), 2222–1719. www.iiste.org

Colmenero-Martinez, J. T., Blanco-Roldán, G. L., Bayano-Tejero, S., Castillo-Ruiz, F. J., Sola-Guirado, R. R., & Gil-Ribes, J. A. (2018). An automatic trunk-detection system for intensive olive harvesting with trunk shaker. Biosystems Engineering, 172, 92–101. https://doi.org/10.1016/j.biosystemseng.2018.06.002

Costa, C., Antonucci, F., Pallottino, F., Aguzzi, J., Sarriá, D., & Menesatti, P. (2012). A Review on Agri-food Supply Chain Traceability by Means of RFID Technology. Food and Bioprocess Technology, 6(2), 353–366. https://doi.org/10.1007/s11947-012-0958-7

Dumanay, A. B., Sakin, R., & İstanbullu, A. (2016). A New Design of Olive Fruit Sorting Machine Using Color Image Processing. Pdfs.Semanticscholar.Org, 9(11), 41–47. https://doi.org/10.9790/2380-0911014147

European Commission. (2021). 2030 Digital Compass: the European way for the Digital Decade. EUR-Lex. https://eur-lex.europa.eu/resource.html?uri=cellar:12e835e2-81af-11eb-9ac9 01aa75ed71a1.0001.02/DOC_1&format=PDF

Feng Tian. (2016). An agri-food supply chain traceability system for China based on RFID & blockchain technology. 2016 13th International Conference on Service Systems and Service Management (ICSSSM). Published. https://doi.org/10.1109/icsssm.2016.7538424

Fernández-Escobar, R., De la Rosa, R., León, L., Gomez, J. A., Testi, F., Orgaz, M., Gil-Ribes, J. A., Trapero, A. (2013). Evolution and sustainability of the olive production systems. Present and future of the Mediterranean olive sector (pp. 11– 42). Zaragoza, Spain: CIHEAM/IOC.

Jiménez-Jiménez, F., Castro-García, S., Blanco-Roldán, G. L., Ferguson, L., Rosa, U. A., & Gil-Ribes, J. A. (2013). Table olive cultivar susceptibility to impact bruising. Postharvest Biology and Technology, 86, 100–106. https://doi.org/10.1016/j.postharvbio.2013.06.024

Kalatzis, N., Marianos, N., & Chatzipapadopoulos, F. (2019). IoT and data interoperability in agriculture: A case study on the gaiasenseTM smart farming solution. 2019 Global IoT Summit (GIoTS). Published. https://doi.org/10.1109/giots.2019.8766423

Kouraba, K., Gil-Ribes, J.A., Blanco-Róldan, G.L., Jaime-Revuelta, M.A., Barranco-Navero, D. (2004). Suitability of olive varieties for mechanical harvester shaking. Olivae, 101, p. 39-43

Leigh, D. (2009). SWOT analysis. Handbook of Improving Performance in the Workplace: Volumes 1 3, 115-140.

MAPA. (2015). Estudios de Costes y Rentas de las Explotaciones Agrarias. ECREA. https://www.mapa.gob.es/es/ministerio/servicios/analisis-y-prospectiva/cultivos_herbaceos_tcm30-428925.pdf

Pigini, D., & Conti, M. (2017). NFC-Based Traceability in the Food Chain. Sustainability, 9(10), 1910. https://doi.org/10.3390/su9101910

Qi Jiangtao, Zhang Shuhui, Sun Yujing, Niu Xutang, Wang Wei, & Wang Lixia. (2010). Experiment research of impact-based sensor to monitor corn ear yield. 2010 International Conference on Computer Application and System Modeling (ICCASM 2010), lCCASM, V6-513-V6-516. https://doi.org/10.1109/ICCASM.2010.5620401

Ravetti, L.M. (2014). Technology for Improving the Efficiency of Mechanical Harvesting in Modern Olive Growing. Acta Horticulturae., 1057, p. 221-229.

Rejano, L., Montaño, A., Casado, F. J., Sánchez, A. H., & de Castro, A. (2010). Table Olives. *Olives and Olive Oil in Health and Disease Prevention*, 5–15. https://doi.org/10.1016/b978-0-12-374420-3.00001-2

Rejano Navarro, L., Sánchez-Gómez, A. H., & Vega Macías, V. (2008). New trends on the alkaline treatment "cocido" of Spanish or Sevillian Style green table olives. *Grasas y Aceites*, *59*(3), 197–204. https://doi.org/10.3989/gya.2008.v59.i3.509

Riquelme, M. T., Barreiro, P., Ruiz-Altisent, M., & Valero, C. (2008). Olive classification according to external damage using image analysis. Journal of Food Engineering, 87(3), 371–379. https://doi.org/10.1016/j.jfoodeng.2007.12.018

Ruiz-Garcia, L., & Lunadei, L. (2011). The role of RFID in agriculture: Applications, limitations and challenges. *Computers and Electronics in Agriculture*, *79*(1), 42–50. https://doi.org/10.1016/j.compag.2011.08.010

Suprem, A., Mahalik, N., & Kim, K. (2013). Computer Standards & Interfaces A review on application of technology systems , standards and interfaces for agriculture and food sector. Computer Standards & Interfaces, 35(4), 355–364. https://doi.org/10.1016/j.csi.2012.09.002

Segovia-Bravo, K.A., García-García, P., López-López, A., Garrido-Fernández, A. (2011). Effect of bruising on respiration, superficial color, and phenolic changes in fresh Manzanilla olives (Olea europaea pomiformis): Development of treatments to mitigate browning. Journal of Agricultural and Food Chemistry, 59,10, p. 5456-5464.

Sjolander, A.J., Thomasson, J.A., Sui, R., Ge, Y., 2011. Wireless tracking of cotton modules. Part 2: Automatic machine identification and system testing. Computers and Electronics in Agriculture 75 (1), 34–43.

Sola-Guirado, R.R., Aragon-Rodriguez, F., Castro-Garcia, S., Gil-Ribes, J. (2019). The vibration behaviour of hedgerow olive trees in response to mechanical harvesting with straddle harvester. Biosystems Engineering, 184, p. 81–89.

Sola-Guirado, R. R., Castro-García, S., Blanco-Roldán, G. L., Jiménez-Jiménez, F., Castillo-Ruiz, F. J., & Gil-Ribes, J. A. (2014). Traditional olive tree response to oil olive harvesting technologies. *Biosystems Engineering*, *118*, 186–193. https://doi.org/10.1016/j.biosystemseng.2013.12.007

Sola-Guirado, R. R., Ceular-Ortiz, D., Gil-Ribes, J. A. (2017). Automated system for real time tree canopy contact with canopy shakers. Computers and Electronics in Agriculture, 143, 139-148.

Tang, Y., Dananjayan, S., Hou, C., Guo, Q., Luo, S., & He, Y. (2021). A survey on the 5G network and its impact on agriculture: Challenges and opportunities. Computers and Electronics in Agriculture, 180, 105895. https://doi.org/10.1016/j.compag.2020.105895

Tous, J., Romero, A., Hermoso, J.F., Msallem, M., Larbi, A. (2014). Olive orchard design and mechanization: Present and future. Acta Horticulturae, 1057, p. 231-246

Particulate Matter Emissions from Soil Preparation Activities as Influenced by Minimum and Strip Tillage Practices

Jacopo Maffia [a*], Massimo Blandino [a], Luca Capo [a], Elio Padoan [a], Luca Rollé [a], Paolo Balsari [a], Elio Dinuccio [a]

[a] Department of Agriculture, Forest and Food Science (DISAFA) University of Torino, Grugliasco, Italy

* Corresponding author. Email: jacopo.maffia@unito.it

Abstract

Land preparation activities are one of the main contributors to particulate matter (PM) emissions from agriculture. Nonetheless, particulate matter emissions from tillage operations are poorly studied, especially in southern Europe, where few assessments have been made. Moreover, it is important to describe the influence of tilling implements and soil preparation practices on the emissions of fine PM (PM_{10}) from fields. A research project, titled "Evaluation of particulate matter emissions from cropping and farm transformation activities in Maize production systems", has been funded by CRT foundation (grant numbers: 2018.2273) to tackle the issue of PM emissions from Maize cropping systems, including land preparation. This study, in particular, presents the results of field trials with assessment of three land preparation scenarios for maize: traditional tillage with ploughing at 30 cm followed by rotary harrow (TT), minimum tillage with disk harrowing (MT) and strip tillage, with soil tilled in strips of 25 cm wide at a working depth of 15 cm (ST). Emissions of PM10 resulted being of 149, 30 and 114 mg m^{-2} respectively for TT, MT and ST. These results give a first insight into reduced soil disturbance practices as mitigation measures for tillage induced direct PM_{10} emissions and highlight MT as the less emitting tillage practice.

Keywords: PM_{10}, emission factors, conservation tillage, air pollution

1. Introduction

Particulate matter (PM) emissions are a growing cause of concern due to their impact on human health and environment. The agricultural sector is responsible of the 17% of the total anthropogenic emission of sub 10 μm PM particles (PM_{10}; EEA, 2016). The main sources of fine PM in agriculture are livestock rearing facilities and field operations, such as tillage, harvesting, manure spreading (Kabelitz et al., 2020; Maffia et al., 2020b). Agricultural PM has been long seen as a risk for field operators and farmers, but it is now also considered for its long range effect on regional air quality (Chen et al., 2017). Many studies have addressed PM emissions from livestock houses (Cambra-López et al., 2010; Winkel et al., 2016), while fewer information is available on open field activities. Moreover, most studies assessing emissions from tillage or harvesting just focus on few of the operations commonly performed by farmers, while others are neglected (Maffia et al., 2020b). Since the amount of PM_{10} emitted, as well as the particles characteristics, varies greatly according to the kind of operation, the environmental conditions (soil humidity and wind speed) and the mechanical implement used (Avecilla et al., 2017; Cassel et al., 2003), it is important to define emission factors (EF) for all different environments and specific activities. After having assessed valid and up to date EF, it is necessary to consider the availability of mitigation measures to reduce the emissions and improve farmer health and general air quality. Minimum and strip tillage are tillage practices that allow seedbed preparation with reduced soil disturbance. These practices have been developed to reduce soil erosion by wind and runoff events and are especially diffused in areas where erosion events are frequent and severe, such as North and South America. Strip tilling, in particular, acts only on the rows of soil where sowing will take place, leaving the inter-rows untouched. This approach allows to grant higher soil coverage (by stalks and leftovers) even during the first growing period of crops, increasing soil protection and reducing seedbed preparation costs and time (Laufer et al., 2016). Few studies addressed of this practices on direct PM emissions during tillage (Baker et al., 2005; Coates, 1996), and none have investigated the emission deriving from sowing itself.

The aim of this study is to assess PM_{10} emissions from land preparation activities in Northern Italy, including sowing, providing new EF figures and evaluating the effect of three different land preparation approaches, Conventional (TT), Minimum (MT) and Strip Tillage (ST), on the emissions.

2. Materials and Methods

2.1. Experimental layout

The trial was performed in an experimental farm situated in Carmagnola, North-west of Italy (44° 53' 10" N 7° 40' 59" E). The experimental field (Figure 1) was divided in three main plots that were subjected to the three different land preparation strategies (TT, MT and ST). The same tillage strategy was applied in each main plot in the previous 5 growing seasons, in which the field was cultivated continuously with maize for grain. The maize

residues from the previous growing season have been totally maintained on the soil surface before the tillage operation. Each plot was divided in six subplots, each one corresponding to one sowing passage (4.5x40 m). The seedbed preparation passages performed for TT, MT and ST thesis are summarized in Table 1. TT consisted of a traditional ploughing (30 cm depth), followed by two rotary harrowing passages before maize sowing. MT consisted of a single two rows disk harrower passage followed by sowing. ST consisted of a strip tillage passage followed by sowing. In all three scenarios, two fertilizer passages were made with potassium chloride, KCl (60%, Pastorelli SPA) and triple superphosphate, $Ca(H_2PO_4)$ (46% of P_2O_5 ; RaFertil Group). Four different tractors were used during the trial, depending on the implement (Table 1). All field operations were performed in one day, in order to reduce environmental variability as much as possible.

Measurements of PM_{10} were carried out at each tractor passage using an optical PM monitor (TSI, DustTrack™ II model 8530), with a sampling frequency of 1 Hz. The PM monitor was placed alongside the tilled area at 5 m distance (Figure 1). The instrument was moved near to the next passage line after each pass. The instrument was always kept downwind (skewed at most by a 30° angle) of the passage line. Background PM_{10} concentration was assessed before and after trials. A weather station was mounted at the corner of the field, far from obstacles, and provided wind measurements by means of two 2D sonic anemometers (GILL, UltraSonic), placed at 2 and 4 m height.
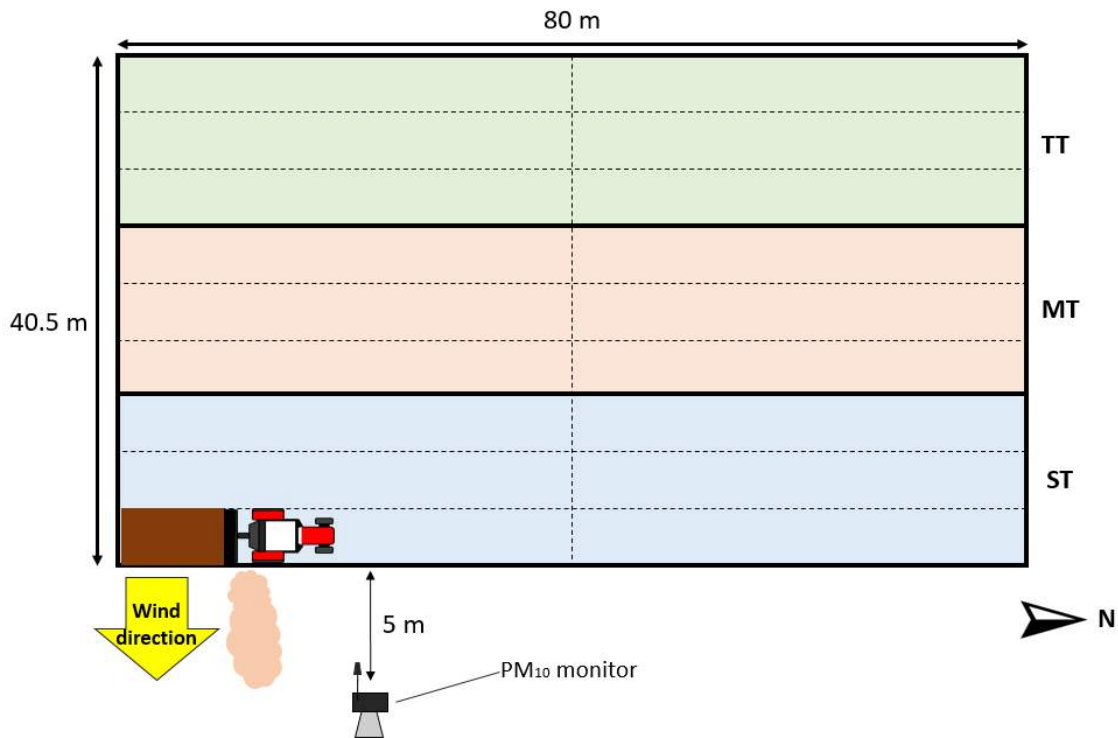
Figure 1. Experimental layout (full lines identify main plots; dashed lines identify sub-plots).

Table 1. Seedbed preparation activities in traditional tillage (TT), minimum tillage (MT) and strip tillage (ST), implements used, working widths and advancement speeds.

	Operation	Implement	Tractor	Working width (m)	Speed (km h⁻¹)
TT	Ploughing	Vittone (two ploughshares)	FIAT 90-90 DT	1.1	2.5
	Rotary harrowing (1st pass)	Breviglieri, MEKFARMER 100	FIAT 70-66	2.5	4.5
	Rotary harrowing (2nd pass)	Breviglieri, MEKFARMER 100	FIAT 70-66	2.5	4.5
	KCl spreading	KUHN, AERO 1120	FIAT 55-66	12	2.5
	P_2O_5 spreading	KUHN, AERO 1120	FIAT 55-66	12	2.5
	Sowing	ALPEGO, Fertidrill ASF	CLAAS 550 ARION	4.5	7.5
MT	Disk harrowing	Harrower (two disk rows)	FIAT 90-90 DT	2.5	2.5
	KCl spreading	KUHN, AERO 1120	FIAT 55-66	12	2.5
	P_2O_5 spreading	KUHN, AERO 1120	FIAT 55-66	12	2.5
	Sowing	ALPEGO, Fertidrill ASF	CLAAS 550 ARION	4.5	7.5
ST	Strip tillage	MOM, Strip Hawk Easy	CLAAS 550 ARION	3	7.5
	KCl spreading	KUHN, AERO 1120	FIAT 55-66	12	2.5
	P_2O_5 spreading	KUHN, AERO 1120	FIAT 55-66	12	2.5
	Sowing	ALPEGO, Fertidrill ASF	CLAAS 550 ARION	4.5	7.5

2.2. Elaboration of wind data

Start and end times of each tractor passage were recorded during field measurements. The passage time intervals were used to clip the output file of the anemometer, to obtain the average wind speed and direction at the time of each PM concentration peaks. The atmospheric stability class was estimated for each passage, according to the Pasquill-Gifford class method (Pasquill, 1961).

2.3. Soil physico-chemical analysis

Three soil samples were collected in each plot (TT, MT and ST), adopting an "X" sampling strategy and quartering subsamples in field. Soil samples were collected at 0–15 cm depth both before the start of the trial and before sowing, to assess the effect of the tillage treatment on soil humidity.

The samples were air-dried and sieved to 2 mm before physico-chemical analyses. We determined soil texture, pH, total carbon and nitrogen content and carbonates. The fraction of particles <10 μm was estimated by repeated sedimentation and decanting. Field capacity was also determined. The methods used for the analysis are described in Padoan et al. (2021).

2.4. Emission factor estimation

EF were assessed using a backward lagrangian model (WindTrax). The input parameters to the model were: wind speed, wind direction, atmospheric stability class, air temperature, average PM_{10} concentration (at 5 m from the operation line) and background PM_{10} concentration. The model was set to simulate the dispersion of 1 million particles and the surface roughness was set to the reference value (1 cm), parameterized for "bare soil" conditions. The emission source was modelled as an area source having the same dimension of the plot tilled at each passage (as in Maffia et al., 2020a).

A simulation was performed per each tractor passage. The output of the model is an Emission Rate (ER, mg m⁻² s⁻¹) referred to the modelled area source. The ER can be later converted in EF (mg m⁻²) according to the following formula:

$$EF = ER \times tpass \qquad (1)$$

where *tpass* is the elapsed time (s) between the start and the end of each passage.

2.5. Statistical analysis

An analysis of variance (ANOVA), followed by a Tukey post hoc test was performed to assess differences in EF among operations and in total emissions among thesis (TT, MT, ST). Wind speed population in the three thesis was also tested. A log transformation was applied to EF data, in order to meet the normality assumption of ANOVA. Normality and homoscedasticity were then confirmed through a Shapiro Wilk test and a Levene test, respectively. All analysis were performed using R (R Core Team, 2019).

3. Results and Discussion

3.1. Wind conditions during field trial

The overall wind conditions observed during the trial are presented in Figure 2. Wind speed averaged at around 1 m s^{-1} and remained among 0.5 and 2.5 m s^{-1} for the length of the trial. These relatively low wind speeds are representative of the area were the experiment took place. Moreover, the post hoc test performed to assess wind speed differences among treatment confirmed no evident significant difference, although during ST tests there was a slight numerical increase in wind speed. Wind direction was constant (WSW, WS) for most of the trial. Nonetheless, it was necessary to move the DustTrak^{TM} monitor to the opposite side of the passage line during few TT and MT passages, since wind was blowing from ESE.
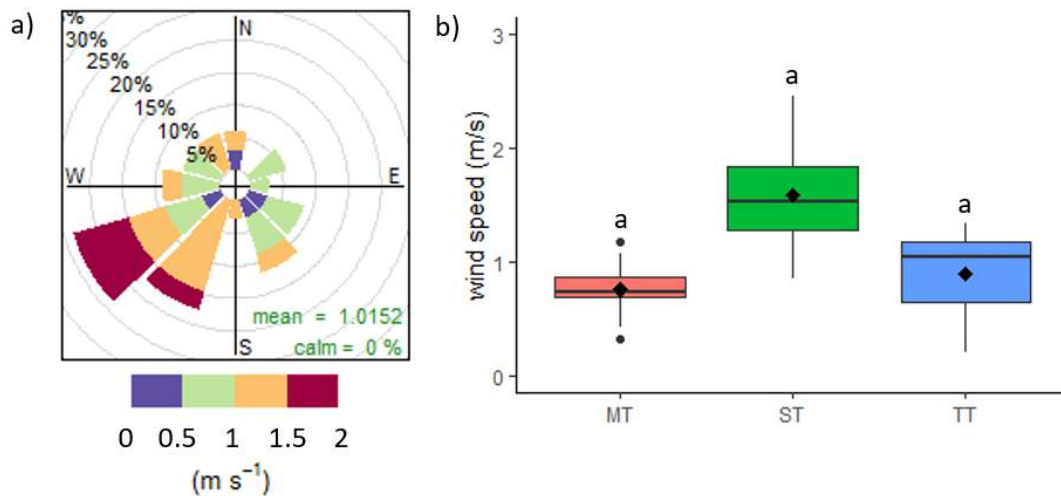
Figure 2. a) WindRose graph highlighting wind speed and direction frequencies during the trial (obtained with OpenAir R package; Carslaw et al., 2012); b) Boxplot graph with post hoc test results (means with the same letter are not statistically different for P<0.05; means are represented by rhombuses).

3.2. Soil characteristics and humidity

Soil characteristics are presented in Table 2. The soil where the trial took place is a silt loam textured soil, with a low organic carbon content. No relevant difference, in terms of soil characteristic was highlighted among plots. Soil humidity at the beginning of the trial was of 18.8±0.6 % on mass in all plots, while humidity before sowing changed slightly, due to the operations performed, and reached 13.9±0.4, 17.6±0.5 and 14.8±0.4 % in TT, MT and ST, respectively. The difference between TT and ST and the MT plot, which was more wet, is probably due, for TT, to the aeration caused by ploughing, which could have caused the soil to dry up faster, while for ST, the type of implement used could have induce less mixing of the upper soil layer (dryer) with the lower one (more wet).

Table 2. Soil characteristics in the three different land preparation approaches, Conventional (TT), Minimum (MT) and Strip Tillage (ST).

		TT	**MT**	**ST**
Sand	%	34.1	34.7	34.0
Silt	%	59.8	58.8	60.0
Clay	%	6.1	6.5	6.0
pH		8.2	8.1	8.2
Total limestone	%	2.8	2.4	2.8
organic C	%	0.9	1.6	0.9
CEC	meq/100g	7.9	8.5	8.0

3.3. Particulate matter emissions as affected by tilling practice

Table 3 shows the results of a post hoc test comparing the PM_{10} EF derived for all operations performed. It was observed that the main tilling operations, ploughing and strip tilling caused the highest emissions, while no significant difference was observed among the other operations. A slight trend of emission increase, although not significant, was observed among the first and second rotary harrowing passage. This result is consistent with the observations of Madden et al. (2009), who highlighted that progressive disaggregation of soil aggregates leads to higher emissions. In general, the observed EF are consistent to those found in literature (summarized in Maffia et al., 2020). An interesting result is the assessment of the EF for fertilizers spreading passages, which have been almost completely neglected in previous literature. PM derived from fertilizer spreading operations could, in fact, have different composition than the one from tillage (composed mainly of soil particles) and should therefore be investigated in further studies for its chemical composition and size fraction range.

Emissions from sowing are reported in Table 4. No significant differences among the three theses were observed. Due to the slightly dryer soil conditions in TT and ST we may expect higher emissions than in MT. However, this effect was not observed. The slightly higher EF value for ST could be due to the passage of tractor wheels on untilled inter rows, which have a particularly dry upper layer (first 2 cm). In general, sowing is, after ploughing, the most emitting operation in terms of PM10. It is therefore important to consider it when assessing seedbed preparation impact, and to propose sowing implements with reduced emission potential. Moreover, previous studies have observed that sowing produces not only resuspension of soil particles, but also of seed and seed coating fragments, with presence of pesticides, which have a potentially higher impact on farmers' and animal (bees) health and environment.

The overall emissions occurred with TT, MT and ST, and the post hoc comparison among them, are presented in Figure 3. A significant difference was highlighted between MT and the other two thesis, with MT emitting 79 and 73 % less PM_{10} than TT and ST, respectively. These results are consistent with a previous study (Coates, 1996), assessing the effect of minimum tillage on total solid particles emitted, observing a 45% reduction as compared to traditional tillage. Baker et al. (2005), instead, observed a reduction of up to two thirds of respirable dust concentration during land preparation with conservation tillage practices as opposed to conventional ones. In this study, the reduction of PM_{10} emissions observed with ST was slighter and did not induce a significant difference in statistical terms. Moreover, it was highlighted that most of PM_{10} emissions are caused by principal heavy-duty operations, such as ploughing and strip tillage, while secondary passages, such as disk or rotary harrowing, are less important. Therefore, as a general rule, to reduce PM10 emissions from seedbed preparation, it would be preferable to avoid principal operation which involve a deeper tilling and profound soil turning and to rely on superficial interventions. In fact, even if, as Coates et al. (1996) suggested, reducing the number of passages is the one of the most effective ways of reducing PM emissions, it is also true that the choice of the implement and the operation type play a vital role in determining dust production. Providing more detailed emission figures is therefore important to inform adequate soil management choices, without forgetting that PM emissions from soils are affected by soil and weather conditions and that the implement choices should be tuned to accommodate for the specific characteristics of the area. Moreover, while addressing PM emissions is should never be forgotten that soil management should first aim to soil preservation and overall agronomic performance and that these should remain the main drivers of management choices made.

Table 3. Post hoc test results highlighting differences among emission factor (EF) of soil tilling operations performed (means followed by same letter are not statistically different for α<0.05).

Operation	EF (mg m^{-2})		Lower CL*	Upper CL*	N**	P
Ploughing	76.1	b	23.7	244.2	12	
Strip tilling	68.0	b	33.3	138.9	5	
Disk harrowing	2.2	a	1.2	4.1	5	
P_2O_5 spreading	2.2	a	0.9	5.3	5	<0.001
2nd rotary harrowing	1.3	a	0.6	2.9	5	
1st rotary harrowing	0.7	a	0.3	1.7	5	
KCl spreading	0.5	a	0.2	1.2	5	

*LowerCL and UpperCL are the lower and upper 95% confidence limits.
**N is the number of tractor passages.

Table 4. Post hoc test results highlighting differences among emission factor (EF) of soil tilling operations performed (means followed by same letter are not statistically different for α<0.05).

	Sowing EF (mg m^{-2})		Lower CL*	Upper CL*	N	P
TT	21.5	a	10.8	42.9		
MT	23.3	a	12.9	42.5	3	0.6
ST	28.2	a	14.1	56.2		

*LowerCL and UpperCL are the lower and upper 95% confidence limits.
**N is the number of tractor passages.
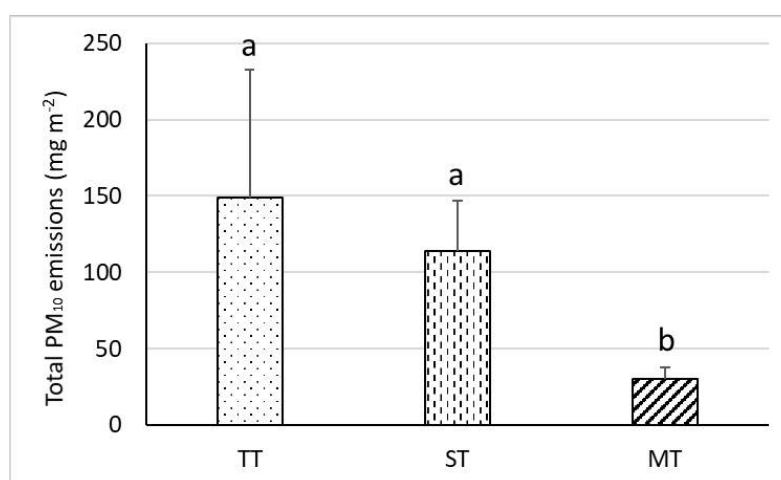
Figure 2. Post hoc test results highlighting differences among total PM10 emissions derived from each tillage practice (means with the same letter are not statistically different for α<0.05).

4. Conclusions

This preliminary study allowed to provide new EF for tillage in Northern Italy, for which no EF were available. Moreover, the effect of different soil tillage approaches on PM_{10} emissions was observed, highlighting a substantial emission reduction, of 79% when applying MT as compared to TT. ST, instead, did not provide a significant emission reduction benefit. It was observed that the operations which are the main drivers of PM_{10} emissions, are principal tillage operations, such as ploughing, strip tillage, and sowing. To improve the knowledge of the processes leading to PM emission from agricultural operations, future studies may address also finer size fractions of PM ($PM_{2.5}$ and PM_1) and the influence of soil moisture on the EF, and may characterize the profile of emitted particulate in order to provide more accurate emission figures.

Acknowledgements

References

Avecilla, F., Panebianco, J.E., Buschiazzo, D.E., 2017. Meteorological conditions during dust (PM 10) emission from a tilled loam soil: Identifying variables and thresholds. Agricultural and Forest Meteorology 244–245, 21–32. https://doi.org/10.1016/j.agrformet.2017.05.016

Baker, J.B., Southard, R.J., Mitchell, J.P., 2005. Agricultural Dust Production in Standard and Conservation Tillage Systems in the San Joaquin Valley. Journal of Environment Quality 34, 1260. https://doi.org/10.2134/jeq2003.0348

Cambra-López, M., Aarnink, A.J.A., Zhao, Y., Calvet, S., Torres, A.G., 2010. Airborne particulate matter from livestock production systems: a review of an air pollution problem. Environ Pollut 158, 1–17. https://doi.org/10.1016/j.envpol.2009.07.011

Carslaw, D. C. and K. Ropkins, 2012. openair --- an R package for air quality data analysis. Environmental Modelling & Software. Volume 27-28, 52-61.

Cassel, T., Trzepla-Nabaglo, K., Flocchini, R., 2003. PM10 Emission Factors for Harvest and Tillage of Row Crops. In 12th International Emission Inventory Conference, San Diego, CA.

Chen, W., Tong, D.Q., Dan, M., Zhang, S., Zhang, X., Pan, Y., 2017. Typical atmospheric haze during crop harvest season in northeastern China: A case in the Changchun region. Journal of Environmental Sciences 54, 101–113. https://doi.org/10.1016/j.jes.2016.03.031

Coates, W., 1996. Particulates generated by five cotton tillage systems. Transactions of the American Society of Agricultural Engineers 39, 1593–1598.

EEA, European Environmental Agency, 2016. EMEP/EEA air pollutant emission inventory guidebook 2016: technical guidance to prepare national emission inventories.

Kabelitz, T., Ammon, C., Funk, R., Münch, S., Biniasch, O., Nübel, U., Thiel, N., Rösler, U., Siller, P., Amon, B., Aarnink, A.J.A., Amon, T., 2020. Functional relationship of particulate matter (PM) emissions, animal species, and moisture content during manure application. Environment International 143, 105577. https://doi.org/10.1016/j.envint.2020.105577

Laufer, D., Loibl, B., Märländer, B., Koch, H.-J., 2016. Soil erosion and surface runoff under strip tillage for sugar beet (Beta vulgaris L.) in Central Europe. Soil and Tillage Research 162, 1–7. https://doi.org/10.1016/j.still.2016.04.007

Madden, N.M., Southard, R.J., Mitchell, J.P., 2009. Soil Water Content and Soil Disaggregation by Disking Affects PM10 Emissions. Journal of Environmental Quality 38, 36–43. https://doi.org/10.2134/jeq2008.0209

Maffia, J., Balsari, P., Padoan, E., Ajmone-Marsan, F., Ricauda Aimonino, D., Dinuccio, E., 2020a. Evaluation of particulate matter (PM10) emissions and its chemical characteristics during rotary harrowing operations at different forward speeds and levelling bar heights. Environmental Pollution 265, 115041. https://doi.org/10.1016/j.envpol.2020.115041

Maffia, J., Dinuccio, E., Amon, B., Balsari, P., 2020b. PM emissions from open field crop management: Emission factors, assessment methods and mitigation measures – A review. Atmospheric Environment 226, 117381. https://doi.org/10.1016/j.atmosenv.2020.117381

Padoan, E., Maffia, J., Balsari, P., Ajmone-Marsan, F., Dinuccio, E., 2021. Soil PM10 emission potential under specific mechanical stress and particles characteristics. Science of The Total Environment 779, 146468. https://doi.org/10.1016/j.scitotenv.2021.146468

Pasquill, F., 1961. The estimation of the dispersion of windborne material. Met. Mag., 90, 33.

R Core Team, 2019. R: A language and environment for statistical computing. R Foundation for Statistical Computing, Vienna,Austria. URL https://www.R-project.org/.

Winkel, A., van Riel, J.W., van Emous, R.A., Aarnink, A.J.A., Groot Koerkamp, P.W.G., Ogink, N.W.M., 2016. Abatement of particulate matter emission from experimental aviary housings for laying hens by spraying rapeseed oil. Poultry Science 95, 2836–2848. https://doi.org/10.3382/ps/pew261

Effect of Mechanical Pruning on Olive Yield in a High Density Olive Orchard - an Account of 14 years

Dias, António B.[ab*], Falcão, J.M.[c], Pinheiro, A.[ab], Peça, J.O.[ab]

[a] Departmento de Engenharia Rural, University of Évora, Évora, Portugal

[b] MED – Mediterranean Institute for Agriculture, Environment and Devlopment, Évora, Portugal

[c] Torre das Figueiras Sociedade Agrícola Lda, Monforte, Portugal

* Corresponding author. Email: adias@uevora.pt

Abstract

In Portugal the study of the use of mechanical pruning in olive orchards began in 1997. The trials were made in traditional olive orchards and the results obtained revealed that the use of mechanical pruning can contribute for the reduction of pruning costs without reduction in yield.

In 2005 the authors started the evaluation of mechanical pruning in an irrigated olive orchard (7m x 3.5m) of Picual cultivar. The trials were organised in a randomised complete block design, with three replications. Four treatments are being compared, leading to a total of 12 plots with 30 trees per plot. The treatments under study were as follow: T1 - manual pruning, using chain saws in 2005, 2010, 2014 and 2017; T2 - mechanical pruning, topping and hedging the two sides of the canopy in 2014 and 2017 followed by a manual pruning complement to remove wood suckers inside the canopy; T3 - mechanical pruning, topping the canopy parallel to the ground in 2005, topping the canopy parallel to the ground and hedging the west side of the canopy in 2008 and 2012, topping the canopy parallel to the ground and hedging the east side of the canopy in 2010, 2014 and 2017, summer topping the canopy in July 2015 (summer pruning) and hedging the west side in winter 2016; T4 - mechanical pruning, topping the canopy parallel to the ground in 2005, topping and hedging the two sides of the canopy in 2010, 2014 and 2017 and topping the canopy in July 2015 (summer pruning).

Common to all treatments were manual pruning to eliminate hanging branches in 2006 and mechanical pruning, topping the canopy parallel to the ground to eliminate 0.50m, in 2007.

The average yield per tree for each treatment was evaluated.

In a first period of 5 years, no significant differences were found between treatments.

In the second period of 4 years, a greater frequency of mechanical pruning (T3) showed a lower yield with significant differences to treatment T2.

In the third period of 5 years a greater severity in pruning interventions reduced the olive yield (2014). A manual pruning complement after mechanical pruning (T2) did not increase olive yield; however, the average yield over this period of time was similar.

The olive yield has been maintained over a period of 14 years only applying mechanical pruning, without manual pruning complement inside de canopy.

Keywords: mechanical pruning, canopy topping, canopy hedging

1. Introduction

In Portugal, the scarcity of labour led to the use of a high level of mechanization to prune olive groves. Long-term tests carried out on traditional olive orchards have shown that the use of disc-pruning machines allows for high pruning rates, which can contribute to reduce pruning costs (Peça *et al.*, 2002). Results obtained by the authors revealed that after mechanical pruning (topping at the uppermost part of the canopy) trees can be kept for 8 years without any significant loss in olive yield and no effect in harvesting efficiency (Dias *et al.*, 2012). For a period of nine campaigns, the selective manual complement, simultaneous with mechanical pruning, brings no pratical advantage in terms of yield (Dias *et al.*, 2014).

In a second period, the selective manual pruning complement to the mechanical pruning, particularly in the year following mechanical pruning, should be regarded as a potentially important technique since it may have contributed to higher yields (Dias eta al., 2014)

The increase in the area of irrigated high density (HD) olive orchards, led the authors to evaluate the use of mechanical pruning in this kind of groves, which had been started in 2005 in an olive orchard of Picual variety.

This paper shows the results from the use of mechanical pruning on olive yield during the 14 years, which can contribute to the definition of a mechanized pruning strategy for HD olive orchards.

2. Materials and Methods

2.1. Olive orchard

The HD olive orchard used in the trial was established in 1996 in Herdade da Torre das Figueiras in the Alentejo region of southern Portugal (lat. 39º 03' 34.04'' N; 07º 28' 22.00'' W). This drip-irrigated, HD olive orchard of the Picual variety was installed in an array of 7m x 3.5m.

The orchard was planted on Chromic Luvisol soil (FAO). This region is semi-arid with a strong continental influence and an annual mean rainfall of 500mm - concentrated in the winter.

The orchard is drip-irrigated twice a week, from May untill October, receiving annually an estimated volume of 1500-2000m3 per hectare.

The HD olive orchard was sprayed to control olive leaf spot (Flusicladium oleaginum (Castagne) Ritschel & U.Braun), olive moth (Prays oleae Bernard), olive fly (Bactrocera oleae Gmelin.) and olive anthracnose (Colletotrichum acutatum Simmons or Colletotrichum gloeosporioides Penz.). Glyphosate was used for weed control in the rows although a shredder machine was also used between rows. A yearly average of approximately 80 units of nitrogen, 30 units of phosphorus and 50 units of potassium were applied to the soil and by drip irrigation.

2.2. Equipment

Mechanical pruning was performed using a Reynolds & Oliveira Ltd. (R&O) disc-saw pruning machine mounted (Fig. 1) on a front loader of a 97 kW (DIN) 4WD agricultural tractor (Dias et al., 2012), (Peça et al., 2002).

The manual pruning complement to the mechanical pruning was executed with the use of telescopic chain saws.

Harvesting was done using an 88kW (DIN) self-propelled multidirectional Orchard Machinery Corporation (OMC) trunk shaker (Dias et al., 2012), except in the period between 2014 -2017 when a prototype of a continuous canopy shaker was employed (Dias et al., 2020).

Figure 1 - Mechanical pruning (topping)

2.3. Treatments

In a randomised complete block design with three replications, four treatments (T1, T2, T3, T4) are being compared leading to 12 plots of one line with 30 trees per plot. The treatments are: T1 - manual pruning, using chain saws in 2005, 2010, 2014 and 2017; T2 - mechanical pruning, topping and hedging the two sides of the canopy in 2014 and 2017 followed by a manual pruning complement to remove wood suckers inside the canopy; T3 - mechanical pruning, topping the canopy parallel to the ground in 2005, topping the canopy parallel to the ground and hedging the west side of the canopy in 2008 and 2012, topping the canopy parallel to the ground and hedging the east side of the canopy in 2010, 2014 and 2017, summer topping the canopy in July 2015 (summer pruning) and hedging the west side in winter 2016; T4 - mechanical pruning, topping the canopy parallel to the ground in 2005, topping and hedging the two sides of the canopy in 2010, 2014 and 2017 and topping the canopy in July 2015 (summer pruning).

Common to all treatments were manual pruning to eliminate hanging branches in 2006 and mechanical pruning, topping the canopy parallel to the ground to eliminate 0.50m, in 2007.

The sequence of pruning interventions made in this trial were in figure 2.

July 4–8, 2021, Évora, Portugal

Trat	2005	2006	2007	2008	2009	2010	2011	2012	2013	2014	2015	2016	2017	2018
T1	Manual	Hanging branches				Manual				Manual			Manual	
T2	No pruning	Hanging branches								+ Manual compl.			+ Manual compl.	
T3		Hanging branches												Summer
T4		Hanging branches									Summer			

Legend: Manual - manual pruning; Manual compl. - manual pruning complement; Summer – summer pruning; hanging branches – removed hanging branches; - mechanical pruning(topping); - mechanical pruning(topping + hedging west canopy side); - mechanical pruning (topping + hedging east canopy side); - mechanical pruning(topping + hedging both canopy sides);

Figure 2 – Sequence of pruning interventions

3. Results and Discussion

Olive yield are significantly ($P<0.05$) influenced by the year (as shows table 1), revealing the common oscillation of this specie. The significantly ($P<0.05$) lower yield obtained in 2012 was due to the lack irrigation water as a consequence of a severe drought. In 2014, a severe pruning intervention was carried out, with a considerable reduction in the canopy volume, contributing to a low level of olive production.

Table 1 – Influence of the year in olive yield

Year	Yield (kg tree-1)
2005	8.9 g
2006	18.0 f
2007	6.7 gh
2008	25.8 cd
2009	26.6 c
2010	33.9 a
2011	27.7 bc
2012	2.0 i
2013	20.4 ef
2014	5.4 h
2015	30.4 b
2016	23.2 de
2017	18.7 f
2018	25.5 cd
Average	19.5

Values followed by the same letter are not significantly different by Tukey multiple range test at the 5% level

Figure 3 shows olive yields by treatment for each year (between 2005-2009) and the average yield for this period. In 2005 and 2006, no significant differences ($P>0.05$) were found in the olive yield per tree between treatments.

In 2007, significant differences ($P<0.05$) were registered between treatments, with a significantly ($P<0.05$) lower yield in treatment T2 compared to treatment T4. No significant differences ($P>0.05$) were found between treatments in

292

2008, showing the light pruning that was carried out on treatment T3 (topping and hedging in the east side of the canopy) did not influenced the olive yield.

In 2009 no significant differences (P>0.05) were found between treatments. On average, during the period 2005-2009, no significant differences (P>0.05) were registered between treatments.
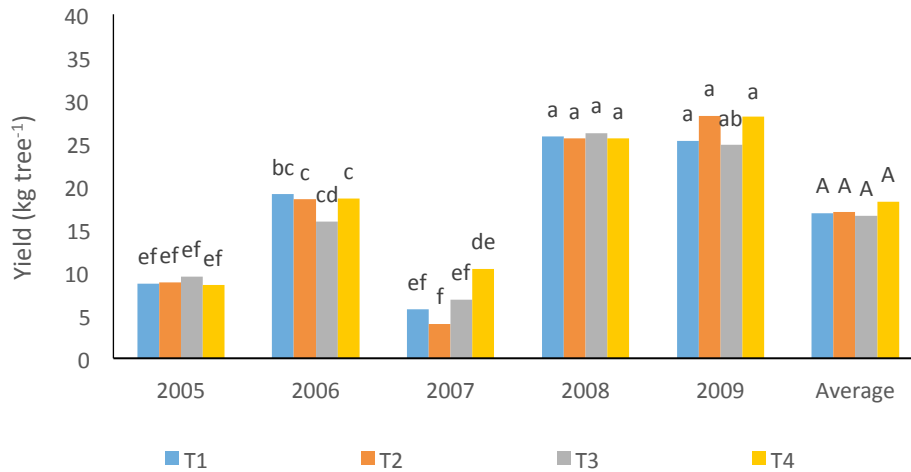
Columns with the same letter are not significantly different by Tukey multiple range test at the 5% level

Figure 3 - Influence of the treatment on olive yield per tree between 2005 and 2009

In the second period (2010-2013), significant differences (P<0.05) were found on the effect of the treatments in yield. Figure 4 shows olive yield by treatment in each year between 2010 and 2013, and the average yield for this period. In 2010, treatment T4 have a significantly (P<0.05) lower yield than other treatments, which did not revealed significant differences (P>0.05) between themselves. This can be explained by the reduction in volume of the canopy imposed by the pruning interventions (topping and hedging the two sides of the canopy).

In the following year (2011) no significant differences (P>0.05) were found between treatments. In 2012 there were no significant differences (P>0.05) between treatments in olive yield, with the highest production in treatment T3. There was a lack of irrigation water that year, so the smaller canopy size in treatment T3 (topping and hedging the west side of the canopy in 2012), may explain the result.
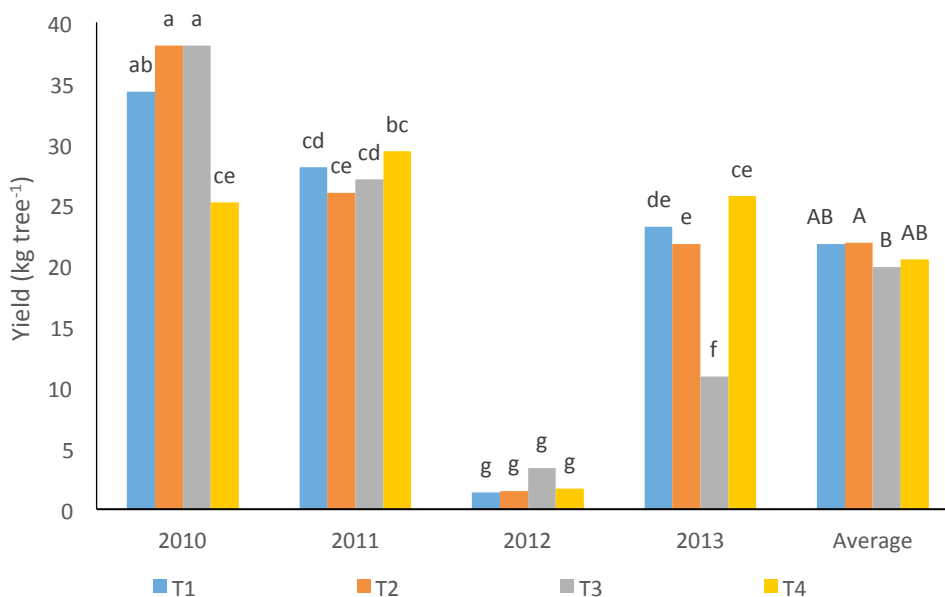
Columns with the same letter are not significantly different by Tukey multiple range test at the 5% level

Figure 4 - Influence of the treatment on olive yield per tree between 2010 and 2013

In 2013 there were significant differences (P<0.05) between treatments in olive yield; treatment T3 registering a significantly (P<0.05) lower production than that obtained in the other treatments, which did not differ from one another. In treatment T3, the trees had a smaller canopy volume than those in the other treatments, because they were pruned in the previous year, while no pruning was done in the other treatments since 2010.

On average, in this period (2010-2013), significant differences (P<0.05) between treatments were found, with a significantly (P<0.05) lower production in treatment T3 than in treatment T2.

It should be noted that in treatment T2, no pruning intervention was performed in this period: This shows that is possible to keep trees unpruned for some years, maintaining productive capacity as had already been seen in traditional olive orchards (Dias et al., 2014).

Figure 5 shows olive yield by treatment in each year from 2014 to 2018 and the average yield of this period. In 2014, significant differences (P<0.05) were registered in olive yield per tree between treatments. Treatment T3 revealed a significantly (P<0.05) higher yield than the other treatments as consequence of the smaller pruning intensity applied. In treatment T3, the significantly higher production may have resulted from the productive branches issued in the previous year on the west side of the canopy, which was left uncut in 2014. In treatments T2 and T4, the lateral cuts on both sides of the canopy eliminated a considerable quantity of the productive branches issued in the previous year, diminishing productive potential in comparison with treatment T3. In the case of treatment T1, despite having been subjected to manual pruning, which has greater selectivity, the elimination of a considerable part of the canopy reduced the productive potential.
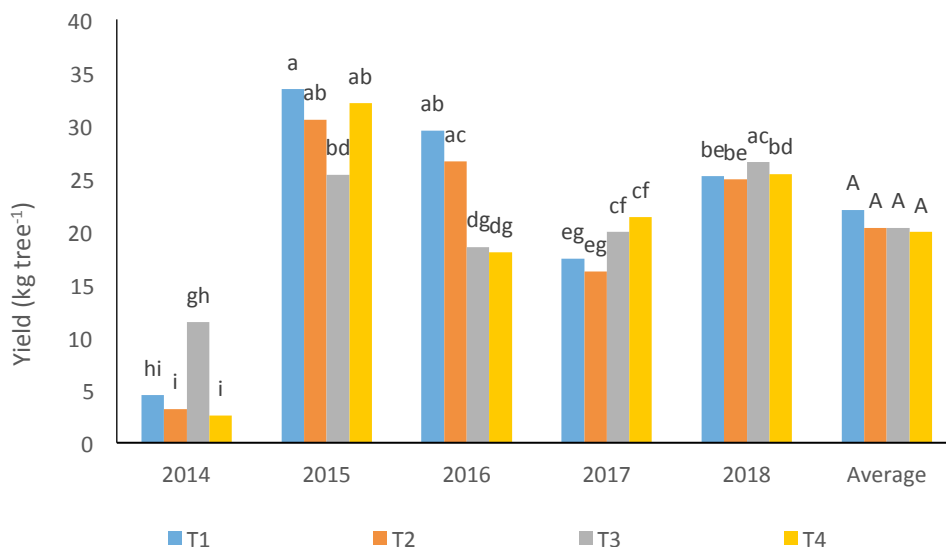
Columns with the same letter are not significantly different by Tukey multiple range test at the 5% level

Figure 5 - Influence of the treatment on olive yield per tree between 2014 and 2018

In 2015 significant differences in olive yield were registered between treatments (P<0.05). Treatment 3 obtained a significantly lower yield (P<0.05) than the other treatments as a consequence of the higher yield obtained in the previous year. Given that the olive tree is characterized by an alternate bearing, a year with low production allows for more vegetative growth. Therefore, the greater leaf mass developed in one year will boost higher yield the following year. This characteristic explains the considerable increase in production that occurred in treatments T1, T2 and T3 from 2014 to 2015. In the case of treatment T3 this increase was not so pronounced since, in 2014, the vegetative growth was conditioned by the existing tree production.

In 2016 significant differences (P<0.05) were found in olive yield between treatments. Treatments T3 and T4 show significantly (P<0.05) lower yield than treatments T1 and T2. The fall in production of treatment T3 compared to treatments T1 and T2 is associated with a reduction in canopy volume due to topping in the summer of 2015 and cutting the west side of the canopy in the winter of 2016, which left these trees with lower leaf mass and consequently with lower fruiting potential. High production in a smaller tree canopy (T4 in 2015) tended to penalize the release of productive branches and, consequently, the production for 2016.

In 2017 production shows the opposite trend to 2016, although no significant differences (P>0.05) between treatments were observed.

The absence of pruning interventions in 2018 contributed to no significant differences (P>0.05) between treatments in olive yield.

On average, over the period 2005 to 2018 significant differences (P<0.05) were found between treatments. Figure 6 shows the average olive yield by treatment during this period. Treatment T3 had registered a significantly (P<0.05) lower yield than treatment T1, but no significant differences (P>0.05) to the other treatments. This result shows that frequent mechanical pruning interventions (T3) tend to penalize olive yield. It can be concluded that performing a more intense mechanical pruning spaced in time is most desirable, as recommended by Pastor and Humanes (1998) for HD olive groves.
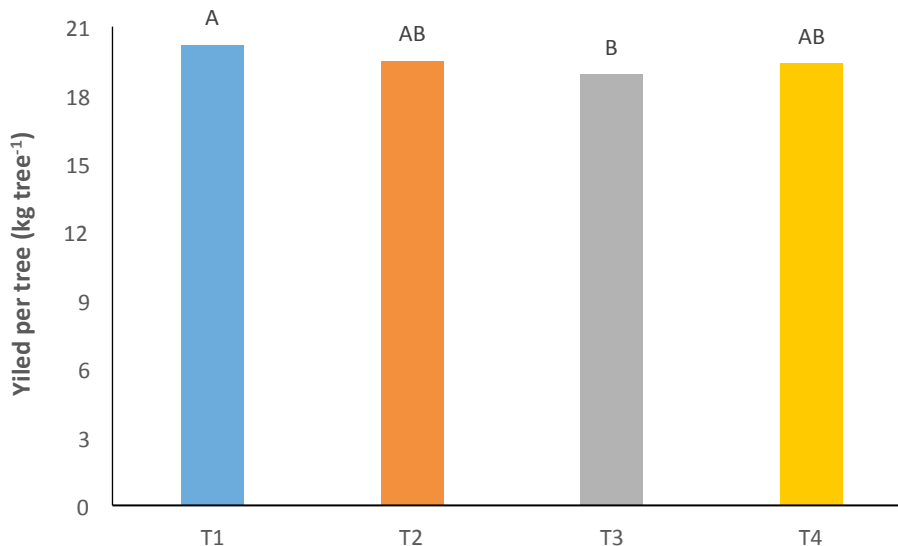
Columns with the same letter are not significantly different by Tukey multiple range test at the 5% level

Figure 6 - Influence of the treatment on olive yield per tree during 14 years period

Applying manual pruning complement to mechanical pruning did not increase olive yield. A manual pruning complement to the mechanical pruning (T2), particularly in years following mechanical pruning, should be regarded as a potentially important technique, since it may contributed to higher yields as verified by Dias *et al.* (2014) on a traditional olive orchard after more than 10 years submitted to mechanical pruning.

These results show the potential of mechanical pruning as a method for reducing labor dependence, without significant negative influence in olive production, in line with the results obtained in traditional olive orchards by Pastor and Humanes (1998), Dias (2006), Dias *et al.* (2012) and Dias *et al.* (2014).

4. Conclusions

In this period of 14 years, on average, mechanical pruning tended to not influence olive yield negatively, except when executed with more frequency.

Given this fact, the following can be concluded:

- the option for pruning with a disc-saw pruning machine on the side faces, in alternate years, is not o good solution since it does not obtain higher production of olives. Carrying out the cuts on the sides of the canopy more frequently- while allowing the canopy volume to be controlled- does not allow for the full-production potential of the regrowth, which appears after the cuts on the side faces.

- manual pruning complement is not useful since it does not lead to an increase in production but tather leads to an increase in pruning costs, as has already occurred in the traditional olive grove trial. Complementary manual pruning interventions only make sense for eliminating excess wood accumulated over a relatively long period of time and should be carried out sporadically. Two supplementary, annual pruning interventions over a period of four years are not advisable.

References

Dias A.B., Falcão, J.M., Pinheiro, A., Peça, J.O. 2020. Evaluation of Olive Pruning Effect on the Performance of the Row-Side Continuous Canopy Shaking Harvester in a High Density Olive Orchard. Front. Plant Sci. 10:1631. doi:10.3389/fpls.2019.01631;

Dias, A.B., Pinheiro, A., Peça, J.O. 2014. Fifteen-Year Evaluation of the Influence of Mechanical Pruning on Olive Yield. Acta Hortic. 1057, ISBN: 978 94 6261 047 7, pp. 335-340, doi:10.17660/ActaHortic.2014.1057.39;

Dias, A.B., Peça, J.O., Pinheiro, A. 2012. Long term evaluation of the influence of mechanical pruning on olive growing. *Agronomy Journal*, Vol. 104, issue 1, 23-25, DOI: 10.2134/agronj2011.0137;

Dias, A.B., Peça, J.O., Santos, L., Pinheiro, A.C., Morais, N., Pereira, A.G. 2008. The influence of mechanical pruning on olive production and shaker efficiency. Acta Hortic. 791, 307-313, DOI: 10.17660/ActaHortic.2008.791.43;

Dias, A.B. (2006) A mecanização da poda da oliveira. Contribuição da máquina de podar de discos. [phd dissertation thesis],Universidade de Évora.

Pastor, M. and Humanes, J., (1998), A poda del olivo – moderna olivicultura, 3ª edición (corregida y actualizada) , Madrid, Editorial agrícola Española S.A.,

Peça, J.O., Dias, A.B., Pinheiro, A.C., Santos, L., Morais, N., Pereira, A.G., Reynolds de Souza, D. 2002. Mechanical pruning of olive trees as an alternative to manual pruning. Acta Hortic. 586, 295-299, doi:10.17660/ActaHortic.2002.586.57.

Comparison of a Light-Weight Experimental Shaker and an Orchard Tractor Mounted Trunk Shaker for Fresh Market Citrus Harvesting

Coral Ortiz[a]*, Antonio Torregrosa[a], Sergio Castro Garcia[b], Jose Miguel Martinez[c], Severiano Real Moreno[b]

[a]Departamento de Ingeniería Rural y Agroalimentaria, Universitat Politècnica de València, Camino de Vera s/n, 46022, Valencia

[b] Escuela Técnica Superior de Ingeniería Agronómica y de Montes, Universidad de Córdoba, Campus de Rabanales, Ed Leonardo da Vinci, Ctra N-IVa, km 396, 14071, Córdoba

[c]Anecoop S. Coop. Valencia

*Corresponding author: Email cortiz@dmta.upv.es

Abstract

In a previous experiment, a designed light weight experimental shaker had been successfully used to collect oranges from ornamental trees. In this study the experimental device has been tested to harvest fresh market citrus. The objective of this work was to evaluate the removal efficiency and operational times of the experimental device compared to an orchard tractor mounted trunk shaker. Fruits were collected using cushioned and elevated canvas to reduce citrus damage. The light weight, linear and low cost, experimental shaker was coupled to a pedestrian tractor.

In a preliminary test, vertical branches from `Navelina´ and `Fukumato´ varieties were tested. In a second step, after a modification in the shaking arm, nine similar trees, according to size and structure, from the Navel group, `Caracara´ variety, were selected and tested. Removal efficiency, vibratory frequency and amplitude, fruit and tree damages and fruit quality were measured. Additionally, a high-speed camera was used to record operational times and to determine cumulative removal percentage over vibration time.

No significant differences in removal efficiency were found between the two harvesting systems (average values of 69 % with the prototype compared to 77 % with the trunk shaker). However, removal efficiency using the experimental device was reduced and working time increased when the access to the main branches to be shaken was difficult. In agreement with previous results, the curve representing the branch cumulative removal percentage in time followed a sigmoidal pattern. A model was developed showing that during the first 5 s more than 50% of the fruits were detached, after 12 s 60% and only 4% more when vibrating 40 s. Regarding fruit damage, slightly damaged fruit percentage was higher when using the experimental shaker, especially little cuts and abrasions. This fact could be due to the fruit friction against thin twigs during the high amplitude vibration.

Keywords: citrus, harvest, vibration

1. Introduction

Mechanical harvesting systems has been studied to solve the problem of the high costs of manual harvesting in Spanish fresh citrus production. Previous results showed the effectiveness of vibration systems for mechanical citrus harvesting (Ortiz and Torregrosa, 2013; Castro-García et al., 2019). Two types of shakers were used: a tractor mounted trunk shaker and a hand-held shaker with a petrol engine. Trunk shakers can be used to harvest citrus fruits using frequencies around 15 Hz to 25 Hz.

Previous laboratory studies have shown the possibility of detaching citrus fruit using lower frequencies and higher strokes to reduce leaf losses (Torregrosa et al., 2014).

A light-weight experimental shaker was developed and successfully tested to harvest ornamental citrus trees (Torregrosa et al., 2019). The frequency used was between 4 Hz to 6 Hz and the stroke was 0.06 m. The gripper is capable to grasp the low diameter trunk to be shaken.

The light-weight experimental shaker was improved to harvest fresh citrus orchards, trees with high trunk diameter and several main branches. In this case, the main branches need to be grasped.

The objective of this work was to evaluate the removal efficiency and operational times of the experimental light-weight shaker compared to an orchard tractor mounted trunk shaker.

2. Materials and Methods

2.1. Materials

Healthy and well-managed trees from the variety 'Caracara' from an ANECOOP experimental orchard in Museros (Valencia) were tested.

The trees were planted in a grid with in-row spacing of 4 m and 5 m between rows. Rows were on trapezoidal ridges (0.3 m in height and 2 m wide at the top). The trunk height was (mean ± SD) 0.41 ± 0.03 m and the trunk diameter was

0.11 ± 0.01 m. The trees had three to five main branches. The canopy height of the aboveground level was 2 ± 0.2 m. The height from the ground to the canopy skirt was 0.35 ± 0.2 m. The canopy diameter perpendicular to the row was 2.9 ± 0.2 m. The canopy diameter parallel to the row was 3.6 ± 0.2 m.

2.2. Methodology

Two different harvesting systems were tested (experimental light-weight shaker and orchard tractor mounted trunk shaker).

The tractor mounted trunk shaker was arranged in two parts: one part (with a mass of 640 kg) was attached at the tractor's rear three-point hitch and included the oil tank and the pumps operated by the tractor's power take-off; the other part (with a mass of 730 kg) was coupled to the front three-point hitch and included an extendable arm and a clamp with two moving fingers, Figure 1. Also included was the hydraulic motor that drives an eccentric mass of 16 kg with an eccentric radius of 0.13 m that produces an orbital vibration (Topavi light shaker, Maquinaria Agrícola Garrido s.l. (Topavi), Autol, Spain, www.topavi.es). In all cases, the tree trunk was clamped at around 0.2 m above the ground. The tractor was a 66 kW four-wheel-drive model.

Figure 1. Tractor and trunk shaker used in the study.

The experimental light-weight shaker (Figure 2) was a light weight, linear and low cost, experimental shaker. The clamp is made of two steel fingers covered with 60 mm thick rubber pads. The fingers were moved by a hydraulic cylinder. The shaker was hitched to the forks of a pedestrian hydraulic tractor (Hinowa, Nogara, VR, Italy; Hinowa.com) 'Hinowa' model 'HS 11000 provided with a fork elevator. The shaker was powered by a hydraulic motor, that received the oil from the external supplies of tractor Lamborghini Plus 990-F that gave a flow of 21 L min^{-1} at 100 bar, or from a John Deere 5820 tractor that gave a flow of 26 L min^{-1} at 100 bar. The vibration amplitude used was 0.60 m.

Nine trees were testes (three with the trunk shaker and six with the experimental shaker. With the trunk shaker two strokes of less than 4 s each of vibration time were applied.

The detachment percentage was calculated by counting and weighing the oranges removed and those remaining on the trees after being picked by hand. To determine the removal percentage according to the vibration time, high-speed video recordings were analyzed. The accumulated number of detached fruits according to the total number of fruits was calculated and related to the vibration time. The actual frequencies were measured using a triaxial accelerometer (type 8763A500, Kistler Instrument Corp., Novi, Mich., ±500 g range, 10 mV g-1 sensitivity, 3.3 g weight, mini-cube design, 0.01 m length) and with highspeed 300 fps video recording (counting cycle time). The video recording was also used to calculate the different working and access times.

Figure 2. Experimental light-weight shaker elements (left) and the shaker vibrating a tree.

3. Results and Discussion

3.1. Detaching times

The registered frequency of the trunk shaker was around 19 Hz with a cumulated time lower than 8 s, with two strokes of less than 4 s each of vibration time.

The experimental shaker worked with a lower frequency (5.7 Hz) with an accumulated time of 50 s. The working time increased when the access to the main branches to be shaken was difficult. The time required to access the vibrated branches were between 16 s to 52 s (37.8 s ± 19.2 s). However, some of the main branches had a very extremely difficult access and the required time was not included. The gripping time was between 3 s to 5 s. And the shaking time was between 14 s to 50 s (31.3 s ±10.5 s).

3.2. Removal percentage

No significant differences were found between the removal percentage using the experimental shaker and the trunk shaker (69% compared to 77 %, respectively), Figure 3. However, the removal percentage of the experimental shaker is lower if the total removal percentage is considered (including the fruit from the non-vibrated branches).
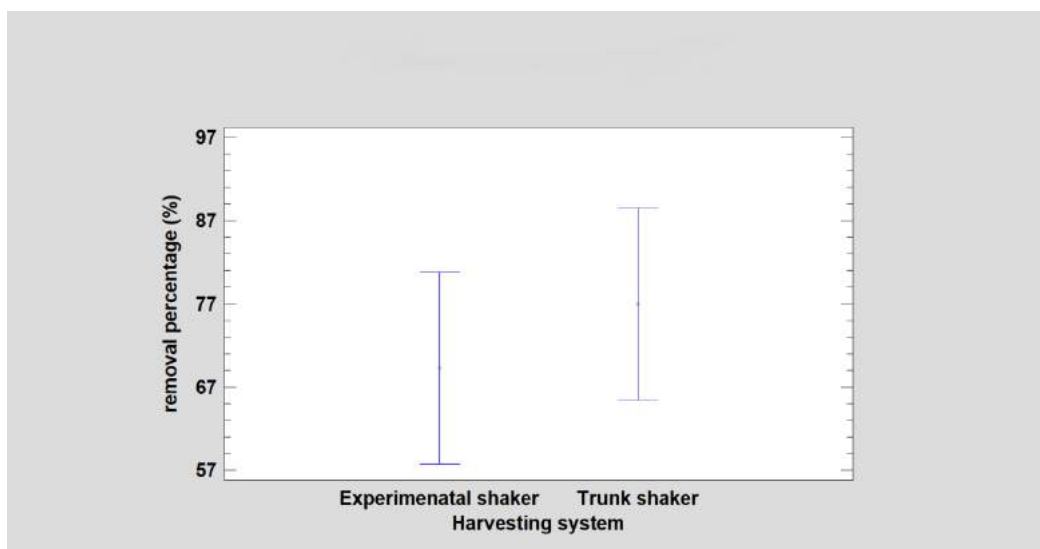
Figure 3. Removal percentage (%) using the experimental shaker and the trunk shaker (average and Fisher LSD intervals)

3.3. Branch removal percentage according to time

The branch removal percentage related time was analysed using the vibration recorded videos. As reported in previous laboratory tests using low frequency and high amplitude (Ortiz and Torregrosa, 2013), the removal percentage change follows a sigmoidal behaviour with the vibration time, Figure 4.
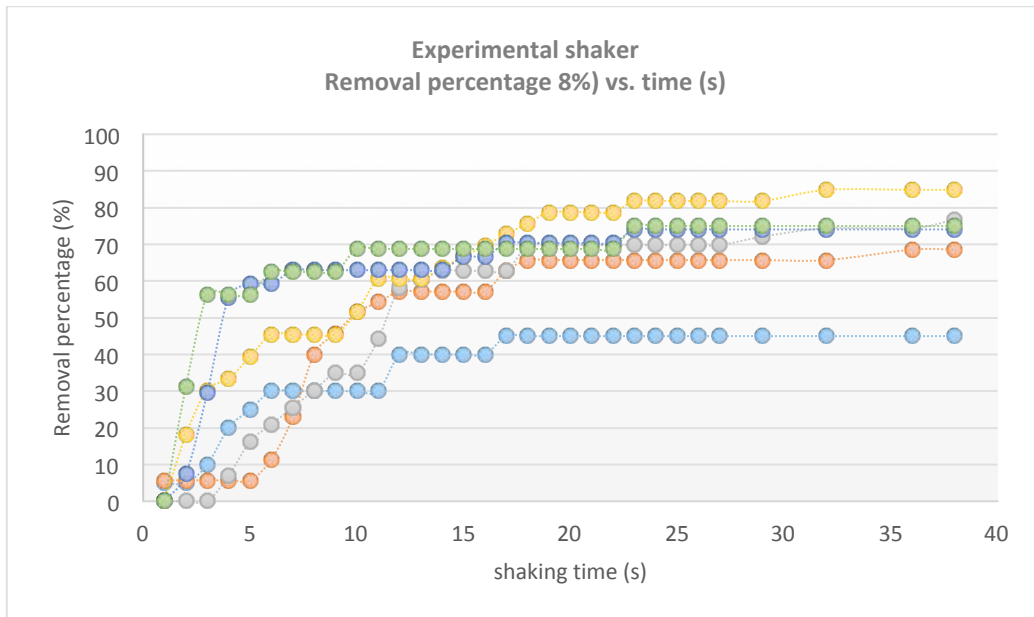
Figure 4. Accumulated branch removal percentage (%) according to time using the experimental shaker in six different branches.

Using the data of the accumulated removal percentage related to time from the different vibrated branches, a modelized curve was built, Figure 5.
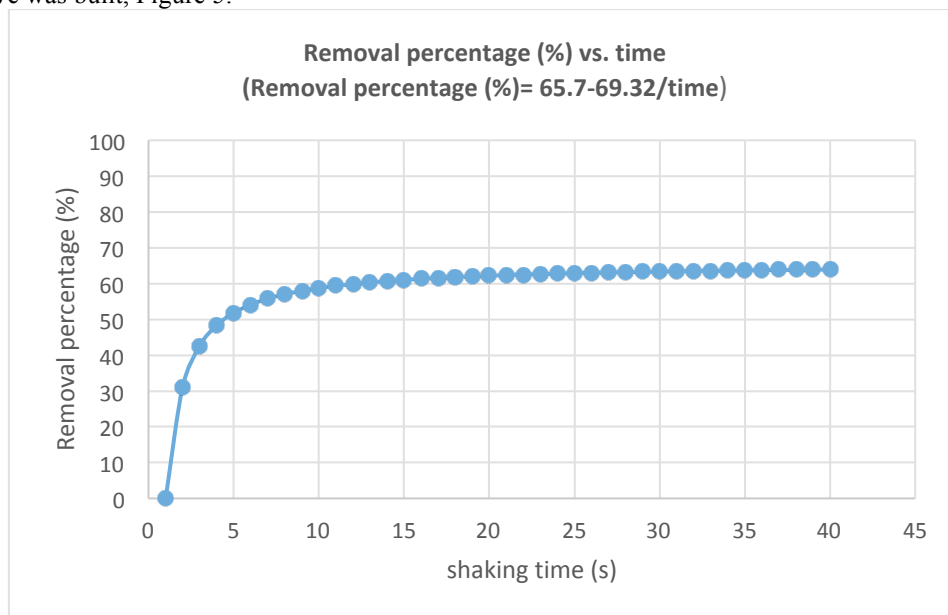
Figure 5. Modelized curve of the branch removal percentage related to time.

In the first 5 s, 50 % of the fruit from the branch was removed, after 12 s 60% of the fruit and after this time only 4% more was removed.

4. Conclusions

The trunk shaker frequency was around 19 Hz and with an accumulated time lower than 8 s, with two strokes of less than 4 s each of vibration time. The experimental shaker worked with a lower frequency (5.7 Hz) and with an accumulated time of 50 s. However, it was proven that the first 12 s were the most important.

The removal percentage (considering the vibrated branches) is slightly lower using the experimental shaker compared to the trunk shaker (69% compared to 77%). With the experimental shaker, the differences in removal percentage are related to the impossibility of vibrating some of the main branches This fact and the difficulty accessing some of the main branches reduced the working capacity of the experimental shaker.

The removal percentage with the experimental shaker follows a sigmoidal behaviour with the vibration time. Most of the fruit was removed in the first 12 s.

References

Castro-Garcia, S., Aragon-Rodriguez, F., Sola-Guirado, R.R., Serrano, A.J., Soria-Olivas, E., Gil-Ribes, J.A. 2019.Vibration Monitoring of the Mechanical Harvesting of Citrus to Improve Fruit Detachment Efficiency. *Sensors*, *19*, 1760. https://doi.org/10.3390/s19081760

Ortiz, C., Torregrosa, A. 2013. Determining adequate vibration frequency, amplitude, and time for mechanical harvesting of fresh mandarins. Transactions of the ASABE, 56(1), 15-22. http://doi: 10.13031/2013.42581

Torregrosa, A., Albert, F., Aleixos, N., Ortiz, C., Blasco, J. 2014.Analysis of the detachment of citrus fruits by vibration using artificial vision. Biosystems Engineering, 119,1-12. https://doi.org/10.1016/j.biosystemseng.2013.12.010

Torregrosa, A., Molina, J.M., Pérez, M., Ortí, E., Xamani, P., Ortiz, C. 2019. Mechanical Harvesting of Ornamental Citrus Trees in Valencia, Spain. *Agronomy*, *9*, 827. https://doi.org/10.3390/agronomy9120827

Estimating Costs of a Chestnut Mechanical Harvester

Arlindo Almeida [a,*], António Borges [b]

[a] Centro de Investigação de Montanha (CIMO), Instituto Politécnico de Bragança, Campus de Santa Apolónia, 5300-253 Bragança, Portugal

[b] Geosil - Empreendimentos Agrosilvícolas, 5300-802 Rebordainhos, Portugal

* Corresponding author. Email: acfa@ipb.pt

Abstract

In some European chestnut producing regions, harvest is mostly manually. However, due to the difficulty to find available labour, a significant number of producers are changing harvesting procedures, adopting mechanical systems.

There is not reliable information about costs associated to this harvesting system. This information can assume great importance for producers decision.

To contribute for the performance assessment of harvesting equipment based on a vacuum harvester, field trials to evaluate work rates has been carried out in Northeast of Portugal.

With the data collected it is possible to estimate associated costs and contribute for a better understanding of the feasibility of this procedure.

To evaluate the equipment work rate, time for each elementary operation was measured.

Work rate is presented by the ratio worked area / time.

Costs are computed under international standards for agricultural machinery management.

In environmental conditions and agriculture systems in the geographical area were field trials took place, vacuum harvesters can reduce harvesting time and associated costs. It can be an answer to the lack of labour required for manual harvesting.

Despite the need for further studies, this seems to be a good solution for lack of manpower problem. It is also necessary to change some agricultural practices in the field to improve the harvesting machines performance, such as soil management.

Keywords: mechanization, fruit harvesting, performance.

1. Introduction

Usually in chestnut (*Castanea sativa*) producing regions, harvest is manually, collecting from the soil previously fallen chestnuts.

With the aging of the rural population and the exodus of young people to other regions and activities, it is difficult to find available labor. Harvest mechanization is one solution to this problem.

Answering to this demand in the last years different chestnut harvesting systems became available in the market.

These harvesting systems can reduce harvesting time through better work rates and enabling to harvest in the optimal timing, improving fruit quality.

Reducing manpower needs is another goal that can be achieved.

To contribute for the performance assessment of harvesting equipment based on one of harvesting systems available, field trials to evaluate work rates has been carried out in Northeast of Portugal.

With the data collected associated costs was evaluated.

The harvesting system studied is based on a self-propelled vacuum harvester.

Results of the study are presented. They can contribute for a better understanding of this procedure feasibility.

2. Materials and Methods

Field trials took place in Northeast of Portugal in November 2018 and 2019 in chestnut orchards with altitudes between 800 and 900 meters, with a slight slope (up to 5%) of the cultivar Judia, with 25 to 35 years of age, spacing 9/10 m x 10/11 m (Figure 1). Soil is not mobilized. Grass cover is maintained.

The mechanical harvesting system studied is based on a self-propelled 74 kW vacuum harvester (Figure 2) (*Facma Cimina 380)*. Harvesting width is 3 m. Chestnuts sucked from the soil, are temporarily stored in an adapted trailer (Figure 2) with a capacity of approximately 1,500 kg, pulled by the harvesting equipment.

The equipment collected fruits in the area between tree lines in three or four parallel strips depending on the distance between rows. After the last of these passages, the equipment proceeded to the next inter row area. Tests were performed using two different harvesting methods. In field tests I, chestnuts are harvested during the three or four trips

and in the turns within each inter row. In field tests II, chestnuts are harvested during the three or four trips between rows, but not during each inter row. There is an interruption in the harvest between the turns between the tree lines, both in tests I and tests II. Field I tests were carried out in the beginning of the harvesting season, with a reduced amount of debris on the soil. Field tests II took place in a late stage of the season, in a repeated harvesting in the same place (double harvest), with a significant amount of debris (leaves, branches and burrs) on the soil. It is on the trailer indicated referred before (Figure 2) that the chestnuts harvested are removed from the orchard.

Figure 1. Orchard were field trials took place

Figure 2. Harvesting equipment and adapted trailer

This harvesting system needs one operator.

To evaluate the equipment work rate, time for each elementary operation was measured in minutes with a chronometer: harvesting time; inoperative time; turning time within two rows (during which harvesting continues) and turning time for switching between rows (during which harvesting stops). Inoperative time refers to the interruption of work to clear the product flow in the internal equipment parts.

Working rate is evaluated in ha h^{-1}.

Costs are evaluated following methodology proposed by Fidalgo et al (2006), Ortiz-Cañavate et al (2003), Hunt (1983); Edward (2015).

According to this methodology, agriculture machinery costs can be divided into two categories: annual ownership costs, which occur regardless of machine use, and operating costs, which vary directly with the amount of machine use. The true value of these costs cannot be known until the machine is sold or worn out. But the costs can be estimated by making a few assumptions about machine life, annual use, and fuel and labor prices.

The following assumptions were taken to evaluate costs:

A total of 250 hours $year^{-1}$ of work is assumed to be the average within the harvesting season, which spreads from mid-September till end of November.

To evaluate the annual total costs it was assumed a purchasing price of 72,320 € for the harvester more 2,000 € for the trailer (a total of 74,320 € for equipment purchasing cost, including taxes). Equipment salvage value estimated as 10% of purchasing cost. An expected economic life time of 10 years for both equipment.

Fuel costs were also assumed as follows: fuel consumption: 7.5 L $hour^{-1}$; fuel cost: 1.3 € L^{-1}. Considered 250 hours $year^{-1}$ of work.

Labour costs were also assumed as follows: cost $year^{-1}$ $person^{-1}$: 9,000 €; social and insurance cost increase: 20%; person total hours $year^{-1}$: 2,000. Work hours for this equipment: 250 hours $year^{-1}$.

Ownership costs (also called fixed costs) include depreciation, interest (opportunity cost), taxes, insurance, and housing.

Depreciation is a cost resulting from wear, obsolescence, and equipment age. To estimate annual depreciation, economic life and salvage value need to be assumed (see assumptions).

Depreciation was computed by the following equation Eq (1):

$$Depreciation = \frac{purchase\ cost - salvage\ value}{economic\ life} \qquad (1)$$

Interest, taxes, insurance, and housing was not considered in this study because these items presume a high level of subjectivity.

Operating costs (also called variable costs) include repairs and maintenance, fuel, lubrication, and operator labor.

Repair costs for a particular type of machine vary widely from one geographic region to another because of soil type, terrain, climate, and other conditions. Within a local area, repair costs vary from farm to farm because of different management policies and operator skill.

Because all these factors and their variability, the best data for estimating repair costs are records of owners past repair expenses: 350 € year[-1] in average for this particular equipment.

Fuel consumption was estimated by records of owners (see assumptions). Actual fuel cost L[-1] was assumed.

Labour cost was computed by the following equation Eq (2), considering assumptions referred previously:

$$Equipment\ annual\ labour\ cost = \frac{Total\ annual\ labour\ cost \times 1.2}{Total\ annual\ hours} \times 250\ hours \qquad (2)$$

The sum of the indicated items represents the equipment annual cost. Equipment cost per hour was calculated considering 250 hours year[-1] of harvesting work.

3. Results and Discussion

Figure 3 shows kg of chestnut harvested hour[-1] and Figure 4 the work rate results in tests 1 and 2.
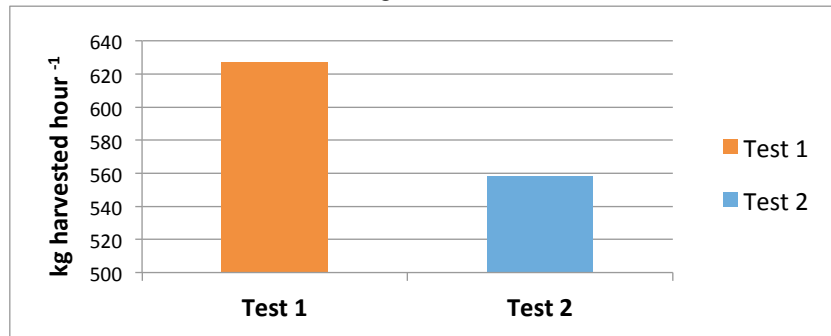
Figure 3. Chestnuts harvested kg h^{-1}
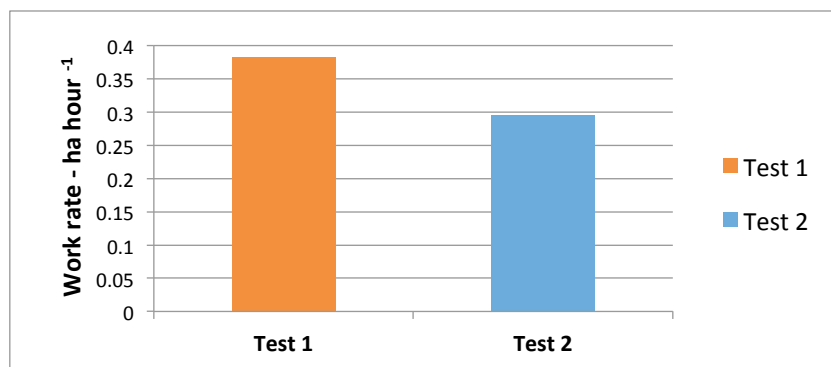
Figure 4. Work rate ha h^{-1}

Field tests 2 took place in a late stage of the season with a significant amount of debris (leaves, branches and burrs) on the soil. This is the reason why in this double harvesting the amount of chestnut harvested is lower. The work rate is lower in consequence of an increase of inoperative elementary time, necessary to clean the chestnut flow inside the equipment (Figures 5 and 6).
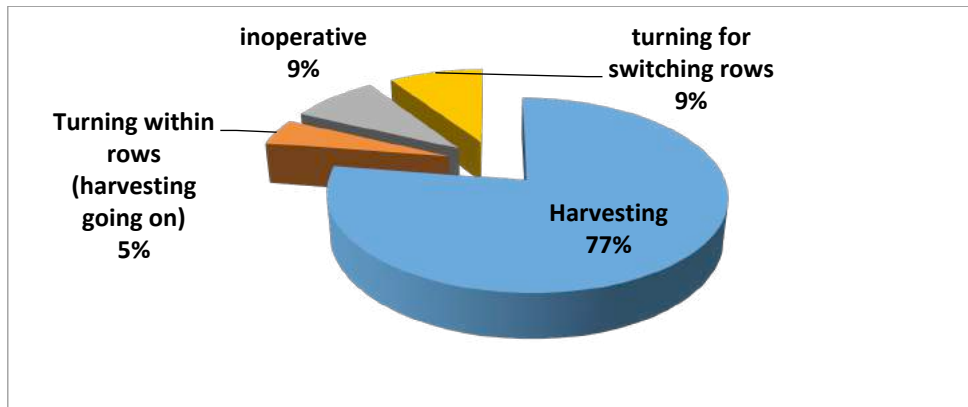
Figure 5. Test 1 – relative importance of elementary operations time.
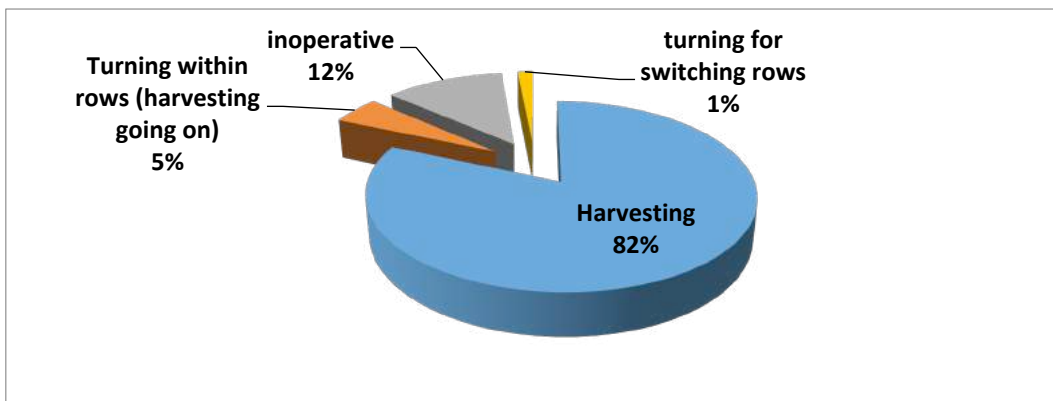
Figure 6. Test 2 – relative importance of elementary operations time.

In Table 1 are presented the annual costs computed under the assumptions mentioned in methods.
Figure 7 represents relative percentage items costs.

Table 1. Annual costs for the harvesting system considered

Annual costs considered	Total costs year^{-1}
Depreciation	€ 6,689
Repairs and maintenance	€ 350
Fuel	€ 2,437
Labour	€ 1,350
total	€ 10,826
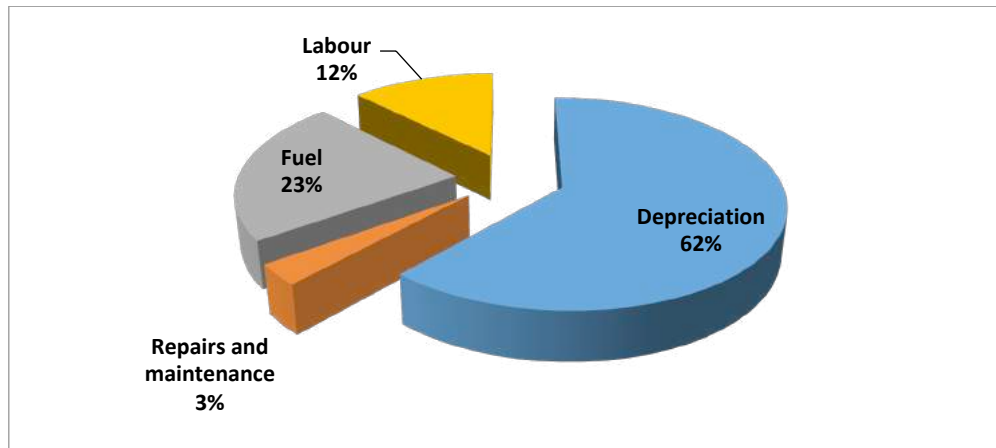
Figure 7. Relative importance of costs items considered.

According these results, cost kg^{-1} chestnut harvested is €0.07 for test 1 and €0.08 for test 2. The increase of cost kg^{-1} in test 2 is consequence of work rate results. Despite the lower performance on double harvesting this procedure is necessary because fruits continuously fall from the trees over the ripening period.

The work rate of manual harvesting expected is 20 kg h^{-1} to 30 kg h^{-1} per person (Monarca D. et al 2003; Monarca D. et al 2014a).Considering a cost of € 7 h^{-1} per operator, it's reasonable to expect a cost € 0.24 to € 0.36 kg^{-1} for manual harvesting.

According mechanical harvesting results presented, a significant cost savings can be achieved (Figure 8).
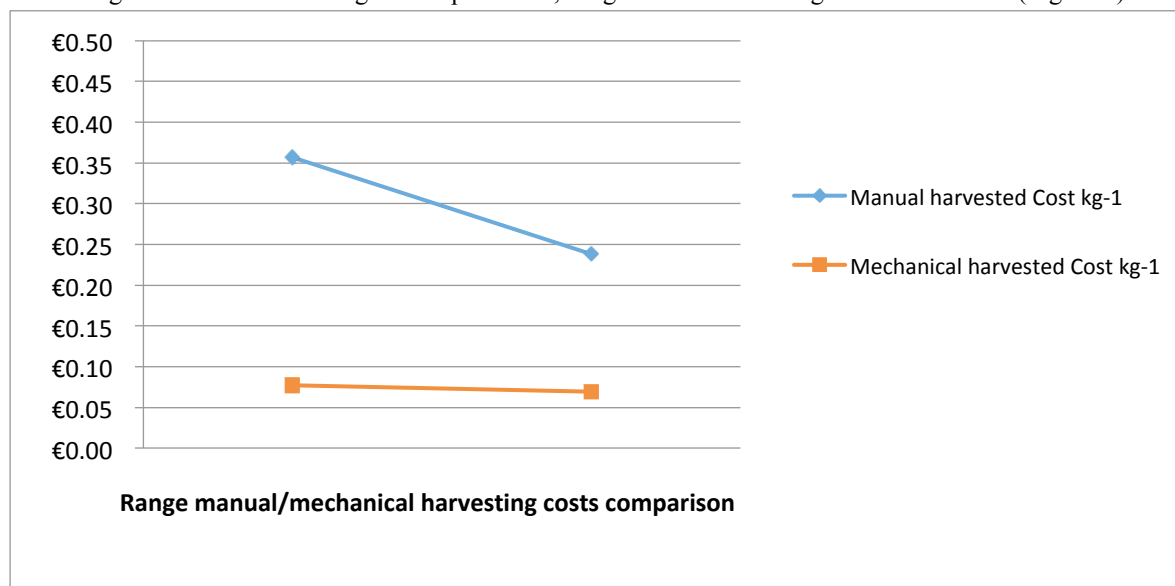
Figure 8. Comparing manual *vs* mechanical costs

4. Conclusions

The results show a work rate vacuum harvester higher, compared with manual harvesting work rate. With the harvesting system studied using a self-propelled vacuum harvester with one operator, it is expected to harvest 593 kg hour^{-1} person^{-1}. With manual harvesting it is expected to harvest 20 to 30 kg hour^{-1} person^{-1} (Monarca et al 2003 and 2014a). This advantage turns easier to match the optimum time to harvest with the area. The reduction in the time facilitates double harvesting procedure (harvest the same area twice), reducing the period of contact of the fruit with the soil, advantageous for the chestnut sanitary status.

The reduction of costs provided by mechanical harvesting is considerable, compared with manual harvesting.

It is possible to conclude that the chestnut mechanical harvesting studied it is possible to achieve considerable advantages:

It is a solution to the labor shortage for this operation.

Significant costs reduction.

Improvement of chestnut sanitary status.

Soil management is a relevant aspect for this operation. For the good suction of the fruits, they must be on an efficient cover of the soil. Soil must have a good grass covering, clean of inert and vegetal residues resulting from agricultural practices. Mechanical harvesting is not compatible with plowed chestnut groves.

Acknowledgements

References

Edward, W. (2015) *Estimating Farm Machinery Costs,* Iowa University Extension and Outreach File A3-29 PM 710 https://www.extension.iastate.edu/agdm/crops/pdf/a3-29.pdf
Accessed May 17, 2021.

Fidalgo, J. Boto (coordenador); Díez, Javier; Gabella, Victor; Santamarta, Pablo; Ordónez, David (2006) *La mecanización agraria, principios y aplicaciones*, 2ª edição, Universidad de León, Secretariado de Publicaciones.

Guyer, D.E.; De Kleine; M.E. and Perry; R.L. (2012). *New approaches in cherry and chestnut harvest systems*. Acta Hortic. 965, 189-194

DOI: 10.17660/ActaHortic.2012.965.25 https://doi.org/10.17660/ActaHortic.2012.965.25

Hunt, Donnel (1983) *Farm Power and Machinery Management*. 8th edition, Iowa State University Press, Ames.

Monarca, D.; Cecchini, M.; Antonelli, D. (2003). *The influence of mechanical harvesting on the quality of chestnuts: experiences in the monti cimini area*. Acta Hortic. 599, 611-616

DOI: 10.17660/ActaHortic.2003.599.79 https://doi.org/10.17660/ActaHortic.2003.599.79

Monarca, D.; Cecchini, M.; Antonelli, D; Mordacchini Alfani, M.L.; Salcini, M.C.; Massantini, R. (2005). *Mechanical harvesting and quality of ´marroni´ chestnut*. Acta Hortic. 682, 1193-1198

DOI: 10.17660/ActaHortic.2005.682.158 https://doi.org/10.17660/ActaHortic.2005.682.158

Monarca, D.; Cecchini, M.; Colantoni, A.; Menghini, G.; Moscetti, R.;Massantini, R. (2014a). *The evolution of the chestnut harvesting technique*. Acta Hortic. 1043, 219-225

DOI: 10.17660/ActaHortic.2014.1043.29 https://doi.org/10.17660/ActaHortic.2014.1043.29

Monarca, D.; Moscetti, R.; Carletti, L.; Cecchini, M.; Colantoni, A.; Stella, E.; Menghini, C.; Speranza, S.; Massantini, R.; Contini, M.; Manzo, A. (2014b). *Quality maintenance and storability of chestnuts manually and mechanically harvested*. Acta Hortic. 1043, 145-152 DOI: 10.17660/ActaHortic.2014.1043.19
https://doi.org/10.17660/ActaHortic.2014.1043.19

Ortiz-Cañavate, Jaime; Ramos J.; Sierra, J. Martos, J.; Altisent, Margarita; Ubierna, Constantino. (2003) *Las maquinas agricolas y su aplicación*, Mundi-Prensa, 6ª edición, Madrid, ISBN: 84-8476-117-7

New application technologies and mechanisation

Lateral Stability Performance of Narrow-track Tractors

Bruno Franceschetti [a], Valda Rondelli [a], Enrico Capacci [a]

[a] Department of Agricultural and Food Sciences (DISTAL), University of Bologna, Viale G. Fanin 50, 40127 - Bologna, Italy

* Corresponding author. Email: bruno.franceschetti@unibo.it

Abstract

A tractor losing lateral stability starts to rollover. It is a matter of fact that tractor lateral rollover accident is one of the most frequent causes of death and injuries for the farmers. Consequently, tractor is fitted with a specific protective structure to minimise the consequences for the driver during the rollover (ROPS). The narrow-track tractor, designed to operate in vineyards and orchards, is a tractor category with a very narrow track width and the risk of rollover is higher.

The aim of the study was to evaluate the compact narrow-track tractor types commercially available, designed to mount a cantilever engine in the forward position with effects on the Center of Gravity (CoG) because more than 50% of the tractor weight is loaded on the front axle, and specifically the articulated narrow-track tractors where the stability is affected by the pivot point connecting the two tractor bodies. As a consequence of the typical tractor design of the articulated tractors, during the steering action the line passing through the front and rear tire contact points on the ground changes influencing the tractor stability. Moreover, the horizontal rotation of the tractor pivot point influences the tractor CoG position and finally the tractor stability. The approach of the research was based on reproducing the lateral stability tractor condition by developing a kinematic model, with the goal to virtual simulate the tractor behaviour and to calculate the lateral stability angle for the steering wheel and the articulated tractors. The model at the tractor design stage will allow adjusting the tractor parameters to improve the lateral stability performance.

Keywords: Articulated tractor, stability angle, mathematical model, safety, rollover.

1. Introduction

Tractor overturning accidents on slopes have serious consequences for the farmer (Hunter & Owen, 1983). Studies indicate that over 80% of tractor accidents are sideways overturns (Rondelli, Martelli, & Casazza, 2018). Determining the lateral stability of agricultural tractor has been a subject to deepen for tractor designers and researchers over the years (Kim & Rehkugler, 1987; Shu, Ahmad, & Akande, 2010). Studies were conducted to determine the factors influencing tractor stability in sloped fields (Franceschetti, Rondelli, & Ciuffoli, 2019; A. Guzzomi & Rondelli, 2013). The tipping event for a tractor in static condition was also analysed (A. L. Guzzomi, 2012). The tractor stability issue on slopes was studied for vehicles designed with fixed-chassis (Grecenko, 1984) and with articulated chassis (Mazzetto, Bietresato, Gasparetto, & Vidoni, 2013); so as for the combination tractor-implement (Yisa, Terao, Noguchi, & Kubota, 1998). Pershing and Yoerger (Pershing R.L. & Yoerger R.R., 1969) investigated the tractor dynamic behaviour on side slopes. Dynamic studies relating inertia properties and energy levels during the tractor rollover were performed (Franceschetti, Lenain, & Rondelli, 2014; A. Guzzomi, Rondelli, Guarnieri, Molari, & Molari, 2009).

Since the last century many research approaches were addressed to develop models for predicting the tractor behaviour in normal operation with the aim to reduce the risk of rollover (Franceschetti, Capacci, & Rondelli, 2016; Li et al., 2016; Spencer, 1978). These attempts were combined to the design of passive protective devices (Roll-Over Protective Structures, ROPS) to be mounted on the tractor to minimize the risk of driver injuries in case of a rollover event. Indeed, over the time it has been recognised that the tractor is really a vehicle prone to rollover because of the high versatility in the use and in the operating conditions (A. L. Guzzomi, Rondelli, & Capacci, 2019; Liu & Ayers, 1999). Nevertheless formulating a tractor lateral stability model is a difficult exercise mainly in properly defining the geometry of the machine and predicting the kinematic effects during its operation in the field, since the forces and moment arms are not coplanar, especially if the case of articulated chassis tractors is considered (Gibson, Elliot, & Persson, 1971). However vector methods provide a powerful analytic tool for the description of 3D motion such as the sideways overturning of a farm tractor (Smith, Perumpral, & Liljedahl, 1974). Basing on this approach, with the aim to calculate the lateral stability angle of a tractor designed with articulated chassis independently on its position on the ground, a kinematic model based on the mass and geometrical tractor data was developed. Often modern compact narrow track tractors are made of two separate bodies centrally joined. These vehicles are frequently in use on sloped areas in orchard, vineyard and forage harvesting operations. Consequently, to analyse the stability performance of articulated chassis tractors is of interest in reason of the specific and wide use currently foreseen in narrow environments and sloped areas.

The model was developed considering the tractor as composed by two rigid elements with different mass and geometry. The two body parts were modelled as joined by two links allowing for two different rotations, horizontal (roll angle) and vertical (yaw angle) rotations. The tractor model evaluates the effect of the two mutual rotations of the

tractor bodies, estimating the influence of the tractor masses repartition. The goal was to determine the unstable equilibrium of the tractor by defining the slope angle of the ground in order to calculate the lateral stability angle of the tractor.

2. Materials and Methods

To identify the unstable equilibrium condition of a compact articulated chassis tractor, a kinematic model was developed to evaluate the tractor lateral stability performance. The model can estimate the critical configuration of the tractor overcoming the unstable equilibrium with the consequence that the rollover event starts.

2.1. Kinematic model for lateral stability test

In developing the kinematic model to study the behavior of a compact articulated chassis tractor, the design of the tractor was simplified considering a rear body, composed of the rear axle and the driver seat, joined to a front body, made of the front axle and the engine. The tractor rear body was allowed to assume an angle of inclination and a position different with respect to the front body because of the pivot point jointing the two bodies. This articulation mechanism in the normal operation of the tractor affects its configuration during the steering action, the rear and front parts can mutually rotate to change the tractor path. Assumptions made to derive the mathematical model of the tractor were: tractor composed of two rigid bodies centrally joined to permit their mutual rotation, the full tractor CoG divided into two distinct portions that are the rear and front tractor body CoG, tractor median longitudinal plane, defined with respect to the two bodies in the straight configuration, symmetrical and parallel to the y-z plane, aerodynamic forces ignored, ground surface nondeformable and slip effect of the tractor on the ground ignored. Five characteristics points were identified to describe the virtual tractor. The approach in modelling the compact articulated tractor was to represent the complex geometry of the vehicle (Figure 1-a) through the decomposition of the tractor into two bodies, front and rear ones, connected with a joint allowing their mutual rotation both on the vertical axis of the tractor (yaw angle – μ, Figure 1-b and Figure 2-b), and on the longitudinal one (roll angle – ϑ, Figure 1-b and Figure 2-c), identifying five parameters related to the geometry and the mass repartition of the tractor (Figure 1-b):

$$\overrightarrow{P_1} = x_{P_1}\hat{\imath} + y_{P_1}\hat{\jmath} + z_{P_1}\hat{k} \tag{1}$$

$$\overrightarrow{P_2} = x_{P_2}\hat{\imath} + y_{P_2}\hat{\jmath} + z_{P_2}\hat{k} \tag{2}$$

$$\overrightarrow{G_1} = x_{G_1}\hat{\imath} + y_{G_1}\hat{\jmath} + z_{G_1}\hat{k} \tag{3}$$

$$\overrightarrow{G_2} = x_{G_2}\hat{\imath} + y_{G_2}\hat{\jmath} + z_{G_2}\hat{k} \tag{4}$$

$$\vec{S} = x_S\hat{\imath} + y_S\hat{\jmath} + z_S\hat{k} \tag{5}$$

where $\overrightarrow{P_1}$ and $\overrightarrow{P_2}$ are the contact points of the rear and front tires on the ground, $\overrightarrow{G_1}$ and $\overrightarrow{G_2}$ specify the position of the CoG of the rear and front bodies of the tractor and $\vec{S}$ is the pivot point of the tractor.
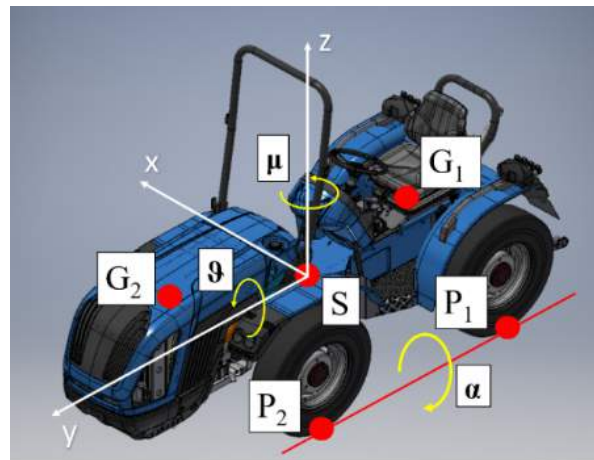
a)   b)

Figure 1. Compact articulated tractor: a) Actual tractor in the straight configuration; b) Graphical representation of the five tractor parameters
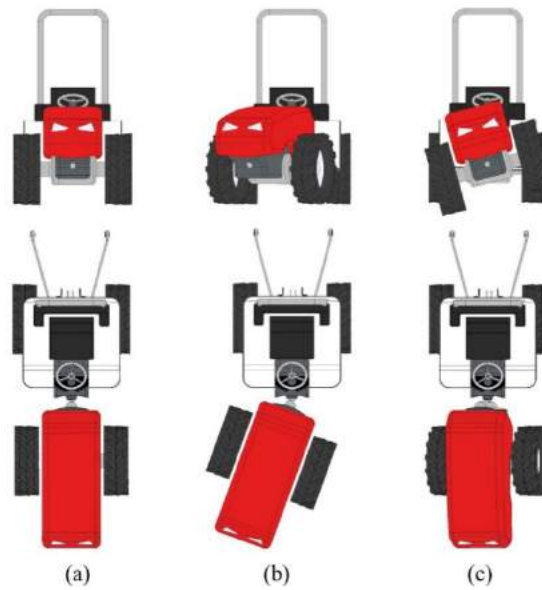
Figure 2. The configurations of the compact articulated chassis tractor:
a) Straight configuration b) Yaw angle limit c) Roll angle limit

When the tractor tip sideways, the first rotation take place about an axis connecting the central pivot point to the contact point of the tire remaining on the ground during the initial tipping motion. Eventually, the tipping body of the tractor strikes a stop on the steady tractor body with further tipping of the whole tractor taking place about an axis connecting the contact points of the front and rear tires on the ground. The lateral stability angle (α) was defined as the angle the full tractor body CoG must assume from the horizontal position on the ground (with the four tractor tires touching the ground) till the inclined position corresponding to the unstable equilibrium of the tractor on the two tires in contact with the ground. The tractor axis of rotation to evaluate the lateral stability angle is varying because affected by the position of the front and rear wheels in contact with the ground plane; these will assume different positions in reason of the mutual rotation of the two tractor bodies, defining the boundary condition the CoG must respect to maintain the stability of the tractor. It is clear, even before analyzing the model results, that the lateral stability angle is linked to the tractor configuration. To represent the complex tractor scenario the first step in modeling was to define a selected configuration based on geometry, masses, and mutual position of the two tractor bodies, to define the roll and yaw angle values. In the second step the corresponding angle of stability was evaluated. Final step will be to identify the worst tractor scenario and to calculate the lateral tractor stability limit angle.

Study development:
a)   Modelling the vertical pivot point (yaw angle)
b)   Modelling the horizontal pivot point (roll angle)
c)   Modelling the lateral tractor stability

2.1.1. Modelling the vertical pivot point (yaw angle)

A fixed chassis tractor typically is designed with front wheels mounted on the steering axle, even if over the years the modern tractors are more and more in the type of four-wheel drive (4WD), where the front axle is at the same time a drive and a steering axle. In the fixed chassis tractor design the yaw angle is equal to zero because the rotation of the front wheels is considered negligible. Taking into consideration the articulated chassis tractor, where the steering action is performed by the rotation of the front body with respect to the rear one, the effect of this rotation needs to be considered. The rotation allowed for the joint defines the yaw angle and affects the two points in Equations (1) and (3). Rotation can be clockwise or anti-clockwise oriented, consistent with a right or a left steering action. Having a maximum value of the yaw angle, a parameter defined at the tractor design stage, tractor bodies can assume positions in between the minimum to the maximum articulation values, with zero value when the two bodies are in the straight configuration, that is a configuration equivalent to a fixed chassis tractor.

The angular orientation of the tractor is related to the rotations about the axes. To model the vertical pivot point, the angular rotation is about the z axis and the following rotation matrix is introducing μ as yaw angle:

$$R_z = \begin{bmatrix} \cos\mu & -\sin\mu & 0 \\ \sin\mu & \cos\mu & 0 \\ 0 & 0 & 1 \end{bmatrix} \tag{6}$$

The new contact point of the rear tire on the ground and the new CoG of the rear body of the tractor are represented by the vector equations, respectively $\overrightarrow{P_1'}$ and $\overrightarrow{G_1'}$:

$$\overrightarrow{P_1'} = \begin{bmatrix} x_{P_1}' \\ y_{P_1}' \\ z_{P_1}' \end{bmatrix} = R_z \begin{bmatrix} x_{P_1} \\ y_{P_1} \\ z_{P_1} \end{bmatrix} \tag{7}$$

$$\overrightarrow{G_1'} = \begin{bmatrix} x_{G_1}' \\ y_{G_1}' \\ z_{G_1}' \end{bmatrix} = R_z \begin{bmatrix} x_{G_1} \\ y_{G_1} \\ z_{G_1} \end{bmatrix} \tag{8}$$

2.1.2. Modelling the horizontal pivot point (roll angle)

The joint connection between the front and the rear body of the tractor allows overcoming the ground unevenness conditions. In the fixed chassis tractor, the joint is designed in the central position of the front axle and its effect on the stability is reduced. In compact articulated chassis tractors, the joint is located in the central part of the tractor chassis causing the mutual rotation of the two tractor bodies when tractor needs to overcome obstacles or ditches. The range of rotation of the two tractor bodies is defined at the design stage but this parameter greatly affects the tractor behavior in terms of stability performance. In critical stability conditions, when the tractor reaches the unstable equilibrium, being the CoGs of the front and rear tractor bodies different, there will be one of the two parts that will represent the worst configuration for the stability effect. A loss of adhesion of a wheel on the ground will be observed and the linked body will rotate of an angle equal to the joint angle, defining a new condition for the tractor. The CoG of the rotated body will be affected. CoG will rotate about the axis defined by the straight line passing through the points, the contact point of the tire on the ground and the pivot point, for an angle equal to the maximum roll angle. In the model, in reason of the geometry and mass repartition of the compact tractor this behavior was ascribed to the front or to the rear tractor body. Nevertheless, to improve the understanding only the event related to the front body of the tractor is considered. Since the initial tipping motion does not take place around either the x, y, or z axes, it is convenient to define the skew coordinate axis about which the tractor is assumed to tip. Introducing ϑ as pivot point angle, following the method of Smith et al. (1974), and let $\vec{v}$ be a unit vector in the direction of the first tipping axis, a rotation matrix can be defined:

$$\vec{v} = (x_v, y_v, z_v) = \frac{x_{P_2}\hat{\imath} + y_{P_2}\hat{\jmath} + z_{P_2}\hat{k}}{\sqrt{x_{P_2}^2 + y_{P_2}^2 + z_{P_2}^2}} \tag{9}$$

$$R_{y'} = \begin{bmatrix} x_v^2 + (1-x_v^2)\cdot\cos(\vartheta) & [1-\cos(\vartheta)]\cdot x_v \cdot y_v - \sin(\vartheta)\cdot z_v & [1-\cos(\vartheta)]\cdot x_v \cdot z_v + \sin(\vartheta)\cdot y_v \\ [1-\cos(\vartheta)]\cdot x_v \cdot y_v + \sin(\vartheta)\cdot z_v & y_v^2 + (1-y_v^2)\cdot\cos(\vartheta) & [1-\cos(\vartheta)]\cdot y_v \cdot z_v - \sin(\vartheta)\cdot x_v \\ [1-\cos(\vartheta)]\cdot x_v \cdot z_v - \sin(\vartheta)\cdot y_v & [1-\cos(\vartheta)]\cdot y_v \cdot z_v + \sin(\vartheta)\cdot x_v & z_v^2 + (1-z_v^2)\cdot\cos(\vartheta) \end{bmatrix} \tag{10}$$

Consequently, the new CoG of the front body of the tractor is:

$$\overrightarrow{G_2'} = \begin{bmatrix} x_{G_2}' \\ y_{G_2}' \\ z_{G_2}' \end{bmatrix} = R_{y'}^T \begin{bmatrix} x_{G_2} \\ y_{G_2} \\ z_{G_2} \end{bmatrix} \tag{11}$$

2.1.3. Modelling of lateral tractor stability

Basing on the CoG of the two tractor bodies, affected by the rotation angles and the masses of the two bodies, the CoG of the whole tractor in the defined scenario is computable. The stability angle of the tractor is calculated by considering the unstable equilibrium when the tractor CoG position falls outside the basis connecting the contact points of the tires on the ground. A determination of the CoG acting on the whole tractor is essential in any prediction of vehicle behavior; it is through the CoG position that the gravity force, if outside the axis connecting the contact points of the front and rear tires on the ground, causes the instability of the tractor. Taking into consideration the distribution of the masses of the tractor, the roll and yaw angles affected the CoG position and the lateral stability angle consequently. Letting W_1 be the weight of the rear tractor body, W_2 the weight of the front tractor body, and W the weight of the full tractor ($W = W_1 + W_2$), the new CoG of the tractor at the instant the tractor begins to tip is located at the point with coordinates:

$$\vec{G} = \begin{bmatrix} x_G \\ y_G \\ z_G \end{bmatrix} = \left(\frac{\sum_{i=1}^{2} W_i x_{G_i}'}{\sum_{i=1}^{2} W_i} \right) \hat{\imath} + \left(\frac{\sum_{i=1}^{2} W_i y_{G_i}'}{\sum_{i=1}^{2} W_i} \right) \hat{\jmath} + \left(\frac{\sum_{i=1}^{2} W_i z_{G_i}'}{\sum_{i=1}^{2} W_i} \right) \hat{k} \qquad (12)$$

The lateral stability angle is a function of the CoG of the full tractor, and the second tipping axis connecting the contact points of the front and rear tires on the ground:

$$\alpha = f\left(\vec{G}, \overrightarrow{P_1'}, \overrightarrow{P_2'} \right) \qquad (13)$$

2.2. Compact narrow-track tractor evaluated

Narrow track tractors are nowadays designed in different configurations affecting the stability performance of the machine (A. L. Guzzomi et al., 2019). In order to better understand the added value of the model developed it is advisable to explain the main behaviour of the articulated chassis tractor and to introduce the tractor configuration data assumed in the simulation. A pivot point is a mechanical tool for the tractor to overcome the ground unevenness. The standard tractor with a fixed chassis is a steering wheel tractor where the pivot point is located in the mid-point of the front axle. Frequently, the compact narrow-track tractor is designed made of two separate bodies joined and the pivot point is close to the geometric center of the tractor. If the tractor is a steering wheel tractor only one degree of freedom is permitted, the longitudinal rotation (roll angle – ϑ). Otherwise, if the tractor is an articulated tractor, two degrees of freedom are permitted, longitudinal and vertical ones (roll angle – ϑ and yaw angle – μ). The values of the input parameters, for a tractor of 55 kW in the unballasted mass configuration, were obtained from Franceschetti et al. (2019). Table 1 lists the geometrical input parameters of the tractor configuration considered.

Table 1. Input tractor parameters.

Identification	Geometric parameter	Unit	Description
$\overrightarrow{P_1}$	(-555; -915; -540)	mm	Rear tire contact point
$\overrightarrow{P_2}$	(-555; 425; -540)	mm	Front tire contact point
$\overrightarrow{G_1}$	(0; -915; 44)	mm	CoG Rear tractor body
$\overrightarrow{G_2}$	(0; 425; 104)	mm	CoG Front tractor body
$\vec{S}$	(0; 0; 0)	mm	Pivot point
W_1	450	kg	Rear tractor body weight
W_2	1090	kg	Front tractor body weight
ϑ	[0 ÷ 7.5]	degrees	Roll angle
μ	[-35 ÷ 35]	degrees	Yaw angle

a)　　　　　　　　　　　　　　　　　　　　　　b)

Figure 3. Tractor configuration: a) Roll angle behaviour b) Yaw angle behaviour

3. Results

The mathematical model was used to examine the behavior of the tractor to variable inputs of the rotation angle to produce a steering effect. By combining the effect of the roll and yaw angles, the critical value of the stability angle was determined and the critical condition for the stability of the tractor was established. The results were split into two tractor configurations: straight configuration and articulated configuration.

3.1. Straight configuration (roll angle)

The tractor in the straight configuration, is comparable to a fixed chassis tractor. The model performs the analysis without considering the yaw angle ($\mu = 0°$) while the roll angle is calculated (Figure 4, $\vartheta \neq 0°$). The model simulates the overturning event by increasing progressively the slope of the ground until a part of the tractor loses stability. In this study, the front body was considered to turn out first ($\alpha = 40.8°$) with respect to the whole tractor ($\alpha = 41.5°$) therefore the overturning starts with the rotation of the front body (Figure 5, $\vartheta = 0°$). The front body rotates till the design angle

(from 0 to 7.5 degrees, Table 1), basically, until the rotating body rests on the stationary body. In Figure 5, the behavior of the front tractor body (black line) and the whole tractor (red line), at different roll angle values, are shown. The loss of stability of the front body with respect to the stability of the complete tractor leads to the change of the CoG tractor and this affects the angle of stability. In addition, not necessarily the loss of stability of the front body will cause the loss of the stability of the complete tractor. In the first step, there is only a reciprocal rotation between the two bodies which can eventually cause the beginning of the tractor overturning. The effect of the velocity of the body due to the loss of stability could cause a different behavior with respect to the simulated one, because of the dynamic effect is not considered here. In Figure 5 it has to be underlined that as the roll angle increases, the stability angle decreases, and the tractor reaches earlier the condition of instability. Calculating the limit of the angle at the tractor design stage, engineers can manage the roll angle with respect to the needs of the end user.
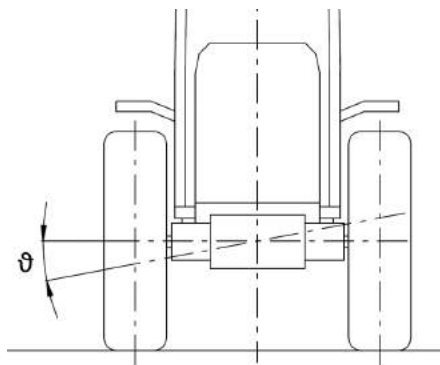
Figure 4. Roll angle graphical representation.
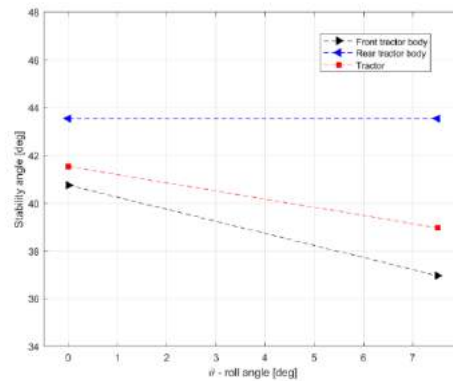
Figure 5. Stability angle vs. roll angle.

3.2. Articulated configuration (yaw angle)

If the tractor steers with the articulation joint the front and the rear tractor bodies, it is necessary to analyze the lateral stability depending on the degree of tractor articulation (Figure 6 - $\mu \neq 0°$). The lateral stability of the tractor is assessed by tilting the tractor till to induce a tip over. The scenario will vary according to the configuration of the tractor, and it will depend on the rotation of the articulation between the front and the rear tractor body. Considering the lower value of yaw angle, equal to -35 degrees (Table 1), the tractor will be fully steered or articulated to the left (Figure 6-a), while for the yaw angle equal to +35 degrees the tractor will be fully articulated to the right (Figure 6-c). The roll angle ($\vartheta \neq 0°$) acts through the rotation of one body on the other.
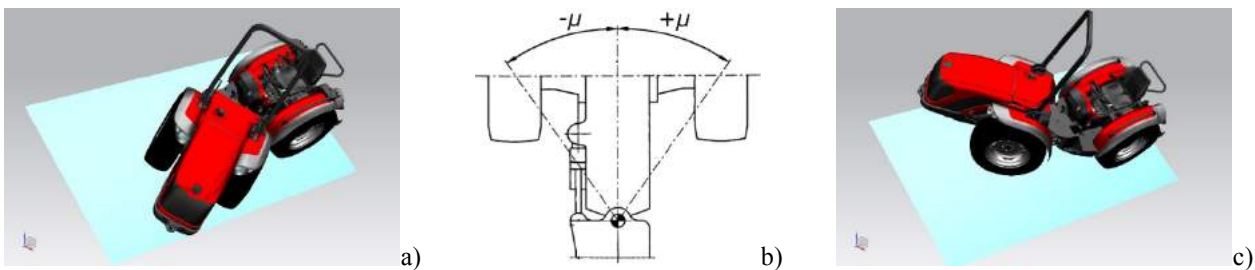
Figure 6. Articulated tractor and yaw angle graphical representations.

The stability angles of the separate bodies and that of the whole tractor are shown in Figure 7. The curves represent the trend of the stability angle as a function of the yaw angle μ and the roll angle ϑ.
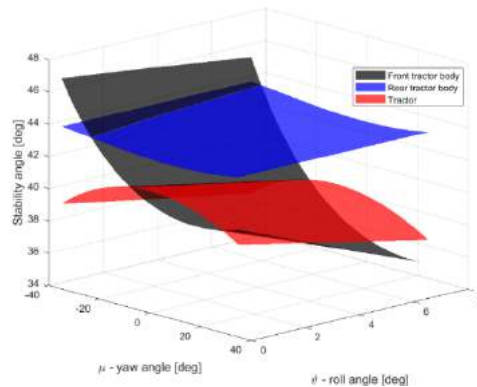
Figure 7. Stability angle vs. yaw and roll angles.

To better figure the part of the tractor losing stability first, the results have been simplified by defining the roll angle equal to zero (Figure 8). The rear tractor body (blue line) will never start the overturning, while the black line representing the front tractor body and the red line representing the whole tractor, are intersecting and this suggests a turnover between the trigger of the overturning cause. Depending on the tractor configuration there are situations where the whole tractor will lose stability first and other cases where the front body will firstly rollover.
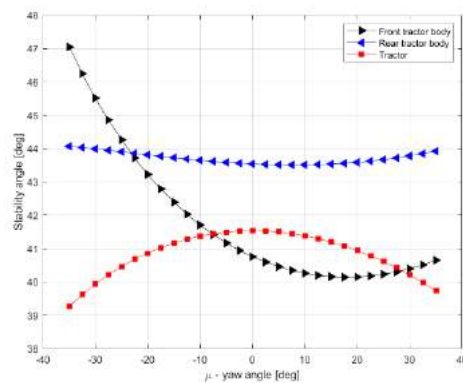
Figure 8. Stability angle vs. yaw angle

4. Discussion

The lateral stability angle of a compact narrow track tractor was calculated using a kinematic model. The results were split into two categories: steering wheel tractor and articulated tractor. The lateral stability angle for the tractor with steering wheel, in the straight configuration, was $\alpha = 41.5°$, when the roll angle $\vartheta = 0°$ (configuration equivalent to a fixed chassis tractor), and $\alpha = 39.0°$ with $\vartheta = 7.5°$. In the case of an articulated tractor, the angle of stability is not unique, and depends on the yaw angle. The lower value of the stability angle is $\alpha = 39.3°$, measured with an angle $\mu = -35°$. These values fulfill the required angle value of the tractors equipped with a front ROPS (the angle must be at least 38 degrees at the moment when the tractor is resting in a state of unstable equilibrium) according to the official OECD procedure (OECD Code 6, 2021). However, difficulties were related to the definition of the lateral stability limit angle of the articulated tractor due to the roll and yaw angle combined effects. The lateral stability angles are theoretically calculated considering the rotation of the tractor with respect to a line passing through the contact points of the tires on the ground. In detail the contact point was considered located in the mid of the tire width. Nevertheless, the tire deformation behavior during an actual rollover can significantly affect the contact points of the tire on the ground. The results presented do not consider all the phenomena of friction, air resistance, internal moving liquids and dynamic behavior that could occur during a real overturn. The dynamic effect of the central pivot point during the rotation of one body of the tractor with respect to the second one, if not properly damped by suitable viscoelastic components, might negatively affect the stability angle leading to an early rollover. Future step will be addressed to compare theoretical and experimental data.

5. Conclusions

This study combines known facts and engineering principles related to compact narrow-track tractor design to predict with a mathematical model the tractor behaviour on sloped ground. The model was set up for the steady-state behaviour, and it predicted the orientation as well as the stability of the vehicle on idealized slopes. Various parameter values were used in a computer analysis to study the effects of tractor geometry, including drive and steer design possibilities. The results highlight critical situations for improvements in design as well as horizons for future study.

Acknowledgements

References

Franceschetti, B., Capacci, E., & Rondelli, V. (2016). Effects of Rubber Tracks on Narrow-Track Tractors on the Non-Continuous Rolling Prediction Model. *Journal of Agricultural Safety and Health*, *22*(4), 262–273. https://doi.org/10.13031/jash.22.11668

Franceschetti, B., Lenain, R., & Rondelli, V. (2014). Comparison between a rollover tractor dynamic model and actual lateral tests. *Biosystems Engineering*, *127*(1). https://doi.org/10.1016/j.biosystemseng.2014.08.010

Franceschetti, B., Rondelli, V., & Ciuffoli, A. (2019). Comparing the influence of Roll-Over Protective Structure type on tractor lateral stability. *Safety Science, 115*. https://doi.org/10.1016/j.ssci.2019.01.028

Gibson, H. G., Elliot, K. C., & Persson, S. P. E. (1971). Side slope stability of articulated - frame logging tractors. *Journal of Terramechanics*, *8*(2), 65–79.

Grecenko, A. (1984). Operation on Steep Slopes: State Of The Art Report. In *Eighth International Conference of the International Society for Terrain-Vehicle Systems* (Vol. 21, pp. 181–194). Cambridge, U.K.

Guzzomi, A. L. (2012). A revised kineto-static model for Phase I tractor rollover. *Biosystems Engineering*, *113*(1), 65–75. https://doi.org/10.1016/j.biosystemseng.2012.06.007

Guzzomi, A. L., Rondelli, V., & Capacci, E. (2019). Operator protection in rollover events of articulated narrow track tractors. *Biosystems Engineering*, *185*, 103–115. https://doi.org/10.1016/j.biosystemseng.2019.04.020

Guzzomi, A., & Rondelli, V. (2013). Narrow-Track Wheeled Agricultural Tractor Parameter Variation. *Journal of Agricultural Safety and Health*, *19*(4), 237–260. https://doi.org/10.13031/jash.19.10249

Guzzomi, A., Rondelli, V., Guarnieri, A., Molari, G., & Molari, P. G. (2009). Available energy during the rollover of narrow-track wheeled agricultural tractors. *Biosystems Engineering*, *104*(3), 318–323. https://doi.org/10.1016/j.biosystemseng.2009.07.005

Hunter, A. G. M., & Owen, G. M. (1983). Tractor overturning accidents on slopes. *Journal of Occupational Accidents*, *5*(3), 195–210. https://doi.org/10.1016/0376-6349(83)90005-6

Kim, K. U., & Rehkugler, G. E. (1987). A review of tractor dynamics and stability. *Transactions of the ASAE*, *30*(3), 615–623. Retrieved from http://agris.fao.org/agris-search/search.do?recordID=US19880008174

Li, Z., Mitsuoka, M., Inoue, E., Okayasu, T., Hirai, Y., & Zhu, Z. (2016). Parameter sensitivity for tractor lateral stability against Phase I overturn on random road surfaces. *Biosystems Engineering*, *150*, 10–23. https://doi.org/10.1016/J.BIOSYSTEMSENG.2016.07.004

Liu, J., & Ayers, P. D. (1999). Off-road vehicle rollover and field testing of stability index. *Journal of Agricultural Safety and Health*, *5*(1), 59–71. https://doi.org/10.13031/2013.5700

Mazzetto, F., Bietresato, M., Gasparetto, A., & Vidoni, R. (2013). Simulated stability tests of a small articulated tractor designed for extreme-sloped vineyards. *Journal of Agricultural Engineering*, *XLIV*(s1), 663–668. https://doi.org/10.4081/jae.2013.(s1):e133

OECD Code 6. (2021). OECD Code 6: Standard Code for the official testing of front mounted Roll-Over Protective Structures on narrow-track wheeled agricultural and forestry tractors. Paris, France: Organisation for Economic Co-operation and Development. Retrieved from www.oecd.org

Pershing R.L., & Yoerger R.R. (1969). Simulation of Tractors for Transient Response. *Transaction of the ASAE*, *12*(5), 715–719. https://doi.org/10.13031/2013.38935

Rondelli, V., Martelli, R., & Casazza, C. (2018). Tractor rollover fatalities, analyzing accident scenario. *Journal of Safety Research*.

Shu, M., Ahmad, D., & Akande, F. B. (2010). A Review of Farm Tractor Overturning Accidents and Safety. *Pertanika Journal of Science and Technology*, *18*(2), 377–385.

Smith, D. W., Perumpral, J. V., & Liljedahl, J. B. (1974). The Kinematics of Tractor Sideways Overturning. *Transactions of the American Society of Agricultural Engineers*, *17*(1), 1–3. https://doi.org/10.13031/2013.36770

Spencer, H. B. (1978). Stability and control of two-wheel drive tractors and machinery on sloping ground. *Journal of Agricultural Engineering Research*, *23*(2), 169–188. https://doi.org/10.1016/0021-8634(78)90047-1

Yisa, M. G., Terao, H., Noguchi, N., & Kubota, M. (1998). Stability criteria for tractor-implement operation on slopes. *Journal of Terramechanics*, *35*(1), 1–19. https://doi.org/10.1016/S0022-4898(98)00008-1

Laboratory Scale Dewatering Analysis of Poultry Manure via a Batch Cylinder-Piston Separator

Peyman Neysari [a,b,*], Akbar Arabhosseini [a], Mohammad Hossein Kianmehr [a]

[a] Department of Agrotechnology, College of Abouraihan, University of Tehran, Tehran, Iran

[b] Farm Technology Group, Department of Plant Sciences, Wageningen University and Research, Wageningen, the Netherlands

* Corresponding author. Email: peyman.neysari@wur.nl

Abstract

Dewatering of poultry manure is one of the most important processes in order to mitigate the environmental impact and ease the transportation. The main objective of this study was to define the optimum design parameters to construct the poultry manure separator. The particle size distribution was defined in order to select the most optimum sieve size. The effects of separator design parameters including the optimum filtering size, pressure (loading) time, manure thickness and loading replication were studied on the final moisture content of manure samples. This was done by using a laboratory scale batch cylinder-piston dewatering set-up. The manure samples were placed in the cylinder-piston set-up and pressed by a universal testing machine (UTM). The result of particle size distribution indicated that the best distribution function for the poultry manure particles was Gaussian distribution. It was also found that the sieves of 2 mm and 1.8 mm had the highest percentage of retained manure of 51.40% and 9.14% respectively. The analyses of variances results for the design parameters showed that all independent factors including filter size, loading time, initial thickness and loading replications had significant effects on the final moisture content at a significant level of 0.01. The Duncan's test results of mean comparison showed that the filter size of 2 mm, 10 s loading time, three times loading and 10 mm initial thickness had the most contribution to reduce the final moisture content of the manure samples. The outcomes of this study can be used as preliminary design magnitudes to construct press-based separators e.g. screw-press separators.

Keywords: Cylinder-piston separator, UTM machine, dewatering, particle size distribution, poultry manure.

1. Introduction

Poultry manure contains main elements including nitrogen (N), phosphorous (P), potassium (K), magnesium (Mg), calcium (Ca), manganese (Mn), copper (Cu), sulphur (S), boron (B), chlorine (Cl), zinc (Zn), molybdenum (Mo), and iron (Fe) essential for different plants (Chastain et al., 1999). The N:P:K ratio for poultry manure is 6:2:3, which makes it an excellent fertiliser (Nicholson et al., 1996). Poultry litter can also be used for energy generation by producing methane as a fuel (Hills and Ravishanker, 1984; Safley et al., 1987). According to the Statistical Bureau of Iran (2012), poultry manure production is approximately 3.5 million tonnes per year. Nowadays, modern and efficient management of manure is environmentally and economically needed for animal farms. The improper manure handling can cause environmental adverse impacts including run-off or leaching the nutrient into the ground water, air pollution, odour and fly problems. The dewatering of poultry manure have been reportedly addressed as one of the most important treatment processes to avoid environmental impacts. Ford and Fleming (2002) stated that the fine organic substances in the liquid part of manure can be removed by dewatering leading less odour problems. Salehion et al. (2013) stated that the effluent from separator had a lower potential to plug transferring pipes as a results of small particle size of the separated manure. Dewatering of poultry manure is mainly carried out in the moisture content ranged from 60-70% (wet basis). Dewatering is one of the most important steps of treatment processes on poultry manure to produce pellet in Iran. This process can be summarised in 1) transporting, 2) mixing 3) dewatering 4) Adding nutrient, 5) mixing, 6) drying and 7) coating. One of the most important characteristics of manure for dewatering purpose is determining the particle size distribution. Particle size distribution can be carried out by different methods including sieving, image processing and laser-based techniques of which sieving is the most simplest and cheapest method. The particle size distribution in agricultural material can be done by using ASABE standard S319.3 (ASABE S319.3, 2003; Bernhart, 2007). The main objective of this study was to define the optimum design properties to construct poultry manure separator. This was done by evaluating the optimum filtering size, pressure (loading) time, manure thickness and loading replication. The preceding properties were tested by using a laboratory scale batch cylinder-piston dewatering set-up pressed by a universal testing machine (UTM).

2. Materials and Methods

2.1. Sampling

The samples used in this study were poultry manure collected from a poultry housing located in Varamin, Iran. The initial moisture content of the samples was determined using the oven method. Based on ASABE Standard, the samples

were dried in an oven at a temperature of 105 ± 3 for 48 h (ASABE S269.4, 2002). The initial moisture content of the sample in the summer was approximately 59% (wet basis).The method proposed by (Kingsly et al., 2007) was used to have a moisture content of the samples at the desired level (70% w.b.), by adding distilled water to the manure samples. The samples were packed in sealed bags and stored in the fridge at 4 for a minimum of 1h to have a unique moisture content in all samples. The required amount of water to add to the samples to let them reach to a desired level of moisture content was calculated through Equation 1 (Valaei et al., 2013).

$$m_w = \frac{m_i (M_{wf} - M_{wi})}{1 - M_{wf}}$$

(1)

where m_w is the amount of added water (g), m_i is the initial mass of the poultry manure (g), M_{wi} is the initial moisture content (%) (wet basis), M_{wf} is the final moisture content (%) (wet basis).

2.2. Particle size distribution

The ASABE Standard S319.3 was used to determine particle size distribution of the particles (ASABE S319.3, 2003). An amount of 100 g of the sample was placed on the sieve set-up containing 6 sieves in series with different size. The sample was then shaken for 10 min by using a shaker (CL 340, Soil Test Engineering Test Equipment Co., Evanston, IL). After shaking the sample, the remaining mass on each sieve was recorded accordingly (Figure 1). The corresponding mass for each sieve was used for determining the particle size distribution of the sample. The particle size distribution was analysed by MATLAB, 2014.

Figure 1. The sieves used for determining the particle size distribution of manure sample

2.3. Cylinder-piston set-up

Manure samples were dewatered by using a cylinder-piston set-up. The set-up was designed in lab-scale dimension (110 mm diameter and 156 mm height) and made of Polytetrahydrofuran (PTF). The set-up consisted of two parts including cylinder and piston. The cylinder had two separable parts capable of keeping different sized sieves during the experiment. The piston had a pressure applying point on which the load-cell of press machine was placed. The internal wall of the piston was sealed by rubber to avoid seeping (Figure 2 and 3).

| (a) | (b) |
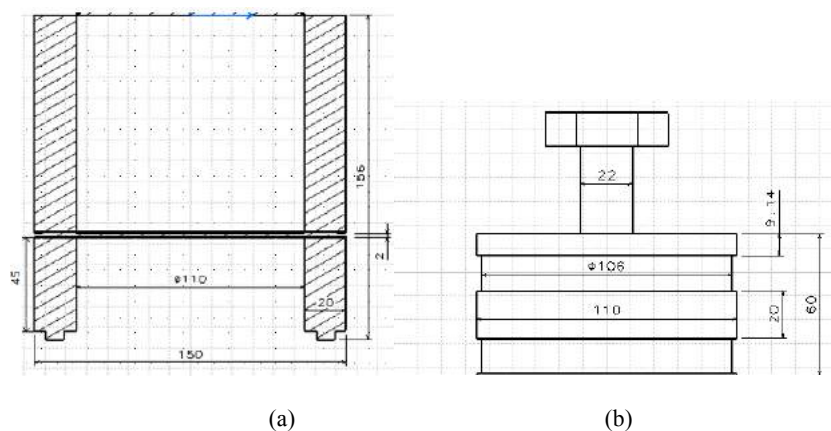
Figure 2. Technical dimensions of cylinder-piston set-up (Dimensions in mm), a) cylinder and b) piston
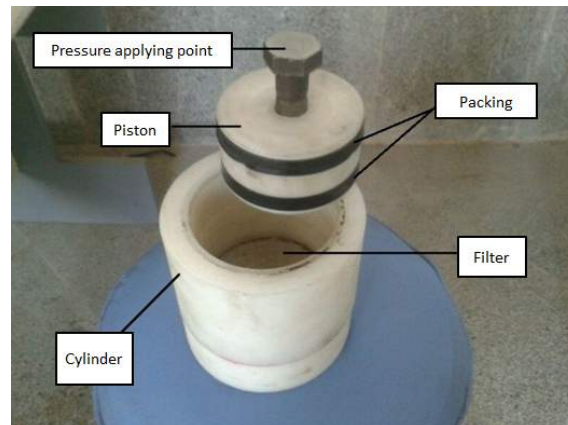
Figure 3. Cylinder- piston set-up for dewatering manure samples

A universal testing machine (UTM) was used as a press machine. The press machine was equipped with a load-cell (DBBP-11, Bongshin) and set at a constant maximum pressure of 110 kg.f. The load-cell was located above piston to record the applied pressure by press machine (Figure 4). The cylinder-piston set-up was filled in by manure samples of 70% moisture content (wet basis) at three thickness levels of 5, 10, and 15 mm. A data-logger was used to collect the pressure data online (Camus, version 1.1).
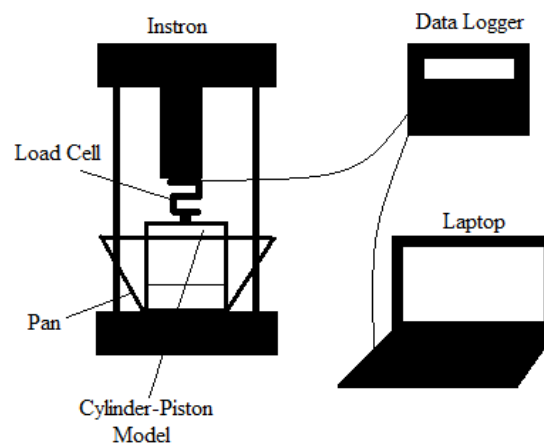
Figure 4. Schematic diagram of the cylinder-piston and press machine set-up (UTM, Instron)

Each sample in the set-up was pressed at three loading time levels of 10, 15 and 20 s. Each loading time level was done in three loading-unloading level of 1, 2 and 3 times. The remaining sample in the cylinder was then weighted (precision of 0.01 g) to calculate the final moisture content. The experiment was conducted in factorial design at three replications. The experiment was carried out for two sieve size of 1 and 2 mm. The analyses of variances were done by using ANOVA. The Duncan's test was used for comparing the sets of means. The analyses were carried out in SAS 9.1. The effects of independent factors were analysed on the final moisture content through ANOVA analysis. The independent factors included filter size, loading time, initial thickness and loading replications. The effects of interaction between independent factors were also analysed by using ANOVA.

3. Results and discussion

Results of particle size distribution indicated that the sieves of 2 mm and 1.8 mm had the highest percentage of retained manure of 51.40% and 9.14% respectively. This filter size is consistent with that of Salehion et al. (2013), who studied the particle size distribution of dairy cattle manure. The retained percentage found in this study can also be compared with a study carried out by Hegg and Larson (1981), who determined the cumulative percentage of retained dry matter of dairy, beef and swine. The result of fitting distribution function showed that the Gaussian distribution was the best distribution function with the sum of squared error (SS_E), R^2 and RMSE of 2.85, 0.99 and 0.97 respectively. Table 1 presents the remained manure in sieves (%) for different sieve sizes.

Table 1. Particle size distribution of poultry manure in percentage for different sieve sizes

Sieve number	Sieve size (mm)	Retained manure (%)
1/2	12.5	6.64
10	2	51.40
16	1.18	9.14
30	0.6	1.22
40	0.42	1.17
50	0.3	0
Pan	0	30.40

The analyses of variances results for independent factors showed that all independent factors including filter size, loading time, initial thickness and loading replication had a significant effects on the final moisture content at significant level of 0.01. The analyses of variances results for the interaction of independent factors including filter size vs. loading time, loading time vs. initial thickness, filter size vs. initial thickness and loading replication vs. filter size showed significant difference on the final moisture content at a significant level of 0.01. In contrast, the interaction of loading replication vs. initial thickness had no significant difference on the final moisture content. Table 2 presents the effects of the independent and the interaction between independent factors on the final moisture content.

Table 2. ANOVA of the effects of independent factors and the interaction of independent factors on the final moisture content of manure samples

Source of Variation	d.f.	mean square Final moisture content
Filter size	1	3669.38**
Loading time	2	108.72**
Initial thickness	2	677.05**
Loading replication	2	436.72**
Filter size × loading time	4	40.05**
Loading time × initial thickness	2	123.80**
Filter size × initial thickness	2	265.72**
Loading repetitions × initial thickness	4	4.80n.s.
Loading repetitions × filter size	2	59.38**
Error	136	3.76
Coefficient of Variations		3.26

**Significant at $p=0.01$, n.s. (non significant).

The Duncan's test of mean comparison for filter size showed that the filter size of 2 mm operated more effective than 1 mm by decreasing the final moisture content by around 15%. The mean comparison for loading time indicated that 10s loading time had the most contribution to dewatering, leading to the final moisture content of 58.3%. The Duncan's also test indicated that three times loading had the highest contribution to the final moisture content reduction to 57.16%. The Duncan's mean comparison of initial thickness revealed that the initial thickness of 10 mm performed more effectively to reduce the final moisture content by 10%.

4. Conclusions

The best distribution function for poultry manure particles was Gaussian distribution. The result of particle size distribution can be used to determine the efficient filter size for poultry manure separators. The outcomes of analysing the effect of filter size, manure initial thickness, loading time of press machine, loading replication can be used as preliminary design magnitudes to construct press-based separators e.g. screw-press separators.

References

Anonymous, 2012. Statistical Bureau of Iran, Tehran, Iran.

ASABE S269.4, 2002. Cubes, pellets, and crumbles – Definitions and methods for determining density, durability, and moisture content.. ASABE .pdf. St. Joseph, MI: ASABE.

ASABE Standard S319.3, 2003. Method of Determining and Expressing Fineness of Feed Materials by Sieving.

Bernhart, M., 2007. Characterization of Poultry Litter for storage and proces design, Degree of Master of Science,

Auburn University.

Chastain, J. P., Camberato, J. J., & Skewes, P. (1999). Poultry Manure Production and Nutrient Content. *Production*, 1–17.

Ford, M. and Fleming, R., 2002. Mechanical Solid-Liquid Separation of Livestock Manure—Literature Review. Prepared for Ontario Pork, Ridgetown College, University of Guelph.

Hegg RO, Larson RE, M. J. A., 1981. Mechanical Liquid-Solid Separation in Beef, Dairy, and Swine Waste Slurries. ASAE 0001-2351 / 81 / 2401-0159:159-163.

Hills, D. J., Ravishanker, P., 1984. Methane Gas from High Solids Digestion of Poultry Manure and Wheat Straw. *Poultry Science*, *63*(7), 1338–1345. https://doi.org/10.3382/ps.0631338.

Kingsly, R. P., Goyal, R. K., Manikantan, M. R., & Ilyas, S. M., 2007. Effects of pretreatments and drying air temperature on drying behaviour of peach slice. *International Journal of Food Science and Technology*, *42*(1), 65–69. https://doi.org/10.1111/j.1365-2621.2006.01210.x.

Nicholson, F. A., Chambers, B. J., & Smith, K. A., 1996. Nutrient composition of poultry manures in England and Wales. *Bioresource Technology*, *58*(3), 279–284. https://doi.org/10.1016/S0960-8524(97)86087-7.

Safley, L. M., Vetter, R. L., & Smith, L. D. (1987). Management and Operation of a Full-Scale Poultry Waste Digester. *Poultry Science*, *66*(6), 941–945. https://doi.org/10.3382/ps.0660941.

Salehion, A. R., Minaei, S., & Razavi, S. J., 2013. Design and performance evaluation of a screw press seperator for separating dairy cattle manure. *International Journal of Agronomy and Plant Production*, *4*, 3849–3858.

Valaei, I., Hassan-Beygi, S. R., Kianmehr, M. H., & Massah, J., 2013. Investigation of Avalanche Time and Carr's Index of Poultry Litter Powder as Flowability Indices. *Cercetari Agronomice in Moldova*, *45*(4), 15–27. https://doi.org/10.2478/v10298-012-0061-2.

Innovative Tractor Hitched Prototype Design from the Demand Side

Francisco J. Castillo-Ruiz [a, b], Sergio Peña Valero [a,c], Gregorio L. Blanco-Roldán [a], Francisco M. Lara del Río [a], Jesús A. Gil-Ribes [a].

[a1] University of Cordoba. R.G. AGR 126 "Mechanization and rural technology". Campus de Rabanales, Edificio Leonardo Da Vinci, Ctra. Nacional IV, km. 396, 14014 Córdoba. Spain.

[b] University of La Rioja. R.G. "Technology, engineering and food safety". Complejo científico tecnológico, C/ Madre de Dios, 53, 26006, Logroño, Spain.

[c] Construcciones Mecánicas Alcay S. L. Calle Barbastro sn., 22310, Castejón del Puente, Spain.

E-mails: FJCR g62caruf@uco.es; GLBR ir3blrog@uco.es; JAGR gilribes@uco.es; SPV ingenieria@serrat.es.

Abstract

In agricultural machinery sector, innovative product development uses to start from an idea conceived by manufacturer or close customers attempting to adequate future product to customer requirements. However, other schedule for innovation could be stablished through Pre-Commercial Procurement in which public procurers act as technologically demanding customers. Innovative prototypes were designed and manufactured by private companies that use their own innovative product development process. In that process a combined swathe rake and mulcher were developed to manage olive pruning residues for both mulching and biomass harvesting. The objective of this work was to define innovative product development process used by farm machinery builders when they face new challenges. This process had six steps: 1. Definition of minimal product features, 2. Prototype outline, 3. Prototype detailed design, 4. Prototype manufacturing, 5. Quality control, 6. No-load test and 7. Test in-field conditions. These steps had different key issues that should be defined properly to avoid unsuccess of future prototype. For instance, on the one hand, tractor features were a key point that must be assessed before prototype design when the future product will be custom manufactured. On the other hand, when the prototype will be mass manufactured tractor features must be considered as minimal features of the targeted market segment. The final step used to imply different machine adjustments and several modifications and adaptations to achieve an adequate performance of the machine. In conclusion, innovative product development process was highly important, but it is not enough to ensure prototype success.

Keywords: Technologically demanding customers, product development, mulcher, development schedule, swathe rake.

1. Introduction

In agricultural machinery sector, innovative product development uses to start from an idea conceived by manufacturer or close customers attempting to adequate future product to customer requirements. Product development could be conceived for custom or mass manufacturing although some farm machinery manufacturers choose hybrid production strategies making possible to attend make-to-order and make-to-stock orders (Köber and Heinecke, 2012). However, other process for innovation could be stablished through pre-commercial procurement (PCP) in which public procurers act as technologically demanding customers. PCP provided technologically advanced products to private companies or enables European public sector to keep updated public services faster and to create opportunities for companies in Europe to take international leadership in new markets (EU, 2020).

The design work of an agricultural machine, according to the demand of the client or of a private or public contract offer begins by collecting as much data as possible. Through the years and experience, Serrat Shredders and Mulchers (www.serrat.es) have been able to optimize data collection, design, and manufacturability, providing greater options and better assembly systems for its different components. In any case, as the difficulty of the machine to be designed increases, further tests and trials are needed, by varying conditions, to achieve a prototype reliable enough to perform the task required by customers in a wide range of situations. Machines manufactured after prototype tests included the advances and improvements determined during prototype development being able to sell mass manufacturing machines with a sufficient guarantee that it will not be occurred excessive breakdowns. In any case, this improvement process is never interrupted, although it is between prototype and next machine where more variations can exist.

The objective of this work was to define innovative product development process used by farm machinery builders when they face new challenges.

2. Materials and Methods

The process to design an innovative tractor hitched shredder or mulcher prototype could be divided into different stages that should be followed in order to complete a successful process.

2.1. Definition of minimal product features.

In a first stage, it is required to find customer or market need that could be satisfied through an innovation. Innovation process should help to perform unsolved tasks, or it should improve current production processes, or it may make more competitive a production process. In this stage, an interview with the customers selected as a market sample was necessary to find out their requirements, available tractors, and type of exploitation in which the machine will work. For this purpose, it is desirable to use a data sheet to fill in the main data for the innovation process (Figure 1).

State of the art is included in this stage. A complete search should be performed to find if there all any available machinery to perform targeted labour, their advantages, and disadvantages. There should be also considered solutions provided by rivals analysing strengths and weaknesses to occupy a specific niche market.

PRE-DESIGN INITIAL SHEET

TRACTOR

PTO Power		C.V.			kW	
PTO RPM	540 rpm		750 rpm		1000 rpm	
HITCH	TYPE		FRONT		REAR	
	CATEGORY		I	II	III	IV
AVAILABLE PUMP FLOW					l/min	
AVAILAPLE PUMP PRESSURE					bar	

MULCHER

GEARBOX RATIO				:	
OUTPUT GEARBOX SPEED					rpm
Øprim GEARBOX PULLEY					mm
Øprim ROTOR PULLEY					mm
PULLEY TRANSMISSION RATIO				:	
BELT PROFILE	A	B	C	SYNCHRO	
QUANTITY / BELT WIDTH					
BELT PROFILE	AX	BX	CX		
	XPA	XPB	XPC		
Øperimetral ROTOR					mm
SPEED ROTOR		rpm			m/s

Figure 1. Data sheet to start fulfilling the features of the innovative machine and available tractor.

2.2. Prototype outline.

It is the most creative stage. Firstly, machine was outlined focused on and adequate final design. During the whole process, desired features should be kept in mind. In this stage, different mechanisms required for machine work start to be sized. Power used to be analysed from available power at tractor power take off, or that available at hydraulic hose couplers. After this task, machine was 2D designed drawing every system periphery (Figure 2) considering different positions for each system that could satisfy the final requirements. Interactions between different options could be considered, assessing machine performance of different considered alternatives if any.
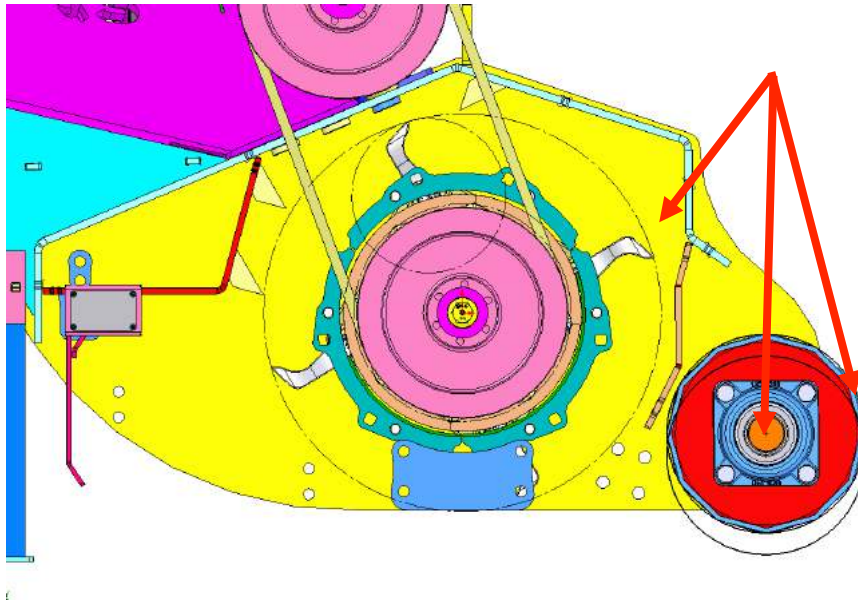
Figure 2. Periphery 2D design for shredding rotor and support roller.

2.3. Prototype detailed design.

In this third stage, after selecting the design that best meets the specifications, the detailed design begins. It works with a 3D design software. At this point, the calculations of the mechanisms and transmissions begin.

To perform the machine design, we always work considering and attempting to use only the machine tool that we have in our facilities for its manufacture. It is also observed if there is any module of our design that can be taken advantage of other elements already designed for other products, completely or partially, with some modifications. If necessary, material strength calculations are made, heat treatments are defined, materials or technical steels are included in the most critical parts of the prototype.

The prototype is designed as modular and versatile as possible (Figure 3). An attempt is made, in its most critical or complex mechanisms, to carry out the design leaving a variability or regulation that allows us to modify the conditions and the behaviour of the prototype in a simple way.
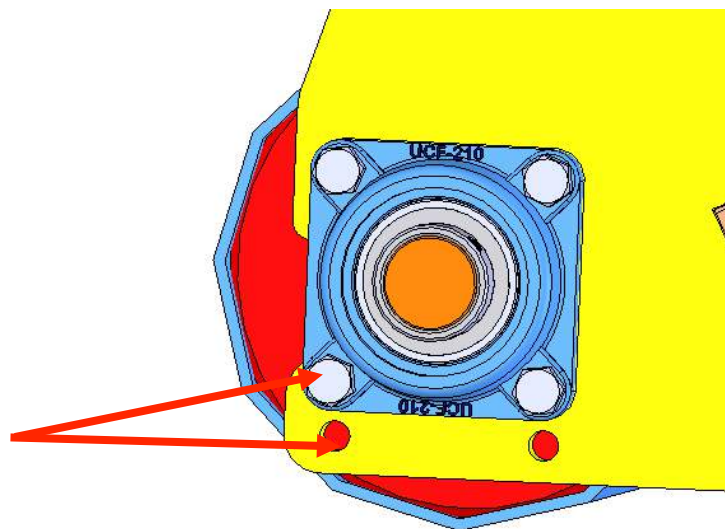
Figure 3. Image of a simple roller regulation

In this step the pieces are grouped into logical and rational assemblies. In turn, those assemblies form more complex ones, which we call functional groups (chassis, rotor, etc.). And the functional groups make up the ultimate prototype machine (Figure 4).
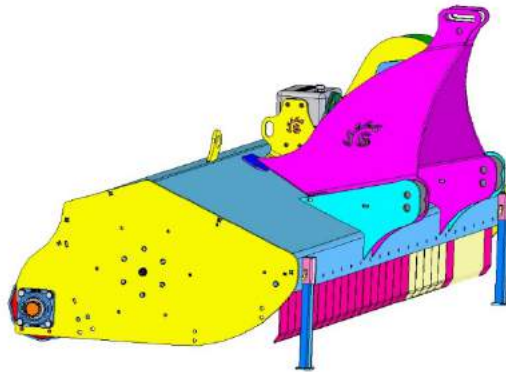
Figure 4. 3D image of a complete prototype in a 3D software.

Finally, for each piece, the production processes involved in its manufacture (laser cutting, bending, multitasking machining and buying normalized pieces) are defined. Each part, assembly and functional group is given an internal code and a brief description of its functionality. Production drawings are made, assigning tolerances to each component so that later, at the time of assembly, the machine works mechanically as it was originally designed.

2.4. Prototype manufacturing.

First, the machine is defined with an internal code, and it is given a unique numbering that will always be associated with the machine. A 3D copy of each machine is computerized as it is manufactured. For later consultation, mainly to be able to give spare parts to our client of the elements that the machine needs due to wear or breakdowns.

Finally, a list of materials is made that includes all the parts that are necessary for the manufacture of the prototype. From there, each piece is manufactured until all pieces are assembled to proceed with manufacturing. Manufacture operators were supported by engineering team, having access to 3D designs. This staff is trained to manage 3D programs to measure, rotate, hide and make sections of pieces or assemblies. An attempt is made to automate as processes as possible, in order to improve manufacturing process quality and competitiveness (Figure5), although some manufacturing processes remained as manual processes (Figure 6). However, introduction of new technologies within the prototype manufacturing is completely integrated in the process, being an important way to ensure prototype quality and enterprise competitiveness (Figure 7).

Figure 5. Machine welded with robot programmed offline.

Figure 6. Image of an operator assembling the machine
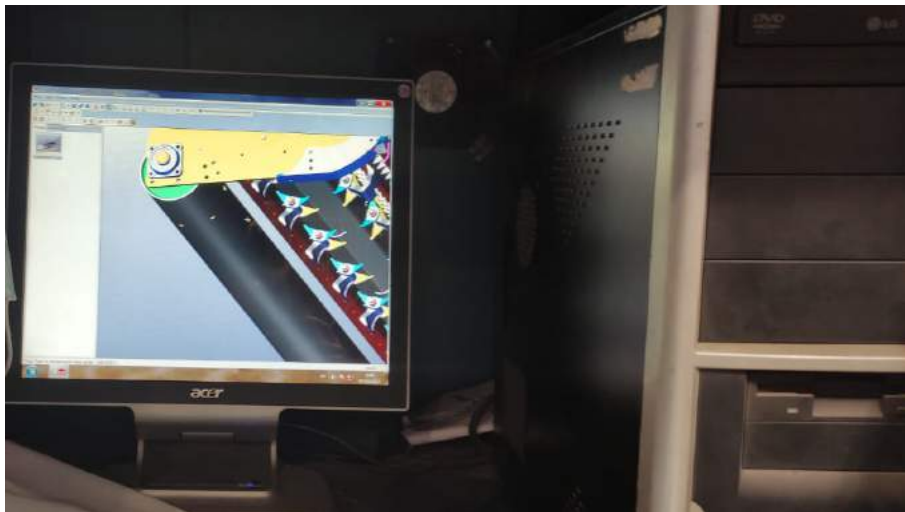
Figure 7. Image of the computer with the application for consultation of operators

2.5. Quality control.

As the different manufacturing processes go through, the parts and assemblies are undergone to quality controls. The operators know the critical points of the machine (Figure 8) and control the assembly to be suitable so that the assembling will be as fast as possible, and the components carry out their work limiting breakdown risk as much as possible.
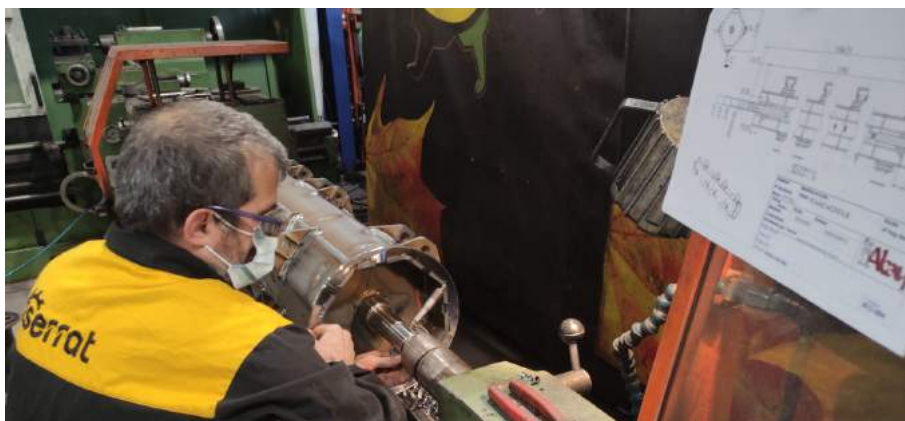
Figure 8. Control of rotor adjustment and balance.

2.6. No-load test.

The prototype is tested on a no-load test machine that we have at our facilities. They try to reproduce the real working conditions of the machine during future work with the greatest possible fidelity (Figure 9). In this process, the correct operation of all mechanisms is assessed, checking noise, vibration, heating of the mechanical elements, etc.

Figure 9. Manufactured machine undergoes no-load test.

2.7. Test in-field conditions.

Before this stage, each machine undergoes a shot peening process and painting process. Once these processes finished, prototype is ready to test in-field conditions in a real working situation, at the customer's own location or other similar situations (Figure 10). Real test starts with simple checking, and conditions difficulty increases as the machine accomplish previously stablished requirements. Once operation was assessed, modifications and regulations available for the prototype are tested to analyse different behaviours and establish the best regulations for the prototype to have a better work performance, looking for the best work results and requiring at least the minimum quality conditions for work. The optimal point should also be affordable for future customers, otherwise, machine could be a great prototype, but it never becomes a successful mass manufacturing machine. Based on this knowledge, the client is advised to choose the best working method through which he should consider, depending on the circumstances of each job, the most economical working method, attempting to maximize fuel savings and machine components wear. Sometimes, it could be also interesting to choose working method with the best result at the highest cost, when cost savings take place at next labours.

Figure 10. Test-in-field conditions

3. Results and Discussion

Currently, Serrat Shredders and Mulchers (www.serrat.es) have over 600 different machines available to manufacture while including discontinued models to date, more than 1000 machines have been designed from the very beginning in the company.

In the last years, the company, has successfully applied these design guidelines, improving these design steps gradually and adapting the process to the Internet of Things (IoT) technologies. This methodology made possible to react as quick as possible when a new machine order is received. According to which custom models, to be able to put the machine into production in a few hours, in the simplest versions. Moreover, it is also possible to give support providing all requested pieces if necessary to our distributors when a machine repair is requested.

All this has been achieved thanks to a production system that preponderated custom manufacturing over the repeatability of series manufacturing. Thus, obtaining competitive prices without having to manufacture the same components and machines in a chain, helping customer to choose the product it needs and not in the one that is manufactured in series.

Since the end of 2018, when we were selected as a participating company in line 4 of the pre-commercial procurement Innolivar, we have put all our capabilities into the development of an innovative prototype that would meet the technological demand provided by University of Córdoba. This new collaboration would be a challenge for our prototype design system due to strict conditions required and the difficult task entrusted. Currently we have the prototype available for in-field testing with windrowing efficiency results of more than 90% of the rest of pruning. Currently, we have finished the prototyping phase, now starting the in-field testing phase, with which the project will be concluded (Figure 11). In this collaboration we have not only developed the prototype but also, we have thought about organizing work and automating the most critical tasks for the operator and the machine. After more than 15 years working with mulching and biomass harvesters as tractor hitched machines, it has helped us to achieve very promising results, in the absence of the definitive tests that will begin with the in-field tests series.
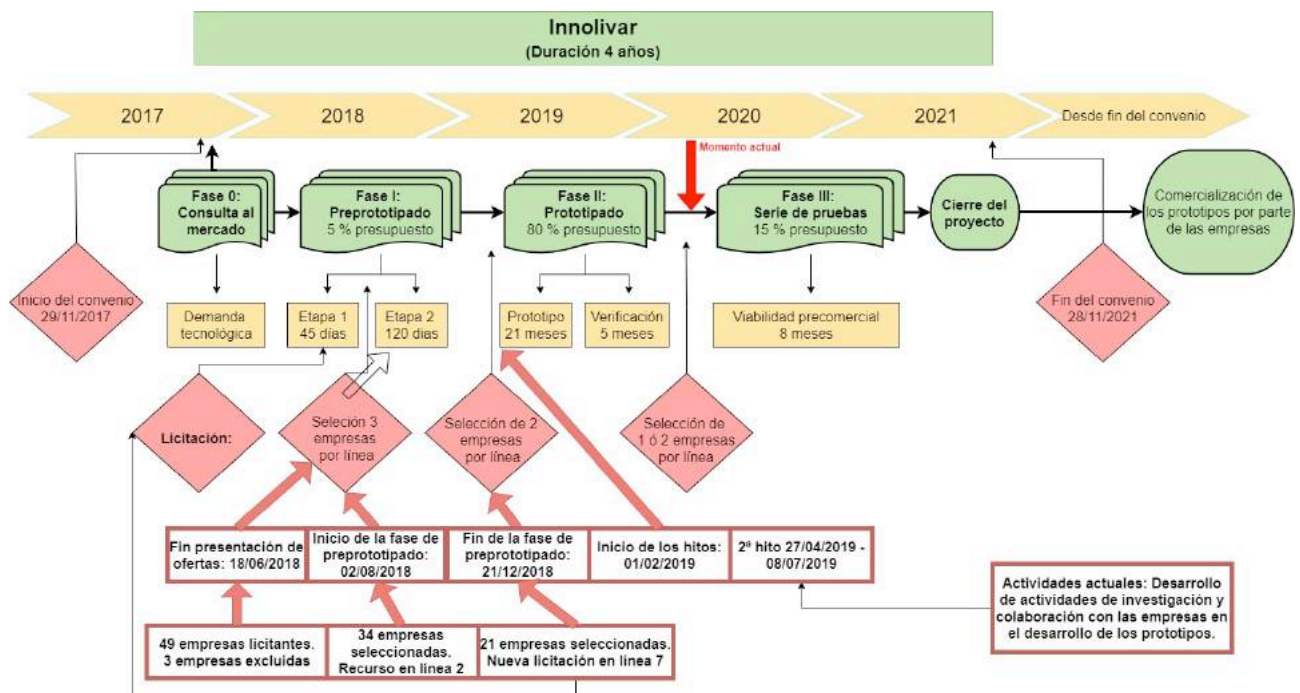
Figure 11. Current situation in CPP Innolivar

4. Conclusions

The objective of this work was to define innovative product development process used by farm machinery builders when they face new challenges. This process was being applied to a shredder-windrower development to meet previously stablished requirements that will made this labour more competitive and efficient. However, innovative product development process for farm machinery is highly important, but it is not enough to ensure prototype success. An economical assessment of machine cost and solved labours should be considered to predict commercial success of each machine series.

Acknowledgements

(https://www.aceitesdeolivadeespana.com/) support. Furthermore, authors want to acknowledge Construcciones mecánicas Alcay S.L. / Serrat trituradoras (https://www.serrat.es/), specially to José Serrat, Pedro Serrat and Raúl Serrat by collaboration and to let several images.

References

EU (European Commision). (2020). Pre-Commercial Procurement. https://ec.europa.eu/digital-single-market/en/pre-commercial-procurement Accessed February 27, 2020.

Köber, J., Heinecke, G. 2012. Hybrid production strategy between make-to-order and make-to-stock–a case study at a manufacturer of agricultural machinery with volatile and seasonal demand. Procedia Cirp, 3, 453-458.

Mechanical Compression Strenght Analysis in Jabre Paths Stabilized with Cement. Comparison CEM I 42.5R with CEM II A-V 42.5N

C. Gilarranz[1], S. Laserna[2], J.E. Gómez, J. Montero[3]

[1] Universidad Politécnica de Madrid; carlosandres.gilarranz@upm.es
[2] Autónomo; santiago.laserna@agroes.es
[3] Universidad de Castilla-La Mancha; JoseEmerito.Gomez@alu.uclm.es
[3] Universidad de Castilla-La Mancha; jesus.montero@uclm.es

Abstract

The aim of the work is to make known this jabre-cement stabilization trial, in this case comparing results of the studies carried out with CEM I 42.5R cements (Portland cement without additions whose basic component is clinker) with other cement called CEM II AV 42.5N having fly ash additions.

Comparison between compression mechanical strengths obtained under the same compression test conditions has been studied. Previously, it was studied optimum humidity that provides the maximum dry density of the jabre material with Normal Proctor compaction energy.

Subsequently, it was analyzed the influence of the cement dosage (from 0 to 10%) with different curing times of cylinder test, that is, repeating the tests with both cements at 2, 7 and 21 days.

This way, not only the differences between cements have been analyzed, but also technical recommendations have been established regarding to the minimum resistance that this type of stabilized paths must have, in order to achieve the rules of the General Technical Specification for Road and Bridge Works (PG-3).

As final conclusion, using CEM I 42.5R under 100% NP compaction, the minimum strength of 1.5 MPa is achieved with a concentration cement of 4.5% at 7 and 21 days.

Under the same conditions, using the other cement with same strength but with fly ash, it would take a smaller cement proportion necessary, 3.5%, to obtain the same resistance. This allows to reduce square meter costs in a path.jabre.

Keywords: jabre. Cement. Stabilization. Paths and roads.

1. Introduction

Jabre can be found in sedimentary deposits as a deposit of fragments of a granite rock that has been disaggregated by the action of atmospheric agents (weathering) and decomposition, which have remained closer to the bedrock. It has a friction angle around 28-32º.

Depending on this level of decomposition, from the granulometric point of view, this material can be grouped into three categories: coarse sand jabre, fine sand jabre and clay jabre.

The main characteristic due to its granite composition is the absence of mud when it is wet. This makes it a material that has many advantages compared to others, as its low cost, high speed in execution and low maintenance cost. It is a material that was traditionally already used in roman times in its roads [1] and that since a few years ago its use has been once again boosted and updated, such as in the rehabilitation of roads in the Parque del Oeste in Madrid or on various roads in the La Moraleja urbanization in Madrid [2], and recently next at Royal Botanical Garden of Madrid in theirs paths under our supervision.

2. Materials

2.1.- Cement, jabre and water

The materials used in this experiment were cement, jabre and water.

Cement is a hydraulic binder, i.e. a finely ground inorganic material which, when mixed with water, forms a paste that sets and hardens through reactions and hydration processes and which, once hardened, retains its strength and stability even under water. Properly dosed and mixed with water and aggregates, it produces a concrete or mortar that retains its workability for a sufficient time, reaching pre-set strength levels and exhibiting long-term stability.

One of the Portland cements is CEM I 42.5R, with the denomination Portland cement, and with the following components[3]: Clinker (95-100%), and minority components (0-5%) such a limestone and gypsum that can be appear or not necessarily. CEM I 42.5R has very low content of C3A, which confers the characteristics such a high compressive strengths at early ages and low specific surface which makes it possible to produce mixes with a lower demand for water, but maintaining plasticity.

This type of cement was chosen because clinker contain is practically 100% and can be used as reference in furthers estudies using others types of cement that contains different types of aditives as fly ashes, limestone, etc. and to be able to compare each other properties in this type of jabre-cement stabilization.

The other Portland cement is CEM II A-V 42.5N, with the denomination Portland cement with fly ash, and with the following components[3]: 85% clinker, 10% fly ash and 5% minority components, which are mostly setting regulators such as 3% gypsum. This type of cement was chosen because it contains a high percentage of fly ash, as this improves workability and provides lower heat of hydration, which reduces shrinkage and cracking by reducing the overall rate of hydration and therefore slows down the setting process. Pozzolanic cements are recommended for road surfaces, as already mentioned [4].

The water to be used, both for mixing and for curing the concrete on site, must not contain any ingredient in such quantities that it negatively affects the properties of the mix. Drinking water is considered suitable for use in addition to cement.

Water must meet the following minimum requirements:

     Hydrogen exponent. PH > 5.
     Dissolved substances < 15 grams per litre (15,000 p.p.m.).
     Sulphates, expressed as SO4, maximum 1 gram per litre (1,000 p.pm.).
     Carbohydrates, must be absent.
     Organic substances dissolved in ether < 15 grams per litre (15,000 p.p.m.).

In this test we have used tap water provided by Canal de Isabel II, which comes mostly from the reservoirs located in the northern part of the Community of Madrid. This water is normally used as drinking water, so it complies with the requirements set out in PG-3.

The mineralogical composition of jabre is made up of granular quartz sands (pseudospherical), feldspars (orthoclase), tourmalines, biotites, etc., linked by clay particles (kaolinite). It is found in the weathered areas of the large granitic batholiths near roman road, from where it is easily extracted by rudimentary mechanical procedures, due to its low degree of compaction [5].

Finally, this material, jabre, according to article 513 of the general technical specifications for road and bridge works, fulfils the previous characteristics that soils should have in order to be stabilised with cement to produce a material with adequate technical characteristics and economically admissible[6].

2.2.- cylinders test and apparatus

The test piece are made with a cylindrical metal mould of 102 mm +/- 0.4 mm inner diameter and 122.4 mm +/- 0.1 mm height, equivalent to a volume of 1000 cm3 and must have a collar with the same diameter and a height of approximately 60 mm, to be placed on the top of the mould at the time of tampping.
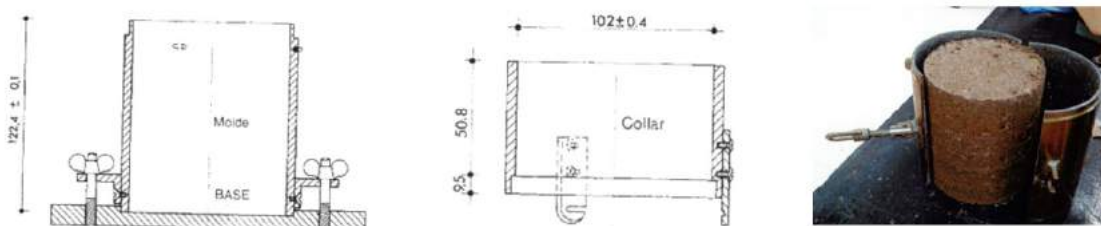
Figure 1. *mould and cylinder test piece*

To be able to carry out the Normal Proctor test, it was necessary to use a compactor with a 2.5kg +/- 0.01kg metal hammer, adapted to a suitable tubular guide with a free fall height of 305mm +/- 2mm. The hammer can be manual, although an automatic compactor was used like the figure. This distributes better the hits on the surface of the cylinder. The experiment procedure was filling the mould (with the upper collar placed) with the portion of jabre-cement mixed with water, distributed in three approximately equal layers, so that each layer, after being compacted, must have a height of more than one third of the height of the mould. The compaction of each of these layers is carried out by 26 hits, evenly distributed. With this procedure, the compaction energy of 0.583 J/cm3 is normalised for each cylinder test.
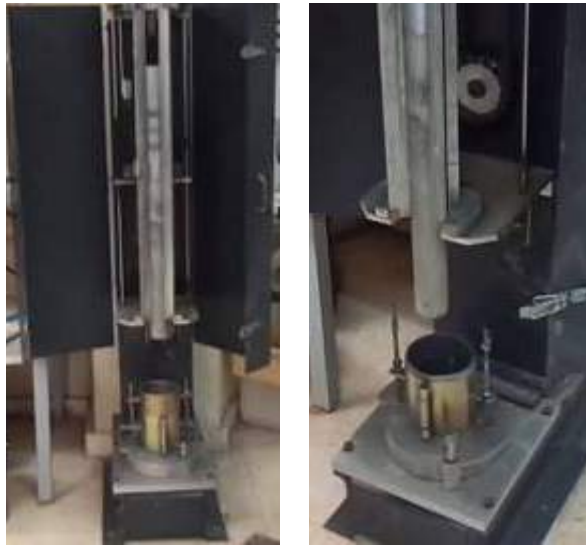
Figura 2. Compactor

The multi-test press was used to break these cylinders. The cylinder is placed between the heads of the press, the system is activated and then, the device moves forward as far as necessary, so that, the head and the cylinder come into contact. Once this contact is rearched, the cylinder loading process starts, so that, the final break time must be between 1 and 10 minutes. Then, the loads and deformations are observed every 30 seconds until the load value begins to decrease, this value is noted down and it coincides with the maximum load that the cylinder can support (breaking value).

Figure 3. Multi-test press rupture

3. Methods

The methodology used was UNE Standard for testing both the jabre and the mixture.

3.1.- Tests methodology carried out on jabre

Granulometry by sieving, according to standard [7].
Determination of the Plastic Limit [8].
Determination of the Liquid Limit [9].
Compaction Test. Normal Proctor [10].

Following this methodology, the aim was to characterise this base material for this type of stabilisation, justifying its suitability for stabilisation with cement.

3.1.- Methodology of tests carried out on the jabre-cement mixture

Unbound aggregate mixtures with hydraulic binder. Part 41: test method for the determination of the compressive strength of hydraulically bound aggregate mixtures [11].

Once the moisture-density curve was determined, the optimum moisture content that provided the maximum density was determined. With this value, three differentiated tests were determined, corresponding to the days of curing of the cylinders (2, 7 and 21 days) to the jabre-cement stabilised mixture. The cement content (%CEM) was also analysed as a variable, from 0-1.5-2.5-3.5-4.5-5.5-6.5-7.5-8.5-10%, with three repetitions per sample, in order to be able to treat the data statistically by an ANOVA analysis of variance.

Both for the jabre and for the mixture, this data obtained are detailed in the results section.

4. Results and discussions

4.1 Granulometric curve of jabre

The granulometric characteristics of this material have been analysed in the laboratory by sieving, following the UNE 103 101:95 (1995) standard with UNE-EN 933-2 sieves, giving the values shown in figure 4.

With these results obtained from the granulometric curve of the material, this type of material could not be stabilised with lime in soils EST1 and EST2, since it does not meet the requirement of table 512.1.a [12] that the percentage passing through the 0.063mm sieve, must be greater than or equal to 15%. In our case it is significantly lower.

In the case of complying with table 512.1.b of the same ministerial order, in this case, it meets all the requirements to be stabilised with cement, and can be S-EST1, S-EST2 or S-EST3.

However, if we go to table 512.3.a, we can discard S-EST1 and S-EST2 since the plastic index of the soap is very low, not exceeding 2%.

Finally, if we look at table 512.3.b, we can only classify this material as S-EST-3.
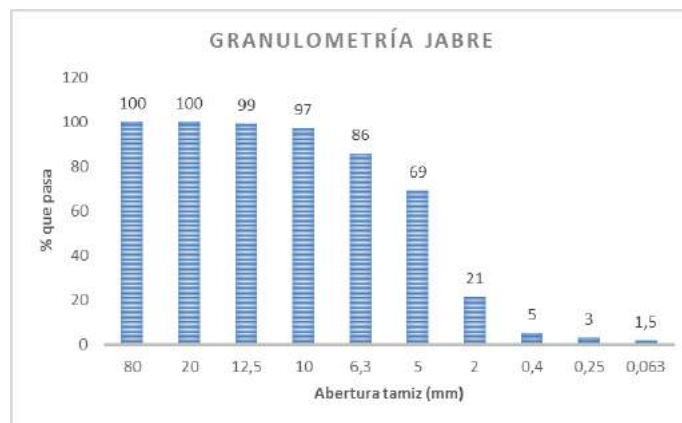
Figura 4*: Granulometric curve of jabre*

In this material there are fractions of all sizes from the smallest to the largest, i.e. with a "continuous grain size".

According to the above, this granular material is optimal for stabilisation with cement, which is why cement was chosen as a binder.

4.2 Plasticity

Casagrande method is used for the liquid limit. It was tested at different humidities, the lowest being 20% and the highest 27%. Results of the test was 16 hits for a humidity of 23% and 35 blows for a humidity of 21%. Therefore the liquid limit value of the jabre can be stablish in 22%.

Plastic Limit test in jabre was analyzed. Results were inconclusive, as it was not possible to establish a moisture value that would make the sample analysed plastic, making this material similar to sands in terms of behaviour, due to the very low proportion of fines. This is a very positive property for jabre, since it will not present significant changes in plasticity in presence of water, being more stable and permeable soil.

4.3 Normal Proctor compaction test

Normal Proctor test was used to determine the optimum moisture content-maximum density curve of the soil. In this test, a total of 15 cylinders were compacted with predefined percentages of water, and once the final water content had been determined, the density was calculated. All these data were taken to the statgraphics programme and the best fitting regression parabola was obtained, so that once this was known, its function was derived and its relative maximum was obtained. This value relates its optimum moisture percentage with its maximum dry density (figure 5).
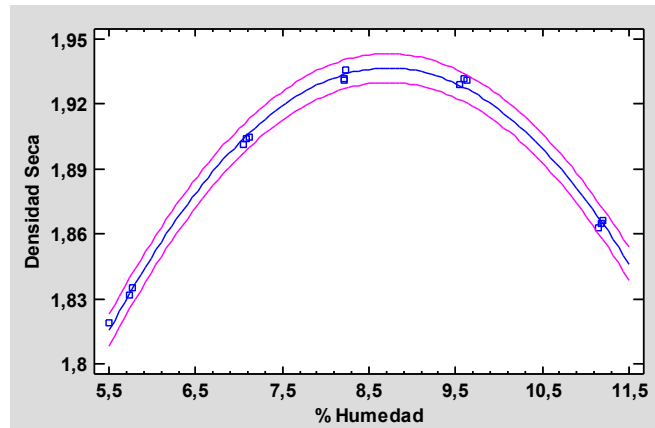
Figura 5*. Normal Proctor model adjusted to jabre*

Normal Proctor parabola explaining the relationship between observed and predicted data has an R^2 correlation of 99.5%. By giving us a p-value of $0.000 < 0.05$, it can be statistically infered that this parabola explains the reality with a confidence level of at least 95%:

$$\text{Ddry} = 1{,}04783 + 0{,}203842 \cdot H - 0{,}0116878 \cdot H^2$$

The maximum density obtained was 1.93 kg/dm3 for an optimum moisture content of 8.7%.

Based on the studies of [13] and [14], an addition of cement induces a slight decrease in dry density and an increase in optimum water compared to the same process without binder. This is due to the hydration that the added cement must have. It is important to take this into account as it would slightly increase the strength values by adding this percentage of hydration water to our study.

In the same way, and as indicated by [15], if the clay content of this material increases due to the over-decomposition of the granite, forming kaolin (hydrated aluminium silicate), the cement content should be increased, since, as indicated by the same author and corroborated by [16] in his book, "Obras en tierra", the addition of cement would reduce the undesired effect of increasing plasticity and attenuate the expansion of the clay, thus reducing the plastic index of the mixture, so that the more cement added, the greater amount of clay it contains.

4.4. Compressive strength of cement-stabilised jabre

4.4.1.- ANOVA analysis of the samples

Jabre, once its geotechnical properties of granulometry, plasticity and compaction had been characterised, was mixed with the cement, and with the optimum percentage of humidity that provides the maximum density, obtained previously

After performing the compression tests (according to UNE-EN 13286-41, 2003), a multifactorial ANOVA analysis was performed to link and discriminate the simple compressive strength (N/cm2) with the percentages of cement used (0-1.5-2.5-3.5-4.5-5.5-6.5-7.5-8.5 and 10%) at the different days to breakage (2, 7 and 21 days) with 3 replicates for each test.

Previously to the analysis, it has been analized independence, normality and homoscedasticity of data in order to verify the three conditions of a good ANOVA analysis.

The values of both analyses for CEM I 42.5R and CEM II A-V 42.5N are shown in both tables, 1 and 2 below:

Source	Sum of squares	Gl	Mean square	F-ratio	P-value
MAIN EFFECTS					
A:% CEM	401912,	9	44656,9	2988,09	0,0000
B:Days of rupture	72394,5	2	36197,3	2422,04	0,0000
INTERACTIONS					
AB	20465,6	18	1136,98	76,08	0,0000
RESIDUES	896,698	60	14,945		
TOTAL (CORRECTED)	495669,	89			

Table 1. *Analysis of Variance for CEM I 42,5R (N/cm2) - Sum of Squares Type III*

Source	Sum of squares	Gl	Mean square	F-ratio	P-value
MAIN EFFECTS					
A:% CEM	800950,	9	88994,4	12814,79	0,0000
B:Days of rupture	120668,	2	60334,2	8687,85	0,0000
INTERACTIONS					
AB	32185,5	18	1788,08	257,48	0,0000
RESIDUES	416,68	60	6,94467		
TOTAL (CORRECTED)	800950,	9	88994,4	12814,79	0,0000

Table 2. *Analysis of Variance for CEM II A-V 42,5 (N/cm2) - Sum of Squares Type III*

According to the values of the analysis of variance (ANOVA), in both cements the values of the independent variables "%CEM" and "Days of rupture", as well as in their interaction, present P-values of 0.0000, which implies that we can reject the null hypothesis, thus, means of the variables are equal and can be accepted the alternative hypothesis, that some of the means are different. This is confirmed by Tukey's Honestly Significant Difference (HSD) procedure in all the contrasts of possible variations of "%CEM", as well as for the contrasts of possible variations of "Days of rupture" with a 95% confidence interval. With this last test we can determine that all means are different, reaffirming the null hypothesis which we have accepted.

4.4.2.- Comparación de las curvas entre cementos a 2, 7 y 21 días

4.4.2.1.- Comparison between CEM I 42,5R and CEM II A-V 42,5N at 2 days

 Based on strengths data of CEM I 42,5R and CEM II A-V 42,5N at 2 days of failure, both data sets have been statistically compared with the program *Statgraphics* and the following analyses of the results have been extracted:

 t-test for comparison of means
  Null hypothesis: mean1 = mean2
  Alt. hypothesis: mean1 <> mean2
   assuming equal variances: t = -1.68254 P-value = 0.0978403
  The null hypothesis is not rejected for alpha = 0.05.
F-Test for comparing Standard Deviations
  Null Hypothesis: sigma1 = sigma2
  Alt. Hypothesis: sigma1 <> sigma2
  F = 0.482131 P-value = 0.0540172
  The null hypothesis is not rejected for alpha = 0.05.
Mann-Whitney (Wilcoxon) W-test to compare medians
  Null Hypothesis: median1 = median2
  Alt. Hypothesis: median1 <> median2
  W = 557.0 P-value = 0.115362
  The null hypothesis is not rejected for alpha = 0.05.
Kolmogorov-Smirnov test
Estimated DN statistic = 0.3
Bilateral K-S statistic for large samples = 1,1619
Approximate P-value = 0.134431
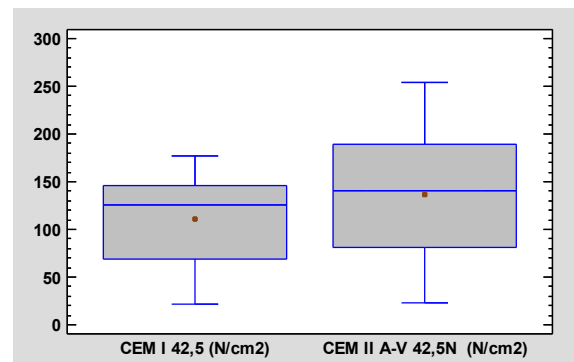
Figure 6. *CEM I 42,5R and CEM II A-V 42,5N 2-day box-and-whisker plot*

 Looking at the values, we cannot reject that the means and medians of the strengths of the two cements at 2 days of curing are equal, so they present similar values, with a very similar dispersion of the data between both cements, except for the last value of strength at 10% of the CEM I 42.5R, but this already coincides with values of use of high % of cement, something that does not practically happen in path construction site, because this type of concentrations are so high and the price of the work would be very elevated

 It is also clear from the previous data that CEM I 42.5R presents a distribution of its strengths with a negative symmetry, as the mean precedes the median value, while CEM II A-V 42.5N has a centred value of the data as the mean and median values coincide.

 It can be concluded with the Kolmogorov-Smirnov test that there is no statistically significant difference between the two distributions with 95% confidence.

4.4.2.2.- Comparison between CEM I 42,5R and CEM II A-V 42,5N at 7 days

Based on strengths data of CEM I 42,5R and CEM II A-V 42,5N at 2 days of failure, both data sets have been statistically compared and the following analyses of the results have been extracted:

t-test for comparison of means
Null hypothesis: mean1 = mean2
Alt. hypothesis: mean1 <> mean2
assuming equal variances: t = -1.54582 P-value = 0.127588
The null hypothesis is not rejected for alpha = 0.05.
F-Test for comparing Standard Deviations
Null Hypothesis: sigma1 = sigma2
Alt. Hypothesis: sigma1 <> sigma2
F = 0.458973 P-value = 0.040004
The null hypothesis is rejected for alpha = 0.05.
Mann-Whitney (Wilcoxon) W-test to compare medians
Null Hypothesis: median1 = median2
Alt. hypothesis: median1 <> median2
W = 547.0 P-value = 0.153667
The null hypothesis is not rejected for alpha = 0.05.
Kolmogorov-Smirnov test
Estimated DN statistic = 0.4
Bilateral K-S statistic for large samples = 1.54919
Approximate P-value = 0.0164595
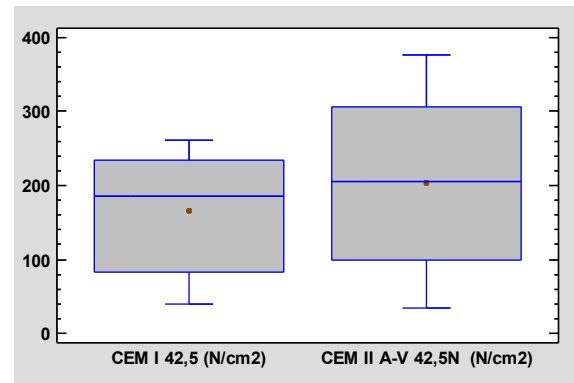
Figure 7. *CEM I 42,5R and CEM II A-V 42,5N 7-day box-and-whisker plot*

Looking at the values, we cannot reject that the means and medians of the strengths of the two cements at 7 days of curing are the same, so they present similar values, although in this case with a different dispersion of the data of both cements.

It is also clear from the previous data that CEM I 42.5R presents a distribution of its strengths with a negative symmetry, as the mean precedes the median value, while CEM II A-V 42.5N has a centred value of the data as the mean and median values coincide.

It can be concluded with the Kolmogorov-Smirnov test that there is a statistically significant difference between the two distributions, so they do not follow a common behaviour in the evolution of the strengths when the percentage of cement added increases.

4.4.2.3.- Comparison between CEM I 42,5R and CEM II A-V 42,5N at 21 days

Based on strengths data of CEM I 42,5R and CEM II A-V 42,5N at 2 days of failure, both data sets have been statistically compared and the following analyses of the results have been extracted:

t-test for comparison of means
   Null hypothesis: mean1 = mean2
   Alt. hypothesis: mean1 <> mean2
   assuming equal variances: t = -1.92223 P-value = 0.0594927
   The null hypothesis is not rejected for alpha = 0.05.
F-Test for comparing Standard Deviations
   Null Hypothesis: sigma1 = sigma2
   Alt. Hypothesis: sigma1 <> sigma2
   F = 0.568721 P-value = 0.134439
   The null hypothesis is not rejected for alpha = 0.05.
Mann-Whitney (Wilcoxon) W-test to compare medians
   Null Hypothesis: median1 = median2
   Alt. Hypothesis: median1 <> median2
   W = 571.0 P-value = 0.0748267
   The null hypothesis is not rejected for alpha = 0.05.
Kolmogorov-Smirnov test
Estimated DN statistic = 0.3
Bilateral K-S statistic for large samples = 1.1619
Approximate P-value = 0.134431
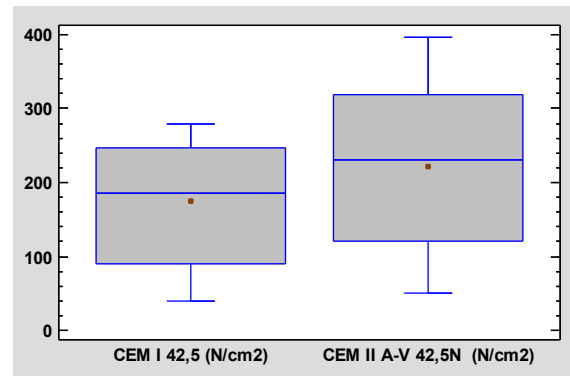
Figure 8. *CEM I 42,5R and CEM II A-V 42,5N 21-day box-and-whisker plot*

Analysing the values, we cannot reject that the means and medians of the strengths of the two cements at 21 days of curing are equal, so they present similar values, with a very similar dispersion of the data between the two cements.

It is also clear from the previous data that CEM I 42.5R presents a distribution of its strengths with a negative symmetry, as the mean precedes the median value, while CEM II A-V 42.5N has a centred value of the data as the mean and median values practically coincide.

It can be concluded with the Kolmogorov-Smirnov test that there is no statistically significant difference between the two distributions with 95% confidence.

Figure 9, corresponding to CEM I 42.5R, shows that there is little difference between the curves at 7 and 21 days, in the same way as in Figure 10 corresponding to CEM II A-V 42.5N, being very similar between them. This means that the worksite can be open at 7 days and not have to wait for 21 days, a very valuable quality in road construction.

As can be seen in both figures, the 2-day rupture curve would require very high cement concentrations to reach the established minimum of 150 N/cm2, so it would be very risky to open the work to traffic with such a short time elapsed or very expensive to have to add almost double the cement dosage.

In both figures 9 and 10, the strength or resistance has been taken as a reference value of 150 N/cm2, since the PG-3, as well as its Order FOM/2523/2014 (2014) defines that the minimum resistance to simple compression in soils stabilised in situ has to be 1.5 MPa (150 N/cm2).

Another thing that can be appreciated in these two graphs is the tendency of the curves, which, although in the case of CEM I 42.5R, the behaviour is more parabolic, providing lower strengths as the amount of cement added increases, with respect to CEM II A-V 42.5N, which has a more linear behaviour and therefore more effective when calculating the dosage of cement to be used depending on the expected strength, since to reach, for example, the minimum strength of 150 N/cm2 in the case of CEM I 42.5R, we would need to apply cement concentrations of 4.5%, with CEM II A-V 42.5N we reach it sooner with 3.5% cement, both, of course, at 7 days of rupture.

This is also demonstrated by the comparison between the two cements at 7 days, using the Kolmogorov-Smirnov test, as we saw above, which shows a P-value of 0.0164595, which, being less than 0.05, there is a statistically significant difference between the two distributions with a confidence level of 95%, considering that the distribution of the means of both series are different.
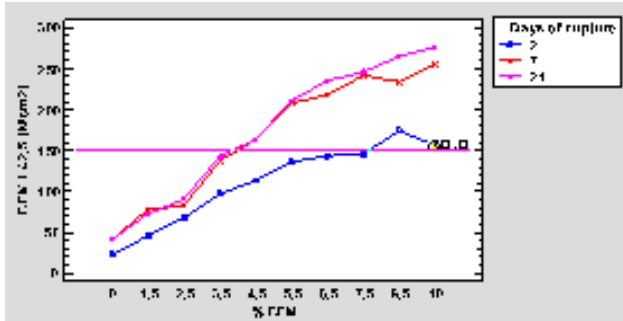
Figure 9. Results of the resistance of jabre - CEM I 42,5R
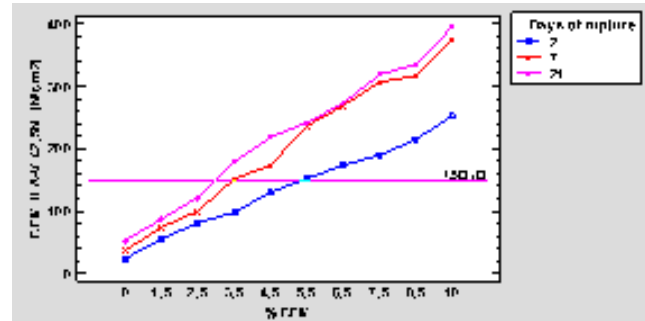
Figure 10. Results of the resistance of jabre - CEM II A-V 42,5N

4.4.3.- Resistencia a compresión y normativa.

In accordance with the minimum required strength for in-situ stabilised soils, according to PG-3 and its Order [17], which defines that this minimum resistance to simple compression must be 1.5 N/mm^2 (150 N/cm2), and considering the statistical model in Figures 9 and 10, it is determined that by applying a Normal Proctor of 100% with a compaction energy of 0.583 J/cm^3 and humidity of 8.7% (optimum humidity/density value), a minimum resistance of 150 N/cm2 is rearched with a minimum concentration depending on each type of cement of:

- **CEM I 42.5R**, a minimum cement concentration of 4.5% would be required with a minimum setting time of 7 days.
- **CEM II A-V 42.5N** with a minimum value of 3.5 % cement, this reference strength is achieved with a minimum setting time of 7 days. This behaviour can be practically explained by the fly ash in this cement that CEM I 42.5R does not have.

A similar conclusion is reached [18] in the case of stabilisation of a phyllite soil stabilised with CEM A-V 32.5 N/mm2 cement, indicating that it is convenient to incorporate 5% cement to improve the soil's punching strength and therefore its resistance, with this proportion registering an increase in the uniaxial compressive strength and reducing the permeability, and thus, being able to meet the minimum requirements of the PG-3. Also, in this study, stabilisation with lime is ruled out, because it increases permeability.

5. Conclusions

It is concluded that jabre is a granular material with good granulometry, plasticity and compaction properties. Mixed with cement, the significant influence of % CEM in the mixture and the curing time was found to be significant.

From the comparative statistical study of averages and the dispersion of the data of both cements, can be seen that the performance of CEM II A-V 42.5N is notably better, as far as resistance is concerned, than CEM I 42.5R, reaching equal resistances with a lower %CEM used.

If the main difference between both cements is that CEM I 42. 5R does not contain any additives and CEM II A-V 42.5N contains fly ash, it would be, a priori, fly ash would be responsible for this better performance in this type of constructions, which are the jabre roads stabilised with cement, since we start from equal initial strengths of 42.5 N/mm2 and although CEM I is R, i.e. with high initial strength, and CEM II is N, with normal initial strength, after 7 days of setting, we can only compare the strength that both have, 42.5 N/mm2.

Last conclusion is a practical recommendation: since the minimum resistance to simple compression, according to PG-3, must be at least 1.5 N/mm2 (150 N/cm2), these values are reached depending on each type of cement with:

RECOMMENDATION	**CEM I 42.5R**	**4,5% at 7 days.** Values lower than 4,5% cement for these curing times would make the construction unviable due to lack of resistance.
	CEM II A-V 42,5N	**3,5% at 7 days.** Values lower than 3.5% of CEM would make the contruction unviable due to lack of resistance.

References

1. Gallo, I.M., Vías romanas: ingeniería y técnica constructiva2004: Isaac Moreno Gallo.

2. Mejora en las aceras con arena de jabre, 2016: La Moraleja, Entidad urbanística de conservación.

3. RC-16, Instrucción para la recepción de cementos. Real Decreto 256/2016, de 10 de junio. Ministerio de la Presidencia, 2016.

4. Calleja, J., Cenizas, cementos y hormigones con cenizas. ETCC/CSlC Madrid, 1982.

5. Montes, J.G., Identificación de una carretera romana a través de la procedencia de los materiales. Elementos de Ingeniería Romana.Congreso Europeo Obras Públicas Romanas, 2004.

6. Pretel, G.B., PG-3 Pliego de prescripciones técnicas generales para obras de carreteras y puentes. Artículo 513, 2010: Ediciones Liteam SL.

7. UNE103101:95, Análisis granulométrico de suelo por tamizado. AENOR, 1995.

8. UNE103103:93, Determinación del Límite Líquido de un suelo. AENOR, 1993.

9. UNE103104:93, Determinación del Límite Líquido de un suelo. AENOR, 1993.

10. UNE103500:94, Geotécnia. Ensayo de compactación. Proctor Normal. AENOR, 1994.

11.UNE-EN13286-41, Mezclas de áridos sin ligante y con conglomerante hidráulico. Parte 41: Método de ensayo para la determinación de la resistencia a la compresión de las mezclas de áridos con conglomerante hidráulico. AENOR, 2003.

12. FOM/2523/2014, O.M., Artículo 512. Suelos estabilizados in-situ. 2014.

13. Kezdy, A., Stabilized earth road. Scientific Pub. Co, Amsterdam, 1979.

14. Miller, G.A., Azad, S., Influence of soil type on stabilization with cement kiln dust. Construction adn Building Materials 14,89-97, 2000.

15. Dal-Ré, R., Caminos rurales. Proyecto y construcción. Ediciones Mundi-Prensa, 1994.

16. Cuadra J., G.C., Obras en tierra. Universidad Politécnica de Madrid. Escuela Universitaria deIngeniería Técnica Agrícola, 2003.

17. FOM/2523/2014, B.d.e.d.O., Orden por la que se actualizan determinados artículos del pliego de prescripciones técnicas generales para obras de carreteras y puentes, relativos a materiales básicos, a firmes y pavimentos, y a señalización, balizamiento y sistemas de contención de vehículos., in Artículo 512.3 tipo y composición del sulo estabilizado2014.

18. Garzón E., C.M.e.a., Effect of cement and lime on phyllites raw materials from SE Spain. 17th International Congress on Proyect Management and Engineering, 2013. Universidad de Almería e Instituto de Ciencia de Materiales, CSIC-US.

Development and Evaluation of a Subsoil Management System to Increase Yield Capacity of Arable Land

Oliver Schmittmann [a,*], Andreas Christ [a], Peter Schulze Lammers [a]

[a] Institut of Agricultural Engineering, University of Bonn, Germany

* Corresponding author. Email: o.schmittmann@uni-bonn.de

Abstract

An increasing challenge for agriculture in times of climate change is to sustainably ensure or increase the yield capacity of crop production. Low-yielding sites are particularly at risk in this respect.

One strategy to counteract is to promote the use of the subsoil through intensification of rooting. This article describes a technical procedure of strip-wise subsoil melioration with an application of compost in a layer of 30-60 cm (www.soil3.de). These strips are each 30 cm wide and 70 cm apart.

A practical technology has been developed for this patented process, which allows the described procedure to be used over a large area. The melioration is carried out in one pass by an implement in an arrangement of 3 rows resulting in a working width of 3 m. The first tool is used to clear the topsoil from these strips. Following, injection coulters bring the compost up to 60 cm into the subsoil and mix it in place. Depending on the soil condition, successive remixing coulters are deployed. Levelling-blades lead the topsoil back to the thoroughly mixed subsoil. The tractor-driven implement is suspended in the rear three-point hitch. During melioration process forward and backward-mounted depth guide wheels are supporting. A hopper with an embedded hydraulic system, agitator shafts and adjustable metering augers was designed to feed the compost into the injection coulter. The compost hopper tank is hooked up on the implements` frame and can be filled by using an over-loading device.

Results from multi-year field trials in different regions of Germany with standard crop rotations verify yield increases of up to 20% still 5 years after melioration. An overview of these trials and results will also be presented. Regional conditions such as soil type and climate will also be considered.

Keywords: Subsoil-management, melioration, compost application, root propagation

1. Introduction

Climate change, combined with higher temperatures, lower precipitation and greater fluctuations, pose problems for crop production (SENEVIRATNE et al., 2006, Davies, 1991). A major future challenge will be to increase or safeguard yields. In addition to water, nutrient availability is also an issue. Nutrients, such as fossil phosphorus, are becoming more limited and therefore more expensive.

Particularly affected are dry, low-yielding sites, whose cultivability is already becoming critical today.

Requirements for cultivation or cultivation systems are therefore obvious: safeguard yields by ensuring sufficient water supply and nutrient availability.

The trend for several decades has been to reduce tillage intensity: flat, energy-saving and as extensive as possible. What has often been disregarded is the function of the subsoil. It represents a huge reservoir of nutrients (P) and is the space where water can be offered to the plant during drought stress (ANGERS, CARON, 1998). The subsoil can thus be seen as its option for 'bad times', provided that the plant is also rooted so deep (BATEY, 2009)! Crop wise this can be done for example by intercrops like oil radish or lucerne. The formed biopores/macropores sustainably promote the root development of the following crops.

Technical procedures are described by SCHNEIDER ET. Al 2019. Their sustainability is to be considered as problematic. Even pure deep loosening tends lead to yield depressions under less optimal conditions since plant roots react very sensitively to heterogeneous soil structure (SCHULZE LAMMERS, 2014).

These findings and relationships led to the development of a process and technology at the University of Bonn, with which artificial 'megapores' are created sustainably through subsoil melioration in conjunction with structure-forming organic material, which stimulates the plant to root through the subsoil more intensively and thus contributes to an increase in biomass formation. Plants above this megapore grow more into the compost-enriched, more biologically active subsoil and can use it to secure water supply and nutrient uptake. Lateral to these strips, roots also grow into the pore. The biomass amount below and above ground will be increased. The biomass pattern across the pore corresponds to a Gaussian distribution.

This paper deals with the development of a subsoil management system for sustainable yield protection in crop production. The patented Bonn method (DEUTSCHES PATENT- UND MARKENAMT, 2018) also was described JAKOBS,

2017, 2019). After melioration in late summer/fall followed by intercrops, the field can be cultivated conventionally without further melioration. The sustainability of the process is currently being investigated by the University of Bonn. In a cereal crop rotation (spring barley - winter wheat - winter barley - oats), additional yields of approx. 20% were achieved in each of the first four years after melioration (SCHMITTMANN, 2021).
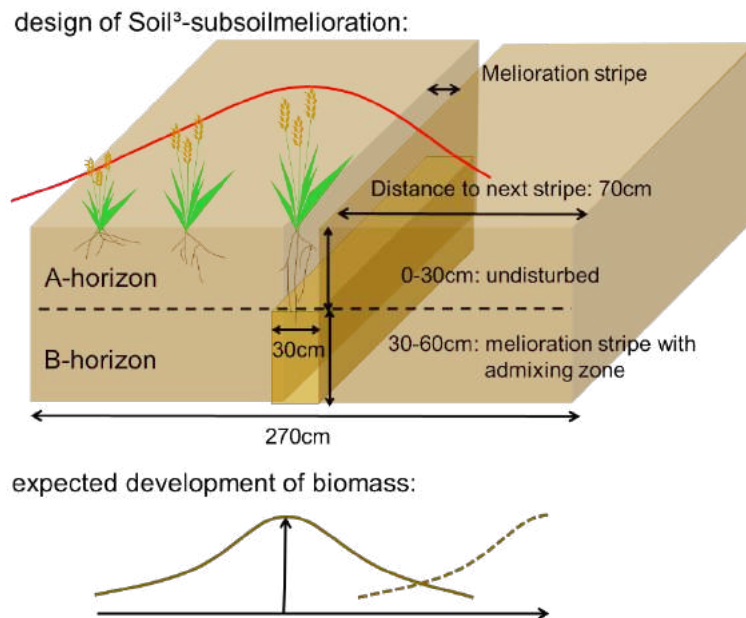
Figure 1. Soil³ subsoil melioration principle

In the Soil³ subsoil melioration process (figure 1), the soil is intensively loosened in strips up to a depth of 60 cm. For structural stabilization, organic material (composts or crop residues) is mixed exclusively into the subsoil (zone 30-60 cm). The topsoil and its structure should not be affected as much as possible and mixing of the A and B horizons should be expressly avoided to prevent degradation of the more fertile topsoil. The amount of compost brought in is about 3-4 kg m^{-2}, so it corresponds to the permissible amount for a conventional above-ground application. The melioration strips have a width of 30 cm. The optimal spacing of these strips from each other was determined in trials. The biomass formed across the strip corresponds to a Gaussian curve, i.e. it decreases with increasing distance from the strip. To produce a homogeneous plant population in terms of yield, quality and maturity, the effects described above must partially overlap. The experimental results have shown an optimal distance of 100 cm (center to center).

The development and evaluation of this now field-proven technology are described in detail in this article. A detailed description of all corresponding yield tests is omitted in this article.

2. Materials and Methods

The development of the subsoil melioration machine was described according to the design methodology.

2.1 Design methodology for technology development

2.1.1 List of requirements

According to VDI 2221 (1993) and VDI 2222 (1997), the requirements are divided into functional requirements, operational requirements and interface requirements. Functional requirements include aspects that are important for the use of the machine. Operational requirements refer to the properties of the machine during operation. The interface requirements cover the handling of the machines. The importance of each requirement is prioritized. P1 denotes requirements that must be met and P2 requirements whose achievement is desirable but not essential.

2.1.2 Design of the development

The conception of the machine results from the list of requirements and is the basis for the following construction phase. The essential structure of the machine is determined.

2.1.3 Working out and designing

From the defined basic conditions and the availability of the machine elements/components, the design is based on physical principles. Product datasheets, material properties (organic material) are consulted. The prototype was designed using CAD software (Autodesk Inventor).

2.1.4 Test and optimization

Test and optimization steps result from the field use of the machine. Essential here are ergonomic aspects and measures to ensure functional and operational safety.

2.2 Technology evaluation

2.2.1 Longitudinal distribution

Determination of the distribution accuracy is mandatory for all application methods in agriculture. It can be carried out by the manufacturer, testing service, or by the user. The quantity to be determined for this purpose from a large number of samples is the coefficient of variation. The classification or evaluation of the coefficient of variation (CV) is regulated in standards.

2.2.2 Mixing quality

The mixing quality describes the homogeneity of the incorporation of the organic material into the subsoil. Cores with a diameter of 10 cm were taken from the subsoil with a depth resolution of 5 cm. In order to eliminate the influence of different soil and substrate moisture contents, the volumetric proportion of the organic material in the respective soil layer was determined and the CV was calculated respectively. The cores were crushed, dried and sieved. To enable this separation, wood ships were used for the test instead of the compost, which in some cases was very small in size.

2.2.3 Working depth

The Melioration was targeted to a layer of 30-60 cm. The working depths was controlled in several places by test digging and measuring with a folding rule.

3. Results and Discussion

The results of the development are presented and discussed according to the construction methodology described.

3.1 Engineering development

3.1 1 List of requirements

The process description is listed in Table 1 for each of the process step.

Table. 1: Demands for the design of the soil³-melioration technology:

			score
Functional demands	1	Working depth 60 cm	P1
	2	Removal of topsoil	P1
	3	Injection of organic material into subsoil	P1
	4	Mixing of different organic substrates only into subsoil	P1
	5	Recompaction	P2
	6	Levelling after injection	P1
	7	Tank for compost	P1
Working demands	1	Process in one phase	P1
	2	Working quality (no mixing of top- and subsoil)	P1
	3	Working quality (no organic material in subsoil)	P2
	4	Blockage-free soil preparation and admixing	P1
	5	Protection against damage and overload	P1
	6	Soil protection	P2
	7	low-maintenance	P2
Interface requirements	1	Compatible for tractor use	P1
	2	Mounted on tractors	P1
	3	Compatible to road traffic	P2
	4	Transportability for truck	P1

3.1.2 Concept of the development

A modular design approach was performed. For each process phase, suitable tools or components were tested separately in preliminary trials. The most favourable variant was selected and improved if necessary. Each assembly should be easily replaceable. The following process phases were defined (Figure 2):

Figure. 2: Phases of the Soil³ melioration process and selected photos of the technology from the preliminary tests for tool selection and design.

Figure 2 also shows photos from the preliminary tests for each process phase. This resulted in the selection and design of the tools and the concept of a single-phase machine with which the subsoil melioration can be carried out in one path (Figure 3).
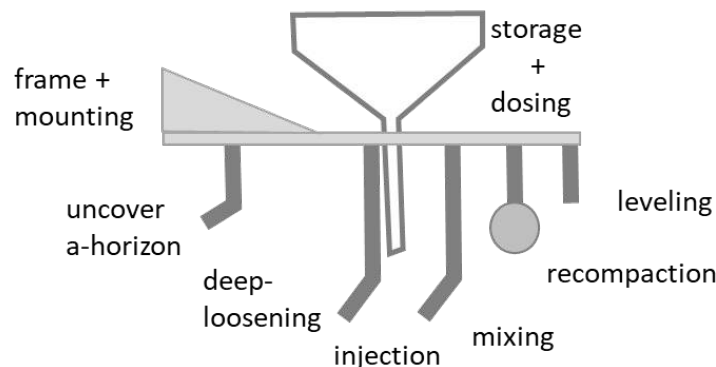
Figure. 3: Concept of the technology to be developed (application in one path).

All assemblies are mounted on a central frame.

(1) The depth control of all tools is ensured by the tractor hydraulics, supported by mounted supporting wheels in the front and rear.

    (2) The first coulter (clearing coulter) removes the topsoil to a depth of 30 cm and places it to the side of the furrow. The furrow should also be 30 cm wide to provide sufficient space for the following tools. The cleared topsoil shall be placed exclusively between the respective furrows on a width of 70 cm.

    (3) An injection tine consists of a share for deep loosening and a drop/injection channel. The tines working depth is 60 cm and is placed within the furrow created by the clearing share: it

      - opens and loosens the soil, lifts it upwards and sideways,

      - directs the compost from the storage tank into the subsoil, and

      - mixes it with the falling back subsoil.

    (4) If necessary, tines with mixing coulters improve the mixing quality

    (5) a tool (compaction wheels) can follow

    (6) Levelling blades guide the set-aside topsoil back into the furrow onto the thoroughly mixed subsoil

    (7) Trailing support wheels control the working depth

    (8) The storage tank with compost is mounted on the frame and supports the feeding of the tools by its weight force.

      a. two agitator shafts homogenize the compost, loosen it up to prevent bridging in the tank and keep the compost flowable

      b. three metering shafts direct the compost into the falling channel behind the injection coulter

3.1.4 Finishing and construction

a. Support frame

The support frame with a 3-point hitch is divided into two parts. The first frame is used to support the tools for furrowing - working depth of 30 cm. The second frame carries the injection equipment (working depth of approx. 60cm) and dozer blades. It is guided on the first frame by a 3-point hitch with a lift and can be coupled and uncoupled, for example, for transport. The compost tank sits on the second frame.

b. Scraper blade

Under the requirement of reducing installation space and power requirements while maintaining high reliability, a conventional plow blade with a large moldboard was selected. To reduce soil throwing force and to allow furrow channel formation of 30x30cm, the moldboard was modified accordingly based on field tests.

c. Injection tine

The injection tine with the drop channel (Figure 4) is the central tool for the process. It runs inside the furrow walls to a depth of 60 cm. The coulter loosens the subsoil intensively and guides the soil upwards, then back along with the tine carrier, where the now loosened soil falls back. The possible coulter width is limited by the available clearance in the furrow. 150 mm has proven to be optimal for loosening and injecting the compost.
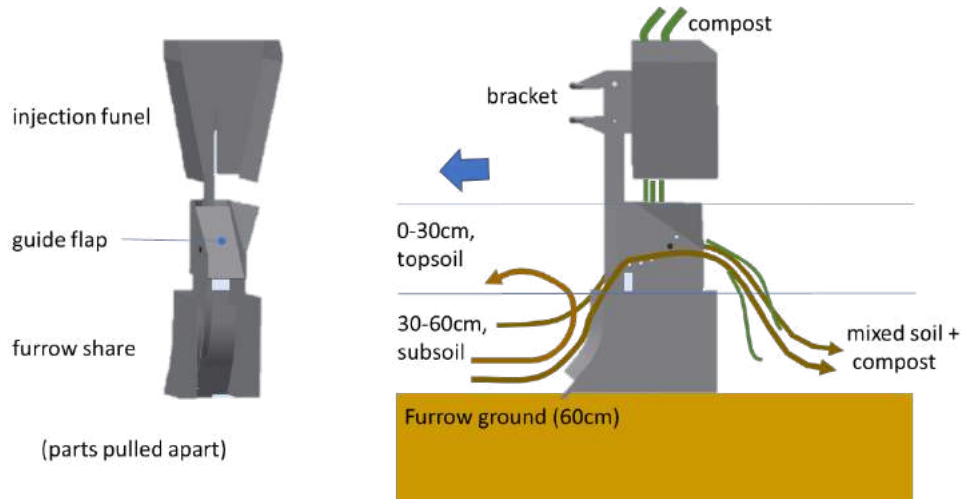
Figure. 4: Injection coulter. Components (left), material flow and mixing process (right).

The drop channel must ensure reliable injection of the compost into the subsoil avoiding clogging or bridging of the material. The optimal design of the channel was stepwise determined in trials. A key consideration was to leave the channel open at the rear. This has several advantages:

- clogging cannot continue upward

- the sides of the open hopper can vibrate slightly, resulting in self-cleaning.

The mixing of subsoil and compost occurs passively - without energy input. The compost is directed into the stream of falling soil through a guide flap installed at the bottom of the falling chute. The point of entry is adjusted by angular adjustment to achieve a mixing of soil and compost. Material (type, particle size and moisture) and soil type, moisture and density are the influencing variables.

a. Post-mix tines

In case of insufficient mixing quality, there is the option to install a post-mix tine on the frame. For remix and not to loosen additional soil, the tine is only approx. 8 cm wide and the working depth is only 55 cm.

b. Levelling blades

The levelling blades guide the topsoil back into the furrow. It is not necessary to adjust the depth of the blades, as the process is defined for one depth. Accordingly, the support is fixed directly to the supporting frame. In order to respond to different soils, the blades can be adjusted in their angle.

c. Depth guidance and support

Due to the high masses and the required constant working depths of the individual tools, depth guidance and support is of major importance. The machine is hooked up by the tractor rear linkage, resulting in better traction efficiency. Support wheels ensure that the desired working depth of the clearing coulters is not exceeded.

The lift on the ground frame ensures a gap between the scraper blade (30 cm) and the injection tine (60 cm) but also allows slight adjustments on uneven surfaces.

d. Compost storage tank

Since compost must be safely fed from the storage tank through the injection tine into the soil, the tank has been placed on the separate frame. Although this concept results in less favourable weight distribution, it is a compromise in favor of functional safety.

Compost and similar organic materials are very difficult to dose: They exhibit high adhesion and cohesion forces and thus tend to clump and bridge. This has to be counteracted technically. Two agitator shafts continuously homogenize the compost material . When designing the tank (Figure 5), care was taken to have as little dead volume as possible in which stirring cannot take place. On the other hand, the drive torques of the agitator shafts must not be too high.
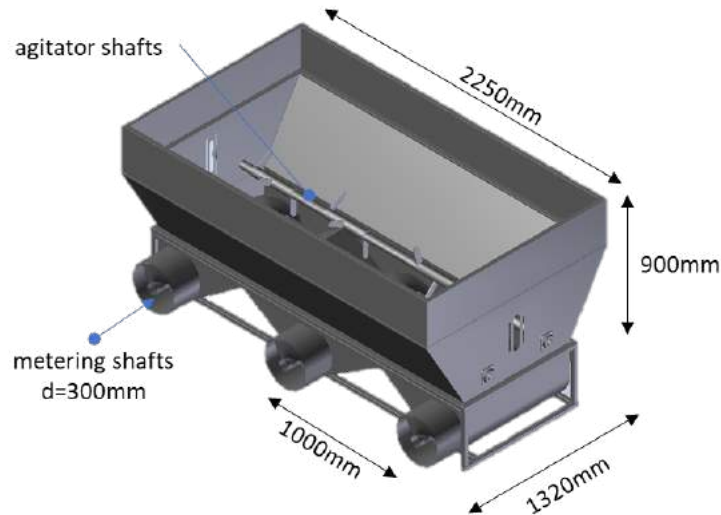
Figure. 5: Compost tank with hydraulically driven mixing and three metering augers.

Three open metering augers at a distance of one meter are placed in the bottom of the tank. They take up the material from the tank and discharge it via the respective injection coulters.

A separate hydraulic circuit has been developed for the mixing and metering operations (Figure 5). A hydraulic pump as propulsion for the hydraulic motors is driven by the tractor PTO. One circuit controls the mixing device in the tank. Synchronization of the two mixing shafts is neither desired nor necessary.

The second hydraulic circuit controls the metering by individual hydraulic motors. The angular speed of the motors and thus the application rate can be controlled via a manually or electrically adjustable flow valve with a downstream flow divider. The flow divider ensures the synchronization of the three shafts.

3.2 Technology evaluation

3.2.1 Dosing quality

Figure 6 shows the throughput of compost determined at different angular speeds of the metering augers. The linear regression has a quality of almost 1.0. The CV of 0.051 is rated 'very good' based on the DLG test standard (DLG, 2011).

3.2.2 Mixing quality

The mixing quality of the compost with the subsoil is influenced by the setting of the guide flap in the injection channel. The angle must be adjusted in a way that the compost is directed into the stream of receding soil. The angle setting is therefore also dependent on the soil type as clay and sandy soils have different flow characteristics. A post-mix coulter can additionally influence the mixing quality.

Accordingly, two flap settings (40 and 52.5°) represented by the angle between soil surface and flap were compared with and without mixing coulter. The means and deviations of the mixed mass for each depth levels and their CVs are shown in Figure 7. The flap angle of 40° and thus higher mixing-in point shows a lower CV than the one at 52.5°. The post-mixing coulter shows the effect of increasing amount in lower layers. The results of the test show that a post-mixing coulter should not be used under these conditions.
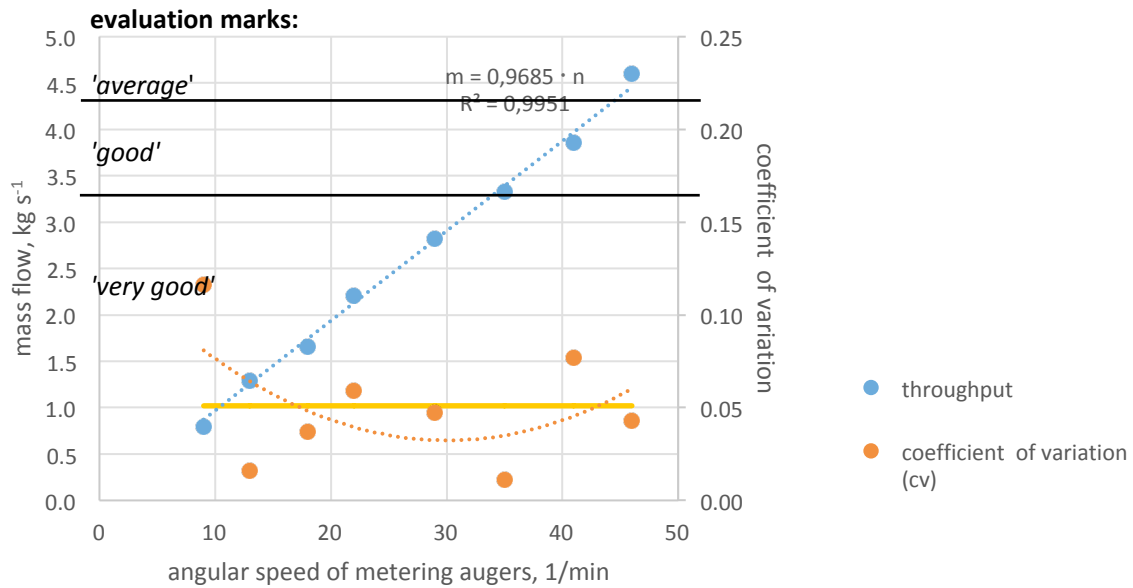
Figure. 6: Mass flow versus angular speed of the metering augers and dosing quality rated by the coefficient of variation according to DLG test framework (DLG, 2011).
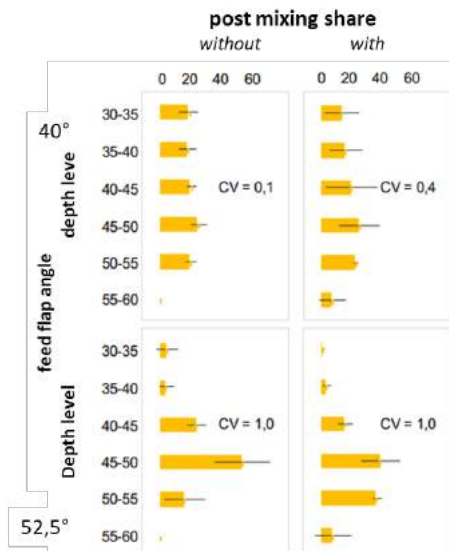
Figure. 7: Mixing quality of compost and subsoil and impact of an additional mixing coulter for different the feed flap settings. rated by the coefficient of variation

3.2.3 Quality of work in the field

In Figure 8 the work quality after the subsoil melioration is illustrated by photos. The strip depth was about 56 cm. It can be seen that the mixing of the compost in the B horizon was successful and there was no mixing of the A and B horizons (left photo). The top layer soil next to the strip is undisturbed and its structure is unaffected.

The levelling blades complete the melioration and ensure that on the one hand the removed A-horizon is returned to the furrow, and on the other hand that the surface of the field is prepared for successive tillage. On the right photo the loosened soil surface with the melioration stripes can be seen. The following tillage can be preferably performed by a cultivator with lower energy demand.

Figure. 8: Melioration strips with mixed compost (left) and field surface after melioration (right).

4. Conclusions

A device for subsoil melioration in strips with simultaneous admixing of organic material has been developed . The individual components have been developed in separate and developed, optimized and tested in the field according to the procedural requirements. The implement has been assessed in field experiments on light and heavy soils with low stone content.

The incorporation of the compost is done in one operation, and is precisely placed on the ground level. The mixing of soil and compost was rated with a CV of ca 0.15 according to the score "very good".

The working width of the implement is 3 m. It was deployed on stubble fields and in standing catch crop with good success. Travel speeds of up to 4 km h^{-1} can be achieved. Higher speeds are not recommended due to the reaction times of the tractor driver in case of disturbances. The power requirement is about 200 kW, depending on the soil. To avoid high wheel-slip the tractor has to be appropriately ballasted in field work.

Acknowledgements

References

Angers, D.A. & Caron, J. 1998. Plant-induced changes in soil structure: processes and feedbacks. Biogeochemistry, 42, 55–72

Batey, T. 2009. Soil compaction and soil management -a review. Soil Use and Management, 25, 335–345.

Davies, W. 1991. Root signals and the regulation of growth and development of plants in drying soil. Annual Review of Plant Physiology and Plant Molecular Biology, 42, 55–76.

DIN EN 13080 2003. Stalldungstreuer – Umweltschutz – Anforderungen und Prüfmethoden, Deutsche Industiernorm. Beuth Verlag GmbH, Berlin

DLG 2011. DLG-Prüfbericht 6045F – Verteilqualität Stallmist und Kompost, S. 1, Deutsche Landwirtschafts-Gesellschaft e.V., Groß-Umstadt

Deutsches Patent- und Markenamt 2018. DE102018120092A1: Verfahren zur Bodenbearbeitung und/oder zur Bodenmodifikation durch Einbringen von wachstumsförderndem organischem Material in einen Ackerboden

Jakobs, I.; Schmittmann, O.; Schulze Lammers, P., 2017. Short-term effects of in-row subsoiling and simultaneous admixing of organic material on growth of spring barley (H. vulgare), Soil Use and Management 2017, 33 https://doi.org/10.1111/sum.12378

Jakobs, I.; Schmittmann, O.; Athmann, M.; Kautz, T.; Lammers, P.S. 2019. Cereal Response to Deep Tillage and Incorporated Organic Fertilizer. Agronomy 2019, 9, 296. https://doi.org/10.3390/agronomy9060296

Schmittmann, O. 2021 Results of Soil³-subsoilmelioration field trials, unpublished

Schneider, F.; Don, A.; Hennings, I.; Schmittmann, O.; Seidel, S.J. 2017.The effect of deep tillage on crop yield—What do we really know? Soil Tillage Res. 2017, 174, 193–204.

Schulze Lammers, P., & Schmittmann, O. 2014. Schlitzsägerät für die einphasige Aussaat von Zuckerrüben. LANDTECHNIK, 69(3), 139–142. 2014 https://doi.org/10.15150/lt.2014.182

July 4–8, 2021, Évora, Portugal

Seneviratne, S.I., Luthi, D., Litschi, M. & Schar, C. 2006. Landatmosphere coupling and climate change in Europe. Nature, 443, 205–209

VDI-RICHTLINIE 2221 1993. Methodik zum Entwickeln und Konstruieren technischer Systeme und Produkte. Düsseldorf: VDI-Verlag

VDI-RICHTLINIE 2222 1997. Methodisches Entwickeln von Lösungsprinzipien. Düsseldorf: VDI-Verlag

Development of a Machine to Remove By-products with Brown Spot Disease Inoculum from Pear Orchards

Dias, António B.[ab*], Garcia, Ana[c], Rasteiro, Carla[d], Isaque, Sónia[e], Gomes, Rafael[e], Batista, Maria J.[f], Antunes, Rosário[g]; Martins, M. Carmo[h], Azevedo, João[i], Luz, João P.[j], Amaro, Conceição[j]

[a] Departmento de Engenharia Rural, University of Évora, Évora, Portugal

[b] MED – Mediterranean Institute for Agriculture, Environment and Devlopment, Évora, Portugal

[c] Frutus - Estação Fruteira de Montejunto CRL, Peral – Cadaval, Portugal

[d] Coopval - Cooperativa Fruticultores Cadaval, Cadaval, Portugal

[e] CPF - Central Produção e Comercial Hortofrutícola Lda, Sobreiral – Bombarral, Portugal

[f] Cooperativa Agrícola do Bombarral, Bombarral, Portugal

[g] Frutoeste - Cooperativa Agrícola de Horticultores do Oeste, Carrascal, Azueira – Mafra, Portugal

[h] Centro Operativo e Tecnológico Hortofrutícola Nacional (COTHN-CC), Alcobaça, Portugal

[i] Associação dos Produtores Agrícolas da Sobrena (APAS), Sobrena, Peral - Cadaval, Portugal

[j] QRural, Escola Superior Agrária de Castelo Branco, Castelo Branco. Portugal

* Corresponding author. Email: adias@uevora.pt

Abstract

In Portugal pear production is located in the Midwest region, occupying an area of about 11000 ha, under the registered designation of origin of "Pera Rocha do Oeste".

In recent years, the incidence of brown spot disease (*Stemphylium vesicarium*) increased, with considerable losses to the growers due to the depreciation of pears both in the orchards and in refrigeration chambers.

The control of the disease based on the use of chemical products was inefficient. In consequence, the development of integrated strategies will be necessary. The reduction of the sources of brown spot disease inoculum from the orchards is one of the strategies evaluated in the project GO – Protecestenfilio. The approach related in this work concerns the removal from the soil surface of the fruits with symptoms of the disease as well as leaves and pruning wood.

No specific technology to remove these by-products from the orchards is available in the market. With the project "GO – Protecestenfilio", a machine was developed for this purpose.

The machine is based on a farm tractor and consists in a front mounted windrow unit and rear semi-mounted lift and storage unit. The windrow unit is provided with two rotary swathers to remove the by-products from the base of the trees to the middle of the alley.

In the lift and storage unit a transversal rotor lifts the by-products from the soil to a conveyor elevator. This conveyer discharges the by-products into a temporary storage box placed at the rear of the unit.

This paper shows the machine developed as well as the limitations identified throughout the field tests performed.

Keywords: mechanization, pear orchard, brown spot disease, inoculum reduction

1. Introduction

In Portugal, pear production is located in the Midwest region, occupying an area of about 11,000 ha (INE,2020), under the registered designation of origin of "Pera Rocha do Oeste".

Since the 2015 campaign, there has been a higher incidence of brown spot disease (Stemphylium vesicarium (Wallroth) Simmons (teleomorph: Pleospora allii (Rabenh.) Ces & De Not) in the region, with a major contribution to the 30% losses in pear production, recorded both in 2015 and 2016, compared to the production in 2014 (Santos, 2019).

The symptoms of this disease are necrotic areas on leaves and fruits that may rot, before, during or after harvest (Luz et al., 2018). At harvest, fruits with symptoms are removed from trees and in most cases left on the soil. Occasionally, producers are able to minimize the economic losses by sending damaged fruits to the transformation industry.

Currently, disease control consists of fungicide applications at fixed schedule (every 7 or 15 days) or using a schedule provided by the brown spot disease (BSP) forecasting system (Llorente *et al*., 2006).

However, chemical control is insufficient under high spread rates of the disease (Llorente *et al*., 2006).

To minimize the risk of reducing the efficacy of fungicide applications, additional measures should be implemented to disrupt the disease cycle at the overwintering sexual phase (Llorente *et al.*, 2012).

The strategy consists in removing biomass (leaves and fruits), left on the orchard soil, that can potentially support the maintenance of inoculum of BSP. The biomass is removed during the autumn/winter season, in combination with the applications of effective Trichoderma strains (Llorente et al.,2012).

In order to contribute to the definition of integrated solutions against BSP, the project GO – Protecestenfilio is underway in Portugal. The project includes the construction of a machine to remove the above mentioned biomass in orchards.

This paper presents the prototype and suggests the next steps of its development.

2. Materials and Methods

2.1. Orchards

The machine field tests were made in two pear Rocha orchards, of about the same age (15 years old), and equal plantation mark (4m×2m): orchard 1, located at Peral - Cadaval (39º 15' 29''N, 9º 05' 00W); orchard 2, located at Quinta do Brejo – Peral – Cadaval (39º 14' 57''N, 9º 03'' 52''W).

2.2. Tractors

New Holland tractors with SuperSteerTM front axle were used in both orchards: model T4050 F of 71kW nominal power (Fig. 1) in orchard 1, and model T4.110 F (Fig. 2) of 79kW nominal power in orchard 2.

Figure 1. Tractor New Holland T4050 F

Figure 2. Tractor New Holland T4.110 F

2.3. Machine to windrow and collect by-products in orchards

The machine is based on a farm tractor and consists of a front mounted windrow unit and rear semi-mounted lift and storage unit.

The windrow unit (Fig. 3) has two rotary swathers with rubber slats hydraulically driven to remove the by-products from the base of the trees to the center of the alley.

Each rotor is mounted on a telescopic arm. These arms are articulated at the centre of the windrower and can be manually adjusted in length. A plate links the windrower to a headstock mounted at the front of the tractor in place of the front counterweights (Fig. 4).

A central mounted hydraulic cylinder, linked to lift chains, folds the articulated arms to the transport position (Fig. 5).

Each rotor is hydraulically driven and has a disc skid on the base (Fig. 6).

Oil for the cylinder and motors is provided by the hydraulic external service of the tractor.
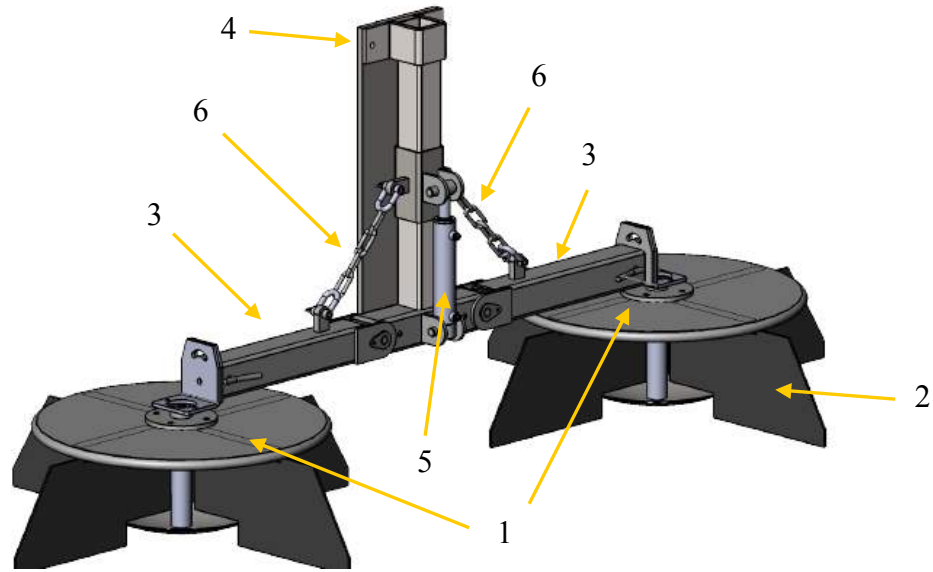
Legend: 1- slat rotors; 2 – slats of reinforced rubber; 3- articulated cross arm;
4 – headstock plate; 5 – arm fold hydraulic cylinder; 6 – link chain

Figure 3. Windrow unit components

Figure 4 Implement headstock mounted
at the front of the tract or

Figure 5. Arms folding

Legend: 1 – disc skid; 2 - hydraulic motors

Figure 6. Rotary swathers of windrow unit in working position

The rear lift and storage unit (Fig. 7) is attached to a drawbar mounted on the tractor three-point linkage.

Figure 7. Lift and storage unit semi-mounted in the tractor

The windrow of by-products are collected from the soil surface by a transversal rubber rotor (Fig. 8) and lifted by a conveyor elevator to a temporary storage box placed at the rear of the unit (Fig. 9). Skids on the base of the unit control the distance of the transversal rotor to soil surface (Fig. 8).
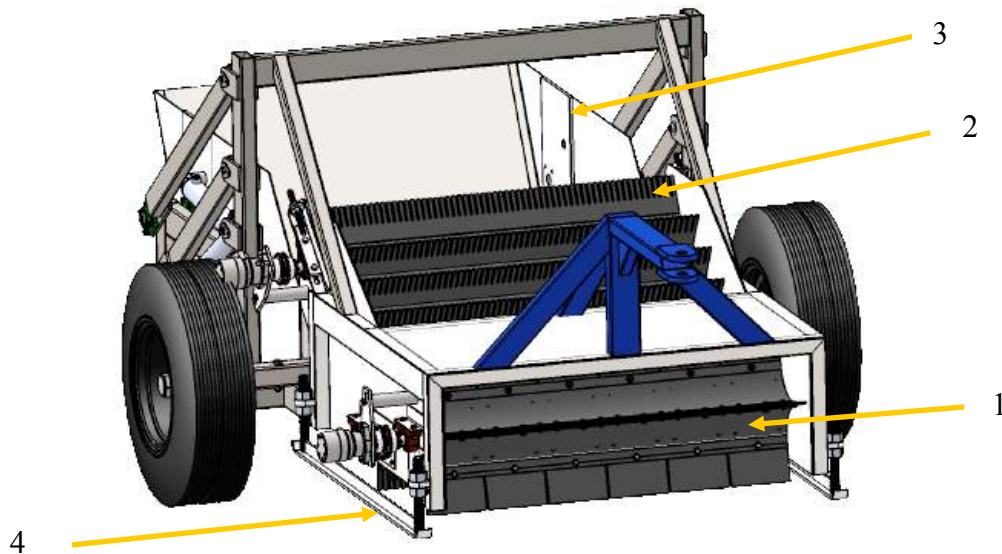
Legend: 1 – transversal rotor; 2 – conveyor elevator;
3 – temporary storage box; 4 - skids
Figure 8. Lift and storage unit

Figure 9. Rear view of conveyor elevator and storage box

Figure 10. Hydraulic motors to drive transversal rotor and conveyor elevator

Transversal rotor and conveyor elevator are hydraulically driven (Fig. 10). Hydraulic cylinders provide lift and tilt movement of the temporary storage box (Fig. 11 and Fig. 12).

Figure 11. Temporary storage box mounted on pantograph arms

Figure 12. Unloading the storage box

3.   Results and Discussion

3.1. Removal of pruning wood and leaves

Tests with the machine were carried out in the orchard 1 (February 2020) and in the orchard 2 (January 2021) to assess the ability to remove pruning by-products and leaves from the soil surface (Fig. 13 and Fig. 14)

Field tests confirmed that the machine was capable for removing by-products from the orchard soil surface in a single pass.

Figure 15 (orchard 1) and figure 16 (orchard 2) shows soil surface after the machine pass.

In the first test (Fig. 13) it was found that rubber slats deformed, jeopardizing the removal of by-products from under the tree canopies and consequently the windrowing at the centre of the alley.

The transversal rotor removes the by-products from soil surface as well as part of the grass growing at the center of the alley (Fig. 15).

The amount of grass removed from the alley does not affect the cover cropping, but tall grass may block the conveyor elevator. Cleaning the conveyor slaters of grass avoids blockage.

Figure 13. Front view of February 2020 trial

Figure 14. Front view of January 2021 trial

Figure 15. - View after machine pass at orchard 1

Figure 16. View after machine pass at orchard 2

In the orchard 2 trial, the use of stiffer rubber slats contributed to a better removal of by-products under the tree canopies despite the large amount of weeds present (Fig. 14).

Figure 17 shows the size of the pruned branches removed by the machine. The test also revealed that the volume of the storage box is insufficient, as it was filled after operating a distance of 80m.

Figure 18 shows that the clearance to the soil of the chassis of the lift and storage should be increased to avoid soil contact in muddy areas.

Tall grass affects the capacity to remove leaves, as they tend to get mixed up in the grass. When the volume of by-products is high, pruning by-products are removed preferentially, leaving smaller material like leaves behind. Adjusting the forward speed of the tractor to the working conditions is a practical way to overcome limitations in the removal of undesired by-products.

Removing by-products from the tree canopies projection area requires the rotary swathers to just touch the ground. Once positioned and bolted to the headstock, the windrower is unable to follow the irregularities of the surface below the set position, which may lead to areas without by-products removal.

Figure 17. Storage box full of pruning by-products

Figure 18. Insufficient clearance to the soil of the chassis

3.2 Simulation of pear removal from orchard soil

In orchard 1 (Fig. 19) and in orchard 2 (Fig. 20), respectively in February and September 2020, were carried out simulation tests of removal of pears previously scattered under the tree canopies.

Figure 19. Windrowing pears – orchard 1

Figure 20. Windrowing pears – orchard2

The tests showed the ability of the windrower to remove fruits from the tree canopy area to the middle of the alley.

In orchard 1 trial (Fig. 21), some fruits remained in the centre of the alley. In orchard 2 fruit removal was very effective in tree canopy projection area (Fig. 22).

Figure 21. Middle of the alley after the machine has passed

Figure 22 – Canopy projection area after the machine has passed

The best removal capacity of the swathers obtained in trial 2 (September 2020) was due to the stiffer rubber slats. Irregularities in the alley surface tend to affect the distribution of the fruits removed from the canopy projection area by the swathers, causing the pears that remain in the path of the tractor to be crushed. In order to prevent this limitation, rubber slats will be placed in the articulated arms to force the fruits to converge to the middle of the alley.

The storage volume of the box proved to be adequate when removing fruits (Fig. 23).

Figure 23. Pears collected in the temporary storage box

4. Conclusions

The most relevant aspects are:

- feasibility of the concept of a machine able to windrow and collect by-products from the ground of the orchards in a single pass;
-       use of the tractor as basic equipment;
- construction of a front mounted windrower.
- construction of a rear semi-mounted lift and temporary storage unit.

Field tests revealed that some details need to be improved to increase the removal capability.

In order to evaluate the durability of the components and the ability to remove by-products under different working conditions, there is a need to ensure funding for a longer period of time.

Acknowledgements

References

Instituto Nacional de Estatistica. (2021). Recenseamento Agrícola - Análise dos principais resultados - 2019 2019, Lisbon,Portugal

Llorent I., Moragrega, C., Ruz, L., Montesinos, E. 2012. An update on control of brown spot of pear. Trees. 26, 239–245. http://dx.doi.org/10.1007/s00468-011-0607-1

Llorent I., Montesinos, E. 2006. Brown Spot of Pear: An Emerging Disease of Economic Importance in Europe. Plant Disease, 90, 1368–1375. http://dx.doi.org/10.1094/PD-90-1368

Luz J.P., Amaro, C., Isabel, R., Jambrek, A., Barrios, D. 2018. Eficácia de fungicidas *in vitro* para *Stemphylium vesicarium* da pereira. *Revista de Ciências Agrárias*, 41(Especial): 97-101.

Santos,R.R., 2019. Incidência e severidade de estenfiliose em pereira 'Rocha' no Oeste e avaliação da eficácia biológica de fungicidas. MS Thesis, Instituto Superior de Agronomia, Lisbon University, Lisbon, Portugal.

Dynamics Assessment of Carbon and Energy Fluxes from Eddy Covariance Time Series in Three Different European Ecosystems

Víctor Cicuéndez[a], Javier Litago[b], Víctor Sánchez-Girón[a], Laura Recuero[c], César Sáenz[a] and Alicia Palacios-Orueta[a,c,*]

[a] Departamento de Ingeniería Agroforestal, ETSIAAB, Universidad Politécnica de Madrid (UPM), Avda. Complutense 3, 28040 Madrid, Spain

[b] Departamento de Economía Agraria, Estadística y Gestión de Empresas, ETSIAAB, Universidad Politécnica de Madrid (UPM), Avda. Complutense 3, 28040 Madrid, Spain

[c] Centro de Estudios e Investigación para la Gestión de Riesgos Agrarios y Medioambientales (CEIGRAM), Universidad Politécnica de Madrid (UPM), C/ Senda del Rey 13 Campus Sur de prácticas de la ETSIAAB, 28040 Madrid, Spain

* Correspondence author: alicia.palacios@upm.es

Abstract

Climate is determinant for understanding ecosystems carbon, water and energy fluxes, but it has to be highlighted that the ecosystem provides a feedback to climate processes. Our overall objective in this research is to assess and model the Gross Primary Production (GPP) dynamics and its bidirectional relationship with meteorological variables and energy fluxes of three different forest European ecosystems by time series analysis. Results show that temperature and solar radiation were the main limiting factors in the Evergreen Needleleaf Forest while water availability was determinant for growth in the Mediterranean ecosystem. The Deciduous Broadleaf Forest showed a different GPP cycle related with an interaction of various factors during all the growing season. In Finland, latent heat was coupled to GPP during all growing season due to the factor of temperature while in Denmark began to be strongly coupled when leaf emergence occurred. In Spain, latent heat was coupled to GPP during all growing season but due to water availability. The vegetation dynamics of the three ecosystems were directly responsible for the energy fluxes partitioning and water fluxes dynamics.

Keywords: GPP, energy partitioning, feedback, time series analysis, Granger causality Test, latent heat, sensible heat.

1. Introduction

Gross Primary Production (GPP) is the largest flux of the global carbon balance and it represents the C fixation of ecosystems through photosynthesis (Beer et al., 2010; Jiang et al., 2013). GPP estimations are necessary to assess the dynamics of the global carbon cycle and to plan a sustainable management of ecosystems (Yuan et al., 2015).

Climate is determinant for understanding ecosystems carbon, water and energy fluxes, but it has to be highlighted that the ecosystem provides a feedback to climate processes modifying these fluxes through evapotranspiration and surface heating (Arora, 2002; Hoek van Dijke et al., 2020). The spatial and temporal variability of this feedback is still uncertain (Seneviratne et al., 2008) and depends on the response of the ecosystems placed in different ecoregions (Wang et al., 2019).

The estimation at field level through Eddy Covariance (EC) measurements from flux towers provides carbon, water and energy fluxes measurements at an ecosystem level with different temporal scales (Baldocchi, 2014). Thus, time series analysis (TSA) is an excellent method to assess these data. Although TSA has been widely used in economics, it is not commonly used in the analysis of environmental variables. TSA has been recently used to assess the phenology of different forest and agricultural ecosystems (Cicuéndez et al., 2015; Recuero et al., 2019). Energy, water and carbon fluxes could be analyzed by TSA to assess the dynamics relationships between them.

Our overall objective in this research was to assess the Gross Primary Production (GPP) dynamics and its bidirectional relationship with meteorological variables and energy fluxes of three different forest European ecosystems by time series analysis (Evergreen Needleleaf Forest (ENF) of Finland, Deciduous Broadleaf Forest (DBF) of Denmark and Mediterranean dehesa ecosystem of Spain).

2. Materials and Methods

2.1. Study area

The research was carried out in three different forests of Europe. The first one is placed in the south of Finland in the experimental station of Hyytiala. It is an ENF located in a boreal climate (Suni et al., 2003). The second one is placed in Denmark and is a DBF called Söroe located in a temperate climate (Pilegaard et al., 2011). The third one is an open Mediterranean forest (i.e. Dehesa) called Las Majadas del Tiétar located in the west of Spain (Casals et al., 2009).

2.2. Flux tower data

In each site there is an eddy covariance flux tower integrated into the global network FLUXNET (Pastorello et al., 2020) and in the European fluxnet database cluster. The study period of Hyytiala and Soroe is from 1996 to 2015 and from 2004 to 2011 in Las Majadas. The following pre-processed daily variables for gap-filling and filtering (Level 4) (Papale and Valentini, 2003; Reichstein et al., 2005) were used: (1) air temperature (Ta, °C),(2) vapour pressure deficit (VPD, hPa), (3) precipitation (PPT, mm day-1), (4) soil water content (SWC,% vol), (5) latent heat (LE, W m-2) (6) sensible heat (H, W m-2) and (7) gross primary productivity (GPP_T, g C m-2 day-1).

2.3. Statistical methods

Firstly, Buys-Ballot tables (Buys-Ballot, 1847) were used to study the intra-annual variability of meteorological data, energy fluxes and GPP. Secondly, the dynamic relationships between variables were assessed through Granger causality tests (Granger, 1969).

The statistical analysis was computed through Statgraphics 18 (StatPoint Technologies Inc., VA, USA), Eviews 10 University edition (IHS Global Inc., CA, USA) and SAS software (SAS 9.4 Software, SAS Institute Inc., NC, USA).

3. Results and Discussion

3.1. GPP, LE and H average year

Figure 1 shows the annual average, i.e. Buys-Ballot, of the time series of daily GPP_T, LE and H of the three ecosystems.

The GPP of the ENF of Scots pine in Finland placed in a boreal climate showed an annual cycle in which the main limiting factors were temperature and radiation (Dass et al., 2016; Mäkelä et al., 2006). Due to extreme low temperatures, GPP was practically zero from mid-November until late March. During spring GPP increased continuously until summer when GPP had its maximum at the beginning of July. At the beginning of August solar radiation began to decrease and subsequently GPP. During September and October, GPP decreased sharply until the beginning of November when low temperatures and radiation became limiting again. The cycle of H was also determined by temperature. Thus, H was negative during winter. During spring, H increased reaching their maximum values in May and before the maximum of GPP due to that temperature had already reached high values enough to begin the process of evapotranspiration, thus the latent heat began to be the most important component of the net radiation. LE is then coupled to the cycle of GPP reaching its maximum in summer and decreasing during autumn.

The DBF of beech in Denmark showed a different cycle. Because beech trees are deciduous, the annual cycle is marked by the emergence and fall of the leaves and this fact is determinant on the seasonal variation of photosynthesis and numerous ecosystem/atmosphere interactions (D'Odorico et al., 2015; Melaas et al., 2013). From November until the mid-March, GPP was very low due to low temperatures and solar radiation. In addition, H was negative during winter indicating that the ecosystem was giving heat to the atmosphere. Then, Ta began to increase and consequently GPP. During this period, sensible heat also increased sharply indicating that energy was being spent on raising temperature. Around the end of April leaf emergence occurs and leaf expansion lasts around one month (Wang et al., 2005). During this period GPP increased sharply together with Ta and this fact leaded to an increase on evapotranspiration and subsequently latent heat. After that, GPP reached its maximum in mid-June and remained high one month when LE reached its maximum. This delay could be explained because Ta and subsequently evapotranspiration continued increasing during summer. Then, GPP decreased gradually during August due to lower Ta and radiation and began to decrease sharply from September to November during the browning and fall of leaves until the offset of the growing season.

The dehesa ecosystem in Spain is composed by two mainly vegetation layers, the tree and the herbaceous layer, which respond to Mediterranean climate in a different way and are responsible of the dynamic of the ecosystem. From December to March, GPP from the herbaceous and tree layer was low due to low temperatures. However, the tree and the herbaceous layer are green and can produce during winter (Chiarielllo, 1989; Ma et al., 2007). Then, Ta began to increase fast and consequently GPP of both strata began to increase reaching its maximum at late April and having maximum values until mid-May. Vegetation in Mediterranean ecosystems, especially grasslands, are adapted to grow earlier in spring to take advantage of lower temperatures, lower VPD and higher SWC than later (Cicuéndez et al., 2015; Evans and Young, 1989). During this period, GPP is strongly coupled to LE and SWC. Other researchers have found that availability of water is the main limiting factors in this ecosystem (Gómez-Giráldez et al., 2018). In late May the species of the herbaceous layer begin to dry due to high Ta and VPD values and consequently GPP and LE decreased during summer and until mid-September. The tree layer can continue to produce a slightly longer period than the herbaceous one due to the deeper roots that can extract water from deeper layers of the soil (Joffre and Rambal, 1988; Pereira et al., 2007), although during summer will close the stomata due to high VPD. H is maximum in summer due to high temperatures and because latent heat is low. During autumn, GPP increased due to rainfall events and the

recovery of water in soil (Cicuéndez et al., 2015; El-Madany et al., 2018) and decreased since mid-November due to low temperatures.
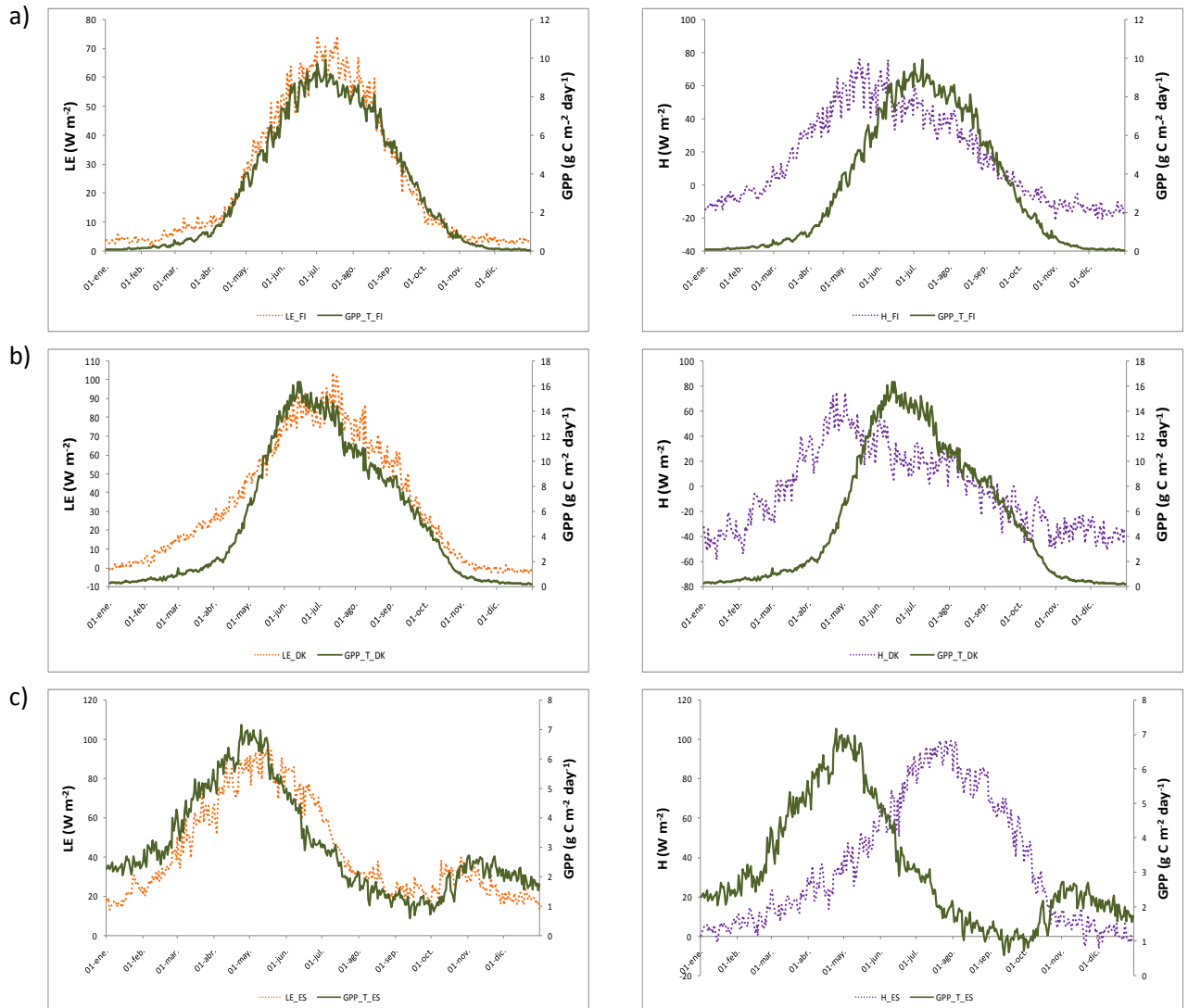
Figure 1. Average year, i.e. Buys-Ballot, of Gross Primary Production GPP_T (g C m-2 day-1) (Right axis) and Latent heat LE (W m-2) and Sensible heat H (Left axis) for a) the Evergreen Needleleaf Forest of Finland (FI), b) the Deciduous Broadleaf Forest of Denmark (DK) and c) the Mediterranean forest of Spain (ES).

3.2. Granger Causality Tests

Figure 2 shows the Granger causality Tests between GPP, LE and H in both directions (i.e., Energy flux variable cause GPP and GPP cause energy flux variable).

The F-tests revealed that GPP cause latent heat more than backwards in the three ecosystems, especially in Denmark and in Finland with values around 500 for the first lag until lag 6 when both directions showed similar F-test values. This fact indicated that vegetation provides a feedback to atmosphere influencing LE at a short term (Forzieri et al., 2020). The differences between sites are due to Leaf Area Index (LAI) and soil water dynamics (Wang et al., 2019).The DBF in Denmark and ENF in Finland showed high LAIs with high soil water contents, this fact entailed more transpiration rates, especially in the Deciduous Forest. Meanwhile, the dehesa ecosystem showed lower GPP, with a lower LAI and less soil water content, subsequently lower transpiration rates.

The F-tests showed that sensible heat causes GPP more than GPP causes sensible heat in Finland and in Spain. This fact indicated that H was controlling GPP more than backwards, although there was also a feedback of vegetation controlling H, especially for the first lags. In both sites, the influence of H on GPP is higher probably due to the effect of temperature controlling GPP. While in Finland the relationship between H and GPP was positive, in Spain was

negative, the maximum of H coincided with the minimum of GPP. In Denmark, the expansion of LAI entailed a reduction of changes on surface temperature and subsequently, affected H. Thus, GPP caused H more than backwards at a very short term (3 lags). Then, H caused GPP evidencing also the effect of temperature on GPP.
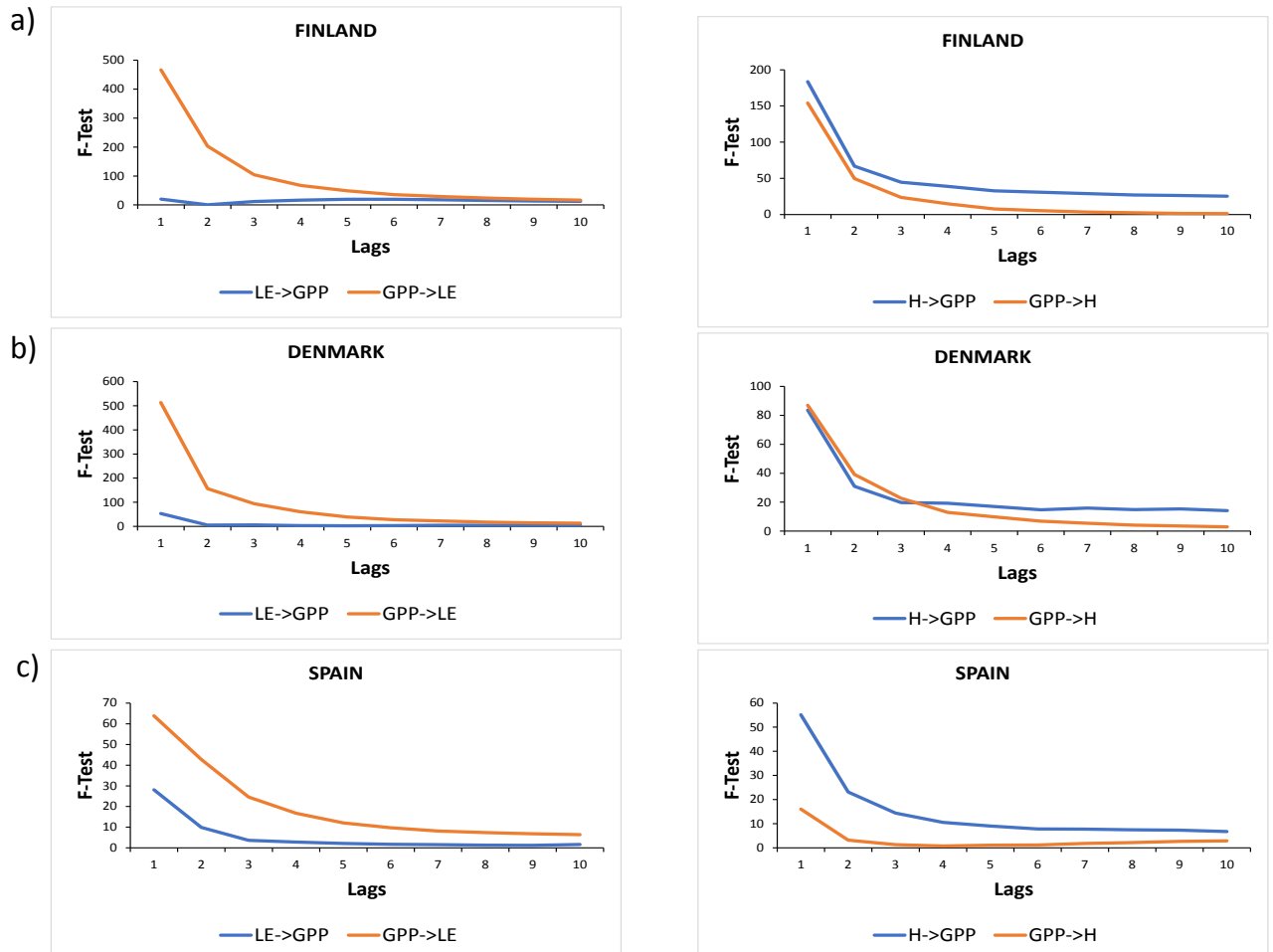
Figure 2. Granger causality Tests between GPP, LE and H in both directions (i.e., Energy flux variable cause GPP and GPP cause energy flux variable).

4. Conclusions

Differences in GPP, LE and H values and dynamics between sites are due to different plant functional types and their interaction with the meteorological variables in each climate. Temperature and solar radiation were the main limiting factors in ENF while water availability was determinant for growth in the Mediterranean ecosystem. The DBF showed a different GPP cycle related with an interaction of various factors during all the growing season.

The three ecosystems are directly responsible for the energy fluxes partitioning and water fluxes dynamics. In Finland, latent heat was coupled to GPP during all growing season due to the factor of temperature while in Denmark began to be strongly coupled when leaf emergence occurred. In Spain, latent heat was coupled to GPP during all growing season but due to water availability.

Different vegetation types provide a feedback to atmosphere influencing the energy partitioning in a different way. GPP causes latent heat more than backwards in the three ecosystems due to LAI and soil water dynamics. However, sensible heat causes GPP more than backwards, especially in Finland and Spain due to that temperature regulated the carbon fluxes but with an inverse pattern in both ecosystems. In Denmark, a forest with a more closed canopy, GPP caused also sensible heat with LAI development.

Acknowledgements

References

Arora, V., 2002. Modeling vegetation as a dynamic component in soil-vegetation-atmosphere transfer schemes and hydrological models. Rev. Geophys. 40, 1006. https://doi.org/10.1029/2001RG000103

Baldocchi, D., 2014. Measuring fluxes of trace gases and energy between ecosystems and the atmosphere - the state and future of the eddy covariance method. Glob. Chang. Biol. 20, 3600–3609. https://doi.org/10.1111/gcb.12649

Beer, C., Reichstein, M., Tomelleri, E., Ciais, P., Jung, M., Carvalhais, N., Rödenbeck, C., Arain, M.A., Baldocchi, D., Bonan, G.B., Bondeau, A., Cescatti, A., Lasslop, G., Lindroth, A., Lomas, M., Luyssaert, S., Margolis, H., Oleson, K.W., Roupsard, O., Veenendaal, E., Viovy, N., Williams, C., Woodward, F.I., Papale, D., 2010. Terrestrial gross carbon dioxide uptake: Global distribution and covariation with climate. Science (80-.). 329, 834–838. https://doi.org/10.1126/science.1184984

Buys-Ballot, C.H.D., 1847. Les Changements périodiques de température, dépendants de la nature du soleil et de la lune, mis en rapport avec le pronostic du temps, déduits d'observations néerlandaises de 1729 à 1846.

Casals, P., Gimeno, C., Carrara, A., Lopez-Sangil, L., Sanz, Mj., 2009. Soil CO_2 efflux and extractable organic carbon fractions under simulated precipitation events in a Mediterranean Dehesa. Soil Biol. Biochem. 41, 1915–1922. https://doi.org/10.1016/j.soilbio.2009.06.015

Chiarielllo, N.R., 1989. Phenology of California grasslands, in: Lieth, H., Mooney, H.A. (Eds.), Grassland Structure and Function: California Annual Grassland (Tasks for Vegetation Science 2.0). Kluwer Academic Publishers, Dordrecht, The Netherlands, pp. 47–58.

Cicuéndez, V., Litago, J., Huesca, M., Rodriguez-Rastrero, M., Recuero, L., Merino-de-Miguel, S., Palacios-Orueta, A., 2015. Assessment of the gross primary production dynamics of a Mediterranean holm oak forest by remote sensing time series analysis. Agrofor. Syst. 89, 491–510. https://doi.org/10.1007/s10457-015-9786-x

D'Odorico, P., Gonsamo, A., Gough, C.M., Bohrer, G., Morison, J., Wilkinson, M., Hanson, P.J., Gianelle, D., Fuentes, J.D., Buchmann, N., 2015. The match and mismatch between photosynthesis and land surface phenology of deciduous forests. Agric. For. Meteorol. 214–215, 25–38. https://doi.org/10.1016/j.agrformet.2015.07.005

Dass, P., Rawlins, M.A., Kimball, J.S., Kim, Y., 2016. Environmental controls on the increasing GPP of terrestrial vegetation across northern Eurasia. Biogeosciences 13, 45–62. https://doi.org/10.5194/bg-13-45-2016

El-Madany, T.S., Reichstein, M., Perez-Priego, O., Carrara, A., Moreno, G., Pilar Martín, M., Pacheco-Labrador, J., Wohlfahrt, G., Nieto, H., Weber, U., Kolle, O., Luo, Y.-P., Carvalhais, N., Migliavacca, M., 2018. Drivers of spatio-temporal variability of carbon dioxide and energy fluxes in a Mediterranean savanna ecosystem. Agric. For. Meteorol. 262, 258–278. https://doi.org/10.1016/j.agrformet.2018.07.010

Evans, R.A., Young, J.A., 1989. Characterization and analysis of abiotic factors and their influences on vegetation, in: Lieth, H., Mooney, H.A. (Eds.), Grassland Structure and Function: California Annual Grassland (Tasks for Vegetation Science 2.0). Kluwer Academic Publishers, Dordrecht, The Netherlands.

Forzieri, G., Miralles, D.G., Ciais, P., Alkama, R., Ryu, Y., Duveiller, G., Zhang, K., Robertson, E., Kautz, M., Martens, B., Jiang, C., Arneth, A., Georgievski, G., Li, W., Ceccherini, G., Anthoni, P., Lawrence, P., Wiltshire, A., Pongratz, J., Piao, S., Sitch, S., Goll, D.S., Arora, V.K., Lienert, S., Lombardozzi, D., Kato, E., Nabel, J.E.M.S., Tian, H., Friedlingstein, P., Cescatti, A., 2020. Increased control of vegetation on global terrestrial energy fluxes. Nat. Clim. Chang. 10, 356–362. https://doi.org/10.1038/s41558-020-0717-0

Gómez-Giráldez, P.J., Carpintero, E., Ramos, M., Aguilar, C., González-Dugo, M.P., 2018. Effect of the water stress on gross primary production modeling of a Mediterranean oak savanna ecosystem. Proc. Int. Assoc. Hydrol. Sci. 380, 37–43. https://doi.org/10.5194/piahs-380-37-2018

Granger, C.W.J., 1969. Investigating Causal Relations by Econometric Models and Cross-spectral Methods. Econometrica 37, 424–438.

Hoek van Dijke, A., Mallick, K., Schlerf, M., Machwitz, M., Herold, M., Teuling, A., 2020. Examining the link between vegetation leaf area and land-atmosphere exchange of water, energy, and carbon fluxes using FLUXNET data. Biogeosciences Discuss. 1–22. https://doi.org/10.5194/bg-2020-50

Jiang, Y., Zhang, J.H., Xu, X. De, Dong, Z.X., 2013. A GPP assimilation model for the southeastern Tibetan Plateau based on CO_2 eddy covariance flux tower and remote sensing data. Int. J. Appl. Earth Obs. Geoinf. 23, 213–225. https://doi.org/10.1016/j.jag.2012.08.015

Joffre, R., Rambal, S., 1988. Soil water improvement by trees in the rangelands of southern Spain. Acta oecologica. Oecologia Plant. 9, 405–422.

Ma, S., Baldocchi, D.D., Xu, L., Hehn, T., 2007. Inter-annual variability in carbon dioxide exchange of an oak/grass savanna and open grassland in California. Agric. For. Meteorol. 147, 157–171. https://doi.org/10.1016/j.agrformet.2007.07.008

Mäkelä, A., Kolari, P., Karimäki, J., Nikinmaa, E., Perämäki, M., Hari, P., 2006. Modelling five years of weather-driven variation of GPP in a boreal forest. Agric. For. Meteorol. 139, 382–398. https://doi.org/10.1016/j.agrformet.2006.08.017

Melaas, E.K., Friedl, M.A., Zhu, Z., 2013. Detecting interannual variation in deciduous broadleaf forest phenology

using Landsat TM/ETM+ data. Remote Sens. Environ. 132, 176–185. https://doi.org/10.1016/j.rse.2013.01.011

Papale, D., Valentini, R., 2003. A new assessment of European forests carbon exchanges by eddy fluxes and artificial neural network spatialization. Glob. Chang. Biol. 9, 525–535.

Pastorello, G., Trotta, C., Canfora, E., Chu, H., Christianson, D., Cheah, Y.-W., Poindexter, C., Chen, J., Elbashandy, A., Humphrey, M., Isaac, P., Polidori, D., Reichstein, M., Ribeca, A., van Ingen, C., Vuichard, N., Zhang, L., Amiro, B., Ammann, C., Arain, M.A., Ardö, J., Arkebauer, T., Arndt, S.K., Arriga, N., Aubinet, M., Aurela, M., Baldocchi, D., Barr, A., Beamesderfer, E., Marchesini, L.B., Bergeron, O., Beringer, J., Bernhofer, C., Berveiller, D., Billesbach, D., Black, T.A., Blanken, P.D., Bohrer, G., Boike, J., Bolstad, P. V., Bonal, D., Bonnefond, J.-M., Bowling, D.R., Bracho, R., Brodeur, J., Brümmer, C., Buchmann, N., Burban, B., Burns, S.P., Buysse, P., Cale, P., Cavagna, M., Cellier, P., Chen, S., Chini, I., Christensen, T.R., Cleverly, J., Collalti, A., Consalvo, C., Cook, B.D., Cook, D., Coursolle, C., Cremonese, E., Curtis, P.S., D'Andrea, E., da Rocha, H., Dai, X., Davis, K.J., Cinti, B. De, Grandcourt, A. de, Ligne, A. De, De Oliveira, R.C., Delpierre, N., Desai, A.R., Di Bella, C.M., Tommasi, P. di, Dolman, H., Domingo, F., Dong, G., Dore, S., Duce, P., Dufrêne, E., Dunn, A., Dušek, J., Eamus, D., Eichelmann, U., ElKhidir, H.A.M., Eugster, W., Ewenz, C.M., Ewers, B., Famulari, D., Fares, S., Feigenwinter, I., Feitz, A., Fensholt, R., Filippa, G., Fischer, M., Frank, J., Galvagno, M., Gharun, M., Gianelle, D., Gielen, B., Gioli, B., Gitelson, A., Goded, I., Goeckede, M., Goldstein, A.H., Gough, C.M., Goulden, M.L., Graf, A., Griebel, A., Gruening, C., Grünwald, T., Hammerle, A., Han, S., Han, X., Hansen, B.U., Hanson, C., Hatakka, J., He, Y., Hehn, M., Heinesch, B., Hinko-Najera, N., Hörtnagl, L., Hutley, L., Ibrom, A., Ikawa, H., Jackowicz-Korczynski, M., Janouš, D., Jans, W., Jassal, R., Jiang, S., Kato, T., Khomik, M., Klatt, J., Knohl, A., Knox, S., Kobayashi, H., Koerber, G., Kolle, O., Kosugi, Y., Kotani, A., Kowalski, A., Kruijt, B., Kurbatova, J., Kutsch, W.L., Kwon, H., Launiainen, S., Laurila, T., Law, B., Leuning, R., Li, Yingnian, Liddell, M., Limousin, J.-M., Lion, M., Liska, A.J., Lohila, A., López-Ballesteros, A., López-Blanco, E., Loubet, B., Loustau, D., Lucas-Moffat, A., Lüers, J., Ma, S., Macfarlane, C., Magliulo, V., Maier, R., Mammarella, I., Manca, G., Marcolla, B., Margolis, H.A., Marras, S., Massman, W., Mastepanov, M., Matamala, R., Matthes, J.H., Mazzenga, F., McCaughey, H., McHugh, I., McMillan, A.M.S., Merbold, L., Meyer, W., Meyers, T., Miller, S.D., Minerbi, S., Moderow, U., Monson, R.K., Montagnani, L., Moore, C.E., Moors, E., Moreaux, V., Moureaux, C., Munger, J.W., Nakai, T., Neirynck, J., Nesic, Z., Nicolini, G., Noormets, A., Northwood, M., Nosetto, M., Nouvellon, Y., Novick, K., Oechel, W., Olesen, J.E., Ourcival, J.-M., Papuga, S.A., Parmentier, F.-J., Paul-Limoges, E., Pavelka, M., Peichl, M., Pendall, E., Phillips, R.P., Pilegaard, K., Pirk, N., Posse, G., Powell, T., Prasse, H., Prober, S.M., Rambal, S., Rannik, Ü., Raz-Yaseef, N., Rebmann, C., Reed, D., Dios, V.R. de, Restrepo-Coupe, N., Reverter, B.R., Roland, M., Sabbatini, S., Sachs, T., Saleska, S.R., Sánchez-Cañete, E.P., Sanchez-Mejia, Z.M., Schmid, H.P., Schmidt, M., Schneider, K., Schrader, F., Schroder, I., Scott, R.L., Sedlák, P., Serrano-Ortíz, P., Shao, C., Shi, P., Shironya, I., Siebicke, L., Šigut, L., Silberstein, R., Sirca, C., Spano, D., Steinbrecher, R., Stevens, R.M., Sturtevant, C., Suyker, A., Tagesson, T., Takanashi, S., Tang, Y., Tapper, N., Thom, J., Tomassucci, M., Tuovinen, J.-P., Urbanski, S., Valentini, R., van der Molen, M., van Gorsel, E., van Huissteden, K., Varlagin, A., Verfaillie, J., Vesala, T., Vincke, C., Vitale, D., Vygodskaya, N., Walker, J.P., Walter-Shea, E., Wang, H., Weber, R., Westermann, S., Wille, C., Wofsy, S., Wohlfahrt, G., Wolf, S., Woodgate, W., Li, Yuelin, Zampedri, R., Zhang, J., Zhou, G., Zona, D., Agarwal, D., Biraud, S., Torn, M., Papale, D., 2020. The FLUXNET2015 dataset and the ONEFlux processing pipeline for eddy covariance data. Sci. Data 7, 225. https://doi.org/10.1038/s41597-020-0534-3

Pereira, J.S., Mateus, J.A., Aires, L.M., Pita, G., Pio, C., David, J.S., Andrade, V., Banza, J., David, T.S., Paço, T.A., Rodrigues, A., 2007. Net ecosystem carbon exchange in three contrasting Mediterranean ecosystems - The effect of drought. Biogeosciences 4, 791–802. https://doi.org/10.5194/bg-4-791-2007

Pilegaard, K., Ibrom, A., Courtney, M.S., Hummelshøj, P., Jensen, N.O., 2011. Increasing net CO2 uptake by a Danish beech forest during the period from 1996 to 2009. Agric. For. Meteorol. 151, 934–946. https://doi.org/10.1016/j.agrformet.2011.02.013

Recuero, L., Wiese, K., Huesca, M., Cicuéndez, V., Litago, J., Tarquis, A.M., Palacios-Orueta, A., 2019. Fallowing temporal patterns assessment in rainfed agricultural areas based on NDVI time series autocorrelation values. Int. J. Appl. Earth Obs. Geoinf. 82, 101890. https://doi.org/10.1016/j.jag.2019.05.023

Reichstein, M., Falge, E., Baldocchi, D., Papale, D., Aubinet, M., Berbigier, P., Bernhofer, C., Buchmann, N., Gilmanov, T., Granier, A., Grunwald, T., Havrankova, K., Ilvesniemi, H., Janous, D., Knohl, A., Laurila, T., Lohila, A., Loustau, D., Matteucci, G., Meyers, T., Miglietta, F., Ourcival, J.-M., Pumpanen, J., Rambal, S., Rotenberg, E., Sanz, M., Tenhunen, J., Seufert, G., Vaccari, F., Vesala, T., Yakir, D., Valentini, R., 2005. On the separation of net ecosystem exchange into assimilation and ecosystem respiration: review and improved algorithm. Glob. Chang. Biol. 11, 1424–1439. https://doi.org/10.1111/j.1365-2486.2005.001002.x

Suni, T., Rinne, J., Reissell, A., Altimir, N., Keronen, P., Rannik, Ü., Dal Maso, M., Kulmala, M., Vesala, T., 2003. Long-term measurements of surface fluxes above a Scots pine forest in Hyytiälä, southern Finland, 1996-2001. Boreal Environ. Res. 8, 287–301.

Wang, P., Li, X., Tong, Y., Huang, Y., Yang, X., Wu, X., 2019. Vegetation dynamics dominate the energy flux partitioning across typical ecosystem in the Heihe River Basin: Observation with numerical modeling. J. Geogr. Sci. 29,

1565–1577. https://doi.org/10.1007/s11442-019-1677-z

Wang, Q., Tenhunen, J., Dihn, N., Reichstein, M., Otieno, D., Granier, A., Pilegaard, K., 2005. Evaluation of seasonal variation of MODIS derived leaf area index at two European deciduous broadleaf forest sites. Remote Sens. Environ. 96, 475–484. https://doi.org/10.1016/j.rse.2005.04.003

Yuan, W., Cai, W., Nguy-Robertson, A.L., Fang, H., Suyker, A.E., Chen, Y., Dong, W., Liu, S., Zhang, H., 2015. Uncertainty in simulating gross primary production of cropland ecosystem from satellite-based models. Agric. For. Meteorol. 207, 48–57. https://doi.org/10.1016/j.agrformet.2015.03.016

Post-harvest technologies

A Comparative Study On Existing Interventions For Tackling Post-Harvest Losses In Developing Countries

Winifred Ereku [a],*, María-Laura Franco-García [b] Michiel A Heldeweg [c]

[a] Department of Governance and Technology for Sustainability,
University of Twente, Enschede, The Netherlands
[b] Faculty of Behavioural, Management & Social Sciences, Enschede, The Netherlands
* Corresponding author. Email: w.e.ereku@utwente.nl

Abstract

Food consumption has grown over the years in tandem with the insistent world population growth forecasted to reach a record high come 2050. As severe hunger remains a present-day challenge, the problem of Post-Harvest Loss and Waste calls for more sustainable solutions especially in developing countries. Although policies and interventions (including smart farming technologies) have been adopted, it is vital to understand the efficacy and limitations of some of these interventions to ensure sustainable outcomes. In this paper, we compare the efficacy and limitations of four different interventions for the reduction of post-harvest food loss (PHL) in developing countries. The main research question tackled in this study is: *How effective are the existing interventions for the reduction of PHL in developing countries*? Also, *what are the primary limitations or drivers of these interventions in developing countries*? In this context, interventions refer to an action or set of actions aimed at positive change. The methodology of this study is both explorative and comparative. Information was gathered through the review of relevant literature and different interventions in various cases were explored and compared. The initial findings of this study reflect the efficacy of interventions created from evidence-based approaches (a pre-informed process) and it also elaborates on the limitations encountered as a result of the adoption of these interventions in areas specifically, Africa. Based on the understanding of the limitations of different interventions, more tailored propositions to solving these malignant issues may suffice, given the potential of such solutions to aid policymaking, reduce hunger, promote sustainable growth and economic development. The mechanism for coping with PHL and how it can be adopted, merged, or form the basis of a new solution is an area recommended for further research.

Keywords: Post-Harvest Loss, Interventions, Sustainable Solutions

1. Introduction

The world has seen a continuous increase in food consumption over the years. This growth is set to increase rapidly considering the forecasted population growth come 2050. The pressure of the potentially rising demand may pave way for an urgent need to increase food production. However, whilst the need to meet rising demand is raising plausible concerns in developing countries, it is imperative to critically examine the processes involved to ensure sustainable outcomes. A primary focus on technological interventions to significantly increase food production without a parallel cause of action to prevent and reduce food loss and waste may potentially result in tragic losses for all the stakeholders involved. Post-harvest food loss can be referred to as measurable qualitative and quantitative food loss along the supply chain, starting at the time of harvest till its consumption or other end uses (Hodges et al., 2011). The reality of the level of postharvest losses (PHL) occurring in developing countries saw a significant increase in 2020 as a result of the effect of the measures taken to fight the COVID 19 pandemic. Abrupt changes and measures including social distancing and transportation restrictions affected the agricultural supply chain and increased postharvest losses in both developed and developing countries alike. In addition, labour shortages, owing to the restriction of movement of key stakeholders in production and transport, are significantly impacting food supply and demand owing to food shortages in some markets, further contributing to food loss and to the unnecessary waste of food supplies in these difficult times (FAO, 2020).

The United Nations Sustainable Development Goal 12.3 (SDG 12.3) reenacts the Importance of ensuring an efficient process from farm to fork. The SDG 12.3 aims to reduce global food waste and food loss across the supply chain, including post harvest losses by 2030. Current interventions for tackling postharvest food loss in developing countries (including technological, financial, process and producer interventions) exist, however, it is important to understand the efficacy and limitations of these interventions within different contexts whilst taking into consideration the geographical and economical differences in the areas where these interventions are implemented. The dynamic of how a postharvest loss intervention is implemented vary from country to country due to a number of factors including but not limited to economic, infrastructural, cultural factors and the level of awareness. Developing countries may share a number of similarities due to developmental challenges that cuts across geographical or cultural contexts even though the differences across these countries stand out.

The aim of this study is to explore, understand and compare current agricultural interventions for curbing postharvest in developing countries. The two questions to be answered within this study is; how effective are the existing interventions for the reduction of PHL in developing countries? Also, what are the primary limitations or drivers of these interventions in developing countries? Understanding the different methods of adoption and the implementation of these interventions in different contexts may contribute to the development and application of a more evidence-based approach in solving similar problems in developing countries with a possibly similar context. The use of a more proven approach with the understanding of the elements that contributed to the successful implementation or limited the efficacy of the given intervention holds the potential of saving time and resources for developing countries when it comes to adopting a new solution to reduce food loss and waste. This may facilitate a more tailored approach to solving the problem of postharvest food loss rather than a more ambiguous or copy-paste approach.

The idea of bringing together different elements to examine and compare in different contexts is not new. As regarding comparative studies and the potential impact it holds, (Esser & Vliegenthart, 2017) states that comparative analysis enhances the understanding of one's own society by placing its familiar structures and routines against those of other systems (understanding); comparison heightens our awareness of other systems, cultures, and patterns of thinking and acting, thereby casting a fresh light on our own political communication arrangements and enabling us to contrast them critically with those prevalent in other countries (awareness); comparison allows for the testing of theories across diverse settings and for the evaluating of the scope and significance of certain phenomena, thereby contributing to the development of universally applicable theory (generalization); comparison prevents scholars from over-generalizing based on their own, often idiosyncratic, experiences and challenges claims to ethnocentrism or naïve universalism (relativization); and comparison provides access to a wide range of alternative options and problem solutions that can facilitate or reveal a way out of similar dilemmas at home (alternatives).

Proffering implementable solutions for tackling postharvest food loss is essential for personal, economical and societal development as the impact of postharvest loss (PHL) spans across a number of areas to include environmental impact, economic impact and health impact. A reduction in PHL means that there is less need to convert more land to farmland because production volumes actually make it to market and thus fulfil demand, reducing the burden on deforestation and offsetting the carbon footprint of crops grown (Deloitte, 2015). Even though the effects of PHL may be seen across the food supply chain, some stakeholders along the supply chain may suffer these impacts in the short term more than other stakeholders in the same supply chain. Nonetheless, the challenges and consequences of food loss and waste is generally evident in developing countries across the world.

2. Materials and Methods

Research Methods

The methodological approach deployed for this study is a comparative qualitative research with a holistic dimension approach. This orientation helps the researcher discover the interrelationships among the various components of the under study (Malhotra et al., 2012). The various elements examined within the study are the four key elements of intervention important for the formulation and implementation of PHL interventions as seen in previous and extensive literature. The systematic interconnectivity of the agricultural supply chain calls for a more combined approach for PHL intervention models if sustainable results are to be achieved. This is one of the reasons for the chosen model developed by (Deloitte, 2015) which elaborates on the integration of the following four Ps: Products (technologies), Processes (procurement channels), Producers (farmers) and Pricing & Payment (financial intervention). Even so, more qualitative data was collected through the review of existing literature which is categorized under the Monitor Deloitte Analysis (see figure 1).
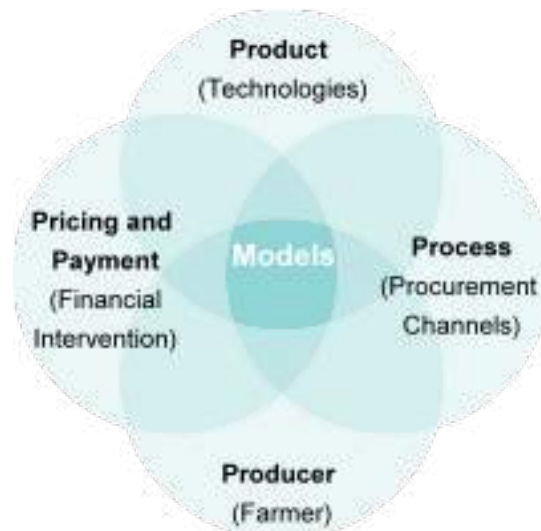
Figure 1. Monitor Deloitte analysis (Deloitte, 2015).

2.1. Sampling Technique

The type of sampling technique adopted for this study is the cluster sampling technique with the specific use of area sampling. According to (Malhotra et al., 2012), area sampling is a common form of cluster sampling in which the clusters consist of geographical areas such as countries, housing tracts, blocks or other area descriptions. This sampling technique creates a broader spectrum to explore and compare the different postharvest loss interventions in these different geographical areas under the specific context, cultural or technological trends that may affect the efficacy of the PHL intervention or limit its potential in these areas (see figure 2). Developing countries are situated in specific continents of the world hence, the need to approach this study from an encompassing view to detect contextual similarities or differences that may be major drivers to consider whilst formulating or implement new or existing PHL solutions.
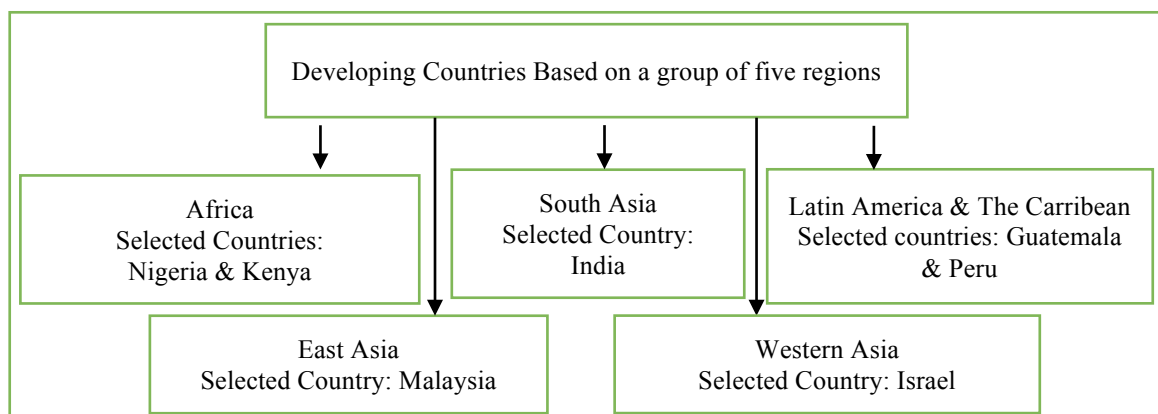
Figure 2. Representation of the sample area using area sampling technique.

The world economic situation and prospects (WESP) classifies all countries of the world into 3 broad categories; developed economies, economies in transition and developing economies (WESP, 2014). The essence of this categorization reflects the economic situation of the countries in their respective categories. For the sake of this study, a subgroup of countries from the developing countries category were selected based on their geographical location in the continents where these developing countries are located as seen in figure 2.

The paper further unravels in the following way; firstly, the reviewed literature is constructively presented to include theoretical background from which the four interventions discussed in the study is based, secondly, these interventions are explored under the context of each individual developing country selected for the aim of this study. Following this, the findings will be compared and discussed in the results and discussion section of this research respectively.

2.2. Data Presentation and Analysis

The paper further unravels in the following way; firstly, the reviewed literature is constructively presented to include theoretical background from which the four interventions discussed in the study is based, secondly, these interventions

are explored under the context of each individual developing country selected for the aim of this study. Following this, the findings will be compared and discussed in the results and discussion section of this research respectively.

3. Results and Discussion

3.1. Findings

The findings and results from reviewed literature are analysed from the Deloitte 4Ps model (products, process, producers and payments and pricing interventions). The countries subject to this analysis were Nigeria, Kenya, India, Malaysia, Guatemala and Peru.

3.1.1.Postharvest Loss Interventions in Nigeria

Nigeria's population is increasing on annual basis and that is putting tremendous pressure on natural resources such as land, water, forest which means food wastage and loss must be avoided in order to avoid food insecurity especially in the face of unstable food prices and slow economic growth (Abbas et al., 2018). In an effort to reduce the level of postharvest food loss over the years, different interventions and policies have been adopted. Product (technological) interventions including reusable plastic crates (RPCs), hermetic bags, silos and charcoal cooler (which is a type of cold storage) are used by some small holder farmers in Nigeria even though some of these technologies are not widely adopted across the country especially by small holder farmers in the grassroots.

Although, the use of certain technologies readily available in the rural areas, (for example, raffia or palm baskets used for bulk tomato storage during transport) is seen to result in significant losses, it is more widely used than its counterpart, the RPCs. In addition, the innovation in the form of the plastic crates showed better results compared to the traditional raffia baskets (Kok et al., 2019). On one hand, financial interventions and process interventions like agricultural crowdfunding platforms and contract farming have sprung up in recent times. These platforms facilities a process that brings the farmers in contact with consumers and investors that invest in farm input for a season in exchange for financial returns or food produce. This has been seen to bridge the gap in the funding needs of many smallholder farmers in Nigeria. On the other hand, producer interventions (including training on postharvest best practices) appear to be needed in the rural grassroots. Farmer and distributor training on the benefits, handling, and use of technologies and processes is important for ensuring adoption, correct usage and thus achieving the desired impact (Deloitte, 2015).

3.1.2.Postharvest Loss Interventions in Kenya

Farmers and suppliers in Kenya presently waste up to 40 % of what they grow, even though it is perfectly good food (Kimiywe, 2015). Given that storage has also been a main challenge. Some existing Interventions in use (inclusive of storage solutions and training interventions) include the Purdue improved cowpea storage bags, metal silos, crates and awareness campaigns to facilitate knowledge transfer and promote best practices at the farm or supply chain level of mitigating postharvest losses. Other interventions driven by a collectively shared solution exist. For example, In Kenya, a new smallholder aggregation and processing centre for mangoes has been established (Hanson et al., 2019). More technological driven interventions include the use of low-cost cold rooms, brick coolers and cool bot systems.

3.1.3.Postharvest Loss Interventions in India

India is second largest producer of food next to China with estimated food processing industry size at US$ 70 billion (Hegazy, 2016). With this level of high food production, India also records a high amount of food waste. Some PHL interventions used in India include hermetic bags for grain storage and crates for carrying fresh fruits. Smallholder farmers' interest in hermetic bags has been driven by the need to reduce grain storage losses due to insect pests and challenges (inefficacy) of current storage methods (Baributsa & Concepcion Ignacio, 2020). Other interventions that kept the grain damage levels at least 20 percentage points lower than the untreated control included mixing synthetic chemicals, botanicals with cowpeas or beans before storing them in sacks (Stathers et al., 2020). In addition to the above-mentioned technological intervention, other products including plastic crates are used to reduce the level of food loss at the initial stages of the food supply chain. Currently, crates are used to carry fruit during harvesting (FAO, 2018). A field trial to test the effectiveness of a zero-energy cool chamber (ZECC) was carried out in India. These were constructed with bricks and sand and were saturated with water to promote evaporative cooling; the units were tested in various locations, weight losses were reduced by 20 percent and vegetable shelf-life increased from one day to between five and six days (Ridolfi et al., 2018).

3.1.4.Postharvest Loss Interventions in Israel

During the growth, production, distribution and marketing of food in Israel, approximately 33% of domestically produced food is lost, becoming waste or surplus (Escajedo & Renobales, 2015). Postharvest loss occurs in Israel like many other developing countries in the world, however, there may be a positive outlook due to the development and adoption of new technologies in the Israeli agricultural sector that has also been adopted in other countries facing

similar challenges. An example of a current PHL intervention is the use of hermetically sealed cocoon storage bags to prevent significant loss and damage resulting from molds, bugs and micro contaminants. New ideas from areas as diverse as efficient dairy farming, post harvest treatments for shelf life extensions to integrated pest management and use of drones for crop monitoring – that were initiated in Israel, inform and upgrade agricultural operations around the world (Tal, 2019).

3.1.5. Postharvest Loss Interventions in Malaysia

Earlier development of postharvest handling technology in Malaysia in the late 1970s to 1980s was targeted mainly at reducing postharvest losses as that was the major issue at that time, however, recent postharvest activities have been focused on quality improvement of produce for both domestic and export markets (Abdullah et al., 2012). Some of the PHL interventions adopted in Malaysia include; product technologies like hermetic storage for grains. Also, financial interventions and process (channels) interventions like contract farming is in use in Malaysia. There are different instances of the adoption of contract farming in developed and developing countries alike. However, these are usually carried out by the private sector, unlike the Malaysian scenario where the government is directly involved as the contractor or buyer of produce from the smallholder farmers (Kaur & Kamarulzaman, 2015).

3.1.6. Postharvest Loss Interventions in Guatemala

Reducing food loss and waste (FLW) would enable Guatemala to increase output of land currently being farmed. Farmers would be able to capture more of what they grow without stressing natural resources or further depleting already marginal land (Cassou et al., 2020). The Government has strategies to strengthen the agricultural sector, through agricultural policies, gender, food fortification, and support for family farming, which contribute to the reduction of poverty and hunger, and contribute to food and nutrition security and the development of a better Guatemala (Feed The Future, 2016). More interventions based on previous research (an evidence-based record from other areas) have been implemented. These include food loss reduction campaigns and hermetic bags. For instance, Farmers that buy maize, or shell it upon drying, prefer to store it in bags (Mendoza et al., 2017). Although there are developmental challenges in Guatemala as experienced in similar developing countries, current efforts in form of PHL interventions and agricultural policies are being developed and implemented to curb the amount of food loss that takes place from farm to fork.

3.1.7. Postharvest Loss Interventions in Peru

Although there is no official food waste and loss data in Peru, reports suggest that the estimated amount of food that is discarded, (33%) of food produced could feed 2 million Peruvians (Broad Leib et al., 2021). Peru is the world's leader in various crops and is becoming an essential player (Bedoya-Perales & Dal' Magro, 2021). PHL solutions have evolved over the years and the level of adoption vary from country to country and form crop to crop. Previous literature show that farmers stored grain in different types of containers: most stored in polypropylene bags and the rest stored their grain in plastic drums or buckets (Díaz-Valderrama et al., 2020). In addition to technological interventions, Peru has developed policies and legal framework to promote the reduction of PHL in the country. In 2016, Peru adopted a Food Donation Law to facilitate and promote the donation of food that has lost commercial value but is still safe for human consumption (Broad Leib et al., 2021).

3.2. Discussion

PHL continues to be a major challenge for developing countries even though some countries may appear to be faring better than others. For instance, information from reviewed literature showed the development of technological interventions in Israel that are adopted in other countries of the world including African countries. India, being the second largest food producer in the world (second to China) experiences a significant amount of PHL as well due to poor handling practices and underdeveloped logistics and transport systems for food produce. A similarity in adopted intervention as seen in all the different country interventions studied in this paper is the use of hermetic storage bags to prevent loss after harvest. This product technological intervention was further developed (hermetically sealed cocoon storage bags) to be more effective in preserving food produce after harvest. It has been observed that the same intervention can vary in success rates depending on prevailing circumstances. For example, metal silos have been a notable success in Central America but have not yet been as successful in Africa (Kimiywe, 2015). In addition, even though a few countries (Guatemala, Kenya and Nigeria) are seen to adopt the use of training interventions and PHL reduction campaigns, more countries seem to take the technological intervention (product centred interventions) approach to tackling PHL in developing countries.

The adoption of process interventions in terms of developing sustainable channels that facilitate the movement of food from farm to fork and also promotes awareness among farmers and growers on PHL best practices could be a step in the direction of combining different forms of PHL interventions to deal with food loss and waste across the supply chain. Developing knowledge and capacity for stakeholders involved in food production and supply (farmers, processors, distributors and retailers) will ensure safety standards are adhered to, thus preventing losses associated with disposal of substandard foods as in the one experienced by Kenyan horticultural products in the European market on the basis of incompliance (Kimiywe, 2015). PHL Interventions as mentioned in this study vary in the level of adoption and

success in the developing countries where they are used. This variation may be credited to the level of awareness of that particular intervention or the incentive for adopting the intervention as perceived by the adopters. A current trend seen is the call for a multi-linked solution that combines different forms of interventions and is also tailored to geographical, cultural and economic context of the adopters.

Whilst it was observed that some interventions were more government-driven in some countries, it was also seen that some PHL interventions were more private-sector driven. Both government and the private sector have their role to play, however, whether an intervention is government or private-sector driven may affect the level of penetration or efficacy of that solution. This situation is evident in Peru (where there is a set legal framework for PHL reduction) or Malaysia where the government is the principal facilitator of the contract farming intervention implemented in that area. On the other hand, in Nigeria, farm-crowdfunding platforms adopt and operate with the contract farming model (this allows the participation of the anyone interested through an online platform) even though the government also facilitates contact farming in some areas within the country but particularly through farm cooperatives and mostly for cash crops (crops available for export).

4. Conclusions

Although, the samples were selected in clusters, the continents with a developing country were to some extent represented. Conclusively, attending to the main questions and aims of this study, the findings indicate that the actualisation of how efficient PHL interventions are in this comparative study is dependent on whether the intervention used is targeted at qualitative or quantitative loss, and also, the time and context where the research on that specific intervention took place. Notwithstanding, the level of adoption of a specific type of intervention across different countries as seen in the adoption of hermetic storage bags could suggest that smallholder farmers who adopt this solution find it useful. In addition to this, the wide adoption (in different countries and continents) of a particular PHL intervention may imply the transferability and adaptability of that intervention in different cultures and contexts.

As enumerated by (World Bank, 2011), one approach to reducing PHL during storage is either by modifying existing store types so that they perform better or by introducing existing traditional but more effective store types to those communities that do not already use them (for example, mud silos). This re-enforces the need for a more tailored approach especially when dealing with rural areas and community grassroots in order to ensure increased adoption of the PHL intervention.

The primary drivers for these interventions in developing countries in this study were seen to be the spread of PHL reduction awareness of existing interventions, affordability of the intervention, adaptability to the geographical and cultural context of the adopters of the PHL intervention (as seen in the use of reusable plastic crates as a replacement for raffia baskets for tomato storage and transport in Nigeria). Contrarily, the Limitation of these PHL interventions in developing countries include lack of awareness, adaptability of the intervention to climatic situations in that area and the cost of adoption. Further research is necessary with a holistic approach but focusing on particular country exhaustively. This will help create more data to build more transformational research that may potentially lead to the recommendation of implementable solutions.

Acknowledgements

References

Abbas, A. M., Abbas, I. I., & Agada, I. G. (2018). Reducing postharvest losses in Nigeria's agricultureal sector: Pathway to sustainable agriculture. *Innoriginal International Journal of Sciences |*, *5*(2), 16–21. https://www.researchgate.net/publication/342920943

Abdullah, H., Razali, M., & Rohaya, M. A. (2012). *Development of postharvest handling technology in malaysia and its impact on the horticultural industry*. *934*, 61–67. https://doi.org/10.17660/ActaHortic.2012.934.4

Baributsa, D., & Concepcion Ignacio, M. C. (2020). *Developments in the use of hermetic bags for grain storage*. *July*, 171–198. https://doi.org/10.19103/as.2020.0072.06

Bedoya-Perales, N. S., & Dal' Magro, G. P. (2021). Quantification of food losses and waste in peru: A mass flow analysis along the food supply chain. *Sustainability (Switzerland)*, *13*(5), 1–15. https://doi.org/10.3390/su13052807

Broad Leib, E. M., Shapiro, M., Jagdagdorj, N., & Hill, J. (2021). *LEGAL* (Issue February).

Cassou, E., Constantino, L., Hou, X., Jain, S., Messent, F., Morales, X. Z., Carlo, J., Pascual, G., De, F. M., Thapa, D., Trinidad, R. Q., Hall, M. F., Quested, T., Parry, A., & Kneller, C. (2020). *Guatemala Food Smart Country Diagnostic*.

Deloitte. (2015). Reducing food loss along African agricultural value chains. In *Deloitte* (Vol. 9, Issue 2).

Díaz-Valderrama, J. R., Njoroge, A. W., Macedo-Valdivia, D., Orihuela-Ordóñez, N., Smith, B. W., Casa-Coila, V., Ramírez-Calderón, N., Zanabria-Gálvez, J., Woloshuk, C., & Baributsa, D. (2020). Postharvest practices, challenges and opportunities for grain producers in Arequipa, Peru. *PLoS ONE*, *15*(11 November), 1–18. https://doi.org/10.1371/journal.pone.0240857

Escajedo, L., & Renobales, S. M. de. (2015). *Food Waste and*. 350.

Esser, F., & Vliegenthart, R. (2017). Comparative Research Methods. In *The International Encyclopedia of Communication Research Methods*. https://doi.org/10.1002/9781118901731.iecrm0035

FAO. (2020). Mitigating risks to food systems during COVID-19: Reducing food loss and waste. *Mitigating Risks to Food Systems during COVID-19: Reducing Food Loss and Waste*, *May*, 1–6. https://doi.org/10.4060/ca9056en

FAO, F. and A. O. (2018). *Food loss analysis : causes and solutions*. www.fao.org

Feed The Future. (2016). *Post-harvest loss technology testing in feed the future innovation lab for the reduction of post-harvest loss*. 1–8. https://www.k-state.edu/phl/what-we-do/FTF Branding- Guatemala Narrative Report FINAL V3-HG-051018.pdf

Hanson, C., Flanagan, K., Robertson, K., Axmann, H., Bos-Brouwers, H., Broeze, J., Kneller, C., Maier, D., McGee, C., O'Connor, C., Sonka, S., Timmermans, T., Vollebregt, M., & Westra, E. (2019). *Reducing food loss: Ten interventions to scale impact*. 84.

Hegazy, R. (2016). *Post-harvest Situation and Losses in India*. *June 2013*, 0–21. https://doi.org/10.6084/m9.figshare.3206851.v1

Hodges, R. J., Buzby, J. C., & Bennett, B. (2011). Postharvest losses and waste in developed and less developed countries: Opportunities to improve resource use. *Journal of Agricultural Science*, *149*(S1), 37–45. https://doi.org/10.1017/S0021859610000936

Kaur, B., & Kamarulzaman, N. H. (2015). the Impact of Public-Assisted Contract Farming. *Journal of Agribusiness Marketing*, *7*(April 2016), 1–15.

Kimiywe, J. (2015). Food and nutrition security: Challenges of post-harvest handling in Kenya. *Proceedings of the Nutrition Society*, *74*(4), 487–495. https://doi.org/10.1017/S0029665115002414

Kok, M. G., Groot, J. J., Dastoum, S., Plaisier, C., Dijkxhoorn, Y., & Wagenberg, C. P. A. van. (2019). A Measurement tool on Food losses and Waste. In *Wageningen Food and Biobased Research*. https://doi.org/10.18174/470201/1906

Malhotra, Naresh. K., Birks, D. F., & Wills, P. (2012). *Marketing Research: An applied approach. Harlow: Pearson.* (4th Editio).

Mendoza, J. R., Sabillón, L., Martinez, W., Campabadal, C., Hallen-Adams, H. E., & Bianchini, A. (2017). Traditional maize post-harvest management practices amongst smallholder farmers in Guatemala. *Journal of Stored Products Research*, *71*, 14–21. https://doi.org/10.1016/j.jspr.2016.12.007

Ridolfi, C., Hoffmann, V., & Baral, S. (2018). *Post-harvest losses: Global scale, solutions, and relevance to Ghana*. Washington, D.C.: International Food Policy Research Institute (IFPRI).

Stathers, T., Holcroft, D., Kitinoja, L., Mvumi, B. M., English, A., Omotilewa, O., Kocher, M., Ault, J., & Torero, M. (2020). A scoping review of interventions for crop postharvest loss reduction in sub-Saharan Africa and South Asia. *Nature Sustainability*, *3*(10), 821–835. https://doi.org/10.1038/s41893-020-00622-1

Tal, A. (2019). *Israeli Agricultural Innovation : Assessing the Potential to Assist Smallholders*. 102. file:///C:/Users/user/Downloads/israeli_agricultural_innovation_assessing_the_potential_to_assist_smallholders.pdf

WESP. (2014). World Economic Situation and Prospects: Country classification system: Data source, country classifications and aggregation methodology. *Dow Jones Indexes*.

World Bank. (2011). Missing food : *The Case of Postharvest Grain Losses in Sub-Saharan Africa*, *60371*.

Potential of NIRS Technology for the Determination of Cannabinoid Content in Industrial Hemp (*Cannabis sativa* L.)

Carmen Jaren[a,*], Paula Zambrana[a], Claudia Perez-Roncal[a], Ainara Lopez-Maestresalas[a], Andrés Abrego[b], Silvia Arazuri[a]

[a] Department of Engineering, Public University of Navarre, Pamplona, Spain
[b] Genscore Navarra S.L., Pamplona, Spain
* Corresponding author. Email: cjaren@unavarra.es

Abstract

Industrial hemp (*Cannabis sativa* L.) is a plant native to Asia, which has been one of the oldest sources of food, textile fiber, and medicines. It is characterized by containing minimal concentrations of delta-9 tetrahydrocannabidol (THC) which is the main psychoactive chemical component and cannabidiol (CBD), a non-psychoactive substance. In most European countries, the maximum concentration legally allowed for cultivation is 0.2% of THC and currently it is under debate whether to increase this level to 0.3%. Also, in many countries its production is being regularized and legalized, increasing the need for a rapid analysis method. The present work evaluates the cannabinoid content in hemp (*Cannabis sativa* L.) using NIRS technology in combination with chemometric techniques. For this, several samples of the Kompolti variety were analyzed. Samples were dried and ground and the content of total THC (%) and total CBD (%) was determined by HPLC-DAD as reference measurements. The spectra were collected with a Luminar 5030 AOTF-NIR instrument. Principal Component Analysis and Partial Least Square Regression Models were developed. Good coefficients of determination of cross-validation (R^2cv) of 0.77 for THC and CBD were achieved and high predictive capacity (RPD) of 7.4 for total THC and 7.8 for CBD. The results obtained show that NIRS technology is an effective tool in the quantitative determination of cannabinoids. Therefore, this analytical method would allow a simpler, more robust, precise and sustainable estimation than the current HPLC.

Keywords: CBD, THC, Near Infrared Spectroscopy, PLS, HPLC

1. Introduction

The non-psychotropic species *Cannabis sativa* L. is called industrial hemp and is characterized by containing minimal concentrations of delta-9 tetrahydrocannabidol (THC), the main psychoactive chemical component, and cannabidiol (CBD), a non-psychoactive substance that is often present in amounts similar to THC. In most European countries the current upper legal limit for cultivation is 0.2 % of THC and the ratio of CBD to THC should be greater than one. It should be notice that thanks to this cannabinoid concentration, hemp is mainly used for medicinal purposes and in the textile and food industries.

Traditionally, cannabinoid content has been determined by high performance liquid chromatography (HPLC). Although HPLC provides a full cannabinoid profile, several disadvantages are associated with its use. Sample destruction, complex instrumentation, hazardous chemicals and longer sample preparation times limit its deployment directly at the grow site where a rapid and non-destructive process is desirable (Townsend et al., 2018) Near-infrared (NIR) spectroscopy, together with chemometric has been developed as a promising method of analysis providing simultaneous, on-line, rapid, and non-destructive qualitative and quantitative analysis of the major components in many plant materials and agricultural products (Valinger et al., 2020).

The cannabis flower is heterogeneous in nature. Therefore, no two parts of the cannabis flower are alike and their cannabinoid content is likely to vary widely. Consequently, it would be highly beneficial to ensure accurate and representative measurement of these chemical compounds using a method capable of addressing the inherent heterogeneity of cannabis flower. In recent years, the interest in NIR spectroscopy applied to hemp has gained importance as moisture, volatile substances and chemical compounds in herbal products absorbed in the NIR region.

Thus, Sanchez-Carnerero et al. (2018) have exploited the potential of NIRS to estimate the content of cannabinoids. They compared the results obtained with Fourier-Transform NIRS and NIR systems 6500 scattering instrument. Similar results were obtained between both NIRS instruments, which confirm that there is enough information in the spectral region of the NIR for the elaboration of cannabinoid prediction models. Daughtry y Walthall (1998) have described a relevant study using NIRS to discriminate leaves of *Cannabis sativa* L. and other plant species. Wilson & Heinrich (2006) discriminated between "drug type" (chemotype I) and "fiber type" (chemotype II) and Borille et al. (2017) predicted the growth stage of Cannabis plants in the early stages of cultivation. Marcel et al. (2004) developed a prediction model of the chemical composition of the fiber and the central fraction of hemp (chemotype III) using NIRS combined witha partial least squares (PLS) analysis method.

More recently, Duchateau et al. (2020) created two classification methods according to the European laws about the discrimination of the legal limits of cannabis spp. using NIRS. Valinger et al. (2020) described the development of artificial neural network (ANN) models for the prediction of the physical and chemical properties of industrial hemp extracts, based on the combination of UV-vis-NIR spectra. Risoluti et al. (2020) developed a real-time detection test for cannabinoids in hemp flour using a MicroNIR spectrometer for the monitoring of cannabinoids in hemp flours.

Therefore, the aim of this study was to evaluate the functionality of the NIR spectroscopy as a tool that allows the quantification of the main cannabinoids present in hemp samples (*Cannabis sativa* L.).

2. Materials and Methods

2.1. Vegetal material

35 hemp samples were obtained in collaboration with the Genscore Navarra S.L. The specimens obtained were of the Kompolti variety, which is among the varieties authorized for the cultivation of industrial hemp in Spain. The plant material was weighed and dried in an oven at 60ºC for 24 hours, until a humidity between 8 and 13% was achieved, as recommended by regulation (EU) 2017/1155 (European Commission, 2017).

2.2. Spectra acquisition

Spectra were collected using a NIR Luminar 5030 Miniature "Hand-held" in the reflectance mode. A spectral range of 1200-2200 nm was used to obtain the spectra, with a sampling interval of 2 nm. In this study, 3 g of each of the 35 hemp powder samples were weighed and placed on the rotating cell of the AOTF-NIR spectrophotometer. As the sample rotates, the spectrum is measured so that different parts of the sample are scanned from above and inhomogeneities averaged. For each individual sample, 3 reflectance spectra were acquired by contacting the probe with the sample.

2.3. Reference Measurements: High Performance Liquid Chromatography

After the acquisition of the NIRS data, the same hemp samples were sent to a certified laboratory where the HPLC-DAD (High Performance Liquid Chromatography with Diode Array Detector) method was used for the determination of cannabinoids.

2.4. Multivariate data analysis

Data analysis was performed using the specific software The Unscrambler® X v.10.4 from CAMO Software Inc. (Norway). In the first place, Principal Component Analysis (PCA) was performed with the full set of samples.

During the pre-model building phase, data pre-processing was carried out to eliminate the non-informative effects of light scattering or system noise. For the development of the models, in addition to working with the raw data, different data pretreatments were applied: Spectra normalization, Standard Normal Variate (SNV), Standard Normal Variate and Detrend (SNV-DT), Multiplicative Scatter Correction (MSC) and First Derivative (1st D).

After that, a PLS regression analysis was applied to the data set to build a model capable of predicting the content of cannabinoids, both for total THC and for total CBD, in the hemp samples and to be able to assess the effectiveness of NIR spectroscopy. For the validation of the model, cross-validation (CV) was used in order to calculate the relationships between spectral and chemical properties.

The performance of the calibration models was evaluated using the root mean square error of the calibration (RMSEC), the root mean square error of cross-validation (RMSECV), the coefficient of determination of calibration (R^2c), the coefficient of determination of cross-validation (R^2cv), and the Residual Predictive Deviation (RPD). The number of latent variables (LV) were used to prevent overfitting.

3. Results and Discussion

3.1. HPLC results

The reference results obtained from the HPLC-DAD analysis can be seen in Table 1. 32 samples out of 35 were analyzed by HPLC-DAD, since 3 hemp plants infected with fungi were identified. Regarding the percentage of humidity, this is among the ranges established in the delegated regulation (EU) 2017/1155 of the commission of February 15 of 2017, which indicates a humidity between 8-13% in the preparation of cannabis samples. All selected samples had a THC value detected between 0.01 and 2.09%. Regarding CBD, which is currently the compound of greatest interest, the results in table 1 show us a maximum value of 7.32% and a minimum value of 2.18%, which indicates the high concentration of CBD in the samples, this being a characteristic of industrial cannabis (United Nations Office on Drugs and Crime, 2010).

Table 1. HPLC-DAD analysis results

Samples	Humidity (%)				THC total (%)				CBD total (%)			
	Min	Max	Mean	SD	Min	Min	Mean	SD	Min	Max	Mean	SD
32	9.02	12.34	10.65	3.16	0.01	2.09	0.20	0.38	2.18	7.32	3.56	1.57

3.2. Spectral Data

In Figure 1, the spectra of the hemp sample set are shown, which correspond to the spectra collected in the Luminar 5030 AOTF-NIR spectrophotometer, where the typical reflectance bands of hemp appear in the NIR region of 1200 to 2200 nm.
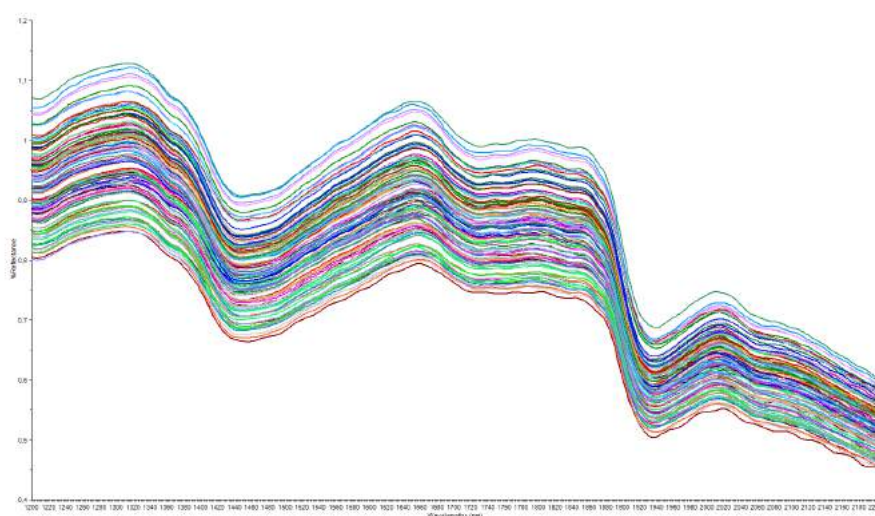
Figure 1. Spectra of the complete set of hemp samples

Principal Component Analysis (PCA) was applied to explore the spectral variability of the population, where no atypical samples were identified. This indicates that the data set is uniformly distributed. Then, PLS analysis was applied to the data set. The results for each PLS model, for total THC and total CBD, applied with each pretreatment, including the number of samples used, were compared based on the values obtained for RMSEC, RMSECV, R^2c, R^2cv, LV, SD, and RPD.

3.3. PLS model for total THC

The results for the R^2cv of the predictive models were higher than 0.72, which indicates that the calibration models can be considered good (Shenk & Westerhaus, 1996).

Similarly, the RPD was considered a good indicator of the predictive capacity and robustness of the model. In the prediction of total THC content RPD values of 7.4 were obtained, which indicates its high predictive capacity and robustness, since it was considered that the values >3 indicated that the equation could be used for high-precision quantitative analysis (Wilson & Heinrich, 2006). The higher the RPD value, the greater the ability of the calibration model to accurately predict the reference parameter values (Table 2).

Table 1. Calibration and validation statistics to predict total THC content

Pretreatment	Nc	RMSEC	RMSECV	R^2c	R^2cv	LV	SD	RPD
Raw data	91	0.010	0.014	0.87	0.77	7	0.103	7.4
Standardization	94	0.011	0.014	0.85	0.75	7	0.103	7.4
SNV	94	0.010	0.014	0.87	0.76	7	0.103	7.4
SNV-DET	94	0.011	0.014	0.84	0.72	6	0.103	7.4
MSC	94	0.010	0.014	0.86	0.76	7	0.103	7.4
1st D	94	0.010	0.014	0.86	0.75	7	0.103	7.4

For total THC (%), the best model was selected according to the highest values of R^2cv and RPD, and the lowest values of RMSECV. Likewise, the results without applying any data pretreatment technique presented higher values of R^2c of 0.87, R^2cv of 0.77 and a RPD of 7.4, which indicates its high predictive capacity and robustness. The lower RMSECV values of 0.014 were also taken into account.

In general, the results showed that the developed models had the ability to predict total THC content, with high R^2 and RPD, and RMSE. Furthermore, the difference between RMSEC and RMSECV was low in all models developed. Therefore, for the determination of total THC, the prediction model obtained without applying any data pretreatment technique presented the best results, taking 7 latent variables. For the rest of the calibration models carried out applying different combinations of data pretreatments, similar results were obtained with minimal differences.

3.4. PLS model for total CBD

The results for the R^2cv of the predictive models were higher than 0.73, which indicates that the calibration models can be considered good, except for the first derivative model that has a R^2cv value of 0.68. The latter would allow adequate discrimination between samples of high, medium and low total THC content (Shenk & Westerhaus, 1996).

Similarly, RPD was considered a good indicator of the predictive capacity and robustness of the model. The standard deviation was equal to 3.367 considering only the samples used for each calibration model and 3.398 for the first derivative model. In general, results obtained for the RPD were higher than 6.9, which indicates its high predictive capacity and robustness (Williams & Sobering, 1996) (Table 3).

Table 2. Calibration and validation statistics to predict total CBD content

Pretreatment	Nc	RMSEC	RMSECV	R^2c	R^2cv	LV	SD	RPD
Raw data	103	0.333	0.431	0.85	0.77	7	3.367	7.8
Standardization	103	0.361	0.459	0.83	0.74	7	3.367	7.3
SNV	103	0.357	0.464	0.84	0.73	7	3.367	7.3
SNV-DET	103	0.358	0.459	0.84	0.74	6	3.367	7.3
MSC	103	0.359	0.465	0.84	0.73	7	3.367	7.2
1st D	98	0.389	0.494	0.79	0.68	3	3.398	6.9

For total CBD (%), the best model was selected according to the highest values of R^2cv and RPD, and the lowest values of RMSECV. Likewise, the results without applying any data pretreatment technique presented higher R^2c values of 0.85, R^2cv of 0.77 and an RPD of 7.8, which indicates its high predictive capacity and robustness. The lower RMSECV values of 0.431 were also considered.

Moreover, as with the prediction of THC, all developed models showed an excellent performance in predicting total CBD content which demonstrate the potential of NIRS for cannabinoid content estimation.

4. Conclusions

Predictive models of the cannabinoid content in hemp have been obtained using NIRS technology, where the reference measurements were based on the concentration of total THC and total CBD obtained with HPLC (carried out in a certified laboratory). The advantage of NIRS is that samples are measured with almost no pretreatment and that the analysis is fast, sustainable and has the potential for on-site analysis.

The near infrared reflectance spectra of the hemp samples indicated that there are slight differences that are significant enough to build quantitative models. Thus, from the results obtained when applying chemometric tools and various data preprocessing techniques, we can conclude that the PLS models developed to determine the cannabinoid content in hemp samples according to their NIR spectra showed a precision of 77% for THC total and for total CBD.

Models for predicting cannobinoid content in hemp plants by NIRS technology could be improved by increasing the number of samples. Although the number of samples in this study was not very high due to the high cost of HPLC, compared with other studies, it has allowed us to demonstrate the potential of NIRS for the determination of these compounds.

The results obtained in this study demonstrate that NIR spectroscopy provides rich information on the chemical composition of the cannabis plant, which allows us to confirm that there is enough information in the NIR spectral region and when combined with chemometrics, for the development of prediction models for total TCH and total CBD in dried and ground *Cannabis sativa* L. plant material. NIRS offers speed and simplicity unmatched by other traditional

techniques and accordingly, it has been tested as an alternative method to conventional HPLC analysis for the evaluation of cannabinoid content with promising results.

References

Borille, B. T., Marcelo, M. C. A., Ortiz, R. S., Mariotti, K. de C., Ferrão, M. F., & Limberger, R. P. (2017). Near infrared spectroscopy combined with chemometrics for growth stage classification of cannabis cultivated in a greenhouse from seized seeds. *Spectrochimica Acta - Part A: Molecular and Biomolecular Spectroscopy*, *173*, 318–323. https://doi.org/10.1016/j.saa.2016.09.040

Daughtry, C. S. T., & Walthall, C. L. (1998). Spectral discrimination of Cannabis sativa L. leaves and canopies. *Remote Sensing of Environment*, *64*(2), 192–201. https://doi.org/10.1016/S0034-4257(98)00002-9

Duchateau, C., Kauffmann, J., Canfyn, M., Stévigny, C., Braekeleer, K. De, & Deconinck, E. (2020). Discrimination of legal and illegal Cannabis spp. according to European legislation using near infrared spectroscopy and chemometrics. *Drug Testing and Analysis*.

European Commission. (2017). Regulation (EU) 2017/1155 as regards the control measures relating to the cultivation of hemp, certain provisions on the greening payment, the payment for young farmers in control of a legal person. *Official Journal of the European Union*, *167*, 1–15. https://eur-lex.europa.eu/legal-content/EN/TXT/PDF/?uri=CELEX:32017R1155&from=ES

Marcel, A. J. T., Chris, M., Theo, H. R., Hilko van der, V., Mastebroek, H. D., Hetty, C. van den B., Michel, J. M. E., Waltraud, K., & Rudolf, W. K. (2004). Predicting the chemical composition of fibre and core fraction of hemp (*Cannabis sativa* L.). *Euphytica*, *V140*(1), 39–45. https://link.springer.com/article/10.1007/s10681-004-4753-z

Risoluti, R., Gullifa, G., Battistini, A., & Materazzi, S. (2020). Monitoring of cannabinoids in hemp flours by MicroNIR/Chemometrics. *Talanta*, *211*(December 2019), 120672. https://doi.org/10.1016/j.talanta.2019.120672

Sánchez-Carnerero, C., Núñez-Sánchez, N., Casano, S., & Ferreiro-Vera, C. (2018). The potential of near infrared spectroscopy to estimate the content of cannabinoids in Cannabis sativa L.: A comparative study. *Talanta*, *190*(July), 147–157. https://doi.org/10.1016/j.talanta.2018.07.085

Shenk, J. S., & Westerhaus, M. O. (1996). Calibration the ISI way. *Near Infrared Spectroscopy: The Future Waves,NIR Publications, Chichester*, 198–202.

Townsend, D., Eustis, I., Lewis, M., Rodgers, S., Smith, K., & Bohman, A. (2018). *The Determination of Total THC and CBD Content in Cannabis Flower by Fourier Transform Near Infrared Spectroscopy*. 1–5. https://doi.org/https://www.perkinelmer.com/lab-solutions/resources/docs/app_determination_of_thc_and_cbd_cannabisflower.pdf

United Nations Office on Drugs and Crime. (2010). Recommended Methods for the Identification and Analysis of Cannabis and Cannabis Products. In *Manual for Use by National Drug Analisis Laboratories*. https://doi.org/10.18356/1e8e4f16-en

Valinger, D., Jurina, T., Šain, A., Matešic, N., Panic, M., Benkovic, M., Gajdoš, G. J., & Jurinjak, T. A. (2020). Development of ANN models based on combined UV-vis-NIR spectra for rapid quantification of physical and chemical properties of industrial hemp extracts. *Wiley*, *July*, 1–13. https://doi.org/10.1002/pca.2979

Williams, P., & Sobering, D. C. (1996). How do we do it: a brief summary of the methods we use in developing near infrared calibrations. *Near Infrared Spectroscopy: The Future Waves*, 185–188.

Wilson, N., & Heinrich, M. (2006). The use of near infrared spectroscopy to discriminate between THC-rich and hemp forms of Cannabis. *Planta Medica*, *72*(11), P_260. https://doi.org/10.1055/s-2006-950060

Smart farming / Precision agriculture

Differentiated Management Center-Pivot Travel Speed Based on Soil Apparent Electrical Conductivity and Remote Sensing

João Serrano [a,*], Shakib Shahidian [a], Carlos Rodrigues [a], Sónia Garcia [b], João Noéme [b], José Palha [c]

[a] MED- Mediterranean Institute for Agriculture, Environment and Development, Instituto de Investigação e Formação Avançada, Universidade de Évora, Pólo da Mitra, Ap. 94, Évora 7006-554, Portugal;

[b] TERRAPRO, Technologies Lda, Av. Nossa Senhora Guadalupe, nº63 Porto Alto 2135-015 Samora Correia, Portugal;

[c] Pereira Palha Agricultura, LDA, Monte de Santo Isidro, 2135-401, Samora Correia, Portugal;

* Corresponding author. Email: jmrs@uevora.pt

Abstract

Climate change, in particular the trend towards global warming, will significantly affect the hydrological cycle leading to a general reduction of the available water for agriculture. In this scenario it is therefore essential that research could focus on the development of 'water saving' technologies and techniques. Conventional irrigation systems are based on the application of a homogeneous input over the field, considered as a uniform spatial unit. However, within the field, can be often recognized a spatial heterogeneity of soil characteristics, topography, microclimate, as well as of crop development. These factors result in spatial variability of irrigation efficiency and a non-uniform irrigation requirement. This work summarizes the methodology followed in a "Precision Irrigation" project for implementation of variable rate irrigation (VRI) systems in large scale application using center pivots. This is based on technologies for monitoring (i) soil electrical conductivity (EC_a), (ii) soil moisture, (iii) vegetation indices (Normalized Difference Vegetation Index, NDVI) obtained from satellite images, and automatic pivot travel speed control technologies. The VRI was achieved by varying the pivot travel speed. EC_a maps were the basis for the definition of irrigation management zones (IMZ) in an experimental corn field of 28ha located in Samora Correia (Portugal). NDVI time-series were used to establish the subsequent prescription irrigation maps. The main result of this study was the reduction of spatial yield variability achieved in the 2017 corn crop campaign with the VRI management compared to the conventional irrigation management. This study demonstrates how a relatively simple solution could be designed and implemented in large scale, showing that precision irrigation techniques are ready to provide tangible results that represent an important contribution to the sustainability.

Keywords: VRI, Precision Agriculture, efficient use of water, EC_a, NDVI

1. Introduction

Climate change will significantly affect the hydrological cycle leading, in many agricultural areas of the planet, to more frequent droughts and heat waves, to alteration of the spatial and temporal patterns of precipitation, to an increase in evapotranspiration, and to a general reduction in the availability of water for agriculture (Ortuani et al., 2019). Given the increase cost of production factors (such as water) and increasing awareness of the need to preserve our natural environment, producers rely more on precision agriculture (PA) technologies to reduce economic costs and environmental impact (Zhang et al., 2010).

The importance of properly managing irrigation is a fundamental factor for sustainable production (Torres–Sánchez et al., 2020). Similar to other agronomic inputs, the conventional management of water is based on the application of a homogeneous input over the field, considered as a uniform spatial unit. However, in any field, one can observe spatial heterogeneity of soil characteristics, topography, microclimate, crop development, water status, and yield, which result in spatial variability of irrigation efficiency and a non–uniform irrigation requirement (Ortuani et al., 2019).

With eight million hectares of the irrigated area, a center pivot system represents 23% of the total area irrigated by sprinkler irrigation systems (Baptista et al., 2019). Center pivot irrigation consists of the application of water through a moving lateral line with several water outlets supported on moving towers, which revolve around a fixed pivot point (center tower) and irrigate a circular area (Baptista et al., 2019). Variable rate irrigation (VRI), sometimes referred to as 'precision' or 'site–specific' irrigation, which is the capacity of an irrigation system to apply different amounts of water to different areas of the field based on site–specific needs, emerges as a potential solution to increase the productivity and reduce the environmental impact of irrigated agriculture (Yari et al., 2017).

The methods for VRI in centre pivots systems include: "speed or sector control" (variable speed irrigation, VSI), where the water application rate is varied in the direction of the moving sprinkler by varying its travel speed, and "zone control" (variable zone irrigation, VZI), which allows watering application rates to be varied along the lateral pipeline

as well as in the direction of the sprinkler movement (O'Shaughnessy et al., 2019). VSI does not require additional hardware on the pivot. It simply uses a more sophisticated control panel that will slow down or speed up the pivot to apply more or less water in different areas of the field and many of the newer pivot control panels already built into them since the overall pivot flow rate remains constant.

VRI assumes that crop water needs to vary spatially. In fact, soil water content varies not only spatially but temporally (Longchamps et al., 2015). In many fields, crop water needs are variable throughout an irrigation season (O'Shaughnessy et al., 2019) due to differences in soil water holding capacity (Zhao et al., 2017), which requires dynamic irrigation prescription maps (Longchamps et al., 2015) to address the variability in the soil available water. Prescription maps, or plans, contain irrigation amounts that vary for the different areas of the field, and, in this case, they should also vary over time, i.e., irrigation decisions must be re–evaluated many times over a season, which corresponds to modify VRI prescriptions in a way that improves the overall profitability (O'Shaughnessy et al., 2019). However, the data collection, analysis, and creation of optimal VRI prescriptions for a specific field's needs can be complex, time consuming, and expensive, especially since many field situations require these prescriptions to vary both in time and in space (O'Shaughnessy et al., 2019). A previous stage in this process involves the establishment of homogeneous management zones (HMZ) (O'Shaughnessy et al., 2019; Zhang et al., 2010). Soil apparent electrical conductivity (EC_a), yield maps, topography, and satellite images are among suggested attributes to delineate HMZ (O'Shaughnessy et al., 2019; Yari et al., 2017). Application of remote sensing is especially attractive because it is non–invasive and relatively inexpensive (Haghverdi et al., 2015). Effective management of VRI will likely require a combination of both remote sensing and proximal sensing to detect spatially and temporally dynamic variable crop water needs (O'Shaughnessy et al., 2019). In general, the following are recognized as necessary to sustain the adoption of site–specific VRI: (i) tools for defining HMZ, (ii) software to write basic prescriptions, (iii) decision support systems, and (iv) technical assistance and training (Evans et al., 2013).

The objective of this case study is to evaluate automatic center pivot travel speed control for dynamic management of irrigation in corn (*Zea mays* L.) based on technologies that monitor (i) soil electrical conductivity (EC_a), (ii) yield maps, and (iii) vegetation indices (Normalized Difference Vegetation Index, NDVI) obtained from satellite images.

2. Materials and Methods

2.1. Experimental Field

In this work, the corn field "Eucalyptus" of 28.2 ha, located at Samora Correia, near Lisbon, Portugal (38°50.68′ N; 8°52.55′ W), was monitored between October 2016 and October 2017. This farm is located in Lezíria do Ribatejo, a characteristic corn producing area under strong influence of the Tejo River Bay. The predominant soil in this parcel is classified as Fluvisols (FAO, 2006), sedimentary formations derived especially from recent fluvial deposits. These are soils with little or no profile differentiation but a distinct topsoil horizon, with good natural fertility, whereby many crops are grown, normally with some form of water control (FAO, 2006).

2.2. Soil Apparent Electrical Conductivity and Altimetric Surveys

In April 2017, an ECa survey was carried out with an electromagnetic induction device (EM38; Geonic, Ltd., Mississauga, ON, Canada). This equipment consists of a receiver and a transmitter coil installed 1.0 m apart at the opposite ends of a nonconductive bar. The measured depth depends on the coil configuration (horizontal or vertical) and the distance between the coils. In this study, the ECa survey was measured at two depths: 0–0.50 m and 0–1.0 m. The sensor was transported by a platform and pulled by an all–terrain vehicle equipped with a global positioning system (GPS) receiver and data collection equipment, at a speed of approximately 12 km h−1. An offset of 10 m between successive parallel paths was guaranteed by a GPS driving support system. This GPS receiver also made it possible to collect the altimetric data for the preparation of the relative field elevation map.

2.3. Vegetation Multispectral Measurements by Remote Sensing

Sentinel–2 optical images (freely available from the European Space Agency, ESA) were used. For this work, Sentinel–2 band 4 (B4, 10 m spatial resolution, 665 nm) and band 8 (B8, 10 m spatial resolution, 842 nm), atmospherically corrected imagery, were extracted from Copernicus data hub and used to calculate the normalized difference vegetation index (NDVI).

A preliminary processing was carried out on these records to remove outliers due to the presence of clouds. Only cloud–free images were used in the analysis. The monitoring of NDVI in the experimental field was carried out between May (date of planting) and October (date of harvest).

2.4. Definition of Homogeneous Management Zones (HMZ)

Homogeneous subfields were delineated using a fuzzy cluster algorithm. The MZ Analyst (MZA) software (Microsoft Corp., Redmond, Washington, United States) was utilized in this study. This software uses procedures for delineating MZs in a field and evaluating the number of homogeneous zones as described by Fridgen et al. (2004). In this study, three MZ maps were defined, one initially based on soil ECa, altimetric surveys, and soil sampling, which has been redefined twice based on NDVI maps (14 June and 23 August) and implemented sequentially during the lifecycle of the crop, as described in the following section. The HMZ obtained from MZA software were later converted into the pie slice format, suitable for pivot irrigation. These new maps were generated by taking into account the area of each homogeneous zone that fall within each circular sector. The calculations were performed for each area corresponding to a slice with 6° amplitude in the irrigation perimeter, thus, totaling 60 slices.

2.5. Definition and Implementation of Variable Rate Irrigation (VRI) Maps

The HMZ defined in a pie slice format identified zones of greater and of lesser potential productivity, constituting the basis for farmer's decision–making. In this work, the knowledge of a spatial variability pattern of 2016 corn yield influenced the farmer's decision in terms of variable irrigation prescription. Corn yield maps of 2016 and 2017 were obtained by a service provider using a John Deere harvester equipped with a crop yield monitor (grain flow meter associated with a GPS receiver). As mentioned, in order to achieve the final goal of reducing the spatial variability of production in this field, three sequential VRI stages were implemented based on three distinct HMZ maps, with each optimized for a specific objective. The initial map was based on the soil ECa survey and soil sampling, and was optimized with the objective of stimulating the productivity of less fertile soils through a greater irrigation prescription. This map was then redefined based on NDVI measurements of 14 June with the objective of stimulating the productivity of the areas with lower vegetative vigour, and then redefined again based on the NDVI measurement of 23 August with the objective of saving water in areas where the crop had reached advanced stages of its vegetative cycle. For the implementation of VRI maps in the 2017 campaign, an electronic "URAPIVOT Irrigation Systems" (Chamsa, Madrid, Spain) controller was used, running the "USENS" software application (app) developed by "TERRAPRO Technologies" (Samora Correia, Portugal), installed on a mobile device. The remote control of pivot travel speed was based on the VRI map, and the actual position (angle) of the pivot. The irrigation frequency was determined by the evolution of soil moisture content (SMC) monitored continuously by two SMC capacitance probes ("TERRAPRO Technologies," Samora Correia, Portugal).

The reduction in the amounts of irrigation water (in %) resulting from the implementation of variable irrigation strategy in lieu of conventional and uniform prescription ("standard" or 100%), which can be calculated based on VRI maps, the number of irrigation events (n), and the established prescription classes (z).

3. Results and Discussion

Mean corn yield in 2016 was $10,510 \pm 4689$ kg ha^{-1} (CV = 44.6%). Figure 1 shows the spatial variability of corn yield at the "Eucalyptus" field with an evident contrast between high productivity areas (>13,000 kg ha^{-1}) and low productivity areas (<5000 kg ha^{-1}). This was the main motivating reason of this study with a purpose, on the one hand, to identify potential causes of low productivity and, on the other hand, to stimulate productivity in these areas, reducing the overall variability of the field.

Figure 2 shows soil EC$_a$ maps at 0–0.5 m depth (**a**) and 0–1.0 m depth (**b**), with average values of, respectively, 12.71 ± 8.12 mS m^{-1} and 20.98 ± 23.08 mS m^{-1}. Soil sampling points are referenced in these maps.

Figure 3 shows eight NDVI maps of the "Eucalyptus" field including two for each month between June (after planting) and September (before harvesting).
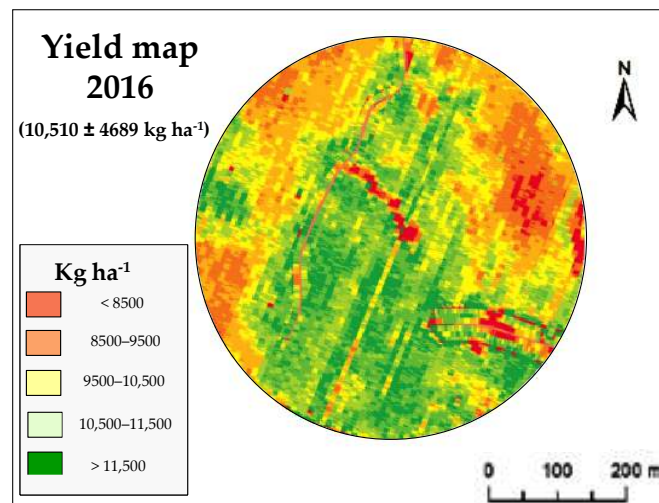
Figure 1. Corn yield map of a "Eucalyptus" field in October 2016.
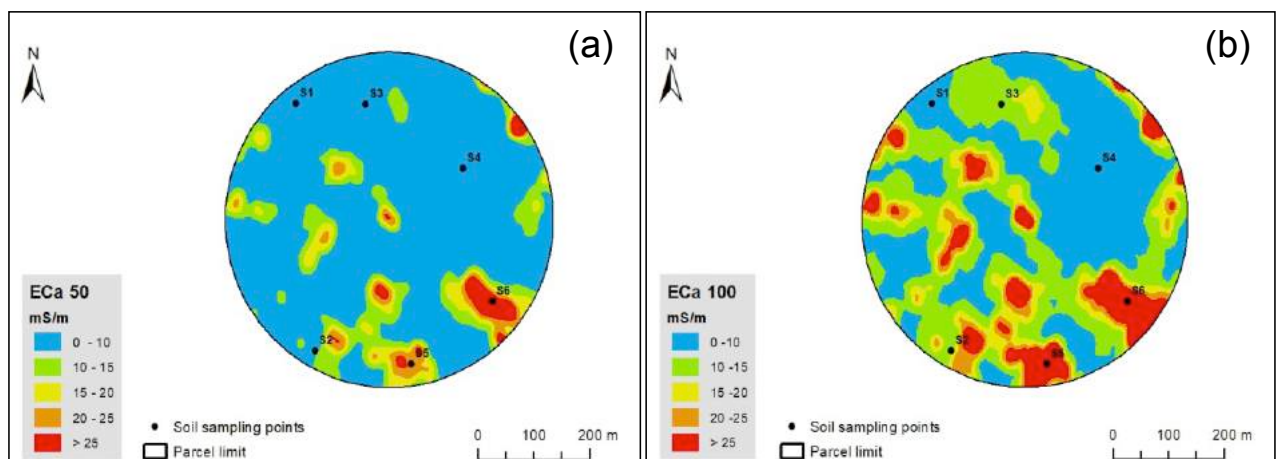
Figure 2. Soil apparent electrical conductivity (EC$_a$) maps of "Eucalyptus" field in April 2017: at 0–0.5 m (**a**) and 0–1.0 m (**b**).

Figure 4 shows the three management zones (MZ) identified in each of the three steps (left) and the corresponding maps converted into the pie slice format (right).

In all maps, the "low class" represents areas with less potential (less fertility in HMZ 1, less vegetative vigour in HMZ 2 and 3), "high class" represent areas with greater potential (greater fertility in HMZ 1, greater vegetative vigour in HMZ 2 and 3) and "medium class" represents areas with an intermediate potential from the previous ones. These maps are tools to support precision crop management, which will always be conditioned by the objectives established in each specific phase. In this case study, the farmer's main objective was to stimulate crop productivity in areas with less productive potential at the expense of applying greater amounts of water, which led to the establishment of the VRI maps presented in Figure 5 and implemented in 14 June (VRI 1), between 17 June and 22 August (VRI 2: 32 irrigation events) and between 24 August and 13 September (VRI 3: 9 irrigation events), as a result of SMC monitoring performed continuously by two capacitance probes. Five prescription classes were defined for the first year, but, in each VRI map, only three classes were used: (i) "standard" corresponds to the amount of irrigation that the farmer normally uses (present in all VRI maps), (ii) "+10%," and (iii) "+20%," respectively, 10% or 20% higher irrigation than the "standard" amount, corresponding to lower center pivot travel speed (classes used only in VRI maps 1 and 2 with the objective of stimulating the productivity of less fertile soils, areas with lower yield potential, and less vegetative vigour), (iv) "−10%" and (v) "−20%," respectively, 10% or 20% less lower irrigation than the "standard" amount, corresponding to faster center pivot travel speed (classes used only in VRI map 3 with the objective of rationalizing the

application of water in areas where the crop is in advanced stages of development). The data indicate an increase of 5.5% in the irrigation amounts as a result of the implementation of this variable irrigation strategy when compared to a conventional and uniform prescription.
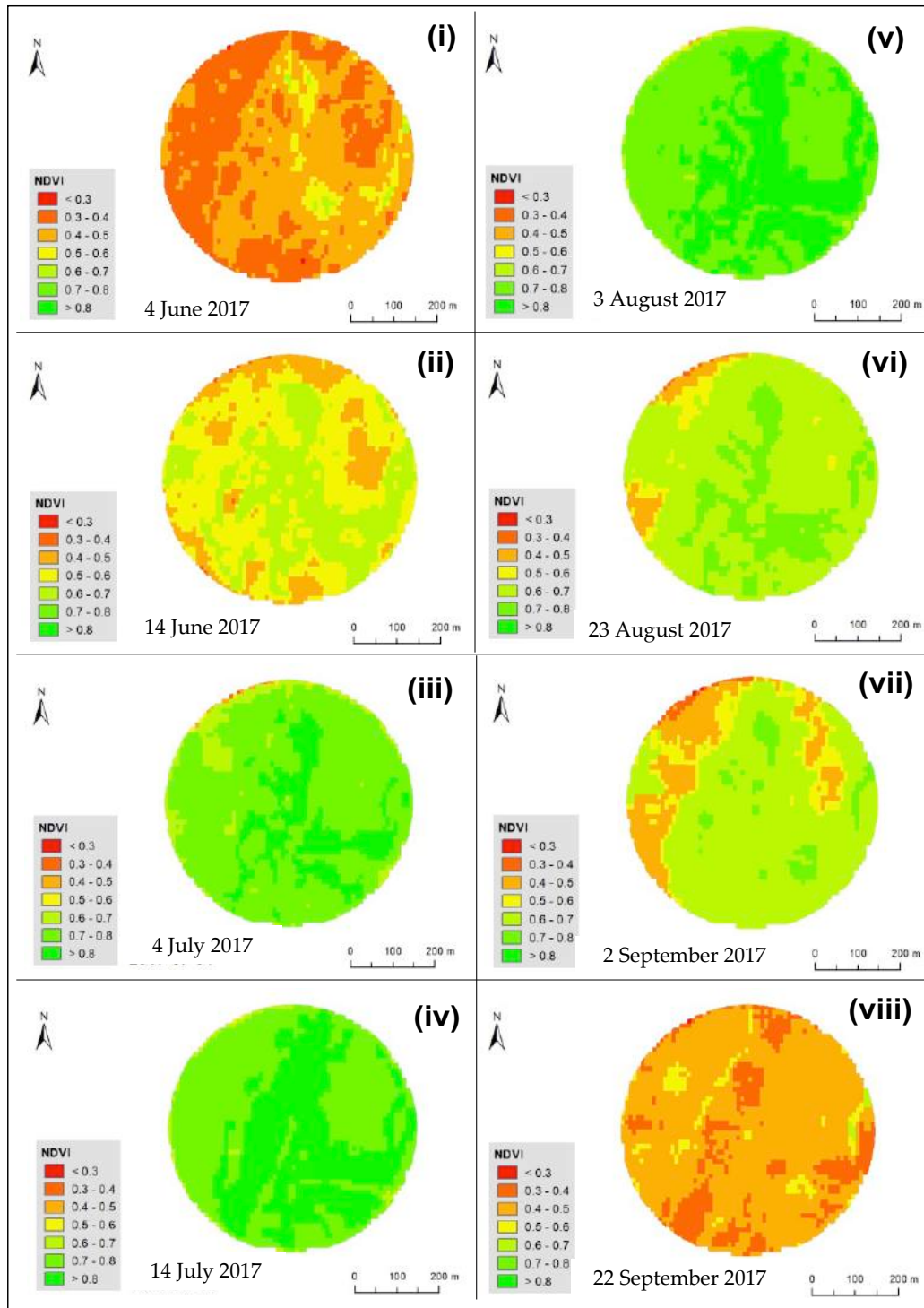
Figure 3. Normalized difference vegetation index (NDVI) maps of the "Eucalyptus" field in different dates (maps i to viii), between June and September 2017.
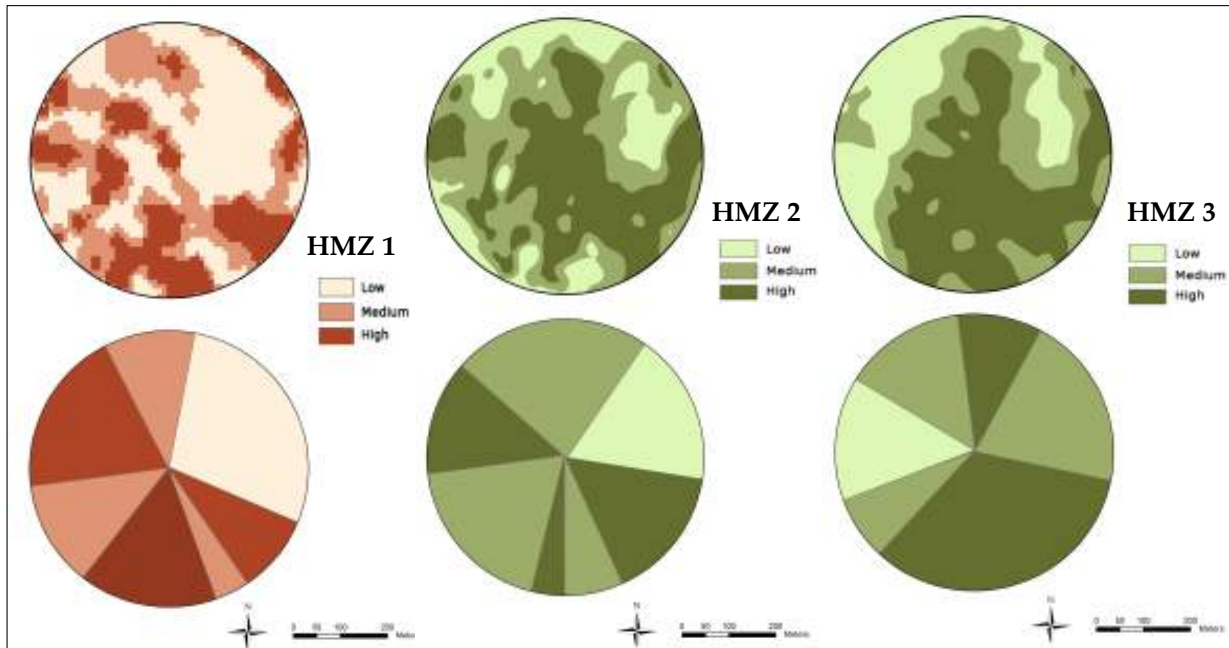
Figure 4. Homogeneous management zones (HMZ) maps 1, 2, and 3 (left) and the correspondent maps converted into the pie slice format (right).
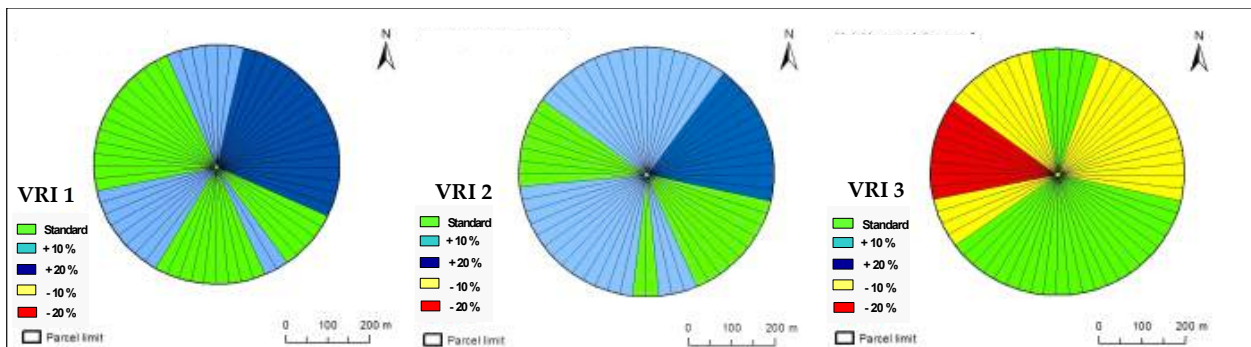
Figure 5. Variable rate irrigation (VRI) maps 1, 2, and 3 implemented in the "Eucalyptus" field between 14 June and 13 September 2017.

The evaluation of the impact of the variable irrigation strategy was also carried out in this first year in terms of crop productivity (total production and spatial variability). Figure 6 shows the corn yield map of the field in October 2017. In addition to the increase of 8% in the productivity (changed from $10,510 \pm 4689$ kg ha^{-1} in 2016 to $11,350 \pm 4097$ kg ha^{-1}), there was also a decrease in spatial variability (CV = 36.1% in 2017, against 44.6% in 2016).

There are usually three paths used to survey variability and define HMZ (Haghverdi et al., 2015; O'Shaughnessy et al., 2019): (i) soil EC$_a$ measurements with proximal sensors (the starting point for variability), (ii) monitoring of vegetation indices based on satellite images, mainly NDVI (the dynamic crop evolution), and (iii) yield data (the final objective of the production process). However, despite similarities between the zones delineated by these three sources (as shown in this study), yield data has less potential because of its inconsistency, since yield is affected by the complex interaction of different factors, which is contrary to what happens with soil EC$_a$ (Corwin et al., 2010), which shows a certain degree of temporal stability (Heil and Schmidhalter, 2017). Additionally, Moral et al. (2010) found that the temporal stability of soil EC$_a$ makes it a better proximal attribute for high resolution zone delineation. This study confirmed similar spatial patterns of EC$_a$ maps in both soil layers (0–0.5 m and 0–1.0 m depth), although with higher soil EC$_a$ values at greater depth (20.98 ± 23.08 mS m^{-1} at 1.0 m depth and 12.71 ± 8.12 mS m^{-1} at 0.5 m), which is due to the cumulative influence of the EC$_a$ measured by the sensor (Serrano et al., 2017). It is evident that the 1.0–m depth

map allows a better stratification of the classes of EC$_a$ and, therefore, a greater potential for the definition of management zones, which is in line with other works (Haghverdi et al., 2015)
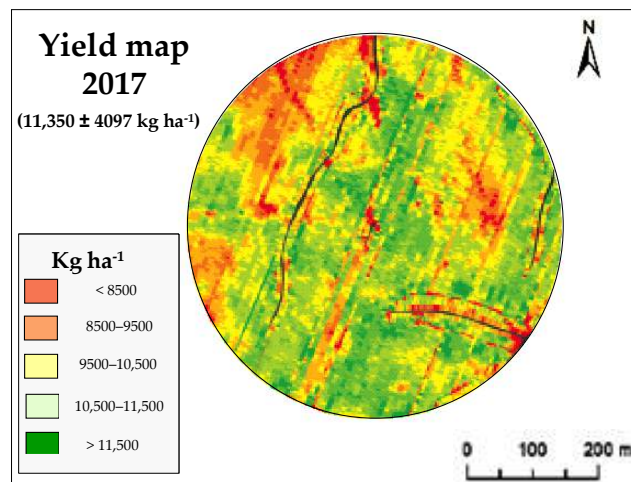
Figure 6. Corn yield map of the "Eucalyptus" field in October 2017.

The results of this first year showed a positive trend in achieving the initial goal established by the farmer, reducing the spatial variability of corn productivity in this field (CV = 36.1% in 2017, against 44.6% in 2016). In addition, this field registered an increase of 8% in the corn productivity at the expense of an increase of 5.5% in the irrigation water amounts when compared to conventional and uniform prescription.

Although these results can be viewed in the perspective of the natural inter–annual variability of crop yield as a result of climatic trends, the data clearly indicate an improvement in the irrigation water use efficiency (IWUE), which relates crop yield produced per unit of water supplied (Chai et al., 2016), and could lead the farmer to readjust his objectives. As part of the precision agriculture (PA) concept, the objectives are revaluated after the end of each crop cycle, and, thus, the farmer can focus on identifying possible structural causes (for example, soil compaction or poor drainage) that help to explain the historically marginal yields in some areas, where the amount of irrigation can be reduced (O'Shaughnessy et al., 2019) instead of increasing the amounts of irrigation water to compensate its lower productive potential. Within the scope of the PA, an approach that addresses the effect of the VRI strategy on crop productivity and the amount of irrigation water used, but also accounts for the costs associated with the technologies and technical support, will be important. For example, in this specific case, the initial cost of "speed control" VRI technology (approximately 3000 €, which can be added to existing moving irrigation systems) must be considered. Additionally, in the first year, the cost of soil EC$_a$ survey (approximately 40 € per ha) should be considered. Annually, a budget of around 1500 € should be considered for the services needed to obtain, process, and integrate all the information as well as capture the satellite images, obtain the respective indices (NDVI), and define and present the VRI maps.

4. Conclusions

The objective of this case study was to evaluate tools for delineating dynamic HMZ and defining dynamic VRI maps needed to automate center pivot travel speed control in corn. The results of this first year showed a positive trend in achieving the initial goal established by the farmer, reducing the spatial variability and increasing corn productivity in this field, at the expense of a light increase in irrigation water amounts. EC$_a$ and topographical information obtained by on–the–go sensors and NDVI obtained by remote sensing proved to be effective in the definition of dynamic management zones and appealing because of the ease with which they can be collected at a field–scale. A contribution to more reliable HMZ may result from the application of the PA concept with the integration of yield maps of several years, averaged to reduce their temporal instability. This relatively simple approach is fairly inexpensive for the farmer and can be implemented on a large scale, which represents an important and sustainable contribution to improved water

use efficiency in Mediterranean agriculture, especially in the current scenario of global warming and reduction of the available water for agriculture.

References

Baptista, V.B.D.S., Córcoles, J.I., Colombo, A., Moreno, M.A. 2019. Feasibility of the use of variable speed drives in center pivot systems installed in plots with variable topography. Water, 11, 2192. doi:10.3390/w11102192.

Chai, Q., Gan, Y., Zhao, C., Xu, H.L.,Waskom, R.M., Niu, Y., Siddique, K.H.M. 2016. Regulated deficit irrigation for crop production under drought stress. A review. Agronomy for Sustainable Development. 36, 3. doi:10.1007/s13593–015–0338–6.

Corwin, D.L., Lesch, S.M., Segal, E., Skaggs, T.H., Bradford, S.A. 2010. Comparison of sampling strategies for characterizing spatial variability with apparent soil electrical conductivity directed soil sampling. Journal of Environmental and Engineering Geophysics. 15, 147–162. doi:10.2113/jeeg15.3.147.

Evans, R.G., LaRue, J., Stone, K.C., King, B.A. 2013. Adoption of site–specific variable rate sprinkler irrigation systems. Irrigation Science. 31, 871–887. doi:10.1007/s00271–012–0365–x.

FAO, 2006. *World Reference Base for Soil Resources*; Food and Agriculture Organization of the United Nations, World Soil Resources Reports No. 103; IUSS Working Group WRB: Rome, Italy.

Fridgen, J.J., Kitchen, N.R., Sudduth, K.A., Drummond, S.T., Wiebold, W.J., Fraisse, C.W. 2004. Management zone analyst (MZA): Software for subfield management zone delineation. Agronomy Journal. 96, 100–108.

Haghverdi, A., Leib, B.G., Washington–Allen, R.A., Ayers, P.D., Buschermohle, M.J. 2015. Perspectives on delineating management zones for variable rate irrigation. Computers and Electronics in Agriculture. 117, 154–167. doi:10.1016/j.compag.2015.06.019.

Heil, K., Schmidhalter, U. 2017. Improved evaluation of field experiments by accounting for inherent soil variability. European Journal of Agronomy. 89, 1–15. doi:10.1016/j.eja.2017.05.004.

Longchamps, L., Khosla, R., Reich, R., Gui, D. 2015. Spatial and temporal variability of soil water content in leveled fields. Soil Science Society of America Journal. 79, 1446–1454. doi:10.2136/sssaj2015.03.0098.

Moral, F.J., Terrón, J., Da Silva, J.M. 2010. Delineation of management zones using mobile measurements of soil apparent electrical conductivity and multivariate geostatistical techniques. Soil Tillage Research. 106, 335–343. doi:10.1016/j.still.2009.12.002.

Ortuani, B., Facchi, A., Mayer, A., Bianchi, D., Bianchi, A., Brancadoro, L. 2019. Assessing the effectiveness of variable–rate drip irrigation on water use efficiency in a vineyard in northern Italy. Water. 11, 1964. doi:10.3390/w11101964.

O'Shaughnessy, S.A., Evett, S.R., Colaizzi, P.D., Andrade, M.A., Marek, T.H., Heeren, D.M., Lamm, F.R., LaRue, J.L. 2019. Identifying advantages and disadvantages of variable rate irrigation: An updated review. Applied Engineering in Agriculture. 35, 837–852. doi:10.13031/aea.13128.

Serrano, J.M., Shahidian, S., Da Silva, J.R.M. 2017. Spatial variability and temporal stability of apparent soil electrical conductivity in a Mediterranean pasture. Precision Agriculture. 18, 245–263. doi:10.1007/s11119–016–9460–y.

Torres–Sánchez, R., Navarro–Hellin, H., Guillamon–Frutos, A., San–Segundo, R., Ruiz–Abellón, M.D.C., Domingo, R. 2020. A decision support system for irrigation management: analysis and implementation of different learning techniques. Water. 12, 548. doi:10.3390/w12020548.

Yari, A., Madramootoo, C.A., Woods, S.A., Adamchuk, V. 2017. Performance evaluation of constant versus variable rate irrigation. Irrigation Drainage. 66, 501–509. doi:10.1002/ird.2131.

Zhang, X., Chen, S., Sun, H., Wang, Y., Shao, L. 2010. Water use efficiency and associated traits in winter wheat cultivars in the north China plain. Agricultural Water Management. 97, 1117–1125.

Zhao, W., Li, J., Yang, R. 2017. Crop yield and water productivity responses in management zones for variable–rate irrigation based on available soil water holding capacity. Transactions of the ASABE. 60, 1659–1667. doi:10.13031/trans.12340.

Determining Critical Points in Order to Reduce Fruit Damages in Fresh Stone Fruit Packing-lines

Rubén Mahiques[a], Coral Ortiz[a]*, Antonio Torregrosa[a]

[a]Departamento de Ingeniería Rural y Agroalimentaria, Universitat Politècnica de València, Camino de Vera s/n, 46022, Valencia
*Corresponding author: Email cortiz@dmta.upv.es

Abstract

Stone fruits are very sensitive and delicate and their evolution is very fast during the last stages of ripening. In certain areas of Valencia region (Spain) citrus packing lines are used during the non-citrus season to process stone fruits. Differences of fruit shape and size, texture, ripening procedure and damage susceptibility between stone fruit and citrus contribute to result in serious product damage after fresh stone fruit postharvest handling. The objective of the present research study was to determine and evaluate the critical points in a citrus packing line used to process stone fruit and propose modifications in order to reduce fruit damages.

A typical citrus packing line in Valencia region (Spain) used to process stone fruit was evaluated using an instrumented sphere. The main aggressive transfer points were: the manual dumping to the elevation conveyor belt, the transfer point between the manual sorting table and the third conveyor belt and the impact to the packing line when it is without fruit, all of them with maximum impacts higher than 95 G, and average impact values higher than 50 G. Several solutions and modifications in the citrus packing line were proposed and analysed to reduce the aggressiveness of the process. In all the transfer points the dropping height should be reduced or the transfer points padded with shock absorbing materials. Besides the fruit speed should be reduced before the transfer point adding deceleration brushes.

Keywords: stone fruit, fruit packing line, damage, bruise, transfer point

1. Introduction

Fruit damage during handling can cause considerable postharvest and economic losses, reduce product quality and result in serious food safety concerns (Hussein et al., 2018).

Mechanical damage to fruits could be produced during harvesting, handling and transport causing fruit bruising (Ahmadi et al., 2010; Tabatabaekoloor, 2013).

Stone fruits are climacteric fruits, sensitive and delicate and their evolution is very fast during the last stages of ripening (Amorós et al., 1989). Due to the high damage susceptibility, stone fruits are usually picked before reaching the highest organoleptic qualities (Martinez-Romero et al., 2002).

In order to evaluate the mechanical damage during handling process, different wireless sensors and electronic spheres have been used to determine the aggressiveness of the fruit postharvest packing lines (García-Ramos et al., 2004; Roa et al., 2015; Xu et al., 2015; Manetto et al., 2017).

The physical and mechanical properties of stone fruit are crucial for the design of the postharvest handling equipment (Hazbavi, 2013). Since currently used systems are designed without taking fruit physical and mechanical properties into consideration, the resulting designs lead to inadequate applications that produce fruit damage and product loss.

In Valencia region (Spain) citrus packing lines are used during the non-citrus season to process other stone fruits. Differences of fruit shape, size, physical and mechanical properties between stone fruit and citrus contribute to result in serious product damage after fresh stone fruit postharvest handling. The objective of the present study was to determine and evaluate the critical points in a citrus packing line used to process stone fruit and propose modifications in order to reduce fruit damages.

2. Materials and Methods

A typical citrus packing line in Llutxent cooperative (Valencia, Spain) used to process stone fruit was evaluated using an instrumented sphere Tuberlog PTR 200 (http://martinlishman.com/tuberlog-electronic-potato/).

2.1. Instrumetal sphere

The instrumented sphere Tuberlog PTR 200 is an acceleration measurement device which records impact forces usually used during harvesting and processing of potatoes. The device locates damage and bruise-causing parts of machinery. It comprises a data logger embedded in a synthetic shape.

The device was placed into the fruit crate and was dumped with the fruit in the packing line.

2.2. Fruit packing line

The fruit packing lines studied is a typical citrus packing line that is adapted during the summer season to process stone fruits.

The main components are:
- Manual dumping
- First conveyor belt (elevation conveyor belt)
- Second conveyor belt (to the manual sorting table)
- Manual sorting table
- Third conveyor belt (conveyor belt to the singulator)
- Singulator
- Chain with plastics
- Electronic Sizer
- Fourth conveyor belt (to the packing tables)
- Manual packing tables

A Casio EX-F1 camera was used to record the images of the electronic sphere registering data from the packing line.

The registering process was carried out twelve times from the manual dumping to the manual packing table. Besides, twenty repetitions of the receiving in the packing table were registered.

3. Results and Discussion

In a first step, the videos were analysed identifying the transfer points, where the possible dangerous impact could be produced.

The identified transfer points were (Figure 1):
- Manual dumping - First conveyor belt (elevation conveyor belt)- O1
- First conveyor belt – Second conveyor belt (to manual sorting table)- O2
- Second conveyor belt (to manual sorting table)-Manual sorting table- O3
- Manual sorting table - Third conveyor belt (conveyor belt to the singulator)- O4
- Third conveyor belt (conveyor belt to the singulator) – Singulator-05
- Singulator – Bicone rollers-O6
- Bicone rollers - Conveyor belt to the packing tables (fourth conveyor belt)-O7
- Fourth conveyor belt (to the packing tables) - Packing table-O8
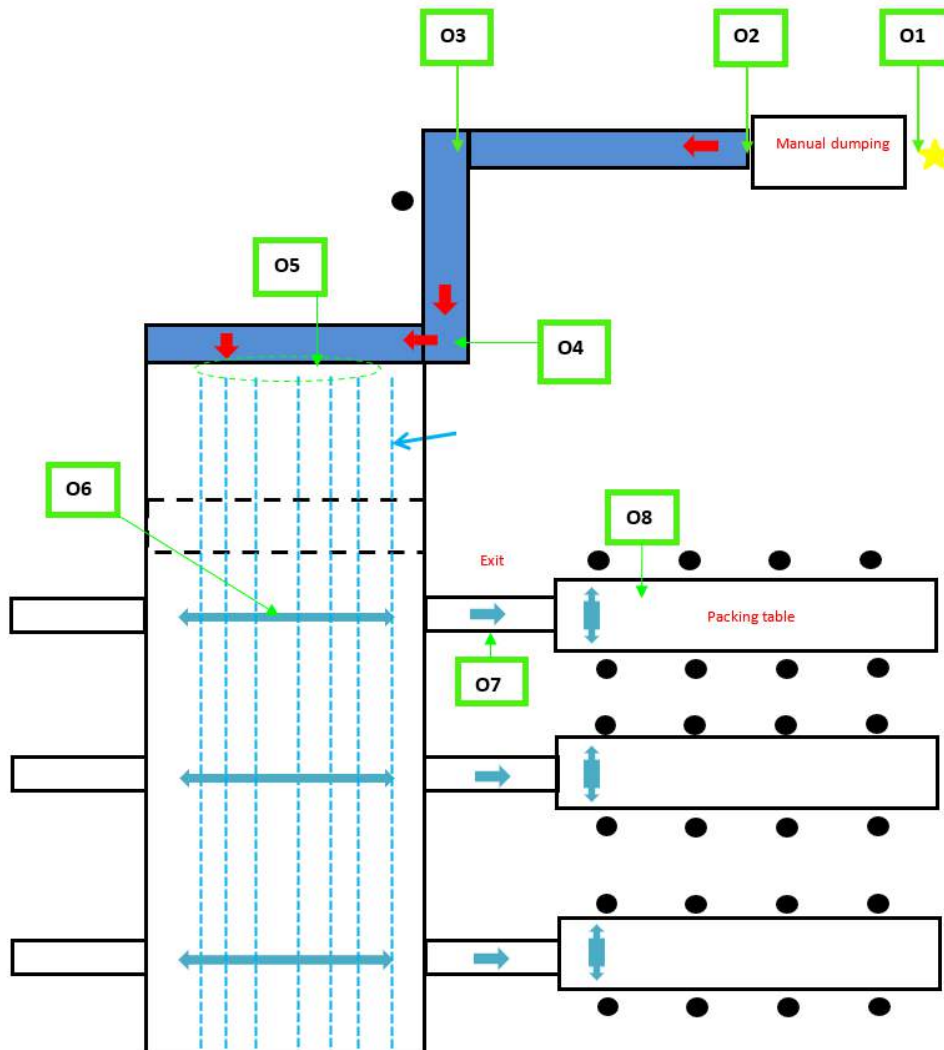
Figure 1. Transfer points of the studied packing line.

Description of the transfer points:

Manual dumping - First conveyor belt (elevation conveyor belt)- O1

In the manual dumping the operator feed the line overturning the 20 kg capacity plastic crate on an elevation conveyor belt, Figure 2. The dropping height ranges from a minimum of few cm to a maximum around 1 m when the operator places the crate on his shoulder before dropping the fruit. The drop is produced on the conveyor belt and on a metallic surface covered by a plastic canvas.
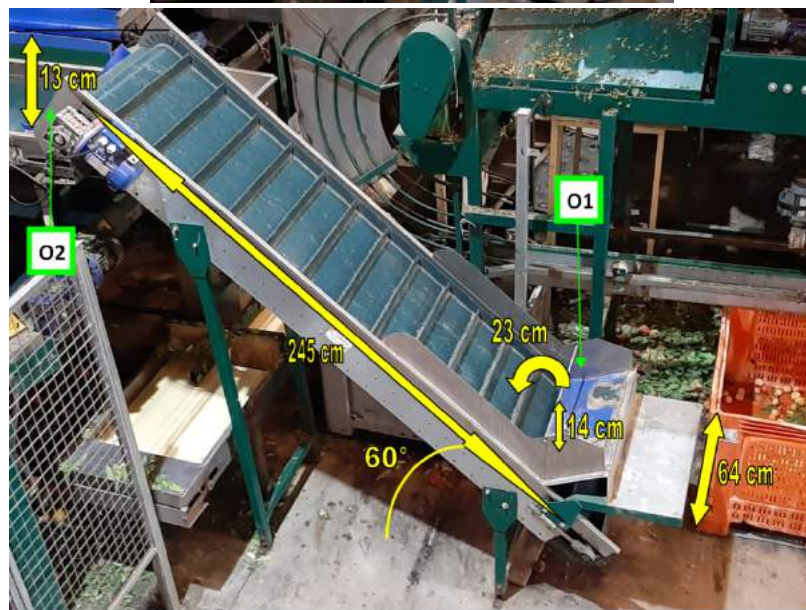
Figure 2. Transfer point O1: Manual dumping - First conveyor belt (elevation conveyor belt)

First conveyor belt – Second conveyor belt (to manual sorting table)-O2

From the elevation conveyor belt to the second conveyor belt there is a 0° horizontal plane transfer point with a 1:1 slope ramp, Figure 3.
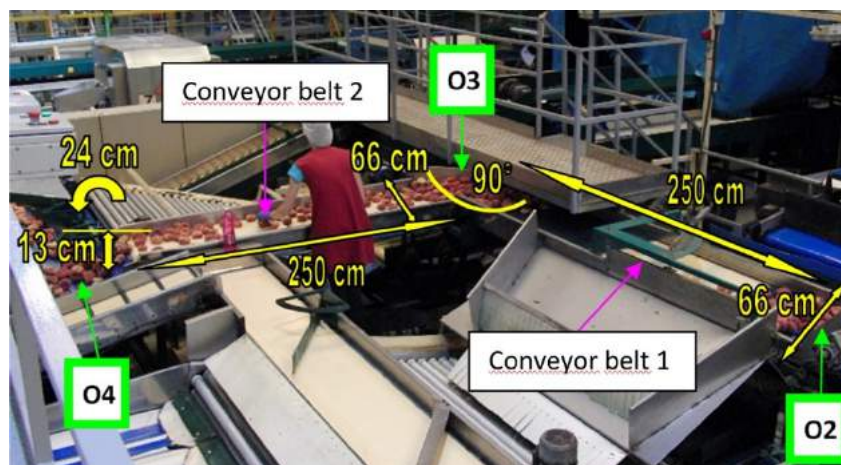
Figure 3. Transfer points O2, O3 and O4: First conveyor belt – Second conveyor belt (to manual sorting table); Second conveyor belt (to manual sorting table)-Manual sorting table; Manual sorting table - Third conveyor belt (conveyor belt to the singulator)- O4

Second conveyor belt -Manual sorting table, O3

From the second conveyor belt to the manual sorting table there is a 90° horizontal plane transfer point protected by a metallic surface, Figure 3.

Manual sorting table - Third conveyor belt (conveyor belt to the singulator)-O4

From the manual sorting table to the conveyor belt to the singulator there is a 90° horizontal plane transfer point with a 8 cm height, protected by a plastic canvas, Figure 3.

Third conveyor belt (conveyor belt to the singulator) – Singulator-O5

From the conveyor belt to the singulator there is a 90° transfer point with a 1:1 metallic ramp and a dropping height of 2 cm to 5 cm, Figure 4 A. The singulator has six "V" shape lines. Only three of the keel structures of the singulator are partly protected by a rubber material.
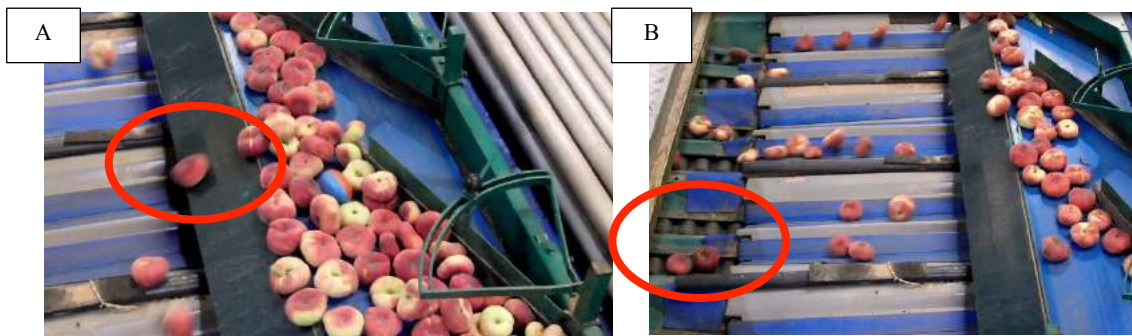
Figure 4. Transfer points: Third conveyor belt (conveyor belt to the singulator) – Singulator-O5 (4A) and Singulator – Bicone rollers-O6 (B)

Singulator – Bicone rollers-O6

From the singulator channels the fruit is directed to the bicone rollers that will carry them to the optical sizer, Figure 4B.

Bicone rollers - Conveyor belt to the packing tables-O7

The exit from the bicone rollers, according to the category assessed in the optical sizer, is a 90° transfer point with a dropping height of 10 cm protected by a tense canvas, Figure 5. The fruit is conducted to a conveyor belt.

Figure 5. Transfer point: Bicone roller - Conveyor belt to the packing tables-O7

Fourth conveyor belt - Packing table-O8

From the fourth conveyor belt to the packing table there is a 90° transfer point, Figure 6. The dropping is helped by a vertical sloping plane that directs the fruit to the sloping packing table. There is a first step in which the fruit impacts the plane and is forced to fall to the packing table, Figures 6 and 7. In a second step the fruit impacts the surface of the sloping packing table. Then, it is possible to have more impacts and a final rolling of the fruit. The level of the impact will depend on the amount of fruit in the packing table. The surface of the sloping packing table is covered with a foam material 2 mm thick and a canvas.

Figure 6: Transfer point: Fourth conveyor belt (to the packing tables) - Packing table

Step 0: movement on the conveyor belt	Step 1: hitting the vertical sloping plane	Step 2: directing to the packing table
Step 3: first impact to the packing table surface	Step 4: second impact to the packing table surface	Step 5: rolling on the packing table surface
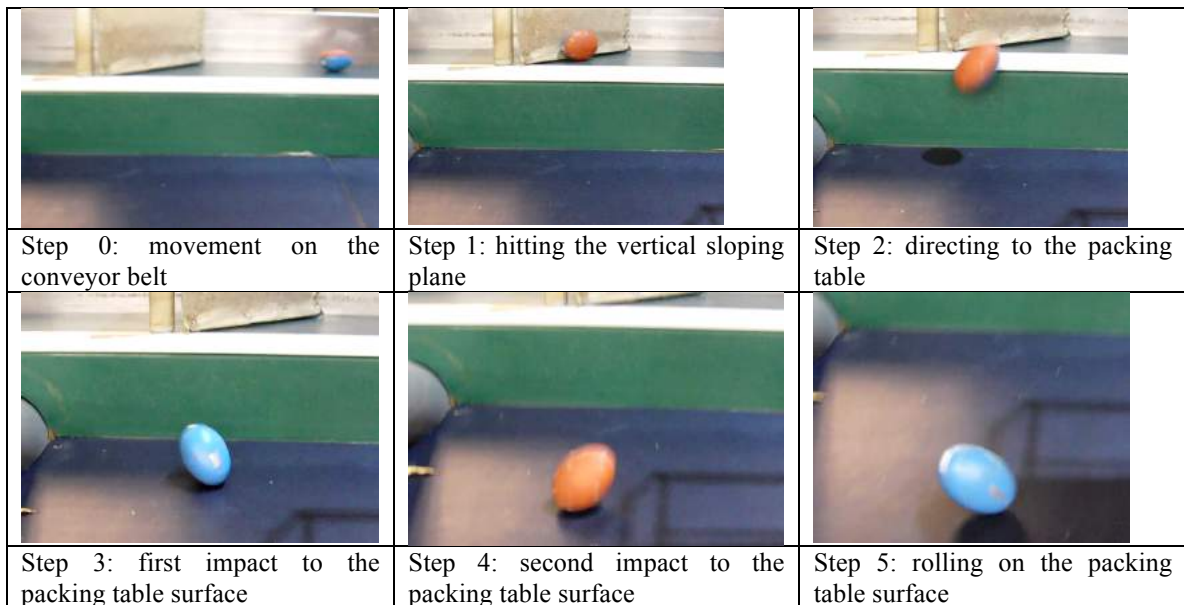
Figure 7: Dropping process from the conveyor belt to the packing table.

In Table 1 the main characteristics of the transfer points and the measured impact levels are shown.

Table 1. Main characteristics of the transfer points and the measured impact values.

Transfer point (from/ to)	Angle (°)	Height (cm)	Slope	Material	Protection	Average Impact (m.s^{-2})	Maximum Impact (m.s^{-2})
Manual dumping – 1st conveyor belt (O1)	0	5-100	-	Canvas Metallic	None	724.2	1319.1
1st conveyor belt – 2nd conveyor belt (O2)	0	10	1:01	Canvas	None	485.1	936.9
2nd conveyor belt – Sorting table (O3)	45	-	-	Canvas, Metallic	None	459.6	682.1
Sorting table – 3rd conveyor belt (O4)	90	8	-	Metallic	Plastic canvas	428.3	1210.3
3rd conveyor belt – Singulator (O5)	90	02-may	1:01	Metallic	Rubber	857.5	8403.5
Singulator – Bicone rollers	0	-	-	Plastic	None		
Bicone rollers – 4th conveyor belt	90	10	>1:1	Canvas	Tense canvas	372.4	3649.5
4th conveyor belt – Packing table (*)	90	60	1:01	Metallic	Foam, Plastic canvas	801.6	7856.1

(*) Considering the worst situation when the packing table is without fruit
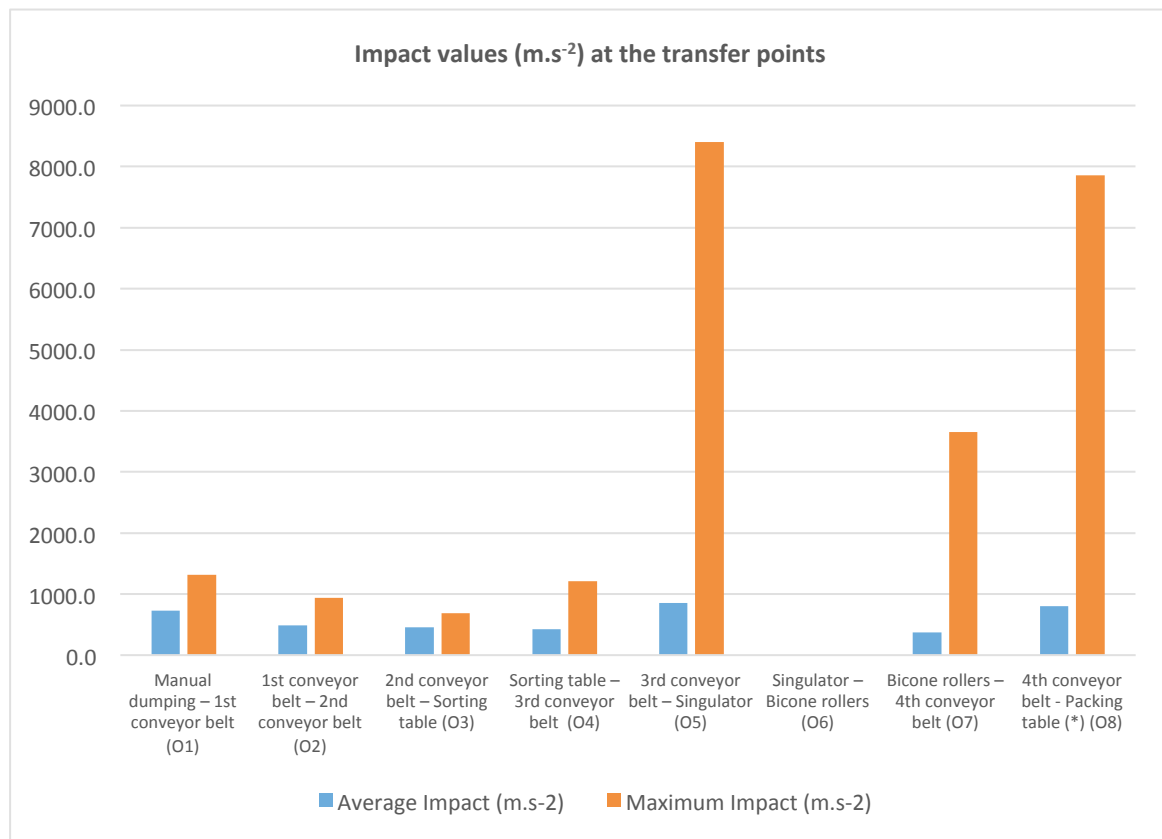
Figure 11. Maximum and average impacts (m.s^{-2}) of the transfer points.

The main aggressive transfer points were: the manual dumping to the elevation conveyor belt, the transfer point between the manual sorting table and the third conveyor belt and the impact to the packing line when it is without fruit, all of them with maximum impacts higher than 95 G, and average impact values higher than 50 G, Figure 11.

Proposals

1) Manual dumping – 1st conveyor belt

The dumping of the fruit overturning the plastic crate on the elevation conveyor belt is always a very aggressive point. And it is worst when the operator places the crate on his shoulder before dropping the fruit and the dropping height drastically increases. Besides, from the point of view of occupational prevention risk it is a very dangerous task for the operator, related to musculoskeletal disorders.

A convenient proposal will be to change the manual dumping by an automated dumper careful with the fruit to reduce impact bruising in the transfer system.

2) Manual sorting table – 3rd conveyor belt

From the manual sorting table to the conveyor belt to the singulator the transfer point is protected by a plastic canvas. The canvas does not reach the 3rd conveyor belt, leaving 4 cm without protection. A possible solution would be to use canvases to the 3rd conveyor belt with a final fringe part.

3) Third conveyor belt – Singulator

From the conveyor belt to the singulator there is a very aggressive transfer point. The metallic ramp could be protected with a shock absorbing foam material. Besides and more important, the keel structures of the "v" shape lines partly protected by rubber material should be totally and carefully protected with the rubber or with another shock absorbing material.

4) Fourth conveyor belt - Packing table

The dropping ramp to the packing table is only protected by a 2 mm foam material and a plastic canvas. A sheet of suitably thick material could be added to reduce the impact when the table is without fruit.

In all the transfer points the dropping height could be reduced or the transfer points padded with shock absorbing materials. Besides the fruit speed could be reduced before the transfer point adding deceleration brushes.

4. Conclusions

The aggressiveness of a citrus packing line adapted during the non-citrus season to process stone fruit has been evaluated using an electronic sphere.

All the transfer points have been studied, being the manual dumping, the dropping of the manual sorting table, the transfer point to the singulator and the dropping to the packing table the more aggressive points. Different solutions reducing dropping height and speed, and padding the receiving surfaces with shock absorbing materials have been proposed.

In order to reduce the bruises caused in stone fruits when handled using citrus packing lines, an important adaptation of the line should be addressed before initializing the process.

Acknowledgements

References

Ahmadi, E., Ghasemzadeh, H.R., Sadeghi, M., Moghadam, M., Zarifneshat, S., 2010. The effect of impact and fruit properties on the bruising peach. J. Food Eng. 97, 110–117. https://doi.org/10.1016/j.jfoodeng.2009.09.024

Amorós, A., Serrano, M., Riquelme, F., Romojaro, F. 1989. Importancia del etileno durante el desarrollo y maduración del albaricoque (Prunus armeniaca L. cv Búlida). Fruits 44, 171-175.

García-Ramos, F.J., Ortiz-Cañavate, J., Ruiz-Altisent, M. 2004. Evaluation and correction of the mechanical aggressiveness of commercial sizers used in stone fruit packing lines. Journal of Food Engineering 63(2), 171-176. https://doi.org/10.1016/S0260-8774(03)00297-8

Hazbavi, I. 2013. Determination of physical properties of apricot fruit and proper box height for storing and handling the apricot fruit. Agric. Eng. Int: CIGR Journal 15(4), 288-292

Hussein, Z., Fawole, O.A., Opara, U.L. 2018. Preharvest factors influencing bruise damage of fresh fruits – a review. Scientia Horticulturae 229, 45–58. https://doi.org/10.1016/j.scienta.2017.10.028

Manetto, G., Cerruto, E., Pascuzzi, S., Santoro, F. 2017. Improvements in Citrus Packing Lines to Reduce the Mechanical Damage to Fruit. Chemical Engineering Transactions, 58, 391- 396. https://doi.org/10.3303/CET1758066

Martínez-Romero, D., Serrano, M., Carbonell, A., Burgos, L., Riquelme, F., Valero, D. 2002. Effects of Postharvest Putrescine Treatment on Extending Shelf Life and Reducing Mechanical Damage in Apricot. Journal of Food Science 67(5),1706-1712. https://doi.org/10.1111/j.1365-2621.2002.tb08710.x

Roa, Y.H.H., Fruett, F., Ferreira M.D. 2013. Real time measurement system based on wireless instrumented sphere. Springerplus 2, 582. https://doi.org/10.1186/2193-1801-2-582

Roa, Y.H.H., Fruett, F., Antoniolli, L.R., Oliveira, T.C., Poletto, F.E.B., Ferreira M.D. 2015. Impact Measurement on Apple and Orange Packinghouses Using a Wireless Instrumented Sphere. Chemical Engineering Transactions 44, 97-102. https://doi.org/10.3303/CET1544017

Stropek, Z., Golacki, K. 2015. A new method for measuring impact related bruises in fruits. Postharvest Biology and Technology 110, 131-139. https://doi.org/10.1016/j.postharvbio.2015.07.005

Tabatabaekoloor, R., 2013. Engineering properties and bruise susceptibility of peach fruits (Prunus persica). Agric. Eng. Int.: CIGR J. 15, 244–252.

Xu, R., Takeda, F., Krewer, G., Li, c. 2015. Measure of mechanical impacts in commercial blueberry packing lines and potential damage to blueberry fruit. Postharvest Biology and Technology 110: 103-11. https://doi.org/10.1016/j.postharvbio.2015.07.013

Predicting the Evolution of Pasture Quality by NIRS: Perspectives for Real-Time Pasture and Grazing Management

João Serrano [a,*], Shakib Shahidian [a], Emanuel Carreira [a], Júlio Nogales-Bueno [a,b] , Ana Elisa Rato [a]

[a] MED- Mediterranean Institute for Agriculture, Environment and Development,Instituto de Investigação e Formação Avançada, Universidade de Évora, Pólo da Mitra, Ap. 94, Évora 7006-554, Portugal,

[b] Food Colour and Quality Laboratory, Área de Nutrición e Bromatologia, Faculdad de Farmácia, Universidad de Sevilla, 41012, Sevilla, Spain,

* Corresponding author. Email: jmrs@uevora.pt

Abstract

Pasture quality monitoring is a key element in the decision making process of the farm manager. Laboratory reference methods for assessing pasture quality parameters such as crude protein (CP) or neutral detergent fibre (NDF) require cutting, collection and analytical procedures involving technicians, time and reagents, making them laborious and expensive. The objective of this study was to evaluate the potential of near infrared reflectance spectroscopy (NIRS) combined with multivariate data analysis as a rapid method to predict and monitor the evolution of pasture quality parameters (CP, NDF and a pasture quality index, PQI=CP/NDF). During the 2018 and 2019 growing seasons a total of 398 composite pasture samples were collected from 9 biodiverse pastures, representing a wide range of botanical composition and phenological states. These samples were scanned with a FT-NIR spectrometer: 315 (collected in 2018) were used in the calibration phase and 83 (collected in 2019) were used during the validation phase. Calibration and validation models were developed and regression equations between predicted and laboratory reference values of CP, NDF and PQI were established. Were used as evaluation parameters the coefficient of determination (R^2), the residual predictive deviation (RPD) and the root mean square errors (RMSE). The best results obtained were: (i) for CP prediction model (R^2=0.844; RPD=4.0; RMSE=1.622); (ii) for NDF prediction model (R^2=0.826; RPD=2.4; RMSE=4.200); and (iii), for PQI prediction model (R^2=0.808; RPD=3.2; RMSE=0.066). The results show the practical interest of portable spectrometry, associated with GNSS, as expeditious tools for monitoring pasture quality. Good prospects and opportunities open up for technology-based service providers to develop remote sensing-based computer applications from satellite imagery that enable dynamic management of animal grazing.

Keywords: near infrared spectroscopy, crude protein, neutral detergent fibre, supplementation, decision making

1. Introduction

Montado is a highly complex agro-forestry-pastoral ecosystem due to the particular climate and soil conditions and the synergies between animals, trees and pasture. In addition, Mediterranean climate presents two very distinct dry and wet seasons accentuated by an increasing inter-annual irregularity (Serrano et al., 2018). Consequently, dryland pasture quality and productivity fluctuate greatly over time as a result of the seasonal distribution of rainfall (Efe Serrano, 2006). Understanding seasonal changes in pasture nutritive value can enhance ruminant production systems and management (Bell et al., 2018).

The value of pasture is a combination of not only pasture production but also its nutritional quality (Bell et al., 2018). Decisions on supplementation are based on the assessment of pasture quantity and quality. The quantification of pasture quality can be done by using measurable parameters. Among them, one must highlight the use of crude protein (CP) content and neutral detergent fiber (NDF) content (Serrano et al., 2018). The conventional method for assessing CP and NDF consists of collecting representative samples and carrying out laboratory analysis. This result in a lengthy and often expensive process, that is not practical for the busy farm manager (Lumbierres et al., 2017). Consequently, there is a demand for express procedures that can monitor pasture variables and provide the farmer with timely information.

In recent years, near-infrared spectroscopy (NIRS) technology, based on the absorption of electromagnetic spectrum (radiation at wavelengths between 780 and 2500 nm), has been used in several industries such as pharmaceutical, petrochemical, agricultural, and food processing (Teye et al., 2019). NIR spectroscopy requires little or no sample preparation (Teye et al., 2019), whereby offering a simple, rapid and reliable way to substitute some routine laboratory procedures, providing a fingerprint of the sample composition. Briefly, energy in the NIR range is directed at the sample and the reflected energy is measured by the instrument. This non-destructive technique requires, however, a calibration procedure using some primary reference methods. The combination of NIR spectroscopy and multivariate data analysis (chemometrics or computational chemistry) provides calibration models that correlate the spectral response of the sample with its compositional profile (Musingarabwi et al., 2016; Véstia et al., 2019). It is also common

knowledge, that a NIR spectra obtained from forage samples has absorption bands that are correlated with specific compounds.

Although the NIR spectroscopy technique has been widely used in Europe to measure feed quality and to predict the nutritional value of forage (Smith and Flinn, 1991), few studies can be found related to its application in dryland biodiverse pastures of Mediterranean region, which highlights the interest of this work.

The purpose of this study was to evaluate NIRS technological approach combined with multivariate data analysis for estimating and monitoring the evolution of the quality parameters in Mediterranean pastures during the 2018 and 2019 growing seasons.

2. Materials and Methods

This work frames the results of several projects conducted by this research team to monitor the pasture in the Montado ecosystem in nine experimental fields in Portugal (Figure 1). These are typical biodiverse dryland pastures which usually grow under a low density plantation of Holm oak or Cork oak, and are used mainly for grazing by sheep or cattle in a rotational or permanent basis.
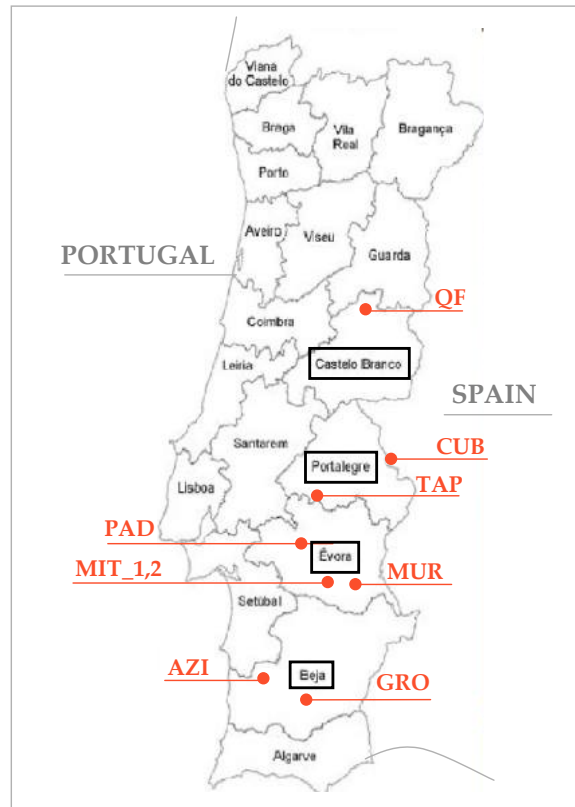
Figure 1. Location of the experimental fields in Portugal.

2.1. Pasture sample collection and chemical processing

Three hundred and ninety eight composite pasture samples were collected between February 2018 and February 2019 in nine different fields. The sampling process consisted of defining, in each point, a 0.5 m × 0.5 m area (through a metal quadrat) and cutting the pasture at 5-10 mm above ground level and preserving in numbered plastic bags. Each composite sample resulted from three representative sub-samples. Once in the laboratory, the pasture sample was weighed to establish total biomass, dried in an oven 72 h at 65 ∘C and weighed again to establish PMC (pasture moisture content, in %). Next, these samples were ground using a Perten instruments mill equipped with 1 mm sieve. CP and NDF were analysed according to standard methods and expressed in percentage on a dry weight basis (AOAC, 2005), constituting the CP and NDF reference values: (i) nitrogen content was analyzed by Kjeldhal, a colorimetric determination in an autoanalyzer Bran + Luebbe with a factor of conversion to CP of 6.25 (method no. G-188-97 Rev 2,

Bran + Luebbe, Analyser Division, Norderstedt, Germany), (ii) the NDF content was analysed according to Goering and Van Soest (1970) method in a Fiberted digester (Foss Tecator AB, Sweden). The pasture quality index (PQI) was then calculated based on the ratio of these two parameters (CP/NDF).

2.2. Sample spectra acquisition and processing

Spectroscopic measurements were made in all samples using a FT-NIR spectrometer (MPA, Opus Bruker, Germany). Pasture ground samples were placed on integrating sphere and spectra was collected in diffuse reflectance mode at room temperature of 20 ∘C, in a small circular cup of 20 mm diameter. Reflectance data (R) were measured as log 1/R (absorbance data) at 1 nm interval and NIR spectra data were obtained. Five spectra were collected from each sample and an average spectrum was used for further mathematical processing and chemometrics analysis. Spectra data were obtained in the entire near infrared region of 12498.66 – 3594.93 cm^{-1} after a total of 32 scans with an average resolution of 16 cm^{-1} following a modification of the method described by Milinovic et al. (2020). Each spectrum was constituted of 1154 points and the background signal was corrected before each set of 20 samples.

2.3. Statistical analysis

The Opus v. 7.5 software (Bruker Optik GmbH, Germany) was employed for spectral data collection and FT-NIR spectra were exported to the Unscrambler software (version 10.5.1, Camo, ASA, Oslo, Norway) for chemometrics analysis, calibration and external validation models were obtained. Prediction models were developed using "Partial Least Square Regression" (PLSR) algorithm, considering an independent validation sample set for the chemometrics analysis (Wold et al., 2001). In order to obtain the best predictive model, for PLSR, samples were split in two sets: a training set (calibration) with 79% of the samples (315 samples of six fields, collected between February and December 2018, day of the year, DOY 39-135) and a test set, with the rest of the samples (83 samples of eight fields collected between January and February 2019, DOY 10-50), used as an external and independent validation set of the NIRS calibration models.

To find the most accurate model to quantify CP, NDF and PQI in pastures, the calibration process was performed in the raw spectra data and after the application of some mathematical algorithms to remove any irrelevant information. Some pre-processing techniques, like standard normal variate (SNV), normalization and normalization followed by SNV (Normalization+SNV) were applied to raw spectra and the best prediction model was selected. Calibration and validation models were developed based on principal components analysis. The quantitative measure for the predictive accuracy from each model was evaluated using coefficient of determination (R^2, an excellent indicator of the accuracy and robustness of model), root mean square errors (RMSE) for calibration and external validation data sets, and the residual predictive deviation (RPD, which corresponds to the ratio between standard deviation (SD) of the results obtained by reference method and the corrected mean error of the prediction of the validation (SEP bias). The value of RPD is usually used as an indicator of the quality of calibration model. The values of RPD higher than 2, 3 or 5 are recommended, respectively, for screening purposes, prediction or quality control (Murray, 1993; Versari et al., 2014).

3. Results

3.1. Pasture moisture content, crude protein and fiber reference values

Table 1 shows PMC, CP and NDF values of pasture samples at each location and each sampling date, determined with the reference method and used in the calibration and external validation models. The first requirement to obtain a good calibration model is to have a wide variation of the chemical composition of the set. The average values of these parameters (PMC between 62.5-89.1%, CP between 10.4-24.3%, NDF between 29.4-60.2%) are characteristic for dryland pastures during the growing season (autumn, winter and spring). The variation ranges of these parameters show, on the other hand, that the samples used in this study are representative of the inherent variability of biodiverse pastures of different fields in different phases of the vegetative cycle.

3.2. Statistics for calibration and external validation models

Table 2 shows statistics for calibration and external validation of prediction models developed using PLSR to correlate NIRS absorbance spectra with the invasive quality measurements (CP, NDF and PQI). The number of latent variables (LV), or components, employed to build the calibration models corresponds to the first minimum value of the predicted residual error sum of squares and the incorporation of new LV does not explain any further variation and may contribute to over-fitted models (Wold et al., 2001). This table indicates the prediction capability of the PLS regression to quantify pasture parameters using the raw spectra and several spectral pre-treatments. Four regression models were developed using the listed mathematical procedure (raw spectra, normalization, SNV and normalization + SNV).

Table 1. Pasture moisture content (PMC), crude protein (CP) and fibre (NDF) reference values of calibration phase (13 tests, 315 samples collected between February and December 2018) and external validation phase (8 tests, 83 samples collected between January and February 2019).

PHASE (field)	DOY (year)	n	PMC (%) Mean±SD	Range	CP (%) Mean±SD	Range	NDF (%) Mean±SD	Range
CAL.	(2018)							
MIT_1	39	24	77.5±7.8	55.6-86.1	18.7±4.9	8.7-25.3	34.3±11.9	18.6-58.9
	66	24	82.2±5.2	66.7-88.9	18.3±4.7	8.3-27.0	36.4±10.4	17.4-52.6
	99	24	84.6±2.4	79.6-88.6	13.2±3.7	8.3-25.5	40.3±7.1	31.3-52.6
	122	24	82.7±2.8	73.3-87.1	15.2±3.2	10.2-24.1	46.8±7.1	33.0-60.3
	155	24	68.5±5.7	54.2-77.8	10.5±2.4	7.3-15.9	60.2±3.4	51.7-66.4
	266	6	89.1±5.0	85.9-93.9	20.5±1.0	19.3-21.8	58.8±3.0	53.0-61.3
	295	35	86.2±2.7	77.8-90.8	24.3±8.8	13.4-52.3	50.5±7.0	28.5-64.5
	310	35	79.0±6.0	58.5-87.8	16.8±5.1	7.7-31.6	51.8±10.1	28.9-71.1
	345	35	82.5±5.6	66.7-88.7	18.4±5.2	13.9-30.0	47.7±8.1	34.2-62.1
MIT_2	130	24	83.7±2.7	77.9-87.1	12.1±1.9	8.9-15.5	51.4±3.6	45.7-58.0
	135	12	83.9±2.5	79.1-86.9	11.5±1.6	9.6-14.9	50.1±4.1	43.2-57.4
TAP	130	24	80.4±3.3	72.9-83.4	10.4±1.7	7.7-14.0	49.0±6.7	41.1-66.1
QF	135	24	72.6±3.7	65.8-77.8	12.8±3.4	7.3-19.1	46.7±7.1	35.1-58.3
VAL.	(2019)							
CUB	10	12	82.2±2.8	77.8-86.5	20.9±4.7	15.3-28.3	29.4±5.4	17.7-37.4
AZI	25	12	71.0±6.5	55.3-79.6	13.0±2.2	10.0-18.9	53.1±5.2	45.8-65.8
GRO	25	12	62.5±6.2	50.0-70.2	11.9±1.1	10.1-13.3	59.9±3.0	55.7-64.2
MUR	45	15	79.7±3.1	72.9-85.3	11.9±2.3	8.8-17.5	44.3±4.3	37.6-53.0
MIT_2	45	8	82.4±2.6	80.2-86.8	17.0±3.8	12.9-24.6	39.6±5.6	30.7-44.9
PAD	55	8	72.8±4.6	63.9-80.0	13.9±5.5	8.4-22.4	52.1±8.8	35.6-60.4
TAP	50	8	75.7±4.9	68.3-81.7	10.7±2.0	7.1-13.5	52.2±5.1	41.5-59.0
QF	50	8	72.8±8.8	57.9-83.3	12.4±3.0	9.1-16.5	48.2±12.6	32.4-67.3

CAL.- Calibration phase, VAL.- Validation phase, DOY- Day of the year , SD- Standard deviation, PMC- Pasture moisture content, CP- Crude protein, NDF- Neutral detergent fibre,

Table 2. Statistics for calibration and external validation models for crude protein (CP), neutral detergent fibre (NDF and pasture quality index (PQI)) using near-infrared spectroscopy (NIRS) spectra and partial least squares regression (PLSR) algorithm (*selected pre-treatment).

Spectral pre-processing	LV	Calibration R^2	RMSE	External validation R^2	RMSE	Bias	RPD
CP							
Raw spectra*	5	0.874	1.882	0.844	1.622	0.057	4.0
SNV	4	0.866	1.894	0.653	2.473	-0.877	3.0
Normalization	4	0.837	1.973	0.817	1.978	0.586	3.4
Normalization+ SNV	5	0.902	1.632	0.753	2.160	-0.421	3.1
NDF							
Raw spectra	7	0.618	6.261	0.607	6.979	4.453	1.9
SNV	7	0.834	4.061	0.802	4.868	0.426	2.1
Normalization	7	0.807	4.446	0.818	4.742	2.015	2.4
Normalization + SNV*	7	0.828	4.163	0.826	4.200	0.701	2.4
PQI							
Raw spectra*	3	0.791	0.071	0.808	0.066	0.009	3.2
SNV	7	0.829	0.079	0.768	0.079	-0.010	2.6
Normalization	7	0.746	0.100	0.747	0.120	-0.024	1.7
Normalization + SNV	7	0.830	0.078	0.736	0.083	-0.015	2.5

LV- Latent variables, SNV- Standard normal variate, R^2- Coefficient of determination, RMSE- Root mean square error, RPD- Residual predictive deviation,

Figure 2 shows measured vs. predicted values for CP, NDF and PQI, in calibration and validation phases. To illustrate the CP, NDF and PQI models robustness, predicted values were plotted against reference values of the validation set. Calibration curves indicate the range within each studied parameter and also show that the quality of the fit differs among parameters. Differences among parameters in prediction accuracy are due to a variety of factors, such as the presence of volatile components which will interfere with the reference determinations (Corson et al., 1999). In this study, with the aim of testing the prediction capability of NIRS and PLSR methodology, a set of samples collected in 2018 was used as calibration and other, external set, collected in 2019, was used as validation set. It is visible in Figure 2 that, despite all, the range of the calibration and validation sets is similar for all parameters which contributes to a good representativeness of the whole group of samples.

4. Discussion

Choosing a proper wavenumber range is an essential pre-processing step to find the most representative wavelengths and eliminate uninformative spectra regions. Considering that the main goals of this study was to obtain predictive models to quantify CP and NDF, and indirectly, pasture quality (PQI), the pasture raw spectra region selected in this study was defined as that within the wavenumber region from 4000 to 9000 cm^{-1}. Actually, many authors refer that the diffuse reflection from this region carries information associated with organic material and structural fibres, typical of a NIRS spectra (Musingarabwi et al., 2016; Smith and Flinn, 1991). Considering the selected wavenumber range used in the NDF prediction model development (4003-5600 and 7050-7300 cm^{-1}) also Givens and Deaville (1999) found two regions around 6066-5988 cm^{-1} and 4424-4385 cm^{-1} that were the most important regions associated with the presence of lignin and cellulose.

On the other hand, Bagchi et al. (2016) found the region around 6798-6535 cm^{-1} corresponded to the absorbance band of protein in molecules. Also in CP calibration model it was observed in this study that the spectra within 4003-7800 cm^{-1} were the most important regions that contribute to the performance of the models. These results indicated that aforementioned wavenumbers may be play important roles in modeling protein content in pasture samples.

Considering that an accurate model should have a high RPD, a high R^2, a low RMSE, a low average difference between predicted and actual values (Bias; Donis-González et al., 2020), and a small difference between RMSE from calibration and external validation models (Aleixandre-Tudo et al., 2018), evaluating all pre-processing methods used to evaluate CP, NDF and PQI in pasture samples, the best results were obtained using:

(i)   The "raw spectra" procedure for CP prediction model, what is justified by the highest RPD (4.0) and R^2 (0.844) and lowest RMSE (1.622) and bias (0.057) of the external validation model (Table 2). Also Garcia and Cozzolino (2006) found similar R^2 values for CP quantification, denoting the high capacity of NIRS to predict this parameter in a wide range of forages and pastures. The RPD greater than 3 is an indicator of good quality of calibration model for prediction of CP (Murray, 1993; Versari et al., 2014).

(ii)   The "normalization + SNV" procedure for NDF prediction model, what is justified by the highest RPD (2.4) and R^2 (0.826) and lowest RMSE (4.200) of the external validation model (Table 2). Successful calibrations have also been made for the prediction of NDF with similar predictive accuracy and using the same spectral region however in other plant species (grasses, cereal, straws) (Givens and Deaville, 1999). The lower calibration accuracy in NDF models, relatively to CP models, might reflect some variability on the reference method due to high starch content on the forage and pasture samples (Garcia and Cozzolina, 2006), once the fibre is a more complex component of forages that protein (Shenk and Werterhaus, 1993). The RPD greater than 2 is an indicator of calibration model for screening purposes of NDF (Murray, 1993; Versari et al., 2014), which suggests that more work needs to be done to build a more robust model.

(iii)   The "raw spectra" procedure for PQI prediction model, what is justified by the highest RPD (3.2) and R^2 (0.808) and lowest RMSE (0.066) and bias (0.009) of the external validation model (Table 2). Given that this parameter is a ratio between the previous ones (CP/NDF), this intermediate behaviour would be expected. This too calibration model, with a RPD greater than 3, like CP, can be used as routine analysis in the prediction of PQI (Batten, 1998; Murray, 1993; Versari et al., 2014).
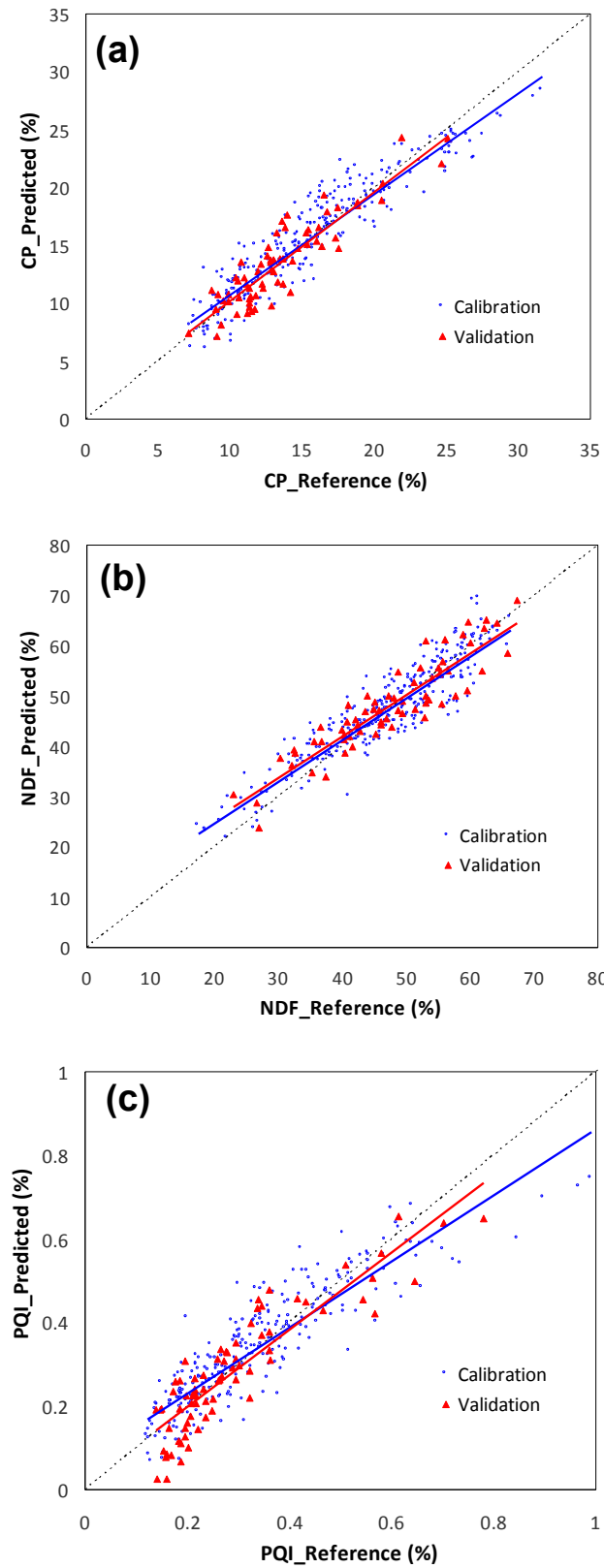
Figure 2. Plot of reference values versus near infrared spectroscopy (NIRS) predicted values for calibration and validation phases: (a) crude protein (CP), (b) neutral detergent fibre (NDF) and (c) pasture quality index (PQI).

Table 2 shows that the PLSR models selected for CP, NDF and PQI quantification in pasture samples exhibited a small difference between RMSE from the calibration and the RMSE from the external validation models. The same small differences between RMSE were obtained by Aleixandre-Tudo et al. (2018), which indicated robust and accurate calibrations. Models are robust when the prediction accuracy is relatively insensitive to unknown changes of external factors. Also, according to Fagan et al. (2011) a model is considered good enough to monitor the quality of individual samples when the R^2 is around 0.90 and the RDP is greater than 3. The R^2 obtained in this study (0.80-0.90) and the RPD (2.4-4.0), indicates that there are very little differences between reference and predicted values in CP, NDF and PQI (Bagchi et al., 2016). In general, the R^2 increase as more information is added to the database, which means that, although these results are encouraging, more accurate models will be built in the future allowing the chemical and nutritional analysis of feed stuffs in a non-destructive and inexpensive way.

5. Conclusions

The development and productivity of dryland pastures depend mainly on the distribution of precipitation throughout the year and on its combination with the air temperature. The important inter-annual variability of rainfall, characteristic of Mediterranean region, places the agricultural decision-maker in a scenario of great unpredictability regarding the availability of food for animals in extensive regime. The results of this study show the practical interest of spectrometry as expeditious tool for monitoring pasture quality and support farmer management decisions in terms of animal supplementation needs in the critical period between the end of spring and the beginning of autumn in Southern of Portugal. Although these are already very interesting results and with immediate practical application, clearly reducing the time and means needed to process pasture samples and obtain quality parameters, we believe that it is still possible to improve the robustness of the NIRS calibration models in estimating pasture quality attributes, resorting either to a greater number of pasture samples, or to portable spectrometry, which allow direct field sampling (green sampling), eliminating the need for sample preparation. Good prospects and opportunities open up for technology-based service providers to develop remote sensing-based computer applications from historical time series of indices obtained by satellite imagery that enable holistic and dynamic management of animal grazing.

Acknowledgements

References

Aleixandre-Tudo, J.L., Nieuwoudt, H., Olivieri, A., Aleixandre, J.L., Toit, W. 2018. Phenolic profiling of grapes, fermenting samples and wines using UV-Visible spectroscopy with chemometrics. Food Control. 85, 11–22.

AOAC. 2005. Official Method of Analysis of AOAC International, 18th ed., AOAC International: Arlington, AT, USA.

Bagchi, T.B., Sharma, S., Chattopadhyay, K. 2016. Development of NIRS models to predict protein and amylase content of brown rice and proximate compositions of rice bran. Food Chemistry. 191, 21–27.

Batten, G.D. 1998. Plant analysis using near infrared reflectance spectroscopy: the potential and the limitations. Australian Journal of Experimental Agriculture. 38, 697–706.

Bell, M.J., Mereu, L., Davis, J. 2018. The use of mobile near-infrared spectroscopy for real-time pasture management. Frontiers in Sustainable Food Systems. 2, 1–10.

Corson, D.C., Waghorn, G.C., Ulyatt, M.J., Lee, J. 1999. NIRS: Forage analysis and livestock feeding. Proceedings of the New Zealand Grassland Association. 61, 127–132.

Donis-González, I.R., Valero, C., Momin, M.A., Kaur, A., Slaughter, D.C. 2020. Performance Evaluation of two commercially available portable spectrometers to non-invasively determine table grape and peach quality attributes. Agronomy. 10, 148.

Efe Serrano, J. 2006. Pastures in Alentejo: Technical Basis for Characterization, Grazing and Improvement, Universidade de Évora—ICAM, Ed., Gráfica Eborense: Évora, Portugal, pp. 165–178.

Fagan, C.C., Everard, C.D., McDonnell, K. 2011. Prediction of moisture, calorific value, ash and carbon content of two dedicated bioenergy crops using near-infrared spectroscopy. Bioresource Technology. 102, 5200–5206.

Garcia, J., Cozzolino, D. 2006. Use of near infrared reflectance (NIR) spectroscopy to predict chemical composition of forages in broad-based calibration models. Agricultural technology. 66, 41–47.

Givens, D.I., Deaville, E.R. 1999. The current and future role of near infrared reflectance spectroscopy in animal nutrition: a review. Australian Journal of Agricultural Research. 50, 1131–1145.

Goering, H.K., Van Soest, P.J. 1970. Forage fibre analysis (apparatus reagents, procedures and some applications). Agriculture Handbook no. 379, USDA-ARS, Albany, USA.

Lumbierres, M., Méndez, P.F., Bustamante, J., Soriguer, R., Santamaria, L. 2017. Modeling biomass production in seasonal wetlands using Modis NDVI land surface phenology. Remote Sensing. 9, 392.

Milinovic, J., Garcia, R., Rato, A.E., Cabrita, M.J. 2020. Rapid assessment of monovarietal portuguese Extra Virgin Olive Oil's (EVOO's) fatty acids by Fourier-Transform Near-Infrared Spectroscopy (FT-NIRS). European Journal of Lipid Science and Technology. 121.

Murray, I. Forage analysis by near infrared spectroscopy. In, Davies, A., Baker, R.D., Grant, S.A., Laidlaw, A.S. (eds.), Sward measurement handbook. 2nd ed., 1993, The British Grassland Society, Reading, UK.

Musingarabwi, D.M., Nieuwoudt, H.H., Young, P.R., Eyeghe-Bickong, H.A., Vivier, M. A. 2016. A rapid qualitative and quantitative evaluation of grape berries at various stages of development using Fourier-transform infrared spectroscopy and multivariate data analysis. Food Chemistry. 190, 253–262.

Serrano, J., Shahidian, S., Marques da Silva, J. 2018. Monitoring seasonal pasture quality degradation in the Mediterranean montado ecosystem: Proximal versus remote sensing. Water. 10, 1422.

Shenk, J.S., Werterhaus, M.O. 1993. Analysis of agriculture and food products by near infrared espectroscopy. Infrasoft International, Pennsylvania, USA, pp. 116–187.

Smith, K.F., Flinn, P.C. 1991. Monitoring the performance of a broad-based calibration for measuring the nutritive value of two independent populations of pasture using near infrared reflectance (NIR) spectroscopy. Australian Journal of Experimental Agriculture. 31, 205–210.

Teye, E., Amuah, C.L.Y., McGrath, T., Elliott, C. 2019. Innovative and rapid analysis for rice authenticity using hand-held NIR spectrometry and chemometrics. Spectrochimica Acta Part A: Molecular and Biomolecular Spectroscopy. 217, 147–154.

Versari, A., Laurie, V. F., Ricci, A., Laghi, L., Parpinello, G.P. 2014. Progress in authentication, typification and traceability of grapes and wines by chemometric approaches. Food Research International. 60, 2–18.

Véstia, J., Barroso, J.M., Ferreira, H., Gaspar, L., Rato, A.E. 2019. Predicting calcium in grape must and base wine by FT-NIR spectroscopy. Food Chemistry. 276, 71–76.

Wold, S., Sjostrom, M., Eriksson, L. 2001. PLS-Regression: A basic tool of Chemometrics. Chemometrics and Intelligent Laboratory Systems. 58, 109–130.

Map-based Site-specific Seeding of Seed Potatoes by Fusion of Proximal and Remote Sensing Data

Muhammad Abdul Munnaf [a], Geert Haesaert [b], Marc Van Meirvenne [a], Abdul Mounem Mouazen [a,]

[a] Department of Environment, Ghent University, Gent, Belgium
[b] Department of Plants and Crops, Ghent University, Gent, Belgium
*Corresponding author. Email: Abdul.Mouazen@UGent.be

Abstract

Uniform rate seeding (URS) is not the optimal approach to utilize the yield potential of different zones of a field. This study examines the potential of map-based site-specific seeding (SSS) of seed potatoes for improving crop yield and economic return. A field (6 ha) was scanned using an on-line visible and near-infrared (vis-NIR) spectroscopy and electromagnetic induction (EMI) sensors. The k-means clustering was used to divide this field into management zones (MZ) using two data sets i.e., apparent electrical conductivity (EMI-MZ), and data fusion of two normalized differential vegetation indexes (NDVIs) retrieved from Sentinel2 images with on-line vis-NIR measured soil pH, organic carbon, available P, K, Mg, Na and moisture content (visNIRSen-MZ). Seed potatoes (*Solanum tuberosum L.* cv. Hermes) were planted at 11, 13, 15, 17 and 19 cm spacing intervals by sowing more seeds to the fertile zones and vice versa. Yield analysis demonstrated that SSS increased overall yield (EMI-MZ: 32.42 Mg ha^{-1}, visNIRsen-MZ: 31.89 Mg ha^{-1}), compared to URS (31.06 Mg ha^{-1}). Although visNIRSen-MZ had a lower gross yield than EMI-MZ, the increased yield of small size (28-45 mm) tubers, having higher market price than other size categories has resulted in an actual market price for the former larger than that of the latter approach. Economic analysis revealed that SSS resulted in a higher gross margin than the URS, whilst both the MZs approaches performed almost equally. The visNIRsen and EMI produced a gross margin of 4995 € ha^{-1} and 4947 € ha^{-1}, respectively while URS's gross margin was 4528 € ha^{-1}. In contrast to URS, visNIRsen-MZ and EMI-MZ increased gross margin by 467 € ha^{-1} and 419 € ha^{-1}, respectively. The visNIRsen-MZ approach saved seeding costs by 14 € ha^{-1} although EMI-MZ consumed 5 € ha^{-1} more compared to URS. Therefore, it is recommended to adopt SSS in seed potato, as a means of increasing crop yield, reducing input cost, and thus maximizing profitability compared to URS.

Keywords: Proximal and remote sensing, Data fusion, Map-based site-specific seeding, Economic analysis, Potato seeding.

1. Introduction

Agricultural soils are spatiotemporally heterogeneous while heterogeneity comes from the inherited field variability of soil origin, topography, weather, and agricultural management practices (Zhang et al., 2002). The traditional practice of Uniform Rate Seeding (URS) does not account for the spatial variability by allocating a unique seed rate over the entire field area. Consequently, it results in improper plant populations, which leads to lower production than the yield potential of a field. Attempts to search for a solution have explored Site-Specific Seeding (SSS), as a seeding approach that takes into account the spatial variation during the seed rate calculation (Heege, 2013). The SSS attempts to optimize seeding density to match the fertility status of different parts of a field. Map-based site-specific seeding is based on an management zone (MZ) approach that devides a field into multiple regions with each having a relatively homogenous fertility level (Nawar et al., 2017). Successful implementation of map-based SSS largely depends on the MZ delineation algorithm and the accurate estimation of MZ proxies used for MZ map delineation (Munnaf et al., 2020).

Key parameters to affect seed spacing are soil-related, which have to be measured at high sampling density to enable assessment of within-field spatial variability during MZ delineation. One of the best sensing technologies to measure soil attributes is Visible and Near-Infrared (vis–NIR) diffuse reflectance spectroscopy, which is a simple, non-destructive and rapid technique that needs no sample preparation for field applications and can be used for off-line and on-line (Kuang et al., 2012) measurement modes. The unique feature of the on-line sensing system (pulled behind a tractor) is that it can offer high resolution (≈2000 samples/ha) measurement of many chemical and physical soil properties (Munnaf et al., 2020). Another sensing technology that is also capable to measure key soil physical attributes related to seed density is Electro-Magnetic Induction (EMI), which is a non-destructive method to measure soil apparent Electrical Conductivity (ECa). Since many factors affect ECa, it is difficult to identify the individual causal effect on soil ECa (Adamchuk et al., 2004). Hence, the majority of EMI applications in precision agriculture were aimed at mapping within-field variability and delineating MZs that can be used for site-specific soil and crop management. The potential of the on-line vis-NIR spectroscopy for the delineation of MZs in comparison to corresponding MZs maps developed with ECa form EMI sensor has not been reported in the literature for SSS of seed potato.

A literature survey has shown that the majority of SSS studies are limited to two MZ proxies i.e., ECa and yield map. Due to the fact that proximal sensors are costly, SSS was often reported as an un-economic seeding approach (Dillon, 2013), though a few studies reported SSS as an economic approach (Bullock et al., 1999). This inconsistent economic conclusion has demotivated the adopters, hence, SSS has not been practiced as widely as other site-specific applications in agriculture.

On the other side, scientists have proved that a single soil or crop property cannot be representative of soil fertility and yield potentiality (Castrignanò et al., 2018). To date, no study has attempted to evaluate map-based SSS for seed potatoes based on the fusion of multiple soils and crop quality indicators. Therefore, this study aims to evaluate the potential of map-based SSS of seed potatoes for improving crop yield and economic return using the fusion of proximal and remote sensing data. Specifically, the current study focuses on (i) assessment of the economic potential of SSS of seed potato, in comparison with URS (ii) comparing the performance of a SSS treatment based on a MZ map developed using EMI data (EMI-SSS) with corresponding SSS treatment based-on a MZ map developed by the fusion of Vis-NIR measured soil data with Sentinel-2 derived normalized difference vegetation index (visNIRsen-SSS).

2. Materials and Methods

2.1. Estimation of soil and crop data

This study was conducted in a 6 ha field located in the Flanders region, Belgium. In August 2018, a soil survey was conducted using an on-line vis-NIR spectroscopy sensor (Tec5 technology, Germany), followed by spectral modeling to establish spectral calibration models of soil pH, Organic Carbon (OC), available-Phosphorous (P), Potassium (K), magnesium (Mg), and Sodium (Na), and Moisture Content (MC). A detailed description of the sensing system and spectral processing to model development can be found in Mouazen (2006) and Munnaf et al. (2020), respectively. Although 20 soil samples were collected during the on-line sensing, additional 102 samples from the local spectral library were merged to create a dataset of 122 samples that were further divided into a calibration (88 samples) and prediction (34 samples) dataset. Partial least squares regression (PLSR) analyses were carried out to establish calibration models of the named soil properties. On-line prediction accuracy was evaluated using the coefficient of determination (R^2), root means square error (RMSE), and the ratio of prediction to deviation (RPD). Another separate survey to measure soil ECa using an EMI sensor (Dualem 21S, Milton, Canada) was carried out in November 2018. Besides, two images (18th and 25th June 2018) of Sentinel-2 were downloaded and processed for the calculation of the previous crop (i.e., wheat) NDVI.

2.2. Spatial soil mapping and management zone delineation

Full points prediction of soil properties using on-line collected vis-NIR spectra and EMI measured ECa were used to develop maps using ordinary kriging followed by variogram fitting. Since on-line measured soil properties were provided at higher sampling resolution (900 samples per ha) than the Sentinel-2 measured NDVI (raster of 10 m), it is ideal to convert all data layers into a common grid to facilitate data fusion. All soil property layers and NDVI data (bi-linear interpolation) were then converted into a common raster of 5 by 5 m grid. The raster analysis was followed by unsupervised classification using *K-means* clustering algorithm. This has resulted in dividing the field into a few homogeneous MZs. On the other hand, soil ECa data were classified into define MZs using the equal interval classifications. Accordingly, two MZ maps were produced in this work, namely, visNIRsen-MZ, and EMI-MZ.

2.3. Site-specific recommendation and experimental plot design

The MZ classes of the visNIRsen-MZ map were ranked, i.e., high (H), medium-high (MH), medium (M), medium-low (ML), and low (L), according to their fertility (productivity) status, which considered the normalized mean values of soil properties and NDVI data as well as the farmers' knowledge of their field. Similarly, the ranking of the EMI-MZ was made assuming that a zone having the highest ECa value would be the most fertile, and the fertility rank declines with the declining of ECa values of the remaining zones.

The field was divided into parallel strips of 6 m width, which was chosen to match the width of the potato planter (GRIMME 860 GL Compacta, GRIMMME UK Ltd, UK). These strips were then divided randomly into three treatments of URS, EMI-SSS, and visNIRsen-SSS. Afterward, the parallel strips were overlaid by each of the two (EMI-MZ and visNIRsen-MZ) developed MZ maps, which resulted in dividing each strip into sub-strips, called plots in this work, whose fertility class and size should match the fertility ranks and size of the corresponding MZ. Accordingly, these plots were designated as H, MH, M, ML, and L fertility, which received seed spacings of 11, 13, 15, 17, and 19 cm, respectively (Fig. 1).
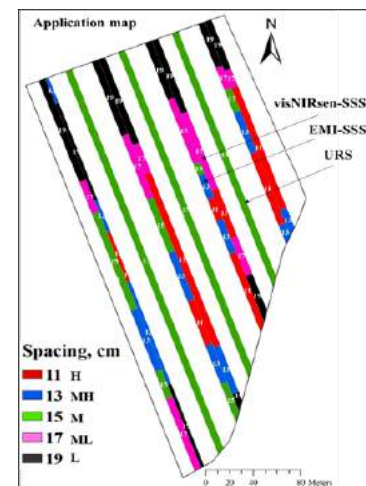
Figure 1. Application map of strip

experiment

This SSS recommendation is known as the "Kings approach" (Munnaf et al., 2020). Finally, the application map was exported as a machine-compatible shapefile and uploaded to the virtual terminal of the potato planter to perform potato planting on 25th April 2019.

2.4. Tuber yield estimation and economic analysis

A total of 100 yield samples were collected across the treatments and kept on an air-circulated floor for two weeks. After sorting out waste, rotten, and under-size tubers (< 28 mm diameter), the net yield was calculated by subtracting 20% of gross yield. The net yield was then graded into five size categories as 28-35 mm, 35-45 mm, 45-50 mm, 50-55 mm, and > 55 mm. The average net yield (Mg ha^{-1}) was calculated for each fertility class considering the samples located within the corresponding MZ and sensor used for MZ delineation.

A cost-benefit analysis was conducted, for which the seeding cost and revenue from yield were considered as production input costs and outcome per unit area i.e., € ha^{-1}, respectively, under few assumptions: (i) unless specified e.g., soil scanning, all other costs were assumed to be equal for both SSS and URS treatments, (ii) tubers of 28-55 mm in diameter were considered as seeds, (iii) tubers of > 55 mm in diameter were considered as consumption potatoes, and (iv) each size category has a specific market price, suggested by commercial potato growers. For example, 600 € Mg^{-1} for 28-35 mm, 450 € Mg^{-1} for 35-45 mm, 300 € Mg^{-1} for 45-50 mm, 200 € Mg^{-1} for 50-55 mm, and 135 € Mg^{-1} for > 55 mm. The revenue (€ ha^{-1}) of URS, visNIRSen-SSS and EMI-SSS treatments were calculated by multiplying the average net yield by the market prices of each size category. Gross margin was derived after subtracting the seeding cost from the revenues.

3. Results and Discussion

3.1. Accuracy of vis-NIR models

Table 1 presents the quality of vis-NIR spectral models obtained from PLSR for the prediction of the seven soil properties. In addition to the overall prediction accuracies for all soil properties that are in good agreement with previous studies, Mg and Na showed better prediction in the current study (Munnaf et al., 2020). Although OC and MC have direct spectral responses in the NIR region, the small range of variability of the reference OC and the high Ca content ($\approx$ 4500 mg 100g^{-1}) in the soil might mask their direct spectral responses, which led to the poorest prediction quality, together with P and K. The similar prediction quality of K and P models might be attributed to covariations they have with OC and MC. Regarding RPD values in prediction, models can be categorized as excellent for Mg and Na, very good for pH and fair for the rest of the properties (OC, P, K and MC) (Viscarra Rossel et al., 2006). The prediction accuracies obtained in this study are good enough for supporting successful MZ delineation for SSS, since an earlier study reported successful site-specific phosphorous management with almost similar vis-NIR model accuracy, using the same on-line soil sensor (Mouazen and Kuang, 2016).

Table 1. Accuracies of on-line visible and near-infrared (vis-NIR) prediction.

Accuracy	pH	OC, %	P, mg 100g^{-1}	K, mg 100g^{-1}	Mg, mg 100g^{-1}	Na, mg 100g^{-1}	MC, %
R^2	0.81	0.63	0.54	0.60	0.90	0.87	0.61
RMSE	0.40	0.16	5.76	5.33	8.97	0.97	1.52
RPD	2.36	1.67	1.49	1.61	3.14	2.76	1.63

LV, Latent variables; R^2, coefficient of determination; RMSE, root mean square error; RPD, residual prediction deviation. OC, organic carbon, P, phosphorous; K, potassium; Mg, magnesium; Na, sodium; M, moisture content.

3.2. Fertility maps and management zone exploration

Figure 2 illustrates the on-line predicted, high-resolution (e.g., 900 readings per ha) soil maps together with crop NDVIs. Soil maps of pH, K, Mg and MC showed distinguished spatial similarity patterns. The NDVI map of the 30th June 2018 shows almost comparable spatial distribution to those of the on-line predicted pH, K, Mg and MC. That's why both the MZ approachs identified the central part of the field as the most fertile, together with the eastern part (Figure 3). In the visNIRsen-MZ, cluster 2 was defined as the H fertility zone, followed successively in descending order by cluster 1, cluster 3, cluster 4 and cluster 5. The highest (ECa = 75.33 - 85.73 ms m-1) and the MH fertility zone (ECa = 66.23 - 75.32 ms m-1) largely overlap with the H fertile zone (cluster 2) in the visNIRsen-MZ map. The M fertile class in the visNIRsen-MZ partially resembles the M fertility class and the second least (MH) fertile classes in the EMI-MZ map. The northern part of the field was marked as the least (M) fertile zone similar to visNIRsen-MZ. Therefore, both the MZ delineation approaches were in good agreement with the 5 MZ classes, which was enough to manage within-field soil variability.

3.3.
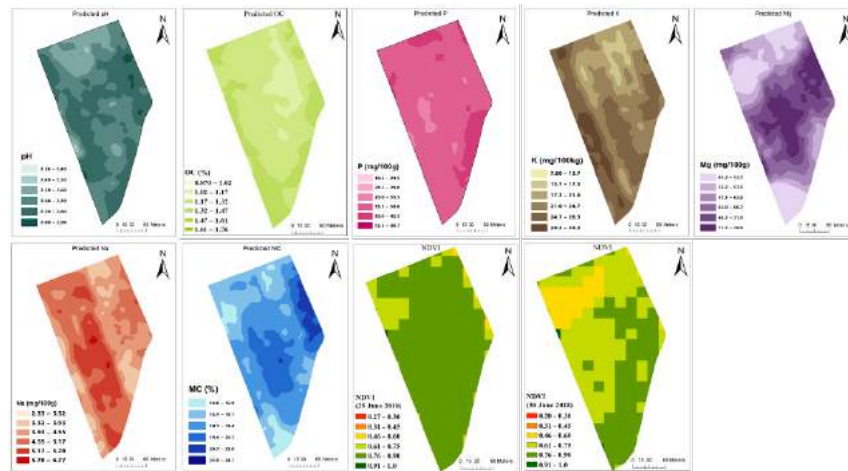
Figure 2. Soil fertility maps of on-line predicted soil pH, organic carbon (OC), available-phosphorous (P), potassium (K), magnesium (Mg), and sodium (Na), and moisture content (MC), and crop normalized difference vegetation index (NDVI).
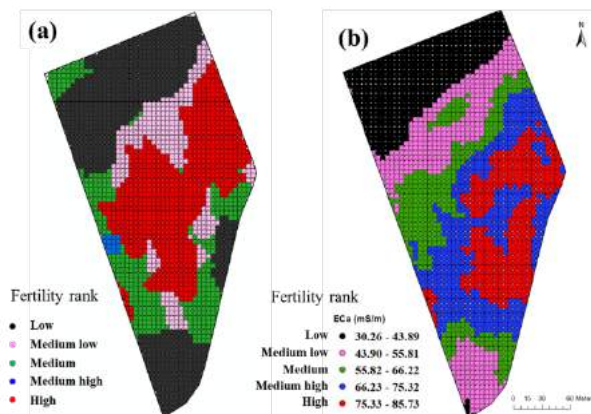
Figure 3. Management zone (MZ) maps delineated with (a) fusion of on-line visible and near-infrared spectroscopy predicted soil attributes with normalized difference vegetation index, retrieved from Sentinel-2 images (visNIRsen-MZ), and (b) apparent electrical conductivity data measured with an electromagnetic sensor (EMI-MZ).

3.4. Tuber yields and cost-benefit results

The yield analysis (Table 2) demonstrated that both SSS approaches have increased overall tuber yield, compared to the URS (28.82 Mg ha^{-1}). The visNIRSen-SSS (32.02 Mg ha^{-1}) produced a slightly lower yield than that of the EMI-SSS (32.54 Mg ha^{-1}). However, this yield increment was not statistically significant at 95% confidence interval (F = 1.054 and P = 0.352) when tested with one-way analysis of variance (ANOVA) and Tukey honestly significant difference (HSD) test. Similarly, the visNIRsen-SSS and EMI-SSS produced a gross margin of 4995 € ha^{-1} and 4947 € ha^{-1}, respectively while URS gross margin was 4528 € ha^{-1}. In contrast to URS, SSS with visNIRsen-MZ and EMI-MZ increased gross margin by 467 € ha^{-1} (10.31%) and 419 € ha^{-1} (9.25%), respectively. Although the visNIRsen-SSS treatment provided a lower gross yield than the EMI-SSS, the increased yield of 28-45 mm sized tubers having high market price, have resulted in an actual market price larger for the former approach than the latter one. Besides, the visNIRsen-SSS approach planted fewer seeds, increasing seed cost saving of 14 € ha^{-1}, though EMI-SSS consumed 5 € ha^{-1} more compared to URS. It indicates that the profitability to growers emerges mainly from the significant yield improved by SSS rather than saving on seed costs. A similar finding was reported by another study (Dwight et al., 2013). Assuming the cost of soil sensing and mapping to be 25 € ha^{-1} per year, the gross margin of SSS treatments would be reduced by 25 € ha^{-1}. Despite the scanning cost, both the SSS approaches would still provide a higher margin than the URS, proving the economic potential of SSS for seed potato production.

3.5. Tuber size distribution

The visNIRsen-SSS has shown a clear and consistent yield increasing trend with the sowing intervals (Fig. 4), particularly for tuber sizes of 50, 55 mm and > 55 mm, a finding that is in good agreement with Knowles and Knowles, (2016). This can be explained by the reduced intra-crop competition for nutrition and solar radiation to produce larger tubers by larger planting intervals. The EMI-SSS provided a higher proportion of larger size tubers than visNIRsen-SSS and URS. For example, the visNIRsen-SSS resulted in higher production for the 28-35 and 35-45 mm categories, whereas the EMI-SSS produced higher yields for the 50-55 mm category. The largest size category tubers (> 55 mm) of the EMI-SSS scenario showed a fluctuated trend in tuber yield with seed spacing. Around 60-70% of the total yield has grown larger than 55 mm sizes tubers, which is not marketable as seeds, and it happened commonly for all three treatments.

This can be explained by the longer cultivation period and delay in harvesting time caused by the wet weather conditions. Therefore, farmers in practice strictly follow the harvest schedule if the weather conditions allow, so that to prevent tubers to grow over the marketable sizes for seeds. In the present study, tubers of larger than 55 mm size should be sold as consumption potato, having much lower market value, compared to seed potato. In this sense, visNIRsen-SSS produced better quality categories for seed potatoes that are marketable as seed by better recommending seeding intervals per MZ class.
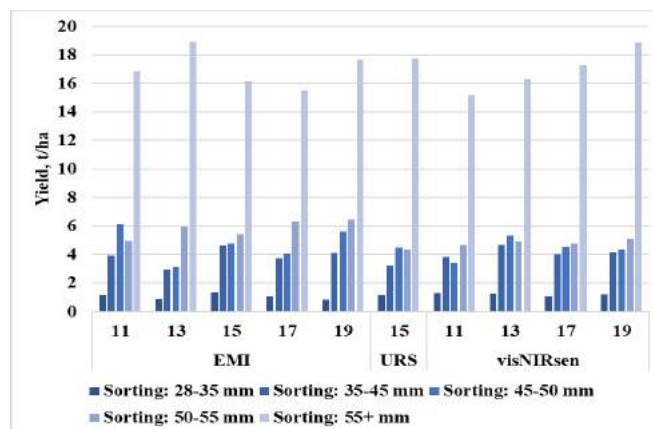
Figure 4. Tuber size distribution across the seeding intervals used in uniform rate seeding (URS) and site-specific seeding treatments: (1) visNIRsen-SSS and (2) EMI-SSS.

Table 2. Results of cost-benefit analysis of site specific seeding (SSS), in comparison with uniform rate seeding (URS) of seed potato.

Treatments	MZs and fertility order	Seed spacing, cm	Seed rate, Mg ha^{-1}	Seeding cost, € ha^{-1}	Yield, Mg ha^{-1}	Revenue, € ha^{-1}	Gross margin, € ha^{-1}	Relative gross margin, € ha^{-1}	Savings seed cost, € ha^{-1}	Increase gross margin, %
URS		15	5.50	2200	28.82	6728.22	4528.22	-	-	-
VisNIRSen-SSS	High	11	6.88	2750	28.57					
	Medium high	13	6.19	2475	32.92					
	Medium	15	-	-	-	7180.82	4994.96	466.69	14.10	10.31
	Medium low	17	4.81	1925	31.85					
	Low	19	4.13	1650	33.72					
	Average			2185.90	32.02					
EMI-SSS	High	11	6.88	2750	33.03					
	Medium high	13	6.19	2475	31.87					
	Medium	15	5.50	2200	32.92	7152.04	4946.95	418.73	-5.09	9.25
	Medium low	17	4.81	1925	30.79					
	Low	19	4.13	1650	34.75					
	Average			2205.09	32.54					

MZ, management zone; visNIRsen-SSS, the fusion of on-line measured soil fertility attributes with normalized difference vegetation index; EMI-SSS, electromagnetic induction measured soil apparent electrical conductivity (EMI-SSS).

3.6. Key soil fertility indicators

The Pearson correlation (Fig. 5) revealed that soil OC, P, and K to have strong correlations (r = 0.22 - 0.91) with the tuber yields from 13, 15 and 17 mm intervals. It explains the association of these underlying soil attributes with potato productivity. Available P serves a prominent role in cellular energy transfer from adenosine triphosphate (ATP) to adenosine diphosphate (ADP) and acts as a structural component of nucleic acids (Naumann et al., 2020). Accordingly, soil P is not only a significant soil attribute for the setting of potato tubers, particularly in the early crop stage (Hopkins et al., 2014), but also accelerates tuber maturity (Rosen et al., 2014). Research also proved that high P fertilization limits the yield of larger size tubers that offsets increased yields of smaller size tubers (Rosen et al., 2014). On the other hand, the basic role of K in regulating the enzyme activity, photosynthesis, and carbohydrates partitioning in the plant body, makes K to have a central association with expected tuber and starch yields (Naumann et al., 2020). A K-deficient soil

exhibited a significant reduction in potato yields (Koch et al., 2019), although K does not positively contribute to increasing potato yield in a K-sufficient soil (Kang et al., 2014). Finally, soil OC is a general but main key soil fertility attribute, as it provides food for micro-organisms and earthworms that play a positive role in improving soil structure and stability. Also, the larger the soil OC (e.g., soil organic matter), the larger is the soil water holding capacity, hence, plant-available water for a longer period during dry conditions. Elevated OC can produce higher tuber yields (Hijbeek, 2017), although intensive potato production results in soil degradation by depleting soil organic matter content (Angers et al., 1999).
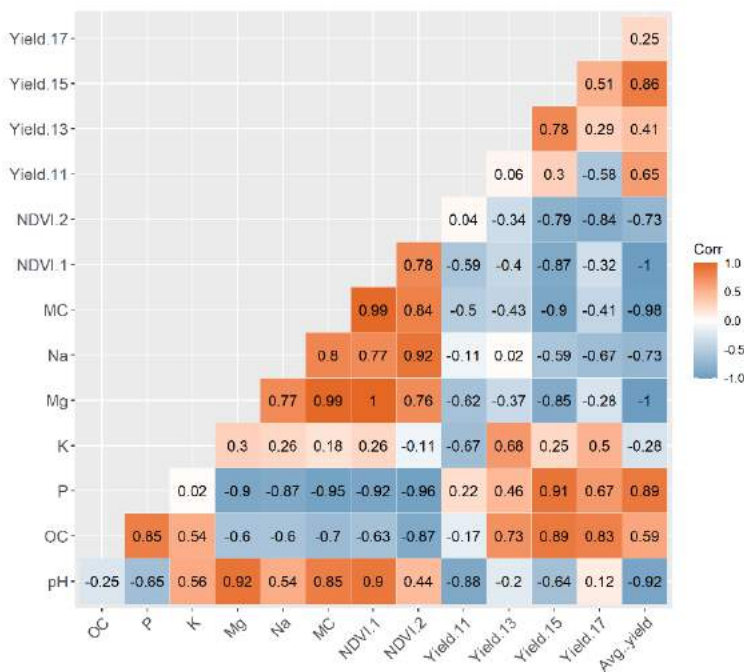
Figure 5. Pearson correlations among on-line measured soil properties, crop normalized difference vegetation index (NDVI), and yield of seed potatoes. OC, organic carbon (%); MC, moisture content (%); P, phosphorus (mg $100g^{-1}$); K, potassium (mg $100g^{-1}$); Mg, magnesium (mg $100g^{-1}$); Na, sodium (mg $100g^{-1}$); Yield-11, Yield-13, Yield-15, Yield-17, tubers yield obtained from 11, 13, 15, 17 cm seeding intervals respectively, NDVI-1 and NDVI-2, normalized difference vegetation index retrieved from Sentinel-2 Level 2A product on 25th and 30th June 2018, respectively.

Besides, soil pH frequently showed positive correlations with soil K, Mg, Na, MC (r = 0.54-0.92) and crop NDVIs (r = 0.44-0.90), though these attributes did not exhibit a positive correlation with tuber yields for any of the seeding intervals. Nevertheless, soil pH has a decisive impact on plant uptake of nutrients. For example, the a pH value between 6.0 and 7.5 is considered as an ideal acidity for soil P uptake and be available to the plants (Pierzynski et al., 1994). Soil pH values in acid and in alkaline ranges can both adversely affect soil P availability (Rosen et al., 2014). Interrupted P availability can restrict crop root growth due to its contribution to cell division (Rosen et al., 2014). However, the ideal range of pH and thus P availability varies according to the soil texture types and crops in question (van Vliet and Giller, 2015). Phosphorus fertilization increases plant growth and tuber yield more in clayey soils than the sandy soils (Martins et al., 2018). The pH level of 6 to 7.5 facilitates soil K availability and a relatively higher pH range (7.0 to 8.5) is good for Ca and Mg uptaking (USDA-NRCS, 2014). Under alkaline soil conditions, P tends to develop poorly soluble mineral precipitates with Mg or Ca (Hopkins, 2013). Based on the above discussion about the contributory role of pH, OC, P, and K on crop nutrient uptaking and potato yield, they could be identified as the key soil properties for seed spacing determination for SSS in potato cultivation.

4. Conclusions

The economic and agronomic performance of two site-specific seeding (SSS) treatments was evaluated and compared with a uniform rate seeding (URS) approach. The first SSS (visNIRsen-SSS) was designed based on MZ delineated with the fusion of on-line vis-NIR estimated soil properties together with crop NDVI retrieved from Sentinel-2A images, while the second SSS (EMI-SSS) was designed based on the soil ECa, data measured with an EMI sensor.

Both SSS treatments increased the overall yield of seed potatoes by 32.54 Mg ha^{-1} (EMI-SSS) and 32.02 Mg ha^{-1} (visNIRsen-SSS), compared to traditional URS (28.82 Mg ha^{-1}). Variable seed spacing has led not only to yield increase but also the quality of tubers suitable for seed potato. Accordingly, higher economic gross margins were calculated for both the SSS treatments, which resulted from not only the increased yield but also larger savings on seed cost as a lower amount of seeds were used compared to the URS. The visNIRsen-SSS and EMI-SSS have resulted in increased gross margins of 467 € ha^{-1} by 419 € ha^{-1}, respectively, in comparison with the URS. The VisNIRSen-SSS treatment has led to a saving on seed costs of 14 € ha^{-1}, whereas the EMI-SSS consumed 5 € ha^{-1} more compared to the URS. The

visNIRsen-SSS approach resulted in the highest marketable seed potatoes for the smallest input of seed rates compared to EMI-SSS and URS treatments. Results showed the potential of the visNIRsen for determining soil fertility level that leads to proper seed distributions over the area under a corresponding MZ. In addition, the vis-NIRsen-SSS approach enabled the evaluation of correlations between key soil attributes and yield at different seeding intervals, suggesting soil pH, OC, P, and K as the key MZ proxies.

After all, it is recommended to adopt SSS in seed potato production, as a means of increasing crop yield, reducing input cost, and thus maximizing profitability. The present study suggests further evaluations of the map-based SSS approaches using proximal and remote sensing data fusion for different cultivars of seed and consumption potatoes under different soil types and agro-climatic conditions.

Acknowledgments

References

Adamchuk, V.I., Hummel, J.W., Morgan, M.T., Upadhyaya, S.K., 2004. On-the-go soil sensors for precision agriculture. Comput. Electron. Agric. 44, 71–91. https://doi.org/10.1016/j.compag.2004.03.002

Angers, D.A., Edwards, L.M., Sanderson, J.B., Bissonnette, N., 1999. Soil organic matter quality and aggregate stability under eight potato cropping sequences in a fine sandy loam of Prince Edward Island. Can. J. Soil Sci. 79, 411–417. https://doi.org/10.4141/S98-033

Bullock, D.S.G., Bullock, D.S.G., Nafziger, E.D., Stafford, J. V, 1999. Variable rate seeding of maize in the Midwestern USA, in: Precision Agriculture '99, Part 2. Papers Presented at the 2nd European Conference on Precision Agriculture, Odense, Denmark, 11 15 July 1999. Precision Agriculture '99, Part 1 and Part 2. Papers Presented at the 2nd European Conference on Precision Agric.

Castrignanò, A., Buttafuoco, G., Quarto, R., Parisi, D., Viscarra Rossel, R.A., Terribile, F., Langella, G., Venezia, A., 2018. A geostatistical sensor data fusion approach for delineating homogeneous management zones in Precision Agriculture. Catena 167, 293–304. https://doi.org/10.1016/j.catena.2018.05.011

Dillon, C.R., 2013. Heuristic optimization for variable rate nitrogen and seeding decisions, in: Precision Agriculture 2013 - Papers Presented at the 9th European Conference on Precision Agriculture, ECPA 2013. pp. 761–768.

Dwight, K., Craig, K., Grant, H., Farrell, A., 2013. Variable Rate Seeding: Easier Than You Think - Crop Quest Agronomic Services [WWW Document]. CropQuest. URL https://www.cropquest.com/variable-rate-seeding/ (accessed 5.7.18).

Heege, H.J., 2013. Site-specific sowing, in: In: Heege H. (eds) (Ed.), Precision in Crop Farming: Site Specific Concepts and Sensing Methods: Applications and Results. Springer Dordrecht, Dordrecht, pp. 171–192. https://doi.org/10.1007/978-94-007-6760-7_8

Hijbeek, R., 2017. On the role of soil organic matter for crop production in European arable farming. Wageningen University, Wageningen, the Netherlands.

Hopkins, B.G., 2013. Russet burbank potato phosphorus fertilization with dicarboxylic acid copolymer additive. J. Plant Nutr. 36, 1287–1306. https://doi.org/10.1080/01904167.2013.785565

Hopkins, B.G., Horneck, D.A., MacGuidwin, A.E., 2014. Improving Phosphorus Use Efficiency Through Potato Rhizosphere Modification and Extension. Am. J. Potato Res. 91, 161–174. https://doi.org/10.1007/s12230-014-9370-3

Kang, W., Fan, M., Ma, Z., Shi, X., Zheng, H., 2014. Luxury absorption of potassium by potato plants. Am. J. Potato Res. 91, 573–578. https://doi.org/10.1007/s12230-014-9386-8

Knowles, L.O., Knowles, N.R., 2016. Optimizing Tuber Set and Size Distribution for Potato Seed (Solanum tuberosum L.) Expressing Varying Degrees of Apical Dominance. J. Plant Growth Regul. 35, 574–585. https://doi.org/10.1007/s00344-015-9562-1

Koch, M., Busse, M., Naumann, M., Jákli, B., Smit, I., Cakmak, I., Hermans, C., Pawelzik, E., 2019. Differential effects of varied potassium and magnesium nutrition on production and partitioning of photoassimilates in potato plants. Physiol. Plant. 166, 921–935. https://doi.org/10.1111/ppl.12846

Kuang, B., Mahmood, H.S., Quraishi, M.Z., Hoogmoed, W.B., Mouazen, A.M., van Henten, E.J., 2012. Sensing Soil Properties in the Laboratory, In Situ, and On-Line, in: Advances in Agronomy. Elsevier Inc., pp. 155–223. https://doi.org/10.1016/B978-0-12-394275-3.00003-1

Martins, J.D.L., Soratto, R.P., Fernandes, A.M., Dias, P.H.M., 2018. Phosphorus fertilization and soil texture affect potato yield. Rev. Caatinga 31, 541–550. https://doi.org/10.1590/1983-21252018v31n302rc

Mouazen, A.M., 2006. Soil Survey Device. International publication published under the patent cooperation treaty (PCT). World Intellectual Property Organization, International Bureau. International Publication Number: WO2006/015463; PCT/BE2005/000129; IPC: G01N21/00; G01N21/00

Mouazen, A.M., Kuang, B., 2016. On-line visible and near infrared spectroscopy for in-field phosphorous management. Soil Tillage Res. 155, 471–477. https://doi.org/10.1016/j.still.2015.04.003

Munnaf, M. A., Haesaert, G., Mouazen, A.M., 2020. Map-based site-specific seeding of seed potato production by fusion of proximal and remote sensing data. Soil Tillage Res. 206, 104801. https://doi.org/10.1016/j.still.2020.104801

Munnaf, M.A., Haesaert, G., Van Meirvenne, M., Mouazen, A.M., 2020. Site-specific seeding using multi-sensor and data fusion techniques: A review, in: Advances in Agronomy. Elsevier Inc., pp. 241–323. https://doi.org/10.1016/bs.agron.2019.08.001

Naumann, M., Koch, M., Thiel, H., Gransee, A., Pawelzik, E., 2020. The Importance of Nutrient Management for Potato Production Part II: Plant Nutrition and Tuber Quality. Potato Res. 63, 121–137. https://doi.org/10.1007/s11540-019-09430-3

Nawar, S., Corstanje, R., Halcro, G., Mulla, D.J., Mouazen, A.M., 2017. Delineation of Soil Management Zones for Variable-Rate Fertilization: A Review, Advances in Agronomy. https://doi.org/10.1016/bs.agron.2017.01.003

Pierzynski, G.M., Sims, J.T., Vance, G.F., 1994. Soils and environmental quality. Lewis Publishers Inc., Boca Raton.

Rosen, C.J., Kelling, K.A., Stark, J.C., Porter, G.A., 2014. Optimizing Phosphorus Fertilizer Management in Potato Production. Am. J. Potato Res. 91, 145–160. https://doi.org/10.1007/s12230-014-9371-2

USDA-NRCS, 2014. Soil pH, Soil health-guide for educators [WWW Document]. Uninated States Dep. Agric. Resour. Conserv. Serv. https://doi.org/10.1017/CBO9781107415324.004

van Vliet, J.A., Giller, K.E., 2015. Mineral Nutrition of Cocoa: A Review, Wageningen University and research centre. https://doi.org/10.1016/bs.agron.2016.10.017

Viscarra Rossel, R.A., McGlynn, R.N., McBratney, A.B., 2006. Determining the composition of mineral-organic mixes using UV-vis-NIR diffuse reflectance spectroscopy. Geoderma 137, 70–82. https://doi.org/10.1016/j.geoderma.2006.07.004

Zhang, N., Wang, M., Wang, N., 2002. Precision agriculture - A worldwide overview, in: Computers and Electronics in Agriculture. Elsevier, pp. 113–132. https://doi.org/10.1016/S0168-1699(02)00096-0

What is needed to build a precision-and task-oriented drone for agricultural use: State-of-the-art and new perspectives

Fateme Bakhshande [a*], Dirk Söffker [b]

[a, b] Chair of Dynamics and Control University of Duisburg-Essen, Duisburg, Germany

* Corresponding author. Email: fateme.bakhshande@uni-due.de

Abstract

Using drones, referred as Unmanned Areal Vehicle (UAV), becoming increasingly common in precision agriculture for increasing crop productivity and quality because of its effectiveness and speed in operation. Agriculture drones are equipped with special sensors, data processing software, and operation instruments for pesticide spraying. The aim of this research paper is first to highlight the importance of semi-autonomous/autonomous drones in precision agriculture and elaborate on the suitable agriculture drones available in the market. Furthermore, the main hardware and software required to build an agriculture drone are elaborated in detail.

Keywords: build a drone.

1. Introduction and overview

According to Pretty et al. (2010) over the next two decades, a technological wave will revolutionize the efficiency of farms all over the world. By the year 2050, the human population will be nearly 10 billion which means doubled the amount of food will be needed. This industry has undergone major developments over the last century. In 1900, about 11 million agricultural workers produced food for 76 million people. Today, just 6.5 million workers feed 321.4 million Americans (Tomlinson (2013)). However, further innovations are necessary for the agriculture field to overcome and solve the predicted problems and issues in the future.

Nowadays, using of drones and robots is becoming increasingly common in precision agriculture for increasing crop productivity and quality because of its effectiveness and speed in operation. Robots or drones that can precisely remove weeds or shoot them with a target spritz of pesticides, using 90 % less chemicals than a conventional blanket sprayer. Tiny sensors and cameras will monitor crop growth and alert farmers on their smartphones if there is a problem or when it is the best time to harvest. The main goal is to grow and harvest without humans ever entering the field. Drones can be used in the agriculture industry for different purposes such as:

- Crop field scanning and health monitoring with compact multi-spectral imaging sensors
- GPS map establishment through on-board cameras
- Heavy payload transportation
- Livestock monitoring with thermal-imaging cameras
- Irrigation equipment monitoring
- Irrigation and pesticide spraying
- Mid-field weed identification

The main goal of this paper is to highlight and elaborate on the importance of semi-autonomous/autonomous drones in the precision agriculture field. Newest agriculture drones available in the market are introduced considering their special sensors, properties, and prices. Additionally, the main hardware and software required to build an agriculture drone are introduced in detail. Finally, the main challenges and limitations in using agriculture drones are summarized. Briefly speaking, the main goal of this literature review research is to deliberate more information about the importance of semi-autonomous/autonomous agriculture drones and to present an actual overview of the different components required for precision agriculture without the presence of humans in the farmlands.

2. Preliminary and advanced technologies for precision agriculture

Precision agriculture or smart farming is an agricultural system in which management practice is performed at the right place, with the right intensity, and at the right time to decrease the amount of nutrient and other crop inputs and to increase performance and productivity. The main tasks considered and performed for using drones in smart agriculture are shown in Fig. 1.
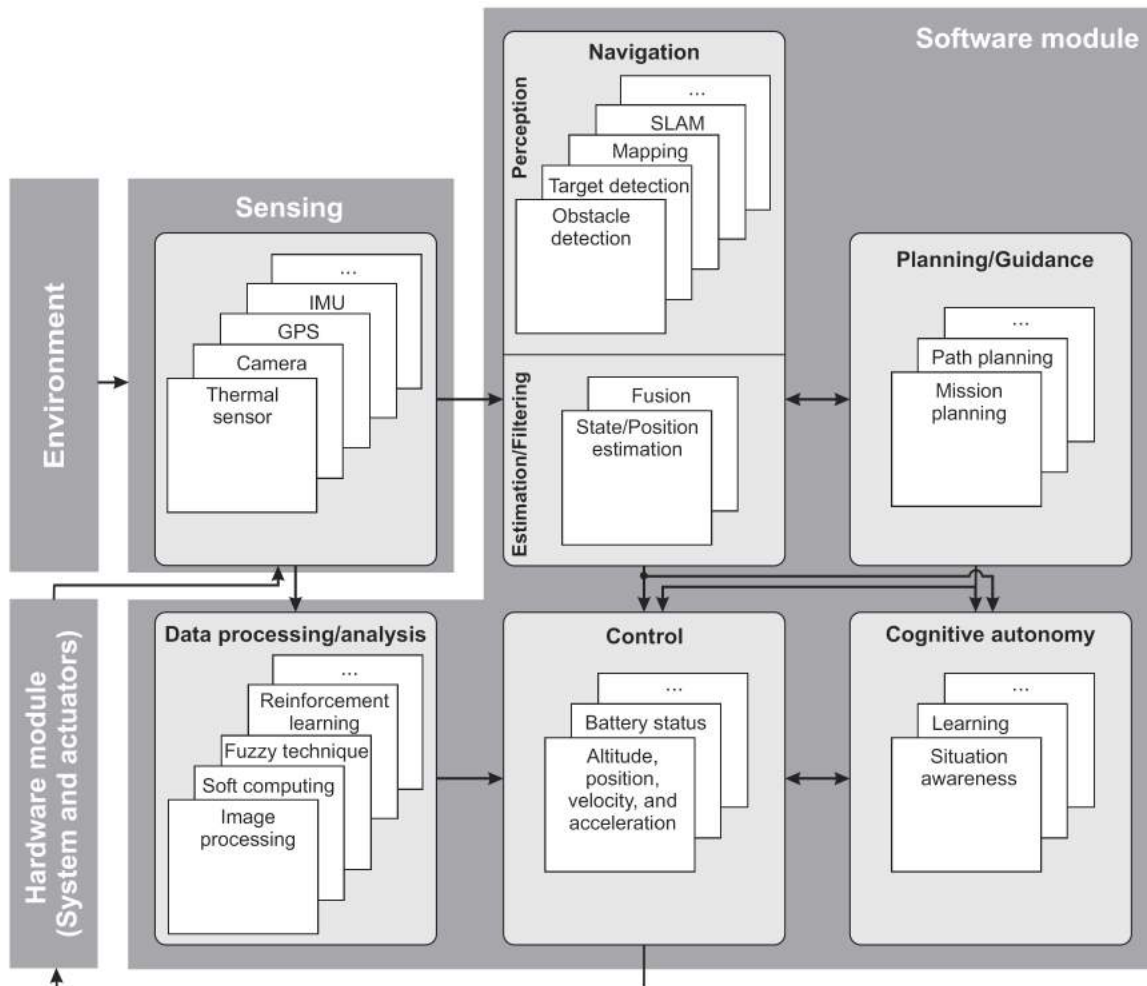
Figure 1. General overview of different modules required for semi-autonomous/autonomous drones in precision agriculture

2.1. Sensors, mapping, and data acquisition

Different sensors can be attached to drones with the purpose of precision agriculture. For instance, Pobkrut et al. (2016) used an electronic nose sensor on the drone. E-nose consists of different chemical gas sensors that can be used for different purposes such as detection of awful smell from swine farm (Lorwongtragool et al. (2010)), hazardous elements from the food industry (Lorwongtragool et al. (2011)), or quality grade identification of green tea (Yu and Wang (2007)). The remote sensing systems for drones can be divided into two main parts, namely active sensing (e.g. laser altimeter, LiDAR, radar, ranging instrument) and passive sensing (e.g. accelerometer, spectrometer, radiometer). The first category can be used for mapping while the second one is used for navigation and control purposes.

Data resources and mapping for precision agriculture can be achieved using different platforms such as (i) satellite constellations, (ii) drones, and (iii) ground-based units. Satellite data can be easily corrupted by cloud cover. Even though the ground-based sensors are less affected by environmental conditions, gathering the data is time-consuming. The drone data resources are more versatile regarding sensor types and flight timings. The images achieved using drones have higher spatial resolution compared to the satellite constellations, capable of improving water stress management in agriculture (Rudd et al. (2017)). Furthermore, drones can gather real-time thermal images to speed up the critical analysis of the crops (Khanal et al. (2017)). The thermal sensors can be used for monitoring crop stresses and diseases, soil water stress, and planning for irrigation scheduling and harvesting operations. In (Elarab et al. (2015)) thermal infrared imagery is used for estimation of chlorophyll concentration and relevance vector machines (RVM) algorithm is used to formulate spatially distributed chlorophyll concentration estimates.

Weed-crop is one of the important issues in precision agriculture. Different methods have been proposed to detect the weeds. In (Santos Ferreira et al. (2017)) Convolutional Neural Network is used to detect the weeds in soybean crop images and to classify the detected weeds among grass and broadleaf. The normalized difference vegetation index (NDVI) sensor data and post/flight image processing can be used to create the weep map. Using this map, the areas of

high-intensity weed proliferation can be distinguished from healthy crop areas (Gago et al. (2015)). The NDVI camera (a combination of an infrared camera and a typical RGB camera) can be easily mounted on the drone to facilitate crop inspection and reduce manual efforts. In (Mahajan and Bundel (2017)) NDVI is used to measure the stressed and well-watered crop as a cheaper alternative for spatial satellite sensors.

The crop health can be monitored using NDVI data in combination with other indexes such as the Crop-Water Stress Index (CWSI) and the Canopy-Chlorophyll Content Index (CCCI). The mechanism of using NDVI is that the leaves reflect a lot of light in the near-infrared (NIR) in the normal situation. In the case that the plant is dehydrated or stressed the amount of NIR reflects by the leaves reduces despite the fact that the amount of reflection in the visible range remains the same. Therefore, using these two signals (RGB and NDVI) helps to differentiate a plant from non-plant and healthy plants from the sickly plants. Multispectral sensors are another type of drone sensor that can be used to detect invisible objects in the visual spectrum, such as wet patches on the ground (Tu et al. (2019)).

Solving the localization problem for the drone system means estimating the drone pose (state) with respect to a map of the environment. Localization is an important part of drone navigation besides perception, cognition, and motion control. This process can be done using the Kalman filter. A more difficult subclass of localization is when no map is available from the environment. In this case, the sensor information is used to build a map from the environment and to localize the drone in this map simultaneously. The SLAM techniques, implemented successfully on mobile robots, can be developed for drones to enhance their autonomous navigation and exploration capacity (Stumberg et al. (2017)). In (Dijkshoorn (2012)) two maps are produced by the AR. Drone namely feature map and texture map. The feature map is used by drones for localization purposes and the texture map is used for human navigation. An extra elevation map is derived using an ultrasound sensor to be combined with the texture map.

2.2. Data processing and analysis

Data processing and analyzing, namely translating the high-resolution images into the information that can be used for agriculture purposes, is one of the most challenging parts of the agriculture drone process. The operators need to analyze and process hundreds of visual, thermal, and multi-spectral images to detect and identify changes in crop health. Image processing and machine learning techniques are powerful tools that help farmers to enhance the data processing procedure.

In (Zhou et al. (2012)) a recognition algorithm based on color features is used to early predict the apple yield by using two different color models for segmenting the ripening period apple images. The super-pixel clustering is used to divide the leaf image into a few compact super-pixels to be used by the K-means clustering approach to segment the lesion image from each super-pixel with the purpose of disease detection. Different studies conducted using image processing together with different techniques like machine learning, deep learning, and artificial intelligence approaches. In (Liu et al. (2016)) the aphids in wheat fields are detected using computer vision techniques. Patricio and Rieder (2018) summarized a general review of the application of computer vision and artificial intelligence techniques in precision agriculture.

2.3. Flight planning, control, and navigation

Flying the drone based on a pattern over the desired field needs to be performed by software that can combine the captured sensor information across the field with geo-referenced to make it possible for the users to get walk into the field and inspect specific problem areas. However, successfully using drones to fly over the field is challenging mainly because of the limited resources (battery autonomy, onboard memory, and processing load). To improve resource utilization 'path planning' is taking into account. On the other side, drones have to be able to avoid collisions with moving obstacles to have a safe operation. In the case of dynamic obstacles, the time dimension is added to the space configuration, and planning is termed 'motion planning' or 'trajectory planning'. The goal is to reach the final target position in a specific time besides minimizing or removing the risk of collision. If perfect information about the dynamic or static obstacle is available, then safe path planning can be constructed by solving an optimization problem using different algorithms like Particle Swarm (Patley et al. (2019)). In (Rokhsaritalemi et al. (2018)) path planning has been considered during the generation of high-resolution 3D urban models. The geometric information system (GIS) is used to determine the best trajectory for the drone.

The GIS can be used for capturing, storing, manipulating, and analyzing spatial and geographic data. In (Lin and Saripalli (2017)) motion model is used to simulate the trajectory of drone besides the trajectories of dynamic obstacles for identifying the potential of collisions. The collision-free trajectories are stored for a fixed amount of time and the shorter one is selected finally as the collision free trajectory.

The drones are remote-controlled devices without any onboard human pilot. The pilot controls the drone via a ground control station through wireless and gets the sensor information via wireless linkages. The drones can be controlled manually or programmed to be operated automatically or fully autonomous. Real-time control of the drones includes take-off, landing, flight mode, hovering mode, and safety in each operation mode. All the aforementioned modes require the main information of the drone such as real-time data on the flight path, position, altitude, aircraft

performance, and battery life. The information from different sensors can be fused by using different approaches like the Kalman filter to achieve the real-time position and altitude of the drone without influence from measurement noise or data lost during the flight. For instance, in (Guerra et al. (2018)) different features of vision and laser sensors are combined for inspection and monitoring operation in industrial applications when the environment is not accessible for humans. The LiDAR sensor is used in this contribution as a range finder sensor with great robustness at the detection and segmentation task. In agriculture, the LiDAR sensor can be used to create a high-resolution topographic map of the fields for further purposes such as determining where to apply costly fertilizer.

The State-Dependent Riccati Equation (SDRE) nonlinear filtering is used by Nemra and Aouf (2010) as an alternative to extended Kalman filter for the sensor fusion task and the information of inertial navigation systems (INS) and global positioning systems (GPSs) are fused to improve the overall sensing system. Furthermore, soft computing approaches are used in the literature as fusion techniques for different sensor information. In (Bostanci et al. (2018)) a novel fuzzy logic-based motion model prediction method is proposed to fuse the information of motion estimation from vision-based measurements, GPS, and IMU to improve the tracking accuracy in outdoor environments.

The autonomous drone has to be able to translate the human commands (i.e. the desired altitude, perform a circular trajectory, maintain the current position) to the control signals namely pitch, roll, yaw angles, or speed and follow the trajectory that comes from the flight planning module. It should also be able to react autonomy for example in the case of perturbations (such as wind or any electromechanical failure) it should be able to keep the predefined trajectory, avoid obstacles, maintain the safety issues such as predefined distance to the ground, and safe take-off and landing. The drone can be equipped with cognitive autonomy capacities like performing simultaneous localization and mapping, resolving conflicting information, planning for battery recharge, object recognition, and learning new situations. These levels of autonomy are introduced in (Floreano and Wood (2015)). Open research fields in this part are related to achieving a fully autonomous drone able to make a 3D high-resolution map from the environment besides collision avoidance in the agriculture field. What has been done before is mostly related to semi-autonomous drones (Otto et al. (2018)).

3. Build your own agriculture drone

The existing agriculture drones in the market are divided into fixed-wing and multi-rotors. Common agriculture drones are equipped with sensors, hardware, and software required for the precision of agriculture. The average price for complete, ready-to-fly agriculture drone systems in the market can be estimated in the range from $5000 to well over $25000 (see Table 1). The main goal of this section is to introduce the conceptual procedure to build up an agriculture drone from a low-cost everyday drone. For this purpose, the standard drones with the known sensors (e.g. gyroscope, accelerometer, magnetometer, ultrasound), cameras (front and down-facing), and motors are taking into consideration (like original Parrot Ar.drone 2.0 up to $200). In Fig. 2 the main components required to build an agriculture drone are illustrated. The standard drones are equipped with control and communication boards that can be used for flight control and sensor data transfer. Arduino or Raspberry Pi can be used to interactively communicate with the drone, getting the sensor's information, controlling the drone, and analyzing the data (up to $100). Additional sensors for agriculture purposes can be installed on the drone and connected to the control board (like NDVI, NIR, or multispectral sensors, up to $400). MultiWii is an open-source software project to be used as the brain of RC controlled multi-rotor flying platform. This software is compatible with several hardware boards and sensors and can easily be used on the Arduino or Raspberry Pi platforms (Ebeid et al. (2018)).

In Price (2018) construction of a sprayer drone is proposed. The free open-source software (https://diydrones.com) is used to hold the height and position of the drone to the exact levels with a good range finder including builtin sprayer functions. Additionally, available sprayer kits (http://www.innofpv.com) including landing gear frame, boom, pump, and nozzles is used with the price of $250 able to operate at 8- to 10-foot flying height. According to the recent article written by Price (2018) sprayer and plant-protection drones to apply pesticides to small land areas and acreages cost $15,000 or more. This type of drone can operate in those areas that are inaccessible or hardly accessible by humans. The main problem of using this type of drone is the limitation in the amount of liquid that can be carried by the drone. Summarizing the price information above, the whole agriculture drone equipped with special sensors and spraying tools costs under $1000 which shows a big difference in the price compared to the ones on market (see Table 1).
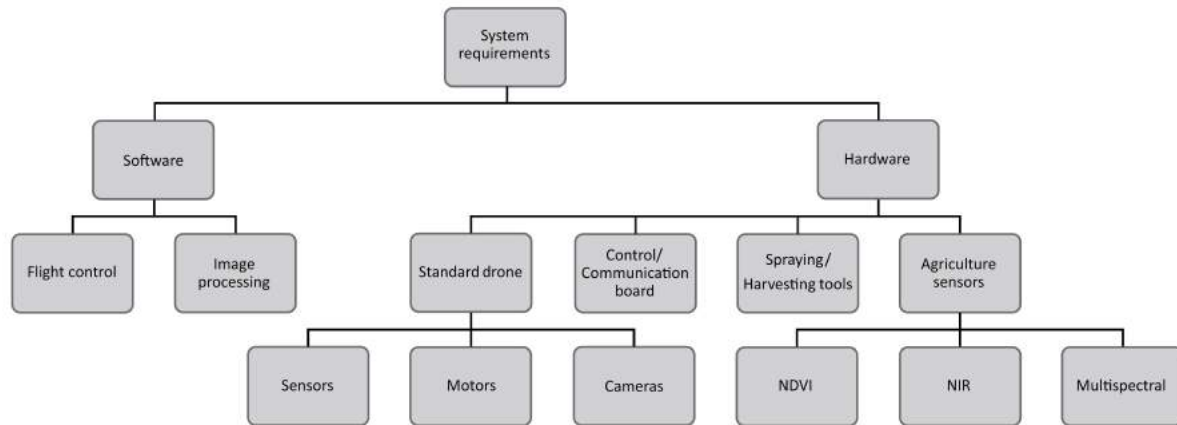
Figure 2. Required equipment to build a (simple) agriculture drone for precision agriculture

4. Main challenges and limitations

As the use of agricultural drones increases, their challenges and limitations become larger and more precise. One of the most challenging issues in precision agriculture and specially using drones is storing, processing, and analyzing of big data. The following dimensions are defined by Chi et al. (2016) to characterize agriculture big data:

- **Volume (quantities of data)**: Size of the data to be analyzed
- **Velocity (real-time applicability)**: Time window that the data is useful and relevant
- **Variety (various heterogeneous sources)**: Multisource, temporal, resolution, and format data
- **Veracity(quality of data)**: Accuracy and reliability

In (Kamilaris et al. (2017)) the authors summarized almost 30 papers and accordingly categorized the gathering data based on the first three levels (volume, velocity, and variety) using three indicators low, medium, and high. For example, remote sensing data (using drones) has high, medium, and medium ranking for volume, velocity, and variety correspondingly. In the mentioned paper common software tools for big data analysis in agriculture are introduced for different applications like image processing tools, machine learning tools, statistical tools, etc.

One of the main limitations of using autonomous or semiautonomous drones in the agriculture field or other application fields is privacy and security issues. As mentioned before drones can be used in different applications like inspection and monitoring, aerial imaging, surveying and mapping, civil engineering, military, and of course precision agriculture. The Federal Aviation Administration (FAA) has defined the certificate of authorization with a provision for Beyond Visual Line of Sight (BVLOS) for the public safety organization in the US. Other countries also address privacy protection and clauses in the use of drones. However keeping legislation up to date with drone technology, which is growing very fast, is always a challenge.

Besides privacy issues, safe behavior assurance for the autonomous and semi-autonomous aerial systems should be taking into consideration. According to (Hägele and Söffker (2019)) system safety assurance can be realized based on hazard detection, risk estimation, and system adjustment using safety instrumented systems (SIS). The SIS is used to implement one or more safety instrumented functions and consists of any combination of sensor(s), logic solver(s), and final element(s). The FAA provides preflight assessment including risk mitigation actions. This assessment ensures that in the case of losing control or other safety issues the drone produces no hazard to the other aircraft or people. More information can be found in (Belcastro et al. (2017)).

Table 1. Agricultural drones: World market and prices

	Agriculture drones	Price $	Sensors	Additional features
	senseFly eBee SQ	12,000	- Four spectral bands RGB - Multi-spectral sensor	- Image processing software - Topography/3D mapping (limited/not survey quality) - Flight planning and management
Fixed wing	PrecisionHawk Lancaster 5	25,000	- Multispectral sensor - Lancaster carries on-board sensors	- Measuring the humidity, temperature, and air pressure - Artificial intelligence to react to changing weather conditions, payload, wind loads, etc. - Flight planning & control
	AgDrone by HoneyComb	10,000	- NDVI - Visual stereoscopic - NIR (thermal imaging)	- Flight planning/control software - Equipped with an advanced autopilot system
	Sentera Phoenix 2	18,000	- RGB visual - NIR - NDVI, live streaming NDVI	- Near-real time reading and analysis of the data
	Trimble UX5	25,000	- Superior multispectral image quality with the MicaSense RedEdge - Downwelling light sensor	- Fight plan - Change landing location during flight - Self-check and failsafe procedures - Automatic takeoff, flight, and landing
Multi rotor	PrecisionHawk Crop Scouting Package (including Phantom 4 PRO)	2,000	- Visual sensors - No multispectral sensor to capture NDVI data	- Flight & image processing software - Sentera NDVI Upgrade for about $3,000 - Starter-level quadcopter package
	DJI Smarter Farming Package	8,300	- Visual sensor - Multispectral sensor	- Image processing package
	AGCO Solo	7,850	- GoPro Hero 4 camera for color imaging - GoPro near-infrared camera for monitoring plant health	- Auto take off and landing
	Sentera Omni Ag	16,995	- High resolution RGB visual - NIR - NDVI, live streaming NDVI	- Image processing package

5. Summary and conclusion

In this paper a general overview of autonomous drones is elaborated with the focus on precision agriculture drones. The best agriculture drones available in the market are introduced besides all the expenses to be paid to improve crop productivity and quality. Additionally, the main hardware and software required to build an agriculture drone are introduced in detail to decrease the costs for those who are interested in building their own agriculture drone. The main challenges and limitations in using agriculture drones are summarized to demonstrate that with the development of UAVs, although much progress is being made in different fields, on the other hand, it leads to greater constraints and problems like storing, processing, and analyzing of big data or privacy and security issues.

References

Belcastro, C.M., Newman, R.L., Evans, J., Klyde, D.H., Barr, L.C., and Ancel, E. (2017). Hazards identification and analysis for unmanned aircraft system operations. In 17th AIAA Aviation Technology, Integration, and Operations Conference, 3269.

Bostanci, E., Bostanci, B., Kanwal, N., and Clark, A.F. (2018). Sensor fusion of camera, GPS, and IMU using fuzzy adaptive multiple motion models. Soft Computing, 22(8), 2619–2632.

Chi, M., Plaza, A., Benediktsson, J.A., Sun, Z., Shen, J., and Zhu, Y. (2016). Big data for remote sensing: Challenges and opportunities. Proceedings of the IEEE, 104(11), 2207–2219.

Dijkshoorn, N. (2012). Simultaneous localization and mapping with the AR. drone. Masters thesis, Universiteit van Amsterdam.

Ebeid, E., Skriver, M., Terkildsen, K.H., Jensen, K., and Schultz, U.P. (2018). A survey of open-source UAV flight controllers and flight simulators. Microprocessors and Microsystems, 61, 11–20.

Elarab, M., Ticlavilca, A.M., Torres-Rua, A.F., Maslova, I., and McKee, M. (2015). Estimating chlorophyll with thermal and broadband multispectral high resolution imagery from an unmanned aerial system using relevance vector machines for precision agriculture. International Journal of Applied Earth Observation and Geoinformation, 43, 32–42.

Floreano, D. and Wood, R.J. (2015). Science, technology and the future of small autonomous drones. Nature, 521(7553), 460.

Gago, J., Douthe, C., Coopman, R., Gallego, P., Ribas Carbo, M., Flexas, J., Escalona, J., and Medrano, H. (2015). UAVs challenge to assess water stress for sustainable agriculture. Agricultural water management, 153, 9–19.

Guerra, E., Munguia, R., and Grau, A. (2018). UAV visual and laser sensors fusion for detection and positioning in industrial applications. Sensors, 18(7), 2071.

Hägele, G. and Söffker, D. (2019). Risk areas determination for autonomous- and semi-autonomous aerial systems considering run-time technical reliability assessment. In Journal of Intelligent & Robotic Systems, 97(3), 511-529.

Kamilaris, A., Kartakoullis, A., and Prenafeta-Boldu, F.X. (2017). A review on the practice of big data analysis in agriculture. Computers and Electronics in Agriculture, 143, 23–37.

Khanal, S., Fulton, J., and Shearer, S. (2017). An overview of current and potential applications of thermal remote sensing in precision agriculture. Computers and Electronics in Agriculture, 139, 22–32.

Lin, Y. and Saripalli, S. (2017). Sampling-based path planning for UAV collision avoidance. IEEE Transactions on Intelligent Transportation Systems, 18(11), 3179–3192.

Liu, T., Chen, W., Wu, W., Sun, C., Guo, W., and Zhu, X. (2016). Detection of aphids in wheat fields using a computer vision technique. Biosystems Engineering, 141, 82–93.

Lorwongtragool, P., Wisitsoraat, A., and Kerdcharoen, T. (2011). An electronic nose for amine detection based on polymer/swnt-cooh nanocomposite. Journal of Nanoscience and Nanotechnology, 11(12), 10454–10459.

Lorwongtragool, P., Wongchoosuk, C., and Kerdcharoen, T. (2010). Portable artificial nose system for assessing air quality in swine buildings. In ECTI-CON2010: The 2010 ECTI International Confernce on Electrical Engineering/Electronics, Computer, Telecommunications and Information Technology, 532–535. IEEE.

Mahajan, U. and Bundel, B.R. (2017). Drones for normalized difference vegetation index (NDVI), to estimate crop health for precision agriculture: A cheaper alternative for spatial satellite sensors. In International Conference on Innovative Research in Agriculture, Food Science, Forestry, Horticulture, Aquaculture, Animal Sciences, Biodiversity, Ecological Sciences and Climate Change (AFHABEC-2016), At Jawaharlal Nehru University.

Nemra, A. and Aouf, N. (2010). Robust ins/gps sensor fusion for UAV localization using SDRE nonlinear filtering. IEEE Sensors Journal, 10(4), 789–798.

Otto, A., Agatz, N., Campbell, J., Golden, B., and Pesch, E. (2018). Optimization approaches for civil applications of unmanned aerial vehicles (UAVs) or aerial drones: A survey. Networks, 72(4), 411–458.

Patley, A., Bhatt, A., Maity, A., Das, K., and Ranjan Kumar, S. (2019). Modified particle swarm optimization based path planning for multi-UAV formation. In AIAA Scitech 2019 Forum, 1167.

Patricio, D.I. and Rieder, R. (2018). Computer vision and artificial intelligence in precision agriculture for grain crops: A systematic review. Computers and Electronics in Agriculture, 153, 69–81.

Pobkrut, T., Eamsa-Ard, T., and Kerdcharoen, T. (2016). Sensor drone for aerial odor mapping for agriculture and security services. In 2016 13th International Conference on Electrical Engineering/Electronics, Computer, Telecommunications and Information Technology (ECTI-CON), 1–5. IEEE.

Pretty, J., Sutherland, W.J., Ashby, J., Auburn, J., Baulcombe, D., Bell, M., Bentley, J., Bickersteth, S., Brown, K., Burke, J., et al. (2010). The top 100 questions of importance to the future of global agriculture. International journal of agricultural sustainability, 8(4), 219–236.

Price, R.R. (2018). Build your own sprayer drone. LSU AgCenter Dean Lee Research and Extension Center.

Rokhsaritalemi, S., Sadeghi-Niaraki, A., and Choi, S.M. (2018). Drone trajectory planning based on geographic information system for 3d urban modeling. In 2018 International Conference on Information and Communication Technology Convergence (ICTC), 1080–1083. IEEE.

Rudd, J.D., Roberson, G.T., and Classen, J.J. (2017). Application of satellite, unmanned aircraft system, and ground-based sensor data for precision agriculture: a review. In 2017 ASABE Annual International Meeting, 1. American Society of Agricultural and Biological Engineers.

Santos Ferreira, A., Freitas, D.M., Silva, G.G., Pistori, H., and Folhes, M.T. (2017). Weed detection in soybean crops using convnets. Computers and Electronics in Agriculture, 143, 314–324.

Stumberg, L., Usenko, V., Engel, J., Stückler, J., and Cremers, D. (2017). From monocular slam to autonomous drone exploration. In 2017 European Conference on Mobile Robots (ECMR), 1–8. IEEE.

Tomlinson, I. (2013). Doubling food production to feed the 9 billion: a critical perspective on a key discourse of food security in the UK. Journal of rural studies, 29, 81–90.

Tu, Y.H., Johansen, K., Phinn, S., and Robson, A. (2019). Measuring canopy structure and condition using multispectral UAS imagery in a horticultural environment. Remote Sensing, 11(3), 269.

Yu, H. and Wang, J. (2007). Discrimination of longjing green-tea grade by electronic nose. Sensors and Actuators B: Chemical, 122(1), 134–140.

Zhou, R., Damerow, L., Sun, Y., and Blanke, M.M. (2012). Using colour features of cv.'gala'apple fruits in an orchard in image processing to predict yield. Precision Agriculture, 13(5), 568–580.

Development of the Technical Structure of the "Cow Energy" Concept

Heinz Bernhardt [a,*], Jörn Stumpenhausen [b]

[a] Agricultural System Engineering, Technical University of Munich, Freising, Germany

[b] Department of Sustainable Agriculture and Energy Systems, University of Applied Sciences Weihenstephan Triesdorf, Freising, Germany

* Corresponding author. Email: heinz.bernhardt@wzw.tum.de

Abstract

Regional energy supply is an important topic in the context of the energy transition in Germany. The "CowEnergy" project aims to combine the production of energy and milk for the farmer. In order to take the different needs into account, a central energy management system (EMS) is being established. This system records and simulates how much electricity is generated from renewable sources (biogas, solar, wind, etc.) on the farm. This is compared with the consumption of the barn technology (milking robot, feeding robot, etc.). This energy management is regulated according to the needs of the cows. In order to balance the fluctuations between energy production and energy consumption, the EMS regulates various battery systems. One goal is to network this energy system with the region and to establish regional energy networks.

Keywords: energy management, regional grids, energy storage, energy simulation, dairy barns.

1. Introduction

The energy transition poses multiple challenges for Germany. In order to convert the previous centralised energy producers based on nuclear energy and coal to renewable energy, regionalised energy production is necessary. This also offers corresponding opportunities for agriculture. There is thus the possibility of coupling a regional resource-oriented energy supply with the social demands for modern, sustainable and animal welfare-oriented dairy cattle stables. This complex of topics is to be the focus of the "CowEnergy" research initiative.

The research concept envisages designing integrated milk and energy production (Integrated Dairy Farming) for dairy farms and installing it on pilot farms, whereby synergy potentials are to be optimally utilised through goal-oriented networking.

New barns must meet increased requirements in terms of labour management, ethology, resource efficiency, ecology and economy. In practice, this leads to a high degree of automation (milking robots, feeding robots, disposal technology, climate control, etc.) in dairy farming. At the same time, agricultural animal husbandry is predestined for the production of renewable energies like no other economic sector.

The complexity of this system leads to the demand for communication between the system elements, analogous to industrial cyber-physical production systems "Industry 4.0". The special features of dairy production result in very specific technical requirements for such a comprehensive energy management system with special consideration of the animal-technology-human interactions. In addition, an intelligent load management system must be developed that enables integration into an agricultural-specific demand side management system so that the farm can act as an energy source and sink for regional suppliers and thus support the development of decentralised, remunicipalised power generation.

2. Materials and Methods

Overall, the research initiative provides for a holistic approach to the further development of dairy farming systems. The essential components of CowEnergy are:

- Barn automation and central control of the systems
- Energy efficiency and use of various energy storage solutions
- integration into the regional power supply to serve the grid
- Sustainable barn construction
- Safeguarding food quality and animal health
- Animal welfare criteria and ethical aspects
- Impact on agriculture and rural regions in southern Germany

The conception and realisation of the Energy Management System (EMS) necessary for this from a technical point of view is one of the decisive challenges of the research and development projects. (Figure 1)
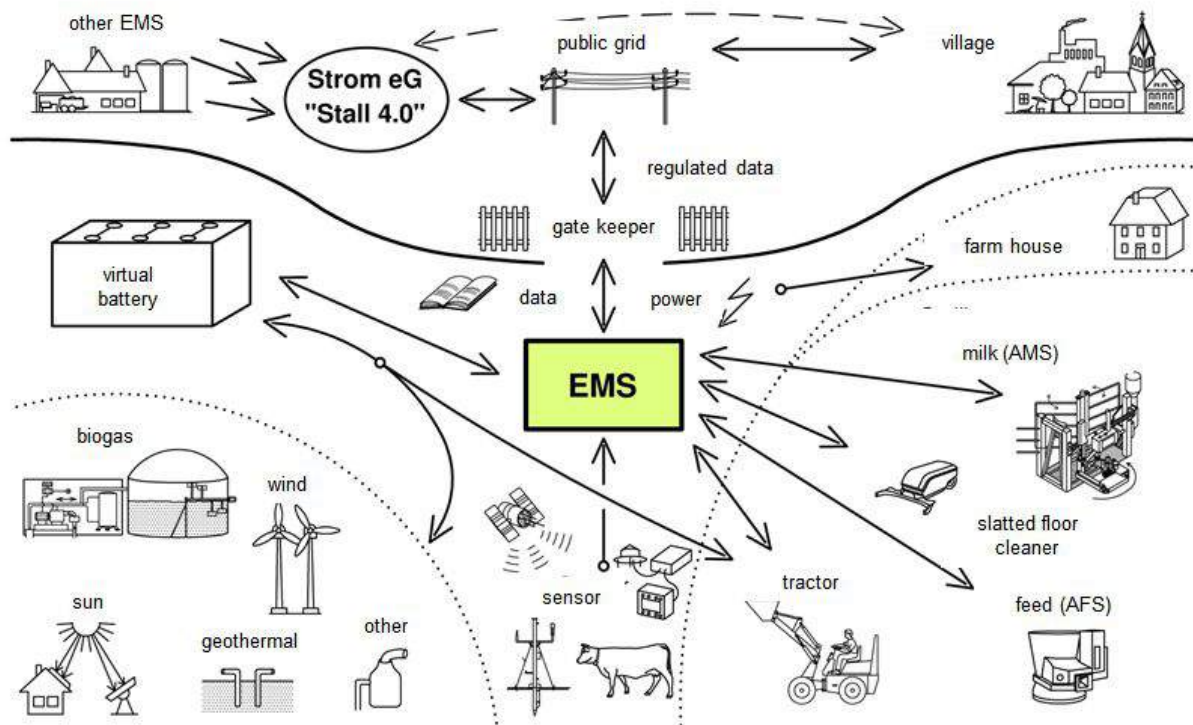
Figure 1. Energy Management System.

The energy and production management system should enable a balanced and sustainable production of energy and milk at the same time. The innovation in agricultural technology thus created serves to increase resource efficiency. By analysing the data of existing sensors and new sensors to be integrated into the overall system, decision-making algorithms for the effective control of the EMS are to be created using Big Data analysis. In the context of agricultural production, milk and meat as well as regenerative energy are to be produced. On the one hand, this energy will be used for self-sufficient self-sufficiency and on the other hand to cover the demand of a regional energy supply network.

3. Results and Discussion

The development of this intelligent self-controlling energy management system is the focus of this research project. The system must collect a large amount of data from a wide range of areas and in a wide range of structures. In the area of barn components, energy consumption and work structures are recorded as characteristic values. It becomes apparent that here, in contrast to arable farming, there is no uniform data interface in the form of the ISOBUS standard. Each system such as milking robot or feeding robot are self-contained. Therefore, all information important for the process must be collected via a separate sensor network. The machine's own sensors can only be used to a limited extent. This naturally limits the functionality. The lowest level of functionality is therefore considered to be switching on and off and recording energy consumption. In contrast to common practice, the energy consumption must be recorded every 10 seconds and not every 15 minutes, so as not to undermine the energy management system (EMS) through high, unrecorded start-up currents. In the area of energy generation via biogas, wind turbines, solar energy and others, the recording is easier because sensor networks from the industrial sector are often used here, for which corresponding interfaces already exist. However, a general standard does not exist here either and every system is put together differently. The power data is recorded here.

In order to balance energy consumption and energy generation, the respective values in the EMS must be planned in advance via simulations. Weather forecasts, barn climate data and data from the dairy cows in particular are used as planning data (Höhendinger, 2018a). Due to the extensive automation of the barn technology, the power consumption is balanced. With AMS, there is an even power demand throughout the day and there are no longer the two power peaks as with the milking parlour. Thus, a power requirement for the individual consumers can be planned in advance

throughout the day. The individual regenerative energies can be planned differently. Biogas enables a steady and constant energy supply, but can also be used as an energy store. Solar energy is only produced during the day when the sun is shining. So for short-term planning over three days, a weather forecast is always necessary. The weather forecast is also necessary to plan for the loss of solar energy due to snow on the modules. When setting up the photovoltaic system, the modules were oriented to the east and west. This reduces the peak power, but leads to more energy yield in the morning and evening hours, which again balances out the energy production. In the case of wind energy, the approach is also to plan ahead using weather forecasts. The third factor to be mentioned in the simulation, in addition to energy consumption and energy production, are the cows. In the case of the cows, this is particularly the individual animal performance data, which is transferred from the herd management systems via an interface. In addition, the animals' behavioural data is recorded individually. These are movement activity via pedometer, chewing activity, animal position via a positioning system and also possibly body temperature and rumen pH value via a bolus. These data are mostly used for short-term planning.

From this data, the EMS can predict behavioural structures of individual cows and cow herds and thus draw conclusions about the future energy demand of the barn components. If, for example, many cows are lying in the cubicles, it would be a good time for the slat cleaning robot to clean the then empty walkways. The energy needed for this must be available via the energy production or storage units. (Figure 2)
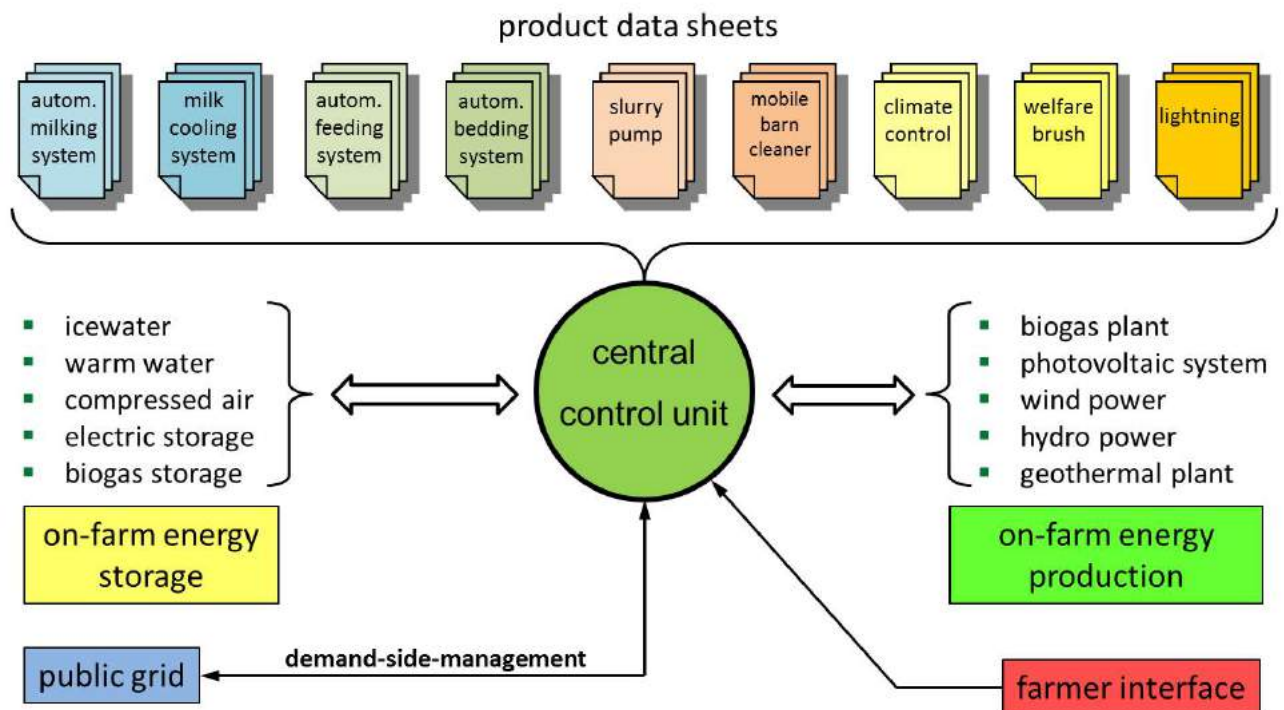
Figure 2. Simulation data for EMS.

The EMS also offers the possibility to better coordinate the individual robots. For example, it is possible to block the cleaning robot at the feeding area when the feeding robot presents new feed. In this way, the systems can be coordinated with each other.

The recording of energy consumption, energy supply and animal data represents the barn level of the EMS. Since the energy generators in the barn are designed in such a way that they produce more energy on average than the barn alone needs, the rest can be fed into the municipal grid. For a secure regional electricity supply, storage and power purchase are therefore also of crucial importance. For grid-serving integration into the power supply network, the farm offers a variety of possibilities due to its different forms of energy. The algorithms to be developed for the EMS control the various storage systems. Classic batteries are available as short-term storage - as stationary accumulators or in mobile implements; here, electricity can be stored for a few hours. As medium-term storage, ice water can be used for milk cooling. Here, the storage period is one to two days. As a long-term storage facility, biogas can be used during the day, which can be converted into electricity as needed. Other storage facilities for emergencies are, for example, the energy reserves of hybrid vehicles. The task of the EMS in the central storage control system is to distribute the energy

flows between the individual storage units and to manage them according to demand and supply.

Internally, the EMS can also be used to optimise own power consumption. For example, in the test operation, the electrically driven feed mixer is only needed at two fixed times per day, in between which it can be charged. This charging process can now be controlled by the EMS so that it is only charged when there is a surplus of energy. The EMS also takes into account that the feed mixer wagon must be charged at a certain time. If not enough energy is generated during the charging period, the EMS can use its own storage in time or use energy from the grid, depending on what makes more economic sense.

With the help of the storage facilities, an offer can also be made to the regional energy suppliers via the operational level. The EMS coordinates with the regional energy supplier via a data gatekeeper. The latter can make requests to the EMS for the supply, storage or absorption of energy. The energy supplier does not have direct access to the energy production, as is currently the case, for example, with the decoupling of biogas plants, but the EMS coordinates these requests. In doing so, the EMS proceeds according to a decision hierarchy. First, the energy demand for the dairy cows is forecast from the collected data. There are components such as the AMS, who's switching off has a considerable impact on animal welfare and must therefore be avoided, and components such as the slat cleaning robot or the cow brush, which can be shifted within certain limits if necessary. These shifts then lead to a change in prioritisation; these shifts are always only possible over certain periods of time. This expertise and decision-making basis are integrated into the EMS via algorithms to be defined. Subsequently, the energy storage level, the storage combined in a virtual battery and the simulated energy generation potential are included in the calculation. The EMS then decides how far the requests can be satisfied without straining the operational energy management.

Since the data exchange with the energy suppliers is continuous and a wide variety of requests for delivery, storage and consumption of energy can arise at very short notice, correspondingly high data query rates must be run for a good simulation and decision-making basis for the EMS, which requires a corresponding data connection (Höhendinger, 2018b).

As an additional benefit, the EMS offers the farm manager the possibility to be continuously informed about the current process and energy status of the barn, to use documented data as planning data for farm development and to ensure the legal and market requirements of traceability of products and processes.

4. Conclusions

Since the EMS shows that battery systems are fundamentally necessary to compensate for fluctuations in renewable energies, this is a future field of work. An interesting approach is the multiple use of energy storage in electric machines, such as feed mixers or wheel loaders. These machines are often only used for 4 hours a day. This means that 80% of the time the battery could be used in the energy storage system. Two developments are necessary for this. The current charging system must be further developed into a bidirectional charging and discharging system and it would be good if these systems were standardised to enable universal use.

Additional energy storage systems should also be analysed in agriculture. One possible approach would be a heat exchanger in the slurry tank.

The use of EMS also offers possibilities in other farm types besides dairy cattle. Pig and poultry farming would be further possible applications. Here, however, flexibility does not play such a large role, as the processes here are even more uniform. One main aspect here is the reliable provision of emergency power.

Another expansion step is the cooperation of several farms with EMS to form an energy cooperative. Here, energy peaks between individual farms could be balanced out. The use of biogas for energy storage would then also become easier, as the balancing in the grid would reduce the start and stop cycles. The next expansion step would then be integration in villages. Here, the generated electricity could be stored temporarily, since farms usually have better possibilities for energy storage than single-family homes. In addition, there is the possibility of integrating the regional black start capability for the energy grids into the farm. For these energy cooperatives, however, a further development of the existing legal and fee structure for energy supply and grid transmission is still necessary.

Acknowledgements

References

Höhendinger, M.; Wörz, S.; Krieg, H.J.; Dietrich, R.; Frech, L.; Stumpenhausen, J.; Bernhardt, H. 2018a. Integration of weather influences into an on-farm energy management system, 46. Symposium „Actual Tasks on Agricultural Engineering", Opatija, Kroatien

Höhendinger, M.; Stumpenhausen, J.; Wörz, S.; Krieg, H.-J.; Dietrich, R.; Frech, L.; Bernhardt,H. 2018b. Einbindung externer Datenquellen und Komponenten in ein On-Farm Energiemanagementsystem, 38. GIL-Jahrestagung: Digitale Marktplätze und Plattformen, 26.-27 Februar 2018, S. 107-110, Kiel

State-machine Based Model for Estimation and Prediction of Above-ground Biomass in Corn During Vegetative Stage

Lina Owino [*], Dirk Söffker

[a] Chair of Dynamics and Control, University of Duisburg-Essen, Duisburg, Germany

* Corresponding author. Email: lina.owino@uni-due.de

Abstract

Ensuring optimal yield from a corn crop requires information about the growth and development of the plants at various stages. Plant biomass measurements offer in combination with models (such as FAO Aquacrop) the option for predictive indication of expected yield, allowing timely decision making with regard to resource allocation. Existing biomass estimation models are primarily targeted at forecasting of biomass at harvest, generating a cumulative value which does not allow intermediate estimates at different phases of crop growth. This makes them unsuitable for applications requiring continuous monitoring and/or real time intervention.

An existing state machine model employed to predict total leaf length in growing corn plants is expanded through the inclusion of leaf width measurements to allow improved estimation of biomass. This is necessitated by the wider applicability of biomass to assess plant growth compared to leaf length. The model is trained using experimental data obtained from corn plants grown in an indoor greenhouse under varying irrigation conditions. Above ground biomass is estimated using leaf length and width measurements. A modification of the original model is introduced, retaining the leaf length estimations and applying a linearized model to describe the relationship between total leaf length and biomass.

The model accuracy is evaluated through comparison with estimates made using the FAO Aquacrop model for corn growth as well as comparison with actual values obtained from sampled plants harvested during the growth experiments.

The large errors produced by the directly trained model are alleviated by the introduction of a linearized model working with leaf length estimates generated by the state machine model. The composite model generates a continuous progressive estimation of above ground biomass of corn plants during the entire vegetative stage, allowing for monitoring of crop growth, timely intervention as required as well as early projection of final yield.

Keywords: Deficit irrigation, growth modeling, biomass estimation, finite state machine.

1. Introduction

The production and consumption of maize has shown an upwards trend over the years, with a constant demand for human consumption in addition to a rising demand for animal feed and commercial uses (Ranum et al., 2014). To meet the constantly increasing demand, greater efficiency in the use of limited resources such as land, water, and fertilizer is necessary. A key requirement in the achievement of higher levels of efficiency is receiving accurate information regarding the status of the crop both during the growing period and at harvest time. Biomass is one of the key indicators used by maize producers to assess the growth and development of the growing crop throughout its growth stages.

The growth and development of maize had been described by a number of growth models, with the most commonly used such as WOFOST (Diepen et al.,), and CERES-MAIZE (Jones and Kiniry, 1986) and its variants such as APSIM (Keating et al., 2003), CSM-IXIM (Lizato et al., 2011) requiring comprehensive data on the climate, soil, genotypes and management to simulate crop growth during an entire growth cycle. Further developments have seen rise to simplified models, primarily relying on characterization of maize growth and development as a function of thermal time (Yang et al., 2004, Kim et al., 2012). The effect of climatic variations on the reliability of maize growth models has also been explored (Bassu et al., 2014), with an emerging concern that changes in temperature and CO_2 levels have a significantly high impact on the performance of crop growth models so as to necessitate further research in how to adapt the models to varying conditions. Additionally, constraints to freshwater resources and the accompanying extensive adoption of deficit irrigation require a shift in growth modeling approaches to account for the effect of water stress and recovery on biomass accumulation in C4 plants such as maize (Ma et al., 2017).

Estimation approaches based on imaging are also a key area of research interest, with studies involving use of RGB and infrared photographs (Sakamoto et al., 2012, Calou et al., 2019), LIDAR (Li et al., 2015, Wang et al., Jin et al., 2020). Prediction of biomass on a larger scale is achieved by use of satellite imagery (Herbei and Sala, 2016, Battude et al., 2016). While certainly advantageous for extensive fields, application on small scale, and particularly indoors is at the moment still an open area of study.

To exploit the advantages of precision irrigation and its potential for facilitating not just the monitoring and

management, but also the control of growth and development in plants, it is necessary to explore growth models that give adequate weight to the role of water consumption in the growth and development of maize. This plays an even more pivotal role in the case of possibly fully controlled environments such as smart greenhouses, or in environments where the dynamics of water availability play a more dominant role than thermal variations, which tend to be the most common foundation for crop growth modeling.

This study examines the potential of applying a state machine model with optimized deficit irrigation parameters developed for the prediction of leaf length (Jihin et al., 2019) to the estimation of leaf area and biomass in maize plants at the early vegetative stage. The obtained results are compared to the FAO Aquacrop model (Steduto et al., 2008), which is one of the most widely used crop growth models focusing on the effect of water deficit on growth and development in plants. Aquacrop was also selected because the model allows for stepwise calculation of parameters of interest, thus allowing for comparison with values obtained in the early vegetative stage as opposed to yield at harvest.

2. Materials and Methods

2.1. Experimental conditions

Experimental data for training and validation of the models was obtained from an indoor greenhouse situated in the Chair of Dynamics and Control at the University of Duisburg-Essen in 2019 (KW 44 to 50). The greenhouse is located in a climate-controlled room with temperature maintained between 18° C and 29° C. Artificial lighting was supplied by a set of eight 75W 9500K fluorescent grow lights at each of four tables set up, with the illuminated area under each lighting set covering approximately 0.5 m by 0.5 m. The height of the lamps above the growing plants is manually adjustable, and was maintained as close as possible to the leaf canopy without making contact with the leaves. The windows in the room are blacked out and sealed with silicone for prevention of air currents from outside, and there is a single point of entry into the room, which was kept closed except for access to the plants for measurements.

The maize seed used in the experiment was KWS Ronaldinio variant. The seed was sowed in 500 ml PET tumblers filled with 175 g of Seramis® clay granulate as the growth substrate. "Seramis Vitalnahrung" liquid fertilizer for green plants was mixed into the irrigation water for fertigation. The plants received 14 hours of illumination daily.

Daily minimum and maximum temperature and relative humidity were recorded using a digital temperature and humidity sensor, and leaf length and width measurements were done using a flexible meter rule. Fresh above ground biomass was determined at the end of the growth experiment through the use of a precision weighing balance with a sensitivity of 0.01 g.

For all growth experiments, a control group of fully irrigated plants was maintained at the experimentally predetermined full holding capacity of the substrate. Training of the state-machine model was carried out using a sample of data from the two experiments for which leaf width measurements (twenty plants in total) were available throughout the growth period. Test data was sampled from the remaining 260 plants. To investigate the accuracy of the proposed prediction model, data from two growth experiments carried out from October to December 2019 was used.

For each experiment, plants were divided into four groups each containing 35 plants, equally distributed on the four growing tables within the greenhouse. The control group was supplied with enough irrigation water daily to replenish evapotranspiration losses, bringing the substrate to full capacity, which was determined to be 145 g of water. Mild stress and severe stress states were determined based on threshold values obtained from an NSGA-II algorithm that was trained with data from previous growth experiments under identical conditions. Plants were considered to be under no stress (hence fully irrigated) for water content above 115 g and 113.42 g respectively for the first and second set of experiments. The lower boundary for the mild stress region for the two experiments was similarly determined to be 67 g and 62.97 g respectively. Plants required to be maintained at mild stress were reirrigated to achieve water content of 100 g. Irrigation was manually performed once daily using syringes, with the weight of the complete potted plant measured using a precision balance. During the later stages of the experiment where expanded leaf area resulted in daily evapotranspiration values high enough to trigger initiation of mild stress in the control group, or severe stress in the test groups, additional water was supplied to the plants with the quantities calculated based on projected evaporation rate and predetermined stress boundary values.

All plants were maintained under no stress until the appearance of the third leaf, after which irrigation was carried out as per the predetermined sequences. For the first growth experiment, the test duration started 10 days after planting and ran for 12 days. During the second growth experiment, the testing phase began 6 days after planting and ran for 16 days. The plants were harvested upon reaching the maximum height achievable within the growing space. The irrigation sequences for the two growth experiments are shown in Table 1, with 0 representing no stress and 1 representing mild stress. For the first experiment, each digit represents three consecutive days, while for the second experiment each digit represents a 2-day period.

Table 1. Irrigation sequences during maize growth experiments

Group	Experiment 1	Experiment 2
A	0 – 0 – 0 – 0 – 0	0 – 1 – 0 – 1 – 0 – 1 – 0
B	0 – 1 – 1 – 0 – 1	0 – 1 – 1 – 0 – 0 – 1 – 1
C	0 – 0 – 1 – 0 – 0	0 – 1 – 1 – 1 – 0 – 0 – 0
D	0 – 1 – 0 – 1 – 1	0 – 0 – 0 – 0 – 0 – 0 – 0

2.2. Aquacrop modeling parameters

The Aquacrop model [Steduto et al., 2008] was developed to allow the modeling of plant growth and yield with a focus on the relationships between supplied water and evapotranspiration losses. Biomass calculations are accomplished stepwise, with the relationship between biomass and water consumption expressed as

$$B = WP * \sum Tr, \qquad (1)$$

where B is the calculated plant biomass, WP is the water productivity and Tr is the transpiration from the plant. Due to the direct linking of biomass production to the water supplied to the plant, the model is able to effectively factor in effects of deficit irrigation strategies, allowing for prediction of in-season plant growth, which provides a source of valuable information for allocation and management of water supply to the crop.

For the configuration of the growth simulation using Aquacrop, the irrigation water supplied was converted to irrigation depth by division of the supplied volume by the cross-sectional area of the pots used in the greenhouse. The substrate was represented as a clay-loam granulate, and groundwater level was set to zero, because the only source of water to the growing plants was irrigation water supplied from above.

2.3. State machine model

The growth of a maize plant was described using a state machine model as described in Owino & Söffker, 2019. Optimization of the model parameters was carried out using an NSGA-II algorithm, resulting in the determination of level and temporal thresholds describing the stress condition of the growing plants. Level thresholds defined the demarcation between the three different water stress levels described in the plant growth model- no stress, mild stress and high (or severe) stress. The temporal thresholds consist of a maximum mild stress duration threshold, which leads to a transition into high stress, and a recovery threshold, which leads to loss of memory acquired during previous periods of stress.

Biomass was estimated directly by training of the state machine model using intermediate biomass values calculated from leaf length and width, expressed by Mokhtarpour et al., 2010 as

$$Ln(B) = \sum_1^n a + b \, Ln(L)_n + c \, Ln(W)_n, \qquad (2)$$

where B is the calculated biomass, L is the leaf length, W is the leaf width, a, b, and c are crop related constants, and n is the leaf number.

The model was additionally applied for determination of total leaf area based on the relationship developed by Montgomery (1911) as

$$LA = kL * W, \qquad (3)$$

where LA is the leaf area, k is a crop-specific constant, with a value of 0.79 used in this work following Birch et al. (1998), L is the length of the leaf from the base to the tip, and W is the width at the broadest part of the leaf.

3. Results and Discussion

3.1. Leaf area estimation

Leaf area estimation by the state machine was able to follow the trajectory of observed leaf area for the test group. Absolute error and root squared error values were calculated for the entire set of generated values, as reported in Table 1. In Figure 1 the trajectory of growth of individual leaves for a sample of the test individuals in the group is shown.

Table 2. Sample error metrics for leaf area estimation using a state-machine based model

Parameter	Test 1	Test 2	Test 3	Test 4	Test 5
Absolute error	6.543	2.685	2.977	0.325	1.158
RMSE	2.334	0.958	1.062	0.116	0.413
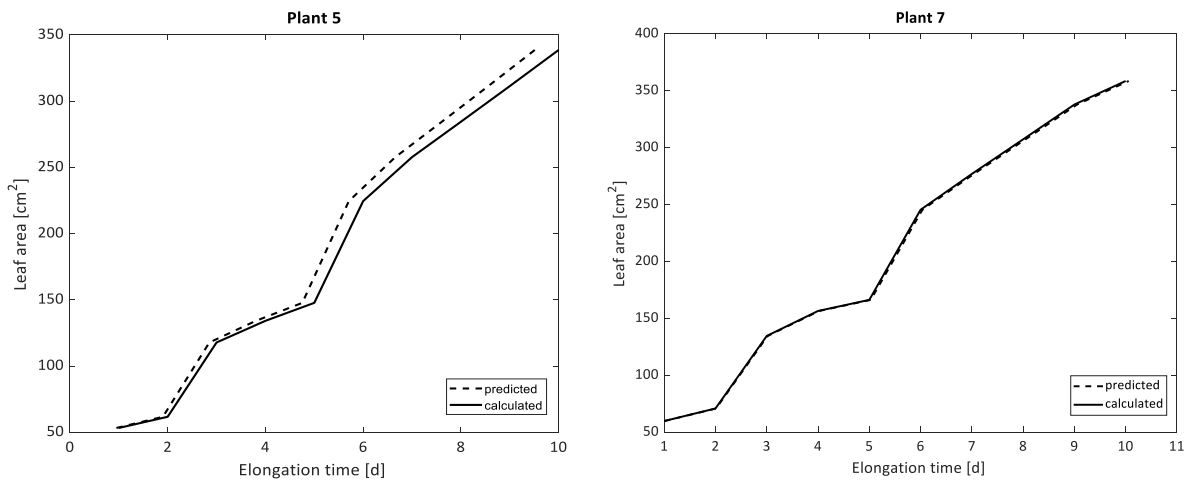
Figure 1. Leaf area growth trajectories predicted by the modified state machine model.

For the range of leaf areas represented, the error values are small enough to be insignificant, indicating that this model can be applied in projection and estimation of leaf area under deficit irrigation conditions, with minimal input requirements, and at very early stages of vegetative growth.

It has however to be noted that since the calculated leaf area is reliant on existing theoretical models, the accuracy of the results is closely tied to the equation selected for calculation of training values. Further improvement of the model could be achieved by employing more accurate destructive or optical-based techniques for generation of more reliable training data, which would improve the accuracy of the predicted

3.2. Biomass estimation

Estimation of biomass directly using the state machine model showed significant deviations from measured values, with the time axis exhibiting a contraction of up to 50%, resulting in biomass estimates that were up to 100% larger than measured values (Figure 2). This result may be due to the limited number of training values for which accurate biomass values were available, or could also be an indication of systemic errors with the approach selected. For this reason, this approach was abandoned, and an estimation approach based on the generated total leaf length was applied instead.
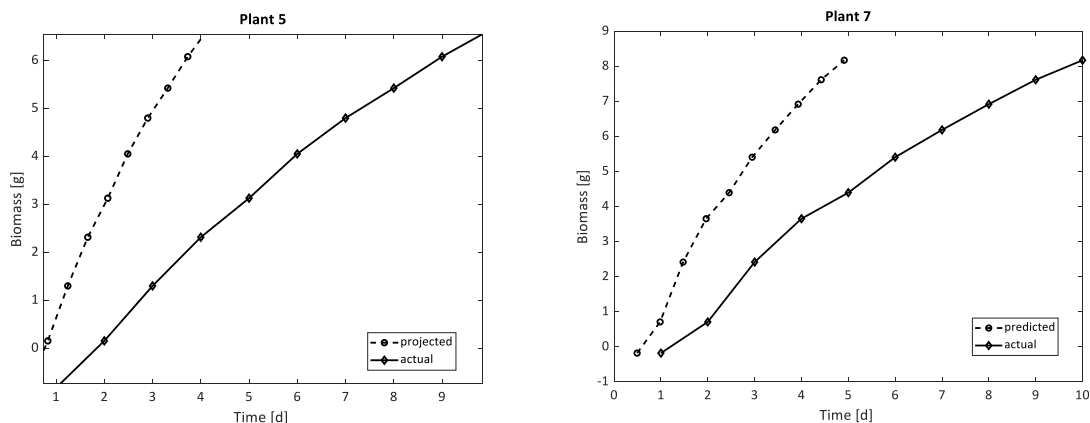
Figure 2. Leaf area growth trajectories predicted by the modified state machine model.

A linear model was trained using measured total leaf length and biomass values obtained at the end of the two experiments. The resultant equation took the form:

$$B = k_1 TLL + k_2, \qquad (3)$$

where k_1 and k_2 are constants obtained by fitting leaf length and biomass data. The linear model was trained with two sets of data- one including samples from six different sets of experiments conducted between 2017 and 2019, and a second set of data restricted to the two experimental periods from which the test data was also obtained. The

distribution of error values obtained is illustrated in Figure 2, with 5-I and 5-II using test data from the first experiment and training data from the expanded and restricted sets respectively. The variables 6-I and 6-II similarly illustrate the test data from the second experiment evaluated using parameters obtained from the two respective sets of training data. The accuracy was quantified using the error metrics shown in Table 3.

Table 3. Error metrics of linearized biomass prediction model based on total leaf length

Parameter	k_1	k_2	R^2	RMSE
Dataset I (2017-2019)	0.09179	-8.311	0.8002	1.389
Dataset II (2019)	0.079	-5.38	0.9462	0.6026

From Figure 3, it can be observed that the median values of the estimated biomass are relatively close to zero, and the distribution of the data between the 25th and the 75th percentile is uniform for all combinations of test and training data. Although it can be seen estimates for test data from the first experiment tended towards under-estimation while test data from the second experiment tends towards over-estimation, the absolute values of the error are relatively small, allowing for reasonable confidence in the reliability of the estimates.
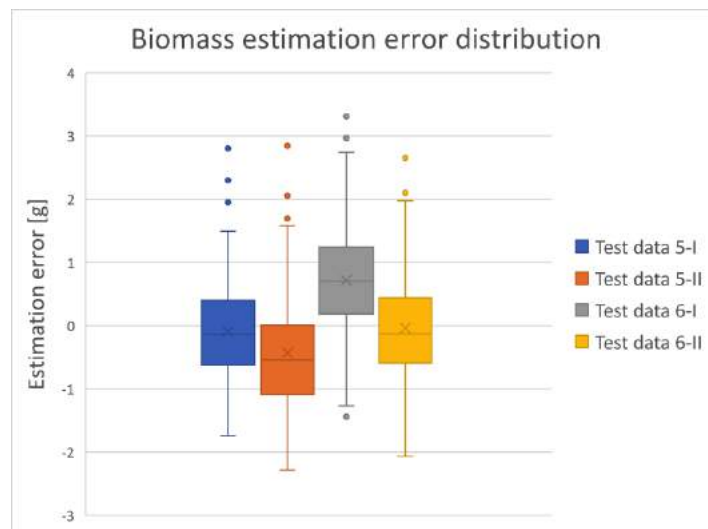
Figure 3. Error distribution for biomass estimation using linearized equation with measured total leaf length values

The next step involved applying the linearized estimation of biomass to total leaf length values generated by the state machine model, with the results then compared to values obtained from the Aquacrop model. Figure 4 shows this comparison, with both models displaying a tendency towards underestimation of the biomass value, as seen by the position of the median line. The modified state-machine generated for this set of data a median error value closer to zero as compared to Aquacrop, but produced a larger number of outliers, suggesting a need for additional refinement of the model to enable its application to plants in earlier growth stages, where total biomass is relatively small.
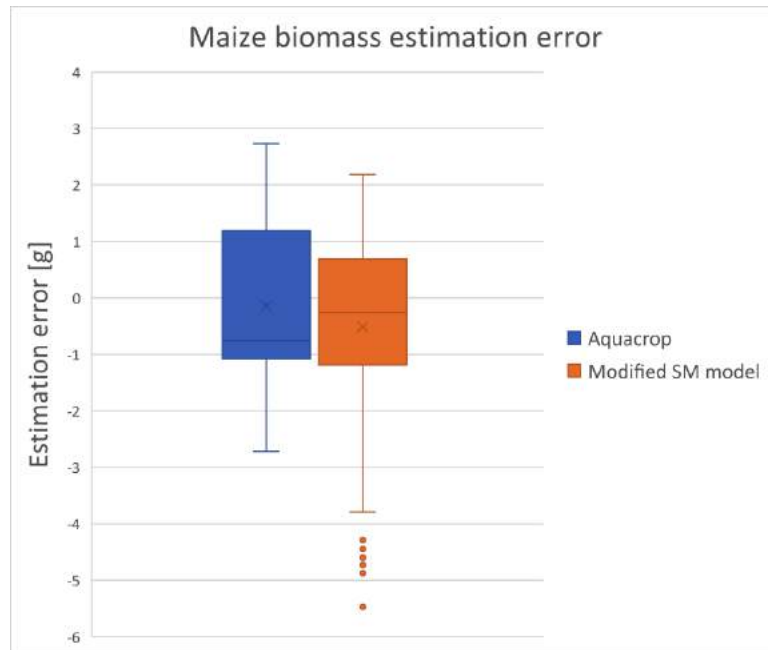
Figure 4. Error distribution in biomass estimates: comparison between introduced approach and Aquacrop

4. Conclusions

Values of above ground biomass were seen to vary even in plants grown from the same cultivar, under identical conditions, during the same growth period. This leads to a reduced reliability of prediction accuracy for models that rely on common variables such as temperature, day length and available radiation, particularly in controlled environments or for purposes of research. Approaches using primarily plant-based signals have proved useful in predicting plant development down to the individual level. Additionally, considering global developments in the availability of freshwater and advances in precision irrigation, employing models that take into account variations in water status of plants is the key to keeping predictive models up to date while exploring the control possibilities offered by new irrigation techniques and technology.

The implemented state machine-based growth prediction model has been applied to successfully predict leaf area by training the model using leaf length and width data. Significant drawbacks were however experienced in direct application of the model for use in estimation of biomass, indicating a need to examine the underlying equations used to generate incremental biomass values in response to plant water status with a view to building a link between the leaf length, leaf area and above ground biomass. The simplicity of the linearized relationship between total leaf length and biomass observed during the early vegetative stage in this case allows for rapid estimation of biomass during the early stages of development, and, coupled with a predictive algorithm, enables for forecasting of expected biomass based on irrigation quantities and sequencing.

Further research is required to assess the relationship between leaf area and biomass, which would facilitate simplified methods of estimating biomass at individual plant level. This would be especially helpful laboratory settings for furthering research on the control of maize growth and development.

Acknowledgements

References

Bassu, S., Brisson, N., Durand, J.-L., Boote, K., Lizaso, J., Jones, J.W., Rosenzweig, C., Ruane, A.C., Adam, M., Baron, C., Basso, B., Biernath, C., Boogaard, H., Conijn, S., Corbeels, M., Deryng, D., De Sanctis, G., Gayler, S., Grassini, P., Hatfield, J., Hoek, S., Izaurralde, C., Jongschaap, R., Kemanian, A.R., Kersebaum, K.C., Kim, S.-H., Kumar, N.S., Makowski, D., Müller, C., Nendel, C., Priesack, E., Pravia, M.V., Sau, F., Shcherbak, I., Tao, F., Teixeira, E., Timlin, D. and Waha, K., 2014. How do various maize crop models vary in their responses to climate change factors? Glob Change Biol, 20: 2301-2320. https://doi.org/10.1111/gcb.12520

Battude, M., Al Bitar, A., Morin, D., Cros, J., Huc, M., Sicre, C., Le Dantec, V., Demarez, V., 2016. Estimating maize biomass and yield over large areas using high spatial and temporal resolution Sentinel-2 like remote sensing data. Remote Sensing of Environment. 184. 668-681. https://doi.org//10.1016/j.rse.2016.07.030.

Birch, C., Hammer, G., Rickert, KG., 1998. Improved methods for predicting individual leaf area and leaf senescence in maize (Zea mays). Australian Journal of Agricultural Research. 49. http://dx.doi.org/10.1071/A97010

Calou, V.B.C., Teixeira, A. dos S., Moreira, L.C. J, da Rocha Neto, O. C., da Silva, J. A., 2019. Estimation of Maize Biomass using Unmanned Aerial Vehicles. Engenharia Agrícola [online]. 2019, v. 39, n. 6 [Accessed 09 June 2021], pp. 744-752. https://doi.org/10.1590/1809-4430-Eng.Agric.v39n6p744-752/2019.

Diepen, C.A., Wolf, J. van, and Keulen, H. van, 1989. WOFOST: a simulation model of crop production. Soil Use and Management, 5: 16-24.

Herbei, M.H. & Sala, F., 2016. Biomass prediction model in maize based on satellite images. 1738. 350009. https://doi.org/10.1063/1.4952132

Jihin, R., Kögler, F., and Söffker, D., 2019. Data Driven State Machine Model for Industry 4.0 Lifetime Modeling and Identification of Irrigation Control Parameters, *2019 Global IoT Summit (GIoTS)*, pp.1-6, https://doi.org/10.1109/GIOTS.2019.8766393.

Jin, S., Su, Y., Song, S. et al., 2020. Non-destructive estimation of field maize biomass using terrestrial lidar: an evaluation from plot level to individual leaf level. Plant Methods 16, 69. https://doi.org/10.1186/s13007-020-00613-5

Jones, C.A., and J.R. Kiniry (Eds.). 1986. CERES-Maize: A simulation model of maize growth and development. Texas A&M Univ. Press, College Station.

Keating B.A., P.S. Carberry, G.L. Hammer et al. 2003. An overview of APSIM, a model designed for farming systems simulation. *European Journal of Agronomy*, 18, 267–288.

Kim, S.H., Yang, Y., Timlin, D.J., Fleisher, D.H., Dathe, A., Reddy, V.R. and Staver, K., 2012. Modeling Temperature Responses of Leaf Growth, Development, and Biomass in Maize with MAIZSIM. Agronomy Journal, 104: 1523-1537. https://doi.org/10.2134/agronj2011.0321

Li, W., Niu, Z., Wang, C., Huang, W., Chen, H., Gao, S., Li, D. & Muhammad, S., 2015. Combined Use of Airborne LiDAR and Satellite GF-1 Data to Estimate Leaf Area Index, Height, and Aboveground Biomass of Maize During Peak Growing Season, IEEE Journal of Selected Topics in Applied Earth Observations and Remote Sensing, 8 (9): 4489-4501, https://doi.org/10.1109/JSTARS.2015.2496358.

Lizaso, J.I., Boote, K.J., Jones, J.W., Porter, C.H., Echarte, L., Westgate, M.E., Sonohat, G., 2011. CSM-IXIM: A New Maize Simulation Model for DSSAT version 4.5. *Agronomy Journal* 103:766-779

Ma, L., Ahuja, L.R., Islam, A., Trout, T.J., Saseendran, S.A., Malone, R.W., 2017. Modeling yield and biomass responses of maize cultivars to climate change under full and deficit irrigation, Agricultural Water Management, 180(A):88-98, https://doi.org/10.1016/j.agwat.2016.11.007.

Montgomery EG (1911). Correlation studies in corn. Agricultural Experiment Station of Nebraska, Lincoln.

Ranum, P., Peña-Rosas, J.P., Garcia-Casal, M.N., 2014. Global maize production, utilization, and consumption. Annals of the New York Academy of Sciences. 1312:105-112. http://doi.org/10.1111/nyas.12396.

Sakamoto, T., Gitelson, A.A., Wardlow, B.D. et al., 2012. Application of day and night digital photographs for estimating maize biophysical characteristics. Precision Agric 13, 285–301 https://doi.org/10.1007/s11119-011-9246-1

Steduto, P., Raes, D., Hsiao, T., Fereres, E., Heng, L., Izzi, G., Hoogeveen, J., 2008. AquaCrop: A New Model for Crop Prediction Under Water Deficit Conditions. FAO, Rome. 33.

Wang C, Nie S, Xi X, Luo S, Sun X, 2017. Estimating the Biomass of Maize with Hyperspectral and LiDAR Data. *Remote Sensing*. 2019, 9(1):11. https://doi.org/10.3390/rs9010011

Yang, H.S., Dobermann, A., Lindquist, J.L., Walters, D.T., Arkebauer, T.J., Cassman, K.G., 2004. Hybrid-maize—a maize simulation model that combines two crop modeling approaches, Field Crops Research, 87(2–3): 131-154, https://doi.org/10.1016/j.fcr.2003.10.003.

Jihin, R., Kögler, F., and Söffker, D., 2019. Data Driven State Machine Model for Industry 4.0 Lifetime Modeling and Identification of Irrigation Control Parameters, *2019 Global IoT Summit (GIoTS)*, pp.1-6, https://doi.org/10.1109/GIOTS.2019.8766393.

Modeling and Prediction of Corn Growth during Vegetative Phase

Lina Owino [a,*], Dirk Söffker [a]

[a] Chair of Dynamics and Control, University of Duisburg-Essen, Duisburg, Germany
* Corresponding author. Email: lina.owino@uni-due.de

Abstract

The stages of corn growth and development are characterized by different demands that are affected by natural and artificial resources, including those requiring partial or full water management. Accurate prediction of specific growth variables during each stage is helpful in allowing proper resource planning and facilitating better prediction and control of growth targets, possibly in combination with watering requirements.

In this work, the appearance of new corn leaves as a measure for developmental stages is estimated/approximated using a linear modeling approach. This approach allows prediction of the time at which a system variable will achieve a predetermined value, and is adapted from prognostic monitoring approaches. The approach is applied to estimate new leaf appearance based on the measured growth trajectory of previously developed leaves. The established model parameters are defined and thereafter trained using experimental data obtained from corn plants grown in an indoor greenhouse under varying irrigation treatments. Based on the obtained experimental results, it can be stated that prediction of leaf appearance from the 4th leaf to the 7th leaf can be accurately realized using the linear model. It is hypothesized that the established model can be used to predict leaf appearance during the complete vegetative phase. This knowledge can be combined with growth control approaches to realize targeted timing of the transition from the vegetative to the reproductive phase.

Keywords: growth modeling, maize growth, leaf appearance, prediction

1. Introduction

Maize is one of the key agricultural crops globally, contributing to 19.5% of global food consumption in addition to serving as a fodder crop and an industrial raw material in the production of biofuels, industrial sweeteners and oil. The production of maize has shown a steady increase over the past decades, with a 20% increase in output expected by the year 2050 [Alexandatro and Bruinsma, 2012]. Increased pressure on available arable land and growing constraints on freshwater supply predicate a need for more efficient management of growth inputs, which can be aided by better accuracy in projection of crop growth and related resource demands.

The growth cycle of maize can be divided into two major phases- the vegetative stage, covering the period from seedling emergence to tasselling, and the reproductive stage, covering the development of kernels up to maturity. A key growth indicator during the vegetative phase is leaf emergence, which is the most commonly used method of identifying the specific growth stage of a maize plant.

Cereal plants have been observed to exhibit a distinct pattern during vegetative growth, with resources concentrated on a fixed number of growing leaves at different stages of development [Etter, 1951; Hesketh et al., 1988]. Studies on the timing and rate of leaf appearance in maize plants have primarily focused on the influence of temperature, with observations indicating that the duration between appearance of successive leaf tips for a specific maize cultivar can be represented as a fixed thermal time, referred to as phyllocron, with modifications to the determination of thermal time to account for different temperatures during the growing period [Kiniry et al., 1991; Giauffret et al., 1995; Birch et al., 1998]. A causal link is suggested between the emergence of the collar in maize leaves and the end of active elongation [Fournier and Andrieu, 2000, Fournier et al., 2005].

A modified approach developed by Jame et al. introduces a non-linear temperature response function that allows the determination of leaf appearance rate under a wider range of temperatures by accumulating leaf appearance rates calculated hourly rather than daily [Jame et al., 1998]. In more recent work, the contribution of genotypic factors [Birch et al., 2002, Padilla and Otegui, 2005] and water stress [Bennouna et al., 2004] to the timing and rate of leaf appearance has been investigated, albeit with the main focus primarily on the relationship between thermal time and maize leaf development.

Studies on effect of water stress on leaf appearance in maize indicate a delay in appearance of new leaves resulting from periods of water deficit [Song et al., 2019; NeSmith and Ritchie, 1992; Traore et al., 2000]. When periods of water deficit are followed by periods of full irrigation, the growth of previously water stressed plants exhibits a recovery phenomenon, with leaf appearance rates greater than control plants that have not experienced water stress [Muchow and Carberry, 1989; Kögler and Söffker, 2018]. Further research is however needed to establish a causative link between the increased elongation rate experienced during recovery from water stress and the accelerated leaf appearance observed in

recovered plants, with the possibility of introducing optimal water management strategies for control of biomass production and timing of leaf appearance.

This work investigates the link between the decreasing rate of leaf elongation as the older leaves approach maturity, and the appearance of new leaves, marked by the visual observation of leaf tips. Experimental data is used to determine threshold values of leaf elongation rate that serve as markers to predict appearance of new leaves. The estimated values of leaf appearance time and duration of leaf elongation are compared to experimentally observed values as well as to calculated values present in literature [Kiniry et al., 1991]. The work is intended to serve as a basis for control of leaf appearance by appropriate scheduling of periods of water stress and recovery.

2. Materials and Methods

2.1. Experimental conditions

Experimental data for training and validation of the models was obtained from an indoor greenhouse situated in the Chair of Dynamics and Control at the University of Duisburg-Essen in 2019 (KW 19 to 23). The greenhouse is located in a climate-controlled room with temperature maintained between 18° C and 29° C. Artificial lighting was supplied by a set of eight 75W 9500K fluorescent grow lights at each of four tables set up, with the illuminated area under each lighting set covering approximately 0.5 m by 0.5 m. The height of the lamps above the growing plants is manually adjustable, and was maintained as close as possible to the leaf canopy without making contact with the leaves. The windows in the room are blacked out and sealed with silicone for prevention of air currents from outside, and there is a single point of entry into the room, which was kept closed except for access to the plants for measurements.

The maize seed used in the experiment was KWS Ronaldinio variant. The seed was sowed in 500 ml PET tumblers filled with 175 g of Seramis clay granulate as the growth substrate. Seramis Vitalnahrung liquid fertilizer for green plants was mixed into the irrigation water for fertigation. The plants received 14 hours of illumination daily.

Daily minimum and maximum temperature and relative humidity were recorded using a digital temperature and humidity sensor, and leaf length measurements were done using a flexible meter rule. Leaf appearance was indicated by appearance of leaf tips, and leaf emergence was taken to represent the appearance of the collar on the growing leaf. Estimation and observation of leaf appearance was performed in growing degree days with a base temperature of 10° C as indicated for calculating thermal time in maize plants.

For all growth experiments, a control group of fully irrigated plants was maintained at the experimentally predetermined full holding capacity of the substrate. Data from a range of seven experiments with the number of test subjects ranging from 20 to 140 was used to generate an overview of phyllocron ranges for the first seven leaves. To investigate the accuracy of the proposed linear prediction model, data from a single growth experiment carried out in May 2019 was used.

For the May 2019 experiment, plants were divided into seven groups each containing 20 plants, equally distributed on the four growing tables within the greenhouse. The control group was supplied with enough irrigation water daily to replenish evapotranspiration losses, bringing the substrate to full capacity, which was determined to be 145 g of water. Mild stress and severe stress states were determined based on threshold values obtained from an NSGA-II algorithm that was trained with data from previous growth experiments under identical conditions. Plants were considered to be under no stress (hence fully irrigated) for water content above 111.26 g. Water content between 51.49 g and 111.26 g was indicative of mild stress, and water content below 51.49 g was considered to induce severe stress in the growing plants. Plants required to be maintained at mild stress were reirrigated to achieve water content of 100 g, while plants required to experience full stress were allowed to dry out to 0 g before being reirrigated as necessary. Irrigation was manually performed once daily using syringes, with the weight of the complete potted plant measured using a precision balance with a resolution of 0.01 g.

All plants were maintained under no stress until the appearance of the third leaf, after which irrigation was carried out as per the predetermined sequences. For this growth experiment, the period from sowing to appearance of the third leaf was eight days, and the subsequent irrigation treatment took 20 days. The plants were harvested on the 21st day upon achieving the maximum height allowable within the growing space. The irrigation sequences for the seven groups are shown in Table 1, with 0 representing no stress, 1 representing mild stress and 2 representing severe stress. Each digit represents two days.

Table 1. Irrigation sequences during May 2019 maize growth experiment

Group	Irrigation sequence
A	0 – 0 – 0 – 0 – 0 – 0 – 0 – 0 – 0 – 0
B	0 – 1 – 2 – 0 – 1 – 2 – 0 – 1 – 2 – 0
C	0 – 1 – 2 – 0 – 0 – 0 – 0 – 0 – 0 – 0
D	0 – 1 – 2 – 1 – 0 – 1 – 2 – 1 – 0 – 1
E	0 – 1 – 2 – 2 – 2 – 2 – 2 – 2 – 2 – 2
F	0 – 0 – 1 – 0 – 1 – 0 – 1 – 0 – 1 – 0
G	0 – 0 – 1 – 1 – 1 – 1 – 1 – 1 – 1 – 1

2.2. Linear prediction model

The prediction of the appearance of a leaf N is performed by estimating the duration it takes for the elongation rate of the older leaf N-3 to reach a predefined threshold as it approaches maximum length, at which point the daily elongation rate becomes zero. The specific threshold is determined from past experimental data, from which observations of the overlap between elongation of older leaves and growth of newly appeared leaves are used to determine a cut-off elongation rate below which parallel growth of both sets of leaves can no longer be observed. The 3-leaf interval for prediction of leaf appearance was selected by visual analysis of growth data from the first to the sixth leaf, as shown in Figure 1.
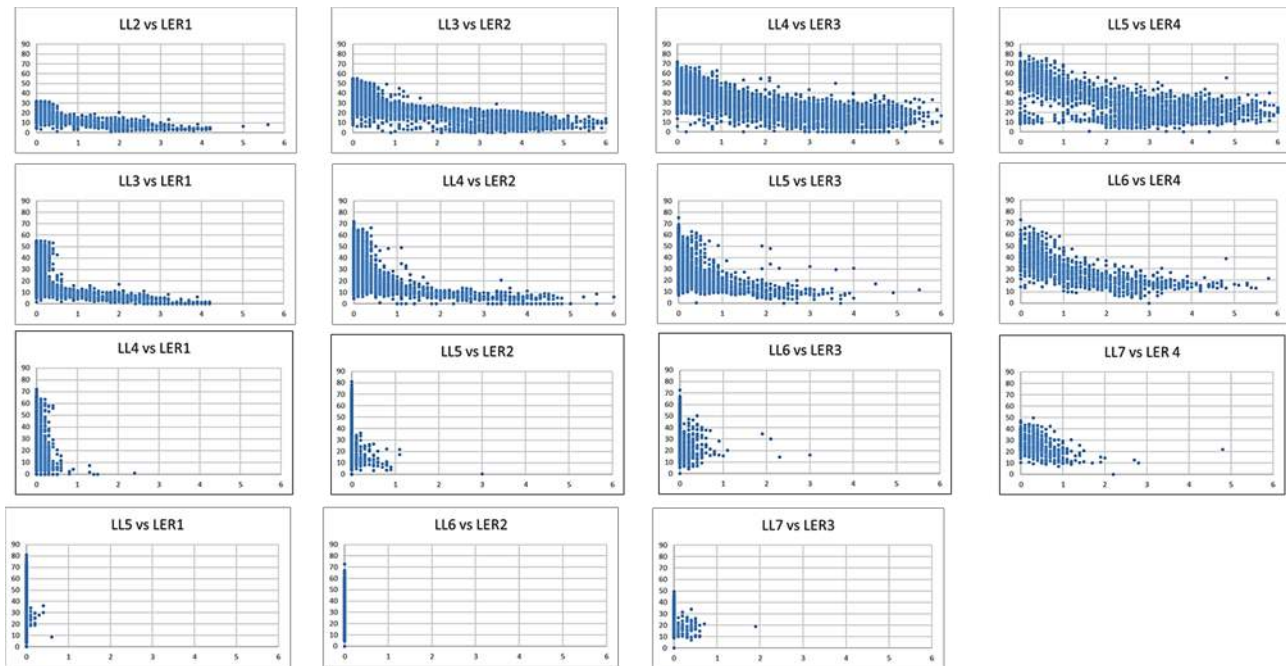
Figure 1. Leaf lengths compared to elongation rates of older leaves. The number in the title indicates the leaf number, with LL denoting length of the individual leaf and LER denoting the elongation rate in cm.

A linear degradation model based on MATLAB's predictive maintenance toolbox [Chakraborty et al., 2009] was applied to the elongation rate data of leaves 1 and 2, with thresholds obtained from visual observation used to determine "remaining useful life", which in this case translates to the remaining elongation time before the specific leaf reached its terminal length. Based on the highlighted charts in Figure 1, a threshold elongation rate of 0.5 cm/day for leaf 1 was selected for prediction of appearance of leaf 4, while for leaf 5 and 6, a threshold of 1 cm/day in the growth rate of leaves 2 and 3 respectively were considered adequate for accurate prediction results.

3. Results and Discussion

3.1. Experimentally observed phyllocron

The timing between the appearance of successive leaf tips was calculated in growing degree days using a base temperature of 10°C [Kiniry et al., 1991] for all seven growth experiments conducted between February 2018 and November 2019 (Figure 2) and for the May 2019 growth experiment (Figure 3).

Significant variation was observed in the duration of the interval between appearance of successive leaves, despite the plants being grown under nearly identical environmental and nutritional conditions as well as being the same cultivar. This illustrates the challenge of using a statically calculated value of phyllocron based on thermal time for prediction of leaf appearance, and is hypothesized that environmental conditions other than temperature may play a more significant role in the appearance of new leaves than proposed by existing research.
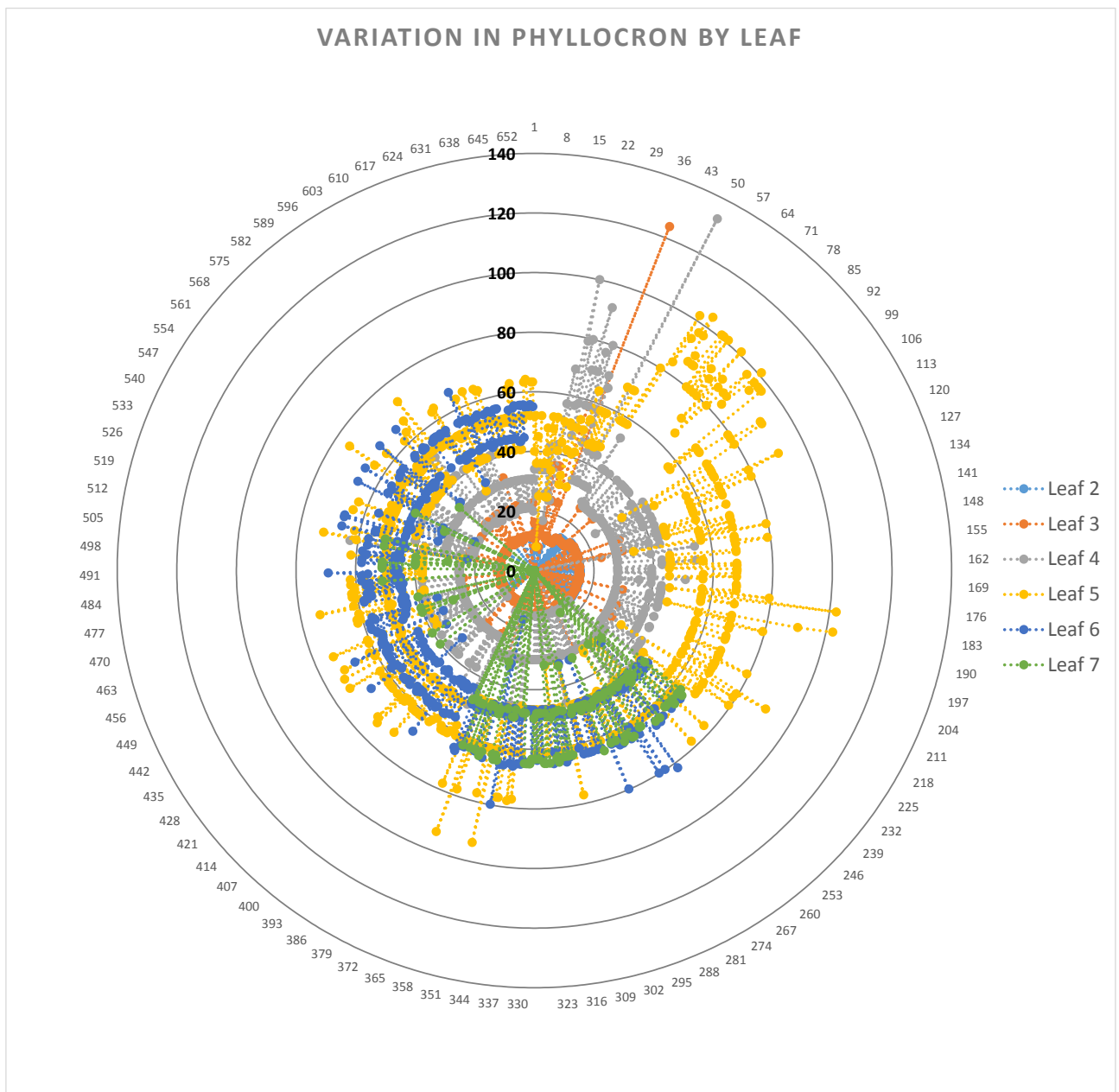
Figure 2. Distribution of phyllocron by leaf in test plants. All values are in GDD, with each point representing the time difference between successive leaf appearances on an individual plant.
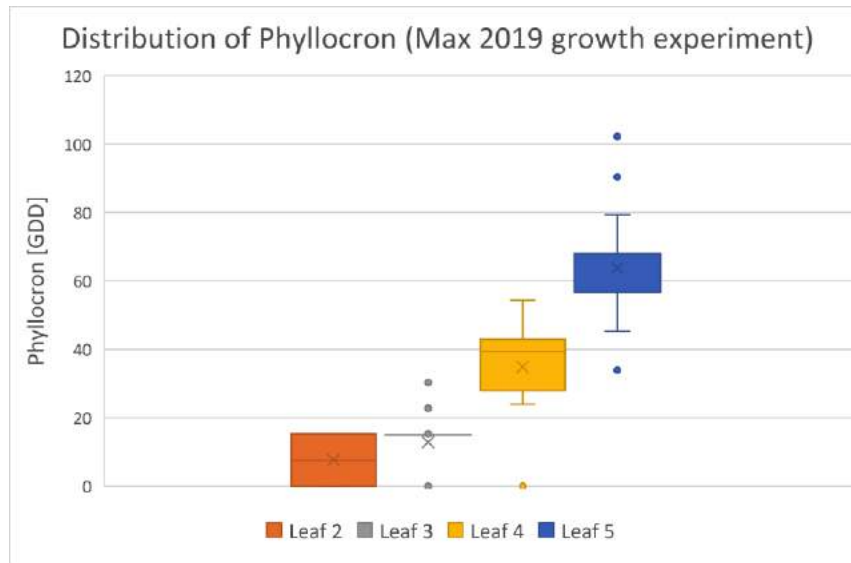
Figure 3. Phyllocron values for May 2019 growth experiment (combined results for control and test groups)

The observations recorded highlight the challenges of applying a static phyllocron value based on thermal time for prediction of leaf appearance. Despite identical maize cultivars growing under almost identical conditions in terms of nutrition and environmental conditions, there was a large variation both overall, and even for appearance of specific leaves during the same experiment.

An analysis of the phyllocron data segmented by stress treatment is shown in Figure 4.
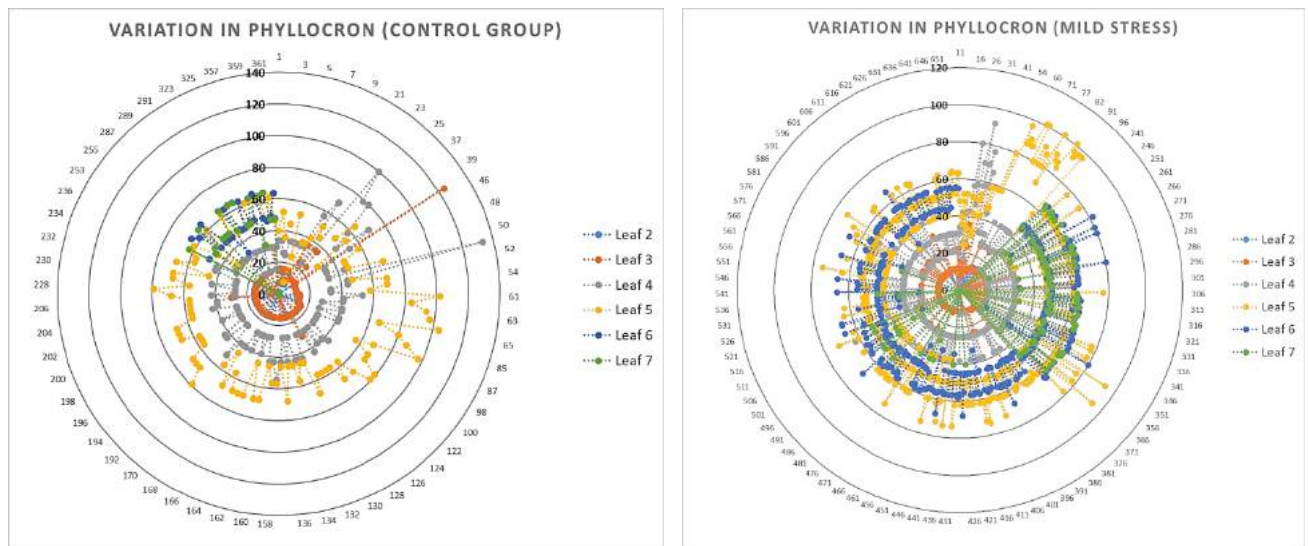
Figure 4. Phyllocron values segmented by water stress conditions during growth period

Values of phyllocron in the control group were comparable to values obtained in the mild stressed group, with more outliers observed in the control group as compared to the mild stressed group. This confirms the observations made by Muchow and Carberry, 1989 and Kögler and Söffker, 2018, indicating a catch-up phenomenon in leaf growth and appearance rate during recovery periods after water stress, resulting in a neutralization of the delay effects witnessed during the period of stress.

3.2. Linear model-based prediction of leaf appearance

Application of the linear model to the prediction of appearance of leaf 4 and 5 resulted in prediction accuracies to within 2 calendar days, with prediction of leaf 5 appearance consistently yielding a closer result to observed times as compared to predictions for appearance of leaf 4. This is graphically illustrated in Figure 5.
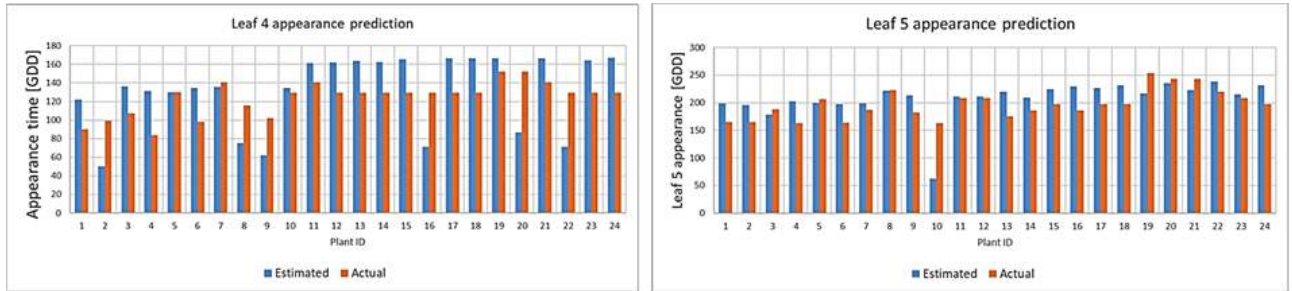
Figure 5. Leaf appearance prediction using linear model with predetermined threshold

Analysis of the observations by stress levels showed greatest consistency in prediction of leaf 4 (Figure 6) appearance for plants that were subjected to high (severe) stress, followed by reirrigation. The control group showed the greatest variability, with predictions both lower and greater than the observations occurring within the data set.
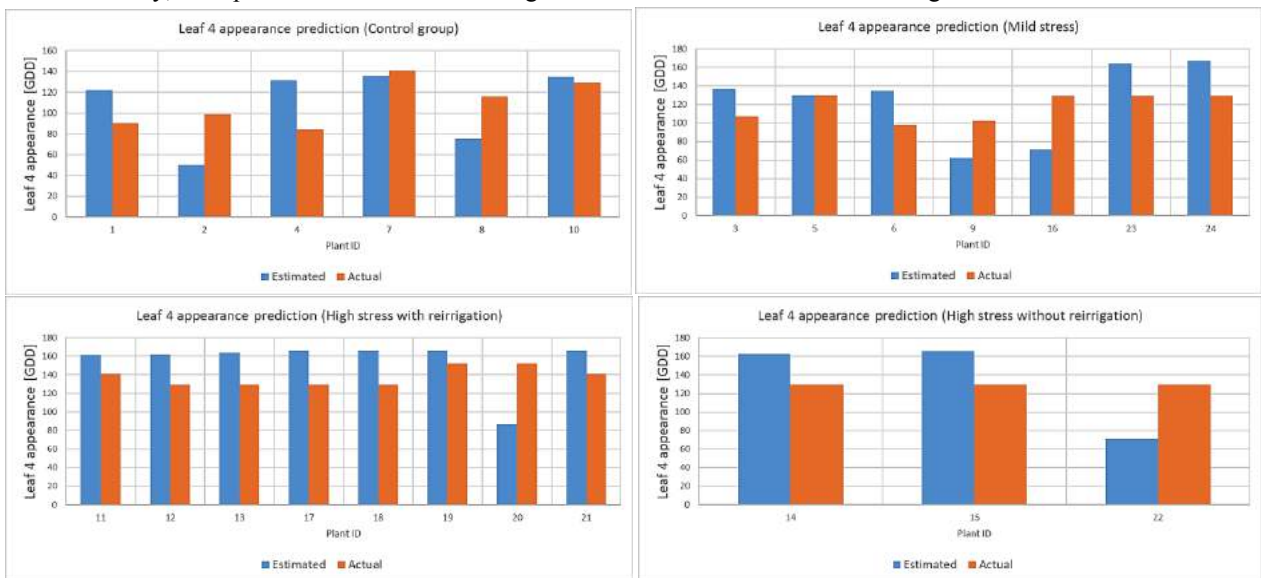
Figure 6. Leaf 4 appearance prediction by stress treatment.

A similar segmentation of leaf 5 appearance predictions by stress treatments showed relatively good performance for all groups with the exception of a few outliers within the data set (Figure 7). There is a tendency towards overestimation of the appearance date of the new leaf. The improvement in accuracy is likely due to the availability of more data for leaf 2 growth, as well as the relative ease in accurately measuring the length (and hence determining the elongation rate) of the leaf, due to the sharpness of the leaf tip, as opposed to the more rounded tip observed for the first maize leaf. The effect of stress treatment on the actual timing of leaf appearance or on the accuracy of the predictions made could not be evaluated due to insufficient growth data for leaf 6 and beyond, which is expected to show the trajectory of plant growth in the test groups without the influence of the initial full irrigation applied before stress treatments commenced.
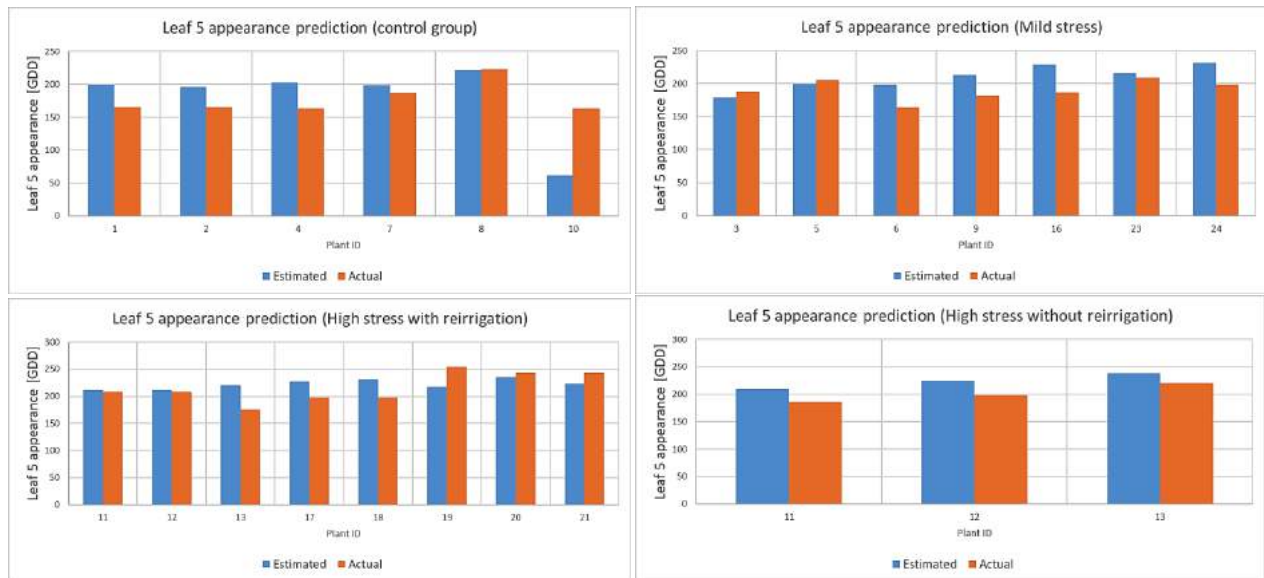
Figure 7. Leaf 5 appearance prediction under different water stress conditions

4. Conclusions

Experimental observations of maize cultivated under controlled greenhouse conditions, both under well-watered and water stressed conditions indicate that the application of static values of phyllocron based purely on thermal time (or on thermal time and levels of illumination) are insufficient to accurately predict appearance of leaves, with significant variations observed in plants grown under identical thermal and lighting conditions. It is proposed that other environmental conditions, in particular, exposure to water stress, may play a role in the appearance of new leaves in growing plants, hence an approach that is independent of the growing conditions, relying purely on the growth characteristics of the plant itself offers significant improvement in prediction of development of new leaves in maize plants.

The link between growth of different leaves on the same plant has been conclusively observed. Further exploration of effects of mild stress as well as severe stress with and without recovery periods would be vital in determining the possibility of realizing targeted leaf appearance through strategical sequencing of stress and recovery periods. This would allow control of both the actual growth of maize plants and the timing of developmental stages, resulting in a fully controllable plant growth by precision deficit irrigation. Additionally, the simplicity of the linear prediction function lends itself to ease of automation, which is one of the main goals of precision irrigation approaches.

References

Alexandratos, N. and J. Bruinsma., 2012. World agriculture towards 2030/2050: the 2012 revision. ESA Working paper No. 12-03. Rome, FAO.

Bennouna, B., Lahrouni, A., Bethenod, O., Fournier, C., Andrieu, B., and Khabba, S., 2004. Development of Maize Internode under Drought Stress. Journal of Agronomy, 3: 94-102. https://dx.doi.org/10.3923/ja.2004.94.102

Birch, C.J., Vos, J., Kiniry, J., Bos, H.J., and Elings, A., 1998. Phyllochron responds to acclimation to temperature and irradiance in maize, Field Crops Research, 59(3): 187-200. https://doi.org/10.1016/S0378-4290(98)00120-8.

Chakraborty, S., N. Gebraeel, M. Lawley, and H. Wan, 2009. Residual-Life Estimation for Components with Non-Symmetric Priors, IIE Transactions, 41(4): 372–387. https://doi.org/10.1080/07408170802369409

Etter, A., 1951. How Kentucky Bluegrass Grows. Annals of the Missouri Botanical Garden, 38(3), 293-375. https://dx.doi.org/10.2307/2394639.

Fournier, C., Durand, J.L., Ljutovac, S., Schäufele, R., Gastal, F. and Andrieu, B., 2005. A functional–structural model of elongation of the grass leaf and its relationships with the phyllochron. New Phytologist, 166: 881-894. https://doi.org/10.1111/j.1469-8137.2005.01371.x

Fournier, C., Andrieu, B., 2000. Dynamics of the Elongation of Internodes in Maize (*Zea mays* L.): Analysis of Phases of Elongation and their Relationships to Phytomer Development , Annals of Botany, 86(3):551–563. https://doi.org/10.1006/anbo.2000.1217

Giauffret, C., Bonhomme, R., Derieux, M., 1995. Genotypic differences for temperature response of leaf appearance rate and leaf elongation rate in field-grown maize. Agronomie, EDP Sciences, 15 (2): 123-137. ffhal-00885676

Hesketh, J.D., Warrington, J., Reid, J.F., Zur, B., 1988. The Dynamics of Corn Canopy Development: Phytomer Ontogeny. Biotronics, 17: 69-77.

Kiniry, J.R., Rosenthal, W.D., Jackson, B.S. and Hoogenboom, G., 1991. Predicting Leaf Development of Crop Plants. In: Hodges, T., Ed., Predicting Crop Phenology, CRC Press, Boca Raton, 29-42.

Kögler, F.; Söffker, D., 2018. Steuerung des Pflanzenwachstums durch Bewässerung. *61. Jahrestagung der Gesellschaft für Pflanzenbauwissenschaften e.V*, Kiel, September 25-27. Verlag Liddy Halm, Göttingen. Eds., Stützel, H., Fricke, A., Francke-Weltmann, L., 116-119. ISSN 0934-5116

Muchow, R.C., Carberry, P.S., 1989. Environmental control of phenology and leaf growth in a tropically adapted maize. Field Crops Research, 20(3): 221-236. https://doi.org/10.1016/0378-4290(89)90081-6

NeSmith, D. and Ritchie, J. (1992), Short- and Long-Term Responses of Corn to a Pre-Anthesis Soil Water Deficit. Agron. J., 84: 107-113. https://doi.org/10.2134/agronj1992.00021962008400010021x

Padilla J.M., Otegui M.E., 2005. Co-ordination between Leaf Initiation and Leaf Appearance in Field-grown Maize (Zea mays): Genotypic Differences in Response of Rates to Temperature, Annals of Botany, 96(6):997–1007. https://doi.org/10.1093/aob/mci251

Song L, Jin J, He J., 2019. Effects of Severe Water Stress on Maize Growth Processes in the Field. Sustainability, 11(18):5086. https://doi.org/10.3390/su11185086

Traore, S.B., Carlson, R.E., Pilcher, C.D. and Rice, M.E. (2000), Bt and Non-Bt Maize Growth and Development as Affected by Temperature and Drought Stress. Agron. J., 92: 1027-1035. https://doi.org/10.2134/agronj2000.9251027x

OPTIMA - Optimised Pest Integrated Management to Precisely Detect and Control Plant Diseases in Perennial Crops and Open-field Vegetables

A. Balafoutis[1], M. Moraitis[1], N. Mylonas[2], S. Fountas[2], D. Tsitsigiannis[2], P. Balsari[3], M. Pugliese[3], E. Gil[4], D. Nuyttens[5], G. Polder[6], F. Freire[7], J. P. Sousa[7], M. Briande[8], V. L. Clerc[8], J. P. Douzals[9], A. Caffini[10], L. Berger[11], Z. Tsiropoulos[12], D. Eberle[13], R. Warneys[14], M. Roth[15]

[1]Institute for Bio-economy and Agri-technology, Center for Research and Technology Hellas, Volos, Greece

[2]Agricultural University of Athens, Athens, Greece

[3]University of Torino, Torino, Italy

[4]Universidad Politecnica de Cataluna, Barcelona, Spain

[5]Instituut voor Landbouw-, Visserij- en Voedingsonderzoek, Merelbeke, Belgium

[6]Wageningen University & Research, Wageningen, the Netherlands

[7]Universidade de Coimbra, Coimbra, Portugal

[8]Institute for life, food and horticultural sciences and landscaping – AGROCAMPUS OUEST, Rennes, France

[9]INPAE, Paris, France

[10]CAFFINI, Verona, Italy

[11]Pulverizadores FEDE, Valencia, Spain

[12]AGENSO, Athens, Greece

[13]Terre da Vino, Barolo, Italy

[14]INVENIO, France

[15]ropLife Europe, Brussels, Belgium

* Corresponding author. Email: a.balafoutis@certh.gr

Abstract

OPTIMA is an H2020 research project that develops an environmentally friendly Integrated Pest Management (IPM) framework for vineyards, apple orchards and carrots by providing a holistic integrated approach which includes all critical aspects related to integrated disease management, such as i) use of novel biological Plant Protection Products, ii) disease prediction models, iii) spectral early disease detection systems and iv) precision spraying techniques. It will contribute significantly to the reduction of the European agriculture reliance on chemical Plant Protection Products resulting in reduced use of agrochemicals, lower residues and reduced impacts on human health.

Keywords: lPM, biological plant protection products, disease prediction models, spectral disease detection, precision spraying

1. Introduction

As the global population approaches 9 billion by 2050 (UN, 2015), the UN Food and Agriculture Organization (FAO) expects that demand for agricultural outputs will increase by 60% compared with the annual average from 2005 through 2007, representing an increase of approximately 1% per year. Furthermore, the total crop yield reduction caused by all crop pest species (estimated to be around 67,000 —including plant pathogens, weeds, invertebrates and some vertebrate species) reaches 40% (Oerke et al., 1994). Therefore, global food security is undermined by pests alongside other constraints, such as inclement weather, poor soils and farmers' limited access to technical knowledge (Chandler et al., 2011). Ways to make crop protection more sustainable are required and Integrated Pest Management (IPM) is promoted as the best way forward, shown also by its central position in the 2009/128/EC Sustainable Use Directive on Plant Protection Products (PPPs) (EU, 2009).

IPM could make a difference in this effort, as it emphasizes on the growth of a healthy crop with the least possible disruption to agro-ecosystems, and encourages natural mechanisms for pest management (Lamichhane et al., 2016). IPM is a systems approach that combines different crop protection practices and subsequent integration of appropriate measures that discourage the development of populations of harmful organisms and keep the use of plant protection products and other forms of intervention to levels that are economically and ecologically justified and reduce or minimize risks to human health and the environment (Flint and van den Bosch, 1981).

Synthetic PPPs have been common practice in industrialised countries for pest management since the Green Revolution and together with optimised crop varieties, intensive mechanization, irrigation and crop nutrition through rigorous fertilization, they increased agricultural yields significantly (70% in Europe and 100% in the USA (Lamichhane et al., 2016)). Ideally, PPPs are used to exterminate the targeted pests. Unfortunately, the application of PPPs worldwide is being executed with limited consideration to the dosage rate, optimum number of applications,

timing and frequency resulting in rampant use of these agrochemicals, under the axiom: "if little is good, much more will be better" (Wasim Aktar et al., 2009), having as result the contamination of natural resources by PPPs, including soil, water, turf and all vegetation types. On the contrary, Bio-PPPs are a particular group of crop protection tools that can substitute or support synthetic PPPs and are ideal for IPM schemes. Bio-PPPs are defined as a mass-produced agent manufactured from a living microorganism or a natural product and sold for the control of plant pests (EU, 2009). That said, Bio-PPPs show attractive properties, such as their selectivity, their little or no toxic residue production, and the significantly lower development costs in comparison to synthetic PPPs (Hajek, 2004).

PPPs are mainly applied, especially in conventional agriculture, using hydraulic and hydro-pneumatic sprayers. The principle of operation is to convert a PPP formulation that in most cases is diluted in water (or another liquid carrier) into droplets that will be sprayed upon the canopy of the selected crop to spread the chemical compound. Unfortunately, dose-transfer to the biological target (i.e. the pest) through PPP spraying has high inefficiencies and significant amounts of the active ingredient end up elsewhere in the environment (Graham-Bryce, 1977) contaminating natural resources (water, soil, air). There are numerous routes of environmental contamination from PPPs (Figure 1). Contamination can be either point source which is mainly related to the handling of PPPs on a farm during cleaning, filling, remnant liquid management, transport and storage (TOPPS, 2008a) or diffuse source which is mainly related to run-off from field after application, discharge from drainage and off target deposition of spray due to wind (spray drift) (TOPPS, 2008b). Therefore, diffuse sources can be mainly reduced through optimization of spraying technology. Novel spraying equipment targeting to a precise application spraying process uses only the approved and advised amount of PPPs reducing therewith both wastes – such as remnants in the sprayer – and risks, yet ensuring optimised biological efficacy with the greatest input cost effectiveness.
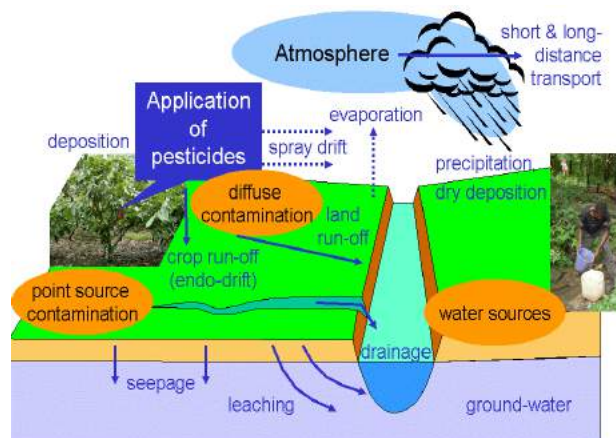
Figure 1. Routes of environmental con tamination from PPPs [Source: Wikipedia]

The overall objective of OPTIMA is to develop an environmentally friendly Integrated Pest Management (IPM) framework for use-cases in orchards, vineyards and open-field vegetables by providing a holistic approach which includes the major elements related to integrated disease management: (i) combined use of bio-PPPs and synthetic PPPs, (ii) DSS for disease prediction, (iii) spectral disease detection systems and (iv) precision spraying techniques.

OPTIMA advanced IPM framework will consist of 4 main pillars (Prediction, Detection, Selection and Application), and will focus on plant diseases that annually damage high-value crops and demand high amounts of fungicides to be applied in numerous spraying applications. OPTIMA will work on apple scab, grape downy mildew and Alternaria leaf blight of carrot, based on the importance of these diseases and crops for European agriculture.

To accomplish OPTIMA's vision, the specific project objectives are:
- **Objective 1:** Optimize plant disease prediction models and develop advanced early disease detection methods.
- **Objective 2:** Evaluate and screen biological and synthetic PPPs and assess plant and pathogen resistance mechanisms for successful disease control.
- **Objective 3:** Enhance and develop innovative precision spraying technologies.
- **Objective 4:** Test and evaluate the proposed new IPM elements under field conditions.
- **Objective 5:** Assess health, environmental and socioeconomic impacts and risks of the proposed IPM system.

2. Methodology

To achieve all objectives of OPTIMA and deliver a fully functional IPM system, the following actions are taken:
1. End-users' requirements are being assessed following the co-creation approach, while participating in the

design and evaluation of the developed products, tools and strategies throughout the project life-time. End-users are also evaluating the features of the demonstrated IPM system in the pilot areas.

2. A Decision Support System (DSS) is designed and developed for the prediction of grape downy mildew, apple scab and Alternaria leaf blight of carrots based on agro-climatic, pathogen biological cycle algorithms and users' testimonies and a portable advanced Early Detection System (EDS) is also developed for in-field localization and monitoring of the selected diseases using state of the art machine learning;

3. Novel sustainable IPM strategies are also being developed, to be applied as preventive or therapeutic control methods for the selected plant diseases both at experimental and commercial scale. Several biological and chemical intervention strategies for Alternaria leaf blight in carrots, grape downy mildew in vineyards and apple scab in apple orchards are being tested experimentally to expand the range of available tools and the best performing options will be optimised for the optimum application strategy to be pilot testing.

4. Technological advancement are being brought together to identify and develop optimal spray configuration and parameters for the different crop-disease combinations and reduce spray drift. These findings together with different variable rate application technologies are being used to develop three smart sprayers for each disease/crop combination.

5. All above mentioned components of the IPM system are being evaluated separately and as a whole. The DSS and EDS are tested in three selected pilot areas, while the efficacy of selected synthetic and bio-PPPs is evaluated as well. The smart sprayers for each crop are tested to quantify the improvements on deposition, coverage and drift reduction in comparison to conventional sprayers, at commercial fields. Finally, all IPM system components as a whole are tested in-field and compared with conventional crop protection methods.

6. Finally, an extended Life-Cycle Assessment (LCA) is performed combined with Human and Environmental Risk Assessment (HERA) using a Multi-Criteria Decision Analysis (MCDA) to identify and quantify the human health, environmental and socio-economic impacts and risks of treatments of the selected crops, comparing the conventional with the proposed IPM crop protection system

3. Expected Results

OPTIMA is expected to produce specific results that will cover its goals. More particularly, OPTIMA will:

1. **Follow the co-creation process** to take advantage of the end-users' experience in its functions. After the technical validation and evaluation of the proposed IPM system and according to the assessment of the benefits that will be obtained from the system evaluation in terms of farm economics, environmental and human health protection and social aspects, the pragmatic depiction of the impacts of such system will become clear.

2. **Optimise already existing disease prediction models** using agro-climatic and biological algorithms; users' testimonies; and geostatistical methods, which will be used for the development of a DSS.

3. **Develop advanced spectral detection systems** for in-field localisation and monitoring of the selected diseases in the use-case crops. OPTIMA's detection system will be used as standalone system providing information at site-specific level that can be used to export the variable rate spraying prescription maps; or as embedded to the three developed in the course of the project smart sprayers for the three crop types, where the image detection results will be transferred directly to the control unit of the sprayer in real-time to adjust the spraying quantity on site.

4. **Evaluate a collection of 10 different bio-PPP agents** per host of commercial (market-ready) and under development bio-PPPs (from partner's culture collections) together with selected new generation synthetic fungicides against apple scab, downy mildew in vineyards and Alternaria leaf blight in carrots to identify the most efficient combinations to efficiently control the diseases.

5. **Develop three smart prototype sprayers** for carrots, vineyards and apple orchards actuating different nozzle types, sprayer settings and adopting variable rate application control based on optimal selection of spray parameters, canopy and disease characteristics, together with the integration of innovative drift reducing technologies in order to minimize losses to the environment.

6. **Pilot test the OPTIMA developed IPM approach** in three selected use case areas. Trials of the OPTIMA IPM system and its individual components (DSS, disease detection system, combinations of PPPs and smart sprayers) will be carried out to evaluate the improvements and benefits when compared with the normal practices applied in the specific areas. Field experiments will be conducted in close collaboration with the three farmers' cooperatives that participate in the project and will follow the field experiments on a daily basis. Primarily, the developed standalone early disease detection system will be evaluated and optimised in field assessment by correlation with conventional field scouting techniques. At the same time, a data collection procedure will be arranged to quantify the savings on PPPs, water and time. The prediction model will be

evaluated in two growing seasons (year 1 and 2) and tested with the other IPM system components in year 3.

7. **Field-evaluate the selected synthetic and bio-PPPs combination** using the developed three smart sprayers for each crop. Depending on the crop characteristics, and following the EPPO guidelines for every single crop, a complete evaluation strategy of disease control will be conducted. Good spraying practices and the most accurate working parameters developed by OPTIMA will be demonstrated and compared with conventional practices. Benefits in terms of less PPP amount and less contamination will be measured and explained to the end-users for the purposes of system evaluation.

8. **Test and evaluate the three smart sprayers** developed in field conditions to define their ability to generate a safe, efficient and improved spray application process. Over the established experimental plots, field trials will be conducted in order to evaluate the spray quality distribution (deposition on leaves, coverage, penetration, etc.), the risk of drift, the potential reduction of PPP loses, and the capability of the three developed sprayers to adapt the spray distribution to the canopy characteristics. During the field trials a complete canopy characterization using different electronic sensors (ultrasonic, LiDAR, etc.) will be performed to collect the necessary information about the intended target. Once the canopy will be characterized, the smart sprayers will be ready to arrange the Variable Rate Application process that will be executed either based on previously generated canopy and risk maps, or on the on-going measurements provided by the on-board sensors.

9. **Evaluate and quantify the disease incidence severity** of the three selected diseases at the end of the experimental session.

10. **Conduct an extended Life-Cycle Assessment** (LCA) of the complete OPTIMA IPM framework, and a full Human and Environmental Risk Assessment (HERA), together with Social LCA and the economic viability to address life-cycle costs together with scenario and sensitivity analysis.

11. **Conduct a Multi-Criteria Decision Analysis** (MCDA) to fully assess the proposed crop protection systems for apple scab, grape downy mildew and Alternaria leaf blight in carrots based on the complementary use of LCA and HERA.

4. Latest progress

In the context of **Community Building and User Requirement analysis**, the two first sessions of the focus group meetings was conducted successfully in the three countries (Spain, Italy, France), while the third and last series carried out face-to-face in Spain and in Italy on June 10th and on July 7th, 2021, respectively. Farmers were able to see and evaluate the latest developments of the IPM system for the apple and vineyard crops, operating in the field. Attendants were very interested and evaluated very positively the different OPTIMA IPM components (Figure 2). The meeting of the French case will take place in early September. As a next step end-users will follow the pilot trials and assess the quality of the whole, deployed IPM system.

Figure 2. OPTIMA 3rd Focus Group in Spain

Regarding **advanced methods for prediction and early detection of plant diseases**, the OPTIMA DSS (Figure 3) uses weather forecast data and growth models for Downy mildew in vineyards, Apple scab in apple orchards and Alternaria leaf blight in carrots, in order to predict and display the best timeframes for spraying to prevent pest outbreaks. A weather station has been installed in all 3 pilot sites in order to compare the performance of the OPTIMA DSS with local weather data and data acquired by weather services (Figure 3).

Figure 3. Decision Support System Interface

Figure 4. Weather stations in Italy, Spain and France

As regards the EDS, an RGB imaging setup together with deep learning algorithms to identify OPTIMA crop/disease combinations was developed. It was tested in the Netherlands with images from apple leaves and sent to Greece to be tested by capturing vineyards and carrot plants images under field conditions. RGB based smart cameras were developed and sent to Spain and Italy for the pilot testing phase (Figure 5). Soon a 3rd system will be sent to France as well. The 3 smart cameras systems are being tested in field conditions mainly as for their ability to detect diseases with high precision. Detections and localization information through GPS are automatically sent to the DSS where prescription maps are constructed for the smart sprayers.

Figure 5. Details from the EDS

A series of tests regarding **combined synthetic and biological PPPs application and assessment of host and PPP resistance mechanisms** has been conducted with more than 12 bio-PPPs per selected crop. The results showed that:

- **Alternaria leaf blight in carrots** trials in Greece and France under controlled conditions (4 trials) highlighted several efficient biological products and pathogen resistance inducers. Additional carrot field experiments that were carried out in France and Greece led to efficient IPM strategies to control Alternaria leaf blight that are currently being tested in large scale field experiments.
- **Apple scab** trials in Italy were carried out under controlled conditions (potted plants) and highlighted several products controlling the disease, however, their efficiencies must be also confirmed in field conditions and new trials are under progress.
- **Grape downy mildew** trials in Italy and in Greece under controlled conditions showed that some of the tested biological control agents, resistance inducers and low-risk substances were effective in reducing the disease. As the active compounds of the tested bio-PPPs are very different, dissimilar mechanisms of action are expected. Current experimentation in vineyards involve the combination of different efficient PPPs in IPM schemes to evaluate the level of protection against grape downy mildew (Figure 6).

Figure 6. Details from the experiments carried out

As for the **developed and optimized innovative spraying technologies**, the individual smart components of the OPTIMA IPM system have already by now been developed and tested. The communication between the OPTIMA controller and the various subcomponents has been established and the physical integration of the smart components in the prototype smart sprayers has been finalized for the carrot, vineyard & orchard sprayer (Figure 7). Unfortunately, COVID-19 related travel restrictions complicated the simulations and the functionality testing, causing a delay in assembly and resulting in some field spray applications being missed in the orchard and vineyard case field trials. In the next period, the smart components and communication protocols will be fine-tuned where needed and additional deposition and drift trials using the PWM (Pulse Width Modulation) system will be performed.

Figure 7. The three OPTIMA smart sprayers (for vineyards, apple orchards and open field carrots respectively)

Besides sprayer developments, viability trials with bio-PPPs containing bacteria were performed. Temperatures of 40°C or higher were found to significantly decrease the viability or even cause total inactivation, whereas no effect of mechanical stress was found. Therefore, very little to no effect of the spray application on bio-PPP viability is expected in real field conditions. Droplet characterization measurements with bio-PPPs, to determine the effect of these products on the droplet size and velocity distribution, are ongoing.

Pilot testing of developed technologies is currently ongoing as the field trials to assess the biological efficacy of treatments have already begun for the apple case in a compilation of 3 farms with a total size of 15.27ha in Epila, Zaragoza (Spain) and for the vineyard case in a 5.9ha farm with Barbera, Moscato and Chardonnay varieties in Canelli

(Asti, Italy) (Figure 8). The trials for the carrot case in France are yet to begin; the trial is set up in the middle of a 30ha plot of seasonal carrots in the commune of Marcheprime, in the Landes de Gascogne region.

In short, the references that are / will be evaluated are: (0) conventional sprayer, representative practice of the zone, (1) Adjusted conventional sprayer according to Best Management Practices, (2) Smart sprayer, based on information from the DSS and the EDS, (3) Adjusted conventional sprayer, using combination of synthetic and selected bio-PPPs, (4) Smart sprayer, developed in the project for the specific crop and (5) Smart sprayer, based on information from the DSS and the EDS, using synthetic and bio-PPPs (complete OPTIMA IPM system).

Figure 8. Snapshots from the OPTIMA field trials.

The developed smart sprayers will also be evaluated in terms of deposition, coverage, drift and ground losses compared to the conventional ones (normal practice and adjusted one), in order to quantification the application improvement.

Human Health, Environmental and Socioeconomic Life-Cycle Analysis & Risk Assessment carries out a multilateral analysis. An extended life-cycle assessment (LCA) of the three OPTIMA crops is currently being implemented based on data collected from the field trials for three system boundaries: i) full crop system, ii) the IPM system and iii) a crop-disease focus. The figure below shows a diagram with the PPP application and distribution per environmental compartment, which is part of the approach developed to calculate the impacts, which is sensitive to different crops, PPPs, plant growth stages and sprayer configurations (Figure 9).
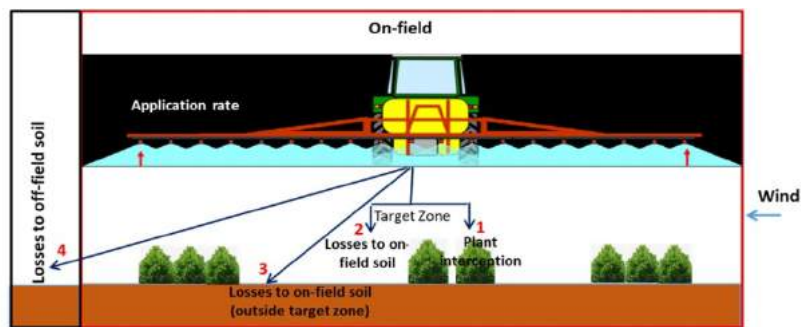
Figure 9. Framework of the environmental impact of spraying in carrots

The work to assess the potential risks of PPP application on soil organisms, beneficial arthropods (pest control agents) and pollinators (ERA) continued, focusing on the different OPTIMA references in the vineyards field trials (Italy). Refined risk values, including crop interception parameters according to the different sprayers used and the BBCH score of the crop, and different refinement exposure coefficients for the different organism groups, were derived based on planned application dosages. In the laboratory, testing different PPPs to fill the data gaps for honeybees and in soil organisms continues, focusing on products used in vineyards and carrots (Figure 10).

Human Health Risks regarding the use of PPPs under conventional practices for three cultures have been assessed. Long-term exposure Human Risks have been estimated in accordance to ASTM E2081: Standard Guide for RBCA (Risk-Based Corrective Action) standard approach and site-specific models, using toxicological data obtained from regulatory documents and scientific publications, while personal exposure data has been provided by OPTIMA partners. The planning field data for the Italian vineyard has been used to a sensitivity assessment of risks. Preliminary results indicate that (i) the substitution of some synthetic PPPs by bio-PPPs, (ii) the use of the DSS and (iii) the combination of the DSS and the use of bio-PPPs may lead to reductions in the Hazard Index and in the Total Carcinogenic Index. OPTIMA is currently working on the definition of a strategy to include fate models addressing wind-drift transport of PPPs on the moment of the application on the field (Figure 11).

Figure 10. Tests of impact on different organism groups
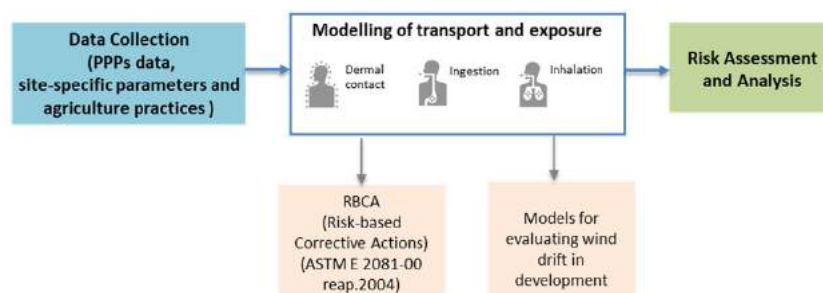
Figure 11. Human health impact assessment

The team focused on building a coherent set of evaluation criteria for a Multi-Criteria Decision Analysis (MCDA) of alternative OPTIMA systems. Based on the literature, the team's expertise, and inputs from focus groups in France, Italy and Spain, potential criteria were listed, trimmed (dropping criteria considered to be less relevant), and organized as a hierarchy.

Acknowledgements

References

Chandler, D., Bailey A.S., Tatchell G.M., Davidson G., Greaves J., Grant W.P. (2011). The development, regulation and use of biopesticides for integrated pest management, Phil. Trans. R. Soc. B, 366 (1573):1987-1998. doi: 10.1098/rstb.2010.0390

EU. (2009) http://eur-lex.europa.eu/LexUriServ/ LexUriServ do?uri=OJ:L:2009:309:0071:0086:en:PDF

Flint, M.L. & van den Bosch, R. (1981). Introduction to integrated pest management. New York: Plenum Press. doi: 10.1017/S0014479700013715

Graham-Bryce, I.J. (1977) Crop Protection: A Consideration of the Effectiveness and Disadvantages of Current Methods and of the Scope for Improvement, Philosophical Transactions Royal Society London, Series B, Biological Sciences, 281 (980): 163-179. doi: 10.1098/rstb.1977.0131

Hajek, A. (2004). Natural enemies: an introduction to biological control. Cornell University, New York Cambridge University Press, doi: 10.1017/CBO9780511811838

Lamichhane J.R., Dachbrodt-Saaydeh S., Kudsk P., Messéan A. (2016). Toward a Reduced Reliance on Conventional Pesticides in European Agriculture, Plant Disease, 100 (1), 10-24. doi: 10.1094/PDIS-05-15-0574-FE

Oerke E.C., Dehne H-W., Schonbeck F., Weber A. (1994). Crop production and crop protection: estimated losses in major food and cash crops. Elsevier doi: 10.1016/C2009-0-00683-7

TOPPS.   (2008a)   http://www.topps-life.org/uploads/8/0/0/3/8003583/_topps_best_management_practices_findoc_070613.pdf

TOPPS (2008b) http://www.topps-life.org/uploads/8/0/0/3/8003583/ansicht_drift_book_englisch.pdf

UN. (2015) http://www.un.org/en/development/desa/news/ population /2015-report.html, accessed on April 25th, 2019

Wasim Aktar, Dwaipayan Sengupta, Ashim Chowdhury (2009). Impact of pesticides use in agriculture: their benefits and hazards, Interdiscip Toxicol. 2(1): 1–12. doi: 10.2478/v10102-009-0001-7

Encouraging the Adoption of Precision Fertilization Technologies: Steps from Theory to Practice

M. Cutini, M. Brambilla, A. Assirelli, E. Romano, C. Bisaglia

CREA Consiglio per la ricerca in agricoltura e l'analisi dell'economia agraria (Research Centre for Engineering and Agro-Food Processing), Via Milano, 43 -24047 Treviglio (BG), Italy

*Corresponding author. Email: maurizio.cutini@crea.gov.it

Abstract

Studies report low levels of smart farming technologies and precision agriculture (PA) adoption due to cultural barriers, the average size of farms, and the difficulty of appreciating the resulting benefits. Following these last findings, the present study focuses on farmers' decision process to provide a fleet of PA machines. The used study case is the experimental arable farm of the CREA research centre of Treviglio, Italy, which has started a process to introduce precision agriculture technologies and digital fleet management.

The CREA experimental farm, 15 ha large, is entirely geo-referred and completely analysed under geophysical parameters through electrical-resistivity sensor mapping. With this background, the state of the art of different mechanization levels dedicated to precision agriculture was assessed. A 117 kW nominal power tractor was provided with commercial PA technologies and gradually set to have the full controlling options of the technology from different levels of guidance precision (from 150 to 25 mm) till the highest levels of PA capability, i.e., section control, variable rate (VR) seeding, fertilising and spraying.

Keywords: variable rate, smart farming, ergonomy.

1. Introduction

Precision agriculture is based on a series of observations from different sources periodically updated in order to performe operations to manage the variability of plots in terms of texture, organic substance content, and pH to bring each area of a field to express its maximum sustainable production. Studies report low levels of smart farming technologies (SFTs) and precision agriculture (PA) adoption due to several reasons. Young farmers, who operate larger farms (often owning more than the land they cultivate), are more prone and optimistic to adopt variable-rate input application technology because of their higher awareness about the costs and benefits of precision farming. Computer use was not significant, possibly because custom hiring shifts the burden of computer use to agribusiness firms (Roberts, 2015).

A study on improving land and water efficiency on corn concluded that PA offers the potential to automate and simplify the collection and analysis of the information. It allows management decisions to be made and quickly implemented on management zones within the fields (El Nahry, 2011).

Employing PA provides access to a large amount of data that can be used to inform farm management decisions. The term *farming 4.0* has been coined to characterise this new type of information-based farming (Clasen 2016). Of course, the tremendous amounts of data farmers have to deal with following PA adoption may also lead to difficulties. Moreover, agricultural machinery must often be modified, and modern computer technology is required. Furthermore, the correct interpretation of PA data is a challenge. The study also identifies which farmers do not apply PA solutions so that future research and development activities can purposefully address the needs of the current non-adopters by bringing up simpler and, therefore, cheaper technological solutions that address smaller farms and less high-tech oriented farmers. The study also provides starting points for future research.

About the economic and environmental gains of PA technologies, it was shown that 30% of farmers and 69% of crop farmers running larger farms (i.e., of more than 500 ha) had adopted PA technologies, while the group with smaller arable land holdings (i.e., 1 to 99 ha) had significantly fewer PA adopters (Zhang et al., 2002; Paustian, 2016).

This discrepancy between a pretty common use of information and communications technology (ICT) in everyday life and its low adoption in agricultural business in the studied sample stresses the importance of identifying the reason. Working alone on a farm and having low education was positively associated with the perception of economic and commercial barriers, which predict the adoption of SFTs via the mediation of such perceived economic barriers (Caffaro, 2019). As with any business, farmers are interested in maximising production and making a profit; the governmental supporting policies can reduce the current economic barriers; however, they may not be sufficient to capture the full complexity of farmers' attitudes and beliefs. Such failure pointed out the importance of providing extension services capable of effectively assisting farmers in building knowledge about the benefits of new technologies and promoting their adoption. Concerning farm size, the study showed that working on a small farm lowered the

adoption of SFTs. Smaller farmers are typically unable to keep up with the new technologies because of a lack of investment capital or knowledge, thus creating a significant digital divide between big and small farmers.

According to the survey of 72 farmers in Hungary, 11% of the interviewed farmers use precision farming technology, and the rate of "non-users" was 89%. However, some of the "non-users" adopted GPS-based soil sampling (7%) or GPS tractor guidance (12%), which are part of precision farming technology, but did not use any other elements to achieve site-specific and variable rate treatment (Lencses, 2014).

Precision fertilisation and precision plant protection were the most frequently used elements of precision farming technology according to the ranking of "users". Tractor guidance and grid soil sampling were not among the most common elements in the "user" sub-sample. Otherwise, tractor guidance was a widely used element among "non-users". So many "non-users" had tractor guidance because the operation of this element does not need additional work, and its advantages are appreciable in a short time. With tractor guidance, farmers can treat their fields without overlapping the worked area, with a subsequent potential decrease of the inputs by about 30%. Although tractor guidance bases on an ICT solution, it is not a site-specific or variable rate operation, so this is the reason why precision farming technology elements do not include it. The relationship between the adoption of precision farming technology and some parameters of farms or farmers was examined with cross-table analysis. It resulted that the adoption of precision farming technology only depends on the quantity of the cultivated land and the age of the farmers. Precision farming technology has mostly been adopted by farms with more than 300 hectares of cultivated land and farmers younger than 40 years of age (Lencses, 2014).

Comparing conventional weed control strategies with precision farming technologies pointed out that: 1) weed hoeing using automated steering technologies reduced weed densities in soybean by 89% and in sugar beet by 87% compared to 85% weed control efficacy in soybean and sugar beet with conventional weeding systems; 2) the speed of weed hoeing could be increased from 4 km h^{-1}, in case of conventional hoes, to 7 and 10 km·h^{-1}, following the adoption of automatic steering systems; 3) precision hoeing technologies increased soybean yield by 23% and sugar beet yield by 37%. Moreover, after conventional hoeing and harrowing, soybean yields increased by 28% and sugar beet yield by 26% (Kunz, 2015).

To fully understand the needs of farmers or contractors to move to precision agriculture, it is good to define the current required operations and what they entail. We, therefore, analysed the primary operations required and the main requirements that must be performed during the cultivation year. They resulted: 1) the relief of the borders: it is necessary to trace and digitise the position of the different parcels on software in order to view their location and record the activities that are carried out during the season; 2) terrain mapping: knowing the variability of the land is the first step to better manage production inputs and calculate its maximum production; 3) automatic driving: it allows the operator to set the work passes so that the machine automatically follows the direction to avoid overlapping; 4) variable rate fertilisation: having information on the variability of the field, it is possible to create prescription maps to distribute the fertilizer in a differentiated way according to the characteristics of the soil and the vegetative state of the crop; 5) the seeding at variable rate: as the soil is able to feed the plant according to its degree of fertility, it allows to plan the suitable investment in plants m^{-2}; 6) variable rate spraying: to make weed management efficient and environmentally friendly, systems have been adopted that are able to close the bar sections that are not needed or that overlap areas already sprayed; 7) the harvesting maps: knowing the final result of the management allows to monitor each area of the field and analyse how much precision farming techniques have influenced the yield and quality of the harvested product; 8) the reporting: the data collected allow the farmer and company technicians to understand how the cultivation took place and to plan improvements for the following season to further improve yields and sustainability (Casa, 2017).

The first step that is recommended is the soil mapping of the farm. The result of this step is reported hereafter briefly. Figure 1 represents the geo-referenced output of the soil mapping carried out using Automatic Resistivity Profile (ARP). These were associated with punctual soil samplings, that throughout the experimental site, different soil conditions do exist because of soil structure and the changes farming activity went through during the time. When comparing soil mapping with crop production characteristics (amounts and quality), a good correlation exists between these features (Figure 1).

In order to manage such physical soil differences, the non-uniformity of the geometry of the fields and to introduce controlled traffic, several choices are available. The preliminary investigation highlighted that the decision was highly dependent on the chosen tractor's level of technology. This research defined four levels of tractor technologies. In order to save money, it could be possible to earn an old used tractor, hereafter T1. However, in front of such an expensive optional, there is no possibility of managing 'tractor's ECU with the ISOBUS, acting electrohydraulic of the implement could be impossible and has to be done manually, there no possibility of transmitting tractor's data to software (telemetry).

Another choice could be to adopt a used tractor predisposed for ISOBUS, hereafter T2. In this case, the problems

could regard some implement action and, again, the possibility of transmitting the tractor's engine data (telemetry).
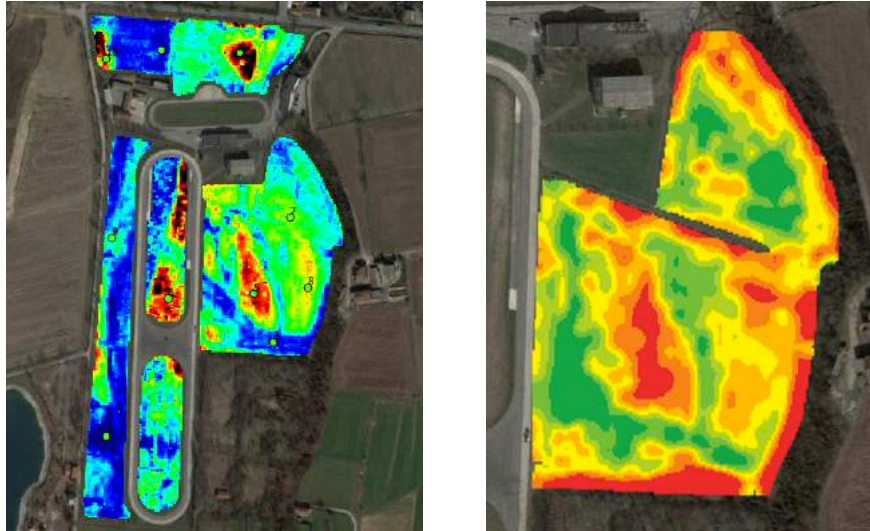
Figure 1. Representation of soil texture, and sampling points, and crop (Triticale) yield maps in the experimental fields at the CREA experimental farm (Treviglio).

The third choice, T3, is the purchase of a new tractor wholly geared toward the required needs, but with the optional parts to be purchased (Global Navigation Satellite System -GNSS- receiver, terminal unit, ISOBUS system). The same tractor can also be purchased entirely full-optional (T4 option). The choice of the tractor is a fundamental step to achieve the desired level of PA: the available options cannot suffice in increasing the technology level of a tractor up to a given performance level.

CREA decided to adopt a T1 tractor purchasing as optional an *entry-level* navigation system (GNSS receiver, low precision antenna L1, a low level of terminal unit, electric system at the drive-wheel for auto-guidance).

The CREA of Treviglio chose a 117 kW nominal power tractor with CVT transmission provided with commercial PA technologies. It was adopted to acquire the field boundaries to develop the guidelines for working soil and the primary operations with conventional implements. In order to read data, developing the guidelines for working, to have access to the tractor's path and working time, it was necessary to have access to the manufacturer software that required an annual fee.

Additional services and fees are often necessary to reach higher precision levels or have access to tractor and field data management systems. This level of precision agriculture allowed to change the farm approach, above all, considering the data available and in terms of operator comfort. Then it was decided to improve the mechanisation with specific implements for operating precision agriculture in a cereal zootechnic farm (i.e., a fertilizer, a sprayer and a seeder).

Following such choices, the enabling of controlled traffic became somehow mandatory, requiring the upgrade of the system to manage specific PA implements and achieving a precision of 2 cm. In practice, to upgrade the system's precision, it was necessary to adopt a double frequency antenna L1 and L2 (on the tractor) and place an RTK fixed antenna with additional fees. Even the software required upgrading (paying an additional fee) to have the possibility of managing additional tools.

Moreover, it was necessary to adopt an ISOBUS system that, considering the current state of the art for the operator, has been associated with only one monitor and one terminal unit able to manage tractor, guidance, implement.

The purpose is to underline that some technologies are ready to be adopted, and other could require additional efforts or consultants. So, the project evaluates the differences between the different levels of technologies in terms of cost, indicating the economic impact and the necessity of adopting software, fixed fees, and consultants.

2. Materials and Methods

At the start of the project CREA experimental farm had two tractors with a completely mechanic driveline, a 4WD 80 kW (1988) and a 2WD 66 kW (2003), one four rows seeder for maize, a conventional rotational fertilizer of 14 meters spread width and a sprayer with 12 meters spraying boom. The farm was not adopting GNSS or auto-guidance system.

A virtual fleet was developed, focusing on a zootechnical cereal farm and analysing the results of introducing different levels of precision agriculture at the agro-mechanical level entailed.

Three implements were considered: seeder (Si), fertilizer (Fi), sprayer (Bi). Consequently, it was considered to adopt a 110 kW tractor, considering that heavy drawbar works and transport, usually in a farm, are performed with another, more powerful tractor. Four tractors type were analysed and adopted for the simulation:

- T1: 15-year tractor, completely mechanic, not predisposition for auto guidance, ISOBUS or GNSS system
- T2: 10-year tractor with continuously variable transmission, the possibility of adopting ISOBUS, GNSS, and auto-guidance system.
- T3: new tractor, fully predisposed for ISOBUS, GNNS system, and auto-guidance, but with optional PA tools.
- T4: a new full optional tractor.

The study hypothesizes that by establishing different levels of PA technology adoption, it could be easier its adoption for the operator.The fertilizer resulted in the implementation of a certain level of technology, so it was decided to divide the technology of this implement in two classes, conventional (F1) and at variable rate in four sections (F2).

The seeder technology presents a high range of options: conventional (S1), with the possibility of excluding some rows (S2), to choose the seed density and the possibility of choosing the seed depth (not considered in this study).

Also, the sprayer can be considered in different classes, mainly conventional (D1), with the possibility of adopting four sections (D2) or with the possibility of managing every single nozzle (not considered in this study).

The variables taken into account are the following:

- Level of precision
  - L1: low precision GNNS (20 cm)
  - L2: RTK precision GNNS (2 cm)
- Virtual terminal
  - V1: Base level
  - V2: High level (more precision and the possibility of managing the tractor and the implement on the same screen)
- Implement
  - S1; F1; B1: Traditional
  - S2; F2; B2: ISOBUS VRT
- Auto-guide system
  - G1: Assisted
  - G2: Auto-guide (T3 at the steering wheel; T4 at the steering cylinders)

In this paper, five possibilities correlated to the desired level of technology are presented, but several other configurations are, obviously, possible.

Total equipment costs include all costs accrued from buying, owning and operating equipment. Fixed costs, operating costs and labour costs have been considered following the method proposed by Miyata (Miyata, 1979).

The adopted scheme is reported in table 1.

In order to evaluate the advantages potentially resulting from the different levels of PA technologies, an experimental test has been carried out in the following settings:

1. C1 (Conventional): T1N- F1
2. C2 (Precision Agriculture): T1Y-L2-V2-F2-G2

The experimental layout involved two fertilizers (F1; F2), both with two rotors. F1 is not ISOBUS and could be regulated with the setting of 12 or 24 meters wide, manually, with a hydraulic distributor; the calibration system followed the table of the implement and tractor speed. F2 is an ISOBUS VRT fertilizer, is automatically controlled with the possibility of 6, 12, 18, 24 meters wide and had a balance continuously monitoring the given dose as the weight of the distributed and that in the implement container.

Both the tractors were 4WD, 117 kW, and CVT. Tractor one (T1N) had not a GNNS system or an auto-guide.

T1Y was fitted with a high precision GNSS system (RTK, L2), auto-guide system and ISOBUS system.

Table 1. The virtual fleet setting taken into account

Setting code	Variables code	Description	Task characteristics
S0	T1-S1-F1-B1	Not ISOBUS implement No GNSS system	Tasks are developed without PA technologies
S1	T2-L1-V1- S1-F1-B1-G1	Not ISOBUS implement Assisted guide	Positional reference for the operator for all the tasks
S2	T2-L1-V1- S1-F1-B1-G2	Not ISOBUS implement Auto-guide GNSS with low precision	Positional reference for the operator and auto-guide, the advantages are mainly in terms of comfort
S3	T3-L1-V1- S1-F2-B2-G2	The implement adopted are ISOBUS. GNSS with low precision	This configuration is interesting also for working soil operations but is not suitable for maise.
S4	T4-L2-V2- S2-F2-B2-G2	The implement adopted are ISOBUS. The precision is 2 cm	This configuration allows operations that require high precision. ' 'It's suitable also for maise.

It was practically not possible to spread fertilizer on the same fields two times, so in order to compare the results, it was followed the method:

- T1N and T1Y had to work 9 hours in the same day starting together;
- T1N and T1Y had to fertilize at the same speed of 10 km h^{-1};
- The fields with the less regular shape were assigned to T1Y. This could appear penalising T1Y, but it was retained a priority not to favour this last;
- Tractors started with the full fuel tank and the fuel consumption was measured at the end of the day;
- The tractors did not have telehandler assistance close to the field for refurnishing fertilizer, therefore they had to come back to the farm;
- T1N had to give the same dose for all the fields, T1Y worked at different dose, depending on the field. T1Y worked with variable section technology but not following prescription maps.

The measured variables resulted: hectares worked, fertilizer distributed, fuel consumption, working precision as fertilizer distributed.

Considering the choice of adopting precision system, it has to be considered that there is a need to acquire the field boundaries. Moreover, field mapping is necessary too and these operations were not taken into account during the experimental test because the maps were already present in T1Y tractor. Effectively this operation has to be done only one time.

3. Results and Discussion

The cost analysis confirmed a wide possibility of setting the agro-mechanic fleet as the desired task.

In particular, considering the conventional tractor and implement, for a 200 ha farm, the cost may start from 31,800 €y^{-1} up to 46,800 €y^{-1} of the full-optional setting comprising ISOBUS VRT implements, use of prescription maps, software, fees and consultants. This evaluation does not cover the different field capacity that PA technology offers (time and fuel consumption savings, product saving), so it has been supposed that the several different fleets would have taken the same time for performing the same task. These costs have been based on prices observed in Italy and with a mean price of similar machines.

Moreover, the Italian policy of incentives provides farmers with 40% support for the purchase of precision farming machines, this has not been considered in table 2. Following these considerations, the difference of 47% more of cost, also considering the full optional configuration confirms that the topic is worth of deepening.

The main advantages that users already equipped with PA technologies reported on agricultural machine is the better way of managing the work and the improved operator comfort. Unfortunately, such considerations are not straightforwardly measurable and there is the arising sensation that the benefits from PA are several and not uniquely determinable or measurable. The analysis of one implement in detail, i.e. the fertilising machine, helps overcoming such difficulty.

Table 2. Virtual fleet setting annual costs (without considering money saving offered from the PA technologies) for a 200 ha farm.

Setting code	Variables code	Main technical of the fleet	Task possible advantages	Annual cost € y⁻¹
S0	T1_F1_S1_D1	Conventional	Conventional	31,800
S1	T2_F1_S1_D1_G1_V1	Assisted guide Low precision GNSS No ISOBUS Basic virtual terminal	Working soil Fertilisation	33,000
S2	T2_F1_S1_D1_G2_V1	Auto guide Low precision GNSS No ISOBUS Basic virtual terminal	Working soil Fertilisation Operator comfort	34,800
S3	T3_F2_S1_D2_G2_V1	Auto guide Low precision GNSS No ISOBUS Basic virtual terminal	Fertilisation VRT Sprayer VRT (i.e. wheat, no maise)	44,300
S4	T4_F2_S2_D2_G2_V2	Auto guide High precision GNSS ISOBUS High level virtual terminal	Fertilisation VRT Sprayer VRT (also maise) Seeding Prescription maps Farm and fleet management software	46,800

Even though the fertilizer could seem unsuitable for such assessment because in terms of precision it is difficult to immediately appreciate the advantages resulting from a machine designed to distribute the product random broadcast in a defined dose per hectare. The reason is in the broad area covered during the operation that is difficult, time consuming, and tiring for the operator to control.

The result of the experimental test carried out with the two tractors and fertilizer are reported in table 3.

Table 3. Experimental test result of a VRT fertilizer (C2) vs conventional (C1)

Setting code	C1	C2
Variables code	T1N_F1	T1Y-L2-V2-F2-G2
Total working time (h)	9:00	9:00
Worked soil (ha)	27	41
Error of distributed fertilize (%)	+18	+4.9
Fuel consumption (l)	75	80
Fuel consumption (l ha⁻¹)	2.8	2.0

The results appear immediately excessively good in favour of the PA tractor and fertilizer.

The 52% of worked soil more is complicated to understand, considering that a hypothesis was that could be expected 20%. Also, the fertilizer distributed shows a strange, not immediate data, is far to be proportional to the worked soil. With PA technologies, considering the dose distributed per hectare, is 22% less, anyway closer to what expected. In order to evaluate and appreciate these data is not enough considering the precision of the system or the hypothesis of the overlapping.

In fact, the PA system has differentiated the dose per hectare following the requirement of the agronomist for the different fields.

The operator with the conventional implement has not changed the dose depending on the different field and has chosen to give the highest dose to all the fields. It is possible to split these two questions. An error of about 18% more than the desired. The PA operator (C2) could achieve the target mean of the different fields.

The PA operator set a theoretical target, but it's an ideal value ,not performable in practice. He distributed with a difference of 4.9% more. At the end of the work, the measured dose from the software of the implement differed the distributed dose of 0.6%. The possibility for the PA operator to easily change the dose for each field and the lowest

error explain the difference between the two performances.

But also considering these factors could not be clear why the first operator had an error of 18% and the 52% of field capacity of C2 that, perhaps, could really explain the advantages of the PA technology. Commonly, is considered the problem of overlapping or of the borders, but it's better to explain what does it mean in practice for the operator.

The Conventional operator (C1) has always worked giving more fertilizer than the target because:

- he was afraid to give less and approximated in excess;
- if C1, in some fields or part of fields, can't forward at 10 km h^{-1}, i.e. 6 or 8, he must perform and calibrate the F1 for all that part of the work at the minimum allowable speed.
- for C2 the last question is not a problem because the F2 change the dose distribution following the speed;
- C1 doesn't fill the container but loads the quantity necessary for the target field (hectares*kg*hectares^{-1} = n° of bag) in order to verify that is correct, C2 loads all the product that is possible because is not important where the container is empty;
- in case C1 arrived at the end of the field and the dose distributed was less (looking into the implement container) he had to pass again on the same field, losing time and precision;
- when the C1 container was empty and he hadn't covered the target surface he had to turn to the farm, fill again the container and return to the same field losing time and forwarding more road.
- C2 cares automatically the precision close to the borders or to the country roads;
- as expected, the overlapping;
- each time there's a pause of the tractor there's a moment that F1 continues distributing and has to be stopped, for F2 is automatic;
- another important question is that the path followed from C1 and C2 are different. Generally, C1 follows before the borders and then the S path in the middle thanks to the VRT technology, for C2 it means losing product and performs directly the S path with a higher error in turnings;
- if the dimensions of the field would require several full containers, C1 has to divide, approximately, the fields in smaller surfaces in order to check the distributed dose.

Substantially, the described situations don't happen with the PA implement thanks to the complete systems of weighing in a continuous mode the fertilizer in the container. The dose is continuously adapted with the target. When the container is empty the target soil surface is correct. This is one of the main advantages of this technology that explain the 52% of more hectares worked and, consequently, of fuel saving and operator's working hours.

The advantages described from this experience are immediately clear looking at the distributed dose map of one of the experimental fields (Figure 2).

Without considering subsidies, the money savings of the process and of the fertilizer, allows achieving economic parity for a farm of 40 ha. Different if the fertilizer was not counted, which would require 220 ha. It is quite easy to pinpoint the results on specific situations, but if in the present experience already with 40 ha the purchase could be justified, although the state contributions have not been counted, the interest in this technology is confirmed.

Figure 2. Map of the distributed dose (on the left in kg ha^{-1}) from the C2 operator (MyJohnDeere). It's immediately clear the followed path and the practical advantages of the use of this technology.

4. Conclusions

The discrepancy between a common use of information and communications technology (ICT) in everyday life and its low adoption in agricultural business stresses the importance of identifying the reason. The apparent difference of the costs required for reaching higher levels of PA technologies discourages farmers to deepen the discussion. This study presents the possibility of establishing different levels of precision agriculture technology adoption to facilitate the operator's approach starting from a base-level of PA technology up to stages of greater complexity and cost if the operating conditions require or suggest it. The experience performed with an ISOBUS fertilizer confirms that some technologies are already set to be adopted and the cost of which is accessible above all in view of the environmental and economic advantages related to the containment of agronomic inputs.

Acknowledgements

References

Caffaro, F., E. Cavallo, 2019. The Effects of Individual Variables, Farming System Characteristics and Perceived Barriers on Actual Useof Smart Farming Technologies: Evidence from the Piedmont Region, Northwestern Italy. Agriculture, 9, 111; doi:10.3390/agriculture9050111

Casa, R. 2017. Agricoltura di precisione: metodi e tecnologie per migliorare l'efficienza e la sostenibilità dei sistemi colturali. Edagricole ISBN 9788850655106, 885065510X

Clasen, M., 2016. Farming 4.0 und andere anwendungen des internet der dinge. In Ruckelshausen, A. et al. (Eds.), Proceedings of GIL annual meeting 2016. Informatik in der Land-, Forst- und Erna ̈hrungswirtschaft. Fokus: Intelligente Systeme—Stand der Technik und neue Mo ̈glichkei-ten (pp. 15–18). Bonn: Koellen.

El Nahry, A.H., R.R. Ali, A.A. El Baroudy, 2011. An approach for precision farming under pivot irrigation system using a remote sensing and GIS techniques. Agricultural Water Management 98, 517-531. Doi:10.1016/j.agwat.2010.09.012

Kunz, C., J.F. Weber, R. Gerhards, 2015. Benefits of Precision Farming Technologies for Mechanical Weed Control in Soybean and Sugar Beet—Comparison of Precision Hoeing with Conventional Mechanical Weed Control. Agronomy, 5, 130-142; doi:10.3390/agronomy5020130.

Lencses, E., I. Takacs, K. Takacs-Gyorgy, 2014. Farmers' Perception of Precision farming Technology among Hungarian Farmers. Sustainability, 6, 8452-8465; doi:10.3390/su6128452

Miyata, E.S., 1980. Determining fixed and operating costs of logging equipment. USDA Forest Service, General Technical Report NC-55, 16 p

Paustian, M., L. Theuvsen, 2017. Adoption of precision agriculture technologies by German crop farmers, Precision Agriculture 18:701–716 DOI 10.1007/s11119-016-9482-5

Roland, K.R., C. Burton, J.A. Larson, R.L. Cochran, W.R. Goodman, S.L. Larkin, M.C. Marra, S.W. Martin, W.D. Shurley, J.M. Reeves, 2015. Adoption of Site-Specific Information and Variable-Rate Technologies in Cotton Precision Farming Published online by Cambridge University Press: 28 April 2015 Volume 36, Issue 1, April 2004, pp. 143-158 DOI: https://doi.org/10.1017/S107407080002191X

Simulation for Variable-rate Nitrogen Fertilization with Different Application Schemes

Angela Guerrero [a], Abdul M. Mouazen[a*]

[a] Department of Environment, Faculty of Bioscience Engineering, Ghent University, Coupure Links 653, 9000-Gent, Belgium

* Corresponding author. Email: Abdul.Mouazen@UGent.be

Abstract

Optimizing variable-rate nitrogen (N) fertilization (VRNF) is required to minimize input, maximize output, and reduce environmental footprint. This study aims at comparing the amount of N used by traditional uniform N fertilization (URNF) against three VRNF treatments of map-based (MB), sensor-based (SB) and map-sensor-based (MSB) in four commercial fields using a new simulation software. Under the three VRNF treatments, two different application schemes were evaluated: applying more N fertilizer to the more fertile zones (Kings scheme, KS) and more N fertilizer to the least fertile zone (Robin Hood scheme, RHS). Simulations were made after imposing N legislation limits and without imposing them. Finally, VRNF applications were evaluated for a full boom, a section control sprayer and a nozzle control sprayer. Results showed that the VRNF did not exceed the traditional URNF approach, but only if the N limit by legislation is imposed. The RHS consumed 16.4-118.1% less N fertilizer than the KS and 33.3-56.2% less than URNF approach. The best performing RHS-VRNF without imposing N limits was the SB followed by the MSB treatment. However, the KS without N limit always exceeded the applied N fertilizer, compared to the URNF approach, imposing large risks of N leaching. When imposing the N limit, both KS and RHS consumed less N than the traditional URNF approach, except for the MSB under the KS, which used the same N as the URNF. Spatial variability can be observed in the MB approach, temporal variability in the SB approach and both variabilities in the MSB approach. Regarding the spatial variability, no significant differences between section and nozzle control options could be observed, whereas it was minimized when using the full boom control. We concluded that the optimal VRNF is a combination of the RHS and section control, which is expected to result in saving on N fertilizer cost, minimal risk of N leaching, and ensuring N applied is under the set legislation limits.

Keywords: Variable rate N fertilization, simulation, software, uniform rate N fertilization.

1. Introduction

The "application of local resources management in the sense of transferring the site-specific plant nutrient demand into variable rates in dependence on the spatial variability of soil and crop parameters" is defined as site specific or variable rate nitrogen (N) fertilization (VRNF) (Srinivasan, 2007). The core objective of VRNF systems is to optimize economic, environmental and yield factors of the fertilization process. This method has been partially proven to show significant positive differences when compared to uniform rate nitrogen application (URNF) (Basso et al., 2016a; Havlin and Heiniger, 2009; Koch et al., 2004). VRNF systems are divided into map-based (MB) and sensor-based (SB) approaches. When using MB treatment, an assessment of soil fertility is performed by measuring key soil parameters and a fertilization recommendation map is created in advance (offline) with the aim to be implemented by a VRNF machine. In the case of SB approach, the measurements can be done in real-time by using optical reflectance sensors over the crop with the aim to capture information of the crop's nutrient status. This is then used to estimate the nutrient requirements and control the doses in real-time VRNF system (e.g., Commercial Yara System) (Boyer et al., 2011). A new approach of VRNF that accumulates the advantages of MB and SB was recently introduced by Guerrero et al. (2021a), [named map-sensor-based (MSB) VRNF], which merges soil fertility information measured a prior with real-time crop normalized difference vegetation index (NDVI). Through data fusion, different recommendation rates are calculated to supply the right amount of N fertilization that the crop needs at the moment of the application. Additionally, a common concern in VRNF systems is whether to apply more N fertilizer to the most fertile zone [Kings scheme (KS)] or to the least fertile zone [Robin Hood scheme (RHS)]. A study developed by Guerrero et al. (2021b) has partially answered this question by proving that the RHS is a more environmentally responsible and profitable solution, compared to KS or URNF schemes in two commercial fields where barley and wheat were grown. However, further research is required to account for the three VRNF approaches (MB, SB and MSB). The use of URNF might lead to overapplication of N in some parts of a field, which can end up in N-leaching causing several environmental problems. Therefore, in Flanders, Belgium, the Flemish Society of Soil and Land has set the Action Program for the Implementation of the Nitrate Directive 2019–2022 (MAP6), in which strict limits for N fertilization were determined according to the location, the type of soil and the crop to be cultivated. These limits were necessary to avoid the contamination in surface- and groundwaters (Vlaamse Landmaatschappij, 2019b, 2019a). Furthermore, to the best of our knowledge, no literature was found on the evaluation of different VRNF treatments and schemes considering the N limits set by the MAP6. Finally, to fully optimize the performance of VRNF systems, the variable rate machinery resolution plays an important role. In liquid fertilization, the resolution of application can be defined at three levels,

namely, individual nozzle, section control and full spray boom control (Grisso et al., 2011). The full boom control option allows for lower resolution spraying, compared to the section and nozzle control options. Section and nozzle control permit more precise spraying of fertilizers adapting to the field variability and crop needs, making them able to increase yield and farm profitability and reduce environmental risks (Chattha et al., 2014). Simulating the effect of control type on N application during VRNF under the different approaches and schemes mentioned above is necessary to avoid overapplication of N, while providing appropriate resolution of N applied at reasonable cost.

To optimize VRNF, it is necessary to evaluate the aspects mentioned above and all of their combinations, together with different VRNF treatments, schemes, N-limitations and VR dosage at several machine resolutions. However, the evaluation of each of these aspects in VNRF systems in commercial fields, requires intervention in agricultural practices and years of experiments considering several different scenarios. Therefore, a simulation software can be a suitable alternative that can reduce time, effort and costs. The aim of this work is to evaluate three different VRNF treatments (e.g., MB, SB and MSB) using both VRNF schemes (e.g., KS and RHS), based on simulations that consider the soil variability, the crop needs, the N limits set by legislations and the technical specification of variable rate spraying machinery. The study will present the results of a new simulation software which produces VRNF recommendation maps, based on data fusion of soil and crop data acquired at high sampling resolution from four commercial fields in Flanders, Belgium, growing cereal crops.

2. Materials and Methods

2.1. Soil and crop data acquisition

This study was carried out on four commercial fields in three different locations in Flanders, Belgium. Two fields located in Veurne named Beers (12 ha – sandy loam) and Fabrieke (8 ha – loam), one field located in Huldenberg named Kouter (12 ha - silty loam) and a field located in Landen named Gimgelomse (11 ha – loam). The data on soil and crop were collected in 2018-2019 (Kouter) and 2019-2020 (other three fields), with barley grown in Fabrieke and Kouter (2019) and wheat in Beers and Gimgelomse. The soil data was collected by using the online multisensor platform designed and developed by Mouazen (2006), which uses a visible and near infrared (vis-NIR) sensor to produce high resolution data of soil attributes. The detailed description of the sensor and data acquisition can be found in Guerrero et al. (2021b). The historical yield data was only available in Kouter and Fabrieke, where yield was obtained using a combine harvester equipped with a yield sensor. The normalized difference vegetation index (NDVI) data was collected with Sentinel 2 satellite imagery for Beers, Fabrieke and Gimgelomse and by six Green Seeker® sensors installed on a liquid fertilizer spraying machine in Kouter field.

2.2. Data processing and management zone delineation

During online measurements, random soil samples were taken to develop prediction models for soil organic carbon (OC), pH, phosphorus (P), potassium (K), magnesium (Mg), calcium (Ca), sodium (Na) and soil moisture content (MC). The prediction models were developed after vis-NIR spectra pre-treatment and partial least squares regression (PLSR) analysis in RStudio (RStudio Inc, USA) with open-source libraries (Stevens and Ramirez Lopez, 2014). Principal component analysis (PCA) was done before PLSR to examine similarity or differences between soil samples. A total of 179, 121 and 155 soil samples collected from different fields with similar soil texture in three farms were used to develop three groups of models for Veurne, Huldenberg and Landen farms, respectively. Only leave-one-out cross-validation was possible for the Kouter field (in Huldenberg farm), as limited data from this field was available to support independent validation. Both leave-one-out cross-validation and independent validation were possible in the remaining three fields. To this end, the entire data set was divided into calibration (70%), and validation (30%) sets. The prediction performance of the developed models was evaluated by means of the coefficient of determination (R^2), root mean square error (RMSE), and the ratio of performance to inter-quartile distance (RPIQ). Data fusion of yield data (if available), online predicted soil properties and crop NDVI was performed to delineate management zones (MZ) in each field. For Kouter field, yield data collected in 2017, online measured soil properties (excluding MC, Mg, and Na) collected in summer 2018 and NDVI measured in three growth stages of wheat in 2017 were used for MZ delineation. In Fabrieke field, yield data from 2018, online measured soil properties in 2019 and NDVI obtained in spring 2020 were used. For Gimgelomse field, no yield data was available, hence, the delineation of MZ was performed using the online measured K, MC, Mg, OC, P and pH in 2019 and the NDVI obtained from Sentinel 2 satellite imagery in spring 2020. For Beers field, only the online measured properties and the NDVI obtained from Sentinel 2 satellite imagery in spring 2019 were used, as no historical yield was available. The first step for the MZ delineation was a raster analysis, which allowed resampling of the soil, NDVI, and yield data (if available) in a common grid of 5 by 5 m resolution. This was followed by K-means clustering, dividing each field into a limited number of clusters, each having similar soil and crop characteristics. The ranking of the MZ classes into different fertility areas was done according to the online measured soil fertility properties and crop NDVI measurements, in addition to the historical yield information or the farmers experience in case the yield was not available.

2.3. Implementation of simulation software

The maximum effective N rates in kg/ha are generally determined according to area classifications according to MAP6, soil texture and the crop grown. Lands are divided into two subclasses according to soil texture, namely, sandy and not sandy. All four fields in this study were of none-sandy soil textures. MAP6 classifies agricultural soils in Flanders into 4 areas according to run-off potential and dictates additional measures such as the sowing of catch crops after harvest where possible, to achieve the target value of nitrate in agricultural areas in the long term (Vlaamse Landmaatschappij, 2019b). Depending on the area classified by MAP6, strong limitations are required to avoid extra contamination in the soils. Areas 0 and 1 refer to zones where any additional measurements are required while areas 2 and 3 refer to zones where strongest limitations (low effective N dose) need to be applied. Fabrieke, Beers and Kouter are located under area 0, while Gimgelomse is located under area 1. Therefore, according to the Standards and Guidelines of January 2020 (Vlaamse Landmaatschappij, 2020), the maximum allowed effective N rate for non-sandy soils is 175 kg/ha per year for wheat and 125 kg/ha per year for barley. These limits were used to calculate the recommendation of the total N rate by running two fertilization applications along the cropping season. The maximum allowed N fertilizer was 300 kg/ha for wheat (corresponding to 78 kg/ha effective N) and 200 kg/ha for barley (corresponding to 52 kg/ha effective N). In the simulation software, two scenarios were implemented. In the first one the N limits were ignored, and the recommendation doses were calculated based on the VRNF treatments and schemes. In the second scenario, the N limits were implemented, so that the maximum allowed N rate should not exceed these limits, regardless of the calculated VRNF according to treatments and schemes.

Two different schemes are evaluated in this study to understand which approach is the optimal application for VRNF. The RHS applies more fertilizer to the least fertile zones and less fertilizer to the most fertile zones while the KS applies more fertilizer to the more fertile zones and less fertilizer to the less fertile zones. In the VRNF treatments, N rates oscillated between +50% and -50%, depending on RHS or KS scheme that is being used (Table 1). The VRNF treatments of MB, SB and MSB were compared with the traditional URNF treatment.

The recommended N rate was provided by the farmer according to his experience, traditional soil analysis and guidelines of the nitrate directive. This recommended rate was used as URNF treatment. The MB treatment is based on the MZ delineation and the variation of recommended rate percentages was determined according to the fertility class (high, medium high, medium low or low) and the VRNF scheme. In the SB treatment, NDVI obtained from Sentinel 2 satellite images was used to calculate the N rates, dividing the NDVI value in four groups, under the RHS or KS schemes (Table 1). Since the new proposed MSB combines the MB and SB treatments, the in advance determined fertility zones by MZ maps and the NDVI values measured in real-time were combined to calculate the N recommendation rates. Table 1 details the calculation of N rates for each of the four treatments.

In this work three sprayer control options, namely, full boom, section and nozzle control were evaluated. The full boom control is the application of the same rate along the entire spraying boom (33 m or 39 m depending on the commercial machinery). The section control, divides the entire boom into sections of 3 m, where the same rate is applied along the section but varies between sections. Finally, the nozzle control allows to cover 0.5 m and different doses can be applied at higher resolution. The VRNF machine automatically adjusts the rate while driving along the field by using the geo-localized variable-rate map. However, the VRNF machinery requires a stabilization time (lag time) while changing between doses. This period is a lapse in time that the nozzles require to adjust and achieve the next desired rate. For a regular sprayer, driving at an average speed of 8 km/h, the stabilization period is approximated 30s or 15m driving distance. In the simulation software, the N dose will be maintained for this 15m before changing to a new N dose.

The simulation software was designed using Labview programming language (National Instruments, USA). The software performed several tasks: 1) prediction of online soil properties using online collected raw spectra, 2) development of maps of soil and crop parameters, 3) implementation of clustering analysis for MZ delineation, and 4) calculation and simulation of recommendation maps for VRNF treatments (MB, SB, MSB and URNF), under both RHS and KS schemes. The software also allows to impose or ignore the legislative N limits while setting the desired control option (full boom, section control or nozzle control). The system inputs are georeferenced online collected soil spectra, and satellite Sentinel 2 data or proximal sensor measured NDVI. To create an application map for VRNF, the software interface allows the user to indicate the tramline direction, crop type and select the width of sprayer and its control option. The simulation output included the calculated N fertilizer in kg per field, the calculated N fertilizer in kg per MZ and recommendation maps for each option of VRNF. Since N fertilization was performed in two applications (two different dates) along the cropping season, then the final N rate in each VRNF treatment is calculated and compared with the final N rate of the URNF. The traditional URNF treatment designated as the control rate (CR) treatment in this study, corresponds to the recommended rate (obtained from soil analysis) that a crop would receive if only URNF scheme was used. The calculated rates for the URNF were 104 kg/ha effective N for barley and 156 kg/ha effective N for wheat. The final N rates per field and per MZ for the MB, SB and MSB treatments were calculated by adding the amount of N applied in the two applications (assuming equal rates of 50% each).

Table 1. Calculation of nitrogen (N) rate (in %) for map based (MB), sensor based (SB) and map sensor based (MSB) treatments, presented for the Robin Hood (apply more on poor zones) and Kings (apply less on fertile zones) schemes under 3 and 4 management zones (MZ) and differentiated by fertility classes. Each N Rate presents the value for Robin Hood scheme (RHS) followed by the value of Kings scheme in blue color: RHS/KS

VRNF Scheme	Number of MZ	MB treatment		SB treatment		MSB treatment				
		Fertility Class	N Rate (%)	NDVI	N Rate (%)	Fertility Class	NDVI			
							0 - 0.34	0.34 - 0.67	0.67 - 1	
Robin Hood Scheme / Kings Scheme	3	Low	50/-50	0 - 0.25	50/-50	Low	50/-50	25/-25	0*/0*	
		Medium	0*/0*	0.25 - 0.5	37/-37	Medium	25/-25	0*/0*	-25/25	
		High	-50/50	0.5 - 0.75	-37/37	High	0*/0*	-25/25	-50/50	
				0.75 – 1	-50/50					
							0 - 0.25	0.25 - 0.5	0.5 - 0.75	0.75 - 1
	4	Low	50/-50	0 - 0.25	50/-50	Low	50/-50	44/-44	0*/0*	-25/25
		Med low	25/-25	0.25 - 0.5	37/-37	Med low	44/-44	37/-37	-25/25	-37/37
		Med high	-25/25	0.5 - 0.75	-37/37	Med high	37/-37	25/-25	-37/37	-44/44
		High	-50/50	0.75 – 1	-50/50	High	25/-25	0*/0*	-44/44	-50/50

*Refers to the same N rate applied for the URNF.

3. Results and Discussion

3.1. Accuracy of prediction models and management zone delineation

Results results for cross-validation presented high prediction accuracies for OC and MC in Huldenberg, MC in Landen and pH, Mg, Ca and Na in Vernue (R2 > 0.80) and moderate to good prediction for the rest of soil properties (R2 > 0.52). For online prediction using the prediction set, high prediction accuracies (R2 > 0.80) were obtained for MC in Landen and pH, Mg, Ca and Na in Vernue, while moderate to good prediction accuracies were observed for the rest of soil properties (R2 > 51). Veurne models obtained the best prediction results for both cross-validation and online-validation. The fusion of online predicted soil properties, with crop yield and NDVI developed by the k-means cluster analysis explained the spatial variability of the fields by dividing them in three (Kouter and Fabrieke) or four classes (Beers and Gimgelomse) as can be observed in Figure 1. The ranking of the fertility classes in Kouter and Fabrieke were determined mainly based on the historical yield while in Beers and Gimgelomse a meeting with the farmer was held to determine the proper classification.
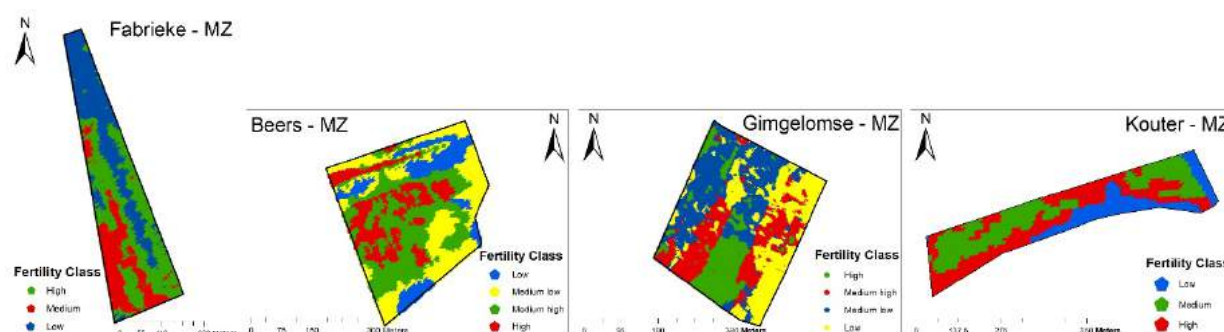
Figure 1. Management zone delineation and fertility classes per field obtained from the K-means clustering analysis.

3.2. Simulation results

3.2.1.Application rates

The output of the simulation software regarding the calculated N rates for each field is presented in Figure 2 for MB, SB, MSB and URNF and under both RHS (Figure 2a) and KS (Figure 2b). VRNF treatments exceed the URNF in the majority of cases (especially for the KS), when the N limit is not considered (Figure 2). When the N limits were imposed all RHS-VRNF treatments presented lower N rates than the CR treatment. Nevertheless, the N rates exceeded

the CR for all KS-VRNF treatments in Kouter and for MSB in Fabrieke and MB in Beers. The published literature based on field experiments in commercial farms have proven to have the potential to improve N fertilization practices by reducing the amount of fertilizer applied (Basso et al., 2016b; Colaço and Molin, 2017; Guerrero et al., 2021b; Kitchen et al., 2010; Link et al., 2006). However, results presented for VRNF when the N limit is not imposed and particularly under KS imply that not always VRNF lead to the reduction of amount of fertilizer but on the contrary might lead to an over-application with both economic and environmental costs. SB treatment seems to have less influence on MSB than MB, since the latest two have the same tendency (Figure 2), which is different than that of the SB. This can be explained by the effect of spatial variability of soil and crop properties, as soil data and subsequently the MZ maps were of higher resolutions. The rates of all VRNF treatments fluctuated along the fields, this can be attributed to the degree of spatial and temporal variability affecting the degree of fluctuation in respect to the URNF. Consequently, the spatial and temporal variability in soil and crop needs to be understood by using proximal and remote sensing tools to be able to capture the interactions between soil-plant-environment, which permits the optimization of VRNF systems (Amaral et al., 2017; Basso et al., 2016c) and can result in both economic and environmental benefits (Kitchen et al., 2010).
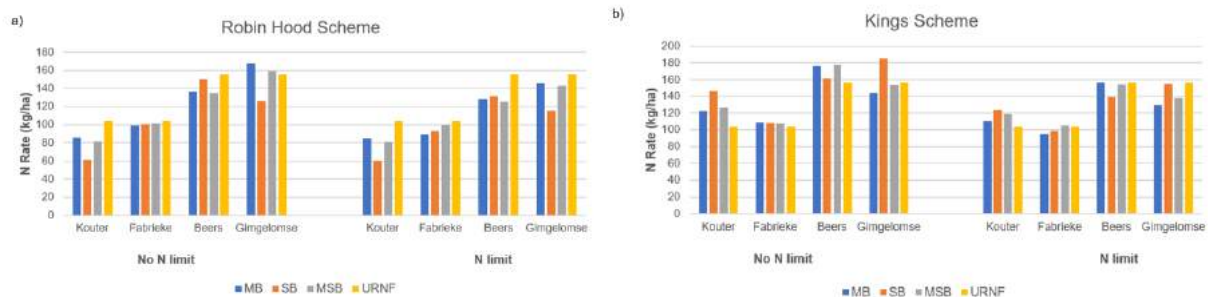
Figure 2. Fertilizer rates applied in each field according to a) Robin Hood scheme and b) Kings scheme. MB: Map-based treatment. SB: Sensor-based treatment. MSB: Map-sensor-based treatment. URNF: Uniform rate nitrogen fertilization. Barley was assumed in Fabrieke and Kouter and wheat in Beers and Gimgelomse.

The calculated N rate of KS-VRNF when the N limits are ignored exceeded the maximum allowed rate of effective N of 125 kg/ha per year for barley and 175 kg/ha per year for wheat. In Beers field, the MB and MSB treatments slightly exceeded the limit (total of 176.41 kg/ha and 177.44 kg/ha per year respectively); in Gimgelomse, the SB treatment exceeded the limit (185.88 kg/ha per year) and in Kouter field, the MSB treatment exceeded it as well (126.86 kg/ha per year). Nevertheless, as expected the calculated N rates did not exceed the maximum allowed N rates for neither RHS or KS, when the legislative N limits were imposed. By imposing the N limits on the VRNF (KS in particular), one can guarantee that the N applied does not exceed the legislative limits and that the nitrate target of 50 mg/l proposed in the nitrate directive can be achieved, which is important since the nitrate target proposed in the nitrate directive is still exceeded in practice in some sand regions (Van Grinsven et al., 2016).

3.2.2. Application maps

The VRNF application maps obtained from the simulation software are presented in Figure 3 for RHS and in Figure 4 for KS. It is clear that in both cases, MB and MSB treatments allow detailed spatial variability which is attributed to the high-resolution data obtained during the soil online scanning. In the case of SB treatment, the application maps are less detailed compared to the MB and MSB maps, and reflect the temporal variability associated with NDVI captured at two different growth stages of the crop (SB_1 and SB_2 maps in Figure 6 and Figure 7). The resolution of the online measurements with the multi-sensor platform (1 m by 12 m) is different than that of satellite images (10 m by 10 m), a difference that is eliminated during the delineation of the MZ by the raster analysis by constructing a common grid of 5 m by 5 m. In the SB treatment no MZ was used hence the sampling resolution was 10 m by 10 m, which is bigger than both the MB and MSB (e.g., 5 m by 5 m). The different resolution may partially explain the coarser resolution of the SB maps. Moreover, more detailed maps are reported to be necessary for more accurate management of within-field variability (Pantazi et al., 2015). But, it is important to note that the resolution of the application map should match or at least not exceed the machine dimension. Still it is true that the SB solution based on crop NDVI data only is not ideal, as no soil data was included in the analysis and recommendation establishment. The fusion between proximal soil sensing and crop remote sensing (in case of MB and SMB) is important not only to evaluate spatial variability and define crop yield limiting factors but to improve within field management of farming input resources (Nawar et al., 2017; Shaddad et al., 2016).
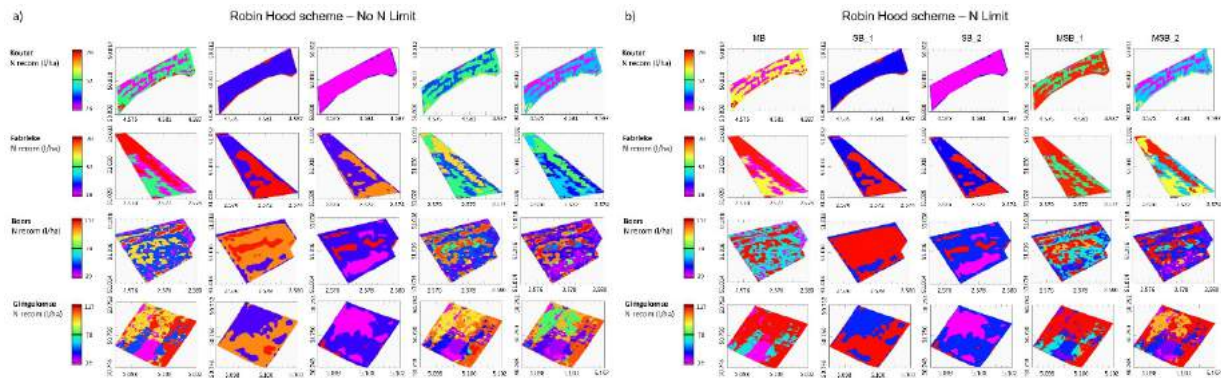
Figure 3. Nitrogen fertilization recommendation (N recom) maps (in l/ha) under Robin Hood scheme per variable-rate treatment. a) Maps ignoring the nitrogen legislative limit. b) Maps considering the nitrogen limit imposed. MB: Map-based treatment. SB_1: Sensor-based treatment first application. SB_2: Sensor-based treatment second application. MSB_1: Map-sensor-based treatment first application. MSB_2: Map-sensor-based treatment second application.
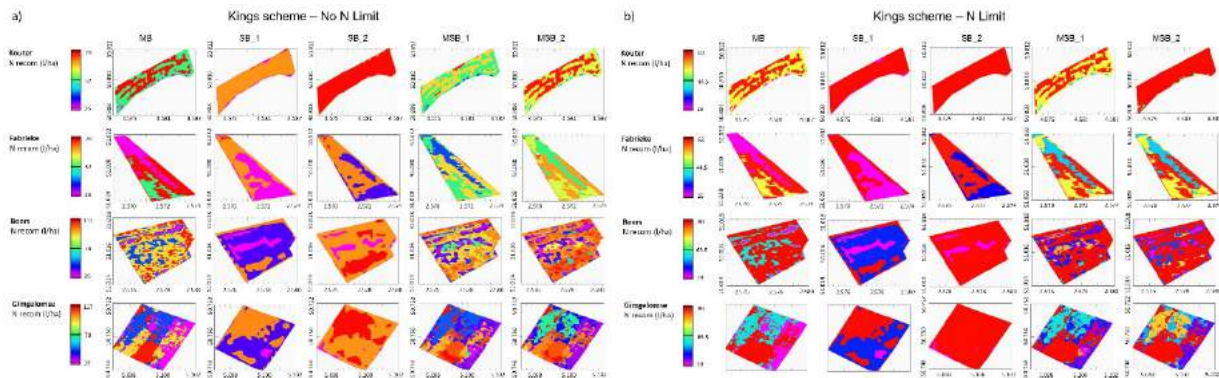
Figure 4. Nitrogen fertilization recommendation (N recom) maps (in l/ha) under Kings scheme per variable-rate treatment. a) Maps ignoring the nitrogen legislative limit. b) Maps considering the nitrogen limit imposed. MB: Map-based treatment. SB_1: Sensor-based treatment first application. SB_2: Sensor-based treatment second application. MSB_1: Map-sensor-based treatment first application. MSB_2: Map-sensor-based treatment second application.

In general, if the N limit is ignored, the fertilization rates exceeded the limit without losing variability in the case of MB and MSB, with the latter showing the lowest N recommended rate (Figure 3). Moreover, in RHS, the maximum rates (red color zones) are observed in SB and slightly less in MB treatment. In contrast, after imposing the N limit, the maximum rate was calculated in large parts of the field in almost all treatments. This can be observed when comparing the variability of the maps when the limit is ignored (Figure 3a) and considered (Figure 3b). Still, the maximum recommended N decreased from 78 to 63 l/ha in Kouter and Fabrieke and from 117 to 88 l/ha in Beers and Gimgelomse, after imposing the legislative N limit (including the RHS). This indicates that even if the N limit is applied and it leads to decrease the maximum rate, the spatial variability is affected in the sense that the rates has the tendency to be uniform limiting the full benefit of the agronomic-optimal VRNF scheme. There are visible larger differences in some areas of KS which are receiving the maximum N rate before and after imposing the limit in comparison with RHS (Figure 4a). Nevertheless, using KS and imposing the N limit, the total areas that should receive the maximum rate increased considerable comparing with the corresponding maps using RHS. This means that the VRNF will be more restricted by KS than RHS, since it will increase the uniformity after imposing the N limits. Some examples of this uniformity in the N application rates can be observed in Kouter and Gimgelomse (Figure 4b). The relative use of N by VRNF treatments compared to the URNF treatment can be analysed by calculating the % of per field recommended N rate in VRNF divided by that of URNF (Table 2). Higher values mean that more fertilizer was used. The relative N use can go over 100%, if the VRNF is larger than that of the URNF. It can be observed that RHS consumed 16.4-118.1% less N fertilizer than the KS and 33.3-56.2% than URNF treatment. As explained before, all the RHS scenarios under-applied N rate compared to the URNF treatment, except in two cases in the Gimgelomse field (Table 2). Additionally, in the KS, the application rates were lower than those of URNF in two cases (e.g., MB and SB with N limit) only the Gimgelomse field (Table 2). The KS consumes more fertilizer than the RHS for both imposing or

ignoring the N limits. The KS with the limits, led to increases in N recommended over the URNF treatment for MB, SB and MSB in Kouter; for MSB in Fabrieke; for MB in Beers and never in Gimgelomse. This means if VRNF treatments are implemented without imposing the legislative N limits, KS will always result in over application compared to the URNF, a result which is supported by the finding of Guerrero et al. (2021b). The RHS will be always an environmentally friendly treatment, as it will result in reducing the amount of N applied per field with or without imposing the legislative N limits.

Table 2. Comparison of % relative fertilizer use by different variable rate nitrogen fertilization (VRNF) treatments and schemes, compared to the uniform rate (URNF) application.

	Robin Hood Scheme - No N Limit	Robin Hood Scheme - N Limit	Kings Scheme - No N Limit	Kings Scheme - N Limit
Map-based (MB)	66.7%	56.3%	142.9%	72.7%
Sensor-based (SB)	46.7%	43.8%	157.1%	90.9%
Map-sensor-based (MSB)	53.3%	50.0%	171.4%	100.0%
Uniform rate (URNF)	100.0%	100.0%	100.0%	100.0%

3.2.3. Effect of variable rate machinery

Recommendation maps for RHS developed for a full boom application (33 m in Kouter and Gimgelomse and 39 m in Beers and Fabrieke), section control (3 m) and nozzle control (0.5 m), are presented in Figure 5. It can be observed that the resolution in application between section (3 m) and nozzle (0.5 m) control are not significant (Figure 5), and these are of much finer resolution than that of the full boom control. It is noteworthy that in SB there are no spraying pattern differences, particularly in Kouter and to a smaller extend in Beers. This can be attributed to the spatial resolution of the NDVI obtained from satellite imagery (10 m by 10 m), which turned out to be larger than the width of the spray boom. Nevertheless, in Fabrieke and Gimgelomse, there are clear differences in SB applications between the three control options. It can be observed that the lapse between two successive rates is highly visible in the recommendation maps. During these laps the crop will not receive the accurate dose of N, which is a limiting factor with large negative effects for the full boom control option, as larger area will be receiving the incorrect amount of N fertilizer compared to the nozzle and section control options. This might lead to over- or under-application and possible agronomic and environmental negative consequences. Nevertheless, the simulation results show that MSB and MB can be implemented in variable rate machinery and that it will match the detailed spatial variability of soil and crop parameters by using section and nozzle control which will guarantee high precision spraying.
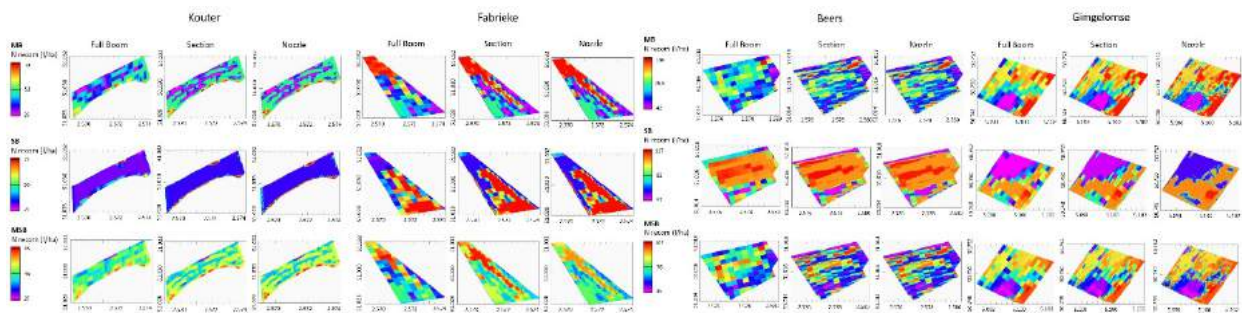
Figure 5. Comparison of Robin Hood scheme with nitrogen limit of variable rate nitrogen fertilization patterns between sprayer three control options demonstrated for the four different fields and variable-rate treatments of MB: Map-based treatment, SB: Sensor-based treatment and MSB: Map-sensor-based treatment. N recom: Nitrogen recommendation.

4. Conclusions

A new software to simulate VRNF under different variable rate scenarios, treatments and spray boom control width was established and used to set the optimal solution from the environmental, economic, and technical points of view. The simulation was carried out using soil and crop data collected at high sampling resolution from four commercial wheat and barley fields. Simulations were also done for the cases of imposing and neglecting the legislative N limit. Results allowed the following conclusions to be drawn: 1) Both VRNF schemes consume less amount of N if the legislative N limit is imposed, with KS consumes consuming more fertilizer than RHS. If the limit is not considered, the fertilizer use in general was higher with KS than with both RHS and URNF. The N limit should be imposed in all scenarios of KS treatment to prevent over-application of N with potential negative environmental consequences.

Although in RHS it is not necessary to impose the legislative N limit, as the field VRNF used less N than the recommended URNF in the top majority of cases, it is recommended to impose them to eliminate any risk of over-application of N above the legislative limits. 2) Spatial variability was optimally managed by the MB treatment, temporal variability by the SB treatment and both variabilities by the MSB treatment. 3) Both the section and nozzle control provided similar spatial resolution of N recommendation maps, while using the full boom control was of poor resolution. 4) The combination of RHS (with or without N limit) with section control is the best VRNF solution, as it minimizes the use of N and subsequently environmental impacts, while maximizing precision of application to best manage within-field variability. Future study should validate the proposed optimal solution under field experimental conditions to allow the evaluation of the crop responses. This will be necessary for full economic, agronomic and environmental evaluation of the VRNF. Development in the hardware and software might be necessary to minimize the lapse time between each pair of successive recommendation rates.

Acknowledgements

References

Amaral, L.R., Trevisan, R.G., and Molin, J.P. (2017). Canopy sensor placement for variable-rate nitrogen application in sugarcane fields. Precis. Agric. 1–14.

Basso, B., Dumont, B., Cammarano, D., Pezzuolo, A., Marinello, F., and Sartori, L. (2016a). Environmental and economic benefits of variable rate nitrogen fertilization in a nitrate vulnerable zone. Sci. Total Environ. 545–546, 227–235.

Basso, B., Fiorentino, C., Cammarano, D., and Schulthess, U. (2016b). Variable rate nitrogen fertilizer response in wheat using remote sensing. Precis. Agric. 17, 168–182.

Basso, B., Dumont, B., Cammarano, D., Pezzuolo, A., Marinello, F., and Sartori, L. (2016c). Environmental and economic benefits of variable rate nitrogen fertilization in a nitrate vulnerable zone. Sci. Total Environ. 545–546, 227–235.

Boyer, C.N., Wade Brorsen, B., Solie, J.B., and Raun, W.R. (2011). Profitability of variable rate nitrogen application in wheat production. Precis. Agric. 12, 473–487.

Chattha, H.S., Zaman, Q.U., Chang, Y.K., Read, S., Schumann, A.W., Brewster, G.R., and Farooque, A.A. (2014). Variable rate spreader for real-time spot-application of granular fertilizer in wild blueberry. Comput. Electron. Agric. 100, 70–78.

Colaço, A.F., and Molin, J.P. (2017). Variable rate fertilization in citrus: a long term study. Precis. Agric. 18, 169–191.

Van Grinsven, H.J.M., Tiktak, A., and Rougoor, C.W. (2016). Evaluation of the Dutch implementation of the nitrates directive, the water framework directive and the national emission ceilings directive. NJAS - Wageningen J. Life Sci. 78, 69–84.

Grisso, R.B., Alley, M., Thomason, W., Holshouser, D., and Roberson, G. (2011). Precision Farming Tools : Variable-Rate Application. Virginia Coop. Ext. 1–16.

Guerrero, A., De Neve, S., and Mouazen, A.M. (2021a). Current sensor technologies for in situ and on-line measurement of soil nitrogen for variable rate fertilization – A review. Adv. Agron.

Guerrero, A., Neve, S. De, and Mouazen, A.M. (2021b). Data fusion approach for map-based variable-rate nitrogen fertilization in barley and wheat. Soil Tillage Res. 205, 104789.

Hassan, M.A., Yang, M., Rasheed, A., Yang, G., Reynolds, M., Xia, X., Xiao, Y., and He, Z. (2019). A rapid monitoring of NDVI across the wheat growth cycle for grain yield prediction using a multi-spectral UAV platform. Plant Sci. 282, 95–103.

Havlin, J.L., and Heiniger, R.W. (2009). A variable-rate decision support tool. Precis. Agric. 10, 356–369.

Kitchen, N.R., Sudduth, K.A., Drummond, S.T., Scharf, P.C., Palm, H.L., Roberts, D.F., and Vories, E.D. (2010). Ground-based canopy reflectance sensing for variable-rate nitrogen corn fertilization. Agron. J. 102, 71–84.

Koch, B., Khosla, R., Frasier, W.M., Westfall, D.G., and Inman, D. (2004). Economic Feasibility of Variable-Rate Nitrogen Application Utilizing Site-Speicific Management Zones. Agron. J. 96, 1572–1580.

Kuang, B., and Mouazen, A.M. (2011). Calibration of visible and near infrared spectroscopy for soil analysis at the field scale on three European farms. Eur. J. Soil Sci. 62, 629–636.

Link, J., Graeff, S., Batchelor, W.D., and Claupein, W. (2006). Evaluating the economic and environmental impact of environmental compensation payment policy under uniform and variable-rate nitrogen management. Agric. Syst. 91, 135–153.

Mouazen, A.M. (2006). Soil Survey Device. International publication published under the patent cooperation treaty (PCT). World Intellectual Property Organization, International Bureau. International Publication Number: WO2006/015463; PCT/BE2005/000129; IPC: G01N21/00; G01N21/0.

Nawar, S., Corstanje, R., Halcro, G., Mulla, D., and Mouazen, A.M. (2017). Delineation of Soil Management Zones for Variable-Rate Fertilization: A Review.

Pantazi, X.E., Moshou, D., Mouazen, A.M., Alexandridis, T., and Kuang, B. (2015). Data fusion of proximal soil sensing and remote crop sensing for the delineation of management zones in arable crop precision farming. CEUR Workshop Proc. 1498, 765–776.

Shaddad, S.M., Madrau, S., Castrignanò, A., and Mouazen, A.M. (2016). Data fusion techniques for delineation of site-specific management zones in a field in UK. Precis. Agric. 17, 200–217.

Srinivasan, A. (2007). Handbook of precision agriculture: Principles and applications. Euphytica.

Stevens, A., and Ramirez Lopez, L. (2014). An introduction to the prospectr package. 1–22.

Vlaamse Landmaatschappij (2019a). Overzicht wijzigingen MAP 6.

Vlaamse Landmaatschappij (2019b). 6de actieprogramma in uitvoering van de nitraatrichtlijn 2019-2022.

Vlaamse Landmaatschappij (2020). Normen en richtwaarden 2020. 1–19.

Detection of Leek Rust and White Tip Disease Under Field Conditions Using Hyperspectral Proximal Sensing and Supervised Machine Learning

Appeltans Simon [a], Pieters Jan[b] , Mouazen Abdul M.[a,*]

[a] Department of Environment, Faculty of Bioscience Engineering, Ghent University, 9000 Ghent, Belgium

[b] Department of Plants and crops, Faculty of Bioscience Engineering, Ghent University, 9000 Ghent, Belgium

* Corresponding author. Email: Abdul.Mouazen@UGent.be

Abstract

Crop diseases remain one of the key yield-limiting factors in leek production, causing the need for continuous fungicide applications, resulting in socio-economic and environmental costs. Precision agriculture aims at reducing these costs, while maintaining or improving farmer revenues. The first requirement for the implementation of variable rate fungicide application is in-field measurement of the spread of disease. In this work, a disease detection methodology was created that could detect early stages of disease development in field conditions for two main diseases: leek rust and white tip disease. A hyperspectral training library was constructed for both diseases separately, containing spectra corresponding to healthy leek, weed plants, diseased leek plants and soil. A custom preprocessing and soil pixel removal strategy was constructed for each disease. An evaluation of 11 common classifiers was performed, of which a logistic regression classifier provided the highest classification accuracy. This logistic regression supervised machine learning classifier was then trained on the hyperspectral library. For leek rust disease, the focus was on detecting early infection (i.e. single rust pustules). For white tip disease, the model was used to classify the data into four classes: healthy plant material, early (pre-visual) disease, moderate disease, severe disease and fully developed disease. The overall accuracy of the disease model was 98.14% for rust and 96.74% for white tip disease. It can be concluded that the results in this work are an important step towards the mapping of leek rust and white tip disease, and that future research is needed to overcome certain challenges before variable rate fungicide applications can be adopted against leek diseases.template is designed to assist a high quality proceedings book editing and printing.

Keywords: Hyperspectral, Disease Detection, Leek White Tip Disease, Leek Rust Disease, Machine learning.

1. Introduction

Despite modern crop protection strategies, crop diseases remain one of the most important yield and revenue limiting factors in crop production. For leek (*Allium porri*), rust (*Puccinia allii* Rud) and white tip disease (*Phytophthora porri* Foister) cause economic losses due to cosmetic damage, yield reduction and secondary infections (Bart Declercq et al. 2012). This leads farmers to apply regular fungicide treatments once every 1 to 5 weeks to prevent disease incidence. However, these fungicides are costly and put a strain on the environment (Geiger et al. 2010). To deal with the economic and environmental costs associated with crop protection, researchers have developed the principles of precision agriculture. Using precision agriculture, farmers aim to apply the right amount of inputs, in the right place at the right time (Archbold Taylor et al. 2019; Anne-Katrin Mahlein 2016; Nawar et al. 2017). This, in theory, leads to lower operational costs while maintaining or even increasing yields and thus improving revenues. In addition to being profitable, this strategy also aims at reducing the environmental impact of agriculture.

Despite the recent surge in research on precision agriculture, its basic principles have been in practice for many years in leek cultivation, dating back to 1995 (P. D. de Jong, Daamen, and Rabbinge 1995). Farmers at the time mainly relied on visual inspection of the field, after which they could decide to apply full-field fungicides or focus the application on specific areas. Because this method is too laborious for modern crop protection, scientists are looking towards automating disease detection (Zhang et al. 2019; Behmann et al. 2015). Among the most promising novel technologies for disease detection are hyperspectral sensors (Grisham, Johnson, and Zimba 2010; Zhang et al. 2012; Anne-Katrin Mahlein 2016; Zhang et al. 2019). These sensors are able to provide fast, high quality reflectance measurements in dozens up to hundreds of wavebands in the visible (VIS) and near-infrared (NIR) spectrum, making them suited for early disease detection and mapping. However, to the best of our knowledge, no work has been published regarding the detection of leek diseases. Most authors in literature have instead focused on developing resistant cultivars and effective fungicides (Clarkson et al. 1997; P. D. de Jong, Daamen, and Rabbinge 1995; Doherty and Preece 1978; Jennings, Ford-lloyd, and Butler 1990; Smith et al. 2000; Theunissen and Schelling 1996).

The aim of the current work is to introduce and validate a novel method of detecting rust and white tip disease in field conditions using hyperspectral imaging machine learning. It will provide the first step towards mapping the spread of the named diseases throughout the field, to be used as input for applying variable rate fungicides.

2. Materials and Methods

2.1. Test field

The first measurement site was the experimental field of the 'Provinciaal Proefcentrum voor de Groenteteelt Oost-Vlaanderen' (PCG), Kruishoutem (Kruisem), Belgium, with coordinates of 50° 56' 40.3404" N, 3° 31' 26.4108" E. This field was used by the experimental centre to conduct a) a leek rust fungicide trial, whereby the Lucretius cultivar was cultivated under normal farming conditions and the efficacy of a range of fungicides was assessed by comparing levels of naturally occurring infection under different spraying regimes, and b) a leek white tip disease sensitivity trial for several cultivars by comparing levels of naturally occurring infection. Leek plants were planted in ridges with a width of 0.65 m and a within row distance of 0.10 m, with four ridges per crop row. Plots were delineated with a length of 2.5 m per plot (Figure 1). Measurements were taken in December 2018 and in February 2019. Data was measured at 6 points along the crop row for leek rust disease, and 5 points for leek phytophthora disease (Figure 1), scanning in the direction perpendicular to the crop row (Figure 1, A). The soil type in this field was loamy sand, with a relatively dark colour.

The second data collection site was the Bottelare experimental farm (Merelbeke, Belgium) of Ghent University and Ghent University College with coordinates of 50°57'45.2"N, 3°45'36.3"E. The soil type in Bottelare consisted of a sandy loam, with a reddish-brown colour. Leek plants of cultivar Pluston were pre-germinated and grown in pots, then transplanted to the field in ridges with a width of 0.75 m, height of 0.30 m and within-row distance of 0.12 m. The field was divided into plots of 3 by 3 m and inoculated on March 18th 2019. The inoculation consisted of four treatments: rust disease, leek white tip disease, both diseases simultaneously and a healthy control, with a total of 16 plots in a randomized block design. Since the first inoculation proved unsuccessful, a second inoculation attempt was performed on April 4th 2019, which was relatively successful. Still, disease pressure in the Bottelare experimental field remained below a few plants infected per plot. Measurements were taken at one-week intervals between March 2019 and May 2019, along the middle two crop rows of each plot (Figure 1, B).
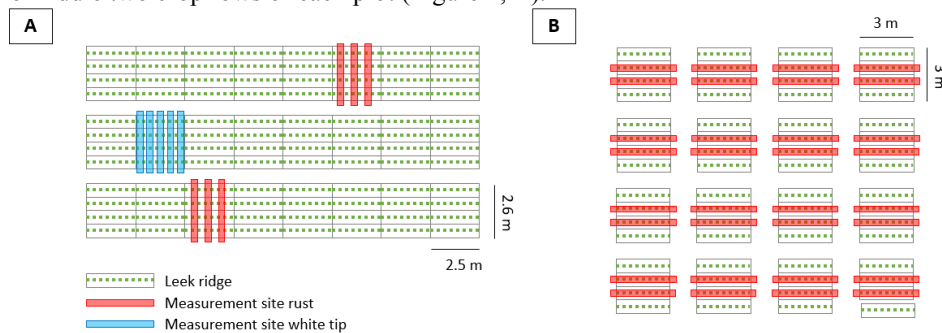
Figure 1: measurement sites at the (A) "Provinciaal Proefcentrum voor de Groenteteelt Oost-Vlaanderen" (PCG) and (B) Bottelare experimental farm.

3.2   Visual assessment of disease severity

Five measurement sites were selected based on the presence of white tip disease in the field at the PCG experimental centre (Figure 1). The level of infection was assessed by technical staff at the centre following the EPPO PP 1/120(2) – guideline on 28/01/2019 and 28/02/2019, showing disease pressures of 1.44% on the first and 2.84 % on the second measurement day. For the Bottelare experimental farm, the disease pressure was too low to be assessed following the EPPO protocol. The methodology described in Clarkson et al. (1997) was therefore followed, by which individual leaves can be assessed for disease severity (Clarkson et al. 1997). The low infection rate was likely due to the weather conditions, which were unusually dry for the time of year and is known to limit infection (Bart Declercq et al. 2012). Most plants in the Bottelare dataset contained zero lesions, with some plants showing signs of early white tip infection (less than 5 lesions per plant).

Six measurement sites were selected based on the presence of rust disease in the field at the PCG experimental centre (Figure 1). The level of infection was assessed by technical staff at the centre following the EPPO PP 1/120(2) guideline on 20/11/2018, showing 0.84% in one plot and 10.32% in the second plot. For the Bottelare experimental farm, the disease pressure was too low to be assessed following the EPPO protocol, so the protocol described in Clarkson et al. (1997) was followed (Clarkson et al. 1997). Most plants contained zero rust pustules, but there was some early disease development with some plants showing 0-10 rust pustules on average.

2.2. Sensor setup

The sensor setup used in these experiments is described in detail in Appeltans et al. (2020) (Appeltans et al. 2020). Hyperspectral data was collected using an FX10e pushbroom sensor (Specim, Finland) from a proximal perspective

(0.30 m above crop canopy), measuring reflectance in 224 bands between 400 and 1000 nm with an integration time of 1 ms.

2.3. Hyperspectral library building

To build the hyperspectral library, the methodology of Xie et al. (2015) was followed in which regions of interest were visually identified containing healthy, diseased and background pixels (Xie et al. 2015). Then, the spectra belonging to these pixels were labelled and exported into separate datasets using ENVI software (Harris Geospatial, USA). The final composition of each training set was 7,436 spectra for each class of the white tip disease model (white tip disease, healthy leek crops both shaded and unshaded, weeds and soil), leading to a total training library of 29,744 spectra, and 10,854 spectra for each class of the leek rust disease model (rust disease, healthy leek crops both shaded and unshaded, weeds and soil), leading to a total training library of 43,416 spectra.

2.4. Preprocessing and model selection

Using the hyperspectral training library, an iterative process was started in which the optimal combination of preprocessing, feature selection and model selection was determined (Figure 2). 11 classifiers were examined using standard and slightly altered parameter settings, including K-nearest neighbors, support vector machine, gaussian process, decision tree, random forest, multilinear perceptron, AdaBoost, gaussianNB, logistic regression, linear discriminant analysis (LDA) and quadratic discriminant analysis (Pedregosa et al. 2011). These classifiers were combined with a variety of preprocessing techniques, including Savitzky-Golay smoothing, normalisation, derivation and feature selection. SelectKBest and SelectFromModel feature selection algorithms were tested (scikit-learn package), but they suffered from high correlation of neighbouring bands (Pedregosa et al. 2011). To solve this, these algorithms were used per region of the spectrum separately, to determine the optimal features for each spectral region of interest. Other dimensionality reduction strategies were tested, including principle component analysis (PCA), LDA, decision tree feature selection, support vector machine feature selection, selection based on highest variance, and visual identification of interesting spectral features.

The first step in the modelling cycle was white/dark reference correction, using a calibrated white reference target (SphereOptics, Germany, Alucore reflectance target, 500 × 500 mm, 95% reflectance). After selecting a combination of smoothing, derivation and normalisation, the data was fed to each of the classifiers. 70% of the dataset was used for model training, while 30% was used for model validation. The highest performing models were retained and used to classify images with known rust or white tip disease infection. Misclassified pixels were examined, and the preprocessing was altered based on the spectral characteristics of these misclassified spectra.
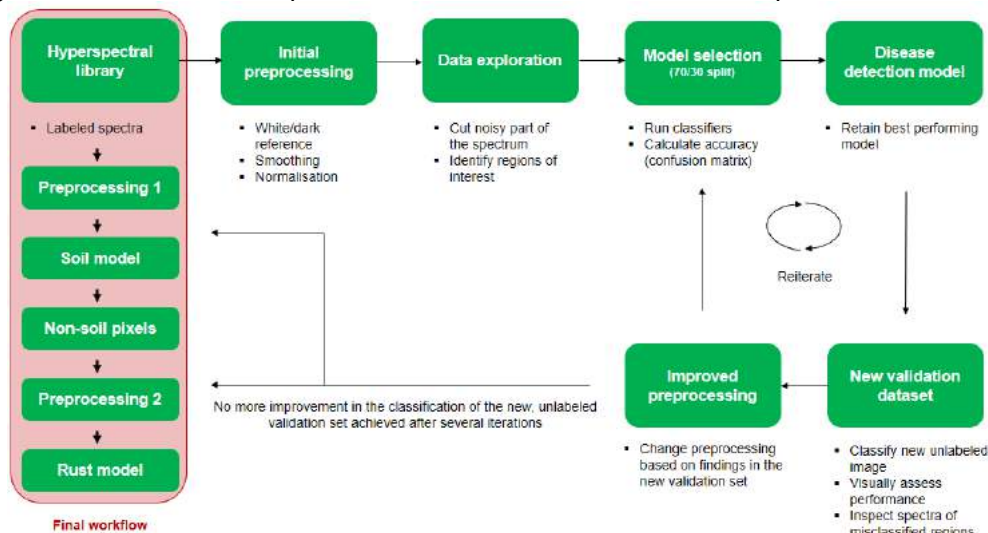
Figure 2: preprocessing and model selection cycle. The area highlighted in the leftmost square box with wording 'Final workflow' represents the final workflow. The rest of the chart represents the steps taken to determine this final workflow.

2.5. Leek rust disease

For leek rust disease, this resulted in a final disease detection workflow containing two models, one for soil and background classification and one for leek rust disease classification. Each of these models had its proper preprocessing step, marked as "preprocessing 1" and "preprocessing 2" in Figure 2. Preprocessing 1 included white/dark reference correction, Savitzky-Golay smoothing algorithm (window 33, polyorder 2), cutting wavebands before 445 nm and after 914 nm, and first derivation. This dataset was then used as input for the soil classification model. The feature used was the 702 nm band of the first derivative spectrum. The model used was a standard LDA algorithm (Pedregosa et al. 2011). Other soil classification strategies such as using normalized difference vegetation index (NDVI) values were also

assessed. The result of the soil classification was used to retain only crop and disease pixels for further modelling. The dataset was then subjected to preprocessing 2. This included white/dark reference correction, Savitzky-Golay smoothing algorithm (window 33, polyorder 2), cutting wavebands before 445 nm and after 914 nm, normalisation (range between 0 and 1), and first derivation.

Certain rust spectra in the hyperspectral library with a low reflection (below 0.13) in the 661 nm waveband showed misclassification issues. Because reflection in the 661 nm band was observed to typically be high in rust pustule pixels, the training labels of these pixels were changed from 'rust' to 'weed'. This reduced misclassification by teaching the model to associate only high reflectance in this waveband with rust disease.

Three features were selected from this dataset: reflectance values at 556 and 661 nm and the value of the first derivative at 511 nm. The model used to identify diseased pixels was a logistic regression model with class weights 0.4 for rust, 1 for healthy leek tissue and 1 for weeds. The LogisticRegressionCV function was used to automatically optimize the C-value parameter, given seven possible values as input (0.1, 0.5, 1, 1.5, 2, 4, 10). A C value of 0.5 was retained. During modelling, 70% of the dataset was used for model training and 30% (randomly selected) was used for model validation.

2.6. Leek white tip disease

The final white tip disease detection workflow contained two models, one for soil and background classification and one for disease classification, each with its own preprocessing strategy. The first preprocessing steps were the same for both soil and disease classification and consisted of: white/dark reference correction, Savitzky-Golay smoothing (window 33, polyorder 2), and min-max normalisation (between 0 and 1), similar to the leek rust disease model. Then, LDA classification was used to distinguish soil from non-soil pixels using the full spectrum as an input. Other soil classification strategies such as using normalized difference vegetation index (NDVI) values were also assessed. The presence of vertical striped noise, interfered with soil classification in the leek white tip disease dataset. A noise removal algorithm was built to remove this noise, by iteratively checking each linescan for noisy pixels and setting their classification result equal to neighbouring pixels.

Since white tip disease causes widespread damage on the leaf surface, it is expected that the pathogen is present in the green tissue surrounding white lesions, before visible symptoms appear. To examine this characteristic of the disease, a cross-section of pixels over a white tip lesion was plotted to examine the development of the spectral signature from healthy to highly diseased. Based on this cross-section, it was observed that the 594 nm band (and surrounding bands) varied greatly as disease progressed. The training data was therefore divided into four training datasets containing the full spectrum, based on the reflection in the 594 nm band: reflectance between 0 and 0.2 = 'early disease', between 0.2 and 0.4 = 'moderate disease progression', 0.4 to 0.6 = 'severe disease progression' and reflectance greater than 0.6 = 'fully diseased. This dataset was then subjected to LDA transformation, which performed best out of all dimensionality reduction techniques. This reduced the dataset to four features, which was then used as input for a logistic regression algorithm to classify different disease stages from healthy leek tissue (Pedregosa et al. 2011). The LogisticRegressionCV function was used to automatically optimize the C-value parameter, given seven possible values as input (0.1, 0.5, 1, 1.5, 2, 4, 10). A C-value of 0.5 was retained. 70% of the dataset was used for model training and 30% (randomly selected) was used for model validation.

3. Results

Figures 3 and 4 show the spectral signatures of leek rust disease and leek white tip disease, respectively.
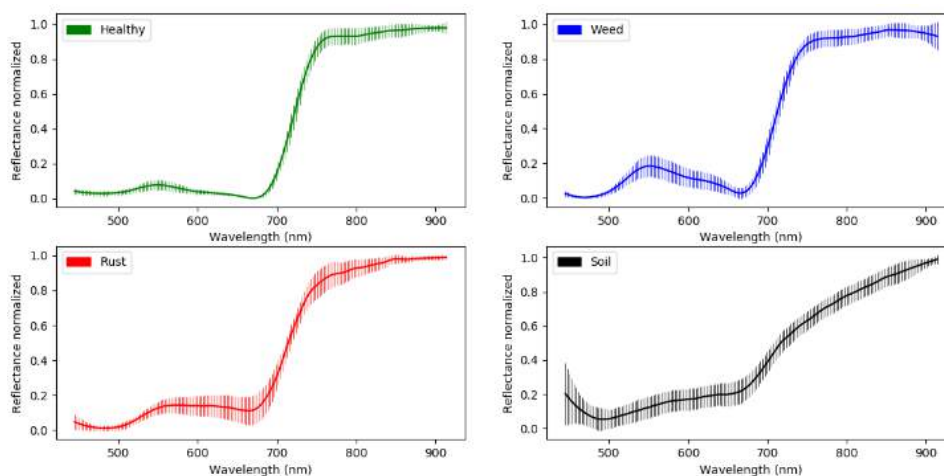
Figure 3: average reflectance curve for each of the four data classes included in the hyperspectral training library, after preprocessing. Error bars show standard deviation, giving an indication of the variability of the data per waveband and per class.
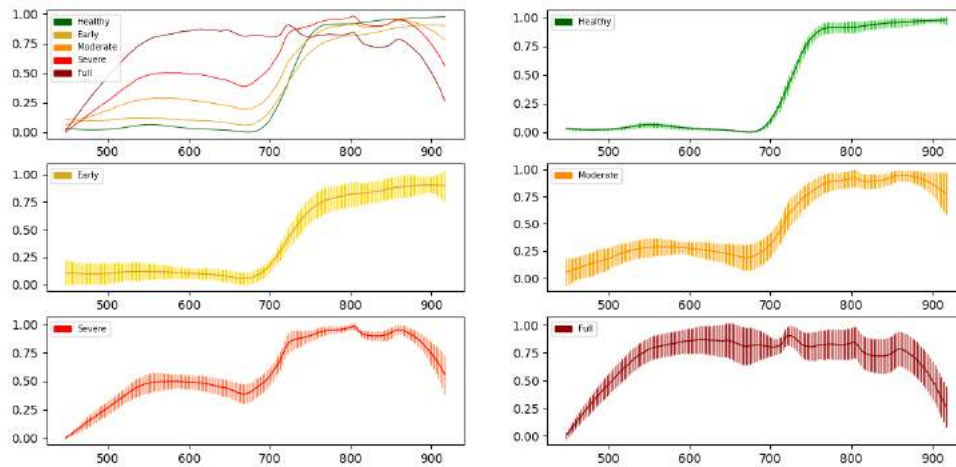
Figure 4: development of the average hyperspectral signature of leek white tip disease from early symptoms to fully diseased lesion. Training data was separated into four disease categories (early, moderate, severe, full) based on the reflectance of the 594 nm band. Spectra were subjected to Savitzky-Golay smoothing and min-max normalisation that scaled them between 0 and 1. X-axis shows wavebands (nm), y-axis shows relative reflectance.

3.1. Leek rust disease detection

The diagnostics of the soil classification model of the rust dataset were calculated based on the confusion matrix for the soil class (not shown), with 30% of the dataset reserved for model validation. Despite the soil classification model achieving a classification accuracy of 94.3%, the true positive rate was 1. This means that the 5.7% accuracy loss was due to misclassification of non-soil spectra, which is insignificant given that the only goal of this model is to accurately classify soil pixels.

Table 1 shows the diagnostics of the leek rust classification model, calculated based on the confusion matrix for the rust class (not shown), with 30% of the dataset reserved for model validation. The rust disease classification model showed an overall classification accuracy of 98.1%. The precision was 99%, meaning 99% of positive 'rust' disease classification results were accurate. This shows the model has been trained to be prone to 'miss' more rust spectra, but to have a high certainty that when a spectrum is classified as rust, it really is rust disease and not a false positive. This can be seen in the true positive rate that indicates that 84.4% of condition positives were correctly classified. The true negative on the other hand was 99.9%, indicating that 99.9% of the condition negatives were correctly classified.

Table 1: Diagnostics based on the confusion matrix (not shown) for the leek logistic regression rust detection model, trained using the reflectance value at 556 and 661 nm and the value of the first derivative at 511 nm. Class weights were set to 0.4 for rust, 1 for healthy and 1 for weeds. The training set was randomly split with a 70/30 ratio for training/validation.

Precision (%)	99%	True pos. rate	84.4%
Accuracy (%)	98.1%	False pos. rate	0.10%
PLR*	812.780	False neg. rate	15.58%
F1 score	0.9115	True neg. rate	99.90%

* PLR = Positive Likelihood Ratio

3.2. Leek white tip disease detection

Since the leek white tip disease model aimed at detecting different stages of disease, the model diagnostics based on the confusion matrix (not shown) have been calculated for each class separately (Table 2). The final classification accuracy of the leek white tip disease detection model was 96.74%. No confusion matrix or diagnostics are shown for the soil classification model. A soil segmentation model had to be chosen that would not affect phytophthora lesions (which show low NDVI, for example). For this reason, there was striped noise in the classified image that had to be removed by a custom-built filter algorithm.

Table 2: diagnostics of the white tip disease detection model derived from the confusion matrix for the results obtained by means of the logistic regression model.

	TPR	TNR	PPV	NPV	FPR	FNR	FDR	ACC
Healthy	99.23	96.41	98.19	98.46	3.59	0.77	1.81	98.28
Early	91.00	98.68	93.92	98.00	1.32	9.00	6.08	97.28
Moderate	86.57	99.21	87.44	99.14	0.79	13.43	12.56	98.45
Severe	88.41	99.89	95.39	99.71	0.11	11.59	4.61	99.61

| **Full** | 99.79 | 99.87 | 98.32 | 99.98 | 0.13 | 0.21 | 1.68 | 99.87 |

*TPR = true positive rate, TNR = true negative rate, PPV = positive predictive value, NPV = negative predictive value, FPR = false positive rate, FNR = false negative rate, FDR = false discovery rate, ACC = accuracy

3.3. Classification of field images

Figure 5 shows a classified image of the leek rust disease. Figure 5A shows the hyperspectral image (RGB representation from the hypercube). Figure 5B shows the classified hyperspectral image. Note that the model was trained specifically to be precise in classifying rust pixels, causing significant misclassifications in weeds vs. healthy leek tissue. Figures 6C and 6D show a close-up of rust pustules with a dimension of 2 mm^2 that have been detected by the model.
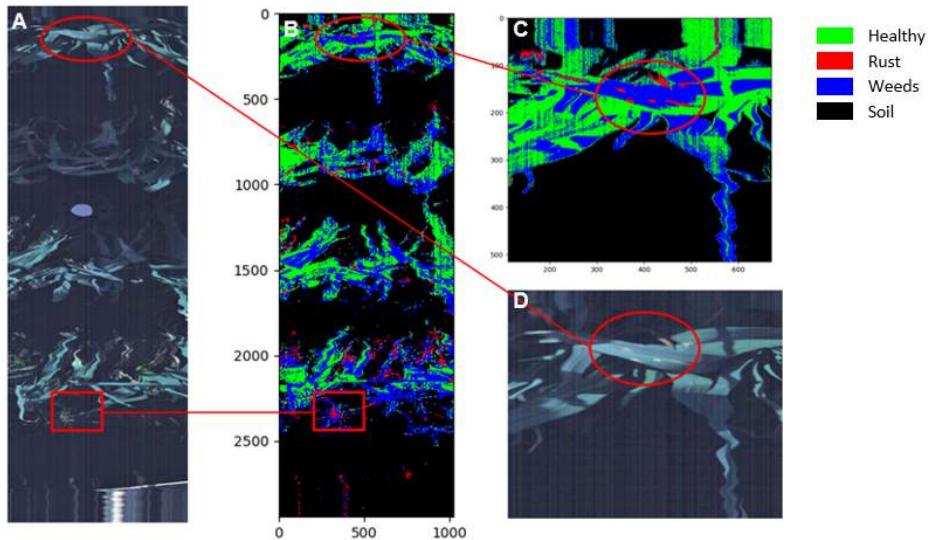
Figure 5: classification of a hyperspectral field image using the soil and leek rust classification models. Red, green, blue (RGB) images shown (A, D) corresponding to the full classified image (B) and a close-up (C). Circles indicate a typical rust infected leaf. Rectangle corresponds to a weed plant that appeared to contain rust disease after classification.

Figure 6 shows the final disease detection workflow. First, soil classification was used to segment the image (Figure 6B). The result was subject to striped noise, which was misclassified as 'crop'. This was solved by a custom noise filter (Figure 6C). Figure 6D shows a close-up of the classified image, showing the concentric pattern of the disease as it spread through the leaf from the initial infection site.
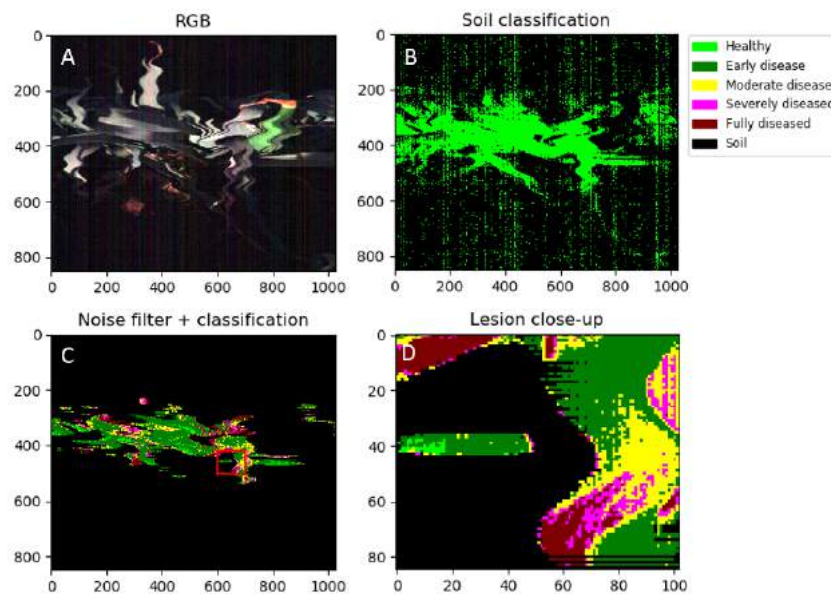
Figure 6: classification of a hyperspectral image of infected leek plants with white tip disease. X and Y axis values represent pixels (0.4 mm pixel size). RGB image is shown as a visual reference for disease severity (A). The soil classification step is shown,

exhibiting striped noise (B). This was solved by a noise filter, after which classification was done (C). A close-up of the classified lesion in the red square area is shown with pre-visible disease detection (D).

4. Discussion

Comparing to literature, there is an absence of available works on hyperspectral-based leek white tip and rust disease detection. It was therefore necessary to compare the classification of the current work with rust or phytophthora diseases on other crops. White tip disease causes more extensive tissue damage ,spreading throughout the leaf, while leek rust disease produces small pustules for propagation, rather than growing throughout the leaf surface. Extensive leave damage opens perspectives for early, pre-symptomatic disease detection before damage becomes visible to the human eye. For leek rust disease, early detection could be considered detecting single rust pustules, as this is the start of infection and causes relatively negligible damage to the crop. Comparing accuracy of disease detection, the leek rust model and white tip disease models perform comparably, with 98.14% and 96.74%, respectively. It needs to be noted however that the overall classification accuracy of the leek white tip model is less significant as an indicator of model performance in the context of variable rate fungicide applications since it is based on 4 disease classes. For these applications, fungicides will be applied as soon as disease is found in any stage of development, making the true negative rate (TNR) of the healthy class a more interesting statistic, because the TNR signifies the ability to detect 'healthy' negative – i.e. 'diseased' – spectra in the population. For this model, the TNR of 96.41% means that only 3.59% of diseased pixels (regardless of the disease stage) were identified as 'healthy'. Modelling the spread of disease throughout the crop in four disease classes is still useful, since it gives an indication on the growth pattern of the disease, and whether the pathogen is still actively growing.

For hyperspectral detection of rust diseases, a large amount of work has been done by authors working on winter wheat (Moshou et al. 2005; Whetton et al. 2018; Whetton, Waine, and Mouazen 2018; Bock et al. 2010; L. S. Huang et al. 2015). Huang et al. (2015) used reflectance in the 704, 1423 and 1926 nm bands to assess yellow rust severity on detached leaves with a coefficient of determination of 88% (L. S. Huang et al. 2015). Zhou et al. (2016) used two wavebands (558 nm and 856 nm) to classify yellow rust disease with an accuracy of 90.6%. Moshou et al. (2005) fused hyperspectral data in the 450 – 900 nm range with fluorescence imaging to detect yellow rust with an accuracy of 94.5%. These results show that the classification accuracy of leek rust disease of 98.14% in the current work appears to be promising and comparable to other rust diseases. The fact that it was possible to detect single rust pustules (Figure 5), means there is potential for identifying early rust infections and therefore possibly variable rate fungicide applications. Moreover, the fact that only three features were used in the current work (556 and 661 nm and the value of the first derivative at 511 nm), all of which are located in the green and red colour region, indicates a potential to replace costly hyperspectral cameras with cheaper multispectral or even RGB cameras. This is in line with findings by Zhou et al. (2015), who were able to detect yellow rust on wheat using RGB cameras at 74% and 81% accuracy (Zhou et al. 2015). The fact that mainly the green and red regions appear interesting for rust disease detection seems logical, given the red appearance of rust pustules. This shows the disadvantage of the LDA transformation that was used to classify white tip disease, whereby the features used can no longer be interpreted.

Hyperspectral detection of *Phytophthora* diseases on other crops than leek has received more attention in literature, with special interest for early disease detection (Franceschini et al. 2019, 2017; Gold et al. 2020; Rumpf et al. 2010; Xie et al. 2015; Fernández et al. 2020). Gold et al. (2020) for example report classification accuracies near 80% for *P. infestans* on potato, depending on the disease stage. However, these results were obtained in laboratory conditions. Fernandez *et al.* (2020) made a notable effort with a classification accuracy of 91.11% on infected potato leaves in controlled conditions. These works achieved disease detection in early conditions, but were executed under laboratory conditions. It is well-described in literature that the transference of disease detection data from laboratory to field conditions can be challenging (Behmann et al. 2015; Bohnenkamp, Behmann, and Mahlein 2019; A.-K. Mahlein et al. 2018; Mishra et al. 2017; Paulus and Mahlein 2020). Comparing these results to the leek white tip disease detection presented in the current work, the accuracy of 96.74% seems promising towards variable rate fungicide applications, given that it was obtained in field conditions.

5. Conclusions

The results presented in this work show that there is potential for early, pre-symptomatic detection of leek white tip disease with a classification accuracy of 96.74%. Detection of leek rust disease is also promising, with a classification accuracy of 98.14%, although no early disease detection was possible. The biggest challenge for variable rate fungicide applications lies in the development of a practical method to use these models in field conditions. Both data processing and storage needs are a concern, as well as image and spatial resolution. Further studies should focus on exploring the best methods to apply the disease detection models in this work to field conditions, focusing on a environmental and economic cost-benefit. Future experiments should focus on mapping the spread of disease in commercial fields,

adapting crop management strategies and then performing a cost-benefit analysis for the farmer and the environment. Trials in controlled conditions could additionally be beneficial to study early, pre-visible disease progression using this model. Finally, the possibility of expanding the results of disease detection in leek to other allium crops, like garlic and onion, is poorly explored and could provide insights towards creating a more universally applicable disease detection model.

References

1. Appeltans, S., A. Guerrero, S. Nawar, J. Pieters, and A.M. Mouazen. 2020. "Practical Recommendations for Hyperspectral and Thermal Proximal Disease Sensing in Potato And." *Remote Sensing* 12, 1939.: 1–19. https://doi.org/10.3390/rs12121939.
2. Archbold Taylor, George, Hector Beltran Torres, Fredy Ruiz, Margarita Narducci Marin, DIego Mendez Chaves, Luis Trujillo Arboleda, Carlos Parra, Henry Carrillo, and Abdul M. Mouazen. 2019. "PH Measurement IoT System for Precision Agriculture Applications." *IEEE Latin America Transactions*. https://doi.org/10.1109/TLA.2019.8891951.
3. Behmann, Jan, Anne Katrin Mahlein, Till Rumpf, Christoph Römer, and Lutz Plümer. 2015. "A Review of Advanced Machine Learning Methods for the Detection of Biotic Stress in Precision Crop Protection." *Precision Agriculture* 16 (3): 239–60. https://doi.org/10.1007/s11119-014-9372-7.
4. Bock, C. H., G. H. Poole, P. E. Parker, and T. R. Gottwald. 2010. "Plant Disease Severity Estimated Visually, by Digital Photography and Image Analysis, and by Hyperspectral Imaging." *Critical Reviews in Plant Sciences* 29 (2): 59–107. https://doi.org/10.1080/07352681003617285.
5. Bohnenkamp, David, Jan Behmann, and Anne Katrin Mahlein. 2019. "In-Field Detection of Yellow Rust in Wheat on the Ground Canopy and UAV Scale." *Remote Sensing* 11 (21). https://doi.org/10.3390/rs11212495.
6. Clarkson, J. P., R. Kennedy, K. Phelps, J. Davies, and J. Bowtell. 1997. "Quantifying the Effect of Reduced Doses of Propiconazole (Tilt) and Initial Disease Incidence on Leek Rust Development." *Plant Pathology* 46 (6): 952–63. https://doi.org/10.1046/j.1365-3059.1997.d01-82.x.
7. Declercq, Bart, Jasper Devlamynck, David de Vleesschauwer, Nathalie Cap, Joris de Nies, Sabien Pollet, and Monica Höfte. 2012. "New Insights in the Life Cycle and Epidemics of Phytophthora Porri on Leek." *Journal of Phytopathology* 160 (2): 67–75. https://doi.org/10.1111/j.1439-0434.2011.01860.x.
8. Doherty, Maureen A., and T. F. Preece. 1978. "Bacillus Cereus Prevents Germination of Uredospores of Puccinia Allii and the Development of Rust Disease of Leek, Allium Porrum, in Controlled Environments." *Physiological Plant Pathology* 12 (1): 123–32. https://doi.org/10.1016/0048-4059(78)90025-5.
9. Fernández, Claudio Ignacio, Brigitte Leblon, Ata Haddadi, Keri Wang, and Jinfei Wang. 2020. "Potato Late Blight Detection at the Leaf and Canopy Levels Based in the Red and Red-Edge Spectral Regions." *Remote Sensing*. https://doi.org/10.3390/RS12081292.
10. Franceschini, Marston Héracles Domingues, Harm Bartholomeus, Dirk Frederik van Apeldoorn, Juha Suomalainen, and Lammert Kooistra. 2019. "Feasibility of Unmanned Aerial Vehicle Optical Imagery for Early Detection and Severity Assessment of Late Blight in Potato." *Remote Sensing*. https://doi.org/10.3390/rs11030224.
11. Franceschini, Marston Héracles Domingues, Harm Bartholomeus, Dirk van Apeldoorn, Juha Suomalainen, and Lammert Kooistra. 2017. "Intercomparison of Unmanned Aerial Vehicle and Ground-Based Narrow Band Spectrometers Applied to Crop Trait Monitoring in Organic Potato Production." *Sensors (Switzerland)* 17 (6). https://doi.org/10.3390/s17061428.
12. Geiger, Flavia, Jan Bengtsson, Frank Berendse, Wolfgang W. Weisser, Mark Emmerson, Manuel B. Morales, Piotr Ceryngier, et al. 2010. "Persistent Negative Effects of Pesticides on Biodiversity and Biological Control Potential on European Farmland." *Basic and Applied Ecology*. https://doi.org/10.1016/j.baae.2009.12.001.
13. Gold, Kaitlin M., Philip A. Townsend, Adam Chlus, Ittai Herrmann, John J. Couture, Eric R. Larson, and Amanda J. Gevens. 2020. "Hyperspectral Measurements Enable Pre-Symptomatic Detection and Differentiation of Contrasting Physiological Effects of Late Blight and Early Blight in Potato." *Remote Sensing* 12 (2). https://doi.org/10.3390/rs12020286.
14. Grisham, Michael P., Richard M. Johnson, and Paul V. Zimba. 2010. "Detecting Sugarcane Yellow Leaf Virus Infection in Asymptomatic Leaves with Hyperspectral Remote Sensing and Associated Leaf Pigment Changes." *Journal of Virological Methods*. https://doi.org/10.1016/j.jviromet.2010.03.024.

15. Heaton, Jeff. 2016. "An Empirical Analysis of Feature Engineering for Predictive Modeling." In *Conference Proceedings - IEEE SOUTHEASTCON*. https://doi.org/10.1109/SECON.2016.7506650.
16. Huang, Lin Sheng, Shu Cun Ju, Jin Ling Zhao, Dong Yan Zhang, Qi Hong, Ling Teng, Fan Yang, and Yan Zuo. 2015. "Hyperspectral Measurements for Estimating Vertical Infection of Yellow Rust on Winter Wheat Plant." *International Journal of Agriculture and Biology* 17 (6). https://doi.org/10.17957/IJAB/15.0034.
17. Jennings, D. M., B. V. Ford-lloyd, and G. M. Butler. 1990. "Effect of Plant Age, Leaf Position and Leaf Segment on Infection of Leek by Leek Rust, Puccinia Allii." *Plant Pathology*. https://doi.org/10.1111/j.1365-3059.1990.tb02538.x.
18. Jong, P. D. de, R. A. Daamen, and R. Rabbinge. 1995. "The Reduction of Chemical Control of Leek Rust, a Simulation Study." *European Journal of Plant Pathology* 101 (6): 687–93. https://doi.org/10.1007/BF01874873.
19. Mahlein, A.-K., M.T. Kuska, J. Behmann, G. Polder, and A. Walter. 2018. "Hyperspectral Sensors and Imaging Technologies in Phytopathology: State of the Art." *Annual Review of Phytopathology* 56 (1): 535–58. https://doi.org/10.1146/annurev-phyto-080417-050100.
20. Mahlein, Anne-Katrin. 2016. "Plant Disease Detection by Imaging Sensors - Parallels and Specific Demands for Precision Agriculture and Plant Phenotyping." *Plant Disease* 100 (2): 1–11. https://doi.org/10.1007/s13398-014-0173-7.2.
21. Mishra, Puneet, Mohd Shahrimie Mohd Asaari, Ana Herrero-Langreo, Santosh Lohumi, Belén Diezma, and Paul Scheunders. 2017. "Close Range Hyperspectral Imaging of Plants: A Review." *Biosystems Engineering*. https://doi.org/10.1016/j.biosystemseng.2017.09.009.
22. Moshou, D., C. Bravo, R. Oberti, J. West, L. Bodria, A. McCartney, and H. Ramon. 2005. "Plant Disease Detection Based on Data Fusion of Hyper-Spectral and Multi-Spectral Fluorescence Imaging Using Kohonen Maps." *Real-Time Imaging* 11 (2): 75–83. https://doi.org/10.1016/j.rti.2005.03.003.
23. Nawar, Said, Ronald Corstanje, Graham Halcro, David Mulla, and Abdul M. Mouazen. 2017. *Delineation of Soil Management Zones for Variable-Rate Fertilization: A Review*. Advances in Agronomy. Vol. 143. https://doi.org/10.1016/bs.agron.2017.01.003.
24. Paulus, Stefan, and Anne Katrin Mahlein. 2020. "Technical Workflows for Hyperspectral Plant Image Assessment and Processing on the Greenhouse and Laboratory Scale." *GigaScience*. https://doi.org/10.1093/gigascience/giaa090.
25. Pedregosa et al. 2011. "Scikit-Learn: Machine Learning in Python." *JMLR 12*, 2825–30.
26. Rumpf, T., A. K. Mahlein, U. Steiner, E. C. Oerke, H. W. Dehne, and L. Plümer. 2010. "Early Detection and Classification of Plant Diseases with Support Vector Machines Based on Hyperspectral Reflectance." *Computers and Electronics in Agriculture* 74 (1): 91–99. https://doi.org/10.1016/j.compag.2010.06.009.
27. Smith, B M, T C Crowther, J P Clarkson, and L Trueman. 2000. "Partial Resistance to Rust (Puccinia Allii) in Cultivated Leek (Allium Ampeloprasum Ssp.Porrum): Estimation and Improvement." *Annals of Applied Biology* 137 (1): 43–51. https://doi.org/10.1111/j.1744-7348.2000.tb00055.x.
28. Theunissen, J., and G. Schelling. 1996. "Pest and Disease Management by Intercropping: Suppression of Thrips and Rust in Leek." *International Journal of Pest Management* 42 (4): 227–34. https://doi.org/10.1080/09670879609372000.
29. Whetton, Rebecca L., Kirsty L. Hassall, Toby W. Waine, and Abdul M. Mouazen. 2018. "Hyperspectral Measurements of Yellow Rust and Fusarium Head Blight in Cereal Crops: Part 1: Laboratory Study." *Biosystems Engineering* 166: 101–15. https://doi.org/10.1016/j.biosystemseng.2017.11.008.
30. Whetton, Rebecca L., Toby W. Waine, and Abdul M. Mouazen. 2018. "Hyperspectral Measurements of Yellow Rust and Fusarium Head Blight in Cereal Crops: Part 2: On-Line Field Measurement." *Biosystems Engineering* 167: 144–58. https://doi.org/10.1016/j.biosystemseng.2018.01.004.
31. Xie, Chuanqi, Yongni Shao, Xiaoli Li, and Yong He. 2015. "Detection of Early Blight and Late Blight Diseases on Tomato Leaves Using Hyperspectral Imaging." *Scientific Reports* 5: 1–11. https://doi.org/10.1038/srep16564.
32. Zhang, Jingcheng, Y. Huang, Ruiliang Pu, P. Gonzalez-Moreno, Lin Yuan, Kaihua Wu, and Wenjiang Huang. 2019. "Monitoring Plant Diseases and Pests through Remote Sensing Technology: A Review." *Computers and Electronics in Agriculture*. https://doi.org/10.1016/j.compag.2019.104943.
33. Zhang, Jingcheng, Ruiliang Pu, Wenjiang Huang, Lin Yuan, Juhua Luo, and Jihua Wang. 2012. "Using In-Situ Hyperspectral Data for Detecting and Discriminating Yellow Rust Disease from Nutrient Stresses." *Field Crops Research*. https://doi.org/10.1016/j.fcr.2012.05.011.
34. Zhou, B., A. Elazab, J. Bort, O. Vergara, M. D. Serret, and J. L. Araus. 2015. "Low-Cost Assessment of Wheat Resistance to Yellow Rust through Conventional RGB Images." *Computers and Electronics in Agriculture* 116. https://doi.org/10.1016/j.compag.2015.05.017.

A Regenerative Agricultural System at Scale: an Outline of Required Outcomes for the Netherlands

Peter Groot Koerkamp [a,*], Wouter-Jan Schouten [b], Loekie Schreefel [a b], Niko Wojtynia [c b], Alfons Beldman [a], Imke J.M. de Boer [a], Marjolijn de Boer [e], Bram Bos [a], Marjolein Derks [a], Jerry van Dijk [c], John Grin [d], Antoine Heideveld [e], Marko Hekkert [c], Gerard Korthals [a], Jan Peter Lesschen [a], Annemiek Pas-Schrijver [a], Walter Rossing [a], Rogier Schulte [a], Bert Smit [a], Hannah van Zanten [a]

[a] Wageningen University & Research, Wageningen, the Netherlands
[b] TiFN Food & Nutrition, Wageningen, the Netherland
[c] Utrecht University, Utrecht, the Netherlands
[d] University of Amsterdam, Amsterdam, the Netherlands
[e] Het Groene Brein, The Hague, the Netherlands
* Corresponding author. Email: peter.grootkoerkamp@wur.nl

Abstract

Regenerative agriculture is considered a more sustainable alternative to current farming practices, but it is not yet well defined. Building on scientific literature we have defined regenerative agriculture as 'an approach to farming that uses soil conservation as the entry point to regenerate and contribute to multiple provisioning, regulating and supporting ecosystem services, with the aspiration that this will enhance not only the environmental, but also the social and economic dimensions of sustainable food production'. In addition to this definition at farm level we propose the following vision for a regenerative agricultural system at landscape or higher system levels: A regenerative agricultural system enables production of food and biomass and enables ecosystems to maintain a healthy state and evolve, while contributing to biological diversity, integrity of the biosphere, human and farm animal well-being and economic prosperity of society. Based on this long-term vision we have defined a comprehensive outline of a regenerative agricultural system that includes, and takes into account, all ecosystem services, soil functions and planetary boundaries. This outline covers fourteen topics and describes the 'outcomes' that are needed to meet the objectives of a regenerative agricultural system, without being prescriptive on 'how' these outcomes should be achieved. Therefore, we use the term 'required outcomes' which precisely and quantitatively describe the target performance of the regenerative agricultural system. These 'required outcomes' are related to the inputs and use of resources, the output (i.e. food, biomass) and losses/emissions, and the preferred state of soils, water bodies, animals, biodiversity and society. The outcomes encompass environmental, social, and economic aspects, and are defined at five different system levels: 1) field (above and below ground), 2) farm, 3) local landscape (including air and water bodies), 4) the Netherlands and 5) international. All required outcomes are based on and supported by scientific literature.

Keywords: Sustainable agriculture, required outcomes, ecosystem services, soil conservation, vision on regenerative agriculture

Introduction

The Netherlands is known for its highly efficient agricultural sector, with high production levels per unit of input, low resource use and low emissions and losses to the environment per kilogram of food produced. Over the last decades impressive results have been achieved in the reduction of environmental impacts per kilogram of food produced.

Despite these results, Dutch agriculture faces serious challenges to achieve the sustainability goals of the UN, the EU and the Dutch government with respect to planetary boundaries (climate change, biodiversity, freshwater use, nutrient cycling and losses, and land system change), as well as to society (consumer and societal acceptance, risk of zoonoses). Furthermore, many farmers are facing significant challenges to earn a living income. A team of researchers from universities in Wageningen, Utrecht and Amsterdam, coordinated by the Top Institute Food and Nutrition (TiFN), explored how the Dutch agricultural system can become regenerative, with positive impact on nature and the living environment, and with healthy farmer business models.

Regenerative agriculture is considered a solution to a more sustainable way of farming, but not yet well defined. As a result, an integrated long term (year 2050) outline of what a regenerative agricultural system at scale looks like is missing. The aim of this paper is to specify the concept of a 'regenerative agricultural system' i.e. to define the goals as precisely and concretely as possible and provide an integrated science-based overview of long-term required outcomes it has to achieve, without describing and prescribing how these goals should be achieved. This paper will present a summary of these required outcomes, though not all detailed background and supporting material and references. The outline of a regenerative agricultural system can be used to evaluate and compare current agricultural practices, assess

the potential impact of existing best practices and to design future scenarios that can meet the required outcomes.

1. Defining objectives for a regenerative agriculture

1.1 Review of existing definitions in scientific literature

A review of scientific literature on regenerative agriculture by Schreefel et al. (2020) showed that, thus far, there is no shared common definition of regenerative agriculture, nor of its objectives. Most definitions rather describe aspirations and activities of regenerative agriculture at farm and/or local level, with a notable absence of objectives and quantified outcomes for a regenerative system at larger scales.

Focussing first on the environmental pillar of farm-level sustainability, we observed a convergence of definitions, all of which mentioned objectives and/or practices to reduce environmental externalities and specifically soil-related issues, as shown in Figure 1. Objectives above farm level and aspirations regarding socio-economic aspects were also found, but without associated operationalisation into specific activities. Overall, the articles found in the literature describe regenerative agriculture as a farming approach which can contribute to ecosystem services in which the entry point is soil health and which stimulates a system change in which primary productivity should be balanced with its ecological and human surroundings. For the outline of a regenerative agricultural system, we will elaborate on this common ground in the relevant literature to create a vision for regenerative agriculture.
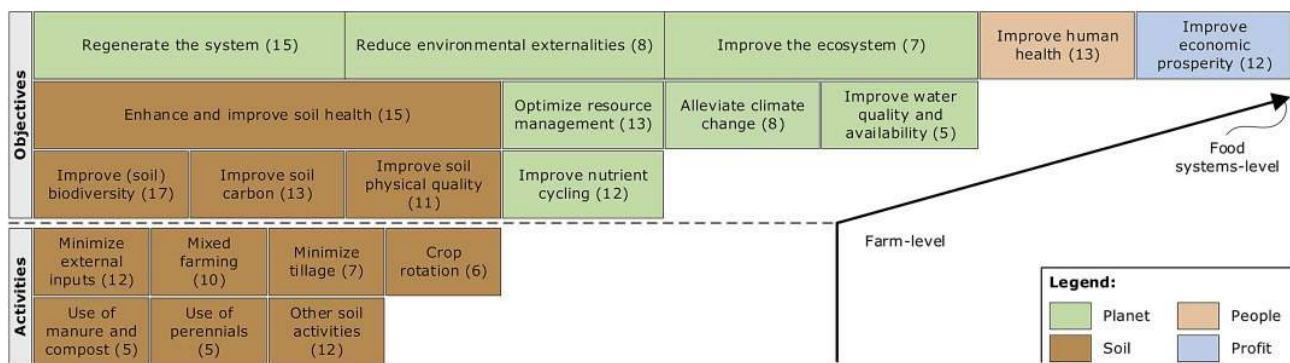
Figure 1. The core themes of regenerative agriculture as identified in Schreefel et al. (2020), categorized (indicated by colors) according the three pillars of sustainability, and soil; 'the number between brackets' represents the number of peer-reviewed articles referring to each theme.

1.2 Vision

Building on the literature review we defined the following definition of *regenerative agriculture* as formulated by Schreefel et al. (2020):

> An approach to farming that uses soil conservation as the entry point to regenerate and contribute to multiple provisioning, regulating and supporting ecosystem services, with the aspiration that this will enhance not only the environmental, but also the social and economic dimensions of sustainable food production.

In addition to this definition at farm level we propose the following vision for a *regenerative agricultural system* at landscape or higher levels:

> A regenerative agricultural system enables production of food and biomass and enables ecosystems to maintain a healthy state and evolve, while contributing to biological diversity, integrity of the biosphere, human and farm animal well-being and economic prosperity of society.

1.3 Explanation and justification of the formulation of this vision

Most existing agricultural systems are aimed at maximizing efficiency per unit of input (energy, nutrients, labour, land), thereby minimizing land use footprint and negative impacts per kilogram of produced food and biomass (de Boer and van Ittersum, 2018). Across the globe, impressive efficiency gains have been achieved towards this aim: the global crop production index has grown almost 300% since 1960 (World bank, 2020a), while arable land area increased with only 12% (World Bank, 2020b). Land use footprint per kilogram of produced food and biomass has thus been reduced by 70% or more. These efficiency gains were essential to feed the growing world population. Despite these efficiency gains food production contributes significantly to the crossing of planetary boundaries (Eat-Lancet, 2019). In order to produce the amount of food that is needed for today's world population within planetary boundaries, many sustainable agriculture efforts aim to optimize the current systems and gradually try to comply to stricter conditions on e.g. inputs and emissions/losses. Current production systems, however, do have their limitations in reaching these stricter conditions and better performance, and many trade-offs are encountered; improvements on one aspect lead to negative

side-effects and lower performance on another aspect (Kanter et al., 2018; Zwetsloot et al, 2020).

For the reasons mentioned above, we think it is no longer enough to minimize land use footprint and negative impacts per kilogram of produced food and biomass. We therefore propose with our vision that the aim of agricultural systems needs to be broadened from 'maximizing production and efficiency' towards 'reaching the goals of food and biomass production, and at the same time contributing positively to biosphere integrity, human well-being and economic prosperity'. This vision addresses all three pillars of the People-Planet-Profit concept, and a series of Sustainable Development Goals (SDGs) and specific targets of the UN, in particular SDG2 (zero hunger), SDG3 (good health and well-being), SDG6 (clean water and sanitation), SDG8 (decent work and economic growth), SDG12 (responsible consumption and production), SDG13 (climate action), SDG14 (life below water), and SDG15 (life on land).

1.4   Objectives for a regenerative agricultural system

To deliver on the vision we propose three overarching objectives for a regenerative agricultural system:

1. <u>Natural Capital Stocks</u>: all natural capital stocks used in agricultural systems are regenerated to and subsequently maintained above threshold levels that are required for a resilient agro-ecosystem i.e. "a system that has the capacity to recover from disruption of functions, and the mitigation of risks caused by disturbance" (Jackson, Pascual and Hodgkin, 2007);

2. <u>Natural Capital Flows</u>: the biophysical conditions and processes in the agro-ecosystem allow that all ecosystem functions and ecosystem integrity in agricultural areas are enabled perpetually;

3. <u>Impact beyond agriculture</u>: The agro-ecosystem has neutral or positive impact on natural capital stocks in natural ecosystems outside the agricultural ecosystem, and on health and well-being in human settlements and public spaces (OECD, 2020).

2.   Required outcomes of a regenerative agricultural system

2.1   Different scales in the biophysical system

To define the required outcomes that are needed to meet these overarching objectives we need to first define the relevant systems, subsystems and the elements in the system (objects and subjects), and with that the various system levels. Most work on regenerative agriculture to date is aimed at describing the aspired impact of regenerative practices at farm or field level. In this paper we will propose required outcomes at higher system levels as well. We distinguish five relevant scales in the system:

1. Field;
2. Farm;
3. Local landscape;
4. National (the Netherlands);
5. International (Europe/Global).

2.2   Frameworks used for the required outcomes of a regenerative agricultural system

The list of required outcomes for a regenerative agricultural system that we propose is developed by combining the objectives that are described by Schreefel et al. (2020) with three existing frameworks: the list of ecosystem services according to TEEB (2019), the planetary boundary targets from EAT-Lancet (2019) and the soil functions in the Landmark study (Schulte et al., 2014) (see figure 2).
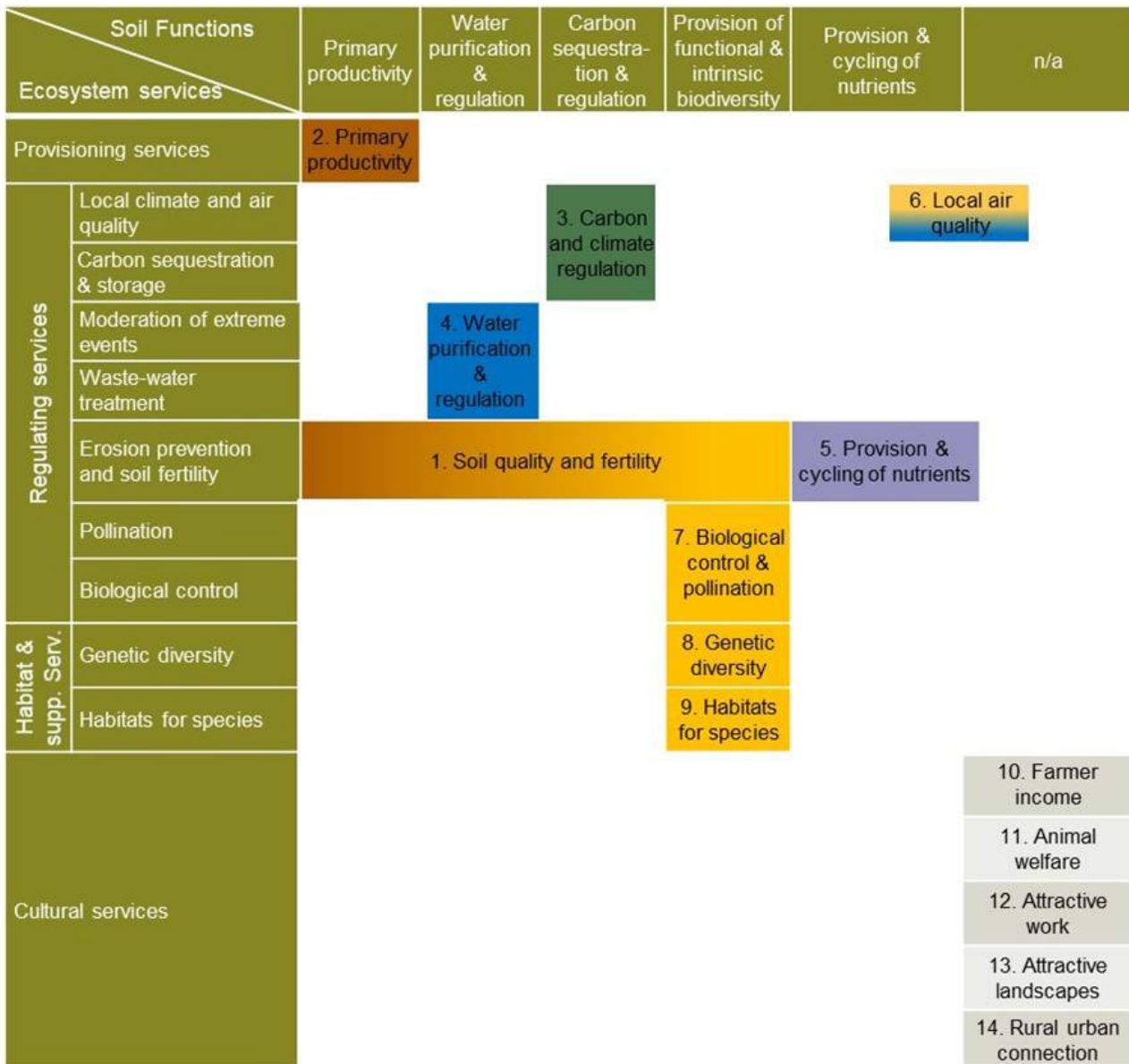
Figure 2. The fourteen identified topics for the outline of a regenerative agricultural system plotted against the five soil functions of the Landmark Study (horizontal axis), the ecosystem services according to TEEB (vertical axis) and linked to the planetary boundary targets from EAT-Lancet (in colour, see legend).

By combining these existing frameworks we identified fourteen topics for which we need to define required outcomes and conditions:

Biophysical outcomes and conditions of a regenerative agricultural system:

1. Soil quality and fertility (biological, physical and chemical soil quality);
2. Primary production of food and biomass;
3. Carbon and climate regulation;
4. Water purification and regulation;
5. Provision and cycling of nutrients;
6. Local air quality;
7. Biological control and pollination;
8. Genetic diversity (diversity and abundance of species)
9. Habitats for species;

Required socio-economic outcomes

10. Farmer income;
11. Animal welfare & health;
12. Safe and attractive work;
13. Attractive landscapes;
14. Rural – urban connection.

The defined required outcomes for these fourteen topics link to various aspects and describe what is needed to meet the overall objectives, without being prescriptive on how these outcomes should be achieved. In addition it needs to be noted that we do not expect that individual farms can contribute to all the outcomes above farming systems levels. For a regenerative system at scale it will be necessary to create symbiotic mixes of diverse farming and natural systems. As a mosaic, these systems can generate a net outcome that meets all the requirements at the appropriate scales, for example: regional scale for nitrogen deposition and (inter-)national scale for greenhouse gas (GHG) emissions.

2.3   Required outcomes of a regenerative agricultural system

For each of these fourteen topics we distinguished and defined required outcomes at the five identified system levels. In formulating these required outcomes we combined the best available scientific insights. Most notably we built on the following sources:

- The extensive work that has been done with the development of the 'Landmark Soil Navigator'. This is a decision support system, developed by Debeljak et al. (2019). The soil navigator is based on a qualitative multi-criteria decision analysis that has been applied using the Decision EXpert (DEX) integrative modelling methodology. Five teams of scientific experts from across Europe have structured, calibrated and validated DEX models for the five soil functions: primary productivity (Sanden et al., 2019), water purification and regulation (Wall et al, 2020), carbon sequestration and climate regulation (van den Broek et al., 2019), nutrient cycling (Schröder et al., 2016) and biodiversity and habitat provision (van Leeuwen et al., 2019). More information about the Soil Navigator can be found on http://www.soilnavigator.eu/;

- The application of the Functional land management framework to map competing expectations of agricultural soils in Europe (Schulte et al., 2019);

- The work by de Boer and van Ittersum (2018) and van Zanten et al. (2019) on circular food systems; see also https://www.circularfoodsystems.org;

- The work by many scientists across Europe in the development of the EU Water framework directive (EC, 2019);

- The work by Lesschen et al. (2020) supporting the Dutch climate agreement;

- The biodiversity monitors that have been developed for dairy farming (Anonymous, 2018) and arable farming (BO-Akkerbouw, 2020).

In Table 1 we present the summary of the required outcomes. The outcomes are partly qualitatively described, but wherever possible the goals were quantified based on available scientific knowledge and insights. For a number of goals, science-based quantification was not (yet or completely) possible. Details of the scientific underpinning can be obtained from the authors and are left out here for reasons of readability and brevity. Table 1 also indicates at which system level the required outcomes need to be met. The required outcomes at field or farm level need to be met by every farm, i.e. farms cannot compensate for each other on these requirements. The required outcomes above farm level are requirements that cannot all be met by individual farms. For a regenerative agricultural system at scale there will be a need to create symbiotic mixes of a diversity of farm systems, as well as nature, that together generate a net outcome that meets all the requirements at the appropriate scales. Adequate monitoring and governance mechanisms will need to

be established to ensure the outcomes are met.

Table 1. Summary of required outcomes at different scale levels for a regenerative agricultural system (relevance for each level indicated with a black box or grey box if preferable but not strictly essential).

Ecosystem service/ soil function	Required outcome at indicated level	Field	Farm	Local landscape	National (NL)	EU/Global
1. Soil quality + fertility, **2. Primary productivity** **3. Carbon & climate regulation**	• A resilient soil food web with functional redundancy; high abundance and richness of soil micro-biome	■				
	• Resilient soil physical quality; a.o. dry bulk density < 1.6 g/cm³ of dry matter	■				
	• Soil organic matter > 4%-8% (soil and farm type dependent)	■				■
	• Average production per ha high enough to produce sufficient food and biomass on < 11-15 M km² cropland, globally				▦	■
	• Circular system; input/output ratio of human digestible protein <1			▦		■
	• Agriculture and nature combined are a 'net carbon sink'				▦	■
	• Intermediate steps: Deliver on commitments in climate agreement, i.e. reduce net GHG-emissions from Dutch Agri + land use with > 6MT by 2030				■	
4. Water purification & regulation **5. Provision & cycling of nutrients** **6. Local air quality**	• Water usage ≤ naturally available (net water replenishment)		■			
	• Water infiltration and storage capacity of soil sufficient to prevent water erosion (soil and crop type dependent)	■				
	• Water quality good/very good according to EU water framework directive			■		
	• Water surpluses are collected as buffer (in soil, groundwater, pond)			■		
	• No negative impacts on water in natural areas and for local communities			■		
	• N and P accumulation in soils limited to levels that minimize the risk of leaching and high emissions to the environment	■				
	• All N, P and micro-nutrients inputs in system come from renewable sources (air, manure, organic rest streams or recovered from sewage/environment)	■				
	• No accumulation of persistent organic pollutants (POPs) in soils, water or air	■				
	• N deposition in natural habitats < critical deposition levels for ecosystems			■		
	• NO, NH₃ and NO₂ concentrations and emissions within EU directives			■		
	• Particulate matter concentrations < WHO limits			■		
7. Biological control & pollination **8. Genetic diversity** **9. Habitats for species**	• >10% of *each* square km landscape (all land uses combined) is semi natural habitat			■		
	• Year-round diversity of habitat and resource provision for farmland species for all stages of the life cycle (providing habitat for farmland species and enabling natural pest control)			■		
	• Maintain abundance and diversity of populations for effective natural pest control	■				
	• Migration of species between all nature areas enabled			■		
	• Maintain abundance and diversity to sustain healthy populations of farm-land species and pollinators			▦		
	• Diversity of gene pool for locally well adapted crops and farm animals				■	
10. Farmer income	• Farmer incomes ≥ living income adequate for local circumstances		■			
11. Animal welfare	• Farm animals have a life worth living		■			
12. Attractive work	• Farms provide safe, attractive and meaningful work		■			
13. Attractive landscapes	• Agricultural ecosystems and nature combined provide attractive landscapes			■		
14. Rural/urban connection	• Good connection between rural and urban communities			■	■	

15. Discussion and conclusions

To ensure sufficient food production within planetary boundaries we think that agricultural systems should aim for 'reaching the goals of food and biomass production, and at the same time contributing positively to biosphere integrity, human and farm animal well-being and economic prosperity'. In this paper we have specified the required outcomes of such agricultural systems that need to be met. It will be challenging to reach this list of required outcomes in practice, which cannot be met with incremental efficiency gains nor with prescribing a few standardized agricultural practices. On the contrary: there will be a need for a diversity of agricultural practices that, combined, can deliver on all the required outcomes. In addition, structural adaptations in e.g. legislation, value chains and water management will be needed (e.g. Bos & Grin, 2008; Morel et al., 2020; Romera et al., 2020). The next step in our research will be to design systems at scale (landscape level and national level) that meet all the required outcomes. In such a design we will use design-principles as described in Figure 3. In parallel, we invite readers to provide input on this outline and collaborate with us to further build and improve it.
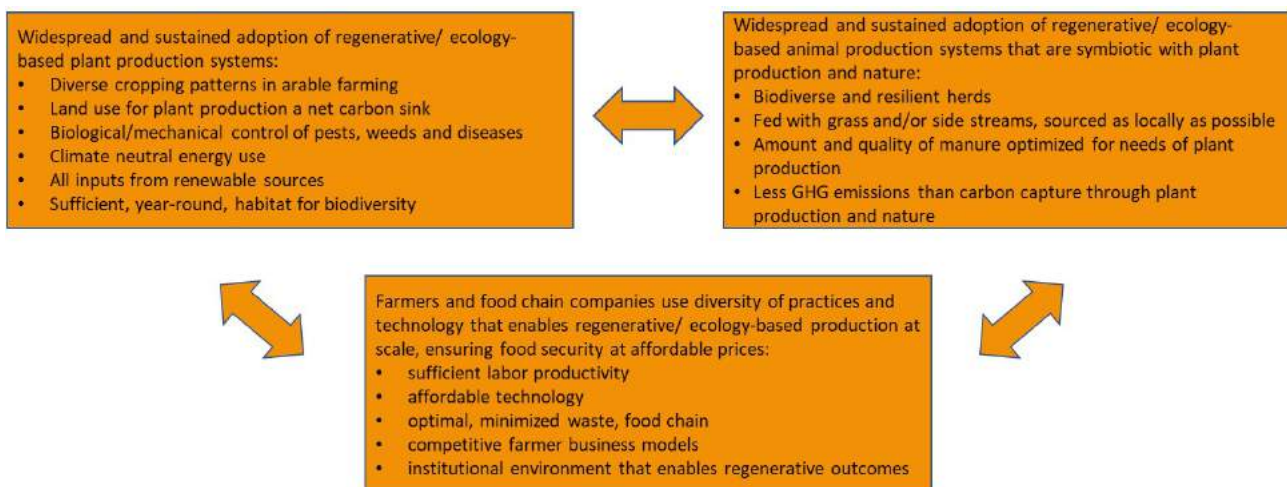
Figure 3. Design principles for a regenerative agricultural system at scale.

Acknowledgements and disclaimer

References

Anonymous, 2018. Biodiversity monitor by FrieslandCampina, Rabobank and WWF. http://biodiversiteitsmonitormelkveehouderij.nl

BO-Akkerbouw, 2020. https://bo-akkerbouw.nl/NL/diensten/Actieplan_Plantgezondheid/Biodiversiteitsmonitor

Bos, A.P. and J.Grin, 2008. '"Doing" Reflexive Modernization in Pig Husbandry: The Hard Work of Changing the Course of a River ', Science, Technology & Human Values , vol. 33, no 4, p. 480-507

Debeljak, M., Trajanov, A., Kuzmanovski, V., Schröder, J., Sandén, T., Spiegel, H., Wall, D.P., Van de Broek, M., Rutgers, M., Bampa, F., Creamer, R.E. and C.B. Henriksen, 2019. A Field-Scale Decision Support System for Assessment and Management of Soil Functions. Front. Environ. Sci. 7:115. doi: 10.3389 / fenvs.2019.00115

de Boer, I.J.M. and M.K. van Ittersum, 2018. Mansholt lezing 2018 - Circularity in agricultural production.

Eat-Lancet, 2019. https://eatforum.org/eat-lancet-commission/eat-lancet-commission-summary-report/

Kanter, D. R., Musumba, M., Wood, S. L. R., Palm, C., Antle, J., Balvanera, P., Dale, V. H., Havlik, P., Kline, K. L., Scholes, R. J., Thornton, P., Tittonell, P., & Andelman, S., 2018. Evaluating agricultural trade-offs in the age of sustainable development. Agricultural Systems, 163, 73–88. https://doi.org/10.1016/j.agsy.2016.09.010

Lesschen, J.P., Reijs, J., Vellinga, T., Verhagen, J., Kros, H., de Vries, M., Jongeneel, R., Slier, T., Gonzalez Martinez, A., Vermeij, I. and C. Daatselaar, 2020. Scenariostudie perspectief voor ontwikkelrichtingen Nederlandse landbouw in 2050. Wageningen Environmental Research Rapport 2984.

Morel K., Revoyron E., San Cristobal M., Baret P.V. (2020). Innovating within or outside dominant food systems? Different challenges for contrasting crop diversification strategies in Europe. PLoS ONE 15(3): e0229910. https://doi.org/10.1371/journal.pone.0229910.

OECD, 2020. How's Life? -edition 2020. Measuring Well-being. Paris.

Romera, A.J., A.P. Bos, M. Neal, et al. (2020). Designing future dairy systems for New Zealand using reflexive interactive design. Agricultural Systems 181, doi.org/10.1016/j.agsy.2020.102818;

Sanden, T., Trajanov, A., Spiegel, H., Kuzmanovski, V., Saby, N., Picaud, C., ... and M. Debeljak, 2019. Development of an agricultural primary productivity decision support model: a case study in France. Frontiers in Environmental Science, 7, 58.

Schreefel L., Schulte R.P.O., de Boer, I.J.M., Pas Schrijver, A. and H.H.E. van Zanten (2020). Regenerative agriculture – the soil is the base. Global Food Security 26: 100404

Schröder, J. J., Schulte, R. P. O., Creamer, R. E., Delgado, A., Van Leeuwen, J., Lehtinen, T., ... and D.P. Wall, 2016. The elusive role of soil quality in nutrient cycling: a review. Soil Use and Management, 32(4), 476-486.

Schulte, R. P., O'Sullivan, L., Vrebos, D., Bampa, F., Jones, A., and J. Staes, 2019. Demands on land: Mapping competing societal expectations for the functionality of agricultural soils in Europe. Environmental Science & Policy, 100, 113-125.

Schulte R.P.O. et al., 2014. http://landmark2020.eu/soil-functions-concept/

TEEB, 2019. The Economics of Ecosystem services and Biodiversity, http://www.teebweb.org/

van Leeuwen, J., Creamer, R., Cluzeau, D., Debeljak, M., Gatti, F., Henriksen, C., ... and N. Saby, 2019. Modeling of soil functions for assessing soil quality: soil biodiversity and habitat provisioning. Frontiers in Environmental Science, 7, 113.

Van Zanten, H. H. E., Van Ittersum, M. K. and I.J.M. De Boer, 2019. The role of farm animals in a circular food system. *Global Food Security*, *21*, 18-22.

Van de Broek, M., Henriksen, C. B., Bhim, G. B., Lugato, E., Kuzmanovski, V., Trajanov, A., ... R. Creamer, 2019. Assessing the climate regulation potential of agricultural soils using a decision support tool adapted to stakeholders' needs and possibilities. Frontiers in Environmental Science, 7, 131.

EC, 2019. https://ec.europa.eu/environment/water/water-framework/index_en.html

World bank, 2020a. https://data.worldbank.org/indicator/AG.PRD.CROP.XD

World bank, 2020b. https://data.worldbank.org/indicator/AG.LND.ARBL.ZS

M.J. Zwetsloot, van Leeuwen, J., Hemerik, L., Martens, H., Simó Josa, I., Van de Broek, M., Debeljak, M., Rutgers, M., Sandén, T., Wall, D.P., Jones, A., Creamer, R.E., 2020. Soil multifunctionality: Synergies and trade offs across European climatic zones and land uses. European Journal of Soil Science.

Study on Deployment of a TrueColor Sensor Array for Dual Use - N-Fertilizer Application

Andreas Christ [*], **Oliver Schmittmann, Peter Schulze Lammers**

Institute of Agricultural Engineering, University of Bonn, Germany

* Corresponding author. Email: andreas.christ@uni-bonn.de

Abstract

In agriculture, efforts are being made to reduce pesticides and fertilizers because of the possible negative environmental impacts, high costs, political requirements, and declining social acceptance. With precision farming, significant savings can be achieved via the application of herbicides and fertilizers to individual plants. In contrast to currently available single systems, the capacity of a dual sensor is much higher and promises significant potential for faster profitability. Moreover, the high spatial resolution of 1 cm² is remarkable.

In this study, experiments were performed to evaluate the applicability of a TrueColor sensor array for site-specific nitrogen application of winter barley and weed detection in low growth stages. The sensor is based on recording the spectral reflection of plants in the CIELab color space and by one IR channel (850 nm). The unique selling point of this sensor is the reflection measurement without influence of ambient light.

Reflection properties (L, a, b, IR) of various weed and crop plants were recorded in greenhouse. A spectrometer was used to reference the reflection values of the sensor array. According to our study, the sensor array can detect weed plants from a minimum size of 125 mm² in real-time. To underline the sensitivity of the array, the increase of leaf area and IR value of the array correlates with $R^2 = 0.97$ for small growth stages of daisy plants. The differentiation of sugar beet and cleaver, as well as daisy, is clearly possible for different growth stages using the CIELab color space sensor.

In field experiments, strong correlations were found between the four reflection channels and the nitrogen level ($R^2 = 0.959$), plant coverage ($R^2 = 0.907$), and fresh mass yield ($R^2 = 0.866$) for winter barley plants.

The fast signal processing allows this sensor to meet stringent demands for the operating speed, spatial resolution, and price structure.

Keywords: CIELab Color Space, Variable Rate Technology, Plant Classification, Pesticide Reduction, Site-specific Nitrogen Fertilization

1. Introduction

Sensors for plant-specific application serve to reduce the application rates for both herbicide and nutrients application. In addition to the ecological aspects that are the subject of much political and social debate, there are also monetary aspects in modern agriculture. Both aspects are taken into account by sensor-based application technology. The combination of several working processes in one sensor unit strengthens these approaches. On the one hand, the utilization and thus the profitability of the investment is increased; on the other hand, a combi-sensor also saves resources by eliminating further required components, in contrast to single sensors.

In our study, the array includes five single sensors with lenses each, as well as TrueColor (CIELab) and IR diodes as defined active light sources. With a detection width of 50 cm, the array fits to the spray width of a conventional sprayer nozzle. This compact technology can be extended to any working width by cascading them. Due to the fast signal processing, the sensor principle meets the high demands on working speed, spatial resolution, robustness against ambient light conditions, and price structure of practical plant recognition systems.

To give a short thematic introduction, the fundamentals of electromagnetic radiation and the used color space will be explained. A prerequisite for the representation of color spaces is visible light. Its electromagnetic oscillations have wavelengths of about 380 nm to 780 nm. This wavelength range is located between ultraviolet (UV) and infrared (IR) and has only a narrow frequency range compared to the rest of the electromagnetic spectrum. Color is neither a property nor the condition of an object, but a subjective sensory perception. For this reason, the detection and display of colored objects depend on environmental conditions and lighting (Marggraf 2019). Technical measuring methods serve to convert subjectively perceived light into physical quantities. In photography as well as in spectroscopy the influence of the illumination spectrum is eliminated by white balance (Marggraf 2019). Color values in different display modes take brightness and saturation into account in different ways. As an example, we look on the CIELab color space in more detail, because it is used in this study.

In the color system developed in 1931 by the CIE (Commission Internationale de l'Éclairage), the color space is defined by a three-dimensional coordinate system. The luminance L (brightness) is displayed on the z-axis, with values between L = 0 (black) and L = 100 (diffuse white). The x-axis has a value range from a = -128 (green) to a = +127

(red). Correspondingly, the opposite colors from b = -128 (blue) to b = +127 (yellow) are plotted on the y-axis (DIN Deutsches Institut für Normung e.V. 2017). In contrast to the tristimulus values X, Y and Z, this type of color representation differs in the consideration of brightness and is, therefore, more similar to the color perception of the human eye (Ganesan et al. 2010). From the CIE's 1931 procedure for measuring the color valence of a light source, statements can be made about the brightness sensitivity of an observer.

Ambient light has a high influence on field measurements. The advantage of using the CIELab color space is the consideration of the brightness through the L channel. Fluctuations in brightness result from characteristic leaf positions of the examined plants and are reflected by the L value. Thus, the color values in the a and b channel are recorded independent of ambient light and represent the true color values of the test objects to be examined (Schmittmann and Schulze Lammers 2017).

Part A: Systematization of weed detection systems and their use in practice

Plant differentiation places minimum demands on the resolution accuracy of the used sensor array. The differentiation of covered to uncovered soil, as well as the influence of the background has been investigated in detail in past studies (Bioucas-Dias et al. 2012), (Ma et al. 2014), (Schmittmann and Schulze Lammers 2017). The challenge with all technical solutions in the field of plant detection is a certain minimum size of the objects to generate a sufficient contrast between plant and background. Limitations arising from this when using the present TrueColor sensor array are discussed in chapter 3.1.

Plant differentiation implies a distinction between crop and weed plants. While in row crops the seed is deposited by singling organs in predetermined rows (Schmittmann et al. 2010), the seed is deposited in area crops by drill sowing without singling technology. This results in different demands on the technique for plant differentiation. Systems such as AmaSelect (Amazonen-Werke H. Dreyer, Hasbergen-Gaste, Deutschland), Selective Spraying (GeoLine, Reggio Emilia, Italien), or See & Spray (BlueRiver, Sunnyvale, Kalifornien) are able to differentiate weeds from crops in row cultures. In geo-referenced sowing, the position of the planted rows is known. If there are plants with a certain deviation near the deposited rows, the evaluation algorithm assigns them to the crop plants. Registered plants between the rows are thus directly classified as weeds, only weeds in the row must be differentiated.

For weed control in row crops, mechanical measures in the form of sensor-controlled hoes are used in addition to the above-mentioned techniques for selective pesticide application. The direction of movement of the actuators can be used as a distinguishing feature. All mentioned hoeing tools, the Robocrop (Garford, Peterborough, Great Britain), as well as the IC-Weeder (Steketee, Stad aan 't Haringvliet, Netherlands), and the actuators of the Robovator system (F. Poulsen Engineering, Hvalsø, Denmark) have a vertical rotation axis. The only difference is the hydraulic or electric drive. Across manufacturers, the soil between the rows is treated with conventional hoeing tools.

The image processing technology of the Robocrop includes an RGB camera with a resolution of 320 x 240 pixels, which communicates with the on-board computer via a serial interface. An algorithm based on two-dimensional wavelet transformations is used to detect the individual plant (Schmeelk 2002). Depending on the weather conditions, the weed reduction in this system is between 66 % and 74 % (Tillett et al. 2008).

At the camera-controlled IC-Weeder, they use one RGB camera per row, which is shielded from natural sunlight by housing and illuminated by a white light-emitting diode (LED). The image processing is based on Fast Fourier Transformations (FFT) (Bontsema et al. 1991).

The company F. Poulsen has developed the third camera-controlled hoe under the brand name Robovator. Analog to the IC-Weeder, they installed one camera per row. To distinguish between weeds and crops, different reflective properties are used due to differences in size. For this reason, either different growth stages or differences in plant-specific size between weeds and crops are necessary conditions for the use of this chopping technique.

By contrast, the camera system from Bilberry (Gentilly, France) is also able to identify weeds not only in row crops but also in field crops. Up to now, this system has mainly been used in grassland, for example for the detection of sorrel (Bilberry 2020). The advantage here is the striking appearance of broad-leaved dock plants (*Rumex* L.) in narrow-leaved grass (Schmittmann and Schulze Lammers 2017).

Part B: Systematization of N-fertilization sensors and their use in practice

Nitrogen from crop fertilizer that is not absorbed by plants has negative effects on the environment, such as groundwater pollution. However, nitrogen deficiency can affect plant health and result in lower yields. Inadequate fertilization can be reduced by combining new technologies with farming practices to adapt to specific needs (Cameron et al. 2013). For more than two decades, digitized solutions have been introduced for site-specific field operations to save resources and protect the environment (Auernhammer 1999). Sensor data can be applied to crop management to improve the yield of agricultural products, which has economic benefits. The challenge for sensor-based applications is to develop valid algorithms for the relationships between the sensor data and crop yield. The indices developed so far for sensor-controlled fertilization are based on computing spectral channels in the visible and near-infrared (IR) wavelength range (Hedley 2015). Spectral analysis is based on the reflection behavior of plant cell compartments. The

pigments within chloroplasts are divided into two photosystems: I (absorption maximum at a wavelength $\lambda = 700$ nm) and II (absorption maximum at $\lambda = 680$ nm) (Nelson and Yocum 2006). A reflection over the entire visual range of electromagnetic radiation appears white to the human eye and can be used for the white balance when calibrating optical reflection sensors. The absorption properties of pigments in the blue and red wavelength range produce the complementary color green, which results in the human perception of leaf color (Reckleben 2014).

Various modelling approaches for spectral analysis are available in the literature. A distinguishing feature is the number of frequency bands. One approach to the development of indices is the multivariate calculation of up to three ranges of the reflection spectrum. Although healthy vegetation has low reflection in the wavelength range of $\lambda = 600$–700 nm (red visible light), its reflection at $\lambda = 700$–1300 nm (near-IR light) is much greater (Carlson and Ripley 1997). A cost-effective approach to estimating the nitrogen content according to reflection ratio R_{ratio} (R870/R620) achieved coefficients of determination (R^2) of 0.70 (Diacono et al. 2014) and 0.82 (Adhikari et al. 2020). (Westermeier and Maidl 2019) showed that quality indices for determining the nitrogen content depend on both the crop type and growth conditions at the test sites. The partial least squares method is commonly used for the detection of herbal ingredients (Wedding et al. 2012). In contrast to approaches using index calculations, this type of multivariate regression requires pre-treatment of the datasets. The signal noise is reduced by differentiating the raw signal; the second derivative eliminates outliers, which results in the highest R^2 values for nitrogen prediction (Wang et al. 2019).

Besides the reflection spectrum of the plant cells themselves, both the fresh mass and degree of coverage influence the assessment of the plant condition. Online measurements of the fresh mass have shown strong correlations with the plant condition and thus the yield (Padilla et al. 2019). An independent and early yield assessment adapted the cultivation strategy (Ehlert et al. 2003), (Gianquinto et al. 2011). A prerequisite for increasing the yield by nutrient supply is the yield potential of the soil. In case the soil is the limiting factor for plant growth, the specifics of the nutrient supply should be determined (Arregui and Quemada 2008). In this context, the main focus is on the nutrient absorption capacity of the plants (Gianquinto et al. 2010). The basis for the nutrient supply of crops such as cereals is the agronomic relationship between the nitrogen uptake and yield uptake. High grain yields depend on the number of ear-bearing stems, grain/ear ratio, and thousand kernel weight. To increase the number of grains per ear, applying fertilizer at the beginning of longitudinal growth is necessary. Grain filling is strongly influenced by nitrogen fertilization after the end of ear pushing. Meanwhile, the degree of plant cover is a good reflection of the number of ear-bearing stems and thus the stocking (Yara 2019).

Statistical analysis has found strong correlations between the degree of coverage and the biomass in the red wavelength range ($\lambda = 678$ nm with a correlation coefficient $r = -0.724$) and near-IR range ($\lambda = 721$–1050 nm with $r = 0.68$) (Zheng et al. 2015). Studies have shown a correlation between the biomass and yield of up to $R^2 = 0.56$ (Ehlert and Dammer 2006). This leads to the hypothesis that present sensors meet the requirements for accurately assessing plant coverage and facilitating early fertilization. Four different models for sensor-controlled nitrogen fertilization are currently available commercially. Across all manufacturers, the measurement spot size covers less than 20 % of the working width: 17 % for the Yara N-Sensor ALS, 11 % for GreenSeeker, 5.5 % for Fritzmeier ISARIA, and 5 % for AgLeader OptRx (Drücker 2016). However, with the TrueColor sensor array, a coverage of 100 % is possible. Using the implemented optical elements in broad segments of industry, induces low unit costs and therefore a cost-effective production of the sensor array.

The appearance of the plants has a significant influence on infrared value, luminance as well as on true color values. Therefore, this study describes the developed TrueColor sensor array with visual and NIR signal outputs. The aim of the present study is to analyze the suitability of weed detection and N-fertilization by CIELab color space and one IR channel. These investigations serve as a basis for practical field applications, where a combined solution for herbicide application and N-fertilization can increase the demand on technique for plant-specific applications.

The main target of this study is to evaluate a TrueColor array as a low-cost dual sensor on suitability for weed detection (Part A) and determination of N-supply (Part B). The performance of this sensor array is analyzed using the following scientific issues:

- Part A: Evaluation of blind spot areas to determine the resolution accuracy of the sensor for weed detection
- Part B: Comparison of the reflection quality of sensor channels by the agronomic parameters N level, plant coverage, and fresh mass

2. Materials and Methods

2.1. TrueColor sensor array

The measurement principle of the TrueColor sensor is based on recording the reflected radiation on a true color scale (Schmittmann and Schulze Lammers 2017). The sensor was developed in collaboration with Premosys GmbH (Kalenborn-Scheuern, Germany) and was designed as an array with the type designation PR0262. Five individual sensors, each with its own light source and a segment width of 10 cm, are arranged next to each other (see Figure 1). The frequency-controlled light sources perform constant light–dark adjustment, which is necessary for daylight-

independent color measurement. The system is supplied with a 24 V DC voltage source.
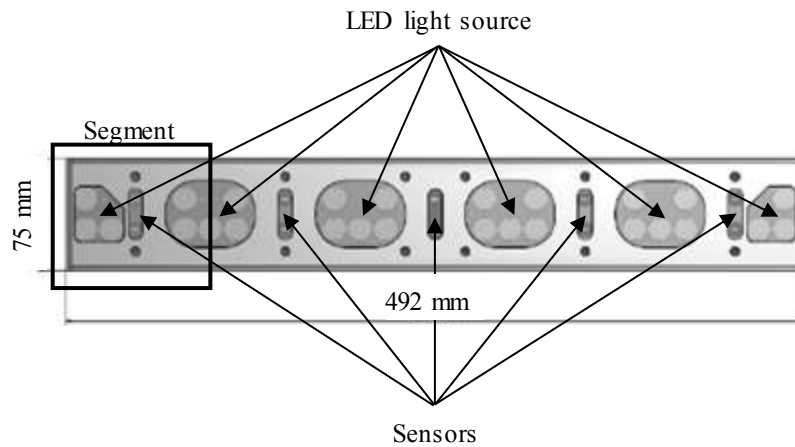
Figure 1. Design and dimensions of the TrueColor sensor array

Light-emitting diodes with a color temperature of 5700 K (daylight white) provide active illumination of the measured objects for the acquisition of the true color values. This sensor is sensitive in the IR channel to a wavelength λ = 850 nm. This results in four output variables per sensor with the tristimulus values X, Y, Z, and IR = 850 nm. With a housing width of 492 mm, the detection range of the array is 500 mm, which corresponds to the standardized nozzle distance for field sprayers. In practical applications, an array can control a single nozzle valve. A master array can be connected with up to four slaves and transmit the recorded reflection data to a computer.

Software developed at the Institute of Agricultural Engineering is used to convert the reflection values from the tristimulus values X, Y, and Z into the CIELab color space; this is saved as a csv file together with the recorded IR channel. In the color system developed in 1931 by the Commission Internationale de l'Éclairage (CIE), the color space is spanned by a three-dimensional coordinate system. The values of the luminance L channel (brightness) are displayed on the z-axis with values between 0 (black) and 100 (diffuse white). The values of the a channel are displayed on the x-axis with a range of −128 (green) to 127 (red). The values of the b channel are displayed on the y-axis with the range of −128 (blue) to 127 (yellow) (DIN Deutsches Institut für Normung e.V. 2017). In contrast to the tristimulus values X, Y, and Z, the CIELab color space differs by considering the brightness; thus, it is more similar to the color perception of the human eye (Ganesan et al. 2010). The influence of ambient light should be eliminated to ensure the reproducibility of field measurements. Fluctuations in brightness result from the characteristic leaf positions of the plants, and they are reflected by the L value. Thus, the color values in the a and b channels are recorded independently of the ambient light and represent the true color values of the test objects to be examined (Schmittmann and Schulze Lammers 2017).

2.2. Part A: Design of the glasshouse experiment for weed detection

To differentiate crops from weeds using TrueColor sensor array, three different plant species were grown in the greenhouse with a day/night temperature of 23 °C/ 20 °C, relative humidity of 60 ± 10 %, and an illumination time of 16 hours. Besides daisy (*Bellis perennis* L.) and cleaver (*Galium aparine* L.) as representatives of dicotyledonous weeds, sugar beet (*Beta vulgaris* L.) was chosen as dicotyledonous crop plant. An overview of the number and phenological growth stages (Biologische Bundesanstalt, Bundessortenamt and Chemical industry BBCH) of the investigated plants gives Table 1 in the following.

The sowing of daisy and cleaver was carried out in trays. To ensure that the seeds emerged as evenly as possible, a lawn support layer was used, whose fine-crumbly soil aggregates ensured rapid run-up. At the different measuring dates of daisy and cleaver, the plants were separated and planted in glass trays, also filled with a lawn base layer. The sugar beets were grown in propagation substrate (Einheitserdewerke Werkverband e.V., Sinntal-Altengronau, Germany) due to the higher demands on seedbed and nutrient requirements. This is a mixture of natural clay, white peat, and perlite and has a nutrient salt content of 1 kg m^{-3}.

The measurement of the individual plants was carried out by means of a tripod with bogie, to which a point laser as well as a camera and TrueColor sensor array are attached (see Figure *2*).

Table 1. Overview of the investigated plant species, their plant growth stages, and number of replicates

| Test object | Measurement 1 | | Measurement 2 | | Measurement 3 | | Measurement 4 | | Total |
	Growth stage	Rep.	Growth stage	Rep.	Growth stage	Rep.	Growth stage	Rep.	
Bellis perennis L.	10	10	11	10	12	10	13	10	40
Galium aparine L.	10	10	11	10	12	10			30
Beta vulgaris L.	10	20	12	10	14	10			40
									110
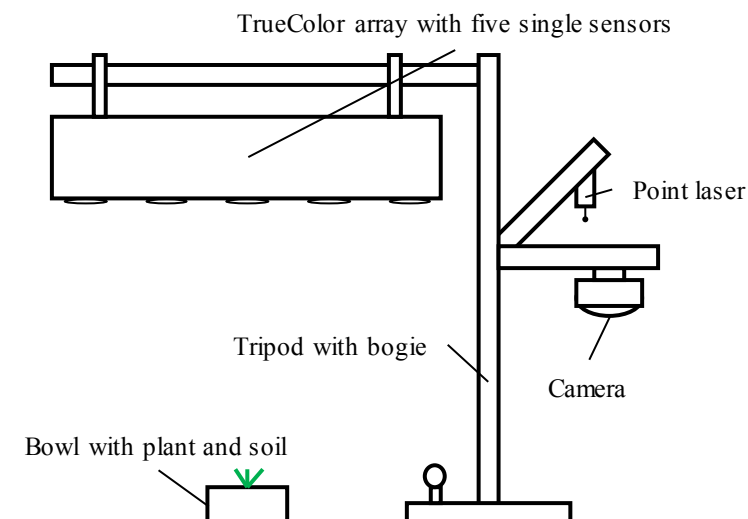
Figure 2. Static test setup for reproducible recording of the reflection behavior of different plant species including soil as background

The plants were aligned reproducibly under the central individual sensor of the array, by using the point laser to keep environmental influences as constant as possible. The glass trays filled with lawn support layer as well as pots filled with propagation substrate were also measured without plants as a reference of the background. The leaf area was determined from the RGB images of the camera, which allows conclusions about the sensitivity of the TrueColor sensor array.

In each case, the latest fully developed leaves were examined. The spectral evaluation of the TrueColor sensor is described in more detail under (Christ et al. 2021). The measurements were performed with n = 10 replicates for statistical verification and better reproducibility, and form the basis of the results presented in the chapter Results and Discussion.

2.3. Part B: Design of the field experiment for N-fertilizer application

The experimental setup was equivalent to a block plantation and comprising four plots with different nitrogen fertilization levels (see Figure 3). The experimental field had a total area of 468 m² with homogeneous soil conditions. The plots had a length of 15 m and width of 6 m; they were separated by a distance of 6 m and were laid out next to a tramline to allow field traffic. Plot I represented the control unit without a nitrogen supply. In Plot II, standard nitrogen fertilization was applied after the nitrogen demand was determined. The winter barley received 160 kg N ha^{-1}, which corresponds to the standard farming practice. Plot III created a shortage in the nitrogen supply by reducing the application by 50 % to 80 kg N ha^{-1}. Plot IV considered a 50 % increase in the nitrogen supply to 240 kg N ha^{-1}.
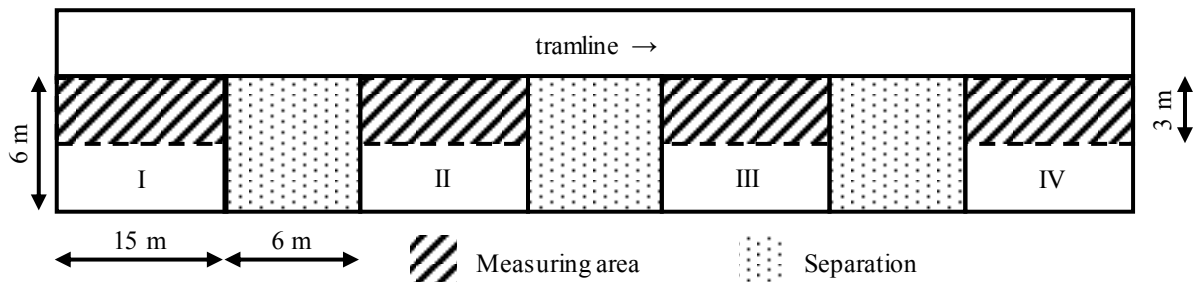
Trial plot	Variant	1. Application [kg N ha^{-1}]	2. Application [kg N ha^{-1}]	3. Application [kg N ha^{-1}]
I	**without N**	0	0	0
II	**100 % N**	60	50	50
III	**50 % N**	30	25	25
IV	**150 % N**	90	75	75

Figure 3. Experimental setup (left) and fertilizer rates per application (right)

The first nitrogen application for tillering regulation was in mid-March after the vegetation dormancy. At the beginning of April, the second dose followed the elongation growth of the plants. Finally, the third application was conducted at the end of April during the grain-filling phase (i.e., quality fertilization). The measuring dates were at growth stages BBCH 32, BBCH 39 and BBCH 59.

The hatched areas in Figure 3 show where the TrueColor sensors were deployed. Six arrays with a total of 30 sensor units, each with a measurement range of 500 mm, were mounted side by side on an aluminium profile rail. The entire working width was 3 m, which corresponds to a standard boom section of a field sprayer, and the total measurement area was 45 m² per plot. The measurement area was not changed throughout the test period to facilitate the comparability of the results. The distance from the sensor to the canopy was typically 50 cm. Crossings were conducted at a constant speed of 0.1 m s^{-1}, and four replicates were obtained. The remaining 45 m² of the plot (white areas in Figure 3) were used to assess the reference measurements. To determine the degree of plant coverage, 10 images were taken per plot at a distance of 50 cm from the canopy. The photographs were analyzed with the software ImageJ (Public Domain). The reflection properties of the background (soil) were recorded as a reference. Samples of the fresh mass were taken on an area of 0.5 m² with 3 replicates per plot.

2.4. Statistical analysis

Statistical analysis was conducted with the software SPSS Statistics (IBM, Armonk, USA). The data were tested by single-factor analysis of variance and a post hoc test according to Scheffé with a significance level of $\alpha < 0.05$. This test is suitable for use with databases of different sample sizes. The regression models presented in the results and discussion section for the entire study period comprising 48 value pairs: three measurement dates with four nitrogen levels and four passes with the sensor array. The reflection values were recorded at a log interval of 60 ms. The raw data were used to calculate the arithmetic mean per plot and generate the regression models.

3. Results and Discussion

3.1. Part A: Studies on the resolution accuracy of the TrueColor sensor array for weed detection

Figure 4 displays the magnitude of signals for the four channels of the TrueColor sensor array. The signals on cleaver, daisy, and sugar beet at growth stages BBCH 10 to BBCH 14 can be compared with the reflection values of soil for reasons of discrimination. The horizontal dashed bars in this graph outline the blind range of the sensor on the possible application for plant detection. Blind range means that the reflection values of plants are within the standard deviation of the arithmetic mean of the soil reflection. In this range, the reflection values of plant and soil do not differ significantly, thus a differentiation is not effectively possible. The scale of each y-axis was chosen in such a way that the represented interval is equal in amount. Thus, the blind areas are displayed without distortion and their dimension is comparable.
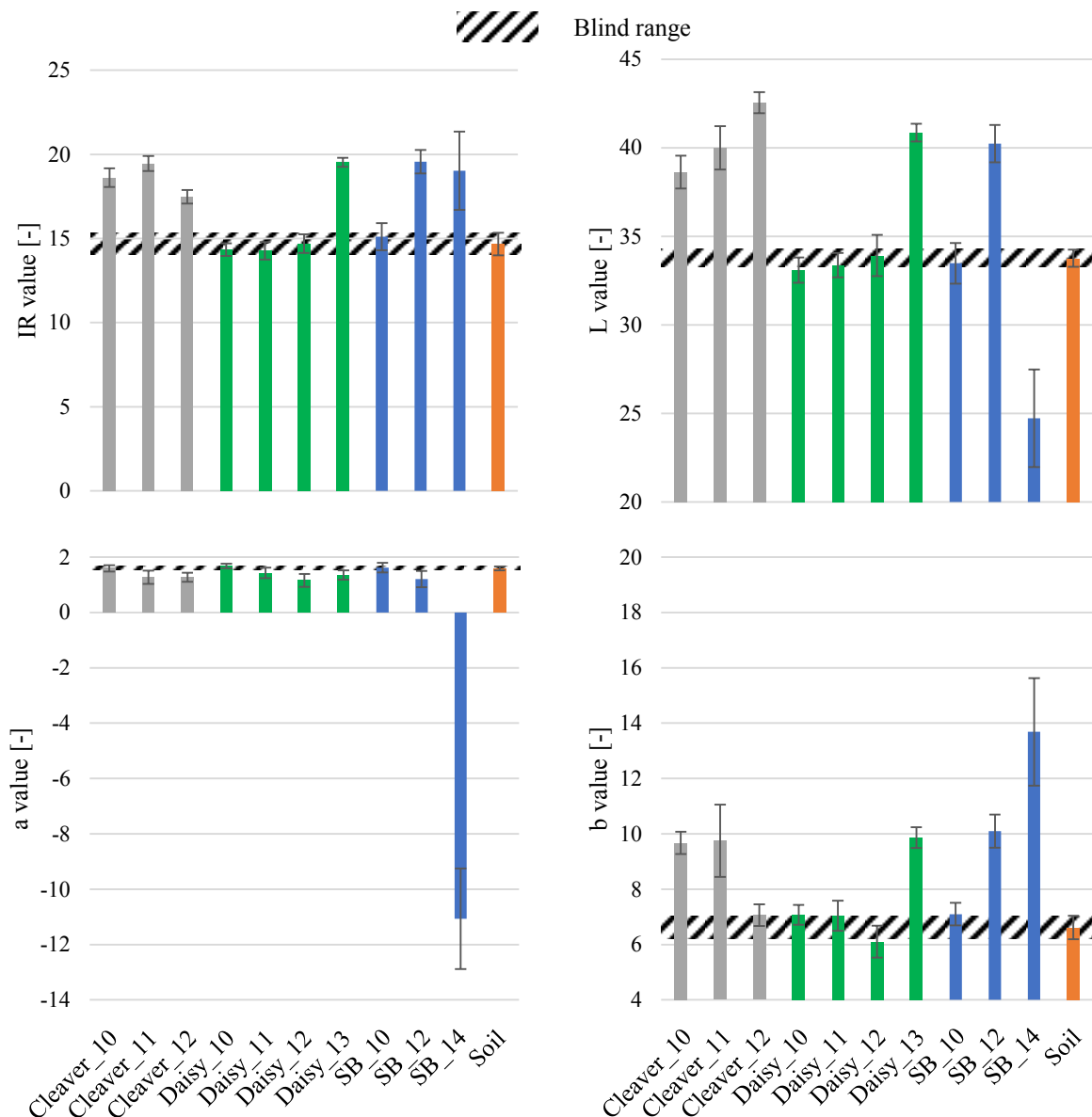
Figure 4. Reflection channels IR and CIELab of the TrueColor sensor array for cleaver, daisy and sugar beet in comparison to soil with resulting blind areas

The reflection values of the IR channel ($\lambda = 850$ nm) differ from the background (ground reflection) in all investigated growth stages of cleaver, daisy in growth stage BBCH 13 (daisy_13), and sugar beet in BBCH 12 (sb_12) and 14 (sb_14). Only few growth stages of daisy and sugar beet are not differentiable by this reflection channel.

Remarkable for the a channel is the small standard deviation of soil reflection, used as threshold range leading to the smallest blind spot of all reflection channels. In relation to the other reflection channels, most of the weeds can be detected by the a channel. In this reflection channel, seven different plant samples are significantly different to the reflection values of soil. At the same time, the plant reflection values do not differ significantly between each other for most of the plant samples. Only sb_14 has a distinct lower a value, which results from the increase of leaf area in this growth stage. From sb_12 with an average surface of 493 mm² to sb_14 with an average surface of 4,824 mm², there is an increase of approx. 10 times. Therefore, the a value becomes much more negative, because of the green(-)/red(+)-axis in the CIELab color space. A differentiation by the dominating green color of plants is not possible in this case. Because of this fact, the other reflection channels of the dual-sensor lead to additional information for this use case.

For the L channel, the dimension of blind spot area corresponds to the IR channel and the detectable growth stages are the same. The differentiation between plant species is most possible by comparing the L channel values. This reflection channel distinguishes strongly the multiple growth stages, which is an important advantage as compared to

other spectral sensors, e.g. based on RGB color space. Not only the color of leaves, but also reflection properties of the plant habitus are important for plant classification by TrueColor sensors. Therefore, discrete wavelengths are not suitable, because it does not include the luminance. The value of luminance depends on the leaf angle and is a differentiating feature (Schmittmann and Schulze Lammers 2017). As Figure *4* shows, cleaver_10, cleaver_12, daisy-_13, and sb_14 are differentiable only by L reflection, when skipping the plant species, which are within the blind area of L channel.

For a robust weed detection, the combination of a values ('detection channel') lead to the discrimination of plant and soil. The L values ('differentiation channel') give the answer on which plant has to be treated. The b channel covers the blue(-)/yellow(+)-axis of CIELab color space and does not give an additional information about weed detection. In contrast to this, chapter 3.2 deals with the importance of b channel values for N-fertilization measurements. For this reason, a combined application of TrueColor sensor arrays, based on CIELab color space, is presented in this study.

3.2. Part B: Comparison of the quality of the reflection channels on basis of agronomic parameters in N-fertilizer application

In addition to the study on deployment of the sensor for weed detection, the informative value of the reflection channels on the recorded agronomic parameters is the focus of Part B in our study. In the following, the coefficient of determination (COD) is used as an indicator for the evaluation of the specific sensitivity. Figure *5* displays the CODs of the reflection channels regarding N level, plant coverage, and fresh mass for each BBCH stage.

N level

The N level correlates most to the a channel for BBCH 39 ($R^2 = 0.959$) and little less to the b channel for BBCH 32 ($R^2 = 0.956$) and BBCH 39 ($R^2 = 0.919$). Moreover, the L channel has a high accuracy for mapping the N level in BBCH 32 with $R^2 = 0.899$. With $R^2 > 0.75$, the correlation between N level and the reflection channel is high, with exception of the IR channel.

Plant coverage

From the beginning of elongation growth in BBCH 32, the L, a, and b values are well suited to represent the plant coverage. Since N-fertilization up to BBCH 32 has an influence on tillering and on the number of ear-bearing stems, the CIELab reflection channels are highly suitable for the first fertilization. With $R^2 = 0.907$, the b channel has the highest correlation for BBCH 39. Similar results show the b channel for BBCH 32 and BBCH 59 with $R^2 = 0.85$, as well as the a channel for BBCH 39 and BBCH 59. These results fit to the findings (Diacono et al. 2014) stating, that strong correlations regarding N level and plant coverage are highly indicative for yield prediction.

Fresh mass yield

Fresh mass has a strong correlation regarding plant health and yield (Ehlert and Dammer 2006). In addition to this, it is a strong indicator for plant growth (Padilla et al. 2019). In our study, the highest correlation to fresh mass displays the a value for BBCH 39 ($R^2 = 0.866$). High CODs of a and b channel with fresh mass yield are promising for a yield-oriented fertilization over the entire fertilization period.

The IR values achieve conspicuously poor level for all investigated agronomic parameters in the individual BBCH stages. The CODs for the IR channel does not exceed $R^2 = 0.5$ for all investigated growth stages and agronomic parameters. Because of that, the IR channel is more attributable to part A and provides the possibility for technical combination of weed detection and N-fertilization for dual use of the sensor array.

In contrast to the results in part A, N-fertilization correlates more with the color axes of the CIELab color space, than with the luminance or IR channel. This implies another algorithm for fertilizer rate application. Therefore, the measurement values have to be compared to the thresholds of a and b values, which are mentioned in the paragraphs before.
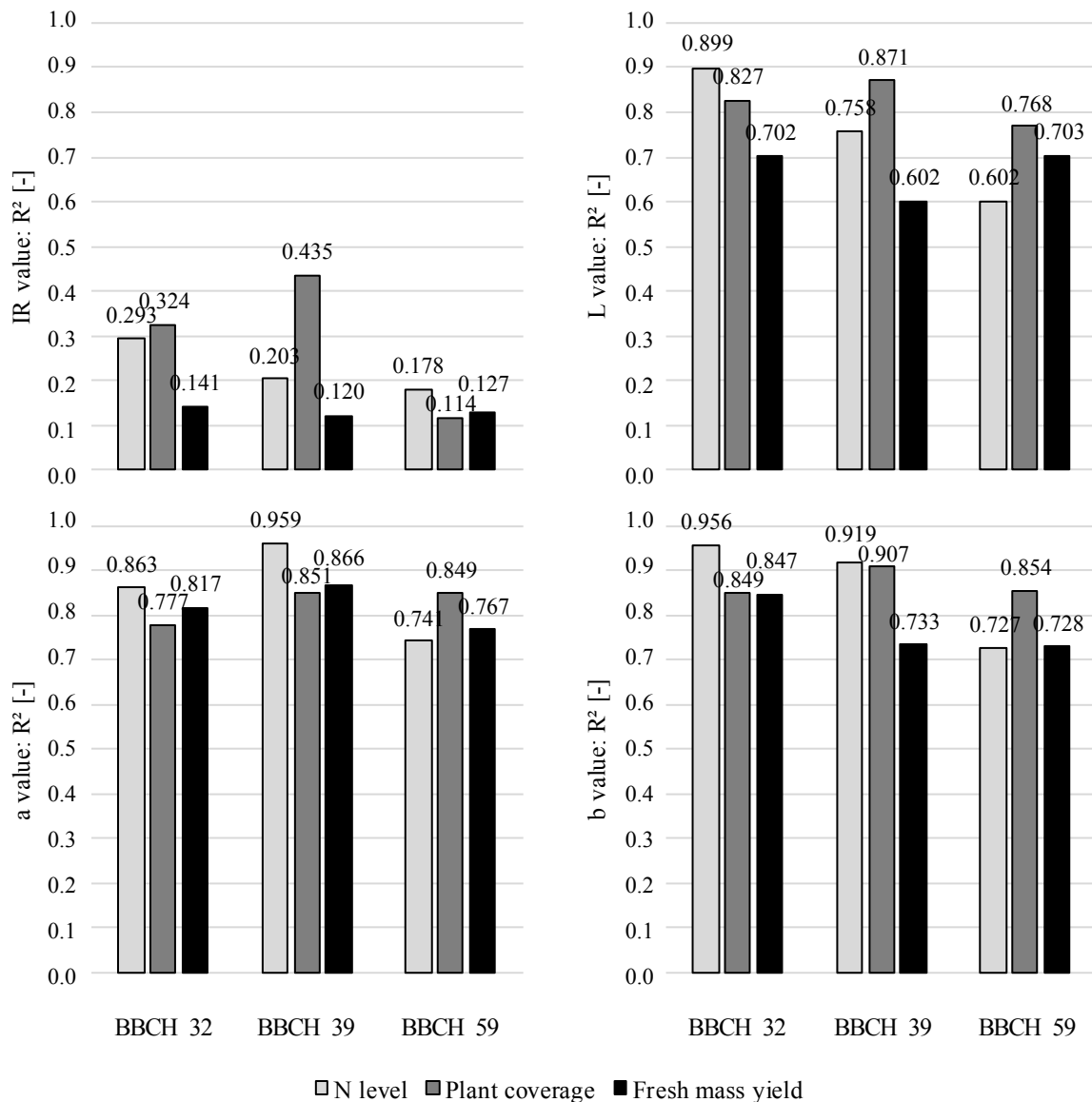
Figure 5. Coefficients of determination of the reflection channels with respect to the agronomic parameters N level, plant coverage and fresh mass yield for the inquired BBCH stages

4. Conclusions

In part A of this study, fundamentals for plant classification in the cultivation of sugar beet by a low cost CIELab sensor are presented. The test setup served as a basic investigation of the general suitability of a TrueColor sensor array for selective herbicide treatment in sugar beet cultivation. In contrast to the practical application, the described measurements were carried out under controlled conditions without dynamic influence. The IR channel shows particularly good feature with regard to differentiation between crop and weed plants at the cotyledon stage. Taking the L or a channel into account, plant differentiation in later growth stages is also possible.

In Part B, the reflection values of the CIELab color space, as well as the IR values, show significant differences between the applied fertilizer levels for the investigated BBCH stages. The values of the L, a, and b channels decreased with increasing fertilization, which is in contrast to the results for the IR channel. The values of the IR channel were lowest at the maximum nitrogen level and highest without fertilizer application. Meanwhile, the values of the IR channel were higher at the 50% nitrogen level than at the 100% nitrogen level. This non-monotonic course and consistently lower R^2 with the agronomic parameters indicate that the IR channel should not be used to control nitrogen fertilization.

The sensor array should be calibrated against an unknown background (soil) and crop (growth stage, genotype) for

demand-controlled nitrogen supply. This is much easier if there is a strong relationship between the nitrogen level and reflectance value, which was observed for the *L*, *a*, and *b* channels. Additionally, the data basis for all reflection channels can be reduced, so the measurement area can be enlarged without affecting the signal quality.

The hypothesis that the TrueColor sensor array can achieve good results when measuring the plant coverage was confirmed. Additionally, a strong correlation was observed between the fresh mass yield and the *a* and *b* channels.

Overall, the TrueColor sensor array is suitable for determining the nitrogen supply of winter barley. High field performance can be achieved with large working widths when cascading the sensor arrays. With fast signal processing combined with high spatial resolution, this sensor technology is able to promote precision agriculture. Furthermore, the use of low-cost components and increased yield due to more plant-specific fertilizer supply at low yield levels improve the cost-effectiveness of this sensor application.

The next development steps include the implementation of the sensor arrays in a standard field sprayer for the application of herbicides and liquid fertilizer in an online process. We are going to extend the sensor system to other crop species for herbicide application and evaluate the suitability of the sensor array for N-fertilization in perennial field experiments and other crop species.

References
Adhikari, R., Li, C., Kalbaugh, K., & Nemali, K. (2020). A low-cost smartphone controlled sensor based on image analysis for estimating whole-plant tissue nitrogen (N) content in floriculture crops. *Computers and Electronics in Agriculture, 169*, 105–173. doi:10.1016/j.compag.2019.105173.

Arregui, L. M., & Quemada, M. (2008). Strategies to Improve Nitrogen Use Efficiency in Winter Cereal Crops under Rainfed Conditions. *Agronomy Journal, 100*, 277–284. doi:10.2134/agronj2007.0187.

Auernhammer, H. (1999). Informationssystem Kleinräumige Bestandesführung Dürnast. 214–215 Seiten / LANDTECHNIK, Bd. 54 Nr. 4 (1999) / LANDTECHNIK, Bd. 54 Nr. 4 (1999). doi:10.15150/LT.1999.2214.

Bilberry. (2020). Intelligent Agriculture Technology for a better Environment. https://bilberry.io.

Bioucas-Dias, J. M., Plaza, A., Dobigeon, N., Parente, M., Du, Q., Gader, P., et al. (2012). Hyperspectral Unmixing Overview: Geometrical, Statistical, and Sparse Regression-Based Approaches. *IEEE Journal of Selected Topics in Applied Earth Observations and Remote Sensing, 5*, 354–379. doi:10.1109/JSTARS.2012.2194696.

Bontsema, J., Grift, T., & Pleijsier, K. (1991). Mechanical weed control in sugar beet growing: The detection of a plant in a row. *IFAC Mathematical and Control Applictions in Agriculture and Horticulture, 24*, 207–211. doi:10.1016/B978-0-08-041273-3.50041-0.

Cameron, K. C., Di, H. J., & Moir, J. L. (2013). Nitrogen losses from the soil/plant system: a review. *Annals of Applied Biology, 162*, 145–173. doi:10.1111/aab.12014.

Carlson, T. N., & Ripley, D. A. (1997). On the relation between NDVI, fractional vegetation cover, and leaf area index. *Remote Sensing of Environment, 62*, 241–252. doi:10.1016/S0034-4257(97)00104-1.

Christ, A., Schmittmann, O., & Schulze Lammers, P. (2021). Plant Differentiation with TrueColor Arrays for Online Precision Plant Protection. *48th International Symposium of Actual Tasks on Agricultural Engineering, 2nd - 4th March 2021, Opatija, Croatia*, 347–359.

Diacono, M., Castrignanò, A., Vitti, C., Stellacci, A. M., Marino, L., Cocozza, C., et al. (2014). An approach for assessing the effects of site-specific fertilization on crop growth and yield of durum wheat in organic agriculture. *Precision Agriculture, 15*, 479–498. doi:10.1007/s11119-014-9347-8.

DIN Deutsches Institut für Normung e.V. (2017). Farbmessung - Teil 1: Grundbegriffe der Farbmetrik (01.040.17; 17.180.20). Berlin: Beuth Verlag, *01.040.17; 17.180.20*(DIN 5033-1). Accessed 7 February 2019.

Drücker, H. (Ed.). (2016). *Precision Farming: Sensorgestützte Stickstoffdüngung* (KTBL-Heft, Vol. 113). Darmstadt: Kuratorium für Technik und Bauwesen in der Landwirtschaft e. V.

Ehlert, D., & Dammer, K.-H. (2006). Widescale testing of the Crop-meter for site-specific farming. *Precision Agriculture, 7*, 101–115. doi:10.1007/s11119-006-9003-z.

Ehlert, D., Hammen, V., & Adamek, R. (2003). On-line Sensor Pendulum-Meter for Determination of Plant Mass. *Precision Agriculture, 4*, 139–148. doi:10.1023/A:1024553104963.

Ganesan, P., Rajini, V., & Rajkumar, R. I. (Eds.). (2010) *2010 International Conference on Emerging Trends in Robotics and Communication Technologies (INTERACT 2010), Chennai, India, 12/3/2010 - 12/5/2010*. Piscataway, NJ: IEEE.

Gianquinto, G., Fecondini, M., Mezzetti, M., & Orsini, F. (2010). Steering nitrogen fertilisation by means of portable chlorophyll meter reduces nitrogen input and improves quality of fertigated cantaloupe (Cucumis melo L. var. cantalupensis Naud.). *Journal of the science of food and agriculture, 90*, 482–493. doi:10.1002/jsfa.3843.

Gianquinto, G., Orsini, F., Sambo, P., & D'Urzo, M. P. (2011). The Use of Diagnostic Optical Tools to Assess Nitrogen Status and to Guide Fertilization of Vegetables. *HortTechnology, 21*, 287–292. doi:10.21273/HORTTECH.21.3.287.

Hedley, C. (2015). The role of precision agriculture for improved nutrient management on farms. *Journal of the Science of Food and Agriculture, 95*, 12–19. doi:10.1002/jsfa.6734.

Ma, W.-K., Bioucas-Dias, J. M., Chan, T.-H., Gillis, N., Gader, P., Plaza, A. J., et al. (2014). A Signal Processing Perspective on Hyperspectral Unmixing: Insights from Remote Sensing. *IEEE Signal Processing Magazine, 31*, 67–81. doi:10.1109/MSP.2013.2279731.

Marggraf, U. (2019). *Ermittlung der Prozessqualität bei der Vermischung der Wirkstoffe in Pflanzenschutzspritzen* (1st ed., Forschungsberichte aus dem Institut für mobile Maschinen und Nutzfahrzeuge). Düren: Shaker.

Nelson, N., & Yocum, C. F. (2006). Structure and function of photosystems I and II. *Annual review of plant biology, 57*, 521–565. doi:10.1146/annurev.arplant.57.032905.105350.

Padilla, F. M., Souza, R. de, Peña-Fleitas, M. T., Grasso, R., Gallardo, M., & Thompson, R. B. (2019). Influence of time of day on measurement with chlorophyll meters and canopy reflectance sensors of different crop N status. *Precision Agriculture, 20*, 1087–1106. doi:10.1007/s11119-019-09641-1.

Reckleben, Y. (2014). Sensoren für die Stickstoffdüngung - Erfahrungen in 12 Jahren praktischem Einsatz. 1,41 MB / Journal für Kulturpflanzen 66(2) 2014 / Journal für Kulturpflanzen 66(2) 2014. doi:10.5073/JFK.2014.02.02.

Schmeelk, J. (2002). Wavelet transforms on two-dimensional images. *Mathematical and Computer Modelling, 36*, 939–948. doi:10.1016/S0895-7177(02)00238-8.

Schmittmann, O., Kam, H., & Schulze Lammers, P. (Eds.). (2010) *2nd International Conference on Machine Control & Guidance, Bonn* .

Schmittmann, O., & Schulze Lammers, P. (2017). A True-Color Sensor and Suitable Evaluation Algorithm for Plant Recognition. *Sensors (Basel, Switzerland), 17*(8).

Tillett, N. D., Hague, T., Grundy, A. C., & Dedousis, A. P. (2008). Mechanical within-row weed control for transplanted crops using computer vision. *Biosystems Engineering, 99*, 171–178. doi:10.1016/j.biosystemseng.2007.09.026.

Wang, C., Li, X., Wang, L., Yang, C., Chen, X., Li, M., et al. (2019). Prediction of N, P, and K Contents in Sugarcane Leaves by VIS-NIR Spectroscopy and Modeling of NPK Interaction Effects. *Transactions of the ASABE, 62*, 1427–1433. doi:10.13031/trans.13086.

Wedding, B. B., Wright, C., Grauf, S., & White, R. d. (2012). The Application of Near Infrared Spectroscopy for the Assessment of Avocado Quality Attributes. In T. M. Theophanides (Ed.), *Infrared spectroscopy*: Life and biomedical sciences. Rijeka, Croatie: InTech.

Westermeier, M., & Maidl, F.-X. (2019). Vergleich von Spektralindizes zur Erfassung der Stick-stoffaufnahme bei Winterweizen (Triticum aestivum L.). Journal für Kulturpflanzen, Bd. 71 Nr. 8/9 (2019) / Journal für Kulturpflanzen, Bd. 71 Nr. 8/9 (2019). doi:10.5073/JFK.2019.08-09.02.

Yara. (2019). *Düngefibel: effizient düngen*. Dülmen.

Zheng, L., Zhu, D., Liang, D., Zhang, B., Wang, C., & Zhao, C. (2015). Winter wheat biomass estimation based on canopy spectra. *International Journal of Agricultural and Biological Engineering, 8*, 30–36. doi:10.25165/ijabe.v8i6.1311.

Estimating Soybean Yield Spatial Variability Within-field Scale through Google Earth Engine in Northeast Italy

Alessandro Zanchin[*], Marco Sozzi, Francesco Marinello, Ahmed Kayad

Department TESAF, University of Padova, Legnaro (PD), Italy

* Corresponding author. Email: alessandro.zanchin@phd.unipd.it

Abstract

The study of spatial variability within agricultural fields is essential for all farmers who want to apply modern precision agriculture. This study investigated the possibility of estimating soybean yield spatial variability at field scale through different vegetation indices (VIs) derived from Sentinel-2 satellite images at different crop growth stages. The study considered yield records from seven fields located in North-East of Italy, with areas ranging between 10 to 19 ha and cultivated by soybean from 2016 to 2018. Sentinel-2 satellite images were used to calculate eight VIs through Google Earth Engine (GEE) between June to October. One-way ANOVA tested the linear correlation between yield and VIs measured at different soybean phenological stages corresponding to the available cloud-free Sentinel-2 images. Results showed that Green Chlorophyll Vegetation Index (GCVI), Green Normalized Difference Vegetation Index (GNDVI) and Wide Dynamic Range Vegetation Index (WDRVI) were the best correlated VIs with soybean yield variability. The highest correlation was observed between 85 and 105 days after sowing corresponding to grains forming and filling (phenological stage R4-R6). R^2 values ranged between 0.21 and 0.68 across whole fields and growth stages. The study proved the effectiveness of a linear model exploiting the equation of the regression line between the VIs and soybean yield from the field with the highest correlation. The model showed high yield estimation accuracy results in 2018 and 2017 seasons with root mean square error (RMSE) of 0.47 and 0.49 Mg/ha respectively compared to less accuracy in 2016 where RMSE was 1.02 Mg/ha. This study approach proved the ability to estimate the within-field variability of soybean yield which could be applied to other Sentinel-2 archived images starting from 2015, while a new model should be calculated each year for each geographic region to ensure the estimation accuracy.

Keywords: Remote sensing, within-field variability, Sentinel-2, soybean.

1. Introduction

Yield maps provide a representation of the crop response to spatial patterns from soil features and topography and temporal patterns as weather conditions or pests and diseases spreading. The recent availability of low-cost (Srbinovska et al. 2015) and freely available high-resolution images from satellites (Sishodia et al., 2020) increased all that helpful data to explain the within-field variability of agricultural areas. All this information is a key factor for all farmers and technicians who target the proper agricultural management of their fields according to precision agriculture (PA). Moreover, the accurate estimation can provide information for insurances and market decision purpose (Lobell 2013). PA is an integrated way of farming to improve the efficiency of agricultural resources through minimising the uncertainty of fields variability management (Liaghat and Balasundram 2010). PA can increase yield and reduce environmental impact and input costs through the site-specific management of homogenous zones (Basso et al. 2016; Kayad et al. 2021). Considering the aforementioned concepts, PA is one of the farming methods with the lowest environmental impact per food unit, ensuring the healthiness of goods simultaneously (Tellaeche et al. 2008). Variable-rate technology (VRT) is an example of precision agriculture tools to manage the within-field variability. VRT allows changing the spreading rate of agricultural inputs and soil tillage according to prescription maps. Monitoring variables of interest lead to estimate the within-field variability and subsequently the required application rate according to crop needs (Leroux and Tisseyre 2019). A common way for monitoring fields and crops is remote sensing (RS). RS is a science, technology, and art that allows the detection and analysis of objects on the earth's surface and below, without any physical contact between the sensor, the operator who collects data, and the targets (Thomas et al., 2015). Satellites are available to monitor agricultural areas for decades (Sishodia et al., 2020). For agricultural applications, the bands within the visible and near-infrared (NIR) reflectance from the crops play a crucial role in crops monitoring. The study of the NIR region allows detecting crop vigour, stress and health issues (Thomas et al.,1997). The reflection of NIR frequencies changes according to the chemical composition of the vegetal tissues, for examples, different plant species, different crops phenological stage and plant health (Foley et al. 1998). Many vegetation indices (VIs) have been proposed to monitor crops, forests and natural areas (Xue and Su 2017). VIs represent a powerful tool to monitor and assess crop variability (Bolton and Friedl 2013). VIs means a mathematical function between the absorbance value of specific frequencies of light reflected by the canopy of both crops and plants and catches by an optical sensor. The ratio between the quantity of

light absorbed by the chlorophyll and other pigments with the light reflected by vegetal tissues is directly related to plants biomass and health status (Zhang et al. 2012). VIs clearly portray these crops features. Normalized vegetation index (NDVI) was proposed by Rouse et al., in 1973, and it retrieves the concentration of chlorophyll expressed from 0 to 1 on plant tissues. It is considered a base method to detect vigour plants rich in chlorophyll than weak plants. Many other VIs was proposed for several purposes. EVI is an example of formula built by Liu and Huete to improve NIR detection avoiding atmospheric interferences. Soil-Adjusted Vegetation Index (SAVI) separates the soil background noise from the light reflected by the crop canopies (Huete 1988). Gitelson designed the Wide Dynamic Range Vegetation Index (WDRVI) that is more sensitive at high chlorophyll concentration while NDVI easily reaches saturation (Xue and Su 2017). Each change on plants tissues has a different effect on the reflected light spectrum (Mahlein et al. 2013). Many indexes were proposed to identify different causes of stress according to the changes in the spectrum of emitted light by the crops. Many authors studied the spatial distribution of stress correlation with the trend of VIs in the same field. If this correlation is significant, it means that VIs is suitable to assess and monitor the spreading of a stress factor (Oumar and Mutanga 2013). As mentioned above, VIs let to detect nutrient deficit and identify in which area of the field they are much required (Basso et al. 2016). Health status monitoring (Xue and Su 2017) and yield estimation (Schwalbert et al. 2018) are some examples of the power of RS for crops monitoring. exploiting VIs. Many studies proved the effectiveness of using Sentinel-2 images to compute VIs and then estimate yield and within-field crop variability (Hunt et al. 2019). Sentinel-2 represents two satellites of the mission Copernicus Sentinel-2 launched by the European Space Agency (ESA). First images of the earth surface have been available since June 2015. Sentinel-2 mount a multispectral sensor. Four bands have a spatial resolution of 10m, six 20m and three 60m and the revisit time is five days at the equator. All data are freely available through ESA and Google earth engine (GEE) platforms. Comparing yield maps with VIs maps from satellite images is a proven method to explore the availability of detecting within-field variability of agricultural areas from RS (Schwalbert et al. 2018; Bolton and Friedl 2013; Al-Gaadi et al. 2016). Schwalbert et al., used NDVI maps from Sentinel-2 to estimate corn yield with a forecast model. This study retrived better results at farm scale than larger areas. Bolton et al., estimated corn and soybean variability at country-level in the Unites states thanks to MODIS (Moderate Resolution Imaging Spectroradiometer), a satellite owned by NASA (National Aeronautics and Space Administration). In this case, Enhanced Vegetation Index (EVI) fit better with their forecasting models than NDVI. Al-Gaadi et al., explored potato yield variability in Saudi Arabia at field-level comparing two satellite, Landsat-8 and Sentinel-2, and two VIs, NDVI and SAVI. Kayad et al., focused their research on the study of within-field variability of corn in the North Italy comparing many VIs from several Sentinel-2 images. Green Normalized Difference Vegetation Index (GNDVI) provided the highest correlation with corn yield variability. However, more investigations from real farms data, different field crops, different crop growth stages and at the field scale are needed.

Therefore, this study focused on the correlation analysis between VIs and the yield of soybean crop. The main objectives were to

1. Identify VIs that better estimates soybean yield spatial variability within field scale.
2. Verify in which phenological stage the correlation between VIs and soybean yield is higher.

2. Materials and Methods

2.1. Study area

This study considered seven fields located in the Veneto region in North-East of Italy, in the province of Rovigo, figure 1. These fields are located in an alluvial plain, and they have a clayey soil texture. The nearby distance between the seven study fields minimizes soil features and crop difference. In addition, the nearby distance helps to avoid any errors in monitoring due to the different incidence angle between the reflected light and the satellite position. The chosen fields have areas higher than 10ha, and they have a regular and polygonal shape. The same farmer cultivated these areas with soybean in 2016, 2017, and 2018 according to conventional management practices. He sowed soybean only once in three years per field, so no repetitions were available for the same field. Soybean is a summer crop (Legumes in Cropping Systems), and Italian farmers usually cultivate soybean from April to October. The seven field features are summarized in table 1.
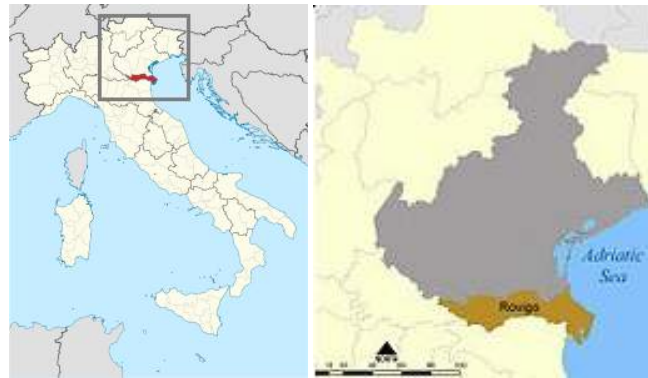
Figure 1. Study area, where the 7 fields considered as case studies were localized.

Table 1. Features of the seven areas considered for this study.

Field Name	Area (ha)	Crop	Sowing Date	Harvest Date	Average Yield (Mg/ha)
CNS	18.4	Soybean	May 20, 2018	Sept 18, 2018	4.15
RFS	12.5	Soybean	May 20, 2018	Sept 18, 2018	3.75
PVS	10.8	Soybean	May 12, 2017	Sept 17, 2017	3.42
AFS	9.4	Soybean	May 11, 2017	Sept 23, 2017	3.06
PAS	11.4	Soybean	Apr 25, 2017	Sept 21, 2017	3.05
RZS	15.1	Soybean	May 15, 2016	Sept 16, 2016	4.31
BDS	10.5	Soybean	May 8, 2016	Sept 13, 2016	4.74

2.2. Yield data

Yield records and maps were provided by Mantovani Lino & Loris agricultural companies. The farmer harvested each field with the same combine "Case IH AXIAL-FLOW 9230", thanks to the "AFS Harvest Command™" technology, that retrieved yield maps from its monitor "AFS Pro 700". Considering that the system records yield data per second, and the harvester works at 7 km/h mounting a header of nine meters wide, the monitor recorded at least 570 data points per hectare. SMS basic (AgLeader) is the software that lets to download the yield maps from the combine monitor. Raw yield maps have been cleaned from non-representative data in ArcMap10.3.1 (Esri), excluding all points less than 10m from the field border, and deleting all data further than three standard deviations from each field yield mean (Amidan et al., 2005; Córdoba et al. 2016). Yield records weredata interpolated in ArcMap10.3.1 with the kriging function to generate a continuous raster instead of a point data. Finally, the maps were resampled to match with the exact resolution of the satellite maps. All available yield maps were treated with the same procedure mentioned above.

2.3. Satellite monitoring

The monitoring started from the first week of June corresponding to 20 to 40 days after sowing (DAS) depending on the sowing date, and ended at soybean harvest. Sentinel-2 Level 2A (L2A) images were available on Google Earth Engine (GEE). GEE is a free Google LLC service available on the cloud, and it provides images from many satellite missions. It lets many transformations and computations on maps and satellite images and download the elaborated products. For this study, the bands one, three, four, five, and eight (Table 2) corresponding to blue, green, red, red-edge and near-infrared bands were used to compute eight VIs from Sentinel-2 images (Table 3). The eight VIs chosen for this research was the most common found in the literature review. For this study EVI formula was modify to obtain values from -1 to +1 adding a factor as showed in equation (1). Satellite images from June to October were suitable to monitor soybean during each developing growth stage. GEE filtered all pictures with more than 20% of the pixel covered by clouds. Summer is the best period of the year to monitor crops exploiting remote sensing because of the high number of available images in low cloudy cover; nevertheless, only a foggy day could affect the study results. GEE provided a raster with the same border of the field including the eight VIs values computed in each data when images were available and resampled at 10m pixel, the lowest available resolution from Sentinel-2 bands.

$$EVI = \frac{B8 - B4}{B8 + 6B4 - 7{,}5B1 + 10000} \qquad (1)$$

Table 2. Sentinel-2 bands features, from www.sentinels.copernicus.eu.

Sentinel-2 Bands	Central Wavelength (nm)	Spatial resolution
B1 – Coastal Aerosol	443	60
B3 – Green	560	10
B4 – Red	665	10
B5 – Vegetation Red Edge	705	20
B8 - NIR	842	10

Table 3. Acronym, full name, equation and references of all vegetation indexes used in this research.

Acronym	Full name	Formula	Reference
NDVI	Normalized difference vegetation index	$(B8 - B4)/(B8 + B4)$	(Rouse et al., 1973)
NDRE	Normalized Difference Red Edge	$(B8 - B5)/(B8 + B5)$	(Barnes et al. 2000)
GNDVI	Green Normalized Difference Vegetation Index	$(B8 - B3)/(B8 + B3)$	(Gitelson et al., 1996)
GARVI	Green Atmospherycally Resistant Vegetation Index	$\dfrac{B8 - (B3 - B1 - B5)}{B8 - (B3 + B1 - B5)}$	(Gitelson et al., 1996)
EVI	Enhance Vegetation Index	$(B8 - B4)/(B8 + 6B4 - 7{,}5B1 + 1)$	(Liu and Huete 2019)
WDRVI	Wide Dynamic Range Vegetation Index	$(\alpha * B8 - B4)/(\alpha * B8 + B4)$	(Gitelson 2004)
GCVI	Green Chlorophyll Vegetation Index	$(B8/B3)-1$	(Gitelson et al., 2003)
mWDRVI	Wide Dynamic Range Vegetation Index	$\begin{cases} NDVI & NDVI \le 0.6 \\ WDRVI & NDVI > 0.6 \end{cases}$	(Sakamoto et al., 2013)

2.4. Data analysis

Each yield map of the seven fields has been compared with its eight VIs rasters per all available dates. Each pairing was used for determining the correlation between yield and the VIs spatial trend by computing the R-squared value (R^2) and the regression line equation. Finally, ANOVA tested the significance of correlations between the two variables. The acquisition date of satellite images was expressed in days after the crop sowing (DAS) to compare the three different years. A time-series analysis let to understand which was the best VIs and when the correlation between yield and VIs was higher. The time-series also showed the field with the highest correlation. Once determined the field and the date with the highest R^2 values, the regression line between the most correlated VIs with soybean yield variability was chosen as a linear model to estimate the yield variability in the other six fields, by applying the model on the VIs map. The estimated yield was compared with the actual yield to test the accuracy of the model. Hence the Root Mean Square Error (RMSE), equation (2) and the correlation between estimated and actual yield proved the effectiveness of the estimation thanks to the linear model.

$$RMSE = \sqrt{\frac{\sum_{i=1}^{n}(y_i - x_i)^2}{n}} \qquad (2)$$

3. Results and Discussion

Figure 2 shows the time-series analysis, once per each field, included all VIs computed in all dates. In the graph, the *x*-axis represents the DAS, while the *y*-axis represents the R^2 between VIs and yield in each date. In general, correlations were very low at the very early growth stages because most of the reflected light collected by the satellite comes from soil portions. In Figure 2, correlations were good at the development stages, decreasing at later

stages. This could be explained by the fact that in the more productive parts of the field, the crop grows with high vigour started since the first stages, while in the less productive areas, the crop developed slowly since the beginning. The same trend has been proved in other fields where correlations had a peak at the early stages. Then the curve decreases, probably due to a higher crop uniformity during the higher growth rate stages. In all the seven time-series the trend of the R^2 values was very similar. The highest correlation observed between 80 and 105 DAS. After that the trend usually decreases due to the end of ripening and the following senescing of all green tissues. According to the Italian crops calendar, 80 - 105 DAS coincide with August. In this period, soybean was at the phenological stage R4/R6, it means respectively pods forming, seeds forming, and pods filling. During R4, soybean plants set the number of pods and so the potential productivity. During R5 and R6, soybean metabolism is most focused on grain production and the dry matter increasing has still a positive linear trend. Both in R5 and in R6, most of the dry matter gained and the N storage are due to pods growing and grain forming (Bender et al., 2015). Hence, these are very susceptible stages for soybean development, and any factor of stress in this period could strongly affect the final production (Clay et al. 2013). This could mean soybean health status and chlorophyll content at this range of time is highly related to final production. GCVI, GNDVI, and WDRVI were the highest VIs related to soybean yield and comparing the time-series from all the seven fields. These three indexes explain crops variability better than the others do when vegetation is very dense, the LAI of the canopy is higher than 2 (Gitelson 2004) or LAI is higher than 3 (Viña et al. 2011). This concept is explained in the graph of Figure 3. Figure 3 shows the correlation line between GCVI and NDVI with yield from the field, and date, which shows the highest values. GCVI, which is the best VIs, always maintains a linear trend Figure 3 (a), while NDVI is scattered at higher values Figure 3 (b). Figure 4 illustrates the comparison between the soybean yield map and two VIs maps in the date of maximum correlation. The colours graduation separates lower production areas from higher ones in the same way. In this example, it was easy to understand how strong the relation between the yield variability with VIs maps is. The two fields studied in 2016 show lower correlation values than 2017 and 2018, and the R^2 between GCVI and yield resulted respectively 0.25 and 0.27 in the two fields. Nevertheless, in the two 2016 fields, the highest correlation values are verified at the same DAS range of 80-105, such as in all the other cases. Many answers could explain this issue. There are many constraints that nobody can detect, considering yield maps and satellite images. Many unknown patterns could affect crops production or the light reflected by a crop. For example, severe weather events, pest or disease could damage the crop. GEE filtered the cloudy images above a threshold, but fog or some cirrus could interfere with the actual crop reflected radiation. Moreover, it must be taking into account how the field variability is distributed. Knowing Sentinel-2 observe the average value of a 10 m pixel means large homogeneous zones are easily detected by remote sensing than small and isolated ones. If variability is randomly spread on a field surface, remote sensing could not be the right way to monitor that field. The correlation line between GCVI and the yield has been exploited as the function of the linear model to estimate yield variability. Figure 5 illustrates the actual yield and the predicted yield by the model and the equation used. Table 4 resume the statistical analysis of the products of the linear model, CNS area missed because its GCVI equation was exploited in the model, and the results were already known. The results were good in terms of R^2 and RMSE in the fields cultivated in 2018 and 2017 while the results were not so satisfactory in 2016 fields. First of all, the correlation between yield and VIs was very low this year. It could also mean a linear model could be acceptable to estimate the variability among areas cultivated in the same year but was not accurate enough to do it across the different year. Each year has different weather condition, sowing and harvest date, and any other factor interfering with the correlation between the crop variability and the VIs.

Table 4. RMSE and R^2 values computed between actual yield and predicted yield by the linear model.

	RFS 2018	PVS 2017	AFS 2017	PAS 2017	RZS 2016	BDS 2016
RMSE Mg/ha	0.47	0.61	0.53	0.49	2.07	1.02
R^2	0.49	0.41	0.63	0.52	0.25	0.27
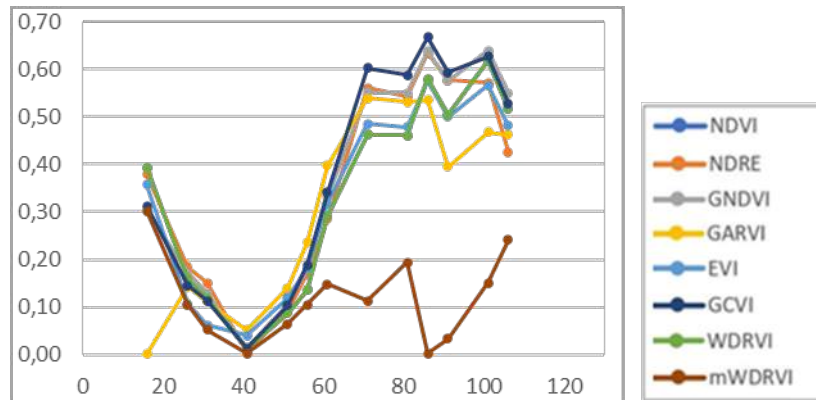
Figure 2. Time-series analysis of the area which showed the higher correlation between soybean yield with eight vegetation indexes computed in all available satellite images. Horizontal axis represents the days after sowing (DAS), while vertical axis means the value of R² computed on a different date.
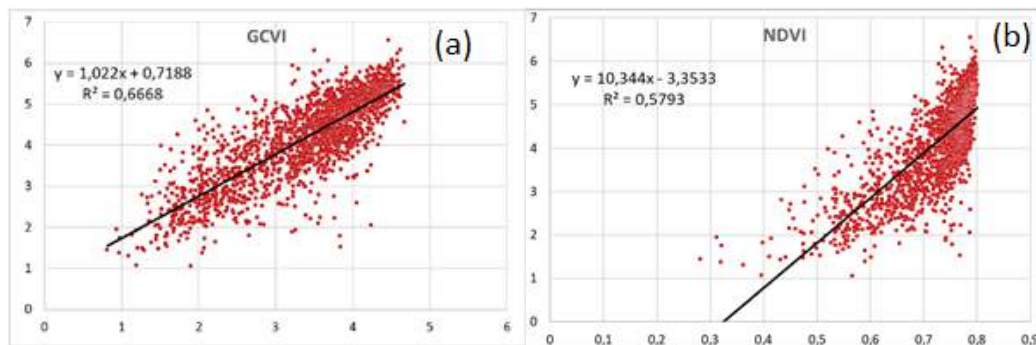
Figure 3. The Scatter plot includes the regression line between GCVI (a) and NDVI (b) values (horizontal axis) and yield (vertical axis). Data comes from the area and the date which showed the highest R² value.
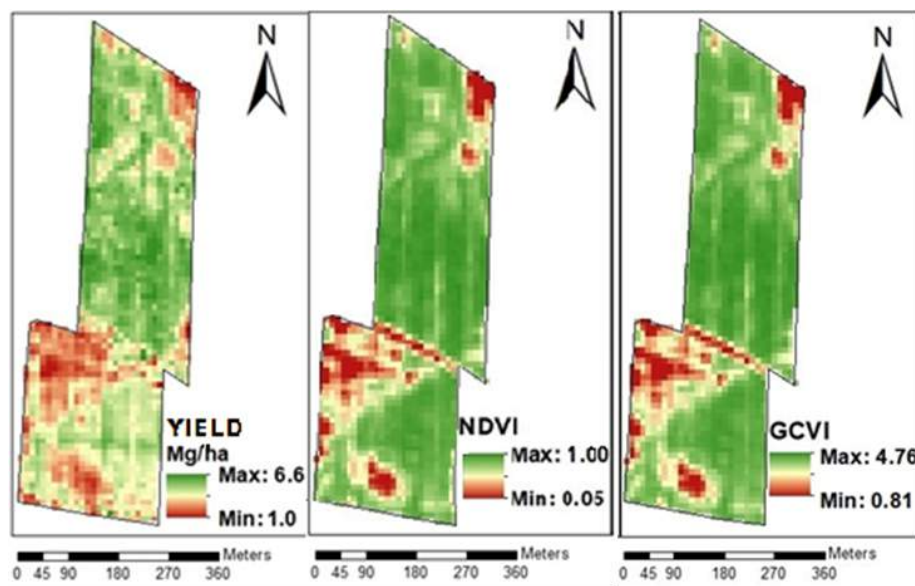
Figure 4. Soybean yield map (10m resolution) from the field with the highest correlation (a), NDVI (b), and GCVI (c) maps of the date with the highest correlation with yield.
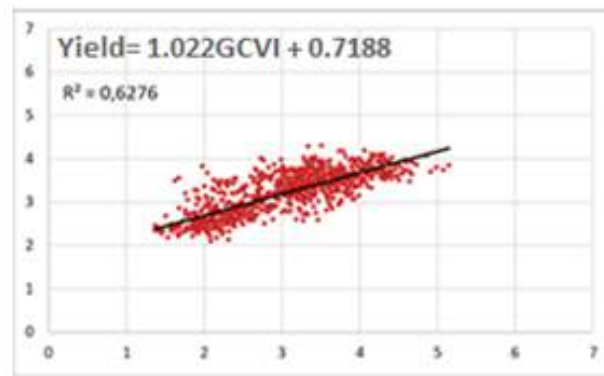
Figure 5. The scatter plot compares the yield predicted by the model on the vertical axis with the actual yield on the horizontal axis; yield is expressed in Mg/ha. (Regression line: yield= 1.022GVI+0.7188)

4. Conclusions

A total of seven yield maps from soybean fields located in North-East of Italy were correlated with eight different VIs derived from Sentinel-2 images. The overall objective was to investigate the ability of Sentinel-2 images to estimate soybean yield variability within-field scale. This research study verified that GCVI, GNDVI, and WDRVI were the best VIs to estimate soybean within-field variability from free Sentinel-2 images. The time-series analysis identified 80 to 105 DAS as the best range of time to detect within-field yield variability from remote sensing. A linear model estimates yield variability in the same area from the VIs raster, but it showed promising results only two years out of three. It suggests a new linear model should be proposed each year to address all the temporal constraints affecting yield and VIs correlation. The use of freely available remote sensing data allows farmers to monitor the within-field variability even though they miss yield maps of their fields or have no other way to monitor their crops. Defining the within-field variability, is essential to all farmers who want to apply precision agriculture: in particular temporal stability of within-field variability can drive farmers decision and support more effective precision farming approaches.

References

Al-Gaadi, Khalid A., Abdalhaleem A. Hassaballa, Elkamil Tola, Ahmed G. Kayad, Rangaswamy Madugundu, Bander Alblewi, and Fahad Assiri. 2016. "Prediction of Potato Crop Yield Using Precision Agriculture Techniques." *PLoS ONE* 11 (9): e0162219. https://doi.org/10.1371/journal.pone.0162219.

Amidan, Brett G., Thomas A. Ferryman, and Scott K. Cooley. 2005. "Data Outlier Detection Using the Chebyshev Theorem." In *IEEE Aerospace Conference Proceedings*. Vol. 2005. https://doi.org/10.1109/AERO.2005.1559688.

Barnes, E M, T R Clarke, S E Richards, P D Colaizzi, J Haberland, M Kostrzewski, P Waller, et al. 2000. "Coincident Detection of Crop Water Stress, Nitrogen Status and Canopy Density Using Ground Based Multispectral Data." *Proc. 5th Int. Conf. Precis Agric*, no. July 2015.

Basso, Bruno, Benjamin Dumont, Davide Cammarano, Andrea Pezzuolo, Francesco Marinello, and Luigi Sartori. 2016. "Environmental and Economic Benefits of Variable Rate Nitrogen Fertilization in a Nitrate Vulnerable Zone." *Science of the Total Environment* 545–546 (March): 227–35. https://doi.org/10.1016/j.scitotenv.2015.12.104.

Bender, R. R.; Haegele, J. W.; Below, F. E. 2015. "Modern Soybean Varieties' Nutrient Uptake Patterns." *Better Crops with Plant Food* 99 (No.2): 7–10.

Bolton, Douglas K., and Mark A. Friedl. 2013. "Forecasting Crop Yield Using Remotely Sensed Vegetation Indices and Crop Phenology Metrics." *Agricultural and Forest Meteorology* 173 (May): 74–84. https://doi.org/10.1016/j.agrformet.2013.01.007.

Clay, David, Charles Carlson, Sharon Clay, Larry Wagner, Darrell Deneke, and Christopher Hay. 2013. "IGrow Soybeans: Best Management Practices for Soybean Production." *Agronomy, Horticulture, and Plant Science Books*, January.

Córdoba, Mariano A., Cecilia I. Bruno, José L. Costa, Nahuel R. Peralta, and Mónica G. Balzarini. 2016. "Protocol for Multivariate Homogeneous Zone Delineation in Precision Agriculture." *Biosystems Engineering* 143 (March): 95–107. https://doi.org/10.1016/j.biosystemseng.2015.12.008.

Foley, William J., Allen McIlwee, Ivan Lawler, Lem Aragones, Andrew P. Woolnough, and Nils Berding. 1998. "Ecological Applications of near Infrared Reflectance Spectroscopy - A Tool for Rapid, Cost-Effective Prediction of the Composition of Plant and Animal Tissues and Aspects of Animal Performance." *Oecologia*. Oecologia. https://doi.org/10.1007/s004420050591.

Gitelson, Anatoly A. 2004. "Wide Dynamic Range Vegetation Index for Remote Quantification of Biophysical Characteristics of Vegetation." *Journal of Plant Physiology* 161 (2): 165–73. https://doi.org/10.1078/0176-1617-01176.

Gitelson, Anatoly A., Yuri Gritz, and Mark N. Merzlyak. 2003. "Relationships between Leaf Chlorophyll Content and Spectral Reflectance and Algorithms for Non-Destructive Chlorophyll Assessment in Higher Plant Leaves." *Journal of Plant Physiology* 160 (3): 271–82. https://doi.org/10.1078/0176-1617-00887.

Gitelson, Anatoly A., Yoram J. Kaufman, and Mark N. Merzlyak. 1996. "Use of a Green Channel in Remote Sensing of Global Vegetation from EOS- MODIS." *Remote Sensing of Environment* 58 (3): 289–98. https://doi.org/10.1016/S0034-4257(96)00072-7.

Huete, A. R. 1988. "A Soil-Adjusted Vegetation Index (SAVI)." *Remote Sensing of Environment* 25 (3): 295–309. https://doi.org/10.1016/0034-4257(88)90106-X.

Hunt, Merryn L., George Alan Blackburn, Luis Carrasco, John W. Redhead, and Clare S. Rowland. 2019. "High Resolution Wheat Yield Mapping Using Sentinel-2." *Remote Sensing of Environment* 233 (November): 111410. https://doi.org/10.1016/j.rse.2019.111410.

James Wilson Rouse, Schell J. A., Donald W. Deering, Robert H. Haas. 1973. "Monitoring Vegetation Systems in the Great Plains with ERTS." In *Proceedings of the Third ERTS Symposium, Goddard Space Flight Center, December 1973, NASA SP-351, NASA, Washington*, edited by NASA, 309–17. Washington: NASA.

Kayad, Ahmed, Marco Sozzi, Simone Gatto, Brett Whelan, Luigi Sartori, and Francesco Marinello. 2021. "Ten Years of Corn Yield Dynamics at Field Scale under Digital Agriculture Solutions: A Case Study from North Italy." *Computers and Electronics in Agriculture* 185 (June). https://doi.org/10.1016/j.compag.2021.106126.

Leroux, Corentin, and Bruno Tisseyre. 2019. "How to Measure and Report Within-Field Variability: A Review of Common Indicators and Their Sensitivity." *Precision Agriculture* 20 (3): 562–90. https://doi.org/10.1007/s11119-018-9598-x.

Liaghat, S., and S. K. Balasundram. 2010. "A Review: The Role of Remote Sensing in Precision Agriculture." *American Journal of Agricultural and Biological Science*. Science Publications. https://doi.org/10.3844/ajabssp.2010.50.55.

Liu, Hui Qing, and Alfredo Huete. 2019. "A Feedback Based Modification of the NDVI to Minimize Canopy Background and Atmospheric Noise." *IEEE Transactions on Geoscience and Remote Sensing* 33 (2): 457–65. https://doi.org/10.1109/tgrs.1995.8746027.

Lobell, David B. 2013. "The Use of Satellite Data for Crop Yield Gap Analysis." *Field Crops Research* 143 (March): 56–64. https://doi.org/10.1016/j.fcr.2012.08.008.

Mahlein, A. K., T. Rumpf, P. Welke, H. W. Dehne, L. Plümer, U. Steiner, and E. C. Oerke. 2013. "Development of Spectral Indices for Detecting and Identifying Plant Diseases." *Remote Sensing of Environment* 128 (January): 21–30. https://doi.org/10.1016/j.rse.2012.09.019.

Oumar, Zakariyyaa, and Onisimo Mutanga. 2013. "Using WorldView-2 Bands and Indices to Predict Bronze Bug (Thaumastocoris Peregrinus) Damage in Plantation Forests." *International Journal of Remote Sensing* 34 (6): 2236–49. https://doi.org/10.1080/01431161.2012.743694.

Sakamoto, Toshihiro, Anatoly A. Gitelson, and Timothy J. Arkebauer. 2013. "MODIS-Based Corn Grain Yield Estimation Model Incorporating Crop Phenology Information." *Remote Sensing of Environment* 131 (April): 215–31. https://doi.org/10.1016/j.rse.2012.12.017.

Schwalbert, Rai A., Telmo J.C. Amado, Luciana Nieto, Sebastian Varela, Geomar M. Corassa, Tiago A.N. Horbe, Charles W. Rice, Nahuel R. Peralta, and Ignacio A. Ciampitti. 2018. "Forecasting Maize Yield at Field Scale Based on High-Resolution Satellite Imagery." *Biosystems Engineering* 171 (July): 179–92. https://doi.org/10.1016/j.biosystemseng.2018.04.020.

Sishodia, Rajendra P., Ram L. Ray, and Sudhir K. Singh. 2020. "Applications of Remote Sensing in Precision Agriculture: A Review." *Remote Sensing* 12 (19): 1–31. https://doi.org/10.3390/rs12193136.

Srbinovska, Mare, Cvetan Gavrovski, Vladimir Dimcev, Aleksandra Krkoleva, and Vesna Borozan. 2015. "Environmental Parameters Monitoring in Precision Agriculture Using Wireless Sensor Networks." *Journal of Cleaner Production* 88 (February): 297–307. https://doi.org/10.1016/j.jclepro.2014.04.036.

Tellaeche, Alberto, Xavier P. BurgosArtizzu, Gonzalo Pajares, Angela Ribeiro, and César Fernández-Quintanilla. 2008. "A New Vision-Based Approach to Differential Spraying in Precision Agriculture." *Computers and Electronics in Agriculture* 60 (2): 144–55. https://doi.org/10.1016/j.compag.2007.07.008.

Thomas, G, J Taylor, and G Wood. 1997. "Mapping Yield Potential with Remote Sensing."

Thomas Lillesand, Ralph W. Kiefer, Jonathan Chipman. 2015. *Remote Sensing and Image Interpretation, 7th Edition*. Edited by Wiley. 7th ed. New York.

Viña, Andrés, Anatoly A. Gitelson, Anthony L. Nguy-Robertson, and Yi Peng. 2011. "Comparison of Different Vegetation Indices for the Remote Assessment of Green Leaf Area Index of Crops." *Remote Sensing of Environment* 115 (12): 3468–78. https://doi.org/10.1016/j.rse.2011.08.010.

Xue, Jinru, and Baofeng Su. 2017. "Significant Remote Sensing Vegetation Indices: A Review of Developments and Applications." *Journal of Sensors*. Hindawi Limited. https://doi.org/10.1155/2017/1353691.

Zhang, Jingcheng, Ruiliang Pu, Wenjiang Huang, Lin Yuan, Juhua Luo, and Jihua Wang. 2012. "Using In-Situ Hyperspectral Data for Detecting and Discriminating Yellow Rust Disease from Nutrient Stresses." *Field Crops Research* 134 (August): 165–74. https://doi.org/10.1016/j.fcr.2012.05.011.

Linear Models for Predicting Ammonia Concentration in the Animal Zone of a Weaned Piglet Building

Tamara Arango[a]*, Roberto Besteiro[b], Juan A. Ortega[c], María D. Fernández[b], M. Ramiro Rodríguez[b],

[a]Estación Experimental del Zaidín, Consejo Superior de Investigaciones Científicas, Granada, Spain

[b]Department of Agroforestry Engineering, University of Santiago de Compostela, Lugo, Spain

[c]Xunta de Galicia, Department of Rural Environment, Pontevedra, Spain

*corresponding author. Email: manuelramiro.rodriguez@usc.es

Abstract

Measuring ammonia inside livestock buildings poses many challenges that hinder the incorporation of this variable into environmental control systems. The aim of this study was to measure various environmental variables inside a weaned piglet building and analyse their interactions with NH_3 concentrations for setpoint temperatures of 26 and 25ºC, in order to control NH_3 concentrations based on other easily measurable variables. The experimental test was conducted on a conventional farm in Northwest Spain. NH_3 concentrations in the animal zone were best correlated with CO_2 concentrations in the animal zone (0.91 and 0.55) and velocity of air extracted through the fan (0.72 and 0.65) for setpoint temperatures of 26 and 25ºC, respectively. Similarly, strong correlations were found with relative humidity in the animal zone and temperature of inlet air. Because NH_3 concentration in the animal zone is related to the performance of the ventilation system, strong positive correlations were found between NH_3 concentration and temperature of inlet air whereas negative correlations were found between NH_3 concentration and ventilation rates. Linear regression models based on CO_2 concentrations in the animal zone and temperature of inlet air are recommended, insofar as they provide a good fit for both setpoint temperatures using variables that can be readily measured.

Keywords: Setpoint temperature, ammonia concentration, carbon dioxide concentration.

1. Introduction

In recent years, the gradual intensification of animal production has brought about many new environmental problems. At the same time, there has been a growing public awareness of the need to protect, respect and defend animals, which has led to market initiatives for pork production systems with increased animal welfare (De Greef et al., 2011). In the near future, animal welfare, food safety and respect for the environment will be major challenges for livestock production. In this context, indoor climate control in livestock buildings becomes crucial to the welfare, health and productivity of animals. Among other parameters, indoor climate control includes temperature, relative humidity, and air velocity and quality, which is defined in terms of airborne dust and harmful gases such as ammonia (NH_3), hydrogen sulphide (SH_2) or carbon dioxide (CO_2) (Park et al., 2013). Therefore, indoor climate in livestock buildings deserves particular attention insofar as it affects animal health and welfare, animal production, workers' health and the environment. In this sense, a successful environmental control system must provide good air quality. Indeed, a well-designed environmental control system is the most efficient tool to ensure optimal production in livestock housing (Garcimartín et al., 2007).

From among all the gases found in livestock buildings, NH_3 requires an in-depth analysis because of the potential adverse effects of emissions (Rong and Aarnink, 2019) and the impact of high NH_3 concentration levels on animal health and production (Wang et al., 2020; Xie et al., 2017; Kim et al., 2008) and farm workers' health (Xie et al., 2017). Generally, the responses of pigs to their environment are complex and difficult to assess, and there is relatively little information available on their reaction to air pollutants (Michiels et al., 2015). Yet, it has been shown that ammonia can affect animal health and productivity, its effects depending on concentration levels and exposure times (Gustafsson et al., 2013; Banhazi et al., 2008a; Cargill et al., 2002). A number of authors have shown that exposing pigs to NH_3 concentrations of 6 and 13 ppm (Lee et al., 2005) or up to 37 ppm (Wathes et al., 2002) does not affect production efficiency. Such disparate concentrations suggest that more research is needed in order to find more conclusive values (Michiels et al., 2015). Hence, no official NH_3 exposure limits have been established for the occurrence of adverse health effects on pig growth (Kim et al., 2008) even though many authors have recommended maximum NH_3 levels in swine buildings between 7 and 15 ppm (Costa, 2017; Banhazi et al., 2008b) or even 20 ppm (Donham et al., 2002; Whates et al., 2002). In any case, many authors have reported measured ammonia concentration levels below those values (Rodríguez et al., 2020; Zong and Zhang, 2015).

Measuring gaseous emissions from livestock buildings, particularly under commercial conditions, is a challenging task that is subject to various uncertainty sources (Calvet et al., 2013). Actually, gas concentrations vary according to the airflow pattern and depend greatly on the ventilation system, among other variables (Rosa et al., 2021; Tabase et al.,

2020; Rong and Aarnink, 2019). Ammonia concentrations can be measured with a variety of sensors, among which semiconductor, infrared, photoacoustic and electrochemical detectors. However, all of them show weaknesses for real-time monitoring of ammonia and many of them show a limited useful life, and require continuous maintenance and frequent calibration. In addition, the effect of sensor location is affected by the time and duration of measurements due to variations in the level of animal activity through time across different life stages (Takai et al., 2013) and to daily and seasonal variations in gas concentrations (Rodríguez et al., 2020; Calvet et al., 2011). As a result, considerable efforts have been made to: (1) understand the mechanisms of ammonia emission (Rosa et al., 2021; Rong and Aarnink, 2019; Ni et al., 2017), (2) solve measurement accuracy issues (Calvet et al., 2013; Takai et al., 2013; Ogink et al., 2012) and (3) reduce ammonia emissions (Calvet et al., 2017; Takai et al., 2013). Because current knowledge and measurement techniques can only provide reasonable estimates of ammonia emissions, there is a need for improved measurement techniques that allow for more accurate emission rate inventories (Takai et al., 2013). Nevertheless, electrochemical sensors are often used in real-time monitoring of gaseous emissions in livestock buildings (Rodríguez et al., 2020; Ogink et al., 2012; Banhazi et al., 2008b) because of their small size and fast response times (Zhang et al., 2013).

The aim of this paper is to analyse the interactions between environmental variables, focusing on NH_3 concentration and its prediction from other easily measurable environmental variables, such as humidity, temperature, CO_2 concentration or air velocity inside the building.

2. Materials and Methods

2.1. Experimental test

2.1.1. Animals and housing

An experimental test was conducted on a commercial pig farm located in northwest Spain (ETRS89. 43º10'12''N, 8º19'30''W). The farm housed weaned piglets of 20 kg live weight and was the largest in the study area, with a maximum capacity of 4985 sows.

The weaner room, with an area of 69.26 m^2 and a volume of 164.50 m^3, consisted of twelve 2.55 m x 1.97 m pens on both sides of a central aisle. The room could hold a maximum of 300 piglets, with an area of 0.20 m^2 per piglet. The piglets, which were Large White x Landrace hybrids weaned at 3 weeks of age, entered the room on February 25 and exited the room on April 8. The floor was completely slatted over a pit with a depth of 45 cm. The ventilation system was composed of a 500 mm helical extractor fan with a volume of 8746 m^3h^{-1}. Fan speed was adjusted by changing the voltage using a temperature-based digital controller, which allowed ventilation rates between 25% and 100% and bandwidth temperatures of ±1.5°C. Additionally, the ventilation rate was modulated with a manual system that reduced the area of the air outlet through the fan and provided volumes of between 1.03 and 10.58 m^3h^{-1} per piglet. Fresh air entered the room through two 0.70 m^2 windows with manually controlled air deflectors. The radiant floor heating system was composed of two 1.20 m × 0.50 m polyester spreader plates for water, with 19 l capacity, placed at the centre of each pen. The average temperature of the plates was 30.60°C, with a mean difference between inlet and outlet temperature of 5.80°C. The heating system was controlled with a manual valve.

2.1.2. Variables and measurement

The following environmental variables were measured (figure 1): Temperature of air in external corridor (T_{CA}), velocity of the air extracted through the ventilation system (V_{EX}), and temperature, relative humidity, air velocity and CO_2 and NH_3 concentrations in the animal zone (T_{AZ}, HR_{AZ}, V_{IN-AZ}, CO_{2-AZ}, NH_{3-AZ}). T_{CA} was recorded using a BetaTherm 100K6A1B Thermistor sensor (Campbell Scientific©), with a measurement range of -5°C – 95°C and ±0.5°C accuracy from -5°C to 90°C. The sensor was placed at 1.80 m height outside the room, in the external corridor. V_{EX} was measured using a Delta Ohm HD2903TTC310 active air speed transmitter with a measurement range of 0.20 – 20 m s^{-1} and an accuracy of ±0.4 ms^{-1} +3% of measurement. The transmitter was installed in a 0.55 × 0.55 m duct with a length of 1.20 m, fixed to the fan outlet, according to the method proposed by Hinz and Linke (1998), and was adapted to the hotwire probe used.

The sensors located in the animal zone were placed in a pen that was representative of room conditions. Sensors were arranged inside a protection cage at 0.2 m height above the slats to reduce the risk of destruction by the animals. T_{AZ} and relative HR_{AZ} were measured using a Temperature/HR smart sensor (ONSET® S-THB-M002) with a measurement range of -40ºC – 75ºC and accuracies of ±0.2ºC for temperature and ±2.5% for humidity. To measure V_{IN-AZ}, a Delta Ohm HD103T.0 hotwire probe with a measurement range of 0 – 5 ms^{-1} and ±0.06 ms^{-1} accuracy was used. CO_{2-AZ} was measured using a Delta Ohm HD37BTV.1 transmitter, with a measurement range of 0 – 5000 ppm and 50 ppm ±4% accuracy. Finally, NH_{3-AZ} was measured by using an electrochemical sensor MGS 150 (Murco ©), with a measurement range of 0 – 100 ppm and accuracy from -40 to +40ºC <1ppm. The 10-min averages of the measured values were stored at 1-sec intervals in a HOBO® data logger, and a CR-10X Campbell Scientific. The electrochemical sensors used were suitable for use in livestock housing. Nevertheless, the sensors showed some problems, among which saturation after long exposures, need for regular maintenance and low sensitivity. The first two issues were minimized

by using the equipment in short periods, with the required maintenance tasks. However, sensitivity is inherent to the sensor and affects mainly measurements of low concentrations. In order to improve data accuracy, each day with the same T_S was considered as a repeated measurement. Under this consideration, two standard days were prepared, one for each T_S (26 and 25ºC), by calculating the hourly average for every day, which resulted in values more indicative of daily variation.
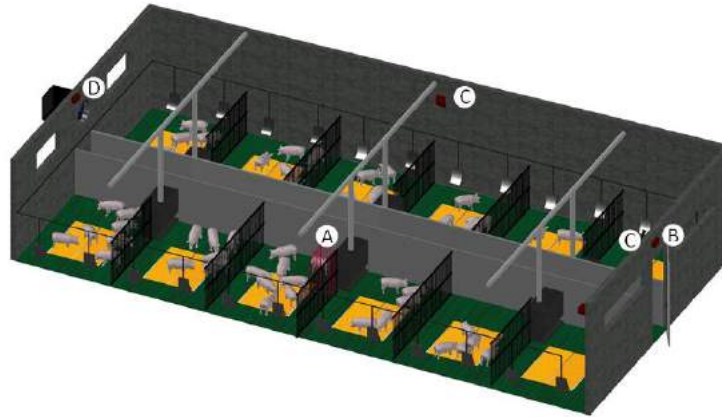
Figure 1: View of the room in which measurements were taken and location of sensors. (A) Sensors in the animal zone (CO_{2-AZ}, HR_{AZ}, NH_{3-AZ}, T_{AZ}, V_{IN-AZ},); (B) T_{CA} and (D)V_{EX}.

2.2. Data analysis

Data were collected at setpoint temperatures (T_S) of 26 and 25ºC between March 2 and March 17, which corresponded to days 5 to 22 after weaning. We chose this study period because of the type of sensor used, which saturates and loses reliability for continuous measurements performed in long periods (more than 20 days). The 10-min averages of the measured values were transformed into hourly averages because the dynamics of the processes associated with the distribution of heat and diffusion of gases did not allow us to establish good linear relationships at shorter times. A statistical analysis was carried out using SPSS 22.0.0 for Windows. To demonstrate the effect of T_S on NH_{3-AZ}, an independent-samples T test was conducted. After that, we worked with two different datasets based on T_S, $T_S = 26$ºC or $T_S = 25$ºC (Rodriguez et al, 2020).

The correlations between the seven study variables were assessed by examining the correlation matrices and testing the significance between variables (N_{H3-AZ}, CO_{2-AZ}, T_{AZ}, T_{CA}, RH_{AZ}, V_{IN-AZ}, V_{EX}).

Data analysis was performed by using multiple regressions, in which the dependent variable was NH_{3-AZ}. The maximum number of independent variables that could be included in the regression model was nine. However, this did not mean that the effect of all the parameters was necessarily significant. In this work, we used a SPSS procedure that performed all possible subset regressions.

3. Results and Discussion

3.1. Concentration of NH3-AZ for TS = 26ºC and TS = 25ºC

For both setpoint temperatures, daily mean NH_{3-AZ} concentrations (figure 2) were well below the strict safe exposure limits set by Cargill et al. (2002) at 10 ppm, and most of the time below the 7 ppm established by Donham et al. (2002). Piglets were in a clean environment, with concentrations below 6 ± 0.5 ppm (Lee et al., 2005), for 85.32% and 66.67% of the time for 26 and 25ºC, respectively, and exceeded this limit only for 14.68% (26ºC) and 33.33% (25ºC) of the time.

3.2. Correlations between the study variables for TS = 26ºC and TS = 25ºC

Except for V_{IN-AZ}, stronger correlations were found for $T_S=26$ºC than for $T_S=25$ºC (table 1), which suggests an important effect of T_S on the dynamics of mass and energy flows that occur in the building. A strong correlation was found between NH_{3-AZ} and CO_{2-AZ} concentrations, with values of 0.91 and 0.55 for 26 and 25ºC, respectively. These values are in agreement with the values reported by other authors (Philippe et al., 2007; Jeppsson, 2002; Duchaine et al., 2000).
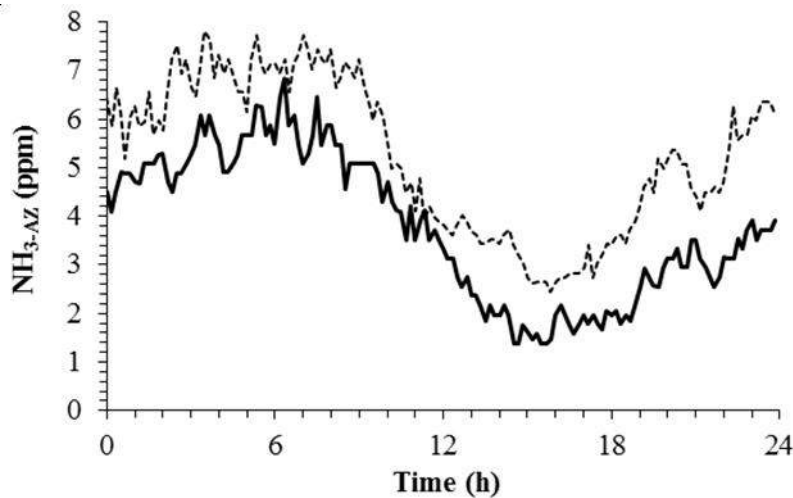
Figure 2: Evolution of hourly mean values of $NH_{3\text{-}AZ}$ for T_S of 26ºC (—) and 25ºC (- -).

Table 1: Correlation matrix based on hourly data for the variables: $NH_{3\text{-}AZ}$, $CO_{2\text{-}AZ}$, RH_{AZ}, $V_{IN\text{-}AZ}$, V_{EX}, T_{CA}, T_{AZ} for T_S = 26ºC and T_S = 25ºC.

	$CO_{2\text{-}AZ}$	RH_{AZ}	$V_{IN\text{-}AZ}$	V_{EX}	T_{CA}	T_{AZ}
			T_S = 26ºC			
$NH_{3\text{-}AZ}$	0.91**	0.78**	0.01	-0.72**	-0.80**	0.03
			T_S = 25ºC			
	$CO_{2\text{-}AZ}$	RH_{AZ}	$V_{IN\text{-}AZ}$	V_{EX}	T_{CA}	T_{AZ}
$NH_{3\text{-}AZ}$	0.55**	0.16*	-0.35**	-0.65**	-0.29**	-0.08

* $p \leq 0.05$. ** $p \leq 0.01$

The difference between the correlations found for the concentrations of $NH_{3\text{-}AZ}$ and $CO_{2\text{-}AZ}$ for the two T_S was evident and was related to the performance of the ventilation system. The lowest T_S (25ºC) showed lower correlations because the ventilation system was much more efficient in removing NH_3 than CO_2, due to the dynamics of the gases in the building.

The correlation between T_{AZ} and $NH_{3\text{-}AZ}$ was near zero for both T_S, which is in contrast with the findings reported by other authors (Jeppsson, 2002). Such a null correlation was due to the capacity of the climate control system –which was composed of ventilation and heating– to keep temperature in the animal zone (T_{AZ}) almost constant at the desired values.

For both T_S, a negative correlation was found between $NH_{3\text{-}AZ}$ and T_{CA}, with higher values for 26ºC (-0.80) than for 25ºC (-0.29), which is in agreement with Rosa et al., 2021. This effect can be explained by the ventilation rates (Koerkamp et al., 1998). When the outdoor temperatures drop, there is a decrease in the ventilation rate inside the building, with the consequent increase in NH_3 concentration. This has been confirmed in our study, insofar as the correlations between ventilation (V_{EX}) and $NH_{3\text{-}AZ}$ were -0.72 and -0.65 for 26 and 25ºC, respectively.

For $V_{IN\text{-}AZ}$, which indirectly characterizes ventilation, correlations with $NH_{3\text{-}AZ}$ were -0.35 for 25ºC and almost null for 26ºC. The high values of $NH_{3\text{-}AZ}$ during the night are indicative of a low ventilation rate, which suggests that the system could not extract all the NH_3 produced.

Correlations between RH_{AZ} and $NH_{3\text{-}AZ}$ were in the range 0.78 and 0.16 for T_S = 26 ºC and T_S = 25ºC, respectively. The value obtained for 26ºC was similar to the value reported by Jeppsson (2002), and intermediate with respect to the values reported by Choi (2005) and Ni et al. (2017).

3.3- Linear regression models of NH3-AZ from mean hourly data

The first model proposed in our study predicted the interactions between $CO_{2\text{-}AZ}$ and $NH_{3\text{-}AZ}$ concentrations and yielded an adjusted R^2 value of 0.83, with a standard error (SE) of the estimate of 0.97 ppm. Model 26H-2 considered RH_{AZ} as the independent variable and yielded an R^2 of 0.60 with an SE of 1.49 ppm. Despite the poorer fit of Model 26H-2 with respect to the first model, Model 26H-2 is interesting because it reveals that keeping humidity at low levels ensures low concentrations of NH_3.

Table 2. Non-standardized coefficients (B), standardized coefficients (β), constants (CTE), correlation coefficients (R), adjusted determination coefficients (R^2), standard errors (SE), collinearity statistics (T' and VIF) and Durbin Watson statistics (DW) for the estimation of $NH_{3\text{-}AZ}$ from multiple regressions with the variables (V): $CO_{2\text{-}AZ}$, RH_{AZ}, T_{CA} and V_{EX} for hourly data and T_S = 26ºC or T_S = 25ºC.

T_S = 26ºC	V	B	β	CTE	R	R^2	SE	T'	VIF	DW
26H-1	$CO_{2\text{-}AZ}$	0.00**	0.91	-6.34	0.91	**0.83****	0.97	1.00	1.00	1.70
26H-2	RH_{AZ}	0.30**	0.78	-13.44	0.78	**0.60****	1.49	1.00	1.00	1.72
26H-3	T_{CA}	-0.26**	-0.74	8.63	0.80	**0.64****	1.41	1.00	1.00	1.80
26H-4	V_{EX}	-10.59**	-0.72	7.96	0.72	**0.52****	1.63	1.00	1.00	2.01
26H-5	$CO_{2\text{-}AZ}$	0.00**	0,71	1.65	0.93	**0.86****	0.89	0.43	2.34	1.80
	T_{CA}	-0.39**	-0,27					0.43	2.34	
26H-6	$CO_{2\text{-}AZ}$	0.00**	0.80	-4.15	0.92	**0.84****	0.94	0.50	1.98	1.70
	V_{EX}	-2.34**	-0.16					0.50	1.98	
26H-7	T_{CA}	-0.74**	-0.50	5.78	0.85	**0.71****	1.26	0.45	2.28	1.85
	RH_{AZ}	0.16**	0.40					0.45	2.28	
26H-8	$CO_{2\text{-}AZ}$	0.00**	0.63	2.91	0.87	**0.87****	0.86	0.33	3.07	1.80
	T_{CA}	-0.36**	-0.25					0.42	2.38	
	V_{EX}	-1.92**	-0.13					0.50	2.02	
T_S = 25ºC	V	B	β	CTE	R	R^2	SE	T'	VIF	DW
25H-1	V_{EX}	-14.57**	-0.65	12.55	0.65	0.42**	1.81	1.00	1.00	1.81
25H-2	V_{EX}	-11.20**	-0.50	4.70	0.71	0.50**	1.69	0.78	1.29	1.90
	$CO_{2\text{-}AZ}$	0.00**	0.32					0.78	1.29	
25H-3	V_{EX}	-10.18**	-0.49	5.29	0.72	0.51**	1.65	0.73	1.37	1.88
	$CO_{2\text{-}AZ}$	0.00**	0.31					0.78	1.29	
	$V_{IN\text{-}AZ}$	-58.33**	-0.16					0.91	1.11	
25H-4	V_{EX}	-9.80**	-0.43	9.86	0.73	0.53**	1.63	0.72	1.40	1.90
	$CO_{2\text{-}AZ}$	0.00**	0.40					0.58	1.74	
	$V_{IN\text{-}AZ}$	-62.25**	-0.17					0.90	1.11	
	RH_{AZ}	-0.11**	-0.14					0.71	1.40	

* $p \leq 0.05$. ** $p \leq 0.01$

Model 26H-3, for the relationship between T_{CA} and $NH_{3\text{-}AZ}$, yielded an R^2 of 0.64 and improved the prediction of $NH_{3\text{-}AZ}$ slightly as compared to model 26H-2. This finding is interesting because Model 26H-3 incorporates an easily measurable variable, T_{CA}. Model 26H-3 considerably improves the model proposed by Pereira et al. (2012) who, using non-continuous measurements, reported values between 0.95 and 0.97 for dairy cattle. Such an improvement could be explained in terms of the differences between forced ventilation and natural ventilation.

Model 26H-4 included V_{EX} as the independent variable and showed poorer results (R^2= 0.52) that were in agreement with the values reported by Sousa and Pedersen (2004) and below those reported by Blanes-Vidal et al. (2008).

Incorporating T_{CA} (26H-5) or V_{EX} (26H-6) into Model 26H-1 slightly improved the predictions, with R^2 values of 0.86 and 0.84, respectively. Model 26H-8 yielded the best results, with an R^2 of 0.87 and an SE of 0.86 ppm, Yet, as with the previous models, Model 26H-8 is not interesting from a practical standpoint because only the models requiring fewer, easily measurable variables can be incorporated into environmental control systems. The standardized coefficients suggest that RH_{AZ} has a slightly greater effect on the prediction of $NH_{3\text{-}AZ}$ than T_{CA}.

As regards the regression models for T_S = 25ºC, Model 25H-1, with V_{EX} as the independent variable, showed an R^2 of 0.42, which is lower that the value reported by Blanes-Vidal et al. (2008). Incorporating new variables into the model produced slight improvements, such that the best results were obtained with Model 25H-4, which yielded an R^2 of 0.53. Yet, the main drawback of Model 25H-4 is the need to incorporate four variables into the control system. For a setpoint temperature of 25ºC, the standardized coefficients suggest that V_{EX} is the variable with the greatest impact on the dependent variable, which implies that ventilation is essential in the determination and prediction of $NH_{3\text{-}AZ}$ concentrations, which is in agreement with the findings reported by Blanes-Vidal et al. (2008).

3.4. Linear regression models of NH3-AZ from mean daily data

Models built from mean daily data (table 3) using a single variable did not improve the results for T_S = 26ºC, even though the SE was considerably lower. On the contrary, models built from mean daily data improved considerably for

$T_S = 25ºC$.

Table 3. Non-standardized coefficients (B), standardized coefficients (β), constants (CTE), correlation coefficients (R), adjusted determination coefficients (R^2), standard errors (SE), collinearity statistics (T' and VIF) and Durbin Watson statistics (DW) for the estimation of NH_{3-AZ} from multiple regressions with the variables (V): CO_{2-AZ}, RH_{AZ}, T_{CA} and V_{EX} for mean daily data and $T_S = 26ºC$ or $T_S = 25ºC$.

$T_S = 26ºC$	V	B	β	CTE	R	R^2	SE	T′	VIF	DW
26D-1	CO_{2-AZ}	4E-03**	0.82	-7.14	0.82	0.66**	0.78	1.00	1.00	1.50
26D-2	RH_{AZ}	0.37**	0.70	-17.34	0.69	0.46**	0.99	1.00	1.00	1.55
26D-3	T_{CA}	-1.12**	-0.89	20.30	0.89	0.79**	0.62	1.00	1.00	1.56
26D-4	V_{EX}	-19.78**	-0.79	11.85	0.79	0.60**	0.87	1.00	1.00	1.86
26D-5	CO_{2-AZ}	1E-03*	0.31	11.70	0.91	0.82**	0.58	0.37	2.71	1.74
	T_{CA}	-0.81**	-0.65					0.37	2.71	
26D-6	CO_{2-AZ}	2E-03*	0.54	1.04	0.89	0.76**	0.66	0.57	1.75	2.32
	V_{EX}	-10.83**	-0.43					0.57	1.75	
26D-7	RH_{AZ}	0.12*	0.23	10.57	0.91	0.82**	0.58	0.63	1.60	1.78
	T_{CA}	-0.94**	-0.75					0.63	1.60	
26D-8	RH_{AZ}	0.22**	0.41	-2.58	0.87	0.72**	0.72	0.77	1.31	2.52
	V_{EX}	-14.81**	-0.60					0.77	1.31	
26D-9	T_{CA}	-0.91**	-0.73					0.38	2.66	
	V_{EX}	-0.60**	-0.02	10.33	0.91	0.81**	0.59	0.45	2.23	1.82
	RH_{AZ}	0.13*	0.24					0.62	1.61	
$T_S = 25ºC$	V	B	β	CTE	R	R^2	SE	T′	VIF	DW
25D-1	V_{EX}	-18.97**	-0.85	14.80	0.85	0.71**	1.04	1.00	1.00	1.73
25D-2	T_{CA}	-2.55**	-0.84	33.13	0.84	0.70**	0.87	1.00	1.00	1.49
25D-3	V_{EX}	-17.49**	-0.79	4.88	0.87	0.73**	0.82	0.87	1.15	2.02
	CO_{2-AZ}	3E-03*	0.18					0.87	1.15	
25D-4	CO_{2-AZ}	6E-03**	0.37	13.34	0.92	0.83**	0.65	0.99	1.02	1.72
	T_{CA}	-2.41**	-0.80					0.99	1.02	

* $p \leq 0.05$. ** $p \leq 0.01$

Overall, the accuracy of the models built from mean daily data (table 3) did not improve for $T_S = 26ºC$, even though these models showed a notably lower SE. Conversely, for $T_S = 25ºC$, the goodness of fit increased considerably and the SE decreased. For both T_S, the models incorporating V_{EX}, T_{CA} or CO_{2-AZ} as the single control variable produced remarkable results, which did not sensibly improve by adding new variables to the model. Consequently, these models provide an efficient and inexpensive method for the control of NH_3 concentrations insofar as they use a single variable that can be readily measured.

4. Conclusions

The following conclusions can be drawn from the analysis of environmental variables, particularly NH_3 concentration and its prediction from other inexpensive, easily measurable environmental variables:

NH_3 concentration in the animal zone correlates positively with CO_2 concentration and relative humidity in the animal zone for setpoint temperatures of 26 and 25ºC. In addition, because NH_3 concentration is directly related to the performance of the ventilation system, the correlation coefficients are strong and negative for air velocity extracted through the ventilation system and positive for temperature of air in the external corridor, which is not environmentally controlled and, therefore, shows a linear relation with outdoor temperature.

For a setpoint temperature of 26ºC, the variables that yield the best linear models are temperature of air in external corridor and CO_2 concentration, both for daily and hourly data. For 25ºC, the velocity of the air extracted through the ventilation system gains relevance and can be compared to the temperature of air in the external corridor.

Based on these differences, we recommend linear regression models based on CO_2 concentration in the animal zone and temperature of air in external corridor using mean daily values, insofar as these models provide good fits for both setpoint temperatures using variables that can be readily measured.

References

Banhazi, T.M., J. Seedorf, D.L. Rutley, W.S. Pitchford, 2008a. Identification of risk factors for sub-optimal housing conditions in Australian piggeries: Part 1. Study justification and design. Journal of Agricultural Safety and Health. 14(1), 5-20. https://doi.org/10.13031/2013.24120.

Banhazi, T. M., J. Seedorf, D.L. Rutley, W.S. Pitchford, 2008b. Identification of risk factors for sub-optimal housing conditions in Australian piggeries: Part 2. Airborne pollutants. Journal of Agricultural Safety and Health. 14(1), 21-39. https://doi.org/10.13031/2013.24122.

Blanes-Vidal, V., M.N. Hansen, S. Pedersen, H.B. Rom, 2008. Emissions of ammonia, methane and nitrous oxide from pig houses and slurry: Effects of rooting material, animal activity and ventilation flow. Agriculture, Ecosystems & Environment. 124(3), 237-244. https://doi.org/10.1016/j.agee.2007.10.002.

Cargill, C., T. Murphy, T. Banhazi. 2002. Hygiene and air quality in intensive housing facilities in Australia. Animal Production in Australia. 24, 387-393.

Calvet, S., R.S. Gates, G. Zhang, F. Estelles, N.W. Ogink, S. Pedersen, D. Berckmans, 2013. Measuring gas emissions from livestock buildings: A review on uncertainty analysis and error sources. Biosystems Engineering. 116(3), 221-231. https://doi.org/10.1016/j.biosystemseng.2012.11.004.

Calvet, S., M. Cambra-López, F. Estelles, A.G. Torres, 2011. Characterization of gas emissions from a Mediterranean broiler farm. Poultry Science. 90(3), 534-542. https://doi.org/10.3382/ps.2010-01037.

Calvet, S., J. Hunt, T.H. Misselbrook, 2017. Low frequency aeration of pig slurry affects slurry characteristics and emissions of greenhouse gases and ammonia. Biosystems Engineering. 159, 121-132, https://doi.org/10.1016/j.biosystemseng.2017.04.011.

Choi, H. L., K.Y. Kim, H. Kim, 2005. Correlation of air pollutants and thermal environment factors in a confined pig house in winter. Asian-Australasian Journal of Animal Sciences. 8(4), 574-579. https://doi.org/10.5713/ajas.2005.574.

Costa, A., 2017. Ammonia concentrations and emissions from finishing pigs reared in different growing rooms. Journal of Environmental Quality. 46(2), 255-260, https://doi.org/10.2134/jeq2016.04.0134.

De Greef K.H., H.M. Vermeer, H.W.J. Houwers, A.P. Bos, 2011. Proof of principle of the comfort class concept in pigs: experimenting in the midst of a stakeholder process on pig welfare. Livestock Science. 139, 172-185. https://doi.org/10.1016/j.livsci.2011.03.005.

Donham, K., Thorne, P., Breuer, G., Powers, W., Marquez, S., Reynolds, S., 2002. Exposure limits related to air quality and risk assessment. In *Iowa Concentrated Animal Feeding Operations Air Quality Study*. Iowa State University and The University of Iowa Study Group, p 164.

Duchaine, C., Y. Grimard, Y. Cormier, 2000. Influence of building maintenance, environmental factors, and seasons on airborne contaminants of swine confinement buildings. AIHAJ-American Industrial Hygiene Association. 61(1), 56-63.

Garcimartin, M. A., I. Ovejero, E. Sanchez, V. Sanchez-Giron, 2007. Application of the sensible heat balance to determine the temperature tolerance of commercial poultry housing. Worlds Poultry Science Journal. 63(4), 575-584. https://doi.org/10.1017/S0043933907001626.

Gustafsson, G., T. Banhazi, K.H. Jeppsson, 2013. Control of emission from livestock buildings and the impact on health, welfare and performance of animals: A review. In: *Livestock housing: Modern management to ensure optimal health and welfare of farm animals*. Wageningen, Netherlands. Wageningen. Eds. A. Aland and T. Banhazi. 261–280 https://doi.org/10.3920/978-90-8686-771-4.

Hinz, T., S. Linke. 1998. A comprehensive experimental study of aerial pollutants in and emissions from livestock buildings. Part 1. Methods. Journal of Agricultural Engineering Research 70 (1), 111-118. https://doi.org/10.1006/jaer.1998.0282.

Jeppsson, K. H., 2002. Diurnal variation in ammonia, carbon dioxide and water vapour emission from an uninsulated, deep litter building for growing/finishing pigs. Biosystems Engineering. 81, 213-224. 10.1006/bioe.2001.0025.

Kim, K.Y., Ko, H.J., Kim, H.T., Kim, C.N., Byeon, S.H., 2008. Association between pig activity and environmental factors in pig confinement buildings. Australian Journal of Experimental Agriculture 48, 680–686. https://doi.org/10.1071/EA06110.

Groot Koerkamp, P.W.G., J.H.M. Metz, G.H. Uenk, V.R. Phillips, M.R. Holden, R.W. Sneath, J.L. Short, , J. Hartung, J. Seedorf, M. Schröder, K.H. Linkert, S. Pedersen, H. Takai, J.O. Johnsen, C.M. Wathes, 1998.

Concentrations and emissions of ammonia in livestock buildings in Northern Europe. Journal of Agricultural Engineering Research. 70(1), 79-95. https://doi.org/10.1006/jaer.1998.0275.

Lee, C., L.R. Giles, W.L. Bryden, J.L. Downing, P.C. Owens, A.C. Kirby, P.C. Wynn, 2005. Performance and endocrine responses of group housed weaner pigs exposed to the air quality of a commercial environment. Livestock Production Science. 93(3), 255-262, https://doi.org/10.1016/j.livprodsci.2004.10.003.

Michiels, A., S. Piepers, T. Ulens, N.Van Ransbeeck, R.D.P. Sacristán, A. Sierens, F. Haesebrouck, P. Demeyer, D. Maes, 2015. Impact of particulate matter and ammonia on average daily weight gain, mortality and lung lesions in pigs. Preventive Veterinary Medicine. 121(1-2), 99-107. https://doi.org/10.1016/j.prevetmed.2015.06.011.

Ni, J.Q., S. Liu, C.A. Diehl, T.T. Lim, B.W. Bogan, L. Chen, A.J. Heber, 2017. Emission factors and characteristics of ammonia, hydrogen sulfide, carbon dioxide, and particulate matter at two high-rise layer hen houses. Atmospheric Environment. 154, 260-273. https://doi.org/10.1016/j.atmosenv.2017.01.050.

Ogink, N.W., J. Mosquera, S. Calvet, G. Zhang, 2013. Methods for measuring gas emissions from naturally ventilated livestock buildings: Developments over the last decade and perspectives for improvement. Biosystems Engineering. 116(3), 297-308. https://doi.org/10.1016/j.biosystemseng.2012.10.005.

Park, J.H., T.M. Peters, R. Altmaier, R.A. Sawvel, T.R. Anthony, 2013. Simulation of air quality and cost to ventilate swine farrowing facilities in winter. Computers and Electronics in Agriculture. 98, 136-145. https://doi.org/10.1016/j.compag.2013.08.003.

Pereira, J., T.H. Misselbrook, D.R. Chadwick, J. Coutinho, H. Trindade, 2012. Effects of temperature and dairy cattle excreta characteristics on potential ammonia and greenhouse gas emissions from housing: A laboratory study. Biosystems Engineering. 112(2), 138-150, https://doi.org/10.1016/j.biosystemseng.2012.03.011.

Philippe, F.X., M. Laitat, B. Canart, M. Vandenheede, B. Nicks, 2007. Comparison of ammonia and greenhouse gas emissions during the fattening of pigs, kept either on fully slatted floor or on deep litter. Livestock Science, 111(1), 144-152. https://doi.org/10.1016/j.livsci.2006.12.012.

Rodriguez, M.R., E. Losada, R. Besteiro, T. Arango, R. Velo, J.A, Ortega, M.D. Fernandez, 2020. Evolution of NH$_3$ Concentrations in Weaner Pig Buildings Based on Setpoint Temperature. Agronomy. 10(1), 107. https://doi.org/10.3390/agronomy10010107.

Rong, L. A.J.A. Aarnink, 2019. Development of ammonia mass transfer coefficient models for the atmosphere above two types of the slatted floors in a pig house using computational fluid dynamics. Biosystems Engineering. 183, 13-25. https://doi.org/10.1016/j.biosystemseng.2019.04.011.

Rosa, E., J. Mosquera, H. Arriaga, G. Montalvo, P. Merino, 2021. Ammonia emission modelling and reduced sampling strategies in cage-based laying hen facilities. Biosystems Engineering. 204, 304-311. https://doi.org/10.1016/j.biosystemseng.2021.02.002.

Sousa, P., S. Pedersen, 2004. Ammonia Emission from Fattening Pig Houses in Relation to Animal Activity and Carbon Dioxide Production. Agricultural Engineering International: The CIGR Journal of Scientific Research and Development. Vol.VI.

Tabase, R.K., S. Millet, E. Brusselman, B. Ampe, C. De Cuyper, B. Sonck, P. Demeyer, 2020. Effect of ventilation control settings on ammonia and odour emissions from a pig rearing building. Biosystems Engineering. 192, 215-231. https://doi.org/10.1016/j.biosystemseng.2020.01.022.

Takai, H., S. Nimmermark, T. Banhazi, T. Norton, L.D. Jacobson, S. Calvet, M. Hassouna, B. Bjerg, G. Zhang, S. Pedersen, P. Kai, K. Wang, D. Berckmans, 2013. Airborne pollutant emissions from naturally ventilated buildings: Proposed research directions. Biosystems Engineering 116 (3), 214-220. https://doi.org/10.1016/j.biosystemseng.2012.12.015.

Wang, X., M. Wang, S. Chen, B. Wei, Y. Gao, L. Huang, C. Liu, T. Huang, M. Yu, S.H. Zhao, X. Li, 2020. Ammonia exposure causes lung injuries and disturbs pulmonary circadian clock gene network in a pig study. Ecotoxicology and Environmental Safety. 205, 111050. https://doi.org/10.1016/j.ecoenv.2020.111050.

Wathes, C.M., T.G.M. Demmers, N. Teer, R.P. White, L.L. Taylor, V. Bland, P. Jones, D. Armstrong, A.C.J. Gresham, J. Hartung, D.J. Chennells, S.H. Done, 2004. Production responses of weaned pigs after chronic exposure to airborne dust and ammonia. Animal Science. 78(1), 87-97. https://doi.org/10.1017/S135772980005387X.

Xie, Q., J.Q. Ni, Z. Su, 2017. A prediction model of ammonia emission from a fattening pig room based on the indoor concentration using adaptive neuro fuzzy inference system. Journal of Hazardous Materials. 325, 301-309. https://doi.org/10.1016/j.jhazmat.2016.12.010.

Zhang, S.R., J.H. Wang, D.M. Dong, W.G. Zheng, X.D. Zhao, 2013. A review of contact sensors used for monitoring malodorous gas in animal facilities. Advanced Materials Research. 629, 655-661. https://doi.org/10.4028/www.scientific.net/AMR.629.655.

Zong, C., H. Li, G. Zhang, 2015. Ammonia and greenhouse gas emissions from fattening pig house with two types of partial pit ventilation systems. Agriculture, Ecosystems & Environment. 208, 94-105. https://doi.org/10.1016/j.agee.2015.04.031.

The Effect of Laser Radiation on Selective Blossom Removal in Apple

Prud Netsawang[a,c,]*, Lutz Damerow[a], Michael Blanke[b] and Peter Schulze Lammers[a]

[a] Institute of Agricultural Engineering, University of Bonn, Germany

[b] Institute of Crop Sciences and Resource Conservation (INRES), Horticultural Sciences, University of Bonn, Germany

[c] Faculty of Engineering, Rajamangala University of Technology Lanna, Chiang Mai, Thailand

* Corresponding author. Email: prud@rmutl.ac.th

Abstract

This study presents a technique for selective flower removal in apple by applying laser radiation for removing flowers. A 4-watt blue diode laser with 450 nm wavelength was deployed in a prototype of laser blossom destroyer. An exposure time of between 500 to 3,000 ms was adjusted by a microcontroller. A distance between flower cluster and laser device of 15 cm was used as focal length with a constant laser spot area of 3.92 mm^2. Ca. 350 flower clusters on pollinator apple cv. 'Hilieri' branches including untreated control were exposed to this laser in a laboratory at institute of agricultural engineering, University of Bonn, Germany. Two phenological stages a) at balloon stage (BBCH 59) and b) at full bloom (BBCH 65) were examined with regard to the efficacy of blossom removal at four laser spot positions with a) from side of the bottom of flower cluster, b) from front of the flower cluster, c) from side of the flower bud at ovary and d) from front of the flower bud. The effect of laser energy density on the number of damaged flowers was additionally studied at positions of laser spot from the front of flower cluster. The damage on flowers was examined for 7 days after application; untreated flowers were monitored for flower abscission over the same time. The results demonstrate that the low power laser radiation is a possible alternative technique for selective flower removal. There was no significant difference in efficacy of flower removal between treatments at balloon stage and full bloom. Emitting of laser radiation with the position of laser spot from the front of flower clusters had the greatest effect on flower removal and succeeded most to reduce the number of flowers in the flower clusters. The efficacy of flower reduction was enhanced by increasing the energy density of laser. The higher laser energy density (3.06 J mm^{-2}) caused lethal damage up to 50% more flowers as compared to the damage with the lower energy density (1.02 J mm^{-2}).

Keywords: Apple, Crop load management, Selective blossom removal, Laser radiation, Precision horticulture

1. Introduction

Crop load management (CLM) is an important method to improve fruit quality (Seehuber et al., 2011). Thinning of flowers is a common CLM method to control the number of fruit, which has a positive effect on fruit size, colour, sugar content, firmness and storability (Meland, 2009; Solomakhin and Blanke, 2010). An early reduction of flowers by thinning can overcome alternate bearing in pome fruit (Meland and Gjerde, 1993). In some years apple trees can have generally an abundance of flowers, but not all of flowers are required for a sufficient harvest of high fruit quality (Costa et al., 2013). Untiedt and Blanke (2001) informed that only 7% of flowers are necessary in apple trees to achieve a sufficient yield with high fruit quality.

The number of unwanted flowers is generally reduced by three main techniques. Firstly, the flower buds can be removed by hand at an inflorescence emergence (Breen et al., 2015; Tustin et al., 2012). This technique requires extensive manpower. Secondly, chemical agents are applied to remove excess flowers such as ammoniumthiosulfate (ATS) and ethephon (Maas, 2016; Wertheim, 2000). Chemical blossom thinning has been found to improve fruit quality, but its efficiency is unpredictable and dependent upon weather conditions and cultivar (Wertheim, 2000; Williams, 1979). Thirdly, the flowers can be removed mechanically e.g. string thinners, which is regarded as an environmentally friendly method (Seehuber et al., 2011). Several machines were designed to be used for blossom thinning in the bio-orchards and with special regard to save labor requirements (Damerow et al., 2007; Kon et al., 2013; Lopes et al., 2019; McClure and Cline, 2015; Solomakhin and Blanke, 2010; Wouters, 2014). However, disadvantages of mechanical blossom thinning have been reported in many studies. Kong et al. (2009) reported that there was a 7% damage of branches and flower buds after applying mechanical thinning using a first prototype. As part of CLM, mechanical blossom thinning offers the option of subsequent additional chemical and/or hand thinning at a later stage for fine-tuning fruit set (Basak et al., 2016; Seehuber et al., 2014).

Laser radiation is applied for disaggregating materials not in industry but also in agricultural and horticultural sector. Marx et al. (2013) investigated lasers as a herbicide for weed control. Their results indicate that using suitable lasers marking energy succeeds to reduce damaging of horticultural product surfaces and correspondingly the risk of fungal infection. Laser beam affects a water loss in the tissue of products without toxic effects (Sood et al., 2008, 2009). In addition, laser application is an alternative method in weed control in arable farming successfully reducing the use of chemicals (Bauer et al., 2020; Marx et al., 2012; Mathiassen et al., 2006).

As a different technique for flower thinning in apple as one of the most important fruit crops in Germany, this study aims to explore an alternative approach for selective flower removal by applying laser radiation to flowers and study under laboratory conditions the efficacy of flower deterioration on three different factors as the phenological growth stages of apple flower, the positions of laser spot and the density of laser energy.

2. Materials and Methods

2.1. Laser set up and energy measurement

A blue (450 nm) diode laser with 4 W optical power was applied for a prototype of laser flower remover. The laser system was installed on the aluminium frame (Figure. 1). An apple branch was placed in front of the laser device with a focal length of 0.15 m for a constant laser spot area of 3.92 mm². Two line lasers with low power were applied for targeting the position of laser spot on the flower clusters and flower buds. The laser diode was operated in continuous mode emitting a laser beam with a Gaussian profile to transfer energy horizontally toward the flower cluster. An Arduino Uno microcontroller board was connected with a laser driver by an interface for adjusting the exposure time.
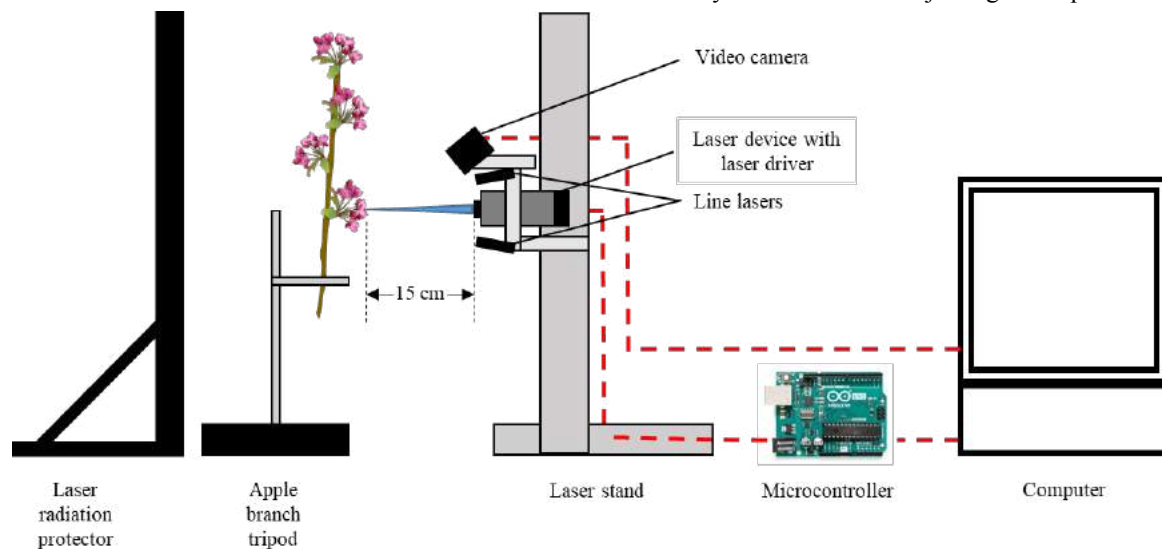
Figure 1. Experimental setup of laser application for flower removal

The optical power of the laser was measured by a laser power meter (PM100A, Thorlabs GmbH., Dachau, Germany) with a thermal power sensor (S425C-L, Thorlabs GmbH., Dachau, Germany) and the laser energy was calculated by Eq (1). The beam profile was measured by a beam diagnostic (LaserCam-HR II, Coherent Inc., USA) with a beam view software (Coherent Inc., USA) to determine the laser spot area on the flower tissue. The laser energy density (Table 1) was determined based on laser energy and laser spot area by Eq (2) (Mathiassen et al., 2006).

$$E = P \times T \tag{1}$$

and

$$I = \frac{E}{A} \tag{2}$$

where E is the laser energy in J, P is the laser power in W, T is the exposure time in s, A is the laser spot area in mm² (3.92 mm² spot area) and I is the laser energy density in J mm⁻².

Table 1. Energy density of the 4 W laser in different exposure times

Exposure time (ms)	Energy (J)	Energy density of laser (J mm⁻²)
500	2	0.50
1,000	4	1.02
1,500	6	1.53
2,000	8	2.04
2,500	10	2.55
3,000	12	3.06

2.2. Apple flower cluster and experimental design

The apple cv. 'Hilieri' flower cluster of one-year-old branches with 1m length from Klein-Altendorf Research Centre of University of Bonn, Germany (50°37', 51 N, 6°59', 32 E) were cut in April 2020 to preserve the flower clusters for the experiments. All apple branches were immersed in water in buckets for storage before tested in the laser laboratory at institute of agricultural engineering, University of Bonn. Two phenological growth stages of apple flower at balloon stage (BBCH 59) (Figure. 2) and full bloom (BBCH 65) (Figure. 3) were investigated with regard on the efficacy of flower removal at four positions of the laser spot with a) from side of the bottom of flower cluster (FSC), b) from front of the flower cluster (FFC), c) from side of the flower bud at ovary (FSB) and d) from front of the flower bud (FFB). Each treatment including untreated control consisted of 25 flower clusters (1 flower cluster = 1 replicate). The 25 flower clusters per each phenological growth stage of flower were applied for the untreated control. Four different positions of laser spot and untreated control were randomly set up on 5-6 flower clusters per branch at the middle of the branch. The effect of laser energy density (Table 1) on the damage of flowers was further investigated by using 10 flower clusters per treatment at the laser spot position from front of flower cluster (FFC).

(a)   (b)
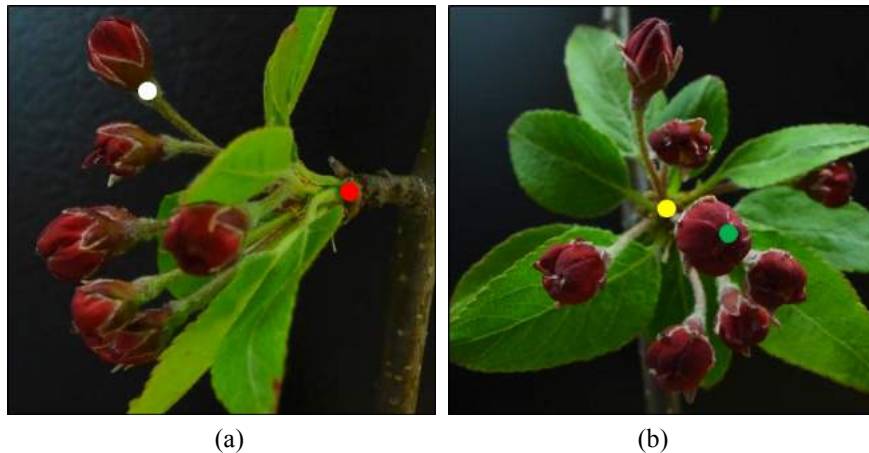
Figure 2. Two photographs as a) from the side of flowers and b) from the front of flowers at **balloon stage** (BBCH 59) with four laser targeting positions (red point: at the laser spot position from side of flower cluster (FSC); white point: at the laser spot position from side of flower bud at ovary (FSB); yellow point: at the laser spot position from front of flower cluster (FFC) and green point: at the laser spot position from front of flower bud (FFB))

(a)   (b)

Figure 3. Two photographs as a) from the side of flowers and b) from the front of flowers at **full bloom** (BBCH 65) with four laser targeting positions (red point: at the laser spot position from side of flower cluster (FSC); white point: at the laser spot position from side of flower bud at ovary (FSB); yellow point: at the laser spot position from front of flower cluster (FFC) and green point: at the laser spot position from front of flower bud (FFB))

2.3. Flower damage assessment and statistical analysis

After laser treatment, the apple branches were immersed in water and took a place in the laboratory with a temperature of 20-25°C. The damage of flowers after laser treatment was evaluated visually every other day. The damage of flowers was monitored until the untreated flowers showed damage to prevent the effect of natural damage on the flower assessment. The number of damaged flower clusters were counted after emitting the laser spot from the side

(FSC) and the front (FFC) of a flower clusters, while the number of damaged flowers were collected for the positions from the side (FSB) and the front (FFB) of the single flower.

To identify the damage, the flowers were divided into two categories depending on the position of damage. The damage of flower at the stigma, style, and ovary was classified as damaged flowers, while the damage at other parts of the flowers such as petal was recorded as undamaged flowers. The number of damaged flowers or flower buds was statistically evaluated using SPSS Statistics (SPSS Co., USA). The LSD test determined the difference between group means at the 95% confidence level.

3. Results and Discussion

3.1. Effect of the laser spot position on the efficacy of flower removal

After treatment, damaged flowers were evaluated visually and recorded every other day. The natural damage on the flower clusters in the untreated control from both phenological growth stages of flower appeared after 5th day after application. Therefore, the results during 1-5 days after application (DAA) were considered in this experiment to prevent natural damage on the assessment of apple flowers. The significant greatest number of the damaged flowers was found on the 5th day after application in both stages (Figure 4 and 5). Thus, the number of damaged flowers on the 5th day of the assessment was applied in this experiment to clarify the influence of the phenological growth stages of flower and the position of the laser spot on the efficacy of laser flower removal.
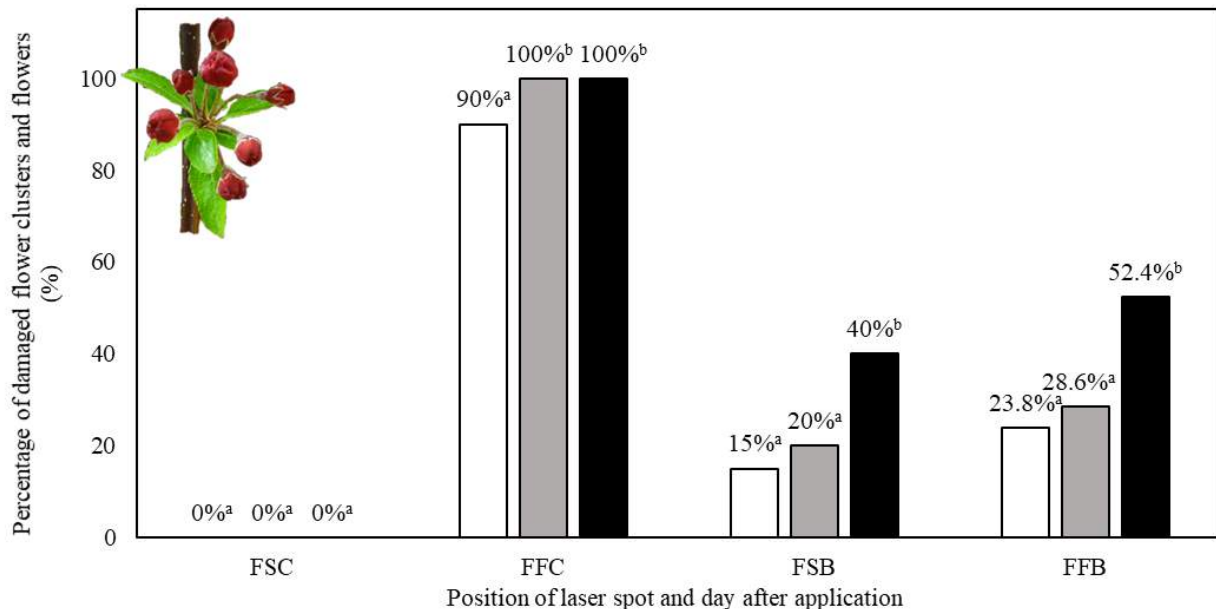
Figure 4 Percentage of damaged flower clusters and flowers on different laser spot positions at balloon stage (white colour: 1st DAA, grey colour: 3rd DAA; black colour: 5th DAA; [a,b] significant difference according LSD with 95% confidence level)
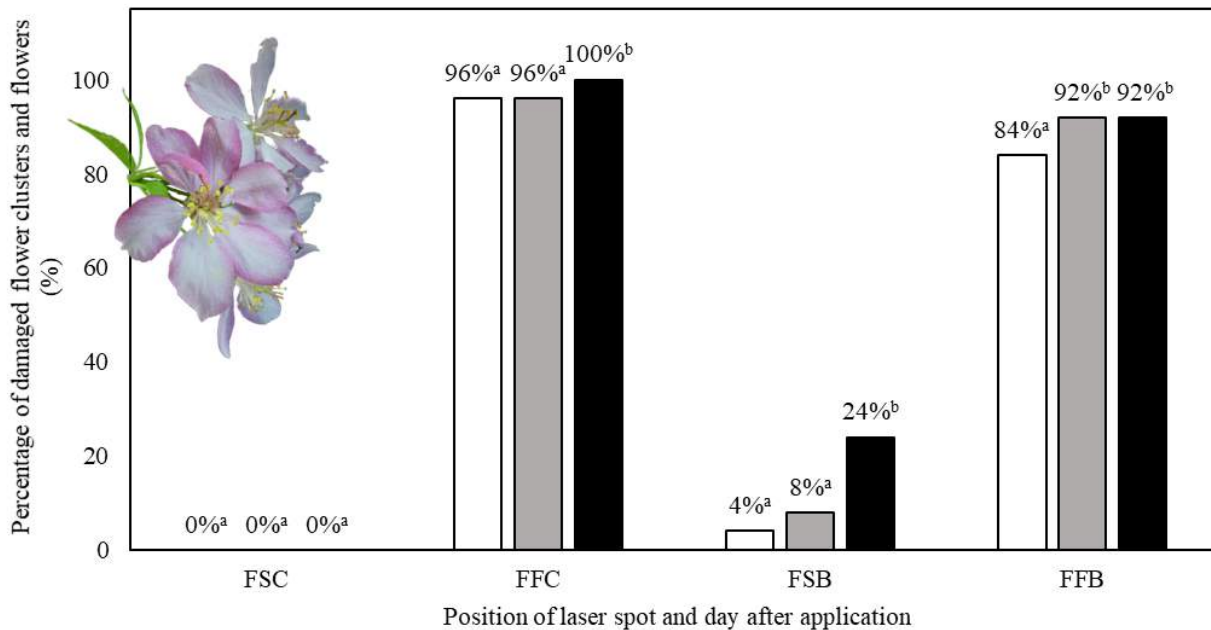
Figure 5 Percentage of damaged flower clusters and flowers on different laser spot positions at full bloom (colour coding as for Fig. 4; [a,b] significant difference according LSD with 95% confidence level)

The position of the laser spot is expected to have an important role in the efficacy of flower removal and affects different damages on flower clusters and flowers. The percentage of damaged flower clusters and flowers at the different laser spot positions has a similar trend at both balloon stage and full bloom (Table 2). From the results, emitting laser radiation with an energy density of 1.06 J mm^{-2} (1,000 ms exposure time) on two positions of laser spot at the base of a flower cluster from the side (FSC) and from the front (FFC) had a significant difference in the percentage of damaged flower. The laser emitting at the position from the front of the flower cluster (FFC) induced the greatest percentage of damaged flowers. It caused lethal damage to the flowers and was able to reduce the partial flower buds on the inflorescences. While emitting of laser radiation at the position from the side at the bottom of flower clusters (FSC) did not damage flower clusters.

Table 2. Efficacy of flower removal by laser radiation with laser energy density of 1.06 J mm^{-2} on four different positions of laser spot at balloon stage and full bloom

Position of laser spot	Percentage of damaged flower clusters and flowers	
	Balloon stage (BBCH 59)	Full bloom (BBCH 65)
FSC	0[c]	0[c]
FFC	100[a]	100[a]
FSB	40[b]	24[b]
FFB	52.4[b]	92[a]

[a, b and c] significant difference according LSD with 95% confidence level

In addition, emitting laser radiation at two positions of the laser spot on an individual flower bud with a) from side of the flower bud at ovary (FSB) and b) from front of the flower bud (FFB) affected the damage of flower buds. The damage on some parts of flower structure at the ovary, stigma, and petals appeared when laser radiation was applied from the side of the flower bud at the ovary (FSB) accounted to by 40% of damaged flowers (at balloon stage) and of 24% (at full bloom) (Table 2). Emitting laser radiation at the position of laser spot from the front of flower bud (FFB) caused damage at stigma and style. It induced a percentage of damaged flowers of 52.4% (at balloon stage) and 92% (at full bloom).

3.2. Effect of phenological growth stage of flower on the efficacy of flower removal

Two phenological growth stages of flower at balloon stage (BBCH 59) and full bloom (BBCH 65) were examined in this experiment to investigate the suitable period for flower removal by using laser radiation. From the results, applying laser radiation with the energy density of laser of 1.06 J mm^{-2} was successfully in both stages of phenological growth to reduce the number of flowers at the laser spot position from the front of flower cluster (FFC) and from the front (FFB) and side (FSB) of flower bud (Table 2). Emitting laser on the laser spot position from front of flower cluster (FFC) at

balloon stage could have more effective than at full bloom because most flowers still have petals forming as hollow ball (Figure 2), which is easier to detect and target precisely the laser spot on the flowers.

Emitting laser radiation from the front of flower bud (FFB) at full bloom improved the efficacy of flower removal in comparison with balloon stage, by 92% and 52.4%, respectively (Table 2). Because of flowers opened at full bloom and all stigmas are located in the center of flower without eclipsed by petals, which has a positive effect for targeting the laser beam at the position of stigma. In contrast, emitting laser radiation at the position from the side of the flower bud at the ovary (FSB) at balloon stage (40%) approached more effective than at full bloom (24%).

The flower removal by laser radiation is effected by the laser spot position in accordance with the phenological growth stage of flower. Two conditions would be recommended for a greater efficacy of deterioration to apply laser radiation at the laser spot position from front of flower cluster (FFC) at balloon stage and at the position from front of flower buds at full bloom (FFB).

3.3. Effect of laser energy density on the efficacy of flower removal

The most successful treatment with the laser spot position from front of flower cluster (FFC) was further investigated in terms of the effect of laser energy density on the efficacy of flower removal. The average number of damaged flowers is summarized in table 3. The efficacy of flower removal by using laser radiation is highly related to the laser energy density. The number of damaged flowers was enlarged when increased the density of laser energy. The lowest density of laser energy of 1.02 J mm^{-2} (4 W laser power with 1,000 ms exposure time) has already a small impact to apply for flower removal. In addition, the higher laser energy of 3.06 J mm^{-2} (4 W laser power with 3,000 ms exposure time) provided lethal damage and reduced up to 50% more flowers as compared to the damage with the lower energy density (1.02 J mm^{-2}). The laser energy density in this experiment was increased by the extension of exposure time. Laser power can also increase the laser energy density and opens up higher accuracy on targeting, but worsen the applicability of laser emitting in orchards because of higher user safety requests.

Table 3. The effect of different density of laser energy at balloon stage and full bloom on the number of damaged flowers in flower cluster with the position of laser spot from the front of flower cluster (FFC)

Energy density of laser (J mm^{-2})	Number of damaged flowers in a cluster	
	Balloon stage (BBCH 59)	Full bloom (BBCH 65)
0.51	0.2[a]	0.2[a]
1.02	2.55[b]	1.96[b]
1.53	2.60[bc]	2.60[bc]
2.04	2.80[cd]	2.60[cd]
2.55	3.20[de]	3.10[de]
3.06	3.30[e]	3.20[e]

[a, b, c, d and e] significant difference according LSD with 95% confidence level

4. Conclusions

Laser radiation can be used as an alternative technique aiming at selective removal of flowers. The efficacy of the laser flower removal was related to the position of the laser spot and laser energy density. The low power laser diode with 4 W and at least 1.02 J mm^{-2} laser energy density led to lethal damage of the flowers at balloon stage and full bloom on three different spot positions as a) from front of flower cluster (FFC), b) from side of the flower bud at ovary (FSB) and c) from front of the flower bud (FFB). Emitting of laser beam at a spot from the front of flower cluster was the most suitable position for flower removal. The lowest applicable laser energy density of 1.02 J mm^{-2} reduced approximately 2 flowers in a flower cluster. The efficacy of flower removal was increased by the laser energy density increment. The laser energy density of 3.06 J mm^{-2} provided lethal damage up to 50% more flowers compared to the damage with the lower energy density of 1.02 J mm^{-2}. Finally, it must be stated that laser application for flower removal in apple farming is still challenging because of unsolved technical problems such as flower recognition and targeting of the laser. Consequences arise from potentially adverse effects of the laser radiation on fruit development and other nearby flowers as well as approval of the laser technology in the field with potentially harmful effects on animals and humans.

References

Basak, A., Juraś, I., Białkowski, P., Blanke, M.M., Damerow, L., 2016. Efficacy of mechanical thinning of apple in Poland. Acta Horticulturae 1138, 75–82.

Bauer, M.V., Marx, C., Bauer, F.V., Flury, D.M., Ripken, T., Streit, B., 2020. Thermal weed control technologies for conservation agriculture-a review. Weed Research 60 (4), 241–250.

Breen, K.C., Tustin, D.S., Palmer, J.W., Close, D.C., 2015. Method of manipulating floral bud density affects fruit set responses in apple. Scientia Horticulturae 197, 244–253.

Costa, G., Blanke, M.M., Widmer, A., 2013. Principles of thinning in fruit tree crops - needs and novelties. Acta Horticulturae 998, 17–26.

Damerow, L., Kunz, A., Blanke, M., 2007. Mechanische Fruchtbehangsregulierung (Regulation of fruit set by mechanical flower thinning). Erwerbs-Obstbau 49 (1), 1–9.

Kon, T.M., Schupp, J.R., Winzeler, H.E., Marini, R.P., 2013. Influence of mechanical string thinning treatments on vegetative and reproductive tissues, fruit set, yield, and fruit quality of 'Gala' apple. HortScience 48 (1), 40–46.

Kong, T., Damerow, L., Blanke, M., 2009. Einfluss selektiver mechanischer Fruchtbehangsregulierung auf Ethylensynthese als Stressindikator sowie Ertrag und Fruchtqualität bei Kernobst (Influence on apple trees of selective mechanical thinning on stress-induced ethylene synthesis, yield, fruit quality, (fruit firmness, sugar, acidity, colour) and taste). Erwerbs-Obstbau 51 (2), 39–53.

Lopes, M., Gasper, P.D., Simões, M.P., 2019. Current status and future trends of mechanized fruit thinning devices and sensor technology. International Journal of Mechanical and Mechatronics Engineering 13 (1), 43–57.

Maas, F.M., 2016. Control of fruit set in apple by ATS requires accurate timing of ATS application. Acta Horticulturae 1138, 45–52.

Marx, C., Barcikowski, S., Hustedt, M., Haferkamp, H., Rath, T., 2012. Design and application of a weed damage model for laser-based weed control. Biosystems Engineering 113 (2), 148–157.

Marx, C., Hustedt, M., Hoja, H., Winkelmann, T., Rath, T., 2013. Investigations on laser marking of plants and fruits. Biosystems Engineering 116 (4), 436–446.

Mathiassen, S.K., Bak, T., Christensen, S., Kudsk, P., 2006. The effect of laser treatment as a weed control method. Biosystems Engineering 95 (4), 497–505.

McClure, K.A., Cline, J.A., 2015. Mechanical blossom thinning of apples and influence on yield, fruit quality and spur leaf area. Can. J. Plant Sci. 95 (5), 887–896.

Meland, M., 2009. Effects of different crop loads and thinning times on yield, fruit quality, and return bloom in *Malus × domestica* Borkh. 'Elstar'. The Journal of Horticultural Science and Biotechnology 84 (6), 117–121.

Meland, M., Gjerde, B., 1993. The effect of handthinning on return bloom of 'Summered' and 'Aroma' apples. Acta Horticulturae (349), 219–224.

Seehuber, C., Damerow, L., Blanke, M., 2011. Regulation of source: sink relationship, fruit set, fruit growth and fruit quality in European plum (*Prunus domestica* L.)-using thinning for crop load management. Plant Growth Regulation 65 (2), 335–341.

Seehuber, C., Damerow, L., Kunz, A., Blanke, M., 2014. Mechanische Fruchtbehangsregulierung bei Apfel verbessert Fruchtgröße, Fruchtfestigkeit, Fruchtausfärbung und die Source: Sink-Verhältnisse mit mehr Einzelfruchtständen (Singlets) bei 'Gala' (Mechanical thinning improves source: sink relationships, fruit quality viz fruit size, fruit firmness and fruit colouration and portion of singlets of cv. 'Gala' apple). Erwerbs-Obstbau 56 (2), 49–58.

Solomakhin, A., Blanke, M., 2010. Mechanical flower thinning improves the fruit quality of apples. Journal of the Science of Food and Agriculture 90 (5), 735–741.

Sood, P., Ference, C., Narciso, J., and E. Etxeberria. 2008. Effects of laser labeling on the quality of tangerines during storage. In *Proceedings of the 121st annual meeting*. Ft. Lauderdale, Florida, USA, June 1-4. Florida State Horticultural Society. Eds. E. Etxeberria et al. 297–300.

Sood, P., Ference, C., Narciso, J., Etxeberria, E., 2009. Laser etching: a novel technology to label florida grapefruit. HortTechnology 19 (3), 504–510.

Tustin, D.S., Dayatilake, G.A., Breen, K.C., Oliver, M.J., 2012. Fruit set responses to changes in floral bud load-a new concept for crop load regulation. Acta Horticulturae 932, 195–202.

Untiedt, R., Blanke, M., 2001. Effects of fruit thinning agents on apple tree canopy photosynthesis and dark respiration. Plant Growth Regulation 35, 1–9.

Wertheim, S.J., 2000. Developments in the chemical thinning of apple and pear. Plant Growth Regulation 31, 85–100.

Williams, M.W., 1979. Chemical thinning of apples. In *Horticultural Reviews 1*. New Jersey, USA. Wiley-Blackwell. Ed., J. Janick. 270–300.

Wouters, N., 2014. Mechatronics for efficient thinning of pear. Ph.D. dissertation, Department of biosystems, Catholic university of Leuven, Leuven, Belgium.

A Vision-Based Road Detection System for the Navigation of an Autonomous Tractor

Sristi Saha [a], Ricardo Ospina [b], Noboru Noguchi [b, *]

[a] Graduate School of Agriculture, Hokkaido University, Sapporo, Japan

[b] Research Faculty of Agriculture, Hokkaido University, Sapporo, Japan

* Corresponding author. Email: noguchi@cen.agr.hokudai.ac.jp

Abstract

RTK-GNSS (Real-time Kinematic-Global Navigation Satellite System) signal is necessary for the navigation of an autonomous tractor. However, the main problem associated with the GNSS is that the RTK correction signal might not be available at all geographical locations. While most RTK services require an internet connection, many rural areas have limited broadband and even cellular connections. In addition, several other factors such as separation between base and rover sites, and signal obstructions cause time delays, as well as signal loss at certain times, especially in the rural areas. These situations can lead the autonomous tractor to travel outside of its predetermined path, which is unsafe. To avoid such situations, this study aims to develop a vision-based road detection system, which does not rely on RTK-GNSS.

The system aims to detect both paved and unpaved roads in rural farm areas. The system takes the RGB images obtained from an HD on-board camera and segments the road surface and road edges. The segmentation is performed by using several image filters, the sliding window method, and a set of rules that are determined manually. Finally, the lateral error obtained from the machine vision system is transmitted to the tractor's automatic navigation system.

Experimental runs performed at the experimental farm of Hokkaido University showed that the lateral error calculated by this system is less than 0.1 m for unpaved roads. In the case of paved roads, manually driven sample videos recorded inside the university campus were tested in the system and it showed that the system is able to detect paved roads as well. Weather conditions and road conditions such as illumination and reflectance of the road surface, affect the detection to some extent. Future work addresses considerations to make the system more robust.

Keywords: image filters, sliding window method, lateral error, precision agriculture.

1. Introduction

At present, the agricultural working population of Japan is continuously decreasing. According to the Agriculture and Forestry census of Japan (2020), the number of key agricultural workers has decreased by 22.4% compared to 5 years ago, amounting to about 1.36 million, of which about 69% are aged 65 years or above, and the average age has increased by 0.8 years to 67.8 years. Due to these circumstances, agriculture in Japan is facing many problems. To solve this, it is necessary to start a new type of agriculture that realizes labour-saving and high-quality production. Therefore, the development of automated or autonomous agricultural equipment is considered to be of the utmost commercial and societal importance. Several autonomous tractors that can be operated in open sky fields using an RTK-GNSS and an inertial measurement unit (IMU) as navigation sensors have been developed (Kise et al., 2001, Noguchi et al., 2001, Takai et al., 2014).

Although RTK-GNSS positioning has numerous benefits, the system has some usability problems. There are generally two methods of using RTK-GNSS- 1) A user places a reference station on the site and transfers the data to the rover by wireless transmission; and 2) A user calculates the rover position by receiving the correction data from a reference station located at a known position (Network-based RTK) (Tsuji et al., 2013). However, with the former, the data transmission is inevitably limited to a few hundred metres in radius from the transmission antenna and it is technically difficult to establish a reference station and determine its position to within 1 cm (Namie et al., 2010). In addition, the Network-based RTK method requires a fast data communication link, which requires good internet connectivity. However, 70% of Japan's land area is occupied by mountains & hills and agricultural land accounts for 14% of the total land area. Thus, rural areas, which are characterized by small population and small industrial activities, have limited or no internet connectivity in many locations. Furthermore, operating range, which refers to the maximum separation between the base and rover sites, often gets determined by the characteristics of the data communications link. There is no maximum limit on the baseline length for RTK with the receiver, but accuracy degrades and initialization time increases with range from the base (Trimble, n.d.). Also, RTK positioning techniques have a weakness due to the obstruction of the satellite signals under the tree canopies. Therefore, the usage of RTK positioning techniques will be dependent on the error tolerance of the applications (Lee and Ge, 2006).

For the navigation of an autonomous tractor on the road, precise data transmission without any obstructions is an essential requirement, which if not met, can lead the tractor out of its predetermined path, which is unsafe. Therefore, at these times a backup method is necessary, which can prevent any dangerous situations from happening in the absence of

RTK-GNSS. Various systems based on different sensors have been developed for road surface detection; mostly for paved, well-marked, well-maintained roads. Among these sensors, monocular vision sensors are one of the highly used sensors as vision data can provide abundant information about the driving scenes (Sivaraman and Trivedi, 2013). Furthermore, a vision sensor coupled with traditional image processing can often solve a given problem with greater accuracy, as colour-thresholding and pixel counting algorithms are very general and perform the same for any image (Mahony et al., 2020). Using a vision sensor, many researchers have developed autonomous driving systems that can track the lane markings on highways and urban roads (Schneiderman and Nashman, 1992, Wang et al., 2002, Chiu and Lin, 2005, Nguyen et al., 2017). However, a tractor mostly travels on unstructured roads, such as rural roads, which are less amenable to standard building techniques for a variety of reasons. There may be no lane markings and the edges may be spatially fuzzy and have low-intensity contrast. The overall road shape may not follow smooth curves and the appearance of the road itself can change drastically since mud, clay, sand, gravel and asphalt may all be encountered (Hu et al., 2004). Therefore, this research proposes to create a vision-based road detection system that can detect both paved and unpaved roads, regardless of their type (structured or unstructured).

The remainder of this research is organized as follows. Firstly, section 2 introduces the methodology in detail. Then, section 3 describes the experimental results and analysis. Finally, we draw the conclusions in section 4.

2. Materials and Methods

The system architecture is outlined in Figure 1. The system relies on the HD RGB image frames (720p, 24 FPS) obtained from a camera (KODAK, PixPro) on-board the tractor. These image frames are then processed in a computer, which is equipped with an Intel Core i7-9750H (@2.6 GHz) processor, 16 GB RAM, and Windows 10 Pro (64 bit) operating system. The computer does not have a graphics card. The road detection algorithm is run on this computer using Python 3.7.0 in the Anaconda distribution. The whole process is comprised of 6 main processes, which are described below. All these processes are performed in real-time.

KODAK PixPro camera **Tractor** **RGB image (1280x720 pixels)** **Road Detection computer**

Lateral error sent to automatic navigation system through **Serial COM Port RS-232**

GNSS + IMU

Automatic navigation system computer **Output image frame (10 FPS)**
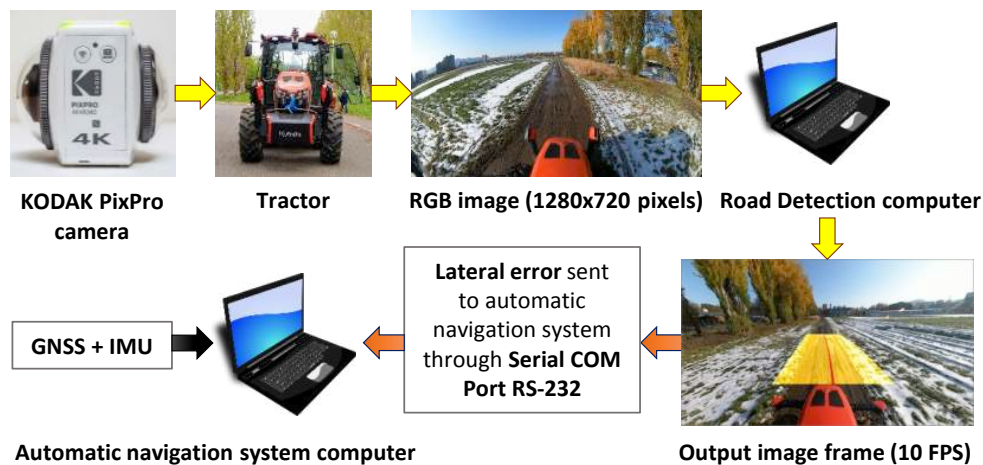
Figure 1. Overview of the road detection system

2.1. Camera calibration

(a) (b) (c)

Figure 2. a) 9x6 grid chessboard, b) input image with camera distortion, c) resulting image without camera distortion

The main process starts from capturing the HD image frames by using the OpenCV (version 4.2.0) library's 'VideoCapture' function. As all cameras introduce significant distortion to the images, it is necessary to remove the camera distortion. To do that, the camera intrinsic parameters are calculated by using a 9x6 grid chessboard (Figure 2a). The KODAK PixPro camera has a fisheye lens, which causes the input image to look curved (Figure 2b). This curvature makes it difficult to obtain real-world distances in the final steps of the process. To avoid that, the OpenCV's 'fisheye'

camera model is used to remove the distortion with the camera's intrinsic parameters taken into consideration. In Figure 2c, it is evident how the image is stretched compared to the distorted image; both the road and horizon lines do not look curved, they look straight.

2.2. Image processing

The images (without camera distortion) are filtered using a combination of several image filters. An overview of the whole image processing method is shown in Figure 3. The OpenCV's 'GaussianBlur' function is first applied to smooth out the images. The image frames are then processed in two ways to separate the road surface from the surrounding. The first process comprises converting the RGB image frames to HSV (Hue, Saturation, and Value) colour space. Then the resulting image frames are morphologically transformed to obtain the filtered image 1 in Figure 3. The goal of this process is to detect white lane markings (in case of paved road), snow etc. The second process is comprised of converting the RGB image frames to HSL (Hue, Saturation, and Lightness) colour space, which results in the filtered image 2 in Figure 3. The goal of this process is to detect the grass, trees etc. In both processes, the values of Hue, Saturation, Value, and Lightness are defined manually through fine-tuning. Finally, a threshold is applied on both filtered image 1 & 2 and the final output image is obtained, which shows the road surface in black and the surrounding in white in Figure 3.
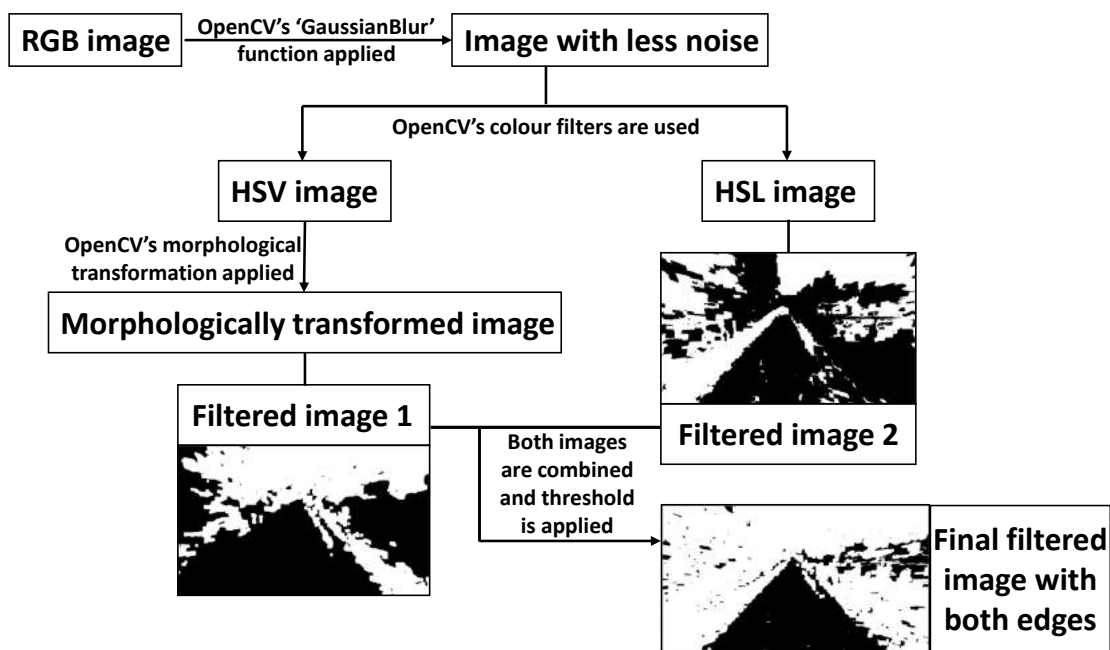
Figure 3. Image processing flowchart

In the same way, by applying different values and threshold to the whole image processing method, the road surface is obtained in white and the surrounding in black as shown in Figure 4. This step aims to detect the colour of the road surface, which can be grey or brown (mostly) depending upon the type of road. This step is necessary as sometimes the road may not have a proper edge.

Figure 4. Final filtered image showing the road surface

2.3. Selecting the region of interest

In this step, the region of interest is selected manually by fine-tuning. Usually, this depends on some external factors such as the field of view and the width of the road. Next, OpenCV's 'warpPerspective' function is applied to the filtered images obtained from the previous step. This step results in a bird's eye view of the region of interest, which facilitates the estimation of the road edges and the centre of the road surface. The resulting images are shown in Figure 5.

(a)   (b)
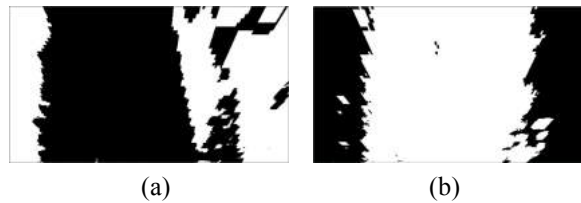
Figure 5. Warping operation: a) Road edges, b) road surface

2.4. Road edge/surface detection: sliding window method

The next step consists of applying the sliding window method to these warped images, which in turn returns two image results. In the sliding window method, a window of specified length *Len*, moves over the image frame data, sample by sample. These windows are represented by the yellow rectangles shown in Figure 6b. The statistic is computed over the data in each window. The output for each input sample is the statistic over the window of the current sample and the length of the previous sample defined as *Len-1*. In the first-time step, to compute the first *Len-1* outputs when the window does not have enough data yet, the algorithm fills the window with zeros. In the subsequent time steps, to fill the window, the algorithm uses samples from the previous data frame. The moving statistics algorithms have a state and remember the previous data (MathWorks, 2021).

OanaGaskey (2020) proposed a sliding window algorithm, which was a starting point in developing the current algorithm. For this algorithm, the OpenCV, the NumPy and the Pandas libraries are used. There are 9 sliding windows along the height (720 pixels) of one image frame. Each window searches for the non-zero pixels inside that window; note that the pixels in black are assigned zero value and one is assigned to the pixels in white. Next, these non-zero pixel values are stored in an array and a second-degree polynomial is fit on these pixel values. These second-degree polynomials represent the left & right edges of the road and also help in determining the centre of the road. Figure 6b shows the detection results for both the road edges and the road surface.

(a)   (b)   (c)
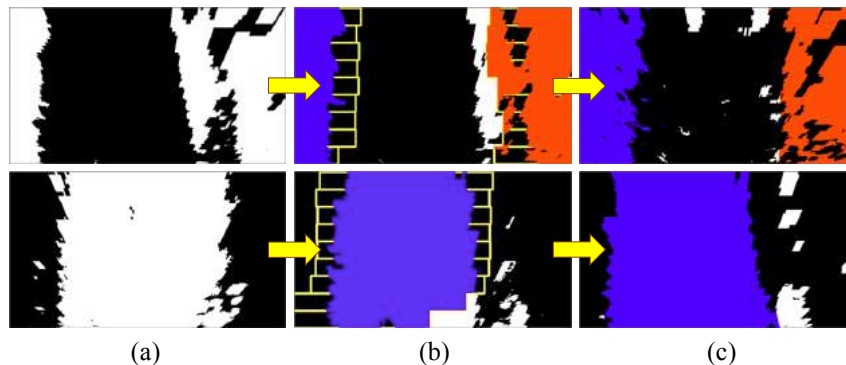
Figure 6. a) Warped images, b) sliding window detection, c) sliding window method – stabilized

While searching for the non-zero pixels, the sliding windows create a region of interest inside the frame. If non-zero pixels are continuously found inside this region of interest, the sliding window method gets stabilized (Figure 6c).

2.5. Displaying the final result

(a)   (b)

Figure 7. Display of the final result: a) paved road, b) unpaved road

After getting the second-degree polynomials from the warped images, the coordinates in the polynomial are converted to real-world coordinates by inverting the warping. The same OpenCV function "warpPerspective" is used to invert the warping. Then, the final result is overlapped with the image shown in Figure 2c; this is the image without any camera distortion. In Figure 7, the yellow polygon shows the road surface detected in the region of interest with respect to the left and right edges. The red polyline shows the centre of the road.

2.6. Calculation of lateral error

The lateral error is estimated from the tractor position relative to the road. To achieve this, the real-world distances were manually calculated using a chessboard to relate the pixel distances with the real-world distances. At first, the horizontal and vertical lengths of the chessboard are measured in meters. Then the same lengths are measured in pixel values from the image shown in Figure 8a. Finally, these two lengths are co-related to get the real-world distances from the image frames.

(a)   (b)
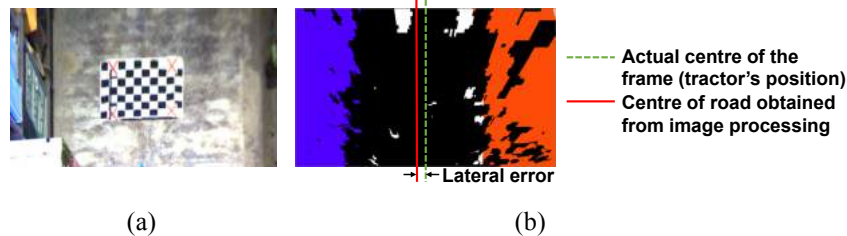
Figure 8. a) Manual calculation of real-world distances from chessboard, b) lateral error estimation

Figure 8b represents the calculation of lateral error by using the real-world distances obtained from the above-mentioned method and the pixel values obtained from the image frames. The left edge is shown by the blue area, the right edge is shown by the orange area and the detected centre of the road is represented by the red line. The green dashed line represents the actual centre of the image frame. The distance between the green dashed line and the red line represents the lateral error in pixel values. It is then converted to real-world distances and can be transmitted to the tractor's automatic navigation system pc using serial port communication as shown in Figure 1.

3. Results and Discussion

The experimental procedure can be divided into two parts. Firstly, manually driven sample videos of paved and unpaved roads were recorded inside Hokkaido University, Japan, as shown in Figure 9. Then the vision-based algorithm was desktop-tested inside the laboratory using these sample videos. Next, the same algorithm was tested in automatic mode at the experimental farm inside the university. This automatic run was performed on an unpaved (dirt) road. The results are discussed in the following sections.

Figure 9. Image frames from the video samples

3.1. Paved road

By using the sample videos taken inside the university, it was seen that the algorithm works for paved road. The road in this case is the same as the road seen in Figure 2b. The lateral error result can be seen in Figure 10. In this figure, in the beginning, a lateral error value of 0.95 m can be seen. The reason behind this big value of lateral error is that, in the beginning, the algorithm starts searching for the non-zero pixels and defines the left and right edges. After determining the edges, the system gets stabilized and the lateral error is within 0.20 m for most of the times. The values are not constant over time as the road doesn't have proper lane markings and the edges are uneven (covered with snow and grass). Also, a big lateral error of 1.2 m can be seen in the latter part. The possible reason behind such a large value of lateral error is the presence of potholes, which reflect light and causes misdetection (Figure 11).
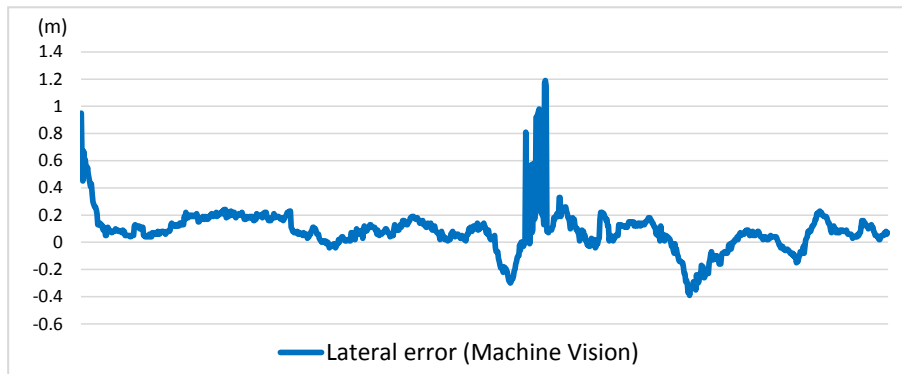
Figure 10. Lateral error result obtained from sample video (paved road with no lane markings)

Figure 11. Potholes present on the road surface causes a large value of lateral error

3.2. Unpaved road
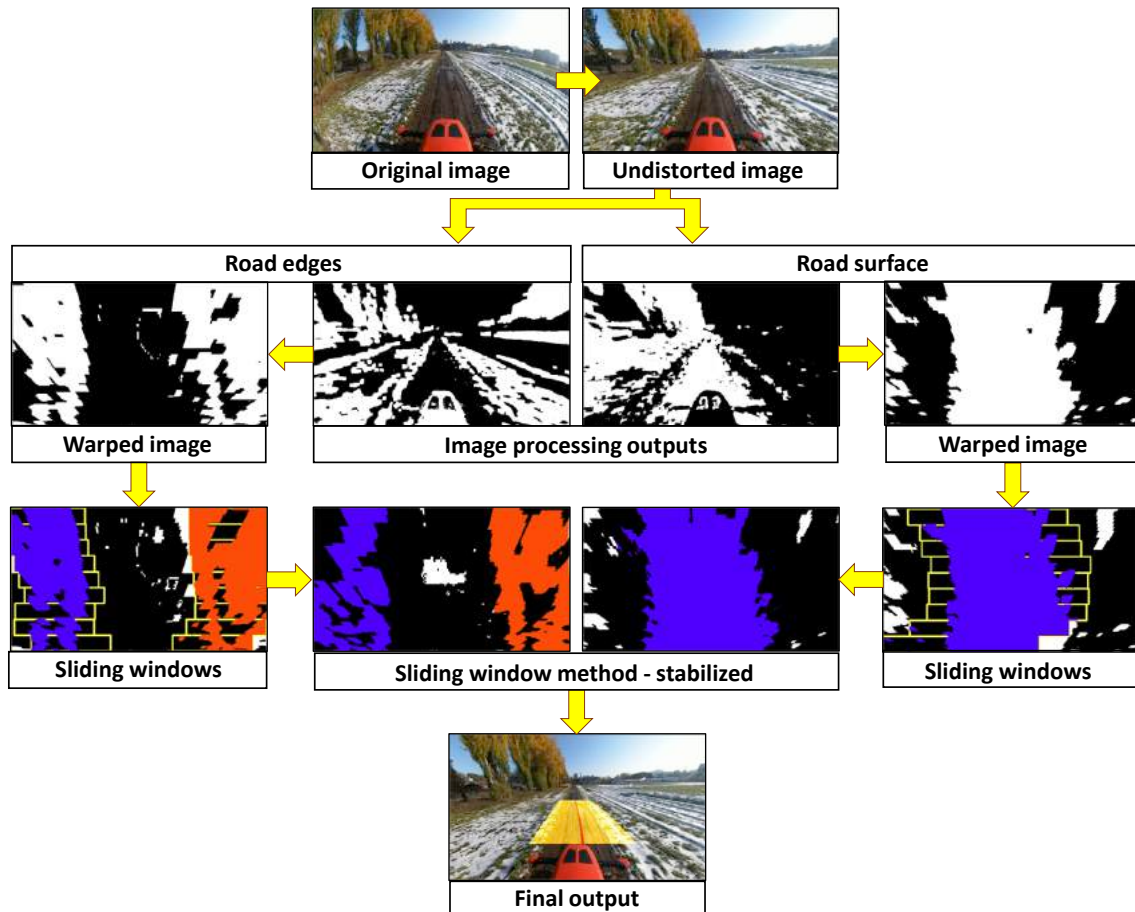
Figure 12. Road detection process for unpaved (dirt) road

At first, the proposed algorithm was applied to the sample videos of the unpaved (dirt) road, which is the same road as shown in Figure 12, illustrating the detection process for both the road and edges step by step. Figure 12 illustrates how both processes take place simultaneously, and finally results in the yellow trapezoid that indicates the road area and the red polyline, which indicates the centre of the road. This experiment produced the lateral error results shown in

Figure 13. As seen in this figure, the values of the lateral errors were less than 0.20 m for most of the time. But, the lateral error is not consistent over time, it displays small oscillations within 0.05m. The reason behind this is that the unpaved (dirt) road has rough & uneven edges. Also, as shown in Figure 8, the lateral error calculation depends on the tractor's relative position and the centre of the road as calculated by the system. Therefore, the resulting values of lateral error have a strong dependence on these two factors.
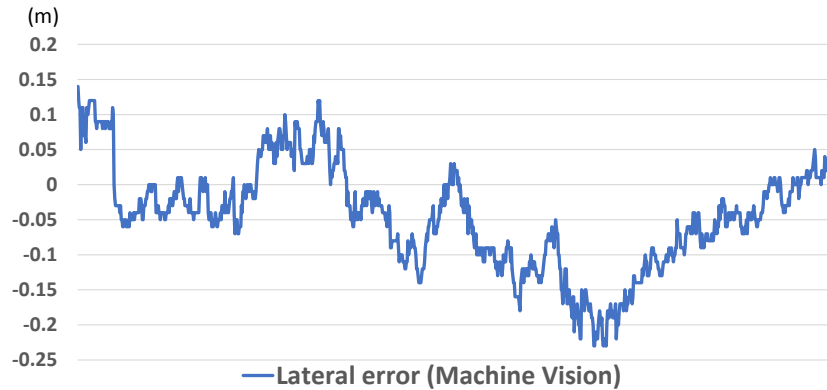
Figure 13. Lateral error result obtained from sample video (unpaved road)

As the method worked with the sample videos, real-time experimental runs were performed. These experimental runs consisted of travelling a straight path in an unpaved (dirt) road at the experimental farm in Hokkaido University, Japan. This road is the same as the road shown in Figure 9. At first, one automatic run was performed using RTK-GNSS as the input of the automatic navigation system. Next, several experimental runs were performed using the vision-based system instead of the RTK-GNSS. In both cases, the starting position of the tractor was approximately in the middle of the road. The average output frame rate was 10 frames per second, which corresponds to a 10 Hz update rate to the tractor's automatic system. Finally, the lateral errors obtained from these experimental runs were compared to the lateral errors produced by the RTK-GNSS.

Figure 14 shows the lateral error results for one travelled path. The lateral errors produced by RTK-GNSS is less than 0.05 m, which serves as reference data for assessing the accuracy of the vision-based system. The lateral error from the machine vision system is less than 0.10 m. Sometimes, it goes over 0.10 m as the road shape is uneven. In this experiment, the tractor travelled a straight path without steering much towards both sides.

Also, as many external factors are affecting the detection procedure, misdetection happened sometimes. In Figure 15, it can be seen that the road surface and the patch of ground to the left, looks similar. This resulted in the tractor going towards the left side of the road, which is dangerous for autonomous driving.
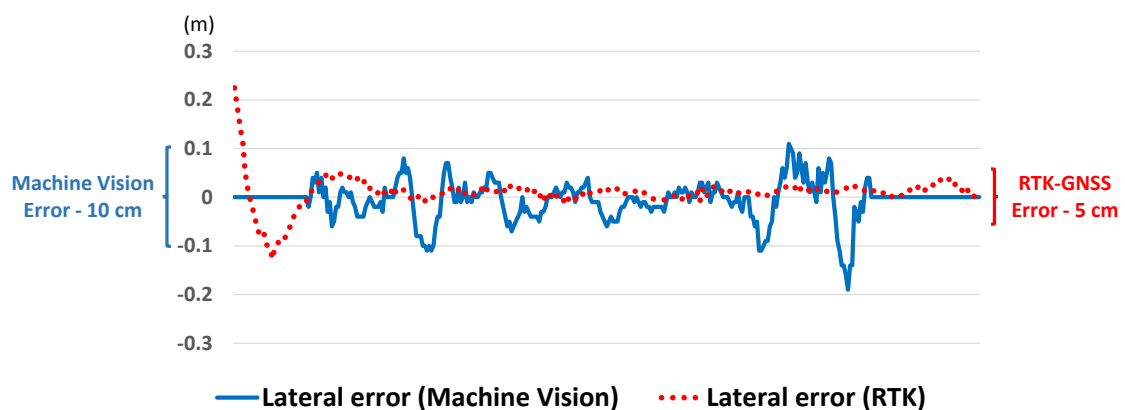
Figure 14. Lateral error result comparison (unpaved road)

Figure 15. Wrong detection by the system

525

4. Conclusions

In this paper, a vision-based road detection system has been presented. This system makes use of the colour information obtained from the camera and defines the edges of the road. This leads to the calculation of the lateral error, which is then provided to the automatic navigation system of the tractor for autonomous driving. From testing with the sample videos, it can be stated that the system can detect many kinds of structured and unstructured roads. Also, the experimental run performed on the unpaved (dirt) road showed that the system can perform in real-time.

It is to be kept in mind that this method is developed to act as a backup method for situations when the RTK correction signal cannot be received. So, this method needs to be robust enough to achieve that objective. However, a system based on RGB images and traditional image processing has some limitations. Many external factors affect this system to some extent, especially in the case of unpaved road scenes (e.g., variable light conditions, the sudden growth of vegetation in the middle of the road, presence of large potholes etc.). Future work includes additional tests to increase the robustness of the system. This might be achieved by using sensor fusion technologies and deep learning techniques.

Acknowledgements

References

Agriculture and Forestry Census, Ministry of Agriculture, Forestry and Fisheries, Japan, 2020. https://www.maff.go.jp/j/tokei/sihyo/data/08.html Accessed May 19, 2021.

Chiu, K., S. Lin, 2005. Lane detection using color-based segmentation. In *IEEE Proceedings Intelligent Vehicles Symposium*. 706-711. https://doi.org/10.1109/IVS.2005.1505186

Hu, M., W. Yang, M. Ren, J. Yang, 2004. A Vision Based Road Detection Algorithm. In *IEEE Conference on Robotics, Automation and Mechatronics, 2004*. Singapore. December 1-3. 2, 846-850. https://doi.org/10.1109/RAMECH.2004.1438028

Kise, M., N. Noguchi, K. Ishii, H. Terao, 2001. Development of the Agricultural Autonomous Tractor with an RTK-GPS and a Fog. IFAC Proceedings Volumes. 34(19), 99–104. https://doi.org/10.1016/S1474-6670(17)33120-8

Lee, I., L. Ge, 2006. The performance of RTK-GPS for surveying under challenging environmental conditions. Earth, Planets and Space. 58, 515-522. https://doi.org/10.1186/BF03351948

Mahony, N.O., S. Campbell, A. Carvalho, S. Harapanahalli, G.V. Hernandez, L. Krpalkova, D. Riordan, J. Walsh, 2020. Deep Learning vs. Traditional Computer Vision. In *Advances in Computer Vision Proceedings of the 2019 Computer Vision Conference (CVC)*. Springer Nature Switzerland AG. 943, 128-144. https://doi.org/10.1007/978-3-030-17795-9_10

Namie, H., O. Okamoto, C. Fan, A. Yasuda, 2010. Development of a Network-Based RTK-GPS Positioning System using FKP via the Internet. Journal of the Institute of Positioning, Navigation and Timing of Japan. 1(1), 9-15. https://doi.org/10.5266/ipntj.1.9

Nguyen, V., C. Seo, H. Kim, K. Boo, 2017. A study on detection method of vehicle based on lane detetction for a driver assistance system using a camera on highway. In *11th Asian Control Conference (ASCC)*. 424-429. https://doi.org/10.1109/ASCC.2017.8287207

Noguchi, N., J.F. Reid, Manager, Q. Zhang, J.D. Will, K. Ishii, 2001. Development of Robot Tractor Based on RTK-GPS and Gyroscope. In *2001 ASAE Annual Meeting*. ASAE. https://doi.org/10.13031/2013.7297

OanaGaskey. "Advanced-Lane-Detection." *GitHub*. Jan 10, 2020. https://github.com/OanaGaskey/Advanced-Lane-Detection.git Accessed May 25, 2021.

Schneiderman, H., M. Nashman, 1992. Visual processing for autonomous driving. In *Proceedings IEEE Workshop on Applications of Computer Vision*. Palm Springs, CA, USA. 164-171. https://doi.org/10.1109/ACV.1992.240315

Sivaraman, S., M.M. Trivedi, 2013. Looking at Vehicles on the Road: A Survey of Vision-Based Vehicle Detection, Tracking, and Behavior Analysis. IEEE Transactions on Intelligent Transportation Systems. 14(4). 1773-1795. https://doi.org/10.1109/TITS.2013.2266661

"Sliding window method and exponential weighting method." *MathWorks*. 2021. https://www.mathworks.com/help/dsp/ug/sliding-window-method-and-exponential-weighting-method.html Accessed May 25, 2021.

Takai, R., L. Yang, N. Noguchi, 2014. Development of a crawler-type robot tractor using RTK-GPS and IMU. Engineering in Agriculture, Environment and Food. 7(4), 143–147. https://doi.org/10.1016/j.eaef.2014.08.004

Tsuji, H., K. Miyagawa, K. Yamaguchi, T. Yahagi, K. Oshima, H. Yamao, T. Furuya, 2013. Modernization of GEONET from GPS to GNSS. Bulletin of the Geospatial Information Authority of Japan. 61. https://warp.da.ndl.go.jp/info:ndljp/pid/8440829/www.gsi.go.jp/common/000085715.pdf Accessed May 19, 2021.

Wang, R., Y. Xu, Libin, Y. Zhao, 2002. A vision-based road edge detection algorithm. In *Intelligent Vehicle Symposium*. IEEE. 1, 141-147. doi: 10.1109/IVS.2002.1187942.

Development of Electrical Vehicle Robot for Orchard Application

Yoshitomo Yamasaki [a], Tomoaki Hizatate [a], Noboru Noguchi [b,*]

[a] Graduate School of Agriculture, Hokkaido University, Sapporo, Japan

[b] Research Faculty of Agriculture, Hokkaido University, Sapporo, Japan

* Corresponding author. Email: noguchi@cen.agr.hokudai.ac.jp

Abstract

Hybrids and electric vehicles have rapidly widespread in the automotive industry, but in the agricultural sector still have been underdeveloped. The purpose of this research is to develop an electric vehicle robot for agricultural use by utilizing the powertrain system of a hybrid automobile. We aim to develop speed and steering controllers that enable the vehicle robot to run on sloping terrain and bumpy fields. In this study on speed control, a feedback controller with added rolling resistance and climbing resistance as the feedforward term was developed. P-control has been implemented in steering control based on lateral and directional errors. In order to solve the problem that the turning radius is larger than that of a normal tractor, we adopted a pass skip turning method that does not include backward movement. The vehicle robot could run at the set speed from 2 km/h to 6 km/h with a coefficient of variation under 25 % in the real vineyard. Even though there was an area with an inclination of nearly 10 degrees, the robot speed was stable and slightly fluctuated. Although the lateral error increased with the set speed increase, the root mean squared error (RMSE) was within 0.10 m at all set speeds, and the maximum lateral error was under 0.21 m. Since the vehicle's width was approximately 1.7 m, the developed automatic controller was accurate enough to travel autonomously in tree rows with 2.5 m space. The robot was also able to conduct spraying in the vineyard without any damages to the trees. Future work includes a prospect of automation in an orchard, such as variable-rate spraying, and also mowing or harvesting based on the electric vehicle robot.

Keywords Vineyard, Autonomous Driving, Speed Control, Steering Control, Smart Farming

1. Introduction

Recently, sustainable development has been required to protect global environment according to some goals such as the Paris Agreement and SDGs. As the development of passenger cars reducing exhaust gas, such as a hybrid electric vehicle (HEV) and an electric vehicle (EV), the electrification of the agricultural vehicle was expected as well. It is expected that an electric tractor (ET) will be widespread in the future because an ET has the advantage of having fewer parts and better maintainability, compared to an internal combustion engine (ICE) tractor. However, a survey reported that an ET was limited for now to use in orchards or greenhouses which have relatively small areas due to its shorter driving time than an ICE tractor (Caban et al., 2018).

Many studies have been conducted on the autonomous driving for agricultural vehicles. Regarding research on a tractor for a flat field, Noguchi et al. developed autonomous field working robots (Noguchi et al., 2001), and Zhang and Noguchi developed multiple cooperative robots (Zhang and Noguchi, 2017). Research on autonomous driving for rice transplanters conducted in a paddy field (Nagasaka et al., 2002) and research on combine harvester automation was conducted in a flat field as well as a tractor (Choi et al., 2014; Rovira-Más et al., 2007). Although these agricultural robots are in the practical stage, there are few studies on an agricultural robot for orchards. Orchards in Japan are relatively steeper and narrower than other crop or paddy fields. An agricultural vehicle such as a tractor cannot enter in such a steep and narrow field. Although there are vast orchards in the world (Moorehead et al., 2012), some researchers have studied on relatively small and lightweight vehicle robots in orchards (Bayar et al., 2015; Zhang et al., 2020).

EVs that use a motor as a driving force have the advantages of faster torque response and accurate measurement of torque from motor current compared to ICE vehicles (Harada and Fujimoto, 2013). Some studies have been conducted to improve the running performance of vehicles such as slip ratio control and driving force control thanks to these advantages (Harada and Fujimoto, 2013; Maeda et al., 2014). An important factor of agricultural vehicles is that the vehicle must keep its speed constant to carry out agricultural work such as spraying and mowing. In the vehicle speed controller on EVs, Higasa et al. performed automatic gain tuning in a PI controller by a neural network (Higasa et al., 1994). Harada et al. reported that the theoretic acceleration was calculated from the set speed and the result was combined with the value from the PI controller. This is an example of speed control by applying a driving force in a feedforward manner (Harada and Fujimoto, 2013). However, these studies target regular paved roads. The road conditions are fundamentally different from rough terrain such as orchards and muddy field environments. In addition, there are few studies that evaluate the speed controller exactly. It is needed to verify the speed controller for agricultural applications where it is important to travel at a constant speed.

In this paper, in order to solve the workforce shortage in orchards, we have developed an agricultural EV robot for orchards that autonomously travels in a narrow and sloping orchard and performs spraying or mowing. Using a golf cart as the base of the car body, it was converted into an agricultural EV robot equipped with a motor, inverter and battery.

The target orchard was a vineyard which is recently popular in Hokkaido, northern area of Japan. The purpose of this research is to verify the accuracy of speed control and steering control on slopes and rough terrain fields.

2. Materials and Methods

2.1. Robot configuration

The overview of the EV robot for orchards developed in this paper and the specifications of the vehicle are shown in Figure 1 and Table 1, respectively. An RTK-GNSS (SPS855, Trimble, US) receiver and an IMU (VN-100, VectorNav, US) were used as navigation sensors. The RTK-GNSS antenna was installed near the front wheels to improve steerability, and the IMU was installed near the center of gravity, ignoring the height direction. In addition to the navigation sensor, a camera for remote monitoring and vegetation monitoring and a LiDAR for obstacle detection were installed in the front. The EV robot used in this paper was equipped with a tank, a pump, nozzles, and fans in the rear for spraying.

The vehicle system of the EV robot was made using the powertrain mechanism of a HEV. The EV robot has three shafts, engine (EG), motor/generator 1 (MG1) and motor/generator 2 (MG2) shaft. The EV robot also has a planetary gear to interact with each shaft. When a certain gear is fixed, the rotation speed of the remaining two gears is determined from the gear ratio. Generally, when used as an HEV, the EG is the main control target, and MG1 or MG2 are also controlled to minimize EG use. The remaining MG1 or MG2 functions as a generator for charging to achieve both running and charging allowing optimum driving efficiency. However, in this paper, the EG shaft is used not as an engine but as an output for spraying pump. Therefore, the EG is not controlled, but the MG1 shaft that strongly acts on the EG shaft and the MG2 shaft that strongly acts on the tires are controlled. The EG shaft which was directly connected to the pump for spraying was driven by rotating the MG1. By controlling MG2 as a traveling motor and MG1 as a working motor, both traveling and spraying work were achieved.

Communication with the EV robot was performed by Controller Area Network (CAN) bus protocol by using a control PC. The control PC received the rotation speed of MG1 and MG2, the actual steering angle, the positioning from the RTK-GNSS and the attitude angle from IMU. The autonomous driving was performed by calculating the torque value of MG1 and MG2, and the steering angle via CAN-BUS based on the received data.
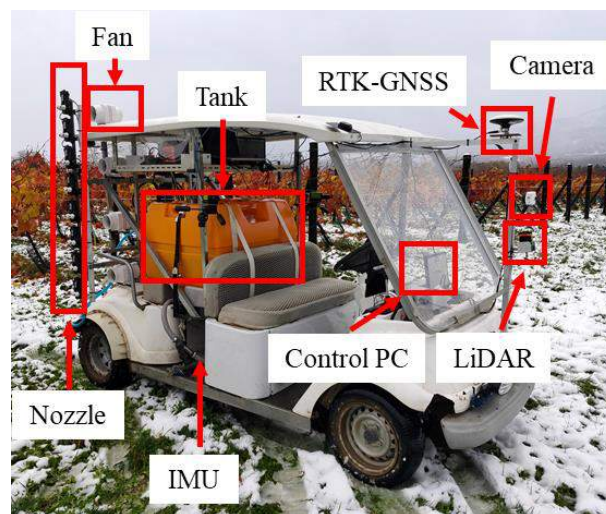
Figure 1. Overview of the smart EV robot for orchards

Table 1. Specification of the vehicle

Vehicle mass	700	kg
Wheelbase	2.15	m
Max torque	400	Nm
Controllable torque resolution	0.125	Nm
Max steering	±40	deg
Input steering resolution	0.1	deg

2.2. Speed control

Figure 2 shows the speed controller used in this paper. The error from the set speed was calculated using the vehicle speed measured by RTK-GNSS, and the calculation was performed by the PID controller. The sum of the value obtained by compensating for the driving resistance and the result of the PID calculation was used as the driving force

F, and the value obtained by multiplying the tire radius *r* and the reciprocal of the reduction ratio *ξ* was input to MG2 as the torque value *T*. In this paper, we tried to restrict the proportional gain to prevent vibration of the vehicle speed by considering the driving resistance particular to rough and slope fields. There are many factors of driving resistance such as rolling resistance, road gradient resistance, air resistance, acceleration resistance, starting resistance, curve resistance, and resistance associated with overcoming obstacles. Both rolling resistance and road gradient resistance were considered in this study because air resistance, acceleration resistance, and curve resistance could be ignored, considering the vehicle run at less than 10 km/h and worked almost in a straight line. Rolling resistance was defined as the product of the rolling resistance coefficient C_r, the load *W*, and the cosine of the road gradient angle *θ* as shown in Eq. (1). Here, C_r is a coefficient that depends on the characteristics of the tire and the condition of the ground, and changes greatly depending on the road surface condition. Especially when a vehicle travels off-road, the bulldozing resistance increases due to subsidence of tires, which has a great effect on driving. Bulldozing resistance can be interpreted as resistance based on the relationship between the field surface and the tires. In this paper, bulldozing resistance is also included in the rolling resistance coefficient C_r, and the rolling resistance is compensated by predetermining the appropriate rolling resistance coefficient C_r from several test driving. Road gradient resistance is defined as the product of the sine of the road inclination angle *θ* and the load *W* as shown in Eq. (2). In this paper, the pitch angle (-90 ° ≤ θ ≤ 90 °) obtained from the IMU was used as the road inclination angle. The final input torque is represented as Eq. (3).
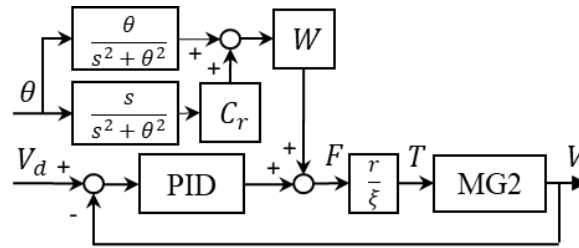
Figure 2. Diagram of the speed controller

$$F_{Rolling} = C_r W cos\theta \tag{1}$$

$$F_{Inclination} = W sin\theta \tag{2}$$

$$T = \frac{r}{\xi}(f_{PID}(v) + F_{Rolling} + F_{Inclination}) \tag{3}$$

2.3. Steering control

A method reported by Kise et al. was adopted in which a navigation map with absolute coordinates created in advance was read, and the steering angle was determined from the lateral deviation and the heading error between the current position and the navigation map (Kise et al., 2001). This method is proportional control based on the lateral deviation and the heading error as shown in Eq. (4). Here, *δ* is the steering angle, *d* is the lateral deviation, *Δφ* is the heading error, and a_1 and a_2 are the control gains. According to Kise et al., the lateral deviation was up to about 0.15 m. In this experiment, thus, the steering gains a_1 and a_2 were adjusted for the lateral deviation less than 0.15 m.

$$\delta = a_1 d + a_2 \Delta\phi \tag{4}$$

2.4. Turning method

A switchback turning method like Kise et al. was common for a tractor because the maximum steering angle was large enough and it was necessary, when cultivating, to enter the next path in order. However, a path skip turning method that includes only travelling forward was adopted because stopping and moving backward was a complicate operation (Figure 3). This method is unique to autonomous driving because the EV robot did not miss to enter paths which were not worked.

The pass skip turning method is divided into three steps: When the EV robot reached the end of the path, steps (1) to (3) were conducted. This method can be applied to any orchard by checking the total number of paths for each orchard and dynamically determining the number of skips.

(1) Turning 90 degrees from current heading
(2) Travelling forward until the distance between the robot and the next path reaches minimum turning radius *r*
(3) Turning according to the steering angle *δ* as shown in Eq. (5), where *Δφ* is calculated from the start point of the next path and the current vehicle heading, and *a* is a control gain.

$$\delta = a\Delta\phi \tag{5}$$
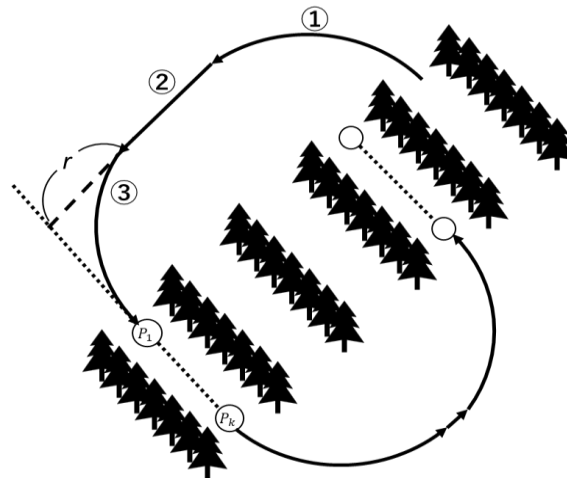
Figure 3. Pattern diagram of the path skip turning

2.5. Implement control

As mentioned above, the EV robot for orchards used in this paper had a pump for spraying mounted on the EG shaft. The rotation speed of the EG shaft was controlled by the PID controller to conduct spraying constantly. The rotation speed of the EG shaft was calculated from the amount of rotation and gear ratio of MG1 and MG2 according to the principle of the planetary gear mechanism. Since the EV robot developed in this paper travels at low speed, MG2 does not affect EG, it is possible to control the EG shaft rotation by controlling only MG1. In this paper, the PID control was performed so that the EG rotation speed would be 1000 rpm according to the requirement of the pump for spraying.

2.6. Field trial

Field trial was conducted at Tsurunuma Winery, Hokkaido Wine Co., Ltd in Hokkaido to evaluate the speed controller and steering controller as shown in Figure 4. The distance between the vines was 2.5 m and the path distance was about 120 m (max gradient: 6.2 [deg.]). In this experiment, the EV robot travelled three paths including two turns at a set speed of 2 km/h. Autonomous driving was performed both while driving MG1 and while not driving it to investigate the effect of driving MG1 on running. A test was also conducted after deleting the second and third terms of Eq. (3), which means the EV robot was controlled by only PID-control, to verify the effect of the feedforward terms of the speed controller.

Field trial was also conducted at Noto Vineyard, Hokkaido Wine Co., Ltd in Ishikawa to verify the speed controller and steering controller. The vineyard has a gradual slope field whose path distance was about 250 m (max gradient: 4.4 deg.) and a steep slope field whose path distance was about 40 m (max gradient: 10.5 deg.). The set speed was changed to 3 km/h, 4 km/h, 5 km/h, and 6 km/h to evaluate the performance of speed during actual work, because the mowing and spraying are usually conducted at a speed between 3 km/h and 6 km/h.
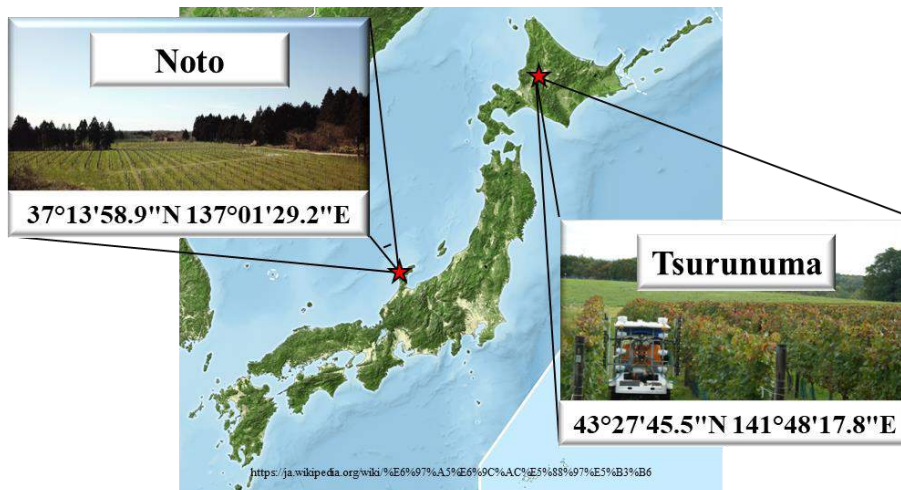
Figure 4. The location of the field trial at Noto and at Tsurunuma in Japan

3. Results and Discussion

3.1. Travelling trajectory

Figure 5 shows the result of the travelling trajectory in Tsurunuma Winery. From now, the paths described as Path 1, Path 2, and Path 3 refer to the paths with the numbers shown in the navigation map of Figure 5. Starting from Path 1 on the upper right of the navigation map in Figure 5, a total of three paths were travelled. In the figure of the navigation map, the solid line should follow the path and the dotted line is the trellis of the grapes. In the figure of the travelled trajectory shown as the solid line, the EV robot can be seen to run safely without crashing into the grapes. It was possible to complete the autonomous driving without any problems such as crash into the vine trunk through a straight path and turning.
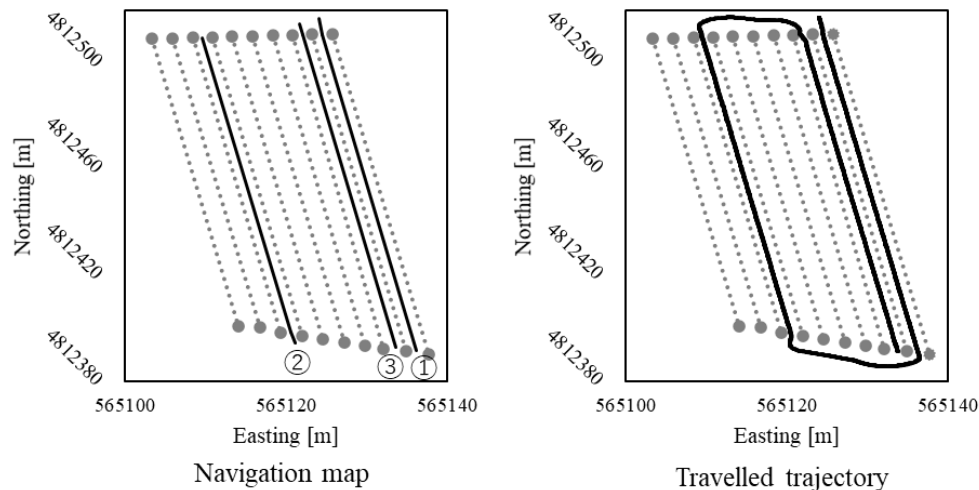
Figure 5. The navigation map (left) and the travelled trajectory (right) in the vineyard: Dotted lines show the vine rows and solid lines show the navigation map (left) and the travelled trajectory (right).

3.2. Speed control

Figure 6 shows the measured speed and the measured pitch angle in Path 1 and Path 2. As shown in Figure 6, the EV robot travelled at a constant speed without any particular change on uphill and downhill slopes. Table 2 shows the vehicle speed on each path. As Figure 6 shows, the vehicle speed in the uphill around 520 seconds fluctuated greatly and dropped to 0 km/h due to the slip, which resulted from the muddy field condition. However, by the PID controller, the EV robot responded to such a disturbance and converged to the set speed of around 2 km/h. Figure 7 shows the vehicle speed when the road gradient resistance was not taken into consideration. As can be seen from Figure 7, the vehicle speed increased as the downhill slope became steeper, and finally the vehicle speed could not be controlled. This is because the controllable range in the PID-control was exceeded. The controllable range could be enlarged by increasing the P gain, but in this experiment, the limit value was adopted not to fluctuate. In other words, the vehicle speed cannot be controlled only by the PID-control in the slope field. It is necessary to consider the road gradient resistance.

Figure 8 shows the vehicle speed when MG1 was driven or not and Table 3 shows statistical values. As mentioned above, MG1 and MG2 affect each other due to the internal friction of the gears. In this experiment, an input torque of up to 4 Nm was applied and MG1 was driven to conduct spraying so that the EG shaft would have a constant rotation speed by the PID controller. As a result, MG1 did not affect the vehicle speed during the spraying work. It was possible to keep a stable vehicle speed during spraying.

In other set speeds, the EV robot was also able to travel with a constant vehicle speed following its set speed as shown in Table 4. Although the coefficient of variation of the vehicle speed increased as the road gradient increased as shown in Table 5, the EV robot was able to be controlled by the same speed controller.

Table 2. Maximum, minimum, average, standard deviation (SD), and coefficient of variation (CV) of the measured vehicle speed in each path.

	Max [km/h]	Min [km/h]	Average [km/h]	SD [km/h]	CV [-]
Path 1	4.86	0.04	2.01	0.46	22.9%
Path 2	3.89	0.07	2.16	0.50	23.1%
Path 3	3.06	0.83	2.05	0.32	15.6%
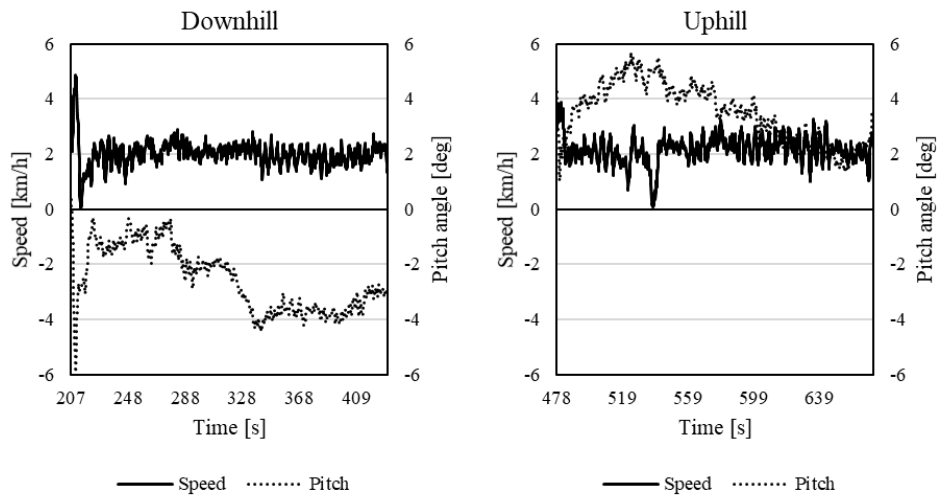
Figure 6. The measured speed and the pitch angle in the downhill and the uphill.
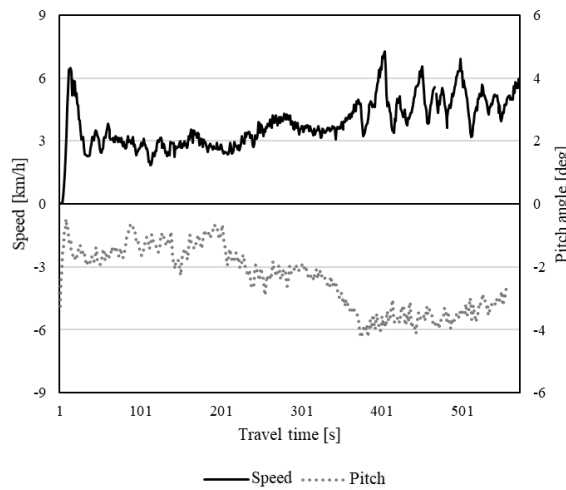
Figure 7. The measured vehicle speed when the vehicle travelled by only PID controller as a set speed of 3 km/h.
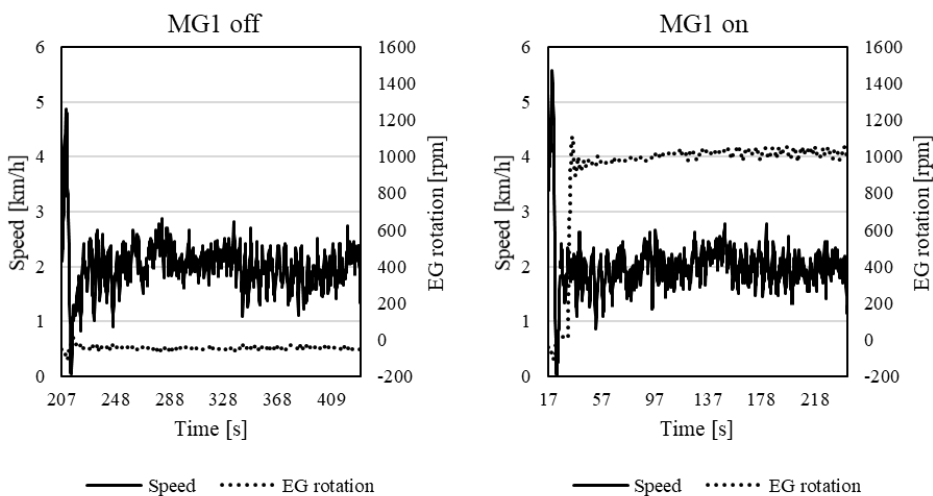
Figure 8. The measured vehicle speed when the MG1 was turn on or off.

Table 3. Maximum, minimum, average, standard deviation (SD), and coefficient of variation (CV) of the measured vehicle speed when the MG1 was turn on and off.

	Max [km/h]	Min [km/h]	Average [km/h]	SD [km/h]	CV [-]
MG1 on	5.58	0.00	1.99	0.49	24.7%
MG1 off	4.86	0.04	2.01	0.46	22.9%

Table 4. Average, standard deviation (SD) and coefficient of variation (CV) of the measured vehicle speed at a different set speed in the gradual slope (max gradient: 4.4 deg.) field at Noto Vineyard.

	3km/h	4km/h	5km/h	6km/h
Average [km/h]	3.0	4.0	4.9	6.2
SD [km/h]	0.6	0.5	0.7	0.9
CV [-]	19%	13%	13%	15%

Table 5. Average, standard deviation (SD) and coefficient of variation (CV) of the measured vehicle speed at a different set speed in the steep slope field (max gradient: 10.5 deg.) at Noto Vineyard.

	3km/h	4km/h	5km/h	6km/h
Average [km/h]	3.0	4.0	4.8	5.7
SD [km/h]	0.7	0.8	1.1	1.4
CV [%]	24%	21%	22%	25%

3.3. Steering control

Figure 9 shows the lateral deviation on each path. Table 6 shows the results of the maximum lateral deviation and the root mean square error (RMSE). In all paths, the RMSE was less than 5 cm. In Path 3, the lateral deviation increased to 20.7 cm in the entrance area, because the soil condition near the start of Path 3 was poor and a lot of lateral slip occurred in the latter of the turn. The lateral deviation recovered to 10 cm in about 5 seconds from the end of the turn, and then the lateral deviation was constant to around 0 in 1 minute. In this experiment, the permissible lateral deviation was 30 cm due to the relationship between the vehicle width and the trellis of vines, so that the vehicle body did not crash into the vines. Although it was unstable when entering next path sometimes, the EV robot developed in this study could drive autonomously in the actual vineyard without any collision.

The EV robot was able to travel autonomously in other set speeds as well as 2 km/h as shown in Table 7. Although the RMSE increased as the vehicle speed increased, it was the predictable result because the control resolution decreased in case of the constant steering rate. However, the maximum deviation did not increase a lot. This result is applicable in agricultural work in orchards.
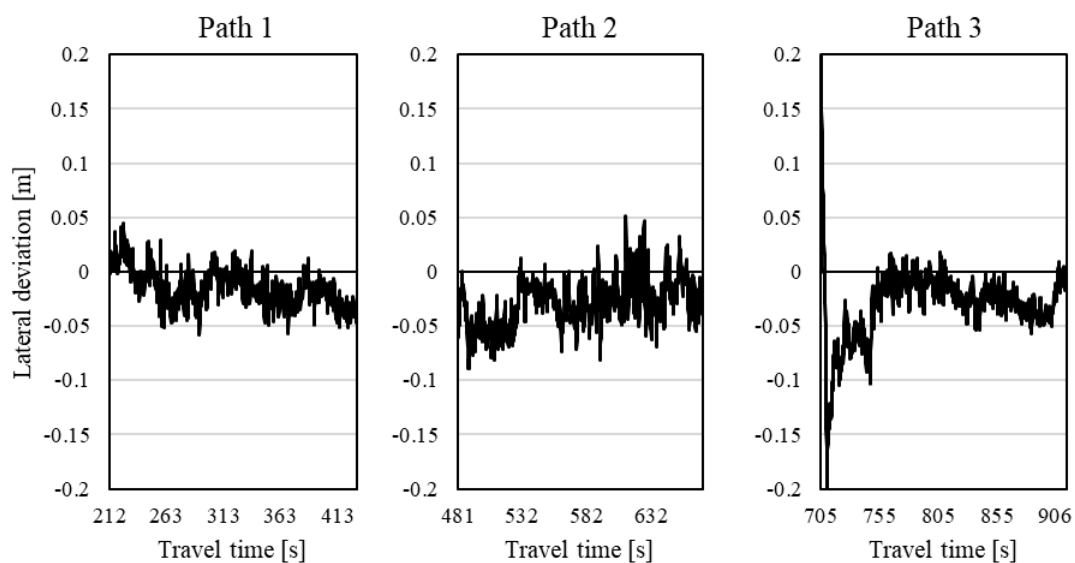
Figure 9. Lateral deviation in path1, path2 and path3.

Table 6. The max deviation and the root mean square error (RMSE) at a set speed of 2 km/h in each path.

	Max deviation [m]	RMSE [m]
Path 1	0.06	0.02
Path 2	0.09	0.04
Path 3	0.21	0.05

Table 7. The max deviation and the root mean square error (RMSE) at a different set speed in gradual slope field (max gradient: 4.4 deg.) in Noto Vinery.

	3km/h	4km/h	5km/h	6km/h
RMSE [m]	0.07	0.07	0.10	0.10
Max deviation [m]	0.21	0.17	0.18	0.21

4. Conclusions

In this study, we developed a speed controller and a steering controller for an EV robot for orchards. The developed speed controller was able to keep a stable vehicle speed from 2 km/h to 6 km/h in a rough slope field during spraying work. The RMSE was within 0.10 m and the maximum lateral deviation was within 0.21 m in the set speed from 2 km/h to 6 km/h. This was sufficient accuracy for the actual vineyard environment. We plan to conduct experiments in a steeper slope vineyard and develop a more accurate turning algorithm as future works.

References

Bayar, G., Bergerman, M., Koku, A.B., Konukseven, E.I., 2015. Localization and control of an autonomous orchard vehicle. Computers and Electronics in Agriculture 115, 118–128. https://doi.org/10.1016/j.compag.2015.05.015

Caban, J., Vrabel, J., Šarkan, B., Zarajczyk, J., Marczuk, A., 2018. Analysis of the market of electric tractors in agricultural production. MATEC Web of Conferences 244, 1–10. https://doi.org/10.1051/matecconf/201824403005

Choi, J., Yin, X., Yang, L., Noguchi, N., 2014. Development of a laser scanner-based navigation system for a combine harvester. Engineering in Agriculture, Environment and Food 7, 7–13. https://doi.org/10.1016/j.eaef.2013.12.002

Harada, S., Fujimoto, H., 2013. Range Extension Control System for Electric Vehicle during Acceleration and DecelerationBased on Front and Rear Driving/Braking Force DistributionConsidering Slip Ratio and Motor Loss. IEEJ Transaction on Industry Application 134, 6626–6631. https://doi.org/10.1541/ieejias.134.1

Higasa, H., Matsumura, S., Omatu, S., 1994. Tuning of PI Gains for Speed Control of Electric Vehicle Testing System. The tramsaction of the Institute of Electrical Engineers of Japan. C 114, 1078–1083. https://doi.org/10.1541/ieejeiss1987.114.11_1078

Kise, M., Noguchi, N., Ishii, K., Terao, H., 2001. Field Mobile Robot navigated by RTK-GPS and FOG (Part 2) - Autonomous operation by applying navigation map -. Journal of the Japanese Society of Agricultural Machinery 63, 80–85.

Maeda, K., Fujimoto, H., Hori, Y., 2014. Driving Force Control of Electric Vehicles with Estimation ofSlip Ratio Limitation Considering Tire Side Slip. Transactions of the Society of Instrument and Control Engineers 50, 259–265. https://doi.org/10.9746/sicetr.50.259

Moorehead, S.J., Wellington, C.K., Gilmore, B.J., Vallespi, C., 2012. AUTOMATING ORCHARDS: A SYSTEM OF AUTONOMOUS TRACTORS FOR ORCHARD MAINTENANCE, in: IEEE/RSJ International Conference on Intelligent Robots and Systems (IROS) Workshop on Agricultural Robots. Vilamoura, Algarve, Portugal. https://doi.org/10.3406/espos.1988.1292

Nagasaka, Y., Taniwaki, K., Otani, R., Shigeta, K., 2002. An Automated Rice Transplanter with RTKGPS and FOG. the CIGR Journal of Scientific Research and Development IV, 1–7.

Noguchi, N., Reid, J.F., Zhang, Q., Will, J.D., Ishii, K., 2001. Development of Robot Tractor Based on RTK-GPS and Gyroscope, in: 2001 American Society of Agricultural Engineers Annual Meeting. Sacramento, California, USA, pp. 1–8.

Rovira-Más, F., Han, S., Wei, J., Reid, J.F., 2007. Autonomous Guidance of a Corn Harvester using Stereo Vision. Agricultural Engineering International: the CIGR Ejournal IX, 1–13.

Zhang, C., Noguchi, N., 2017. Development of a multi-robot tractor system for agriculture field work. Computers and Electronics in Agriculture 142, 79–90. https://doi.org/10.1016/j.compag.2017.08.017

Zhang, S., Guo, C., Gao, Z., Sugirbay, A., Chen, J., Chen, Y., 2020. Research on 2D Laser Automatic Navigation Control for Standardized Orchard. Applied Sciences 10, 2763. https://doi.org/10.3390/app10082763

Low Power GPS-Based Systems to Support Herd Management in Extensive Livestock Systems

Simona M.C. Porto [a], Francesca Valenti [a] *, Cascone Giovanni [a]

[a] Department of Agriculture, Food and Environment (Di3A), University of Catania, Catania, Italy

* Corresponding author. Email: francesca.valenti@unict.it

Abstract

The use of wearable sensors to record animal activity in intensive livestock systems has become more and more frequent for both early detection of diseases and improving quality of production. Their application may be also significant in extensive livestock systems, where there is an infrequent farmer-to-animal contact.

The aim of the present study was to prove the feasibility of a novel automatic system for locating and tracking cows in extensive livestock systems based on space-time data provided by a low power global positioning system (LP-GPS). A customised device was equipped with a LP-GPS omnidirectional system, an integrated SigFox communication system and a power supply. The experimental trial was carried out in an existing semi-natural pasture characterized by good availability of meadow and cultivated grazing areas. Ten cows were embedded with LP-GPS collars and the data, i.e., geographical coordinates and the time intervals related to each cow detection, were recorded every 20 minutes. Data were collected through a developed AppWeb to be further imported and elaborated by using a GIS software tool. In GIS environment, the daily distances travelled by each cow were correlated with heatmaps obtained by applying Kernel Density Estimation models. The results of the study made it possible to obtain information on some relevant aspects for livestock's management. In detail, it was possible to acquire information on the use of the pasture, e.g., the area of the pasture most frequently used during day, individual use of the pasture, possible animal interaction. These findings represent a first step towards further insights and research activities. The LP-GPS system could be further integrated with other sensors for monitoring a wider range of animal behaviour such as that related to feeding and oestrus.

Keywords: grazing cows, IoT, cow behaviour, GIS, spatial analysis.

1. Introduction

Animal location and tracking have been topics of interest for both wildlife biologists and livestock researchers for a long time. The monitoring of animal location allows researchers to evaluate some key aspects, such as the movements of animals around the landscape [Gordon, 2001], the spatial heterogeneity of field occupancy by animals [Liu et al., 2012], the pasture utilization, the animal performance and behaviour [Turner et al., 2000; Porto et al, 2015] or the social affiliations within a herd [Veissier et al., 1998; Sennek et al., 2004; Arcidiacono et al., 2020].

In the last years, studies moved from very high frequency (VHF) tracking technologies, commercially available for gathering location data, to global positioning systems (GPS) by allowing the possibility of collecting large amounts of high-quality location data, 24 h per day under all weather conditions, with accuracy ranging from 5-30 m depending on several factors, e.g., vegetation cover, topography, etc. [Rodgers et al., 1996; D'Eon et al., 2000; Frair et al., 2004]. In literature several research studies were carried out by adopting GPS positioning [Van Beest et al., 2010; Schieltz et al., 2017; Fogarty et al., 2018]. Almost all the carried-out studies demonstrated the necessity of miniaturizing the sensor technologies and developing higher energy-dense batteries [Arcidiacono et al., 2020]. Another drawback highlighted by Tomkiewicz et al., [2010] is related to the development of telecommunication infrastructures, since at today there are many large areas throughout the world, mostly rural areas, scarcely covered by telecommunication networks based either on wired or wireless infrastructures. In this regards, tailored sensor networks, based on peer-to peer-routing, have been applied for gathering location data of several animals in those areas where GSM service were not available [Pelusi et al., 2006; Arcidiacono et al., 2018]. To overcome the above cited problems and enhancing the development of real-time applications for monitoring animal behaviour, low-power wide-area network (LPWAN), such as SigFox and LoRa, are being considered for developing Internet of Things (IoT) technologies also in the field of precision livestock farming (PLF) [Berckmans, 2017; Dieng et al., 2017] with reference to the continuous and real-time monitoring of health and welfare of animals in extensive livestock systems. In fact, despite the advances achieved in these recent years in tracking objects by GPS-based technology, several constraints limit the use of GPS-based systems in commercial farms for identifying, locating, and monitoring animals in large pastures [Evans, et al., 2016; Nóbrega et al., 2018]. First of all, both the high cost of the GPS devices and the lifetime of battery, not adequate to monitor the herd for several months a year [Davis et al., 2011].

The animal location retrieved by GPS devices could be used to develop anti-theft control systems. Livestock theft

is a relevant issue in herd management and farmers spend high economic resources for insurances, to reduce the financial burden whenever livestock does get stolen. Moreover, since GPS devices could retrieve also animal identification, each identified animal position could be tracked during the monitored period. This could allow for monitoring animal walking activity which is a relevant parameter for a first remote screening of animal well-being. For example, in farms for dairy cows or in the cow-calf systems of beef production, the increment of cow walking activity could be an index of some physiological status such as heat or calving. On the contrary an extended stationary time interval could alert the farmer for some disease activity or an accident.

 Extensive breeding of dairy cows and cows in the cow-calf line generates various environmental impacts, among which the most significant one concerns greenhouse gas emissions and soil degradation. As regards the issue of the impact of extensive livestock farming on soils, it should be stressed that the degradation processes can be triggered by incorrect agricultural practices for livestock food production or by the adoption of non-rational grazing systems, with consequent phenomena caused by animal activity of compaction, pathways, and erosion.

In this context, on the one hand a IoT-based solution that enables the location and tracking of cows in grazing fields could be adopted by farmers for a long-distance monitoring of herd position. On the other hand, such a solution could provide a large dataset of geo-spatial information to be integrated in a Geographical Information System (GIS) in order to model the environmental impacts of extensive livestock systems.

Therefore, the main objective of this paper was to investigate the feasibility of a novel automatic system for locating and tracking cows in extensive livestock systems based on space-time data provided by a low power global positioning system (LP-GPS). SigFox telecomunication network was used to manage position information received by a low power global positioning system (LP-GPS) attached to the collars of the cows. The methodology developed in this study can be used also for both investigating possible cow interactions and analyzing potential environmental impacts of the herd.

2. Materials and Methods

2.1. The herd under study

Livestock transhumance represents a way for adapting breeds at the variable climatic conditions. In detail, summer transhumance to highland pastures is still highly widespread in Sicily, the largest island of the Mediterranean Sea, characterised by continental climate in the inland areas, where winters become moderately cold, and summers are still hot. Transhumance is relevant for farmers as it integrates the normal annual forage and allow access to public economic aids. Moreover, transhumance has important economic externalities because increase the cultural values of a territory, by improving landscape quality, promoting local products, such as milk and cheese, maintaining local tradition, supporting the biodiversity through the conservation of native species of high values [Zendri et al., 2016].

The breed considered in this study generally moves from the Nebrodi mountains, located in the province of Messina, to the Margilupo district belonging to the municipality of Melilli within the province of Syracuse (Figure 1a) at an altitude of 200 m a.s.l. (Figure 1a). The climate is typically Mediterranean, with mild, humid winters and hot, dry summers.

The experimental activity was carried out during December 2019 and cows were free of grazing in area of about 100 hectares, delimited by an electrified fence for avoiding cattle's trespassing. The breeding consists of 90 animals: 1 limousine breed bull, 70 suckler cows aged between 5 and 10 years, 13 heifers that are 1 to 4 years old, 10 calves under 1 year of age.

(a) (b)
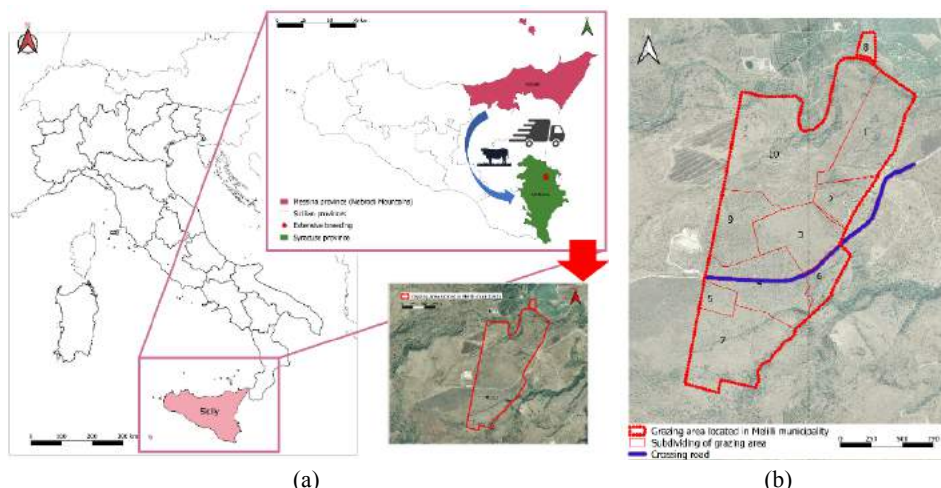
Figure 1. (a) The territorial area by the localisation of the grazing area. (b) Grazing area subdivisions after visual inspection.

The pasture is mostly made up of permanent natural fodder, typical of the Mediterranean climate since no processing is carried out. It origins from the interaction of climatic, pedological and species adaptation factors. By visual analysis it emerged that vegetation cover of the soil is characterised by many thorny shrubs, several species of cruciferous and composite grasses which due to their morphological characteristics such as the presence of thorns on the stems, are not eaten by animals. These conditions, combined with the lack of water resources, contributed to define a medium-low production potential of the pasture (Figure 2). Animals influence the vegetation cover of soil by taking of plants and seeds, the restitution through the manure. Furthermore, animal trampling modifies the natural form of the soil; in fact, it was possible to observe the presence of well-established paths in the direction of the few watering points.

Figure 2. Grazing survey carried out in December 27 of 2019.

The cattle breeds considered in this study are rustic and not very used to wearing equipment. Therefore, to select a sample of cows for the experiment, the breeder chosen 10 animals among the tamest, that generally wear the collar with the cowbell. The collar is made by the breeder by using a very resistant plastic material but able to mould itself based on the required shape. Each collar is provided by a bell that makes a sound when the animal is moving and, therefore, allows the breeder to track the animal (Figure 3).

Each bell (Figure 3) is produced with a specific shape and size in order to be adapted to animals by considering different ages and furthermore it could emit different sounds, which allow the breeder to identify and locate the animal. Even today, especially in the Nebrodi mountain areas, this very ancient method of tracking animals is the most used by breeders to retrieve the animals.

Figure 3. Bell and collars adopted during the study.

2.2. Data collection system

The Low Power GPS-Based System (LP-GPS system) developed in this research study is composed of wearable devices the receive position information from up to three global navigation satellites systems (GPS, Galileo, GLONAS) and send it to a cloud server by using SigFox telecommunication network.

This system allowed the collection of position data, e.g., latitude and longitude, of ten cows, as well as date, time of detection and distance travelled by each animal. The time interval of acquisition was 20 minutes as well as the time interval of sent messages to the cloud server.

All the information were sent to a developed AppWeb running either on mobile devices or on Personal Computer. Data were then imported for further elaborations trough both statistical and geo-spatial analyses. In detail, geo-spatial analysis was carried out by using the QGIS software tool (v.3.10.11), a free software provided by Open-Source Geo-Spatial Foundation (Chicago, USA), which allows the organization, the analysis and visualization of data at territorial level in order to deeply understand the link between livestock and environment.

By applying the Kernel Density Estimation (KDE) tools, available in QGSI land use analyses were carried out by considering the positions of each animal equipped with the devices. In detail, the KDE analysis, frequently used in biology studies, allows the calculation of the home range of the species (the area of the agricultural land in which a species lives) and provides a density estimation of the use of the territory. The result of the KDE analysis consists of a map (i.e., a raster or a vector image) that represents the area of the territory most frequently used by animals, in terms of density. The density levels are 95% (home range) and 50% (core home range); the Home Range (HR) represents the area in which the probability of finding the monitored items is 95%; while the Core Home Range (CHR) represents the

area in which the probability is 50%. These maps were obtained both for each animal of the sample and for the whole group, in order to classify the areas most used by the herd. The device developed in this study was equipped with an omnidirectional GPS antenna and receiver with -167 dBm sensitivity and 72 channels, an ultra-low power microcontroller, a SigFox radio module 868MHz, 14dBm E.R.P., an omnidirectional SigFox antenna, a powered by high-capacity Li-SOCL2 batteries. The device can operate at a range of temperature between -20 and 50 ° C and was put into a commercial case of small dimension 119x66x43 mm having an IP degree equal to 68 (Figure 4).

Figure 4. Low Power GPS-Based System.

The analysis began on December 27, 2019, but the data recording took place from January 1, 2020, and continued until January 22, 2020, when for technical reasons the LP GPS devices were removed from the collars. In detail, due to the weakness of the anchor points, some devices began to come off and fall to the ground. Therefore, in order not to damage the instrumentation, it was decided to remove the devices from the collars and reattach them with a safer system. However, due to the COVID-19 emergency, it was no longer possible to return to the company due to the lockdown. However, it is believed that the data collected are in any case sufficient to describe the functionality of the system and its potential applications both for the management of the herd and, in a broader context that concerns the analysis, monitoring and management of the territory. Therefore, data monitoring was recorded for 22 days at time-intervals of 20 minutes.

Ten of these devices (Figure 4) were put to the collars (Figure 3) of ten female cows, differing in age (from 2 to10 years old) and number of births, selected as sample because of they were easier approachable by the breeder. Knowing the animals individually, the breeder chose which ones needed to be monitored and took care of arranging the collar equipped with a GPS device on each selected animal.

3. Results and Discussion

3.1. Environment observation

Through direct surveys and visual inspections carried out in the study area, it was possible to investigate the floristic composition of the field, which appears to be homogeneous in all areas of the pasture. The whole grazing area had a northern exposure that generates a poor exposure of animals to solar radiation. In detail, the visual inspections of the grazing areas, due to their direct link with the environment, land, and species, were carried out between the end of December and the first ten days of January, which is a well-known time period of medium-low production, because the climate conditions. Almost all the vegetation is dominated by the Mediterranean scrub, with carob, olive and citrus trees. Dwarf shrubs and herbaceous plants including *calicotome villosa, sarcopoterium spinosum and cynara cardunculus altilis* are the main species characterising the pasture. The excessive presence of these species highlighted a high exploitation by animals as the pabulary species become more and more sparse and the non-pabulary species take over.

Firstly, the study area was subdivided into ten different areas (i.e., 1, 2, 3, 4, 5, 6, 7, 8, 9, 10) (Figure 1b).

The grazing areas i.e., 3, 4, 5, 6 were considered as polyphite pasture close to the road network and characterised by not excessively thick soil coverage, with different pabulary species of legumes, cruciferous and composite grasses but also species that due to their morphological characteristics such as the presence of thorns on the stems are not eaten by the animals. The scarce vegetation cover recorded for these areas is due to the fact that the exploitation by animals combined with road-crossing inhibited the growth of the pabulary species by implementing the development of shrubs spinescent.

The grazing areas i.e., 1, 8, 9, 10 that are placed far from the road network, are much richer in forage due to their proximity to the dam (Figure 2). These areas and the area 7 are quite homogeneous, characterised by grasses and pabulary legumes (i.e., composites, asteraceae, umbelliferae and chenopodiacee). Among the grasses predominate: *Bromus sp.*, *Avena sp.*, *Hordeum sp.* Among the legumes predominant were *Trifolium subterraneum*, *Trifolium campestre* and *Medicago arabica* and *hispida*.

3.2. Analyses of data acquired by the LP GPS-Based System

Data collected during the 22 day-monitoring period were used to locate and track the ten cows equipped with the LP GPS-Based System. By applying KDE algorithm to the dataset acquired by the LP GPS System, 9 thematic maps were obtained by using QGIS software tools, one for each monitored cow (Figure 5). Each map reports the perimeter of the whole grazing area, a dirt road that crosses the grazing area and divides it into parts, the home range and core range areas obtained by KDE algorithm, the subdivision of the whole pasture into ten classes.

Moreover, after the statistical analysis, the spatial analysis was carried out through QGIS software. It allowed to obtain the heatmap for each of the monitored cow. Figure 8a showed the cow1-tracking during the 22 day - time detection.

In each Heatmaps (Figure 5) relating to the use of the grazing within the 22 days of monitoring, it is possible to visualise the areas preferred by the animals.

From Figure 8 it is possible to notice that both areas, namely the CHR area and the HR area determined by the KDE application, are located mostly in the northern part of the land in those areas classified as 9 and 10. This confirms that the animal remained within the CR area for the entire period due to the high forage availability. Within the HR area the cow has been remained for more time since it found favourable microclimatic conditions in addition to the available forage.

By elaborating data recorded from the developed AppWeb, for each animal through its device it was possible to locate and track, as detailed below, by taking into account the three weeks of monitoring.

As regard Cow 1, by analysing data acquired from the device, during the first week of monitoring, from January 01 to January 07, about 12 km-distance has been travelled. Instead of during the second week an increment was recorded related to the daily km-distance travelled, with about a weekly distance of 16 km, due to the necessity of moving for looking for finding better forage areas. Instead, both Cow 2 and Cow 4 kept almost unchanged their daily distance, about 2 km per day, except for Cow 2 during January 4 and 5, in which reaches more than 3 km per day. By comparing data of Cow 1 and Cow 2, it emerged that it has travelled more kilometres, as it is possible to see also from the Heatmap reported in Figure 5b. In detail Cow 2 remained for longer in those areas close to the crossing road (i.e., areas 4, 6, 3). This difference is due to the fact that Cow 2 is younger than Cow 1 and prefers group-life.

As shown in Figure 5c, the recurrent positions of Cow 3, obtained through the heatmap, highlighted an HR area, which was far from the central grazing area due to the necessity to move to an area richer in forage and closer to the natural drinking source (i.e., area 10). In this regard, it was observed that the kilometres per day travelled by Cow 3 were kept unchanged during the three weeks of monitoring, about 17 km. The Heatmap reported in Figure 5d shows only few HR areas close to the road network (i.e., areas 4, 3, 6), due to the Cow 4 rural attitude, that prompts the preferences of those areas placed in north-west of the grazing area as they are further away from the road and therefore by the human presence.

Similar behaviour was observed for Cow 6 and Cow 8. In detail, by elaborating data, a stable daily-distances travelled was recorded during the first week, while during the second week, about 4-km daily travelled, respectively on January 12 and January 10 were achieved, due to the possible heat state during oestrus cycle. As regard their heatmaps (Figure 5e and Figure 5g) the Cow 6's CR area is mainly located close to the road network, while the HR one was located along the road which explains its preference for the forage located in this area. Cow 8's CR and HR areas are both far from the crossing road, placed within the inner part of the grazing area (i.e., area 10), due to this cow's solitary and rural attitude (Figure 5g).

Cow 7 recorded data, in comparison with the others, show a different travelled distances during the three weeks by travelling two kilometres distance per day more than others. As regards Cow 9 and Cow 10, different behaviours were observed. In particular, a reduction of the Cow 9 travelled distance per day was registered, from 2 km per day (as those recorded also for Cow 2 and Cow 4) during the first week to less than 1 km per day during the second week.

From the observation of this sudden reduction in travelling distance the breeder promptly recognised a lameness in the right anterior limb of the Cow, which was therefore transferred for medical treatments. The heatmap reported in Figure 5h shows that the CR areas are widely distributed throughout the entire grazing area, instead as related to the HR areas, the largest one shows that the animal remained there for longer and represents the equipped shelter area where the animal was transferred for medical treatments due to the limb lameness.

Conversely from the other cows, Cow 10 shows a fluctuating motor activity. During the first week of monitoring about 3 km per day were travelled, by revealing a no meek attitude. During this first week, as reported on Figure 5i it is possible to identify the widest HR area in which the cow stays until starting the second week (i.e., January 6) which registered a highly decrease of the travelled daily distances by reaching about less than 1 km per day as observed also for Cow 9. During the third week, the travelled distances again increase due to the necessity of finding new grazing areas richer in forage.

By merging the KDE maps of each cow (Figure 5), it was possible to create a heatmap (Figure 5l) aimed at detecting

the most preferred territorial areas from all cows.

From Figure 5l it is possible to see that, among the detected six areas (i.e., A, B, C, D, E, F), that one called as "area D" was mostly occupied since it is the flattest, far from the road network, and far from the humans' presence, with a great supply of forage, as observed during the visual inspection.
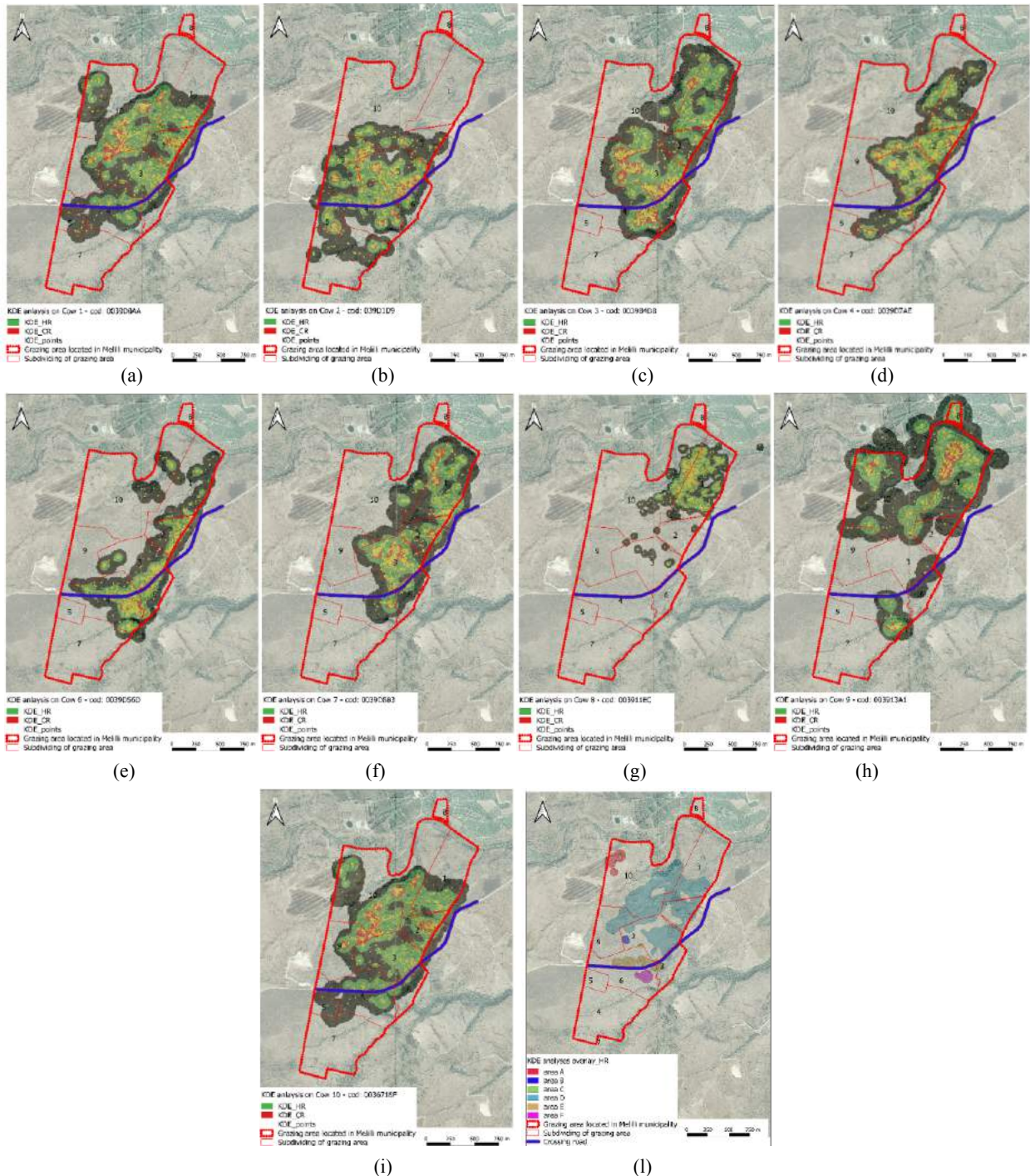
Figure 5. Heatmaps of the ten cows. (a) Cow 1. (b) Cow 2. (c) Cow 3. (d) Cow 4. (e) Cow 6. (f) Cow 7. (g) Cow 8. (h) Cow 9. (i) Cow 10. (l) Merged heatmaps.

As shown from the heatmaps reported in Figure 5, during the monitoring period only nine of the ten adopted devices collars recorded data, since one LP GPS device detached from the collar (Cow 5). The heatmaps, carried out by elaborating the data acquired by the LP GPS system, could represent a fundamental aspect for the livestock

management since farmers can have a feedback on the type of forage ingested as well as on the soil conditions of the grazing areas. Moreover, the comparison of the daily distances travelled by each animal could be useful for the farmer to discover anomalies in their trend which can be an alarm for possible diseases. This occurred in the experiment described in this paper, when Cow 9 had a drastic reduction of the daily travelled distance due to a right limb lameness. The farmer promptly acted by transferring the cow for the medical treatment by preventing further diseases.

4. Conclusions

Prompt reaction to any change in health, welfare and production status is the key factors helpful for both reducing management difficulties and improving animal welfare. The achieved results demonstrate the potential of LP GPS devices for locating and tracking grazing cattle. Real-time monitoring of positions and tracking represents a simple way to measure those variables that can provide farmers with a clear and adequate timely alert.

Potential applications of the proposed LP GPS monitoring system may be of interest also for stakeholders, local authorities and regional environmental protection agencies. In fact, the system can allow the monitoring of any important variations within the structure of the vegetation and in the composition and variety of plant species that may arise due to food selection of essences, trampling and release of manure. Through these actions the animals modify the habitats and the populations of invertebrates and other organisms. Changes in the intensity of grazing or in the animal species involved can therefore have important consequences on biodiversity. Furthermore, from the social, economic, and cultural point of view, the identification of the most exploited grazing areas can be useful in the context of the assessment procedures of the landscape characteristics (relationship of the areas subject to grazing and the characteristics of the landscape of the area). In general, the relationship between animal husbandry and landscape quality can be positively configured, as can happen in the case of rationally conducted grazing farming systems where the maintenance of the grass in good clean conditions, together with the presence of grazing animals contribute to landscape amenities. On the other hand, the presence of marginal areas, which from the analyses may not be used by animals, could lead to a reduction in the aesthetic value of the landscape due to the effect of abandonment that could result.

Acknowledgements

References

1. Gordon, I.J. Foreword. In Tracking Animals with GPS: An International Conference Held at the Macaulay Land Use Research Institute; Macaulay Land Use Research Institute: Aberdeen, Scotland, 2001; p. III.
2. Liu, T.; Rodríguez, L.F.; Green, A.R.; Shike, D.W.; Segers, J.R.; Maia, G.D.N.; Norris, H.D. Assessment of cattle impacts on soil characteristics in integrated crop-livestock systems. In Proceedings of the American Society of Agricultural and Biological Engineers Annual International Meeting, Dallas, TX, USA, 29 July–1 August 2012.
3. Porto, S.M.C., Arcidiacono, C., Anguzza, U., Cascone, G. The automatic detection of dairy cow feeding and standing behaviours in free-stall barns by a computer vision-based system (2015) Biosystems Engineering, 133, 46-55.
4. Arcidiacono, C., Barbari, M., Benni, S., Carfagna, E., Cascone, G., Conti, L., di Stefano, L., Guarino, M., Leso, L., Lovarelli, D., Mancino, M., Mattoccia, S., Minozzi, G., Porto, S.M.C., Provolo, G., Rossi, G., Sandrucci, A., Tamburini, A., Tassinari, P., Tomasello, N., Torreggiani, D., Valenti, F. Smart Dairy Farming: Innovative Solutions to Improve Herd Productivity (2020) Lecture Notes in Civil Engineering, 67, 265-270.
5. Turner, L.W.; Udal, M.C.; Larson, B.T.; Shearer, S.A. Monitoring cattle behavior and pasture use with GPS and GIS. Can. J. Anim. Sci. 2000, 80, 405–413.
6. Porto, S.M.C., Arcidiacono, C., Giummarra, A., Anguzza, U., Cascone, G. Localisation and identification performances of a real-time location system based on ultra wide band technology for monitoring and tracking dairy cow behaviour in a semi-open free-stall barn, Computers and Electronics in Agriculture, 2014, 108,221-229.
7. Arcidiacono, C., Mancino, M., Porto, S.M.C. Moving mean-based algorithm for dairy cow's oestrus detection from uniaxial-accelerometer data acquired in a free-stall barn (2020) Computers and Electronics in Agriculture, 175.

8. Veissier, I.; Boissy, A.; Nowak, R.; Orgeur, P.; Poindron, P. Ontogeny of social awareness in domestic herbivores. Appl. Anim. Behav. Sci. 1998, 57, 233–245.

9. Rodgers, A.R.; Rempel, R.S.; Abraham, K.F. A GPS-based telemetry system. Wildlife Soc. B 1996, 24, 559–566.

10. D'Eon, R.G.; Serrouya, R.; Smith, G.; Kochanny, C. GPS radiotelemetry error and bias in mountainous terrain. Wildlife Soc. B 2000, 30, 430–439.

11. rair, J.L.; Nielsen, S.E.; Merrill, E.H.; Lele, S.R.; Boyce, M.; Munro, R.H.M.; Stenhouse, G.B.; Beyer, H.L. Removing GPS collar bias in habitat selection studies. J. Appl. Ecol. 2004, 41, 201–212.

12. Van Beest, F.M.; Loe, L.E.; Mysterud, A.; Milner, J.M. Comparative space use and habitat selection of moose around feeding stations. J. Wildl. Manag. 2010, 74, 219–227.

13. Schieltz, J.M.; Okanga, S.; Allan, B.F.; Rubenstein, D.I. GPS tracking cattle as a monitoring tool for conservation and management. Afr. J. Range For. Sci. 2017, 34, 173–177.

14. Fogarty, E.S.; Swain, D.L.; Cronin, G.; Trotter, M. Autonomous on-animal sensors in sheep research: A systematic review. Comput. Electron. Agric. 2018, 150, 245–256.

15. Tomkiewicz, S.M.; Fuller, M.R.; Kie, J.G.; Bates, K.K. Global positioning system and associated technologies in animal behaviour and ecological research. Philos. Trans. Roy. Soc. B 2010, 365, 2163–2176.

16. Pelusi, L.; Passarella, A.; Conti. Opportunistic networking: Data forwarding in disconnected mobile ad hoc networks. IEEE Commun. Mag. 2006, 44, 134–141.

17. Arcidiacono, C., Porto, S.M.C., Mancino, M., Cascone, G. A software tool for the automatic and real-time analysis of cow velocity data in free-stall barns: The case study of oestrus detection from Ultra-Wide-Band data, Biosystems Engineering, 2018, 173, 157-165.

18. Dieng, O.; Diop, B.; Thiare, O.; Pham, C. A study on IoT solutions for preventing cattle rustling in an African context. In Proceedings of the Second International Conference on Internet of Things, Data and Cloud Computing, Cambridge, UK, 22–23 March 2017.

19. Berckmans, D. General introduction to precision livestock farming. Anim. Front. 2017, 7, 6–11.

20. Evans, J.C.; Dall, S.R.X.; Bolton, M.; Owen, E.; Votier, S.C. Social foraging European shags: GPS tracking reveals birds from neighbouring colonies have shared foraging grounds. J. Ornithol. 2016, 157, 23–32.

21. Nóbrega, L.; Tavares, A.; Cardoso, A.; Gonçalves, P. Animal monitoring based on IoT technologies. In Proceedings of the IoT Vertical and Topical Summit for Agriculture, Tuscany, Italy, 8–9 May 2018.

22. Davis, J.D.; Darr, M.J.; Xin, H.; Harmon, J.D.; Russell, J.R. Development of a GPS herd activity and well-being kit (GPS HAWK) to monitor cattle behavior and the eᴚect of sample interval on travel distance. Appl. Eng. Agric. 2011, 27, 143–150.

23. Frost, A.R., Schofield, C.P., Beaulah, S.A., Mottram, T.T., Lines, J.A., Wathes, C.M.A review of livestock monitoring and the need for integrated systems, Computers and Electronics in Agriculture, 1977, 17, 2, 139-159.

24. Zendri F., Ramanzin M., Bittante G., Sturaro E. 2016. Transhumance of dairy cows to highland summer pastures interacts with breed to influence body condition, milk yield and quality, Italian Journal of Animal Science, 15:3, 481-491.

Evaluation of a Sensor-based System for Monitoring Rumination in Dairy Cows with Access to Pasture

Lara Schmeling[a,b,*], Golnaz Elmamooz[c], Daniela Nicklas[c], Stefan Thurner[a], Elke Rauch[b]

[a] Institute for Agricultural Engineering and Animal Husbandry, Bavarian State Research Center, Freising, Germany

[b] Chair of Animal Welfare, Ethology, Animal Hygiene and Animal Husbandry, Faculty of Veterinary Medicine, Ludwig-Maximilians-University Munich, Munich, Germany

[c] Chair of Mobile Systems, University of Bamberg, Bamberg, Germany

* Corresponding author. Email: lara.schmeling@lfl.bayern.de

Abstract

Monitoring the health and welfare of animals is time consuming, especially on pasture. Monitoring systems can assist the farmer in detecting the oestrous and emerging health disorders by continuously predicting the animal behaviour and its changes. Rumination behaviour has proven to be a useful indicator. As most of the monitoring systems available on the market were either developed for the stable or for pasture and fail to detect the behaviour reliably in the other location, our goal was the development of a monitoring system for dairy cows kept on pasture as well as in the stable. As a first step, a model for the prediction of rumination behaviour was developed and evaluated. Up to eleven cows on three different farms were equipped with the collar-based prototype of the monitoring system. The system contained a 3D accelerometer and a gyroscope, both collecting data at 10 Hz. Ground Truth data were collected by recording the animals with cameras and labelling the video data based on an ethogram. The data from three animals (30.4 h) on farm 1 were used for training the model. Random Forest and a window size of 5 s without overlap proved to achieve the highest accuracy compared to other classifiers and window sizes. An orientation-independent feature set with 26 features was chosen. The model was evaluated on data from the remaining animals (184.8 h). The output of the model and Ground Truth were compared second by second. Overall accuracy of the model in detecting rumination behaviour was 97.4 %. Lying without rumination was the behaviour confused the most with rumination by the model. From individual rumination bouts, 97.1 % were successfully predicted by the model. The duration of rumination bouts did not differ (p = 0.70) between model output and video observation. Compared to other models for the prediction of rumination behaviour, our model achieved high accuracies both on pasture and in the stable.

Keywords: PLF, accelerometer, gyroscope, grazing, behaviour recognition

1. Introduction

Rumination behaviour increases the saliva production which buffers the acids produced in the rumen within the bacterial carbohydrate decomposition. Besides, masticating the feed increases the surface available for bacterial decomposition in the rumen. Eventually, rumination enables (dairy) cows to use fibrous plant material as energy source. Healthy dairy cows show approximately 7 to 8 h of rumination behaviour per day depending, e.g., on the husbandry system (Gregorini et al. 2013), the size of the animal (Bae et al. 1983), the parity (Miguel-Pacheco et al. 2014), the phase of lactation (Gáspárdy et al. 2014) and the milk yield (Soriani et al. 2013). Rumination behaviour is shown in 13 to 15 bouts per day (Dado and Allen 1994).

Rumination behaviour is a useful indicator for the health and welfare status of dairy cows. Deviations in daily rumination time and the frequency and the duration of rumination bouts provide valuable information for the detection of the oestrous as well as for the identification of emerging health disorders or health challenges. Abeni and Galli (2017) found a decrease in rumination time, especially during the day, in cows exposed to heat stress. Also on the day prior to calving and on the calving day itself, dairy cows show a reduced rumination time (Clark et al. 2015) making it a useful indicator for the detection of calving. Mayo et al. (2019) and Minegishi et al. (2019) found a reduction of rumination time on the day of oestrous, confirming that by assessing rumination behaviour, oestrous can be detected. Besides, various health disorders lead to decreased rumination times, e.g. subclinical ketosis (Kaufman et al. 2016), lameness (Miguel-Pacheco et al. 2014), mastitis (Stangaferro et al. 2016b) and metritis (Stangaferro et al. 2016a).

To detect changes in rumination time in dairy cows, rumination behaviour must be recorded continuously. The automated and continuous measurement of rumination time can be realized with monitoring systems. With different sensors, e.g. accelerometers, pressure sensors or microphones, those systems detect movements of the head, neck, jaw, or ear or sounds associated with movements of the jaw. By training and applying suitable machine learning models on the sensor data, behavioural patterns like rumination can be predicted automatically. For the stable, various systems have proven to reliably detect rumination behaviour. Martiskainen et al. (2009) developed a model that predicted rumination behaviour with high accuracy in dairy cows kept in a barn. Borchers et al. (2016) evaluated the performance of an accelerometer sensor attached to the ear and found high correlations between visual observation and the system

output for rumination behaviour. A collar-based monitoring system was assessed by Grinter et al. (2019) and Werner et al. (2018) evaluated the performance of a halter containing a pressure sensor. Both systems performed well in predicting rumination behaviour in dairy cows. Hamilton et al. (2019) successfully developed a model for the automated detection of rumination periods with an accelerometer integrated into a rumen bolus. On pasture, on the other hand, most of the systems developed for the stable perform weakly (Ambriz-Vilchis et al. 2015; Elischer et al. 2013). González et al. (2015) developed an algorithm for the detection of rumination behaviour in steers kept on pasture with a collar-based system and achieved high accuracies in the evaluation of the algorithm. An algorithm for the automated prediction of rumination behaviour from sound data collected with a microphone was developed and evaluated by Chelotti et al. (2020). The algorithm detected rumination behaviour as well as individual rumination bouts with high accuracies. Both studies focused on behaviour data from pasture and did not include data from the stable. Kononoff et al. (2002) on the other hand evaluated the performance of a noseband sensor which was developed for pasture on dairy cows in a barn and found significant differences in the rumination time predicted by the system compared to visual observation.

As the available monitoring systems developed for the detection of rumination behaviour in dairy cows were either developed for the stable or for pasture, exclusively, and fail to reliably predict rumination in the other location, the goal of the presented study was to develop a model for the automated detection of rumination behaviour in dairy cows kept on pasture as well as in the stable.

2. Materials and Methods

2.1. Animals and farm management

All performed procedures followed the EU directive 2010/63/EU and the German Welfare Act. Data collection methods were previously described in Schmeling et al. (2021). Data collection was conducted on three different dairy farms in Upper Bavaria, Germany. On all farms, calving was seasonal, the herds consisted of dairy cows mainly from the Simmental breed and the animals had access to pasture during the summer months. All cows were kept in or had access to a free stall barn. On farm 1, access to the barn was limited to two hours around each milking. Permanent access to the barn was granted during the day on farm 2, while during the night, the cows were kept on a smaller pasture without access to the barn. As observations on farm 3 were made during winter, the cows were kept in the barn all day long without access to pasture. Details on the three farms and their management can be found in Table 1.

Two observation rounds of two consecutive days each were conducted on farm 1. On farm 2 and 3, one observation round of three and four consecutive days, respectively, were performed. For the trials, animals in the second to fifth lactation were chosen randomly from each herd. Only cows free from clinical symptoms of any kind were included in the trial. Details on the selected cows can be found in

Table *2*.

Table 1 – Details on farms and farm management.

Farm	No. of cows in the herd	Size of pasture [ha]	Type of milking parlour	Milking times	Feed (feeding times)	Type of cubicles	No. of cubicles
1	40	17	herringbone	6 am / 5 pm	-[4]	deep, straw-bedded	40
2	34	12[1] / 3[2]	herringbone	7 am / 4 pm	-[4]	deep, litter	34
3	52	-[3]	tandem	6 am / 6 pm	TMR (10 am / 6 pm)	high, rubber mattresses	48

[1]access during the day, [2]access during the night, [3]observations made during winter, [4]main feed derived from pasture

Table 2 – Details on the dairy cows included in the trials.

Farm	No. of round	No. of chosen animals	Parity (mean ± sd)	DIM[1] (mean ± sd)
1	1	7	3.1 ± 0.7	233 ± 30
	2	8	3.5 ± 1.2	285 ± 40
2	1	8	4.0 ± 1.2	101 ± 46
3	1	11	4.0 ± 0.9	273 ± 16

[1]Days in milk (DIM) on the first day of the trial

2.2. Behaviour data collection

On all three farms, the selected animals were equipped with the prototype of a monitoring system (Blaupunkt Telematics GmbH, Hildesheim, Germany) attached to a collar. The system contained a three-dimensional accelerometer and a triaxial gyroscope (BNO055, Bosch Sensortec GmbH, Reutlingen, Germany). Data sampling frequency was set to 10 Hz. Raw data was stored on an integrated SD memory card (32 GB; SanDisk; Western Digital Deutschland, GmbH, Aschheim, Germany) and downloaded after each round.

In parallel with the sensor data, behaviour data were collected. Therefore, the selected animals were observed with five (pasture) to seven (barn) cameras (GoPro HERO5, GoPro, Inc., San Mateo, USA) for 5 to 8 h per day. After the observation rounds, the video data were analysed. The behaviour of each cow was classified at every second based on an ethogram. Video analysis was conducted by one observer only, avoiding errors between observers. Rumination behaviour was defined as the time between the regurgitation of the first and the re-swallowing of the last bolus of a rumination bout. A gap of 60 s in between two boli separated two rumination bouts based on the criteria used by Werner et al. (2018) and the findings from Kononoff et al. (2002). Besides rumination behaviour, lying, grazing, walking, standing and additional behaviours like chewing, social, comfort and explorative behaviour were labelled (Schmeling et al. 2019). The data from all animals on all days from farm 1, all animals on one day from farm 2 and three animals on one day from farm 3 were analysed in detail with rumination behaviour being labelled.

2.3. Model development

The data sets consisting of sensor data from the accelerometer and the gyroscope and the Ground Truth data (= behaviour data) derived from the video observation served as basis for the development of the machine learning model for rumination behaviour. Data from two animals from farm 1 from the first round and one animal from farm 1 from the second round were chosen for the development. From the chosen data, 20 % were used for the training of the model and 80 % served as the basis for the evaluation within the model development. The goal was to develop a binary model that is able to distinguish between rumination and non-rumination behaviour. Lying without ruminating, grazing, standing, and walking were considered as non-rumination behaviour. Each behavioural pattern shared 25 % of the training data set. Down-sampling from 10 to 9, 7, 5 and 3 Hz was examined by calculating the mean. Different algorithms (Random Forest, Decision Tree, Support Vector Machine and Naïve Bayes), window sizes (5, 6, 8, 10 and 12 s) and strides (50 %, 75 %, 100 %) were assessed. Various features were applied to the magnitude of the accelerometer and the gyroscope data and given to the classifiers. Different combinations of model characteristics were regarded to find the best combination for a successful prediction of rumination behaviour. As the output of the model was noisy, a filter was applied to the model data. All rumination and non-rumination sequences with a duration of <60 s were disregarded and added to the behaviour classified in the preceding sequence.

2.4. Model evaluation and statistical analysis

The model output and the Ground Truth data were compared second by second. Seconds of rumination behaviour correctly identified as rumination were considered as true positive (TP). Seconds correctly predicted as non-rumination behaviour were considered as true negative (TN). Seconds of rumination in Ground Truth that were predicted as non-rumination behaviour by the model were defined as false negative (FN) and seconds of non-rumination falsely predicted as rumination behaviour as false positive (FP). These values were used to calculate the sensitivity, specificity, and accuracy of the model in predicting rumination behaviour. Regarding duration, only rumination bouts that were observed without an interruption of >60 s in Ground Truth were compared to the duration predicted by the model. Only beginnings and endings of bouts preceded or followed by 60 s of non-rumination behaviour in Ground Truth (= threshold that divided two bouts from each other) were compared between Ground Truth and model output.

The statistical analysis was performed in RStudio 1.3 (RStudio, Inc., Boston, USA). Data was tested for normality using Shapiro-Wilk test. For normally distributed data average and standard deviation is given as $\bar{x} \pm$ sd. For data that was not normally distributed the median is given. The difference in rumination time and the duration of rumination bouts between Ground Truth and model output, as well as the difference between rumination time in the stable and on pasture and the rumination time during the day and during the night were assessed with a two-sample t-test. P-values <0.05 were considered as significant.

3. Results and Discussion

3.1. Collected data

With the chosen methods, 1516.0 h of sensor data were collected. From the videos, 219.3 h of corresponding Ground Truth data where rumination behaviour was labelled were collected. This share was available for the development and the evaluation of the model for the prediction of rumination behaviour in dairy cows. The final model was applied to all sensor data collected for the assessment of rumination time. One animal was excluded because it showed oestrous symptoms within the observation round.

A share of 14.1 %, equalling 30.4 h of data sets were chosen for the model building and the remaining 184.8 h were used for evaluation of the model. While for the development of the model all data were derived from the pasture, the data for the evaluation was divided among pasture (120.1 h) and stable (64.7 h). The available time both for model development and evaluation exceeded the one in the study of González et al. (2015) where 18 h of continuous behaviour data was used for the development of the model and 25 h were collected for the evaluation for the model. Borchers et al. (2016) evaluated an ear tag-based sensor in detecting rumination behaviour and had a similar amount of time (48 animals, 4 h, equalling 192 h) available for the evaluation.

In total, 105 rumination bouts were observed in Ground Truth. For 46 bouts the duration between Ground Truth and model output could be compared. The beginning of 82 bouts and the ending of 72 bouts was included in the evaluation and compared between Ground Truth and model output.

3.2. Developed model

Down-sampling did not bring any benefit and the sampling frequency was left at 10 Hz. The same sampling frequency was used in the study of Martiskainen et al. (2009) and González et al. (2015) for the development of a rumination model. Random Forest proved to be the most accurate algorithm for the prediction of rumination behaviour compared to other classifiers (Decision Tree, Support Vector Machine and Naïve Bayes) in our study. In contrast, Support Vector Machine (Hamilton et al. 2019; Martiskainen et al. 2009) and Decision Tree (González et al. 2015) were used but not compared with other algorithms in other studies. A window size of 5 s without overlap and an orientation-independent feature set with 26 features achieved the highest accuracy. A window size of 10 s without overlap was used by González et al. (2015) who showed that longer windows result in lower accuracies. An orientation-independent feature set ensures high accuracies regardless of sensor shifting caused by movement of the animals (Kamminga et al. 2018). By applying a filter of 60 s the model data was smoothed. As non-rumination bout lasted less than 60 s in Ground Truth, no information was lost by deploying the filter. In contrast, only with the filter individual lying bouts could be identified in the model output.

3.3. Performance of the model and rumination behaviour

In total, the developed model predicted rumination behaviour with a sensitivity of 92.6 %, a specificity of 99.3 % and an accuracy of 97.4 %. Performance on pasture (sensitivity: 91.7 %, specificity: 99.7 %, accuracy: 97.6 %) was slightly higher than in the stable (94.6 %, 98.4 %, 97.0 %). In total, variation between animals was small (min. accuracy: 94.9 % vs. max. accuracy: 99.1 %). The accuracy and sensitivity of our model exceeded the performance values of a model developed by Martiskainen et al. (2009) for dairy cows kept in a barn. Lower performance was achieved by the model developed by Hamilton et al. (2019). The model developed by González et al. (2015) for steers on pasture reached similar specificity (99.4 %) but a higher sensitivity (98.4 %). In this study, the development and the evaluation of the model were limited to data from pasture. Ambriz-Vilchis et al. (2015) evaluated a system for the monitoring of rumination behaviour in dairy cows both in the barn and on pasture. For the barn, they found a high correlation between video and visual observation and the system output for rumination time but on pasture correlation was poor. This finding is supported by the results of Elischer et al. (2013) who evaluated a collar-based system on a mixed data set from the barn and the pasture and found major differences in rumination time recorded by the system in comparison with visual observation. In contrast to other studies, our model performed well in detecting rumination behaviour in dairy cows kept in a barn as well as on pasture.

The FN time (= time when model predicted non-rumination behaviour, but the animals were showing rumination behaviour in Ground Truth) amounted up to 3.8 h (2.1 %). The FP time (= time when model predicted rumination behaviour, but animals were not ruminating in Ground Truth) on the other hand totalled only 1.0 h (0.5 %) of the observed time. The behavioural patterns that were confused the most with rumination by the model were lying without ruminating (46.2 %), standing without additional behaviour (22.8 %) and standing with additional behaviour like feeding, drinking, or chewing (18.7 %). These findings correspond to the results obtained by Martiskainen et al. (2009). Their model confused rumination behaviour with lying and standing the most as well.

Rumination time per animal per observation day was slightly overestimated by the model but did not differ significantly between Ground Truth and model output (1.7 vs. 1.6 h; p = 0.70; see Figure 1). In contrast, the system evaluated by Grinter et al. (2019) underestimated rumination time compared to visual observation. In our study, the share of rumination time of the total observed time in Ground Truth and model output was similar (29.8 vs. 28.3 %).

The model correctly detected 105 out of 109 rumination bouts, equalling 97.1 %. Of the 105 bouts, two (1.9 %) were merged to one and six (5.7 %) were divided into two or three bouts by the model. The model missed three rumination bouts that were observed in Ground Truth. More rumination bouts were not recognized, recognized too much, merged or divided by different models evaluated by Chelotti et al. (2020) for the automated detection of rumination behaviour from sound data derived from cows on pasture.

There was no significant difference between the duration of rumination bouts in the model output compared to Ground Truth (33.4 vs. 34.6 min.; p = 0.70; see Figure *2*). Variation of rumination bout duration was large (Ground

Truth min.: 6.7 min, Ground Truth max: 75.6 min; model output min: 5.7 min, model output max: 74.6 min). Dado and Allen (1994) found a slightly higher rumination bout duration (36.0 min) but variation was larger. In a study conducted by Kononoff et al. (2002), high agreement was found between the duration of rumination bouts predicted by a noseband-based system with visual observation as well, but the difference (+1.9 min) was slightly higher than in our study (+1.2 min). As our observations were limited to daytime, rumination bout duration could vary when night-time is considered as well.

From the compared beginnings of the rumination bouts, 29.3 % were detected ± 5 s from the beginning in Ground Truth. Most of the rumination bout beginnings were detected too late (56.1 %), a few beginnings were detected too early (14.6 %). Median difference in the beginning detected by the model compared to the beginning in Ground Truth was 53 s. The model detected the endings of 34.1 % of the rumination bouts within ± 5 s from the ending in Ground Truth. Part of the endings was detected too early (23.2 %) and part too late (30.5 %). Median time deviation between the endings of rumination bouts was -1 s. To our knowledge there is no study evaluating the detection of rumination bout beginnings and endings with a sensor-based system.

By applying the model to the entire sensor data (1516.0 h), the rumination behaviour could be assessed. In general, significantly more time per day was spent ruminating in the stable (farm 3) than by cows with access to pasture (farm 1 and 2; 8.2 vs. 7.1 h; $p < 0.05$). In a study conducted by Beer et al. (2016), higher rumination times were found for German Holstein cows kept in a stable. Similar rumination times were found in the study of Gregorini et al. (2012) for cows in the stable and cows that spent 24 h on pasture. On pasture, significantly more time was spent ruminating during the night (6 pm to 6 am) compared to the day (6 am to 6 pm; 4.2 vs. 3.2 h; $p < 0.05$). This finding is supported by the results of Gregorini et al. (2012) where cows showed more rumination time during the night than during the day as well. More time was spent ruminating during the day than during the night in the stable as well, but the difference was not significant (4.3 vs. 3.9 h; $p = 0.07$).
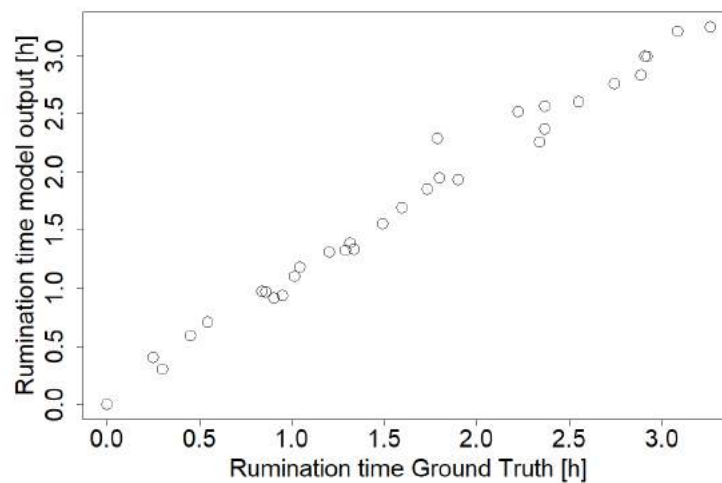
Figure 1 – Comparison of rumination time per animal and observation day (6-8 hours of total time observed per day) between Ground Truth and model output.
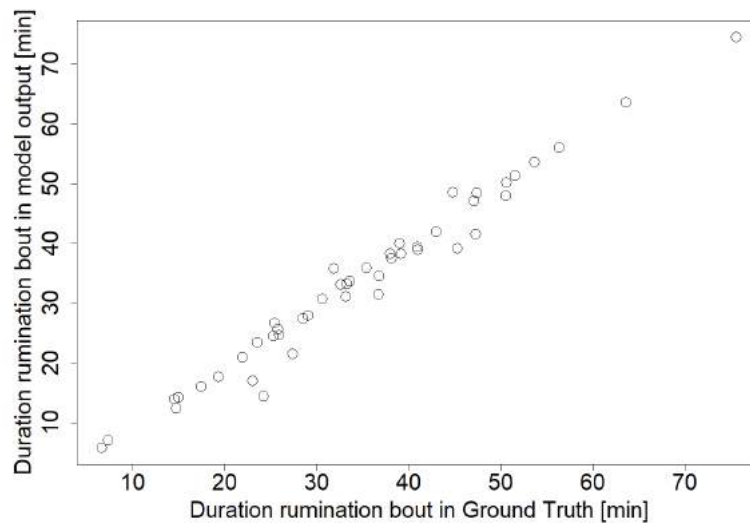
Figure 2 – Comparison of rumination bout duration between Ground Truth and model output

4. Conclusions

To summarize, the model developed for the collar-based prototype monitoring system predicted rumination behaviour in dairy cows with high accuracy. No significant differences in rumination time were found compared to rumination time recorded by video analysis. Also, the model was able to accurately detect individual rumination bouts and their duration. The good performance of the rumination model enables the sensor system to reliably detect rumination behaviour and changes in rumination behaviour caused, e.g., by oestrus, emerging health disorders, calving, or health challenges like heat load. Unlike previously assessed systems, the model was tested both on data from the stable and pasture and performed similarly well in both locations. Therefore, it is applicable on farms with either or both husbandry systems.

Acknowledgements

References

Abeni, F., and Galli, A. (2017) Monitoring cow activity and rumination time for an early detection of heat stress in dairy cow. International journal of biometeorology, 61 (3), 417–425, DOI: 10.1007/s00484-016-1222-z

Ambriz-Vilchis, V., Jessop, N.S., Fawcett, R.H., Shaw, D.J., and Macrae, A.I. (2015) Comparison of rumination activity measured using rumination collars against direct visual observations and analysis of video recordings of dairy cows in commercial farm environments. Journal of dairy science, 98 (3), 1750–1758, DOI: 10.3168/jds.2014-8565 (

Bae, D.H., Welch, J.G., and Gilman, B.E. (1983) Mastication and Rumination in Relation to Body Size of Cattle. Journal of dairy science, 66 (10), 2137–2141, DOI: 10.3168/jds.S0022-0302(83)82060-8

Beer, G., Alsaaod, M., Starke, A., Schuepbach-Regula, G., Müller, H., Kohler, P., and Steiner, A. (2016) Use of Extended Characteristics of Locomotion and Feeding Behavior for Automated Identification of Lame Dairy Cows. PloS one, 11 (5), e0155796, DOI: 10.1371/journal.pone.0155796

Borchers, M.R., Chang, Y.M., Tsai, I.C., Wadsworth, B.A., and Bewley, J.M. (2016) A validation of technologies monitoring dairy cow feeding, ruminating, and lying behaviors. Journal of dairy science, 99 (9), 7458–7466, DOI: 10.3168/jds.2015-10843 (eng).

Chelotti, J.O., Vanrell, S.R., Martinez Rau, L.S., Galli, J.R., Planisich, A.M., Utsumi, S.A., Milone, D.H., Giovanini, L.L., and Rufiner, H.L. (2020) An online method for estimating grazing and rumination bouts using acoustic signals in grazing cattle. Computers and Electronics in Agriculture, 173 (2), 105443, DOI: 10.1016/j.compag.2020.105443

Clark, C.E.F., Lyons, N.A., Millapan, L., Talukder, S., Cronin, G.M., Kerrisk, K.L., and Garcia, S.C. (2015) Rumination and activity levels as predictors of calving for dairy cows. Animal : an international journal of animal bioscience, 9 (4), 691–695, DOI: 10.1017/S1751731114003127

Dado, R.G., and Allen, M.S. (1994) Variation in and Relationships Among Feeding, Chewing, and Drinking Variables for Lactating Dairy Cows. Journal of dairy science, 77 (1), 132–144, DOI: 10.3168/jds.S0022-0302(94)76936-8

Elischer, M.F., Arceo, M.E., Karcher, E.L., and Siegford, J.M. (2013) Validating the accuracy of activity and rumination monitor data from dairy cows housed in a pasture-based automatic milking system. Journal of dairy science, 96 (10), 6412–6422, DOI: 10.3168/jds.2013-6790

Gáspárdy, A., Efrat, G., Bajcsy, A.C., and Fekete, S.G. (2014) Electronic monitoring of rumination activity as an indicator of health status and production traits in high-yielding dairy cows. Acta veterinaria Hungarica, 62 (4), 452–462, DOI: 10.1556/AVet.2014.026

González, L.A., Bishop-Hurley, G.J., Handcock, R.N., and Crossman, C. (2015) Behavioral classification of data from collars containing sensors in grazing cattle. Computers and Electronics in Agriculture, 110, 91–102, DOI: 10.1016/j.compag.2014.10.018

Gregorini, P., DelaRue, B., McLeod, K., Clark, C., Glassey, C.B., and Jago, J. (2012) Rumination behavior of grazing dairy cows in response to restricted time at pasture. Livestock Science, 146 (1), 95–98, DOI: 10.1016/j.livsci.2012.02.020

Gregorini, P., Dela Rue, B., Pourau, M., Glassey, C., and Jago, J. (2013) A note on rumination behavior of dairy cows under intensive grazing systems. Livestock Science, 158 (1-3), 151–156, DOI: 10.1016/j.livsci.2013.10.012

Grinter, L.N., Campler, M.R., and Costa, J.H.C. (2019) Technical note: Validation of a behavior-monitoring collar's precision and accuracy to measure rumination, feeding, and resting time of lactating dairy cows. Journal of dairy science, 102 (4), 3487–3494, DOI: 10.3168/jds.2018-15563

Hamilton, A.W., Davison, C., Tachtatzis, C., Andonovic, I., Michie, C., Ferguson, H.J., Somerville, L., and Jonsson, N.N. (2019) Identification of the Rumination in Cattle Using Support Vector Machines with Motion-Sensitive Bolus Sensors. Sensors (Basel, Switzerland), 19 (5), 1165, DOI: 10.3390/s19051165

Kamminga, J.W., Le, D.V., Meijers, J.P., Bisby, H., Meratnia, N., and Havinga, P.J. (2018) Robust Sensor-Orientation-Independent Feature Selection for Animal Activity Recognition on Collar Tags. Proceedings of the ACM on Interactive, Mobile, Wearable and Ubiquitous Technologies, 2 (1), 1–27, DOI: 10.1145/3191747

Kaufman, E.I., LeBlanc, S.J., McBride, B.W., Duffield, T.F., and DeVries, T.J. (2016) Association of rumination time with subclinical ketosis in transition dairy cows. Journal of dairy science, 99 (7), 5604–5618, DOI: 10.3168/jds.2015-10509

Kononoff, P.J., Lehman, H.A., and Heinrichs, A.J. (2002) Technical Note—A Comparison of Methods Used to Measure Eating and Ruminating Activity in Confined Dairy Cattle. Journal of dairy science, 85 (7), 1801–1803, DOI: 10.3168/jds.S0022-0302(02)74254-9

Martiskainen, P., Järvinen, M., Skön, J.-P., Tiirikainen, J., Kolehmainen, M., and Mononen, J. (2009) Cow behaviour pattern recognition using a three-dimensional accelerometer and support vector machines. Applied Animal Behaviour Science, 119 (1-2), 32–38, DOI: 10.1016/j.applanim.2009.03.005

Mayo, L.M., Silvia, W.J., Ray, D.L., Jones, B.W., Stone, A.E., Tsai, I.C., Clark, J.D., Bewley, J.M., and Heersche, G. (2019) Automated estrous detection using multiple commercial precision dairy monitoring technologies in synchronized dairy cows. Journal of dairy science, 102 (3), 2645–2656, DOI: 10.3168/jds.2018-14738

Miguel-Pacheco, G.G., Kaler, J., Remnant, J., Cheyne, L., Abbott, C., French, A.P., Pridmore, T.P., and Huxley, J.N. (2014) Behavioural changes in dairy cows with lameness in an automatic milking system. Applied Animal Behaviour Science, 150, 1–8, DOI: 10.1016/j.applanim.2013.11.003

Minegishi, K., Heins, B.J., and Pereira, G.M. (2019) Peri-estrus activity and rumination time and its application to estrus prediction: Evidence from dairy herds under organic grazing and low-input conventional production. Livestock Science, 221, 144–154, DOI: 10.1016/j.livsci.2019.02.003

Schmeling, L., Thurner S., Maxa, J., and Rauch, E. (2019) Recording the behaviour of grazing dairy cows to develop a sensor based health monitoring system. In Organising Committee of the 9th European Conference on Precision Livestock Farming and Teagasc, Animal & Grassland Research and Innovation Centre, Eds., Precision Livestock Farming '19: Papers presented at the 9th European Conference on Precision Livestock Farming, Proceedings of the 9th European Conference on Precision Livestock Farming, Cork, Ireland, 26.-29.08.2019, p. 707–713, Fermoy, Cork

Schmeling, L., Elmamooz, G., Hoang, P.T., Kozar, A., Nicklas, D., Sünkel, M., Thurner, S., and Rauch, E. (2021) Sensor-based Monitoring of Lying Behavior in Dairy Cows on Pasture. Computers and Electronics in Agriculture. Under Review

Soriani, N., Panella, G., and Calamari, L. (2013) Rumination time during the summer season and its relationships with metabolic conditions and milk production. Journal of dairy science, 96 (8), 5082–5094, DOI: 10.3168/jds.2013-6620

Stangaferro, M.L., Wijma, R., Caixeta, L.S., Al-Abri, M.A., and Giordano, J.O. (2016a) Use of rumination and activity monitoring for the identification of dairy cows with health disorders: Part III. Metritis. Journal of dairy science, 99 (9), 7422–7433, DOI: 10.3168/jds.2016-11352

Stangaferro, M.L., Wijma, R., Caixeta, L.S., Al-Abri, M.A., and Giordano, J.O. (2016b) Use of rumination and activity monitoring for the identification of dairy cows with health disorders: Part II. Mastitis. Journal of dairy science, 99 (9), 7411–7421, DOI: 10.3168/jds.2016-10908

Werner, J., Leso, L., Umstatter, C., Niederhauser, J., Kennedy, E., Geoghegan, A., Shalloo, L., Schick, M., and O'Brien, B. (2018) Evaluation of the RumiWatchSystem for measuring grazing behaviour of cows. Journal of neuroscience methods, 300, 138–146, DOI: 10.1016/j.jneumeth.2017.08.022

M2M Communication in a Dairy Barn - Identifying Farmers' Needs and Requirements

Jernej Poteko [a,*], Pia Lübke [a], Jan Harms [a]

[a] Institute for Agricultural Engineering and Animal Husbandry, Bavarian State Research Center for Agriculture, 85586 Grub - Poing, Germany

* Corresponding author. Email: jernej.poteko@LfL.bayern.de

Abstract

Digital technologies in the dairy barn produce a lot of data during its operation and provide the information basis for appropriate decisions to be made at the right time. Although many decisions could be based on logical relations of this information, farmers cannot hand over the decision to the technologies due to the lack of machine-to-machine (M2M) communication. This frequently excludes the possibility to adapt the barn technology to the current conditions in the barn without the farmer's direct intervention. The actual requirements for networking and interacting barn technologies from a view of farmers as end user are still scarce. The aim is to identify these requirements through a survey on farmer's expectations, experiences, and barriers of M2M networking and interacting of barn technology. The online survey was answered by dairy farmers in Germany. Nearly 90% of all respondents identified opportunities in the use of a cross-system (herd) management program, e.g. for technology setting. Inter alia, the subset of farmers who are highly familiar with an automatic milking system prioritised feeding operation and cow tracking as a new feature in an (herd) management program among the possible technology settings. Approx. 70% of them (or slightly more than 30% if additional costs are involved) expressed willingness to use the networked operation of milking, feeding, dung removal and barn climate control technologies. Networking of automatic bedding delivery system or cow locating technologies was less attractive (around 50% or under 20% in case of additional investment). The priorities can possibly be attributed to the intensity of the use or the availability of certain technology on the farm. This and further results surround the farmer's requirements on M2M networking in the dairy barn.

Keywords: Digital Barn Technology, M2M Interaction, Networking, Survey

1. Introduction

Nowadays, the digitalisation has a strong impact on the dairy barn technology. This modern technology in the dairy barn not only enables the automation of work processes, but commonly also produce a lot of data during their operations. The increasing use of digital technologies in dairy barn results in an increasing need for communication between devices and/or with farm management system (Ipema et al., 2012). This is where the machine-to-machine (M2M) networking of the barn technology comes into consideration.

The dairy farmers express evidently a strong interest in digital barn technologies, for example, by the increasing number of installed automatic milking systems (AMS) and by the investment interest in upgrading existing technology with digital technology such as automatic feeding systems and herd management programs (Barkema et al., 2015, Egger-Danner et al., 2020, LKV Bayern, 2019). These technologies relieve the farmer the monotonous routine activities and help him to ensure that the (physical) workload does not increase (Schick, 2014). On the other side, new devices require continual support and adjustment. Currently, the farmer takes over this task by deriving settings for these devices and scheduling the work process based on his experience. When several devices in the barn require coordinated interaction, the farmer acts as connector between individual devices.

In practice, communication between devices in the barn is still very limited and the data usually only flows in the direction of the control software or herd management program. Direct data exchange between complex devices such as automatic milking or feeding systems is rarely possible due to different communication standards and incompatibility between manufacturers (Wöber et al., 2014, Tomic et al., 2014). Smaller devices such as dung removal robots or robots for feeding are often overlooked and are not intended for data exchange with other devices. This prevents efficient operation of the devices. The result is "isolated solutions" that often do not pass on information relevant to agricultural processes. The networking of devices from different manufacturers and thus the optimization of agricultural processes is therefore difficult or impossible. Wischenbart (2018) states that the costs for the development and maintenance of data integration from systems of different manufacturers are simply too high due to the large number of available products. Some of them are produced in small quantities, what requires additional expense. Neither producer companies nor farmers are willing to pay for this additional expense. Hence there is a need to cut the Gordian knot and undertake the initial steps to demonstrate the digital barn technology in the sense of M2M.

M2M networking refers to a communication between two or more devices that occurs almost without direct human intervention. The wireless connecting devices between software or data sources aim to provide communication and to enable decision-making processes by using a wide range of communication technologies such as WiFi, LoRaWAN or

cellular communication (Minerva et al., 2015). The dairy farming requires the exchange of data from different systems (e.g. feeding, milking, dung removal, ventilation) and barn internal or external sources (e.g. farm management program, weather forecast) (Ipema et al., 2012, Poteko et al., 2020). Direct data exchange enables the possibility to adapt the barn technology to the current conditions in the barn without the farmer's direct intervention. The new approaches to data analysis such as machine learning (ML) and decision-making algorithms can be developed by taking this work off the farmer's hands and provide the basis for appropriate settings and decisions to be made at the right time (Cockburn, 2020). Unfortunately, the farmers cannot hand over the decision to the individual devices due to the lack of M2M communication (Tomic et al., 2014).

Current on-going research is mainly identifying possibilities for better information of farmers (e.g. sensors for monitoring of animal behaviour, health, …) (Umstätter et al., 2020). Despite a low reflectance by the scientific community, practical experiences indicate a requirement of M2M networking of the barn technology. Based on a survey of milk producers, the networking possibilities and compatibility of new digital technologies with existing technologies and systems would be enormously important for the spread of precision dairy farming (Borchers and Bewley, 2015).

The aim of this study is to identify farmers' needs and requirements for M2M networking of barn technology. For this reason, a survey was conducted to determine the farmers' attitude to the networking of barn technology, with the focus on expectations, experiences, and obstacles to barn technology from the farmers' point of view.

At the Institute of agricultural engineering and animal husbandry at the Bavarian state research centre for agriculture in Germany the experimental field DigiMilch investigates, among other issues, the needs, requirements, and benefits of farmers in relation to the networking of technology in dairy barns. The systematically recorded and evaluated needs and requirements of the networked technology are demonstrated with concrete examples on the project farms during the project, hence the manufacturers can orient development process of barn technology towards the end user.

2. Materials and Methods

2.1. Data collection, data sampling and visualization

The following study present selected issues of M2M requirements with a focus primarily on the importance of an overview of the current device status in the barn and on the possibilities of device settings in a cross-system (herd) management program.

The study based on an online survey on the networking of digital technologies in dairy barns. It was conducted in the period from begin of November 2020 to the end of February 2021. The survey link was shared to the people working on dairy farms by companies in project, project social-media and newsletter, University of Applied Science Weihenstephan-Triesdorf, Germany, and Landeskuratorium der Erzeugerringe für tierische Veredelung in Bayern, Germany.

The survey includes the following elements: the description of the farm situation, such as information about the farmer (e.g. gender, age, residence, education), size of the farm, satisfaction of the farmer with his work, and the barn technology used on the farm, the topics of experiences, expectations and requirements in relation to digital technologies of barn technology. The experiences, expectations, and requirements are asked in the questionnaire, by means of a Likert rating scale. In addition, these questions also offer the option of describing one's own experiences as required in open questions, so that the feedback from practice could be as accurate as possible. The entire data sample included 242 completely answered questionnaires. The subset (n=91) in this study represents the people working on dairy farms in Germany.

The present results are limited to survey participants who have a dairy cattle barn with an AMS in Bavaria (n=93). Likert scales were used to determine the experiences, expectations, and requirements of respondents with the networking of various devices in the barn, as well as their relationship to (herd) management program and its functions. The results are prepared and visualized using the Microsoft 365 Excel program.

3. Results and Discussion

The first results provide an initial impression of the identification of farmers' needs and requirements for M2M networking in a dairy barn. The main question in this context was: which devices should work interactively in a dairy barn? A question in a survey provided possible examples of M2M networking of barn devices. Generally, the majority of respondents would network their devices in the barn (Figure 1). About 70% of the surveyed farmers saw potential for networking between devices of milking, feeding, dung removal and barn climate (e.g. curtains, ventilators). If the M2M networking of this devices would be possible, one third of them would be willing to invest into the M2M networking in their dairy barn additionally.

The automatic bedding delivery system or cow positioning (e.g. with selection gate...) system in interaction with a barn climate system or dung removal system would be used by a half of all surveyed farmers. Whereby, the willingness

to invest in the M2M networking of this areas was less attractive (between 10% and 20% of farmers).

Lower mentions can be attributed to the intensity of the use of certain technology (e.g. several times daily dung removal or milking in contrast to sporadic bedding delivery) or the availability of technology on the farms. AMS or automatic dung removal are more common in Bavarian dairy barns than automatic bedding delivery systems or selection gates (e.g. the straw can be alternatively delivered with mobile technology or in case of free cow traffic no selection gate is needed).
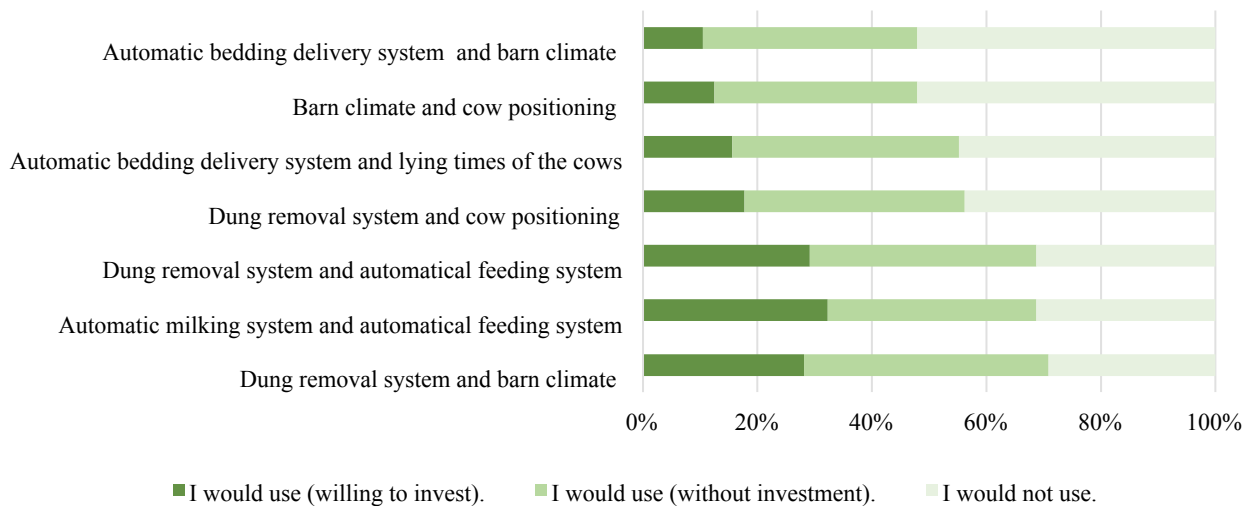
Figure 1: Farmers' requirements for the networking of different barn technologies in dairy farming (n=91).

Almost 90% of all respondent farmers saw opportunities in the use of a cross-system herd management program in their barn, if it would exist. The new required features in the cross-system (herd) management program (additionally to the existing features in their (herd) management program) were chosen in the survey by the farmers from the given examples. The possibility of adjusting individual devices as a new feature in a cross-system (herd) management program were favoured in the areas of feeding and the cow selection (Figure 2). The adjustment of dung removal system or barn climate condition system (e.g. curtains, ventilators) were lower prioritized in such a (herd) management program, but were described as desirable for use by about 70% of the respondents from the networking point of view.
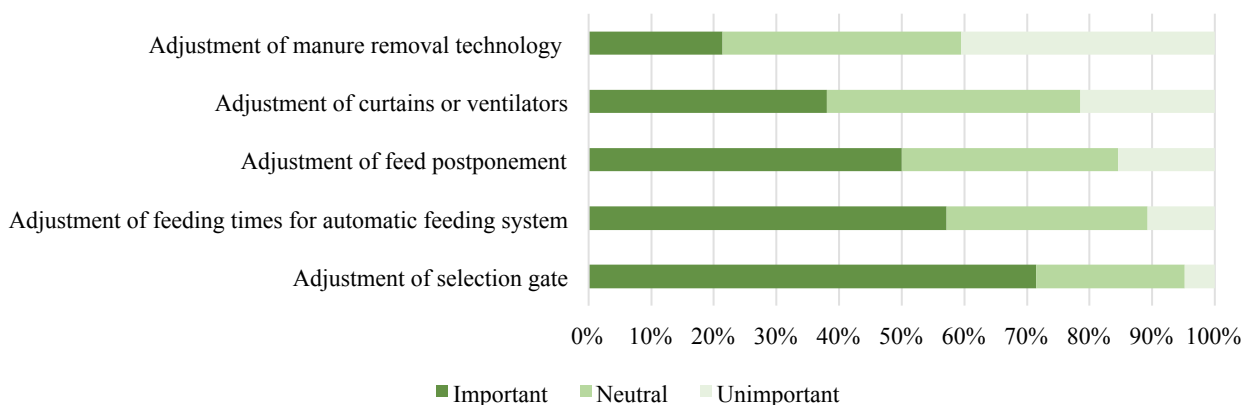
Figure 2: Prioritization of the new features in a herd management program in dairy farming from the farmer's perspective (n=91).

The overviews of device status or of additional information accessed by diverse devices in a cross-system (herd) management program were seen as important features. In none of the examples mentioned in Figure 3 were more than 20% of the farmers recognised it as unimportant. In the context of feeding, more than 70% of respondents attributed an important role to feed delivery. Interestingly, on the other hand the least important role was attributed to overview over

the feed pusher status. From this, it could be deduced that the feed composition and mass were important characteristics for farmers, which they would monitor in a cross-system (herd) management program, than pure process of feed pushing. In general, the importance of features overview - further information related to barn climate, energy consumption or selection of the animals - was classified as neutral by a large part of survived farmers. The reason might be a lack of perception about the (un-) importance of these features, as they are still missing in such an (herd) management program.
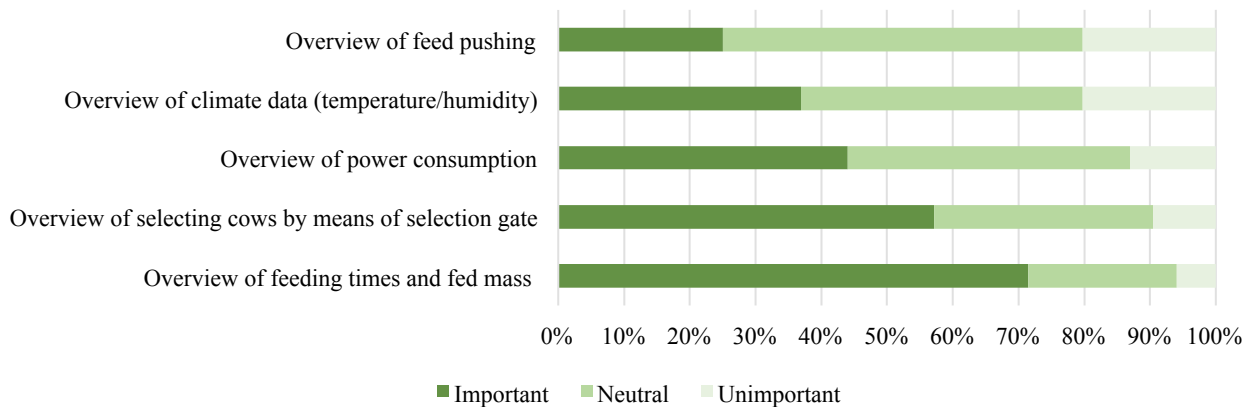
Figure 3: Prioritization of the new features in a herd management program in dairy farming from the farmer's perspective (n=91).

4. Conclusions

Digitalization has now found its way into dairy cattle barns and points to the positive effects on animals, humans, and the environment. Nevertheless, there is a need for development in which the farmer as the end user with practical experience and requirements for the technology must play a central role. The survey on needs of farmers concerning the networking of digital technologies represents a new step on the way of M2M development in the dairy barns.

Acknowledgements

References

Barkema, H. W., M. A. von Keyserlingk, J. P. Kastelic, T. J. G. M. Lam, C. Luby, J. P. Roy, S.J. LeBlanc, G.P. Keefe, D. F. Kelton (2015). Invited review: Changes in the dairy industry affecting dairy cattle health and welfare. Journal of dairy science, 98(11), 7426-7445.

Cockburn, M. 2020. Application and Prospective Discussion of Machine Learning for the Management of Dairy Farms. Animals, 10(9), 1690.

Egger-Danner, C., F. Steininger, M. Suntinger, M. Mayerhofer, M. Koblmüller, F. Grandl, J. Duda, F.-J. Linke, Auer, M. Stegfellner, M. Drillich, F. Papst, O. Saukh, B. Fürst-Waltl, P. Klimek, T. Wittek, 2020. D4Dairy – Datenvernetzung im Kuhstall. In: Digitale Technologien am bäuerlichen Familienbetrieb. Gumpenstein, 22.-23.10.2020.

Ipema, A. H., H. C. Holster, P. H. Hogewerf, E. J. B. Bleumer, 2012. Towards an open development environment for recording and analysis of dairy farm data. Paper presented at ICAR 2012 38th Conference, 28-05-2012 01-062012, Cork Ireland.

LKV Bayern, 2019. Milchleistungsprüfung in Bayern 2019, 55 s.

Minerva, R., A. Biru, D. Rotondi, 2015. Towards a definition of the Internet of Things (IoT). IEEE Internet Initiative, 1(1), 1-86.

Poteko, J., P. Lübke, J. Harms, 2020. DigiMilch: Demonstrationsprojekt 4, Vernetzte Stalltechnik: In: Gandorfer, M., A. Meyer-Aurich, H. Bernhardt, F. X. Maidl, G. Fröhlich, H. Floto (Hrsg.), 40. GIL-Jahrestagung, Digitalisierung für Mensch, Umwelt und Tier. Bonn: Gesellschaft für Informatik e.V. 41-42.

Schick, M. 2014. Arbeitswissenschaft In: Frerichs, Ludger (Hrsg.): Jahrbuch Agrartechnik 2013. Braunschweig: Institut für mobile Maschinen und Nutzfahrzeuge. 1-8.

Tomic, S. D. K., D. Drenjanac, G. Lazendic, S. Hörmann, F. Handler, W. Wöber, K. Schulmeister, M. Otte, W. Auer, 2014. agriOpenLink: Semantic Services for Adaptive Processes in Livestock Farming. In: Proceedings International Conference of Agricultural Engineering, Zurich, 06-10.07.2014 – www.eurageng.eu, C0274

Umstätter, C., D. Martini, F. Adrion, 2020. Opinion Paper: Digital Animal Monitoring–What is on the Horizon?. LANDTECHNIK, 75(1).

Wischenbart, M. 2018. Herausforderungen und Architekturen für Datenintegration in der Landwirtschaft In: Tagungsband 21. Arbeitswissenschaftliches Kolloquium "Arbeit in der digitalen Transformation", 13.-14.3.2018, HBLFA Francisco Josephinum, Wieselburg, 2018, 155-162.

Wöber, W., K.G. Schulmeister, C. Aschauer, A. Gronauer, D.K. Tomic, A. Fensel, T. Riegler, F. Handler, S. Hörmann, M. Otte, W. Auer. 2014. agriOpenLink: Adaptive Agricultural Processes via Open Interfaces and Linked Services. In: Clasen, M., Hamer, M., Lehnert, S., Petersen, B. Theuvsen, B. (Hrsg.), IT-Standards in der Agrar- und Ernährungswirtschaft – Fokus: Risiko- und Krisenmanagement. Bonn: Gesellschaft für Informatik e.V. 157-160.

Unmanned Ground Vehicles in Agriculture: A Bibliometric Review

Johnny Waked[ab*]**, Giuseppe Todde**[a]**, Gabriele Sara**[a]**, Marco Polese**[a]**, Georges Hassoun**[b]**, Filippo Gambella**[a]**,
Maria Caria**[a]

[a] Department of Agricultural Sciences, University of Sassari

[b] Department of Agricultural Engineering and Veterinary Medicine, Lebanese University

* Corresponding author email: jwaked@uniss.it

Abstract

Robotic technologies in agriculture have seen rapid evolution throughout the years. Among these technologies, Unmanned Ground Vehicles (UGV) are becoming increasingly popular especially for on-field monitoring and operational agricultural activities. The introduction of this technology on the field, implemented with specific sensors and components, provides high-accuracy data in line with the precision agriculture principles. Moreover, UGVs may reduce human workload and improves work quality, enabling the automation of agricultural activities. These advantages, increasingly documented in the scientific literature, encounter a lack of reviews on UGVs applied for agricultural purposes. This paper aims to improve the body of knowledge about the application of UGVs in agricultural contexts. Detailed analysis on the interest of the academic community available on Web of Science, Scopus and IEEE Xplore databases was undertaken testing 12 different keywords. In this study, the features of the UGVs available in the market was also evaluated. The results showed that, among the several keywords utilized, the main outcomes were found for terms "Rover" and "Unmanned Ground Vehicles". Across the three scientific search platforms, the studies conducted in this topic area were mostly found as "conference paper". Considering the world distribution of the results for the keywords that included the term "Agriculture", the countries mainly involved were found to be the United States, Italy, India and Spain.

Finally, this paper presented the current challenges and forthcoming trends within the introduction of UGVs in agricultural farms.

Keywords: Rover, Precision Agriculture, Agricultural Engineering, Robotic platform, UGV.

1. Introduction

An Unmanned Vehicle is a device that operates without the human presence on-board, autonomously using artificial intelligence or operated remotely by a human. Unmanned vehicles could be aerial or grounded; the Unmanned Aerial Vehicle (UAV) could fly above obstacles, cross faster and cover a wider area that might not be accessible for the Unmanned Ground Vehicle (UGV). While the UGV could inspect more accurately and closely than the UAV (Tran et al., 2020). These unmanned vehicles could coordinate and function with each other or standalone. These vehicles could be identified with several terms and acronyms other than UGV. According to Scopus, the term "UGV" first appeared in a scientific search in 1974, whereas "rover" appeared in 1896. Other terms newer terms like "agricultural robot" in 1982, "ground robot" in 1994 and "unmanned ground vehicle" in 1991. UGVs are used in space applications, in civilian and commercial activities, as well as for defence and emergency response, for example, during the 2020 pandemic of coronavirus, UGVs were used in Tunisia to enforce new COVID-19 restrictions (Project Ploughshares, 2020). Throughout the time, the use of "UGVs" has been gaining ground for several agricultural and farming practices, ranging from pruning and inspection, disease detection to precise spraying of fertilizers, pesticides, and insecticides (Fotio Tiotsop et al., 2020; Karthik et al., 2018). Other activities that could be accomplished with the use of UGVs are cutting fruits (Rakshitha et al., 2017), mowing (Broderick et al., 2014), field scouting, weed control, harvesting (Quaglia et al., 2019), as well as monitoring animals (Roure et al., 2018; Usher et al., 2015). Depending on their application, these autonomous platforms could be equipped with simple or advanced sensors and equipment such as video and thermal imager, visible and near-infrared cameras, LIDAR, robotic arms and agricultural tools (Bao et al., 2019; Milella et al., 2019; Srisuphab et al., 2019; Wendel and Underwood, 2017).

This paper aims to improve the body of knowledge about the application of UGVs in agricultural contexts. Detailed analysis on the interest of the academic community available on Web of Science, Scopus and IEEE Xplore databases was undertaken testing 12 different keywords. In this study, the main characteristics of the UGVs available in the agricultural domain were also evaluated.

2. Materials and Methods

Unmanned vehicles seemed to show an increase of concern in the scientific community. To study the literature concerning these platforms this study has been structured in two main parts: the first one described and highlights the

trend of topics search for keywords related to UGVs, and their relationship with agriculture; the second one focused on the characteristics of UGVs used in agriculture and available in the market as well as the countries involved in the scientific research. In this study, Scopus, Web of Science, and IEEE Xplore have been chosen as they represent the most reliable scientific database to analyse the main items for a specific set of keywords. Scopus is one of the largest scientific databases of peer-reviewed scientific – literature journals, conference, and books proceedings. While Web of Science's platform provides access to different kind of indexes comprising regional and multidisciplinary citation; specialist subject; patent family; and scientific data sets. Whereas IEEE (Institute of Electrical and Electronics Engineers) Xplore digital library is a resource for technical and scientific publications in computer science, electrical engineering, and electronics. On one hand, a search has been carried out on abstract and citation databases such as Scopus, Web of Science (WoS), and IEEE Xplore on two levels. The first one for a set of keywords related to the term UGVs, while the second one related to the term UGVs and "agriculture", specifically: UGV, UGV and agriculture, Unmanned ground vehicle, Unmanned ground vehicle and agriculture, Robot platform, Robot platform and agriculture, Ground robot, Ground robot and agriculture, Ground robot platform, Ground robot platform and agriculture, Rover, Rover and agriculture.

The analysis has been carried out including different criteria involving: the number of publications per keyword over the years (per year/contribution trend/publication trend); the subject areas (subject area); the document type (document type). All the data concerning the "per year/ publication trend" have been searched for the time frame 2009-2020 due to the increasing interest in these topics in the last years. The most considerable subject areas, obtained for each keyword searched, have been selected for the data analysis. Anyway, the subject area related to the agricultural area has been always included in the results, to show the magnitude of the data obtained.

The data related to the document type has been selected considering the most representative type of document indexed (articles, journals, conference paper, etc.) according to the available time frame covered by each scientific database (Scopus 1896-2020, Web of Science 1985-2020, and IEEE Xplore 1872-2020).

The total number of publications per country were identified for the Scopus database considering the whole years' coverage and putting together all the data obtained for all keywords with the term agriculture. The results have been presented in a Map Chart to determine the countries most involved with scientific research in this topic area. Market research has been carried out to identify the UGVs available for agricultural application. Features and characteristics of the available UGV have been analysed to define the main aptitude of these technologies. Moreover, the interest of the scientific community in the application of effectively available UGVs in agriculture has been analysed using the data gathered from Scopus, Web of Science, and IEEE Xplore.

3. Results and Discussion

3.1 Total number of publications

The number of publications available was much higher for the keywords not including the term "agriculture". The results obtained from the three scientific databases investigated, showed that the highest number of publications were associated with the keywords "rover" followed in order by "robot platform", "UGV", "unmanned ground vehicle", "ground robot" and finally "ground robot platform". Figure 1 shows the percentage of the total number of publications per keyword according to the three scientific databases.

IEEE Xplore shows the highest number of contributions when compared to Scopus and Web of Science for the following keywords: "unmanned ground vehicle and agriculture"; "robot platform and agriculture"; "ground robot and agriculture"; "ground robot platform and agriculture"; "ground robot platform"; "unmanned ground vehicle". For the overall keywords analyzed, the results underlined that Scopus found the highest number of contributions compared to WoS. Table 1 represents the percentage of publications when the searched keywords are associated with the term "agriculture" within the results obtained when searching for the same keywords alone. Scopus and WoS held the highest percentage for the keyword "ground robot platform and agriculture". On Scopus, the second-highest percentage came for "Ground robot and agriculture" with 3.82%, followed by "UGV and agriculture" and for "Unmanned ground vehicle and agriculture" with an average of 3%. On WoS, the second-highest percentage of 2.71 came for "Unmanned ground vehicle and agriculture" and followed with "UGV and agriculture". On IEEE Xplore, the highest percentage of 59.12 came for "Ground robot and agriculture" where 107 publications out of 181 included "agriculture", the second-highest percentage of 16.46 came for "Robot platform and agriculture". Unpredictably, "Rover" keyword with has the highest number of publications had the lowest percentages on Scopus, WoS and IEEE Xplore when the keyword search was associated with agriculture, 0.92%, 0.89% and 1.18% respectively. These results showed that the main outcomes were found for the keywords not including the term "agriculture", underlining that the scientific community is mostly oriented on studies related to other aspects (e.g. technical issues, design and development, path planning, etc.) rather than on-field agricultural applications.
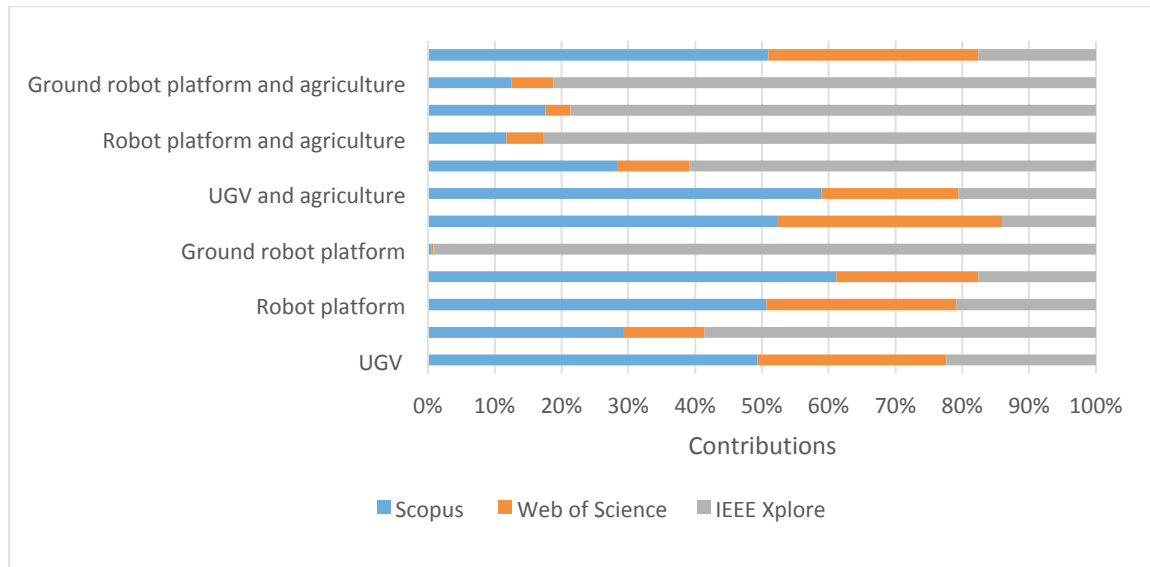
Figure 1. Percentage of the total number of contributions per keyword(s) according to Scopus, Web of Science, and IEEE Xplore

Table 1 Percentage of the contributions per keyword associated with agriculture compared to the keyword(s) search alone in the three different scientific databases

Keyword(s)	Scopus	Web of Science	IEEE Xplore
UGV and agriculture	3.03	1.84	2.33
Unmanned ground vehicle and agriculture	2.99	2.71	3.18
Robot platform and agriculture	0.96	0.81	16.46
Ground robot and agriculture	3.82	2.28	59.12
Ground robot platform and agriculture	50.00	50.00	1.90
Rover and agriculture	0.92	0.89	1.18

3.2 Number of publications per year

Figure 2 highlights the yearly number of results on each of the three scientific databases per keyword. The results were arranged into 2 columns, showing the publication trends, over the last 11 years, of the 12 keywords investigated, containing or not the term agriculture. Overall, an increase from 2009 to 2020 has been found for all the keywords investigated. The highest growth was found for "Ground Robot" and "Agriculture" keywords on IEEE Xplore showing an increase of 35 times. The results obtained clearly show how the keywords that did not include the term agriculture already had a consistent presence of published scientific articles in the past years. Moreover, observing the keywords that also included the term agriculture, there was a considerable increase in the number of publications, mostly in the last 5 years.
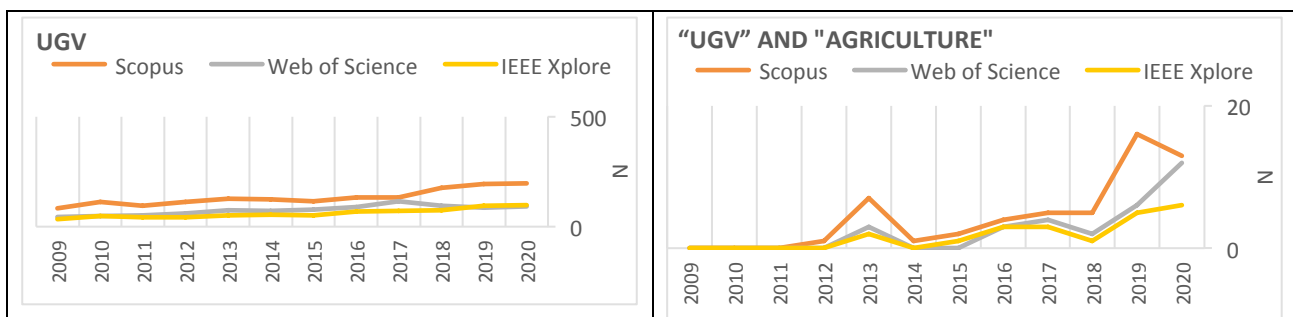
Figure 2. Yearly number of contributions per keyword(s) and per keyword(s) associated with "agriculture" according to Scopus, Web of Science, and IEEE Xplore (N = number of publications)

3.3 Number of publications per subject area

This section will show the number of publications of the keyword(s) alone, then annexed in the search with "agriculture" across the three scientific databases. For the "UGV" keyword, agriculture and related fields represent 0.49% of total subject areas on Scopus, while in WoS 0.41% which both came last among other areas, and in IEEE Xplore none is found. As for "UGV" and "Agriculture" keywords, agriculture and related fields represent 11.39% of total subject areas on Scopus, while in WoS 22.72% which are the lowest in their categories and in IEEE Xplore 30.55% which came equally as "mobile robots" subject area. For "Unmanned Ground Vehicle" agriculture and related fields came last and represent 0.53% of total subject areas on Scopus, while in WoS and IEEE Xplore none were found. As for "Unmanned Ground Vehicle" and "Agriculture" keywords, agriculture and related fields represent 12.24% of

total subject areas on Scopus, while in WoS 20% which are the lowest in their categories and in IEEE Xplore 34.01% which came second after "autonomous aerial vehicles" subject area. For the "Robot platform" keyword, agriculture and related fields came last and represent 0.77% of total subject areas on Scopus, while in WoS and IEEE Xplore none is found. As for "Robot platform" and "Agriculture" keywords, agriculture and related fields represent 11.76 % of total subject areas on Scopus found third after "engineering", while in WoS it's 10% which was found last in its categories and in IEEE Xplore 52.04 % which came first. For the "Ground robot" keyword, agriculture and related fields came last and represent 0.55% of total subject areas on Scopus, while in WoS and IEEE Xplore nothing is found. As for " Ground robot " and "Agriculture" keywords, agriculture and related fields represent 15.79% of total subject areas on Scopus, while in WoS 28.57% which are the lowest in their categories and in IEEE Xplore 24.54% which came first among the subject areas. For "Ground robot platform" keyword, agriculture and related fields are found on any platform. As for "Ground robot platform" and "Agriculture" keywords, agriculture and related fields were found the first subject area and only on IEEE Xplore representing almost the half of total subject areas by 47.62%.

Table 2. Number of publications per subject area across Scopus, WoS and IEEE Xplore for the selected keywords

Database	Subject area	"UGV"	"UGV" and "Agriculture"	"Unmanned Ground Vehicle"	"Unmanned Ground Vehicle" and "Agriculture"	"Robot platform"	"Robot platform" and "Agriculture"	"Ground robot"	"Ground robot" and "Agriculture"	"Ground robot platform"	"Ground robot platform" and "Agriculture"	"Rover"	"Rover" and "Agriculture"
Scopus	Engineering	1,484	27	1,828	34	1,527	12	547	17	4	2	6,478	33
	Computer Science	1,299	31	1,506	36	1,604	14	512	15	2	2	2,733	32
	Mathematics	659	12	787	16	487	4	197	5	1	1	939	7
	Agricultural and Biological Sciences	17	9	22	12	28	4	7	6	0	0	602	9
	Earth and Planetary Sciences	37	2	35	1	17	0	10	0	0	0	3,134	5
Web of Science	Engineering electrical electronic	445	2	374	0	463	3	84	1	1	0	1,040	0
	Robotics	416	7	328	6	556	3	106	3	1	1	893	7
	Automation control systems	343	3	280	2	411	3	71	2	2	1	679	0
	Computer science artificial intelligence	289	6	222	5	407	3	56	1	1	1	726	0
	Agriculture	5	5	0	4	0	1	0	2	0	0	0	6
	Engineering aerospace	33	0	0	0	0	0	6	0	0	0	1,170	0
	Engineering	0	0	0	0	0	0	0	0	0	0	0	16
IEEE Xplore	Agriculture	0	11	0	67	0	102	0	100	0	10	0	18
	Mobile robots	458	11	1130	31	524	68	125	53	445	7	736	9
	Remotely operated vehicles	435	7	1165	23	0	12	18	18	120	4	79	2
	Autonomous aerial vehicles	151	7	1958	76	0	23	38	42	168	4	0	0
	Robot vision	138	3	422	21	187	26	64	32	176	2	174	3
	Path planning	137	4	383	11	118	16	41	16	94	2	233	0
	Humanoid robots	0	0	0	0	125	0	0	0	34	0	0	0
	Planetary rovers	0	0	0	0	0	0	0	0	0	0	1,236	5
	Mars	0	0	0	0	0	0	0	0	0	0	512	1

For "Rover" keyword, agriculture and related fields came last and represent just 4.65% of total subject areas on Scopus, where it is only found on this platform. As for "Rover" and "Agriculture" keywords, agriculture and related fields represent 12.16% of total subject areas on Scopus and came third, while in WoS 16.67% which is the lowest in their categories as well and in IEEE Xplore 54.54% which came first among the subject areas, this could be explained by the interest in publishing documents having agriculture, agricultural machinery, horticulture, crops, and agricultural robots as subject areas on IEEE Xplore.

3.4 Distribution of publications per document type and per Country

This part highlights the total number of publications, of each keyword tested, per document type. The results

illustrated that, across the three scientific databases, about 75% of the publications were published as conference paper, while only 25% is published as article or review paper. IEEE Xplore held the highest number of contributions published as conference paper (90%). The keywords "Ground robot platform" including or not the term agriculture showed 100% of publications as conference paper in Scopus and WoS databases. The keywords "Rover" also when associated with the term agriculture, held the highest contribution as articles compared to the other tested keywords in Scopus and WoS.

Figure 3 shows the number of publications per Country for the keywords including the term agriculture according to Scopus database.
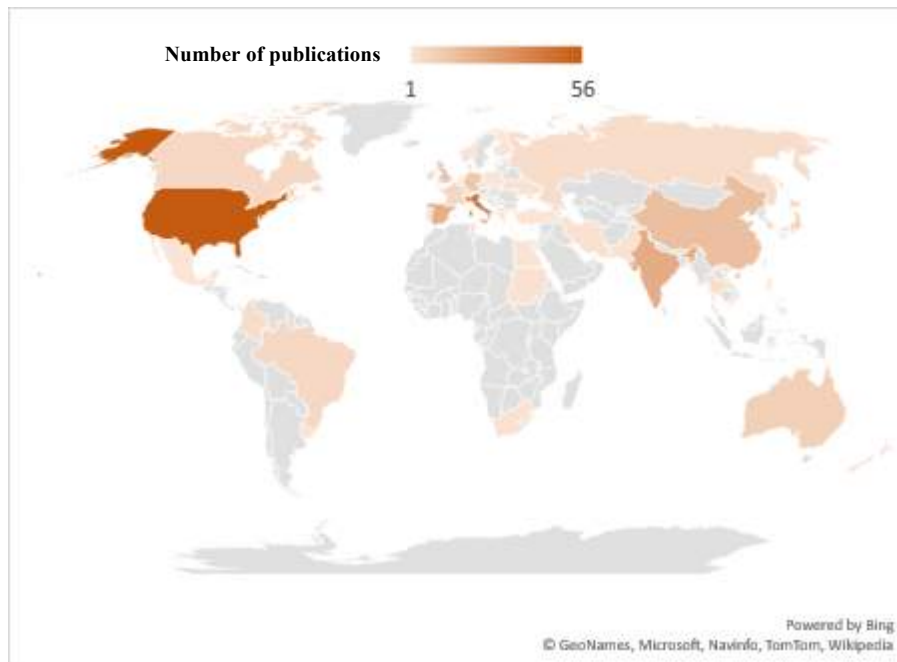
Figure 3. Number of publications per Countries for the keywords including the term agriculture according to Scopus

These all-time results for the selected keywords show the highest interest found in the United States with 56 publications, followed by Italy with 44 publications, India 23, Spain 22, China and the United Kingdom 16 and Germany 13. A total number of 42 countries follow the previous list with fewer publications ranging from 9 to 1.

Most of the countries involved in scientific research having the highest number of publications belong to the countries with developed economies, except India and China according to United Nations' country classification in 2020.

3.5 Technical specifications and key studies indexed on agricultural domain UGVs

Table 3 shows the main features of the analyzed agricultural UGVs which largely differ from each other. One of the first features that most distinguishes these robots were the dimensions. The biggest UGVs were found to be Bonirob, Thorvald, and Robot Dino, reaching up to 3000 mm of width, while Robot OZ was the smaller one. Regarding the traction system, all the UGVs were equipped with 4-wheel drive except the XBot which was found to be an all-terrain tracked robot. The maximum working speed ranged between 1.8 to 18 km/h. the overall UGVs analyzed were powered by batteries, where Bonirob was also equipped with a fuel generator, while Vitirover was furnished with photovoltaic solar panels.

The main topics studied across Scopus, WoS and IEEE Xplore for the agricultural domain UGVs are discussed below. Husky robot held the highest number of references (32) followed by Bonirob (12) and Thorvald (5). Clearpath's Husky platform has been developed in agriculture with an Autonomous Driving Systems Using State Estimator with Multi-rate Sampled data collected by an onboard sensor (Jin et al., 2019). The accuracy of posture detection was improved with a specific Kalaman filter (Lin et al., 2018) while driving it indoors and outdoors on several surfaces (Dogru and Marques, 2018). Franco et al. (2019) embedded a new algorithm for visual path, while Gopi et al. (2017) worked to develop a prototype for gesture-based communication between untrained humans and mobile robots. Husky robot has been widely used for monitoring activities in polluted and contaminated soils (Akhil et al., 2019; west et al., 2019), for localization, mapping, and planning (Abdul-Rahman et al., 2019; Lenac et al., 2017; Wang et al., 2013).

The main research topics studied with the use of Bonirob, an autonomous robot for plant phenotyping, deals, in the first stage, with mapping of plant diseases based on spectral imaging information, navigation and plant-sensors also

using a 3D LIDAR (Ruckelshausen et al., 2009; Rahe et al., 2010; Weiss et al., 2010; Wunder et al., 2011). Moreover, Peveling and Schulze (2011) presented a sensor system based on Ultra-Wideband-RADAR which can evaluate the properties and dimensions of the plants.

Table 3. Main features, power, performances, and communication of the agricultural domain UGVs

	Robot	XBOT	BONIROB	VITIROVER	WARTHOG	HUSKY	THORVALD	ROBOTNIK	WEEDING ROBOT OZ	WEEDING ROBOT DINO	VINEYARD ROBOT TED
Main Features	Dimensions (L x W x H) [mm]	1250 x 1266 x 723	2800 x 2400 x 2200	750 x 390 x 290	1520 x 1380 x 830	991 x 671 x 370	1500-1750 x 1000-3000 x 825	720 x 614 x 417	130 x 47 x 83	2500 x 1400 – 1800 x 1300	450 x 142-185 x 200
	Ground Clearance [mm]	350	-	-	254	127	Variable	-	7	-	-
	Weight [Kg]	500	1100	20	280	50	180	65	150	800	1700
	Traction system	All Terrain Tracks	4 Wheel Drive	4 Wheel Drive	4 Wheel Drive	4 Wheel Drive	4 Wheel Drive	4 Wheel Drive	4 Wheel Drive	4 Wheel Drive	4 Wheel Drive
	Max Payload [kg]	350	150	-	272	75	250	65	90-300	-	-
	Max Speed [km/h]	3	5.4	1.8	18	3.6	5.4	10.8	1.8	4	4
	Climb capacity	< 40°	-	< 8.53°	< 45°	< 45°	-	< 45°	< 5.71°	-	-
Power Performances	Total Power [W]	4800	-	~20	192- 480	192	2000	2000	-	-	-
	Power Options	Battery Pack	Battery Pack, Fuel generator	Solar panel+ battery pack	Battery Pack	Battery Pack	Battery Pack	Battery Pack	Battery Pack	Battery Pack	Battery Pack
Communication	Communication Interface	USB, RS-232, Wi-Fi, Ethernet, CAN bus, RC pulses	USB (6 ports outside, up to 14 ports inside), WiFi (2.4 & 5 GHz), Bluetooth 4.0	-	Ethernet, USB, Remote Control, Wi-Fi	-	I/O ports and CANbus	WiFi 802.11n Internal: USB, RS232, GPIO y RJ45	Communication with user via text message	text message communication with anti-theft tracking device	communication via SMS and anti-theft tracking device

Another work illustrated how the Bonirob system was employed for the task of mechanical weed control in organic farming and the determination of soil parameters (Michaels et al., 2012; Scholz et al., 2016). To evaluate which configuration can be used to distinguish root plants and weeds through the use of specific sensors, images were acquired with the autonomous field robot Bonirob (Haug and Ostermann, 2015a-b; 2016; Knoll et al., 2016). Lastly, Fleckenstein et al. (2017) studied the path planning problem for BoniRob agricultural robot with adjustable relative wheel positions to increase the navigation capabilities. Thorvald platform was developed as a versatile and modular robot for a wide variety of agricultural operations such as seeding, weeding, and harvesting. It can carry a large variety of tools and is lightweight so that it can operate during wet periods without being stuck or damaging the structure of the soil (Grimstad et al., 2016). Moreover, Grimstad and From (2016, 2017a, 2017b, 2018a, 2018b) presented detailed studies on the characteristics of the hardware and software components of the Thorvald II mobile robotic platform.

4. Conclusions

The present bibliometric review illustrates the literature evolution of Unmanned Ground Vehicles and their application with the agriculture domain. This study showed an increasing interest of the scientific community with the topics related to the autonomous robot in agriculture throughout the time (2009 - 2020), where the main findings are reported as follow:

- The keywords that resulted more used was "Rover" including or not the term "Agriculture" compared to the other keywords tested;
- Across the three scientific databases utilized in this study, main results were found in the subject area related to

Engineering fields;

- Analysing the number of the studies developed on these topics, the document type much published was found the conference paper (75%) rather than articles or reviews;
- The all-time results for the selected keywords, which included the term agriculture, showed that the highest interest was found for the United States followed by Italy and India;
- The main characteristics of the UGVs implemented in the agricultural context highlights a high variability in terms of size, weight and max speed, while the main traction system and power source adopted were the 4 wheels drive and the battery pack, respectively.

Concluding, this bibliometric review aims to motivate and promote the interest of the scientific community towards the design, development and application of autonomous robots in the agricultural sector. These technologies represent a valuable opportunity for farms to implement precision agriculture practices in their production system.

Acknowledgements

References

1. Abdul-Rahman, S., Razak, M. S. A., Mohd Mushin, A. H. B., Hamzah, R., Bakar, N. A., & Aziz, Z. A. 2019. Simulation of simultaneous localization and mapping using point cloud data. *Indonesian Journal of Electrical Engineering and Computer Science, 16*(2), 941-949. doi:10.11591/ijeecs.v16.i2.pp941-949

2. Bao, Y., Zarecor, S., Shah, D. *et al.* 2019. Assessing plant performance in the Enviratron. *Plant Methods* 15, 117, https://doi.org/10.1186/s13007-019-0504-y

3. Broderick, J.A., Tilbury, D.M. & Atkins, E.M. 2014. Optimal coverage trajectories for a UGV with tradeoffs for energy and time. *Auton Robot* 36, (pp. 257–271), https://doi.org/10.1007/s10514-013-9348-x

4. Dogru, S. & Marques, L. 2018. A Physics-Based Power Model for Skid-Steered Wheeled Mobile Robots. *IEEE Transactions on Robotics,* vol. 34, no. 2. (pp. 421-433). doi: 10.1109/TRO.2017.2778278

5. Fleckenstein, F., Dornhege, C. & Burgard, W. 2017. Efficient path planning for mobile robots with adjustable wheel positions. *Proceedings - IEEE International Conference on Robotics and Automation*. (pp. 2454).

6. Fotio Tiotsop, L., Servetti, A. & Masala, E. 2020. An integer linear programming model for efficient scheduling of UGV tasks in precision agriculture under human supervision. *Computers and Operations Research, vol. 114.*

7. Franco, I. J. P. B., T. T. Ribeiro and A. G. S. Conceição. 2019. A Novel Approach for Parameter Extraction of an NMPC-based Visual Follower Model. *19th International Conference on Advanced Robotics (ICAR)*, Belo Horizonte, Brazil, 2019. (pp. 117-122). doi: 10.1109/ICAR46387.2019.8981666

8. Gopi, S., Muir, A. & Bhavani, R.R. 2017. Naturalistic gestures based Human Robot Interaction on a UGV for outdoor use. *2017 1st International Conference on Electronics, Materials Engineering and Nano-Technology, IEMENTech 2017*. (pp. 1-6). doi: 10.1109/IEMENTECH.2017.8077017

9. Grimstad, L., Pham, C.D., Phan, H.T. & From, P.J. 2016. On the design of a low-cost, light-weight, and highly versatile agricultural robot. *Proceedings of IEEE Workshop on Advanced Robotics and its Social Impacts, ARSO*, Lyon, 2015. (pp. 1-6). doi: 10.1109/ARSO.2015.7428210

10. Grimstad, L., & From, P. J. 2017a. The thorvald II agricultural robotic system. *Robotics, 6*(4) doi:10.3390/robotics6040024

11. Grimstad, L., & From, P. J. 2017b. Thorvald II - a modular and re-configurable agricultural robot. Paper presented at the *IFAC-PapersOnLine, , 50*(1) 4588-4593. doi:10.1016/j.ifacol.2017.08.1005

12. Grimstad, L., & From, P. J. 2018a. Software components of the thorvald II modular robot. *Modeling, Identification and Control, 39*(3), 157-165. doi:10.4173/mic.2018.3.2

13. Grimstad, L., & From, P. J. 2018b. A configuration-independent software architecture for modular robots. Paper presented at the *2018 International Conference on Reconfigurable Mechanisms and Robots, ReMAR 2018 - Proceedings,* doi:10.1109/REMAR.2018.8449834

14. Haug, S. & Ostermann, J. 2015a. Plant classification for field robots: A machine vision approach. *Computer Vision and Pattern Recognition in Environmental Informatics*. (pp. 248-272).

15. Haug, S. & Ostermann, J. 2015b. A crop/weed field image dataset for the evaluation of computer vision based precision agriculture tasks. *Conference: European Conference on Computer Vision.* (pp. 105-116). DOI: 10.1007/978-3-319-16220-1_8.

16. Jin, Y., Han, S., Lee, E.M., Lee, S.M., Shin, C. & Yun, J. 2019. Development of Autonomous Driving Systems Using State Estimator with Multi-rate Sampled-data. *2019 IEEE International Conference on Consumer*

Electronics, ICCE 2019. (pp. 1-6). doi: 10.1109/ICCE.2019.8661985

17. Karthik, M., Singh, N., Sinha, E., Anand, B.S. & Gowreesh, S.S. 2018. Design and development of unmanned chemical spraying rover for agriculture application. *International Journal of Engineering and Advanced Technology, vol. 8, no. 2*. (pp. 18-21).

18. Knoll, F.J., Holtorf, T. & Hussmann, S. 2016. Investigation of different sensor systems to classify plant and weed in organic farming applications. *Proceedings of 2016 SAI Computing Conference, SAI 2016. (*pp. 343).

19. Lenac, K., Kitanov, A., Cupec, R., & Petrović, I. 2017. Fast planar surface 3D SLAM using LIDAR. *Robotics and Autonomous Systems, 92*, 197-220. doi:10.1016/j.robot.2017.03.013

20. Lin, W., Ren, X., Hu, J., He, Y., Li, Z. & Tong, M. 2018. Fast, robust and accurate posture detection algorithm based on Kalman filter and SSD for AGV. *Neurocomputing,* vol. 316. (pp. 306-312).

21. Michaels, A., Albert, A., Baumann, M., Weiss, U., Biber, P., Kielhorn, A. & Trautz, D. 2012. Approach towards robotic mechanical weed regulation in organic farming", *Informatik aktuell*. (pp. 173).

22. Milella, A., Reina, G. & Nielsen, M. 2019. A multi-sensor robotic platform for ground mapping and estimation beyond the visible spectrum. *Precision Agriculture*, vol. 20, no. 2. (pp. 423-444).

23. Peveling-Oberhag C., Schulze Lammers P. 2011. In-Soil measuring of root-crop properties using UWB-RADAR. *Conference Agricultural Engineering 2011, Land.Technik - AgEng 2011, VDI-MEG*. (pp. 423-430). Hannover.

24. Project Ploughshares. 2020. Using drones and UGVs to fight COVID-19—but then what? https://ploughshares.ca/2020/04/using-drones-and-ugvs-to-fight-covid-19-but-then-what/. Accessed 25 April 2020.

25. Quaglia G., Visconte C., Scimmi L.S., Melchiorre M., Cavallone P., Pastorelli S. 2019. Design of the positioning mechanism of an unmanned ground vehicle for precision agriculture. In: Uhl T. (eds) *Advances in Mechanism and Machine Science. IFToMM WC 2019. Mechanisms and Machine Science, vol 73.* Springer, Cham.

26. Rahe, F., Heitmeyer, K., Biber, P., Weiss, U., Ruckelshausen, A., Gremmes, H., Klose, R., Thiel, M., Trautz, D. 2010. First field experiments with the autonomous field scout BoniRob. *Proceedings 68th International Conference Agricultural Engineering 2010*. (pp.419 – 424).

27. Rakshitha, N., Rekha, H.S., Sandhya, S., Sandhya, V. & Sowndeswari, S. 2017. Pepper cutting UGV and disease detection using image processing. *RTEICT 2017 - 2nd IEEE International Conference on Recent Trends in Electronics, Information and Communication Technology, Proceedings*. (pp. 950).

28. Ruckelshausen, A., Biber, P., Dorna, M., Gremmes, H., Klose, R., Linz, A., Rahe, R., Resch, R., Thiel, M., Trautz, D. & Weiss, U. 2009. BoniRob: An autonomous field robot platform for individual plant phenotyping. *Precision Agriculture 2009 - Papers Presented at the 7th European Conference on Precision Agriculture, ECPA 2009*. (pp. 841).

29. Roure, F., Moreno, G., Soler, M., Faconti, D., Serrano, D., Astolfi, P., Bardaro, G., Gabrielli, A., Bascetta, L., Matteucci, M. 2018. GRAPE: Ground Robot for vineyArd Monitoring and ProtEction. In: Ollero A., Sanfeliu A., Montano L., Lau N., Cardeira C. In ROBOT 2017 (eds), *Third Iberian Robotics Conference. ROBOT 2017. Advances in Intelligent Systems and Computing,* vol 693. Springer, Cham

30. Scholz, C., Ferhadbegovic, B., Hinck, S., Litfin, T. & Ruckelshausen, A. 2016. Model-based efficiency analysis for the determination of soil parameters using the autonomous field robot BoniRob. *Lecture Notes in Informatics (LNI), Proceedings - Series of the Gesellschaft fur Informatik (GI)*. (pp. 185).

31. Srisuphab, A., Silapachote, P., Tantratorn, W., Krakornkul, P. & Darote, P. 2019. Insect Detection on an Unmanned Ground Rover. *IEEE Region 10 Annual International Conference, Proceedings/TENCON* (pp. 954).

32. Tran, V.P., Garratt, M. & Petersen, I.R. 2020. Switching time-invariant formation control of a collaborative multi-agent system using negative imaginary systems theory. *Control Engineering Practice, vol. 95*.

33. Usher, C., Daley, W., Webster, A.B., & Ritz, C.W. 2015. A Study on Quantitative Metrics for Evaluating Animal Behavior in Confined Environments. doi:10.13031/aim.20152190148

34. Wang, S., Panzica, A. C., & Padir, T. 2013. Motion control for intelligent ground vehicles based on the selection of paths using fuzzy inference. Paper presented at the *IEEE Conference on Technologies for Practical Robot Applications, TePRA,* doi:10.1109/TePRA.2013.6556354

35. Weiss, U., Biber, P., Laible, S. & Zell, A. 2010. Plant detection, mapping and differentiation for autonomous agricultural robots", *4th International Conference on Cognitive Systems, CogSys 2010*.

36. Wendel, A. & Underwood, J. 2017. Illumination compensation in ground based hyperspectral imaging, ISPRS. *Journal of Photogrammetry and Remote Sensing, 129* (pp. 162-178).

37. Wunder, E., Ruckelshausen, A., Klose, R., Thiel, M., Kielhorn, A. 2011. GIS- and sensor-based technologies for individual plant agriculture. *Proceedings 69th International Conference Agricultural Engineering, 2011, VDI-Verlag*, pp. 493-498, ISSN 0083-5560.

Design and Evaluation of Two New Seed Chutes for a Stanhay Webb Precision Seed Drill using Discrete Element Modelling.

William J Hook [a], David R White [a,*]

[a] Engineering Department, Harper Adams University, Newport, Shropshire, UK

* Corresponding author. drwhite@harper-adams.ac.uk

Abstract

Stanhay Webb Ltd, UK design and manufacture precision seed drills for over 200 different types of produce. In order to improve the performance of a Stanhay Pro Air Multiline drill whilst seeds are transferred to the soil, two new seed chutes made from 3D printed ABS plastic, and stainless-steel were designed. Altair EDEM Discrete Element Modelling (DEM) simulation software was used to evaluate the new designs at forward speeds of 1.0 m s^{-1}, 1.5 m s^{-1}, and 2.0 m s^{-1} with carrot and cabbage seeds. One-way and two-way ANOVA tests were used to evaluate the QFI, Miss Index, Multiples Index, and CP3 values for each seed chute. The ABS 3D printed chute performed best with the highest QFI value of 99.1%, the lowest Multiples index of 0.47%, and the lowest Miss Index of 0.47%, and the highest CP3 value of 87.6%.

Keywords: seed metering, precision seeder, Discrete Element Modelling.

1. Introduction

Precision seed drills typically consist of a hopper which carries the seed, a metering mechanism to sow the seeds evenly, a coulter which opens up the soil, and a device to cover and consolidate the soil over the seed. One of the most precise and reliable seed metering mechanisms at picking up and transferring seed with a uniform seed spacing is a vacuum metering device. Stanhay Webb Ltd produce a range of such drills, Figure 1.
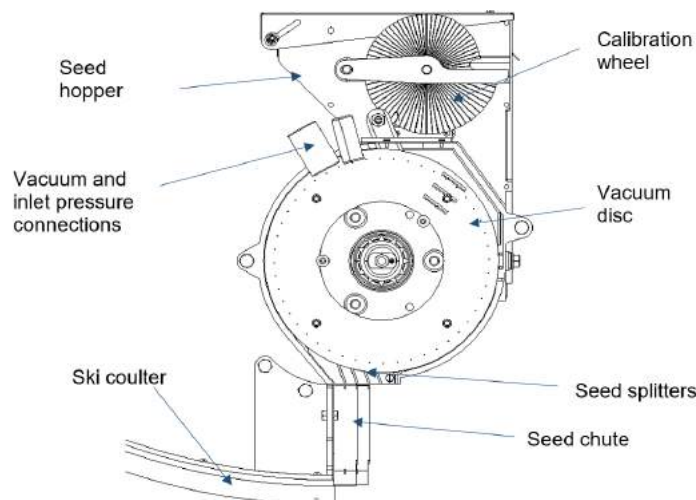
Figure 1. Stanhay Webb Ltd Pro Air Multiline Pneumatic Precision Seed Drill.

The ski coulter produces three furrows and the seed chute device containing three separate chutes drops the seed into each of the furrows. This is known as a 'multiline' precision seed drill. One problem is that when lighter seeds, such as carrot seed, pass through the seed chutes from the seed splitters, the seed spacing achieved by the vacuum disc is reduced.

Seed spacing uniformity is expressed by a series of indices, namely; Miss Index, the absence of a seed where there should theoretically be one; Multiples, the presence of two seeds or more where there should only be one (spacings less than 0.5 times the theoretical seed spacing are a recorded as a multiple); the Quality of Feed Index (QFI) which is the ratio of normally sown seeds to the number of intervals (ISO, 2020; BSI, 1988); and the Coefficient of Precision (CP3). CP3 is the percentage of seeds which fall within ±1.5 cm of the theoretical seed spacing (Mapoka *et al.*, 2018; Searle *et al.*, 2008; Smith and Kocher, 2008).

Bracy *et al.* (1999) stated that a minimum value of 85% for the QFI is acceptable for precision seeders such as the Stanhay Pro Air, while other authors have argued that this should be a minimum of 95% (Bateman, 1972; Halderson, 1983; Snyder and Hummel, 1985; Irla and Heusser, 1991). Önal (2006) states that the upper limit of the Miss and

Multiples index should be 4.75% for precision seed drills.

This paper discusses research designed to improve the seed spacing uniformity for a Stanhay Pro Air Multiline precision seed drill by designing and evaluating two new seed chutes using Altair EDEM discrete element method (DEM) software.

2. Materials and Methods

Two new chutes, a stainless-steel, and a Acrylonitrile Butadiene Styrene (ABS) 3D printed chutes were designed and evaluated against the current stainless-steel design, using Altair EDEM software with carrot and cabbage seeds, at forward speeds of 1.0 m s^{-1}, 1.5 m s^{-1}, and 2.0 m s^{-1} since these are the most common speeds for drilling carrot and cabbage seeds. The three chute designs are shown in Figure 2.

Figure 2. The 3D models (from L to R) of the original stainless-steel design, the improved stainless-steel design, and the ABS 3D printed design with acetone smoothing.

Random variability such as particle position and particle size were integrated into the simulation, so that each seed had a unique inherent behaviour and dimension.

Each of the seed chute designs were modelled using Solidworks. These, together with the complete drill unit (Figure 3), were then imported into the Altair EDEM simulation software as a STEP file.

Updated seed chute design
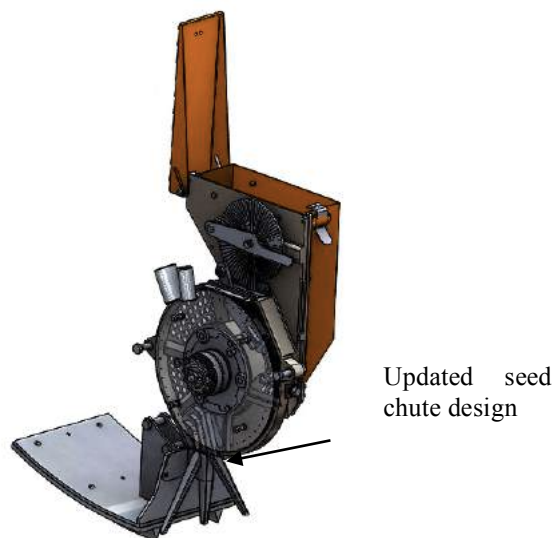
(Source: Stanhay Webb Ltd)

Figure 1. 3D CAD model of the Stanhay Pro Air Multiline drill unit used for the Altair EDEM Simulation.

2.1 Material properties

A Poisson's ratio of 0.4 was used for this study for both carrot and cabbage seeds. The bulk density of carrot seeds were determined to be 357 kg m^{-3} (Gautam *et al.*, 2016) and those for cabbage seeds were determined to be 732 kg m^{-3} (Jadhav *et al.*, 2017).

The Modulus of Elasticity and bulk density for the stainless-steel 316 was 190 GPa and 7610 kg m^{-3} respectively and the values for ABS plastic were 2.08 GPa and 1030 kg m^{-3} (CES EduPack, 2019). The Poisson's ratio values used were 0.265 for stainless-steel 316 (AZO Materials, 2020) and 0.35 for ABS plastic (Engineers Edge LLC, 2020).

For cabbage seeds interacting with steel, the coefficient of restitution, e, and the coefficient of static friction, μ_s, were quoted as being 0.93 and 0.32 respectively (Saracoglu and Ozarslan, 2012). The rolling friction value, μ_r, for cabbage seeds had not been determined, but Kaliniewicz *et al.* (2015) stated that the value for agricultural seeds in contact with steel was in the range of 0.277 and 0.353, with a pea seed having a μ_r value of 0.286. Hence, this value was used for the rolling friction between the cabbage seed and the stainless-steel, since a pea seed has similar sphericity to cabbage seed.

For carrot seeds, the e value could not be found in literature. A value of 0.1 was used, based on Jinwu *et al.* (2017) findings for maize seed. Gautam (2016) concluded that the μ_s value for carrot seed was 0.86 for interactions with stainless-steel surfaces. Due to the non-spherical shape of carrot seed the coefficient of rolling friction of carrot seed was not included. For the interactions of the seeds with the ABS material, the coefficient of static friction was reduced in accordance with the findings of Ivkovic *et al.* (2000).

2.2 Defining particle geometry in Altair EDEM

Huang *et al.* (2018), Ramírez-Aragón *et al.* (2018), and Abbaspour-Fard (2000) all used the Hertz-Mindlin (no slip) model to predict seed behaviour. It was therefore employed in this study. The particle contact and behaviour particles of carrot and cabbage seeds were constructed in the Altair EDEM simulation software using spheres.

A sample of seeds were measured and the dimensions were used to construct the particles in Altair EDEM. Since the sphericity value of cabbage seed is high, this was modelled as a sphere with a radius of 1000 μm. The carrot seeds were created using the multi-sphere method also adopted by Han *et al.*, (2018) using 32 spheres each with a radius of 400 μm. The two particles are shown in Figure 4.
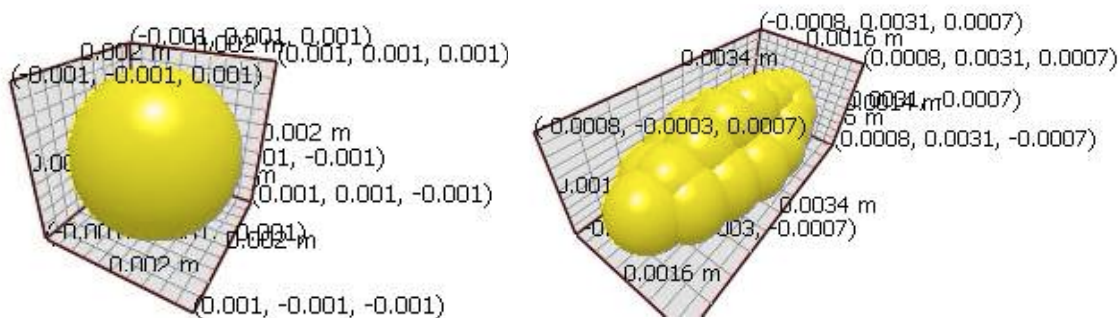
Figure 2. The 3D models of a cabbage seed (left) and carrot seed (right) used in the Altair EDEM software.

To account for the random variability associated with the samples of this study, the dimensions of the seeds had a standard distribution of ±0.05 standard deviations from the mean size. 288 seeds were entered into each simulation.

3. Results

Results were exported as csv files and the measurements of particles positions were given as the measures between the geometric centres (±0.00001 mm) of two adjacent seeds in Cartesian form (x and y value) as per BS 6978-2:1990 and ISO 7256-2:1984. The particle positions were plotted on a scatter plot; an example is shown in Figure 5.
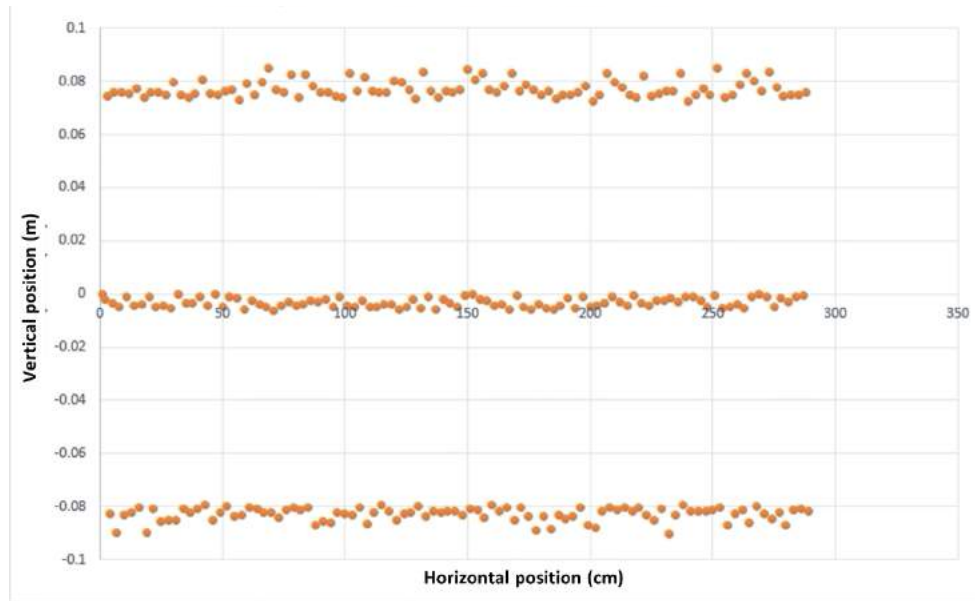
Figure 5. Scatter plot for carrot seeds with steel chute at 1 m s^{-1} using Altair EDEM simulation results.

One-way and two-way ANOVA tests were used with a post-hoc Tukey test to determine if the independent variables of chute, forward speed, and seed were statistically significant in their difference with a confidence level of ($p<0.05$). A three-way ANOVA test was applied to the displacement of seed value in the y direction (direction of travel). Statistical analysis was conducted in Genstat 19th Edition (64-bit). The mean QFI, Multiples Index, Miss Index, and CP3 simulation results are shown in Figure 6.
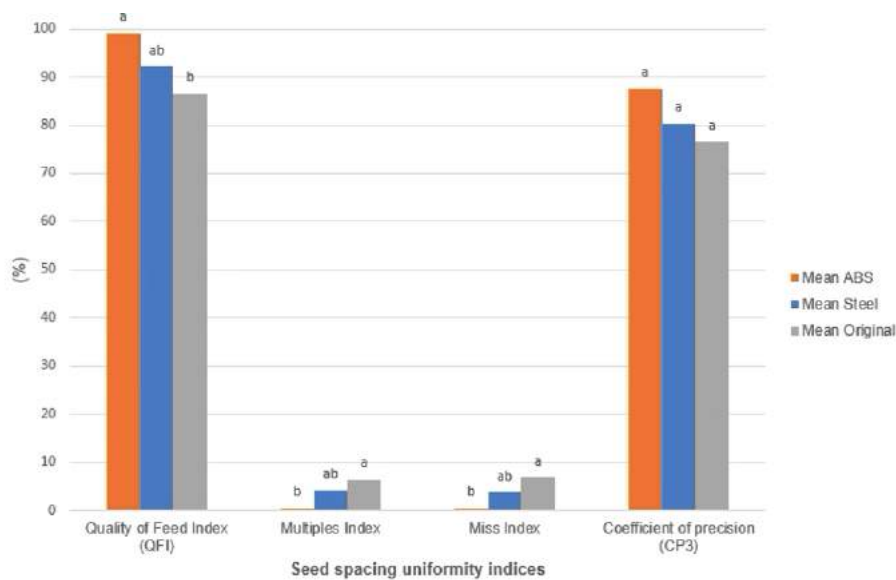
Figure 6. The mean index values for each of the seed chutes across all seed types and forward speeds. Values not followed by the same letter are significantly different at 5% probability level.

The ABS 3D printed chute performed the best with the highest QFI value of 99.1%, the lowest Multiples index of 0.47%, the lowest Miss Index of 0.47% and the highest coefficient of precision at 87.6%. The CP3 value of the ABS chute did not prove to be significantly different from the other values. The stainless-steel design was not statistically different from the other two designs. The original chute performed the worst with a QFI value of 86.6%, a Multiples index of 6.5%, a Miss Index of 6.8%, and a CP3 value of 76.6%.

Forward speed of drill had no significant effect upon the index values, since all index values across forward speed were statistically similar, Figure 7. As forward speed increased, the QFI reduced by 3% while the Miss and Multiple Indices both increased by 1.5%.
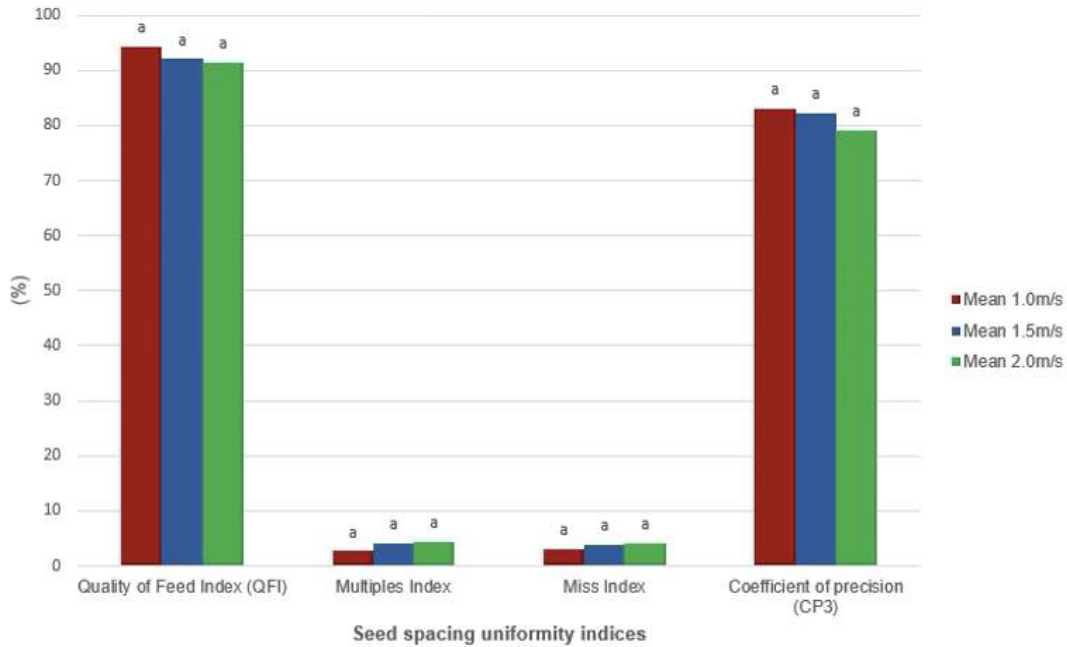
Figure 7. The mean index values for the forward speeds 1.0 m s^{-1}, 1.5 m s^{-1} and 2.0 m s^{-1}. Values not followed by the same letter are significantly different at 5% probability level.

Figure 8 shows that there was a greater seed spacing uniformity for cabbage seed than carrot seed with the QFI value of 95.4% compared to 80.9% for carrot and the CP3 value of 92.3% compared to 63.6% for carrot. The Multiples Index was lower for cabbage at 2.3% compared to 4.6% for carrot, and the Miss Index was lower for cabbage at 2.4% compared to 4.5% for carrot.
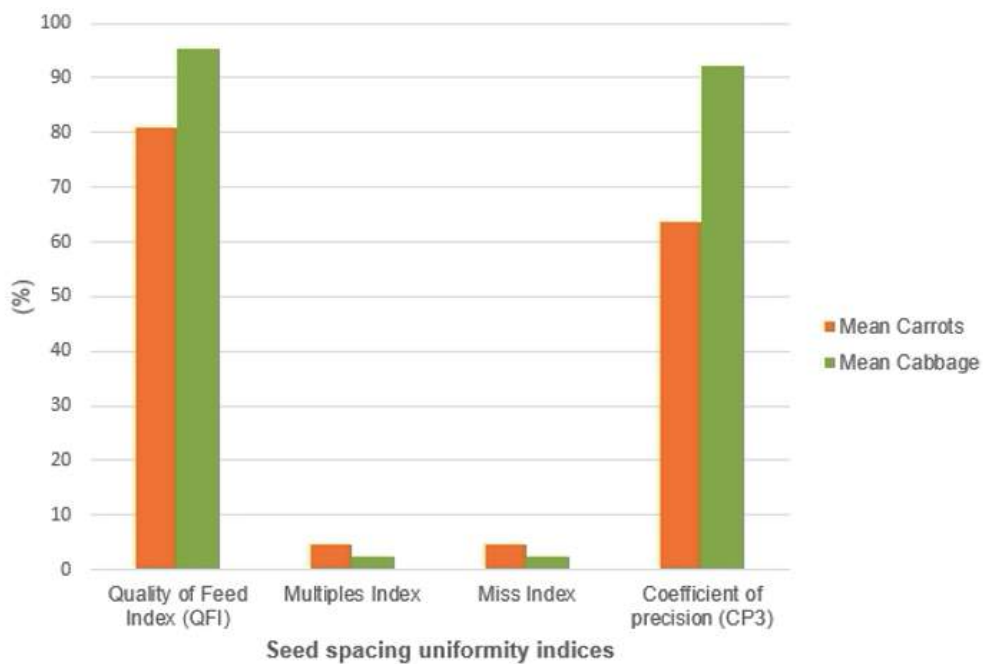
Figure 8. The mean index values for carrot and cabbage seeds.

4. Discussion

Several studies have been conducted investigating the difference in values between the results produced by Altair EDEM software and real-world experiments of seed metering mechanisms (Jinwu *et al.*, 2017; Marcinkiewicz *et al.*, 2019; Li *et al.*, 2013). Jinwu *et al.*, (2017) showed Altair EDEM simulations to be consistent with bench tests, with an error of the QFI value being 1.95%, for a precision metering device for maize. Guzman *et al.* (2020) compared simulated and experimental values for fluted roller metering devices using DEM, determining that the error of mass flow rate from the metering unit was 16.5%. Huang *et al.* (2018) found an average relative error of 10.3% for the coefficient of variation for a fluted roller metering unit for DEM results compared to real-world results.

The chute made from ABS produced the greatest seed spacing uniformity due to its non-uniform shape and its low value of the coefficient of static friction. The original design had the worst seed spacing uniformity with higher Miss and Multiples Indices. This may be because the coefficient of friction for steel is greater than for smoothed ABS, resulting in more 'sticking' of seeds to the internal walls of the chute resulting in two or more seeds coming out of the chute at the same time. Also, the ABS chute had a smaller cross sectional area (CSA). Kocher *et al.* (2011) showed that a 10% increase in CSA resulted in a 3% increase in the Multiple Index and Miss Index, i.e. the CSA of a seed chute has an effect on seed spacing uniformity.

Carrot seed, being a flat seed, showed a mean CP3 value of 63.6% compared to 92.3% for cabbage, a round seed. These values are greater than those found by Kocher *et al.* (2011) (35.3% and 49.6% respectively) but they show a similar relationship.

At a forward speed of 1.0 m s^{-1} the mean QFI, Miss Index, and the Multiples Index for all chutes were 94.3%, 3.05%, and 2.66% respectively. For the same vacuum pressure and forward speed of 1.0 m s^{-1}, Karayel *et al.* (2004) recorded values of 90%, 3.6%, and 3.6% respectively for laboratory testing using real seed and equipment. This gives the authors some confidence in the validity of the simulation data.

Humidity, temperature, wind speed, and mechanical vibration were not modelled in the simulation software. A number of assumptions based on similar seeds were made for the carrot and cabbage seed. Future research should aim to determine these properties.

5. Conclusions

A new ABS seed chute with acetone smoothing improved the seed spacing uniformity (QFI increased by10%, and the Miss Index and the Multiples Index reduced by 5%), and is undergoing evaluation in field trials. A new stainless steel chute design showed no statistically significant improvement compared to the original steel design.

References

Abbaspour-Fard, M.H. 2000. Discrete element modelling of the dynamic behaviour of non-spherical particulate materials. Doctoral dissertation, Newcastle University.

AZO Materials. 2020. *Stainless Steel - Grade 316 (UNS S31600)*. [Online]. Available from: https://www.azom.com/properties.aspx?ArticleID=863. [Accessed 27th March 2020].

Bateman, H.P. 1972. Planter metering, soil and plant factors affecting corn ear populations. *Transactions of the ASAE*, 15 (6), pp.1013-1020.

Bracy, R.P., Parish, R.L. and McCoy, J.E. 1999. Precision seeder uniformity varies with theoretical spacing. *HortTechnology*, 9(1), pp.47-50.

BSI (British Standards Institution). 1988. *Seed drills- Part 1: Methods of test for single seed drills.* London: BSI.

CES EduPack. 2019. *Level 1 Database*. Granter Design Limited.

DEM Solutions Ltd. 2020. *EDEM Applications in the Design of Agricultural Machinery*. [Online]. Available from: https://www.edemsimulation.com/edem-applications-agricultural-machinery-design-ebook-download

Engineers Edge LLC. 2020. *Common Plastic Moulding Design Material Specification*. Available from: https://www.engineersedge.com/plastic/materials_common_plastic.htm [Accessed 28th March 2020].

Gautam, A., Khurana, R., Manes, G.S. and Dixit, A.K. 2016. Studies on engineering properties of pelleted carrot (Daucus carota L.) seeds. *International Journal of Bio-resource and Stress Management*, 7(5), pp.1044-1048.

Halderson, J.L. 1983. Planter selection accuracy for edible beans. *Transactions of the ASAE*, 26(2), pp.367-0371.

Huang, Y., Wang, B., Yao, Y., Ding, S., Zhang, J. and Zhu, R. 2018. Parameter optimization of fluted-roller meter using discrete element method. *International Journal of Agricultural and Biological Engineering*, 11(6), pp.65-72.

Irla, E. and Heusser, J.1991. Comparison of precision grain sow machines. Swiss Federal Institute for Business Administration and Agricultural Engineering.

ISO. 2020. Available from: https://www.iso.org/about-us.html [Accessed November 14th 2020].

Ivkovic, B., Djurdjanovic, M. and Stamenkovic, D. 2000. The influence of the contact surface roughness on the static friction coefficient. *Tribology in industry*, 22, pp.41-44.

Jadhav, M.L., Mohnot, P. and Shelake, P.S. 2017. Investigation of engineering properties of vegetable seeds required for the design of pneumatic seeder. *International Journal of Current Microbiology and Applied Sciences*, 6(10), pp.1163-71.

Jinwu, W., Han, T., Jinfeng, W., Xin, L. and Huinan, H. 2017. Optimization design and experiment on ripple surface type pickup finger of precision maize seed metering device. *International Journal of Agricultural and Biological Engineering*, 10(1), pp.61-71.

Kaliniewicz, Z., Markowski, P., Anders, A. and Jadwisieńczak, K. 2015. Frictional properties of selected seeds. *Technical Sciences/University of Warmia and Mazury in Olsztyn*.

Karayel, D., Barut, Z.B. and Özmerzi, A. 2004. Mathematical modelling of vacuum pressure on a precision seeder. *Biosystems Engineering*, 87(4), pp.437-444.

Kocher, M.F., Coleman, J.M., Smith, J.A. and Kachman, S.D. 2011. Corn seed spacing uniformity as affected by seed tube condition. *Applied Engineering in Agriculture* 27(2).

Li, Y., Xiantao, H., Tao, C., Dongxing, Z., Song, S., Zhang, R. and Mantao, W. 2015. Development of mechatronic driving system for seed meters equipped on conventional precision corn planter. *International Journal of Agricultural and Biological Engineering*, 8(4), pp.1-9.

Mapoka, K.O., Birrell, S.J. and Eisenmann, D.J. 2018. Application of Ground-Penetrating Radar in measuring Corn seeds (CS) Spacing and Planting depth in different soils. *2018 ASABE Annual International Meeting*, pp .1.

Marcinkiewicz, J., Selech, J., Staszak, Ż., Gierz, Ł., Ulbrich, D. and Romek, D. 2019. DEM simulation research of selected sowing unit elements used in a mechanical seeding drill. *MATEC Web of Conferences* 254, p. 02021).

Önal, I. 2006. Mathematical-Statistical Principles of Sprinkling and Use of Sowing Machines in Trials. *Journal of Agricultural Machinery Science*, 1 (2), pp.93-100.

Ramírez-Aragón, C., Ordieres-Meré, J., Alba-Elías, F. and González-Marcos, A. 2018. Comparison of cohesive models in EDEM and LIGGGHTS for simulating powder compaction. *Materials*, 11(11), p.2341.

Saracoglu, T. and Ozarslan, C. 2012. Moisture-Dependent Geometric, Frictional and Mechanical Properties of Cabbage (Brassica oleraceae L. var. capitata) Seeds. *Philippine Agricultural Scientist*, 95(1), pp.53-63.

Searle, C.L., Kocher, M.F., Smith, J.A. and Blankenship, E.E. 2008. Field slope effects on uniformity of corn seed spacing for three precision planter metering systems. *Applied Engineering in Agriculture*, 24(5), pp.581-586.

Smith, J.A. and Kocher, M.F. 2008. Evaluate planter meter and seed tube systems for seed spacing performance of confection sunflower seed to improve plant spacing in the field. *National Sunflower Association,* 762.

Snyder, K.A. and Hummel, J.W. 1985. Low pressure air jet seed selection for planters. *Transactions of the ASAE*, 28(1), pp.6-0010.

Stanhay Webb Ltd. 2020. *ProAir*. Stanhay Webb Ltd . [Online]. Available from: https://www.stanhay.com/proair [Accessed 4th February 2020].

Understanding the Barriers to Uptake of Precision Livestock Farming (PLF) in the UK Sheep Industry

Amy L Boothby [a], David R White [a,*]

[a] Engineering Department, Harper Adams University, Newport, Shropshire, UK

* Corresponding author. drwhite@harper-adams.ac.uk

Abstract

The UK has the largest number of sheep in Europe. Despite the sheep industry being worth £2.2 billion per annum, profitability on sheep farms in the UK remains low. The combination of Electronic Identification (EID) of sheep (obligatory since 2010) and increased awareness of precision livestock farming (PLF) in other agricultural industries, offers the opportunity for UK sheep farmers to raise productivity by increasing their use of PLF techniques. However, the use of PLF on UK sheep farms remains low.

The aim of this study was to understand the barriers restricting the uptake of PLF, explore existing technologies available to the industry, and make recommendations for increasing uptake in the future, through the use of a questionnaire.

A total of 193 responses were received from the online questionnaire of which 50.3% of the respondents said they were currently using PLF technologies with their sheep enterprise, which included EID technologies, automatic weighing and drafting technologies, management software, and livestock cameras. Flock size and position in the stratified system were the two main influencing factors as to whether PLF technologies are being used. The results also suggest that the initial investment cost of the equipment is the largest barrier to entry, while the age and attitude of sheep farmers was also perceived as a barrier. To increase future uptake, the biggest incentive to respondents was for the technology and equipment to be subsidised through Government funded schemes.

Keywords: Precision livestock farming, sheep industry, barriers, questionnaire.

1. Introduction

The UK has the largest number of sheep across all European countries. In 2019 the total number of sheep and lambs in the UK was 33.6 million on approximately 72,000 holdings (Duchy College, 2018; DEFRA, 2019A), and are estimated to be worth £2.2 billion (Duchy College, 2018). Aside from its value, the sheep sector is a large employer within the agricultural industry, employing 34,000 people directly on farms and 111,400 in contributing industries, which includes veterinarians, shearing contractors, equipment dealerships, and feed merchants. The estimated contribution to employment is £291.4 million (Duchy College, 2018). However, on average, farms grazing livestock (including sheep farms) rely on EU payments for more than 90% of their profits (Abbound, 2018).

The UK sheep industry is stratified into three tiers: lowland, upland, and hill (NSA, not dated). This system is unique to the UK and aims to best utilise the strengths of different breeds and the varying habitats, climates and environments across the country. Sheep farming in the UK also plays an important role in providing sustainable land management, especially in areas inaccessible to machinery (e.g. hill sides and mountains).

Precision Livestock Farming (PLF) technology and equipment may offer the opportunity to streamline the UK sheep industry into one that is more efficient and sees a better return on its products and investment. Many labour and anthelmintic savings are available from operating with PLF techniques, which in turn offers raised health and welfare standards of flocks, making it possible to demand more for money for higher quality products (Morgan-Davies *et al.*, 2018). Brexit may further offer the opportunity to reshape the UK sheep industry. As well as profits in the farming sector, a viable sheep industry is essential for encouraging tourism and helping to support rural businesses in the UK countryside (Woodland Trust, not dated).

Despite the many benefits of PLF techniques, which have been recognised by the dairy and beef industries, uptake within the UK sheep industry has been relatively poor with very few farmers investing in the technology (Pierpaoli *et al.*, 2013 and Bucci *et al.,* 2018). This is linked to the fact that sheep are not considered to be as economically valuable as other livestock animals (Carpentier *et al*., 2018).

However, since 2010, it *is* mandatory for all small ruminants that are not destined for slaughter before the age of 12 months, to be EID tagged (Waterhouse *et al.*, 2013; Lima *et al.,* 2018). Adult sheep are required to have two identifiers (one in each ear) with the same individual identification number. One tag must be an EID tag, while the other is a standard tag (UK Government, 2014). Lambs who are intended for slaughter only require one tag, which must include EID and contain the individual number of the flock. They are not required to be uniquely identified. These EID tags can be used in conjunction with EID readers, electronic weighing units, unmanned aerial vehicles (UAV), automatic

drafting gates, livestock monitoring cameras, and concentrate feed management, in a PLF system.

A study undertaken by Morgan-Davies *et al.* (2018) aimed to establish the feasibility of introducing PLF techniques into a commercial hill flock. Mountain based flocks suffer from high rates of lamb mortality and poor ewe survival over winter because of the harsh environment and bleak climate which exists all year round. The study concluded that managing a large hill flock would benefit from implementing PLF techniques because sheep would be considered on an individual basis. The benefits brought about included better labour efficiency, better anthelmintic control and better animal welfare (Morgan- Davies *et al.*, 2018).

In a survey conducted by Gautier *et al.* (2019), across the 6 main EU sheep producing countries (UK, France, Ireland, Italy, Spain, Romania, and Turkey), only 38% were appropriately equipped to use PLF techniques despite 64% of respondents stating that PLF was an opportunity for the sheep industry. Across the countries, France and Ireland were the best equipped with technology, while the rest of the countries, including the UK scored very poorly. It is thought that farmers rejected the idea of implementing PLF techniques into their daily operations was mainly due to the equipment cost and accessibility (Morgan-Davies *et al.*, 2019).

The aim of this research was to review existing PLF technologies for sheep industry, determine through the use of a questionnaire the main barriers to adoption of PLF techniques, and make recommendations for increasing the uptake of PLF technologies within the UK sheep industry in the future.

2. Materials and Methods

Following on from the work of Russel and Bewley (2013), Borchers and Bewley (2015), Gargiulo *et al.* (2018), Lima *et al.* (2018), Abeni *et al.* (2019), and Gautier *et al.*(2019), a questionnaire was designed to investigate the perceptions of PLF amongst UK sheep farmers who consider sheep farming to be their primary or secondary enterprise.

Kelley *et al.(*2003) states that postal questionnaires do not generate good response rates (<20%). Therefore, the questionnaire was designed online. This questionnaire was split into three main sections (based upon the work of Morgan-Davies et al. (2019)).

Section one consisted of profile questions, that aimed to establish background of respondents – these are an important aspect of research as age, gender, education and other factors contribute greatly to people's opinions (Fitzpatrick, 1991). Section two investigated the respondent's perceptions of technology and PLF. Section three included Likert-scale type questions as they are best used for capturing opinions on how strongly someone feels about a particular matter (Saunders *et al.,* 2009). Respondents were provided with a list of ten statements that were all perceived to be entry barriers to using PLF, and asked to rate them as to how larger a barrier they perceived them to be, on a five point scale.

In total, the questionnaire consisted of 16 questions. Where possible, multiple choice questions were used as they are the least time consuming questions to answer (Chudoba, not dated). However, some open ended questions were required to fully capture the opinions of each respondent. The questionnaire was live for four weeks in July/August 2020. In order to maximise response rates, reminders were posted on the forums seven days before the questionnaire was due to close.

Data analysis was completed using Microsoft Excel. A Chi Squared test was used to determine the statistical significance between two quantitative variables (Saunders *et al.,* 2009). For qualitative data, an inductive approach was used (Saunders *et al.*, 2009), to explore which themes were reoccurring and should be focused upon.

3. Results

A total of 193 responses were received to the online questionnaire.

3.1. Quantitative Data.

A Chi Squared test found that there was no significance (p=0.893) between age and the level of technology/automation being used on the farm specifically for sheep, Table 1.

A Chi Squared test found that there was no significance (p=0.768) between the level of education of the respondent and the level of technology/automation being used on the farm specifically for sheep, Table 2.

A Chi Squared test found that there was a significance (p<0.001) between the number of breeding ewes and the level of technology/automation being used on the farm specifically for sheep, Table 3.

A Chi Squared test found that there was no significance (p=0.203) between the position in the stratified system and the level of technology/automation being used on the farm specifically for sheep, Table 4.

Table 1. Cross tabulation of the age of the respondent and the current level of use of technology/automation on their sheep farm.

Age	Are you currently using any PLF technologies in sheep production?		Total
	Yes	No	
16-24	35	35	**70**
25-35	28	22	**50**
36-45	14	16	**30**
46-55	12	13	**25**
>55	8	10	**18**
Total	**97**	**96**	**193**

Table 2. Cross tabulation of the highest level of education of the respondent and the current level of use of technology/automation on their sheep farm.

Level of Education	Are you currently using any PLF technologies in sheep production?		Total
	Yes	No	
Level 2 (e.g. GCSEs, O-levels)	18	21	**39**
Level 3 (e.g. A-Levels, Level 3 NVQs)	30	25	**55**
Level 4 (e.g. Higher National Certificate)	6	6	**12**
Level 5 (e.g. Foundation Degree)	15	8	**23**
Level 6 (e.g. Bachelor's Degree)	24	29	**53**
Level 7 or higher (e.g. Master's Degree, PhD)	4	7	**11**
Total	**97**	**96**	**193**

Table 3. Cross tabulation of the number of breeding ewes and the current level of use of technology/automation on the respondents' sheep farm.

Number of Breeding Ewes	Are you currently using any PLF technologies in sheep production?		Total
	Yes	No	
<50	3	24	**27**
51-100	6	23	**29**
101-300	22	28	**50**
301-500	13	9	**22**
501-1000	30	8	**38**
>1000	23	4	**27**
Total	**97**	**96**	**193**

Table 4 Cross tabulation of the position in the stratified tier of the farm and the current level of use of technology/automation on their sheep farm.

Are you currently using any PLF technologies in sheep production?	Stratified System Tier		Total
	Lowland	Upland & Hill	
Yes	68	29	**97**
No	75	21	**96**
Total	**143**	**50**	**193**

While there is no significance between the two variables, there was a 79.8% level of confidence that the level of technology/automation used on sheep farms is affected by the location of the farm, as to whether it is lowland or upland/hill, with those farming in the upland or hill tiers being more likely to use technology for their sheep.

3.2 Qualitative Analysis

An important aspect of the research was to determine what technologies UK sheep farmers were aware of and how much they are utilising them.

50.3% of the respondents said that they were using some form of PLF technology or automation for their sheep enterprise. This indicates that technology and automation on UK sheep farms is under-utilised. These 50.3% of respondents also revealed several consistent themes in the technologies used. The three main technologies that were used were identification technologies such as readers (48%), automated weighing technologies (21%) and computer management software (24%) for managing the flock whilst the next two technologies, automatic drafting and sheep surveillance, only accounted for 7% and 1% respectively.

To understand the primary entry barriers to PLF in the UK sheep industry, respondents were asked to rate ten statements in terms of how much they deemed them to be a barrier. Each level of barrier was assigned a numerical value (5 = major barrier, 4 = substantial barrier, 3 = a barrier, 2 = minor barrier, and 1 = not a barrier). Using the numerical values for the ordinal choices allowed a mean value of each barrier to be calculated to give an approximate overall value. Each statement was then ranked, the largest barrier being the initial investment cost which scored an average of 3.81, Figure 1.
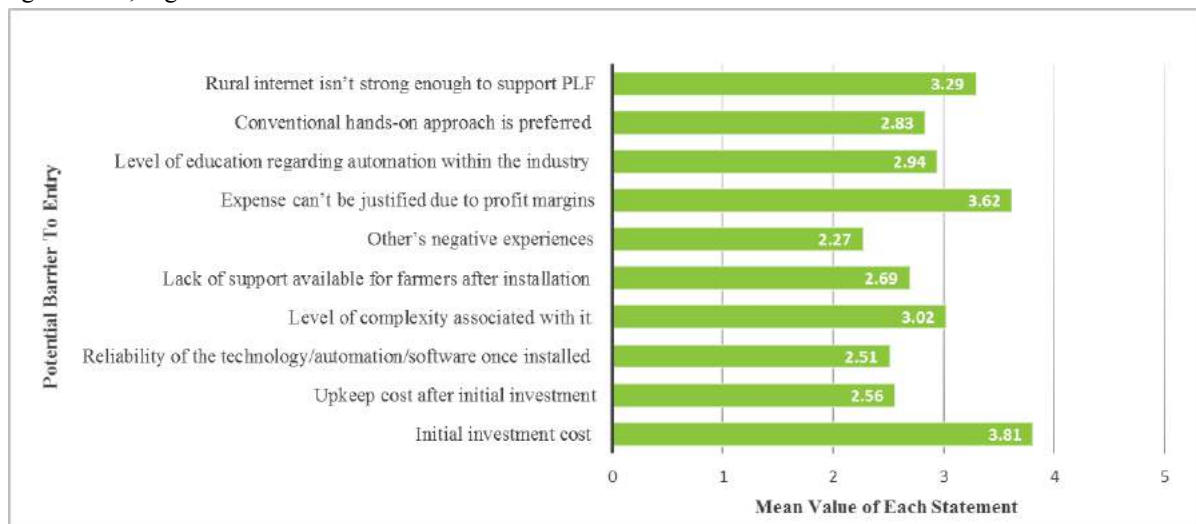
Figure 1. The mean value of each proposed barrier to adopting PLF in the UK sheep industry, as ranked by the survey respondents.

From the open ended questions capturing the opinions of each respondent, the top five barriers were; age and attitude of sheep farmers (34%); profitability or investment concerns (30%); concerns regarding technology (18%); UK climate, geography and location of sheep farms (10%); and flock size (9%). Many stated that the age of UK sheep farmers is considerably higher than those within other farming enterprises who are not willing to pass the farm onto the younger generation who would be more inclined to adopt new technology.

In order to make recommendations of how to increase the use of PLF techniques in the UK sheep industry, it is important to understand what incentives UK sheep farmers need in order to invest. As part of the questionnaire, the respondents were asked to rate eight individual statements regarding the use of PLF techniques. For each statement, respondents had the choice of five answers which ranged from very unlikely to extremely likely with appropriate intermediary stages.

The mean value of each statement was calculated, by giving each ordinal statement a value, which enabled the statements to be ranked. Means ranged between 3.2 and 4.06, indicating that all of the statements had some validity and would positively influence a farmer's choice of whether to invest or not. The most popular statement was "subsidising the technology as part of various government schemes". The results can be seen in Figure 2.
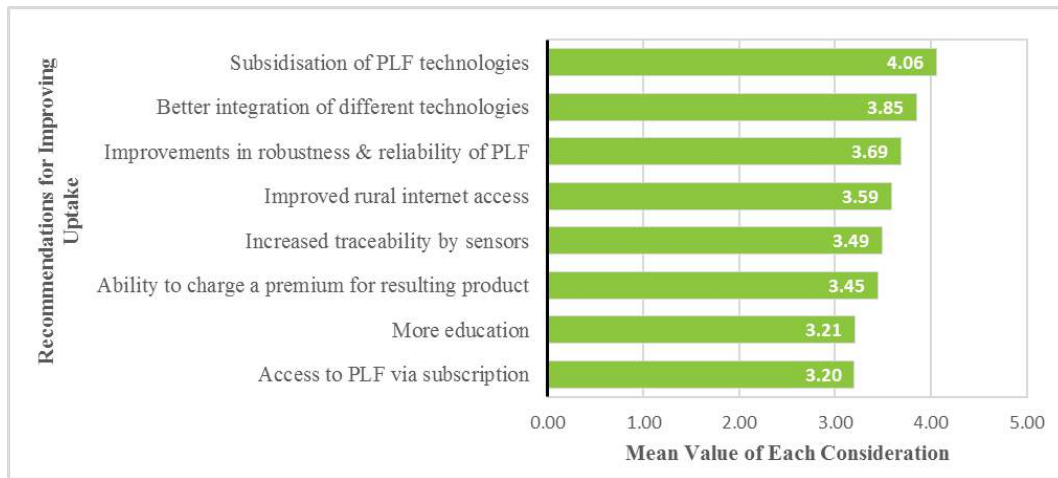
Figure 2. The mean value of each proposed recommendation for increasing the adoption of PLF in the UK sheep industry, as ranked by the survey respondents.

4. Discussion

4.1 Respondent Profile

45% of all respondents were male and under the age of 45. However, the age profile was skewed, as shown in Figure 3. When compared to the results of a similar survey conducted by Lima *et al.* (2018), their age profile was dominated by 46-55 year olds with only 3% of their respondents being under the age of 25.
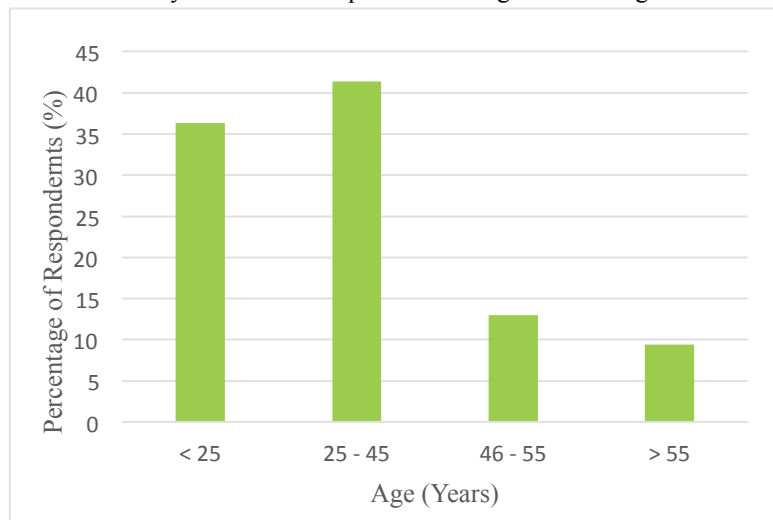
Figure 3. Age profiles of respondents

The difference in age profile may be accounted for by the method of questionnaire distribution. The questionnaire in this study was distributed online via social media to generate responses quickly, however Lima *et al.* (2018) distributed a printed questionnaire via the post with a pre-paid envelope to return the completed questionnaire. Subsequently, the data was likely skewed due to the fact that 94.6% of all social media users are under the age of 44 (Talkwalker, 2020). Social media is under-utilised by people over the age of 44 and, therefore, this age group could have been underrepresented in the questionnaire results.

Previous studies by Borchers and Bewley (2015) in the dairy cattle industry and Lima *et al.* (2018) in the sheep industry both identified that the age of the farmer has no significance to the current level of use or adoption of technology/automation on sheep and dairy cattle farms. The results from this study identified the same conclusion (p=0.893).

The average flock size observed during this study was comparable to the average flock size observed by Gautier *et*

al. (2018). 34% of respondents had more than 501 breeding ewes, whereas Gautier *et al.* (2019) found that only 23% of EU respondents had a flock size larger than 501 breeding ewes. This could be linked to the average size of European farms, where the average UK is the largest being 68ha (EuroStat, 2019). Therefore, sheep farmers in the UK have the land capacity to farm larger flocks compared to their European counterparts. Abeni *et al.* (2019), Russel and Bewley (2013) and Gargiulo *et al.* (2018) in dairy cattle industry, and Gautier *et al.* (2019) in the sheep industry have all concluded that herd or flock size is an important factor in determining the use and adoption of PLF on farms across Europe, Australia and America.

The results of this study identify that the flock size is significant to the level of use of PLF equipment on UK sheep farms (p<0.001). This is explained by the fact that maintaining larger flocks is time consuming and labour intensive - one way to reduce this is to implement PLF equipment (Morgan-Davies *et al.,* 2018). Further to this, this study found a relationship between the position in the stratified system and the level of technology present on UK sheep farms, with uplands/hill farms being more likely to be using technology. This may be explained by high rates of lamb mortality and poor ewe survival rates over winter due to the harsh environment and bleak climate of hill farms. Using PLF allows for better, individual management of sheep, allowing farmers to target weaker ewes, providing them with treatment or food required to keep them at their fittest. Healthy ewes are more likely to survive harsh winters (Morgan-Davies *et al.,* 2018).

4.2 Perceptions of Technology

45.08% of all respondents who considered themselves to be advocates of the use of technology in general were also currently using PLF equipment with their sheep enterprise. Despite UAVs appearing in the market research they did not appear as a technology currently being used by UK sheep farmers in the questionnaire. This was expected because the use of UAVs with sheep is still in the development phase.

4.3 Barriers to entry and Increasing uptake.

The initial investment cost of the equipment and technology was identified as being the largest barrier to uptake of PLF in the UK sheep industry. For example, automatic drafting equipment is the most expensive and therefore the least utilised within the UK. A typical entry-level Sheep Auto Drafter produced by Shearwell Ltd is priced at £9,997 (Shearwell Ltd, not dated). This agrees with Gautier *et al.* (2019) who also found initial investment cost to be the main barrier to entry of PLF in the European sheep industry. If the technologies were subsidised through schemes such as the Environment Land Management scheme (ELMs) (Defra, 2020) in England, farmers would be more inclined to invest because the probability of making a return on the investment is higher (Carpentier *et al.,* 2018; Morgan-Davies and Lambe, 2015).

4.4 Changing attitudes

Mandatory EID identification for all small ruminants in the European Union appeared to be an additional burden to farmers who did not recognise the opportunity EID offered for better management and welfare of sheep. Gautier *et al.* (2019), identified that 62% of European sheep farmers in the top seven producing sheep countries and Turkey were not interacting with EID technologies.

The results obtained by this study identified that only 49.7% of UK sheep farmers are not using any kind of technology or automation. This indicates that either the UK as a whole is making better use of PLF and EID technologies than the other seven countries within the study conducted by Gautier et al. (2019), or that the opinions of sheep farmers on a UK, European and Global scale are slowly beginning to change to realise the benefits that PLF on offers. Opinions may change further as awareness of precision agriculture rises (Bucci *et al.,* 2018).

5. Conclusions

50.3% of all respondents used some form of technology on their sheep enterprise. The level of equipment was influenced by the flock size, and to some extent, by the position of the farm in the stratified tier system.

The main barrier to uptake of PLF in the UK sheep industry is the initial investment cost of the technology or automation. Also, farmers were not able to justify the expense due to the lack of profitability within the UK sheep industry compared with other sectors of farming. Rural internet not being able to support the technologies was also perceived to be a significant barrier for UK sheep farmers. Other people's negative experiences with PLF and the reliability of the equipment were not perceived to be a significant barrier.

In order to increase the uptake of PLF on UK sheep farms the technology needs to be made available at a subsidised rate through the use of government funded schemes, such as the new ELM scheme. Better integration of different technologies, software, and brands could greatly increase the use of PLF as they would provide improved management information.

References

Abbound, L. 2018. *UK Farmers prepare for overhaul to farm subsidies after Brexit.* Financial Times. [Online]. Available from: https://www.ft.com/content/db2a28e2-c175-11e8-95b1-d36dfef1b89a [Accessed 12/07/2020]

Abeni, F., Petrera, F., Galli, A. 2019. A survey of Italian Dairy Farmers' Propensity for Precision Livestock Farming Tools. *Animals (Bevel),* Vol 9(5). [Online]. MDPI. Available from: https://www.mdpi.com/2076-2615/9/5/202/htm [Accessed 21/08/2020]

Borchers, M., and Bewley, J. 2015. An assessment of producer precision dairy farming technology use, prepurchase considerations, and usefulness. *Journal of Dairy Science.* Vol 98 (6) pp. 4198-4205. [Online]. Elsevier. Available from: https://reader.elsevier.com/reader/sd/pii/S0022030215002490?token=BAF05141D81305C61193F80420BFBE5D59CE641110D1D74CE7F92BD2A2601DA46A9DAA3D1116F4A53D051B672F891494 [Accessed 21/08/2020]

Bucci, G., Bentivoglio, D., Finco, A. 2018. *Precision agriculture as a driver for sustainable farming systems: State of art in literature and research*. *PhD.* Ancona, Italy: Università Politecnica delle Marche

Carpentier, L., Berckmans, D., Youssef, A., Berckmans, D., Van Waterschoot, T., Johnston, D., Ferguson, N., Earley, B., Fontana, I., Tullo, E., Guarino, M., Vranken, E., and Norton, T. 2018. Automatic cough detection for bovine respiratory disease in a calf house. *Journal of Agricultural Engineering Research*, 173, pp 45-56. [Online]. Elsevier. Available from: https://www.sciencedirect.com/science/article/pii/S1537511017304762 [Accessed 17/08/2020]

Chudoba, B. Not dated. *How long should a survey be?.* [Online]. SurveyMonkey. Available from: https://www.surveymonkey.co.uk/curiosity/survey_completion_times/ [Accessed 11/08/2020]

DEFRA (Department of Environment, Food and Rural Affairs). 2019A. *Farming Statistics Crop areas and cattle, sheep and pig populations At 1 June 2019 – England*. [Online]. UK Government. Available from: https://assets.publishing.service.gov.uk/government/uploads/system/uploads/attachment_data/file/868939/structure-june19-eng-28feb20.pdf [Accessed 26/08/2020]

DEFRA (Department of Environment, Food and Rural Affairs). 2020. New details of the flagship Environmental Land Management scheme unveiled by Environment Secretary. [Online]. UK Government. Available from: https://deframedia.blog.gov.uk/2020/02/25/new-details-of-the-flagship-environmental-land-management-scheme-unveiled-by-environment-secretary/ [Accessed 26/08/2020]

Duchy College. 2018. *The value of the sheep industry.* Callington: Duchy College. Available from: https://www.nfuonline.com/assets/106083 [Accessed 11/07/2020]

Fitzpatrick, R. 1991. Surveys of patient satisfaction: II—Designing a questionnaire and conducting a survey. *British Medical Journal,* Vol 302. [Online]. BMJ. Available from: https://www.ncbi.nlm.nih.gov/pmc/articles/PMC1669839/pdf/bmj00125-0039.pdf [Accessed 11/08/2020]

Gargiulo J., Eastwood, C., Garcia, S., Lyons, N. 2018. Dairy farmers with larger herd sizes adopt more precision dairy technologies. *Journal of Dairy Science,* Vol 101 (6) pp. 5466-5473. [Online]. Elsevier. Available from: https://reader.elsevier.com/reader/sd/pii/S0022030218302066?token=F544E88A88A0B78DBF82128B5F592C7FB727B27E83057B12E9DD51B6C4E1681856D02295901114CE8D04B3BDA9C87219 [Accessed 21/08/2020]

Gautier, J., Morgan-Davies, C., Keady, T., Bohan, A., Lagriffoul, G., Ocak, S., Beltrán De Heredia, I., Carta, A., Gavojdian, D., Rivallant, P., Francois, D. 2019. *Use of electronic identification and new technologies on European sheep farms. Presented at the 12th European Federation of Information Technology in Agriculture, Food and the Environment, June 27-29, Rhodes.* [Online]. INFITA. Available from: https://economics.agri.huji.ac.il/ict-agriculture [Accessed 19/08/2020]

Kelley, K., Clark, B., Brown, V., Sitzia, J. 2003. Good practice in the conduct and reporting of survey research. *International Journal for Quality in Health Care*, Vol 15 (3), pp. 261-266. [Online]. Oxford Academic. Available from: https://academic.oup.com/intqhc/article/15/3/261/1856193 [Accessed 25/08/2020]

Lima, E., Hopkins, T., Gurney, E., Shortall, O., Lovatt, F., Davies, P. 2018. Drivers for precision livestock technology adoption: A study of factors associated with adoption of electronic identification technology by commercial sheep farmers in England and Wales. *PLoS ONE* 13(1). Available from: https://doi.org/10.1371/journal.pone.0190489 [Accessed 16/08/2020]

Morgan-Davies, C and Lambe, N. 2015. *Investigation of barriers to uptake of Electronic Identification (EID) for sheep management.* Scotland: Scotland's Rural College (SRuC)

Morgan-Davies, C, Lambe, N, Wishart, H, Waterhouse, T, Kenyon, F, McBean, D, McCracken, D. 2018. Impacts of using a precision livestock system targeted approach in mountain sheep flocks. *Livestock Science*, 208, 67-76. [Online]. Elsevier. Available from: https://www.sciencedirect.com/science/article/abs/pii/S1871141317303670 [Accessed 31/07/2020]

Morgan-Davies, C., Dwyer, K., Frater, P. 2019. *SheepNet farmers' views on Precision Livestock Farming for sheep production.* [Press Release]. SheepNet. 24 October. Available from: http://www.sheepnet.network/index.php/node/654

[Accessed 31/07/2020]

Pierpaoli, E., Carli, G., Pignatti, E., and Canavari, M. 2013. Drivers of precision agriculture technologies adoption: A literature review. *Procedia Technology*, 8, pp 61–69. [Online]. Elsevier. Available from: https://www.sciencedirect.com/science/article/pii/S2212017313000728 [Accessed 20/08/2020]

Russel, R. and Bewley, J. 2013. Characterization of Kentucky dairy producer decision-making behavior. *Journal of Dairy Science.* Vol 96 (7) pp. 4751-4758. [Online]. Elsevier. Available from: https://reader.elsevier.com/reader/sd/pii/S0022030213003159?token=73EF684171C07D56EEF9037F5B444A3AD139 CBA8997FFAA8D3781B428C9ECC0EEFFDB5DB3897AE2F8BF2B2C612395EBF [Accessed 21/08/2020]

Saunders, M., Lewis, P., Thornhill, A. 2009. *Research methods for Business Students.* 5th Edition. Essex: Pearson Education Limit.

SHAWG (Sheep Health and Welfare Group). 2018. *Sheep Health and Welfare Report.* 2nd Edition. SHAWG. Available from: http://beefandlamb.ahdb.org.uk/wp-content/uploads/2018/11/SHAWG-REPORT_2018_11_19_WEB.pdf [Accessed 22.07.2020]

Shearwell Ltd. Not dated B. *Shearwell EID Sheep Automatic Drafting Crate.* Shearwell Ltd. Available from: https://www.shearwell.co.uk/eid-sheep-automatic-drafting-crate [Accessed 21/08/2020]

Talkwalker. 2020. *Social media statistics in the UK*. [Online]. Talkwalker. Available from: https://www.talkwalker.com/blog/social-media-statistics-in-the-uk [Accessed 23/08/2020]

UK Government. 2014. *Sheep and goats: types and combinations of identifier*. [Online]. Publisher. Available from: https://www.gov.uk/guidance/sheep-and-goats-types-and-combinations-of-i/dentifier [Accessed 25/08/2020]

Waterhouse, A., Morgan-Davies, C., Lambe, N., Umstaetter, C., Kenyon, F., McBean, D. and Stevens, H. 2013. *Integrating Electronic Identification into Hill Sheep Management. Presented at the Precision Livestock Farming Conference 2013, Belgium.* [Online]. ResearchGate. Available from: https://www.researchgate.net/publication/259283557_Integrating_Electronic_Identification_into_Hill_Sheep_Managem ent [Accessed 19/08/2020]

Woodland Trust. Not dated. *The role of trees in sheep farming.* Woodland Trust: Grantham.

Evaluation of Smart Glasses for Augmented Reality: Technical Advantages on Their Integration in Agricultural Systems

Gabriele Sara[*], Giuseppe Todde, Marco Polese, Maria Caria

Department of Agriculture, University of Sassari, Sassari, Italy

* Corresponding author. Email: g.sara2@studenti.uniss.it

Abstract

Recently the interest in augmented reality (AR) technologies and smart glasses (SG) has grown considerably in all production sectors. In agriculture, new technologies are being adopted to improve productivity and reduce farm input. In this perspective, the SG may be considered a valuable device to support modern farms. In the last decade, head-wearable devices with different characteristics e.g. display types (optical see-through, video see-through), interaction methods (external joypad, touchpad, voice control) and features (battery life, weight, camera definition, flash memory, etc.) have been developed. These aspects may affect SG experience, leading to different performance levels by the users and its integration on the farm. The aims of this study were to compare different types of SGs for AR and evaluate the technical advantages of their integration in agricultural systems. In this work, SGs with optical or video visualization systems, representing the main discriminating feature for augmented reality devices, were adopted. The tests were carried out on the available functionality of the SGs (e.g. QR code scanning time and distance, audio-video quality, battery life). The results showed that the devices, in relation to their operating system, have different performance detecting the markers and thus the augmented information in terms of time and distance. The audio-video quality performances result comparable for all devices, allowing to share detailed farm information in real-time. The present study demonstrated that the SG features and technical characteristics significantly differ between devices, highlighting how these should be carefully considered when selecting the most appropriate device for the farm.

Keywords: Digital farming, precision agriculture, augmented reality, remote assistance, support system.

1. Introduction

The augmented reality (AR) consists in the enhancement of the real objects, physical things even more living organisms with virtual information or data, that could help working profitably or live comfortably (Azuma et al., 2001; Azuma 1997; Milgram and Kishino, 1994). Several devices, such as smartphone, tablet, and laptop could be used to view the information in an augmented way (ElSayed et al., 2016).

The smart glasses (SG) are a specific device suited for augmented reality applications. In the last years many step forward, have been done developing new SG, also thank to the spreading of the smartphone that reduced the cost of micro electronical components (Lee and Hui 2018; Chatzopoulos et al., 2017).

Essentially, the SG are head wearable computers provided by a display placed in front of the wearer's eye (monocular), or both eyes (binocular). Moreover, the SG have been developed with different characteristics e.g. operating system (Linux, Android, Microsoft), user interface, interaction methods (external joypad, touchpad, voice control), features (battery life, weight, camera definition, flash memory, etc.), and price. But, one of the main discriminating features concern the visualization system that can be an optical see-through display composed by semi-reflective or semi-transparent surface where the virtual contents are projected, or a video see-through display composed by a video camera for the real-world image acquisition and a screen where the augmented information, blended with the real environment, are showed (Lee and Hui, 2018; Syberfeldt et al., 2017; Billinghurst et al., 2015).

The overlaying process of the virtual information on the real can be implemented in various ways. In relation to the device sensors used, can be considered vision-based (marker-based) AR, or sensor-based (marker-less) AR (Billinghurst et al., 2015). The vision-based process uses markers (template, Data Matrix, QR Code, barcode) or features of the environment to estimate and track the position information, whereas the sensor-based process uses inertial, magnetic, electromagnetic or ultrasonic sensors (GPS, gyroscope, accelerometer) to measure and pose the information.

A growing trend in the number of scientific papers in the bibliography related to AR and AR in agriculture has been published, highlighting the interest in this new technology also in the agricultural sector. Until now the main topics of investigation for the AR, with the biggest number of publications were research & development, strictly linked to the implementation of AR technology, healthcare, education, and industry sectors (Munoz-Saavedra et al., 2020). Moreover, many manufacturers of SG are making devices for industrial use (GlassUp; Vuzix; Epson, RealWear).

There are several scientific studies related to the application of AR in agriculture, mainly related to the development of support systems for the farmers, providing them with augmented information on the field. One of the first study by King et al. (2005) developed a system for displaying geo-referenced yield data and NDVI on vine. Another systems

concerns the tractor driving assistance, displaying the optimal trajectory to be followed on a head wearable device (Santana-Fernández et al., 2010), or the use of an AR device to control the operation of two autonomous agricultural machines (Huuskonen and Oksanen 2019). Moreover, Cortazar et al. (2015) developed a system for the quantification of chlorophyll in the leaves with the support of the Google Glass, whereas Huuskonen and Oksanen (2018) developed a real-time navigation system to guide the farmer rightly in the soil sampling area. Furthermore, the applications in the livestock sector were showed (Caria et al., 2019) with systems to help farmer in the management of the flock while milking (Caria et al., 2020). Finally, another example concerns the development of an AR-based application to promote sustainable development in hydroponic cultivation (Garzón et al., 2020) and for plot diagnosis activities in vineyards (Larbaigt and Lemercier, 2021).

The published scientific works underlined that the range of AR applications and SG in the agricultural field are multiple and dynamic. Nevertheless, the SGs are still in their infancy and not ready for agricultural stable use, therefore it is important to evaluate their performance and how different SG might be adapted to an agricultural environment, to help both manufacturers and farmers to make a SG with the features suited for the agricultural field, and, to choose the more appropriate device for their needs respectively.

Then the purpose of this work was to compare different types of SGs for AR and evaluate the technical advantages of their integration in agricultural systems.

2. Materials and Methods

In this study, different smart glasses for augmented reality was adopted: the GlassUp F4 (F4), produced by the GlassUp company (Modena, Italy); the Vuzix M400 (M400), produced by the Vuzix Corporation (25 Hendrix Road West Henrietta, NY 14586, USA); and Moverio BT-300 (BT300), produced by Seiko Epson Corporation (Figure 1).

The three smart glasses (SGs) have the same basic functionality, but different technical characteristics (Table 1). All SGs have been built for professional use, particularly for the industrial sector, and adapted in this study to agricultural applications.
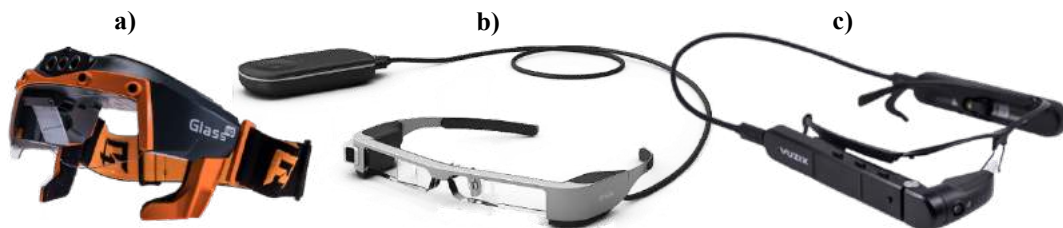
Figure 1. The three smart glasses' models used in this study: a) GlassUp F4; b) Epson Moverio BT-300; c) Vuzix M400.

The devices used can be divided in relation to them visualization system. The F4 are monocular SG with transparent optical see-through display. The M400 are also monocular SG, but with video see-through display. Instead, the BT300 are binocular SG with transparent optical see-through display.

The SGs tested have also different interaction systems, such as, external joypad, touchpad, key button, and different frame design.

To compare the performances of the devices, several tests were carried out at the laboratory of the Agricultural Department of the University of Sassari. The common functions of the SGs, useful for agricultural applications, such as, the scanning of AR marker (QR codes) and the audio-video transmission, were tested. Moreover, the battery life during the tests were monitored.

Table 1. Technical features (as reported by the producers) of the smart glasses used in this study.

Item	Technical features		
	F4	M400	BT300
Processor	Cortex A9	8 Core 2.52 GHz Qualcomm XR1	4 Core 1.44 GHz Intel Atom
Flash memory	8 Gbytes	64 Gbytes	16 Gbytes
Operating System	Linux	Android 8.1	Android 5.1
Display	LCD (on right eye) Full colour 640 x 480	Occluded OLED, 24-bit colour, 640x360	Si-OLED 24-bit colour, 1.280x720
Sensors	Accelerometer-gyroscope-compass (9 axis), lux sensor	Gyroscope-accelerometer-magnetometer (3 axis)	Gyroscope-accelerometer-magnetometer (3 axis), lux sensor
Connectivity	Wi-Fi, Bluetooth	GPS, Wi-Fi, Bluetooth, USB-C	GPS, Wi-Fi, Bluetooth, micro-USB
Camera	5 Megapixel, 15fps	12.8 Megapixel, 30fps	5 Megapixel
Battery Life	6 - 8 h	2 - 12 h	4 h
Controller input	Joypad, one button on the glasses	Touch pad, 3 buttons, voice command	Joypad (touch pad)
Weight	251 g	190 g	69 g

2.1. QR code scanning test

The scan function, available to all devices, was used to compare the performance of the SGs to detect the augmented information. The selected AR marker was the QR code where the farm information was entered. Two types of QR code tests were carried out: scanning time and scanning distance.

The scanning time trial consists of the measurement of the time needed to open the augmented information associated to the marker. The time interval measured range from the scan function or app activation to the augmented farm information visualization on the SG display. In this trial, three different printed size of QR codes were used 3.5 x 3.5 cm (3.5), 4 x 4 cm (4), and 7.5 x 7.5 cm (7.5). The scans were carried out at 40 cm of distance from the QR codes.

The scanning distance trial concerned the measurement of the minimum and maximum distance at which the QR codes were detectable from the SGs' camera and thus the AR information. The printed size of the QR code used were 1.5 cm, 3.5 cm, 4 cm, 7.5 cm, 13 cm, 15 cm, and 20 cm. per side.

For both tests two different versions of QR codes, in term of the number of modules (black and white squares) were used, to test if the complexity of the marker might affect the scanning performance. A simple (SI) and complex (CX) QR code versions was generated for each device, with respectively 29 x 29 modules and 61 x 61 modules. In Figure 2 an exemplification of the versions used is showed. In the CXs code were overwritten farm information directly on the QR using 272 characters, instead in the SI one the same information was written on a file (i.e. PDF, web page) and in the QR code was overwritten the file name or web page link.
The markers were placed on the vertical plane at eye level for both tests.
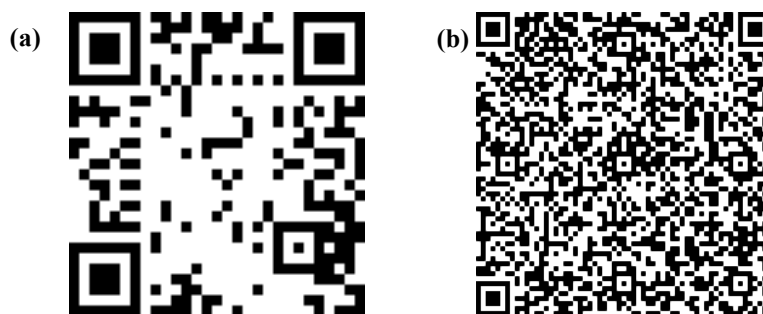
Figure 2. Example of the two version of QR codes used during the trials. Simple (SI) code version (a) and CompleX (CX) code version (b).

2.2. Audio-video quality transmission test

Two tests were performed in order to evaluate the audio-video quality of the transmitted audio-visual image from the SGs to a remote device (PC). The first test concerned the lag times measurement to evaluate the delay to transmit image and audio between SGs and laptop. This trial was carried out by a VOIP (Voice over Internet Protocol) remote video call using the specific app for each device. The lag times were measured by synchronizing the clocks of the two users and recording the emission and receiving time of a fixed signal for audio and a programmed position for the video.

The second test concerned the evaluation of the observable level of detail of transmitted images through the SGs camera. It was performed using a standard Snellen chart placed at 50 cm from SGs and displaying the characters on the laptop's 16-inch screen. The error rate was measured and related to the decreasing size of the character (Muensterer et al., 2014).

The lag times were measured 20 times, whereas the Snellen chart test was performed three times from different receiving operators.

2.3. Battery life Test

During the previous trials, the status of the battery was checked to evaluate how long the tested devices might be work with one battery charge. Two usage situations were evaluated: using the SGs only with the scan function to detect the markers and open the augmented information; or considering a mixed-use (scanning, video calling, etc.).

2.4. Statistical analysis

Descriptive statistics (arithmetic average, standard deviation values) were calculated and reported for the QR code performance test, and for the lag time test. Statistical analysis was carried performing a Kruskal-Wallis rank sum test for the scanning time and audio-video quality transmission data and a multiple comparison after Kruskal-Wallis test ($P < 0.01$). The analyses were performed with R Studio software (version: 4. 0. 5).

3. Results and Discussion

3.1. QR code scanning smart glasses' performance

Table 2 states the results of the QR codes scanning times. Different performance, in relation to the version (SI, CX) and size of the code, were recorded. Significance differences in the scanning times comparing the three devices within the QR code size were observed. The best performance was recorded for the M400 that required on average 2.00 s to show up the augmented farm information. Moreover, the QR code version used did not influence the scanning time, as there are no significant differences within the three QR size. Considering the BT300, the scanning time for the SI QR codes was 6.10 s on average and significantly different from the CX code (3.83 s). The other two CX QR codes (3.5 and 4) resulted unscannable from the BT300 app. Contrary to what one might expect, the scanning time of 7.5 CX code was lower than SI QRs, probably due to the different detection systems. In fact, in the CX code, the farm information was directly encoded, as characters, into the QR code and therefore faster available. But, on the other hand, it was only possible to encode a limited number of data (259 alphanumeric digits).The F4 showed a general scanning time of about 9.50 s, almost always significantly different from the corresponding scanning time of the other devices. Considering the scanning time within the F4, despite the size seem to influence the scanning time, the QR code version not. The higher time required for the F4 was probably due to the different scanning system that needs more time to start the scan app, to focus, and detect the QR code.

Table 2. Average scanning time (s) and standard deviation (SD) of the two QR code version (SI = simple, CX = complex) for the three devices (F4, BT300, M400). Values in the same row with diverse superscript letters are statistically different ($P < 0.01$). Values in the same columns with diverse capital letters are statistically different ($P < 0.01$)

QR size (cm)	3.5		4		7.5		Tot. scan
Device	SI	CX	SI	CX	SI	CX	N
F4	12.03[aA]	12.12[aA]	8.10[bA]	8.99[bA]	7.28[bA]	7.46[bA]	288
SD	±6.10	±4.33	±2.76	±3.33	±3.26	±0.93	
BT300	6.02[aB]	-	6.28[aB]	-	6.19[aA]	3.83[bB]	192
SD	±1.02	-	±1.22	-	±1.02	±0.83	
M400	2.05[abC]	2.05[abB]	1.99[abC]	2.09[aB]	1.84[bB]	1.90[abC]	288
SD	±0.34	±0.35	±0.28	±0.33	±0.31	±0.31	

Figure 3 shows the results of the QR code scanning distance comparison between SGs. This test underline at which distance the augmented farm information will be detectable with different AR devices through a specific marker. Considering the QR code versions, regardless of the size, resulted that the SI codes were scannable at a higher distance than CX codes for all devices as expectable. The BT300 was not able to scan the CX codes smaller or equal to 4 cm size, whereas the F4 and M400 were able to detect also 1.5 QR codes, even though at close distances, up to 5 cm and 22 cm respectively. The highest scanning distances were measured for the M400 considering both QR code versions (SI, CX). Using this device and a SI code (29 modules) it is possible detect a marker 4, and thus the augmented information, at about 2 meters. Moreover, a 20 cm size QR code can be scanned at about 10 meters away. Besides, the minimum scanning distance was recorded for all devices and QR codes versions. The ratio between the scanning distance and QR size was constant for the two versions of codes considering each SGs since the minimum distance was strictly dependent to the camera frame of the device.
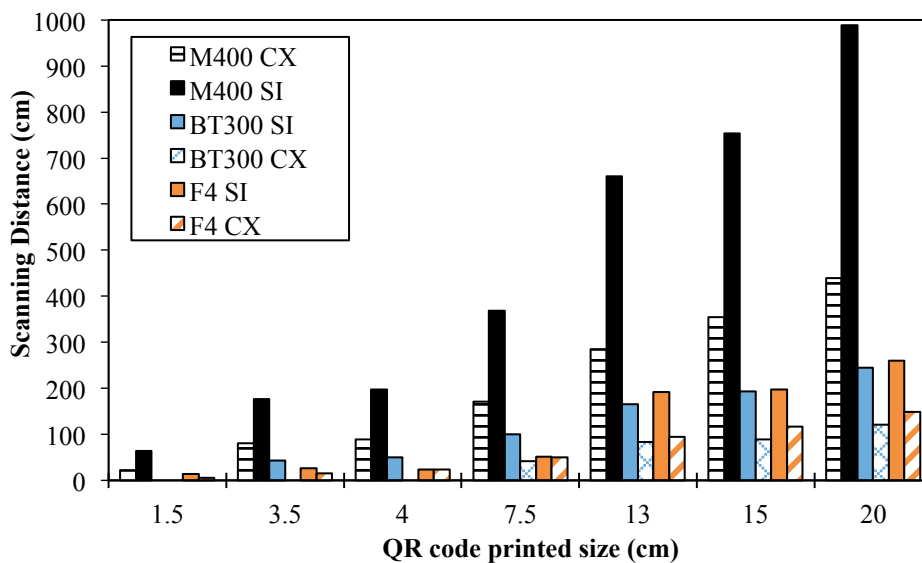
Figure 3. Maximum scanning distance of two QR code versions: SImple (solid color fill) and CompleX (pattern fill) with increasing printed size.

The QR codes scanning tests represent a primary step in understanding the capabilities of the SGs to detect and provide AR information to the farmers on the field. In fact, the markers could be coupled with several production units (crops, animals, orchards, protected crops) and contexts (open field, milking shad, greenhouse) of the farm. Three SGs were compared and each device was observed to perform differently by detecting QR codes at different times and distances. Moreover, the QR code versions influence only the scanning distance due to the higher number of modules that make the marker more difficult to distinguish at a great distance. So, if the farmer wants to obtain AR information from long distances (e.g. from tractor cabin) it will be advisable to use simple QR codes and a SG with the features of M400 that showed great marker detection capabilities. The time requested to visualize augmented information, especially in an agricultural work context, could be one of the parameters that influence the farmer's performance while working with the SG on the field, and then its acceptability. The less time will take, the more satisfied the operator is, especially when the farmer needs augmented information in short intervals of time i.e. selecting animals during the milking sessions.

3.2. Audio-Video Quality transmission performance

Table 3 reports the results on the lag time registered during a video call between the SGs and a laptop. Comparing the three devices resulted that M400 and BT300 had less than one second of delay both for audio and video transmission. Whereas the F4 showed a delay grater of 1 s for audio transmission and greater than 2 s for video transmission in both cases significantly different from the other two devices. The lag times recorded for all SGs should not affect the farmer's field performance, as the ultimate goal of this feature is to share the farmer's point of view with a technician (agronomist, veterinarian, mechanic), although the lower the delay the better.

Table 3. Lag time (s) and standard deviations (SD) measured to transmit audio and video from the smart glasses (F4, M400, BT300) to a laptop during a videocall. Values in the same column with diverse superscript letters are statistically different ($P < 0.01$).

Device	Audio (s)	SD	Video (s)	SD
F4	1.24[a]	±0.81	2.21[a]	±0.11
BT300	0.43[b]	±0.81	0.55[b]	±0.68
M400	0.44[b]	±0.22	0.91[b]	±0.29

Figure 4 shows the results of the video quality evaluation during a video call. Despite all the SGs tested were able to clearly discriminate characters or elements greater or equal to 1.3 cm size, the BT300 and F4 showed a better performance allowing users to completely discriminate elements greater or equal to 0.7 cm. Moreover, the BT300 allowed discriminating with a high percentage (96 %) the 4 cm size characters. The farmers using the SGs will be able to share their point of view with technicians during crops or animal dieses control, maintenance procedures (e.g., milking parlor or tractor inspections), with a good level of details and a reduced delay to solve issues more efficiently.
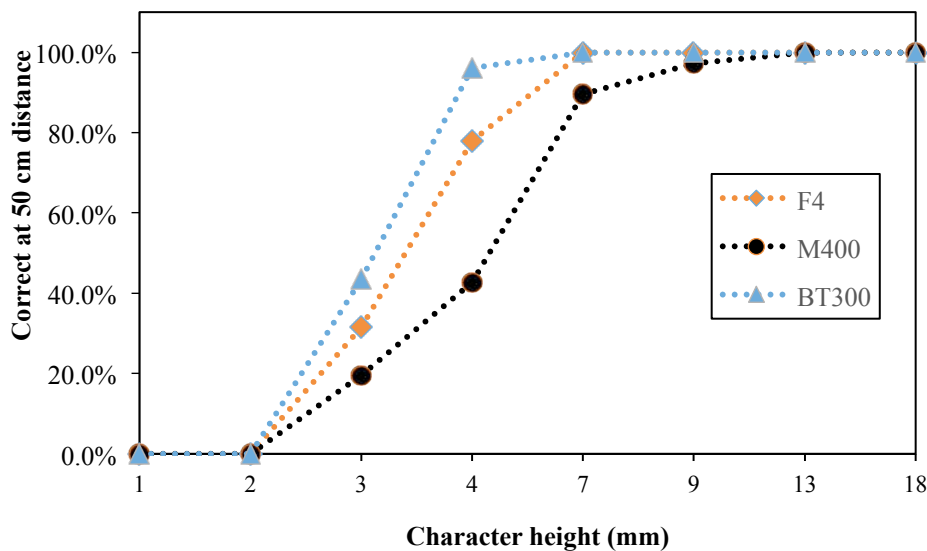
Figure 4. Snellen chart vision test, describing the percentage of correct letter read on the laptop screen during a videocall from the smart glasses. Reading was carried out on a 16 inches display. Three smart glasses were used: Epson Moverio BT300 -▲-; Vuzix M400 -●-; and GlassUp F4 -♦-. The distance between smart glasses camera and the chart was of 50 cm.

3.3. Battery life

Table 4 states the results on the SGs battery performance. All the devices, as expectable, have shorter battery life in a mixed-use situation. The BT300 and M400 showed a higher difference in the duration, respectively of about 12 and 18 minutes than the scanning usage. The F4 showed the best performance in the battery life, close to the working day hours, and a reduced difference comparing the two-usage situation. This fact was probably due to the simplest F4 interface that probably did not consume great energy, contrary to the other two devices that have a different and more complex interface, like the smartphone one, that drains the battery more.

The tested devices cannot support the activities of the farmer during the whole working day but only during specific tasks e.g. selecting the animals or the feed, connecting with a technician to receive support on the field etc., but for a limited time.

Table 4. Battery life expressed in working hours (h) of the three smart glasses (F4, BT300, M400) considering two type of usage situation: Scanning (QR code repeated scans); Mixed-Use (both scanning, video calling, etc.)

	Usage type	
Device	Scanning (h)	Mixed-Use (h)
F4	6.91	6.87
BT300	2.32	2.02
M400	3.58	3.37

4. Conclusions

This study compared three different SGs for AR with different characteristics and tested their available functionality, i.e. scan code, video call, etc., from an agricultural use perspective. It was found that the tested SGs had different performances in the marker detection, both in terms of time and distance. However, all the devices could allow the farmer to obtain the augmented information from the main on-farm activities (e.g. on tractor operations, animal selection, and on-field production, etc.), in relation with the type and version of the markers used. The audio-visual transmission quality was suitable for discriminating small details during remote assistance among the SGs tested. However, the internet connection might influence the quality of the transmitted contents. Finally, different performances in the battery life were found, ranging from 2 to 7 hours. Finally, the technical characteristics differ considerably among devices, highlighting how these aspects should be carefully considered when selecting the SGs depending also from the specific farm activities.

Acknowledgements

References

Azuma, R. 1997. A survey of augmented reality. Presence Teleoper. Virtual Environ. 6, 355–385.

Azuma, R., Y. Baillot, R. Behringer, S. Feiner, S. Julier, B. MacIntyre, 2001. Recent advances in augmented reality. IEEE Comput. Graph. Appl. 21, 34–47. doi:10.1109/38.963459.

Billinghurst, M., A. Clark, G. Lee, 2015. A survey of augmented reality. Found. Trends Hum. Comput. Interact. 8, 73–272. doi.org/10.1561/1100000049.

Caria, M., G. Sara, G. Todde, M. Polese, A. Pazzona, 2019. Exploring smart glasses for augmented reality: A valuable and integrative tool in precision livestock farming. Animals, 9 (11), 903. doi:10.3390/ani9110903.

Caria, M., G. Todde, G. Sara, M. Piras, A. Pazzona, 2020. Performance and Usability of Smartglasses for Augmented Reality in Precision Livestock Farming Operations. Applied Sciences, 10 (7), 2318. doi.org/10.3390/app10072318.

Chatzopoulos, D., C. Bermejo, Z. Huang, P. Hui, 2017. Mobile augmented reality survey: From where we are to where we go. Ieee Access, 5, 6917-6950. doi:10.1109/ACCESS.2017.2698164.

Cortazar, B., H.C. Koydemir, D. Tseng, S. Feng, A. Ozcan, 2015. Quantification of plant chlorophyll content using Google Glass. Lab on a Chip, 15 (7), 1708-1716. doi.org/10.1039/C4LC01279H.

ElSayed, N. A., B.H. Thomas, K. Marriott, J. Piantadosi, R.T. Smith, 2016. Situated analytics: Demonstrating immersive analytical tools with augmented reality. Journal of Visual Languages & Computing, *36*, 13-23. doi.org/10.1016/j.jvlc.2016.07.006.

Epson. Product, Smartglass. Available online: https://www.epson.it/products/see-through-mobile-viewer. Accessed May 5, 2021.

Garzón, J., S. Baldiris, J. Acevedo, J. Pavón, 2020. Augmented Reality-based application to foster sustainable agriculture in the context of aquaponics. In *2020 IEEE 20th International Conference on Advanced Learning Technologies (ICALT)* (pp. 316-318). IEEE.

GlassUp F4 Smart Glasses. https://www.glassup.com/en/. Accessed: May 5, 2021.

Huuskonen, J., T. Oksanen, 2018. Soil sampling with drones and augmented reality in precision agriculture. Computers and Electronics in Agriculture, 154, 25-35. doi:10.1016/j.compag.2018.08.039.

Huuskonen, J., T. Oksanen, 2019. Augmented Reality for Supervising Multirobot System in Agricultural Field Operation. In *IFAC-PapersOnLine*. 52 (30), 367-372. doi.org/10.1016/j.ifacol.2019.12.568.

King, G.R., W, Piekarski, B.H, Thomas, 2005. ARVino–Outdoor Augmented Reality Visualization of Viticulture GIS Data. In *Proceedings of the 4th IEEE/ACM International Symposium on Mixed and Augmented Reality.* Washington, DC, USA, 5–8 October 2005; pp. 52–55.

Larbaigt, J., C. Lemercier, 2021. An Evaluation of the Acceptability of Smart Eyewear for Plot Diagnosis Activity in Agriculture. Ergonomics in Design, 10648046211018541.

Lee, L.H., P. Hui, 2018. Interaction Methods for Smart Glasses: A Survey. IEEE Access. 6, 28712–28732. doi**:**10.1109/ACCESS.2018.2831081.

Milgram, P., F.A. Kishino, 1994. Taxonomy of Mixed Reality Visual Display. IEICE Trans. Inf. Syst. 77, 1321–1329.

RealWear. Product. https://realwear.com/products/hmt-1/. Accessed: May 5, 2021.

Santana-Fernández, J., J. Gómez-Gil, L. Del-Pozo-San-Cirilo, 2010. Design and implementation of a GPS guidance system for agriculture tractors using augmented reality technology. Sensors. 10, 10435–10447. doi:10.3390/s101110435.

Syberfeldt, A., O. Danielsson, P. Gustavsson, 2017. Augmented Reality Smart Glasses in the Smart Factory: Product Evaluation Guidelines and Review of Available Products. IEEE Access. 5, 9118–9130. doi:10.1109/ACCESS.2017.2703952.

Vuzix. Products. Compare products. https://www.vuzix.com/products/compare-vuzix-smart-glasses. Accessed May 5, 2021.

Granulometric Parameters of Solid Blueberry Fertilisers and Their Suitability for Precision-Fertilisation

Tormi Lillerand [a,*], Indrek Virro [a], Viacheslav V. Maksarov [b], Jüri Olt [a]

[a] Institute of Technology, Estonian University of Life Sciences, Tartu, Estonia

[b] Department of Mechanical Engineering, Saint-Petersburg Mining University, St. Petersburg, Russia

* Corresponding author. Email: tormi.lillerand@emu.ee

Abstract

For precise-fertilisation of blueberry plants by using granulized fertilisers, it is essential to know parameters such as: the size of the fertiliser particles and their bulk density. This research involves measuring up three different fertilisers (SQM Qrop K, Memon Siforga, Substral): width, height and length of randomly selected 100 fertiliser particles, also volumes and weights of 100 particles in 10 repetitions. According to the measurements, average diameters of fertiliser particles were found, also average mass, volumes and bulk density. Turned out that the average diameters and bulk densities of the 3 fertilisers differed far from each other, meaning that the given volume could be filled with different amount of fertiliser. Equations between mass and weight were formed according to the measurements. The results could be used to select a suitable doser for fertilizing blueberry plants precisely and adjust the doser each time in the situation, defined by the variety of blueberry plants: their age, size and health.

Keywords: agricultural robotics, berry plantation, dosing, product design and development.

1. Introduction

In a blueberry plantation, the plants are fertilised two or three times during the vegetation period, ie. in spring, summer, and autumn (Starast et al, 2002). This can be done both with mineral and liquid fertilisers. The fertilisation rate depends upon the age of the blueberry plants; it is lower at first, but higher later as the plants grow. In the first few years, the dose is about 20-30 g per plant, while it reaches up to about 60 g for each plant in later years (Starast et al, 2007; Virro et al, 2020).

Three mineral fertilisers are commercially available for fertilising blueberry plants on plantations; these are Agro NPK SQM QROP TOP K, Substral, and Agro Organic Memon Siforga. This article focuses mainly on the granulometric characterisation of these fertilisers. Blueberry fertilisers differ in their chemical composition and therefore in their areas of use. The Agro NPK fertiliser has a high nitrogen (N) content (12%), which activates the plant's growth and is therefore more suitable for spring fertilisation when the plants need to be stimulated to grow. It is certainly not wise to fertilise blueberry plants with this fertiliser in the autumn.

Substral fertiliser has a low nitrogen (N) content, but is high in phosphorus (P) and potassium (K), which makes it more suitable for autumn fertilisation, as P and K help the plant to prepare for winter. Substral is usually given to plants in early August. Of course, this fertiliser can also be applied in spring, if the soil has a low P and K content.

Agro Organic is a fertiliser which contains organic material (chicken manure). It actually contains all three elements, but in a relatively low concentration. It can be used for spring, summer, and autumn fertilisation. Consequently, all of the fertilisers shown in Table 1 are included in the list of fertilisers which are suitable for blueberry cultivation.

According to the authors of this paper, volumetric dosing is the most technologically suitable and simplest way in which to use precision fertilisation. There is reason to assume that, with the use of this technique, the volumetric doser is able to dispense the prescribed amount of fertiliser (in grams) to each blueberry plant. In order to set the volume metering unit, it is necessary to know the mechanical properties of the material that is to be dosed, ie. the fertiliser granules, including their granulometric properties, meaning the size of the fertiliser's particles (granules) and its bulk density.

The size and mass of the fertiliser particles (granules) are also important when spreading with a disc spreader, as these parameters affect the uniformity of fertiliser spreading (Aphale et al, 2003; Yule & Pemberton, 2009; Villette et al, 2010; Biocca et al, 2013). According to the available literature (Dintwa et al, 2003; Bulgakov et al, 2021), the particles of granulised fertilisers are not all of the same size. Particle size is estimated by the median diameter of those particles, d_{50} (Fulton & Port, 2016). Typically, the experimental determination of the granular composition involves the screening of a fertiliser sample using a set of sieves (Ivell & Nguyen, 2014; Fulton & Port, 2016). In the case at hand, this method of determination is unsatisfactory because it is not the fractional composition and surface uniformity of the application that are important for volumetric dosing, but the uniformity of the (individual) amounts to be dosed per plant.

The aim of this research was to determine and characterise specific blueberry fertilisers by their granulometric properties and provide possible uses for the data in order to choose a suitable doser.

2. Materials and Methods

1. The particle size of blueberry fertilisers

Although the fertiliser particles are depicted as spherical (Valius & Simutis, 2009), the fertiliser granules are rather ellipsoidal on visual inspection. In any case, the fertiliser particles are three-dimensional and can be characterised in the approximation of a sphere by three diameters which are measurable in three transverse planes (Fig 1). It is more convenient to evaluate different fertilisers according to the mean size of these granules, ie. their mean diameter. In order to characterise the size of the granules, this parameter is quite approximate, whereas the mean diameter d_m of the fertiliser granules must be understood as the geometric mean dimension, which can be determined as follows:

$$d_m = \sqrt[3]{d_1 \cdot d_2 \cdot d_3},\qquad(1)$$

where d_1, d_2 and d_3 are the diameters of the granules according to the scheme (Fig 1), with d_1 being the largest diameter and d_3 being the smallest.
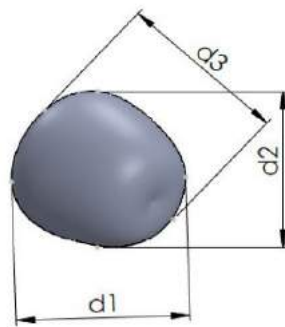
Figure 1. Schematic for measuring the geometrical parameters of a fertiliser granule.

To determine the mean diameter d_m of the blueberry fertiliser granules, ten random samples were taken from several different layers of each 1,000kg large bag of said mineral fertiliser; the diameters d_1, d_2 and d_3, for the hundred random granules from the sample were measured according to Fig 1. The mean diameter d_m of each granule was found according to formula (1). Then the mean statistical diameter of the hundred granules $d_{m,100}$ and the lower and the upper limits were determined: $d_{m,min}$ and $d_{m,max}$ respectively. All fertiliser samples were collected in separate cups. A Mahr Digital Caliper 16EWRi 0-150 mm was used to measure the diameters of the fertiliser granules with an accuracy of ± 0.01 mm. The caliper was connected to a computer, and the software used was MarCom Professional.

2. Bulk density of the blueberry fertilisers

Although the fertiliser manufacturers have indicated the bulk density of the fertiliser on the packaging for those fertilisers, it was appropriate for the sake of accuracy to specify it further within the context of this research. To be able to determine bulk density, the mass of a hundred fertiliser granules m_{100} was measured by weighing them. Their volume, V_0, was measured by means of a measuring glass; then their bulk density $\gamma_{f,i}$ was determined as follows:

$$\gamma_{f,i} = \frac{m_{100}}{V_0}.\qquad(2)$$

The mass m_{100} of a hundred granules of each fertiliser was determined in ten replicates, and their statistical mean was calculated. The analytical scale, Kern ABJ 220-4NM, was used to determine mass.

The volume V of a hundred fertiliser granules was then determined in ten replicates. The volumes were measured, using measuring glasses which had been manufactured to the GOST 1770-74 standard, with one measuring glass having a maximum volume of 10 ml in 0.2 ml increments and another having a maximum volume of 100 ml in 1 ml increments.

3. The mass-to-volume dependency of the fertilisers

According to the fertiliser dose Q, the fertiliser is precision-dosed by mass, within the range of $Q = 20\text{-}60$ g per plant. Based on this and the measurement results, the mass-to-volume dependency was determined for the fertiliser. For this purpose, a corresponding graph was prepared which contained approximation functions.

3. Results and Discussion

1. Granule size in blueberry fertiliser

The summary results are given in Table 1 for the measurement of the blueberry fertiliser granule diameters.

Table 1. Geometrical parameters of blueberry fertiliser granules.

Parameter \ Fertiliser	Substral	Agro NPK	Agro Organic
Diameter of granule d_1	3.98	4.82	5.11
Diameter of granule d_2	3.65	4.32	3.18
Diameter of granule d_3	3.45	3.82	2.64
Mean diameter of granule $d_{m,100}$, mm	3.68	4.29	3.64
Minimum diameter $d_{m,min}$, mm	2.52	3.08	2.66
Maximum diameter $d_{m,max}$, mm	4.86	6.09	5.07
Sample variance	0.22	0.28	0.19
Standard deviation	0.47	0.53	0.44
Standard error	0.047	0.053	0.044

The information in Table 1 is illustrated in Fig 2, which shows that different blueberry fertilisers have different mean diameters. While the mean diameters of the Agro Organic and Substral fertilisers are relatively similar, ie. 3.64 mm and 3.68 mm respectively, the mean diameter of the Agro NPK fertiliser is about 15% larger, or 4.29 mm.
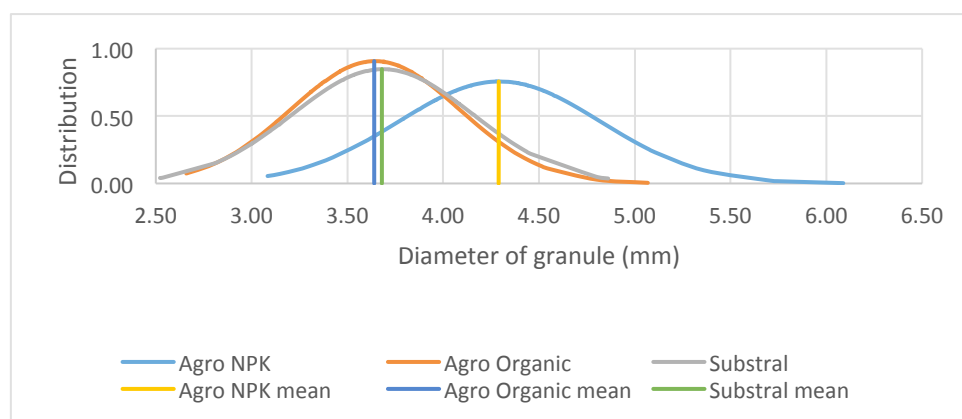
Figure 2. Distribution curves for the mean diameters of fertiliser granules.

In addition, the Agro Organic fertiliser contains a good deal of smaller granule debris inside. Knowing the granule diameter alone does not help us to set the doser so that it can dose the prescribed fertiliser amount; for that we also need to know the bulk density of the fertiliser in question.

2.The bulk density of blueberry fertiliser

The masses and volumes of a hundred pellet samples were determined in ten replicates in order to be able to identify the bulk density of the blueberry fertilisers. The measurement results are summarised in Tables 2, 3 and 4.

Table 2. The hundred-granule sample mass, volume, and bulk density for the Agro NPK fertiliser

Parameter	Mass m, g	Volume V_{avg}, ml	Bulk density γ_{avg}, g cm^{-3}
Mean	5.21	5.61	0.928
Standard error	0.22	0.22	0.007
Median	5.20	5.63	0.928

Standard deviation	0.70	0.68	0.022
Sample variance	0.49	0.47	0.0005
Range	2.18	2.20	0.073
Minimum	4.02	4.53	0.886
Maximum	6.20	6.73	0.959
Count	10	10	10

Table 3. The hundred-granule sample mass, volume, and bulk density for the Agro Organic fertiliser

Parameter	Mass m, g	Volume V_{avg}, ml	Bulk density γ_{avg}, g cm^{-3}
Mean	2.37	3.76	0.631
Standard error	0.11	0.17	0.003
Median	2.40	3.80	0.631
Standard deviation	0.35	0.53	0.010
Sample variance	0.12	0.28	0.0001
Range	1.16	1.73	0.033
Minimum	1.73	2.80	0.616
Maximum	2.88	4.53	0.649
Count	10	10	10

Table 4. The hundred-granule sample mass, volume, and bulk density for the Substral fertiliser

Parameter	Mass m, g	Volume V_{avg}, ml	Bulk density γ_{avg}, g cm^{-3}
Mean	3.31	4.01	0.824
Standard error	0.11	0.14	0.004
Median	3.34	4.03	0.820
Standard deviation	0.34	0.44	0.013
Sample variance	0.12	0.19	0.00017
Range	1.03	1.27	0.042
Minimum	2.69	3.27	0.809
Maximum	3.71	4.53	0.851
Count	10	10	10

The information in Tables 2, 3 and 4 shows that the masses and volumes for the hundred granule samples in all three fertilisers, as well as their bulk density, are clearly different. Statistical data processing shows that the results which were obtained are indeed reliable. The actual measured bulk densities would provide possibility to use a simple volumetric doser to precisely dose the fertiliser by determined weight. The granulometric properties enable the farmers to choose from many different dosers. Hereby, a doser with a grooved roller (Fig 3.) which rotates around its horizontal axis, is suggested as one of the possible solutions. It is recommended that the width of the dispensing roller would be adjustable for increased precision.

Figure 3. Grooved roller of a volumetric filler.

Fig 4 shows that, for all of the fertilisers which are under consideration, the volume increases linearly with mass. If, for example, we need to apply a dose of 50 g of fertiliser for each plant, for example the volumetric doser must be set to 50.6 ml for Substral, 54.9 ml for Agro NPK, and 66.35 ml for Agro Organic, ie. the volumetric doser must be adjustable and must also ensure that dosing is possible for the prescribed amount of fertiliser in grams for each plant.
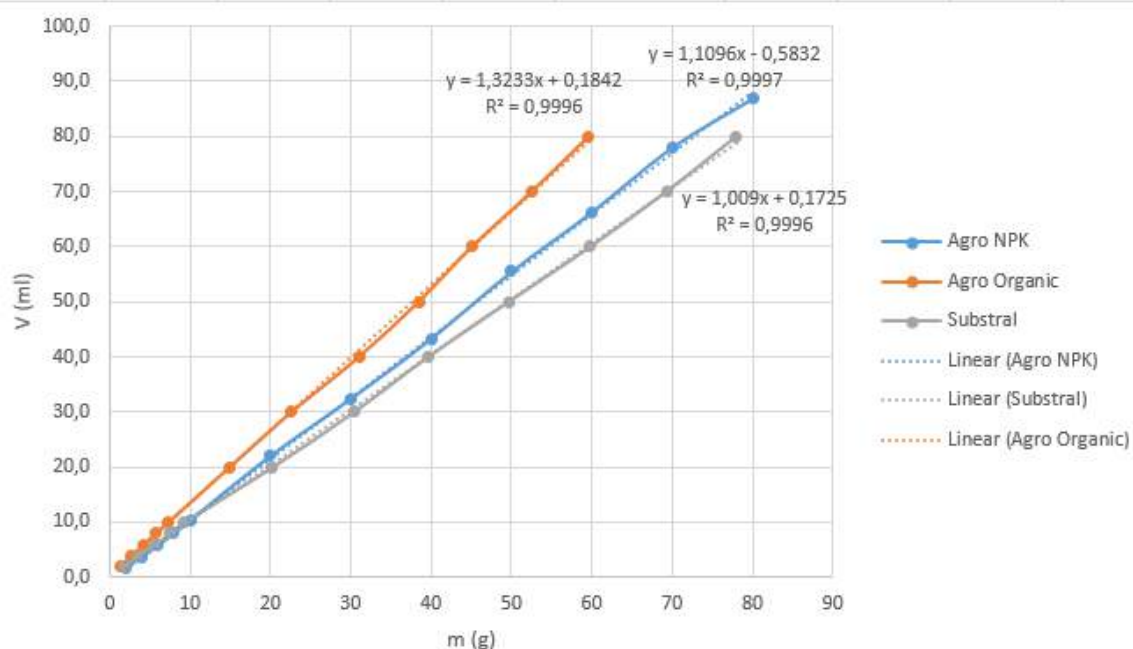
Figure 4. The mass-to-volume dependency of blueberry fertilisers.

4. Conclusions

Granulated fertilisers with different chemical properties (NPK) are used in berry cultivation. It turns out that these fertilisers also have different granulometric parameters. In the precision fertilisation of blueberry plants, the fertiliser must be dosed at the prescribed fertilisation rate, in grams per plant. The aim of this research was to determine the granulometric parameters: the mean diameter d_m and the bulk density $\gamma_{f,i}$ of Agro NPK, Agro Organic, and Substral fertilisers. The parameters enable to choose a suitable doser. It was suggested that it is expedient to carry out the dosing by mass, by for example using a simple volumetric doser, and in particular, a doser with a grooved roller which rotates around its horizontal axis. A mass-to-volume dependency was determined for the blueberry fertilisers, which can be used to set the volumetric doser for dosing granular fertilisers which have different parameters.

References

Aphale, A., Bolander, N., Park, J., Shaw, L., Svec, J., Wassgren, C. 2003. Granular fertiliser particle dynamics on and off a spinner spreder. Biosystems Engineering, 85(3), 319-329. doi: 10.1016/S1537-5110(03)00062-X.

Biocca, M., Gallo, P., Menesatti, P. 2013. Aerodynamic properties of six organo-mineral fertilizer particles. *Journal of Agricultural Engineering*, 44, Art. E83, 411-414.

Bulgakov, V., Adamchuk, V., Arak. M., Petrychenko, I., Olt, J. 2020. Theoretical research into the motion of combined fertilizing and sowing tractor-implement unit. *Agronomy Research* 15(4). 1498-1516. doi: 10.15159/AR.17.059.

Bulgakov, V., Adamchuk, O., Pascuzzi, S., Santoro, F., Olt, J. 2021. Research into engineering and operating parameters of mineral fertilizer application machine with new fertilizer spreading tools. Agronomy Research 19(S1), 676-686, doi: 10.151519/AR.21.040.

Chen, C., Pan, J., Lam, S.K. 2014. A review of precision fertilization research. *Environ Earth Sciences* 71, 4073-4080, doi: 10.1007/s12665-013-2792-2.

Dintwa, E., Van Liedekerke, P., Olislagers, R., Tijskens, E., Ramon, H. 2004. Model for simulation of particle flow on a centrifugal fertiliser spreader. Biosystems Engineering, 87(4), 407-415. Doi: 10.1016/j.biosystemseng.2003.12.009.

Ehret D. L., Frey B., Forge T., Helmer T., Bryla D. R., Zebarth B. J. 2014. Effects of nitrogen rate and application method on early production and fruit quality in highbush blueberry. *Canadian Journal of Plant Sciences,* 94: 1165-1179.

Farooque A. A., Zaman Q. U., Schumann A. W., Madani A. Percival D. C. 2012. Delineating management zones for site specific fertilization in wild blueberry fields. Applied Engineering in Agriculture, 28 (1): 57   70.

Fulton, J., Port, K. 2016. Physical properties of granular fertilizers and impact on spreading. The Ohio State University. FABE-550.1, 9 p.

Ivell, D.M., Van Nyugen, T. 2014. The Evolution of Screening Systems for Optimum Granular Fertilizer Product Quality. Procedia Engineering, 83, 328-335. DOI: 10.1016/j.proeng.2014.09.024.

Leit, I. 2017. Effect of genotype and fertilization on the chemical composition of blueberries under organic farming conditions: master thesis. Eesti Maaülikool, Tartu, Estonia, (in Estonian), 46 p.

Paal T., Starast M., Noormets-Šanski M., Vool E., Tasa T., Karp K. 2011. Influence of liming and fertilization on lowbush blueberry in harvested peat field condition. *Scientia Horticulturae*, 130 (1): 157−163.

Retamales J. B., Hancock J. F. 2018. Blueberries (2nd ed.). Crop Production Science in Horticulture Agriculture, book 29. CABI, 424 p.

Starast M., Karp K. Noormets M. 2002. The effect of foliar fertilisation on the growth and yield of lowbush blueberry in Estonia. Acta Horticulturae, 594: 679–684.

Starast M., Karp K., Vool E., Paal T., Albert T. 2007. Effect of NPK fertilization and elemental sulphur on growth and yield of lowbush blueberry. Agricultural and Food Science, 1: 34–45.

Vainura K. 2018. The influence of Monterra Malt fertilizers on the productivity and fruit chemical composition of blueberry's selections (*Vaccinium*): master thesis, Eesti Maaülikool, Tartu, Estonia, 63 p. (in Estonian).

Valius, G., Simutis, R. 2009. Modeling of continuous fertilizer granulation-drying circuit for computer simulation and control purposes. In: Proceedings of the 6th International Conference on Informatics in Control, Automation and Robotics – Signal Processing, Systems Modeling and Control, 98-103. Doi: 10.5220/0002206300980103.

Villette, S., Gee, C., Piron, E., Martin, R., Miclet, D., Paindavoine, M. 2010. Centrifugal fertiliser spreading: velocity and mass flow distribution measurement by image processing. In: Proceedings International Conf. on Agricultural Engineering, AgEng2010, Clermont-Ferrand, France, 6-8 September, 10 p.

Virro, I., Arak, M., Maksarov, V., Olt, J. 2020. Precision fertilisation technologies for berry plantation. *Agronomy Research*, 18 (S4), 2797−2810. DOI: 10.15159/AR.20.207.

Yamamoto, S., Hayashi, S., Yoshida, H., Kobayashi, K. 2014. Development of a Stationary Robotic Strawberry Harvester with a Picking Mechanism that Approaches the Target Fruit from Below, Japan Agricultural Research Quarterly: JARQ, 2014, Volume 48, Issue 3, 261-269 , https://doi.org/10.6090/jarq.48.261

Yule, I., Pemberton, J. 2009. Spreading Blended Fertilisers. 22nd Annual FLRC Workshop In: Nutrient management in a rapidly changing world. Eds L-D. Currie and C.L.Christensen. Occasional Report No 22. Fertiliser and Lime Research Centre, Massey University, Palmerston North, New Zealand, 243-249.

Comparison of Different Growing Substrates for the Vegetative and Reproductive Growth of Strawberry Plants

Bolappa Gamage Kaushalya Madhavi[a], Anil Bhujel[a], Na Eun Kim[a], Hyeon Tae Kim[a*]

[a]Department of Bio-systems Engineering, Gyeongsang National University (Institute of Smart Farm), Jinju 52828, Republic of Korea

* Corresponding author. Email: bioani@gnu.ac.kr

Abstract

The optimum production of strawberries requires the essential nutrients and an appropriate substrate for growth. The present study sought to determine the effectiveness of growth parameters in two phases of strawberries in different substrates growing in a controlled greenhouse. The significant effect substrates on the growth assessed by four treatments such as control soil (CS), bio plus compost (T_1), the combination of bio plus compost and synthetic nutrient applied soil substrate (T_2), and synthetic nutrient applied soil substrate (T_3). Morphology parameters like plant height, fresh weight, and dry weight of roots and canopy area were measured after eight weeks and sixteen weeks for each treatment and analyzed using completely randomized block designs through the variance with a significance level of $p < 0.05$. The canopy area was evaluated using an image processing technique applied in HSV colour space. Correspondingly, the maximum plant height, fresh weight, dry weight, and canopy area in the vegetative and reproductive phase attained $16.93+0.31$ cm and $19.34+0.21$ cm, $18.00+3.06$ g and $20.15+3.49$ g $5.15+1.26$ g and $6.66+2.34$ g, $23.02+1.94$ cm^2 and $28.78+0.93$ cm^2 observed in T_2 followed by T_1, T_3, and CS respectively. A comparison of the relative growth parameters T_2 exhibited better growth performance of the strawberry plants.

Keywords: Bio plus compost; Image processing technique; Strawberry plants; Substrate; Synthetic nutrient

1. Introduction

Strawberry (*Fragaria × ananassa*) is the leading fruit in the category of soft berries and cultivation under the protected structures in South Korea has gained momentum in the recent past. Strawberry is famous due to its glamorous red colour, the fragrance of sweet as well as delectable fruit among consumers. Since strawberry is a soft fruit, perennial plant that can be grown successfully at a day temperature of 22 °C to 25 °C and night temperature of 7 °C to 13°C. Specifically, the winter season is appreciable for the growth and productivity of strawberries in South Korea.

Growing substrate plays an intriguing role as a media and influences the water holding and nutrient dynamic to the plants. Nowadays, researchers are encouraged to find out alternatives for high-quality and low-cost soil substrates to apply for agricultural purposes. Correspondingly, the most commonly used soilless growing substrate for strawberries are peat moss, rock wool, perlite, and cocopeat (Thakur *et al.*, 2018). Moreover, commercial compost namely Bio plus (coco peat 68.86%, peat moss 11.00%, perlite 11.00%, and zeolite 9.00%) used as a standard compost in South Korea made from coconut and other biodegradable materials such as leaves and grass clipping, etc (Khan *et al.*, 2019). Concurrently, the application of compost improves the soil's physical and chemical properties as well as water retention ability especially addition in sandy loam soil as mentioned by Elanchezian *et al.*, 2019.

Growing substrate empirically related to the growth of strawberry plants and analyzing the growth rate is of paramount importance in the evaluation of primary productivity, which links crop yield and understanding of physiological phenomena that determine yield. A major reward of growth analysis lies in the ease of raw data measurements which is relied on growth parameters like plant height, canopy area, root fresh weight, and dry weight (Casierra *et al.*, 2012). Furthermore and even more importantly, growth analysis is essential to achieving a better understanding of physiological processes such as photosynthesis, respiration, and transpiration. Specifically, photosynthesis is logarithmically related to the leaf area expansion and biomass accumulation of plants and it influences the better reproductive structure development and yield performance of plants. Simultaneously, canopy area measurement is a key index in crop growth and breeding practices and the non-destructive measurement method of image processing technique already gives accurate and rapid information to modern agriculture production as reported by Easlon *et al.*, 2014. HSV (Hue, Saturation, Value) colour space is one of the digital image processing methods to determines the colours that exist in one part of the plant and this part will produce information about the plant canopy area as revealed by Setyawan *et al.*, 2018. Considering the above facts, the present study work was carried out to determine the growth performance of strawberries in the vegetative and reproductive phases under the different growing substrates.

2. Materials and Methods

2.1. Experimental design

This present experiment was laid out at the controlled greenhouse at Smart Farm Research Center of Gyeongsang National University, South Korea during the winter season in 2020. The overall experiment time was 120 days in winter (from the beginning of November to the end of February). The important environmental parameters such as temperature, CO_2 concentration, and humidity were daily monitored using a specific high accurate sensor unit MCH 383SD (Lutron Electronic Enterprises Co. Ltd., Taiwan), (Elanchezhian *et al*., 2019). In this investigation, four kinds of soil substrates such as control soil (C: N ratio-12:0.3), bio plus compost soil (C: N ratio- 30:1), the combination of bio plus compost, and synthetic nutrient applied soil substrate and synthetic nutrient applied soil substrate were assayed. In the beginning, 32 daughter plants of strawberry were planted with a distance of 0.5 m, and growth parameters in two stages (vegetative and reproductive) were measured after 8 weeks and 16 weeks of planting.

Plant height was measured in 25 plants of each treatment in two different growth phases using a metric ruler as reported by Basak *et al*., 2019. Generally, fresh weight and dry weight of 6 root samples from each treatment in two different growth phases were measured using a digital balance (Model-FX-300iWP, A&D Company Limited, Tokyo, Japan) and drying oven (Shelves for 5E-DHG6310: 2 layers, Changsha Kaiyuan Instruments Co., Ltd, Changsha 410100, PR China). The weight of roots was measured after drying at 80 ^{o}C for 48 h (Khan *et al*., 2019).

Subsequently, the canopy area measurement RGB camera (HZ 35 W, WB 650, Korea) was used to capture the images from every 6 plant samples from each treatment from bottom to top 50 cm working distance, and end of the experiment RGB images convert to black and white image using Python programming language. Every image taken from the RGB camera was downscaled into a 0.25 ratio and extract the green, yellow and brown colour threshold using the HSV colour model and converted into a black and white image (Chumuang et al., 2016). Concurrently, the Field of view was calculated by using camera focal length, sensor size, and working distance. Eventually, the smallest feature was calculated employing image resolution and field of view value. Total pixel counts were used to estimating the canopy area, according to the equation proposed by "Calculating Camera Sensor Resolution and Lens Focal Length", 2021.

2.2. Statistical analysis

The vegetative and reproductive phase data of strawberry plants were collected in MS Excel (Microsoft Office 2019, Seattle, WA, USA) and standard statistical methods were used in SPSS for data evaluation including analysis of variance (one-way ANOVA) to practice with a significance level of $p < 0.05$. The significant differences between the mean values of experimental data were tested with a Post-Hoc Tukey's HSD test in Statistics 10 (SPSS Version: 22.0.0, IBM, New York, USA).

3. Results and Discussion

The relevant to growing substrate T_2 in the vegetative and reproductive phases were observed the maximum plant height followed by T_1 and T_3 and the lowest plant height CS as represented in Table 1. Treatments (CS, T_1, T_2, T_3) were significantly different ($p < 0.05$) among each other, T_2 increased plant height might due to the better uptake of nutrients as mentioned by Khan *et al*., 2019.

The maximum fresh weight of root was measured in T_2 in the vegetative and reproductive phases followed by T_1, T_3, and CS respectively as presented in Table 1. Nevertheless, there was no significant difference ($p < 0.05$) between T_1 with T_2 and T_3 due to the synthetic nutrient solution which contains phosphorous that also directly correlated with the root growth promotion as revealed by Barita *et al*., 2018. Moreover, with regards to the dry weight of root in the reproductive phase, T_1 was no significant difference between T_2 and T_3 due to the root biomass increased in bio plus compost and synthetic nutrient contain soil at the same rate.

Table 1. Effect of different growing media on the growth of the strawberry plant in the vegetative and reproductive phases. Values in the columns with the same letters are not significantly different at p = 0.05.

Plant height (cm)		Fresh weight of the root (g)		Dry weight of the root (g)		Canopy area (cm^2)	
Vegetative phase	Reproductive phase	Vegetative phase	Reproductive phase	Vegetative phase	Reproductive phase	Vegetative phase	Reproductive phase
CS 7.97$\pm$0.36^d	9.82$\pm$0.52^d	6.74$\pm$1.33^c	7.74$\pm$1.19^c	1.95$\pm$0.26^c	2.21$\pm$0.29^c	15.58$\pm$0.79^c	19.29$\pm$1.03^d
T$_1$ 12.76$\pm$0.34^b	14.94$\pm$0.37^b	13.52$\pm$1.97^{ab}	16.09$\pm$3.28^{ab}	3.40$\pm$0.23^b	4.33$\pm$1.35^{ab}	21.46$\pm$0.31^a	24.28$\pm$0.80^b
T$_2$ 16.93$\pm$0.31^a	19.34$\pm$0.21^a	18.00$\pm$3.06^a	20.15$\pm$3.49^a	5.15$\pm$1.26^a	6.66$\pm$2.34^a	23.02 $\pm$1.94^a	28.78$\pm$0.93^a
T$_3$ 9.38$\pm$0.44 ^{c}	12.14$\pm$0.44^c	11.15$\pm$1.08^b	12.63$\pm$0.63^b	3.09$\pm$0.29^b	3.03$\pm$0.12^b	18.69$\pm$1.12^b	22.69$\pm$0.56^c
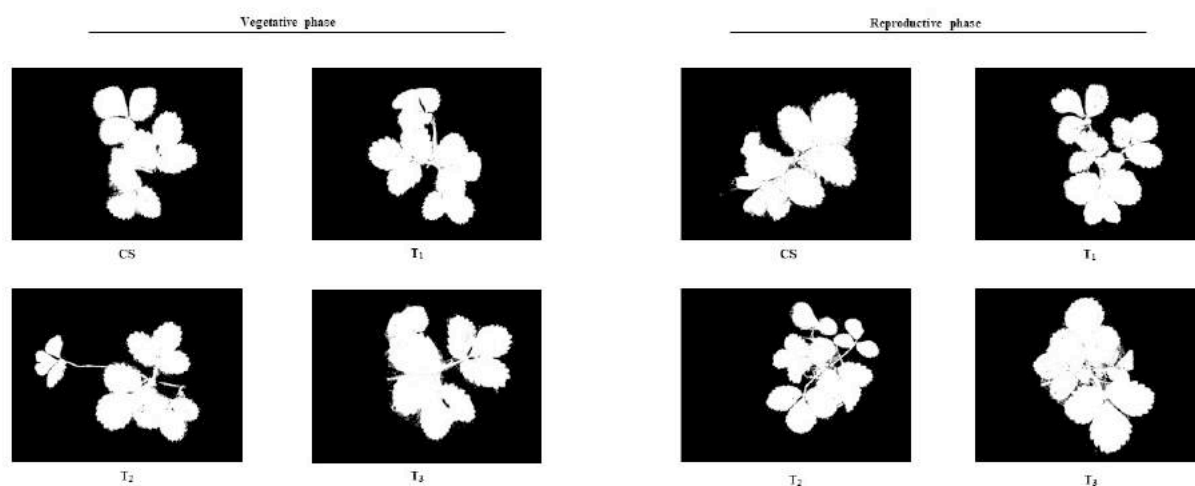
Figure 1. HSV developed images for canopy area calculation of strawberry plants in the vegetative and reproductive phases

The maximum canopy area for growing substrate in both phase T$_2$ was observed the highest followed by T$_1$, T$_3$, and CS as represented in Table 1 and the HSV developed images for canopy area calculation demonstrated in Figure 1. However, there was no appreciable difference between T$_1$ and T$_2$ canopy area in the vegetative phase at (p<0.05) level due to the release of a similar amount of nitrogen (N), phosphorous (P), and potassium (K) level and subsequently develop the leaf area with the same rate. Furthermore and even more importantly, the canopy area was gradually increased in the reproductive phase due to the composting process slowly release the minerals from the soil as revealed by Odongo *et al*., 2008. In addition to that higher microbial biomass in bio plus compost containing substrates which are T$_1$ and T$_2$ influence, the mineralization process and humic acid production during the composting process, and this substance correlates with the production of plant growth regulators which increase the growth rate of strawberry plants. Moreover, T$_2$ exhibited the highest growth rate compared to T$_1$ due to the containing of a synthetic nutrient solution except to bio plus compost. On the other hand, N in synthetic nutrients stimulates bud formation and gradually develops into leaves and crowns, P facilitates cell division and membrane development, and K increases the growth rate and considerably enhances the leaf area (Madhavi *et al*., 2021).

4. Conclusions

The findings of the present investigation concluded that a comparable growing pattern and the increasing trend in the plant height, canopy area, root fresh weight, and dry weight in T$_2$ treatment. Furthermore, T$_2$ has enriched with higher available minerals and beneficial microbes that lead to producing humic substances and growth regulators which

increase significantly for the vegetative and reproductive growth of strawberry plants grown under protected conditions.

References

Barita, Y., Prihastanti, E., Haryanti, S. and Subagio, A., 2018, May. The influence of granting npk fertilizer and nanosilic fertilizers on the growth of Ganyong plant (Canna edulis Ker.). In *Journal of Physics: Conference Series* (Vol. 1025, No. 1, p. 012054). IOP Publishing.

Basak, J.K., Qasim, W., Okyere, F.G., Khan, F., Lee, Y.J., Park, J. and Kim, H.T., 2019. Regression analysis to estimate morphology parameters of pepper plant in a controlled greenhouse system. *Journal of Biosystems Engineering*, *44*(2), pp.57-68.

Calculating Camera Sensor Resolution and Lens Focal Length. Ni.Com, 2021. Retrieved 23 February2021. https://www.ni.com/enus/support/documentation/supplementa l/18/calculating-camera-sensor-resolution-and-lens-focal-length.html.

Casierra-Posada, F., Peña-Olmos, J.E. and Ulrichs, C., 2012. Basic growth analysis in strawberry plants (Fragaria sp.) exposed to different radiation environments. *Agronomía Colombiana*, *30*(1), pp.25-33.

Chumuang, N., Thaiparnit, S. and Ketcham, M., 2016. Algorithm design in leaf surface separation by degree in hsv color model and estimation of leaf area by linear regression. In 2016 12th International Conference on Signal-Image Technology & Internet-Based Systems (SITIS) (pp. 628-631). IEEE.

Easlon, H.M. and Bloom, A.J., 2014. Easy Leaf Area: Automated digital image analysis for rapid and accurate measurement of leaf area. *Applications in plant sciences*, *2*(7), p.1400033.

Elanchezhian, A., Khan, F., Basak, J.K., Park, J., Okyere, F.G., Lee, Y.J. and Kim, H.T., 2019, June. Analysis of water retention capacities of various compost and its relationship to strawberry moisture level. In *International Symposium on Advanced Technologies and Management for Innovative Greenhouses: GreenSys2019 1296* (pp. 899-906).

Khan, F., Okyere, F.G., Basak, J.K., Qasim, W., Park, J., Arulmozhi, E., Lee, Y.J. and Kim, H.T., 2019, June. Comparison of different compost materials for growing strawberry plants. In *International Symposium on Advanced Technologies and Management for Innovative Greenhouses: GreenSys2019 1296* (pp. 869-876).

Madhavi, B.G.K., Khan, F., Bhujel, A., Jaihuni, M., Kim, N.E., Moon, B.E. and Kim, H.T., 2021. Influence of different growing media on the growth and development of strawberry plants. *Heliyon*, p.e07170.

Odongo, T., Isutsa, D.K. and Aguyo, J.N., 2008. Effects of integrated nutrient sources on growth and yield of strawberry grown under tropical high altitude conditions. *African Journal of Horticultural Science*, *1*.

Setyawan, T.A., Riwinanto, S.A., Nursyahid, A. and Nugroho, A.S., 2018, September. Comparison of HSV and LAB Color Spaces for Hydroponic Monitoring System. In *2018 5th International Conference on Information Technology, Computer, and Electrical Engineering (ICITACEE)* (pp. 347-352). IEEE.

Thakur, M. and Shylla, B., 2018. Influence of different growing media on plant growth and fruit yield of strawberry (Fragaria× ananassa Duch.) cv. Chandler grown under protected conditions. *International Journal of Current Microbiology Applied Sciences. 2018a*, *7*, pp.2724-2730.

Challenges for Agriculture Through Industry 4.0

Heinz Bernhardt [a,*], Mehmet Bozkurt [b], Reiner Brunsch [c]; Eduardo Colangelo [d], Andreas Herrmann [b], Jan Horstmann [e], Martin Kraft [f], Johannes Marquering [g], Thilo Steckel [h], Heiko Tapken [i], Cornelia Weltzien [c], Clemens Westerkamp [i]

[a] Agricultural System Engineering, Technical University of Munich, Freising, Germany

[b] VDI – The Association of German Engineers, Düsseldorf, Germany

[c] ATB Leibniz-Institut für Agrartechnik und Bioökonomie, Potsdam, Germany

[d] Fraunhofer IPA, Stuttgart, Germany

[e] Krone, Spelle, Germany

[f] Johann Heinrich von Thuenen Institute, Braunschweig, Germany

[g] University of Applied Sciences Jade, Wilhelmshaven, Germany

[h] CLAAS E-Systems, Dissen a.T.W., Germany

[i] University of Applied Sciences Osnabrueck, Osnabrueck, Germany

* Corresponding author. Email: heinz.bernhardt@wzw.tum.de

Abstract

Industry 4.0 is currently considered the structural implementation of networked and cooperative digitalisation and the next step in technological and social development. The aim is to examine how these structures are also suitable for agriculture and whether there are already approaches to this. Therefore, the main aspects of Industry 4.0 will be analysed and compared with agricultural examples from arable farming and livestock farming.

The study shows that the approaches of Industry 4.0 are also useful for agriculture. However, they must be adapted to agriculture, as it has a different basic structure. As in industry, it is also evident in agriculture that there is still a need for action in the organisational and technical networking of systems.

Keywords: agriculture 4.0, digitisation, networks, smart farming

1. Introduction

The terms industry 4.0 and agriculture 4.0 are currently the subject of much public debate on the future development of the sectors. However, a more detailed analysis shows that both the content of the individual terms and their possible interrelationships are not sufficiently clarified. In many cases, everyone associates them with his or her own image and imagination. (Ghobakhloo, 2020; Schmidt, 2018; Rose, 2018; Ozdogan, 2017) As a result, although everyone uses the same term, very different ideas are associated with it. This is a very poor basis for a common orientation that the pair of terms is intended to achieve. (Weltzien, 2016)

Here, a structure is to be created within the framework of a VDI/VDE guideline committee on the subject of "State of Industrial Use 4.0 - Technologies in Agricultural Engineering". The discussion covers several levels. It is based on the current understanding of the term Industrie 4.0 with its structure and objective for the industrial sector. In the transition from Industry 4.0 to agriculture, the sectoral differences between industry and agriculture must be analysed. This includes not only technology, but also the different orientations in economics, ecology and sociology. Based on this, the current state of the structures of Industry 4.0 in agriculture will be presented in practice and theory using various examples from arable and livestock farming. In summary, it can be seen that the contents of the terms used still need to be coordinated in many areas. (Rojko, 2017)

The term "Industry 4.0" became widely known with the Hannover Fair 2013. It goes back to an initiative of the Federal Government in Germany in 2011. (Kagermann, 2011) To date there is still no binding definition of the term "Industry 4.0", but a generally accepted understanding is emerging. (Müller, 2017; Saurabh, 2018; Frank, 2019) The term "Agriculture 4.0" has developed from this. However, this term is even more difficult to grasp. So far, "Agriculture 4.0" has been little more than a kind of advertising slogan, claiming state-of-the-art IT and production concepts and techniques for agriculture. Often "Agriculture 4.0" is just a new coat that means digital techniques in agriculture and precision farming, as in Roland Berger Focus - Agriculture 4.0 (Aulbur, 2019). In order to find a well-founded definition of "Agriculture 4.0" as a revolutionary stage of agricultural production, the generations 1.0 to 3.0 of agriculture must first be defined. At first glance, it looks relatively easy to name the individual stages with threshing machine, tractor and ISO-BUS for machine communication. However, others also mention mineral fertiliser or the green revolution as corresponding stages. It is therefore relatively difficult to describe the revolution that led to 4.0 - if there is a revolution at all that justifies a new generation 4.0. On the other hand, some authors already see a coming "Agriculture 5.0" on the horizon. (Fraser, 2019; Murugesan, 2019) In the absence of such general clarification, the term "Agriculture 4.0" is avoided in this paper.

2. Materials and Methods

In order to check the transferability of Industry 4.0 applications to agriculture, it is first necessary to clarify how the system is understood in the industry. Over the last 270 years, industry has developed in the context of the so-called "industrial revolutions". The first industrial revolution began in the second half of the 18th century with the development of the steam engine. The second revolution took place towards the end of the 19th century with the development of mass production and the use of electrical energy. In the second half of the 20th century, the third industrial revolution began, characterised by the automation of production using electronic and IT approaches.

Each industrial revolution brings about a fundamental change in the production paradigm, made possible by the development of one or more technologies which trigger a fundamental change in established ideas and practices. However, their impact is not limited to production; they touch and influence the whole of society.

The current stage, caused by the fourth industrial revolution, is known as Industry 4.0. It differs from the third industrial revolution in that it focuses on networking the various automation modules. (Li Da, 2018)

Despite the current widespread use of the Industry 4.0 concept, it is difficult to find a clear definition. The term is best described by its components.

From a purely technical point of view, the Industry 4.0 approaches can be summarised under the term networking. Instead of managing different machines, sensors etc. individually, as was previously the case, Industry 4.0 is based on cyber-physical systems (CPS), which can be connected and used flexibly, and on the equally flexible service-oriented architecture (SOA), which enables the use of the necessary software components. (Bauernhansel, 2017) This also improves the possibility of simulating processes up to the digital twin of the process. However, the networked and service-oriented character of Industry 4.0 goes beyond the boundaries of purely technical aspects and enables the design of new business models (Demot, 2017).

From this, the following implementation options (Bauernhansel, 2015) can be derived for the intelligent products and services to be offered by Industry 4.0:

Digital individualisation: Digital media considerably simplify the offer of individualised products and services. This includes the entire production chain from customer request to realisation.

Flexibilisation: Industry 4.0 offers, for example, the possibility to react quickly to fluctuations in demand by making production capacities more easily scalable (e.g. through more intelligent plants and simplified capacity procurement) and by making more data available about the environment and the company itself.

Demand orientation/ "X-as a service": Service orientation will be transferred to business models, which in turn will be facilitated by increasing data volume and flexibility. For example, products and services can be offered and billed according to the extent of use.

Sustainability: Better planning and control of production processes through digitisation can save resources, e.g. through cost- and load-optimised production programmes for energy-intensive processes. The availability of extended and timely data from production and the supply chain, e.g. through the early detection of quality problems, allows an additional reduction in resource requirements.

Consistent process orientation: The networking capability enables each value-added stage in the supply chain (internal and external to the company) to call up information on the overall process. This enables a customer- and employee-oriented work organisation.

Automated knowledge and learning: The increase in data volume and the degree of automation in Industry 4.0 environments prove to be ideal prerequisites for the use of self-learning functionalities. The data can come from outside the company boundaries, for example through IoT approaches. In addition, the systems in question enable extended and simplified knowledge management in companies.

Collaboration competence: In terms of end-to-end process optimisation, Industry 4.0 approaches reduce the amount of cooperation between value-added partners. For example, it is possible to know the current stock and available capacity of suppliers.

Productivity optimisation: All the above-mentioned implementation options contribute to an increase in productivity. Optimisation options can be found at various levels, from the strategic orientation of the company to the operational management of production processes.

Although these implementation options have been analysed for the machinery and equipment sector, the identified benefits are also relevant for agriculture. However, implementing a highly flexible and distributed architecture is not without its challenges. The desired fast connection in the production chain also requires a corresponding data exchange. However, this requires appropriate standardisation or standardised interfaces and data formats between components from different manufacturers.

The processing and storage of data on distributed systems, often outside the company, gives cause for concern about

data security. Both software-based and methodical approaches are being developed for this purpose. While the former are based on novel security applications and protocols, the latter focus on issues such as intelligent data control and anonymization. The analysis of the definition of Industry 4.0 shows that this definition is still under development and discussion.

If the definition of Industry 4.0 is applied to agriculture, it quickly becomes clear that agriculture is still characterised by additional aspects. (Sonnen, 2019) Particularly striking here is the environmental character of agriculture, which includes not only society and the state, but also to a large extent nature, the environment, people, farm animals and the weather. The organisation of work is also structured differently in agriculture than in industry. This shows that the socio-economic, technical and ecological systems in agriculture are much more closely interwoven, which makes the definition of "Agriculture 4.0" more difficult than in industry.

3. Results and Discussion

In order to explain the current status of Industry 4.0 approaches in agriculture, examples from arable farming and livestock farming are therefore used and a differentiation and description possibility based on technological levels is created.

3.1. Approaches for Industry 4.0 in arable farming

3.1.1.Focus on combine harvesters

Combine harvesters are among the most complex agricultural machines. Several hundred measurement and control variables have to be taken into account in order to achieve the desired result in the harvest. The combine harvester has the advantage that it is a single machine. It does not have to communicate with several machines for the process, as is the case with the tractor with soil cultivation and sowing. Assistance systems such as automatic steering systems were used early on to manage the complexity in the combine. This level of automation shows a certain similarity to industry, which simplifies the analysis with Industry 4.0 approaches.

There are limits to digital individualisation in numerous cultures and forms of exploitation. In the area of large crops such as wheat, maize and soya, it is important to realise the greatest possible mass flows while complying with certain limit values. Individualisation can be found in the areas of area planning, vehicle design and straw processing. Methods for selective harvesting would be a good example of individualisation; it has not yet become established.

For climatic reasons, there are narrow limits to the flexibility of harvesting in the open field. Greater flexibility can be achieved if it is possible to limit the variability of the environment, which is not necessarily in the spirit of sustainable agriculture, or to design the specificity of machines in such a way that they can follow the variability of the environment as well as possible.

The advent of sensors and corresponding telematics systems has led to a corresponding transparency of information in combine harvesters. The general availability of mobile devices contributes to the fact that this data is now also available to all participants at the same time.

The high investment volume and short service life associated with combine harvesters for individual farms have long led to service offers for harvesting capacities. In most cases, the entire harvest is contracted out on the basis of the harvested area. The offer of peak load capacities for fluctuating harvest volumes hardly exists. Increasing digitalisation could provide the basis for more precise recording and evaluation and enable new offers here.

The current state of harvesting technology has different impacts on sustainability. Currently, larger machines and increased efficiency save resources, but these larger machines can also lead to increased ground pressure.

Combine harvesters are already highly process-oriented. Currently, this is still associated with a high degree of internal complexity. Methods from the Industry 4.0 toolbox can improve this.

The high degree of digitalisation in combine harvesters already creates an extensive basis for generating and using automated knowledge and learning. This provides a good basis for the training of employees, as the operating time of the machine is limited and high performance must be achieved during this period.

Collaboration skills as well as productivity optimisation are a central point in the further development of the combine harvester. So far, the combine harvester has been optimised as an individual machine. To enable productivity increases in the future, interaction with other process participants, such as logistics, is necessary. This offers corresponding opportunities for Industry 4.0 applications.

The concept of services and interoperability in harvesting processes is complex. Harvesting as a mechanised process is offered as a service for the reasons already mentioned. Service engineering methods can be used to further develop such services into hybrid service bundles. Service platforms for trading harvesting capacities, offers for breaking peak loads, individualised billing modalities and special data offers are examples of diverse possibilities.

3.1.2.Focus on logistics

Almost all processes in agriculture contain logistical components. Nevertheless, little attention is paid to this area. Agriculture describes itself as a "transport industry against its will". This fact makes it particularly interesting with regard to Industry 4.0 aspects.

Unlike industrial logistics, logistical processes in agriculture do not run according to a timetable. Due to local conditions and boundary conditions that are difficult to plan, individualisation inevitably results. Digital individualisation in Industry 4.0 is an active measure, whereas in agriculture it is more of a reactive measure. In order to implement digital individualisation in agricultural logistics, it is necessary to apply complex methods due to the complex influencing factors.

Flexibility is a basic structure in agricultural logistics due to the multitude of product and process requirements. In contrast to industry, agriculture has never succeeded in standardising these, so the Industry 4.0 approach to flexibilisation is advantageous for agriculture.

Information transparency is insufficient in agricultural logistics. As there are hardly any digital processes in this area, data can hardly be exchanged. However, this would be absolutely necessary to support the upstream and downstream processes.

Legal regulations are leading to an increasing contracting out of logistics services to agricultural contractors. Further forms of demand-oriented trading are not to be seen. Exchanges for the procurement of services and capacities have been tested, but have not yet become established.

In logistical processes, there are significant losses in efficiency due to lack of transparency and the compulsory parallelism of sub-processes. As a result, waste leads to unnecessary consumption of resources and can thus be described as unsustainable. Transparency can improve this situation.

Process orientation is an outstanding goal in logistics, but it is only partially achieved for the reasons mentioned above. Process orientation and sustainability are mutually dependent.

The planning and control of logistical processes is almost exclusively experience-based. If it is possible to create additional knowledge and possibilities for action with methods of automated knowledge and learning, further potential can be raised. This will also benefit the documentation and analysis of processes, e.g. by automatically recognising defined states and providing recommendations for action in the next step.

So far, collaboration has mainly taken place through informal communication. The development of tools to improve transparency is one step that enables improved collaboration. Building on this, however, it is necessary to offer decision support with quantitative methods.

The networking of process participants in logistical processes is a basic prerequisite for creating transparency and improving processes. In contrast to industrial processes, permanent availability and sufficient bandwidth for the transmission of messages cannot be assumed. Therefore, it is important here to achieve the highest possible robustness in communication with the help of suitable technologies and methods.

Interoperability is the basic prerequisite for establishing networking in logistical processes. The standardisation of messages, such as in the context of ISOBUS, is one way. Self-describing interfaces, e.g. in the context of web services, enable further flexibility.

3.2. Approaches for Industry 4.0 in livestock farming

Animal husbandry in agriculture has many more parallels to industry than arable farming. Production takes place in buildings with regulated structures and a continuous process throughout the year. This suggests that there may already be more approaches to Industry 4.0 to be found here.

Automation is widespread in dairy farming due to the clearly structured and recurring daily processes. This has led to a large number of automated systems and sensors in dairy farming. The most important building blocks are the Automatic Milking System (AMS), the Automatic Feeding System (AFS) and automatic cleaning and bedding systems. In addition, a variety of sensors can be found in the barn, such as animal identification, animal location, heat detection, calving detection or barn climate. (Höhendinger, 2019) The situation is similar in pig and poultry farming. Here, feeding, climate control and manure removal are also automated.

In the area of digital individualisation, there are a wide variety of approaches in animal husbandry. One system that is already widely used for dairy cows and sows is the individualised distribution of concentrated feed via a station with identification of the animal via transponder. Another is the matching of cows in the AMS on the basis of the stored body measurements, among other things. However, it is apparent that many points of individualisation are not yet being used. For example, there is still no individual marketing of milk according to the protein pattern of the cow, and in the case of poultry and pigs, work is only done in groups and individuality is not taken into account.

There are hardly any signs of flexibilisation in livestock farming. The trend is currently still towards standardisation as it corresponds to Industry 3.0. The potential for flexibility is not being used.

In terms of its basic structure, livestock farming is actually predestined for comprehensive information transparency. In the individual systems, the data is also collected and used accordingly. But unfortunately there is no general and open data interface to make the data sufficiently public and share it with other systems. In some cases, the necessary information transparency is not even given between different systems of one manufacturer.

The lack of demand orientation is currently a major problem in livestock farming in Germany. Production structures are relatively inflexible and therefore have difficulty adapting to changes in demand. The easiest application would still be in poultry farming due to the short production cycles, and correspondingly difficult in pigs and dairy cows due to the longer production cycles.

Due to its structure, farm animal husbandry is fundamentally process-oriented, with the main processes such as meat, milk or egg production being linked to correspondingly complex secondary processes.

A common problem in livestock farming is that these processes are usually not documented in a structured way that is comprehensible to others. This means that measuring points and links are not optimally recognised, which makes the use of decision models and their implementation more difficult. Methods from the Industry 4.0 toolbox would offer fundamental approaches to improving process orientation here.

In the area of automated knowledge and learning, current automation in animal husbandry offers great potential, as animal-specific data series are continuously generated. However, this data is not yet consistently used in the sense of Industry 4.0. The situation is similar with collaboration skills. Here, the networking of various automatic systems in the barn would result in many approaches for Industry 4.0. For example, a measured change in the movement activity of fattening pigs could lead to an automatic adjustment of the climate control. This intelligent linking of different automated systems also enables an optimisation of productivity, which can simultaneously lead to a change in the farmer's work structure in the system.

In principle, livestock farming offers good conditions for networking the individual systems due to its fixed spatial structure. In many cases, networking can be done via cables to a central point. Difficulties are often encountered here in the recording of individual data on the animal in wireless networks, as there is no uniform data standard.

Areas such as piglet production, chick production, feed production and manure spreading can be outsourced as animal husbandry services. However, it is often the case that although the process or product is outsourced, no arrangements are made for data exchange or it does not take place. As a result, these areas are often underrepresented on the farm in terms of data and thus cannot be used for networked decisions.

4. Conclusions

When analysing the applications of Industry 4.0 in agriculture, it is noticeable that although many things initially look like 4.0, on closer inspection decisive aspects such as cross-sector networking or the individualisation and flexibilisation of production are missing. These technical solutions are therefore more likely to be classified as automated stand-alone solutions of Industry 3.0.

The challenges for the implementation of Industry 4.0 in agriculture can be identified as process orientation, standardisation, data communication and knowledge transfer. In the case of process orientation, it can be seen that this has not yet fully penetrated agriculture and tools such as digital twins cannot be sufficiently implemented. This is also reflected in standardisation. Here, the ISO bus is available in arable farming, but adapted development is also necessary here. Unfortunately, a similar system is lacking in livestock farming. The individual systems are mostly self-contained and do not communicate and cooperate with each other. In addition, the transitions between the individual links in the production chain are not standardised across the board. Here, even in the case of in-house management systems, the step back to the paper level is taken.

In addition to the organisational structure of data exchange, the technical infrastructure must also be expanded accordingly, as both wired and radio-based data networks still have performance gaps, especially in rural areas. In order to be able to understand and appropriately use the possibilities of Industry 4.0 applications, a corresponding structure for the further training of users is also necessary. New and flexible learning structures that adapt to the requirements of the users are also necessary here.

Another aspect that is often pointed out is the gap between the practical implementation and the technologically possible realisation. An example of this is TIM for balers and tractors. Here, implementation is slow, although it would be technically possible. With a view to Industry 4.0 approaches, there are also other possible aspects, such as track shifting via process steps, track planning based on the combine harvester's performance or logistics planning based on yield estimates. This can also be observed in livestock farming. Here, quarter-individual milking based on past milking cycles or the route optimisation of cleaning robots based on the current movement data of cows would correspond to the basic idea of Industry 4.0.

In many cases, these technological developments would only require corresponding adjustments and coordination.

However, this requires a cross-manufacturer will, which is often hindered by company-specific interests. It is obvious that without cross-manufacturer networking, no application of Industry 4.0 in agriculture is possible, but only the automation of individual machines.

References

Aulbur, Wilfried; Henske, Robert; Morris, Gillian; Schelfi, Giovanni 2019. Farming 4.0: How precision agriculture might save the world. Roland Berger Focus, Roland Berger GmbH, München.

Bauernhansl, Thomas 2017. Industry 4.0. in the field of tension between market, technology and organisation. In: Organisational Development: Journal for Corporate Development and Change Management (2), pp. 32-38.

Bauernhansl, Thomas; Schatz, Anja 2015. Industry 4.0 for business model innovations. Procedure for developing industry-specific business model scenarios. In: wt Werkstattstechnik online 105 (3), pp. 79-83.

Bernhardt, Heinz 2019a. Livestock Engineering Machinery and Techniques for Cattle Husbandry. In: Frerichs, Ludger (Ed.): Jearbook Agricultural Engineering 2018. Braunschweig: Institut für mobile Maschinen und Nutzfahrzeuge, 2019, pp. 1-13, https://doi.org/10.24355/dbbs.084-201901211151-0

Bernhardt, Heinz, Martin Höhendinger, Anja Gräff, Omar Hijazi, Manfred Höld, Matthias Reger, Jörn Stumpenhausen 2019. Development of Automatic Milking in Germany, 2019 ASABE Annual International Meeting 1900127. https://doi.org/10.13031/aim.201900127)

Demont, Anja; Paulus-Rohmer, Dominik 2017. Developing Industry 4.0 business models systematically. In: Daniel Schallmo, Andreas Rusnjak, Johanna Anzengruber, Thomas Werani and Michael Jünger (eds.): Digital Transformation of Business Models, vol. 3. Wiesbaden: Springer Trade Media Wiesbaden, S. 97-125.

Fraser, Evan D. G.; Campbell, Malcom 2019. Agriculture 5.0: Reconciling Production with Planetary Health. One Eart (1). p 278-280.

Germán, Frank Alejandro; Lucas Santos Dalenogare, Néstor Fabián Ayala 2019. Industry 4.0 technologies: Implementation patterns in manufacturing companies, International Journal of Production Economics (210) p15-26, https://doi.org/10.1016/j.ijpe.2019.01.004.

Ghobakhloo, Morteza, 2020. Industry 4.0, digitization, and opportunities for sustainability. Journal of Cleaner Production (252), 119869. https://doi.org/10.1016/j.jclepro.2019.119869.

Höhendinger, Martin, Natascha Schlereth, Maximilian Treiber, Manfred Höld, Jörn Stumpenhausen, Heinz Bernhardt 2019. Potential of cyber-physical systems in German dairy farming, 2019 ASABE Annual International Meeting 1900221. https://doi.org/10.13031/aim.201900221

Kagermann, H., Lukas, W. D., Wahlster, W. 2011. Industrie 4.0: Mit dem Internet der Dinge auf dem Weg zur 4. industriellen Revolution. VDI Nachrichten, 13(1).

Li Da Xu, Eric L. Xu & Ling Li 2018. Industry 4.0: state of the art and future trends, International Journal of Production Research, (56)8, p. 2941-2962, https://doi.org/10.1080/00207543.2018.1444806

Müller J., Dotzauer V., Voigt K. 2017. Industry 4.0 and its Impact on Reshoring Decisions of German Manufacturing Enterprises. In: Bode C., Bogaschewsky R., Eßig M., Lasch R., Stölzle W. (eds) Supply Management Research. Advanced Studies in Supply Management. Springer Gabler, Wiesbaden. https://doi.org/10.1007/978-3-658-18632-6_8

Murugesan, Rajkumar; Sudarsanam, S. K.; Malathi G.; Vijayakumar, V.; Neelanarayanan .V; Venugopal R.; Rekha, D.; Saha, Sumit; Bajaj, Rahul; Miral, Atishi; Malolan, V. 2019. Artificial Intelligence and Agriculture 5.0. Int. J. Recent Technology and Engineering (8) p. 1870-1877.

Ozdogan, B, Gacar, A, Aktas, H. 2017. DIGITAL AGRICULTURE PRACTICES IN THE CONTEXT OF AGRICULTURE 4.0. Journal of Economics Finance and Accounting 4 (2), 186-193. http://doi.org/10.17261/Pressacademia.2017.448

Rojko, Andreja. 2017. Industry 4.0 Concept: Background and Overview. International Journal of Interactive Mobile Technologies (iJIM) 11(5) p. 77-90. http://dx.doi.org/10.3991/ijim.v11i5.7072.

Rose David Christian, Chilvers Jason 2018. Agriculture 4.0: Broadening Responsible Innovation in an Era of Smart Farming, Frontiers in Sustainable Food Systems. (2) p. 87, https://doi.org/10.3389/fsufs.2018.00087

Saurabh Vaidya, Prashant Ambad, Santosh Bhosle 2018. Industry 4.0 – A Glimpse. Procedia Manufacturing (20) p 233-238, https://doi.org/10.1016/j.promfg.2018.02.034.

Schmidt C. 2018. Landwirtschaft 4.0 – Digitalisierung als Chance für eine nachhaltige Landwirtschaft. In: Bär C., Grädler T., Mayr R. (eds) Digitalisierung im Spannungsfeld von Politik, Wirtschaft, Wissenschaft und Recht. Springer Gabler, Berlin, Heidelberg. https://doi.org/10.1007/978-3-662-55720-4_38

Sonnen, Johannes 2019. Digitization and Automation Digitization and networking. In: Frerichs, Ludger (Ed.): Jearbook Agricultural Engineering 2018. Braunschweig: Institut für mobile Maschinen und Nutzfahrzeuge, pp. 1-11, https://doi.org/10.24355/dbbs.084-201901211129-0

Weltzien Cornelia 2016. Digital agriculture – or why agriculture 4.0 still offers only modest returns. Landtechnik 71(2). p. 66–68. https://doi.org/10.15150/lt.2015.3123

New Approaches for Improving Nitrogen Efficiency based on Clustering Algorithms

Philipp Kastenhofer [a, *], Peter Prankl [a], Peter Riegler-Nurscher [a], Johann Prankl [a]

[a] Josephinum Research, Rottenhauser Straße 1, Wieselburg, Austria

* Corresponding author. Email: philipp.kastenhofer@josephinum.at

Abstract

Site-specific fertilization attempts to address the heterogeneities within a field by supplying plants with their respective nutrient requirements while also taking account of the heterogeneous yield capacity of the soils. This is intended to increase efficiency which, in addition to economic advantages, also brings ecological benefits.

To determine the actual nutrient requirements of plants, data from the local site and the vegetation condition must be interpreted and processed. Among other things, the use of satellite-based multispectral images (Sentinel-2) is being investigated and applied for the site description.

Fertilization models often assume a compensatory site which means that poorly developed areas of cereal fields in the spring can be compensated with a higher amount of fertilizer. In years with dry periods, especially in soils with low water holding capacity, the possibility of misinterpretation arises and thereby increases the ecological risks. These low-yield sites must be excluded from the existing system and treated separately. For this purpose, historical vegetation patterns and anomalies are examined, and corresponding areas are identified with the help of clustering algorithms like k-means clustering.

Low-yield areas could be detected in the fields of supporting farmers with an F1 score of 0.4. There were mainly differences in the expression of the areas, while the location was mostly well detected. This value was achieved by using the vegetation index NDVI with data from April to July, a modified, more robust distance function and with three clusters. In general, it has been shown that a smaller number of clusters leads to better results as the low-yield cluster here is very different from the other clusters.

Keywords: site-specific fertilization, precision farming, machine learning, remote sensing

1. Introduction

Nitrogen plays a major role in crop production from both a productivity and an environmental perspective. Nitrogen is an essential component of proteins and other compounds and is converted into large quantities in the agricultural nutrient cycle. These conversion processes can be associated with high losses. Nitrogen translocations to water bodies and outgassing into the air cannot often be avoided and contribute to environmental problems. Especially in areas where nitrogen fertilizers are used on a large scale (such as in America, China or Europe), these losses create an ecological risk (Basso *et al.*, 2019) Therefore, plants must be supplied with nutrients according to their needs and adapted to their location in order to keep these losses as low as possible and to keep the N balance at equilibrium (Spiess and Richner, 2005). One approach is site-specific fertilization which involves measuring the heterogeneities of a field and then adapting the amount of nutrients depending on the respective yield potential and the current nutrient requirements of the subfield (Isensee, Thiessen and Treue, 2003)

Sensor based crop measurements serve as the basis for nitrogen fertilization models. A correlation is estimated between the N uptake of the crop (determined via biomass measurements and N content analyses) and the measured sensor data (for example, from multispectral images from an UAV or a satellite)(Söderström *et al.*, 2017). Repeated measurements over time and regression analyses can be used to record the N uptake over time(Sharif, 2020). Depending on the yield expectations, a growth-adjusted amount of N can be administered through an idealized N uptake curve and a measured sensor value. An N uptake that is too high or too low can be detected and then compensated for with fertilization. The different yield potentials within a field must be taken into account by adjusting the uptake curves. Yield potentials can either be determined by the soil information and/or multi-year multispectral reflectance measurements(Yuzugullu *et al.*, 2020). It is especially important that low-yield areas be excluded.

In the existing fertilization model, it is assumed that the N uptake of the site can be compensated for, i.e. partial areas in winter wheat that are poorly developed in the spring (Spicker, 2016), by higher fertilization rates at the first application. In years with dry periods or at very sandy sites, there is however a risk of misinterpretation. Poorly developed sites might not be capable of being compensated with higher fertilization rates. To illustrate this, Figure 1 compares a compensable site with a non-compensable site. It can be seen that the non-compensable site contains sub-areas that are always under-developed and cannot be compensated for in the current growing season. However, the deficit in the sub-area of the compensable site is almost compensated for by May.

Compensable site (2018, near Wieselburg, Austria)		
March	April	May
Non-compensable site with low yield areas (2019, near Tulln, Austria)		
March	April	May
low EVI high		
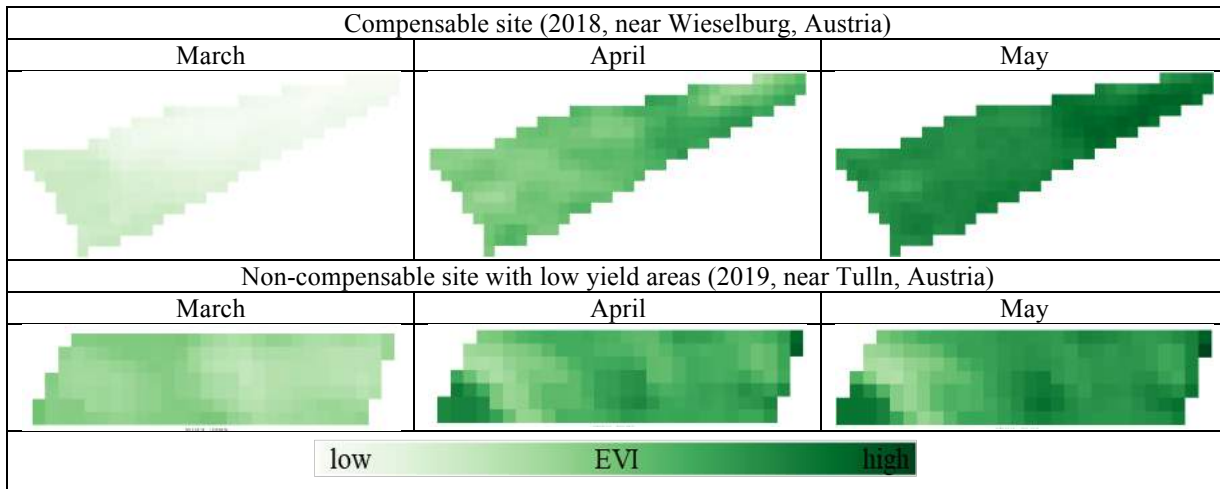
Figure 1. Comparison of the vegetation index EVI of a compensable site with a non-compensable site with winter wheat at three points in time

Low-yield sites must be detected and treated separately by excluding them from the existing fertilizer system regardless of the crop. In this research, only data from the winter wheat were used for a corresponding zonation. The mapping of low-yield sites can be used in crops other than winter wheat as well. The prerequisite for this is that a historical winter wheat vegetation course of the site must be used for zoning.

2. Materials and Methods

Unsupervised learning methods like clustering are used for the detection of low yield areas. An extensive dataset serves as the basis to derive sensor data over the vegetation periods from Sentinel-2 images. Clustering algorithms will be used to detect and interpret the patterns and the structures within the sensor data. Validation will be performed in pilot plots by comparing the model estimation with the farmers' assessments. Additionally, the consistency of the results over several years will be investigated.

2.1. Creating the dataset

In order to carry out a cluster analysis, a data set was created that represents the growth of plants as generally as possible and allows clustering into the main growth patterns. To ensure this, winter wheat fields in the main arable regions in Austria (Upper Austria, Lower Austria, and Burgenland) were observed from 2018 to 2020. The data set INVEKOS plots Austria 2018 to 2020 (Agrarmarkt Austria, 2020) was used as the basis for selecting the fields. To avoid border effects, a buffer of -20 m was first created for each observed field. From the resulting polygon, a random point was chosen which lies within the polygon. For the training data set, 95,235 random points in Austria were selected (see Figure 2 a). A similar approach was used for the test dataset. However, some of the fields were selected specifically in pilot farms. When possible, sensor data was selected from the same field over two years to assess the consistency of the cluster results. In addition, rather than selecting one random point in the field, multiple points were selected in a 20 x 20 m grid arrangement (see Figure 2 b). Vegetation trajectories in the growing season of winter wheat (February to July) were formed for these selected points. For this purpose, the vegetation indices EVI, MSAVI2 and NDVI were calculated from Sentinel-2 data. The atmospheric correction and cloud detection was done with the tool Sen2Cor. Only images with a cloud-probability of 0 were used. To obtain a uniform temporal resolution and to simplify the further processing steps with a uniform input vector, the data was linearly interpolated to a grid of 15 days (see Figure c).

a)	b)

year	Id	Idp	02-16	03-03	03-18	04-02	04-17	05-02	05-17	06-01	06-16	07-01	07-16	07-31	geometry
2019	540	688	0.261897	0.276435	0.329420	0.401629	0.563764	0.675833	0.732078	0.822661	0.821004	0.670011	0.237132	0.233410	MULTIPOINT (446379.468 476098.537)
2019	632	816	0.322201	0.275323	0.375910	0.490433	0.632544	0.721569	0.784494	0.847419	0.763430	0.455773	0.146230	0.173269	MULTIPOINT (583564.253 518553.527)
2019	1087	1540	0.295098	0.328827	0.421391	0.560957	0.728458	0.853641	0.847284	0.851555	0.685834	0.339712	0.217985	0.162311	MULTIPOINT (628345.275 443537.261)
2019	1283	1808	0.340247	0.330125	0.490328	0.650531	0.790783	0.813364	0.864623	0.915883	0.653522	0.254515	0.167053	0.147356	MULTIPOINT (629309.092 477505.659)
2019	1353	1899	0.397068	0.471790	0.546512	0.621234	0.792974	0.795177	0.768310	0.741442	0.832977	0.604610	0.219660	0.178343	MULTIPOINT (463565.995 474953.295)

c)

Figure 2. a) Random section of the point selection for the training dataset with a buffer of -20 m; b) gridded field from the test data set with a buffer of -20 m; c) ready dataset excerpt

2.2. Filtering incorrect vegetation trends

Although all satellite images with a cloud probability > 0 were sorted out during the creation of the dataset, there are still erroneous vegetation trends (especially in the year 2020). These erroneous trends must be removed in order to achieve a good clustering result. For this purpose, erroneous courses were manually annotated in both the training data set and the test data set (training data set annotation n = 162). Subsequently, a support vector classifier was trained (cost factor = 5, gamma = 0.6, kernel = radial basis function). Inaccurate trajectories could be detected reliably with an accuracy of >90%.

After filtering out the incorrect vegetation trends with the support vector classifier, 49,613 to 50,460 instances remained depending on the vegetation index. Especially in 2020, many instances were discarded due to the frequent occurrence of bad weather periods with a high cloud coverage.

2.3. Cluster analysis

The k-Means method, implemented in scikit learn, was used for clustering. Several indicators were decisive for the result, including the hyper-parameters cluster number, vegetation index, number of dimensions (= number of days) and the distance function for the later assignment of the test instances to a cluster. The Euclidean distance is usually used as distance function for k-Means clustering. A new distance function was implemented to get a more robust distance function with respect to the outliers. For this purpose, the L1 distance from the cluster centroid to the instance of the test data set was calculated for each dimension and the maximum distance was discarded. The remaining dimensions are used for the distance calculations to the clusters where the test instances are assigned to the clusters based on the lowest Euclidean distance.

2.4. Cluster validation

For the validation of the clustering results, we introduced two approaches called "Permanence" and "Farm." In the "Permanence" approach, the clustering results of a point from 2018 and 2019 were compared. The resulting clusters were thereby converted into a binary categorization (0...no low-yield point, 1...low-yield point). Finally, the confusion matrix was formed to calculate the Precision, Recall, F1 score and Accuracy. In the "Farm" approach, three farmers from Lower Austria were asked to annotate their areas for low-yield sites. Again, the cluster result was converted into a binary categorization (0...no low-yield site, 1...low-yield site). The annotated areas were compared with the cluster result. From this a confusion matrix was formed to calculate the metrics Precision, Recall, F1 score and Accuracy.

The number of instances of the datasets was 32,108 for the permanence approach and 7,212 for the farm approach after filtering out the incorrect instances.

2.5. Grid search hyper-parameter optimization

All possible variants were calculated in a grid-search analysis to evaluate the effects of the hyper-parameters on the cluster result and to finally find the best variant. The performance metrics of the "Farm" evaluation and the "Permanence" evaluation were determined in each case. The hyper-parameters vegetation index (NDVI, EVI, MSAVI2, NDVI+EVI), distance function (normal, robust), temporal dimensions (April to July, May to July) and the cluster number (3, 4, 5, 6) thus result in 64 variants.

3. Results and Discussion

The following chapter discusses the results of the grid search based hyper-parameter optimization of the "Farm" and "Permanence" evaluation.

3.1. F1 score

Figure 3 shows the variant with the best "Farm" F1 score. The variant is based on the vegetation index NDVI from April to July with the robust distance function and three clusters. In the line graph, the clusters centroids are shown. The low-yield cluster can be clearly differentiated from the other clusters. The low-yield points were drawn by the farmer with a red line in the selected fields. Some low-yield points were also classified as low-yield points by the estimation (=points). The sensitivity of the variant is slightly too low to fully detect even the small areas as shown in the right panel.

Vegetation-Index: NDVI Dimensions: April to July		Clusters: 3 Distance function: Robust	
	Permanence		Farm
Precision	0,59		0,33
Recall	0,40		0,52
F1 score	0,48		0,40
Accuracy	0,84		0,71
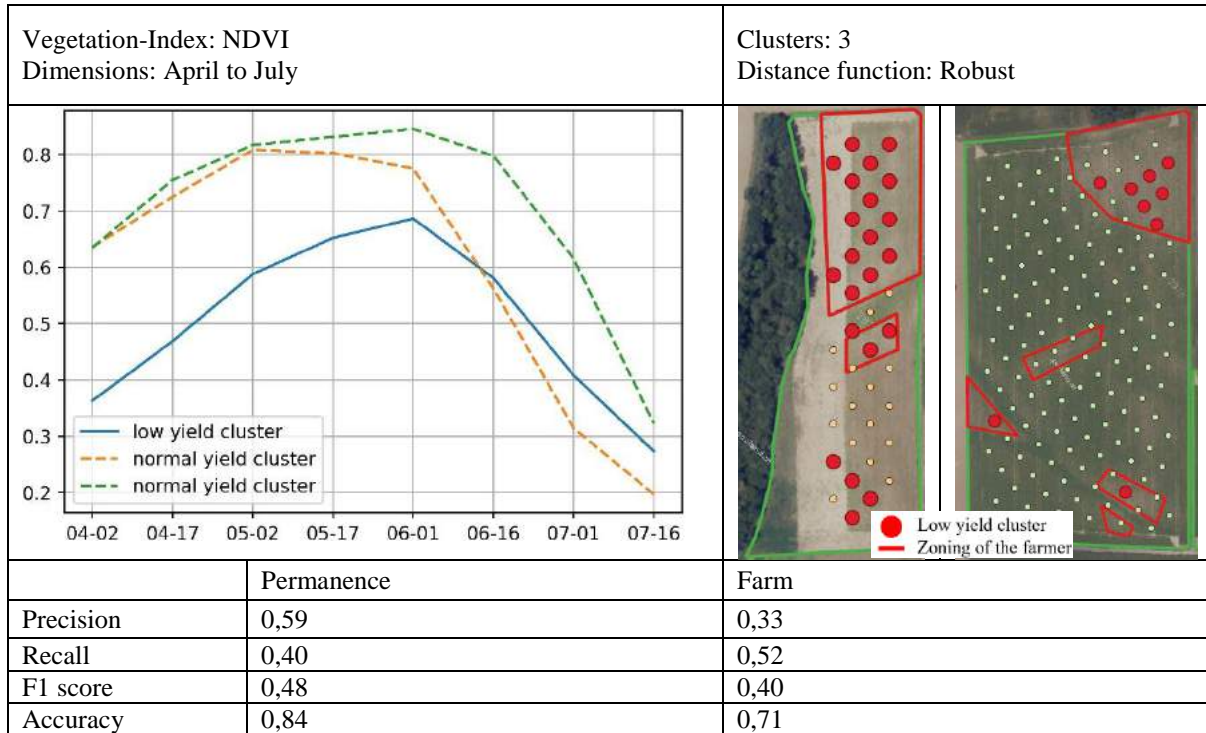
Figure 3. Variant with best Farm F1 score: top) variant description; upper left) cluster centers; upper right) example fields of farm dataset; bottom) performance metrics of permanence and farm approach

Figure 4 shows the variant with the best "Permanence" F1 score. It is based on the MSAVI2 index from May to July with three clusters and the robust distance function. It can be seen that the lower yield cluster stands out less from the other clusters than the previously presented variants in the line plot. It can also be observed that in the sample plots the low-yield locations cannot be satisfactorily detected. It is also noticeable that the "Permanence" Precision is very close to 1 with 0.98 while the "Farm" Precision is very low with 0.17. The Farm F1 score is also rather low.

Vegetation-Index: MSAVI2 Dimensions: May to July		Clusters: 3 Distance function: Robust	
	Permanence		Farm
Precision	0,98		0,17
Recall	0,37		0,35
F1 score	0,53		0,23
Accuracy	0,44		0,56
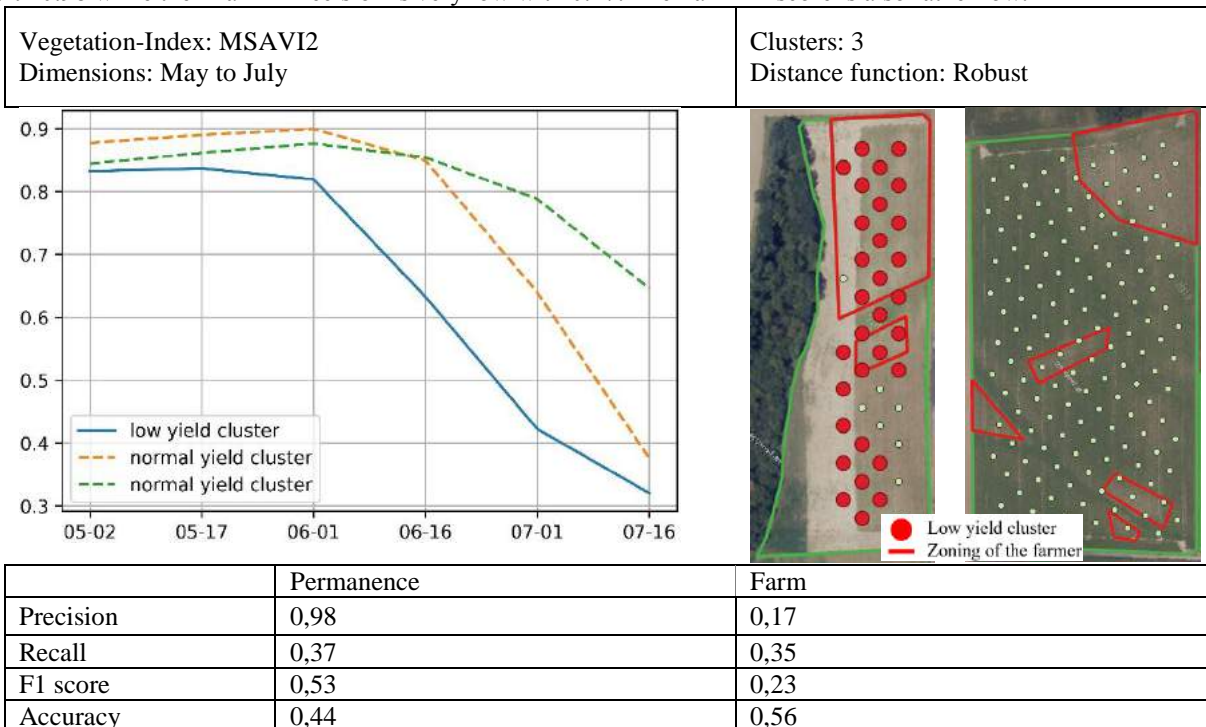
Figure 4. Variant with best Permanence F1 score: top) variant description; upper left) cluster centers; upper right) example fields of farm dataset; bottom) performance metrics of permanence and farm approach

3.2. Other metrics (Recall, Precision, Accuracy)

It turns out that the F1 score is possibly the best metric to rank the performance of the cluster analysis. Accuracy is not a good metric since the dataset is very unbalanced. Depending on the variant, the number of true negatives is about 5 to 10 times larger than the true positives. The recall would serve as a good metric if the low-yield areas could be reliably detected and if a classification of normal areas into a low-yield area is subordinate. However, variants with a high recall are somewhat too sensitive to low-yield points, and often entire fields are detected as such (see Figure 5 a). When optimizing for the precision metric, the exact opposite is the case. Hardly any areas are detected as low yield areas (see Figure 5 b) because the sensitivity of variants with high precision is too low.
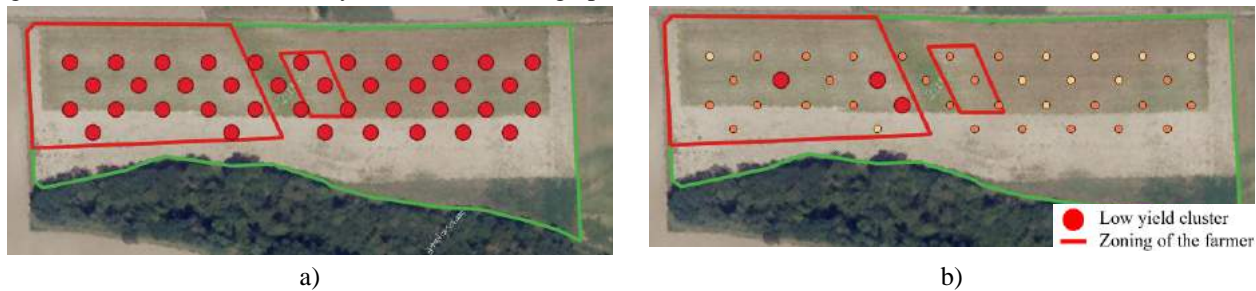
Figure 5. a) selected field with best farm recall (EVI, robust distance function, 3 cluster, May to July); b) selected field with best farm precision (NDVI, robust distance function, 6 cluster, April to July)

3.3. Influence of the individual hyperparameters on the result

The next step (in our research) involved grouping the results of the variants according to their vegetation index, distance function, temporal dimensions, and number of clusters to draw further conclusions on the influence of the parameters. The mean of the F1 scores was calculated from the resulting groups. There are no significant differences in the grouping according to the vegetation index and the distance function. The other two hyperparameters, dimension and number of clusters, influence the results. For the temporal dimensions, the variants using data from April to July generally perform better (mean "Permanence" F1 score: 0.43, mean "Farm" F1 score: 0.32). Those variants that use results from May produce lower F1 scores (mean "Permanence" F1 score: 0.35, mean "Farm" F1 score: 0.28). When grouped by the number of clusters, variants with a lower number of clusters perform better. Variants with 3 clusters produce the best results (mean "Permanence" F1 score: 0.43, mean "Farm" F1 score: 0.34). For example, variants with 6 clusters produce a mean "Permanence" F1 score of 0.35 and a mean "Farm" F1 score of 0.24. As the number of clusters increases, it is observed that the low-yield cluster no longer differentiates itself as strongly from the other clusters as in variants with fewer clusters.

3.4. Example fields

Figure 6 gives some overview of the zoning of the variant with highest F1 score (=0.4). It is observed that the location of the low yield points can be detected and that there is a partial correlation between the estimated zones and the zoning of the farmer. However, there are also the following error factors: low-yield points that are located in the border area of the field (e.g., in field 1 and field 3) cannot be detected due to the border area correction. The low-yield sites detected by the cluster analysis often have a different expansion than the areas classified by the farmer as indicated by a decrease in the F1 score. The areas classified by the farmer are a subjective assessment and may differ from the actual location and expansion under certain circumstances. In addition, there is also the issue that the 20 x 20 m data set has a low spatial resolution. Thus, there may be an influence by adjacent areas with higher yield potential in the border region of the low-yield area classified by the farmer. It is important to take note that each point is assigned to a cluster after only one year of observation which can lead to year-specific influences, such as weather, management practices, varietal influence, diseases, and nutrient deficiencies (not nitrogen-related).
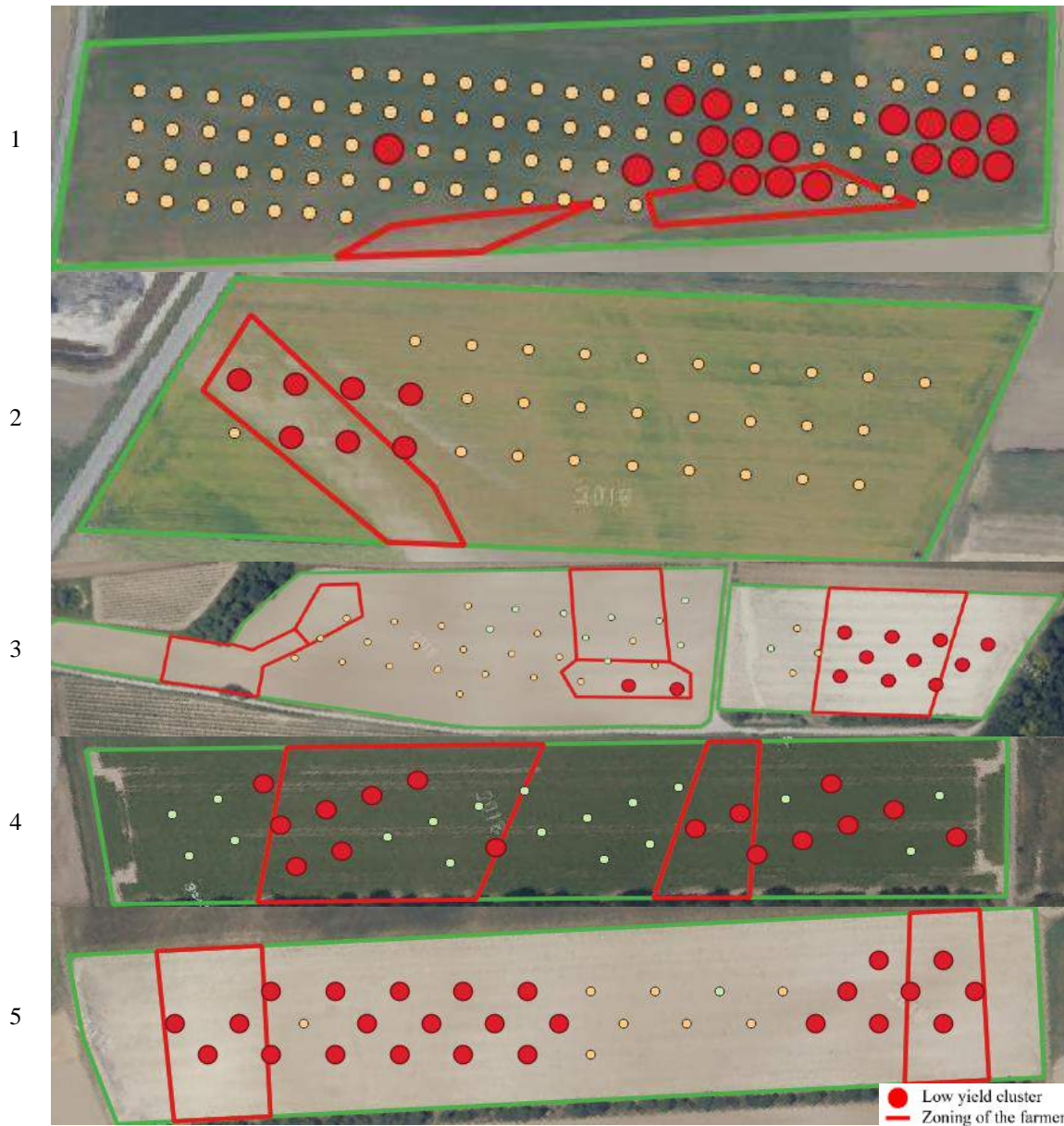
Figure 6. Example fields with best farm F1 score (=0.4), (NDVI, robust distance function, April to July, 3 cluster)

4. Conclusions

The detection and separate treatment of low-yield sites is an important ecological component of fertilizer models. The method used to detect low-yield sites is based on Unsupervised Learning methods. This involves examining historical vegetation patterns and anomalies and identifying corresponding areas using clustering algorithms such as k-means clustering. The advantages of this approach are that large amounts of data can be generated for a training and test data set, and it does not have to be labelled with soil samples or complex and cost-intensive analysis methods. It is difficult to validate the model, but initial comparisons with zoning or farmers' assessments are promising.

Future research could improve this model through optimized validation like conducting and measuring soil or yield parameters. Multi-year observations of a site would weed out year-dependent factors (e.g. climate). The disadvantage here is the lack of area coverage of a crop (for example, winter wheat). This could be remedied by including other crops (e.g. maize) and adding more years to the data set (beginning in 2021). A further improvement can be achieved by expanding the scope of the data to include more data points which could lead to a higher generalization. More relevant characteristics could be extracted by increasing the bands used and calculating more indices. Additionally, a higher temporal resolution of the data, or the integration of earlier months, could lead to the extraction of even more relevant data. These suggestions must also be accompanied by improved pre-processing and improved handling of clouds.

References

Agrarmarkt Austria, 2020 *INVEKOS Schläge Österreich 2018, 2019, 2020*. Available at: https://www.data.gv.at/katalog/dataset/35e36014-ec69-439b-8629-389f52ffaa92

Basso, B., Shuai, G., Zhang, J. et al., 2019. Yield stability analysis reveals sources of large-scale nitrogen loss from the US Midwest. Sci Rep 9, 5774 https://doi.org/10.1038/s41598-019-42271-1

Isensee, E., Thiessen, E. and Treue, P.,2003. 'Mehrjährige Erfahrungen mit der teilflächenspezifischen Düngung und Ernte', *Agrartechnische Forschung*, 9

A. Sharifi, 2020. "Using Sentinel-2 Data to Predict Nitrogen Uptake in Maize Crop," in IEEE Journal of Selected Topics in Applied Earth Observations and Remote Sensing, vol. 13, pp. 2656-2662, doi: 10.1109/JSTARS.2020.2998638

Söderström, M., Piikki, K., Stenberg, M., Stadig, H., & Martinsson, J., 2017. Producing nitrogen (N) uptake maps in winter wheat by combining proximal crop measurements with Sentinel-2 and DMC satellite images in a decision support system for farmers. Acta Agriculturae Scandinavica Section B: Soil and Plant Science, 67(7), 637–650. https://doi.org/10.1080/09064710.2017.1324044

Spicker, A. B., 2016. Entwicklung von Verfahren der teilflächenspezifischen Stickstoffdüngung zu Wintergerste (Hordeum vulgare L.) und Winterraps (Brassica napus L.) auf Grundlage reflexionsoptischer Messungen (Doctoral dissertation, Technische Universität München)

Spiess, E. and Richner, W., 2005. 'Stickstoff in der Landwirtschaft', *Schriftenreihe der FAL*, 57.

Yuzugullu O, Lorenz F, Fröhlich P, Liebisch F., 2020. Understanding Fields by Remote Sensing: Soil Zoning and Property Mapping. Remote Sensing. 12(7):1116. https://doi.org/10.3390/rs12071116

Data Fusion Modelling of Visible-near-infrared and Mid-infrared Spectra

S. Hamed Javadi [a] and Abdul M. Mouazen [a,*]

[a] Precision Soil and Crop Engineering Group, Faculty of Bioscience Engineering, Ghent University, Gent, Belgium.

* Corresponding author. Email: Abdul.mouazen@ugent.be

Abstract

Spectroscopy has emerged as a solution to estimate key soil attributes in precision agriculture (PA) during recent decades. Chemometrics and machine-learning methods are used in order to extract useful information out of the spectra. In this paper, the performance of visible-near-infrared (Vis-NIR) and mid-infrared (MIR) spectrophotometers for the prediction of pH, organic carbon (OC), phosphorous (P), potassium (K), magnesium (Mg), calcium (Ca), sodium (Na), moisture content (MC), and cation exchange capacity (CEC) were evaluated. Using 267 soil samples measured with a CompactSens spectrometer (tec5 technology, Germany) with 350-1700nm spectral range and a 4300-FTIR (Agilent, US) with 650-4000cm^{-1} spectral range, we compared single-sensor partial least squares (PLS) regression after feature selection. To take advantage of both sensors, the combined use of them were evaluated in three fusion scenarios: 1. Spectral concatenation (SC) in which the raw vis-NIR and MIR spectra are concatenated; 2. Feature fusion (FF) wherein the features (i.e., selected spectral ranges) of vis-NIR and MIR are concatenated; and 3. Fusion of the predictions given by vis-NIR and MIR PLS-based models by linear regression (LR). The validation results showed that the vis-NIR model outperforms the MIR model in the prediction of all studied attributes, except for pH, Ca, and CEC. Furthermore, the single-sensor accuracies were improved in all cases by LR while SC and FF enhanced the single-sensor accuracies just in cases of OC, Ca, and CEC with FF being superior to SC. However, the improvement achieved by fusion was not significant. Accordingly, it is suggested to use just vis-NIR for prediction of the studied soil attributes since it showed more robustness than MIR.

Keywords: Data fusion; precision agriculture; spectroscopy; visible-near-infrared; mid-infrared.

1. Introduction

Precision agriculture (PA) has emerged as a sustainable and profitable solution (Mouazen et al., 2019). In PA practices, it is essential to identify variability within the field by assessing soil properties for which spectroscopy is a fast and inexpensive method (Ben-Dor and Banin, 1994; Guzmán Q. et al., 2018; Stenberg et al., 2010). Different kinds of spectrometers, including visible-near-infrared (vis-NIR), mid-infrared (MIR), and X-ray fluorescence (XRF), are being used for this purpose, each potentially providing information about different soil attributes. Accordingly, the potential of single-sensor and combined use of these devices in prediction of different soil fertility attributes needs to be evaluated. While single-sensor of each of these spectroscopy sensors were studied intensively, the fusion of their output is still in its early stage of research. A common hypothesis is that the fusion data of multiple sensors can improve the overall prediction accuracy, compare to the single-sensor solution. However, it has been shown in (Javadi et al., 2021; Javadi and Mouazen, 2021; Tavares et al., 2021) that this cannot always be the case when using vis-NIR and XRF, as there might be no synergy between vis-NIR and XRF data.

While there is an extensive literature on soil analysis by vis-NIR (Chabrillat et al., 2019; Fidêncio et al., 2002; Kodaira and Shibusawa, 2020; Mouazen et al., 2005; Mouazen and Kuang, 2016; Shepherd and Walsh, 2002), a review of soil analysis with a focus on MIR has been provided by (Janik et al., 1998). Normally, machine-learning-based algorithms are exploited in order to predict the soil attributes out of the vis-NIR and MIR spectra. Mostly, instead of using all the reflectance values all over the whole spectral ranges, the relevant latent variables are used since the high-dimensional spectra are highly correlated. To this end, either principal components regression (Chang et al., 2001) or partial least squares (PLS) regression (Javadi et al., 2021; Javadi and Mouazen, 2021; Tavares et al., 2021) are used. The PLS model is more advantages since it considers covariance maximization between the latent variables of the predictors and the predicted values. Nevertheless, both vis-NIR and MIR sensors have shown limited performance in soil analysis and the potential in combined use of them needs to be studied using different types of soil and in different prediction methodologies.

In this paper, we studied potential of the vis-NIR and MIR spectra in prediction of key soil fertility attributes including pH, organic carbon (OC), phosphorous (P), potassium (K), calcium (Ca), magnesium (Mg), moisture content (MC), sodium (Na), and cation exchange capacity (CEC). Especially, we used the PLS-based prediction model and incorporated feature selection based on the regression coefficients in order to make the models simpler and more efficient. This also facilitates studying the potential synergy between the two spectral kinds. Furthermore, three fusion schemes were evaluated including low-level fusion, feature fusion, and high-level fusion. In the low-level fusion scheme – spectra concatenation (SC), the raw spectra are concatenated to each other forming a single spectrum which

covers vis-NIR and MIR spectral ranges. In the feature fusion (FF) scheme, the selected spectral ranges of vis-NIR and MIR are concatenated and subjected to a PLS model. Finally, in the high-level fusion, the predictions given by the single-sensor PLS-based models are fused according to linear regression (LR).

2. Materials and Methods

2.1. Study sites and soil sampling

In this study, we used totally 267 soil samples from different locations of nine fields in Flanders, Belgium. The soil samples were collected at 10-20 cm soil depth, with an average spatial sampling rate of 3.25 samples/ha during 2018. The fields included Bottelare (5ha), Thierry (3ha), Watermachine (6ha), Beers (12ha), Kouter (13ha), Gingelomse (11ha), Dal (6ha), Kattestraat (5ha), and Grootland (21ha). The information of the study fields has been provided in Table 1. Topographically, the Gingelomse and Bottelare fields had mild undulations but other fields' surfaces were rather flat. Also, there was a high percentage of salt (Ca++) in the soil of Watermachine and Beers located close to North Sea. Across all fields, a general cropping rotation of maize, potato, sugar beets, and barley/wheat is being performed with an intermittent short duration cover crop.

Table 1. The information of the study fields in different areas of Flanders in Belgium.

Field name	Location	Date of sampling (2018)	No. of Samples	Crop Type	Soil Texture	Average MC* (%)	Average OC** (%)
Bottelare	Melle	Nov.	23	Maize	Silt Loam	14.64	1.60
Thierry	Moeskroen	Aug.	13	Wheat	N.A.*	15.56	1.66
Watermachine	Veurne	Aug.	19	Wheat	Loam	19.86	1.35
Beers	Veurne	Aug.	38	Oil seed rape	Sandy Loam	19.30	1.29
Kouter	Huldenberg	Jul./Aug.	40	Burley	Silt Loam	3.63	1.10
Gingelomse	Landen	Dec.	37	Barley	Silt Loam	22.79	1.34
Dal	Landen	Dec.	21	Sugar beet	N.A.	23.02	1.38
Kattestraat	Landen	Aug.	19	Barley	N.A.	8.75	1.47

* N.A.: not available

2.2. Laboratory soil measurement

Each soil sample was reduced to 400g following standard coning and quartering methods [29]. Each fresh sample was mixed well and stones/gravels, grass, and stubble, were removed. Then, it was divided into two parts of 200g each. One part was used for optical measurements in laboratory while the chemical analysis was performed on the other part. For optical measurements, samples were air-dried for more than two weeks, then they were crushed using an agate mortar and pestle and then they were sieved using a 2mm stainless steel sieve.

2.3. Measurement by visible and near infrared (vis-NIR) and mid-infrared (MIR) spectrometers

We placed about 50g of each dried and sieved soil sample into three Petri dishes (diameter = 2cm and depth = 1cm). In order to ensure maximum diffuse reflection and increase signal-to-noise ratio [30], each soil sample was gently pressed and levelled using a spatula. We scanned the Soil samples using a CompactSpec vis-NIR spectrophotometer (Tec5 Technology for spectroscopy, Germany) in diffuse reflectance mode, with wavelength range of 305 - 1700nm. A 100% reflectance ceramic disc was scanned or the device calibration every 30 minutes. Ten spectra per Petri dish were collected and the resultant 30 spectra per three dishes were averaged in one spectrum per sample.

The soil samples were then scanned using an Agilent 4300 handheld Fourier transfer infrared (FTIR) spectrometer (Agilent Technologies, Santa Clara, CA, United States), with a spectral wavenumber range of 4000 cm^{-1} to 650 cm^{-1} with 8 cm^{-1} resolution. The background spectrum was taken out using a silver-plated reference cap provided by the manufacturer every 30 min during scanning. The background scan provides a baseline profile of the system conditions with no sample loaded on the instrument, and helps to correct for changes in the environment (e.g., changes in local atmospheric composition) influencing measurement as well as potential instrument drift. The spectral data were collected as absorbance using the Microlab software V5.0 provided by the manufacturer together with the spectrometer. Average absorbance of the three scans was used for spectra pre-treatment and model establishment.

2.4. Chemical analysis in laboratory

The other half part of each soil sample dedicated for the laboratory chemical analysis was kept at 4 ^{o}C within a

cooling room and then was given to the Soil Survey of Belgium (BDB, Heverlee, Belgium) for chemical analysis of soil OC, pH, Ca, and Mg. OC was obtained using the dry combustion following Dumas principle (ISO 10694; CMA/2/II/A.7; BOC). Before OC measurement, total inorganic carbon compounds were removed by treating the soil samples with hydrochloric (HCl) acid. Soil pH, after shaking and equilibrium for 2h in mol/l potassium chloride solution (KCl), was measured in the supernatant, using 1:2.5 soil to solution ratio. The available Mg and Ca were determined in ammonium lactate extract with inductively coupled plasma atomic emission spectroscopy (ISO 11885; CMA 2 / I / B1). Table 2 has listed the statistics of the laboratory measured soil attributes for the soil samples of each field.

Table 2. The results of the laboratory measured soil organic carbon (OC), pH, magnesium (Mg), calcium (Ca), phosphorous (P), potassium (K), sodium (Na), moisture content (MC), and cation exchange capacity (CEC).

	pH	OC (%)	P (mg/100g)	K (mg/100g)	Mg (mg/100g)	Ca (mg/100g)	Na (mg/100g)	MC (%)	CEC (%)
mean	6.93	1.31	27.2	30.02	27.85	597.53	5.76	16.45	33.22
Standard deviation	0.58	0.28	9.47	11.03	19.85	794.09	4.58	6.77	40.95
Minimum	5	0.77	8	10	7	83	0.94	2.28	5.92
maximum	8	2.4	69	69	85	4210	30	28.81	215.09

2.5. Single-sensor modelling

Out of the 267 soil samples, 13 samples were detected as outliers using the Mahalanobis distance criterion (De Maesschalck et al., 2000). Using Kennard-Stone algorithm (Nawar and Mouazen, 2018), the whole dataset was divided into calibration and validation sets of 200 and 55 samples each, respectively.

The PLS model was adopted for predicting the soil attributes using single sensors. The number of the latent variables was optimized for each soil attribute according to the leave-one-out cross-validation results. Then, the optimal wavelength ranges for vis-NIR and MIR, respectively were obtained by grid search through all the regression coefficients with the RMSE of the leave-one-out cross-validation as the objective. More specifically, the regression coefficients were sorted first. Then, in each step, the variables with coefficients more than a threshold were used for cross-validation. The set of the variables giving the minimum RMSE was selected and used for calibrating the prediction models. After having the model calibrated, it was validated using the soil samples of the validation set.

2.6. Fusion models

Three fusion schemes (shown in Figure 1) were evaluated which are discussed in the following.
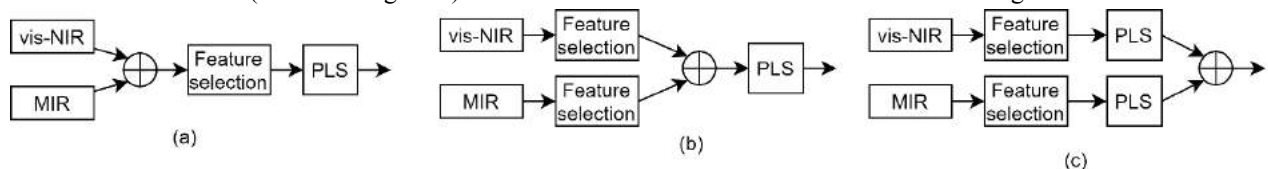
Figure 1. Studied schemes for fusion of visible-near-infrared (vis-NIR) and mid-infrared (MIR) spectra using partial least squares (PLS) modelling. (a) spectra concatenation (SC); (b) Feature fusion (FF); (c) Fusion of the single-sensor predictions based on linear regression (LR).

2.6.1.Spectra concatenation (SC)

In this scheme (Figure 1-a), the vis-NIR and MIR spectra are concatenated to each other to form a single spectrum covering the vis-NIR and MIR spectral range. Note that the spectral range between 1650 nm to 2550 nm was not covered due to limitation of the devices used and also due to edge cutting of the spectra in preprocessing. The concatenated spectrum is treated the same as a single spectrum and the same procedure as the vis-NIR and MIR modelling is applied on it. More specifically, the optimal number of latent variables is obtained according to the cross-validation results. Then, the optimal features (i.e., the optimal wavelength ranges) are obtained based on which the PLS model is established. SC has been examined in several works (Javadi et al., 2021; Tavares et al., 2021) but here we applied feature selection on the concatenated spectra rather than applying the raw concatenated spectra directly to the prediction model.

2.6.2.Feature fusion (FF)

Feature fusion (FF) – shown in Figure 1-b – is based on concatenating the selected spectral ranges of vis-NIR and MIR spectra to each other. FF is based on the fact that instead of fusing the raw data, as in SC, their features which are more informative can be used. This simplifies the fusion prediction model as well.

2.6.3. Linear regression (LR)

The highest level of fusion includes just the predictions given by the single-sensor models. The method – referred to as model averaging (O'Rourke et al., 2016) and Granger-Ramanathan (GR) (Granger and Ramanathan, 1984; Xu et al., 2019) as well – gives the final prediction of the soil attributes based on linear regression (LR) of the single-sensor predictions. We tag this fusion scheme by LR in order to highlight the prediction method used, i.e., LR. LR is simply a weighted sum of the single-sensor predictions with the more accurate single-sensor prediction weighed more.

2.7. Evaluation criteria

The prediction accuracies of the above listed individual and fusion models were evaluated in terms of root mean square error (RMSE), ratio of performance to deviation (RPD), and Lin's concordance correlation coefficient (LCCC). RPD is defined as the ratio of the standard deviation of the measured soil property divided by the RMSE of the prediction. LCCC is a measure of concordance between new measurements, y, and the reference values, r, and is given by (Lin, 1989):

$$LCCC = \frac{2\rho\sigma_y\sigma_r}{\sigma_y^2 + \sigma_r^2 + (\bar{y} - \bar{r})^2} \tag{1}$$

wherein σ_y and σ_r denote the standard deviation of the measurements and the reference values, respectively, and ρ is the related Pearson correlation coefficient. Indeed, LCCC modifies the Pearson correlation coefficient by measuring how far the best-fit line is from the 45-degree line through the origin in addition to assessing the closeness of the data to the best-fit line.

3. Results and Discussion

The selected spectral ranges and spectral bands for the single-sensor models and also for SC are shown in Figure 2, Figure 3, and Figure 4. OC and MC have spectra responses in NIR spectra. As shown in Figure 2, the optimal wavelength ranges of OC and MC include their corresponding range in vicinity of 1000 nm and 1400 nm, respectively (Chabrillat et al., 2019). The other soil attributes do not have direct impact on the spectral data but can still be estimated with vis-NIR spectroscopy, as they are known to be correlated with properties have direct spectral responses in the NIR range.
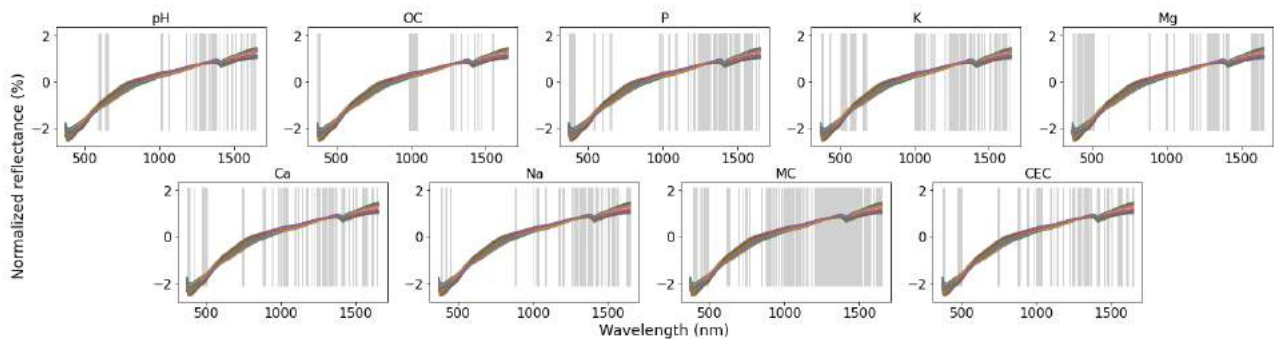
Figure 2. The normalized visible-near-infrared (vis-NIR) spectra and their selected spectral ranges for studied soil attributes. OC: organic carbon; P: phosphorous; K: potassium; Mg: magnesium; Ca: calcium; Na: sodium; MC: moisture content; CEC: cation exchange capacity.

In the MIR selected features (Figure 3) for the OC prediction model include its important range in vicinity of 3200 nm (Cañasveras Sánchez et al., 2012). For other soil attributes, also the optimal spectral ranges have been used, especially for Ca which include the range in vicinity of 4000 nm. The selected features of vis-NIR and MIR (Figure 4) were concatenated and subjected to a PLS-based model in the FF scheme. On the other hand, in SC, the optimal wavelength ranges are selected from the whole concatenated spectra.
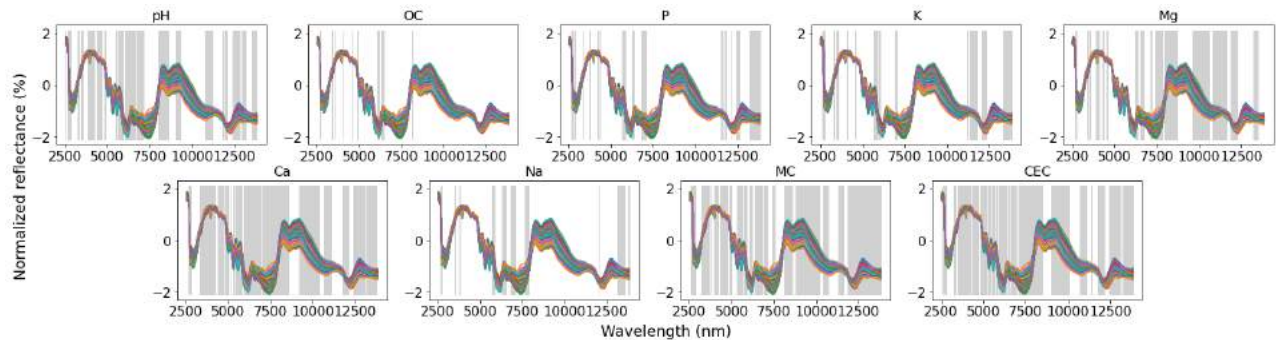
Figure 3. The normalized mid-infrared (MIR) spectra and their selected spectral ranges for studied soil attributes. OC: organic carbon; P: phosphorous; K: potassium; Mg: magnesium; Ca: calcium; Na: sodium; MC: moisture content; CEC: cation exchange capacity.
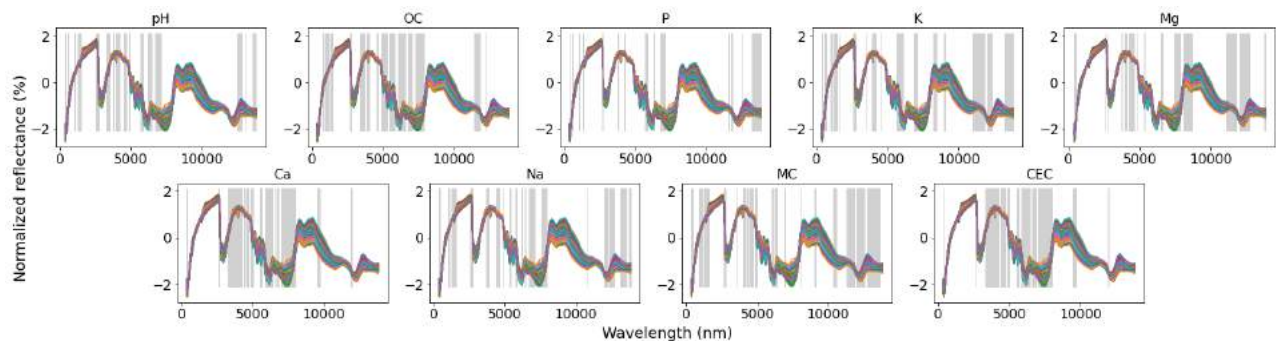
Figure 4. The normalized concatenated visible-near-infrared (vis-NIR) and mid-infrared (MIR) spectra and their selected spectral ranges in the spectra concatenation (SC) scheme for predicting the studied soil attributes. OC: organic carbon; P: phosphorous; K: potassium; Mg: magnesium; Ca: calcium; Na: sodium; MC: moisture content; CEC: cation exchange capacity.

The performance of the single-sensor and the fusion models is shown in Figure 5 in terms of RPD and LCCC. Also, the RMSE values of the models are listed in Table 3. Comparing the single-sensor models shows that MIR outperforms vis-NIR just in prediction of pH, Ca, and CEC while the vis-NIR performance is also acceptable in all these cases. As can be seen, fusion was effective in all cases, especially with regard to LR and FF. LR outperformed the single-sensor accuracies for all soil attributes. With FF and SC, the predictions were improved in OC, Ca, and CEC wherein FF outperformed SC which indicates that the features selected in single-sensor models expose synergy. All single-sensor and fusion models gave excellent performance (RPD ≥ 2) in pH, Mg, Ca, and CEC. However, the LCCC value for all models are more than 0.4, which indicates an appropriate response of all models, even in cases of P, K, and Na whose RPD might not seem acceptable (RPD < 2). It is worth mentioning, as has also been pointed out in (Javadi and Mouazen, 2021; Tavares et al., 2021), that when a single device performs satisfactorily, its fusion with a poorly-behaving sensor may degrade the performance. A good example of this is the MC case where vis-NIR model gave an excellent accuracy while its fusion with the MIR model degraded the accuracy in FF and SC fusion schemes; though the overall performance was more enhanced using LR. Note that the LR performance was just slightly better than the best single-sensor model in cases where SC and FF were not able to enhance the overall accuracy (cf. Table 3). Accordingly, it can be concluded that each of the vis-NIR and MIR spectra are not capable of complementing each other for all soil properties investigated, so their combined use for all properties except Ca and CEC is not advantageous, as also pointed out by (Rossel et al., 2006).

(a)   (b)
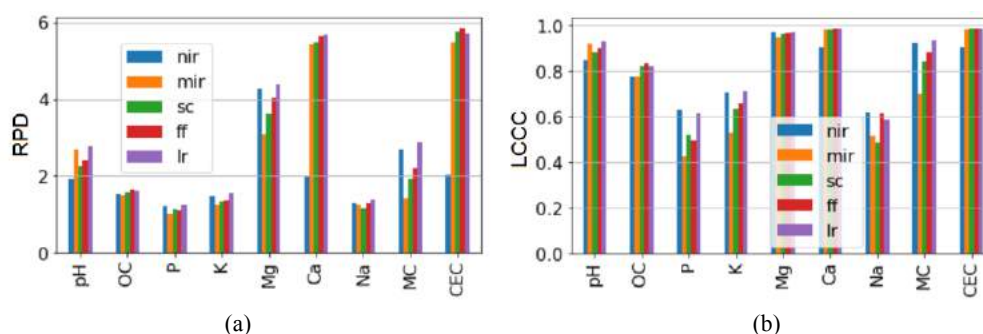
Figure 5. The (a) ratio of performance to deviation (RPD) and (b) Lin's concordance correlation coefficient (LCCC) of single-sensor modelling of visible-near-infrared (NIR), mid-infrared (MIR), and the studied three fusion scheme including spectra concatenation (SC), feature fusion (FF), and linear regression (LR). OC: organic carbon; P: phosphorous; K: potassium; Mg: magnesium; Ca: calcium; Na: sodium; MC: moisture content; CEC: cation exchange capacity.

Table 3. The root mean squared error (RMSE) of single-sensor modelling of visible-near-infrared (NIR), mid-infrared (MIR), and the studied three fusion scheme including spectra concatenation (SC), feature fusion (FF), and linear regression (LR). OC: organic carbon; P: phosphorous; K: potassium; Mg: magnesium; Ca: calcium; Na: sodium; MC: moisture content; CEC: cation exchange capacity.

	vis-NIR	**MIR**	**SC**	**FF**	**LR**
pH	0.25	0.18	0.21	0.2	0.18
OC (%)	0.15	0.15	0.14	0.14	0.14
P (mg/100g)	6.45	7.78	7.06	7.19	6.42
K (mg/100g)	7.6	8.91	8.37	8.15	7.21
Mg (mg/100g)	3.73	5.16	4.39	3.95	3.67
Ca (mg/100g)	273.44	99.82	98.78	95.85	96.19
Na (mg/100g)	3.27	3.38	3.67	3.3	3.12
MC (%)	2.41	4.55	3.33	2.92	2.25
CEC (mg/100g)	13.82	5.12	4.88	4.82	4.99

4. Conclusions

In this paper, the potential of vis-NIR and MIR and their combined use in prediction of key soil fertility attributes [e.g., pH, OC, P, K, Ca, Mg, Na, MC, and CEC] were studied. Notably, optimal wavelength ranges of the vis-NIR and MIR spectra were obtained by cross-validation through the regression coefficients. More specifically, those spectral ranges with significant regression coefficient that gave the best PLS-based cross-validation results were used while the other ranges were neglected. Furthermore, three fusion schemes were assessed: 1. Spectra concatenation (SC) in which the whole vis-NIR and MIR spectra are concatenated after feature selection (based on regression coefficient – similar to single-sensor modelling), and are subjected to a PLS model; 2. Feature fusion (FF) which concatenates the selected spectral ranges of the vis-NIR and MIR spectra and subjects it to a PLS model; and 3. Fusing the single-sensor prediction by linear regression (LR). The validation results showed that all single-sensor and fusion models performs satisfactorily in prediction of pH, Mg, Ca, and CEC. Comparing the single-sensor models showed the superiority of vis-NIR in all cases except for pH, Ca, and CEC wherein its performance was also acceptable with RPD $\geq$ 1.98. While LR was effective in enhancing the single-sensor accuracies, SC and FF were successful just in cases of OC, Ca, and CEC wherein FF outperformed SC. However, we noted that the improvement achieved by fusion was not significant. Accordingly, the information provided by the vis-NIR spectra did not complement that of the MIR spectra and just vis-NIR would be sufficient for prediction of the studied soil attributes since it exhibited more robustness than MIR. As future directions, it is suggested to examine the studied models with a wider range vis-NIR spectrometers and detector types. Moreover, feature selection was done here based on the regression coefficient since a linear prediction model (i.e., PLS) was adopted. Feature selection by an evolutionary algorithm – e.g., the genetic algorithm (GA) – together with a nonlinear prediction model – such as random forest or artificial neural network – can be considered as a future study topic.

Acknowledgements

References

Ben-Dor, E., Banin, A., 1994. Visible and near-infrared (0.4–1.1 µm) analysis of arid and semiarid soils. Remote Sens. Environ. 48, 261–274. https://doi.org/https://doi.org/10.1016/0034-4257(94)90001-9

Cañasveras Sánchez, J.C., Barrón, V., del Campillo, M.C., Viscarra Rossel, R.A., 2012. Reflectance spectroscopy: a tool for predicting soil properties related to the incidence of Fe chlorosis. Spanish J. Agric. Res. Vol 10, No 4 (2012)DO - 10.5424/sjar/2012104-681-11 .

Chabrillat, S., Ben-Dor, E., Cierniewski, J., Gomez, C., Schmid, T., van Wesemael, B., 2019. Imaging Spectroscopy for Soil Mapping and Monitoring. Surv. Geophys. 40, 361–399. https://doi.org/10.1007/s10712-019-09524-0

Chang, C.-W., Laird, D.A., Mausbach, M.J., Hurburgh, C.R., 2001. Near-Infrared Reflectance Spectroscopy– Principal Components Regression Analyses of Soil Properties. Soil Sci. Soc. Am. J. 65, 480–490. https://doi.org/10.2136/sssaj2001.652480x

De Maesschalck, R., Jouan-Rimbaud, D., Massart, D.L., 2000. The Mahalanobis distance. Chemom. Intell. Lab. Syst. 50, 1–18. https://doi.org/https://doi.org/10.1016/S0169-7439(99)00047-7

Fidêncio, P.H., Poppi, R.J., de Andrade, J.C., 2002. Determination of organic matter in soils using radial basis function networks and near infrared spectroscopy. Anal. Chim. Acta 453, 125–134. https://doi.org/https://doi.org/10.1016/S0003-2670(01)01506-9

Granger, C.W.J., Ramanathan, R., 1984. Improved methods of combining forecasts. J. Forecast. 3, 197–204.

Guzmán Q., J.A., Rivard, B., Sánchez-Azofeifa, G.A., 2018. Discrimination of liana and tree leaves from a Neotropical Dry Forest using visible-near infrared and longwave infrared reflectance spectra. Remote Sens. Environ. 219, 135–144. https://doi.org/https://doi.org/10.1016/j.rse.2018.10.014

Janik, L.J., Merry, R.H., Skjemstad, J.O., 1998. Can mid infrared diffuse reflectance analysis replace soil extractions? Aust. J. Exp. Agric. 38, 681–696.

Javadi, S.H., Mouazen, A.M., 2021. Data Fusion of XRF and Vis-NIR Using Outer Product Analysis, Granger– Ramanathan, and Least Squares for Prediction of Key Soil Attributes. Remote Sens. . https://doi.org/10.3390/rs13112023

Javadi, S.H., Munnaf, M.A., Mouazen, A.M., 2021. Fusion of Vis-NIR and XRF spectra for estimation of key soil attributes. Geoderma 385, 114851. https://doi.org/https://doi.org/10.1016/j.geoderma.2020.114851

Kodaira, M., Shibusawa, S., 2020. Mobile Proximal Sensing with Visible and Near Infrared Spectroscopy for Digital Soil Mapping. Soil Syst. . https://doi.org/10.3390/soilsystems4030040

Lin, L.I.-K., 1989. A Concordance Correlation Coefficient to Evaluate Reproducibility. Biometrics 45, 255–268. https://doi.org/10.2307/2532051

Mouazen, A.M., Alexandridis, T., Buddenbaum, H., Cohen, Y., Moshou, D., Mulla, D., Nawar, S., Sudduth, K.A., 2019. Monitoring, in: Agricultural Internet of Things and Decision Support for Precision Smart Farming. pp. 36–138.

Mouazen, A.M., Kuang, B., 2016. On-line visible and near infrared spectroscopy for in-field phosphorous management. Soil Tillage Res. 155, 471–477. https://doi.org/https://doi.org/10.1016/j.still.2015.04.003

Mouazen, A.M., Saeys, W., Xing, J., Baerdemaeker, J. De, Ramon, H., 2005. Near Infrared Spectroscopy for Agricultural Materials: An Instrument Comparison. J. Near Infrared Spectrosc. 13, 87–97. https://doi.org/10.1255/jnirs.461

Nawar, S., Mouazen, A.M., 2018. Optimal sample selection for measurement of soil organic carbon using on-line vis-NIR spectroscopy. Comput. Electron. Agric. 151, 469–477. https://doi.org/https://doi.org/10.1016/j.compag.2018.06.042

O'Rourke, S.M., Minasny, B., Holden, N.M., McBratney, A.B., 2016. Synergistic Use of Vis-NIR, MIR, and XRF Spectroscopy for the Determination of Soil Geochemistry. Soil Sci. Soc. Am. J. 80, 888–899. https://doi.org/10.2136/sssaj2015.10.0361

Rossel, R.A.V., Walvoort, D.J.J., McBratney, A.B., Janik, L.J., Skjemstad, J.O., 2006. Visible, near infrared, mid infrared or combined diffuse reflectance spectroscopy for simultaneous assessment of various soil properties. Geoderma 131, 59–75. https://doi.org/https://doi.org/10.1016/j.geoderma.2005.03.007

Shepherd, K.D., Walsh, M.G., 2002. Development of Reflectance Spectral Libraries for Characterization of Soil Properties. Soil Sci. Soc. Am. J. 66, 988–998. https://doi.org/https://doi.org/10.2136/sssaj2002.9880

Stenberg, B., Rossel, R.A.V., Mouazen, A.M., Wetterlind, J., 2010. Chapter Five - Visible and Near Infrared Spectroscopy in Soil Science, in: Sparks, D.L. (Ed.), Advances in Agronomy. Academic Press, pp. 163–215.

Tavares, T.R., Molin, J.P., Javadi, S.H., Carvalho, H.W., Mouazen, A.M., 2021. Combined Use of Vis-NIR and

XRF Sensors for Tropical Soil Fertility Analysis: Assessing Different Data Fusion Approaches. Sensors . https://doi.org/10.3390/s21010148

Xu, D., Chen, S., Viscarra Rossel, R.A., Biswas, A., Li, S., Zhou, Y., Shi, Z., 2019. X-ray fluorescence and visible near infrared sensor fusion for predicting soil chromium content. Geoderma 352, 61–69. https://doi.org/https://doi.org/10.1016/j.geoderma.2019.05.036

Simulation of Variable Rate Manure Application under Different Schemes

Jian Zhang, Angela Guerrero, Abdul M. Mouazen[*]

Department of Environment, Ghent University, Coupure Links 653, 9000 Gent, Belgium

*Corresponding author. Email: Abdul.Mouazen@UGent.be

Abstract

In order to implement variable rate manure (VRM) in fields correctly, at rates that do not exceed the maximum allowable limits set by legislations, simulations are needed for different VRM scenarios [e.g., map-based (MB), sensor-based (SB) and map-sensor-based (MSB)]. This study aims at the evaluation of these VRM scenarios based on simulation taking into account soil variability and manure limits set by legislations. A simulation software was designed and developed to allow the calculation of recommendations for variable rate manure application. Then, it was used to compare traditional uniform rate manure (URM) application against two VRM treatments in three commercial fields in Flanders, Belgium. Under each of the three treatments, two VRM schemes were evaluated, e.g., applying more manure to the more fertile zone (Kings scheme - KS) and more manure to the least fertile zone (Robin Hood scheme - RHS). Results revealed that RHS consumed 8.0% -15.3% less manure than the UR and 10.5% -15.8% than the KS approach only in one field. Due to the fact that rich parts were of larger area than the poor part, the KS method consumed more manure, hence, this was more expensive than RHS. When imposing the "MAP6" legislation limits, both KS and RHS consumed less than the case of without restrictions, reducing environmental risks due to reducing both nitrogen (N) and phosphorus (P) applied. Simulation results also presented that non-sensor-based methods (MB and URM) exceeded sensor-based (SB and MSB) rates by 2.8%-6.6%, when the mean value of real-time sensed P in manure was higher than the nominal P (measured by laboratory methods) value used for calculating the manure recommendation. We concluded that the manure consumed in VRM application depends on treatment approaches (MB, SB or MSB), application schemes (RHS or KS), measured manure quality, and the proportion of rich, medium, and poor fertility areas in a field.

Keywords: Variable rate manure application; software package; simulation; uniform rate manure application.

1. Introduction

Although manure is an excellent organic fertilizer source containing nitrogen (N), phosphorus (P) and other elements that not only provides essential nutrients for soil but benefits soil physical properties as well (Edmeades, 2003). Despite this, it poses more of a challenge such as nutrient enrichment, P accumulation in soils, and water contamination due to over application and/or its low N/P ratio. Conventional manure application methods tend to treat all areas of a field with the uniform manure rate, regardless of variations in soil nutrients and some parts of landscape features. Such a uniform-rate manure application (URMA) often leads to issues related to over-application or under-application of manure to different parts of a field, than necessary according to crop needs. A promising solution is by implementing variable rate manure application (VRMA) as this will ensure the nutrient inputs match exactly the crop needs by considering small-scale variations of soil fertility under the legal restriction on manure application.

A key requirement for such a VRMA is to depict the within-field variations in soil fertility attributes with a management zones (MZs) map. Among the different kinds of proximal soil sensing tools, visible and near infrared (vis-NIR) spectroscopy is one of the most adopted optical techniques for in-situ soil scanning, as it is fast, cost-effective, robust and enables the collection of quantitative values on key soil fertility attributes at high sampling resolution (Kuang et al., 2013). Even if the site-specific recommendation map for VRMA is already created successfully based on vis-NIR sensors (e.g., Mouazen, 2006), there are still significant differences in manure consumption, economic cost, and applied nutrients among treatments, e.g., VRMA versus URMA. (Guerrero et al., 2021) summarised three different variable rate applications schemes are possible for nitrogen fertilisation, e.g., apply more in the high fertility zones (feeding the rich) and less in the low fertility zones (feeding the poor) of a field, according to the King scheme (KS) and Robin-Hood scheme (RHS), respectively. Authors concluded based on simulation that RHS less risky in overapplying of nitrogen above the set limits by legislations in Flanders, Belgium. Similar simulations for VRMA is necessary, to allow farmers or agricultural service providers to assess which scheme fits their needs prior to practical application. While there are a few methods to determine a URMA, to our best knowledge, there is no automatic tool for calculation and evaluation of VRMA (Loro et al., 2008).

The present work aims to evaluate the performance of different VRMA schemes, e.g. RHS and KS, against uniform rate scheme (URS) under different application scenarios, e.g. map-based (MB), map-sensor-based (MSB), and sensor-based (SB), from economic, environmental and technical points of view. The aim was to find the optimal VRMA method that will ensure the optimal use of manure according to the crop needs at different parts of a field without exceeding the legislation limits.

2. Materials and Methods

In this work, a software package was firstly developed as a simulation tool by combining the LabVIEW programming environment with Matlab. The software can not only automatically create fertiliser or manure recommendation maps, but also simulate a manure application for different treatments and schemes, providing statistical output. Then, the software was used to evaluate traditional URS against RHS-VRMA and KS-VRMA, based on the MZs maps generated from the vis-NIR data collected in three commercial fields, named Beers (12 ha-sandy loam), Gimgelomse (13 ha-loam), and Bottelare (5 ha - silt loam) in Flanders, Belgium. This study intended to provide tools and insights to assess VRMA schemes by means of numerical simulation. Detailed description of the methods used are provided below.

2.1. Field description and online soil sensing

The three commercial fields located at three different farms in Flanders, Belgium shown in Figure 1 are considered in this study. The three fields are under arable cropping system, with crop rotation of of wheat, barley, oilseed rape, sugar beet and potatoes with a short duration autumn cover crop. A multi-sensor platform developed and patented by Mouazen (Mouazen, 2006) was utilized to collect on-line visible and near infrared (vis-NIR) spectra. The platform is equipped with a subsoiler that penetrates the soil, creating a ditch at a depth range of 15 - 25 cm. Appended to the back of the subsoiler chisel, an optical probe connected to a vis-NIR sensor (TEC5 Technology for Spectroscopy, Germany) with a measurement range of 305 – 1700 nm was used to collect soil spectra in diffuse reflectance mode. Every 30 minutes, a 100% ceramic disc was used as the white reference to correct the soil spectra. A differential global positioning system (DGPS) (CFX-750, Trimble, USA) with a datalogger (Compact Rio 9082, National Instruments, USA) was used to synchronically log and record GPS positions and reflectance spectra at a frequency of 1 Hz through a multi-sensor data logging and acquisition software developed under the Labview programming environment. During the field scan, the platform was driven by a tractor along 12 meter apart parallel scanning transects in all fields, with an average travel speed of around 3.5 km/hour. This means that the data consisting of both GPS readings and vis-NIR spectra was collected at one frame per meter.
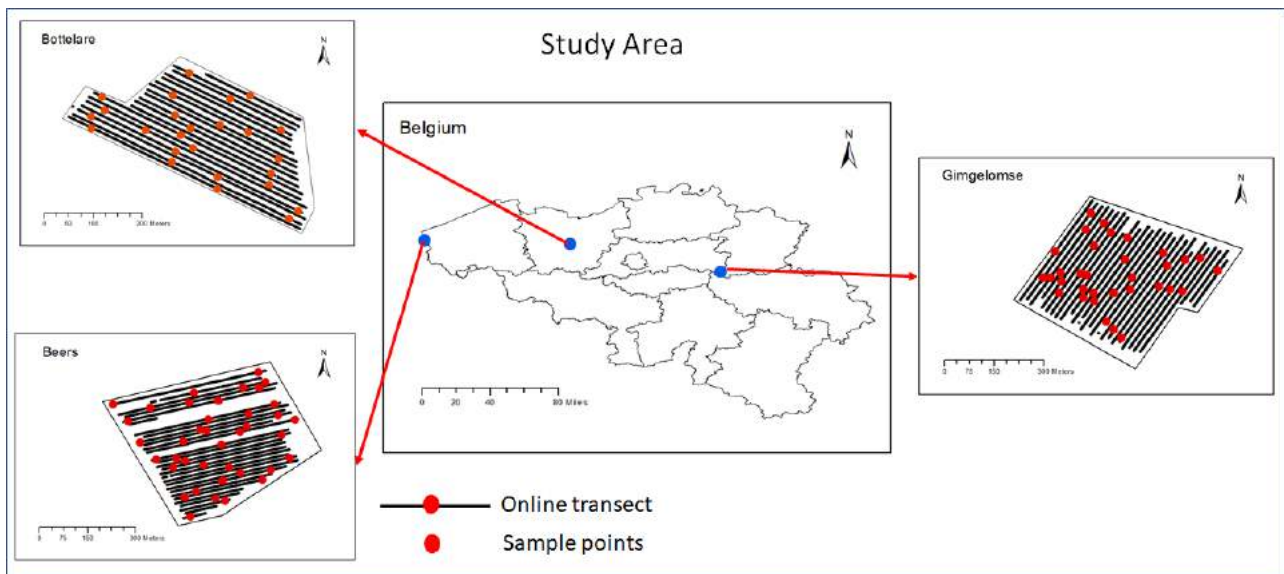
Figure 1. Location of experimental sites in Flanders, Belgium, on-line measured lines and locations of the randomly collected soil samples.

2.2. Pre-processing spectra and modelling

Each soil sample was mixed thoroughly and reduced to a sub-sample of 150g with the quartering method (Geriach, et al., 2002) after removing visible crop residues, roots or stones. Each sub-sample was used for chemical analysis using traditional laboratory methods of the Soil Survey of Belgium (BDB, Leuven, Belgium). More details about the methods used for soil analyses are available in Guerrero et al. (2021).

Spectra modelling was performed on online collected spectra and laboratory measured values of organic carbon (OC), pH, phosphorous (P), potassium (K), magnesium (Mg), calcium (Ca), sodium (Na) and moisture content (MC). Modelling included spectra pre-processing, followed by regression analysis using partial least squares (PLSR) analysis. The pre-processing of vis-NIR spectra included removal of the jump at the joining point of the two detectors at 1045 nm. Additionally, the noisy parts at both edges of spectra were excluded in all soil spectra. The following pre-processing steps were carried out successively Beers and Gimgelomse: moving average to reduce high frequency noise,

a standard normal variate transformation, a Savitzky-Golay (SG) first-order derivative filter and finally a SG smoothing. Besides, the multiplicative scatter correction (MSC) and de-trending were also included in the pre-treatment of spectra for the Bottelare field. The PLSR analyses performed after spectra pre-processing was done using R software (RStudio Inc, USA) with open-source libraries.

Since the number of soil samples collected from each the three study sites were not sufficient to build three field-specific calibration models, their samples were merged with the other samples collected from samples collected from fields in the same farms to form three datasets of 138, 122, and 179 soil samples, for Beers, Gimgelomse, and Bottelare models, respectively. The data of the three datasets were spitted into calibration (70%), and validation (30%) sets by means of the Kennard-Stone algorithm (Kennard, et al., 1969). The prediction performance of the developed models by PLSR was evaluated using the coefficient of determination (R2), root mean square error (RMSE), and the ratio of performance to inter-quartile distance (RPIQ).

2.3 Management zones map

Management zones (MZs) delineation was performed by fusion of data of online measured K, MC, Mg, OC, P and pH and the crop normalised difference vegetation index (NDVI) obtained from Sentinel 2 satellite that is a 13-wavebands multi-spectral earth observation asset distributed in the spectral range of 433nm-2190 nm with 5-day revisit frequency. It started with raster analysis in ArcGIS (ESRI ArcGIS^{TM} , version 10.8.1, CA, USA), which allowed resampling of the soil and NDVI in a common grid of 5 by 5 m resolution. K-means clustering was performed by the developed automatic software, dividing each field into a limited number of clusters, each having similar soil and crop characteristics. Since yield data for Gimgelomse and Beers was not available to rank the groups into different fertility classes, MZs classification was based-on farmers' knowledge of their fields, the measured and online predicted soil properties as well as crop NDVI.

2.4 Numerical simulation

A soft package was developed by combining the LabVIEW programming environment with Matlab. It has a user-friendly simulation interface as shown in Figure 2 - (a), which is flexible and extendible. All of the parameters can be easily set and selected to configure treatments, schemes and application scenarios to be simulated. It also enables the various soil, crop and MZ maps to be plotted and the final statistical results to be exported as output file. With this tool, a simulation usually consists of three steps: 1) loading a MZs map and selecting the direction of tramlines, 2) calculating a fertilizer/manure recommendation map according to the treatments and schemes and creating a fertilizer recommendation map, and 3) simulating the manure applications (both uniform and variable rates) under different application scenarios and calculating the statistical results of applied manure in an output file.

Firstly, the MZs maps of three fields with the geographic and projection coordinates were loaded as displayed in Figure 2 b)-d). It can be observed from the MZs maps that both Beers and Gimgelomse fields, were classified into four fertility classes and the Bottelare field was divided into five classes that were denoted as high (H), medium-high (MH), medium (M), medium-low (ML), and low (L).

In the second step, stripy fertilizer recommendation maps were automatically generated according to three RHS, KS, and URS treatments. In these schemes, the P_2O_5 recommendation was calculated per MZ according to the indexes of fertile classes by applying 30% and 15% more manure in the H and MH areas for RHS (opposite for KS), and 30% and 15% less manure in the L and ML areas of the recommended application rate (RAR) of URS. The medium fertile class received the same application rate as the RAR of the URS that was set as 60 kg P_2O_5 per hectare (ha). The SB also shared the same uniform rate map with the URS. The width of strips was set to be equal to the width of a manure applicator machine that was chosen to be 12 meters. Following the manure action program (MAP6) in Flanders, the legislative P_2O_5 limit of 70 kg/ha was chosen in this work.

The simulations will also be done for sensor based (SB), map-based (MB) and sensor-map-based VRMA scenarios. In the SB scenario, variation in manure P values is considered as input for VRMA, whereas in MB scenario, MZ maps developed with fusion of online soil properties and NDVI is used as input. In the MSB scenario, both the MZ and manure P values are combined in the simulation. While MZ maps were developed based on online measured soil properties and crop NDVI, P variation in manure was randomly developed and fed into the simulation. The randomly generated manure P values were used for SB and SMB simulations.

There are two kinds of practical options to implement VRMA, which are tractor speed control or manure flow rate control. Altering the ground speed to compensate for nutrient variations in applied manure is one implementation scheme that is commercially adopted e.g., by John Deere company. The practical P_2O_5 application of the speed-control option for MSB scenario will be somewhat different from the P_2O_5 recommendation map by the MB scenario. The main difference is time delay in change the recommendation rates between two successive plots within a strip. In the simulation, the time delays was accounted for by the speed-control, which was simulated by iteratively calculating the tractor position as follows:

$$\begin{cases} Tr_{Longti}^{(i+1)T} = Tr_{Longti}^{iT} + S_{iT} \cdot cos\theta \\ T_{Lati}Tr_{Lagti}^{(i+1)T} = Tr_{Lagti}^{iT} + S_{iT} \cdot sin\theta \end{cases} \tag{1}$$

where θ is the angle of the tramline determined in the first step, $Tr_{Longti}^{(i+1)T}$ and Tr_{Longti}^{iT} denote the location of the applicator at the ith and $(i + 1)$th update period along the longitude direction, correspondingly, $Tr_{Lati}^{(i+1)T}$ and Tr_{Lati}^{iT} denote the location along the latitude direction, and S_{iT} means the tractor speed at the moment iT.

In both MSB and SB scenarios, the manure was set randomly to vary in the range of 2.0 kg/ton and 2.2 kg/ton, with the mean value of 2.1 kg/ton, whereas the manure to be applied in MB was assumed to be a fixed value of 2.0 kg/ton that was usually measured by a chemical analysis, and therefore referred to as the nominal value. Based on the above parameters and formulas in the previous two steps, a dynamic simulation for nine cases namely MB-RH, MB-KING, MB-UR, MSB-RH, MSB-KING, MSB-UR, SB-RH, SB-KING, SB-UR, were performed and the statistical results of manure applied were calculated.
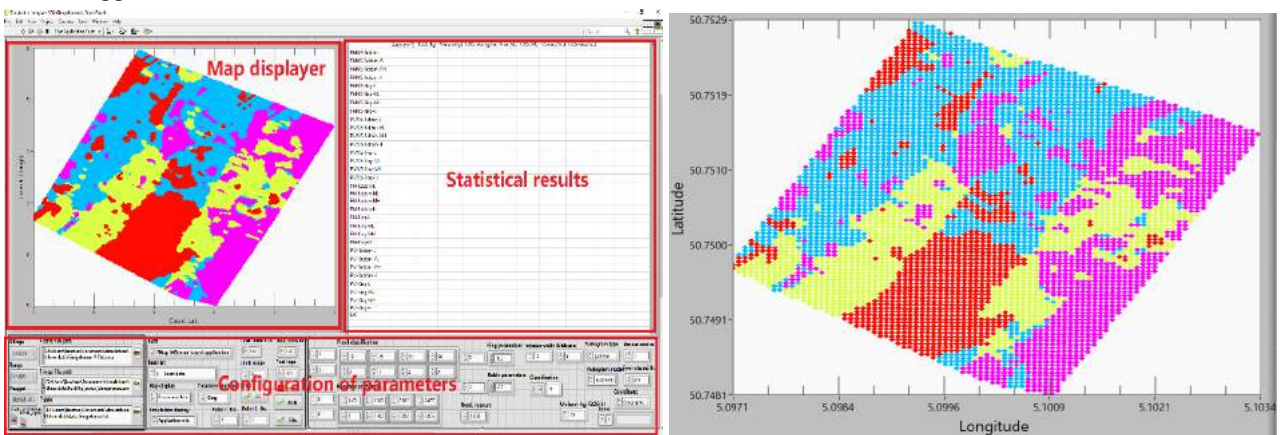
a)   Interface of the simulation program package   b) Management zones map of the Gimgelomse field
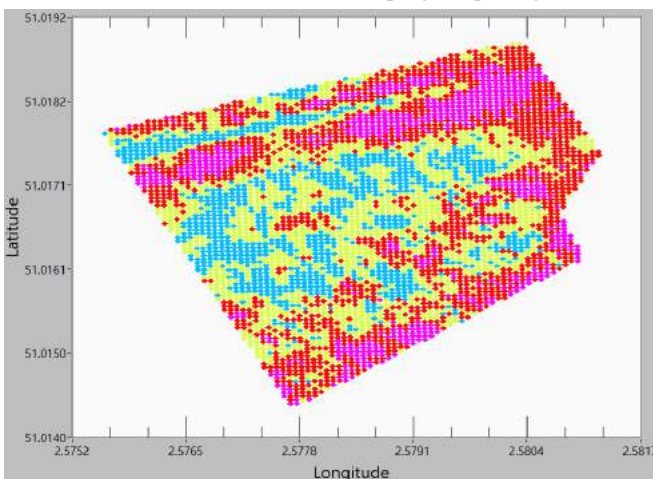
c)   Management zones map of the Beers field   d)   Management zones map of the Bottelare field
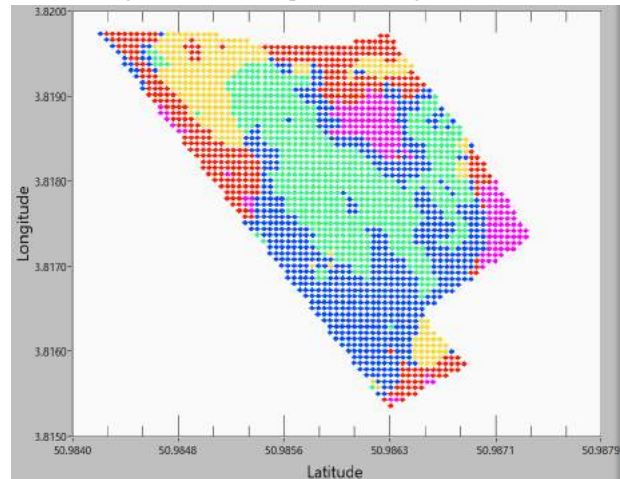
Figure 2. Interface of the simulation program package (a) and the management zone maps for the studied fields (b, c and d)

3. Results and Discussion

3.1 Manure recommendation map

The strip recommendation maps extracted from the simulation software for different treatments, schemes and scenarios are shown in Figure 3 for nine cases. The numbers of strips were different among different strips, depending on the field length perpendicular to the tramline, divided by the machine width. The maximum number of lines was in the Gimgelomse field, having the largest area of 13 hectares. Comparing Figure 2 with Figure 3, although the strips were generated with a lower resolution of 12 m by 5 m in Figure 3, than the grid size of 5 m by 5 m in the MZs maps in Figure 2, the spatial variations were similar. It implies the width of manure applicator machine has limited impacts on

the variations of MZs. If the resolution of sampling along a strip was chosen to be larger than 5 m, although spatial variations becomes coarser the frequency of control (changing) the speed or manure flow decreases with advantageous linked with implementation. Different operating options can be tried with this software until a balance between the spatial resolution and control frequency is obtained.

When the P_2O_5 limit was imposed, it could be observed that the application rate of the richest and poorest areas in RHS and KS treatments respectively were decreased to a maximum of 70 kg P_2O_5 per hectare. In Figure 2, there were four P2O5 fertilization levels of 78, 69, 51, and 42 kg/ha implemented in both Beers and Gimgelomse fields, and five levels of 78, 69, 60, 51, and 42 kg/ha in Bottelare field. Due to the fact that the highest application rate of 78 kg occurred at the most fertile zones (H) in KS and the least fertile zones (L) in RHS, respectively, the legislative P_2O_5 limit was actually imposed on these two classes. It means that the magnitude of impact the legislation limit has on P_2O_5 fertilizer application depends on the proportion of the most fertile (H) or least fertile (L) zones in a field. Since most legislative limits were prescribed by government usually to protect soil and water from contamination, the resulted map in Figure 3 could be considered as a balance between minimizing environmental risks and provide sufficient nutrient inputs to the crops.
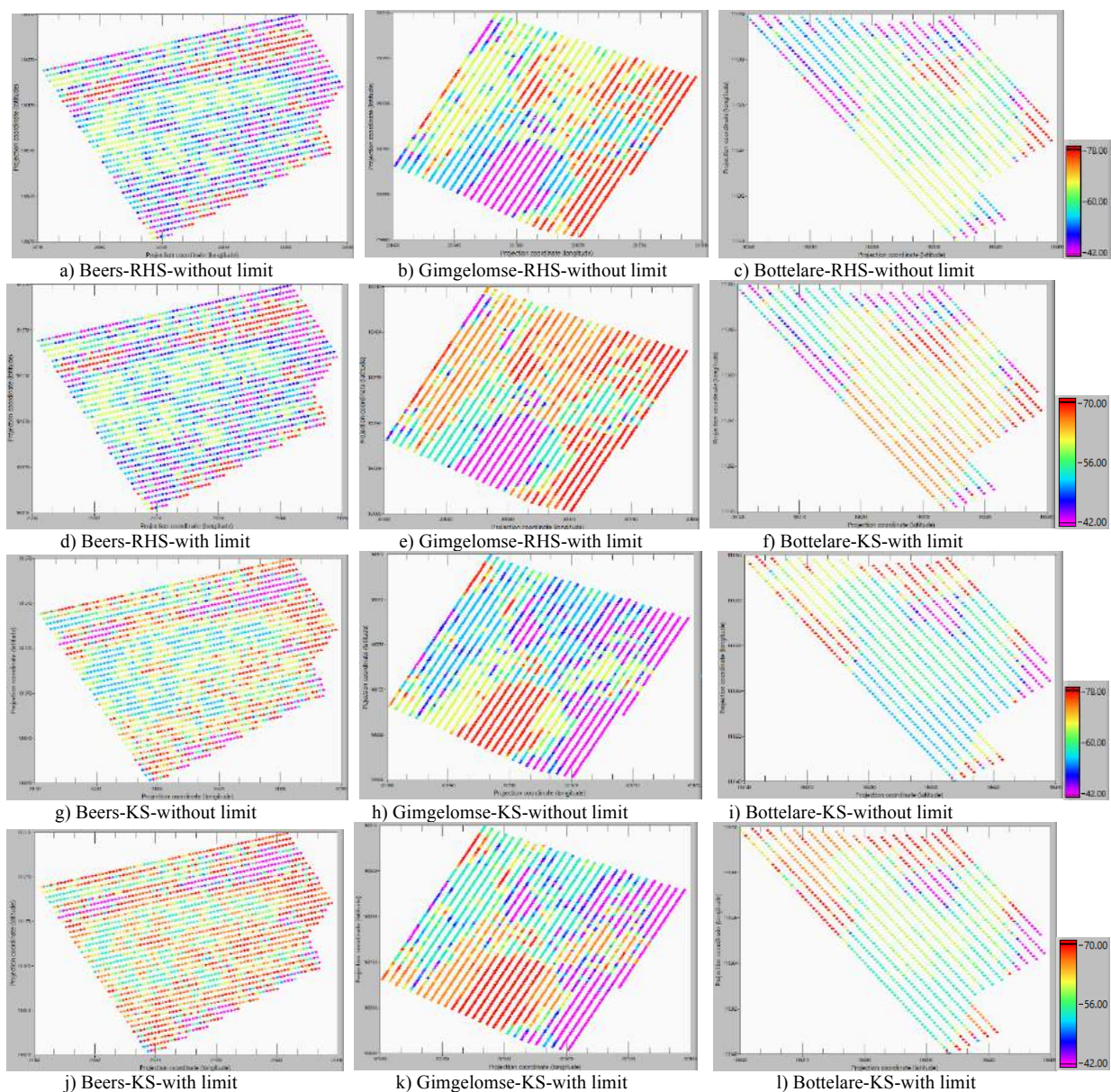
Figure 3. The strip P_2O_5 (kg/ha) recommendation maps of RHS and KS with and without limit imposing the legislation limits.

3.2 Statistical Results

The calculated P_2O_5 applied per hectare in each of the three fields using the three application scenarios of MB, MSB, and SB for RH, KS and URS, under with and without the legislative P_2O_5 limits, are depicted in Figure 4. Under both MB and MSB, RHS consumed 8.0% -15.3% less manure than the URS and 10.5% -15.8% than the KS only in Beers. This means that it is not always correct to assume that VRMA will decrease the amount of manure applied and RHS will be
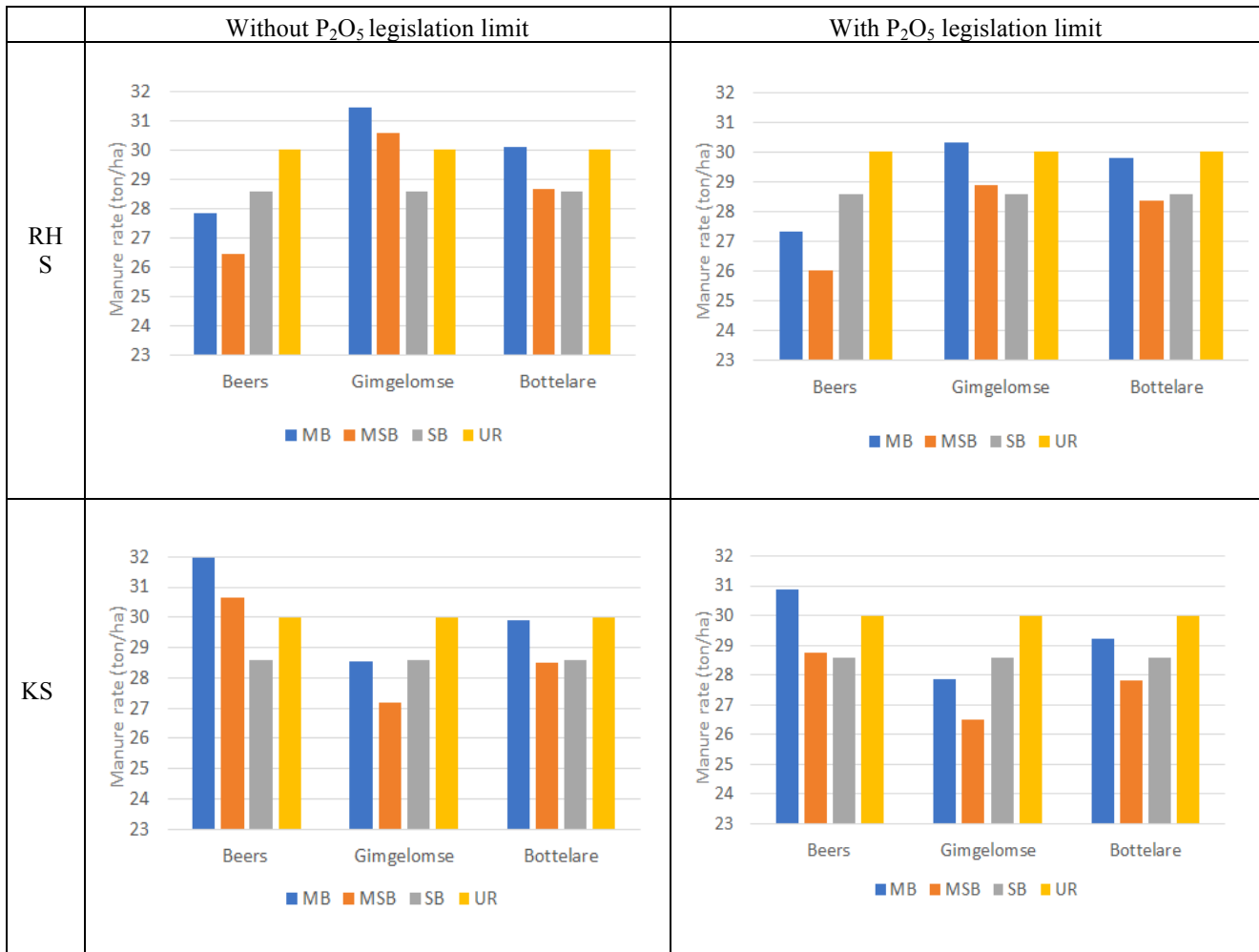
Figure 4. Statistical comparison

better than KS in terms of saving on manure consumption. On the contrary, the application rate in KS was lower than not only RHS but URS as well in both the Gimgelomse and Bottelare fields. This was particularly true for MB and SMB scenarios. This was simply because poor parts were of larger area than the rich parts in both fields. The KS consumed least amount of manure in the poor zones compared to RHS and URS, hence, was the cheapest in these two fields. Moreover, the KS still showed the lowest application rates in the both fields even with the P_2O_5 limit was imposed. Therefore, the manure consumption is dependent on the area proportion of different fertile levels over a whole field. Since MB and MSB are based on split of a field into MZs, the accuracy of the clustering algorithms used would affect the manure rate applied. In this study, only k-means clustering algorithm was tested, and further work should test other clustering algorithms if more accurate simulation can be targeted.

As mentioned in the previous section, the SB scheme was simulated based the same uniform rate map as the URS. The difference was that random manure values with the mean value of 2.1 kg P_2O_5/ton, the maximum value 2.2 kg P_2O_5/ton, and the minimum value 2.0 kg P_2O_5/ton, were utilized in SB instead of the homogeneous one with the chemical analysis of 2.0 kg P_2O_5/ton in URS. Such a chemical analysis value was usually received prior to the practical fieldwork and then used for the calculation of uniform application rate in URS. Since the chemical analysis value of URS was less than that adopted for SB, manure applied in URS is poorer than the one in SB, which is the reason why

the latter consumed less manure than the URS. A similar situation also happened to MB and MSB where the former consumed higher application rates by 2.8%-6.6%. However, this result will not be true if proposed mean manure P_2O_5 content is less than the chemical analysis value. Therefore, whether sensor-based approaches are more economical than non-sensor-based approaches depends on the relation between the average value of real-time sensed P_2O_5 in manure and the nominal P_2O_5 content in manure measured by laboratory methods. As it is hard and expensive to take a large number of samples for chemical analysis in each manure application, a vis-NIR sensor adopted for manure sensing is more likely to arrive at accurate estimation of manure quality at high sampling resolution, necessary for more accurate simulation in a future work.

Although imposing the P_2O_5 limit has resulted in reducing the application rate, only both most fertile and least fertile zones, i.e. H and L zones, in KS and RHS respectively, were affected because the limit value was lower than P_2O recommendation only in H and L zones. This is the reason why imposing the legislative limit caused a relatively large decrease in applied rate only in the Beers field where the richest areas account for a larger percentage (L：14%，ML：21%，MH：33%，H：31%），of the field total area compared to the other two fields. The lower percentages of both H and L zones in the Gimgelomse and Bottelare fields decreased the impacts of the legislative P_2O_5 limit. Again, this means that delineating accurate MZ maps are essential for accurate estimation of the influence of the legislation limit on VRMA application. On the other hand, more classes would be affected by the limit if the prescribed P_2O_5 recommendation in medium (M) zones is below the limit value. In this case, the application rate over a whole field would be decreased significantly when the same P_2O_5 limit is imposed.

Although the URS was not worst among the four treatments displayed in Figure 4 in terms of manure consumption, it did not mean the URS was competent to VRMA. A holistic assessment criterion should account not only for the amount of manure applied to soil as the input, but should also include crop yield as the output. If a scheme with a slightly higher consumption of manure can bring a significant increase in yield, it would be better than the one that applies less manure but along with a lower crop yield. In order to further discuss the results in Figure 4, a quantitative analysis was carried out based on a simplified VRMA example shown in Table 1.

Table 1. Specific parameters for a demonstrative example

	Low fertile zones ($p\%$)	Medium fertile zones ($q\%$)	High fertile zones ($r\%$)
Robin-Hood scheme	$+ s\%$	0%	-
King scheme	$- s\%$	0%	$+ s\%$
Uniform rate scheme	Cr kg P_2O_5 per hectare		

Cr: the used manure application rate in URS; s%: the percentage of deviated manure application rate.

Here we assume that there was a K hectares of field with $p\%$ low fertile area, $q\%$ medium fertile area, $r\%$ high fertile area, and $p\%+ q\%+ r\%$ =1. Three schemes, RH, KS, and URS, were applied according to the parameters included in Table 1 where the legislative limit was assumed as Fr of P_2O_5 kg/ha. Table 2 summarized the results, which allows the conclusions to be made:

1) In the case of no P_2O_5 limit imposed,

   the total field applied manure for RHS-VRMA is not smaller than the one of KS-VRMA and URS if $p\% \geq r\%$,

   the total field applied manure for RHS-VRMA is not larger than the one of KS-VRMA and URS if $p\% \leq r\%$,

   the total field applied manure of KS-VRMA is not smaller than the one of URS if $p\% \leq r\%$,

   the total field applied manure of KS-VRMA is not larger than the one of URS if $p\% \geq r\%$,

   the application rates of RHS-VRMA, KS-VRMA, and URS are equal to each other if $p\% = r\%$.

2) In the case of P_2O_5 limit imposed, compared to the case of no P_2O_5 limit imposed will result in:

   the total field applied manure of RHS-VRMA decreases as: $(Cr(1 + s\%) - Fr) \cdot K \cdot p\%$,

   the total field applied manure of KS-VRMA decreases as: $(Cr(1 + s\%) - Fr) \cdot K \cdot r\%$,

   the total field applied manure of URS decreases as: $(Cr - Fr) \cdot K$,

   In particular, If $Fr = Cr(1 + s\%)$, there would be no reduction in the amount of fertilizer applied because the schemes meet exactly the legal requirements.

Table 2. Specific parameters for a demonstrative example

	No P$_2$O$_5$ limit	P$_2$O$_5$ limit
Robin-Hood scheme	$Cr \cdot K \cdot [(1+ s\%) \cdot p\% + q\% + (1- s\%) \cdot r\%]$	$Cr \cdot K \cdot [(q\% + (1- s\%) \cdot r\%] + Fr \cdot K \cdot p\%$
King scheme	$Cr \cdot K \cdot [(1- s\%) \cdot p\% + q\% + (1+ s\%) \cdot r\%]$	$Cr \cdot K \cdot [(q\% + (1- s\%) \cdot p\%] + Fr \cdot K \cdot r\%$
Uniform rate scheme	$Cr \cdot K$	$Cr \cdot K$

Cr: manure application rate used in URS; Fr: the legislative P$_2$O$_5$ limit; K: field size; $s\%$: the percentage of deviated manure application rate.

4. Conclusions

A software package based on Labivew and Matlab programming languages was developed for the simulation of different VRMA treatments and schemes under different application scenarios. The software was used to automatically create fertilizer recommendation map, simulate manure application rates applied at different zones of a field, and generate statistical results as output file. Results allowed the following conclusions to be drawn:

1) The manure consumed in VRMA was directly related to the proportion of rich, medium, and poor fertility areas in a MZs map;
2) Non-sensor-based methods consume more manure than sensor-based schemes, when the mean value of real-time sensed P$_2$O$_5$ content in manure was higher than the nominal P$_2$O$_5$ measured by laboratory methods, and vice versa;
3) Both RHS and KS consumed less amount of manure when the legislative P$_2$O$_5$ limit was imposed.

The future work will aim at the integration of crop yield in the simulation to evaluate different VRMA schemes, taking into account not only the amount of manure used but also yield output in a comprehensive, cost-benefit, environmental and agronomic analysis.

Acknowledgements

References

Edmeades, D.C., 2003. The long-term effects of manures and fertilizers on soil productivity and quality: a review. Nutrient Cycling in Agroecosystems, 66, 165-180.

Geriach, R.W., Dobb, D.E., Raab, G.A., Nocerino, J.M., 2002. Gy sampling theory in environmental studies. Journal of Chemometerics, 16, 321-328.

Guerrero, A., De Neve, S., Mouazen, A.M., 2021. Current sensor technologies for in situ and on-line measurement of soil nitrogen for variable rate fertilization : a review. Advances In Agronomy. https://doi.org/10.1016/bs.agron.2021.02.001.

Kennard, R.W., Stone, L.A., 1969. Computer-aided Design of Experiments. Technometrics, 11, 137-148.

Kuang, B.Y., Mahmood, H.S., Quraishi, M.Z., Hoogmoed, W.B., Mouazen, A.M., van Henten, E.J., 2012. Sensing soil properties in the laboratory, in Situ, and on-Line: a review. Advances in agronomy, 114, 155-223.

Loro, P., et al., 2008. Manure application rate calculator MARC 2008 User's Manual - Version 2.1.3. Manitoba Agriculture, Food and Rural Initiatives, Canada.

Mouazen, A.M., 2006. Soil survey device. International publication published under the patent cooperation treaty (PCT). World Intellectual Property Organization, International BureauWO2006/015463,PCT/BE2005/000129, IPC: G01N21/00; G01N21/00.

Benefit of the Variable Rate Technology in a Top-Dressed Fertilization of a Fodder Crop in a Nitrate Vulnerable Area

Luis Alcino Conceição [a,b*], Luís Silva[a] Susana Dias [a,b], Luís Loures [a,b] Benvindo Maças[c]

[a] VALORIZA—Research Center for Endogenous Resource Valorization, Polytechnic Institute of Portalegre, 7300-110 Portalegre, Portugal

[b] Polytechnic Institute of Portalegre, 7300-110 Portalegre, Portugal

[c] Research Unit of Biotechnology and Genetic Resources (INIAV), 7300 Elvas, Portugal

* Corresponding author. Email: luis_conceicao@ipportalegre.pt

Abstract

The need to control the concentration of nitrates in vulnerable areas of the Alentejo region and the poor efficiency of nitrogen top-dressed fertilizations in winter crops, because of the rainfed characteristics of the Mediterranean regions, suggest new forms of mechanization based on precision farming technologies namely variable rate application (VRA). Overall, VRA technology is primarily used to detect information about a given landscape and to have a system make decisions based on that information.

The study was carried out in a 7,5ha plot located at Herdade Experimental da Comenda in Elvas, Southeast Portugal between October 2020 and April 2021. Surveys of apparent soil electrical conductivity (EC_a) were conducted with an EM 38 soil sensor. A total of 8 sampling areas (95mx95m) were georeferenced to allow normalized difference vegetation index (NDVI) and normalized difference water index (NDWI) readings. Historical time series of these indices were obtained from satellite imagery (Sentinel-2) since crop early stem elongation, and crop biomass content in N was determined in a laboratory. Based on the obtained results, three homogeneous management zones were defined, and three N rates were applied in opposition to a conventional fixed N rate. The obtained results highlight the contribution of VRA to the environmental control of nitrates in vulnerable areas using precision management technology.

Keywords: GIS, environment, remote sensing, mechanization, crop production.

1. Introduction

The careful management of natural resources and the rational use of production factors are increasingly imposed on agricultural practices. Since 1991 the EU Nitrates Directive aims to protect water quality across Europe by preventing nitrates from agricultural sources polluting ground and surface waters and by promoting the use of good farming practices. According to the Portuguese legislation (Decreto-Lei n. º 235/97) the continental territory has 9 nitrate vulnerable zones, 3 of which are in the Alentejo region.

Nitrogen (N) application required in large quantities is one of the most important factors in maximizing yields and economic profits for farmers. Because of it is the most mobile and dynamic nutrient in soil systems, depending on soil physical and chemical properties N dynamics are subjected to mechanisms for its losses. In Mediterranean regions such as Alentejo in Portugal because farmers are forced to supplement cattle during wintertime and end of summer with preserved annual fodder crops, the efficiency of N fertilization in its production is usually low, due to climatic and edaphic restrictions (Carvalho, 2016). On the one hand, the intra-annual variability of the climate makes it very difficult to calculate N fertilization, on the other hand, the low levels of organic matter of the soil, together with its poor capacity to retain nutrients, lose it with the risk of contamination of surface and deep waters.

Thus, assessing soil and crop variability must become an important issue to determine the right strategy to determine homogeneous management zones (HMZ) to a profitable crop production and long-term soil and environmental quality. Currently, site-specific management and the use of variable rate products in the framework of Precision Agriculture gives farmers the possibility to increase yield, reduce inputs, and minimize environmental impact (Robertson et al., 2012; Basso et al., 2016). The first step for implementing strategies for management of this variability requires the determination of the spatial and temporal patterns of the main soil properties and crop response by determining apparent soil electrical conductivity (ECa), the Normalized Difference Vegetation Index (NDVI) and Normalized Difference Water Index (NDWI) (Serrano et al., 2019).

The objectives of this study were to: i) identify HMZ to define crop optimal N fertilizer rates; ii) demonstrate the environmental benefits of precision nitrogen management in fodder crops in a nitrate vulnerable zone.

2. Materials and Methods

2.1. Site Characteristics and initial conditions of the trial

The study was carried out in a nitrate vulnerable area in Caia (Elvas) on a 7,5-ha plot at the Comenda Experimental farm, owned by the National Institute of Agricultural and Veterinary Research (NIAVR). According to the Portuguese legislation in this area, no more than 55 units of N are allowed considering mix fodder crops.

Climate, according to Köppen-Geiger is Mediterranean Csa where the average annual precipitation observed at the Elvas weather station is 535.4 mm, divided by a rainy season from October to February with 64% of the average annual precipitation. Figure 1 show the Ombrothermic diagram in 2021 campaign.
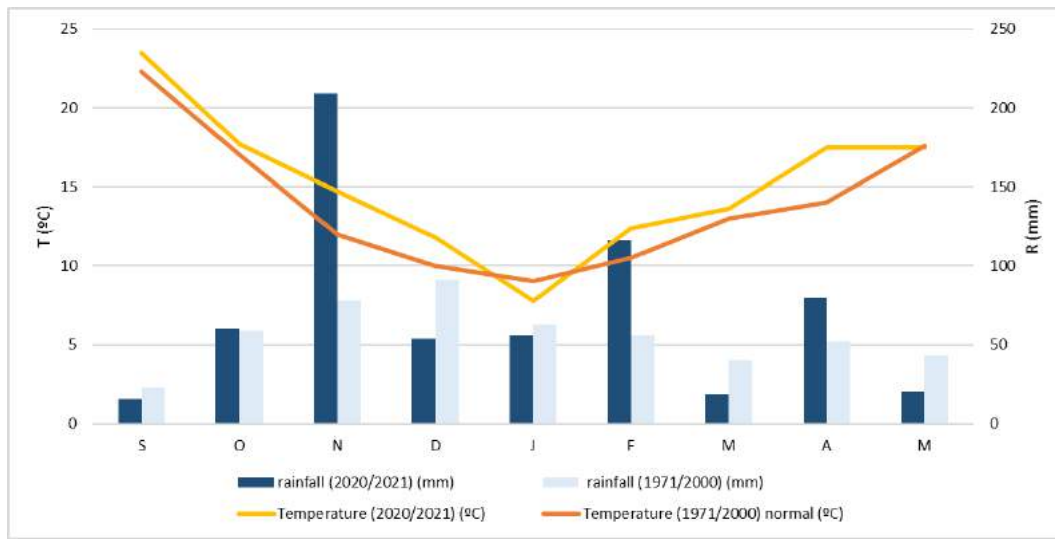
Figure 1. Ombrothermic diagram in 2021 campaign.

The predominant soil of the field is, according to the FAO classification, a Luvisol matching to a Pag and Sr Mediterranean soil types (Cardoso, 1974). Pag is characterized by brown to brownish or light grey color, sandy or loamy sandy sometimes with coarse elements of quartz throughout its profile and a structure without aggregates or weak fine granules and Sr of brown or reddish-brown color, usually with many coarse elements throughout its profile, of moderate or weak fine granular structure.

2.2 Soil and crop Assessments

Soil was surveyed to apparent electrical conductivity (EC_a) by an EM-38 soil sensor (Geonics. Ltd., Mississauga, ON, Canada) in the $0 – 0.5m$ depth. In October, the 20th after a weed control of a glyphosate-based herbicide a mixed grass (67%) and legume (32%) fodder crop was sown under no-till. Table 1 show the fodder crop seed rate.

Table 1. Fodder crop cultivars and corresponding seed rate.

Grass/Legume Cultivar	Seed rate (%)
Lolium multiflorum	12
Avena sativa	35
x Triticosecale Wittmack	53
Trifolium suaveolens	25
Vicia villosa	75

To allow soil and crop analysis the plot was divided in 8 georeferenced sampling areas (95mx95m, approximately). For each of the sampled points a standard soil characterization was made of soil gravimetric moisture, texture, bulk density, pH, organic matter content, phosphorus, and potassium.

Crop evaluation was made since early stem elongation using Normalized Difference Vegetation Index (NDVI) and

Normalized Difference Water Index (NDWI) readings from satellite imagery (Sentinel-2). NDVI was calculated according to Rouse et al. (1974) (Eq.1) and NDWI (Eq.2) according to Gao (1995) (Eq.2).

$$NDVI= ((NIR-Red))/((NIR+Red)) \qquad (1)$$

$$NDWI= ((NIR - SWIR))/((NIR +SWIR)) \qquad (2)$$

Where NIR-Near infrared band; Red – Red infrared band; SWIR - Short Wave Infrared

Fodder samples of $0,25m^2$ were harvested 3 cm height immediately before top dressing application, and approximately 22- and 40-days later to determine Fresh (FM) and Dry Matter (DM) yield (Lancashire *et al.* 1991). The collected samples were weighted to determine the FM production per hectare, and subsamples in small paper bags placed in 65 °C until constant weight to determine moisture content and DM. To determine the amount of top-dressed fertilization, leaf total N content was determined in laboratory using the Kjeldahl method. Nitrogen fertilizer (Nitro 27%) was applied at a variable rate using a tractor New Holland T5 120 Dynamic Command equipped with a monitor IntelliView IV, and a mounted spreader Amazone ZAV, both equipped with ISOBUS.

Statistical data were performed using Statistica software, version 12.0 (StatSoft®, Tulsa, USA), and digital cartography using Qgis 3.10.10 version.

3. Results and Discussion

Soil EC_a interpolated map showed two main areas for 25 to 35 mS/m and 70 mS/m corresponding to a sandy loam and loam texture, respectively (Figure 2).

Figure 2. Soil EC_a interpolation map of the field trial.

Table 2 show the soil analysis results of the experimental field corresponding to each soil EC_a range.

Table 2. Soil analysis results corresponding to ECa range 25 to 35 mS/m and 35 to 70 mS/m

EC$_a$ Class (mS/m)	Soil Texture	Sand (%)	Silt (%)	Clay (%)	Available Phosphorus (mg kg^{-1})	Available Phosphorus (mg kg^{-1})	pH	Organic Mater (%)	Gravimetric moisture (%)	Bulk Density
25-35	Sandy loam	74.6	10.4	15	168.2	99.3	6.8	1.5	7	1.3
35 - 70	Loam	51.2	29	20.1	162	79	6.5	1.10	9	1.4

At the sowing moment, considering the fodder crop mix and soil physical and chemical characteristics, one third of the total nitrogen fertilization was applied at a variable rate: 1/3 in the zone of the highest electrical conductivity and 2/3 in the zone of lowest electrical conductivity corresponding approximately to 9 and 16 units of N fertilizer.

Immediately before the top-dressed fertilization, the analysis of the values of the NDVI and NDWI maps, and the relationship between the NDVI and the leaf total N content in the crop samples showed a positive and significant coefficient of determination (R^2) of 0.57 and 0.51, respectively (Figures 3 and 4).
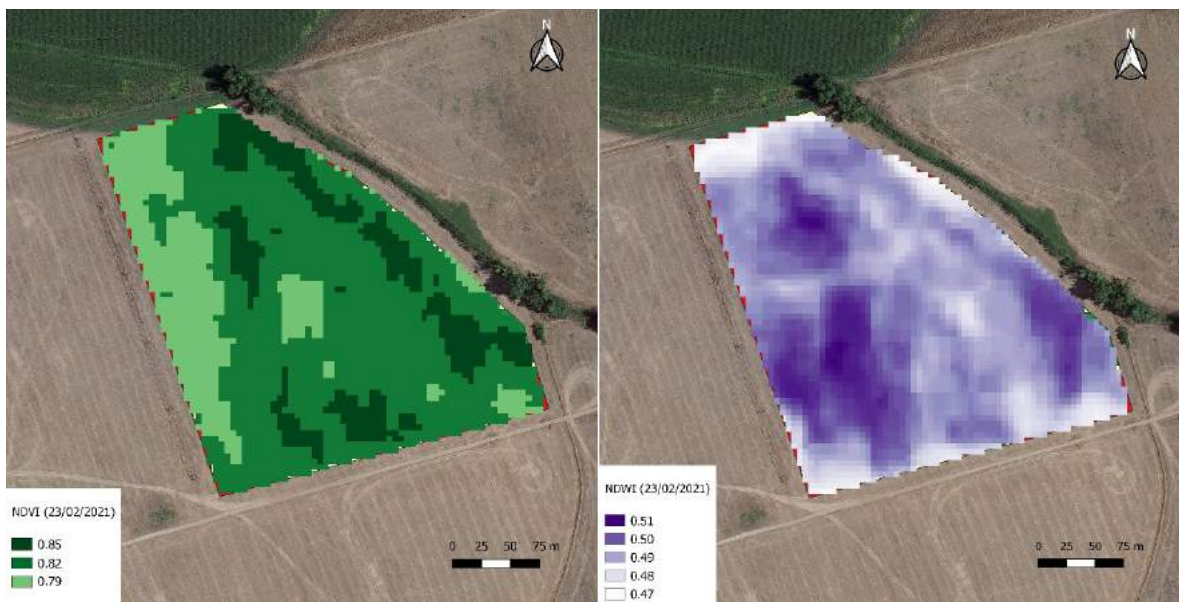
Figure 3. Spatial variation in NDVI (left) and NDWI (right) crop values before top-dressed fertilization.
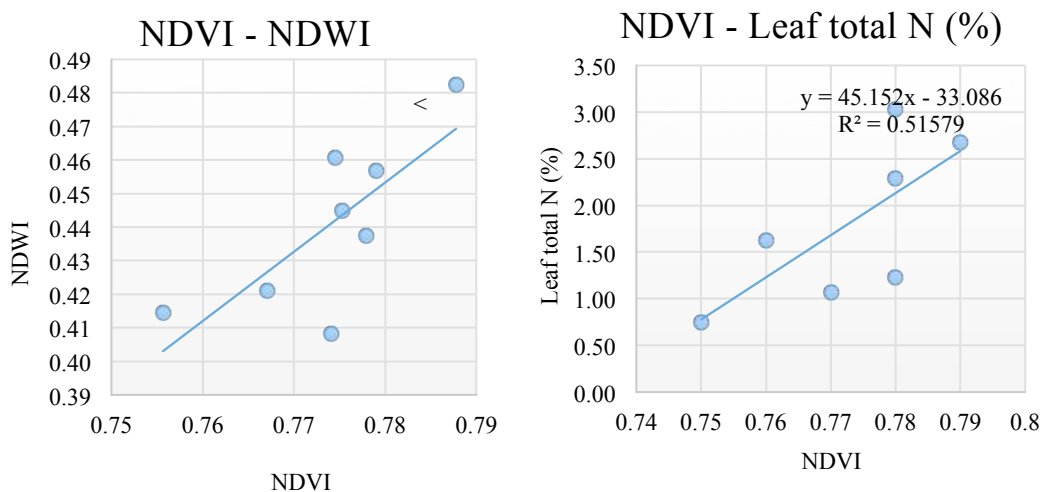
Figure 4. Relationship between the crop NDVI X NDWI (left) and NDVI X Leaf total N content before top-dressed fertilization.

Three HMZ were determined for the top-dressed fertilization (Figure 5). Considering the crop needs and the limit amount of N in the plot, a variable rate of 10 units in zone 1, 15 units in zone 2 and 20 units in zone 3 were applied corresponding to the average values of NDVI 0.89, 0.85 and 0.79, respectively.

Figure 5. Three HMZ

Figure 6 and Table 3 show the evolution of the crop's NDVI minimum, maximum and average values, and the evolution of the FM and DM values after de VRA along the crop cycle, respectively.

	23rd Feb	28th Feb	2nd Marh	7thMarch	10th March	19th Apr
Mín	0.79	0.77	0.74	0.77	0.83	0.87
Max	0.85	0.81	0.78	0.80	0.86	0.89
Average	0.82	0.79	0.76	0.79	0.85	0.88
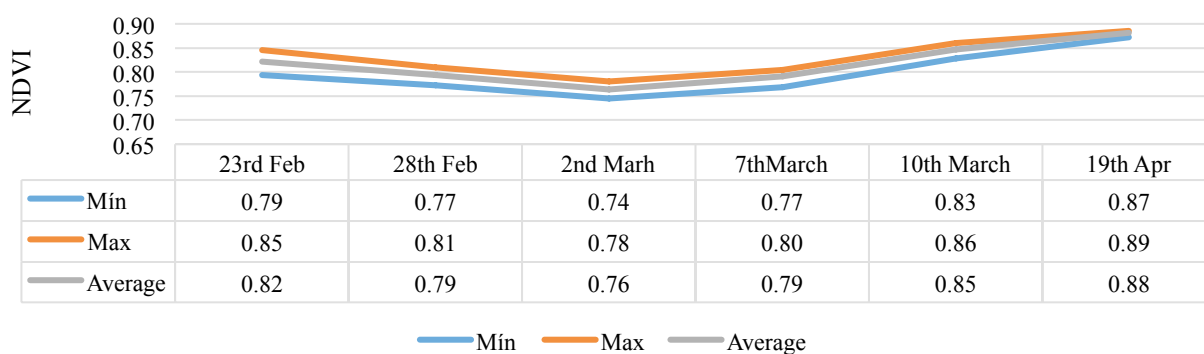
Figure 6. Evaluation of the minimum, maximum and average values of NDVI after the VRA along the crop cycle.

Table 3. Minimum, maximum, average, standard deviation and coefficient of variation of the FM and DM

	FM (kg/ha)			DM (kg/ha)		
	18th Feb	22nd Mar	19thApr	18th Feb	22nd Mar	19thApr
Mín	16400,0	10213,3	28578,7	1125,3	2306,7	**5360,0**
Max	37933,3	18546,7	41417,3	2493,3	4626,7	**8245,3**
Average	29025,0	13858,3	35016,3	1943,7	3203,3	**6701,8**
Sd	7538,2	3157,3	5261,7	463,7	748,8	1015,0
CV	26,0	22,8	15,0	23,9	23,4	15,1

Twenty to forty days after the VRA not only there was an increasing value of the crop NDVI as well throughout the crop cycle, but there was also a reduction in the coefficient of variation of the NDVI, FM and DM, regardless of the constant increase in the DM content, whether in the min, max or average values. Considering the different levels of fertilization FM and Dm yield are in line with some of other trials at a fix rate (Bueno *et al.* 2007; Akdeniz *et al.*, 2019).

4. Conclusions

In Mediterranean regions due to local edaphoclimatic conditions the alternative for a better use of nitrogen fertilizers in vulnerable areas to nitrates is their distribution along the crop cycle; currently with sensory technologies in precision agriculture is also the use of variable application rates considering soil and crop variability.

In this trial, due to soil ECa evaluation and lab analysis two HMZ were delimited for the application of N at a variable rate at the sowing moment. Based on the ratio of the NDVI, NDWI and leaf total nitrogen content, three HMZ were defined for the application of the top-dressed fertilization following a crop standardizing strategy.

According to the bibliography, results showed that maintaining regular yield values for fixed N rates, the use of VRT allowed a decrease in the standard deviation and the coefficient of variation of FM and DM values, this one maintaining a crop productivity growth curve.

In this way, and unlike the use of a fixed rate of fertilizer, a direct response to the needs of the crop is achieved, avoiding overdoses, and so reducing the risks that this represents for environmental and local biodiversity.

Acknowledgements

References

Akdeniz, H., Ali Bozkurt, M., Hosaflioglu, I., Islam,M.S., Hossain, A., Elsabagh, M.,Iqbal, M.A., El Sabagh, A. 2019. Fresenius Environmental Bulletin. 28 (12), 8986-8992. ISSN 1018-4619

Basso, B., Dumont, B., Cammarano, D., Pezzuolo, A., Marinello, F., & Sartori, L. (2016). Environmental and economic benefits of variable rate nitrogen fertilization in a nitrate vulnerable zone. The Science of the total environment, 545-546, 227–235. https://doi.org/10.1016/j.scitotenv.2015.12.104

Bueno, J., Amiama, C., Hernanz, J.L., 2007. No-tillage drilling of Italian ryegrass (*Lolium multiflorum* L.): Crop residue effects, yields and economic benefits. Soil and Tillage Research, Volume 95, Issues 1-2: 61-68, doi: 10.1016/j.still.2006.11.002

Cardoso, J.C., 1974. A classificação dos solos de Portugal. Portuguese soil classification. Nova versão – Boletim de solos do S.R.O.A, 17, 14-46.

Carvalho, M. 2016. A adubação do trigo em Portugal: o problema do seu uso eficiente. Agrotec. 18, 40-43.

Gao, B.C. 1995. A normalized difference water index for remote sensing of vegetation liquid water from space. SPIE's 1995 Symposium on OE/Aerospace Sensing and Dual Use Photonics. 2480.

Lancashire, P.D., Bleiholder, H., Langeluddecke, P., Stauss, R., van den Boom, T., Weber, E., Witzen-Berger, A., 1991. A uniform decimal code for growth stages of crops and weeds. Ann. Appl. Biol. 119 (3), 561–601. doi:10.1111/j.1744-7348.1991.tb04895.x

Robertson, M.J., Llewellyn, R.S., Mandel, R., Lawes, R., Bramley, R.G.V., Swift, L., Metz, N., O'Callaghan, C. 2012.

Adoption of variable rate fertiliser application in the Australian grains industry: status, issues and prospects

Precision Agric. 13, 181-199.

Rouse, J.W., Haas, R.H., Schell, J.A., Deering, D.W., 1974. Monitoring vegetation systems in the Great Plains with ERTS, In: S.C. Freden, E.P. Mercanti, and M. Becker (eds) Third Earth Resources Technology Satellite–1 Syposium. Volume I: Technical Presentations, NASA SP-351, 309-317.

Characterizing Lactating Sow Posture in Farrowing Crates Utilizing Automated Image Capture and Wearable Sensors

Asya Macon [a], Dr. Sudhendu Sharma[a] Bernard Lee[b], Dr. Eric Markvicka[b], Dr. Gary Rohrer[c], Dr. Jeremy Miles[c], Dr. Tami Brown-Brandl[a]

[a] Department of Biological Systems Engineering, University of Nebraska-Lincoln, Lincoln, NE, USA

[b] Department of Mechanical Engineering, University of Nebraska-Lincoln, Lincoln, NE, USA

[c]USDA Agricultural Research Service Meat Animal Research Center, Clay Center, NE USA

Corresponding Author: Dr. Tami Brown-Brandl. Email: tami.brownbrandl@unl.edu

Abstract

Pre-weaning mortality is a major economic and welfare issue in swine production, and one of the major causes is the crushing of the piglets by the sow. This experiment's objective is to track lactating sow static posture changes and activity in three different farrowing crate layouts using wearable accelerometer sensors. The accelerometer sensor integrates an electronic sensing circuit with rigid, waterproof enclosure to monitor the posture of the sow. The electronic sensing circuit contains 1) microcontroller for signal processing, 2) non-volatile flash data storage, 3) real-time clock, 4) rechargeable battery, 5) and three-axis accelerometer with integrated temperature sensor. The wearable sensors were placed in denim pockets with a Velcro enclosure affixed to the sow using livestock tag cement. Three Brinno BCC100 time-lapse cameras were utilized for validation of the wearable sensors. The Brinno camera collected data at 1 frame/sec. The image data was used to assess major movements associated with six static posture changes (standing, lying-left, lying-right, lying-other, kneeling, and sitting). The accelerometer data can be used to assess general activity level movement and to determine postures and precise movements. The temperature data can be used to assess the microenvironment surrounding the sow. The system provides a path towards the collection of phenotypic data related to maternal ability. The X-, Y-, and Z-acceleration orientation values were analysed using statistical analysis to determine the significant difference between the six static postures. There was a significant difference between sitting and standing in acceleration X and a significant difference between lying-left and lying-right in accelerations Y and Z. In addition, it was also found that in all three acceleration values, the sow in the offset crate was significantly different from the sows in the expanded and diagonal crates. A combination of the X-, Y-, and Z-values will be used to determine different static postures by comparing the significant differences.

Keywords: Accelerometer, swine, well-being, movement, PLF

1. Introduction

Precision livestock farming (PLF) applies technology and real-time automated processes to provide a continuous data stream to aid in management decisions such as animal reproduction, welfare, health, and production. Farmers are using this method to retrieve real-time data from their herds using sensors and other applications. PLF has the potential to be an extremely useful technique because farmers are not always around to continuously observe their animals, and it assists them in monitoring the health of their herds. These technologies and managements are growing increasingly popular where it is also being used by producers, animal scientists, veterinarians, and physiologists. The need for these technologies is growing with decreases in labour sustainability.

Accelerometers are one of the most used sensors to improve animal production and welfare. They are electromechanical devices that measure acceleration. The acceleration forces include static which is gravity, and dynamic which is caused by vibrations and movement of the accelerometer. These sensors can be placed in a variety of places on the animal such as the ears, body, neck collar, and limbs. Animal's behaviours are indicative of their health and welfare, and monitoring their behaviours can help assess physiological status, well-being, and preference to different housing systems. These wearable sensors have been shown to be beneficial in several different species including dairy, poultry, and swine.

Accelerometers have been used in dairy cattle to detect lameness, determine estrus, and classify behaviours. Thorup et al. (2015) used accelerometers to detect activity patterns. They showed longer-lying durations, and a decrease in total walking time and walking speed were all indicative of lameness. Shahriar et al. (2016) fitted accelerometers to the neck collars of pasture-based dairy cows who were in heat to identify increased activity levels. A heat detection algorithm was created based on the accelerometer data, and there was an overall accuracy of 82-100% with 100% sensitivity when the change detection technique was applied to the activity index level. Tamura et al. (2019) utilized tri-axial accelerometers mounted to the neck of dairy cattle to identify the association between behaviour and the acceleration data. The behaviours were also observed visually, and recorded behaviours include eating, rumination, and lying. The study provided high precision results of 99.2% and a sensitivity and specificity of 100% using the decision-tree method

as a behaviour classification algorithm based on the acceleration data. Based on these studies and others, accelerometers have proven to be a useful tool in dairy cattle herd management.

Accelerometers have also been used to determine behaviours in poultry. In a study done at Mississippi State, lightweight triaxial accelerometers were used to determine specific behaviours in broilers including resting, walking, feeding, and drinking (Yang et al., 2021). Behaviours were detected with a greater than an 80% accuracy (Yang et al., 2021). Murillo et al. (2020) harnessed three-axis accelerometers on the backs of laying hens to continuously record movement before, during, and after inoculation with northern fowl mites. Their goal was to evaluate how these mites affected laying hens' normal behaviours using accelerometers to record the magnitude of acceleration of the hens. Specific bird behaviours such as pecking, preening, and dustbathing were identified with a Nearest-Neighbour Classifier algorithm. Using the algorithm, the model's F-score for dustbathing and preening was 1.00, whereas pecking 0.88 (Murillo et al., 2020). From the statistical analysis of the accelerometer data, it was shown that mite infestation increased hen preening behaviour and skin lesions, which was a direct assessment of animal welfare.

Using accelerometers on sows has been a topic of interest for several authors. Grégoire et al. (2013) used accelerometers fixed to the rear leg to quantify lameness in sows by analysing their stepping and postural behaviour. Through posture analysis, they found that lame sows spent less time standing over a 24-hour period compared to non-lame (6.33 vs. 14.53%, respectively) and non-lame sows spent 15.2 minutes and more standing after feeding than lame sows. Lame sows also took more steps per minute in the hour after a meal than non-lame sows (10.12 vs 5.37 steps per minute, respectively). Pastell et al. (2016) aimed to measure sow activity before farrowing by using a wireless three-dimensional accelerometer attached to neck collars of the sows. Based on the accelerometer data, a model was created to detect the approach of farrowing based on the increase of activity within 24 hours before the start of farrowing. The model was proven to be effective by detecting a rise in activity before farrowing in sows housed in crates and pens with a sensitivity of 96.7% and specificity of 100%. Thompson et al. (2016) used accelerometers mounted to a sow's hind leg and hip area to determine sow postures and posture transitions. Postures included standing, sitting, lying-left, lying-right, and sternal-lying. All postures except for the siting class had a precision and recall score greater than 0.74, while sitting was at 0.542. Unfortunately, this manuscript did not look for the posture of kneeling or the sow's transitional posture when changing postures from standing to lying. The time spent kneeling was determined to play a significant role in preweaning mortality (Al Kiyumi et al., 2021). In addition, accelerometers play a role in identifying lameness, which has an economic impact on swine production as well as a pig's welfare

Therefore, the objectives of this paper were to determine if three-axis accelerometers could be used to determine static postures in sows housed in farrowing crates. Postures will be specifically focusing on sitting, kneeling, standing, and lying- left, right or other.

2. Materials and Methods

2.1. Animal and Housing Specifics

The experiment was conducted in a farrowing building of the U.S. Meat Animal Research Center (USMARC), from the Agriculture Research Service-ARS of United States Department of Agriculture – USDA located in Clay Center, Nebraska. All animal husbandry and experimental protocols were performed in compliance with federal and institutional regulations regarding proper animal care practices and were approved by the U.S. Meat Animal Research Center Institutional Animal Care and Use Committee (2021).

The farrowing facility at USMARC consists of 3 rooms. Each farrowing room has 20 individual farrowing stalls positioned in two rows of ten stalls with the heads of the sows facing each other. The building was designed with a hallway to temper the incoming air, so heaters and evaporative cooling pads are using to pre-heat or to cool the air. The temperature control setup in the room was a linear decrease such that the first week of lactation the set point was 24 °C and was slowly lowered to 20°C by the end of the farrowing cycle. The environmental conditions (temperature, dew point, and light) were independently verified using three portable data loggers (XR440, Pace Scientific, Boone, NC, USA) one located in the hallway, and two located in the farrowing room (between the first and last two farrowing stalls and the other between the 9 and 10 farrowing crate both at a height of 1.3 m). Information was recorded every 5-minutes. In addition, manure was managed through fully slatted metal floors and a shallow pit, and each room contained two 1900 L dump tanks that were flushed manually twice per day The room was also lit with a row of lights above each farrowing crate and were automatically programmed to power on and off between the hours of 4:30 and 18:00.

Nine sows of a mix of Landrace x Yorkshire breeds were used in a 5-week long data collection period. The sows were placed in in three different farrowing crate layouts (Figure 1). Although a total of 9 sows have been collected, this conference proceedings will focus on only 3 sows. All sows had ad libitum access to feed and water throughout the farrowing and lactation period. Three Brinno BCC100 time-lapse cameras (Brinno Inc., Zhou Zi St.,Taipei City 11493, Taiwan) were placed behind each sow and were utilized for validation of the wearable sensors. The Brinno camera collected data at one frame/sec. The image data was used to observe and label static acceleration forces associated with

changes in posture. This conference proceedings will focus only on the static postures; future work will also focus on the dynamic changes.
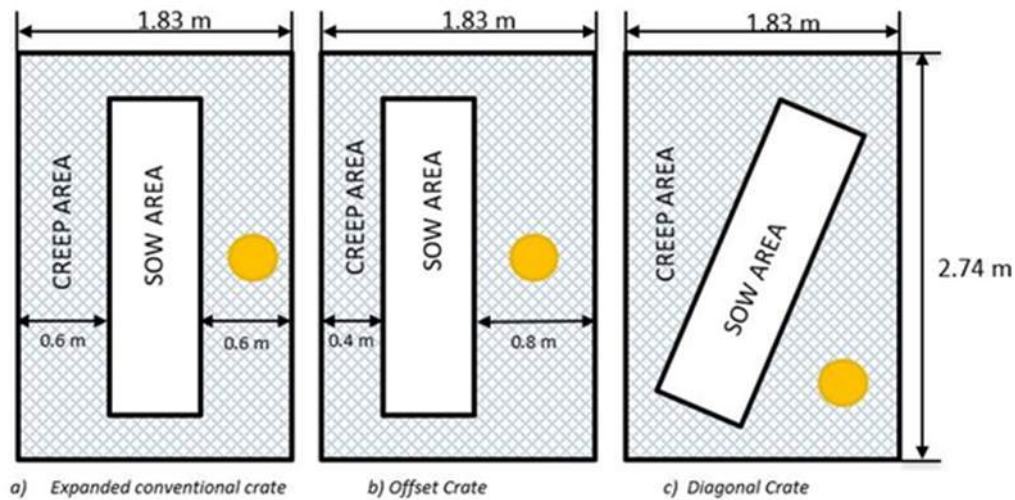
Figure 1. Three farrowing crate layouts: expanded conventional, offset, and diagonal. The yellow circle represents a heat lamp for the piglets.

2.2. Wearable accelerometer sensors

The experiment used one wearable sensor per sow. The wearable sensor consisted of an electronic sensing circuit with rigid, waterproof enclosure to monitor the posture of the sow (Figure 2). The electronic sensing circuit contains 1) microcontroller for signal processing, 2) non-volatile flash data storage, 3) real-time clock, 4) rechargeable battery, 5) and three-axis accelerometer with integrated temperature sensor. The six-direction function sensitivity threshold was set to 0.250 g (acceleration of gravity), and data was continuously collected. The sampling frequency was set to 300 Hz. Each accelerometer was powered by a 3.7V 500MAH lithium battery (Adafruit Industries LLC) that had an overall life of approximately 72 hours. These batteries were recharged using a USB LIION/LIPOLY charger (Adafruit Industries LLC). The three-axis accelerometer (X, Y, Z) data was stored on a 32GB Micro SD card and exported as text files. The accelerometer data was used to not only assess general activity level but to also determine precise movements. The temperature data was used to assess the microenvironment surrounding the sow and to assess the temperature differences when the sows' back was towards or away from the heat lamp. In this paper, the wearable sensor will be referred to as an accelerometer.
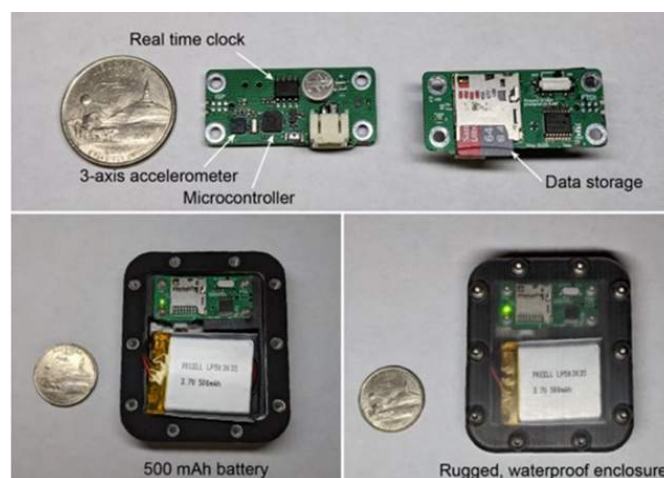
Figure 2. Three-axis accelerometer, battery, and enclosure

The accelerometer was affixed to the sow in a denim pocket with a Velcro enclosure (Figure 3), which was affixed on each sow in between the shoulder blades (Figure 4) with Livestock ID Tag Cement (The Ruscoe Company, 485 Kenmore Blvd Akron, OH 44301, 330-253-8148). The accelerometers were placed faced down inside of the denim pocket with the SD card facing the sow cranially. The SD cards in the accelerometers were changed every other day during the week to ensure proper data collection.

Figure 3. Denim pocket with Velcro enclosure

Figure 4. Denim pocket application

2.3. Posture description and Labelling and Data Processing

The time-lapse images from the Brinno cameras were analysed using a Behavioural Observation Research Interactive Software (BORIS, University of Torino Department of Life Sciences and Systems Biology). A total of six static sow postures were visually labelled from the recorded time-lapse videos. Prior to labelling the postures, descriptions of each posture were created. Standing (Figure 5c) was categorized as the sow is standing on all four feet, and kneeling (Figure 5f) is when the sow's front legs are bent, and she is on her knees and is standing on her back legs. Sitting (Figure 5d) is where the sow's rear end is on the ground, her head is head up, and her feet are supporting her. Lying-left (Figure 5e) and lying-right (Figure 5a) is when the sow was lying-down on her left or right side with all four legs extended and her udder visible. Lying-other is any other sow lying-position that is not lying- left or right (Figure 5b).

Figure 5. Illustrations of the 6 postures that were observed for this study: a) lying-right, b) lying-other, c) standing, d) sitting, e) lying-left, and f) kneeling.

For this initial work, a total of five observations of each static posture were extracted from each sow using a MATLAB (Mathworks Inc., USA), script. Data was extracted between the dates of March 10-12, 2021 and each posture was segmented into short windows ranging from 10 to 30 seconds to ensure the appropriate static acceleration and reduce extra noise. The X-, Y-, and Z-acceleration values were passed through a low-pass filter in MATLAB to clean up the signals and remove extra noise. For each observation of the static postures, the X-, Y-, and Z-acceleration values were averaged and converted to meters per second squared.

A one-way analysis of variance was performed to test the effect of crate design (confounded with sow) and postures for the X-, Y-, and Z-acceleration using R-Studio Version 1.2.5033. A Tukey multiple pairwise comparisons was used to determine differences between crate designs and between postures.

3. Results and Discussion

The results presented in this paper is a subset of the data and results collected for this study. The 3 sows used in this analysis were placed in the farrowing crates on March 1st, 2021, and the piglets were farrowed between March 6th, 2021 and March 9th, 2021. All three sows were first parity sows. The sows and piglets remained in the farrowing crate until April 3rd, 2021. The average dry-bulb temperature within the room was 22.7 °C, and dew point temperature was 11.10 °C. The lights in the farrowing room were on from 4:30 to 18:00. The posture data used in this manuscript were captured on March 10th, 2021, through March 12th, 2021, between the times of 5:00 and 17:00. Besides, the days piglets were farrowed, caretakers' activity was concentrated between 7:00 and 9:00. The caretakers' main duties consisted of feeding and medicating the sows and piglets, removing excess manure from the crates, and overall regular husbandry procedures to ensure that the pigs are in great health. The accelerometer batteries and SD cards and the Brinno camera SD cards were changed every 2-3 days. This was completed between the hours of 8:00 and 10:00 to minimize the distractions to the sows' natural behaviours.

3.1 Behaviour

The overall tagged data from the BORIS software was compiled for all three sows on March 10th, 2021, from 8:00 to 21:00. The number of occurrences of each static posture and the average duration was calculated. Table 1 shows a summary of posture changes per sow in the offset, diagonal, and standard crates in the analysed time. The sow in the offset farrowing crate layout farrowed on March 6th. This sow spent the most occurrences in the lying-other position more than any other postures with an average of 6 minutes but stayed in the lying-right posture for more time with an average of 113 minutes.

The sow in the expanded conventional farrowing crate layout farrowed on March 7th. This sow did not kneel or stand up throughout the day on March 10th. She was in the lying-other position more than any other postures with an average duration of 8 minutes but was also in the lying-right position that lasted for an average of 62 minutes slightly like the sow in the offset farrowing crate layout. According to the tagged data from this day, it seems as though the sow preferred lying on its right side for a longer period rather than lying-other or the left (Table 1 and Figure 6).

The sow in the diagonal farrowing crate layout farrowed on March 8th, 2021. This sow had the greatest number of occurrences of each posture out of the three sows. This could be since the sow had just farrowed, or that the diagonal crate layout provides the most space for movement. Like the two sows in the other farrowing crate layouts, lying-other had the most occurrences with an average duration time of 3 minutes. Lying-left had one less occurrence than lying-right but had a longer average duration time of 57.4 minutes. This sow also had the longest standing average duration time with a time of 5 minutes (Table 1). Further data analysis is being done to calculate the number of occurrences of each posture and average duration time over a longer period for each sow in the experimental study.

Table 1. Number of occurrences, average duration (min), total duration (min) for all six static postures during the analyzed hours (8:00 – 20:00) on March 10th, 2021

Posture	Expanded Conventional Crate			Offset Crate			Diagonal Crate		
	Number	Average Duration (min)	Total Duration (min)	Number	Average Duration (min)	Total Duration (min)	Number	Average Duration (min)	Total Duration (min)
Kneeling	0	0	0	1	0.13	0.13	13	0.05	0.67
Lying-left	4	26	102	4	86.3	345	6	57.4	344
Lying-other	21	8	177	11	6	70	31	3	84
Lying-right	6	62	373	2	113	227	7	24	171
Sitting	11	2	18	6	4	25	11	0.93	10.28
Standing	0	0	0	2	2	4	13	5	65

A time budget of simplified behaviours is shown in Figure 6. The sows spent most of the day lying. It can be noted that the sows spent the most time in other postures (sitting, standing, and kneeling), between the hours of 8:00 and 9:00, while caretakers were generally in the room, 13:00 hours (after the caretakers' lunch break), and immediately following light turning off at 18:00. Although there was kneeling behaviour in the data – it does not show up on the graph, due to the short time segments. Kneeling behaviour was observed between 8:00 and 9:00 by sows in the Offset and Diagonal Crates. Then kneeling was observed at 10:00, 11:00, 13:00, 14:00, 15:00, 18:00, and 20:00. These results are similar to other literatures that suggest that pig behaviour is cued by light cycles (Brown-Brandl et al., 2014; Hyun et al., 2002).
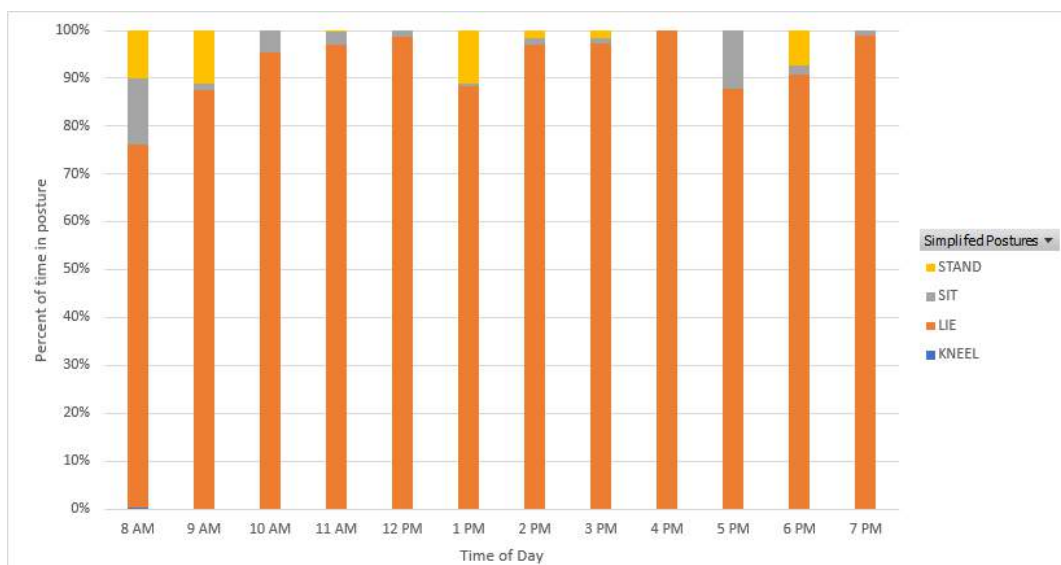
Figure 6. Percentage of the simplified static postures (standing, lying, sitting, kneeling) during the analyzed hours (8:00 – 19:00) on March 10th, 2021.

3.2 Wearable Sensor Data

Five 10-30-second-long accelerometer data segments were extracted for each posture for each sow. So, a total of 15 data segments for each posture were analyzed. There were significant effects of crate (sow) and posture. The mean and standard deviation of accelerations X, Y, and Z of each static posture of all sows were found (Table 2). Using the analysis procedure, it was found that there was a significant difference between sitting and standing in the X-acceleration and a significant difference between lying-left and lying-right in the Y- and Z-acceleration. It was also found that accelerations X, Y, and Z of the sow in the offset crate were significantly different from the sows in the expanded conventional and diagonal crates. In the X-acceleration, there was a significant difference between sitting and standing where these mean values were extremely positive and negative. According to the raw accelerometer data, when the sow was sitting, the x-axis varied between 0.12 and 5.17 while when standing the acceleration varied from 0.39 and −5.93. When lying-left, the y-axis varied between 6.49 and 9.53 while when lying-right the acceleration varied from -0.12 and −9.75. As shown in Figures 5e and 5a, the left and the right laying postures can be differentiated from each other by the values of the y-axis. Both Y and Z mean acceleration values displayed a significant difference in both lying-left and lying-right. In acceleration Y, the lying-left mean value was positive and in acceleration Z the mean value was negative. In acceleration Y, the lying-right mean value was negative and in acceleration Z the mean value was positive. This is what we expected as the accelerometer should have been nearly vertical in the y-axis. Laying on the

left should be opposite in the y-axis compared to laying on the right. As the accelerometers may have moved a bit or the sow posture may not have allowed the accelerometer to be collected vertical in the y-axis, the values varied slightly.

Table 2. Mean±standard deviation of accelerations X, Y, and Z of each static posture per sow.

Posture	Acceleration X	Acceleration Y	Acceleration Z
Kneeling	-0.51±1.42[a]	-0.33±6.73[a]	-6.01±2.36[a]
Lying-left	-0.45±1.80[a]	7.60±2.40[b*]	-1.95±5.70[b*]
Lying-other	-0.51±1.37[a]	-0.73±6.94[a]	-5.78±2.30[a]
Lying-right	0.56±0.86[a]	-8.63±2.38[c*]	0.82±3.13[c*]
Sitting	3.36±1.59[b*]	-1.35±1.68[a]	-7.67±2.26[a]
Standing	-2.16±2.03[c*]	-1.32±2.83[a]	-8.12±1.08[a]

* Differing superscripts are significantly different at P < 0.10

When kneeling the X-, Y-, and Z-acceleration values were between 0.09 and –2.51, 1.75 and –9.26, and –0.59 and –8.93 respectively. Further data analysis and processing for the kneeling posture must be conducted to determine which axes are indicative of the kneeling posture. When in the lying-other posture, the X-, Y-, and Z-acceleration values were between 2.69 and –3.32, 9.00 and –9.54, and –0.87 and –8.50. Determining the lying-other posture using static values independently could be challenging due to its similarity with other postures. Lying other can resemble lying- left or right because there are three legs extended instead of four. Per the statistical analysis, we could use acceleration X to determine sitting and standing, and accelerations Y and Z to determine lying-left and lying-right.

Table 3. Mean±standard deviation of accelerations X, Y, and Z of each sow in the three farrowing crates

Farrowing Crate:	Acceleration X:	Acceleration Y:	Acceleration Z:
Offset	-1.15±2.22[a*]	-2.48±5.53[a*]	-5.51±3.78[a*]
Expanded conventional	0.38±2.25[b]	0.25±6.30[b*]	-5.10±4.15[ab]
Diagonal	0.91±1.85[b]	-0.15±7.06[ab]	-3.75±5.21[b*]

*. Differing subscripts are significantly different at P < 0.10

The mean and standard deviation of accelerations in the X-, Y-, and Z-planes of each sow in the three different farrowing crate layouts were also evaluated using ANOVA and Tukey's HSD Test (Table 3). For all accelerations, the sow in the offset crate was significantly different from the sows in the expanded and diagonal crates and all the means were negative values. This was found to be extremely interesting but could be due to the accelerometer orientation in the denim pocket or the crate layout.

As can be seen in Figure 7 lying-left and lying-right formed very distinct and separable clusters. Lying-other's values were scattered across the graph and varied, but this was expected due to the variety of lying-other positions. For kneeling and standing the acceleration values varied and were spread apart in the plot. Sitting showed some similarities represented by the small cluster, but also varied across the plot.

These results are comparable to the research of Radeski & Ilieski (2017). Radeski & Ilieski (2017) used horizontal and vertical axes acceleration values recorded by tri-axial accelerometers mounted to the hind legs of the sheep to create a method to identify walking, trotting, galloping, standing, and lying. Sampling duration, total duration, and total accelerometer readings were used for the gait and posture discrimination. A forward stepwise discriminant function analysis model was applied to evaluate the significant differences between the groups of postures. In this manuscript, acceleration values in the vertical axis showed large variances between standing and lying of the animal; however, the vertical axis values could not be used to determine differences between lying-left or lying-right. Our data showed a large difference between lying-left and lying right. This is possible due to the differences in animal behavior between sows and sheep. Sows lie completely laterally, while sheep lie mostly sternally with their legs on the left or on the right. Radeski and Ilieski (2017) were able to classify walking and galloping movements with high accuracy (great than 90%) using vertical and horizontal axis.
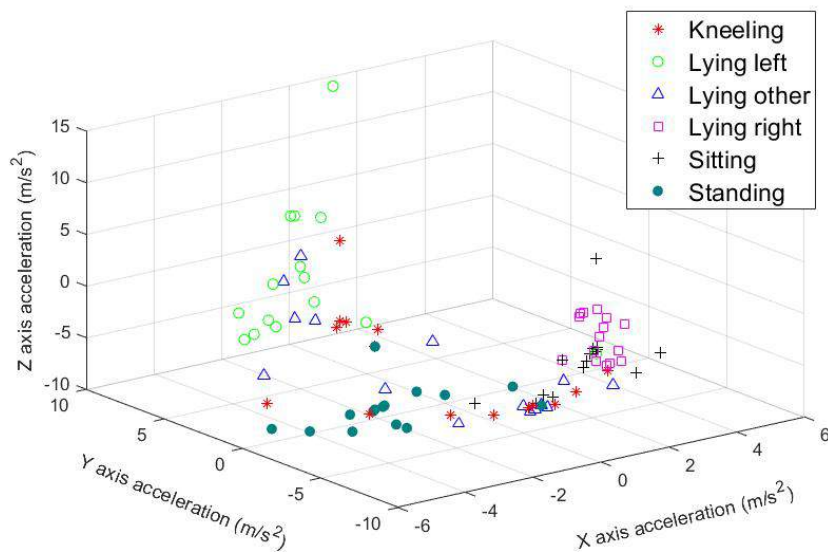
Figure 7. 3D scatter plot of the X-, Y-, and Z- mean acceleration values of all the analyzed segments corresponding to each of the six postures.

3.3 Future Analysis

At the end of our experiment, we want to be able to look at the different acceleration values to determine what postures that sows are in and if transitional changes occurred. An algorithm will not be created, but a program will be made to analyze these values. We will use the labeled video camera data to validate the program and estimate duration times of the postures that the sows are in. As we move forward with the experiment, we will be looking at thresholds of each posture and its values. Some thresholds included for when lying-left, the Y-acceleration values are between 6.49 and 9.53 while when lying-right its Y-acceleration values are between -0.12 and –9.75. In addition, when lying-left the acceleration values are between 14.44 and –8.26 while when lying-right its Z-acceleration values are between –8.30 and 3.78. Most of the Z-acceleration values in the lying-left position were negative numbers lower than or equal to –1.64, and the 14.44 value was the outlier. In addition, majority of the Z-acceleration values in the lying-right position were greater than 0.82 while –8.30 was the outlier. Further analysis of the six static postures and their X-, Y-, and Z-acceleration values must be done to ensure the correct thresholds for each posture. When automated these ranges of values can be used to determine lying- left and right. Kneeling requires further data collection and analysis to determine their accurate acceleration values. When sitting the acceleration values in the X-acceleration were between 0.12 and 5.17 while standing was from 0.39 and -0.53. After automation these ranges of values can help determine if the sow is sitting or standing.

Our future work will focus on the dynamic changes and transitional postures of the sows utilizing the same method of evaluating the X-, Y-, and Z- acceleration values. We will also determine the correct sampling frequency by down sampling while ensuring that we are getting the appropriate amount of data. In addition, the application and design of the denim pockets will be re-evaluated to achieve maximum wearable time. In the next round of data collection, the denim pockets with the accelerometers will be placed on the front and rear of the sows. The different placements of the accelerometers will allow us to assess the differences in the static and dynamic posture changes and acceleration values. The long-term objective of this study is to provide a simple sensor-based system that can be automated to determine static and dynamic postures. These data streams can be used in several different ways. First, the impacts of farrowing crate design can be determined. Second, once a baseline is determined, the overall health and well-being of each sow can be tracked. Third, behavioral phenotypes can be determined for each individual sow to aid in genetic selection.

4. Conclusion

In conclusion, the goal of our study is to prove that accelerometers and the acceleration of gravity values can be used to determine postures and posture changes of sows in production settings. By determining posture and posture changes, farmers can determine the health status of the animal, activity level, and help decrease pre-weaning mortality. Ultimately, for this method to be applied in industry we must move the accelerometer from the body to an ear tag. A combination of these values will help us decide the different static postures that the sows are in. Thresholds will be set to determine the different postures. Per the statistical analysis' results and the significant differences this method could be used to determine lying-right, lying-left, sitting, and standing.

Acknowledgements

References

Al Kiyumi, A., Shi, Y, Brown-Brandl, T.M., Condotta, I, Bolman,R (2021). Understanding sow's mothering ability by analyzing their behavioral phenotypes from overhead sensor images. University of Nebraska, UCARE Project.

Brown-Brandl, T. M., Hayes, M. D., Xin, H., Nienaber, J. A., Li, H., Eigenberg, R. A., .Stinn, J.P. & Shepherd, T. (2014). Heat and moisture production of modern swine. Transactions of the ASHRAE 120(1):469-489.

Dawson, M. D., Lombardi, M. E., Benson, E. R., Alphin, R. L., p; Malone, G. W. (2007). Using Accelerometers to Determine the Cessation of Activity of Broilers. Journal of Applied Poultry Research, 16(4), 583–591. https://doi.org/10.3382/japr.2007-00023

Hyun, Y., & Ellis, M. (2002). Effect of group size and feeder type on growth performance and feeding patterns in finishing pigs. *Journal of Animal Science*, *80*(3), 568-574.

Grégoire, J., Bergeron, R., D'Allaire, S., Meunier-Salaün, M.-C.; Devillers, N. (2013). Assessment of lameness in sows using gait, footprints, postural behaviour and foot lesion analysis. Animal, 7(7), 1163–1173. https://doi.org/10.1017/s1751731113000098

Murillo, A. C., Abdoli, A., Blatchford, R. A., Keogh, E. J., Gerry, A. C. (2020). Parasitic mites alter chicken behaviour and negatively impact animal welfare. Scientific Reports, 10(1). https://doi.org/10.1038/s41598-020-65021-0

Pastell, M., Hietaoja, J., Yun, J., Tiusanen, J.; Valros, A. (2016). Predicting farrowing of sows housed in crates and pens using accelerometers and CUSUM charts. Computers and Electronics in Agriculture, 127, 197–203. https://doi.org/10.1016/j.compag.2016.06.009

Radeski, M., & Ilieski, V. (2017). Gait and posture discrimination in sheep using a tri-axial accelerometer. Animal, 11(7), 1249–1257. https://doi.org/10.1017/s175173111600255x

Shahriar, M. S., Smith, D., Rahman, A., Freeman, M., Hills, J., Rawnsley, R., Henry, D.; Bishop-Hurley, G. (2016). Detecting heat events in dairy cows using accelerometers and unsupervised learning. Computers and Electronics in Agriculture, 128, 20–26. https://doi.org/10.1016/j.compag.2016.08.009

Tamura, T., Okubo, Y., Deguchi, Y., Koshikawa, S., Takahashi, M., Chida, Y.; Okada, K. (2019). Dairy cattle behavior classifications based on decision tree learning using 3‑axis neck‑mounted accelerometers. Animal Science Journal, 90(4), 589–596. https://doi.org/10.1111/asj.13184

Thompson, R., Matheson, S. M., Plötz, T., Edwards, S. A.; Kyriazakis, I. (2016). Porcine lie detectors: Automatic quantification of posture state and transitions in sows using inertial sensors. Computers and Electronics in Agriculture, 127, 521–530. https://doi.org/10.1016/j.compag.2016.07.017

Thorup, V. M., Munksgaard, L., Robert, P.-E., Erhard, H. W., Thomsen, P. T.,; Friggens, N. C. (2015). Lameness detection via leg-mounted accelerometers on dairy cows on four commercial farms. Animal, 9(10), 1704–1712. https://doi.org/10.1017/s1751731115000890

Yang, X., Zhao, Y., Street, G. M., Huang, Y., Filip To, S. D.; Purswell, J. L. (2021). Classification of broiler behaviours using triaxial accelerometer and machine learning. Animal, 15(7), 100269. https://doi.org/10.1016/j.animal.2021.100269

Tracking Grow-Finish Pigs Across Large Pens Using Multiple Cameras

Aniket Shirke[a,*], Aziz Saifuddin[a], Angela Green-Miller[c], Isabella Condotta[b], Achleshwar Luthra[e], Jiangong Li[c], Xiaodan Hu[d], Tawni Williams[b], Aneesh Kotnana[a], Okan Kocabalkanli[a], Narendra Ahuja[d], Ryan N. Dilger[b], Matthew Caesar[a]

a Department of Computer Science, University of Illinois at Urbana-Champaign, Champaign, USA

b Department of Animal Sciences, University of Illinois at Urbana-Champaign, Champaign, USA

c Department of Agricultural and Biological Engineering, University of Illinois at Urbana-Champaign, Champaign, USA

d Department of Electrical and Computer Engineering, University of Illinois at Urbana-Champaign, Champaign, USA

e Department of Electrical and Electronics Engineering, BITS Pilani, India

* Corresponding author. Email: anikets@illinois.edu

Abstract

Increasing demand for meat products combined with farm labour shortages has resulted in a need to develop new real-time solutions to monitor animals effectively. Significant progress has been made in continuously locating individual pigs using tracking-by-detection methods. However, these methods fail for oblong pens because a single fixed camera does not cover the entire floor at adequate resolution. We address this problem by using multiple cameras, placed such that the visual fields of adjacent cameras overlap, and together they span the entire floor. Avoiding breaks in tracking requires inter-camera handover when a pig crosses from one camera's view into that of an adjacent camera. We identify the adjacent camera and the shared pig location on the floor at the handover time using inter-view homography. Our experiments involve two grow-finish pens, housing 16-17 pigs each, and three RGB cameras. Our algorithm first detects pigs using a deep learning-based object detection model (YOLO) and creates their local tracking IDs using a multi-object tracking algorithm (DeepSORT). We then use inter-camera shared locations to match multiple views and generate a global ID for each pig that holds throughout tracking. To evaluate our approach, we provide five 2-minutes long video sequences with fully annotated global identities. We track pigs in a single camera view with a Multi-Object Tracking Accuracy and Precision of 65.0% and 54.3% respectively and achieve a Camera Handover Accuracy of 74.0%. We open-source our code and annotated dataset at https://github.com/AIFARMS/multi-camera-pig-tracking

Keywords: computer vision, continuous, surveillance, precision livestock monitoring, homography.

1. Introduction

Pigs are one of the most raised livestock animals in the world, forming a primary protein source for millions of people across numerous cultures and geographical regions (Shahbandeh, 2020). The increase in demand for high-quality protein has resulted from growing populations combined with increasing incomes across the globe.

Health is a contributor to efficient production, and ideally could be best done by monitoring them individually. Behavior has been well-established as a strong indicator of pig health (Stephen et al., 2016). Manual monitoring of individual behavior in a commercial livestock farm is not practical or sustainable with existing farm staffing and workflow (Swan, 2019). Each animal typically receives no more than a few seconds of observation time on an average day (PIC North America, 2014).

Monitoring pigs automatically requires tracking each animal and identifying and interpreting its behavior. This presents several key challenges. Pens often contain a large number of pigs, that are similar in appearance and thus difficult to visually distinguish from each other. Moreover, pens are often in buildings with low ceilings or otherwise congested areas, making it difficult to see the entire pen from a single vantage point, requiring monitoring across different views, from different vantage points.

To address this challenge, we have developed a system to monitor pigs using multiple cameras with adjacent cameras having overlapping fields of view. We detect and track pigs in each view using state-of-the-art object detection and tracking models. We then use homography between adjacent camera views to identify a pig in their overlapping views, transitively match different camera views of the same pig, and thus assign a global identity to each pig, thereby achieving global tracking. In order to validate our methods, we have monitored two grow-finish pens using a set of appropriately chosen and placed cameras.

Our primary contributions in this paper can be summarized as follows:

- We present a multi-camera pig tracking system for identifying each pig across all camera views. We are not aware of any other such system.

- We present a multi-camera, multi-pen dataset containing videos of pigs in multiple pens captured from multiple viewpoints and make it publicly available. We are not aware of any such publicly available dataset.

2. Related Work

Individual tracking of animals in group housing is a demanding task. Uninterrupted tracking poses significant challenges when there is a lack of discernible differences in the physical characteristics of the animals. To address these challenges, tracking-by-detection methods have been proposed. Psota et al. (2014) cast detection as a segmentation task. The four semantic parts of pig (ears, shoulder, and tail) are detected and tracked using a Fully Convolutional Network and the Hungarian algorithm. In addition, the authors provide a dataset with 2000 images from multiple pens, which is publicly available.

In Seo et al. (2020), a TinyYOLO (Redmon et al., 2016) architecture is employed to detect pigs from infrared videos, with emphasis on execution speed as the target platform is an embedded device. Jaewon et al. (2019) propose a method to detect pigs under various illumination conditions, by combining information from the depth and infrared images using spatio-temporal interpolation. Similarly, in Johannes et al. (2020) the bounding boxes are replaced with ellipses, which are detected through a segmentation network. Zhang et al. (2019) use an SSD (Wei et al., 2016) architecture coupled with the MOSSE (Bolme et al., 2010) algorithm to perform animal tracking.

Prior work in multi-camera, multi-target tracking typically assumes that the target has distinguishing features, which can be used for re-identification across multiple views (Cabrera et al., 2011; Ristani and Tomasi, 2018). But this has not led to a similar ability to track pigs because of the lack of such visual features on pigs. To the best of our knowledge, our work is the first application of multi-camera tracking to pigs. Moreover, the only few publicly available datasets for pig monitoring consist of a single-camera view (Psota et al. 2014; Bergamini et al. 2021; Riekert et al. 2020), with no open-source implementations. To address this need, we have collected and open-sourced our multi-camera view dataset, along with our implementation.

3. Methods

3.1. Detection and Local Tracking

For each camera view, pig detection is achieved by using the state-of-the-art YOLOv4 (Bochkovskiy et al., 2020) model. In order to generate tracking IDs in a single camera view, the detections provided by YOLOv4 are tracked using DeepSORT (Wojke et al., 2017). The following subsections describe how local tracking IDs are processed to obtain global tracking IDs for pigs.

3.2. Homography Estimation

Any two images of the same planar surface are related by a homography. In our case, the planar surface is the pen floor, observed from a *Ceiling* view and an *Angled* view, as depicted in Figures 1a and 1b, respectively.

Assuming that the *Angled* view is aligned with the world coordinate axes and has no translation, a 3-D point P is mapped to the 2-D pixel point p_{angled} in the *Angled* view using the following relation:

$$\lambda_1 * p_{angled} = K [I \mid 0] P$$

where K is the intrinsic parameter matrix, I is a 3x3 identity matrix, and p_{angled} and P are homogeneous coordinates defined as follows:

$$p_{image} = \begin{bmatrix} x_{image} \\ y_{image} \\ 1 \end{bmatrix} \qquad P = \begin{bmatrix} X_{world} \\ Y_{world} \\ Z_{world} \\ 1 \end{bmatrix}$$

Similarly, the same 3-D point P is mapped to the 2-D pixel point $p_{ceiling}$ in the *Ceiling* view using the relation:

$$\lambda_2 * p_{ceiling} = K [R \mid t] P$$

where R and t is the relative rotation and translation of the *Ceiling* view with respect to the *Angled* view. Note that λ_1 and λ_2 are free parameters as multiple 3-D points can get mapped to the same 2-D point in the image due to single-view ambiguity.

Our task is to estimate a homography $H(.)$ such that

$$p_{angled} = H(p_{ceiling})$$

In an ideal scenario, having many 3D-2D correspondences between the floor pen and the corresponding image views can help in obtaining the homography accurately. Obtaining those correspondences is challenging at a farm due to the large numbers of pigs occluding the floor. In the absence of such correspondences, multiple methods can be potentially used to estimate homography between two camera views.

| *(a) Track detected in Ceiling view* | *(b) Perspective warp using homography* | *(c) Matching track in Angled view* |

Figure 1: Simplified depiction of the Multi-Camera Tracking algorithm

We adopt the following method to estimate the homography $H_{ceiling \to angled}$:

1. Using a perspective transformation, the *Ceiling* view is first transformed into a top-down view parallel to the pen floor. The homography between these two views is denoted as $H_{ceiling \to top-ceiling}(.)$

2. The *Angled* view is then transformed into a top-down view using a similar perspective transformation. The homography between these two views is denoted as $H_{angled \to top-angled}(.)$

3. Since both the top-down views are parallel to the pen floor, key points from the overlapping regions of both these views are matched. These keys points can be detected as well as matched automatically. But in this paper, we perform these steps manually, by inspection, and estimate a homography using RANSAC (Derpanis, 2010). The homography is denoted as $H_{top-ceiling \to top-angled}(.)$

Thus, a pixel point $p_{ceiling}$ in the *Ceiling* view can be mapped to a point $p_{estimated}$ in the *Angled* view as follows:

$$p_{estimated} = H^{-1}_{angled \to top-angled}(H_{top-ceiling \to top-angled}(H_{ceiling \to top-ceiling}(p_{ceiling})))$$
$$= H_{ceiling \to angled}(p_{ceiling})$$

3.3. Track Aligning Algorithm

Algorithm 1: Multi-Camera Tracking algorithm

Data: Set of c and a local pig IDs and bounding boxes in *Ceiling* view and *Angled* view respectively: `ceiling_tracks`, `angled_tracks`

Result: Dictionary of matches between `ceiling_ids` and `angled_ids`: matches

/* Generate `transformed_ceiling_tracks` by using the homography $H_{ceiling \to angled}$*/

```
matrix = []       //size of the matrix will be c x a
For (ceiling_id, bbox) in transformed_ceiling_tracks:
    matrix.append(intersection(bbox, angled_tracks))

```

/* Greedily pop the max value from the matrix and enter in matches*/

```
matches = {}
While non-zero entry in matrix exists:
    ceiling_id, angled_id = matrix.argmax()
    matches[:, angled_id] = 0
    If ceiling_id not in matches:
        matches[ceiling_id] = angled_id
```

We use the homography $H_{ceiling \to angled}$ computed in the previous subsection to develop a multi-camera tracking algorithm, by aligning tracks in the *Ceiling* view and the *Angled* view.

The bounding box from the *Ceiling* view can be treated as a quadrilateral on the pen floor in which the corresponding pig is contained. The bounding box from the *Ceiling* view is then projected under the homography to a quadrilateral in the *Angled* view, as depicted in Figure 1c. The transformed quadrilateral is then matched with a bounding box in the *Angled* view with which it has significant overlap in terms of the pixel area. As seen in Figure 1b, ID 56 in the *Ceiling* view will be matched with ID 6 in the *Angled* view.

4. Evaluation

4.1. Camera Deployment
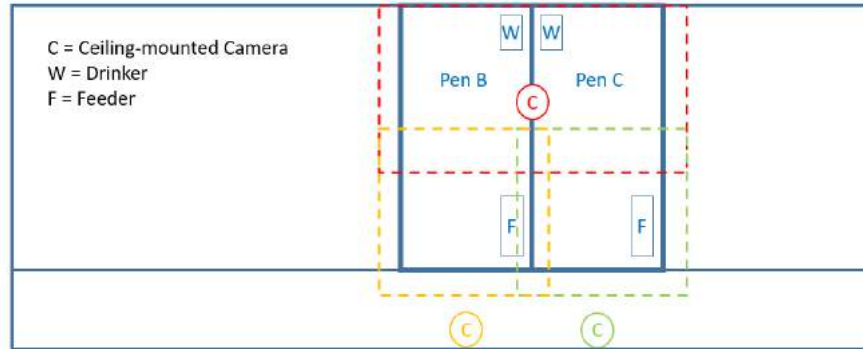
Figure 2: Camera Deployment at the Imported Swine Research Laboratory, UIUC

Figure 3: (Left) Angled view of Pen C. (Right) Ceiling view of Pens B and C.

Videos were recorded in two grow-finish pens (B and C) at the University of Illinois, Urbana-Champaign's Imported Swine Research Laboratory (ISRL), which serves as the research testbed for our experiments. Our surveillance setup monitored 17 and 16 pigs raised in pens B and C respectively. Three wide-angle lens cameras were strategically placed to cover the drinkers and feeders in the visual field, as shown in Figure 2. The *Ceiling* camera covered the drinkers and was placed at a height of 4 metres. The *Angled* cameras covered the feeders and were placed at a height of 2.2 metres. Figure 3 depicts the *Angled* and *Ceiling* camera views. Infrared floodlights were deployed to enhance the existing night vision capabilities of the cameras. The video feed was captured 24x7 at 4k resolution and 15 frames per second.

4.2. Dataset

For training the YOLOv4 model, we sample and annotate 429 images using the VGG Image Annotator (Dutta et al., 2016). The images were randomly split in an 80:20 between the training set (343 images) and the validation set (86 images). To evaluate the tracking efficacy, five 2-minutes long video sequences were annotated with global pig IDs using a custom MATLAB tool. The annotations for two camera views are made every 15th frame, thus (5*2*60*2) 1200 annotated frames are available, in addition to the 429 images for object detection.

4.3. YOLOv4 detection

We train the YOLOv4 model on an Nvidia V100 GPU provided by the HAL computing cluster (Kindratenko et al., 2020). The model was configured for an input resolution of 608x608 and optimized for 2000 iterations with a batch size of 64, a learning rate of 0.001, and momentum of 0.95. We evaluate the model using standard object detection metrics. A mean Average Precision of 99.5% and an average Intersection over Union of 80.52% is achieved on the validation set.

4.4. Tracking evaluation

We evaluate the efficacy of the single-camera tracking algorithm (DeepSORT) using standard Multi-Object Tracking Metrics (Ristani et al., 2016). The Multi-Object Tracking Accuracy (MOTA) takes into account three sources of errors and can be defined by the following equation: MOTA = $1 - [\Sigma_t (FN_t + FP_t + IDSW_t)/\Sigma_t GT_t]$ where FN_t, FP_t and $IDSW_t$ are False Negatives, False Positives and Identity Switches, and GT_t is the ground truth number of bounding boxes at time t. Multi-Object Tracking Precision (MOTP) captures the localization precision of the object detector. Standard metrics such as Precision and Recall measure the number of mismatched or unmatched detection-frames,

regardless of where the discrepancies start, or end or which cameras are involved. We also report identity related metrics computed after global min-cost matching: IDF1, IDP, and IDR. IDF1 is the ratio of correctly identified detections over the average number of ground-truth and computed detections, IDP (precision) is the fraction of computed detections that are correct whereas IDR (recall) accounts for correctly identified ground truth detections.

Table 1:Local and Global Tracking metrics

Type	Local Tracking (DeepSORT)							Global Tracking
	IDF1	IDP	IDR	Recall	Precision	MOTA	MOTP	CHA
Day	66.1	61.8	71.0	98.0	85.4	80.6%	61.3%	92.4%
Night	53.2	49.9	56.9	85.6	75.1	55.2%	44.5%	46.3%
Overall	58.2	54.5	62.3	90.4	79.0	65.0%	54.3%	74.0%

We evaluate our multi-camera tracking approach by reporting the Camera Handover Accuracy (CHA). CHA is defined as the fraction of predicted identity matches for two camera views out of the total ground truth matches. Intuitively, MOTA and MOTP quantifies how accurately the algorithm is tracking pigs with minimal false positives, and CHA quantifies how accurately identities are exchanged between cameras using homography. As seen in Table *1*, we observe that tracking is relatively easier during day as the quality of video feed degrades at night. We achieve an MOTA, MOTP and CHA of 65%, 54.3% and 74% respectively.

5. Discussion

5.1. Issues in Detecting Pigs using YOLOv4
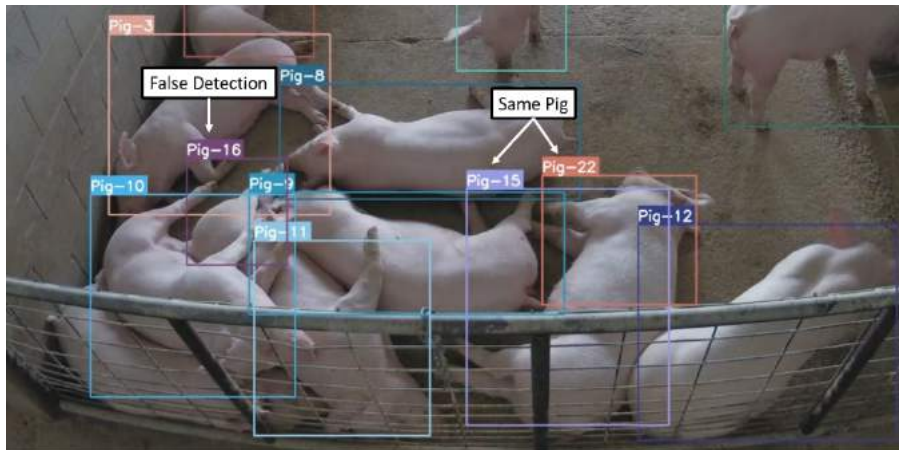
Figure 4: False Positives and False Negatives in Detection

Occlusions are a primary source of false negatives. Even though detecting pigs by a direct application of state-of-the-art deep learning models, such as YOLOv4, yield great results, there are several scenarios where detection of pigs becomes very challenging. One of the most common impediments to detection is occlusion. If a pig is partially or completely occluded in any of the views, then the model tends to either miss the pig completely or predicts a bigger bounding box, encompassing more than one pig, which leads to missed detections. Having two camera views helps in partially alleviating this problem.

False positives result from part of pig being recognized as a whole pig. Pigs tend to huddle in pens to keep themselves warm as a group, which creates a challenge for recognition. Usually, a post-processing non-maximal suppression step during object detection helps in selecting the best bounding box with the maximum confidence score. But often, the model considers a part of the pig to be the whole pig and predicts a box that is not suppressed during non-maximal suppression.

One can see both kinds of errors, as described above, in Figure 4. The pig in the bottom left of the frame is not detected by the model due to heavy occlusion from other pigs and the pen door. One way to mitigate this issue can be to augment the dataset by emulating the artifacts encountered in the pen environment, such as occlusions from grid-like doors in this case. Additionally, detections 'Pig-22' and 'Pig-15' in Figure 1 belong to the same pig. Here, 'Pig-22' predicts a bounding box for a part of a pig and should be ideally suppressed. It is also worth noting that 'Pig-16' is a false detection as the two hind legs of two different pigs confuse the model into believing that it is a single pig.

5.2. Issues in Tracking Pigs using DeepSORT
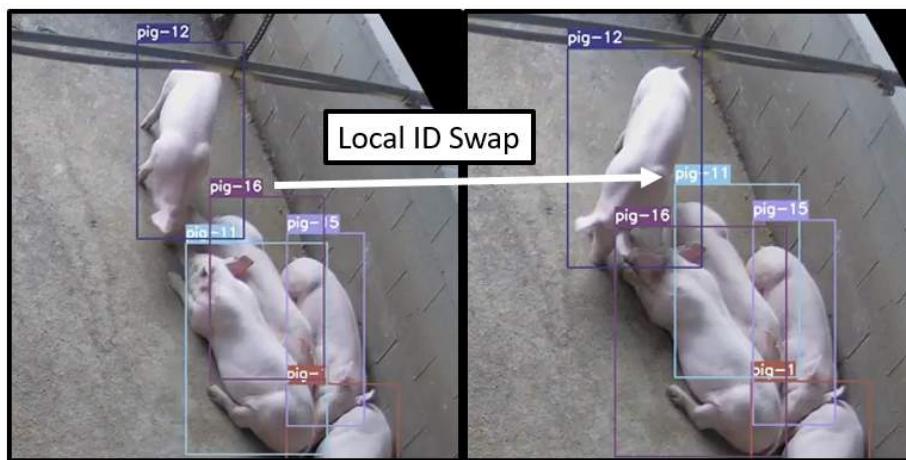
Figure 5: Identity Swap in DeepSORT

The detection issues described in the previous subsection affect the tracking performance of DeepSORT, as false positives lead to an extra number of tracks and false negatives lead to premature termination of tracks. Another primary source of tracking errors is induced by rapid movements in a pig huddle. As seen in Figure 5, the identity of Pigs 11 and 16 get swapped due to a rapid social interaction with Pig 12. Theoretically, DeepSORT should tackle and minimize such identity swaps as it uses an appearance model for re-identification. But the lack of visually distinguishing features between pigs calls for advanced re-identification algorithms while tracking. One potential solution might be to apply another recognition approach, such as a gait analysis, to reidentify them upon occlusion.

5.3. Issues in Global Tracking

The inherent problems in detection and tracking described in the previous subsections affect global tracking, as false detections can lead to false correspondences between different views. The algorithm is also sensitive to variations in detections from a pig huddle, as any error in homography estimation can magnify and lead to an identity swap between multiple pigs. This issue can be mitigated by precise homography estimation and by only assigning a global ID for pigs that have higher overlapping confidence. But that can lead to missed opportunities of matching, leading to a low recall value. Additionally, the multi-camera algorithm described in section 3.3 works under the assumption that all the cameras are synchronized with each other. But in actual deployments, there is a variable delay of several minutes between the capture times of the Ceiling and the Angled views. The delay needs to be fixed manually as such homography-based multi-camera trackers need tight synchronization between the two views.

6. Conclusions

Livestock monitoring is becoming increasingly important in precision livestock management. In order to tackle the problem of monitoring livestock residing in large pens, we propose a scheme for homography-based multi-camera tracking. We achieve a single-camera tracking accuracy and precision of 66.7% and 76.2% respectively, along with a camera handover accuracy of 74%. We plan to further enrich our multi-camera tracking dataset with key focal points and a validated ethogram for pig behavior. We open-source this dataset so that it can be leveraged to build educational applications for pig tracking and behavior monitoring.

References

[1] PIC North America. Standard animal care: Daily routines. Wean to Finish Manual, pages 23–24, 2014. 1

[2] Luca Bergamini, Stefano Pini, Alessandro Simoni, Roberto Vezzani, Simone Calderara, Rick BD Eath, and Robert B Fisher. Extracting accurate long-term behavior changes from a large pig dataset. In 16th International Joint Conference on Computer Vision, Imaging and Computer Graphics Theory and Applications, VISIGRAPP 2021, pages 524–533. SciTePress, 2021.

[3] Alexey Bochkovskiy, Chien-Yao Wang, and Hong-Yuan Mark Liao. Yolov4: Optimal speed and accuracy of object detection, 2020.

[4] David S Bolme, J Ross Beveridge, Bruce A Draper, and Yui Man Lui. Visual object tracking using adaptive correlation filters. In 2010 IEEE computer society conference on computer vision and pattern recognition, pages 2544–2550. IEEE, 2010. 2

[5] Johannes Brünger, Maria Gentz, Imke Traulsen, and Reinhard Koch. Panoptic instance segmentation on pigs. arXiv preprint arXiv:2005.10499, 2020.

[6] Reyes Rios Cabrera, Tinne Tuytelaars, and Luc Van Gool. Efficient multi-camera detection, tracking, and identification using a shared set of haar-features. In CVPR 2011, pages 65–71, 2011.

[7] A. Dutta, A. Gupta, and A. Zissermann. VGG image annotator (VIA). http://www.robots.ox.ac.uk/ vgg/software/via/, 2016. Version: X.Y.Z, Accessed: 04/14/2021.

[8] Wei Liu, Dragomir Anguelov, Dumitru Erhan, Christian Szegedy, Scott Reed, Cheng-Yang Fu, and Alexander C. Berg. Ssd: Single shot multibox detector. Lecture Notes in Computer Science, page 21–37, 2016.

[9] Stephen G. Matthews, Amy L. Miller, James Clapp, Thomas Plötz, and Ilias Kyriazakis. Early detection of health and welfare compromises through automated detection of behavioural changes in pigs. The Veterinary Journal, 217:43–51, 2016.

[10] J. Redmon, S. Divvala, R. Girshick, and A. Farhadi. You only look once: Unified, real-time object detection. In 2016 IEEE Conference on Computer Vision and Pattern Recognition (CVPR), pages 779–788, 2016.

[11] Martin Riekert, Achim Klein, Felix Adrion, Christa Hoffmann, and Eva Gallmann. Automatically detecting pig position and posture by 2d camera imaging and deep learning. Computers and Electronics in Agriculture, 174:105391, 2020.

[12] Ergys Ristani, Francesco Solera, Roger S. Zou, Rita Cucchiara, and Carlo Tomasi. Performance measures and a data set for multi-target, multi-camera tracking, 2016.

[13] Ergys Ristani and Carlo Tomasi. Features for multi-target multi-camera tracking and re-identification. In Proceedings of the IEEE Conference on Computer Vision and Pattern Recognition (CVPR), June 2018.

[14] Jaewon Sa, Younchang Choi, Hanhaesol Lee, Yongwha Chung, Daihee Park, and Jinho Cho. Fast pig detection with a top-view camera under various illumination conditions. Symmetry, 11(2):266, 2019.

[15] Jihyun Seo, Hanse Ahn, Daewon Kim, Sungju Lee, Yongwha Chung, and Daihee Park. Embeddedpigdet—fast and accurate pig detection for embedded board implementations. Applied Sciences, 10(8):2878, 2020.

[16] M Shahbandeh. Number of pigs worldwide from 2012 to 2020. https://www.statista.com/statistics/263963/number-of-pigs-worldwide-since-1990.

[17] M. K. Swan. Swine human resources: Managing employees. https://swine.extension.org/swine-human-resources-managing-employees.

[18] Eric T Psota, Ty Schmidt, Benny Mote, and Lance C Pérez. Long-term tracking of group-housed livestock using key-point detection and map estimation for individual animal identification. Sensors, 20(13):3670, 2020.

[19] N. Wojke, A. Bewley, and D. Paulus. Simple online and realtime tracking with a deep association metric. In 2017 IEEE International Conference on Image Processing (ICIP), pages 3645–3649, 2017.

[20] Lei Zhang, Helen Gray, Xujiong Ye, Lisa Collins, and Nigel Allinson. Automatic individual pig detection and tracking in pig farms. Sensors, 19(5):1188, 2019.

[21] Volodymyr Kindratenko, Dawei Mu, Yan Zhan, John Maloney, Sayed Hadi Hashemi, Benjamin Rabe, Ke Xu, Roy Campbell, Jian Peng, and William Gropp. Hal: Computer system for scalable deep learning. In Practice and Experience in Advanced Research Computing, PEARC '20, page41–48, New York, NY, USA, 2020. Association for Computing Machinery

[22] Derpanis, Konstantinos G. "Overview of the RANSAC Algorithm." Image Rochester NY 4, no. 1 (2010): 2-3.

Bluetooth Low Energy (BLE) and passive RFID integration for obstacle avoidance and autonomous vehicles management in Agriculture

Danilo Monarca [a], Pierluigi Rossi [a,*], Pier Luigi Mangiavacchi [a], Marco Pirozzi [b], Luciano Di Donato [b], Laura Tomassini [b], Pierluigi Febo [c], Filippo Cossio [a], Massimo Cecchini [a]

[a] Department DAFNE Tuscia University, Viterbo, Italy

[b] University of Palermo, Palermo, Italy

[c] INAIL, Laboratorio Macchine e Attrezzature, Rome, Italy

* Corresponding author. Email: pierluigi.rossi@unitus.it

Abstract

Inadequate or poor interaction between operators and machines in agriculture and forestry operations can lead to severe accidents and thus represents one of the most relevant dangers. The simultaneous presence of autonomous vehicles and workers on foot calls indeed for inherently safer designs and major developments of safety devices meant to reduce the risk of crush and risk of being run over. In addition, the emerging technological advances could make common agricultural machinery harder to understand and to control, thus increasing the probability of accident.

To cope with such an evolving context, the "SMARTGRID" project described in this paper aims to deploy an integrated, multilayer, and wireless safety network infrastructure based on the integration of Bluetooth Low Energy (BLE) devices and passive Radio Frequency IDentification (RFID) tags. Funded by the Italian National Institute for Insurance against Accidents at Work (INAIL), the smart system is based on antennas placed on every vehicle which scan and eventually detect the presence of nearby RFIDs attached on workers' personal protective equipment. Every machine is also provided with BLE beaconing system which allows the transmission of alerts to any mobile device in its range and to a backend server on the working site. Such notifications generated by the system can activate an emergency stop of the machines involved and get through a cloud-based software which keeps track of hazardous activities and near-misses, preventing further dangers by sending alerts to every worker at risk on their mobile phones.

Early results of project's test programs show a detection range of passive RFIDs within 8 and 12 metres, distances that will be further verified in tests scheduled by the end of 2021, to be carried out in an experimental farm.

Keywords: smart farming, work safety, wireless, remote control, tractor.

1. Introduction

Agriculture and forestry are hazardous work sectors due to the large use of machinery and to the need to perform high risk operations with dedicated equipment, which carry their own specific hazards. Smallholding farmers often work in solitary and therefore face additional issues when accidents happen and rescues are needed; on the other hand, mechanization is vital for larger farms and dangers derived by poor interaction between workers on foot and vehicles eventually arise. With the coming of smart devices further evolution of farming equipment has been achieved but the described hazards did not melt away at all: with the increasing usage of remotely controlled vehicles and automated equipment, a previous research has already shown that safety plays a key role even at design stage and its management needs to be embedded with quality in every agricultural practice (Pirozzi et al., 2020).

The first attempt to describe the development of a remote-control system for an agricultural tractor belongs, according to Scopus Database, to Kubota (Okuyama et al., 1987). With a lack of the major advances by that time of the technology on which we can rely nowadays like electronic sensors and modern wireless communication protocols, the hardware components simply consisted in solenoid valves operated via a Radio-Frequency controller but despite such technical limits the system was already focused on the need to perform safety and emergency procedures.

Another approach which exploits the benefits of using wireless communication in agriculture can be found in attempts to sense any kind of machine anomalies and intervene before the occurrence of an accident, with the usage of low-cost electronic devices in order to integrate them even in the smallest equipment (Gubiani et al., 2013).

The general purpose of this project is to provide INAIL a possible solution to the hazards which strongly depend by the presence of autonomous remote-controlled vehicles, workers on foot and various obstacles that can be found in agricultural and forestry working environments. To achieve this result, an integrated network made of passive RFID tags placed on obstacles and a set of antennas placed on vehicles to scan for other vehicles and RFID tags has been studied and developed.

2. Materials and Methods

The SMARTGRID project has a multidisciplinary dimension which required a wide range of know-how's but also a detailed definition of activities carried out by the involved departments in order to avoid possible overlapping. One of the goals of the SMARTGRID project is to provide a deep analysis of the working environment and its inherent hazards. A specific focus has been required on the risks of run-over and impact against obstacles or between remote-controlled machines. This part of the project followed a specific process which aimed to define the domain and some of the system requirements for its wireless infrastructure. The steps have been:

- Bibliographic research of previous attempts to tackle safety issues in agriculture with the use of smart/wireless sensors and applications;
- Statistical research on accident databases to define a certain background for hazard analysis;
- Hazard identification in some well-known agricultural processes with Hierarchical Task Analysis (HTA);
- Scan for single point of failures (SPOFs) with Failure Mode and Effects Analysis(FMEA).

2.1. State of the art

The first step focused on bibliographic research on Scopus Database. Specific criteria have been selected in order to include as much as relevant papers on the subject and to avoid activities that were not of interest for the project.

Criteria	Content	Field(s)
Wireless communication protocols and infrastructures	Mobile devices, remote, wireless, BLE, bluetooth, RFID, internet of things	Title, abstract or keyword
Selected sectors	Agriculture, tractors	Keyword
Excluded sectors: markets and traceability	Markets, traceability, supply chain, water purification, breeding, products	Title, abstract or keyword
Excluded sectors: transportation	Road safety, maritime safety, plane crash, automotive, public works, traffic control, road accidents	
Excluded sectors: disasters and emergencies	Asbestos, terrorism, suicide, acid rain, forest fire, radiation	
Excluded sectors: others	Medical applications, mining, spectroscopy, environmental education, occupational health, testbeds	

Table 1: Scopus search criteria

As a result of the previously described Scopus search in table 1, a set of 10 papers has been selected to analyse what has been attempted in previous years. Technology obviously improved every safety system design and this comes clear when discussing how a new wireless network protocol played a key role for the success of every projects.

Title	Citations
The Radio-controlled Tractor From Kubota (Okuyama S. et al., 1987)	0
An Obstacle Identification Algorithm For A Laser Range Finder-based Obstacle Detector (Kise, M. et al., 2005)	35
Child Safety Driver Assistant System And Its Acceptance (Quendler, E. et al., 2009)	1

Title	Citations
Method For An Electronic Controlled Platooning System Of Agricultural Vehicles (Zhang et al., 2009)	4
Safedriving: A Mobile Application For Tractor Rollover Detection And Emergency Reporting (Liu et al., 2013)	21
A Wii-controlled Safety Device For Electric Chainsaws (Gubiani et al., 2013)	0
Application Of The Zigbee Wireless Communication Technology On The Endless Rope Continuous Tractor Derailment Monitoring System (Wan et al., 2013)	0
Smart Machines, Remote Sensing, Precision Farming, Processes, Mechatronic, Materials And Policies For Safety And Health Aspects (Monarca et al., 2018)	9
Agricultural Security Monitoring And Safety Alert System: Implementation Of Wireless Video On The Farmstead (Ehlers et al., 2019)	0
Data Collection From Outdoor Iot 802.15.4 Sensor Networks Using Unmanned Aerial Systems (Allen et al., 2019)	0

Table 2: Scopus search results for wireless and smart solutions in agricultural safety

Through analysis of papers listed in table 2 has been carried out to understand strengths and weaknesses of every solution that has been tried before. As a result, it has been found that a reliable and fault-tolerant safety system has always been considered one of the core processes for all the papers, while major differences are seen between network protocols and infrastructures:

- the usage of mobile phone applications can be of great help in sending automatic alerts in case of accident, while Bluetooth specific devices can even communicate additional info to nearby devices even without an available internet connection;
- ZigBee networks, since they allow every device to share information with each other without the need of communicating through an access point can increase the feasibility of wireless networks in harsh conditions, but this also comes with a lower communication speed and an inferior number of available channels;
- Unmanned Aerial System can play a key role in improving connectivity among machines working on large areas and in areas with lack of a good GSM mobile connection, but still require an active communication network with vehicles and workers on foot to perform safety functions;
- low-energy and passive modules, in association with a reliable wireless infrastructure for longer ranges, can prove to be robust enough to enhance detection capabilities and safety alert systems.

2.2. Statistical research on accident databases

Authors have first performed a deep statistical research on workplace accidents which involved such hazards (INAIL national database, SPISAL AULSS9 of Verona, Veneto), gathering a wide dataset of accidents descriptive details. In addition, the research provides a solid scientific perspective of the state-of-art safety advances for agricultural vehicles, identifying the most prominent enhancements in smart technologies, automations, remote-control systems, remote sensing and alarm notification systems adopted on existing machines or at design stage.

Some injury and mortality statistics have been found on INAIL's database (called Infor.Mo.) which collects data from accidents all around Italy. As shown in the following table, consequences have always been quite harsh for the involved workers with an average loss of 185 workdays.

Accident year	Gender	Missed workdays	Body part of injury	Injury type
2012	Female	194	Feet	crush
2015	Male	110	Head	wound
2016	Male	250	Leg	amputation

Table 3: Runover accident statistics with severe consequences from InforMo database

The Infor.Mo. database also provides data for fatal accidents, as shown in the following table with 5 casualties which involved runover of workers between years 2003 and 2016.

Accident year	Gender	Years of employment	Body part of injury	Injury type
2003	Male	not specified	leg	wound
2005	Male	more than 3 years	more than one	crush
2008	Male	not specified	head	Bone fracture
2009	Male	more than 3 years	thorax	crush
2016	Male	more than 3 years	more than one	crush

Table 4: Runover accident statistics with fatal consequences from InforMo database

Occupational Health Service for workplaces of Verona provincial area (SPISAL AULLS9 "Scaligera") provides some valuable data over a wide period of 15 years (2006-2020) over a population of 926.497 inhabitants. The database gives accident information in terms of type of injury, severity, age of the worker and many other relevant details which help to understand accident dynamics. Data has been deeply analysed and resulting statistics are shown in the following table.

	Accidents involving vehicles	Fatal	Fatal runover
Cases (2006-2020)	37	25	1
Percentage	74,00%	67,57%	2,70%
Annual average frequency	2,467	1,667	0,0667

Table 5: Runover accident statistics from SPISAL AULSS9 Verona

The type of activity carried out during accidents and average age of involved workers also show critical information, since almost every case happened in solitary activities while 60 years old workers were involved in 46% of the accidents reported in the database.
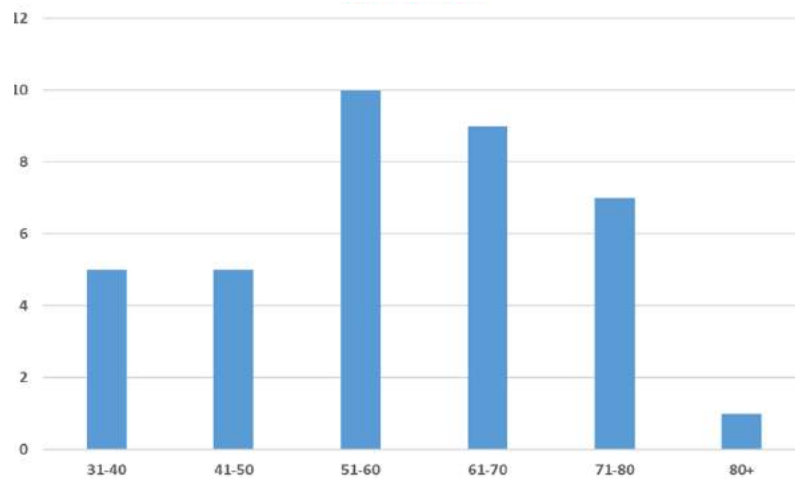
Figure 1: distribution of accidents by age of the involved workers

The statistical analysis on accidents showed the importance of prevention since protection devices are often absent and a large amount of time can be necessary for rescues to intervene. Another aspect that needs to be highlighted is the percentage of fatal accidents, a substantial majority of the total accidents which involve vehicles and their equipment.

2.3. Hazard identification in agricultural processes with Hierarchical Task Analysis (HTA)

SMARTGRID project is focused on particular risks that are part of the everyday practice in agriculture and this needs hazards to be identified consequently. The analysis has been carried out accordingly for three kinds of hazards:

- Run-over and impact with obstacles;
- Contact between workers on foot and tractor's equipment;
- Contact between workers on foot and trails or towed equipment.

Further analysis has been provided then by the describing the activities workflows for some the agricultural processes linked accidents to the previously identified hazards. Such work has been done by performing a Hierarchical Task Analysis (HTA) oriented to understand dependencies and to identify which steps can play a relevant role in triggering the accidents that have been found in statistical research.

For this step of the analysis three well known agricultural activities have been considered in order to identify the most safety-related concerns for possible accidents. The activities are:

- Mechanical harvest of shell fruits
- Mechanical fertilization with manure spreaders
- Mechanical pruning, for example in vineyards
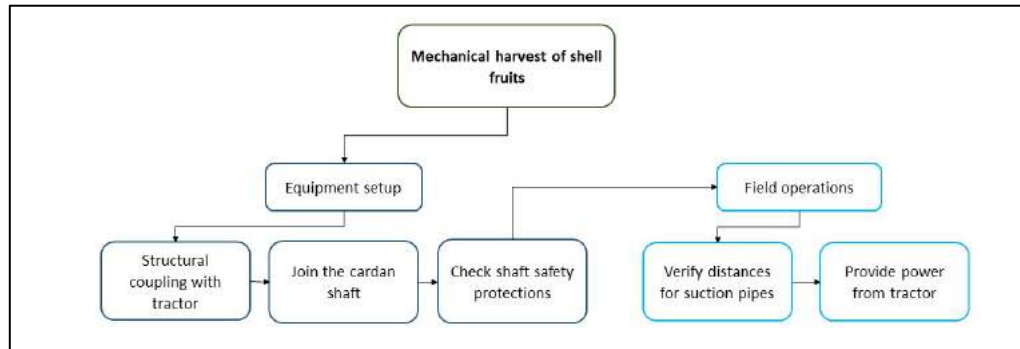
Figure 2: basic HTA for mechanical harvest of shell fruit
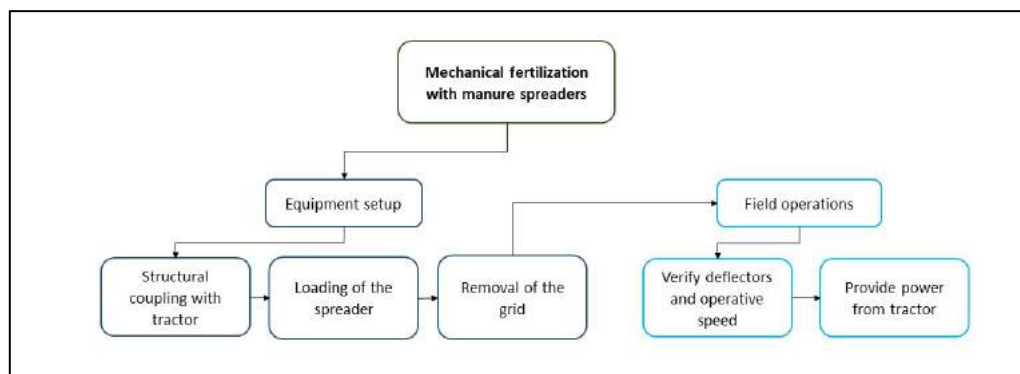
Figure 3: basic HTA for mechanical fertilization with manure spreaders
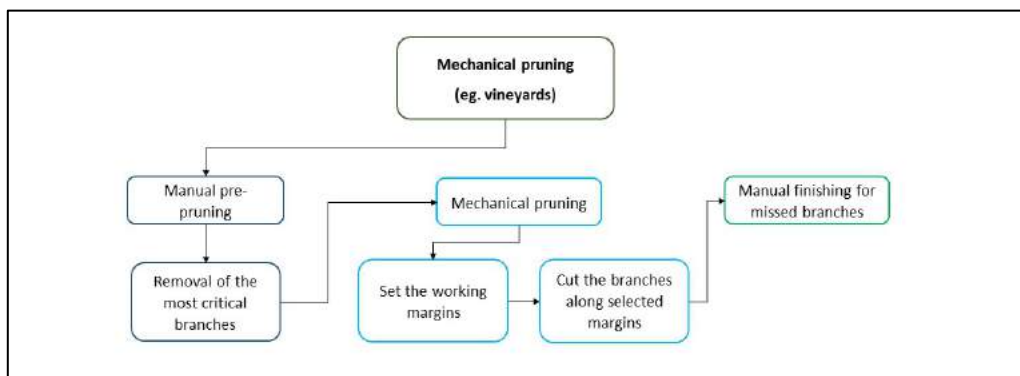
Figure 4: basic HTA for mechanical pruning in vineyards

The result of this analysis provided a good basis for the identification of the single points of failure (SPOFs): while the term naturally belongs to analysis at design level to remove flaws which may result in severe accidents, the goal for the project is to identify any flaws in the everyday practice that may lead to an accident even if the machine's design would not normally let it happen. This can be due to a major difference between the way work has been imagined and they way work gets actually carried out in reality but could also be due to absence of redundancies in accident prevention.

2.4. Scan for single points of failure (SPOFs) with Failure Mode and Effects Analysis (FMEA)

Given the importance of human factor in agriculture and forestry activities a deep analysis of accident causes is paramount to any progress in designing the system itself. The domain of the analysis has however been restricted to the most relevant activities as previously described and to the failure modes which lead to risks that SMARTGRID project aims to reduce. In order to do so a modified FMEA has been carried out and the result of this brand-new approach allowed to understand how a safety system should perform to overcome the SPOFs which have been found.

Activity	Requirements	Single Points Of Failure	Failure mode	Severity
Mechanical harvest of shell fruits	Equipment setup and margin definition	Workers on foot getting run over by machines	Wrong distances or wrong maneuvring	Severe injury or death
		Physical contact with active mechanical parts of the equipment	Wrong distances with the equipment while working	Severe injury or death
Use of manure spreaders with vertical axes rotors	Maintenance and cleaning	Activation of equipment during maintenance activities	Power still present on the equipment	Severe injury or death
Setup of manure spreading equipment	Need to be done before the use on field	Physical contact with moving parts like conveyor belt carpets while adjusting its speed	Requirement's check has been ignored	Severe injury or death
			Requirements check carried out while using the equipment	Severe injury or death
Mechanical pruning, blades as cutting equipment	Manual pruning to be executed, margins to be set	Physical contact with blades while performing manual activities	Missing alerts for danger zones while approaching equipment	Death
			Wrong maneuvering, impossibility to check for the presence of nearby workers	Severe injury or death
			Failure of blade supports	Injury and material losses
		Physical contact with workers, both on foot and on board, assigned to manual finishing of missed branches	Absence of barriers	Severe injury or death
			Inadequate distance from danger areas	
			Increase of working speed for mechanical pruning that workers cannot cope with	
Mechanical pruning, disks as cutting equipment	Manual pruning to be executed, margins to be set	Physical contact with cutting disks while performing manual activities	Absence of barriers	Severe injury or death
			Wrong maneuvering, impossibility to check for the presence of nearby workers	
			Failure of disks supports	
Mechanical pruning or cutting with telescopic arms	Verify safety distances and working conditions	Side overturn	Staibility check incomplete or not correctly performed	Severe injury or death
		Impact with obstacles or workers on foot	Wrong maneuvering, impossibility to check for the presence of workers on foot	

Table 6: Failure Mode and Effects Analysis for activities of major concern

The analysis showed the importance of redundancies to avoid misinterpretation of how procedures need to be carried out and the need of an integrated system which allows the drivers to identify nearby workers but at the same time workers on foot to be receive notifications as soon as they enter danger zones.

3. Results and Discussion

In order to fulfil the essential requirements that have been discussed and to achieve a reasonably high level of safety, a network infrastructure based on passive RFID tags and Bluetooth Low Energy devices has been designed. When one of the two sides of the network identifies potential danger a notification system promptly intervenes. The following elements have been identified as key system components:

- Passive RFID tags attached to individual protective equipment. To avoid reliability issues with reading of a single tag, several of them have been attached on bigger equipment as redundancy;

- Every vehicle has been equipped with:
  - o sensors to identify other vehicles and vice-versa;
  - o antennas to identify nearby workers;
  - o actuators for emergency stops and signals;
  - o control systems to establish a connection with an on-site server and update the real-time notification.

The integrated network infrastructure has been designed to be managed as shown in the following figure.
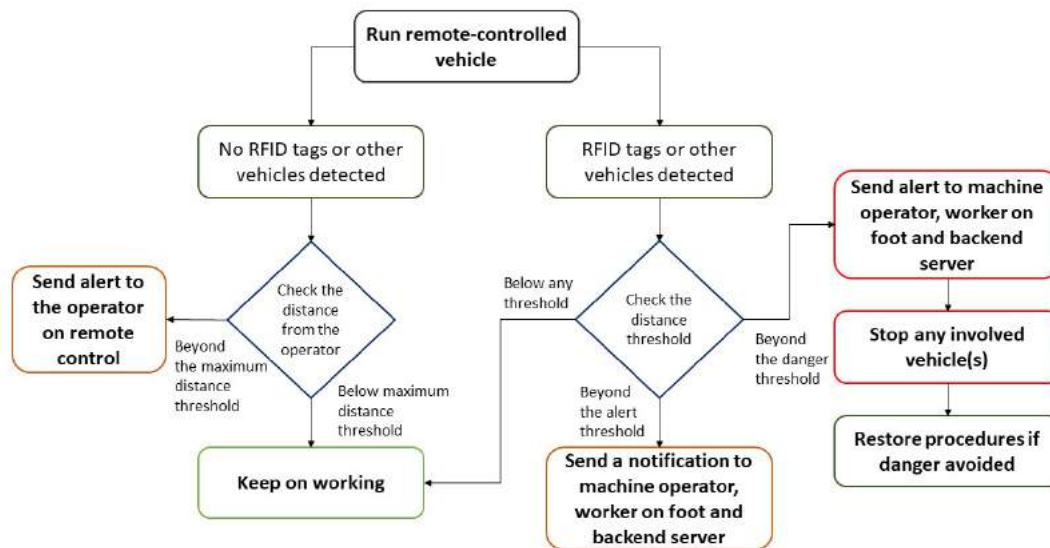
Figure 5: SMARGRID's flowchart of the safety system

The process shown in the previous figure simply works by defining distance thresholds which generate different alerts to the workers, to the backend server which keeps track of every dangerous event and to vehicles for emergency procedures if necessary. Zones can be defined accordingly to risk evaluation, for instance acceptable if no other RFID tags are found nearby the vehicle and the operator's remote control is found within a distance which guarantees safe operations. If other RFIDs can be found around the vehicle, notification can be sent to the operator and if the distance too short danger alerts might even stop any machine in the danger area. Additional checks can be done by scanning RFIDs at the entrance of the working area by dedicated gates and any near-miss information can be stored in the backend server.

4. Conclusions

Preliminary tests have already been carried out to determine the maximum range of beaconing and maximum detection for passive RFIDs in agricultural and forestry working environments. Such tests simulated the presence of a tractor with the required antennas which scanned for the presence of workers on foot and other machines, with a reading capability of around 8-12 metres. Such early results seem to be promising and can demonstrate that wearable smart solutions and low cost and low energy wireless devices can greatly enhance safety in agriculture and forestry if remote controlled or autonomous vehicles are used. The limit of the system has been found in presence of equipment that work within 2-4 metres beyond the vehicle's perimeter, such as telescopic arms or other extendable machineries: such equipment would require additional smart devices like active RFIDs, RFID readers with integrated antennas or similar.

Next step of SMARTGRID project has already planned to test system behaviour in the experimental farm of Tuscia University, in order to provide the necessary feedback needed to set precise thresholds to the whole safety management system.

References

Allen, Ryan, et al. "Data Collection from Outdoor IoT 802.15.4 Sensor Networks Using Unmanned Aerial Systems." *MobiSys 2019 - Proceedings of the 17th Annual International Conference on Mobile Systems, Applications, and Services*, 2019, pp. 564–65, doi:10.1145/3307334.3328627.

Colantoni, Andrea, et al. "Smart Machines, Remote Sensing, Precision Farming, Processes, Mechatronic, Materials and Policies for Safety and Health Aspects." *Agriculture (Switzerland)*, vol. 8, no. 4, 2018, doi:10.3390/agriculture8040047.

Ehlers, S. G., and R. L. Tormoehlen. "Agricultural Security Monitoring and Safety Alert System: Implementation of Wireless Video on the Farmstead." *Journal of Agricultural Safety and Health*, vol. 25, no. 4, 2019, pp. 155–68, doi:10.13031/jash.13004.

Gubiani, R., et al. "A Wii-Controlled Safety Device for Electric Chainsaws." *Journal of Agricultural Engineering*, vol. 44, no. 2s, 2013, pp. 690–94, doi:10.4081/jae.2013.s2.e138.

Kise, M., et al. "An Obstacle Identification Algorithm for a Laser Range Finder-Based Obstacle Detector." *Transactions of the American Society of Agricultural Engineers*, vol. 48, no. 3, 2005, pp. 1269–78, doi:10.13031/2013.18491.

Liu, Bo, and A. Bulent Koc. "SafeDriving: A Mobile Application for Tractor Rollover Detection and Emergency Reporting." *Computers and Electronics in Agriculture*, vol. 98, Elsevier B.V., 2013, pp. 117–20, doi:10.1016/j.compag.2013.08.002.

Okuyama, Shigeaki, et al. "The Radio-Controlled Tractor from Kubota." *SAE Technical Papers*, 1987, p. 871638, doi:10.4271/871638.

Pirozzi, Marco, et al. "Possible Innovative Technical Measures for Risk Prevention during the Use of Mobile Machines with Remote Guide/Control." *Procedia Manufacturing*, vol. 42, 2020, pp. 457–61, doi:10.1016/j.promfg.2020.02.049.

Quendler, Elisabeth, et al. "Child Safety Driver Assistant System and Its Acceptance." *Journal of Agromedicine*, vol. 14, no. 2, 2009, pp. 82–89, doi:10.1080/10599240902779394.

Wan, Li Rong, et al. "Application of the ZigBee Wireless Communication Technology on the Endless Rope Continuous Tractor Derailment Monitoring System." *Advances in Intelligent Systems and Computing*, vol. 181 AISC, 2013, pp. 1313–18, doi:10.1007/978-3-642-31698-2_185.

Zhang, X., et al. "Method for an Electronic Controlled Platooning System of Agricultural Vehicles." *ICVES 2009 - 2009 IEEE International Conference on Vehicular Electronics and Safety*, 2009, pp. 156–61, doi:10.1109/ICVES.2009.5400187.

Soil, land and water engineering

Assessment of Emitter Clogging with Different Sand Media Filter Underdrain Designs Using Reclaimed Effluent

Carles Solé-Torres, Jaume Puig-Bargués [*], Miquel Duran-Ros, Gerard Arbat, Joan Pujol,

Francisco Ramírez de Cartagena

Department of Chemical and Agricultural Engineering and Technology, University of Girona, Spain

* Corresponding author. Email: jaume.puig@udg.edu

Abstract

Sand media filters are recommended when reclaimed effluents are used in drip irrigation systems. These filters usually differ on the design of their underdrain, but the effect of these different designs on emitter clogging has not been widely studied. Three sand media filters with different underdrain designs (wands, inserted domes and drainage with porous media) were used for filtering a reclaimed effluent in a surface drip irrigation system. Pressure-compensating emitters with $2.3 \, l \, h^{-1}$ nominal emitter discharge were placed every 40 cm in 4 irrigation laterals each measuring 90 m in length. Effluents were chlorinated after being filtered. The filters operated for 1000 h with sand media heights of 20 and 30 cm and filtration velocities of 30 and 60 m h^{-1}. At the beginning, after 500 h, and at the end of the experiment the emitter discharge of each one of the 2712 emitters that were installed was experimentally measured under field conditions. Emitter clogging was primarily affected by the interactions between underdrain design, emitter location and irrigation time. Differences on emitter discharge due to underdrain design were only observed at 1000 h, showing a significantly higher flow rate (p <0.05) those emitters protected with the filter with a wand underdrain, despite that this filter did not achieve the highest turbidity removals. Emitter location had also a significant effect after 500 h of operation, being discharge significantly lower (p <0.05) only in the last 2 m of the laterals, with the minimum values found for the final two drippers. The three filters used in the experiment did not show a significant effect on the percentage of completely clogged emitters, which mainly depended on the interaction between irrigation time and emitter location.

Keywords: wastewater, micro irrigation, granular filter, filtration, plugging.

1. Introduction

The best irrigation technique for using wastewater from the public health and environmental points of view is drip irrigation. However, the main problem using drip irrigation with reclaimed effluents is emitter clogging (Ravina et al., 1992), which depends on factors such as wastewater characteristics, emitter type, system operation, maintenance and filtration (Capra and Scicolone, 2004; Duran-Ros et al., 2009). High discharge emitters (Ravina et al., 1992; Trooien et al., 2000) are more resistant to clogging. Clogging could also be reduced with lower irrigation frequencies (Zhou et al., 2015) and lateral flushing (Puig-Bargués et al., 2010; Tripathi et al., 2014). Several authors have studied how biofilm and chemical precipitation, which are the most common clogging causes when reclaimed effluents are reused, affect emitter performance (Gamri et al., 2014; Green et al., 2018). Chlorination has also resulted in being effective in reducing emitter clogging and it has been widely used to prevent biological clogging (Cararo et al., 2006).

Other authors analysed the effect of different filter types on emitter clogging when reclaimed effluents were used (Ravina et al., 1992; Capra and Scicolone, 2004; Duran-Ros et al., 2009; Tripathi et al., 2014). Sand filters are considered those that offer a better protection for drip irrigation systems (Trooien and Hills, 2007). Several authors have studied the influence of underdrain designs on pressure loss (Mesquita et al., 2012; Pujol et al., 2016), but none of them have analysed how filter design affects emitter clogging. On the other hand, sand filters have to be periodically backwashed for releasing those particles retained in the media, which increase pressure loss across filtration time. Backwashing is an important procedure for an effective filter performance (Nakayama et al., 2007) but the media cleaning pattern depends on the underdrain design (Burt, 2010). Usually, filter backwashing is carried out at pre-set pressure loss, nevertheless daily backwashing has been also verified to be a good practice for assuring good emitter performance (Enciso-Medina et al., 2011). Even though filter and backwashing operations in drip irrigation systems have been studied (Elbana et al., 2012) there are few studies which try to improve the design and performance of sand media filters. With this in mind, Bové et al. (2017) designed a new underdrain aiming to reduce pressure loss across sand filters for improving both water and energy use efficiency.

The main objective of this study was to analyse the effect of three sand filters with different underdrain designs (the prototype designed by Bové et al. (2017) and two commercial ones) on emitter clogging when a reclaimed effluent is used.

2. Materials and Methods

2.1. Experimental layout

Reclaimed effluent from the Celrà (Girona, Spain) wastewater treatment plant (WWTP), which treats urban and industrial effluents using a sludge process, was used in the experiment.

The experimental irrigation system consisted of three sand filters with three underdrain different designs (Figure 1): a sand filter model FA1M (Lama, Gelves, Spain), a sand filter model FA-F2-188 (Regaber, Parets del Vallès, Spain) and an experimental sand filter built with an underdrain designed by Bové et al. (2017). Additional details about the different underdrain designs are provided by Solé-Torres et al. (2019). All the filters were filled with silica sand with an effective diameter De of 0.48 mm and a coefficient of uniformity of 1.73.

Figure 1. Different underdrain designs: porous media (A), inserted domes (B) and wand (C).

Each filter had an irrigation subunit associated, which consisted of four laterals, each with a total length of 90 m. Each lateral had 226 emitters, so for each emitter location there were 4 replications per subunit. However, for location 226 only there were 3 emitters per subunit. Commercial integrated and pressure compensating emitters Uniram AS 16010 (Netafim, Tel Aviv, Israel), with 2.3 l h^{-1} of nominal flow discharge, a distance between emitters of 0.4 m, a nominal working pressure of 50-400 kPa and a manufacturing coefficient of variation of 0.03 were used.

The experimental setup allowed that only one filter was operating at a time. A chlorine deposit of 200 l was installed, to continuously inject chlorine for achieving a concentration of 2 ppm in the water after being filtered, using a DosTec AC1/2 membrane pump (ITC, Sta. Perpètua de la Mogoda, Spain). When sand filters were backwashed, backwashing water entering the filters was chlorinated to reach a 4 ppm chlorine concentration. Backwashings were carried out for 3 min when the total pressure drop across the filters reached 50 kPa.

2.2. Operational procedure

The experiment lasted 1000 h for each filter, taking place uninterruptedly between March and November 2018, except for the month of June, where the installation did not work due to a breakdown of turbidity sensors. Whenever possible, six daily irrigation sessions of 4 h each (i.e., two daily sessions of 4 h per filter) were carried out. In practice, it was attempted to establish irrigation sessions as homogeneous as possible, which was not always possible due to small breakdowns that prevented the use of a filter for a certain period of time. When these breakdowns were solved, the operation time of the affected filter was increased to equalize the hours of operation.

During the 1000 h that the experiment lasted, two different media heights were tested (20 and 30 cm), and two different filtration velocities (30 and 60 m h^{-1}) for each one, which made a total of four different operating conditions. The operating conditions were the same for each filter with each being tested for 250 h. Working pressure was set to 172 kPa at drip irrigation subunit inlet. No lateral flushing was carried out during the experiment.

2.3. Assessment of filter and emitter performance

Filter performance for removing turbidity and dissolved oxygen was assessed through the removal efficiency achieved by the filters, computed following Duran-Ros et al. (2009). Flow discharge for all the emitters of all the laterals (i.e., a total of 2712 emitters) was measured in the experimental field at the beginning, after 500 h and at the end of the experiment (1000 h). The experimental determination of emitter discharge lasted for about 20 h after the target time (0, 500 and 1000 h) due to the number of emitters being measured. In addition, the percentage of completely clogged emitters was also computed at each control time.

During the emitter discharge measurements, pressure was also determined in four positions on each lateral (at the beginning, 1/3 of the lateral length, 2/3 of the lateral length and at the end) for computing pressure uniformity coefficient, which for all irrigation subunits was above 98% during the whole experiment. Therefore, the pressure distribution for the driplines was uniform.

2.4. Characterization of inlet water

Effluent electrical conductivity (EC), pH and temperature at filter inlet and turbidity and dissolved oxygen (DO) at both filter inlet and outlet were measured and recorded every minute in a supervisory control and data acquisition system (SCADA). Volumetric flow rate and pressure values were also recorded. Since the filters did not operate

simultaneously, it was necessary to assess if effluent characteristics were different during the experiment. Table 1 presents the mean values of the pH, temperature, EC, DO and turbidity values recorded through the 1000 hours the experiment lasted.

Table 1. Average ± standard deviation of the effluent physical and chemical parameters at filter inlets. Different letters mean that there were significant differences (p<0.05) in the values of each parameter at the different filter inlets.

Filter underdrain design	pH	Temperature (ºC)	EC (dS m⁻¹)	DO (mg l⁻¹)	Turbidity (FTU)
Porous media	7.33 ± 0.20 b	20.61 ± 3.26 a	2.64 ± 0.46 a	3.27 ± 0.83 b	6.22 ± 2.11
Inserted domes	7.43 ± 0.24 a	20.12 ± 3.49 ab	2.46 ± 0.53 b	3.57 ± 1.02 a	5.82 ± 3.08
Wand	7.31 ± 0.22 b	19.68 ± 3.57 b	2.63 ± 0.44 a	3.28 ± 1.04 b	6.42 ± 2.77

Significant differences (p <0.05) were observed for pH, temperature, EC and DO for the reclaimed effluents at each filter inlet. Reclaimed effluent used during the experiment with the dome underdrain filter had a pH significantly higher (p <0.05) than that for both porous media and wand underdrain filters. According to Bucks et al. (1979) classification, there was a moderate chemical clogging hazard regarding the pH for all the filters. Water inlet temperatures when the porous media underdrain was tested were significantly higher (p<0.05) than those for the wand underdrain but not for those of the dome underdrain. These differences between temperatures may have helped the formation and growth of biofilms, which are closely related to emitter clogging (Zhou et al., 2013). EC when porous media and wand filters were used was significantly higher (p <0.05) than that with the dome underdrain. Effluent used during the operation of dome underdrain filter had DO significantly higher (p<0.05) than those for both porous media and wand filters. No significant differences were observed in turbidity values in inlet water for any of the tested filters, meaning that the risk of physical clogging was the same. All these variations are due to the usual variability present when reclaimed effluents are treated in the WWTP.

2.5. Statistical analyses

Statistical analyses carried out using SPSS Statistics 25 software (IBM, New York, USA). In order to analyze emitter discharge and percentage of completely clogged emitters, an analysis of the variance was carried out. The model that was used included as fixed effects the filter underdrain design, the time of measurement and the position of the emitters as well as the double interactions between the filter and time, filter and position, and time and position. Triple interactions were initially assessed but, as they were not significant (p>0.05), they were excluded from the final analyses. To differentiate the averages that were significantly different with a probability of 0.05 or less, the Tukey's pairwise comparison test was used.

3. Results and Discussion

3.1. Filter performance

Table 1 presents the percentages of oxygen and turbidity removals achieved by the different underdrain designs. The porous media underdrain filter showed turbidity removals of 26.3%, significantly higher (p<0.05) than those reached by dome (18.5%) and wand (13.5%) underdrain filters, which were not significantly different from each other. Previous experiments with effluents of the same WWTP and using a dome underdrain sand filter with a filtration media height of 50 cm achieved turbidity removals of 57.6% with an inlet 6.76 FTU (Duran-Ros et al., 2009) and 70.6% with an inlet 9.78 FTU (Elbana et al., 2012). Tripathi et al. (2014) observed turbidity reductions of 51.1% using effluents with inlet 55 FTU. Wu et al. (2015) obtained reduction efficiencies of suspended solids from 11.4 to 48.0% using a sand filter filled with different media with equivalent diameters ranging between 2.1 and 0.45 mm. No details about sand filter design were provided in either of the two previous papers. The smaller turbidity removal observed in the present experiment (19.4% on average) for all of these three underdrain designs may be due to the smaller inlet levels of turbidity of the effluent used (6.15 FTU on average) and to the reduced height of sand media bed in the filters, which was between 40 and 60% lower than the heights used by Duran-Ros et al. (2009) and Elbana et al. (2012) with a dome underdrain filter. Lower media heights used in the present experiment are explained by the limitation caused by reduced maximum height of wand underdrain filter (40 cm) and the need to carry out the experiment under the same experimental conditions for each filter.

The increase of DO achieved by the porous media (11.2%) and wand underdrain (11.0%) filters were greater than that observed with the dome underdrain filter (6.7%), although no significant differences were noted between these values. The smaller increases in DO achieved by the dome underdrain filter might be explained by the significantly (p<0.05) higher values of this parameter at this filter inlet (Table 1). DO increases in the dome underdrain filter were higher than those observed by Duran-Ros et al. (2009) (0.5% for inlet DO values of 2.80 mg/l and working with an effective sand size of 0.40 mm) and Elbana et al. (2012) (3.8% for inlet DO values of 4.00 mg/l and using an effective

sand size of 0.48 mm), which were obtained in an experiment without any chlorination treatment. The main reason for DO increase is related to chlorination of backwashing water, which reduced microbial population (Li et al., 2010) that consumes oxygen.

Table 1. Average ± standard deviation of the removal efficiencies (in % reductions of th e inlet values) of dissolved oxygen (DO) and turbidity achieved by the different underdrain design filters. Negative values indicate an increase of the parameter. Different letters mean that there were significant differences ($p < 0.05$) in the removal efficiency for a parameter.

Filter underdrain design	Removal efficiency (%)	
	Dissolved oxygen	Turbidity
Porous media	-11.20 ± 33.84	26.29 ± 16.50 a
Inserted domes	-6.68 ± 30.53	18.53 ± 24.38 b
Wand	-11.03 ± 35.89	13.45 ± 25.07 b

3.2. Emitter performance

There was a significant effect ($p < 0.05$) on emitter discharge of each fixed factor (time, emitter position and filter underdrain design) as well as the interactions of underdrain design and time, underdrain design and emitter location and time and emitter location. Overall, there was a significant reduction ($p < 0.05$) of emitter discharge, which gradually decreased from an average measured discharge of 2.49 l h^{-1} at the beginning of the experiment, to 2.29 l h^{-1} at 500 h and 2.22 l h^{-1} at 1000 h. Globally, there has been a 10.8% reduction of emitter discharge from the beginning to the end of the experiment. This emitter discharge reduction throughout irrigation time due to clogging incidence has been widely observed (Ravina et al., 1992; Duran-Ros et al., 2009; Tripathi et al., 2014; Wu et al., 2015).

3.3.1. Effect of the underdrain design and irrigation time

Emitter discharge regarding filter underdrain design and irrigation time is shown in Figure 3. There was a significant reduction in emitter discharge over time for all the filter designs. Emitters protected by a wand underdrain sand filter showed a discharge reduction of 7.6% at 500 h and 9.6% at 1000 h from the initial value. These discharge diminutions were smaller than those observed for those emitters protected by the porous media and dome underdrain filters (8.8 and 8.1% at 500 h and 12.4 and 11.3% at 1000 h, respectively). Most of discharge rate reductions took place during the first 500 h, compared with those from 500 to 1000 h (3.9% for the porous media, 3.5% for the dome and 2.2% for the wand underdrain). Wu et al. (2015) also observed major emitter discharge reductions in first testing stages (from 0 to 150 h) compared to reductions in final testing stages (from 150 to 300 h).

At the beginning of the experiment, no differences in emitter discharge between underdrain designs were found (Figure 3). After 500 h, the average discharge of emitters protected by a wand design (2.31 l h^{-1}) was significantly higher ($p < 0.05$) than with the dome underdrain (2.28 l h^{-1}) but not with the porous media design (2.29 l h^{-1}). After 1000 h, the average discharge of emitters protected by the wand design (2.26 l h^{-1}) was significantly higher ($p < 0.05$) than those from both dome and porous media (2.20 l h^{-1}) underdrain filters. However, these differences were only about 3% of emitter discharge, on average. Further research on the hydrodynamics conditions under filtration and, especially, backwashing, since the last has an important effect on filter performance (Burt, 2010; Enciso-Medina et al., 2011), for each underdrain design should be carried out in order to identify different patterns on particle removal that may have an effect on emitter clogging.

3.3.2. Effect of the underdrain design and emitter location

For each underdrain sand filter design, significant differences ($p < 0.05$) in emitter discharge were found, but only for emitters placed at the end of each lateral (Figure 4). In addition, slight variations were observed between filter designs. Thus, for both porous media and dome underdrain designs, emitter discharge of the three last emitters (last 1.2 m of the dripline) was significantly ($p < 0.05$) lower than the discharge of emitters located at the first 88.8 m of the lateral, i.e., emitters 1-222. For the wand underdrain, the smallest emitter discharge was only observed in the two last emitters (last 0.8 m) regarding emitter discharge of emitters 1-223. For all the underdrain designs, last emitter had clearly the lowest emitter average discharge (1.09 l h^{-1} for the porous media, 1.31 l h^{-1} for the dome and 1.57 l h^{-1} for wand designs).
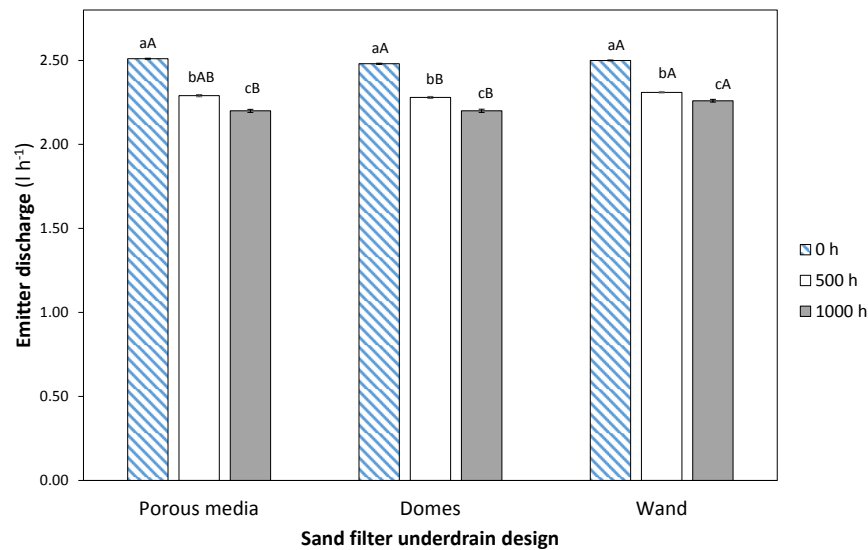
Figure 2. Average emitter discharge and standard error (l h⁻¹) of all the emitters protected by sand filters with different underdrain designs at three measurement times. For each filter underdrain design, different small letters mean significant differences (p<0.05) among times. For each measured time, different capital letters mean significant differences (p<0.05) among filter underdrain designs.
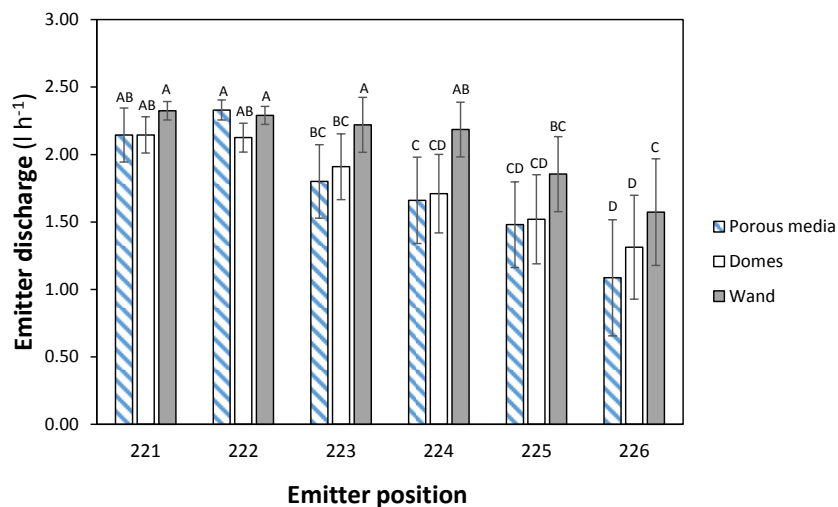
Figure 3. Average emitter discharge and standard error (l h⁻¹) of the last 6 emitters of the lateral for each filter underdrain design. For each underdrain design, different capital letters mean significant differences (p<0.05) among locations.

For each emitter position, differences in emitter discharge between underdrain designs were only found in 11 emitters, which accounted for only 5 % of the emitters on each dripline. The distribution of these emitters did not follow any pattern since they were emitter number 20, 31, 43, 105, 110, 111, 112, 153, 156, 160 and 217. In 27% of these emitters (emitters number 105, 111 and 112), discharge achieved with porous media underdrain sand filter was significantly higher than with wand filter while just the opposite happened with 18% of the emitters (emitters 20 and 217). For another 18% of these emitters (emitters 31 and 110) dome underdrain sand filter achieved more emitter discharge than wand but for emitters 156 and 160 the results was exactly the opposite. These differences might be explained by the randomness that is commonly observed in emitter clogging (Feng et al., 2019).

3.3.3. Effect of time and emitter location

At the beginning of the experiment, there were no significant differences among locations, although after 500 and 1000 h significant differences (p <0.05) appeared (Figure 5), with smaller discharges observed in the emitters at the end of the driplines. After 500 h, the three last emitters (positions 224, 225 and 226) had significantly lower (p<0.05) discharges than the rest of emitters, with average values of 1.83, 1.83 and 1.49 l h⁻¹, respectively. After 1000 h, the last

four emitters (locations 223, 224, 225 and 226) had a lower discharge (p<0.05) than the 222 previous ones, with values of 1.45, 1.22, 0.61 and 0.00 l h^{-1}, respectively. This means that all the final emitters were completely clogged at the end of the experiment, whatever the filter was. In addition, the emitter located in position 221 showed also a smaller discharge than that of the previous 220 emitters, with the exception of emitters 213 and 218. After 1000 h, there was a flow discharge reduction in almost all the emitters compared with 500 h emitter flow rates, with this reduction accentuated along the lateral. Greater discharge reductions at the end of laterals have been widely observed by many authors (e.g. Ravina et al., 1992; Trooien et al., 2000; Puig-Bargués et al., 2010; Wu et al., 2015).
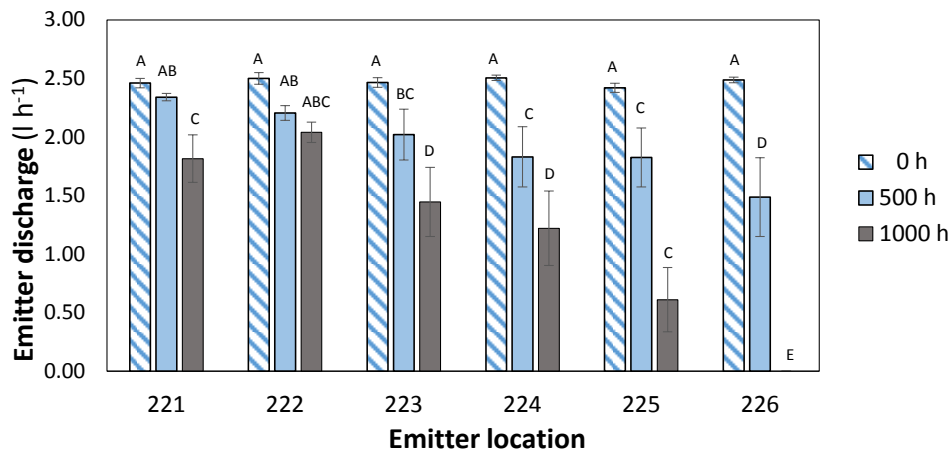
Figure 4. Emitter discharge averages and standard error l h^{-1}) for the last 6 emitters of the lateral at each measured time. For each measured time, different capital letters mean significant differences (p<0.05) among locations.

3.3. Completely clogged emitters

The total number of totally clogged emitters after 500 h was 5 emitters (0.6% of the total) for the laterals protected by the porous media underdrain filter and 2 (0.2% of the total) for the dome underdrain filter. No clogged emitters for the wand underdrain filter were found. After 1000 h, the total number of clogged emitters was 10 for the porous media filter (1.1% of the total), 8 for the dome (0.9% of the total) and 6 for the wand underdrain filter (0.7% of the total). The emitter protected with dome underdrain in location 223 recovered from total clogging after 500 h to a flow rate of 0.36 l/h after 1000 h. Some authors had observed the recovery of clogged emitters and attributed this fact to a release of the material that plugged the emitter (Ravina et al., 1992; Duran-Ros et al., 2009) due to pressure variations or deformation of organic particles. Although the filter with porous media underdrain had turbidity removals significant higher than the other two designs, it presented a higher percentage of completely clogged emitters. A possible explanation could be that other particles such as small sized sand released from the filter might have clogged the emitter, but this was not observed. Thus, the randomness observed in clogging (Feng et al., 2019) might also explain this observation.

The percentage of totally clogged emitters for each location was treated statistically, and there was a significant effect of time, emitter location and the interaction of both. Either the effect of underdrain sand filter design or its interaction between time and emitter location were found to be significant (p>0.05). These means that the different underdrain designs tested in the present experiment did not explain the percentage of completely clogged emitters. Regarding experiment time, after 500 h of irrigation significant differences (p<0.05) of the percentage of completely clogged emitters among locations were found, with locations 224 and 225 (each one with 16.7 % of completely clogged emitters) being significantly different from the rest except emitter number 223 (8.3% of totally clogged emitters) and emitter 226 (22.2% of completely clogged emitters). Completely clogged emitters for location 226 were significantly higher than those observed in locations 1-223. After 1000 h, location 226 had a significantly higher percentage of completely clogged emitters than the rest of emitter locations at this time. Emitter 225 also had a significantly higher percentage of completely clogged emitters (58.3%) than the emitters placed before and emitters 223 and 224 had, at the same time, a higher percentage of totally clogged emitters (25 and 33.3 %, respectively) than that observed for the first 222 emitters (Figure 6).

All the clogged emitters were located at the end of the lateral. Several studies show this same clogging emitter tendency (Trooien et al., 2000; Duran-Ros et al., 2009) which can be attributed to a reduction flow rate at the end of the lateral and a greater concentration of particles (Wu et al., 2015). Despite that reclaimed effluent was chlorinated after being filtered, at the end of laterals emitter discharges were lower and more emitters became fully clogged. Some qualitative measurements of chlorine at the emitter outlet at the end of the lateral were made using chlorine test strips and, as it may be anticipated, the chlorine level was very low at this point since injection was carried out at a long distance away from the filters. Free chlorine levels between 1.5-2.5 mg l^{-1} at the end of the laterals effectively reduced

emitter clogging (Li et al., 2010; Song et al., 2017). It should be pointed out that no lateral flushing was carried out during the experiment in order to have more clogging incidence. Flushing reduces sediment deposition within driplines (Puig-Bargués et al., 2010) as well as biofilm formation (Li et al., 2015). However, the number of completely clogged emitters was relatively small.
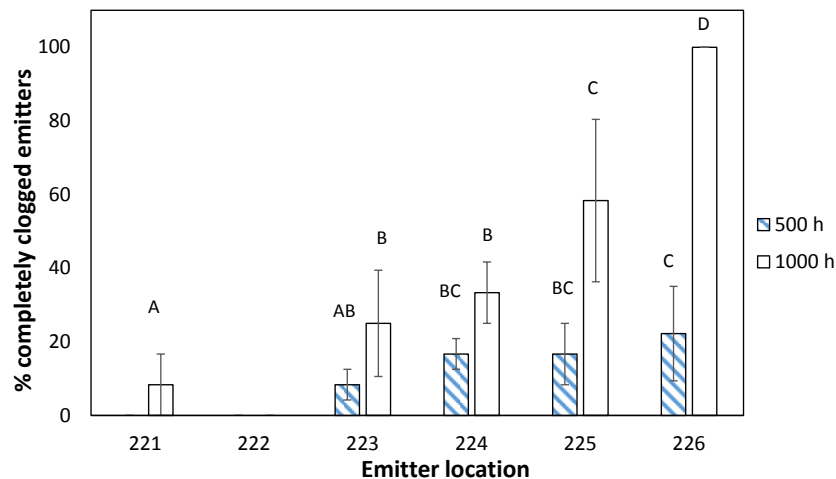
Figure 5. Percentage of completely clogged emitters (%) per emitter location, after 500 and 1000 testing hours. For each time, different capital letters mean significant differences (p<0.05) among locations.

4. Conclusions

The present study was carried out to determine the effect of three different underdrain designs used for sand media filters on emitter clogging when using a chlorinated reclaimed effluent. Emitter clogging was affected by the interactions between underdrain design, emitter location and irrigation time. Emitter location had a significant effect only after 500 h of operation, with significant differences among emitter discharge (p<0.05) in the last three emitters (last 1.2 m of the lateral) and after 1000 h for those emitters located at the last 2 m of the laterals. There was also a significant reduction in emitter discharge that ranged from 9.6% to 12.4% depending on the filter design after 1000 h of irrigation. A significantly higher emitter discharge (p<0.05) was observed in those emitters protected by a sand filter with wand underdrain, although this filter did not achieve the highest turbidity removals. There was also a location effect on emitter discharge among underdrain designs. The emitter discharge values were significantly lower from the final 4, 3, and 2 emitters when sand filter with a porous media, dome and wand underdrains, respectively, were used.

On the other hand, the percentage of completely clogged emitters depended on the interaction between irrigation time and emitter location, without any significant effect of any of the three different sand filter underdrain designs.

Based on the results, a sand filter with a wand underdrain design showed less emitter clogging when reclaimed effluent was used, but only after 1000 h of irrigation. For shorter times, clogging protection between the different tested filters was not different. However, emitter clogging, which is a complex process, depended also on the interaction between irrigation time and emitter location. Further research should be carried out to analyse if different sand filter designs have a specific effect on any of the emitter clogging agents.

References

Bové, J., J. Puig-Bargués, G. Arbat, M. Duran-Ros, T. Pujol, J. Pujol, F. Ramírez de Cartagena, 2017. Development of a new underdrain for improving the efficiency of microirrigation sand media filters. Agricultural Water Management. 179, 296-305. https://doi.org/10.1016/j.agwat.2016.06.031

Bucks, D.A., F.S. Nakayama, R.G. Gilbert, 1979. Trickle irrigation water quality and preventive maintenance. Agricultural Water Management. 2 (2), 149–162. https://doi.org/10.1016/0378-3774(79)90028-3

Burt, C.M., 2010. Hydraulics of Commercial Sand Media Filter Tanks used for Agricultural Drip Irrigation. Irrigation Training & Research Center, California Polytechnic State University, San Luis Obispo, California.

Capra, A., B. Scicolone, 2004. Emitter and filter tests for wastewater reuse by drip irrigation. Agricultural Water Management. 68, 135–149. https://doi.org/10.1016/j.agwat.2004.03.005

Cararo, D.C., T.A. Botrel, D.J. Hills, H.L. Leverenz, 2006. Analysis of clogging in drip emitters during wastewater irrigation. Applied. Engineering in Agriculture. 22 (2), 251–257. https://doi.org/10.13031/2013.20286

Duran-Ros, M., J. Puig-Barguès, G. Arbat, J. Barragán, F. Ramírez de Cartagena, 2009. Effect of filter, emitter and location on clogging when using effluents. Agricultural Water Management. 96 (10), 67–79. https://doi.org/10.1016/j.agwat.2008.06.005

Elbana, M., F. Ramírez de Cartagena, J. Puig-Barguès, 2012. Effectiveness of sand media filters for removing turbidity and recovering dissolved oxygen from a reclaimed effluent used for micro-irrigation. Agricultural Water Management. 111, 27-33. https://doi.org/10.1016/j.agwat.2012.04.010

Enciso-Medina, J., W.L. Multer, F.R. Lamm, 2011. Management, maintenance and water quality effects on the long-term performance of subsurface drip irrigation systems. Applied Engineering.in Agriculture. 27 (6), 969–978. https://doi.org/10.13031/2013.40633

Feng, J., Y. Li, Z. Liu, T. Muhammad, R. Wu, 2019. Composite clogging characteristics of emitters in drip irrigation systems. Irrigation Science. 37 (2), 105–122. https://doi.org/10.1007/s00271-018-0605-9

Gamri, S., A. Soric, S. Tomas, B. Molle, N. Roche, 2014. Biofilm development in micro-irrigation emitters for wastewater reuse. Irrigation Science. 32 (1), 77-85. https://doi.org/10.1007/s00271-013-0414-0

Green, O., S. Katz, J. Tarchitzky, J., Y. Chen, 2018. Formation and prevention of biofilm and mineral precipitate clogging in drip irrigation systems applying treated wastewater. Irrigation Science. 36 (4-5), 257-270. https://doi.org/10.1007/s00271-018-0581-0

Li, J., L. Chen, Y. Li, J. Yin, H. Zhang, 2010. Effects of chlorination schemes on clogging in drip emitters during application of sewage effluent. Applied Engineering in Agriculture. 26(4), 565–578. https://doi.org/10.13031/2013.32067

Li, Y., P. Song, Y. Pei, J. Feng, 2015. Effects of lateral flushing on emitter clogging and biofilm components in drip irrigation systems with reclaimed water. Irrigation Science. 33 (3), 235-245. https://doi.org/10.1007/s00271-015-0462-8

Mesquita, M., R. Testezlaf, J. Ramirez, 2012. The effect of media bed characteristics and internal auxiliary elements on sand filter head loss. Agricultural Water Management.115, 178-185. https://doi.org/10.1016/j.agwat.2012.09.003

Nakayama, F.S., B.J. Boman, D.J. Pitts, 2007. Maintenance. In *Microirrigation for Crop Production. Design, Operation, and Management*. Elsevier, Amsterdam. Eds., F.R. Lamm, J.E. Ayars, J.E. and F.S.Nakayama, 389–430.

Puig-Barguès, J., F.R. Lamm, T.P. Trooien, G.A. Clark, 2010. Effect of dripline flushing on subsurface drip irrigation systems. Transactions of the ASABE.53 (1), 147-155. https://doi.org/10.13031/2013.29513

Pujol, T., G. Arbat, J. Bové, J. Puig-Barguès, M. Duran-Ros, J. Velayos, F. Ramírez de Cartagena, 2016. Effects of the underdrain design on the pressure drop in sand filters. Biosystems Engineering. 150, 1-9. https://doi.org/10.1016/j.biosystemseng.2016.07.005

Ravina, I., E. Paz, Z. Sofer, A. Marcu, A. Shisha, G. Sagi, 1992. Control of emitter clogging in drip irrigation with reclaimed wastewater. Irrigation Science. 13 (3), 129–139. https://doi.org/10.1007/BF00191055

Solé-Torres, C. J. Puig-Barguès, M. Duran-Ros, G. Arbat, J. Pujol, F. Ramírez de Cartagena, 2019. Effect of different sand filter underdrain designs on emitter clogging using reclaimed effluents. Agricultural Water Management, 223, 105683. https://doi.org/10.1016/j.agwat.2019.105683

Song, P., Y, Li, B. Zhou, Z. Zhang, J. Li, 2017. Controlling mechanism of chlorination on emitter bio-clogging for drip irrigation using reclaimed water. Agricultural Water Management, 184, 36-45. https://doi.org/10.1016/j.agwat.2016.12.017

Tripathi, V.K., T.B.S. Rajput, N. Patel, 2014. Performance of different filter combinations with surface and subsurface drip irrigation systems for utilizing municipal wastewater. Irrigation Science. 32 (5), 379-391. https://doi.org/10.1007/s00271-014-0436-2

Trooien, T.P., F.R. Lamm, L.R. Stone, M. Alam, D.H. Rogers, G.A. Clark, A.J. Schlegel, 2000. Subsurface drip irrigation using livestock wastewater: dripline flow rates. Applied Engineering in Agriculture. 16 (5), 505–508. https://doi.org/10.13031/2013.5301

Trooien, T.P., Hills, D.J., 2007. Application of biological effluent. In *Microirrigation for Crop Production. Design, Operation, and Management*. Elsevier, Amsterdam, Eds., F.R. Lamm, J.E. Ayars, J.E. and F.S.Nakayama, 329–356.

Wu, W.Y., Y. Huang, H.L. Liu, S.Y. Yin, Y. Niu, 2015. Reclaimed water filtration efficiency and drip irrigation emitter performance with different combinations of sand and disc filters. Irrigation and Drainage. 64 (3), 362-369. https://doi.org/10.1002/ird.1909

Zhou, B., Y.K. Li, Y.T. Pei, 2013. Quantitative relationship between biofilms components and emitter clogging under reclaimed water drip irrigation. Irrigation Science 31(6), 1251–1263. https://doi.org/10.1007/s00271-013-0402-4

Zhou, B., Y.K. Li, L. Yaoza, X. Feipeng, 2015. Effect of drip irrigation frequency on emitter clogging using reclaimed water. Irrigation. Science. 33 (3), 221-234. https://doi.org/10.1007/s00271-015-0461-9

Hydraulic Performance of a Wand-type Underdrain in a Sand Media Filter for a Drip Irrigation System

Toni Pujol [a], Jaume Puig-Bargués [b,*], Gerard Arbat [b], Miquel Duran-Ros [b], Carles Solé-Torres [b],

Joan Pujol [b], Francisco Ramírez de Cartagena [b]

[a] Department of Mechanical Engineering and Industrial Construction, University of Girona, Girona, Spain

[b] Department of Chemical and Agricultural Engineering and Technology, University of Girona, Spain

* Corresponding author. Email: jaume.puig@udg.edu

Abstract

Sand media filtration is frequently used in drip irrigation systems. Commercial filter designs may use different underdrain models, but wand-type designs provide a large ratio of horizontal area covered by underdrains and are expected to provide a uniform flow of water through the medium. The complexity of these designs makes it difficult to analyse the effects of changing the position of wand and the slot open area. These underdrain effects were studied by means of a computational fluid dynamics (CFD) model assuming clean water conditions. The backwashing process was not considered. The results obtained from the numerical model were validated using experimental data from a commercial sand media filter with 10 wands. Unbalanced flows between underdrains were observed in the original configuration. Two new designs were proposed: (1) a design that uses the same type of wands as the original filter but distributes them so as to have an equal horizontal area served by each wand; (2) a design that uses the same spatial distribution as the original filter but with longer wands in those regions of the original filter with lower volumetric flow. CFD simulations of the two designs indicate that design (1) can reduce the pressure drop through the filter at nominal volumetric flow rates by up to 5.8% with a more uniform flow inside the medium and design (2) could improve the performance of the filter by achieving an up to a 4.9% reduction of pressure drop. Thus, the spatial distribution of underdrains is a key parameter in the hydraulic performance of sand media filters.

Keywords: filtration, granular bed, drip irrigation, computational fluid dynamics, modelling.

1. Introduction

Filtering irrigation water properly and effectively prevents emitter clogging. Sand media filters are the most common used filtration protection for microirrigation systems when low quality waters are used (Trooien and Hills, 2007). Their simplicity and large filtration volumes make them favoured by farmers and designers over other filter types (Burt, 2010). However, substantial differences in pressure loss and media cleaning are found between filters of different designs (Burt, 2010). Thus, the study of the hydraulic performance of the different sand media filters is necessary to improve their designs since they affect particle removal, energy consumption and emitter clogging (Solé-Torres et al., 2019a, 2019b).

The head loss of different sand media filters filled with different grain sizes and operating at different velocities is significantly affected by the filter internal elements, mainly the diffuser plate and the underdrain (Mesquita et al., 2012). Computational fluid dynamics (CFD) is a tool that allows the hydrodynamic simulation of irrigation equipment for assessing its performance and the effect of design improvements. This technique was used by Mesquita et al. (2019) for designing a new diffuser plate that reduced the vortex formation close to the sand bed surface, thereby achieving less bed deformation and avoiding preferential flow paths that can cause filters to be less effective since they are not backflushed sufficiently well when preferential paths are formed (Enciso-Medina et al., 2011). Arbat et al. (2011, 2013) used CFD and analytical equations to assess head losses across a sand media filter with a nozzle underdrain and verified that non uniform flow was produced in the underdrain area. Different improvements of the nozzle design were evaluated with CFD by Bové et al. (2015) and using analytical equations by Pujol et al. (2016) The work produced a new underdrain prototype that reduced pressure loss across the underdrain by 20 - 45% compared to commercial designs (Bové et al., 2017). The improvements carried out by Bové et al. (2017) were assessed by both CFD simulation and experiment and consisted of enlargement of the passage at the underdrain outlet; reduced flow curvature when approaching to the underdrain by changing the underdrain slots; replacing the media size where there is more flow curvature with media of greater size to increase hydraulic conductivity in these areas.

Other common types of underdrain design that can be found in sand media filters used for microirrigation systems use wands (Burt, 2010). High pressure losses and the removal of particles near to the walls have been observed with this type of underdrain design (Mesquita et al., 2012) but these effects have not been fully investigated since a complete hydraulic study of the performance of wand filters has not been carried out.

Thus, the main objective of this paper was to analyse the hydraulic performance of wand-type sand media filter

underdrains during the filtration process using clean water conditions in order to suggest design improvements that could improve flow circulation and reduce pressure loss. The backwashing process was not considered in this study.

2. Materials and Methods

2.1. Experimental layout

A commercial sand media filter with wand underdrains (FA1M, Lama, Gelves, Spain) was installed in a drip irrigation system. The filter was filled either with 62.5 kg or 94 kg of silica sand, providing an effective height over the centre of the wands equal to 20 cm or 30 cm, respectively. Silica with an effective diameter De of 0.48 mm and a coefficient of uniformity of 1.73 was used. No evaluation of possible sand losses during the filtration process was carried out. The filter had 500 mm inner diameter with 10 wand-type underdrains horizontally positioned at 60 mm intervals (Figure 1). Additional details of the wands can be found in Pujol et al. (2020).

The volumetric flow rate was measured using a flowmeter. Pressure values were obtained at 1.44 m head before the filter inlet and 1.29 m after the filter outlet using a pressure transmitter. Data were collected at 1 min interval. Inlet water came from the tertiary effluent of a wastewater treatment plant (see Solé-Torres et al. (2019a) for further details). It was assumed that the hydraulic performance of the filter in clean conditions corresponded to that occurring during the first 5 min after backwashing. The filter was assumed as being far from being clogged during this period and the results were interpreted as equivalent to those obtained when using clean water. Four experimental cases considering two media heights (20 and 30 cm) and two flow rates (6 and 12 m^3 h^{-1}) were analysed, each one obtained from averaging the first five minutes of a minimum of 33 cycles during 20 d.
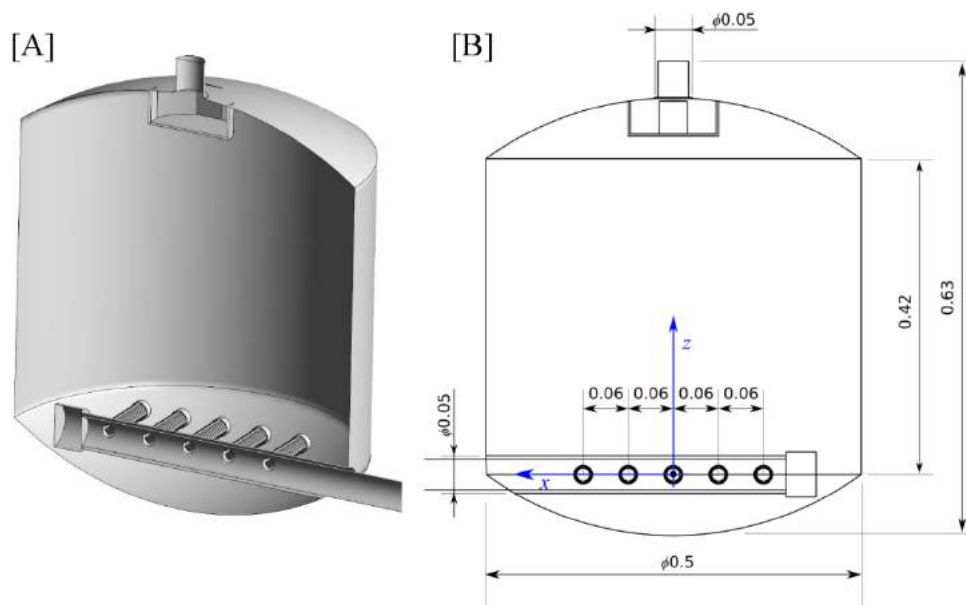
Figure 1. [A] Cross-sectional view of the sand media filter analysed (Lama FA1M type) that uses 10 wands. [B] Main dimensions of the filter (in m). The blue coordinate axes located at the symmetry plane are used in the analysis.

2.2. Model set-up

The numerical model employed was ANSYS-Fluent (version 19.1), a commercial CFD code that has successfully been applied in previous studies of sand media filters (Arbat et al., 2011; Bové et al., 2017). ANSYS-Fluent uses a finite volume method to solve the fluid flow governing equations in a discretised domain formed by small elements (i.e., the mesh) (ANSYS, 2018). The domain analysed was reduced to a half section of the filter (Figure 1) by taking advantage of symmetry. This substantially reduced the computational time without compromising the accuracy of the results. The sand medium was simulated as a porous region with fixed height. Therefore, the filter domain was divided into three main regions: 1) the water-only upper region that includes the inlet; 2) the porous lower region that contains the medium; 3) the water-only region at the filter exit (inner wands and exit pipe).

These regions had unstructured meshes created with ANSYS-Meshing software. The mesh was highly refined near the wands and, also, at both inlet and exit regions. Triangles were used to mesh all surfaces. A layer of five prisms was attached to solid walls that grows towards the fluid volume. Tetrahedrons were employed in the inner volume of all regions. The maximum characteristic size of surface elements (triangles) at the slots of the wands was 0.2 mm and the maximum characteristic size of volume elements (tetrahedrons) ranged from 2 mm at the exit pipe to 7 mm at the inner

zone of the sand media (far from wands and diffuser plate). The number of elements employed per region were: 1.3×10^6 elements for the water-only region at the top of the filter (H = 30 cm case), 11.6×10^6 elements in the sand media (H = 30 cm case), 5.0×10^6 elements for the water-only region at the exit of the filter. Thus, 18.0×10^6 elements were used to mesh the whole filter domain. A detailed mesh sensitivity study was carried out, as it will be explained in subsection 2.4.

Boundary conditions included a fixed pressure at the filter inlet and a fixed mass flow rate at filter outlet, both values were specified to fit with the experimental data. A symmetry boundary condition was applied to the plane of symmetry (x-z plane at y = 0). Finally, all solid walls were defined as non-slip surfaces with a surface roughness value equal to 0.1 mm to simulate slightly corroded steel surfaces.

The numerical algorithm used double precision. The fluid flow governing equations were the classical Navier-Stokes ones for incompressible flows under stationary conditions, with the SIMPLE calculation scheme for the pressure-velocity coupling and second order schemes for the spatial discretization of all variables. The flow in the porous media (region identified as sand) was modelled by adding a sink in the standard momentum equations. This term led to a pressure gradient ∇p in the porous media (Pa m-1) that followed:

$$-\nabla p = \frac{1}{\alpha}\mu v_i + C_2\frac{\rho}{2}|v|v_i \quad for \ i = x, y, z \quad (1)$$

where vi is the i-th component of the flow velocity (m s^{-1}), $|v|$ is the magnitude of the flow velocity (m $^{s-1}$), μ is the fluid viscosity (Pa s), ρ is the fluid density (kg m^{-3}), α is the permeability of the filtration medium (m^2) and C$_2$ is the inertial resistance factor (m^{-1}).

The turbulence model used was the standard k-ω that performs similarly to the realisable k-ε model, but it was expected to have a superior performance in low Reynolds number flows occurring inside the sand filter. For comparison, differences less than 0.5% were obtained for pressure drop values across the filters when using the realisable k-ε turbulence model instead of the standard k-ω one for the H = 30 cm, Q = 6 m^3 h^{-1} case. At both the inlet and outlet boundaries, the turbulent viscosity ratio was set to 10% and the turbulence intensity was set to 5%.

In all simulations the convergence criterion was set to 10^{-5} for the maximum value of the residuals of the variables, including those of the turbulence model. Once this value was achieved, the model ran for a minimum of 500 more iterations. Thus, the variation of the computed values as a function of the iteration was very small. For example, a variation of total pressure drop < 0.5 Pa was found between iteration m-100 and iteration m, m being the last iteration chosen to report the data.

2.3. Model calibration

Both viscous (1/α) and inertial (C$_2$) factors in Eq. (1) were fitted to minimise the difference between experimental data and simulations. The root mean square relative error RMSrE was the function to chosen to be minimised, where,

$$RMSrE = \sqrt{\frac{\sum_{i=1}^{n}\left(\frac{\Delta p_{m,i} - \Delta p_{e,i}}{\Delta p_{e,i}}\right)^2}{n}} \quad (2)$$

with $\Delta p_{e,i}$ the experimental pressure drop obtained in the i-th case (Pa), $\Delta p_{m,i}$ the pressure drop predicted by the model applying the conditions of the i-th case (Pa) and n (= 4) the number of cases experimentally analysed.

The numerical model was run for all the four conditions by varying the values of the viscous α^{-1} and inertial C$_2$ factors at intervals of $\Delta(\alpha^{-1})$ =104 m^{-2} and ΔC_2 =0.2×109 m^{-1}. The pressure drop of the external conduits was added to that simulated for the filter to obtain the $\Delta p_{m,i}$ value used in Eq. (2). These external head losses were required to properly compare with the experimental measurements $\Delta p_{e,i}$ with simulations since field manometers were located at a given distance from inlet and outlet of the filter (see section 2.1). The minimum *RMSrE* value, expressed in %, was attained with α^{-1} = 0 m^{-2} and C$_2$ = 5.6×109 m^{-1} (*RMSrE$_{min}$* < 1.9 %). Although the *RMSrE* value was < 1.9%, the maximum difference of pressure drop between measurement and simulation occurred for the H = 20 cm and Q = 12 m^3 h^{-1} case being equal to 2.3%. Note that simulations tended to underestimate the pressure drop when H = 20 cm and to overestimate it when H = 30 cm. However, the conclusions of the present work are not affected by the exact values employed in Eq. (1).

2.4. Mesh sensitiviy

A mesh sensitivity study was carried out with the values of both viscous and inertial factors determined above. The filter pressure drop when using different meshes was analysed. The coarse mesh was defined by increasing the main characteristic lengths of the finer mesh defined in section 2.2 by a factor of 3. The regular mesh applied an increment by a factor of 1.5 with respect to the finer mesh. Thus, the total number of elements of the course, regular and fine meshes were 2.7×10^6, and 8.9×10^6 and 18.0×10^6 elements, respectively. The difference of the pressure drop value between the fine and the regular mesh was < 0.35% and between the fine and the coarse mesh was < 0.57%. With these values, the

grid independence index (GCI^{21}_{fine}) was therefore < 0.1% with an order p = 7.2 (Célik et al., 2008). Therefore, the results presented below were grid independent.

3. Results and Discussion

3.1. Original filter

Unless otherwise stated, results discussed in this section correspond to the H = 30 cm and Q = 6 m³ h⁻¹ case. Nevertheless, the main findings pointed out below were also observed when analysing the other cases studied.

Here the pressure values inside the filter are first studied. Figure 2 shows the pressure profile in three vertical lines (y = 7, 14 and 21 cm) located at the y-z plane at x = 0 m. Pressure contours at the z < 18 cm are shown for clarity. Pressure values were almost equal for the three lines above z > 20 cm. This height corresponds to 100 mm below the sand surface (located at 30 cm). In this 100 mm layer, the flow behaved as if no underdrain existed, being very uniform throughout the entire cross-sectional area of the filter. Since the velocity of the flow in this region had almost a unique z-component, the pressure decreased linearly with depth following Eq. (1). Below z = 20 cm, the influence of the underdrain on the pressure drop increased with depth, being more intense when approaching the wand. Thus, following a vertical line above the underdrain (y = 7 cm in Figure 2), pressure decreased more rapidly than linear. This was a consequence of the increase in flow velocity within the sand media in the vicinity of the wand slots. By contrast, pressure slightly reduced with depth in a vertical profile far from the underdrain (e.g., y = 21 cm in Figure 2) since the flow velocity in that region was very low.
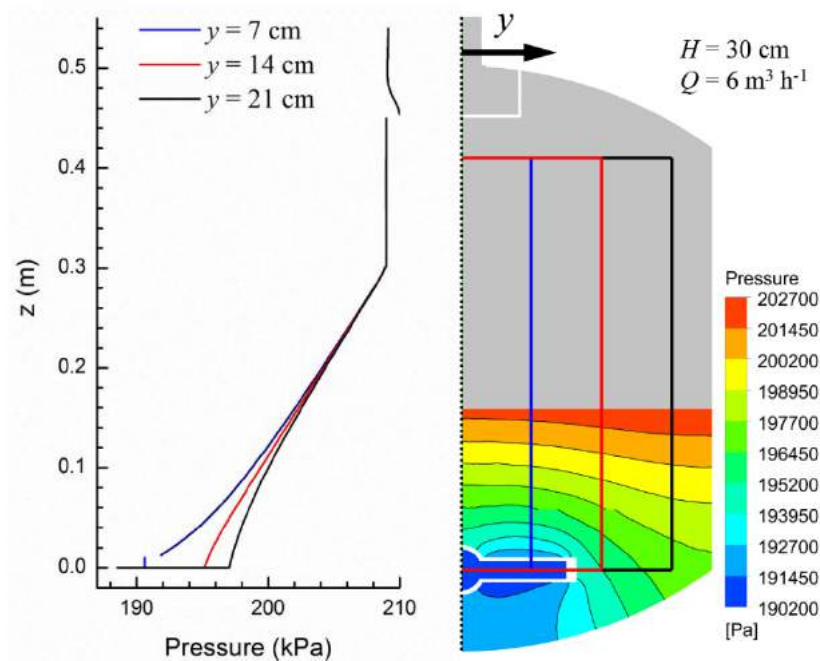
Figure 2. Pressure profiles (left) through the lines shown at right (plane located at x = 0 m). Pressure contours are only displayed at the bottom region for a better visualization. Case H = 30 cm, Q = 6 m³ h⁻¹.

The diffuser plate may have a strong effect on the filter. It substantially increased the pressure of the incoming flow (see Figure 2) and diverted the flow in different directions. When analysing the contours of vertical velocity in the horizontal plane at four different heights, flow primarily descended in the external region close to the walls, and in the central zone close to the sand top surface. Other regions showed upward flows indicating the existence of vortices in the water-only region. An ideal filter design should produce uniform downward flow values close to the top of the medium to avoid causing an uneven sand surface. A bumpy sand surface at the top of the medium may indicate the existence of preferential flow patterns, thereby reducing the hydraulic performance of the filter.

There were also differences in flow patterns at underdrain level. Velocities were maximum at the centre of the first wand (x = 0.12 m), almost doubling the values obtained at the centre wand (x = 0 m). This phenomenon can be clearly seen in Figure 3, where the contour velocities in the horizontal x-y plane (z = 0) are shown. Considering an individual wand, flow velocity increased approaching the connection with the central collector. This effect was more noticeable with wands located at both extreme positions (1 and 5). The maximum velocity of the water flow (= 1.76 m s⁻¹) found in

the filter occurred in the exit collector at the end of wand 1. Figure 3 indicates that this high velocity region is accompanied by a low velocity region with recirculating flow. This hydraulic behaviour (high velocity with an attached recirculation zone) was commonly observed in bending flows exiting surfaces with sharp edges. Although this effect was also observed with all wands, it was intensified at the exit of wand 1 since all the flow from downstream wands was added to the main collector. This increase in volumetric flow rate along the exit collector reduced the pressure along it, reaching a minimum value just after wand 1 (e.g., reduction of 1.8 kPa in the area averaged pressure of the exit pipe cross section from the position of wand 5 to that of wand 1). Once the flow exited the filter, pressure continuously dropped in the pipe following the standard friction losses term. Note from Figure 3 that the flow attains fully developed conditions at the end of the filter exit pipe.

Within the sand, the flow velocity was highly non-uniform when approaching the slots of the wands. This irregular distribution of the water flow reduces the effectiveness of the drainage process as pointed out by Mesquita et al. (2017). Upper slots (-90º < θ < 90º) were the main zones for circulating water. By contrast, slots at the below the wands weakly contributed to the total flow rate. A common feature to all slots is the fact that at both ends the velocities reached their maximum values. This is most likely because at these points there was a larger concentration of volumetric flow from regions not occupied by wands. This was more pronounced at the outer edge of the slot since the area not occupied by the underdrain was substantially larger, especially at wand 3. Comparing wands #1 and 3 showed an unbalanced functioning between them, with a higher contribution to the water flow for the first underdrain since it had to serve a larger sand region. Note that, in comparison with the water-only region, flow velocities within the sand region were, at least, one order of magnitude lower.
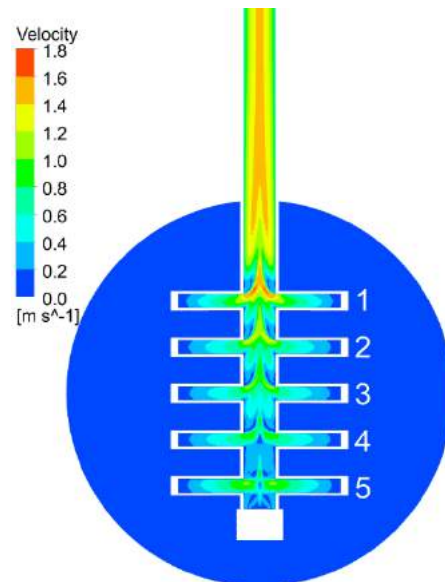
Figure 3. Velocity contours at z = 0. Wands are centred at x = 0.12 m (1), x = 0.06 m (2), x = 0 m (3), x = 0.06 m (4) and x = -0.12 m (5). Case H = 30 cm, Q = 6 m^3 h^{-1}.

The contribution to the volumetric flow rate for each one of the 24 slots per wand was also analysed. The central wand (3) behaved symmetrically, with a maximum flow rate found in the upper slots (= 0.0093 l s^{-1}). The minimum contribution to the flow rate was at angle θ = ±140.7º (= 0.0039 l s^{-1}). The minimum flow rate was not found at the lowermost slot (θ = ±163.6º) since the region served by it is higher than that for the neighbour slots. At wand 1, the behaviour was clearly asymmetrical, with higher volumetric flow rates through the slots facing the exit of filter (θ > 0º; maximum equal to 0.0122 l s^{-1} at θ = 16.4º) in comparison with those at θ < 0º. This was a consequence of the major available area of sand on that zone. For the very same reason, higher values of volumetric flow rates were found through the slots at θ < 0º (maximum equal to 0.0111 l s^{-1} at θ = -16.4º) in comparison with those at θ > 0º for wand 5. Differences between the minimum and the maximum values of flow rates through slots in a single wand were more than 100% for all underdrain positions.

The total amount of volumetric flow rate per wand, weighted by the total flow rate, is shown in Figure 4 for all the experimental configurations. For example, data for case Q = 6 m^3 h^{-1} and H = 30 cm were found by summing the individual contribution of each slot per wand multiplied by 2 (since there are two wands at each position) and divided by Q. The results, in percentage, clearly pointed out the hydraulics imbalance of the underdrain system. Wands at position 1 were responsible of ∼ 25% of water circulation, whereas those at the central position (x = 0 m) only contributed ∼ 17%. The existence of a predominant filtration zone within the media enhanced the probability of partial

clogging and slot damaging and increased the head loss of the entire system. Note that this preferential circulation for the first wand was more remarkable when the flow rate increased. This suggests that the exit collector has a significant influence on the observed imbalance.
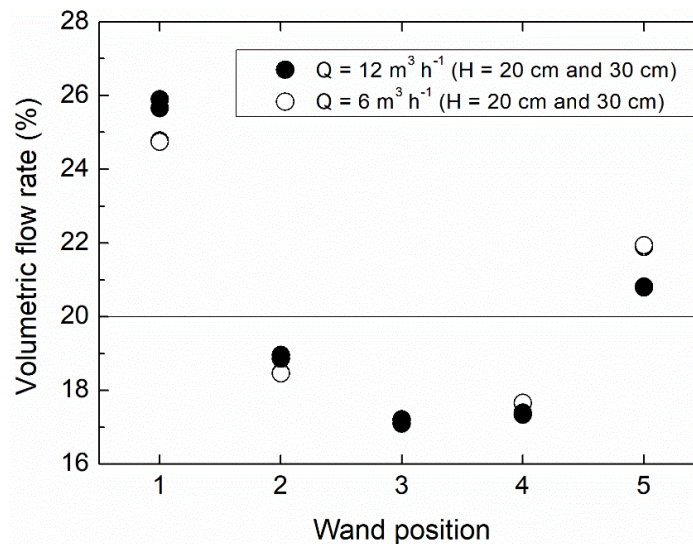
Figure 4. Volumetric flow rate through the wands with respect to the total one (in %) for all cases simulated. Two wands are taken into account at each position. A value of 20% is expected in a filter with perfectly equilibrated wands.

3.2. New filter designs

Ideal hydraulic behaviour should balance the volumetric flow rate through each underdrain, giving a value of 20% in Figure 4 for all wand locations. The purpose here is to propose new designs, that are easy to implement, to improve hydraulic behaviour in the underdrain. From the previous discussion of the results, the designs investigated are based on the following two hypotheses: 1) an equal horizontal area of media served per unit of underdrain would tend to balance the flow rate among wands; 2) an increase in the slot open area in those underdrains with less flow rates would also tend to balance the flow rate among wands. Therefore, two modifications of the original filter were investigated: 1) wands spatially distributed to cover the same horizontal area (equal area design); 2) longer wands at locations 2, 3 and 4 (longer wands design).

In comparison with the original case, the longer wands case enlarged the slot area by 20 mm in wands 2 and 4 and by 40 mm in wand 3. These were the three wand locations with volumetric flow rates less than the expected uniform value in the original filter. In contrast, the equal area design required a slight modification at the blind end of the exit collector, since it was too short to include a new location for wand 5.

Volumetric flow rate per wand position (expressed in % of the total flow) for the three filter designs is shown in Figure 55. For both $Q = 6$ m^3 h^{-1} and $Q = 12$ m^3 h^{-1} cases, the equal area design substantially reduced the differences of flow among wands. Wand 1 maintained the maximum contribution, although with a remarkable reduction (> 10%) in comparison with the original filter. Numerical values showed that the range between the maximum Q_{wmax} and the minimum Q_{wmin} flow rates per wand is < 3.3% ($Q = 6$ m^3 h^{-1}) and <5.5% ($Q = 12$ m^3 h^{-1}). By contrast, the original filter had ranges > 7.5% for all cases. The longer wands case, with a 20% more slot open area than the original configuration, also reduced the contribution of the first wand almost to the same level as in the equal area design. However, the high increase in the slot open area at the central wand (+50% in comparison with the original one) led to a contribution to the total flow rate above 20% in all cases with wand 4 now being the one that contributed least to the total flowrate. As already observed in the original case, almost no differences in the hydraulics behaviour of wands were observed between the 20 cm and 30 cm sand height cases.
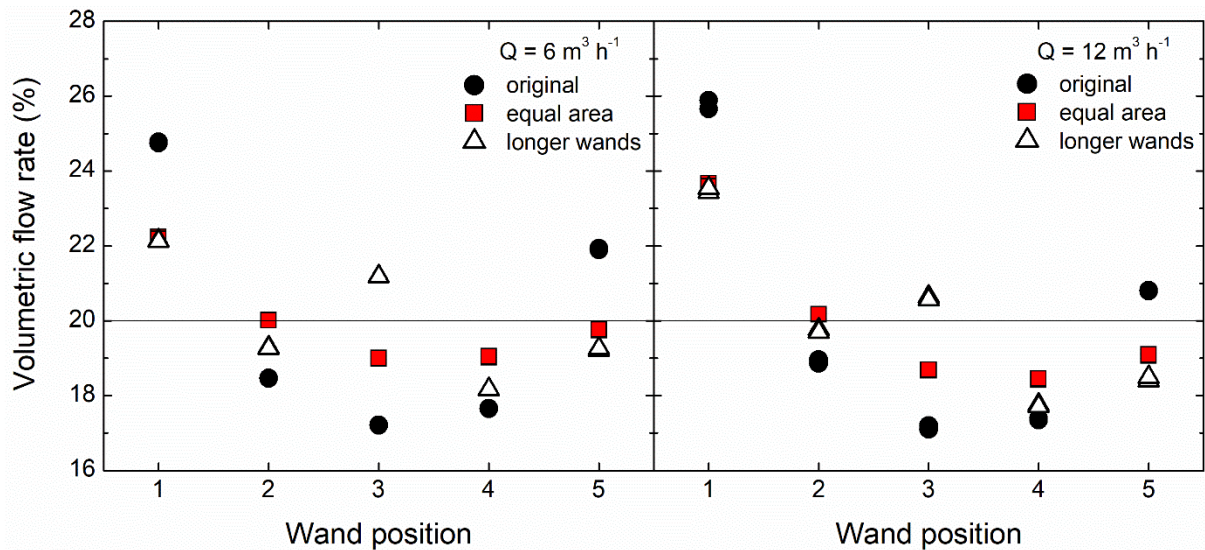
Figure 5. Volumetric flow rate through wands with respect to the total one (in %) for Q = 6 m^3 h^{-1} and 12 m^3 h^{-1} for original filter (closed circles), filter with equal horizontal area served per wand (red squares), filter with longer wands at the centre (blue triangles) (see Fig. 15). Two wands are taken into account at each position. A value of 20% is expected in a filter with perfectly equilibrated wands.

A better balance of the flow that circulates through wands reduced the pressure drop across the filter Δpf. The spatial redistribution of current wands in order to serve equal horizontal areas reduced the pressure drop up to 5.8% in comparison with the original design. The longer wands design also improved the pressure drop although with more moderate values (up to 5.2%). In the equal areas design, the effect of the underdrain on the pressure contours was substantially reduced. Thus, the redistribution of wands made the flow more uniform within the filter medium, diminishing the pressure drop. For the longer wands case, the zone of influence of the underdrain was similar to that from the original case. However, the pressure drop was reduced due to the increase in slot open area and, also, in the horizontal covered area ratio.

4. Conclusions

At the wand level, volumetric flow rates through upper slots (-90º < θ < 90º) were predicted to be more than 1.4 times that through lower slots (θ < -90º, θ > 180º). Maximum vs minimum water flow rate ratios through slots were higher than 2.2.

At the filter level, there is also an imbalance of water flow rate among wands. Wands located closest to the pipe exit were predicted to contribute the most to the total water flow rate. The highest water velocities in the whole filter were found at the exit of these wands, where the flow joints the mainstream of the collector pipe. In the original filter, wands at the centre appear to have the lowest volumetric flow rate. Differences between the maximum and the minimum volumetric flow rates per wand may reach values as high as 44% (6 m^3 h^{-1} cases) and 51% (12 m^3 h^{-1} cases) with respect to the lowest value (central wands).

A very simple and economic spatial redistribution of the original wands to serve equal horizontal areas per unit underdrain is predicted to considerably improve filter performance. With a coefficient of variation equal to 0, differences of volumetric flow rates among wands were reduced to 17% (6 m^3 h^{-1} cases) and 28% (12 m^3 h^{-1} cases). This improvement in the hydraulic equilibrium of wands implies a reduction in the filter pressure drop, being 5.7% smaller than in the original filter (6 m^3 h^{-1} case).

Modifications of the wands in order to increase the slot open area while maintaining the original spatial distribution may not be as beneficial as equalising the horizontal areas per wand. A case with 20% increase in slot open area, and 18% increase in the area covered ratio per wand did not improve the design with equal surface area served per wand. Therefore, the slot open area value and the area covered ratio coefficient may not be as critical as the coefficient of variation for determining the hydraulic performance of sand media filters with wand-type underdrains.

Acknowledgements

References

ANSYS, Inc., 2018. *ANSYS Fluent User's Guide*. Canonsburg, PA, USA: ANSYS Inc.

Arbat, G., T. Pujol, J. Puig-Bargués, M. Duran-Ros, J. Barragán, L. Montoro, F. Ramírez de Cartagena, 2011. Using computational fluid dynamics to predict head losses in the auxiliary elements of a microirrigation sand filter. Transactions of the ASABE. 54(4), 1367 -1376. https://doi.org/10.13031/2013.39038

Arbat, G., T. Pujol, J. Puig-Bargués, M. Duran-Ros, L. Montoro, J. Barragán, J., F. Ramírez de Cartagena, 2013. An experimental and analytical study to analyze hydraulic behavior of nozzle-type underdrains in porous media filters. Agricultural Water Management. 126, 64-74. https://doi.org/10.1016/j.agwat.2013.05.004

Bové, J., G. Arbat, T. Pujol, M. Duran-Ros, F. Ramírez de Cartagena, J. Velayos, J. Puig-Bargués, 2015. Reducing energy requirements for sand filtration in microirrigation: improving the underdrain and packing. Biosystems Engineering. 140, 67–78. https://doi.org/10.1016/j.biosystemseng.2015.09.008

Bové, J., J. Puig-Bargués, G. Arbat, M. Duran-Ros, T. Pujol, J. Pujol, F. Ramírez de Cartagena, 2017. Development of a new underdrain for improving the efficiency of microirrigation sand media filters. Agricultural Water Management. 179, 296-305. https://doi.org/10.1016/j.agwat.2016.06.031

Burt, C.M., 2010. Hydraulics of Commercial Sand Media Filter Tanks used for Agricultural Drip Irrigation. Irrigation Training & Research Center, California Polytechnic State University, San Luis Obispo, California.

Célik, I.B., U. Ghia, C.J. Freitas, H. Coleman, P.E. Raad, P.E., 2008. Procedure for estimation and reporting of uncertainty due to discretization in CFD applications. Journal of Fluids Engineering. 130 (7), 078001. https://doi.org/10.1115/1.2960953

Enciso-Medina, J., W.L. Multer, F.R. Lamm, 2011. Management, maintenance and water quality effects on the long-term performance of subsurface drip irrigation systems. Applied Engineering.in Agriculture. 27 (6), 969–978. https://doi.org/10.13031/2013.40633

Mesquita, M., F.P. de Deus, R. Testezlaf, R., L.M. da Rosa, A.V. Diotto, 2019. Design and hydrodynamic performance testing of a new pressure sand filter diffuser plate using numerical simulation. Biosystems Engineering. 183, 58-69. https://doi.org/10.1016/j.biosystemseng.2019.04.015

Mesquita, M., R. Testezlaf, J. Ramirez, 2012. The effect of media bed characteristics and internal auxiliary elements on sand filter head loss. Agricultural Water Management.115, 178-185. https://doi.org/10.1016/j.agwat.2012.09.003

Mesquita, M., R. Testezlaf, F.P. de Deus, F.P., L.M. da Rosa, 2017. Characterization of flow lines generated by pressurized sand filter underdrains. Chemical Engineering Transactions. 58, 715-720. https://doi.org/10.3303/CET1758120

Pujol, T., G. Arbat, J. Bové, J. Puig-Bargués, M. Duran-Ros, J. Velayos, F. Ramírez de Cartagena, 2016. Effects of the underdrain design on the pressure drop in sand filters. Biosystems Engineering. 150, 1-9. https://doi.org/10.1016/j.biosystemseng.2016.07.005

Pujol, T. J. Puig-Bargués, G. Arbat, M. Duran-Ros, C. Solé-Torres, J. Pujol, F. Ramírez de Cartagena, 2020. Effect of wand-type underdrains on the hydraulic performance of pressurised sand media filters. Biosystems Engineering. 192, 176-187. https://doi.org/10.1016/j.biosystemseng.2020.01.015

Solé-Torres, C., J. Puig-Bargués, M. Duran-Ros, G. Arbat, J. Pujol, F. Ramírez de Cartagena, 2019a. Effect of underdrain design, media height and filtration velocity on the performance of microirrigation sand filters using reclaimed effluents. Biosystems Engineering. 187, 292-304. https://doi.org/10.1016/j.biosystemseng.2019.09.012

Solé-Torres, C. J. Puig-Bargués, M. Duran-Ros, G. Arbat, J. Pujol, F. Ramírez de Cartagena, 2019b. Effect of different sand filter underdrain designs on emitter clogging using reclaimed effluents. Agricultural Water Management. 223, 105683. https://doi.org/10.1016/j.agwat.2019.105683

Trooien, T.P., Hills, D.J., 2007. Application of biological effluent. In *Microirrigation for Crop Production. Design, Operation, and Management*. Elsevier, Amsterdam, Eds., F.R. Lamm, J.E. Ayars, J.E. and F.S. Nakayama, 329–356.

Characterization of Floating Waste in the Vega Baja del Segura District

Carmen Rocamora [a,*], Herminia Puerto [a], Ricardo Abadía [a], Margarita Brugarolas [a], Laura Martínez-Carrasco[a], José Cordero [b]

[a] Centro de Investigación e Innovación Agroalimentaria y Agroambiental (CIAGRO-UMH), Miguel Hernandez University, Ctra de Beniel, km 3.2, 03312 Orihuela, Alicante, Spain

[b] Department of Agro-Environmental Economics, Cartography Engineering and Graphic Expression in Engineering, Miguel Hernandez University, Ctra de Beniel, km 3.2, 03312 Orihuela, Alicante, Spain

* Corresponding author. Email: rocamora@umh.es

Abstract

The region of Vega Baja del Segura is located southeast of Spain, in Alicante province, right at the mouth of the Segura river. The traditional irrigation system consists of a complex net of channels. Small dams located on the river bed divert water to irrigation channels which distribute water to the fields. The excess irrigation water is collected in drainage channels, which in turn are used as irrigation channels when they reach a sufficient height over the fields. The whole region is a great alluvial plain of about 23,000 hectares with a slope of less than 1 per 10000 which makes drainage difficult. Floating solid waste invades the entire water transport system, affecting the water quality and the water transport through the watercourses, and reaching the coastal waters. Great amounts of waste accumulate on dams and retention elements along the river, and on sluices and siphons in channels. The aim of this paper is to characterize the floating residues stacked on the whole system.

Keywords: traditional irrigation, floating debris, litter

1. Introduction

The Vega Baja region is located on the lower course and floodplain of the Segura River in southeastern Spain. It encloses the Vega Baja "huerta", one of the six traditional *huerta* artificial landscapes in Europe. The irrigation infrastructure of this centuries old *huerta* ecosystem is formed by an extensive network of irrigation channels and drainage ditches characterized by scarce slopes and a reutilization system of drainage water, "dead waters", which allow for irrigation of land at lower altitudes towards the river mouth, with drainage waters from upper areas.

Debris from giant reed (*Arundo donax,* L.) cuttings accumulate at certain points of the riverbed, forming a characteristic reed and mud build-up that hinders the natural river discharge. At these points, plant residues favor the accumulation of other garbage, mainly plastics, expanding their negative effects.

Recently, there is an increasing number of papers that have focused on the evaluation of plastic debris in rivers (Gasperi et al., 2014; Lechner et al. 2014; Morritt et al., 2014; Guerranti et al., 2014; Sadri et al., 2014). Jang et al. (2015) identified main points of accumulation of floating debris in the Nakdong River Basin (South Korea), concluding that accumulations closest to the mouth are at significant risk of reaching the ocean if not properly collected. Suaria et al. (2015) reported that natural debris were more abundant than artificial litter in most surveyed locations on the Black Sea, probably due to the proximity of the Danube delta.

Most of the plastic waste found in the seas and oceans originates from the mainland and is transported to the sea by rivers (Andrady, 2011; Dris et al., 2015). In marine debris reported worldwide, plastics are the most abundant waste per number of items (Isangedighi et al., 2018).

The problem of plastic waste and vegetal debris accumulation has been described in natural environments such as rivers, lakes, seas, and oceans, but little information is available regarding the effect of this floating litter on artificial surface irrigation infrastructures.

Floating items of a certain size in the river cause trouble in irrigation infrastructures such as obstruction of the irrigation channel intakes. If these floating debris accumulations make it through the irrigation channels, they hinder the farmers' water management and impede ordinary irrigation operations.

At the irrigation channel level, the irrigators' communities that own the irrigation channels are responsible for their maintenance and they have the duty to keep the channels clean and clear. Since drainage channels discharge drainage waters into the river, the river authority can compel the irrigators' communities to install retention elements and can impose sanctions if waste reaches the river through these drainage channels.

There are numerous references in the local press to the situation of the river and the irrigation and drainage network. Public opinion is sensitized to the subject and sometimes holds the irrigators' communities socially accountable for the incidence of floating debris. Thus, floating debris that invade the entire water transport system on the Segura River are causing environmental, social, and economic problems whose solution requires a multidisciplinary approach. Although

the presence of waste in the river and channels is a years-long problem, it is only recently that it has been subject to public debate.

The objective of this paper is to characterize the floating residues found in the final section of the Segura River and assess their effect on the traditional *huerta* irrigation system. A methodology is proposed as a first approach to characterize the floating debris by means of aerial photography and manual recording and classification of debris extracted in the irrigation and drainage channels. This information will help assess the proper actions that need to be taken in order to eliminate floating litter build-up in the irrigation and drainage channels and the population that should be addressed by these actions.

2. Materials and Methods

2.1. Description of the Studied Area and Location of Litter Accumulation Areas

The region of Vega Baja del Segura is located in southeastern Spain, in Alicante province, along the lower course of the Segura River. The whole region is a great alluvial plain of 42,739 hectares, of which 38,085 are cultivated in irrigated land and 4654 ha in dry land. The surface under traditional irrigation reaches 23,391 hectares, which is 55% of the agricultural area of the entire region (Abadía et al., 2018).

The traditional irrigation system consists of a complex system of irrigation and drainage channels that take water directly from the river Segura through small dams located on the river bed, called Azudes, which divert water to irrigation channels called Acequias, which are responsible for distributing water to the fields. The excess irrigation water is collected in drainage ditches, called Azarbes, which in turn are used as irrigation channels when they reach a sufficient height over the fields. The low slope of the plain, less than 1 per 10,000, hinders greatly the land's natural drainage. In the decade of 1990, channeling works were carried out in several stretches of the river throughout the area. Near the mouth, the Segura River was channeled to the south of the original stretch, but the last section of the old river was maintained to facilitate the drainage of the lands on the north margin of the river.

For the purpose of this work, we selected 6 litter accumulation points along the river where floating retentions occur, either because of the presence of dams, or because of the installation of retention elements (Figure 1). Two accumulation points were selected on the irrigation infrastructure, one located on an irrigation channel (ID6) and the other one located in a drainage ditch (ID7). In both cases, there was a syphon in the intersection with other channel where waste accumulates. Finally, the floating screen at the mouth of the river was chosen as the last accumulation point (ID8).
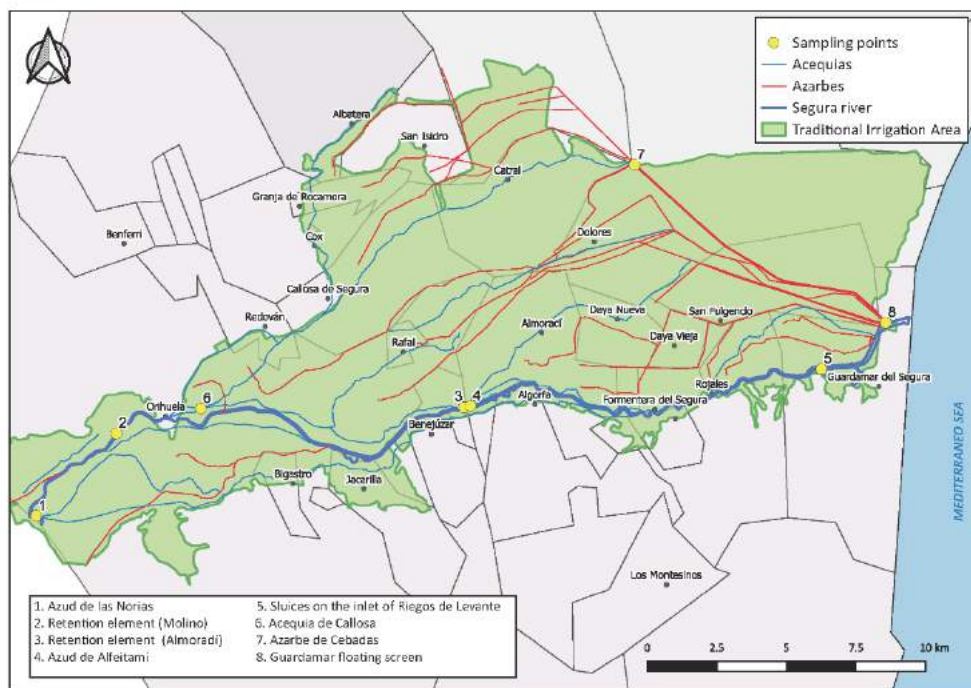

Figure 1. Traditional irrigation area along the lower course of the Segura River. The names correspond to the municipalities in the area. Yellow dots correspond to the sampling points locations as described in the text. Acequias correspond to irrigation channels while Azarbes correspond to drainage ditches.

2.2. Sampling Methodology and Measurements by Image Analysis

The surface area of the river or the channels occupied by floating debris at the 8 selected points was assessed by means of aerial overhead photography. The photographs were taken from a sufficient height for the spot of floating debris to be captured in a single image. In each image, a ranging rod was photographed along the debris for scale determination. Other images were captured from lower heights to obtain better images for the waste characterization.

Measurements were taken on 22 January, 25 February, 8 April, 6 May, and 1 July 2019.

Zenith images were taken using a drone. Drone type was a DJI MAVIC PRO with a weight of 743 g, three-axis stabilization, inclination of −90° to + 30°, and rotation of 0° or 90° (horizontal and vertical). The camera had a 1/2.3″ CMOS sensor; 12.35 effective Mpixels (total: 12.71 Mpixels), and a 2 6 mm lens (35 mm format equivalent) f/2.2 FOV 78.8°.

ImageJ software, based in the software NIH Image for Mackintosh, developed by National Institutes of Health of the United States (https://imagej.net (accessed on 4 February 2019), was used for image analysis.

The scale factor for each photograph was determined with the help of the measure of the ranging rod. The photo scale was entered using the Analyze > Set scale option. The contour of the floating debris was determined by a freehand selection and the surface occupied by the Analyze > Measure option.

For the characterization of floating waste, we defined 11 categories and subdivided them into groups (Table 1). The number of floating residues of each group was manually counted. We used "multipoint" function of ImageJ software to count the elements that are thus marked with correlative numbers. A different counter was used for each category.

Table 1. Waste categories and classes.

	Category	Classes
1	Vegetal material	Reeds, branches, algae, fruits, and vegetables
2	Dead animals	Wild animals, domestic animals, livestock
3	Beverage containers	Water bottles, soft drinks bottles, water cans, soda cans
4	Plastic household containers	Oil bottles, plastic cups and plates, food containers, empty bags, plastic sheeting, full garbage bags, personal hygiene products containers, cleaning products containers
5	Other household containers	Tetrabricks, canned cans, aerosols
6	Industrial waste	Packaging of motor oil and automobile products, rubber, manufactured wood
7	Other materials	Textiles, footwear, balls, toys, paper, and cardboard
8	Others	Medication boxes and blisters, lamps, gas bottles, etc.
9	Glass containers	Glass bottles of beer, wine, liquor or soft drinks, food jars, cosmetic jars
10	Agricultural containers	Cans and bottles of phytosanitary products, fertilizer bags and boxes
11	Other agricultural waste	Transplant trays, drip irrigation pipes

2.3. Manual Counting of Litter

Aerial photography makes it possible to measure the surface occupied by residues at each selected accumulation point and to count the objects of each type that can be distinguished in the surface layer. It is necessary to contrast these results and relate them to the volume of floats and their mass, as well as to make a count of all the retained objects, not only those visible in the aerial photography.

A mechanical extraction of waste was performed in each channel. The extraction for calibration was performed by means of construction machinery in ID6 and with manual means such as nets and hooks in ID7. The waste was spread on the floor, counted, and sorted. Objects less than 3 cm were not considered as they are not retained by extraction means. Manual counting was compared to image analysis counting, performed as described above.

Volume of reeds and non-vegetal waste were estimated from the measured area occupied by reeds and other waste, respectively. Data obtained in the extraction in ID6 was used for these estimations, except for the sampling point ID7, located at a drainage ditch, where only non-vegetal waste was found, and data obtained in the extraction at the same point were used for the estimations of volume.

Although reeds are very abundant on the riverbank, they are not frequently found in channels. However, after episodes of heavy rain, the reeds can go through the intake of the irrigation channels. In April 2019, a heavy rainfall occurred in Orihuela and, as a result, a large number of reeds accumulated at point ID6 in the following weeks. This circumstance allowed us to compare the area of reeds measured by image analysis with the volume and weight of reeds measured in the extraction made in May.

2.4. Classification of Litter

Waste categories were defined on the basis of the most likely material, use, and origin. For this purpose, the type of waste observed in the previous visits to the accumulation points was taken into account, as well as classifications referenced in scientific publications. The list published in Guidance on Monitoring of Marine Litter in European Seas (European Commission, 2013) helped in defining the waste classes. However, many items in this list correspond to articles found at the seashore that do not come from river channels, such as fishing gear and beach items. The document Floating Macro Litter in European Rivers—Top Items (González-Fernández et al., 2018) presents lists of the most frequently found items in European rivers, particularly in the rivers of the Mediterranean basin.

A χ^2 test was performed to assess if there were differences in the proportions of the waste classes found in ID6 and ID7, both on a volume and weight bases. This kind of test was also applied for the results of the repeated measures of waste classes in all the sampling points located in the river and channels.

3. Results and Discussion

Table 2 shows the weights and volumes of different categories measured after classifying the waste extracted in points ID6 and ID7.

Table 2. Weights and volumes of waste extracted for calibration at sampling points ID6 (syphon at Acequia de Callosa) and ID7 (syphon at Azarbe de Cebadas).

	Category	ID6		ID7	
		Volume (m^3)	Weight (kg)	Volume (m^3)	Weight (kg)
1	Vegetal material	7.50	3000 [a]	0.02	0.05
2	Dead animals	0.2 [b]	50 [b]	-	-
3	Beverage containers	2.30	41.41	0.23	7.41
4-8	Plastic household containers, Other household containers, Industrial waste, Other material, Others	1.00	79.76	0.06	7.20
9	Glass containers	0.60	89.80	0.04	15.50
10	Agricultural containers	0.50	17.21	0.05	4.54
11	Other agricultural waste	1.00	14.52	0.10	10.28

[a]: approximate weight [b]: estimated values

Four dead animals (category 2) were found at ID6. Three of them were wild animals whose habitat is the river (a duck and a carp) or that could accidentally fall into the channel (a hedgehog). However, a lamb was also found, which can be considered a residue of livestock activity. These animals were not visible on the zenith images at ID6. On the contrary, several dead animals were seen on images captured at the Guardamar floating screen (ID8). Waste extraction at this point was not viable. However, these animals were apparently goats, that is, waste originating from livestock farming.

A large number of bottles and water drums (category 3) were counted, which occupied between 41% and 48% of the total volume of non-vegetable waste, and a weight close to 15%. This waste was separated from other household waste because the use of this type of packaging is universal, cannot be identified with any segment of the population, and cannot be associated with an economic activity.

The weights and volumes of objects in categories 4 to 8 were measured together. It is in all cases domestic waste. Even products classified as industrial waste were cans of motor products commonly used by the population and they do not necessarily come from a workshop. This set of categories represented between 13 and 15% of the total volume of non-vegetal waste.

Agricultural waste corresponds to categories 10 and 11, basically consisting of containers of phytosanitary products and transplant trays. They represented approximately 30% of total non-vegetal waste volume.

Glass containers, mainly 1 L beer bottles, represented approximately 10% of the total volume of non-agricultural waste.

Items of category 7 were found at ID6. Among them there was a significant number of balls.

Other residues were found, such as medication boxes and blisters, syringes, lamps, lighters, and a 1.8 kg camping butane bottle.

The results of the χ^2 test applied to the distribution of floats extracted in ID6 and ID7, on a weight basis (Table 2), showed that there were very significant differences (p < 0.01) in the proportions of the extracted items between the samples obtained in both places. The same analysis performed on a volume basis showed no statistically significant differences.

Table 3. Results of count of items of different categories in accumulation points ID6 (syphon at Acequia de Callosa) and ID7 (syphon at Azarbe de Cebadas) by image analysis and after extraction of waste.

	Category	ID6		ID7	
		Image analysis	Extraction	Image analysis	Extraction
1	Vegetal material	a	a	a	a
2	Dead animals	0	4	0	0
3	Beverage containers	238	646	67	112
4	Plastic household containers	53	326	18	31
5	Other household containers	6	37	5	15
6	Industrial waste	0	15	0	4
7	Other materials	8	107	0	4
8	Others	0	47	0	3
9	Glass containers	11	184	11	31
10	Agricultural containers	17	50	7	11
11	Other agricultural waste	27	b	25	b

[a] the quantity and characteristics of the vegetal material found, made up entirely of reeds, makes it impossible to count [b] in the extraction the transplant trays are broken into innumerable fragments; their weight and volume have been recorded.

The same χ^2 analysis was applied to the proportion of objects in each category counted in ID6 and ID7 (Table 3). Again, in this case, the differences between the proportions of the different classes showed statistically very significant differences (p < 0.01).

Images obtained at the selected sampling points throughout the study were analyzed. Table 4 shows the results of the counts by image analysis of elements in each category at different points and dates.

According to the number of elements of each class, the most numerous class of waste is made up of 1.5 to 2 L bottles and 5 to 8 L drums of bottled water and soft drink cans (category 3), which represent on average 74.2% of the total number of elements counted. These items belong to the same category stated in Table 2, but they are separated in two columns since they differ significantly in size and also in the number of objects counted. The vast majority of items in this category were 1.5 to 2 L bottles. The number of containers, plastic or not, of purely domestic origin (food, personal care, and cleaning products containers) represented 14.9%. The number of agricultural waste items, that is, bottles and cans of phytosanitary products, represented only 3.8% of elements counted at the sampling points.

Transplant trays appeared broken into a large number of fragments. In the counts, both whole trays and pieces of sufficient size to be identified were added. The number of tray pieces counted cannot be considered since the surface was not measured and the equivalent number of whole trays present cannot be known. For these reasons, the percentages of items reported above were calculated over a total of 1598 items.

For the analysis of the proportions of items of each category counted at different sampling sites (Table 4), we applied a Shapiro–Wilk test that showed that the data were not normally distributed. Therefore, we applied χ^2, a non-parametric test. We pooled together the river locations, ID1 to ID5, and the irrigation infrastructure locations, ID6 and ID7, obtaining the average of all sampling sites and dates. The χ^2 test result showed us that there were no differences (p = 0.94) in the proportion of residues classes found in the river and in the irrigation channels. However, the number of counts was not enough to draw conclusions in this regard.

Throughout the study, large accumulations of reeds were observed on the shore at various points in the river. Occasionally the river authority cuts reeds, which are left aside on the shore. When heavy rain occurs and the water level rises, these reeds are carried away by the river flow. Part of them reach a retention boom located downstream, but others are held in meanders or other points in the river. In the final section of the river, downstream from Rojales, which

was widened in the 1990s, the riverbed is very wide, 60 to 70 m, and a large part is overgrown with reeds and tamarisks. In this stretch, large accumulations of reeds have also been observed, on which other residues are piled up, especially plastics. It is therefore difficult to estimate the total volume of debris that is transported to the sea through the river.

Unfortunately, we also verified the presence of large appliances in the riverbed, such as a TV set and a refrigerator, as well as pieces of furniture, which shows that for some people the river is nothing but a landfill.

Table 4. Result of counting by image analysis of elements at different points and dates.

	Date	Water plastic bottles (1.5 to 2 L)	Water plastic drums (5 to 8 L)	Personal care & cleaning products containers	Cans, tetrabricks & other household containers	Full garbage bags	Other materials (balls, shoes, toys)	Glass bottles	Cans and bottles of phytosanitary poducts	Transplant trays & fragments
ID1	25/02/19	14	2	8	3	0	5	2	0	0
ID1	06/05/19	8	1	3	0	0	1	0	0	4
ID1	01/07/19	7	1	2	0	0	1	1	1	0
ID2	25/02/19	42	4	4	7	0	1	4	6	2
ID2	06/05/19	51	4	2	0	2	0	0	1	5
ID3	08/04/19	109	0	18	0	0	1	6	2	5
ID4	08/04/19	35	2	9	15	4	2	6	5	10
ID4	06/05/19	10	6	3	0	0	1	7	3	0
ID5	06/05/19	63	7	4	3	0	1	1	6	9
ID6	25/02/19	56	0	9	2	0	2	0	2	4
ID6	06/05/19	214	7	10	3	1	8	12	8	22
ID6	24/05/19	112	11	13	10	0	3	10	3	25
ID6	01/07/19	36	0	3	10	0	6	3	0	0
ID7	25/02/19	191	12	6	13	0	1	0	5	18
ID7	08/04/19	39	2	9	15	4	2	6	6	17
ID7	06/05/19	2	0	0	1	0	0	0	1	1
ID7	01/07/19	65	7	10	9	2	0	10	6	16
ID7	08/07/19	58	8	9	11	1	0	11	5	20
Sum counted objects		1112	74	122	102	14	35	79	60	158

4. Discussion

The results show that the volume of reeds is the main component of floating debris on the riverbed. Estimated weight of plant debris on these sampling points was over 98% of total debris weight. These numbers are similar to the results reported by Gasperi et al (2014) for the Seine River, where plant debris represented between 92.0% and 99.1% of total debris by weight.

Floating debris found in drainage ditches are almost exclusively anthropogenic waste. This is favored by the drainage ditches running parallel to roads and pathways and their lower altitude, this makes it easy for any waste thrown on the road to be windblown to the ditch.

The two locations of the irrigation infrastructure, the ID6 and ID7, that were particularly prone to floating waste accumulation are syphons, that is, a U section where irrigation water flows downwards, filling the whole section of the syphon, and then upwards to the following reach of the channel. The floating waste is retained at the upstream side of the syphon as long as the water keeps flowing. When the irrigation shift changes, the water level in the channel reduces gradually and the floating waste is carried into the lower part of the U section. When the new irrigation shift resumes, the waste flows downstream to the following accumulation point. This irrigation dynamics, characteristic of surface

irrigation districts, makes it difficult to assess the effects of waste accumulation on the irrigation infrastructure. Another reason is that, as soon as the person in charge of the irrigation channel realizes that the accumulation of waste reduces the channel discharge, they proceed to the extraction, and thus it is not easy to make an estimate of the reduction in flow caused by the floats and even less a correlation between the volume of floats and the flow of the ditch.

The dynamics of the reed accumulation in the river depends on the type of barrier. Floating booms across the riverbed generate increasing accumulations over time that need to be periodically cleaned. This is the case for ID2, ID3, and ID8. On the other hand, accumulations of waste in weirs and dams are sensitive to river flooding, in which the water drags much of the waste downstream, such as in ID1 and ID4.

The Guardamar floating screen, ID8, is a safe defense to prevent the arrival of plastics into the sea because the retention of floating solids increases through time and is not reduced by heavy rainfall episodes.

The fact that reeds are the biggest part of the floating debris causes no problems to the environment. However, the presence of plastics has important consequences in hindering the irrigation water management at the drainage ditches and the accumulation of plastics at the river mouth poses a hazard to maritime life if they are not periodically removed.

Between 41% and 48% of the total volume of non-vegetable waste was made up by bottles and water drums. This waste can come from household garbage, farmers, walkers, sportspeople, workers, or anyone who discards a bottle of water. Therefore, it cannot be associated with a certain type of human activity, and in particular it cannot be associated with agricultural activities.

Though the layperson's perception is that most of the litter comes from agricultural activity, the results obtained in our area closely resemble those found in South Korea by Jang et al. (2015). They found that 70% of the floating debris consisted of plant debris, 23.4% were household waste, and only 4.5% had an agricultural origin, while a proportion of 90% of natural debris and only 5% of plastic debris in the Three Gorges Reservoir Area (China) was reported by Wan et al. (2018).

Since the Vega Baja is largely an agricultural area, it could be expected that the waste from agricultural activity would be predominant. On the contrary, the number of agricultural waste items, that is, bottles and cans of phytosanitary products, represented only 3% of elements counted at the sampling points.

It is striking that the number of containers of domestic origin of food, personal care, and cleaning products containers represented 17% of the number of items counted in the extractions. This fact, along with the presence in the riverbed of large appliances, such as a TV set and a refrigerator, as well as pieces of furniture, showed that some inhabitants take the river as a sewer.

5. Conclusions

The estimate of the volume of floating debris in certain sections of the river or channels by using aerial photography is reliable, fast, and economical. It allows for making decisions about the need for cleaning or taking the appropriate measures to reduce them. The method also allows for the characterization of floats, although it would be convenient to develop algorithms that eliminate the subjective component in the object counting process.

The results show that the floating waste found along the Segura River and the irrigation channels has diverse origins, predominantly vegetal waste from the banks of the river itself, such as reeds, as well as various types of waste among which plastic predominates.

Most of the anthropogenic waste found in the river and channels is of domestic origin. The agricultural activity is responsible for a small part of the waste present in the river and in the channels.

The responsibility for keeping the river and channels clear generates conflicts between administrations and irrigators' communities, which are detrimental to good water management.

The problems caused by floating waste have important consequences for the region's economy, from an agronomic, environmental, and touristic point of view. It is necessary to take measures to alleviate these problems.

References

Abadía Sánchez, R.; Puerto Molina, H.; Rocamora Osorio, C.; Hernández García, F.; Melián Navarro, A.; Sánchez Zapata, J.A.; Botella Robles, F.; Giménez Casalduero, A. et al., 2018. Modernización de los regadíos tradicionales la Vega Baja del Segura. In Agroalimentación, Agua y Sostenibilidad; Melgarejo, J., Abadía, R., Eds.; Ayuntamiento de Orihuela, Universidad de Alicante: Alicante, Spain, 2018; pp. 141–168, ISBN 978-84-13-02014-3.

Andrady, A.L., 2011. Microplastics in the Marine Environment. Mar. Pollut. Bull. 62, 1596–1605, doi:10.1016/j.marpolbul.2011.05.030.

Dris, R.; Gasperi, J.; Rocher, V.; Saad, M.; Renault, N.; Tassin, B. 2015. Microplastic Contamination in an Urban Area: A Case Study in Greater Paris. Environ. Chem. 2015, 12, 592–599, doi:10.1071/EN14167.

European Commission; Joint Research Centre; Institute for Environment and Sustainability; MSFD Technical Subgroup on Marine Litter. 2013. Guidance on Monitoring of Marine Litter in European Seas; Publications Office: Luxembourg, ISBN 978-92-79-32709-4.

Gasperi, J.; Dris, R.; Bonin, T.; Rocher, V.; Tassin, B. 2014. Assessment of Floating Plastic Debris in Surface Water along the Seine River. Environ. Pollut. 195, 163–166, doi:10.1016/j.envpol.2014.09.001.

González-Fernández, D.; Hanke, G.; the RiLON Network. 2018. Floating Macro Litter in European Rivers—Top. Items; Publications Office of the European Union: Luxembourg.

Guerranti, C.; Cannas, S.; Scopetani, C.; Fastelli, P.; Cincinelli, A.; Renzi, M. 2017. Plastic Litter in Aquatic Environments of Maremma Regional Park (Tyrrhenian Sea, Italy): Contribution by the Ombrone River and Levels in Marine Sediments. Mar. Pollut. Bull. 117, 366–370, doi:10.1016/j.marpolbul.2017.02.021.

Isangedighi, I.; David, G.; Obot, O. 2018. Plastic Waste in the Aquatic Environment: Impacts and Management. Environment 2, 1–31.

Jang, S.-W.; Kim, D.-H.; Chung, Y.-H.; Yoon, H.-J. 2015. A Study on Exploring Accumulation Zone and Composition Investigation of Floating Debris in Nakdong River Basin. J. Korean Assoc. Geogr. Inf. Stud. 18, doi:10.11108/kagis.2015.18.2.045.

Lechner, A.; Keckeis, H.; Lumesberger-Loisl, F.; Zens, B.; Krusch, R.; Tritthart, M.; Glas, M.; Schludermann, E. 2014. The Danube so Colourful: A Potpourri of Plastic Litter Outnumbers Fish Larvae in Europe's Second Largest River. Environ. Pollut. 188, 177–181, doi:10.1016/j.envpol.2014.02.006.

Morritt, D.; Stefanoudis, P.V.; Pearce, D.; Crimmen, O.A.; Clark, P.F. 2014. Plastic in the Thames: A River Runs through It. Mar. Pollut. Bull. 78, 196–200, doi:10.1016/j.marpolbul.2013.10.035.

Sadri, S.S.; Thompson, R.C. 2014. On the Quantity and Composition of Floating Plastic Debris Entering and Leaving the Tamar Estuary, Southwest England. Mar. Pollut. Bull. 81, 55–60, doi:10.1016/j.marpolbul.2014.02.020.

Suaria, G.; Melinte-Dobrinescu, M.C.; Ion, G.; Aliani, S. 2015. First Observations on the Abundance and Composition of Floating Debris in the North-Western Black Sea. Mar. Environ. Res. 107, 45–49, doi:10.1016/j.marenvres.2015.03.011.

Wan, J.; Wang, Y.; Cheng, M.; Engel, B.A.; Zhang, W.; Peng, H. 2018. Assessment of Debris Inputs from Land into the River in the Three Gorges Reservoir Area, China. Environ. Sci. Pollut. Res. 25, 5539–5549, doi:10.1007/s11356-017-0881-6.

VSIM Model Adaption to Qualified Denomination of Origin Rioja Soil and Weather Conditions.

José M. Peña * [a], Julia Arbizu-Milagro [a] Alberto Tascón [a], Francisco J. Castillo-Ruiz [a].

[a] University of La Rioja. R.G. "Technology, engineering and food safety". Faculty of Science and Technology, C/ Madre de Dios, 53, 26006, Logroño, La Rioja, Spain.

* Corresponding author. Email: jmiguel.penya@unirioja.es

Abstract

Irrigation is a key practice for wine grapes production. Both, irrigation in excess and lack of irrigation could produce different wine faults. Traditionally, vineyard irrigation was considered as a way to increase yield although it reduced product quality. The aim of this research was to adapt VSIM model to weather and soil conditions of Qualified Designation of Origin Rioja in northeast Spain. Plots were planted mainly with Tempranillo cultivar, although Graciano, Tempranillo Blanco and Viura were also grown in three plots. Humidity sensors were placed at two depths to assess plant response to water stress. In addition, one weather station was set in each plot and data was transmitted in real time through a host control platform enabling data browsing by wineries technicians and researchers. Grape samples were analyzed during harvest to supplement in real time data. Two treatments were applied: irrigation based on adapted VSIM model and rainfed. Each monitoring system test weekly water balance relating those data with water status of each plant by dendrometry measurements. Adaptations of VSIM model to Rioja soil and weather conditions replaced Leaf Area Index (LAI) by Normalized Difference Vegetation Index (NVDI) along with trunk diameter measurements using dendrometry. Furthermore, crop coefficient was calculated based on NVDI instead of LAI and water stress thresholds were modified from originals. The main problem was to define a desired water stress to obtain an adequate yield without reducing fruit quality, although dendrometry measurements helped to check if the plant suffer or not water stress. In conclusion, adapted VSIM model contributed to optimize water resources through measuring soil humidity, grapevine growing and trunk diameter through dendrometry.

Keywords: Deficit irrigation, dendrometry, grape irrigation, water stress, crop coefficient.

1. Introduction

Irrigation in the vineyard is one of the essential and capital issues at present within the DOC Rioja. Water can be the best ally to get a quality grape or the worst enemy when is inadequately handled. For example, if in full vegetative growth, the plant receives water because it rains a lot or because it is irrigated, the vineyard develops a very exuberant vegetative system, an important cluster and grape size and therefore a potential, with a clear harvest, of grapes of not much quality. However, if in the ripening period you suffer from water stress, the leaves dry out and do not produce enough sugars or polyphenols, which are responsible for the colour, smell and taste of the grape. Therefore, it is necessary to be very careful with the management of water and, if possible, you must have a good technology that allows you to know when and in what amount to water.

Currently, in best cases, irrigation decisions are made based on data recorded by public agroclimatic stations scattered throughout the region. However, these stations are taken as a reference for areas that are too large. The topographical characteristics, the vegetation cover and even the hand of the man are factors that can generate differences in smaller areas within the area so, in many cases, the data are not completely reliable or representative for all the vineyards included in the area and therefore the decisions related to irrigation can be taken in the wrong way, resulting in a decrease of grapes quality.

Therefore, it is necessary to carry out a careful water management and, if possible, develop and adopt technologies that allow us to know when and in what amount to irrigate such as precision irrigation based on physiological methods (Acevedo-Opazo et al., 2010), considering that irrigation management influences growth, yield and grape quality (Santesteban et al., 2011).

In La Rioja, although until a few years ago the use of irrigation was much more restrictive, the Rioja Qualified Designation of Origin (DOCa Rioja) regulation recently authorized (Order AAA/2127/2012, August 2012) to maintain the balance of the plant throughout the vegetative cycle and, therefore, grape quality. However, due to the short time since this authorization, there are hardly any studies that provide the necessary knowledge about irrigation management in Rioja vineyards. Furthermore, it is important to note that currently the irrigation control systems available, are designed for other types of crops in which irrigation is only determined by soil moisture or rainfall and the actual state of the plant is not a variable to take into account. This is because water stress is considered negative in almost all crops, except for some Mediterranean crops among which is the vineyard.

In this sense there are some models such as the VSIM (Vineyard Soil Irrigation Model) for irrigation management and stress control in vineyards, (Johnson, L. et al. 2006, Pierce, L. et al 2015). This model was developed by the University of California Monterey Bay and NASA, is basically a spreadsheet that simulates water balance with climate, soil and plant parameters. User can modify some parameters of the spreadsheet to see the effects of their intervention on soil moisture, crop water needs and irrigation requirements and, in the case of the vineyard, water stress.

The aim of this research was to start VSIM model application on DOCa Rioja vineyards to determine influence of different cultivars, training systems and different model management systems on water requirements.

2. Materials and Methods

2.1. Site description.

The experiment was carried out with the collaboration of different wineries in La Rioja (Northeast Spain) that let plots of their vineyards to measure and irrigate vineyards following VSIM model. Chosen plots represented the variability of varieties, soils, climatology, and formation of the vineyards of the DOCa Rioja (Table 1). Before started tests, Soil samples were taken to determine the texture, which was taken into account in the water balance.

Table 1. Tested plots location and features. Vertically Shoot Positioned (VSP).

Plot	Village	Cultivar	Plant spacing (m)	Training System	Soil texture/lithology
Campo Viejo winery					
La Rad	Logroño	Tempranillo	2.8 x 1.20	VSP	-
	Alfaro	Tempranillo	2.8 x 1.20	VSP	-
Argadiel	Azagra	Tempranillo	2.8 x 1.24	VSP	Alluviums, Drainage Cones, Terraces, Alluvial fans
Caduengo	Azagra	Tempranillo	2.8 x 1.25	VSP	Clay loam
Remolino	Fuenmayor	Tempranillo	2.8 x 1.27	Bush	Gravels with sandy-clay matrix; sands; silts and clays
Riojanas winery					
Monte Real	Cenicero	Tempranillo	2.8 x 1.20	VSP	Clay-silt matrix rotated corners
Graciano	Cenicero	Graciano	2.8 x 1.20	VSP	
Gimileo	Gimileo	Tempranillo	2.8 x 1.20	VSP	Franco
Ontañón winery					
Encina	Quel	Tempranillo	2.9 x 1.1	VSP	Sandy loam
Pozo	Quel	Graciano	2.9 x 1.1	VSP	Sandy loam
Aniceto	Quel	Tempranillo blanco	2.9 x 1.1	VSP	Sandy loam
Altanza winery					
Tomillares	Galilea	Tempranillo	2.8x1.1	Double cordon	Stony with frank matrix
Los Llanos	Galilea	Tempranillo	2.8x1.1	Double cordon	Stony with sandy matrix
Vago	Galilea	Tempranillo	2,8 x 1,1	Double cordon	clayey

2.2. Data collection

An agroclimatic station was installed for each plot at two control points, one without irrigation and another with the possibility of irrigation (Figure 1). Data collected in each plot were:

- Climate data: temperature, relative humidity, solar radiation, rainfall and wind speed and direction.
- Soil data: moisture sensors placed at 25 and 50 cm depth.
- Plant response data: dendrometers in irrigated area and in area without irrigation.

Figure 1: Climatic station in test plot and dendrometer detail

The climate, plant and soil data were collected and processed continuously, and can be consulted through Cesens® platform that allows access to the different data collected quickly. Furthermore, data could be downloaded to work offline. Finally, images of satellite Sentinel 2 were took to determine NVDI throughout the crop in each of the tested plots.

2.3. Adaptation of the VSIM model to the conditions of La Rioja

VSIM is a model for irrigation recommendations that downloads and processes in real time the images of a vineyard and transforms them into irrigation recommendations. The methodology is based on estimating the crop coefficients (Kc) from the Foliar Area Index obtained from satellite images and integrating them into a water balance model in the soil. It provides the evolution of the vegetative growth of the vineyard, evapotranspiration (ETc), soil moisture, drainage, and water stress (leaf water potential). VSIM could be used as a tool for evaluating irrigation daily or weekly program based on soil moisture and water stress.

VSIM model needs to be fed with very few data related to soil texture, considering that calculation follows Saxton et al. (2006) method to determine water balance. Other data were plant spacing, root depth and the values of the pressure chamber to determine plant stress. Water balance was calculated considering that at the beginning, soil was at field capacity, and it was assumed that there was runoff or percolation when the water obtained by the balance is greater than the available water capacity at field capacity. Finally, crop evapotranspiration was calculated following Eq (1).

$$ETc = ET0 \cdot Kcb \cdot Ks \qquad (1)$$

where *ET0* is the reference evapotranspiration obtained from the climatic seasons; *Kcb*, represents the influence of the crop and are obtained by measuring the leaf area obtained by Landsat satellite images; and Ks represents a coefficient of water stress, which was 1 when there is no drought, and 0 during an intense drought. Intermediate values correspond to the intermediate conditions from the beginning of stress to the maximum stress.

Soil featurisation was made from Saxton formulae (Saxton et al. 1986). Furthermore, the model assumes that the potential with which the soil retains water coincided with the potential with which the plant had to suck to obtain it measured with a soil potential on the stem at sunrise (ψt). This potential was an indirect measure of water stress and served to modify Kc values, so that it causes Kc to decrease when the water potential of the stem decreases. Original VSIM model assumed that for California conditions, the value at which the stress measured in the soil potential starts is -5 bar and the maximum stress value was obtained at -12 bar. However, to obtain adequate results, VSIM model was modified to perform better in La Rioja conditions.

- Foliar Area Index had been replaced as a representative parameter of the plant conditions by two parameters: the NDVI (Normalized Diference Vegetation Index) and by main trunk diameter obtained by dendrometry.
- Calculation of Kcb (coefficient of the cultivation of the vineyard) of the original model was based on the Leaf Area Index, but it had been replaced by a Kcb calculated from the NDVI, following the method described by Calera et al. (2014) and Campos et al. (2010).

- Soil potential values in which the strain stress was supposed to start have been modified as it shown:
  - $0 < \psi < -2$. There were not deficit conditions.
  - $-2 < \psi < -4$. Slight deficit. Do not irrigate.
  - $-4 < \psi < -6$. Deficit. Intervention if vegetative production and/or growth want to be increased
  - $\psi < -6$. Notable deficit. Justified irrigation.
  - $\psi < -15$. Maximum deficit. Justified irrigation.

2.4. Model management

Model management had been carried out in three different ways:

1.-Classic method, Kcb fixed by bibliography: it was based on the assignment in the balance of a Kcb obtained from the bibliography. In La Rioja, the coefficients used were:
  - Up to fruit set: Kcb = 0.40
  - From fruit set to veraison: Kcb = 0.30
  - From veraison to harvest: Kcb = 0.20

2.- Method based on the relationship between Kc and NVDI: It was based on the method of Fields et al. (2010), which assigns a value to Kc based on the NDVI according to the expression with weekly measurements of NDVI:

$$Kcb = 1.44 \cdot NVDI - 0.1 \tag{2}$$

3.-Method based on soil potential control: It was based on the calculation that performs the balance of the Water Retention Potential in the soil at 25 cm. Stress and irrigation was considered to start at -6 bar and maximum stress started at -15 bar.

3. Results and Discussion

3.1. Irrigation management in 2018 season

The year 2018 was an especially rainy year during the summer, therefore, VSIM model could be run, but there were no significant irrigation events considering that water stored in the soil was not decrease under intervention value. This fact was due to frequent rain events (Figure 2).

Figure 2. State of soil moisture and rainfall in the Logroño plot during 2018 season.

This fact could be observed by studying trunk diameter evolution during summer of 2018 for the same plot (Figure 3), where there was no decreasing of trunk diameter, therefore stress was not important. Very similar graphs were obtained in all the stations monitored in 2018, regardless of variety, soil type, planting age or any other variable.
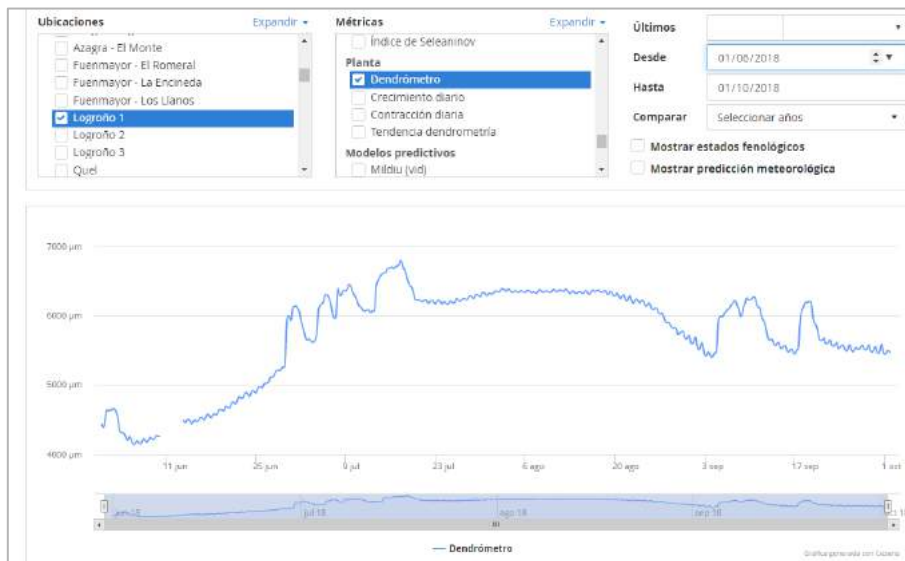
Figure 3. Trunk diameter measured by dendrometry in Logroño plot during summer of 2018

3.2. Irrigation management in 2019 season

2019 was not such a rainy year as 2018 was, hence, water balances in the plots were calculated by means of the VSIM model using different model management adaptations.

3.2.1.   *Classic method: Kc fixed by bibliography*

In the example shown of the plot La Encineda (Figure 4), the model estimated water needs of 164 mm until July 10th, which can be replenished with 2 irrigations of 10 mm and 7 irrigations of 20 mm.
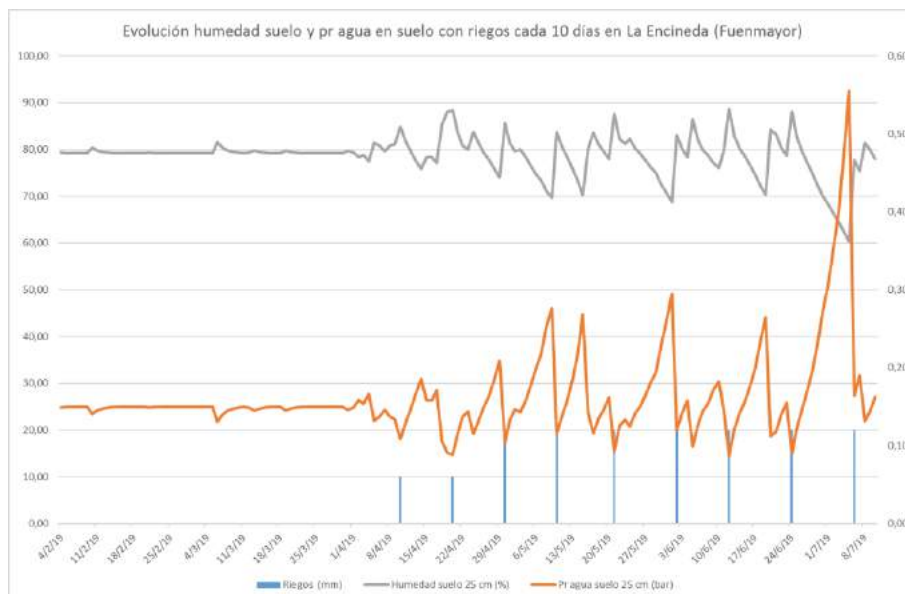
Figure 4.- Simulation of the variation of the water content in the soil from the estimate of the ETc watering from the month of April. Blue bars: Irrigation amount; Orange line: Soil potential (negative values); Grey line: Soil humidity.

The proposed watering schedule allow to maintain the soil with a high humidity and low potential of retention of water in the soil, so that the plant does not suffer any stress. However, in other plot, rain events until the end of June allow the potential of the soil to remain below − 6 bar, and that this value is only exceeded at the beginning of July, so only at that time a stressful situation occurred that justified the only irrigation event. (Figure 5).
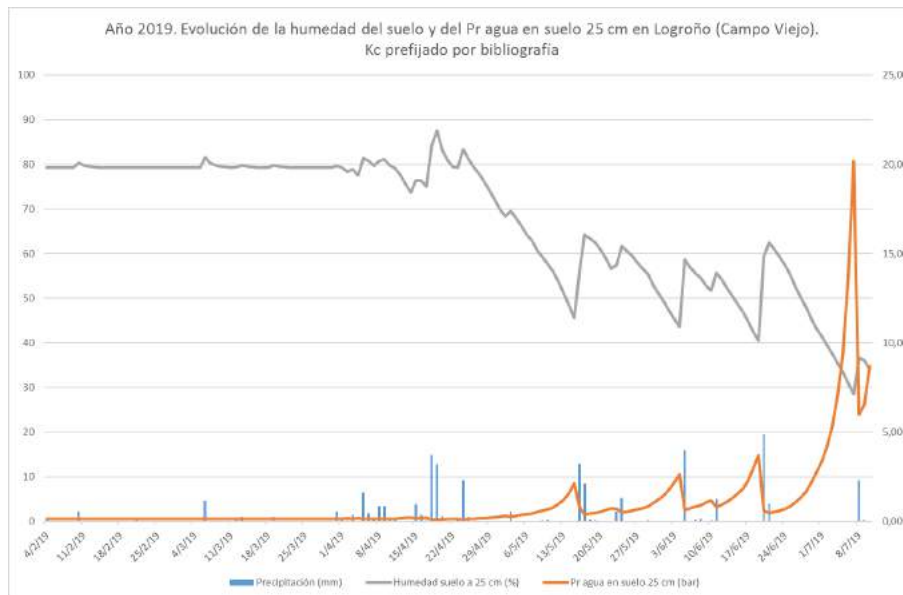
Figure 5.- Variation of the water content in the soil from the estimate of the ETc by the classical method, considering only the rains. Blue bars: Rain events; Orange line: Soil potential (negative values); Grey line: Soil humidity.

3.2.2. Method based on the relationship between Kc and NVDI

In this case the simulation showed lower values of water needs, 113 mm compared to the 164 mm of the classic method. In this case, a lower Etc was considered, hence, the crop did not suffer water stress, so it would not be necessary to apply any irrigation (Figure 6).
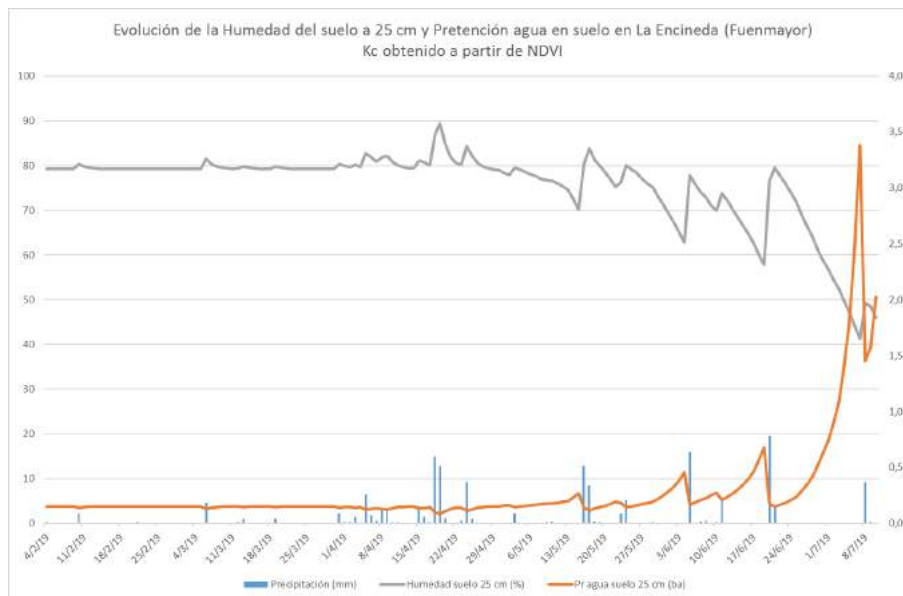
Figure 6.- Variation of the water content in the soil from the estimate of the estimated ETc with a Kc based on the NVDI data. Blue bars: Rain events; Orange line: Soil potential (negative values); Grey line: Soil humidity.

3.2.3. Method based on soil potential control

The model would indicate that from a soil potential above -6 bar irrigation could be justified. In the example above this value was reached on 7th July, but when it rains on 8th July soil humidity was recovered, so that the dendrometer did not show stress for the plants. (Figure 7).
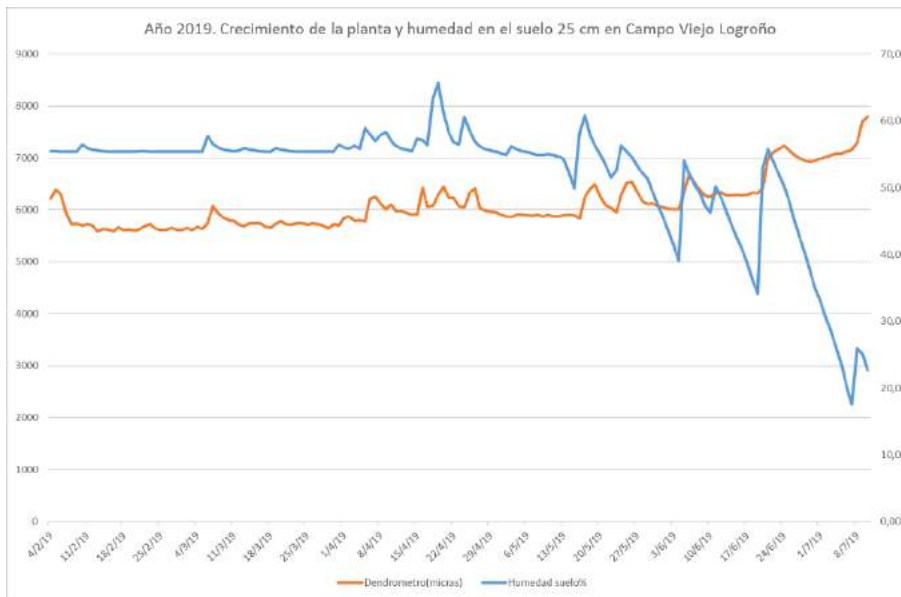
Figure 6.- Trunk diameter and soil water content. Blue line: Soil humidity; Orange line: Trunk diameter measured using dendrometer.

This fact could be seen more clearly other plot, with sandy soil and with less soil available water capacity. It this plot was observed how soil humidity decreasing increases soil water potential exceeding the threshold of -6 bar, which would indicate the beginning of irrigation considering that vineyard reached a severe stress according to the model (above -15 bar) (Figure 7). Rain events on 8th July cause the recovery of moisture in the soil, and soil water potential turned to non-stressed levels, although it quickly rised again.
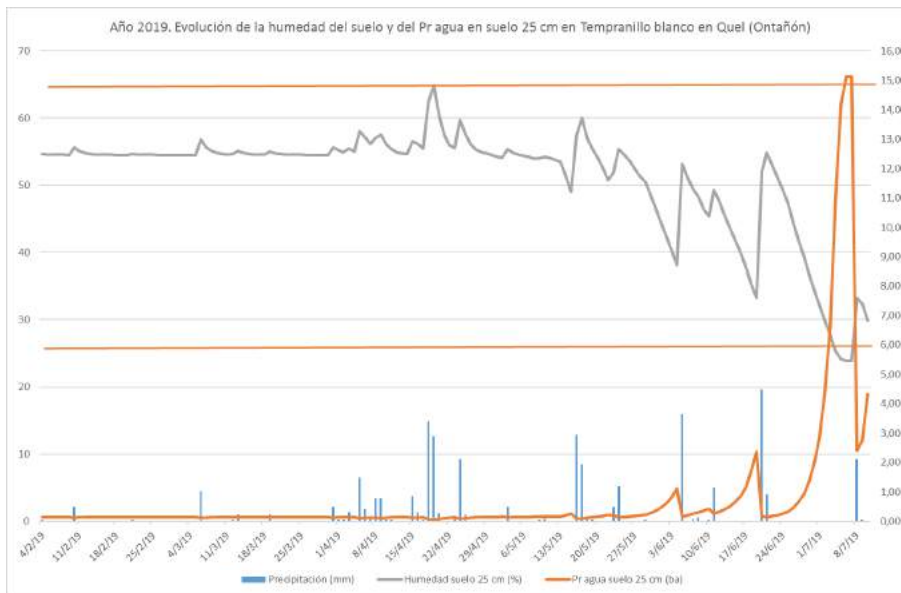
Figure 7.- Variation of the water content in the soil and the potential of water in the soil with the rains in the period studied. Blue bars: Rain events; Orange line: soil potential (negative values); Grey line: Soil humidity.

Plant response to water stress was observed how there was a retraction of the trunk diameter, which recovers slightly with the rain of the 8th July, but as it decreased again the next day indicated that it would be advisable to start the irrigation (Figure 8).
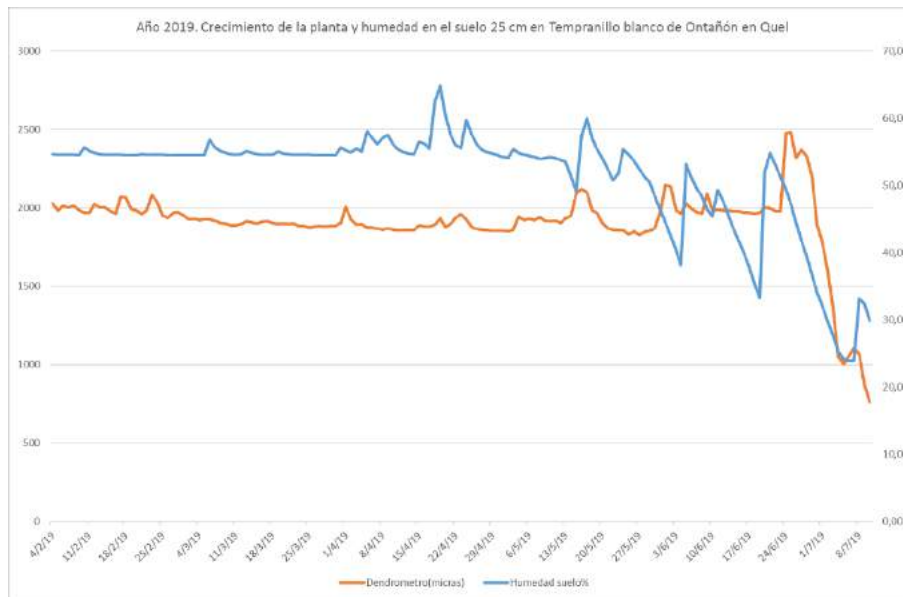
Figure 8.- Variation of the water content in the soil and the potential of water in the soil with the rains in the period studied. Blue line: Soil humidity; Orange line: Trunk diameter measured using dendrometer.

4. Conclusions

Different cultivars, training systems did not show appreciable differences because plants provided similar responses. However, soil texture along with climatology was determinant to predict plants response, for instance, plot location determines the amount of rain during summer, and hence, it influenced irrigation schedule. Model configuration was also important, considering that, different threshold for stress will indicate different moments to start irrigation, and then, it influenced water requirements. Moreover, NDVI will help to obtain Kcb and generated water savings without apparent influence on yield nor plant growth. However, only data from two years were not enough to extract solid conclusions, which stand out the need of further research, mainly to define stress threshold.

Acknowledgements

References

Acevedo-Opazo, C., Ortega-Farias, S., Fuentes, S. 2010. Effects of grapevine (Vitis vinifera L.) water status on water consumption, vegetative growth and grape quality: An irrigation scheduling application to achieve regulated deficit irrigation. Agricultural Water Management, 97(7), 956-964.

Calera, A., Campos, I., Garrido, J., 2014. Determinación de las necesidades de agua y de riego mediante estaciones meteorológicas y series temporales de imágenes multiespectrales. Jornada técnica de innovación en gestión del regadío mediante redes agroclimáticas, teledetección y sistemas de información. CENTER, MAGRAMA.

Campos, I., Neale, C.M.U., Calera, A., Balbontín, C., González-Piqueras, J., 2010. Assessing satellite-based basal crop coefficients for irrigated grapes (Vitis vinifera L.). Agricultural Water Management 98, 45-54.

Johnson, L., Pierce, L., Michaelis, A., Scholasch, T., Nemani, R. 2006. Remote Sensing and Water Balance Modeling in California Drip-Irrigated Vineyards. In Proceedings, ASCE World Environmental & Water Resources Congress, Omaha NE, 21-25 May 2006.

Pierce L., Nemani R., Johnson L. 2015. VSIM - Vineyard Soil Irrigation Model, release 3/1/06: user guide. Available online at http://geo.arc.nasa.gov/sge/vintage/vsim_050103_guide.pdf. Accessed 29 January 2015

Santesteban, L.G., Miranda, C., Royo, J.B. 2011. Regulated deficit irrigation effects on growth, yield, grape quality and individual anthocyanin composition in Vitis vinifera L. cv.'Tempranillo'. Agricultural Water Management, 98(7), 1171-1179.

Saxton, K.E., Rawls, W., Romberger J.S., Papendick R.I. 1986. Estimating generalized soil-water characteristics from texture. Soil Sci. Soc. Amer J. 50(4):1031-1036.

Effects of Regulated and Continuous Deficit Irrigation on Growth and Yield of Super High Density Olive orchard in La Rioja (Spain)

Julia Arbizu-Milagro [a,*], **Francisco J. Castillo-Ruiz** [a,*], **Alberto Tascón** [a,*], **Jose M. Peña** [a]

[a] University of La Rioja. R.G. "Technology, engineering and food safety". Faculty of Science and Technology, C/ Madre de Dios, 53, 26006, Logroño, La Rioja, Spain.

* Corresponding author. Email: juarbizu@unirioja.es

Abstract

This study evaluated four irrigation strategies applied to olive trees (*Arbequina* cv.) in super high density orchard, in order to reduce the consumption of water compared to a fully watered control. The most advantageous strategy has been to prevent the water stress of trees by means of the continuous measurement of trunk diameter fluctuations in which the productive and vegetative variables are not altered with a 31.2 % of average water saving. The production of moderate stress during the pit hardening phase has also been very interesting. Experience shows that trees recover from this moderate stress (18.9 % average water saving) and their vegetative and productive characteristics turn out to be very similar to those of the control treatment.

On the contrary, the strategy that has been based on producing water stress throughout the crop, as well as that which produced severe stress during the pit hardening phase have been shown to significantly alter some of the vegetative and production characteristics. It caused a decrease in oil yield of 16% less compared to the Control, which might not compensate for the water saved.

Keywords: Regulated deficit irrigation, dendrometer, olive oil.

1. Introduction

Over the last years, olive growing has experienced a huge development. Plant densities are changing from 60-100 plants per hectare for wide spacing traditional olive orchards to 1600-2500 plants per hectare for super high density olive orchards. However, current super high density olive orchards increase plant spacing varying from 550 to 850 plants per hectare for rainfed conditions and from 650 to 1150 plants per hectare for irrigated orchards (Todolivo, s.f.). Despite rainfed orchards started to be planted with this olive category, in many cases, irrigation water is required to achieve stablished growth and yield objectives.

The Mediterranean area of cultivation and, in particular, La Rioja, is characterized by suffering from water deficit during the summer. Frequently, plant-watering demand cannot be satisfied with the available resources, so it is necessary to use Continuous Deficit Irrigation (CDI) strategies that remove part of the irrigation water during the entire vegetative cycle, or Regulated Deficient Irrigation (RDI), in which irrigation water amounts are reduced during phenological periods that are non-critical for yield or fruit quality. In the case of the olive tree, it coincides with the pit hardening phase, which takes place in the summer months.

In recent years, some experiments have been conducted to test RDI during the pit hardening phase (Goldhamer, 1999; Motilva et al., 2000; Tovar et al., 2002; Alegre et al., 2002) and continuous deficit irrigation (CDI) (Patumi et al., 2002; Tognetti et al., 2006; Goldhamer et al., 2006). However, these two irrigation strategies have not been compared between them. The studies report no or small differences in yield between fully and deficit irrigated trees. However, the evapotranspiration (ET) was not measured, so the results cannot be easily extrapolated to other situations.

Moriana et al. (2003) compare deficit irrigated trees under CDI and RDI to fully irrigated trees and reported that both deficit irrigation strategies reduce the ET and, consequently, the yield. These authors find an asymptotic yield-ET function, which means that water use efficiency (WUE) is reduced when the amount of irrigation increases. However, ET is different in both deficit irrigation strategies due to different amounts of irrigation applied in CDI and RDI.

On the one hand, Melgar et al. (2008) find no vegetative or productive responses to different irrigation regimes. On the other hand, Grattan et al. (2006) obtain the opposite results. It is demonstrated that less irrigation provokes a reduction in photosynthetic activity, although it does not affect productivity (Kremer et al., 2018) Therefore, definitive conclusions on the performance of the two strategies cannot be deduced.

The aim of the present study was to evaluate the effect of four deficit irrigation treatments productive and vegetative response of a super high density olive orchard cv. "Arbequina". Flowering, number of fruits and oil yield was also assessed to optimize olive water demand.

<div align="center">2. **Materials and Methods**</div>

2.1. Site description.

The experiment was conducted during 3 irrigation seasons from April to December (2006, 2007 and 2008) on a commercial olive orchard located in La Rioja (Spain) (42º 14´57.73" N; 2º 2´58.45" W) trees were 4 years old olive trees and they were drip irrigated. The climate of the zone is continental Mediterranean-type. The average year temperature for the experimental period was 13.8, 13.0 and 13.7 ºC respectively, although summer temperatures often exceed 32ºC. Rainfall during tested seasons were 417 (2006), 416 (2007) and 560 mm (2008) and most rains occurred during non-summer months. ET0 was 1085 (2006), 1047 (2007) and 991 mm (2008).

Olive trees *(Olea europaea)* variety Arbequina i-18 were planted with GPS at high density of 1666 trees ha^{-1} at 4.0 x 1.5 m spacing. Soil was sampled to obtain representative analysis values, soil deep was enough (> 1.5 m), with a loam-clay-sandy texture, alkaline pH, low organic matter and high calcium carbonate content (table 1). Crop management (fertilization, pruning, weed control, tillage and soil maintenance) was carried out following standard grower practices.

<div align="center">Table 1. Soil analysis results in March 2006.</div>

Determinations	Value at 30 cm depth	Value at 60 cm depth
pH	7.9	8.18
Organic matter content (%)	1.3	0.7
Calcium carbonate content (%)	17.8	-
Field capacity (%)	29	28
Permanent wilting point (%)	9	10
Hydraulic conductivity (cm h^{-1})	3.9	1.6
Bulk density (kg m^{-3})	1.52	1.44

2.2. Experimental design and irrigation treatments description

The trial design consisted of a randomized complete block, with 5 treatments of irrigation and 3 repetitions. There were 15 plots in which 7 trees per plot located in a single row with two adjacent guard rows were selected for the measurements.

ETc for Control treatment was calculated according to:

$$ETc = ET0 \times Kc \times Kr \qquad (1)$$

ET0 was calculated using the Penman-Monteith-FAO method (Allen at al., 1998) from an automatic weather station close to the experimental plot. An estimated crop coefficient *Kc=0,7* was taken from Girona, J. (1996) for an intensive crop in full production as we have a perennial leaf crop, and a reduction coefficient (*Kr*) (Fereres and Castel, 1981) was considered to account the area shaded by the canopy. The *Kr* applies to canopies less than 50% ground cover and is described as:

$$Kr = 2 \times Sc/100 \qquad (2)$$

Where *Sc* is the percentage of canopy cover. Measurements made in April 2006 gave *Sc* = 37,5 %, so it was taken as a constant the value of *Kr = 0,75* for the three years of study.

Certain developmental periods in olive are especially sensitive to low soil moisture. Following Girona et al. (2004), during bloom period, olive is very sensitive to dry soil conditions, particularly in warm-dry weather. These conditions also cause excessive fruit thinning, fruit drop and alternate bearing. On the other hand, when moderate water deficit are suffered during the early stages of fruit development, fruit growth is not reduced compared with fully irrigated trees. However, water deficits during the final stages of fruit growth cause a reduction of fruit diameter reducing yield. Those moments were considered for the irrigation scheduling of RDI treatments.

So, from April to early June (growing of inflorescences and flowering period) no deficit was allowed, in order to obtain better flowering and more shoots for the following year. This water status was maintained during spring up to massive pit hardening phase which used to take place in June. From that moment to the beginning of fruit ripening, sensibility to water deficit was expected to be less important because of stomata closing due to high daily Vapor Pressure Deficit (VPD). Thus, during the summer vegetative growth stop, irrigations were limited to those that maintained the photosynthetic functions of leaves. From September to October (fruit ripening and reserve accumulation) water stress sensibility is maximum again, so deficit should be avoided.

Having into account these premises, irrigation treatments were defined as follows:

- T1: Control treatment (C): 100% ETc during the whole irrigation season.
- T2: Moderate regulated deficit irrigation (MRDI): 100% ETc from the beginning of season to massive pit hardening, 50% ETc during summer vegetative growth stop and 100% ETc from the ripening of fruit to the end of season.
- T3: Severe regulated deficit irrigation (SRDI): 100% ETc from the beginning of season to massive pit hardening, 25% ETc during summer vegetative growth stop and 100% ETc from ripening of fruit to the end of season.
- T4: Continuous deficit irrigation (CDI): 50% ETc the whole irrigation season.
- T5: Dendrometer regulated deficit irrigation (Dendro): Irrigation after two consecutive days of decrease of trunk diameter according to dendrometer data (Verdtech dendrometer, Verdesmart CO S.L., Spain) during summer vegetative growth stop. The volume of water contributed to each irrigation was equivalent to the ETc of the previous day. For the rest of the season, 100% ETc was used to irrigate.

2.3. Vegetative Measurements

At the beginning of the experiment, five central trees on each plot were marked to be taken as control trees. Measurements of plant growth consisted on tree height and trunk diameter 15 cm above the soil. At the same time, each season, two lateral branches from the upper third ones per tree were selected to measure its length. Measurements were performed at five different dates, at different phenological stages as follows: 15 days after shoot flush (I), pre-flowering (II), 5 weeks after fruit setting (III), beginning of ripening of fruit (IV) and pre-harvesting (V).

2.4. Production Measurements

Measurements were also made on selected branches (Table 2) to estimated flowering, fruit density (number of fruits per length of branch) and fruit set (percentage of initial flowers with fruit at harvest).

Table 2. Measurements and determinations of production carried out in the control trees along the vegetative growth season.

Measurements	I	II	III	IV	V
Number of inflorescences		X			
Number of flowers/shoot		X			
Number of fruits/ shoot			X		
Weight of 100 olives (g)			X	X	X
Ripening index (RI)					X

2.5. Data analysis

Results were analysed by an analysis of variance using the IBM SPSS Statistics 19.0 for Windows (IBM Corporation, Armonk, NY, USA). Differences and confidential levels were determined by calculating the least significant difference (LSD), and significant difference was defined at $p \leq 0.05$.

3. **Results**

3.1. Consumption of irrigation water

All irrigation strategies have achieved significant water savings compared to Control (Table 3). Higher savings were provided by CDI treatment, although all irrigation treatments provided significant differences ($\rho > 0,05$) compared to control treatment.

Table 3. Irrigation water applied (mm) and saving water (%) to the treatments during the three years of the experience. Treatments: Control treatment; MRDI, Moderate regulated deficit irrigation; SRDI, Severe regulated deficit irrigation; CDI, Continuous deficit irrigation; Dendro, Dendrometer regulated deficit irrigation. Different letters showed significant differences ($\rho > 0,05$) according to Duncan's test.

Treatments	mm/year	mm/year	mm/year	Average water saving (%)
Control	469.8	446.3	430.4	0.0 a
MRDI	383.5	360.8	348.1	18.9 b
SRDI	340.3	318.1	306.9	28.3 c
CDI	234.9	223.2	215.2	50.0 d
Dendro	327.4	306.1	292.5	31.2 c

3.2. Vegetative response

Regardless of the irrigation strategy, trees growth rapidly during phases I to III. Between phases III and IV (pit hardening) growth stops and, at the end of the summer, there is a second vegetative growth increasing. This seems to respond to the adaptation of the olive tree to the Mediterranean climate, which causes the stomas to close in periods of high temperatures and low relative humidity. Vegetative stop intensity seems to be affected by water management, which was more intense in the CDI, Dendro and SRDI treatments, and lower in the Control and MRDI treatment (Figure 1).
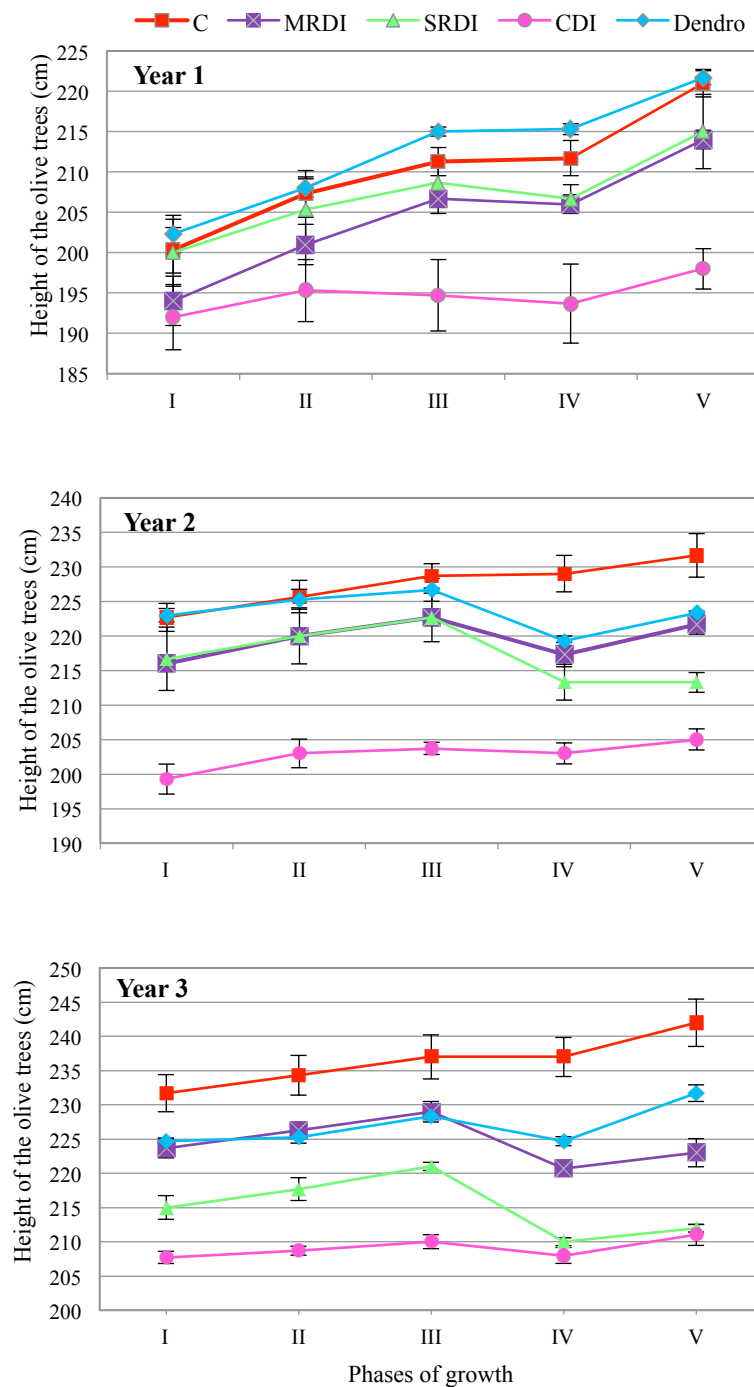

Figure.1. Evolution of the height of the olive trees (cm) in the different treatments of irrigation throughout the phases of growth in the three years of the experiment. The symbols represent the average of 15 measurements of three blocks and the vertical bars indicate the typical error.

A strong decrease in the growth height rate and in the length of lateral branches were observed in the CDI treatment that occurred from the first year (Table 4). This observation, which coincides with the data of Iniesta et al. (2009) and Moriana et al. (2003), seems to indicate that the sustained deficit affects growth adversely, which could be interesting to control vigour in Super high density olive orchards. In addition, SRDI shows a lower tree height and a shorter lateral branch length, although in the first year, differences were less evident. The treatments Control, MRDI and Dendro are the ones in which the plants reach greater height, and the side branches reach a greater length, without there being statistically significant differences between them.

Table 4. Absolute growth in tree height (cm) during the irrigation season in 2006, 2007 and 2008. Different letters showed significant differences ($\rho > 0,05$) according to Duncan's test.

Treatments	Absolute growth in tree height (cm)		
	2006	2007	2008
Control	20.7±3.5 a	9.0±2.1 a	10.3±1.2 a
MRDI	20.0±2 a	5.7±0.3 ab	-0.7±0.7 cd
SRDI	15.0±3.5 ab	-3.3±3.2 c	-3.0±1.2 d
CDI	6.0±1.5 b	5.7±0.7 ab	3.3±2.4 bc
Dendro	19.3±2.9 a	0.3±0.7 bc	7.0±1.5 ab

At the end of the three years of the experiment, the treatments Dendro and MRDI did not affect the height of the tree with respect to the Control. On the contrary, the trees of the CDI and SRDI strategies grew significantly below the previous ones after three years of testing. However, the irrigation strategies only showed a reduction of the thickness reached by the trunk at the end of the three seasons for CDI treatment (50% less), according to previous research, which find the same results: trunk growth is not affected by controlled deficit irrigation (Moriana et al. 2000).

Provided results showed that water restrictions during pit hardening seemed to affect the tree growth, that only took place for CDI treatment. Previous research was in accordance, for instance, Melgar et al. (2008) obtain a significant positive trend ($\rho > 0,05$) between length of the shoots and water applied in 3 of the 9 tested years. However, data showed that Control obtained the highest cumulative growth followed by Dendro and MRDI with no differences between them. SRDI obtained significant ($\rho > 0,05$) lower average growth than previous ones, and finally, CDI was placed with results similar to those obtained by Grattam et al. (2006) in which they observed smaller growths of the branches when they irrigated with doses inferior to 72% of the ETc during the entire vegetative cycle.

3.3. Flowers and fruits

The number of flowers per shoot did not changed significantly over time, but it does depend on the amount of water supplied (Table 6). On the contrary, it has been verified that in 2007 there were significant ($\rho > 0,05$) less fruits than in years 2006 and 2008, which leads us to think that alternate bearing phenomena described for the olive tree, although attenuated, are still present.

Table 6. Average of number of flowers and fruits per shoot, and fruit setting rate, at the end of the experiment. Different letters indicate significant differences ($p < 0.05$) between treatments according to Duncan's test.

Treatments	Number of flowers/shoot	Number of fruits/shoot	Fruit setting rate (%)
Control	716±63 ab	27.0±0.6 a	4.4±0.5 a
MRDI	675±37 ab	25.3±2.0 ab	3.9±0.5 a
SRDI	565±45 bc	20.9±1.7 bc	3.9±0.6 a
CDI	490±21 c	18.8±1.0 c	3.8±0.4 a
Dendro	738±83 a	29.4±2.5 a	4.2±0.8 a

At the end of the experiment, the irrigation strategies Dendro, Control and MRDI obtained a greater number of flowers per shoot without significant differences among them. By contrast, it was observed that CDI and SRDI had a

lower number of flowers per shoot because the number of flowers per panicle was reduced (data not shown). Alegre et al. (2002) obtained similar results and concluded that the water deficit of one year could affect the flowering of successive years. In addition, when the influence of irrigation strategies was studied, it was observed that MRDI and Dendro provided no significant differences ($\rho > 0,05$) for number of fruits.

The results seem to indicate that floral induction phenomena occurring during the pit hardening phase at summer stop are not affected by treatments where the dendrometer is used as a reference and in which the stress is moderate. However, the moment that stress increases, the number of fruits suffers, which would explain the worse results of SRDI. Finally, the data suggest that, if the stress continues after the pit hardening phase in post-summer growth, the initiation phenomena would be affected, and the CDI treatment would have achieved its worst results. However, the rate of setting is not altered, which shows that the fruit set had not been influenced by the irrigation strategies.

Less clear seems to be the relation between the number of flowers and fruits and the vegetative growth of the shoots that Iniesta et al. (2009) indicate. Curdled fruits do not seem to be related to irrigation strategies in 2006 and 2007 (Table 7). Only in 2008 they separated, with the Dendro treatment producing more fruits per branch cm, while CDI had a lower yield.

Table 7. Number of flowers and fruits curdled per cm of branch during the three irrigation campaigns studied. Different letters indicate significant differences (p< 0.05) between treatments according to Duncan's test.

Treatments	Number of flowers/cm shoot			Number of fruits/cm shoot		
	2006	2007	2008	2006	2007	2008
Control	10.8±4.6 a	12.0±0.9 ab	14.7±1.4 a	0.46±0.0 a	0.39±0.1 a	0.52±0.0 ab
MRDI	9.2±0.5 a	12.6±1.0 ab	12.6±1.0 ab	0.47±0.1 a	0.36±0.0 a	0.51±0.0 ab
SRDI	10.6±2.5 a	9.6±0.9 bc	9.2±0.8 b	0.47±0.1 a	0.26±0.0 a	0.41±0.0 b
CDI	9.5±0.8 a	7.2±0.9 c	9.5±0.1 b	0.53±0.0 a	0.28±0.0 a	0.28±0.0 c
Dendro	14.3±3.3 a	14.2±1.8 a	14.2±0.4 a	0.53±0.1 a	0.38±0.0a	0.55±0.1 a

These data would indicate that the differences in the number of fruits would not be due to a higher rate of setting, but to a greater vegetative growth of the fruiting shoots in the Control, MRDI and Dendro strategies. As the shoot growth was greater, the number of fruits was also greater.

3.4. Yield

3.4.1.Evolution of the weight of 100 olives.

The evolution in time of fruit weight has not registered significant variations in the three years. The olives remained equal in size after ripening (III) apart from CDI, but during phases IV and V the fruits of the Control, Dendro and MRDI strategies accumulated more water and gained a greater weight of the olives at the harvest, while the CDI and SRDI treatments obtained significantly lower weights (Figure 2). These results coincide with those by Iniesta et al. (2009) who found that their treatments with deficits (similar to CDI and SRDI) reduced fruit growth. Tognetti et al. (2006) also found that deficit situations in the pit-hardening phase could affect linearly the weight of the fruit and, consequently, the final production.

The olives from CDI treatment always had lower weight, which seems to indicate that the continuous deficit negatively affects the weight of the fruits from the moment of their formation. Also, the SRDI and MRDI treatments increase less weight at time IV (fruit growth stage) than Dendro and Control. This seems to indicate that whatever the level of stress at that stage affects the growth of olives, a situation that has been visually verified in our case since we have observed fruit passages for the three deficit strategies at some point in time. MRDI treatment was capable of recovering the growth in weight in the moments prior to the harvest when the irrigation is restored, whereas SRDI treatment was not.

3.4.2.Production of oil

The production shows annual differences, so that the year 2007 is significantly less productive than 2006 and 2008. This seems to have to do with the data of a smaller number of fruits in that year.

The trees that were not undergone to water stress (Control and Dendro) achieved an olive production significantly (p< 0.05) superior to the rest because of having a greater number of fruits and a greater weight of the olives at harvest. It led to think that greater vegetative development of the productive shoots and increase of the fruit weight were decisive in the final production. According to showed results, Iniesta et al. (2009) also attribute to a lower vegetative growth the reduction of the harvest that they find when irrigation reduces tree growth.
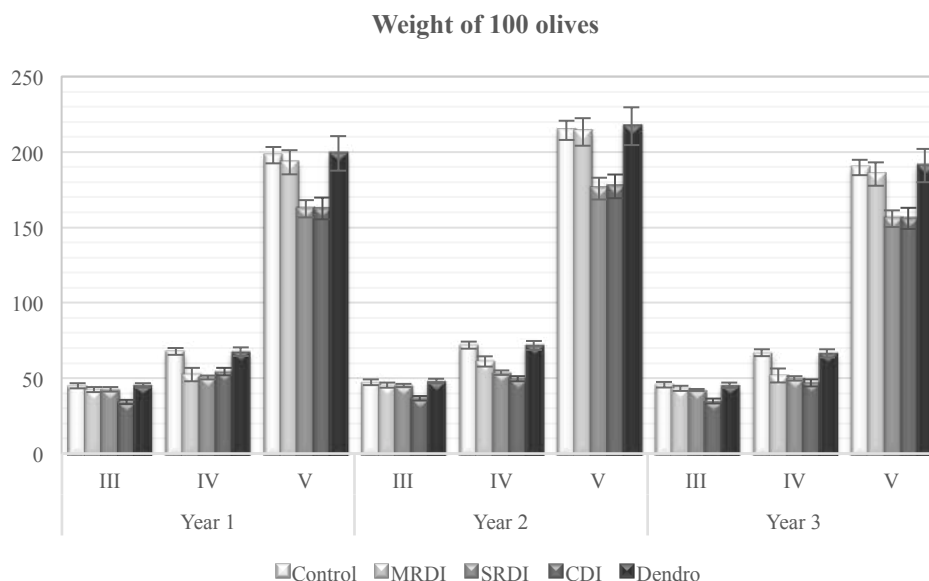
Weight of 100 olives

Figure 2. Evolution of the weight of 100 fruits (g) from the beginning of the summer vegetative stop (mid-July) (III) to the harvest (first of November) (V), in the three years of the experience, year 1 (2006), 2 (2007) and 3 (2008). The vertical bars represent the typical error.

Unlike with the production of olives, the oil yield was higher in more stressed treatments SRDI and CDI and lower in the rest of the irrigation treatments. However, the maximum oil production was achieved with the controlled deficit irrigation strategies Dendro and MRDI, without significant differences ($p < 0.05$) with the Control for yearly production. (Table 8). Similar results were obtained by Girona et al. (2002), which seem be related to the water content of the samples. The production of olive oil accumulated throughout the experiment has also been calculated in order to avoid the distortions that could be produced by the fact that the annual yields are different.

Table 8. Oil production per unit area (Kg oil /ha) for the different irrigation strategies in the three years of experience (Years 2006, 2007 and 2008) and cumulative production of the three years. Different letters indicate significant differences ($p < 0.05$) between treatments according to Duncan's test.

	Oil yield (Kg olive oil/ha)			
Treatments	2006	2007	2008	Cumulative
Control	1196±53.1 a	1075±21.9 a	1438±47.4 ab	3708±30 ab
MRDI	1090±24.4 ab	1037±63.7 ab	1496±80.7 a	3622±115 b
SRDI	963±20.9 b	880±19.0 b	1271±45.1 bc	3114±56 c
CDI	1018±9.8 b	911±51.8 b	1171±20.5 c	3100±81 c
Dendro	1198±64.5 a	1153±68.5 a	1614±79.3 a	3965±116 ab

4. Conclusions

The experiments carried out in a super high density olive orchard showed that there is room to optimize olive irrigation, considering that it is possible to reduce water applied without reducing olive growing nor oil production. Olive oil production in super high density olive orchards depends fundamentally on the vegetative development of the fruiting branches, the fruit set, and the evolution of the fruit weight until the harvest date.

The proposed irrigation strategy Dendro, in which the tree is watered when it is expected to suffer stress, with daily trunk diameter growth acting as an indicator, has obtained olive and oil yields like the fully irrigated Control treatment, providing mean water savings of 31.2 %. Data showed that this water saving strategy was possible because there has been no significant reduction in vegetative growth nor in the production of flowers and fruits. At the same time, olive weight in the summer deep similar to fully irrigated treatment. In the same way, the MRDI strategy has been interesting to achieve water savings of 18.9 % compared to Control. The vegetative parameters have decreased slightly with respect to Control, but not the weight of the olives in the harvest. Finally, SRDI and CDI treatments have altered the length of the shoots and the final weight of the olives, so that, despite achieving significant water savings, they provided lower oil production.

Acknowledgements

References

Alegre, S., Marsal, J., Mata, M., Arbones, A., Girona, J. 2002, Regulated deficit irrigation in olive trees (*Olea europaea* L, cv. "Arbequina") for oil production, Acta Hortic 586: 259-262.

Allen, R.G., Pereira, L.S., Raes, D., Smith, M. 1998. Crop Evapotranspiration. Guidelines for computing crop water requirements. FAO irrigation and Drainage Paper 56. Rome, Italy, 15-27

Fereres, E., Castel, J.R., 1981. Drip Irrigation Management. Division of Agricultural Sciences, University of California, Leaflet 21259.

Girona J (1996) Requerimientos hídricos del olivo. Estrategias de aplicación de cantidades limitadas de agua de riego en 'Arbequina'. Fruticultura Prof 81:32–40.

Girona, J., Luna, M., Arbones, A., Mata, M., Rufat, J., Marsal, J., 2002. Young olive trees responses (Olea europaea, cv "Arbequina") to different water supplies, Water function determination. In: Proceedings of the Fourth International Symposiumon Olive Growing, Vol. 1 and 2, pp. 277–280.

Girona, J., Marsal, J., Mata, M., Arbonés, A., De Jong, T., 2004. A comparison of the combined effect of water stress and crop load on fruit growth during different phenological stages in young peach trees. J Hort Sci Biotech 79: 308-315.

Goldhamer, D. 1999. Regulated deficit irrigation for California canning olives. Acta Horticulturae 474: 369-372.

Goldhamer, D.A.; Viveros, M.; Salinas, M. 2006. Regulated deficit irrigation on almonds: effect of variations in applied water and stress timing on yield and yield components.

Grattan, S.R., Berenguer, M.J., Connel, J.H., Polito, V.S. Vossen, P.M. 2006. Olive oil production as influenced by different quantities of applied water. Agriculture Water Management 85, 133-140.

Iniesta, F., Testi, L., Orgaz, F. and Villalobos, F.J. 2009. The effects of regulated and continuous deficit irrigation on the water use, growth and yield of olive trees. Eur J Agron 30, 258-265

Kremer, C., Reyes, L., Fichet, T., de Cortázar, V. G. and Haberland, J. 2018. Physiological and production responses of olive (Olea europaea L.) cv. Frantoio under regulated deficit irrigation on a semiarid mediterranean weather condition (Cholqui, Maipo Valley, Chile). Revista de la Facultad de Ciencias Agrarias UNCuyo, 50(1), 73-83.

Melgar, J.C., Mohamed, Y., Navarro, C., Parra, M. C., Benlloch, M. 2008. Long-term growth and yield responses of olive trees to different irrigation regimes. Agr. W. Management 95: 968-972.

Moriana A, Fereres E, Orgaz F, Castro J, Humanes MD, Pastor M (2000) The relations between trunk diameter fluctuations and tree water status in olive tree (Olea europea L.). Acta Hortic 537:293–297

Moriana, A. and Orgaz, F. 2003. Yield responses of a mature olive orchard to water deficits. J. Amer. Soc. Hort. Sci., 128(3):425-431.

Motilva, M.J., Tovar, M.J., Romero, M.P., Alegre, S. and Girona, J. 2000. Influence of regulated deficit irrigation strategies applied to olive trees (*Arbequina cultivar*) on oil yield and oil composition during the fruit ripening period. J Sci Food Agric 80: 2037-2043.

Patumi, M., d'Andria, R, Marsilio, V., Fontanazza, G., Morelli, G., Lanza, B. 2002. Olive and olive oil quality after intensive monocone olive growing (*Olea europaea* L., cv. Kalamata) in different irrigation regimes. Food Chemistry, 77: 27-34

Todolivo. S.f. Olivar en seto, los nuevos marcos de plantación. https://www.todolivo.com/olivar-en-seto/los-nuevos-marcos-de-plantacion/ Accessed June 7, 2021.

Tognetti, R., D`Andria, R., Lavini, A. and Morelli, G. 2006. The effect of deficit irrigation on crop yield and vegetative developmet of *Olea europaea* L. (cv Frantoio and Leccino). Europ J Agronomy 25, 356-364

Tovar, M.J., Romero, M.P., Alegre, S., Girona, J., Motilva, M.J., 2002. Composition and organoleptic characteristics of oil from Arbequina olive (*Olea europaea* L.) trees under deficit irrigation. J. Sci. Food Agric. 82, 1755–1763.

Experimental Investigation of Sustainable Water Production by PV-RO Desalination Systems for Crop Irrigation

Evangelos Dimitriou[a,*], Christos – Spyridon Karavas[a], Athanasios T. Balafoutis[b], Dimitris Manolakos[a] and George Papadakis[a]

[a] Natural Resources & Agricultural Engineering Dept, Agricultural University of Athens, Iera Odos 75, 11855, Athens, Greece

[b] Institute for Bio-Economy & Agro-Technology, CERTH, Dimarchou Georgiadou 118, 38333, Volos, Greece

* Corresponding author. Email: vdimt@aua.gr

Abstract

Water is an essential element of life and 844 million people today lack even basic freshwater services; this number is expected to increase due to population growth and growing food demand. Hence, it is imperative to find new solutions for sustainable production of fresh water, aiming at improving and increasing crop production and minimise environmental impact. Desalination powered by renewable energy seems to be a sustainable solution to this problem. Experimental studies have shown that powering a Reverse Osmosis (RO) desalination unit with photovoltaics (PV) that include short term energy storage offers excellent results regarding the specific energy consumption when operating the RO unit in part-load. However, the variable operation of the RO unit leads to production of desalinated water of variable salinity depending on the instantaneous renewable power available. This paper regards the development of an integrated water management system for lettuce irrigation, using a RO unit powered by PV. An experimental study of lettuce irrigation is executed to study the growth rate, the quality characteristics, and the yield under different salinity levels (0.3, 0.8, 1.2, 1.7, 2.2 and 3 dS m^{-1}) of irrigation water produced by such a RO unit. The objective of this work is to identify the optimum relationship between irrigation water salinity and lettuce yield/quality, so to set the RO unit to produce water of proper quality, while allowing it to operate in part-load conditions using the least energy consumption, contributing in more water for irrigation purposes in semi-arid and arid areas. This way, economic development of such areas will be enforced with adapted water production technologies and assist on sustainable crop production.

Keywords: RO Desalination, PV, irrigation, water salinity, lettuce.

1. Introduction

According to United Nations (2019), the world's population is expected to reach 9.7 billion in 2050. The increase in population leads to increasing demand for food, feed, and nutrients. Water is the most used nutrient carrier and at the same time the most important resource. Today, 70% of global freshwater resources are used in agriculture that is expected to continue dominating water consumption due to population growth and growing food demand (Drechsel et. al., 2015). FAO (2017) estimates that about 60 % more food will be needed by 2050. Agriculture in semi-arid and arid regions is highly dependent on irrigation water (Schacht et. al., 2016) and irrigated food production will increase by more than 50% by 2050 (FAO, 2017). The lack of fresh water in these areas has led to increased use of low quality and brackish groundwater (Wada et. al., 2012). The salinity of irrigation water is known to adversely affect both crop growth and yield (Ayers and Westcot, 1985). For this reason, proper irrigation water management is required to maintain proper salinity levels for irrigation, as high salinity leads to osmotic stress that reduces water intake and suppresses plant growth (Grattan, 2002). Irrigation water may have a higher salinity than drinking water, but the salinity level is a function of the crop relative tolerance, the hydraulic properties of the soil, the meteorological conditions, and the type of salts of the irrigation water in order to maintain the productivity of plants (Raveh & Ben-Gal, 2016).

Hence, development of new strategies and technologies for sustainable freshwater production and use is imperative. Desalination is one of these strategies (Yermiyahu et. al., 2007), as it replaces high-salt water with clean water to improve crop yield and reduce irrigation requirements without environmental effects (Martínez-Alvarez, et. al., 2016).

The main desalination method, which is the most popular and widely used today, is Reverse Osmosis (RO) desalination (Lee et. al., 2011). RO is a process in which the feed water enters to a semipermeable membrane at a pressure greater than the osmotic one and the membrane separates the fresh water from the concentrate solution. RO desalination is an energy consuming process due to the high pressure required for fresh water production (Greenlee et. al., 2009). However, coupling RO units with Renewable Energy (RE) technologies such as photovoltaics (PV) is very attractive proposition, especially in remote areas, as they are disconnected from fossil fuels and their constant price increase and the respective environmental impact. Therefore, RO systems powered by RE can lead to the economic and social development of areas that lack fresh water for both drinking and irrigation (Mohamed & Papadakis, 2015).

Connecting RO units with RE could result in lowering specific energy consumption due to the part-load operation of the desalination unit (Greenlee et. al., 2009; Mohamed & Papadakis, 2015; Dimitriou et. al., 2015a; 2015b). However,

variable operation of the RO unit (transient feed flow rate and pressure) has the effect that the flow rate as well as the electrical conductivity (salinity) of the produced fresh water, varies depending on the instantaneous RE power available. Particularly, low available power to the RO unit leads to a low membrane inlet pressure and as a result the product flow rate will be decreased whereas the salinity of the desalinated water will be increased (Dimitriou et. al., 2015a, 2015b).

Regarding irrigated fresh vegetables, lettuce (Lactuca sativa) is categorized as being moderately salt tolerant (Pascale & Barbieri, 1995). Initial studies showed that the threshold for salinity of irrigation water for lettuce crops was 1.3 dS m^{-1} (Maas & Hoffman, 1977). Subsequently, Pascale & Barbieri (1995) studied that the Romaine lettuce variety is salt tolerant, and the lower salinity limit may be 2.7 dS m^{-1}. However, Andriolo et. al. (2005) showed that the use of irrigation water with a salinity level equal to 4.7 dS m^{-1} did not affect crop yield.

In this paper, an experimental study of lettuce irrigation was executed to study the growth rate, the quality characteristics, and the yield under different salinity levels (0.3, 0.8, 1.2, 1.7, 2.2 and 3 dS m^{-1}) of irrigation water produced by a RO unit operated in part-load conditions. The objective of this work is to identify the impact of water salinity on lettuce yield/quality to find the RO unit operation limits to produce water of adequate quality, while operating in part-load conditions using the least energy consumption for irrigation purposes in semi-arid and arid areas.

2. Description of the experimental set up

2.1. Reverse Osmosis Desalination apparatus

The Reverse Osmosis (RO) desalination system consists of a mixing tank, feed water pump, pretreatment system, high pressure pump equipped with two types of Danfoss pumps and four 25 – 40 inch spiral wound seawater Filmtec membrane modules (Figure 1). A detailed description of the sub-systems and components is given in Dimitriou et al. (2015a).

Figure 1. Reverse Osmosis desalination unit

2.2. Plant material, growth conditions and treatments

The water produced by the RO system was stored in six water tanks depending on the salinity of the desalinated water (0.3, 0.8, 1.2, 1.7, 2.2 and 3 dS m^{-1}). The crop irrigation experiment was conducted in spring 2020 in a glasshouse at AUA (N 37°59′10′′, E 23°42′29′′, altitude 24 m). On February 24th, 2021, lettuce (Lactuca sativa) seedlings at the stage of three true leaves were transplanted in 4L pots filled with sandy soil as a substrate. The characteristics of soil are presented in Table 1.

Table 1. Soil Characteristics

Parameter		Value
pH (1:5)		7,36
EC (1:5) μs/cm		280
P-Olsen (μg/g)		0,017652414
K - available (μg/g)		289,23
Organic Matter %		0,15
Soil Texture	Sand %	92,5
	Clay %	4,8
	Silt %	2,7

The experimental set up consisted of 6 irrigation channels (5.3 m in length, 0.42 m in width, and 0.07 m in height) that were supported on scaffoldings with 4% inclination, accommodating 48 plants each. Each channel was divided into 4 groups of fertilization rate. The first group of 10 pots was irrigated with only water, without fertilizer added, whereas the rest three groups treated with a conventional basic nutrient solution (N:12%, P_2O_5:8%, K_2O:16%) in 33%, 66% and 100% of the optimum fertilization rate. The optimum fertilization rate was set to 12 grams of each pot as reference (Gaiapedia, 2015). The experimental layout is shown graphically in Figure 2a. Irrigation flow was set at 32 ml/min*pot and irrigation time was set to 3min/2times per day, in the morning and in the afternoon. Lettuce plants were grown under natural light conditions. Inside the glasshouse, the daily air temperature was always maintained below 25 °C, while the night temperature was always higher than 12 °C. All the experimental conditions in the glasshouse (irrigation, temperature, CO_2 concentration, ventilation, and lighting) were controlled by MACQU software/system (Geomations, S.A.). Figure 2b shows a perspective of crop irrigation experiment in the glasshouse.

| (a) | (b) |
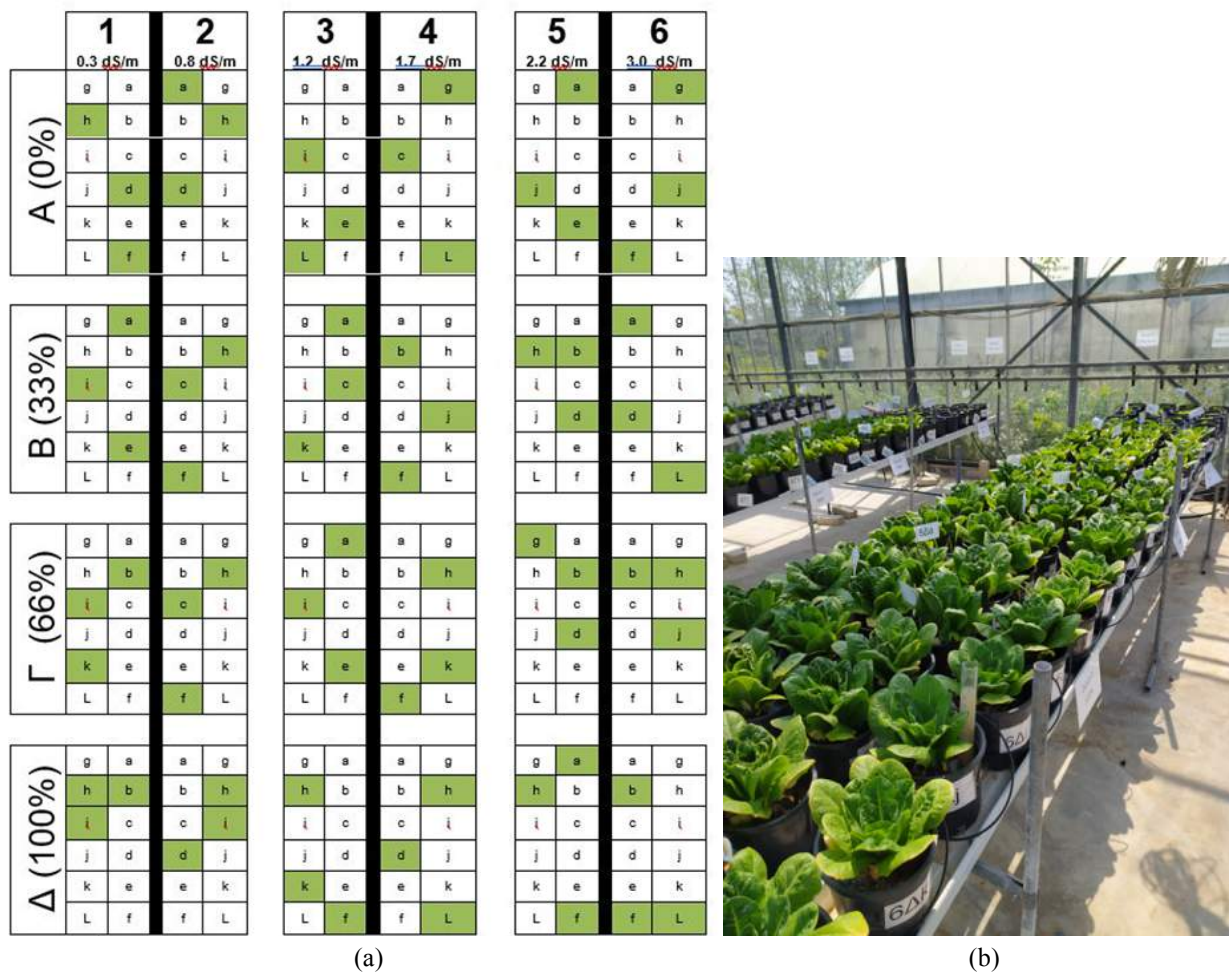
Figure 2. (a) The experimental layout of lettuce cultivation; (b) Lettuce irrigation experiment in the glasshouse

2.3. Biomass determination and growth analysis

During the growing period, height, and diameter of canopy as well as number of leaves were measured every three days to identify the growth rate. For those measures a conventional ruler was used (Figure 3a). After six weeks, plants were harvested, and, after removing soil and dust from the canopies and roots, the fresh weight was measured. The harvested canopies were dried at 70°C for 72h and weighed to account for the dry biomass. The harvesting procedure is presented in Figure 3b.

(a)   (b)
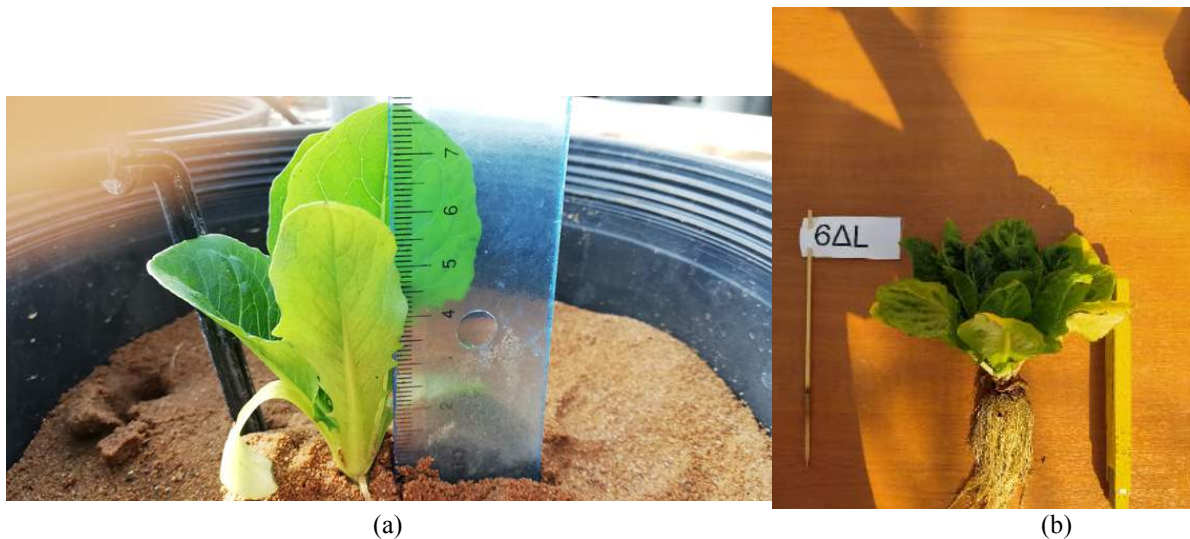
Figure 3. (a) Plant Height measurements; (b) Harvesting procedure of crop irrigation experiment

2.4. Statistical analysis

Analysis of variance (one way-ANOVA) of the experimental data was performed using the software package Statistica for Windows 9.0 (Tulsa, OK, USA). To separate treatment means within each measured parameter, the Duncan's Multiple Range Test was performed at $P \leqslant 0.05$.

3.   Results and Discussion

3.1. RO desalination system results

The main pursue of this experimental work is to determine the optimum operational window of the desalination unit with the lowest specific energy consumption and simultaneously with an acceptable quality of fresh water. The operation of the RO unit is studied in full- and part-load conditions as a simulation of the power produced from PV. To achieve this, the desalination unit was equipped with a DC-driver for DC motor. DC-driver is responsible for the control of the rotational speed of the motor pump assembly. Varying the speed of the motor pump assembly the pressure and the flow rate of the feed water change. Thus, several parameters were measured and recorded such as membrane inlet and outlet pressure, feed/concentrate flow rate, feed/concentrate electrical conductivity as well as the specific energy consumption of the desalination unit.

The specific energy consumption was calculated with the following equation:

$$S_{EC} = \frac{E_m}{Q_p} \qquad \text{(Eq. 1)}$$

where S_{EC} is the specific energy consumption (kWh m^{-3}), E_m is the energy consumed by the motor (kWh), and Q_p is the fresh water production (m^3).

Figure 4 shows the specific energy consumption and the electrical conductivity of the produced water as a function of the membrane inlet pressure of the desalination unit when it operates in part load conditions depending on the available power from the PV system. The experimental results of the desalination unit show that there is an operational window of the RO unit where the specific energy consumption is low (at around 5 Kwh m^{-3}) and the quality of the produced water is also low (below of 1 dS m^{-1}). However, in case of available power from PV system the desalination can continue producing water in higher but possibly acceptable salinity levels for lettuce growth even if the specific energy consumption is high.
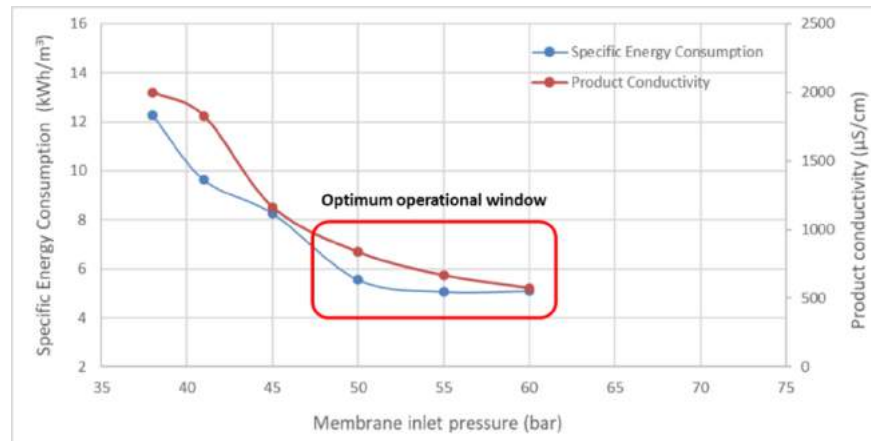
Figure 4. Specific energy consumption and electrical conductivity as a function of the membrane inlet pressure.

3.2. Height and diameter of lettuce canopy

In order to evaluate the lettuce yield/quality in different salinity levels of irrigated water, the height and diameter of canopy were measured every three days during the growing period. The growing rate of lettuce height and diameter, in different salinity levels and fertilization rates, is presented in Figures 5 and 6, respectively. As shown in these figures, the more fertilization rate, the higher and wider gets the lettuce canopy. The height of lettuce leaves ranges from 4 cm for 0% of the optimum fertilization rate, to 24 cm for 100% of the optimum fertilization rate. On the other hand, the diameter of lettuce canopy ranges for 7 cm (at 0% fertilization) to 28 cm (at 100% fertilization). Although the differences in lettuce growth (height and diameter of canopy) between the fertilization rates are obvious, no difference can be noticed between the salinity levels. This was validated by the analysis of variance of the experimental data where there is no statistically significant difference in the mean of height and diameter between the 6 salinity levels of irrigation water in 33%, 66% and 100% of the optimum fertilization rate. Only in the lettuce cultivation group without fertilization (0%) the significance value was $0.0006 \ 10^{-17}$ (i.e. $p < 0.05$), which means that there is a statistically significant difference in the mean of height and diameter between the 6 salinity levels at 0% fertilization.
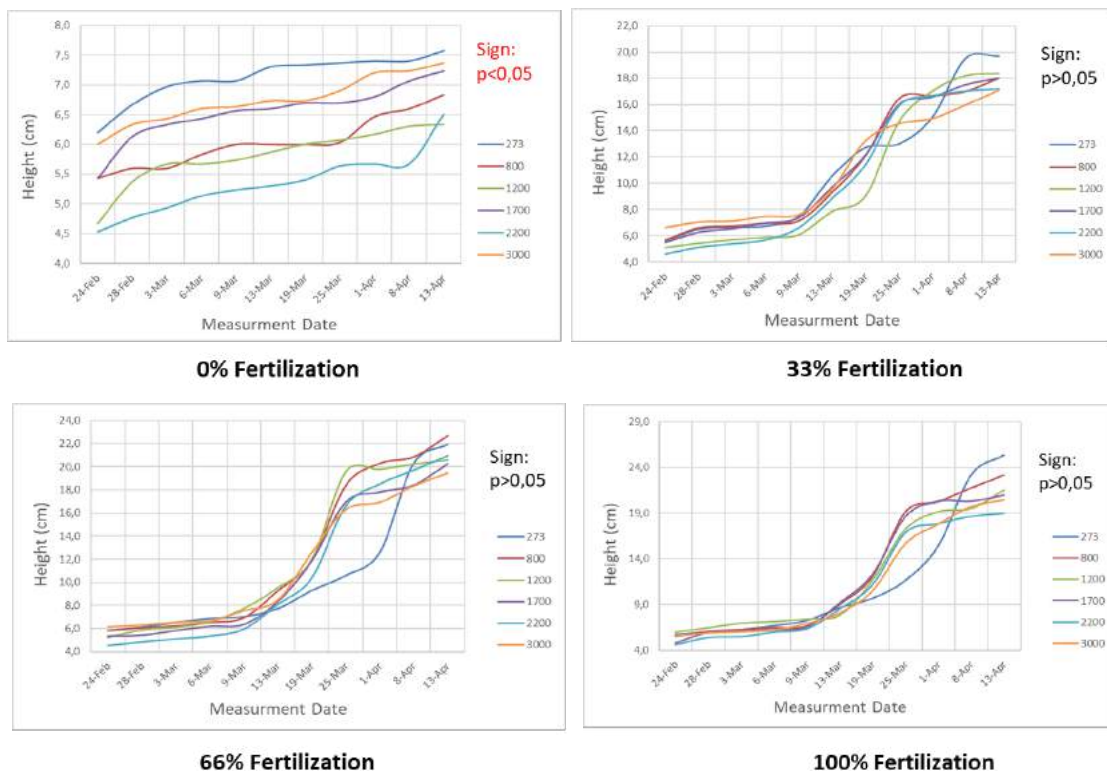
Figure 5. The growing rate of lettuce height in different salinity levels and fertilization rates.
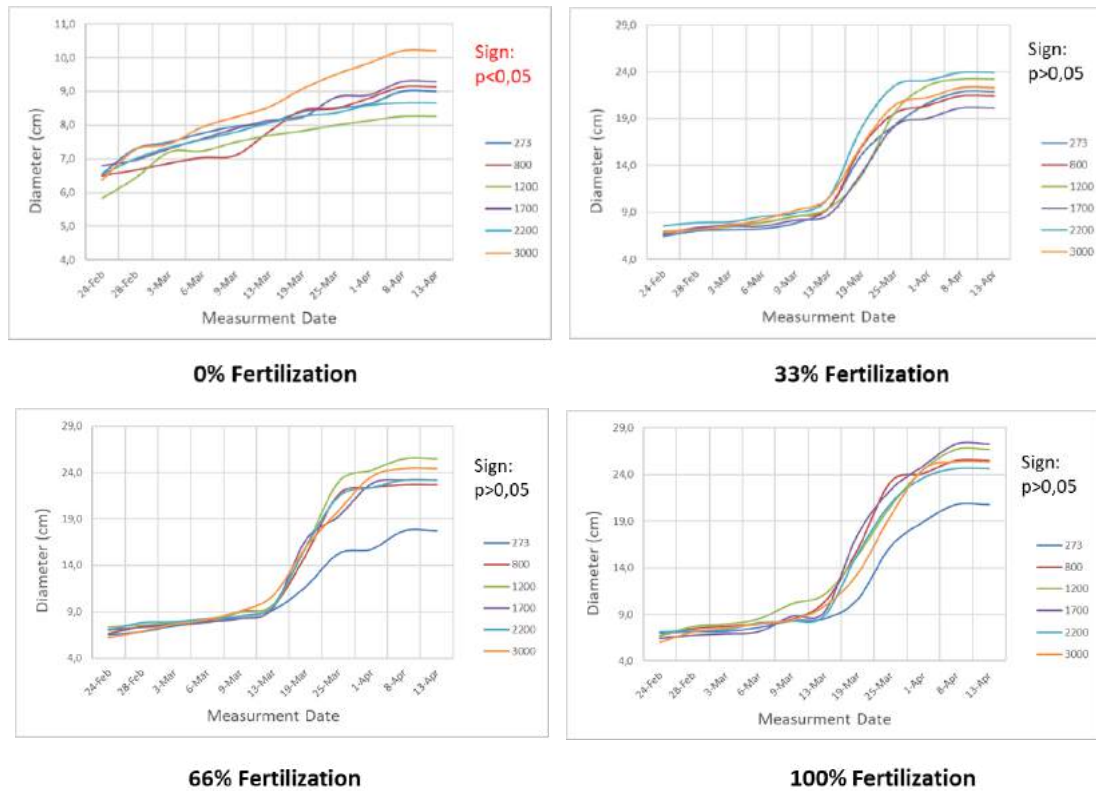
Figure 6. The growing rate of lettuce diameter in different salinity levels and fertilization rates

3.4. Biomass results

Another important parameter for the identification of growth rate was the dry biomass of lettuce leaves. Figure 7 shows the weight of dry biomass of lettuce canopy in different salinity levels and fertilization rates.
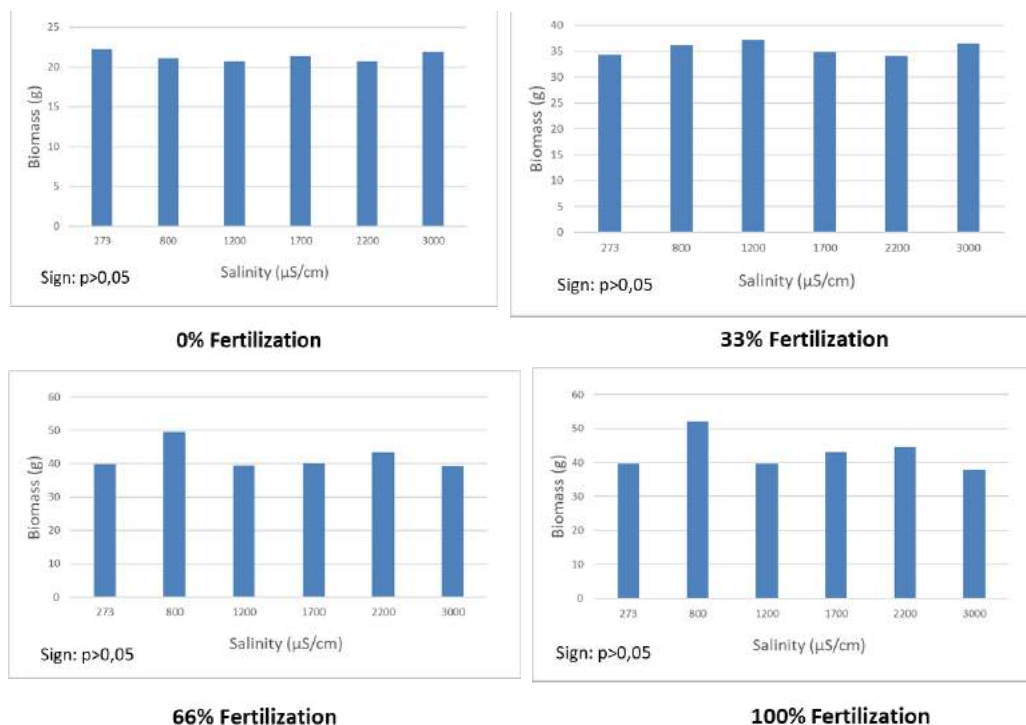
Figure 7. The weight of dry biomass of lettuce canopy in different salinity levels and fertilization rates

Similarly with the height and diameter analysis, the weight of biomass is the same in all 6 salinity levels of irrigation water produced by the desalination unit. According to the analysis of variance of the experimental data there is no statistically significant difference (i.e. $p > 0.05$) in the mean of weight of dry biomass between the 6 salinity levels in any of 4 groups of fertilization. Hence, the lettuce can be grown in any of 6 salinity levels of irrigation water produced by a PV- RO system without any impact on its yield/quality. A concentrated graph regarding the results of weight of dry biomass of lettuce leaves in different salinity levels of irrigation water and different fertilization range is presented in Figure 8.
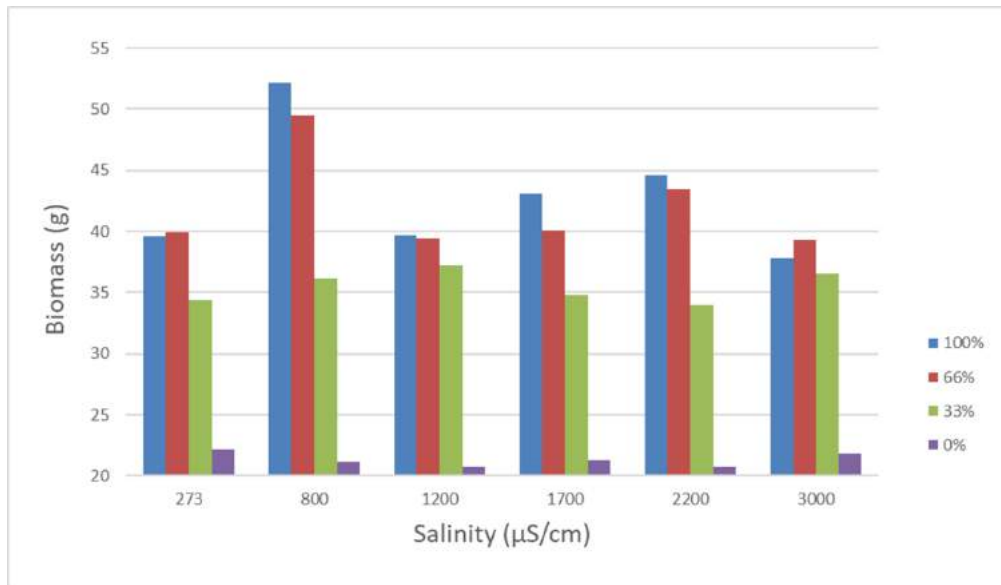
Figure 8. The weight of dry biomass of lettuce canopy in different salinity levels and fertilization rates

4. Conclusions

The conclusions arising from this work could be evaluated with regard to the operating efficiency of an RO desalination unit and the quality of the irrigation water produced by such PV-RO system as well as the impact of irrigation water salinity on lettuce yield/quality.

- There is no statistically significant difference in the lettuce growth rate and yield between the 6 different salinity levels of irrigation water produced by the RO desalination unit.
- The lettuce can be grown in any of 6 salinity levels of irrigation water produced by the PV-RO system without any impact on its yield/quality and with the least energy consumption, contributing to reduced water desalination cost.
- The best salinity level for lettuce irrigation purposes and simultaneously with the least energy consumption for the desalinated water by PV-RO system is 0.3, 0.8 and 1,2 dS m^{-1} with a specific energy consumption around to 5 kWh m^{-3}. In case of available energy produced by PV system the RO unit can continue producing irrigation water in higher salinity without any impact on lettuce growth even if the specific energy consumption is high.

5. Acknowledgements

References

United Nations, 2019, World Population Prospects 2019, https://population.un.org/wpp/Publications/Files/WPP2019_Highlights.pdf, Accessed on May 2021.

Food and Agriculture Organization of the United Nations, 2017, Water for Sustainable Food and Agriculture A report produced for the G20 Presidency of Germany, http://www.fao.org/3/i7959e/i7959e.pdf, Accessed on May 2021.

P. Drechsel, G. Danso, M. Qadir, Wastewater use in agriculture: challenges in assessing costs and benefits, Wastewater, Springer, 2015, pp. 139–152.

K. Schacht, Y. Chen, J. Tarchitzky, B. Marschner, The use of treated wastewater for irrigation as a component of integrated water resources management: reducing environmental implications on soil and groundwater by evaluating site-specific soil sensitivities, Integrated Water Resources Management: Concept, Research and Implementation, Springer, 2016, pp. 459–470.

Y. Wada, L. Beek, M.F. Bierkens, Non sustainable groundwater sustaining irrigation: a global assessment, Water Resources Research, 48 (2012).

R.S. Ayers, D.W. Westcot, Water quality for agriculture, FAO Irrig. Drain. Paper 29, FAO, Rome, 1985.

S. Grattan, Irrigation Water Salinity and Crop Production, UCANR Publications, 2002.

E. Raveh, A. Ben-Gal, Irrigation with water containing salts: evidence from a macrodata national case study in Israel, Agricultural Water Management, 170 (2016) 176–179.

U. Yermiyahu, A. Tal, A. Ben-Gal, A. Bar-Tal, J. Tarchitzky, O. Lahav, Environmental science - rethinking desalinated water quality and agriculture, Science 318 (2007) 920–921.

V. Martínez-Alvarez, B. Martin-Gorriz, M. Soto-García, Seawater desalination for crop irrigation—a review of current experiences and revealed key issues, Desalination 381 (2016) 58–70.

K.P. Lee, T.C. Arnot, D. Mattia, A review of reverse osmosis membrane materials for desalination—development to date and future potential, Journal of Membrane Science, 370 (2011) 1-22.

L.F. Greenlee, D.F. Lawler, B.D. Freeman, B. Marrot, P. Moulin, Reverse osmosis desalination: water sources, technology, and today's challenges, Water research, 43 (2009) 2317-2348.

E.S. Mohamed, G. Papadakis, Advances of Renewable Energy Powered Desalination, Handbook of Clean Energy Systems, (2015).

E. Dimitriou, E.S. Mohamed, G. Kyriakarakos, G. Papadakis. Experimental investigation of the performance of a reverse osmosis desalination unit under full- and part-load operation. Desalination and Water Treatment, 12 (2015) 1-9.

E. Dimitriou, E.S. Mohamed, C. Karavas, G. Papadakis, Experimental comparison of the performance of two reverse osmosis desalination units equipped with different energy recovery devices, Desalination and Water Treatment, 55 (2015) 3019-3026.

S. De Pascale, and G. Barbieri. "Effects of soil salinity from long-term irrigation with saline-sodic water on yield and quality of winter vegetable crops." Scientia Horticulturae 64 (3) (1995), 145-157.

E.V. Maas, and G.J. Hoffman. Crop salt tolerance–current assessment. Journal of the irrigation and drainage division, 103 (2) (1977), 115-134.

J.L. Andriolo, G.L.D. Luz, M.H. Witter, R.D.S. Godoi, G.T. Barros and O.C. Bortolotto. "Growth and yield of lettuce plants under salinity." Horticultura Brasileira 23 (4) (2005), 931-934.

Gaiapedia, "Lettuce Cultivation", 2015, http://www.gaiapedia.gr/gaiapedia/index.php/Καλλιέργεια_μαρουλιού Accessed on February 2020.

Geomations S.A., Measurement Control & Management, http://www.geomations.com/EN/Products/Products.htm

Influence of Irrigation and Nitrogen Fertilization on Kiwifruit Production

Rui Pinto[1,2], M. Isabel Valin[1,2*], L. Miguel Brito[3], Rute Rego[2], Carlos Cardoso[1], Nuno Mariz-Ponte[4], Isabel Mourão[3], Raúl Rodrigues[1,2], Luísa Moura[1,2]

[1]Instituto Politécnico de Viana do Castelo, Escola Superior Agrária, Refóios, 4990-706 Ponte de Lima, Portugal.

[2]Centro de Investigação e Desenvolvimento em Sistemas Agroalimentares e Sustentabilidade (CISAS), Rua Escola Industrial e Comercial de Nun'Álvares, nº 34, 4900-347 Viana do Castelo, Portugal.

[3]Centro de Investigação de Montanha (CIMO). Escola Superior Agrária, Instituto Politécnico de Viana do Castelo, Refóios, 4990-706 Ponte de Lima, Portugal.

[4]LAQV-REQUIMTE, Departamento de biologia, Faculdade de Ciências (FCUP), Universidade do Porto, 4169-007 Porto, Portugal.

* Corresponding author. Email: isabelvalin@esa.ipvc.pt

Abstract

The ineffective water use and nitrogen (N) fertilization increases the cost of crop production and negatively affects the environment. Therefore, the present study aims to access the irrigation scheduling and N fertilization on kiwi production. A field experiment with 7500 m^2 was set up in 2020 as a randomized block design at the farm of Picas in the NW of Portugal with three blocks and factorial treatment structure. Nitrogen fertilization including full fertilization (50 kg ha^{-1}, N50) and deficit fertilization (30 kg ha^{-1}, N30) was combined with two irrigation rates comprising full irrigation (manager's irrigation schedule, FI) and deficit irrigation (DI = 50% FI). During the irrigation period (1st of June to the 9th of September) water supplied by full irrigation was 26 m^3 ha^{-1} day^{-1}. Soil water content and stem water potential were assessed with the multi-depth capacitance probe and the Scholander pressure chamber, respectively.

Soil water content for FI and DI conditions were above field capacity during the irrigation period and stem water potential remained between -0.7 and -0.5 MPa for FI and DI except in the beginning of June for DI (-0.8 MPa). Therefore, these results suggest that the kiwivines were not exposed to water stress for FI and DI. Kiwifruit yield was similar for all treatments. In contrast, the weight of the kiwis with large caliber 25-18 (> 120 g) increased for FI compared to DI. Moreover, the DI-N30 treatment showed a higher total solid soluble (ºBrix) content and caused a higher flesh firmness compared to FI-N50 at harvest.

This study suggests that reducing water supply to 13 m^3 ha^{-1} day^{-1} average and approximately 30 kg ha^{-1} N fertilization may maintain yields and increase kiwifruit quality in the edaphoclimatic conditions of the farm of Picas and following cultural practices used by orchard manager. Nevertheless, further research is needed to make solid conclusions on the effect of irrigation and N fertilization management on kiwi production.

Keywords: *Actinidia deliciosa*, fruit quality, soil water content, nitrogen fertilization, yield

1. Introduction

The kiwifruit production is of economic importance in the region of Entre-Douro e Minho and Beira Litoral situated in the NW of Portugal (Antunes et al., 2018). In this region, actinidia is very sensitive to water stress from June to September, and crop water uptake is high. Yet, it is widely recognized that the fresh water available for agriculture is decreasing (Fitton et al., 2019) and that increasing irrigation will increase N leaching beyond the root zone (Geerts et al., 2009). In addition, the contamination of the ground water is mainly associated with excessive N fertilization (Ju et al., 2007). In this context, it is crucial to develop effective water use and N management to improve water quality, maximizing net economic benefit.

The sensitivity of kiwifruit development to soil water availability has been reported by several authors (Ciordia et al., 1993; Judd et al., 1989; Lagos et al., 2017). Water stress can induce changes in fruit yield and quality. Fruit size is generally reduced by water deficit as opposed to the quality of the fruits, such as the increasing of sugar content or improved colour, which is enhanced by lower irrigation (Steduto et al., 2012). The technical approach to optimize irrigation program is based on monitoring soil water moisture content and plant water status (Steduto et al., 2012). The plant water status is determined by the stem water potential (ψ_{stem}) measured on a non-transpiring leaf that indicates the capacity of kiwivine to conduct water from soil to the atmosphere and is considered the most truthful indicator of plant water stress because is less influenced by environmental variability (McCutchan and Shackel, 1992; Choné et al., 2001).

Nitrogen fertilization is one of the most important factors to promote vigor and obtain large fruits. However, applied in excess can adversely affect fruit quality and the environment (Buwalda et al., 1990; Lu et al., 2018). Furthermore, high level of N induces excessive vigor and delays fruit maturity as well as increases susceptibility to pests and diseases. The role of N in all aspects of cell metabolism and its effect on vine vigor requires an adequate N application rate, but the amount of N fertilizer to apply remains unclear in spite of substantial research over the years (Morton, 2013). Hence, growers need information based on local field experiments to decide on fertilization practices. On the other hand, the orchard management practices change according to the preferred fruit size of the market demand. However, growers need to be aware of the fact that the cultural practices that lead to the increased fruit size tend to lower fruit quality (Foundation et al., 2018). Therefore, the aim of this study was to assess under field conditions the effect of irrigation and N supply reduction on yield and quality of kiwifruit.

2. Materials and methods

This study was carried out at the kiwi commercial orchard (41º31´N; 8º27´W) owned by Kiwi Greensun company located in the NW of Portugal. Kiwifruit vines of cv. Haryward were planted in 1988 with a north-south orientation and 5×2.5 m spacing, trained to a pergola trellis system 1.9 m in elevation. Soil has a sandy clay loam texture with a bulk density of 0.93 and the value of the moisture content retained by the soil at field capacity is 320 mm m^{-1} determined directly in the field using maximum values of soil water content after drainage. The soil organic matter (OM) content was 3.5% and the soil reaction was acidic with a pH (H$_2$O) value of 5.6.

A field experiment was set up as a randomized block design with 3 replicated plots per treatment and a combination of two rates of irrigation and fertilization as a factorial treatment structure. Treatments included full irrigation (manager's irrigation schedule, FI) and deficit irrigation (DI = 50% FI) combined with full fertilization (50 kg ha^{-1}, N50) and deficit fertilization (30 kg ha^{-1}, N30). The kiwivines were planted 1988 with a row-row and plant-plant spacing of 5.0 and 2.5 m, respectively. The experimental site with 7500 m^2 was divided in 12 plots of 625 m^2 and 5 rows each. Three plants of each replicate treatment were collected from the middle row.

The plants were irrigated using a drip system with 2.2 L h^{-1} drippers spacing 50 cm. An amount of 26.4 m^3 ha^{-1} day^{-1} (33 L day^{-1} plant^{-1}) was supplied at full irrigation from the 1st of June until the 9th of September adding up a total of 267 mm applied during this period. The period of irrigation corresponded to the phenological growth stages of kiwifruit development (28th of May to 23rd of July) and maturity (scale BBCH) (Salinero et al. 2009). Soil water content was evaluated every two weeks with the multi-depth capacitance probe (Diviner 2000). One PVC plastic access tube was installed on each plot 0.3 m away from the drip line and three scaled readings were recorded at depth intervals of 0.1 m down to 0.8 m. The stem water potential (ψ_{stem}) was assessed every two weeks with the Scholander pressure chamber. A shaded leaf per tree was selected from three trees in each treatment, leaves were placed inside an aluminium plastic bag for 60 minutes before excision. Measurements were performed according to Scholander et al. (1965) and following the recommendations of Turner (1988).

The fresh weight was recorded for each fruit grade clustered in four classes: (i) waste < 60 g fruit^{-1}; (ii) small 60 g – 80 g fruit^{-1}; (iii) medium 80 g - 120 g fruit^{-1}; and (iv) large > 120 g fruit^{-1}. The fruit dry matter (DM, %), firmness (penetrometer with 8 mm diameter tip, Newton-N) and the total soluble solids content (TSS, ºBrix) were evaluated in 10 fruits per each treatment repetition, immediately after harvest.

All statistical calculations were carried out using SPSS v. 17.0 for windows (SPSS Inc.). Two-way factorial analysis of variance (ANOVA) was performed by the SPSS general linear model procedure, and a probability level of $P < 0.05$ was applied to determine statistical significance between treatment means.

3. Results and Discussion

3.1 Irrigation effects on soil water content and stem water potential

Changes on soil water content between FI and DI were not significant with watering reduction (Figure 1). In addition, the FI (413 to 359 mm m^{-1}) and DI (423 to 340 mm m^{-1}) remained above field capacity between June and September. The volumes of water applied during the irrigation period (267 and 133 mm) were similar to those reported by Currie et al. 2008 (350 to 200 mm). However, these authors reported that the soil moisture levels decreased after applying half irrigation as well as in a study by Lagos et al. (2017) the soil moisture content descended up to 50% when the irrigation was reduced from 960 to 594 mm. Here, the similarity between soil water content for FI and DI is probably due to the presence of high water table. This over-watering increased the soil moisture content at lower levels (data not show). In agreement, there were no significant differences on ψ_{stem} for FI and DI during the irrigation period, except for DI in the beginning of June (Figure 2). The average values were -0,58 MPa and -0,66 MPa for FI and DI, respectively (Figure 2). The values of stem water

potential, between -0.7 and -0.5 MPa, except for DI in the beginning of June (- 0.8 MPa) indicate that kiwivines were not exposed to water stress during the irrigation period (Orellana, 2020), even though there was 50% water saving.
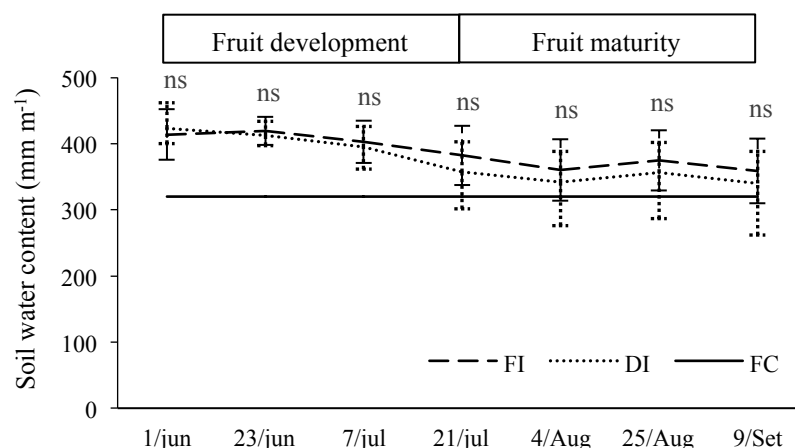
Figure 1. Soil water content for the full and deficit irrigation treatments (FI and DI; mm m^{-1}) and for the field capacity (FC; mm m^{-1}) over the growing season. Means are not significantly different (ns).
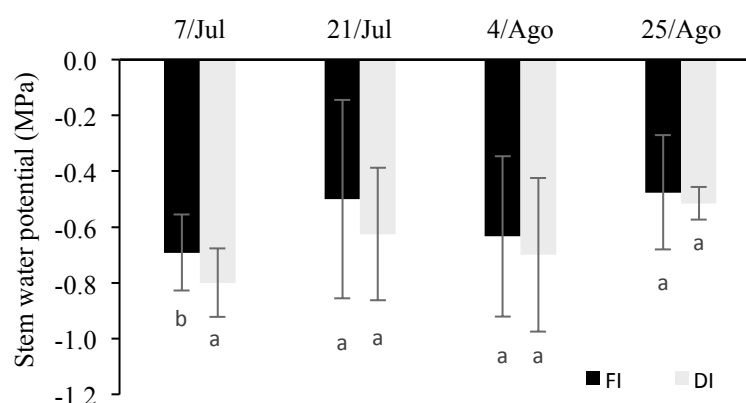
Figure 2. Stem water potential (MPa) for kiwivines with full irrigation (FI) and deficit irrigation (DI) over the growing season. Bars, within each sampling date, with different letters are significantly different (P < 0.05).

3.2 Kiwifruit yield and grade

A large amount of studies has documented a decrease in kiwifruit yield after water reduction (Currie et al., 2008; Lagos et al., 2017). Actually, fruit growth is more closely linked with the water supply than the rate of photosynthesis (Judd et al., 1989). The reduction weight in harvest occurs if the supply of water is limited in the summer but this effect is particularly severe when the water stress is inflicted early in the season due to the competition for carbohydrate after flowering (Miller et al., 1998). In a study by Currie et al. (2008) it was found that applying half irrigation and a quarter irrigation the fruit weight decreased 3.4 g and 8.9 g, respectively, in comparison to full irrigation equivalent to orchards manager irrigation schedule (192 or 384 L on each vine every week, corresponding to a total irrigation of 350 mm). In another study, Ciordia et al. (1993) found that the yield decreased for the vines irrigated on the basis of 36.3% ET (7,68 kg plant[-1]) and 63,5% ET (8,71 kg plant[-1]) compared to 100% ET (9,44 kg plant[-1]). Likewise, Chandel et al. (2004) observed that kiwifruit yield decreased from 86 to 70 kg plant[-1] when the irrigation was reduced from 100% ET to 60% ET. The lower yield can be explained because the soil moisture nearly at field capacity with 100% ET (23%) decreased for values between 23 and 15% when the irrigation was reduced to 60% ET. In the present study the kiwifruit yield for FI (43 kg plant[-1]) and DI (36 kg plant[-1]) were not significantly different because the soil moisture content was maintained above field capacity after 50%

water reduction during the irrigation period (figure 3b). These results are in line with Lagos et al. (2017) that indicated that the irrigation based on 100% ET (960 mm) and different water restriction from 960 to 305 mm during the irrigation period did not significantly affect production.

Nitrogen fertilization is a cultural practice with great effect on kiwifruit yield (Pacheco et al., 2008). However, several authors (Vizotto et al., 1999; Pacheco et al. 2008) found a negative effect of high rates of N supply on kiwifruit yield. A study with three levels of N (30, 60 and 90 kg ha^{-1}) have indicated that the highest yield was obtained with 60 kg ha^{-1} N (Pacheco et al., 2008). Moreover, yield reductions at N rates above 50 kg ha^{-1} were reported by Buwalda et al. (1990). This may be partly explained because reduced N application encourage the removal of carbohydrates from the leaves to the fruit due to the reduction of carbon assimilation via photosynthesis promoting the partitioning of carbon to favor fruit growth (Mills et al., 2009). In addition, the risk of leaching is greatly reduced with moderate N input rates (Lu et al., 2018). The level of N applied in this experiment (between 30 and 50 kg ha^{-1}) and the leaf N content (20 to 25 g kg^{-1}) achieved here were under the recommended N application of 90 kg ha^{-1} N and the optimum N content (25 to 32 g kg^{-1}) to achieve yields of 20 and 25 t ha^{-1} (LQARS, 2005). The higher yields (40 and 39 t ha^{-1}) found here with the application of lower N rates (50 and 30 kg ha^{-1}) by fertigation and the similarity of crop yields achieved with the application of both of these N rates (Figure 3c) may be explained for a number of possible reasons. The mineralization of soil organic matter can be a major source of mineral N. It has been estimated that 1.5 to 3.5% of soil organic N is mineralized annually (Seiter and Horwath, 2004). This means 40 to 105 kg N ha^{-1} for a soil with 3.5% OM. The application of foliar N is an efficient technique to supply N avoiding stimulation of vegetative vigor (Dong et al., 2005) and, a commercial foliar fertilizer (Maxima, Green Iberia) based on amino acids (4% N) was applied 8 times from flowering until the beginning of fruit maturation. Furthermore, N recycled by mulched prunings will eventually be available for crop uptake in the long term (2005; Mills et al., 2009), as well as N inputs by the farm practice of application of 15 to 20 m^3 of an organic amendment with 1,6% N (Fertibom from Resinorte) every 4 years.

Figure 3. Kiwifruit yield (t ha^{-1}) in response to: (a) treatments with deficit irrigation and deficit fertilization (DI-N30), full irrigation and deficit fertilization (FI-N30), deficit irrigation and full fertilization (DI-N50) and, full irrigation and full fertilization (FI-N50); (b) full irrigation (FI) and deficit irrigation (DI) for the average of fertilization rates; and (c) full fertilization (N50) and deficit fertilization (N30) for the average of irrigation rates. Bars with different letters are significantly different (P < 0.05).

Water reduction affected the kiwifruit grade distribution. The weight of the kiwis with Large grade 25-18 (> 120 g) increased for FI (20 kg plant^{-1}) compared to DI (11 kg plant^{-1}) (figure 4). This is consistent with observations by other authors (Ciordia et al., 1993; Bonany and Camps, 1998; Judd et al., 1999). The percentage of kiwi with Large grade (> 110 g) was 80,5% with 100% ET but this percentage was reduced to 49.9% and 24.0% with vines irrigated with 63,5% ET and 36.3% ET, respectively (Ciordia et al. (1993).

3.3 kiwifruit quality at harvest

It is commonly accepted that the quality parameters improve applying less irrigation and less fertilization (Currie et al., 2008; Bonany and Camps, 1998, Chandel et al., 2004). Accordingly, the flesh firmness increased for DI-N30 in comparison to FI-N50 and the total soluble solids (TSS) decreased for FI-N50 compared to the other treatments (table 1). These results are in agreement with Pacheco et al. (2010) that set up an experiment with three levels of N (30, 60 and 90 kg ha^{-1}) and

found out that the lowest flesh firmness was obtained with the highest level of N. Similar results were obtained by Pacheco et al. (2008). Other studies have indicated that TSS content increased applying lower irrigation (Chandel et al., 2004; Currie et al., 2008). Currie et al. (2008) reported that TSS was reduced 0.3% and 0.9%, applying half irrigation and a quarter irrigation, respectively. Miller et al. (1998) pointed out that a moderate water stress late in the season improved fruit quality in terms of higher TSS. This might be due to the dilution effect in the large fruits under high soil moisture content (Chandel et al. 2014). Conversely, there are studies in which TSS content was not affected by N fertilization (Costa et al., 1997; Vizzoto et al., 1999; Pacheco et al. 2008). Pacheco et al. (2008) pointed out that different levels of N fertilization (30, 60 or 90 kg ha^{-1} N) did not influence TSS content.
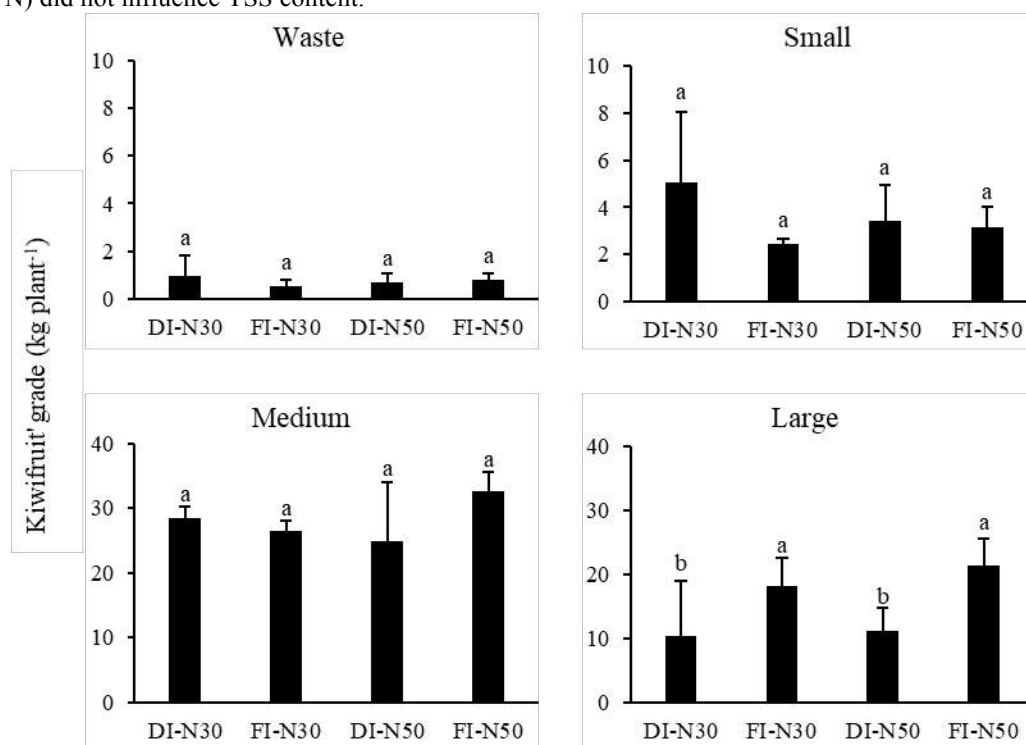
Figure 4. Calibration weights (kg plant^{-1}) of kiwifruit classes (waste < 60 g fruit^{-1}; small 60 g – 80 g fruit^{-1}; medium 80 g – 120 g fruit^{-1}; and large > 120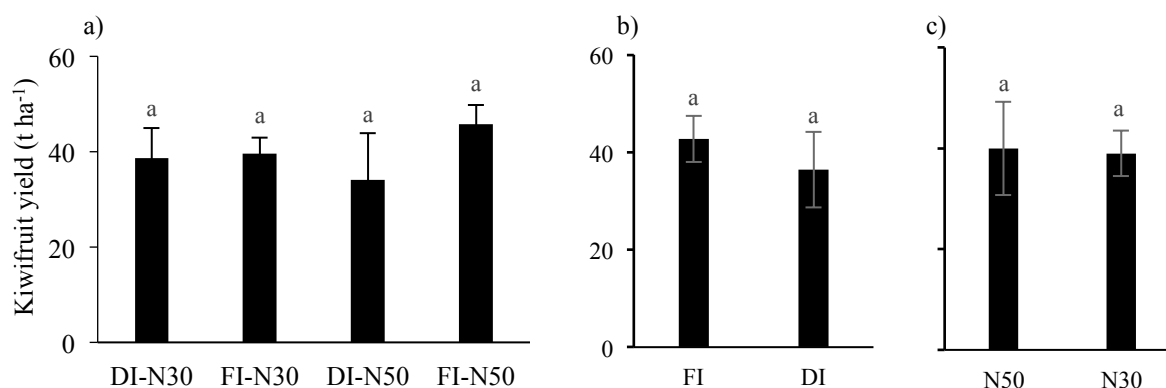 g fruit^{-1}) in response to the treatments with deficit irrigation and deficit fertilization (DI-N30), full irrigation and deficit fertilization (FI-N30), deficit irrigation and full fertilization (DI-N50) and, full irrigation and full fertilization (FI-N50). Bars with different letters are significantly different (P < 0.05).

Table 1. Dry matter (%), firmness (N) and total solid soluble content (ºBrix) response to the treatments with deficit irrigation and deficit fertilization (DI-N30), full irrigation and deficit fertilization (FI-N30), deficit irrigation and full fertilization (DI-N50) and, full irrigation and full fertilization (FI-N50) at harvest. Means in the same row followed by different letters are significantly different (P < 0.05).

Fruit quality		DI-N30	FI-N30	DI-N50	FI-N50
Dry matter	(%)	15.2 a	14.8 a	15.4 a	14.3 a
Firmness	(N)	60.8 a	57.1 ab	58.1 ab	55.3 b
Total soluble solids	(°Brix)	8.3 a	8.6 a	8.4 a	7.5 b

4. Conclusion

The application of half irrigation (133 mm) compared to the orchard manager irrigation schedule (267 mm) during the summer period, and the reduction of N fertigation from 50 kg ha^{-1} to 30 kg ha^{-1}, did not significantly affect crop yield and improved the kiwifruit quality in Quinta das Picas owned by Kiwi Greensun. Thus, for the edaphoclimatic conditions of the farm of Picas in the NW Portugal and following the cultural practices used by typical orchard managers, the deficit irrigation is an alternative for increasing fruit quality without affecting yield.

Acknowledgements

References

Antunes, M.D., J. Franco, F. Veloso, T. Panagopoulos, 2018. The evolution of kiwifruit production in Portugal. Acta Horticulturae 1218, 17-21.

Bonany, J., F. Camps, 1998. Effects of different irrigation levels on apple fruit quality. Acta Horticulturae 466, 47-52.

Buwalda, J.G., G.J. Wilson, G.S. Smith, R.A. Litter, 1990. The development and effects of nitrogen deficiency in field-grown kiwifruit (*Actinidia deliciosa*) vines. Plant and Soil 129, 173-182.

Chandel, J.S., R.K. Rana, A.S. Rehalia, 2004. Comparative performance of drip and surface methods of irrigation in kiwifruit (*Actinidia deliciosa*) cv. Allison. Acta Horticulturae 662, 205-211.

Choné, X., C. Leeuwen, D. Dubourdieu, J.P. Gaudillére. 2001. Stem water potential is a sensitive indicator of grapevine water status. Annals of Botany 87, 477-483.

Ciordia, M., J.G. Aparisi, 1993. The effect of different irrigation rates on kiwifruit growth and cropping. Acta Horticulturae 1993, 235-240.

Currie, M., S. Green, P. Martin, N. Currie, 2008. Thirsty vines can give tasty fruit, but at a cost. New Zeeland Kiwifruit Journal 1(185), 7-12.

Dong, S., D. Neilsen, G.H. Nielsen, L.H. Fulchigami, 2005. Foliar N application reduces soil NO_3^--N leaching loss in apple orchards. Plant and Soil 268, 357-366.

Fitton, N., P. Alexandre, N. Arnell, B. Bajzelj, K. Calvin, J. Doelman, J.S. Gerber, P. Havlik, P.C. West, P. Smith. et al., 2019. The vulnerabilities of agricultural land and food production to future water scarcity. Global Environment Changes 58, 1-10.

Foundation A., A. Baker, B. Luke, B. Hyd, D. Armour, J. Lunan, J. Troughton, J. Benge, K. Lonman et al., 2018. Kiwifruit book. NZKGI press. 138 p.

Geerts, S., D. Raes. 2009. Deficit irrigation as on-farm strategy to maximize crop water productivity in dry areas. Agricultural water management 96, 1275-1284.

Ju X. T., C.L. Kou, P. Christie, Z.X. Dou, F.S. Zhang, 2007. Changes in the soil environment from excessive application of fertilizers and manures to two contrasting intensive cropping systems on the North China Plain. Environmental Pollution 145, 497–506.

Judd, M.J., K.J. McAneney, K.S. Wilson, 1989. Influence of water stress on kiwi growth. Irrigation Science 10, 303-311.

Lagos, L.O., W. Lama, J. Hirzel, C. Souto, M. Lillo, 2017. Regulated deficit irrigation evaluation on kiwi (*Actinidea deliciosa*) production. Agrociência 51, 359-372.

LQARS, 2005. Produção integrada da cultura da actinídea. INIAP, LQARS, Lisboa 56 p.

Lu, Y., T. Kang, J. Gao, Z., Z. Chen, J. Zhou, 2018. Reducing nitrogen fertilization of intensive kiwifruit orchards decreases nitrate accumulation in soil without compromising crop production. Journal of Integrative Agriculture 17(6), 1421-1431.

McCutchan H., K.A. Shackel, 1992. Stem-water potential as a sensitive indicator of water stress in prune trees (Prunus domestica L. cv French). Journal of American Society and Horticulture Science 117(4), 607-611.

Miller, S.A., G.S. Smith, H.L., Bolding, A. Johansson, 1998. Effects of water stress on fruit quality attributes of kiwifruit. Annals of Botany 81, 73-81.

Mills, T., H. Boldingh, P. Blattmann, S. Green, J. Meekings, 2009. Nitrogen application rate and the change in carbohydrate concentration in leaves, fruit, and canes of gold kiwifruit. Journal of Plant Nutrition 32, 2140-2157.

Morton, R.M. 2013. Kiwifruit (ActinidIa spp.) vine and fruit responses to nitrogen fertilizer applied to the soil and leaves. PhD Thesis, Massey University, Palmerston North, New Zealand.

Orellana, A.A., C. Atenas, D. Silva, 2019. Riego en kiwis. Universidade Agronomia Chile Press. 40 p.

Pacheco, C., F. Calouro, S. Vieira, F. Santos, N. Neves, F. Curado, J. Franco, S. Rodrigues, D. Antunes, 2008. Influence of nitrogen and potassium on yield, fruit quality and mineral composition of kiwifruit. International Journal of Energy and Environment 2, 9-15.

Salinero., M.C., P. Vela, M.J. Sainz. 2009. Phenological growth stages of kiwifruit (*Actinidea deliciosa* 'Hayward'). Scientia Horticulturae 121, 27-31.

Scholander P., H. Hammel, E.D. Bradstreet E.A. Hemmingsen, 1965. Sap pressure in vascular plants: negative hydrostatic pressure can be measured in plants. Science 148, 339–346.

Seiter, S., W.R. Horwath, 2004. Soil organic matter in sustainable agriculture. New York, CRC Press, 398 p.

Steduto, P., T.C. Hsiao, E. Fereres, D. Raes, 2012. Crop yield response to water. Food Agriculture Organization Press. 500 p.

Turner N.C., 1988. Measurement of plant water status by the pressure chamber technique. Irrigation Science 9, 289–308.

Vizzoto, O., LG. Costa, 1999. Relationship between nitrogen and fruit quality in kiwifruit. In *4th International kiwi Symposium*. Santiago, Chile, Jan 11-14. Eds. J. Retamales et al. Acta Horticulturae. 498, 165-172.

Calibration of Crop Coefficients of *Vitis vinifera* L. cv. Loureiro Using SIMDualKc

Simão P. Silva [a*] , M. Isabel Valín [a], Susana Mendes [a], Cláudio Araujo-Paredes [b], Javier J Cancela[c]

[a] Centre for Research and Development, in Agrifood Systems and Sustainability (CISAS), Escola Superior Agrária, Instituto Politécnico de Viana do Castelo, Portugal;

[b] Research Unit in Materials, Energy and Environment for Sustainability (PROMETHEUS), Escola Superior Agrária, Instituto Politécnico de Viana do Castelo, Portugal.

[c] GI-1716 Projects and Planification. Agroforestry Engineering Department, Escuela Politécnica Superior de Ingeniería Lugo, University of Santiago de Compostela, Spain;

* Corresponding author. Email: silvasimao@esa.ipvc.pt

Abstract

Vineyard irrigation management in a temperate zone requires knowledge of the crop water requirements. The main objective of this work was to apply the dual crop coefficient approach (K_{cb}) to estimate the crop evapotranspiration (ET_c) of *Vitis vinifera* cv. Loureiro in presence of an active ground cover. The study was carried out in a commercial vineyard during two growing seasons (2019-2020), located in Ponte de Lima, NW of Portugal (41 ° 40'32.16 "N 8 ° 32'6.21" W). Two irrigation treatments were considered, Full Irrigation (FI; 100% of ET_c) and Deficit Irrigation (DI, 50% of ET_c) and a control treatment: rain-fed (R). In this study were calculated soil evaporation, and grapevines and active ground cover transpiration, in the last case using data about active soil ground cover determined during both seasons. The ET_c was estimated using the SIMDualKc model, which performs the soil water balance with the dual-Kc approach. This balance was made by calculating the basal coefficient (K_{cb}), obtained through the coefficients for the grapevine ($K_{cb\ adj}$) and the active soil cover ($K_{cb\ gcover}$), and the soil evaporation coefficient (K_e). The model was calibrated and validated by comparing the simulated available soil water content (ASWC) with the soil water content data measured with a capacitive probe for the years 2019 and 2020.

A good adjustment between the simulated and observed soil water content was obtained in 2019 R strategy (calibration) with a determination coefficient (R^2) of 1. The root mean square error (RMSE), the percent bias of estimation (PBIAS, %) and the modelling efficiency (EF, dimensionless) ranged between 2.57 to 3.44, -1.72 to 2.27 and 0.92 to 0.98 respectively. As for the vine crop, the best fit was obtained for $K_{cb\ full\ ini}$ = 0.33, $K_{cb\ full\ mid}$= 0.79 and $K_{cb\ full\ end}$ = 0.60. Results of assessing of simulation with SIMDualKc model led to conclude that computational procedures are accurate when using field data about active soil ground cover, thus allowing to evaluate the transpiration of the active soil cover, and the crop water requirements, to establish a good management of irrigation.

Keywords: Active ground cover; Available soil water content; Soil evaporation; Vine plants transpiration; Ground cover transpiration

1. Introduction

Wine production must be associated with an economically viable and socially accepted dichotomy where environmental aspects, such as the efficient use of water, must be considered. The efficiency water use is intrinsically related with the estimation of cultural evapotranspiration (ET_c). There are two main approaches to calculate crop evapotranspiration, the use of a single crop coefficient (Kc) that combines the effects of soil evaporation and crop transpiration and, the most accurate approach, adopting a double crop coefficient (dualKc) to determine the effects of soil evaporation and crop transpiration separately. The dualK_c considers a basal crop coefficient (K_{cb}) that includes the crop transpiration component and some diffusive evaporation, and the soil evaporation coefficient (K_e) that describes direct evaporation from the soil surface (Allen et al., 1998).

In many permanent row crops, the density and height of the active soil cover must be considered when calculating evapotranspiration (Paço et al., 2019). In this sense, the dualK_c approach should be used, as it considers that the active soil cover represents a part of the evapotranspiration, therefore, the transpiration of the active soil cover must be added to the transpiration of plants and evaporation (Fandiño et al., 2012). In many permanent row crops, the density and height of active soil cover must be considered when calculating evapotranspiration (Paço et al., 2019). During active growing season variations in the soil cover occur influenced by cultural operations aimed at controlling its vegetative vigor (herbicide application or tillage operations), as well as by climatic factors (Zhuang et al., 2020). The water consumption of the active soil cover is environmentally acceptable when considering the numerous ecosystem services provided by cover crops in vineyards (Garcia et al., 2018). The prevention of erosion and the improvement of infiltration rates during the rainy season (Lopes et al., 2011), the contribution to carbon (C) sequestration, the increase in total nitrogen (N) content and root biomass and also the stimulation of soil biodiversity (Gattullo et al., 2020). As for the benefits for the cultivation of *Vitis vinifera*, in Mediterranean climates, ground cover can mitigate impacts resulting

from dramatic reductions in stomatal conductance on hotter days and contribute to the control of plant vigour and fruit quality (Pou et al., 2011).

The DualK$_c$ approach estimates crop evapotranspiration (ET$_c$) through reference evapotranspiration (ET$_o$) and actual crop coefficient (K$_{c\ act}$). Adopting this DualK$_c$ approach Eq. (1), the K$_{cb\ act}$ results from the sum of the actual basal crop coefficients (K$_{cb}$) and the soil evaporation (K$_e$). The K$_{cb\ act}$ is obtained by correcting the basal crop coefficient (K$_{cb}$) through a stress coefficient (K$_s$) that varies between 0 (maximum stress) and 1 (no stress) (Allen et al., 1998).

$$ET_c = (K_s * K_{cb} + K_e) * ET_o = K_{cb\ act} * ET_0 \qquad (1)$$

The DualKc approach to calculate ETc has developed and improved in several works (Allen et al., 1998; Allen et al., 2005, 2006; Allen & Pereira, 2009; Pereira et al., 2021). In line with this approach, the SimDualKc software was developed, which takes the DualK$_c$ approach and performs soil water balance simulations for irrigation programming (Rosa et al., 2012). Several studies have reported the applicability of the dual Kc methodology to various field crops namely olives (Paço et al., 2019), hop (Fandiño et al., 2015), as well as in the culture of *Vitis vinifera*, where there are studies with the cv. Albariño (Fandiño et al., 2012), Godello e Mencía (Cancela et al., 2015). In these studies, the SimDualKc software has been shown to be appropriate to understand the water fluxes on soil.

Considering the good results obtained with the SIMDualKc model in the studies described, as well as its ability to simulate the use of water in the vine crop, the main objective of this study is to implement the DualK$_c$ approach to the cultivation of *Vitis vinifera* cv. Loureiro. Adopting the DualK$_c$ approach for this cultivar is innovative and interesting, since this approach has never been used in the varieties of the demarcated region of Vinhos Verdes with a controlled designation of origin (DOC).

2. Materials and Methods

2.1. Study area

The study was carried out in a commercial Loureiro vineyard during two growing seasons (2019-2020), located in Ponte de Lima, NW of Portugal (41 ° 40'32.16 "N 8 ° 32'6.21" W, and 170 m altitude). The vineyard were planted in 2001 at 3.0 m × 2.0 m spacing with North–South orientation, trained in a single upward cordon. The irrigation system had a distance between the drippers of 1 m and a nominal flow rate of 4 L h^{-1}.

The climate is of Atlantic type characterized by relatively high annual rainfall (above 1 200 mm) and relatively mild summers (Fraga et al., 2014). The Köppen–Geiger (Kottek et al., 2006) classification is Csb. Agrometeorological data were obtained from a weather station located in the field. Daily data consisted of maximum, minimum and mean temperature, maximum, minimum and mean humidity, wind speed at 2m height, rainfall and net radiation (Rn). The Figure 1 – Figure 1 showed the monthly ETo computed with the FAO Penman–Monteith equation using weather data, as well as the average monthly temperature and the sum of monthly precipitation.

The soil was classified as eutric regosol (WRB, 2014) with a sandy loam texture with, on average, 70.2% sand, 20.3% silt and 9.5% clay, and with 1.95% organic matter content. The total available soil water (TAW) down to 0.8 m depth was 100 was calculated from the difference between the field capacity (ΘFC = 0.246 cm^3 cm^{-3}) and the permanent wilting point (ΘWP = 0.121 cm^3 cm^{-3}) using eight different soil layers (from 10 to 80 cm). Based on successive SWC readings, carried out with a capacitive probe (Diviner 2000) after the occurrence of high precipitation, the drainage depletion curve for the soil was obtained and applying the power regression method (Liu et al., 2006) the parameters a = 287.05 and b=-0.056 were defined. The surface runoff value considered was 60 (Rosa et al., 2012).

Crop heights (from the soil) and the fraction of soil shaded by the crop was determined at noon solar, were observed throughout the active growing season and their values at the dates of the crop growth stages are presented in Table *1*.

The active ground cover was composed of spontaneous species. In 2019, the density of active coverage (performed by observation) varied between 10 and 90% with height between 2 and 25 cm between the rows and there was no active coverage in the row. In 2020, the density of active soil cover in the row ranged between 5 and 15% and the height between 5 and 10 cm, between the rows the density ranged from 20 to 85% and the height between 5 and 30 cm.
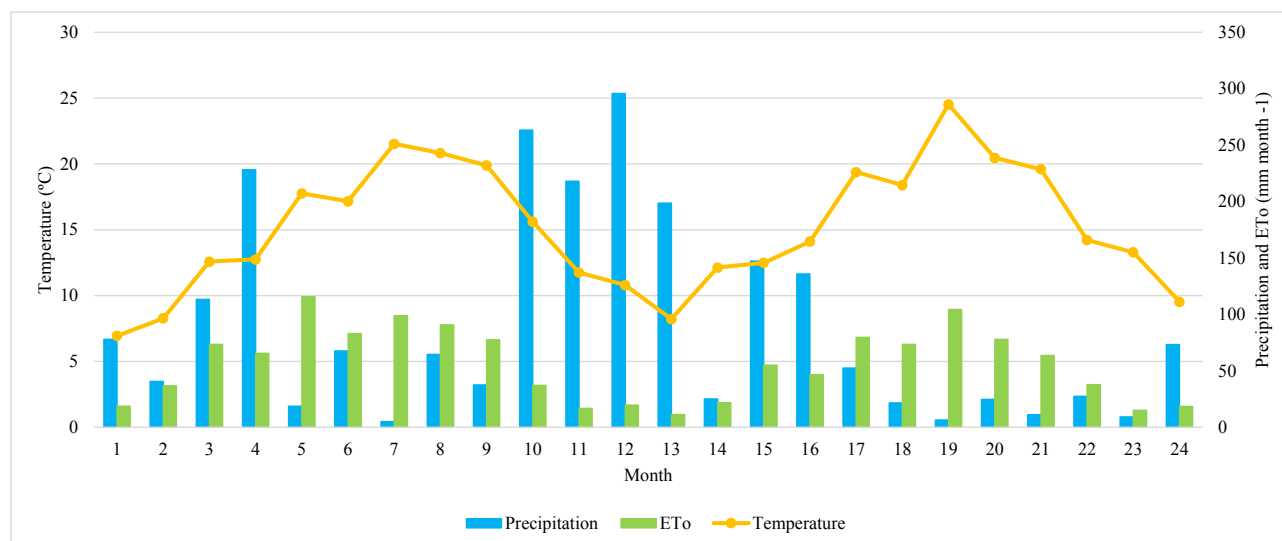
Figure 1 – Monthly mean temperature (●—●), total monthly precipitation (▬), total monthly reference evapotranspiration (▬) in the experimental area during the two experimental seasons.

Table 1 - Vineyard crop growth stages, height (h) and fraction of soil covered by the crop by vineyard (fc)

Crop growth stages	2019			2020		
	Dates	h(m)	f_c	Dates	h(m)	f_c
Initiation	21 March	1	0.01	01 March	1	0.01
Start rapid growth	26 March	1.4	0.05	28 March	1.2	0.05
Start mid-season	06 June	2	0.3	22 June	2	0.3
Start maturity	02 September	2.4	0.4	20 August	2.4	0.4
Harvesting	23 September	2.4	0.4	09 September	2.4	0.4

Two irrigation treatments were considered, Full Irrigation (FI; 100% of ET_o) and Deficit Irrigation (DI, 50% of ET_o) and a control treatment: R-rain-fed. Each treatment had four replicates and each replicate consisted of four rows, the two central rows were used to install the access probe To obtain the SWC readings, 18 probes of 80 cm depths distributed over the treatments and control were used. Irrigation in 2019 began in DOY 202 and was 42.67mm in FI and 17.33mm in DI, in 2020 it began in DOY 190 and was 66.67mm in FI and 32mm in DI.

2.2. Model Calibration and validation

The calibration of the model was performed by adjusting the crop parameters ($K_{cb\ full\ ini}$, $K_{cb\ full\ mid}$ and $K_{cb\ full\ end}$, p depletion fractions), the soil evaporation parameters (Ze, TEW, REW), as well as the local conditions of the cv. Loureiro, through minimizing the residual deviations between simulated and observed soil water content (Cancela et al., 2015). Calibration was performed by minimizing the differences between available soil water content (ASWC) observed and simulated in the control treatment- R, for the year 2019. The validation consisted of the use of previously calibrated parameters ($K_{cb\ full\ ini}$, $K_{cb\ full\ mid}$ and $K_{cb\ full\ end}$ and p) in other treatments, in the years 2019 and 2020.

The procedures to assess the goodness of fit of the model were like those adopted in previous studies (Fandiño et al., 2012; Paredes et al., 2018; Rosa, 2018). A linear regression was performed between observed and simulated ASWC values forced to the origin. A set of goodness of fit indicators were used to assess model fitting during calibration and to evaluate the results of validation. The indicators used were regression coefficient (b), determination coefficient (R^2), root mean square error (RMSE), normalized RMSE (NRMSE, %), average relative error (ARE, %), percent bias of estimation PBIAS (%), modelling efficiency (EF, dimensionless), average absolute error (AAE) and d_{IA} index of agreement.

3. Results and Discussion

The standard values (Allen et al., 1998; Allen and Pereira, 2009) and calibrated values for the parameters $K_{cb\ full\ ini}$, $K_{cb\ full\ mid}$ and $K_{cb\ full\ end}$, p are presented in the Table 2. Initial and mid seasons differences are observed. In addition to these differences in cultural coefficients, the best fit was obtained with equal p depletion fractions except in mid-seasosn where a higher value was used. Total evaporable water (TEW) used was 17mm, for Readily Evaporable Water (REW) used was 10mm and depth of the soil evaporation layer (Ze) was 0.1m.

Table 2 – Standard and calibrated model parameters

Parameters	Standard		Calibrated
$K_{cb\ full\ ini}$ (dimensionless)	0.20		0.33
$K_{cb\ full\ mid}$ (dimensionless)	0.80	(Allen & Pereira, 2009)	0.79
$K_{cb\ full\ end}$ (dimensionless)	0.60		0.60
p_{ini} (dimensionless)	0.45		0.45
p_{mid} (dimensionless)	0.45	(Allen et al., 1998)	0.54
p_{end} (dimensionless)	0.45		0.45

K_{cb} = Basal crop coefficients and p = Depletion fraction

As an example, the result of the calibration of the observed and simulated ASWC values in R 2019 as well as the validation in the FI 2020 strategy can be seen in Figure 2 . In this Figure 2 a good approximation between the simulated and measured ASWC values is observed. It is considered that the model can predict ASWC throughout the vineyard cycle in the various irrigation strategies with little margin of error. It was also found that the rainfed vineyard (a) was subject to periods of water stress (Ks<1), however when applying 100% of ETc (b) there are no water stress.

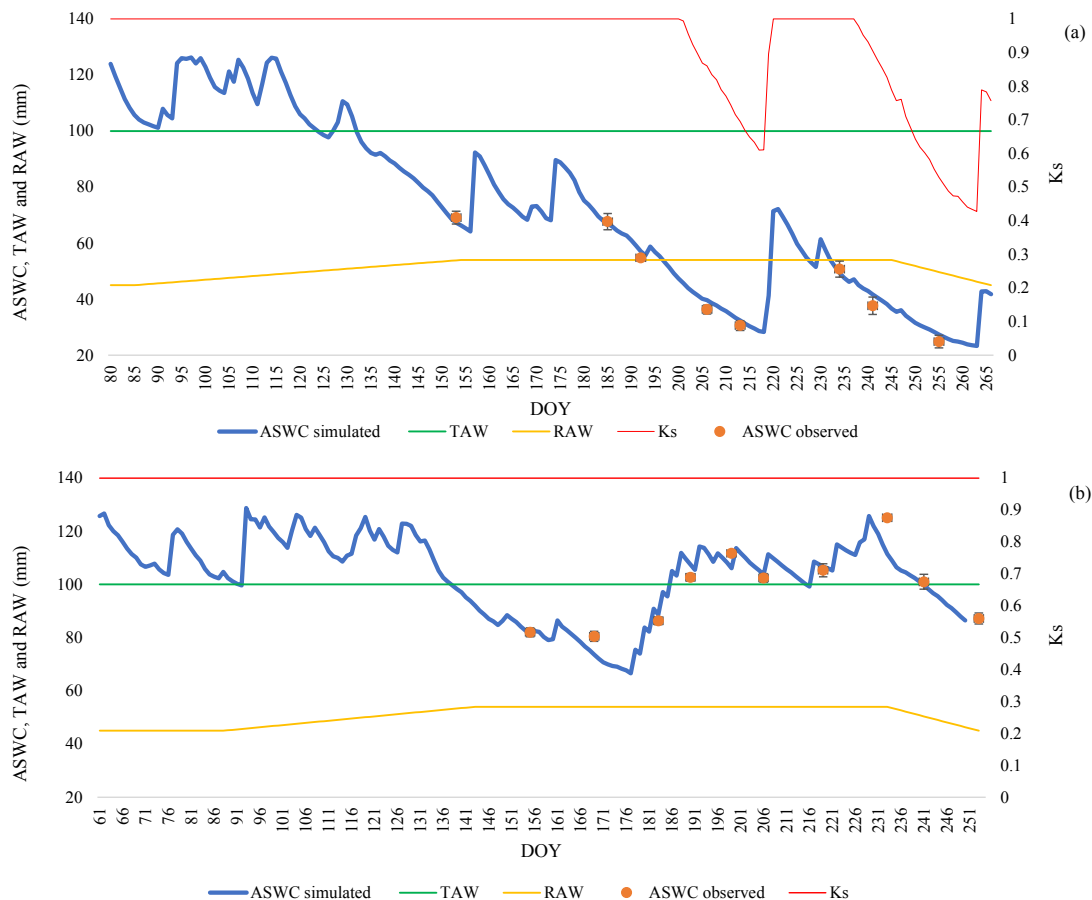Figure 2 - Simulated (——) vs. observed (●) available soil water (ASW): (a) 2019-R, calibration; (b) 2020-FI. (error bars represent the standard deviation of the mean observed values).

The Table 3 shows the goodness of fit of indicators related to the model's calibration and validation. The indicators obtained from the forced regression to the origin show a good agreement between observed and simulated data. The

other indicators (EF, RMSE, NRMSE, PBIAS, dIA e a AAE) demonstrate that the model after a previous calibration becomes efficient in predicting ASWC throughout the crop cycle in the various irrigation strategies with high efficiency. The values b and r^2 in the present work are similar to those reported by Cancela et al., (2015) which obtained values of b between 0.92 and 1.04 and r^2 between 0.87 and 0.97. The efficiency of the model (EF) in the present study ranged between 0.92 and 0.98 and Cancela et al., (2015) obtained slightly lower values between 0.77 and 0.96. Regarding the other indicators, there is a close approximation to those obtained by Fandiño et al., (2012).

Table 3 - Goodness of fit indicators relative to the SIMDualKc model calibration and validations for the different treatments in the 2019 and 2020 growing seasons.

Year		2019			2020		
	Treatment	**R**	DI	FI	R	DI	FI
linear regression	b	**1.00**	0.99	0.99	1.00	0.97	1.00
	r^2	**0.98**	0.94	0.93	0.99	0.97	0.94
goodness of fit indicators	EF	**0.97**	0.93	0.92	0.98	0.97	0.94
	RMSE	**2.57**	3.44	3.18	3.10	3.24	3.37
	NRMSE (%)	**5.58**	6.54	3.26	6.70	5.85	3.42
	PBIAS (%)	**-1.28**	0.41	1.26	-1.72	2.27	0.23
	d_{IA}	**0.99**	0.98	0.98	0.99	0.99	0.98
	AAE	**2.31**	2.77	2.89	2.39	2.69	2.77

R: rainfed; DI: Deficit Irrigation; FI: Full Irrigation; b: regression coefficient, r^2: determination coefficient, EF: modelling efficiency; RMSE: root mean square error, NRMSE (%): normalized RMSE of total available water, PBIAS (%): percent bias of estimation; dIA: index of agreement; AAE: average absolute error. Bold data refer to calibration.

4. Conclusions

Calibration and validation of the SIMDualKc model was successfully performed for *Vitis vinifera* cv. Loureiro considering specific parameters of the study field (soil, climate, crop and irrigation). In the two years of field studies, 2019 and 2020, a goodness of fit was obtained between the ASWC values observed with a capacitive probe and those simulated with the SIMDualKc model.

After making necessary adjustments to the standard values (Allen et al., 1998) a good approximation between the real and simulated values was obtained. We conclude the SIMDualKc model can predict the ASWC. These values allow determining the ASWC in future growth seasons, facilitating irrigation management, adapting it to the levels of water stress that the farmer wants for his vineyard. The use of calibrated parameters for cv. Loureiro in the SIMDualKc model allows to use water efficiently, but still necessary to carry out future studies to determine the vine response to the different levels of water stress generated in each irrigation treatment. To facilitate the application of this calibration, it is recommended to round the values of $K_{cb\ full\ ini}$, $K_{cb\ full\ mid}$ and $K_{cb\ full\ end}$ 0.60 to 0.35, 0.8 and 0.6 respectively.

Acknowledgements

References

Allen, R. G., & Pereira, L. S. ,2009. Estimating crop coefficients from fraction of ground cover and height. *Irrigation Science*, *28*(1), 17–34. https://doi.org/10.1007/s00271-009-0182-z

Allen, R. G., Pereira, L. S., Smith, M., & Raes, D. ,1998. Crop Evapotranspiration. Guide- lines for Computing Crop Water Requirements. *FAO Irrigation and Drainage Paper 56*, 300.

Cancela, J. J., Fandiño, M., Rey, B. J., & Martínez, E. M. ,2015. Automatic irrigation system based on dual crop coefficient, soil and plant water status for Vitis vinifera (cv Godello and cv Mencía). *Agricultural Water Management*, *151*, 52–63. https://doi.org/10.1016/j.agwat.2014.10.020

Fandiño, M., Cancela, J. J., Rey, B. J., Martínez, E. M., Rosa, R. G., & Pereira, L. S. ,2012. Using the dual-K c approach to model evapotranspiration of Albariño vineyards (Vitis vinifera L. cv. Albariño) with consideration of active

ground cover. *Agricultural Water Management*, *112*, 75–87. https://doi.org/10.1016/j.agwat.2012.06.008

Fandiño, M., Olmedo, J. L., Martínez, E. M., Valladares, J., Paredes, P., Rey, B. J., Mota, M., Cancela, J. J., & Pereira, L. S. ,2015. Assessing and modelling water use and the partition of evapotranspiration of irrigated hop (Humulus Lupulus), and relations of transpiration with hops yield and alpha-acids. *Industrial Crops and Products*, *77*, 204–217. https://doi.org/10.1016/j.indcrop.2015.08.042

Fraga, H., Malheiro, A. C., Moutinho-Pereira, J., & Santos, J. A. ,2014. Climate factors driving wine production in the Portuguese Minho region. *Agricultural and Forest Meteorology*, *185*, 26–36. https://doi.org/10.1016/j.agrformet.2013.11.003

Garcia, L., Celette, F., Gary, C., Ripoche, A., Valdés-Gómez, H., & Metay, A. ,2018. Management of service crops for the provision of ecosystem services in vineyards: A review. *Agriculture, Ecosystems and Environment*, *251*(September 2017), 158–170. https://doi.org/10.1016/j.agee.2017.09.030

Gattullo, C. E., Mezzapesa, G. N., Stellacci, A. M., Ferrara, G., Occhiogrosso, G., Petrelli, G., Castellini, M., & Spagnuolo, M. ,2020. Cover crop for a sustainable viticulture: Effects on soil properties and table grape production. *Agronomy*, *10*(9). https://doi.org/10.3390/agronomy10091334

Liu, Y., Pereira, L. S., & Fernando, R. M. ,2006. Fluxes through the bottom boundary of the root zone in silty soils: Parametric approaches to estimate groundwater contribution and percolation. *Agricultural Water Management*, *84*(1–2), 27–40. https://doi.org/10.1016/j.agwat.2006.01.018

Lopes, C. M., Santos, T. P., Monteiro, A., Rodrigues, M. L., Costa, J. M., & Chaves, M. M. ,2011. Combining cover cropping with deficit irrigation in a Mediterranean low vigor vineyard. *Scientia Horticulturae*, *129*(4), 603–612. https://doi.org/10.1016/j.scienta.2011.04.033

Paço, T. A., Paredes, P., Pereira, L. S., Silvestre, J., & Santos, F. L. ,2019. Crop coefficients and transpiration of a super intensive Arbequina olive orchard using the dual Kc approach and the Kcb computation with the fraction of ground cover and height. *Water (Switzerland)*, *11*(2). https://doi.org/10.3390/w11020383

Rosa, R. D., Paredes, P., Rodrigues, G. C., Alves, I., Fernando, R. M., Pereira, L. S., & Allen, R. G. ,2012. Implementing the dual crop coefficient approach in interactive software. 1. Background and computational strategy. *Agricultural Water Management*, *103*, 8–24. https://doi.org/10.1016/j.agwat.2011.10.013

WRB. ,2014. World Reference Base for Soil Resources. World Soil Resources Reports 106. In *World Soil Resources Reports No. 106*.

Zhuang, Q., Wu, S., Feng, X., & Niu, Y. ,2020. Analysis and prediction of vegetation dynamics under the background of climate change in Xinjiang, China. *PeerJ*, *2020*(1), 1–23. https://doi.org/10.7717/peerj.8282

Orchard Level Assessment of Irrigation Performance and Water Productivity of an Irrigation Community in Eastern Spain

Herminia Puerto [a,*], Miguel Mora [b], Bernat Roig-Merino [c], Carmen Rocamora [a], José María Cámara [a], Ricardo Suay [a], Ricardo Abadía [a]

[a] Centro de Investigación e Innovación Agroalimentaria y Agroambiental (CIAGRO-UMH), Miguel Hernández University, 03312 Orihuela, Spain

[b] MOVAL Agroingeniería, Alcantarilla, Spain

[b] Instituto de Investigación Para la Gestión Integrada de Zonas Costeras, Universitat Politècnica de València, 46730 Grao de Gandia, Spain

* Corresponding author. Email: hpuerto@umh.es

Abstract

Over the last three decades, a great investment effort has been made in the modernization of irrigation in the Valencian Community (Spain). The initial change from distribution networks to pressurized ones and the shift towards drip irrigation systems was followed by improvements in irrigation scheduling, based on agrometeorological data, soil water content sensors and remote sensing. These improvements are considered adequate for increasing irrigation water use efficiency but it is difficult to find systematic measurements to assess its impacts on irrigation adequacy along with irrigation productivity in fruit orchards. This work presents the results of a four-year assessment of irrigation water and energy use efficiency along with water productivity of a recently established irrigation community in the province of Valencia (Spain). The study was carried out at the orchard level and focused on two fruit crops: persimmon and peach trees. Five irrigation performance indicators, Relative Water Supply (RWS), Relative Irrigation Supply (RIS), global Water Productivity (WP$_{Overall}$), Output per Unit Irrigation water (OUI), and % of Nitrogen fertilization obtained by irrigation water, were defined and calculated for years 2017 to 2020 in 104 persimmon and peach orchards. The results showed that most of the farmers irrigated below the crop water requirements showing RWS and RIS values below 1, and there was great variability among farmers, especially in WP$_{Overall}$ and OUI indicators.

Keywords: irrigation management, drip irrigation, benchmarking, KPI, efficiency.

1. Introduction

In the last decades, irrigation schemes modernization in Spain has entailed changing from open channels networks for surface irrigation to pressurized pipes networks and drip irrigation systems. This modernization has allowed the reduction of irrigation water use and improved the control of irrigation application by farmers (Berbel et al. 2019; García-Mollá et al. 2019). Many irrigation management and information systems, developed by national and regional governments or commercial solutions are readily available for farmers to perform a sound irrigation management but most of them do not use them in their common practice for convenience or trust reasons.

Nevertheless, the improvement of irrigation management in a modernized irrigation scheme requires the assessment of irrigation performance under different points of view to be able to detect and correct unfit irrigation practices. Irrigation performance assessment is an essential tool to record, compare and improve the water management of irrigation schemes (Malano and Burton 2001). Research in this field has traditionally focused in the hydraulic management of irrigation schemes but scarcer information is available that relates the hydraulic performance to the productivity and the economic performance of irrigated schemes at the plot level. Some examples are provided in the work of (Lorite, Mateos, and Fereres 2004b; 2004a; Dechmi et al. 2003) for data on extensive crops. Regarding fruit crops and following a similar approach of establishing a set of water use and productivity indicators, Parra et al. (2020) assessed the factors that influence irrigation performance and Poveda-Bautista et al. (2021) built a synthetic irrigation efficiency index to assess and rank the global water use efficiency of citrus orchards.

This work proposes a set of irrigation performance indicators aimed at assessing the water use and productivity at plot level and describes a case study of their application to peach and persimmon orchards of an irrigation community in the province of Valencia, Valencian Community, Spain.

2. Materials and Methods

2.1. Irrigated area description

The studied area is located in the south of the Valencia province, Valencian Community (Spain). It encompasses agricultural plots from several municipal terms, serving an irrigated area of around 290 ha. The irrigation community was established in 2008 to exploit the effluents of a water treatment facility serving three municipalities to bring stable irrigation to former dryland crops. The irrigation community has a pumping station at the collection point of the wastewater treatment plant, a booster station to pump water to an elevated reservoir of 170,000 m^3, and another pumping station injecting directly to the irrigation network. The irrigation network is pressurised and fully automated. It is divided into four irrigation sectors serving 72 farmers. 26 farmers with persimmon and peach orchards participated in this study with a total of 55 persimmon and 49 peach plots.

The climate is a Hot-summer Mediterranean climate in the Köppen climate classification, with a yearly average precipitation of 614 mm. The average air temperature is 17,4 ºC on annual basis, and it ranges from a minimum of 10 ºC in January to 26,3 ºC in August (AEMET and Agencia Estatal de Meteorología 2021).

Its cropping pattern is very diverse, including fruit orchards, horticultural crops, olives, wine grapes and nursery gardens. Persimmon (*Diospyros kaki* Thunb.) and peach (*Prunus* persica L.) are the main cultivated crops in terms of surface area and economic income. The varieties cultivated in this area are *Rojo* brillante for persimmon and 26 different peach varieties. Table 1 shows the names of the six main peach varieties, in terms of cropped area and the most common characteristics of the studied plots. The orchards considered in this study comprised 38.23 ha and 23.57 ha of persimmon and peach, respectively, the average size of the studied plots was 0.59 ha, with a maximum of 4.03 ha and a minimum of 0.05 ha. The average size of persimmon plots was bigger than the peach ones (Table 1).

Table 1. Description of orchards and crops monitored.

	Peach	Persimmon
Varieties	*King Zest, Samanta (*flat*), Nazario, Carmina 28 (*nectarine*), Alejandro Dumas, Romea, Leo (*flat*)*	*Rojo brillante*
Number of plots[*]	- Extra- early: 9 - Early: 22 - Mid-season: 13 - Other[**]: 5	55
Average size (Max-min) (ha)	0.48 (1.85 - 0.05)	0.70 (4.03 - 0.09)
Planting framework	5 m x 4 m	5 m x 3 m

[*] In 2017, [**] Late season or unknown earliness.

2.2. Definition of performance indicators

Performance indicators must be adapted to the purpose of the evaluation and the characteristics of the irrigation scheme. So that the process of obtaining and comparing the indicators is effective, the data required for calculations must be recorded customarily by the irrigation community or the cooperative and there must not be added difficulties to the interoperability of the required data. In this case, the following five performance indicators were chosen to assess the results of irrigation practices in each of the studied plots:

a) Annual Relative Water Supply, RWS, relates the amount of water received by the crop from the effective precipitation and irrigation and the crop water requirements, ETc.

$$RWS = \frac{Total\ annual\ volume\ of\ water\ supplied\ to\ the\ crop}{Total\ annual\ volume\ of\ crop\ water\ demand} = \frac{I+P_e}{ET_c} \qquad (1)$$

where ET_c is the annual crop evapotranspiration calculated according to FAO-56 and P_e is the annual effective precipitation or rainfall calculated using the USDA-SCS model.

b) Annual Relative Irrigation Supply, RIS, relates the amount of irrigation water actually applied to the crop, that depends on the farmer's practice and the reliability of the irrigation system, and the theoretical gross volume of irrigation water required to avoid water stress to the crop, which depends on the kind of crop, peach or persimmon, the environmental variables, the irrigation interval and the application uniformity.

$$RIS = \frac{Total\ annual\ volume\ of\ irrigation\ water\ applied\ to\ t\ e\ crop}{Total\ annual\ volume\ of\ crop\ irrigation\ demand} = \frac{I}{I_r} \qquad (2)$$

The total annual volume of crop irrigation demand, the raw irrigation requirement, I_r, was calculated as:

$$I_r = \frac{ET_c - P_e}{UC} \qquad (3)$$

where UC is the uniformity coefficient of the drip irrigation system. In this case we considered a generic UC=0.95 since the drip irrigation systems at plot level are recent and installed by qualified professionals.

The optimal RIS value is 100%, that is when irrigation applied matches the water requirement of the crop.

c) Crop Yield Gap (%) is the actual yield stated as a % of attainable yield under good management conditions.

$$CYG = \frac{Crop\ actual\ yield}{Crop\ attainable\ yield} \qquad (4)$$

This indicator is only calculated for adult trees, i.e., trees of six years or older for peach or eight years or older for persimmon. Young trees or saplings can have a fraction of adult yield depending on their size and not only as a response to irrigation dose. The crop attainable yield should be a value is a

d) Overall water productivity of the irrigated crop (WP$_{Overall}$), is defined as the ratio between the total annual mass of crop production, including all grades, and the annual volume of irrigation water applied (kg/m^3).

$$WP_{Overall} = \frac{Total\ annual\ mass\ of\ crop\ yield}{Total\ annual\ volume\ of\ irrigation\ water\ applied\ to\ t\ e\ crop} \qquad (5)$$

e) Output per unit irrigation delivery, OUI (€/m^3), measures the financial efficiency of the cropped plot:

$$OUI = \frac{Total\ annual\ value\ of\ crop\ production}{Total\ annual\ volume\ of\ irrigation\ water\ applied\ to\ t\ e\ crop} \qquad (6)$$

f) % of N fertilizer provided by irrigation water (N %) is calculated as the actual number of N fertilizer units applied expressed as a % of N fertilizer units requirements under good management conditions.

$$N\% = \frac{N\ FU\ applied\ wit\ irrigation\ water}{N\ FU\ required} \qquad (7)$$

2.3. Measurements and calculations

The values of the total annual volume of irrigation water applied to the crop, I (m^3), were provided by the Irrigation community metering and control software for each of the considered plots for seasons 2017 to 2020.

Daily environmental data, reference evapotranspiration, ET$_o$ (mm), and precipitation, P (mm), were obtained for years 2017 to 2020 from a nearby agrometeorological station of the Spanish Agriculture Ministry (Ministerio de Agricultura n.d.) (UTM X: 720841; UTM Y: 4306490; altitude: 233 m). Total annual volume of irrigation demand was calculated with Cropwat 8.0 (Smith et al. n.d.).

Table 2. Crop data for Cropwat ET$_c$ calculations.

Registration fee	Peach	Persimmon
Growing season period	1st March – 31 October	1st March – 30 November
Kc ini / Kc mid / Kcb final		
- Adult	0.34 / 0.47 / 0.47	0.32 / 1.08 / 0.59
- Young	0.15 / 0.21 / 0.21	0.14 / 0.49 / 0.27
- Sapling	0.06 / 0.09 / 0.09	0.06/ 0.20 / 0.11
Length of initial / development / midseason / late season periods (d)	1 / 90 / 122 / 30	31/ 121 / 92 / 30
Rooting depth (m)		
- Adult	0.60	0.60
- Young	0.40	0.40
- Sapling	0.30	0.30
Critical depletion (fraction)	0.50	0.50
Bud burst date	March 1st	March 1st

The values of total annual mass of crop yield and the average prices of fruit were provided by a commercialisation cooperative where most of the farmers sell their produce. The crop attainable yield of peach and persimmon were obtained from the Spanish Agriculture Ministry agricultural statistics database taking the average yield of "peaches and nectarines" and "persimmon" classes of the Valencia province statistics. Nitrogen,

as NO_3^-, concentrations were obtained from customary irrigation water analysis at the irrigation reservoir at the beginning of the irrigation seasons.

3. Results and Discussion

3.1. Measured and calculated values of environmental parameters

Table 3 summarizes the environmental conditions regarding evapotranspirative demand, ETo, and precipitation, P, along the years considered in this study. Annual ETo values remained quite constant as well as P, except for year 2017 that had the lowest P value. Annual precipitation in the studied years stayed below the yearly average of the area (614 mm). Since crop water requirements calculations take into account the precipitation occurred during the cropping season, we calculated also the sum of precipitation from March to October. There was a difference of 185 mm between year 2019 and the average of 2017, 2018 and 2020. This difference accumulated only along the month of April 2019. In all cases, summer and autumn months registered reduced amounts of rainfall, as typical.

Table 3. Reference evapotranspiration, precipitation and results of the calculated raw irrigation requirements.

	Year			
	2017	2018	2019	2020
ETo (mm)	1,173.2	1,179.2	1,211.2	1,166.4
P (mm)	449.2	590.0	583.4	570.2
P March-October (mm)	252.3	273.1	441.3	243.7

The number of plots considered under the three tree sizes, adult, young and sapling, varied along the studied seasons since trees grew older each year ($I_r = \frac{ET_c - P_e}{UC}$ (3) for both crops and tree sizes showed similar values for 2017, 2018 and 2020 (Table 4). The higher precipitation amount of 2019 did not result in a reduction in irrigation requirements because its occurrence in April did not increase the effective precipitation values. The average values of Annual irrigation depths applied to the crops are well below the calculated values of Raw Irrigation Requirements and show no clear trends along time.

Table 4). The tendencies showed an increase of young persimmon orchards as saplings grew older and a more stable trend in the case of peach orchards. In this latter case, there was a tendency to abandon mid-season varieties for extra-early peach varieties though the most abundant ones remained the early varieties. Also, the availability of irrigation leads to higher planting densities in the young and saplings categories of both crops.

Calculated Raw Irrigation requirements $I_r = \frac{ET_c - P_e}{UC}$ (3) for both crops and tree sizes showed similar values for 2017, 2018 and 2020 (Table 4). The higher precipitation amount of 2019 did not result in a reduction in irrigation requirements because its occurrence in April did not increase the effective precipitation values. The average values of Annual irrigation depths applied to the crops are well below the calculated values of Raw Irrigation Requirements and show no clear trends along time.

Table 4. Number of plots in each category, results of raw irrigation requirement calculations and averages of the annual irrigation depths applied to the different plots for persimmon and peach orchards.

		Persimmon				Peach			
		2017	2018	2019	2020	2017	2018	2019	2020
Number of plots	Adult	10	10	10	11	20	20	21	33
	Young	16	24	35	40	13	15	17	6
	Sapling	29	21	10	4	16	14	11	10
Planting density (trees/ha)	Adult	465	465	465	459	415	415	415	450
	Young	571	565	565	578	515	493	515	463
	Sapling	602	621	699	877	617	680	704	775
Raw	Adult	863.7	823.5	914.1	847.7	481.2	442.1	503.6	379.3

Irrigation requirement (mm)	Young	414.5	340.8	419.8	349.7	239.7	200.1	228.7	181.4
	Sapling	203.1	166.4	198.5	130.2	129.6	104.8	123.7	89.5
Annual Irrigation applied (mm)	Adult	285.6	419.6	162.0	223.2	141.8	251.4	237.6	159.7
	Young	151.3	218.8	149.4	170.3	208.4	124.2	145.3	139.2
	Sapling	129.7	65.8	143.0	110.8	98.6	72.2	110.1	87.6

Table 5 summarises the values of the six performance indicators along the four irrigation seasons. The values of RWS and RIS below 1, except for Peach saplings in 2020, indicate that deficit irrigation is applied in all cases, the maximum evapotranspiration demand of the crops is not met, and reductions of productivity can be expected. Similar results were found in other irrigation schemes in Spain by (Lorite, Mateos, and Fereres 2004b) in Andalusia, and (Dechmi et al. 2003) in Aragon, both for field crops. (Parra et al. 2020) in citrus orchards also report RWS and RIS values much lower than 1.

The CYG indicator shows the ratio of actual to attainable yield, it behaves differently in Persimmon and Peach crops. It is lower than 100% for Persimmon and higher than 100% for peach. The values considered for attainable yield were the ones provided for Persimmon and for Peaches and Nectarines classes by the statistics office of the Agriculture Ministry for the Valencia province. In the case of Persimmon, the low values of CYG may be due to the low RWS and RIS values, though no correlation is noticeable, but it could be also caused by the choice of the attainable yield value. Persimmon is a speciality crop that is mainly cultivated in the *Ribera del Júcar* area where the yields may be higher than in the study area. On the other hand, the study area is a traditional producer of stone fruits which could explain the yields in line with or slightly higher than the average of the Valencia province.

Table 5. Average values of the calculated performance indicators: annual relative water supply, RWS, annual relative irrigation supply, RIS, crop yield gap, CYG, overall water use efficiency, $WP_{Overall}$, output per unit irrigation water, OUI, and percentage of nitrogen fertilization requirement supplied by irrigation water, %N.

		Persimmon				Peach			
		2017	2018	2019	2020	2017	2018	2019	2020
RWS	Adult	0.42	0.60	0.26	0.38	0.41	0.69	0.55	0.62
	Young	0.46	0.77	0.46	0.65	0.93	0.77	0.75	0.88
	Sapling	0.72	0.59	0.80	0.94	0.85	0.84	0.96	1.02
RIS	Adult	0.35	0.54	0.19	0.28	0.31	0.60	0.50	0.44
	Young	0.38	0.68	0.37	0.51	0.92	0.65	0.67	0.81
	Sapling	0.67	0.42	0.76	0.90	0.80	0.72	0.94	1.03
CYG (%)	Adult	67.97	63.64	76.04	61.47	145.34	104.44	86.35	141.61
$WP_{Overall}$ (kg/m^3)	Adult	7.6	8.4	18.7	15.5	28.9	10.5	9.3	11.7
	Young	22.6	11.5	14.7	10.7	14.0	28.4	18.6	13.1
	Sapling	20.0	-	30.2	-	7.1	9.5	2.8	14.3
OUI (€/m^3)	Adult	2.80	3.29	8.59	7.35	16.79	4.19	3.63	5.24
	Young	8.36	4.48	6.77	5.06	8.12	11.34	7.26	5.88
	Sapling	7.40	-	13.88	-	4.14	3.79	1.07	6.42
% N	Adult	25	35	5	16	16	27	10	14
	Young	18	26	7	18	32	18	9	21
	Sapling	30	13	13	24	16	25	15	26

Overall water productivity, $WP_{POverall}$, varied appreciably between years and trees sizes. It showed no apparent relationship with the annual irrigation applied nor with the RWS or RIS indices (Figure 1), this lack of correlation may be due to the higher planting densities of younger orchards that can offset the reduction in $WP_{Overall}$ caused by increased irrigation depths. The data of sapling persimmon $WP_{Overall}$ and OUI are blank due to lack of reliable yield data.
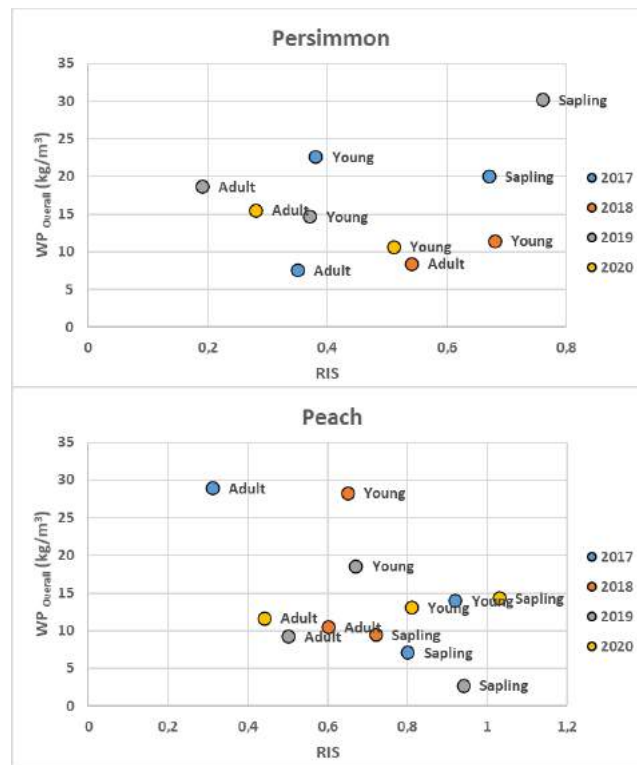
Figure 1. WP Overall vs. RIS for Persimmon and Peach. Each dot corresponds to a tree size for years 2017 to 2020.

Finally, as an environmental indicator, the percentage of N fertilizer units received with irrigation water showed remarkable variability among years. It decreased in 2019 because of the nitrate concentration in the irrigation water that was one third of the values attained the other 3 years. During 2019 and first months of 2020 the irrigation community did not receive water from the municipal wastewater treatment plant for quality reasons. The highest values for %N are 35% and 32% for Persimmon and Peach, respectively. These values indicate N contributions of the irrigation water lower than the crop N requirements so, in the actual conditions, no pollution problems are to be expected associated to nitrate leaching because both the low concentrations in the irrigation water and the low irrigation depths provided to the crops.

4. Conclusions

RWS and RIS values indicate that irrigation practiced in this irrigation community does not balance the crop's water requirements and a reduction in yield is expected caused by water stress. This finding is in line of other irrigation performance analysis done for field crops and for citrus orchards in Spanish irrigation communities.

Both WUE $_{Overall}$ and OUI values are high as compared to values obtained for other field crops and similar or slightly larger than those found for citrus (Parra et al. 2020). It is interesting to consider the effects of a sound irrigation practice in the yield of first quality fruits. Big size peaches are desirable commercial grades, but persimmons are not a commercial target for production since smaller fruits are preferred by consumers.

The shift to higher planting densities of newly established orchards can mask the effects of increased RIS in younger orchards. Modelling the productive response of fruit trees, like peach and persimmon, to water requires a more refined approach in which the different cultural techniques such as planting frames, pruning and fruit thinning can be considered.

References

AEMET, and Agencia Estatal de Meteorología. 2021. "Atlas Climático." Atlas Climático. 2021. http://agroclimap.aemet.es/#.

Berbel, Julio, Alfonso Expósito, Carlos Gutiérrez-Martín, and Luciano Mateos. 2019. "Effects of the Irrigation Modernization in Spain 2002–2015." *Water Resources Management* 33 (5): 1835–49. https://doi.org/10.1007/s11269-019-02215-w.

Dechmi, F., E. Playán, J. M. Faci, and M. Tejero. 2003. "Analysis of an Irrigation District in Northeastern Spain I. Characterisation and Water Use Assessment." *Agricultural Water Management* 61 (2): 75–92. https://doi.org/10.1016/S0378-3774(03)00020-9.

García-Mollá, Marta, Carles Sanchis-Ibor, Llorenç Avellà-Reus, José Albiac, Daniel Isidoro, and Sergio Lecina. 2019. "Spain." *Global Issues in Water Policy*. Springer. https://doi.org/10.1007/978-3-030-03698-0_4.

Lorite, I, L Mateos, and E Fereres. 2004a. "Evaluating Irrigation Performance in a Mediterranean Environment: II. Variablility among Crops and Farmers." *Irrigation Science* 23: 85–92. https://doi.org/10.1007/s00271-004-0096-8.

———. 2004b. "Evaluating Irrigation Performance in a Mediterranean Environment: I. Model and General Assessment of an Irrigation Scheme." *Irrigation Science* 23 (2): 77–84. https://doi.org/10.1007/s00271-004-0095-9.

Malano, Hector, and Martin Burton. 2001. *Guidelines for Benchmarking Performance in the Irrigation and Drainage Sector*. Edited by International Programme for Technology and Research in Irrigation and Drainage. Rome: IPTRID Secretariat Food and Agriculture Organization of the United Nations.

Ministerio de Agricultura, Pesca y Alimentación. n.d. "SIAR. Sistema de Información Agroclimática Para El Regadío." Accessed June 9, 2021. https://eportal.mapa.gob.es/websiar/SeleccionParametrosMap.aspx?dst=1.

Parra, L, M Botella-Campos, H Puerto, B Roig-Merino, and J Lloret. 2020. "Evaluating Irrigation Efficiency with Performance Indicators: A Case Study of Citrus in the East of Spain." *Agronomy* 10 (9). https://doi.org/10.3390/agronomy10091359.

Poveda-Bautista, Rocío, Bernat Roig-Merino, Herminia Puerto, and Juan Buitrago-Vera. 2021. "Assessment of Irrigation Water Use Efficiency in Citrus Orchards Using AHP." *International Journal of Environmental Research and Public Health* 18 (11): 5667. https://doi.org/10.3390/ijerph18115667.

Smith, Martin, Giovanni Muñoz, Gerardo van Halsema, Florent Maraux, Gabriella Izzi, and Robina Wahaj. n.d. "CropWat 8.0." *Cropwat 8.0*. Rome: Food and Agriculture Organization of the United Nations, Land & Water | Food and Agriculture Organization of the United Nations. Accessed January 1, 2020. http://www.fao.org/land-water/databases-and-software/cropwat/en/.

Sustainable production in Farm buildings

Comparing Ammonia Emission Measured Through Impinger Method (Direct) and Total N Loss via N Balance Method (Indirect) for Poultry Litter

Peyman Neysari[a,*], Nico W.M. Ogink[a,b], Jerke W. De Vries[c], Peter W.G. Groot Koerkamp[a,b]

[a] Farm Technology Group, Department of Plant Sciences, Wageningen University and Research, Wageningen, The Netherlands

[b] Wageningen Livestock Research, Wageningen University and Research, Wageningen, The Netherlands

[c] External Supervisor Farm Technology Group, Department of Plant Sciences, Wageningen University and Research, Wageningen, The Netherlands

* Corresponding author. Email: peyman.neysari@wur.nl

Abstract

Ammonia emission from agriculture contributes to acidification, eutrophication, biodiversity decrease through excessive deposition of N in the environment, and it is also a precursor to secondary particulate matter. The main objective of this study was to compare direct and indirect measurements of N emission from stored poultry manure, defined as the N-gap. The N gap between the methods was calculated by establishing the impinger method (direct) to measure NH_3-N and the N balance method (indirect) to calculate total N loss. NH_3-N emission from manure of laying hens was measured for 7 days. In total, 8 vessels each with 200 g litter and 8 primary and 8 secondary impingers each with 0.5 M HNO_3 were used. Litter samples were collected from 8 vessels on the first day (initial) of the experiment and after the 7-day trial (final). The samples were then thoroughly mixed and immediately delivered to the laboratory to be analysed for total N content in duplicate measurements. The NH_3-N emission magnitude by the impinger method accounted for 0.036 ± 0.0034 (SD) g during the trial, whereas, the N balance method registered 0.41 ± 0.11 (SD) g N loss over the 7-day period. Based on measured NH_3 emission in this study, other N compounds were estimated by using a literature-based ratio of NH_3 to N_2O, NO, NO_2 and N_2 (5:1:1:1:5). The N-gap was quantified by comparing the directly measured emission and the total N loss calculated by N balance method. The results demonstrated a substantial gap of 92% between the direct and indirect methods. Further research is needed to determine the possibility of improving estimation/measurement of N_2 from manure.

Keywords: N-gap, NH_3 emission, impinger method, N mass balance, poultry litter.

1. Introduction

Agriculture is currently responsible for the vast majority of anthropogenic nitrogen (N) loss/emission into the environment (Smith et al., 2007), including ammonia (NH_3), nitrous oxide (N_2O), nitric oxide (NO), nitrogen dioxide (NO_2), and leaching or run-off of nitrate (NO_3^-). In 2013, 93.3% of the NH_3 emission in the EU-28 was related to agricultural production (Eurostat, 2018). Nitrogen emissions inflict different impacts on the environment. For example, NH_3 contributes to acidification and eutrophication and is a precursor to secondary particulate matter (Erisman & Schaap, 2004). Ammonia also decreases biodiversity through the deposition of nitrogen creating an N-enriched environment (Larios et al., 2016).

N loss is currently measured through two different approaches: the direct and the indirect. The direct approach consists of those methods that directly measure the volatilization of each individual N compound (e.g. NH_3 via the impinger method), and the sum of the measured compounds is then the total N loss. In contrast, the indirect approach is based on calculating N loss by subtracting the N content of initial sample from the N content of final sample over a period of time (e.g. from excretion to transporting of manure).

In the direct method, N_2O, NO_2, NO and N_2 are mainly estimated by using two main ratios that are presented in Central Bureau of the Statistics in the Netherlands (CBS, 2019) and Oenema et al. (2000). In the CBS report, the ratio of NH_3 to N_2O, NO and NO_2 is given as 5:1:1:1. In Oenema (2000), the emission of ammonia is equal to N_2 and 10 times greater than the emission of N_2O, NO_2 and NO. Results of comparing the sum of the directly measured N compounds and indirectly measured N loss revealed substantial gaps. This gap can be as high as 80% in some poultry houses (CBS, 2019). As to the authors knowledge, some research has been done on comparing direct and indirect methods, but not comprehensively either not including all N compounds or not including a complete mass balance.

The main objective of this study was to do first a trial on laboratory scale to estimate the difference between directly and indirectly measured N emissions, referred to as the N-gap, in a poultry manure case. To do this, the NH_3-N emission was directly measured through the impinger method. The directly measured magnitude was then compared with total N loss calculated by N balance method to quantify the N-gap.

2. Materials and Methods

2.1. Sampling

Poultry litter of laying hens was collected from a barn near Wageningen, the Netherlands, in August 2020. The house measured 95m by 14m, excluding the roofed area outside scratching area. The roofed area was 7m in width and ran along the length of the building. The hens also had a free-range area outside. Additionally, 10 meters of the building's length was used for egg handling and manure removal. The bird area was divided into 6 equal compartments, each separated by a mesh wall. The area also included three rows of aviaries (each 80m long) with a walking area between every two aviaries (Bolegg Terrace, Vencomatic). The aviaries had a lower and upper manure belt, and a litter scraper (0.5 m in width) was installed under each aviary to remove litter over the length of the house. At the start of the production cycle, the floor was covered with wood shavings. The total living area for the hens was 2,826 m^2 or 9 hens per m^2. The total number of hens was around 24,000. In total, 4 samples were collected from the bedding litter of the rows between aviaries. Samples were collected from the middle and borders of each row. The samples were then thoroughly mixed to be as representative as possible of the whole barn's bedding litter. The mixed sample was immediately delivered to the laboratory without being frozen. A sufficient amount of the mixed sample was analysed concurrently with the impinger experiment for initial N content, dry matter (D.M.), organic matter (O.M.), ammoniacal nitrogen and total P content.

2.2. Impinger method (direct)

In total, eight vessels were utilized to ensure sufficient replication for the experiment. Each vessel contained 200 g of litter. The vessels (0.19 m diameter, 0.30 m height) were made from transparent Perspex Acrylate. The cap of each vessel was perforated with 24 small holes (Ø 0.001 m) as air inlet and another hole (Ø 0.005 m) in the middle as an air outlet. Each vessel was connected to a preliminary and a secondary impinger in a series. The impingers contained 0.5 mol l^{-1} (M) nitric acid (HNO_3). The acid concentration was sufficient for the whole experiment (7 days). The secondary impingers served as spare impingers to trap escaped NH_3 when the preliminary impinger was full. One of the preliminary impingers (No. 6) had insufficient bubbling compared to other impingers and was replaced with a new impinger about 24 h after the start of the experiment. The required vacuum for the air flow was produced by a vacuum pump with a capacity of 8 l min^{-1}. In the vessels air flowed continuously over the surface of each substrate at a nominal rate of 1 l min^{-1}, controlled by a corresponding critical orifice. The flow rate of each vessel was measured daily by a flow meter (Defender, 510). This was done for 5 replications and an average magnitude was calculated. The operational headspace was 0.2-0.25 m for each vessel and air was exchanged 5-7 times per hour, which is comparable to the common air exchange rate in poultry houses in the Netherlands. During the experiment the ambient air temperature varied from 22°C to 27°C and relative humidity from 45% to 55%. After 7 days, the pump was stopped and acid samples were collected from the impingers. The samples were then analysed for ammonium concentration by using spectroscopy method at a 655 nm wavelength according to NEM 4672: ISO/DIS 7150 (Krorn, 1970). NH_3-N concentration was calculated on the basis of ammonium (NH_4-N) concentration by using Equation 1:

$$[NH_3\text{-}N] = [NH_4\text{-}N] \times \Delta m \qquad (1)$$

in which, [NH_3-N] is the concentration of ammonia trapped by impinger (µg), [NH_4-N] is the measured concentration of ammonium through spectroscopy method (µg ml^{-1}) and Δm is the mass change of each impinger solution at the end of the 7-day trial. The acid solution contained 1.015 g ml^{-1} including HNO_3 and water. However, NH_4 mass was considered negligible. NH_3 was converted to NH_4 in the presence of HNO_3 in the following steps: first, the volatilised NH_3 was conveyed from vessels to the preliminary impingers by vacuum pump. The air, including NH_3 gas, was directed to the acid solution in impingers. The NH_3 gas was then absorbed into HNO_3 acid and converted to NH_4 through the chemical pathways as shown in Equation 2a and 2b. The remaining vacuumed gas (except NH_3) was exhausted to the consecutive secondary impinger. This gas was then directedly vented to the outside ambient air through a prepared ventilation system. Figure 1 illustrates the schematic diagram of the impinger set-up for measuring NH_3.

$$NH_3 \text{ (g)} \rightleftharpoons NH_4 \text{ (aq)} \qquad (2a)$$
$$NH_3 \text{ (aq)} + HNO_3 \text{ (aq)} \rightarrow NH_4^+ + NO_3^- \qquad (2b)$$
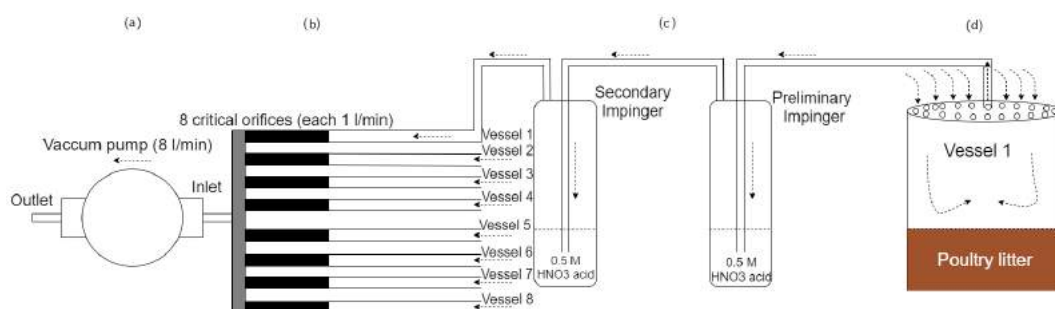
Figure 1 Schematic diagram of ammonia measurement through the impinger method from the poultry bedding litter: a) vacuum pump b) critical orifices c) impingers (preliminary and secondary connected in series) d) vessel containing substrate sample. The dashed arrows indicate the continuous air flow for all vessels. For clarity of the Figure, only one vessel and the corresponding impingers have been drawn

2.3. N balance method (indirect)

The N content was analysed in two steps. First, one representative sample was collected from the initial thoroughly-mixed sample at the beginning of the impinger experiment (initial sample). Second, the remaining substrates in the 8 vessels were thoroughly mixed at the end of the impinger method, and one representative sample was collected to be analysed for N content (final sample). Additionally, other specifications, including D.M., O.M., ammoniacal nitrogen and total P, were analysed based on the initial and final collected samples. Table 1 illustrates the results of the laboratory analyses for the initial and final samples of bedding litter. In this experiment, total N content for both the initial and final samples was analysed through chemical destruction in duplicate experiment according to NEM 4672: ISO/DIS 7150 (Krorn, 1970). Using Equation 3, total N loss was calculated by subtracting the initial sample N content from the final sample N content, under the assumption that the mass change of substrate in each vessel was negligible during 7-day trial.

$$[N]_{loss} = W \times [n_1] - W \times [n_2] \tag{3}$$

where, $[N]_{loss}$ is the total N loss (g), W is the initial sample mass at the beginning of the experiment (g), $[n]_1$ and $[n]_2$ are initial and final N content measured at the beginning and the after 7-day trial respectively (g/kg).

Table 1. laboratory composition analyses of the initial sample (beginning of the impinger experiment) and final samples (7 days after the impinger experiment).

Sample	Dry matter (g/kg)	O.M. (g/kg)	N content (g/kg)	Ammoniacal nitrogen (g/kg)	Total P (g/kg)
Initial	844	606.3	27.70	1.38	8.80
Final	924	642.7	25.65	1.32	8.13

2.4. Statistical Analyses

NH_3-N loss measured by the impinger method and total N loss calculated by the N balance methods were compared by using Welch's t-test. The Welch's t-test (unpaired or independent t-test) was performed to evaluate whether the data from two methods had significant differences. This test is reliably used when two samples have different variances and/or sample sizes (Ruxton, 2006). The normality of NH_3-N data from the 8 impingers were tested through the Shapiro-Wilk normality test at a confidence level of 0.95, under the null hypothesis that the data follow a normal distribution. The N balance data was assumed normal without establishing the Shapiro-Wilk test because there were only limited data points available.

2.5. Quantification of the N-gap between impinger and N balance methods

The N-gap was quantified by comparing sum of the directly measured/estimated N compounds (NH_3-N, N_2O-N, NO-N, NO_2-N and N_2) and N loss calculated through N balance method. The N compounds were estimated based on NH_3-N magnitude measured by the impinger method and the ratio used was based on CBS (2019). The magnitude of all N compounds, including measured and estimated, then summed up to a total N loss (direct). The summed up magnitudes was then divided over the N loss magnitude calculated by N balance over the same period of time. The resulting value indicated the N-gap between the methods.

3. Results and Discussion

The average NH_3-N (g) emission measured by direct method and total N loss (g) calculated by indirect method was compared including error bars as shown in Figure 2. The Welch's t-test result for NH_3-N and N loss data at a confidence level of 95% showed a significant difference of 0.368 (the difference between means = 0.402 g (total N) - 0.036 g (NH_3-N) = 0.366 g). A p-value of 1.5×10^{-6}, t estimator of -11.44 and pooled standard deviation of 0.0407 were

obtained. The Shapiro-Wilk test for NH_3-N data showed a p-value of 0.7, supporting the normality of data. This normality is visually presented in quantile-quantile plot in Figure 3 by straightness factor (w) of 0.94 (1 is 100% normal).
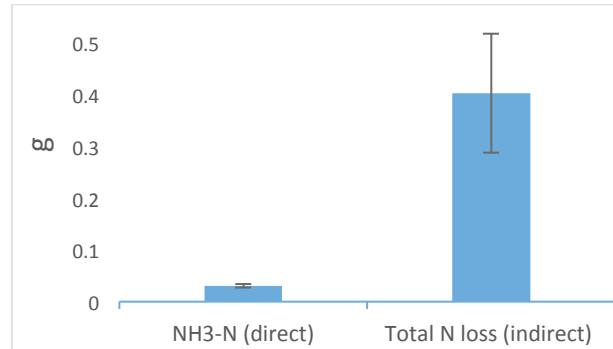

Figure 2 Comparison of average NH_3-N (g) emission and total N loss (g) measured by direct and indirect methods respectively

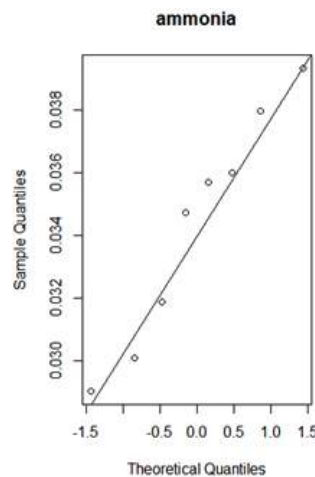Figure 3 QQ-plot for testing normality of ammonia magnitudes measured through the impinger (direct) method

The average NH3-N magnitude measured by the impinger method for 8 vessels during the 7-day experiment accounted for 0.033 ± 0.0036 (SD) g. The N loss during the 7-day experiment was calculated to be 0.41 ± 0.11 (SD) g. The proportion of the total N loss derived from the two methods was calculated to be 0.080 g g-1 resulting in an N-gap of 92%. This N-gap may result from underestimating emission rates of one or more N compounds. This finding is consistent with that of Shah, et al. (2013), who estimated the loss of NH_3-N and N_2O (29.2% of N-input) in a study with 9 flocks of broilers combining measurements and assumptions from literature. This finding was also reported by Coufal et al., (2006), who measured N-balances in 18 consecutive flocks of broilers without emission measurements. They partitioned N input between carcass, mortality, litter, and the remaining part was loss, where N loss, on average, amounted to 21% of N-input. There is also similarity between the current study and the N-gap accounted by Wang et al. (2006) from broiler litter by measuring NH_3-N through acid scrubber method and N balance. The results showed that the acid scrubber method registered 138 mg NH_3-N at an ambient moisture content of 17.8%, while the N balance method accounted for 994 mg in the same period, resulting in an N-gap of 87%.

4. Conclusions

This study set out to quantify the N-gap between direct and indirect methods of measuring N loss from an aviary poultry barn. The results of this research show that there is a substantial N-gap of 92% between the two methods. This study has raised important questions about the nature of estimated ratio between NH_3-N and other N compounds in the literature. All N compounds can be measured through establishing a measurement device. However, the need for measuring N_2 to fill in the N-gap arises remarkably as it is only estimated. Further research is needed to determine the possibility of improving the estimation/measurement of N_2 from manure.

References

CBS. 2019. Stikstofverliezen in stal en opslag. The Central Bureau of Statistics, the Netherlands.

Coufal, C. D., Chavez, C., Niemeyer, P. R., & Carey, J. B. 2006. Nitrogen emissions from broilers measured by mass balance over eighteen consecutive flocks. *Poultry Science*, *85*(3), 384–391. https://doi.org/10.1093/ps/85.3.384.

Erisman, J. W., & Schaap, M. 2004. The need for ammonia abatement with respect to secondary PM reductions in Europe. *Environmental Pollution*, *129*(1), 159–163. https://doi.org/10.1016/j.envpol.2003.08.042.

Eurostat, F., Explained, T. S., Union, E., State, M., & Eurostat, F. 2018. Archive : Agriculture - ammonia emission statistics Main statistical findings, (June 2015), 1–8.

Krorn, M. 1970. The analyst. *Analyst*, *95*(1249), 705. https://doi.org/10.1039/AN9709500705.

Larios, A. D., Kaur Brar, S., Avalos Ramírez, A., Godbout, S., Sandoval-Salas, F., & Palacios, J. H. 2016. Challenges in the measurement of emissions of nitrous oxide and methane from livestock sector. *Reviews in Environmental Science and Biotechnology*, *15*(2), 285–297. https://doi.org/10.1007/s11157-016-9394-x.

Wang Lingjuan, Zifei Liu, David B. Beasley, Roberto Munilla, & Gerald R. Baughman. 2006. Measuring Ammonia Emissions from Broiler Litter. https://doi.org/10.13031/2013.21571.

Oenema, O., Verdoes, N., Groot Koerkamp, P. W. G., Bannink, A., Meer, H. G. van der, & Hoek, K. W. van der. 2000. Forfaitaire waarden voor gasvormige stikstofverliezen uit stallen en mestopslagen.

Ruxton, G. D. 2006. The unequal variance t-test is an underused alternative to Student's t-test and the Mann-Whitney U test. *Behavioral Ecology*, *17*(4), 688–690. https://doi.org/10.1093/beheco/ark016.

Sanhueza, E., Plum, C. N., & Pitts, J. N. 1984. Positive interference of nitrous acid in the determination of gaseous HNO3 by the NOx chemiluminescence-nylon cartridge method: Applications to measurements of ppb levels of HONO in air. *Atmospheric Environment (1967)*, *18*(5), 1029–1031. https://doi.org/10.1016/0004-6981(84)90081-7.

Shah, S. B., Grimes, J. L., Oviedo-Rondón, E. O., Westerman, P. W., & Campeau, D. 2013. Nitrogen mass balance in commercial roaster houses receiving different acidifier application rates. *Journal of Applied Poultry Research*, *22*(3), 539–550. https://doi.org/10.3382/japr.2012-00704.

Smith, P., Cai, Z., Gwary, D., Janzen, H., Kumar, P., McCarl, B.,Sirotenko, O. 2007. Agriculture In Climate Change: Mitigation. *Cambridge University Press*, (4), 1–44.

Winer, A. M., Peters, J. W., Smith, J. P., & Pitts, J. N. 1974. Response of commercial chemiluminescent NO-NO2 analyzers to other nitrogen-containing compounds. *Environmental Science and Technology*, *8*(13), 1118–1121. https://doi.org/10.1021/es60098a004.

Thermal Analysis for an Unrefined Sugar Cane Processing Factory in Colombia by Using CFD.

Juan Alvarez Carpintero [a, *], Robinson Osorio Hernández [b]

[a] Faculty of Engineering, Universidad Nacional de Colombia, Bogotá, Colombia
[b] Faculty of Engineering, Universidad Nacional de Colombia, Bogotá, Colombia

* Corresponding author. Email: juadalvarezcar@unal.edu.co

Abstract

In facilities dedicated to manufacturing, processing and treating agricultural goods, especially in tropical climate it is common to find elevated humidity and temperature levels, factors that can affect the life and productivity of operators, also generating problems in healthiness, therefore spoiling the production. The main goal of this project was to evaluate the existing conditions for the workers in the unrefined sugar cane's juice collector center, located in Caparrapí - Cundinamarca, Colombia, based on temperature to measure the indexes, using CFD tools.

The simulation results showed high temperature levels, consequently demonstrating that the workers are under thermal stress, according to indexes developed in previous investigations. Moreover, the simulations showed that the applied changes to the structure successfully enhance work conditions inside the Center, and the indoor environment, therefore being a good solution for the actual conditions.

Keywords: Unrefined sugar, agroindustry, CFD simulation, higrothermal analysis, bioclimate.

1. Introduction

Unrefined sugar, also known as panela, is an important product in Colombia's economy, being this the third main product produced in agroindustry in the country in 2019, above products like coffee and cocoa (DANE, 2020). According to official data, 198856.83 hectares were sown to produce unrefined sugar cane in year 2020, with around 6.28 tons of unrefined sugar per hectare (Fedepanela, 2020). The most harvested sector for 2020, was Cundinamarca, the region in which the capital is located, with 18% of the national unrefined sugar cane production.

The panela is usually produced in small, artisanal compounds located in each farm dedicated to panela production, with specific characteristics, as described by García B (2020) . Nevertheless, some of the municipalities of the country have unified processes in factories, in order to increase product quality with traceability processes while also ensuring ways to commercialize the panela (Fedepanela, 2016).

The process of manufacturing panela, learned from experience, starts with the receival of juice extracted from sugar cane, also called honey, harvested in small nearby farms. After this, pH and Brix level are determined from the arriving honey, so it can be classified in class A or B honey, being A the highest quality. These characteristics determine the payment the farmers will receive for their production.

The same quality honey received from different farms is combined and placed under a decantation process, in which impurities move to the lower parts of the tanks, purifying and homogenizing the honey. After this, the honey is sent to an elevated tank with 5-ton capacity, to prepare for the distribution.

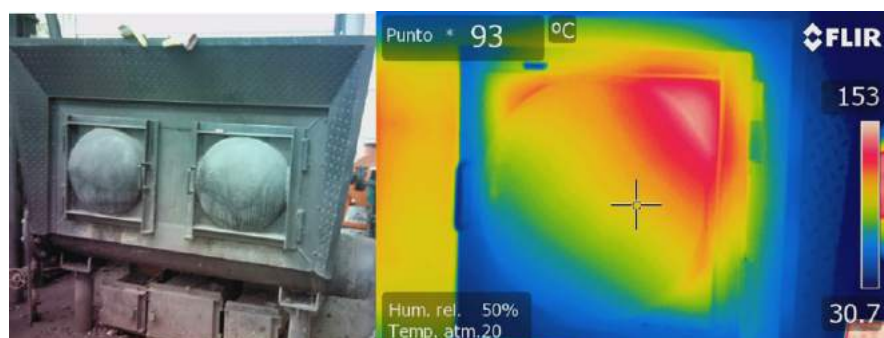Figure 1. Evaporators used in the process of panela manufacturing.

From the distribution tank, honey is driven into the evaporators, shown in Figure 1, where the cooking process takes place, at the most posterior section of the facility. Nevertheless, while the system is still heating, prior to 60°C pH is corrected if necessary. When the desired pH level is reached, the heating process continues normally until the

evaporators reach 105°C. At this point, water inside the honey is evaporated, incrementing the Brix level to around 85° (Fedepanela, 2016).

As soon as the Brix level is reached, the valves are opened for the honey to drop in the concentrators. During this process, honey temperature fluctuates around 120°C, as shown in Figure 2. When the maximum amount of honey is met inside the concentrators, the hitter process begins. Through series of hits, the workers seek to reduce the temperature levels, homogenize the humidity and oxygen content inside the mixture, and changing the panela colour until it reaches the "point of panela", recognized by the experience of the workers. This point is found after 15 minutes, approximately.
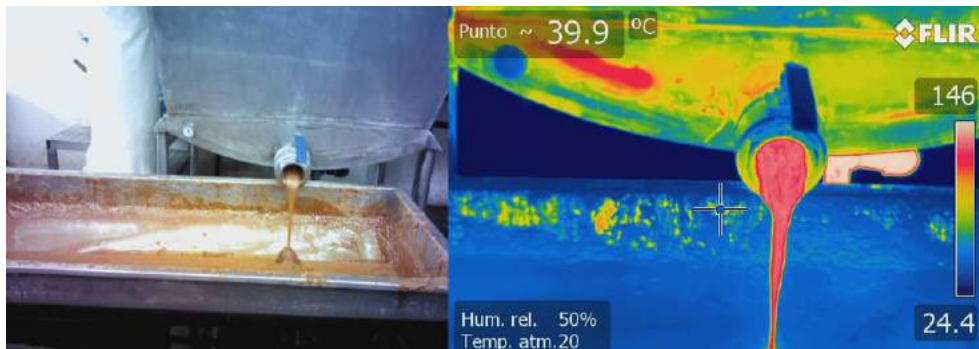

Figure 2. Opening of valves in panela creation process.

When the mixture is ready, the shape process begins by pouring it into moulds, as can be seen in Figure 3, presenting temperatures around 60°C. 3 minutes after the pour in is done, the moulds are lifted, and the panela is left over the table for cooling. Once the panela reaches the environmental temperature, it is ready to be packed or grinded, according to the desired subproduct.

Figure 3. Molding and cooling of panela.

Previous studies using CFD techniques have been applied to a facility destined to wet processing of coffee, in which environmental conditions were evaluated through different opening configurations (Osorio Hernandez, et al., 2020), including comfort indexes (Guerra García, Ferreira Tinôco, Osorio Saraz, & Osorio Hernández, 2019). Additionally, studies in the panela manufacturing process have been developed to investigate the energy efficiency through reuse of bagasse (Quispe & Saavedra, 2015), also simulation for traditional compounds (Osorio Jaraz, Ciro Velasquez, & Espinosa Bedoya, 2010) and design optimization through CFD (Restrepo, Flórez, & Tibaquirá, 2017).

It is important that agro-industrial buildings provide good conditions for workers, optimizing temperature, illumination and ventilation (Rozo, 2013). In Colombia, requirements for environmental conditions in thermal buildings have been developed by ACAIRE (2017), in order to standardize the building construction and guarantee said conditions. High temperatures and vapour production can develop genetic implications and lung diseases (Samet, Marbury, & Spengler, 1987), also having repercussions over the economic incomes of the factories (Cai, Lu, & Wang, 2018). Due to these reasons, the objectives of this investigation are to determine the behaviour of the temperature distribution and air performance inside the building through a CFD simulation for the facility, and a thermal comfort index to analyse the facility environment.

2. Materials and Methods

In this section the model creation process is described as follows.

2.1. Location and geometrical representation of the model

The facility that is the object of this study is in the municipality of Caparrapí - Cundinamarca - Colombia, at coordinates 5° 20′ 39″ N, 74° 29′ 30″ W.

For the model to run, the first design was implemented on the base geometry of the control volume. The measurements of the building were extracted from the original layout drawings and represented in a 3D model created through the software CAD. Height, width and depth were the main data extracted there, including measures from the worktables, evaporators, air extractors and other smaller structures inside the building, as can be observed in Figure 4. , where the geometric model is showed.
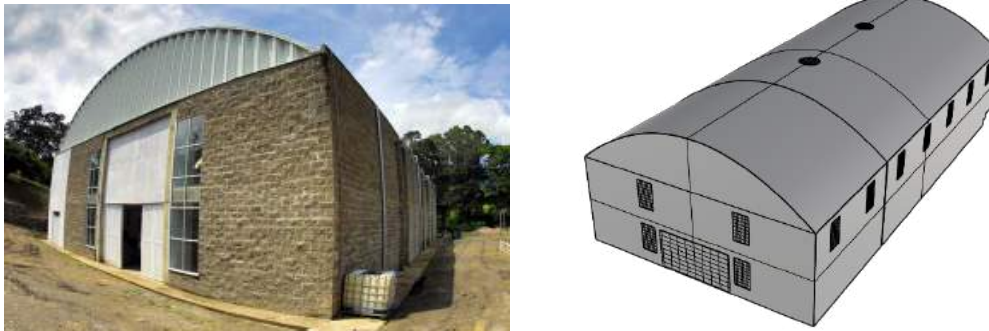

Figure 4. Real building (Gobernación de Cundinamarca, 2018) and geometric model to represent the postharvest factory of sugar cane.

2.2. Mesh programming

Mesh use is an important process in CFD simulation, especially the definition step, in which the number of nodes and elements is determined (Duan, et al., 2015). There are not studies in the area concerning air dynamics in unrefined sugar cane, nor in geometry definition for structures with these processes. For that reason, the number of nodes and elements for this study was defined automatically.

Mesh creation and optimization was realized in the software ANSYS ICEM CFD. A tetrahedral mesh type was selected due to the complexity some edges of the structure represented, especially in curve sections and small elements, such as roofs and tables. The definition of the element's sizes was defined through a sensitivity examination, obtaining smaller elements for the complex areas, in order to assure a better definition during the simulation. In Figure 5, the result of the mesh is shown.

Next step focused in grouping the elements according to their size and utility. Windows were defined as one big lot, while doors were separated each one by their functionality inside the building. The same process was carried with the extractors, worktables and the remaining structure's parts.
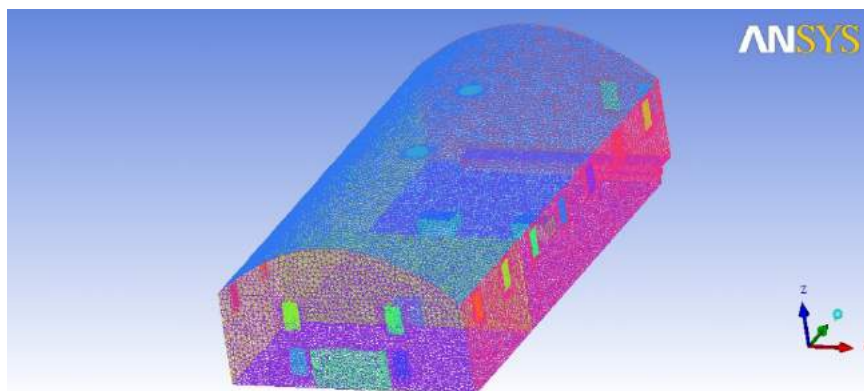

Figure 5. Mesh created for the structure.

For this study, the resultant number of nodes was 85271, while the total number of elements was 480041, which were used to run the simulation, in the next step.

2.3. CFD simulation

For the boundary conditions of simulation, base data had to be gathered. Prior configurations before the start of the simulation, through ANSYS CFX, require the average environmental characteristics including temperature, height over the sea level, daily radiation, wind speed and direction, and local pressure (when required). This data was gathered in the study place with the sensors destined for each task. For this study, an average temperature of 25.4°C was taken, while the average speed of the wind was rounded to 2.0 m/s.

The use of this software requires the definition of the parts conforming the mesh as inlets, outlets, walls or openings. For this investigation, the windows and doors were defined as walls, the same than the floor, roof and divisions in the structure, due to their real use in the factory, as they remain closed all the time. On the other hand, extractors were defined as outlets, while worktables and evaporators were selected as inlets, owing to its contribution of particles and heat to the air. These properties can be seen in Figure 6.
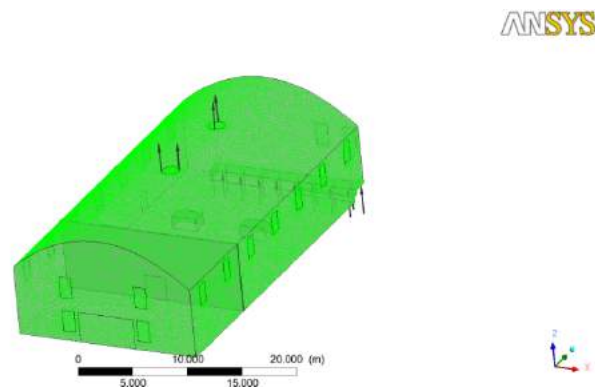
Figure 6. Parts definition for simulation

For the simulation, a non-steady model was chosen in order to assure real air movement results and to be able to add more characteristics for future simulations.

3. Results and Discussion

In this item, the obtained simulations will be analysed, subdivided in three major aspects: air movement focusing on the speed it moves inside the building, temperature distribution inside the building, and thermal comfort.

3.1. Air movement inside the building

For bioclimatic environment it is important to observe air movement, especially from and to where it is moving, in order to act about the behaviour, it has and its effects in the building. Simulation results shown in Figure 7 describe the air moving only through the effect of evaporator and stem of water generation in the process of drying sugar cane of unrefined sugar cane products (panela); simulating in this way, what happens inside the real building.

The air velocity inside the building suffered small variations, due to the lack of air exchange inside the building through windows, doors or openings contributing to this function. Interiorly, the air velocity was close to 0m/s, indicating slow movement and air exchange, whereas in the proximities of the extractors the air speed incremented reaching velocities around 1.7m/s.
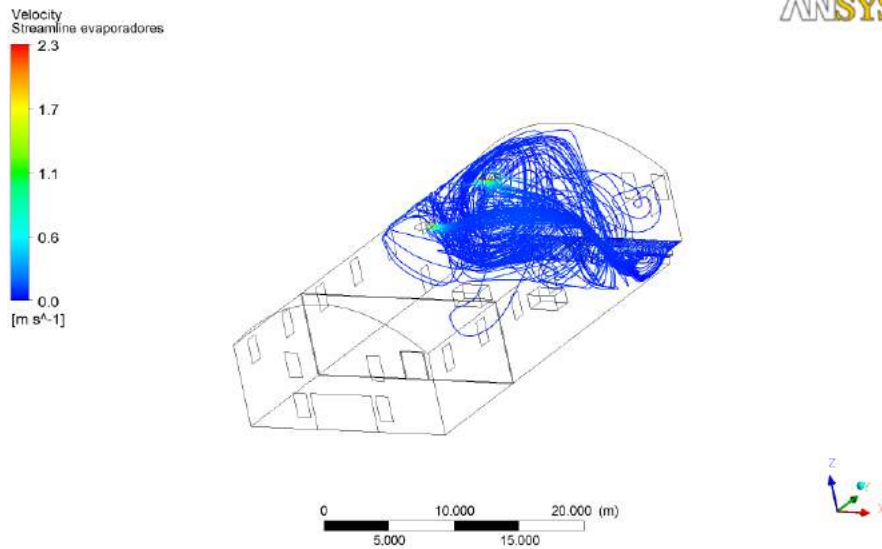
Figure 7. Air speed and direction inside the building, in meters per second.

3.2. Temperature distribution along the structure

To observe the air temperature distribution inside the building a render model was simulated, using as main parameters the air temperature and the amount of exchanged air with the environment surrounding the structure. Temperature variation is shown in Figure 8, where a general scheme can be distinguished.
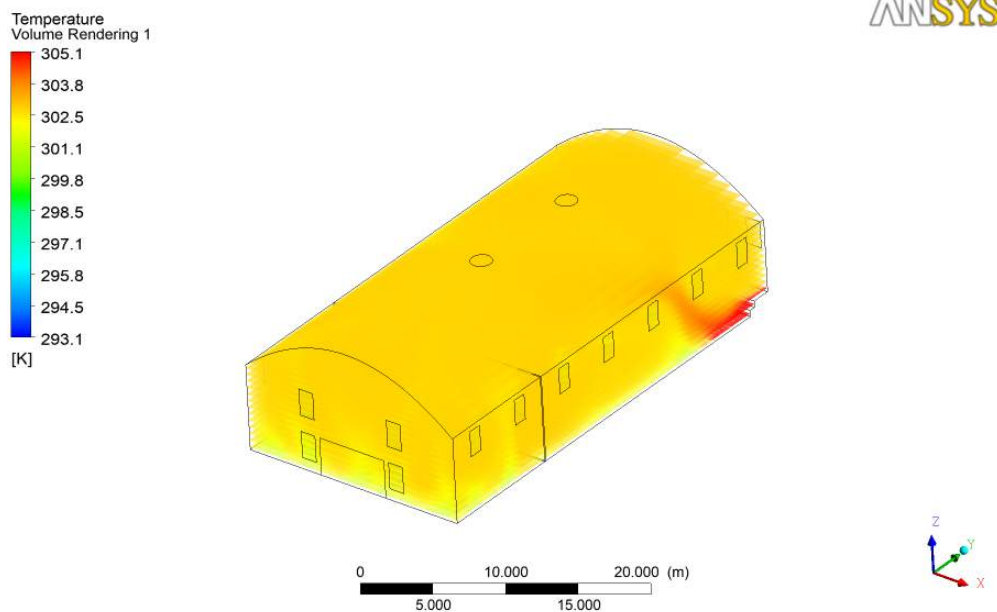
Figure 8. Volume render describing the air temperature inside the building in Kelvin.

Air temperature does not present a high variation on the inside of the building, stabilizing around 30°C. In the contiguities of the floor, the temperature is lower, around 28°C, due to the heat exchange with this surface, whereas close to the evaporators, the temperature rises to temperatures of 32°C and more, in some cases. These results, along with the long shifts they work, show that the workers are exposed to high temperatures for a labour environment, developing a difficult and suffocating atmosphere.

3.3. Laboral comfort

As mentioned in the introduction, thermal comfort is essential to create suitable environments for workers in any factory. According to Chow et al. (2010), for a comfort analysis temperature should be measured at around 1.5m in order to determine the real sensation workers experience.
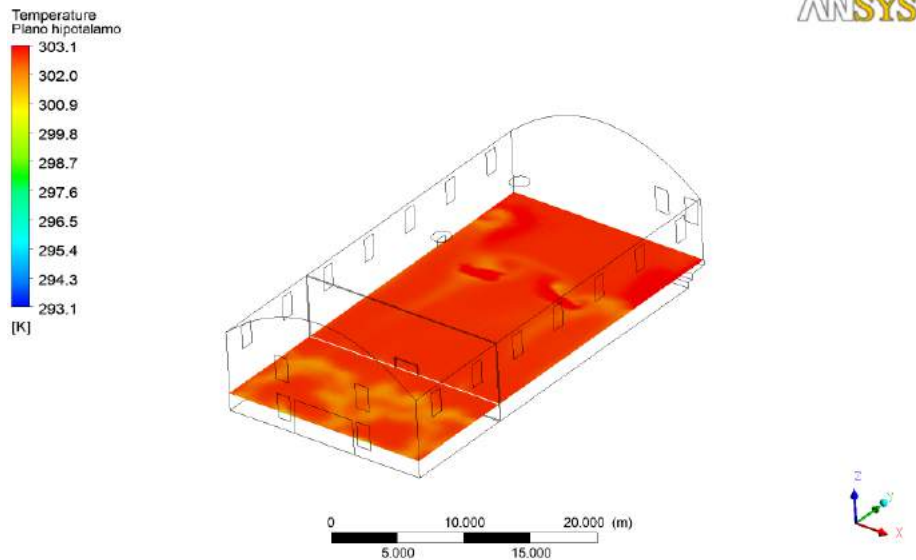
Figure 9. Temperature distribution at a height of 1.5m.

With the results of the simulation, shown in Figure 9, it is possible to determine that temperature levels go from 28°C to 30.1°C. Heat spotlights can be observed throughout the facility especially in areas close to high temperature processes, like the evaporators and worktables. Nevertheless, on the other side of the wall, temperature levels decrease due to the distance to these processes.

To determine numerically whether the workers are under comfortable conditions, or they are suffering thermal stress, a comfort index was applied with the intention to know what actions could be taken, depending on the number of grades that are causing the stress.

For this investigation, the model equation for men was taken from the study made by Chow et al. (2010), in which a comfort temperature is calculated through the application of equation .

$$TS_m = 0.3022T_C - 0.5095v - 7.358 \qquad (3.1)$$

Where TS_m is the thermal sensation, indicating temperature stress or neutral sensation when it is equal to 0. T_c is the comfort limit temperature to which the laborers feel a suitable place to work, for a determined air velocity, indicated by v. In order to assure the thermal comfort, the thermal sensation was set to 0, resulting in equation 3.2.

$$T_c = 24.348 + 1.686v \qquad (3.2)$$

Air velocity inside the building is 0.4m/s approximately, according to the simulation, as shown in Figure 7. Solving the equation with this velocity shows as result a comfort temperature of 25.1124°C. This indicates that the workers are exposed to high temperatures, especially those in charge of operating the evaporators and worktables, thus showing they are under heat stress.

4. Conclusions

As discussed before, it was possible to determine that the conditions in the work environment are not recommended for the workers to perform tasks like those currently done, because of the high temperatures inside the building. Also, ventilation systems do not refresh enough air, nor give it enough velocity to create a correct renewal process.

To continue this investigation, a verification process is required to determine the veracity of the investigation, through confirm the proximity of the simulated data to the real one. Also, to further implement simulations, modifications can be proposed to the facility in order to observe changes in the structure and its environment, aiming to

lower the temperature and create air exchange cycles. Additionally, it is possible to include vapour interaction in the simulations, to identify mass transfer to the environment and determine its impacts on the worker's health.

References

ACAIRE. (2017). *Rite 2017 - Reglamento Técnico de Instalaciones Térmicas en Edificaciones.* Bogotá: Asociación Colombiana de Acondicionamiento del Aire y la Refrigeración.

Cai, X., Lu, Y., & Wang, J. (2018). The impact of temperature on manufacturing workerproductivity: Evidence from personnel data. *Journal of Comparative Economics*, 889-905. doi:doi: 10.1016/j.jce.2018.06.003

Chow, T. T., Fong, K. F., Givoni, B., Lin, Z., & Chan, A. L. (2010). Thermalsensation of Hong Kong people with increased air speed, temperature and humidityin air-conditioned environment. *Building and Environment*, 2177–2183. doi:10.1016/j.buildenv.2010.03.016

DANE. (2020). *Encuesta Nacional Agropecuaria (ENA) Primer Semestre 2019.* Bogotá: DANE.

Duan, R., Liu, W., Xu, L., Huang, Y., Shen, X., Lin, C., . . . Sasanapuri, B. (2015). Mesh type and number for the CFD simulations of air distribution in an aircraft cabin. *Numerical Heat Transfer, Part B: Fundamentals*, 489-506. doi:10.1080/10407790.2014.985991

Fedepanela. (2016). *PLANTA HOMOGENIZADORA DE MIELES - CENTRAL DE MIELES DE CAPARRAPÍ.* Caparrapí: Central de mieles - Caparrapí.

Fedepanela. (2020). *ÁREAS, RENDIMIENTO Y PRODUCCIÓN PROYECCIÓN PARA 2020.* Bogotá: SIPA - Sistema de información panelero.

García B, H. (2020, 08 21). *SIPA - Sistema de Información Panelero.* Retrieved from CURSO BÁSICO DESCRIPTIVO PARA EL DISEÑO, CONSTRUCCIÓN Y OPERACIÓN DE HORNILLAS PANELERAS: http://www.sipa.org.co/wp-content/uploads/Tema1_Hornillas.pdf

Gobernación de Cundinamarca. (2018, 11 20). Inversión de $6.000 millones en nueva central de mieles en Útica. *Inversión de $6.000 millones en nueva central de mieles en Útica*. Bogotá, Cundinamarca, Colombia.

Guerra García, L. M., Ferreira Tinôco, I. d., Osorio Saraz, J. A., & Osorio Hernández, R. (2019). Thermal comfort in buildings for wet processing of coffee. *Revista de Arquitectura*, 101-111. doi:http://dx.doi.org/10.14718/RevArq.2019.21.2.2597

Osorio Hernandez, R., Osorio Saraz, J. A., Sullivan Oliveira, K., Aristizabal, I. D., Arango, J. C., & , . (2020). Computational fluid dynamics assessment of effect of different openings configurations on the thermal environment of a facility for coffee wet processing. *Journal of Agricultural Engineering*, 21-26. doi:10.4081/jae.2020.892

Osorio Jaraz, J. A., Ciro Velasquez, H. J., & Espinosa Bedoya, A. (2010). EVALUACIÓN TÉRMICA Y VALIDACIÓN DE UN MODELO POR MÉTODOS COMPUTACIONALES PARA LA HORNILLA PANELERA GP150. *DYNA*, 237-247. Obtenido de http://www.scielo.org.co/scielo.php?script=sci_arttext&pid=S0012-73532010000200025&lng=en&tlng=es

Quispe, C., & Saavedra, R. (2015). Aplicaciones CFD para el Uso Racional de la Energía del Bagazo en la Agroindustria Panelera. *The Thirteenth Latin American and Caribbean Conference for Engineering and Technology*, 1-8.

Restrepo, Á., Flórez, L. C., & Tibaquirá, J. E. (2017). Diseño, simulación y construcción de un serpentín evaporador para la industria panelera a baja escala en Colombia. *Ingeniería Mecánica*, 51-57. Obtenido de http://scielo.sld.cu/scielo.php?script=sci_arttext&pid=S1815-59442017000200001&lng=pt&tlng=es

Rozo, T. (2013). *Manual técnico de buenas prácticas de manufactura (BPM) para el proceso tecnológico de producción de panela.* Neiva: CORHUILA. Obtenido de https://www.onfandina.com/images/Publicaciones/Panela/ManualTécnicoBPMTrapiches.pdf

Samet, J. M., Marbury, M. C., & Spengler, J. D. (1987). State of Art: Indoor Air Pollution. *The American Review of Respiratory Disease*, 1486–1508.

Evaluation of the Effects of Antidrip and UV Transmission Properties of Polyethylene Films on a Greenhouse Strawberry Crop

Nikolaos Katsoulas[a], Anastasia Bari[a], Theodora Georgopoulou[b], Chryssoula Papaioannou[b]

[a] Department of Agriculture, Crop Production and Rural Environment, School of Agricultural Sciences, University of Thessaly, Volos, Greece

[b] Department of Agrotechnology[2], School of Agricultural Sciences, University of Thessaly, Larisa, Greece

* Corresponding author. Email: nkatsoul@uth.gr

Abstract

Polyethylene covering materials of 84% and 24% transmissions in UV light and permanent anti-drip properties were evaluated examining the size and the overall formation of droplets when the roof was covered by moisture. In addition the effect of these covers on agronomical factors of hydroponic strawberry crop was investigated. The results indicated that the cover which creates an environment with less UV light seems to increase fruit nutrition value in the case of strawberry plants, as it increases their content in certain secondary metabolites. Other agronomical parameters related to crop performance (such as chlorophyll content, photosynthetic rate, yield characteristics, etc.) remained unaffected. As regards the size and type of droplets when moisture condensation occurred on these covers, great differences among the tested films where emerged. In one of the tested films, the appearance of droplets lacked uniformity and the overall condensed water weigh was lesser (15% *vs.* 71%).

Keywords: ultraviolet radiation, greenhouse cover, crop response, fruit quality

1. Introduction

Crop transpiration and soil evaporation generate water vapor, which, if not removed from the greenhouse air, will condensate on surfaces with temperature lower than the dew point temperature. Among others, in these surfaces usually are included the surface of the leaves of the crop as well as the surface of the greenhouse cover. In case that the cover material is hydrophobic, such as the low-density polyethylene (LDPE) greenhouse covering films, then the problem is exacerbated, because due to surface tension, condensation occurs in the form of droplets. Water droplets form an opaque layer on the surface of the film that is harmful to the covered crop because it leads to:

1. reduction of cover light transmission resulting in reduction of photosynthesis rate
2. increase in the incidence of fungal diseases when the droplets drop on the crop leaves
3. increase in the occurrence of burns on the surface of the leaves due to the creation of light focal points
4. reduction of production (both qualitative and quantitative)
5. higher needs for plant protection products use that burden greenhouse crops and the environment with chemical residues.

Schultz and Barting (1996) and later Papadakis et al. (2000), explained how the gathering of condensed water on greenhouses' roof is actually connected to the transmissivity of the cover and when this transmissivity is affected in a bad manner it results in less light, meaning a decreased yield. Therefore, anti-drip (AD) films have been developed which according to Gilby (1990), can avoid transmissivity reduction by 15% in comparison with a material that lacks AD properties. Giacomelli and Roberts (1993) reported that AD properties of PE films for condensation drip control are obtained by modifying the surface tension of the film.

In general, the relative research on covering material with this specific characteristic has been reported many decades before. Jaffrin (1990) and Geolla and Peipper (1994) have thoroughly explained how manufacturers include surface active agents to the basic resin of polymer in order to produce a greenhouse covering material with AD properties, which change its nature, without preventing the formation of condensation. According to the previous mentioned authors, this material spreads the condensation over the surface of the film instead of forming droplets.

However, the AD additive that gives the cover its AD characteristics is gradually washed off by the condensed water during usage. Toneatti (1989) stated that the duration of the AD characteristic is affected by the amount of condensed water, a statement that has been also supported by other authors (Jaffrin and Makhlouf, 1990, Geoola et al.,1994, Geoola et al., 2004). Thus, the creation of a covering material with permanent AD properties is of great importance and a multilayer co-polymer designed for greenhouse cover and characterized by this particular property, is evaluated in this report. This research will focus mainly on the effect of glazing (term adopted by Giacomelli and Roberts, 1993), on strawberry fruit quality and overall plant performance.

2. Materials and Methods

2.1 Greenhouse facilities and plant material

The experiments were performed in the experimental greenhouses shown in Fig. 1. The greenhouses are modified arched type, N-S oriented and are located at the University of Thessaly farm (39°22'N 22°44'E, altitude 85 m), on the

continental area of Eastern Greece. The geometrical characteristics of each greenhouse are as follows: eaves height of 2.9 m; ridge height of 4.1 m; total width of 8 m; total length of 20 m; ground area of 160 m², and volume of 524 m³. The greenhouses were equipped with two continuous side roll-up windows located at a height of 0.6 m above the ground with a maximum opening area of 27 m² (two vents of 15 m length × 0.9 m opening height) for both vents. A flap roof window was also located longitudinally on the whole greenhouse roof (20 m long) with 0.9 m maximum opening height (18 m² opening area). The vents were controlled automatically via a controller and opened in steps; they began to open when greenhouse air temperature exceeded 22°C, and reached their maximum aperture when temperature reached 25°C.
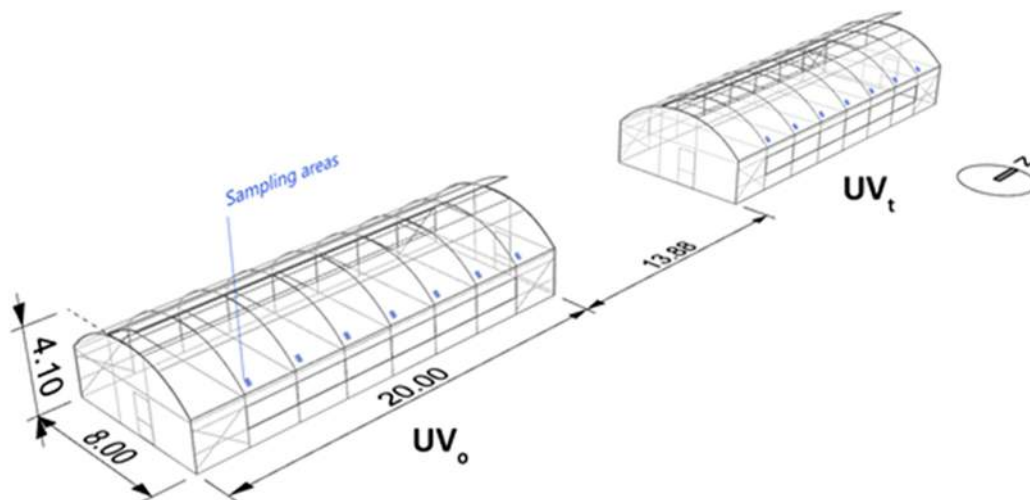

Figure 1. Experimental Greenhouses (sampling areas referred to the condensation when this parameter was examined by weighing paper placed in above marked places to harvest the moisture amount).

Both films had 180 μm thickness and equal amounts of infrared, diffusion and ethyl-vinyl-acetate additives as well as permanent AD properties. All covering materials were made of low-density PE film with equal amounts of infrared, diffusion and ethyl-vinyl-acetate additives. One greenhouse (UV$_o$) had limited UV transmittivity (24%) while the other (UV$_t$) had higher (84%) (Both manufactured by Plastika Kritis S.A., Heraklion, Crete, Greece).

Condensation characteristics were examined, more precisely the percentage of wet per total cladding area, the shape of droplets as well as their max and min dimensions, using the following procedure: photographs of different sample areas were taken on the roof of greenhouses and then they were imported in Rhinoceros 3D software, where calculations were executed using the Grasshopper plug-in, which is a visual programming language (method 1). In addition, another measurement (method 2) concerning film condensation evaluation was performed by collecting and weighing water in certain locations in the interior surface of the roof (Fig.1) of greenhouses.

Strawberry crop (*Fragaria x ananassa*, cv. Victory) was transplanted on 22/02/2020, at a density of 6 plants m⁻². Experiments were carried during spring and summer 2020 (February-July) concerning strawberry fruits harvested 11 times in total at the fully red/ripe maturity stage, from 45 selected plants in each greenhouse, harvesting, once a week, during 9 a.m. to 11 a.m. After every harvest fruit were packed separately in paper bags and transferred in the laboratory where fresh, dry and specific weight, were measured or calculated. Also, total production per plant was calculated weighing harvested fruit of the labelled plants. Nutrition uptake and other cultivation treatment (pruning, spraying etc.) do not differ between the greenhouses.

Figure 2. Harvested fruit in UV_t (right) and UV_o (left) greenhouses

2.2 Elected Agronomical Measurements on plant material (fruit)

In the research regarding UV blocking material on plant performance it has been documented (Kittas et al., 2006; Papaioannou et al., 2012; Katsoulas et al., 2020) that when the same material in chemical structure and properties (mechanical and optical) except the transmission in UV radiation are applied as covering material on greenhouses, then, the different UV light inside those greenhouses mainly affects fruit quality. The fruit colour measurement methodology that was followed was based on the above-mentioned papers.

Photosynthetic rate of strawberry plants was measured by using LCpro + 1.0 ADC (Bioscientific Ltd., Hoddesdon, Hertfordshire, UK) and it was expressed as $\mu molCO_2sec^{-1}$. For each measurement 10 leaves from 10 different plants from each treatment were selected. The measurements took place during the solar noon, from 12.00 p.m. to 02.00 p.m.

Leaf chlorophyll content was estimated by using Chlorophyll Meter SPAD-502Plus (Konica Minolta Europe). Also, for each measurement 10 leaves from each treatment were selected, and chlorophyll content was expressed as SPAD units.

3. Results

3.1 Effect on condensation quantity and morphology (pattern and dimensions)

3.1.1 Effect on condensation quantity

The condensation on greenhouse cover was calculated, according to method 2 (see section 2.1), on springtime 2020 and 2021, when the outside temperature was less than 5^oC. Sampling positions, in which water was collected, did not differ between greenhouses (Fig. 1). According to Table 1, in all measurements (N=24) in greenhouse UV_t the amount of water was almost 40% greater (2.8 g *vs*. 0.6 g).

Table 1. Water collected from greenhouse roof in a 200 cm^2 area (means of 24 measurements) evaluated with IBM SPSS statistical package v.26, according to Prof. Duncan's criterion. ± indicate the standard deviation of the means. Numbers of the same line followed by different letters indicate statistically significant differences.

	UV_o	UV_t
Condensed water (g)	0.64 ± 0.13^b	2.82 ± 0.21^a

3.1.2 Effect on condensation morphology (pattern and dimensions)

Accordingly, when we measured condensation on the UV_t greenhouse roof using the Rhinosceros software (method 1), the levels were also higher (Fig. 2). Condensed water was covering the 71% of the surface of the roof, while in the UV_o greenhouse this amount was lesser (15%). In addition, in the same greenhouse (UV_t) the dropping area pattern was uniform and spherical.

The largest drops in the greenhouse UV_t covering material did not exceed the area of 0.332 mm^2, while in the UV_o greenhouse this wet area was higher by almost 1000% (982%) reaching 3.572 mm^2.

The smallest drops on the UV_t greenhouse had a value of 0.001 mm^2 while in the UV_o greenhouse this value was increased by 3000% (=0.030 mm^2).
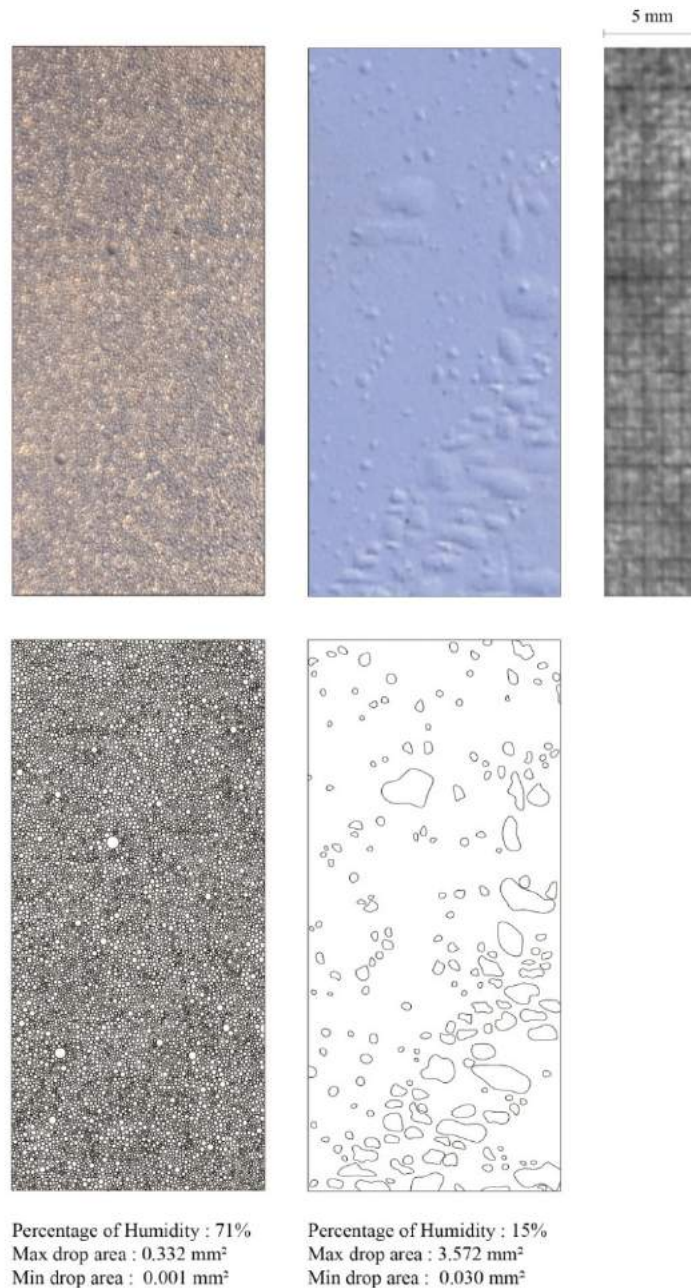
Figure 2. Condensation pattern and dimensions of drops picturing the cladding material of the UV_t (left) and the UV_o (right) greenhouses (sampling area=376.08 mm^2).

3.2 Effect on crop and fruit quality

3.2.1 Effects on Photosynthetic rate and Chlorophyll content

As shown in Table 2, no significant differences were noticed in photosynthetic rate of strawberry plants among the treatments. The same was also observed for leaf chlorophyll content index.

Table 2. Photosynthetic rate A (μmol m^{-2} sec^{-1}) and Chlorophyll content index (CCI) of plants. ± indicate the standard deviation of the means. Numbers of the same column followed by different letters indicate statistically significant differences.

Cover	A (μmol m^{-2} sec^{-1})	CCI (SPAD)
UV_o	15.25 ± 0.23^a	41.36 ± 1.01^a
UV_t	14.41 ± 0.31^a	41.67 ± 1.07^a

3.2.2 Effect on plant yield

Total yield per plant, total number of harvested fruit per plant and mean fruit weight in the two greenhouses for all dates tested, are summarized in Table 3. Significant differences were noticed only for the total number of fruit per plant, where the highest number of fruits recorded in the plants under the UV_t cover. On the other hand, no differences were noticed in total yield per plant (kg plant^{-1}), mean fruit weight and fruit dry matter partitioning.

Table 3. Strawberry Yield characteristics. ± indicate the standard deviation of the means. Numbers of the same column followed by different letters indicate statistically significant differences.

Cover	Yield (kg plant^{-1})	Fruit number per plant	Mean fruit weight (g)	Dry matter (%)
UV_o	0.32±0.02[a]	21.85±7.65[a]	12.47±7.37[a]	9.27±1.12[a]
UV_t	0.28±0.04[a]	17.94±6.06[b]	12.92±7.36[a]	10.02±1.63[a]

3.2.3 Effect on fruit colour

The results of colour measurements on strawberry fruit are presented in Table 4. No significant differences were found in any of the measured parameters.

Table 4. Chroma*, L*, a*, b* values of harvested fruit. ± indicate the standard deviation of the means. Numbers of the same column followed by different letters indicate statistically significant differences.

Cover	L*	a*	b*	Chroma*
UV_o	32.60±1.73[a]	37.24±2.52[a]	19.87±2.45[a]	42.23±3.21[a]
UV_t	32.27±1.76[a]	36.52±2.11[a]	20.21±4.12[a]	41.86±3.34[a]

3.2.4 Effects on secondary metabolites concentration

According to Table 5, the greatest values of all metabolites tested, were found in strawberry fruits harvested from the greenhouse that was covered with the UV_o film. In the UV_t greenhouse strawberries had decreased values in polyphenols by 12% when compared to fruit harvested from the UV_o greenhouse.

Table 5. Physicochemical Analysis of strawberry fruits (Total Polyphenols) in the tested Greenhouses

Secondary metabolites	UV_o	UV_t
Polyphenols calculated as tannic acid equivalent	2500	2190
Polyphenols calculated as gallic acid equivalent	2080	1820
Polyphenols calculated as epicatechine equivalent	1260	1100
Polyphenols calculated as catechine equivalent	1660	1450
Polyphenols calculated as EGCG equivalent	3020	2640

Table 6. Initial measurements of covering material optical properties (transmittance) in spectrum regions, crucial for crop performance.

	UV_o	UV_t
UV (300-400 nm)	24.06	87.42
Blue (400-500 nm)	90.15	89.48
Red (600-700 nm)	89.37	91.09
FR (700-800 nm)	91.67	91.62
NIR (700-1100 nm)	92.16	92.18
PAR (400-700 nm)	90.78	90.33
Total (400-1100 nm)	91.57	91.39

Table 7. Agronomic photochemical factors with direct effects on plant growth (Kittas and Baille, 1998).

Photoreceptor	UV_o	UV_t
Phytochrome $\zeta_0* = \dfrac{\int_{600}^{700}}{\int_{700}^{800}}$	0.975	0.994
Cryptochrome $\dfrac{BLUE}{RED} = \dfrac{\int_{400}^{500}}{\int_{600}^{700}}$	1.009	0.982
$\dfrac{BLUE}{FR} = \dfrac{\int_{400}^{500}}{\int_{700}^{800}}$	0.983	0.977
PAR $\dfrac{PAR}{TOTAL} = \dfrac{\int_{400}^{500}}{\int_{400}^{1100}}$	0.991	0.988
$\dfrac{PAR}{NIR} = \dfrac{\int_{400}^{500}}{\int_{700}^{1100}}$	0.985	0.980

4. Discussion

Greenhouse microclimate was not affected by any of the covers (data not shown), meaning no significant differences in air temperature and relative humidity were observed. Covering material modified only UV light levels in the greenhouses. Other parameters responsible for yield and fruit quality (such as nutrition uptake, spraying, etc.) also did not differ between treatments, therefore any difference in plant performance or fruit quality could be attributed to cover optical properties difference (Katsoulas, et al*.,* 2012; Katsoulas, et al., 2020).

Condensation evaluation was performed partly using one of the three techniques, that reported by Geoola et al. (2004), concerning visual estimation on photos of condensation on the cover. This technique which was followed in the present study was enriched by using Rhinoceros 3D software, aided by Grasshopper visual programming language (for the 1st time in glazing condensation evaluation, to our knowledge). Taking under consideration the precision of the obtained values it can be concluding that this software can be used as a tool for moisture evaluation of condensed water on greenhouse roof because it ends in actual (objective) measurements of related values.

In addition, it was found that on the cover surface with the greater number of condensation droplets (UV_t greenhouse) those droplets were small, which is in agreement with Cemek et al. (2005). The latest authors have used a stereobinoculer microscope to measure the size area of condensation drops.

Finally, when condensation occurs in a cover characterized by permanent AD property and limited transmittance in UV light (the case of the UV_o greenhouse), then the formation of droplets, lacks uniformity. The droplets have large variability in shape and dimensions. Thus, within this research, one can distinguish different kinds of condensation behaviour even between *treated* plastic covers (meaning the special treatment those material have had during manufacturing in order to be enriched by permanent AD property) and not only on *untreated* plastic materials that Elsner et al. (2000) have stated.

As it was mentioned before, the different light conditions inside each tested greenhouse ought to different radiation transmittance properties in many wavebands responsible for crop growth and development it turned out that the tested material is alike, except the one within UV band (Table 6). To verify this conclusion, we proceed in calculations regarding phytochrome, cryptochrome and PAR ratios values which according to Chen et al. (2004) and Kittas and Baille (1998) affect plant growth. The evaluation of these parameters (presented in Table 7) concludes that these values are almost equal among treatments. It seems that a covering material with permanent AD properties had no effect on plants photoreceptors, maybe because it does not attenuate considerably light spectrum that enters the greenhouse. Consequently, we do not expect any differences in crop growth and development, and this is verified in Table 2 where no significant differences were emerged in photosynthetic rate of strawberry plants or on Table 3 where the leaf chlorophyll content indexes values are presented. On the contrary it seems that the different amount of transmitted UV

radiation through the glazing; affect mainly fruit quality rather than quantity. No differences in total yield per plant, mean fruit weight and fruit dry matter partitioning were found, except total number of fruit per plant which was lower in the UV$_t$ greenhouse, where higher UV values were present. This finding is in agreement with other reports' opinion, where higher number of fruit per plant was recorded (Fletcher, et al., 2004; Casal et al., 2009; Behn, et al., 2010; Josuttis, et al., 2010). These authors commented that absence of UV radiation favours this yield characteristic, while the opposite was also declared by others (Ordidge et al., 2012).

Lastly except the above-mentioned effect of UV radiation on yield, UV radiation affects also fruit quality (Tsormpatsidis et al., 2011; Katsoulas et al., 2020). Our results revealed that strawberries in the UV$_o$ greenhouse with lesser UV light perform higher nutrition values, because fruit had 12% more total polyphenol content. Substances such as Epigallocatechin Gallate (EFCG) that was measured and found greater in the UV$_o$ greenhouse is considered among the most effective Cancer Chemopreventive Polyphenol in many fruit (Du et al., 2012).

5. Conclusions

Covering materials with permanent anti-drip properties combined with UV blocking properties seems to increase fruit nutrition values in the case of strawberry plants. All other agronomic values (chlorophyll content, photosynthetic rate, yield characteristics, etc.) remain unaffected when the plant material is strawberry. Also, in the case of the material studied, when condensation occurs, the formation of droplets has no uniformity or regularity.

Acknowledgements

References

Behn, H., S. Tittmann, A. Walter, U. Schurr, G. Noga, A. Ulbrich, 2010. UV-B Transmittance of greenhouse covering materials affects growth and flavonoid content of lettuce seedlings. Europ. J. Hort. Sci. 75, 259–268. ISSN 1611-4426.

Casal, C., C. Vilchez, E. Forjan, B.A. De la Morena, 2009. The absence of UV-radiation delays the strawberry ripening but increases the final productivity, not altering the main fruit nutritional properties. Acta Hort. 842, 159–162. 10.17660/ActaHortic.2009.842.19

Cemek B., Y. Demir, 2005. Testing of the condensation characteristics and light transmissions of different plastic film covering materials, Polymer Test. 24,284–289. https://doi.org/10.1016/j.polymertesting.2004.11.007

Chen, M., J. Chory, F. Fankhauser, 2004. Light signal transduction in higher plants. Annu. Rev. Genet. 38, 87–117. https://doi.org/10.1146/annurev.genet.38.072902.092259

Du G.J., Z. Zhang, X.D. Wen, C. Yu, T. Calway, C.S. Yuan, C.Z. Wang, 2012. Epigallocatechin Gallate (EGCG) is the most effective cancer chemopreventive polyphenol in green tea. Nutrients, Nov. 84 (11), 1679-1691. https://doi.org/10.3390/nu4111679

Von Elsner B., D. Briassoulis, D. Waaijenberg, A. Mistriotis, Chr. Von Zabeltitz, J. Gratraud, G. Russo, R. Suay-Cortes, 2000. Review of structural and functional characteristics of greenhouses in European Union countries, part I: design requirements, Journal of Agricultural Engineering Research 75, 1–16. https://doi.org/10.1006/jaer.1999.0502

Fletcher, J.M., A. Tatsiopoulou, P. Hadley, F.J. Davis, 2004. Growth, yield and development of strawberry cv. 'Elsanta' under novel photoselective film clad greenhouses. Acta Hort. 633, 99–106. 10.17660/ActaHortic.2004.633.11

Geoola, F., U.M. Peiper, 1994. Outdoor Testing of the Condensation Characteristics of Plastic Film Covering Material Using a Model Greenhouse. J. Agric. Engng Res. 57, 167-172. https://doi.org/10.1006/jaer.1994.1016

Geoola, F., Y. Kashti, A. Levi, R. Brickman, 2004. Quality evaluation of anti-drop properties of greenhouse cladding materials, Polym. Testing 23, 755–761. https://doi.org/10.1016/j.polymertesting.2004.04.006

Giacomelli, G. A., W. J. Roberts, 1993. Greenhouse covering systems. Hort. Technology. 3, 50-57. https://doi.org/10.21273/HORTTECH.3.1.50

Gilby, G. W, 1990. Speciality horticultural films, based on polyethylenes, for greater control of the growing environment. XI International Congress on The use of plastics in Agriculturae. New Delhi, India 67-73. ISBN: 9061919983

Jaffrin, A., 1990. Greenhouse light transmission from obstacle analysis and anti-drop film performance. Proceedings of International Seminar and British – Isreal Workshop on Greenhouse Technology, Institute of Agricultural Enginnering, Agricultural Research Organization, Bet Dagan, Israel, 103-118.

Jaffrin, A., S. Makhlouf (1990). Mechanism of light transmissionthrough wet polymer films. Acta Horticulturae 281, 11–24. 10.17660/ActaHortic.1990.281.1

Josuttis, M., H. Dietrich, D. Treutter, F. Will, L. Linnemannstons, E. Kruger, 2010. Solar UVB response of bioactives in strawberry (Fragaria x ananassa Duch. L.): A comparison of protected and open-field cultivation. J. Agric. Food Chem. 58, 12692–12702. https://doi.org/10.1021/jf102937e

Katsoulas N, T. Bartzanas, E. Kitta, 2012. Effects of anti-drip polyethylene covering films on microclimate and crop production. Acta Horticulturae 952, 209–215. 10.17660/ActaHortic.2012.952.25

Katsoulas, N., A. Bari, C. Papaioannou, 2020. Plant responses to UV blocking greenhouse covering materials: a review.

Agronomy 10, 1021. https://doi.org/ 10.3390/agronomy10071021

Kittas, C., A. Baille, 1998. Determination of the spectral properties of several greenhouse cover materials and evaluation of specific parameters related to plant response. J. Agric. Eng. Res. 71 (2), 193–202. https://doi.org/10.1006/jaer.1998.0310

Kittas, C., M., Tchamitchian, N. Katsoulas, P. Karaiskou, Ch. Papaioannou, 2006. Effect of two UV-absorbing greenhouse-covering films on growth and yield of an eggplant soilless crop. Scientia Horticulturae, 2006, 110(1), pp. 30–37. https://doi.org/10.1016/j.scienta.2006.06.018

Ordidge, M., P. Garcia-Macias, N.H. Battey, M.H. Gordon, P. John, J.A. Lovegrove, E. Vysini, A. Wagstaffe, P. Hadley, 2012. Development of color and firmness in strawberry crops is UV light sensitive, but color is not a good predictor of several quality parameters. J. Sci. Food. Agric. 92, 1597–1604. https://doi.org/10.1002/jsfa.4744

Papadakis, G., D. Briassoulis, G. Scarascia Mugnozza, G. Vox, P. Feuilloley, J.A. Stoffers, 2000. Radiometric and thermalproperties of, and testing methods for greenhouse covering materials, and testing methods for greenhouse coveringmaterials. J. Agric. Eng. Res. 77 (1), 7–38. https://doi.org/10.1006/jaer.2000.0525

Papaioannou, C., N. Katsoulas, P. Maletsika, A. Siomos, C. Kittas, 2012. Effects of a UV-absorbing greenhouse covering film on tomato yield and quality. Span. J. Agric. Res. 10, 959–966. http://dx.doi.org/10.5424/sjar/2012104-2899

Schultz, W., K.H. Bartnig, 1996. Evaluation of the non-drip pro-perties of greenhouse cladding films. Plasticulture 111, 23–33, ISSN: 0257-9022

Toneatti, P., 1989. Anti-fog films, facts and fiction. Plasticulture 84(4), 6-12

Tsormpatsidis, E., M. Ordidge, R.G.C. Henbest, A. Wagstaffe, N.H. Battey, P. Hadley, 2011. Harvesting fruit of equivalent chronological age and fruit position shows individual effects of UV radiation on aspects of the strawberry ripening process. Environ. Exp. Bot. 71, 178–185. https://doi.org/10.1016/j.envexpbot.2011.05.017

Novelties in the Revised Eurocode 1991, Part 4: Actions on Silos and Tanks

Francisco Ayuga [a], Eutiquio Gallego [a], José María Fuentes [a]

[a] BIPREE research group, Universidad Politecnica de Madrid, Madrid, Spain

* Corresponding author. Email: francisco.ayuga@upm.es

Abstract

Recently the European Committee for Standardization (CEN) has undertaken the systematic review of the Eurocodes. These standards of European scope are a world reference due to the incorporation of the most advanced knowledge and the participation of experts from all over the world in their preparation and discussion before the final approval. Many of the standards that are currently being revised have an impact on agriculture. One of the most used in this area and from which the final draft has already been prepared is Eurocode 1 part 4 which refers to the actions to be considered in the design of silos and tanks. This paper presents the main changes that have been introduced in the standard, which refer to the load coefficients, combination coefficients, definition of structural typologies for risk consideration, structure of the calculation process in two blocks and the introduction of new cases not considered in the previous version.

The structure of the document includes definitions and symbols used in the standard, actions classification, consequences of the failure and structural complexity. The main body is structured in a Fundamental Silo Load Cases (FSLC) block and a Special Silo Load Cases block (SSLC), which greatly facilitates the calculation in most silos' designs. The FSLC includes the actions in situation of filling and discharging for the different slenderness of silos. SSLCs include eccentric filling loads, large eccentricity filling loads in squat and intermediate circular silos, minor outlet eccentricity loads, unsymmetrical pressures treated by proxy loads (previously patch loads), pipe flow, silos with entrained air, thermal actions, suction and special rectangular silos.

In addition, a hopper calculation section is included, this time also considering special cases, such as the inverted cone, oblique hoppers or pipe flow. A section on material properties and its determination, with some improvements, are included.

Keywords: silo, Eurocodes, hopper, standards

1. Introduction

Eurocodes are a series of 10 European Technical Standards that provide a common approach to the structural design of buildings and other civil engineering works. Eurocodes help make European companies more competitive and increase safety in the construction industry (European Commission, 2021)

The Eurocodes cover:

- Basis of structural design (EN 1990).
- Actions on structures (EN 1991).
- Design of concrete (EN 1992), steel (EN 1993), composite steel and concrete (EN 1994), timber (EN 1995), masonry (EN 1996), and aluminium structures (EN 1999).
- Geotechnical design (EN 1997).
- The design, assessment, and retrofitting of structures for earthquake resistance (EN 1998).

Among them the paper deals on a part of EN 1991. This standard provides the actions to be considered for the structural design of buildings, bridges and other civil engineering works, or parts thereof, including temporary structures, in conjunction with EN 1990 and the other Eurocodes (Joint Research Centre, 2021). It is divided into four parts, the first one devoted to General Actions, the second to Traffic loads on bridges, the third to Actions induced by cranes and machinery and the fourth to Actions on silos and tanks

So, EN 1991-4 gives design guidance for the evaluation of actions for the structural design of silos and tanks, and it is an important standard for the engineering design of many food industries, farm facilities and agricultural infrastructures. In all cases, silos and tanks are common installations.

The standard was first published in 2006 with the complete code EN 1991-4:2006 and it was slightly amended in 2012 (code EN 1991-4:2006_AC:2012). It belongs to the first generation of Eurocodes that were published between 2002 and 2007 after more than two decades of developments and contributions from all over the world.

At this moment, a second generation of the Eurocodes is being developed under Mandate M/515 issued to CEN by the European Commission and the European Free Trade Association. The revision of all Eurocodes is going to be made in four phases starting in different years from 2015 to 2019. Each phase comprises different tasks (Phase 1: 25 Tasks, Phase 2: 22 Tasks, Phase 3 & 4: 26 Tasks). Each Task is the responsibility of a Project Team (PT), under contract, involving more than 300 experts in them. The approval of the drafts produced by the PTs should be made by vote of the National Standardization Bodies, which also participate through the process by commenting on intermediate drafts (CEN/TC 250, 2013). The Project Team working on EN 1991-4 has produced the final draft and it has been circulated to the National Standardization Bodies for final approval. Some changes can still occur, but the main new features of

the standard are known.

In order to keep the Eurocodes internally consistent and given that different Project Teams have been set up for each of the parts, it was necessary to create an Ad Hoc Group (AHG) including representatives from all the Project Teams working on silos and tanks issues in Eurocodes 0,1, 2, 3, 5, 7 and 8. The formal objective was to prepare recommendations on how to enhance the consistency, compatibility and ease of use of provisions specifically related silos and tanks across the Eurocodes. In the case of silos and tanks, some definitions and classifications were different among standards, causing difficulties for designers. Another important issue for this AHG was the coefficients applied to actions and actions combinations in Eurocode 0 as it will be commented on afterwards.

2. Structure of the standard

After introduction words, and some chapters devoted to the scope of the standard and the list of terms and symbols, the new Eurocode 1, part 4 is structured in the following main chapters:

- Classification of silos and tanks.
- Design situations and modelling of actions.
- Properties of particulate solids.
- Symmetrical loads on vertical walls (Fundamental Silo Load Cases).
- Special Silo Load Cases for vertical walls.
- Symmetrical loads on silo hoppers and bottoms (Fundamental Silo Load Cases).
- Special Silo Load Cases for hoppers and silo bases.
- Loads on tanks from liquids.

Besides, there are some annexes:

- Annexes A and B (informative) Actions and combinations of actions on silos and tanks.
- Annexes C, D and E (normative) Values of the properties of particulate solids, measurement of properties and evaluation of properties of solids for certain conditions.
- Annex F (informative) Actions due to dust explosions.
- Annex G (informative) Flow charts to aid in the use of the standard.

The distinction between Fundamental Silo Load Cases (FSLC) and Special Silo Load Cases (SSLC) is a major improvement for the easy-to-use principle. Many silos can be included in the first category (and among them most of the silos designed for agricultural activities or food industries). The rules, equations and conditions, in this case, are simpler, and there is no need to read the rest of the cases. Design flow charts have been included in annex G to help in any case.

Another important issue was the relationship with the Eurocode 0 since this standard in 2006 was a great advance in the design of silos and had a great international recognition (Carson & Craig, 2015), but in its practical application it resulted in excessively robust silos (and therefore costly)

This was mainly due to coefficients in Eurocode 0, which did not consider the particularity of the silos and tanks and in some cases duplicated the safety. Annex 4 in Eurocode 0 will try to solve this problem (Nielsen & Rotter, 2018)

3. Main novelties of the revised standard EN 1991-4

3.1. Material properties and flow

The table of material properties has been improved considering the new experiments and available data. Mechanical properties for additional materials have been incorporated and the procedures for testing materials have been updated.

For the first time, the flow properties of materials have been considered in a standard with different rules accordingly. Four categories of flow from the free flowing (A) to very difficult materials (D) are considered. Definitions and examples can be seen in the annex.

The distinction between mass flow and funnel flow when the silo discharge starts has been updated with new charts according to recent research works. This distinction is important regarding discharge loads.

3.2. Modifying factors and FSLC design

Most of the uncertainties in the actions of the material in the silo are incorporated by means of modifying factors. These include filling and emptying eccentricity (provided it is not too large, because in such case it would be a Special Silo Load Case), slenderness, silo emptying frequency, flow properties of the material (flow group) and variability of material properties in relation to the Action Assessment Class. This is a new approach, better for designers and fitting safety needs.

The basics of silos design present in the Eurocode 1 part 4 published in 2006 are still in force but introducing these factors. Slender and very slender silos are designed by these factors and the classical Janssen equations (Janssen, 1895) (figure 1). Intermediate slenderness and squat silos are designed by these factors and the Rotter/Reimbert equations (Reimbert & Reimbert, 1987; Rotter, 2001).
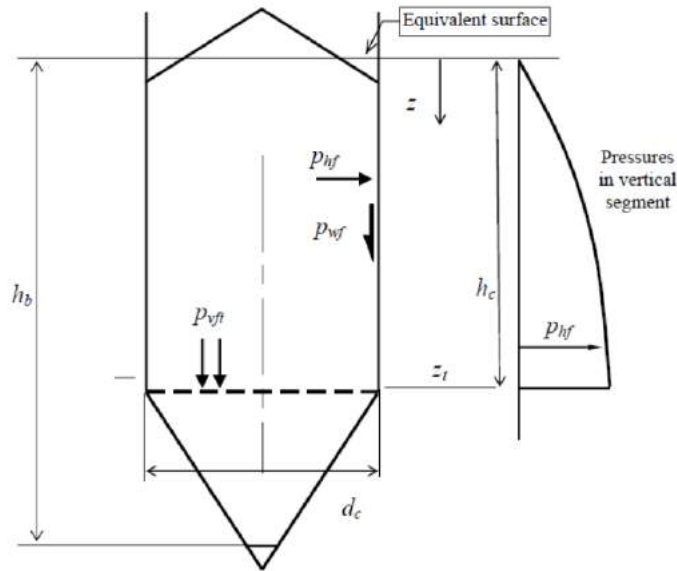

Figure 1. Janssen approach for slender and very slender silos

3.3. Mixed flow

For the first time in a standard, rules are given to design slender silos under mixed flow, which is a very common design situation in FSLC (figure 2). All slender and very slender silos with a flat bottom and many with a hopper discharged with a mixed flow. The upper part of the silo is flowing while the lower remains static. In the transition, a peak pressure can be detected that caused many accidents in the past. This peak pressure is pretty like the one that can be seen in the transition between the vertical wall and the hopper. Most of the silo standards tackle the issue by an overpressure coefficient applied to the whole wall. That means an unnecessary increase of the wall resistance.

In the new Eurocode a free band load of normal pressure is considered just below the effective transition between the static and the flow zone. A simplified approach for the determination of this band load is provided.

The lowest position of the effective transition is determined by a simple equation and any other position above this value should be considered in the design (Sadowski et al, 2020)
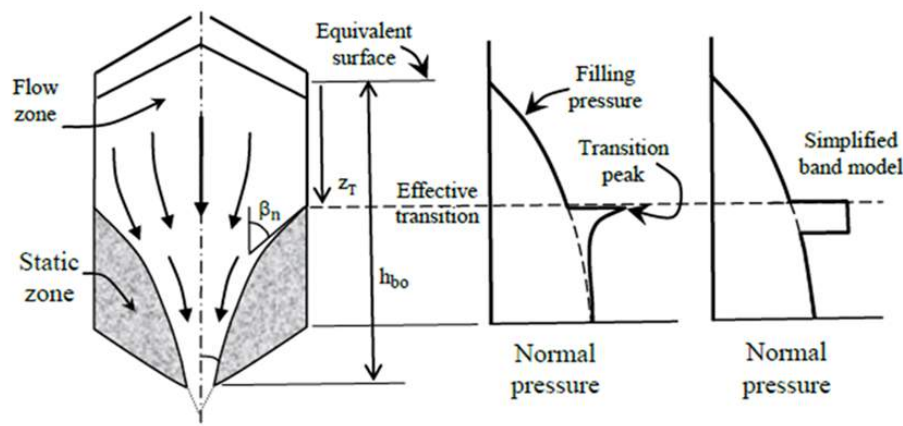

Figure 2. Mixed flow, transition and band model

3.4. Special Silo Load Cases

Several Special Silo Load Cases are considered in the standard:

- Large eccentricity filling loads in squat and intermediate slenderness silos. It remains almost the same than in the older version, but as an SSLC.

- Unsymmetrical pressures treated by proxy loads (patch loads in the previous standard). It is an improvement in the new version because it is only mandatory to check the silos against this SSLC when necessary, while in the previous version, most of the silos needed to be checked against this procedure. Equations have also been simplified in the new Eurocode. (Gallego et al., 2011)

- Pipe flow in all silos with large flow channel eccentricities. This section remains like in the previous version, although some adjustments have been made to consider the recent research on the topic (Sadowski & Rotter, 2012).
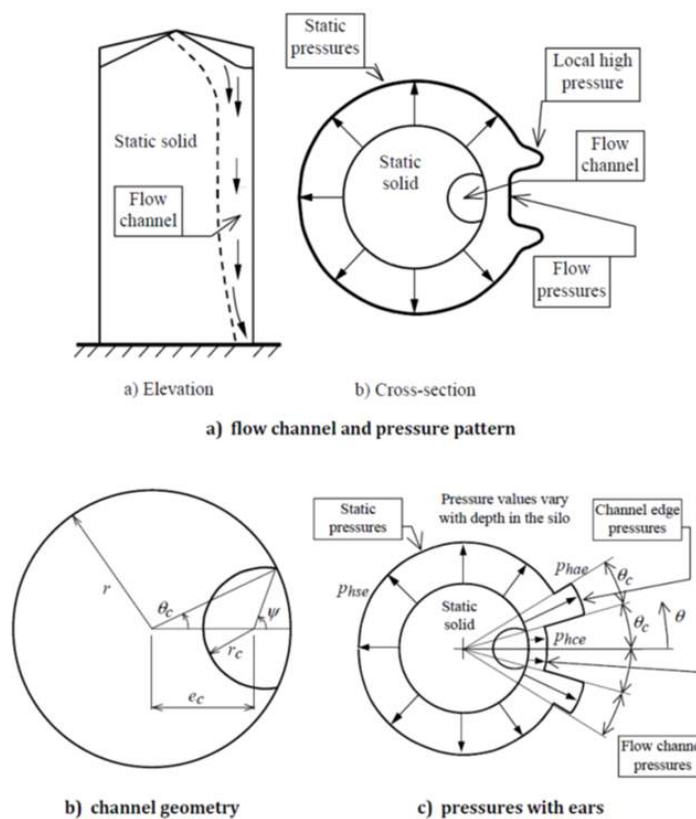
Figure 3. Pipe flow with large flow channel eccentricities

- Silos containing solids with entrained air. No differences.

- Thermal differences between stored solids and the silo structure. This action has been adjusted considering the research made in recent years. New particulate solid parameters have been included and considered in the corresponding section (Lapko, 2005; Moran et al. 2005).

- Suction due to inadequate venting. It was included for tanks and now also for silos.

- Loads on the vertical walls of special rectangular silos. Actions on rectangular silos with rigid walls are the same as other silos with different planforms, but if the walls can bend, then redistribution of pressures can be observed. It is a new section in the standard that helps designers of this kind of silos (Rotter, Goodey, Brown, 2019). The use of internal ties has also been considered in this section.

$$p_{hf}\left(\frac{\alpha}{\tanh\alpha}\right) \qquad p_{hf}\left(\frac{\alpha}{\sinh\alpha}\right)$$
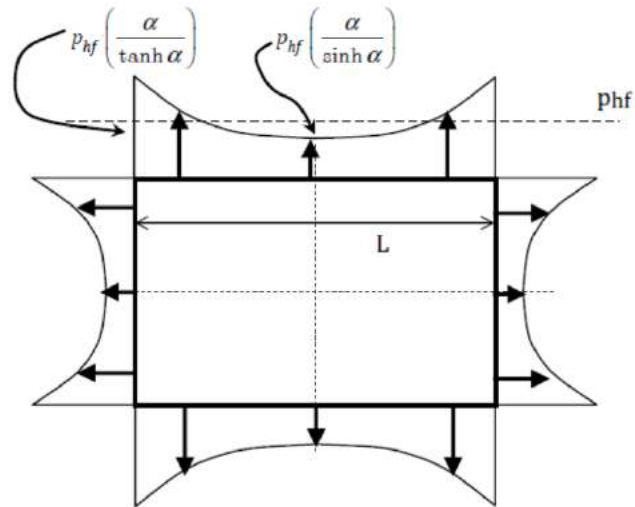
Figure 4. Rectangular silos with flexible walls

Most of the cases were included in the previous standard, but they have been updated and simplified at the present version of the standard. Main novelties come from thermal actions and special (flexible walls) rectangular silos and rectangular silos with internal ties

3.5. Hoppers

Hopper design remains the same in FSLC, but the new standard includes several SSLC.

A section on circular silos with internal inverted cone has been included, which is very common in large concrete silos. Silos for storing cement and other mineral solids, or sugar in the case of agricultural products use this procedure to facilitate the discharge process. Actions on the cone and the adjacent walls need special considerations (Wójcik et al., 2012).

There is also a section on oblique conical hoppers, particularly important in agricultural processing silos and farm silos. Sometimes this shape helps the designers to fit the silos into the production chain. The consequences to the actions on the hopper have been recently studied and can be now incorporated into the standard (Vidal et al. 2006; Ramírez et al., 2010).

Figure 5. Oblique hoppers

Discharge loads for eccentric pipe flow in steep concentric or oblique hoppers complete the equivalent design rules for vertical walls and the same with the section on hoppers in silos containing solids with entrained air.

4. Conclusions

A new Eurocode 1 part 4: Actions on silos and tanks is developing. It will be in force in the coming year
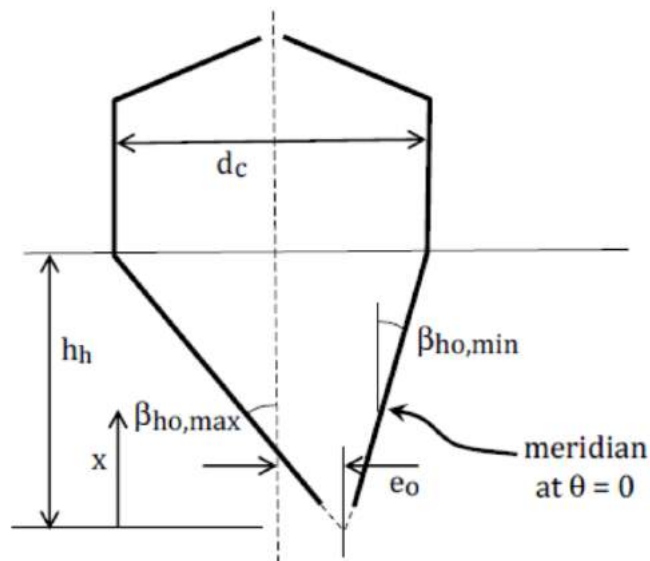
Several changes are expected regarding the previous version to include more design situations and considering the easy-to-use principle

A new Annex 4 in Eurocode 0 will be devoted to silos and tanks. Silos designed accordingly with Eurocode 1 are considered safer and more precisely engineered. With this new annex, they will also be economically competitive with silos designed with other standards

Acknowledgements

Authors acknowledge the access to the drafts of the new standard circulated among experts by the Spanish Standardization Association (AENOR-UNE)

References

Carson, J., Craig, D. 2015. Silo design codes: Their limits and inconsistencies. Procedia engineering, 102, 647-656.

CEN/TC 250 (2013). http://www.psc.ro/wp-content/uploads/2013/07/M515_TC-250-answerAnnexes.pdf . Accessed July 1, 2021

European Commission. 2021. https://ec.europa.eu/growth/sectors/construction/eurocodes_es. Accessed July 1, 2021

Gallego, E., González-Montellano, C., Ramírez, A., Ayuga, F. 2011. A simplified analytical procedure for assessing the worst patch load location on circular steel silos with corrugated walls. Engineering Structures, 33(6), 1940-1954.

Janssen, H. A. 1895. Versuche uber getreidedruck in silozellen. Z. Ver. Dtsch. Ing., 39 (35), 1045-1049.

Joint Research Centre. 2021. https://eurocodes.jrc.ec.europa.eu/showpage.php?id=131. Accessed July 1, 2021

Lapko, A. 2005. Thermal fields in grain during storage-their sources and effects on silo structure reliability. International Agrophysics, 19 (2), 141-146.

Morán, J. M., Juan, A., Ayuga, F., Robles, R., Aguado, P. 2005. Analysis of thermal load calculations in steel silos: A comparison of Eurocode 1, classical methods, and finite element methods. Transactions of the ASAE, 48(4), 1483-1490.

Nielsen, J., Rotter, J. M. 2018. On the definition of design values for loads on silos and tanks. Advances in structural engineering, 21(16), 2499-2506.

Ramírez, A., Nielsen, J., Ayuga, F. 2010. Pressure measurements in steel silos with eccentric hoppers. Powder Technology, 201(1), 7-20.

Reimbert, M. L., Reimbert, A. M. 1987. Silos. Theory and practice. Vertical silos, horizontal silos (retaining walls). Lavoisier Publishing.

Rotter, J. M., Goodey, R. J., Brown, C. J. 2019. Towards design rules for rectangular silo filling pressures. Engineering Structures, 198, 109547.

Rotter, J. M. 2001. Guide for the economic design of circular metal silos. CRC press.

Sadowski, A. J., Rotter, J. M. 2012. Structural behavior of thin-walled metal silos subject to different flow channel sizes under eccentric discharge pressures. Journal of Structural Engineering, 138(7), 922-931.

Sadowski, A. J., Rotter, J. M., Nielsen, J. 2020. A theory for pressures in cylindrical silos under concentric mixed flow. Chemical Engineering Science, 223, 115748.

Vidal, P., Couto, A., Ayuga, F., Guaita, M. 2006. Influence of hopper eccentricity on discharge of cylindrical mass flow silos with rigid walls. Journal of Engineering Mechanics, 132(9), 1026-1033.

Wójcik, M., Tejchman, J., Enstad, G. G. 2012. Confined granular flow in silos with inserts—Full-scale experiments. Powder Technology, 222, 15-36.

Effect of Photoconversion Greenhouse Films Used as 'Double Covers' on Tomato Crop in Almeria (Spain)

Molina-Aiz F.D.[a] [*], Moreno-Teruel M.A. [b], Lemarié S.[b], Valera D.L.[a], Proost Kristof [b], Peilleron F. [b], López-Martínez A.[a]

[a] CIAMBITAL (Centro de Investigación en Agrosistemas Intensivos Mediterráneos y Biotecnología Agroalimentaria),
University of Almería, Ctra. Sacramento s/n, 04120 Almería, Spain.

[b] CASCADE SAS, Centre d'Affaires Emergence, 24 rue du Gouverneur Général Eboué, 92130 Issy les Moulineaux, France.

* Corresponding author. Email: fmolina@ual.es

Abstract

Improving the sunlight spectrum can lead to increased crop yields and quality. The French company CASCADE developed a technology named 'LIGHT CASCADES®' (LC®) that modifies and adapts the sunlight spectrum closer to plant needs. The purpose of this study was to analyse the effect of a new LC® photoconversion film installed as 'double covers' above a tomato crop inside a greenhouse. In the trial, the effects of a photoconversion films were tested on the 'Elcabo' tomato [*Lycopersicon esculentum* (L.) Mill.] variety in Almeria (Spain) in comparison to tomatoes grown under an equivalent colourless control film. The trial was carried out in a winter/spring crop cycle (from February to June 2019) under a multi-span greenhouse divided transversely by a polyethylene sheet. The experimental photoconversion LC® film was installed in the eastern section of the greenhouse and the colourless control film was located at the west side. Morphological plant traits, photosynthetic activity, marketable yield and quality of the fruits production were measured under each films. Results showed that under the photoconversion LC® film, marketable yield gains reached up to +10.8% compared to tomatoes grown under colourless reference film. Average photosynthetically active radiation inside the greenhouse with the LC® film was statistically higher (201 µmol m^{-2} s^{-1}) compared to the control double cover film (184 µmol m^{-2} s^{-1}). Net photosynthetic rate measured at tomato leaves was also greater under the LC® film (8.1 µmol m^{-2} s^{-1}) than under the control film (7.8 µmol m^{-2} s^{-1}). Fruit's weight and sugar content measured on tomato grown under the LC® film tended to be improved. These results on tomato crop confirmed the positive effects of LC® technology photoconversion films observed on other crops such as pepper and berries in Spain.

Keywords: protected crops, optically active dyes, photoconversion film, tomato fruits quality, marketable yield.

1. Introduction

Water-impermeable plastic films are installed as double roof inside unheated greenhouses in the Mediterranean area in autumn-winter cycles to reduce fungal infections (Hernández *et al*., 2017). In 9.7% of greenhouses of Almería (Spain) double roof are used (Valera *et al*., 2016), mainly with crops sensitive to fungal diseases as cucumber. These double roofs can also be used as energy saving technique in heated greenhouse. The fall of condensation onto the crop favoured the proliferation of fungal diseases (Baptista *et al*., 2012), which might reduce crop yield and quality. Double-roof inside greenhouses can reduce fungal infections and increase inside temperature approximately 1ºC (Vargues *et al*., 1994). However, double roof can reduce ventilation airflow and light transmission. Reduction of light transmission can affect the crop production in a negative way (Cockshull *et al*., 1992).

Crop development is dependent on the light spectrum because distinct wavelengths of light are different photosynthetic efficiency (Novoplansky *et al*., 1990). The effective wavelength range of light for photosynthesis is 400-700 nm (photosynthetically active radiation, PAR), with photosynthetic sensitivity in the blue (400-500 nm) and red (600-700 nm) regions (Edser, 2002; Nishimura *et al*., 2012). Blue light (containing a high red/far-red ratio) can reduce the dry weight and plant height in tomato crop (Mortensen and Strømme, 1987). On the other hand, yellow-green light (510–580 nm) is almost completely reflected by plants leaves, and ultraviolet (280–380 nm) light can increase plant diseases and insect pests (Qi *et al*., 2016).

New greenhouse plastic covers have been developed incorporating fluorescent dyes into plastic films (Novoplansky *et al*., 1990; Hammam et al., 2007). Spectrum conversion films can modify the incident solar spectrum to wavelengths that are more suitable for photosynthesis (Yoon *et al*., 2020). Spectral modifications can affect the quality and quantity of solar radiation by using "photoselective" materials as greenhouse cladding (El-Bashir *et al*., 2019).

In materials doped with luminescent components (luminophores) sunlight enters through the top surface, is then absorbed by the luminophores and finally isotropically re-emitted at a longer wavelength and different direction (El-Bashir *et al*., 2019).

Plastic material can be doped with different dye concentrations to absorb radiation in the range that is not used by chlorophylls and re-emit as red or blue light for improve photosynthesis (El-Bashir *et al*., 2019). The red film can

convert the blue–green light (450–550 nm) into the red light (600–700 nm), and the blue film can convert the ultraviolet (UV)–violet light (350–450 nm) into blue–green light (Hidaka *et al.*, 2008).

The French company CASCADE has developed the LIGHT CASCADE® technology (LC®) that are dispersed into plastic greenhouse films. These LC® additives enable the absorption of the UV and green wavelengths of the solar spectrum and reemit them into blue and red wavelengths respectively (Lemarié *et al*. 2018). More than 100 trials with LC® films have been tested since 2013 on several crops such as melon and potato (Lemarié *et al*. 2018) but as well on red fruits and vegetables.

The project "*Improving profitability in greenhouses by increasing photosynthetic activity with passive climate control techniques* (GREENPHOC)" is being developed from 2020 to 2024 with the goal of increasing photosynthetically active radiation within the greenhouses of Almeria. The aim of this study was to analyse the effect of a new blue photoconversion film LC® installed as 'double covers' above a tomato crop [*Lycopersicon esculentum* (L.) Mill.] inside a greenhouse. The effect on the microclimate inside the greenhouse, the photosynthetic activity, the growth and production of the crop on a spring-summer cycle were analyzed.

2. Materials and Methods

2.1. Experimental greenhouse and plant materials

The experiment was carried out in a multispan greenhouse located in the Experimental Station "*Catedrático Eduardo Fernández*" of the Center for Innovation and Technology Transfer "Fundación UAL-ANECOOP" (Latitude: 36° 51' 53.2" N; Longitude: 2° 16' 58.8" W; Altitude: 87 m). The greenhouse, whose main axis is parallel to the northeast-southwest direction (118° in relation to the north direction), has a soil surface of 1080 m^2 (Fig. 1).
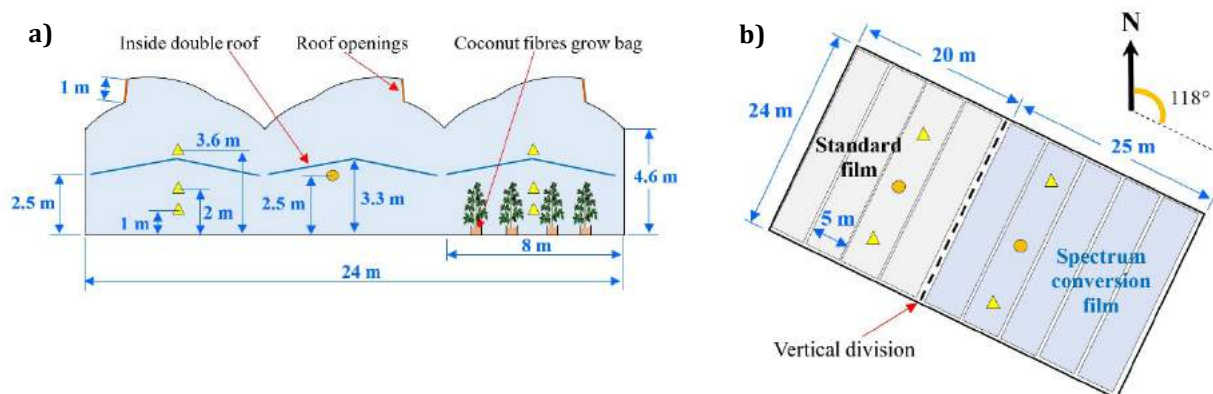

Figure 1. Vertical section (a) and horizontal view of the division (b) of the experimental greenhouse. Temperature and humidity sensor (▨) and PAR radiation sensor (▨).

The experimental greenhouse was divided in two similar sectors with a vertical polyethylene sheet (Fig. 1b). The experimental photoconversion LC® film was installed in the eastern sector of the greenhouse and the standard colourless control film was located at the west sector (Table 1).

Table 1. Dimensions, soil surface S_c and surface of the vent openings S_V of the two sectors of the experimental greenhouse.

Sector	Double roof film	Dimensions	S_c [m^2]	S_V [m^2]	S_V/S_c [%]
East	Spectrum photoconversion LC®	24 m × 25 m	600	67.5	11.3
West	Standard	24 m × 20 m	480	52.5	10.9

The greenhouse has roof vent openings on the ridges of the three spans (Fig. 1a) protected with insect-proof screens of 10 × 20 cm^{-2} threads. Ventilation is controlled by a Synopta software (HortiMax B.V., Maasdijk, The Netherlands) and a centralized climate control and data logging system (HortiMax B.V., Maasdijk, The Netherlands) with a weather station.

On February 11, 2019 a tomato field (*Solanum lycopersicum* L.) of the variety 'El Cabo' (Zeta Seeds, S.L., Alfafar, Spain) was transplanted into the greenhouse. The transplant was carried out on coconut fibre substrate, with a density of 1 plants per m². The plant lines were perpendicular to the ridges of the greenhouse (Fig. 2).

2.2. Microclimate and photosynthesis measurement equipment

To analyse the effect of double roof in the inside microclimate, 12 autonomous HOBO® Pro Temp-HR U23-001 (Onset Computer Corp., Pocasset, USA) dataloggers with temperature (accuracy of ±0.18 °C for a measurement range of –4 to 70 °C) and humidity (accuracy of ±2.5% for the range 0-100%) sensors were located in the mean vertical profiles of both sectors. In the central spans of both sectors, SKP215 quantum sensors (Campbell Scientific Spain, Barcelona, Spain) were also installed for measurement of the PAR radiation in the range of 400-700 nm with accuracy of ±5%. These sensors were connected to two autonomous CR3000 Micrologger (Campbell Scientific Spain, Barcelona, Spain). The outside climatic parameters were measured by a meteorological station located 29 m at the north of the experimental greenhouse.
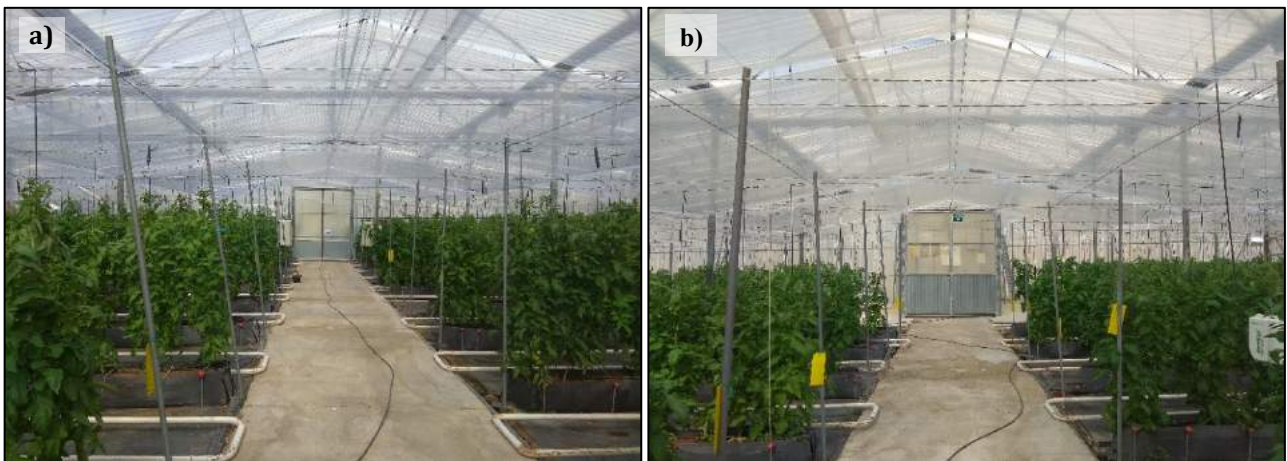

Figure 2. Tomato crop inside the sector East with the double roof with the spectrum photoconversion film LC® (a) and the sector West with the standard transparent film (b) the 16th of April 2019.

To compare the effect of plastic films used as double roofs in the greenhouse on the reduction of PAR and on the photosynthesis of tomato plants, measurements were made with an LCI SD photosynthesis analyser (ADC BioScientific Limited, Hertfordshire, United Kingdom). It is a portable console with a leaf chamber, equipped with CO_2 and H_2O concentration sensors IRGA (infrared gas analysis). The measurement ranges are of 0-2000 ppm for the CO_2 (accuracy ±1 ppm), 0-75 mbar for H_2O (precision ±0.1 mbar) and 0-3000 μmol m^{-2} s^{-1} for PAR radiation.

2.3. Morphological measurements

To evaluate the development of tomato crop, three lines of plants in each sector with 4 plants per line were randomly chosen. Every two weeks, the morphological parameters were measured using a tape measure and a 150 mm digital calliper (Medid Precision, S.A., Spain). Distance from the apical meristem of the plant to the last node (N_T) was measured considering the last node under the last leaf at physiological maturity. Total length of the stem ($L_P=N_T+S_{NA}$) was calculated from N_T and the distance from the last node to the ground (S_{NA}). The number of nodes (N_N) and the length of the two internodes below the last leaf at physiological maturity (L_I) was also measured. Finally, the stem diameter (D_S) and the length of last mature leaf (L_L) were measured.

2.4. Tomato yield and quality

Marketable and non-marketable yield of three lines of plants in each sector (considered statistical replications) was weighed weekly with a Mettler Toledo electronic balance (Mettler-Toledo, S.A.E., Spain) with a sensitivity of 20 g and a maximum capacity of 60 kg. In order to evaluate the quality of the production, three lines of tomato plants were chosen randomly in each sector, selecting 20 fruits for quality analysis. Quality parameters were measured at each harvest using a Pb3002-L DeltaRange electronic scale (Mettler Toledo, S.A., Spain), with a sensitivity of 0.01 g for fruit weight and a 150 mm digital calliper (Medid Precision, S.A., Spain) for fruit diameter. The sucrose fraction (ºBrix) was measured with a PAL-1 refractometer (Atago Co., LTD., Japan) with an accuracy of ±0.2% and pH was measured with a portable multimeter MM 40 (Crison Instruments S.A., Spain) with an accuracy of 0.01. Fresh fruit firmness was measured with a PCE-FM 200 digital penetrometer (PCE-Ibérica S.L., Spain), with an accuracy of ±0.5%.

2.5. Statistical analysis

Statistical analysis of the data was performed with the software Statgraphics Centurion XVIII (STATGRAPHICS, 2021) comparing multiple samples with an analysis of variance (ANOVA) at the 5% significance level (*P*-value < 0.05). The Fisher's LSD (Least Significant Difference) intervals was used to determine if the means were significantly

different. Levene test was used to variance check and when there were statistical differences between the standard deviations of the samples a non-parametric analysis was performed with the Friedman test and using the box-and-whisker plot (STATGRAPHICS, 2021).

3. Results and Discussion

3.1. Photosynthetically active radiation

Mean and daily maximum PAR radiations were statistically greater (9.2% and 7.4%, respectivelly) in the sector with the spectrum conversion film LC[®] as double roof than in the control sector with the transparent film (Table 2).

Table 2. Mean R_{PAR} and average daily maximum R_{PARmax} PAR radiation inside the two greenhouse sectors (mean ± standard deviation).

Inside double roof	R_{PAR}	R_{PARmax}
Spectrum photoconversion film LC[®]	201 [b] ± 280	960 [b] ± 229
Standard film	184 [a] ± 256	894 [a] ± 213

[a] Means with different superscript letters in the same column are significantly different with a confidence level of 95.0% (LSD Test, *P*-value<0.05).

PAR radiation was higher in the compartment with the double roof with the spectrum conversion film LC[®] along all the measurement period (Fig. 3).

a)

b)
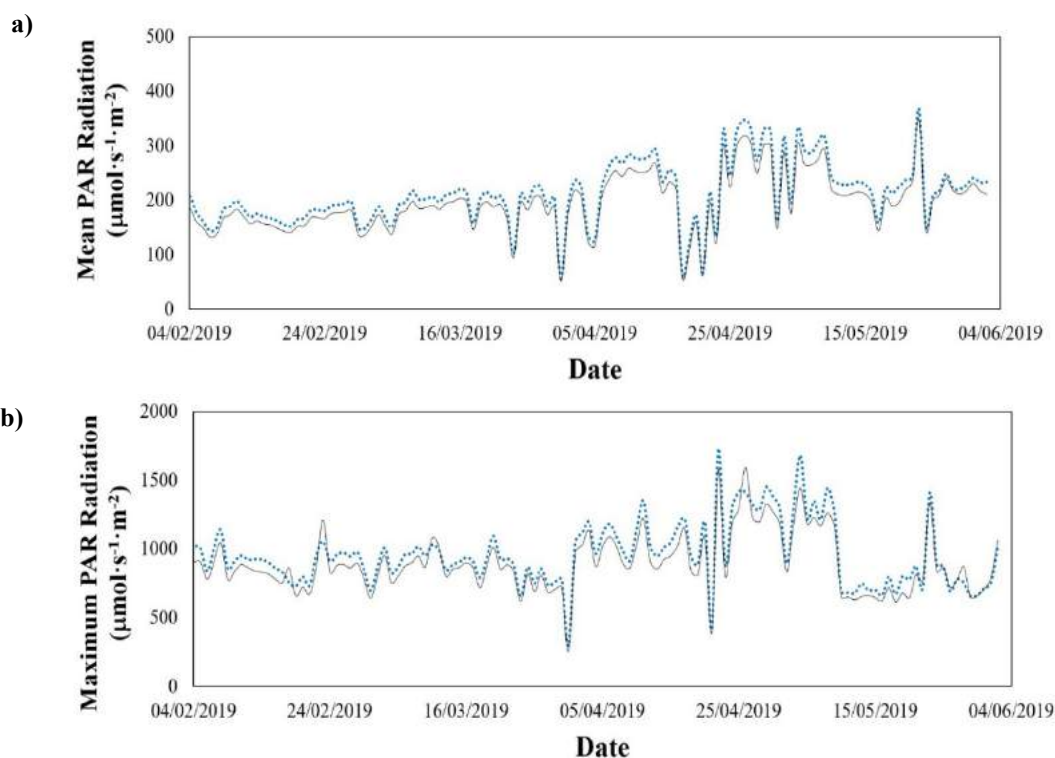
Figure 3. Evolution of the mean (a) and the maximum (b) PAR radiation measured under the double roof with the transparent film (---) and with the blue spectrum photoconversion film LC[®] (---).

3.2. Air temperature

The use of the spectrum conversion film LC[®] increased the average temperature at 1 meter and 2 meter in height, whereas no statistically significant differences was observed in the temperatures over the double roof at 3.6 m (Table 3).

Table 3. Average mean, maximum and minimum indoor temperatures in the greenhouse sectors. Air temperatures over the double roof at 3.6 m height $T_{3.6\ m}$, and under the double roof at 2 and 1 m in height $T_{2\ m}$ and $T_{1\ m}$.

Parameter	Mean temperature		Maximum temperature		Minimum temperature	
Film	LC®	Standard	LC®	Standard	LC®	Standard
$T_{3.6\ m}$ (°C)	21.0 [a] ± 7.3	21.1 [a] ± 7.3	32.9 [a] ± 5.6	32.9 [a] ± 4.7	12.2 [a] ± 4.5	12.1 [a] ± 4.5
$T_{2\ m}$ (°C)	20.9 [b] ± 6.4	20.2 [a] ± 6.4	31.5 [a] ± 4.0	30.9 [a] ± 4.2	12.7 [a] ± 4.6	11.0 [a] ± 5.3
$T_{1\ m}$ (°C)	20.6 [b] ± 5.7	20.1 [a] ± 5.5	29.5 [a] ± 3.8	28.9 [a] ± 3.8	13.1 [a] ± 4.7	12.8 [a] ± 4.6

[a] Means with different superscript letters in the two columns of the same parameter are significantly different with a confidence level of 95.0% (LSD Test, *P*-value<0.05).

3.3. Air relative humidity

The use of the spectrum conversion film LC® increases the relative humidity at the three heights analysed (Table 4), mainly due to an increase of crop transpiration.

Table 4. Average mean, maximum and minimum indoor relative humidity in the greenhouse sectors. Air humidity over the double roof at 3.6 m height $RH_{3.6\ m}$, and under the double roof at 2 and 1 m in height $RH_{2\ m}$ and $RH_{1\ m}$.

Parameter	Mean relative humidity		Maximum relative humidity		Minimum relative humidity	
Film	LC®	Standard	LC®	Standard	LC®	Standard
$RH_{3.6\ m}$ (%)	69.4 [b] ± 17.4	68.2 [a] ± 16.2	89.4 [b] ± 4.2	86.8 [a] ± 4.5	37.6 [a] ± 14.8	39.8 [a] ± 14.7
$RH_{2\ m}$ (%)	73.3 [b] ± 13.1	72.9 [a] ± 13.8	88.5 [a] ± 3.5	87.9 [a] ± 4.2	46.2 [a] ± 16.8	41.1 [a] ± 19.9
$RH_{1\ m}$ (%)	74.1 [b] ± 11.9	71.5 [a] ± 13.1	88.8 [a] ± 4.2	87.6 [a] ± 5.0	43.2 [a] ± 21.9	45.7 [a] ± 16.7

[a] Means with different superscript letters in the two columns of the same parameter are significantly different with a confidence level of 95.0% (LSD Test, *P*-value<0.05).

3.4. Plant's photosynthesis

The use of the spectrum conversion film LC® seems to increase photosynthesis by 3.8% but no statistical significance could be obtained (Table 5). These results may be linked to the increase of PAR radiation underneath the LC® film.

Table 5. Mean values of parameters measured on the leaves of plants growing in the two greenhouse sectors with the two double roof films. Photosynthetic activity P_A [µmol CO_2 m^{-2} s^{-1}], radiation Q_{PAR} [µmol m^{-2} s^{-1}], leaf temperatures T_L [°C], concentration of CO_2 C_O [ppm], transpiration E_L [mmol m^{-2} s^{-1}] and stomatal conductivity C_E [mol m^{-2} s^{-1}].

Inside double roof	P_A	Q_{PAR}	T_L	C_O	E_L	C_E
Spectrum conversion film LC®	8.1 [a]	320 [a]	29.2 [a]	403.0 [a]	2.36 [a]	0.18 [a]
Standard film	7.8 [a]	316 [a]	28.7 [a]	412.6 [a]	2.34 [a]	0.19 [a]

[a] Means with different superscript letters in the same column are significantly different with a confidence level of 95.0% (LSD Test, *P*-value<0.05).

3.5. Plant's morphology

All the analysed morphological parameters were similar in both sectors, without statistical effect produced by the use of the spectrum conversion film LC® (Table 6).

Table 6. Average values of the morphological parameters measured in plants grown in the sectors with different cover plastics. Total length of the stem L_P [cm], length of internodes L_I [cm], diameter of the stem D_S [mm], number of nodes N_N and length of last mature leaf L_L [cm].

Inside double roof	L_P	L_I	D_S	N_N	L_L
Spectrum photoconversion film LC®	120.7 [a]	5.4 [a]	8.5 [a]	13.2 [a]	25.9 [a]
Standard film	123.7 [a]	5.4 [a]	8.6 [a]	13.0 [a]	24.8 [a]

[a] Means with different superscript letters in the same column are significantly different with a confidence level of 95.0% (LSD Test, *P*-value<0.05).

3.6. Tomato production

Although no statistical significance could be obtained, there is a tendency toward an increase in marketable and total cumulative yields of the tomato crop production. A value of 0.5 kg/m^2 (+10.8%) and 0.8 kg/m^2 (+14.0%), respectively, in the eastern sectors could be obtained with the spectrum conversion film LC® as inside double roof (Figure 4).
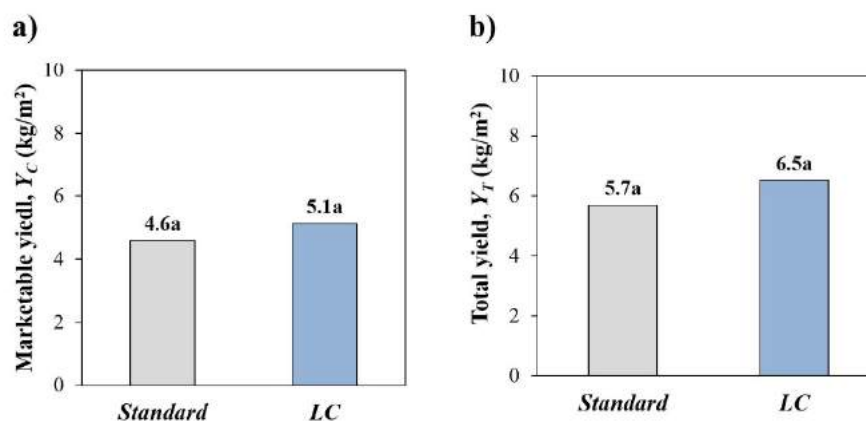

Figure 4. Total (a) and marketable (b) tomato yield of the greenhouse sectors equipped with the double roof whit the standard colourless film (☐) and the spectrum photoconversion film LC® (▨).

It is interesting to note that higher marketable and total tomato yields were obtained in the sector with the experimental LC® film from the starting of the production (Fig. 5).
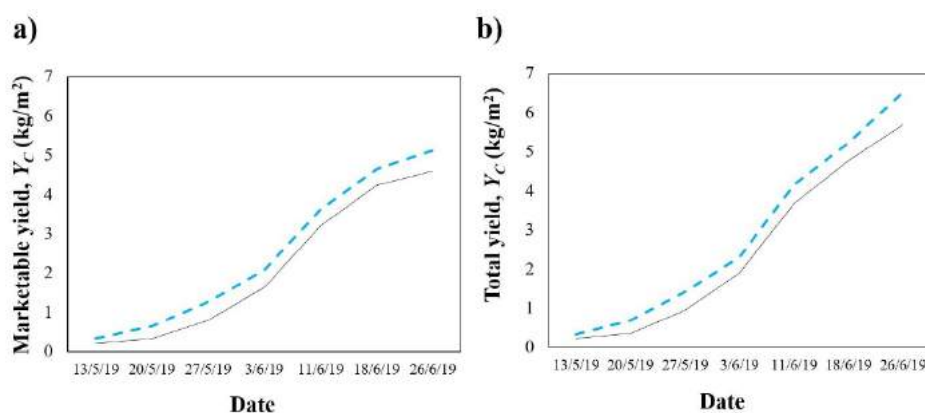
Figure 5. Evolution of the total tomato yield of the greenhouse sectors equipped with the double roof whit the standard colourless film (—) and the spectrum photoconversion film LC® (- - -).

3.7. Fruit quality

No statistical differences were observed for the parameters of quality of fruits growing under the double roofs with the spectrum conversion film LC® or the transparent film (Table 7).

Table 7. Average values of the production quality parameters, measured for plants grown in areas with different cover plastics. Weight W_F [g], equatorial diameter D_F [mm], firmness F_F [kg mm^{-1}], soluble solids content T_{SS} [°Brix], and acidity of fruits *pH.*

Inside double roof	W_F	D_F	F_F	T_{SS}	pH
Spectrum photoconversion film LC®	271.0 [a]	84.9 [ab]	1.43 [a]	4.53 [a]	3.81 [a]
Standard film	268.4 [a]	85.3 [b]	1.71 [a]	4.48 [a]	3.93 [a]

[a] Means with different superscript letters in the same column are significantly different with a confidence level of 95.0% (LSD Test, *P*-value<0.05).

4. Conclusions

From the results presented in this work, we can draw the following conclusions:

- The experimental spectrum conversion film LC® used as double roof inside a multispan greenhouse increased significatively the mean and maximum daily PAR radiation in 9.2% and 7.4%, respectively, in comparation with a commercial transparent film.
- The use of the LC® film increased the mean temperature with approximately 0.6 °C at 1 meter and 2 meter height under the double roof, while similar temperatures were observed using the standard film above the double roof.
- The mean relative humidity was increased with the use of the spectrum conversion film LC® above and below the double roof.
- The use of the LC® film increased the photosynthetic activity by 3.8% which could be explained as a consequence of the increase of PAR radiation; no statistical significance could be proven, however.
- No statistical differences were observed for none of the parameters associated with plant morphology and fruit quality.
- The spectrum conversion film LC® produced an increase in marketable and total tomato yield of 0.5 kg/m^2 (+10.8%) and 0.8 kg/m^2 (+14.0%), respectively.

We can conclude that the use of spectrum conversion film LC®, used as double cover inside greenhouses, can improve tomato production as a response to an increased photosynthetic active radiation in comparison to standard films.

References

Baptista, F.J., Bailey, B.J., Meneses, J.F., 2012. Effect of nocturnal ventilation on the occurrence of Botrytis cinerea in Mediterranean unheated tomato greenhouses. Crop Protection, 32, 144-149. https://doi.org/10.1016/j.cropro.2011.11.005.

Cockshull, K.E., Graves, C.J., Cave, C.R.J., 1992. The influence of shading on yield of glasshouse tomatoes. Journal of Horticultural Science, 67 (1), 11-24. https://doi.org/10.1080/00221589.1992.11516215.

Edser, C., 2002. Light manipulating additives extend opportunities for agricultural plastic films. Plastics, Additives and Compounding, 4 (3), 20-24. https://doi.org/10.1016/S1464-391X(02)80079-4.

El-Bashir, S.M., AlSalhi, M.S., Al-Faifi, F., Alenazi, W.K., 2019. Spectral properties of PMMA films doped by perylene dyestuffs for photoselective greenhouse cladding applications. Polymers (Basel), 11 (3), 494. https://doi.org/10.3390/polym11030494.

Hammam, M., El-Mansy, M.K., El-Bashir, S.M., El-Shaarawy, M.G., 2007. Performance evaluation of thin-film solar concentrators for greenhouse applications. Desalination, 209 (1–3), 244-250. https://doi.org/10.1016/j.desal.2007.04.034.

Hernández, J., Bonachela, S., Granados, M.R., López, J.C., Magán, J.J., and Montero, J.I., 2017. Microclimate and agronomical effects of internal impermeable screens in an unheated Mediterranean greenhouse. Biosystems Engineering, 163, 66–77. https://doi.org/10.1016/j.biosystemseng.2017.08.012.

Hidaka, K., Yoshida, K., Shimasaki, K., Murakami, K., Yasutake, D., Kitano, M., 2008. Spectrum conversion film for regulation of plant growth. Journal of the Faculty of Agriculture, Kyushu University, 53 (2), 549-552. https://doi.org/10.5109/12872

Lemarié, S., Guérin, V., Jouault, A., Proost, K., Cordier, S., Guignard, G., Demotes-Mainard, S., Bertheloot, J., Sakr, S., Peilleron, F., 2020. Melon and potato crops productivity under a new generation of optically active greenhouse films. Acta Hortic. 1296, 517-526. https://doi.org/10.17660/ActaHortic.2020.1296.67

Mortensen, L.M., Strømme, E., 1987. Effects of light quality on some greenhouse crops. Scientia Horticulturae, 33 (1–2), 27-36. https://doi.org/10.1016/0304-4238(87)90029-X.

Nishimura, Y., Wada, E., Fukumoto, Y., Aruga, H., and Shimoi, Y. (2012). The effect of spectrum conversion covering film on cucumber in soilless culture. Acta Horticulturae *956*, 481–487. https://doi.org/10.17660/ActaHortic.2012.956.56

Novoplansky, A., Sachs, T., Cohen, D., Bar, R., Bodenheimer, J., Reisfeld, R., 1990. Increasing plant productivity

by changing the solar spectrum. Solar Energy Materials, 21 (1), 17-23. https://doi.org/10.1016/0165-1633(90)90039-4.

Qi, Y., Wang, Y., Yu, Y., Liu, Z., Zhang, Y., Qi, Y., Zhou, C., 2016. Exploring highly efficient light conversion agents for agricultural film based on aggregation induced emission effects. Journal of Materials Chemistry C, 4, 11291–11297. https://doi.org/10.1039/C6TC04215E.

STATGRAPHICS, 2021. Statgraphics Statgraphics®Centurion 18. User Manual. Statgraphics Technologies. https://cdn2.hubspot.net/hubfs/402067/PDFs/user-manual.pdf.

Valera, D.L., L.J., Belmonte, F.D., Molina-Aiz, A., López, 2016. Greenhouse agriculture in Almería. A comprehensive techno-economic analysis. Ed. Cajamar Caja Rural. Almería, Spain: 408 pp. http://www.publicacionescajamar.es/series-tematicas/economia/greenhouse-agriculture-in-almeria-a-comprehensive-techno-economic-analysis/

Vargues, A.C., Campo, J.L., Monteiro, A. 1994. The effect of greenhouse double-roof on tomato growth and yield. Acta Hortic. 357, 317-324. https://doi.org/10.17660/ActaHortic.1994.357.30.

Yoon, H.I., Kim, J.H., Park, K.S., Namgoong, J.W., Hwang, T.G., J.P., Kim, J.E., Son, 2020. Quantitative methods for evaluating the conversion performance of spectrum conversion films and testing plant responses under simulated solar conditions. Hortic. Environ. Biotechnol. 61, 999–1009. https://doi.org/10.1007/s13580-020-00286-y.

Differences in Yield and Water Consumption in a tomato Crop Irrigated with Desalinated Seawater Blended with Well Water

Patricia Marín-Membrive [a,*], Diego L. Valera [a], Araceli Peña [a], María de los Ángeles Moreno-Teruel [a], Alejandro López-Martínez [a], Francisco Domingo Molina-Aíz [a], Juan Reca [a]

[a] CIAMBITAL (Centro de Investigación en Agrosistemas Intensivos Mediterráneos y Biotecnología Agroalimentaria), University of Almería, Ctra. Sacramento s/n, 04120 Almería, Spain.

* Corresponding author. Email: patriciamarin@ual.es

Abstract

Desalination is an inexhaustible source that provides water with a guarantee of supply in sufficient quantity and quality, regardless of the weather. Today, the costs of treatment and distribution of conventional water have been increasing in many regions around the world and desalination has become more competitive and economically attractive due mainly to advances in technology to reduce desalination costs. The purpose of this study was to quantify the differences in production, water consumption and fertilizer input, derived from the use of desalinated seawater and water from mixing it with well water, in a tomato crop (Lycopersicum esculentum Mill.) transplanted on 09/10/2018, grown in soil and in hydroponics with reuse of drainage. The trial was conducted in an E-W oriented Almería-type greenhouse located at the UAL-Anecoop Experimental Station of the University of Almeria. In total there were 6 different treatments with a total area of 242.4 m2 each, with three replications. The desalinated water was supplied by the Carboneras Desalination Plant (Almería), while the well water was simulated by adding in situ different salts to the desalinated water. The drains were treated in a small desalination plant installed next to the greenhouse, functioning with solar energy. In general, hydroponic crop obtained higher yield than the plants growing in soil, although soilless cultivation was less efficient in the use of water and more fertilizers were added. For the hydroponic crop, treatment with desalinated water obtained the highest productions. In the soil, the highest production and better efficiency of water corresponded to the treatment with the irrigation water of higher salinity, with a lower addition of fertilizers.

Keywords: greenhouse, desalinated seawater, soilless cultivation, tomato, yield.

1. Introduction

The world is in constant transformation, and we are more aware of this now than ever before. Some of the factors affecting these changes are climate change and resource scarcity. Lack of water availability is nowadays one of the main problems for farmers (Jordi Esteve Bargués & Oller, 2019).

According to the United Nations World Water Development Report, a global shortage of drinking water resources of approximately 40% is expected by 2030 (Aznar-Sánchez et al., 2021). Of all, agriculture is the largest consumer of water in the world. It is estimated that more than two thirds of total water use is devoted to irrigating agricultural land (Reca et al., 2018), other studies put this figure at more than 75% from irrigated agriculture (Aznar-Sánchez et al., 2017) or it is even estimated at 80% of water resources (Martinez-Mate et al., 2018).

In addition to scarcity, there is also great concern about the quality of irrigation water (Reca et al., 2018). Many areas are affected by increasing salinization of groundwater resources caused by overexploitation of aquifers and irrigation water returns(Colombani et al., 2016)(Colombani et al., 2016).

The salt stress caused by this increase in salts is one of the main abiotic factors affecting plant growth and limiting crop yields (Köster et al., 2019)(Zörb et al., 2019). The use of saline water as irrigation water, causes there to be a toxic response when Na^+ and Cl^- ions are introduced into the plant, triggering various responses (Yasuor et al., 2020). Sodium has a particularly considerable negative impact on plant growth and development compared to other cations due to its ability to induce Ca and K deficiencies (Butcher et al., 2016). In addition, Na^+ and Cl^- can cause nutrient imbalances, mainly due to interaction with nitrate (NO_3^-) that can affect plant growth and yield (Yasuor et al., 2020).

Agriculture is part of the problem, but it is also part of the solution, as it will have a prominent role within the strategy to combat climate change, for example, by helping to contain erosion and desertification. It will also contribute to the generation of technological advances and innovations, to achieve a more efficient use of water (Calicioglu et al., 2019).

The province of Almeria has the highest concentration of greenhouses in Europe with 32368 hectares (Cajamar Caja Rural, 2020), making it an area where the need for an alternative to the traditional use of irrigation is evident. Within the available solutions, desalinated water has become a competitive option in the supply of quality water for irrigation in arid or semi-arid regions. Desalinated seawater can provide a continuous and abundant water source (Martínez-Alvarez et al., 2016). A technically and economically viable alternative contributes to the sustainability of agriculture and water resources. This water source provides good chemical quality, high reliability of supply and immediate accessibility (Ghaffour et al., 2013). In addition to satisfying the need for good quality water, it allows the possibility of

crop diversification, these being the reasons why farmers would use this type of water (Aznar-Sánchez et al., 2017).

Another positive aspect of desalinated seawater is that minerals that are normally present in a saline water and are necessary for crop development, such as Ca^{2+}, Mg^{2+} and SO_4^{2-}, in desalinated seawater can be reintroduced in case they have been completely removed in the desalination process (Yermiyahu et al., 2007). These nutrients can be reintroduced by adding fertilizers or by mixing desalinated water with high salinity groundwater (Yasuor et al., 2020).

In a case study on a bell pepper crop in Israel, comparing the use of desalinated water versus different blends of desalinated water with brackish water, it was observed that irrigation with blended water (70% desalinated water and 30% brackish water) provided yields higher than 90% of those with fully desalinated water, but it was necessary to increase irrigation rates by at least 50%. In contrast, the use of water with an intermediate conductivity of 1.35 dS·m^{-1} caused up to five times more salt in the soil in the plant root zone than in the case of using desalinated water alone (Ben-Gal et al., 2009).

All studies are directed towards the same objective in the end, which is to find the right ratio of water to obtain the maximum yield at the lowest economic and ecological cost. Some authors suggest that the proportion of brackish water should contribute at least 25% of the total volume to achieve this objective (Grattan & Oster, 2003).

Other authors propose applying water at different conductivities throughout the crop cycle, depending on the plant's stage of maturity. At times when the plant is more sensitive, such as during germination and the first stages of development, use water of lower salinity, and during the subsequent growth of the plant, apply water of higher salinity (Minhas & Gupta, 1993a)(Minhas & Gupta, 1993b).

In terms of fruit quality, studies have shown that the use of desalinated water does not compromise consumer acceptance of tomatoes due to low quality differences. (Antolinos et al., 2020).

On the other hand, it is noteworthy that the south eastern area of Spain has the necessary infrastructure, since of Spain's desalination capacity (1,670,000 m^{3}day^{-1}) 74% corresponds to the south eastern area of the country, of which 54% is destined for agricultural use (García-Rubio & Guardiola, 2012) (Aznar-Sánchez et al., 2017).

In south eastern Spain, alternative water sources and technologies for irrigation are needed, such as hydroponic systems as an alternative to traditional soil in the area (Martinez-Mate et al., 2018). This system in traditional soil, called sanding, consists of covering the surface of the cropland with a layer of sand that acts by retaining the moisture present in the soil. It has different layers: from bottom to top it has a natural layer of soil, above it is the gully soil (40 cm), on top of it is placed manure (10 cm) and finally the sand (15 cm) (Valera et al., 2014). Traditional sanding has a number of advantages over the hydroponic system, and one of these advantages is to conserve soil moisture and, therefore, an estimated saving of 20% in water (Jiménez & Lao, 2002). Although desalinated seawater coupled with hydroponic system could be a valuable strategy to maintain a high productivity agriculture; although also very dependent on energy (Martinez-Mate et al., 2018).

The objective of this study is to compare the yield and quality of a greenhouse tomato crop, irrigated with desalinated seawater and two waters of higher salinity, grown in traditional soil and in hydroponics with reuse of drains.

2. Materials and Methods

The greenhouse is located in the Practice Field of the University of Almeria "Catedrático Eduardo Fernández" of the UAL-ANECOOP Foundation, being its location: Longitude: 2° 17' W, Latitude: 36° 51' N and Altitude: 90 m (Figure 1), specifically in the module called U8.

The "Almeria" type greenhouse is oriented E-W and has a surface area of 1935 m^2. It consists of five troughs 8 m apart, with a height in the trough of 4.7 m (tube + block) and 3.4 m in the band. The greenhouse has zenithally windows (in the three scrapers) with a ventilation surface of 4 % and lateral windows (in the whole sash) with a ventilation surface of 12.9 %. The plastic of the cover is three-layer, 800-gauge, thermal, white and with a duration of 3 seasons.

For the realization of the trial, we have three different irrigation waters, one of them is desalinated water, supplied by the Carboneras Desalination Plant, and the other two are well water. In addition, the greenhouse is divided into subplots in which soil and hydroponic crops are grown.

For each of the three irrigation waters there are three replicates in soil and three replicates in hydroponics. This leaves six plots irrigated with desalinated water at a conductivity of 0.5 dS·m^{-1}, six plots with water at a conductivity of 1.5 dS·m^{-1} and six plots at a conductivity of 3 dS·m^{-1}. Finally, there are eighteen demonstration plots, where three treatments are applied in three replicates in soil cultivation and three treatments in three replicates in hydroponic cultivation. Table 1 shows the parameters of each of the irrigation waters used in this trial.

Figure 1: Layout of the UAL-ANECOOP Experimental Farm Foundation (Google Maps).

Table 1: Irrigation water parameters of the three treatments.

SALINITY LEVELS	CE dS·m⁻¹	mmol L⁻¹									
		NO_3^-	SO_4^{2-}	$H_2PO_4^-$	HCO_3^-	Cl^-	K^+	Ca^{2+}	Mg^{2+}	Na^+	NH_4^+
1	0.6	0.00	0.06	0.01	0.75	4.48	0.12	0.37	0.13	4.39	0.00
2	1.5	0.00	1.47	0.01	3.55	7.28	0.12	3.17	1.54	5.91	0.00
3	3.0	0.00	3.58	0.01	7.75	11.48	0.12	7.37	3.65	8.18	0.00

Fertilizer supply is based on an ideal solution, adapted from Sonneveld and Straver's ideal solution (Sonneveld & Straver, 1994). This fertilizer supply is done by simulating the situation in the field, so that, in the case of desalinated water, the final EC with fertilizers would be 2.2 dS·m⁻¹, in the case of water with intermediate salinity, it is increased to 2.5 dS·m⁻¹ and in the case of water with higher salinity, it is increased to 3.5 dS·m⁻¹. The calculations have been made according to the irrigation water we have in each case (Urrestarazu, 2004), leaving the final composition as shown in Table 2.

Table 2: Theoretical final water composition of each treatment.

SALINITY LEVELS	CE dS·m⁻¹	mmol L⁻¹									
		NO_3^-	$H_2PO_4^-$	SO_4^{2-}	HCO_3^-	Cl^-	NH_4^+	K^+	Ca^{2+}	Mg^{2+}	Na^+
1	2.2	12.00	1.51	1.31	0.75	4.48	0.50	7.12	3.92	1.08	4.39
2	2.5	9.50	1.51	1.47	3.55	7.28	0.00	7.62	4.17	1.54	5.91
3	3.5	4.50	2.01	3.58	7.75	11.48	0.00	4.62	7.37	3.65	8.18

The crop used in the trial was tomato grown as a short cycle, from 09/11/2019 to 02/21/2020. Specifically, the commercial variety Ramyle RZ F1 (74-207), from the company Rijk Zwaan Ibérica S.A. It is a canary tomato, red, for bunch or loose harvesting. The plant is vigorous with good leaf coverage and fruits of M-MM calibre. The bunches are uniform with good fruit firmness and long shelf life. Resistances: ToMV:0-2/Ff:B,D/Fol:0,1/Va:0/Vd:0 and TSWV/TYLCV/Ma/Mi/Mj.

The greenhouse has 1454.4 m² total area to be cultivated, each experimental plot has an area of 80.8 m² and each treatment 727.2 m². Finally, there are eighteen demonstration plots, where three treatments are applied in three replicates in soil cultivation and three treatments in three replicates in hydroponic cultivation.

Both the soil and hydroponic treatments have an area of 727.2 m², the tomato plants will be planted directly every 0.5 m between plants and 0.5 m between rows leaving an aisle every 2 rows 1.5 m. Each plot consists of four crop rows,

distributed in such a way that two aisles are 1.5 m apart, the paired rows are 0.5 m apart and the distance between plants is 0.5 m, corresponding to one plant per dripper in both cases. The planting frame is 1.5 × 0.5 × 0.5 m and the planting density is two plants per square meter. In each row, we have 39 plants and in each plot 156 plants.

Finally, a configuration of the different treatments remains as shown in Table 3.

Table 3: Characteristics of the different treatments.

SALINITY LEVELS	EC Irrigation water	CROPPING SYSTEM	EC Irrigation water + fertilizers
1	0.6 dS·m^{-1}	Hydroponic	2.2 dS·m^{-1}
1	0.6 dS·m^{-1}	Soil	2.2 dS·m^{-1}
2	1.5 dS·m^{-1}	Hydroponic	2.5 dS·m^{-1}
2	1.5 dS·m^{-1}	Soil	2.5 dS·m^{-1}
3	3.0 dS·m^{-1}	Hydroponic	3.5 dS·m^{-1}
3	3.0 dS·m^{-1}	Soil	3.5 dS·m^{-1}

On the one hand, production was recorded and controlled in the different experimental plots, where marketable production was directly quantified. An electronic scale EKS Premium (E.K.S. Spain, S.A., Spain), with a sensitivity of 10 g and a maximum capacity of 40 kg, was used.

On the other hand, a series of parameters were measured for the evaluation of the marketable quality of the production on 18 fruits per treatment:

- Average fruit weight (kg) [Electronic balance PB3002-L DeltaRange® Mettler Toledo, S.A., Spain].
- Diameter (mm) [Digital caliper 150 mm Medid Precision, S.A., Spain].
- Soluble solids content (°Brix) [Refractometer PAL-1 Atago Co., LTD., Japan]
- Firmness (kg·cm^{-2}) [Digital Penetrometer PCE-FM 200 PCE-Ibérica S.L., Spain].

The irrigation head is equipped with a Supra64 ® Hydrocomputer (Hermisan S.A., Alicante, Spain) for the management and control of the irrigation head. With this program, we can download the records of the volume of water supplied to each treatment.

The data were analysed with the statistical program Statgraphics® Centurion 18. Multifactorial ANOVA, Multiple Range Test and Variance Check analyses were performed. The method used to discriminate between means was Fisher's Least Significant Difference (LSD) procedure, with a 5.0% risk of each pair of means being significantly different.

3. Results and Discussion

3.1 Comparison of irrigation water treatments

Comparing the different irrigation water treatments with different salinity levels we obtain the results that can be seen in Table 4.

A multifactorial analysis of variance was performed to determine whether salinity level has a statistically significant effect on the different parameters studied. Type III sum of squares was chosen in the analysis, so that the contribution of each factor is measured having eliminated the effects of all other factors.
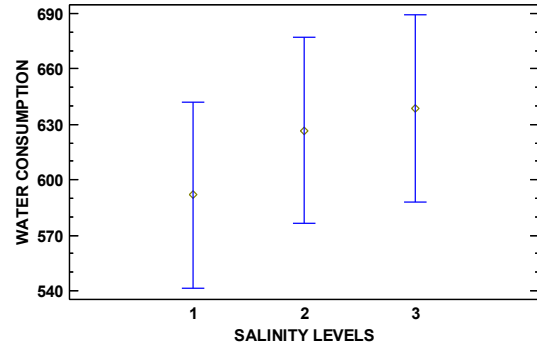
Table 4: Analysis of the parameters measured as a function of the different levels of salinity of the irrigation water.

SALINITY LEVELS	Commercial Yield [kg·m^{-2}]	Water Consumption [m^3·ha^{-1}]	Water Productivity [kg·m^{-3}]	QUALITY PARAMETERS			
				Fresh Weight [g]	Diameter [mm]	Soluble Solids [ºBrix]	Firmness [kg·cm^{-2}]
1	3.55 a	591.77 a	62.04 a	119.45 b	62.69 b	4.79 a	1.57 a
2	3.74 a	626.77 a	60.89 a	130.18 c	64.36 c	5.24 ab	1.75 c
3	3.23 a	638.71 a	50.51 a	113.86 a	61.20 a	5.55 b	1.94 b

In the case of commercial production, there are no statistically significant differences. The highest production was found in the treatment with intermediate salinity levels (Figure 2 a) and the lowest in the treatment with higher salinity (Figure 2 b). These results are to be expected, since in the desalinated water treatment and in the intermediate salinity treatment the final EC is very similar, so similar results are expected, and in the case of the treatment with higher salinity, reaching the tolerant threshold for the tomato crop, production is already reduced, in agreement with the linear relationship between salinity and production of Maas and Hoffman (Maas & Hoffman, 1977).
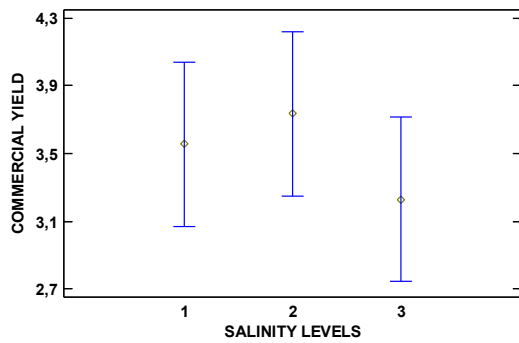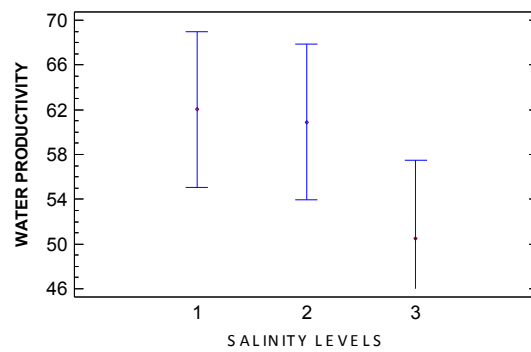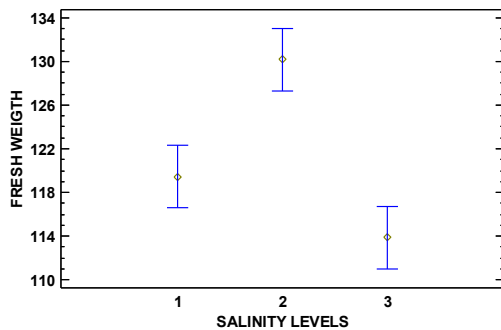
Figure 2. Parameters analysed as a function of the different levels of salinity of the irrigation water (**1**: EC 0.6 dS·m^{-1}; **2**: EC 1.5 dS·m^{-1}; **3**: EC 3.0 dS·m^{-1}). (a) Commercial yield [kg·m^{-2}]. (b) Water Consumption [m^3·ha^{-1}]. (c) Water Productivity [kg·m^{-3}]. (d) Fresh Weight [g]. (e) Diameter [mm]. (f) Soluble Solids [ºBrix]. (g) Firmness [kg·cm^{-2}].

Water consumption was higher in the treatment with higher salinity (Figure 2 b), although without statistically significant differences. The lowest water consumption was in the desalinated water treatment. In addition, if we determine water productivity (Figure 2 c), we see that the treatment with desalinated water has been higher and, as in consumption, water productivity has been lower in the treatment with higher salinity. According to this and as we have discussed, we see how we can reach a balance between economy and ecology. It would be interesting, as other authors did (Grattan & Oster, 2003), to determine the ideal ratio to reach this balance.

Regarding the analysis of fruit quality, there are differences in all the parameters analysed. Fresh weight was higher in the intermediate salinity treatment and lower in the higher salinity treatment, as was the case for fruit diameter and yield (Figures 2 a, d and e); tomatoes with higher soluble solids content and greater firmness were found in the higher salinity treatment (Figures 2 f and g). In all cases, despite the existence of statistically significant differences, we found ourselves within the same commercial ranges established for external and internal fruit quality (Domene Ruiz & Segura Rodríguez, 2014) (Domene R & Segura R, 2014). These results are in agreement with those of Antolinos et al., 2020, where no differences in consumer perception of fruit quality were observed.

3.2 Comparison of cultivation systems

Comparing the different cultivation systems used, we obtain the results shown in Table 5.

A multifactorial analysis of variance was performed to determine whether the cropping system has a statistically significant effect on the different parameters studied. Type III sum of squares was chosen in the analysis, so that the contribution of each factor is measured having eliminated the effects of all other factors.

Table 5: Analysis of measured parameters according to different cultivation systems.

CROPPING SYSTEM	Commercial Yield [kg·m⁻³]	Water Consumption [m³·ha⁻¹]	Water Productivity [kg·m⁻³]	QUALITY PARAMETERS			
				Fresh Weight [g]	Diameter [mm]	Soluble Solids [ºBrix]	Firmness [kg·cm⁻²]
SOIL	3.13 a	495.45 a	63.39 a	121.18 a	62.63 a	5.34 a	1.67 a
HYDROPONIC	3.88 a	742.71 b	52,24 a	121.14 a	62.87 a	5.02 a	1.85 b

In the case of commercial production, it was higher in the hydroponic treatment, although without statistically significant differences (Figure 3 a). Water consumption was much higher in hydroponic cultivation, in our case 33% higher in the hydroponic system (Figure 3 b), a value above that estimated by Jiménez and Lao, 2002. According to our results, we observe that in order to obtain higher yields it is necessary to use more water and consequently more energy, as occurs in a study on lettuce where the use of soilless techniques entails significantly higher energy consumption and emissions than the production of soil-grown crops. However, water productivity is higher in the case of soilless cultivation (Martinez-Mate et al., 2018). This is not so in our case, where water productivity is higher in soil cultivation (Figure 3 c), although there are no statistically significant differences between the two cultivation systems.

Regarding the quality parameters studied, statistically significant differences were only detected in the case of firmness (Figure 3 d), being superior in the hydroponic cultivation system, although always within the same commercial category (Domene R & Segura R, 2014).
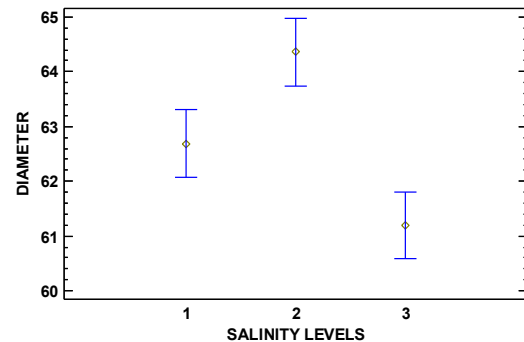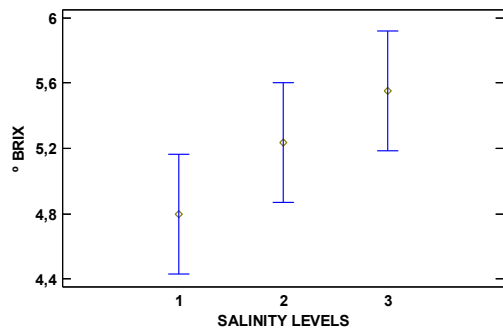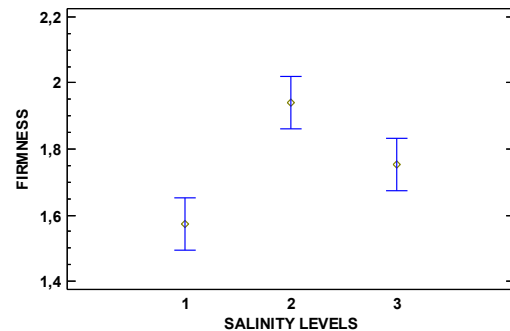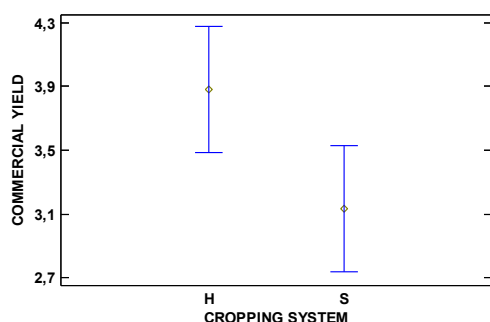

(a)

(b)

(c)

(d)
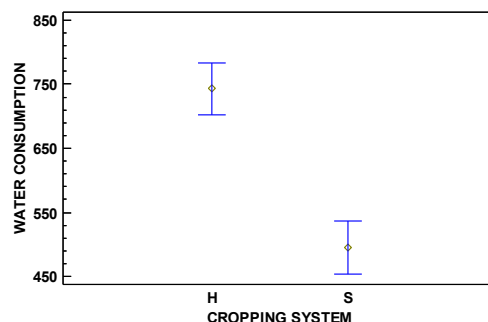
Figure 3. Parameters analysed as a function of the different cropping systems. (**H**: Hydroponic and **S**: Soil). (a) Commercial yield [kg·m^{-2}]. (b) Water Consumption [m^3·ha^{-1}]. (c) Water Productivity [kg·m^{-3}]. (d) Firmness [kg·cm^{-2}].

4. Conclusions

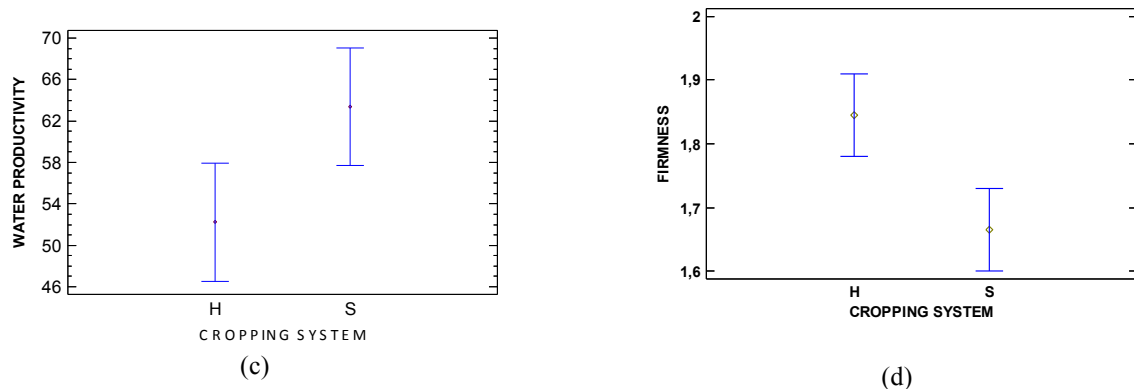The yield, quality and water consumption of a short cycle of tomato, grown in greenhouses in the province of Almeria, irrigated with desalinated seawater and with two irrigation waters of higher salinity were compared. It was observed that there were no significant differences in production and that the treatment irrigated with desalinated seawater had a higher water productivity in terms of kilograms produced. The quality parameters, weight and diameter, were higher in the treatment with water of intermediate salinity, and the parameters of soluble solids content and firmness were higher in the treatment with higher salinity, with statistically significant differences, although in all cases within the same commercial categories.

The yield, quality and water consumption of the same crop, grown in two cultivation systems, traditional soil and hydroponic, were also compared. A higher yield was obtained in the hydroponic system, although in this case the water productivity was higher in the case of the system cultivated in traditional soil. As for the quality parameters, statistically significant differences were only found in the case of firmness, with superior results in the hydroponic system and in all cases within the same commercial categories.

Acknowledgements

References

Antolinos, V., Sánchez-Martínez, M. J., Maestre-Valero, J. F., López-Gómez, A., & Martínez-Hernández, G. B. (2020). Effects of irrigation with desalinated seawater and hydroponic system on tomato quality. *Water (Switzerland)*, *12*(2), 1–16. https://doi.org/10.3390/w12020518

Aznar-Sánchez, J. A., Belmonte-Ureña, L. J., & Valera, D. L. (2017). Perceptions and acceptance of desalinated seawater for irrigation: A case study in the Níjar district (southeast Spain). *Water (Switzerland)*, *9*(6). https://doi.org/10.3390/w9060408

Aznar-Sánchez, J. A., Belmonte-Ureña, L. J., Velasco-Muñoz, J. F., & Valera, D. L. (2021). Farmers' profiles and behaviours toward desalinated seawater for irrigation: Insights from South-east Spain. *Journal of Cleaner Production*, *296*. https://doi.org/10.1016/j.jclepro.2021.126568

Ben-Gal, A., Yermiyahu, U., & Cohen, S. (2009). Fertilization and Blending Alternatives for Irrigation with Desalinated Water. *Journal of Environmental Quality*, *38*(2), 529–536. https://doi.org/10.2134/jeq2008.0199

Butcher, K., Wick, A. F., Desutter, T., Chatterjee, A., & Harmon, J. (2016). Soil salinity: A threat to global food security. *Agronomy Journal*, *108*(6), 2189–2200. https://doi.org/10.2134/agronj2016.06.0368

Cajamar Caja Rural. (2020). *Análisis de la campaña hortofrutícola 2019/2020*. 1–9. https://www.plataformatierra.es/detalle/analisis-campana-hortofruticola

Calicioglu, O., Flammini, A., Bracco, S., Bellù, L., & Sims, R. (2019). The future challenges of food and agriculture: An integrated analysis of trends and solutions. *Sustainability (Switzerland)*, *11*(1). https://doi.org/10.3390/su11010222

Colombani, N., Di Giuseppe, D., Faccini, B., Ferretti, G., Mastrocicco, M., & Coltorti, M. (2016). Inferring the interconnections between surface water bodies, tile-drains and an unconfined aquifer-aquitard system: A case study. *Journal of Hydrology*, *537*, 86–95. https://doi.org/10.1016/j.jhydrol.2016.03.046

Domene R, M. A., & Segura R, M. (2014). Parámetros de calidad externa en la industria agroalimentaria. *Cajamar*

ADN Agro, *3*, 1–12.

Domene Ruiz, M. Á., & Segura Rodríguez, M. (2014). De Hortalizas Y Frutas En La. *Cajamar*, 1–18. https://www.cajamar.es/pdf/bd/agroalimentario/innovacion/investigacion/documentos-y-programas/005-calidad-interna-1410512030.pdf

García-Rubio, M. A., & Guardiola, J. (2012). Desalination in Spain: A Growing Alternative for Water Supply. *International Journal of Water Resources Development*, *28*(1), 171–186. https://doi.org/10.1080/07900627.2012.642245

Ghaffour, N., Missimer, T. M., & Amy, G. L. (2013). Technical review and evaluation of the economics of water desalination: Current and future challenges for better water supply sustainability. *Desalination*, *309*(2013), 197–207. https://doi.org/10.1016/j.desal.2012.10.015

Grattan, S. R., & Oster, J. D. (2003). Use and reuse of saline-sodic waters for irrigation of crops. *Journal of Crop Production*, *7*(1–2), 131–162. https://doi.org/10.1300/J144v07n01_05

Jiménez, S., & Lao, M. T. (2002). Los suelos enarenados en el sureste español. *Vida Rural*, 42–44.

Jordi Esteve Bargués, & Oller, R. A. (2019). *El futuro del sector agrícola español pwc Sobre este estudio*. https://www.pwc.es/es/publicaciones/assets/informe-sector-agricola-espanol.pdf

Köster, P., Wallrad, L., Edel, K. H., Faisal, M., Alatar, A. A., & Kudla, J. (2019). The battle of two ions: Ca2+ signalling against Na+ stress. *Plant Biology*, *21*, 39–48. https://doi.org/10.1111/plb.12704

Maas, E. V., & Hoffman, G. J. (1977). Crop Salt Tolerance - Current Assessment. *ASCE J Irrig Drain Div*, *103*(2), 115–134. https://doi.org/10.1061/jrcea4.0001137

Martínez-Alvarez, V., Martin-Gorriz, B., & Soto-García, M. (2016). Seawater desalination for crop irrigation - A review of current experiences and revealed key issues. *Desalination*, *381*, 58–70. https://doi.org/10.1016/j.desal.2015.11.032

Martinez-Mate, M. A., Martin-Gorriz, B., Martínez-Alvarez, V., Soto-García, M., & Maestre-Valero, J. F. (2018). Hydroponic system and desalinated seawater as an alternative farm-productive proposal in water scarcity areas: Energy and greenhouse gas emissions analysis of lettuce production in southeast Spain. *Journal of Cleaner Production*, *172*, 1298–1310. https://doi.org/10.1016/j.jclepro.2017.10.275

Minhas, P. S., & Gupta, R. K. (1993a). Conjunctive use of saline and non-saline waters. I. Response of wheat to initial salinity profiles and salinisation patterns. *Agricultural Water Management*, *23*(2), 125–137. https://doi.org/10.1016/0378-3774(93)90036-A

Minhas, P. S., & Gupta, R. K. (1993b). Conjunctive use of saline and non-saline waters. III. Validation and applications of a transient model for wheat. *Agricultural Water Management*, *23*(2), 149–160. https://doi.org/10.1016/0378-3774(93)90038-C

Reca, J., Trillo, C., Sánchez, J. A., Martínez, J., & Valera, D. (2018). Optimization model for on-farm irrigation management of Mediterranean greenhouse crops using desalinated and saline water from different sources. *Agricultural Systems*, *166*(March), 173–183. https://doi.org/10.1016/j.agsy.2018.02.004

Sonneveld, C., & Straver, N. (1994). Nutrient solutions for vegetables and flowers grown in water or substrates. *Serie: Voedingsoplossingen Glastuinbouw (Netherlands)*, *8*, 45. http://edepot.wur.nl/237302%0Ahttps://agris.fao.org/agris-search/search.do?recordID=NL8901262

Urrestarazu, G. (2004). Tratado de cultivo sin suelo. *Mundi-Prensa*, *January 2004*, 914. https://www.mundiprensa.com/catalogo/9788484761396/tratado-de-cultivo-sin-suelo

Valera, D.L., Belmonte, L.J., Molina, F.D. y Lopez A. 2014. Los invernaderos de Almeria. Analisis de su tecnologia y rentabilidad. Cajamar Caja Rural, Almeria.

Yasuor, H., Yermiyahu, U., & Ben-Gal, A. (2020). Consequences of irrigation and fertigation of vegetable crops with variable quality water: Israel as a case study. *Agricultural Water Management*, *242*(June), 106362. https://doi.org/10.1016/j.agwat.2020.106362

Yermiyahu, U., Tal, A., Ben-Gal, A., & Bar-Tal, A. (2007). Rethinking Desalinated Water Quality and Agriculture. *Science*, *318*(November), 920–921.

Zörb, C., Geilfus, C. M., & Dietz, K. J. (2019). Salinity and crop yield. *Plant Biology*, *21*, 31–38. https://doi.org/10.1111/plb.12884

Influence of Different Cooling Systems on the Photosynthetic Activity and Yield of Greenhouse Tomato Crops

María Ángeles Moreno-Teruel [a], Alejandro López-Martínez [a], Francisco Domingo Molina-Aiz [a], Diego Luis Valera- Martínez [a*], Araceli Peña-Fernández [a], Patricia Marín-Membrive [a].

[a] CIAMBITAL (Centro de Investigación en Agrosistemas Intensivos Mediterráneos y Biotecnología Agroalimentaria), University of Almería, Ctra. Sacramento s/n, 04120 Almería, Spain.

* Corresponding author. Email: dvalera@ual.es

Abstract

The purpose of this study was to analyse the effect of different evaporative cooling systems compared to natural ventilation on the photosynthetic activity and production of a tomato crop (*Lycopersicum esculentum* Mill.) in a spring-summer cycle. The study was carried out in three multi-span greenhouses: (i) a greenhouse with evaporative pads and fans and natural ventilation (PS+NV); (ii) a greenhouse with a fog system and natural ventilation (FS+NV); (iii) a greenhouse only with natural ventilation (NV). The photosynthetic activity was higher in the greenhouse with natural ventilation (14.7 µmol CO_2 m^{-2} s^{-1}) than in the greenhouse with pad-fan system (14.6 µmol CO_2 m^{-2} s^{-1}; without statistically significant difference) and in the greenhouse with fog system (13.4 µmol CO_2 m^{-2} s^{-1}; with statistically significant difference). The production was higher in the greenhouse with pad-fan system (5.0 kg m^{-2}) than in the greenhouse with natural ventilation (4.8 kg m^{-2}; without statistically significant difference) and in the greenhouse with fog system (4.5 kg m^{-2}; with statistically significant difference). In general, photosynthetic activity and crop production increased as the maximum temperature (and the number of hours of exposure to high temperatures) decreased. It has been observed that the improvement in temperature conditions inside the greenhouses in spring-summer cycles produces increases in the photosynthetic activity of the tomato crop and consequently a growth in production.

Keywords: protected crops, ventilation, evaporative systems, photosynthesis, yield.

1. Introduction

Photosynthesis is the main physiological process that drives plant growth and crop productivity. This physiological process is heavily influenced by environmental conditions (Yin *et al.,* 2009). Air temperature not only affects growth but also nitrogen metabolism in tomato plants, which is related to photosynthetic activity (Liu *et al.,* 2017). For most horticultural crops its yield is adequate in a wide range of temperatures, although the net photosynthesis balance decreases when temperature increase excessively, due to a rise in respiration. An augmentation in temperature between 5 and 10 °C above the optimum can produce a notable impact on net photosynthesis (Camejo *et al.,* 2005), which is closely related to crop yields and can be an important variable when selecting one variety or another of cultivation (Santiago *et al.,* 1998).

In the Mediterranean area the excess of temperature from spring to autumn can damage the yield of crops (Kittas *et al.,* 1995). For this reason, it is necessary to reduce the temperature inside the greenhouses throughout the growing season of the crop. The cooling system to be chosen will depend on the climatic conditions, the technology, and the available resources (Bakker *et al.,* 2008). The greenhouses in the province of Almeria (Spain) that use evaporative-cooling systems are around 20%. The most used is the fog system due to the peculiarities of the greenhouses already built, such as the excessive width and lack of hermeticity (Valera *et al.,* 2016). Water evaporative cooling systems are also associated with an increase in relative humidity inside the greenhouse, being desirable in dry climate zones (Arbel *et al.,* 1999; González-Real *et al.,* 2006). The combination of the reduction in temperature and the increase in relative humidity makes cooling systems more efficient than other climatic controls systems such as shading or forced ventilation (Luchow and Von Zabeltitz, 1992). Fog systems are less efficient than evaporative pad-fans systems (Katsoulas *et al.,* 2009), however, their lower installation cost makes them more attractive for use in greenhouses (Luchow and Von Zabeltitz, 1992). The use of evaporative pad-fan systems normally produces non-uniform climatic conditions (Luchow and Von Zabeltitz, 1992). Significant temperature gradients of around 0.13-0.27 °C m^{-1} have been observed in the direction of airflow (Arbel *et al.,* 2003).

Although more and more active refrigeration systems are being implemented inside the greenhouses, the reality is that practically all farmers in Almeria develop their crops in greenhouses whose only method of climate control is natural ventilation. At present the existing ventilation surface in the greenhouses of Almeria is around 15%. This average value is below the real needs in a greenhouse with insect-proof screens. Recommended ventilation surface values in unscreened greenhouses vary between 15 and 25% of the soil surface (Valera *et al.,* 2002). These percentages should be increased to compensate the decrease of ventilation capacity when insect-proof nets are used (Valera *et al.,* 2016). Efficient natural ventilation of greenhouses is crucial to maintain suitable microclimatic conditions for crops and

to promote photosynthetic activity, being especially important if the outside temperature, global radiation and indoor humidity have high values (Valera *et al.*, 2016). The net rate of photosynthesis increases with the rise of the concentration of CO_2 in a range between 0 and 1000 μmol mol^{-1} (Allen and Amthor, 1995). Therefore, the concentration of CO_2 in greenhouses can be increased during the day, using CO_2 enrichment techniques, up to about 1000 μmol mol^{-1} to promote photosynthesis and plant growth inside greenhouses (Hand *et al.*, 1993; Ceulemans *et al.*, 1997). In the absence of this CO_2 enrichment, net rates of photosynthesis may increase enhancing air circulation by natural ventilation (Shibuya and Kozai, 1998; Kitaya *et al.*, 2003), allowing the entry of CO_2 from the outside to compensate for the CO_2 consumed by plants. The optimal air circulation depends on the plant species, plant structure, canopy depth and wind direction with respect to the position of the plant in greenhouses (Wadsworth, 1959; Sase, 2006). On the other hand, insufficient air circulation above the plant canopy causes limited gas exchange due to increased strength of the leaf boundary layer (Kin *et al.*, 1996; Kitaya *et al.*, 1998).

Cooling greenhouses by means of water evaporative cooling systems implies greater energy and water consumption than the use of the traditional natural ventilation system. According to Franco *et al*. (2011), despite the existence of a higher consumption in the evaporator panel system, the crop requires less irrigation (Montero *et al.*, 2005) since its transpiration rate decreases by 31%. Therefore, the total increase in the water requirement is only 19% (Arbel *et al.*, 2003).

The objective of this work was to determine the influence that different refrigeration systems exert on the inside microclimate, the photosynthetic activity, and the production of a tomato crop in greenhouse. Two cooling systems using evaporation of water combined with natural ventilation were compared to the use of only natural ventilation.

2. Materials and Methods

2.1. Characteristics of experimental greenhouses

The research was carried out in three multi-span greenhouses, located in the experimental farm UAL-ANECOOP "*Catedrático Eduardo Fernández*" of the University of Almeria (36° 51′ N, 2° 16′ W and 87 m.a.s.l.). The greenhouses were divided transversely by a polyethylene wall, constituting two isolated sectors. For our trial we used the experimental sectors located in the east of each greenhouse (Table 1), the west sectors were used for other research work, being the same crop in the two sectors of the greenhouses. Greenhouse 1 consisted of two spans 9 m wide, with two roof windows and two side openings. Greenhouses 2 and 3 have three spans 8 m wide, with three roof windows. Greenhouse 2 has two side openings and greenhouse 3 was equipped with a cellulose pad at the south wall and 8 fans at the north wall.

Table 1. Characteristics of the east sectors of each experimental greenhouse. Total length L_G and width W_G (m), width of each span w_S (m), maximum height of the span h_{max} (m), gutter height h_{gut} (m), surface area S_C (m^2), side ventilation surface S_{VS} (m^2), roof ventilation surface S_{VR} (m^2) and total ventilation surface area S_V/S_C (%).

Greenhouse	Cooling systems	$L_G \times W_G$	w_S	h_{max}	h_{gut}	S_C	S_{VS}	S_{VR}	S_V/S_C
1	Natural ventilation (NV)	18 × 25	9	6.6	4.6	450	40.5	45.0	19.0
2	Fog systems (FS) + NV	24 × 25	8	6.2	4.6	600	34.5	67.5	17.0
3	Pad-fan (PS) + NV	24 × 25	8	6.2	4.6	600	-	67.5	11.3

The side walls of the greenhouses were made up of corrugated sheets of rigid polycarbonate, while for the roof of the greenhouses a three-layer TRIPLAST plastic cover (PE-EVA-PE) of 0.2 mm thickness (Plastimer-Morero & Vallejo Industrial, Almería, Spain) was used. The manufacturer described the technical characteristics of the cover as diffuse colorless, 85% transmittance to visible light, 50% transmittance to diffuse light and 8% transmittance to infrared light. All side and roof openings were protected using insect-proof screens with a density of 10×20 threads cm^{-2} and a porosity of 36.0%.

The sector East of the experimental greenhouse 1 was uses as control, with only natural ventilation as climate control method (Table 1). The sector East of greenhouse 2, in addition to natural ventilation had a fog system at low pressure, composed of a network of pipes with nozzles mixing water and air, located above the crop lines (2.5 m). Air was supplied by a rotary screw compressor RTA10-8 (Puska Pneumatic ®, Vizcaya, Spain) with a power of 7.5 kW, working pressure of 8 bars and an airflow of 1.12 L min^{-1}.

The sector East of greenhouse 3, could use natural ventilation by roof openings and pad-fan cooling. The cooling system was compound of an evaporator pad CELdek 7090-15 (Munters Spain ® Madrid, Spain) and 8 fans EM50d (Munters Spain ® Madrid, Spain) of 735 W of power with a nominal flow of 32500 m^3 h^{-1} (for a pressure difference of

25 Pa). In this case, the natural ventilation and the cooling system do not work simultaneously since when the pad-fan was activated the roof openings were closed.

The different climate control systems were managed by a MultiMa Series II climate controller (Hortimax SL, Almería, Spain) connected to a weather station and microclimate measuring boxes located inside the experimental sectors (Table 2).

Table 2. Characteristics of microclimate measurement equipment.

Parameters	Sensor	Manufacturer	Range	Accuracy
Outdoor climatic parameters measured at the weather station located at 9 m heigth				
Solar radiation	Kipp Solari	HortiMax B.V. (Maasdiijk, Netherlands)	±2000 W m^{-2}	$\pm5\%$
Wind speed	Anemómetro - MII		0 - 40 m s^{-1}	$\pm5\%$
Wind direction	Veleta Meteostation II		0 - 360°	$\pm5°$
Air temperature	Pt1000 IEC 751 1/3B	Vaisala Oyj (Helsinki, Finland)	−25 - 75 °C	±0.2 °C
Air humidity	HUMICAP HMT100		0 - 100%	±2.5 %
Indoor climatic parameters measured at 2 m heigth				
Air temperature	Pt1000 Clase A – Ektron III	Eleltronik Ges. M.b.H. (Engerwitzdorf, Austria)	−10 - 60 °C	±0.6 °C
Air humidity	EE07-04 PFT6 – Ektron III		0 - 100%	$\pm2\%$

Vent openings were managed depending on the climatic conditions, begin opened when inside air temperature rise above 20 °C and closed when the wind speed exceeds 8 m s^{-1}, to avoid structural damage of the greenhouses. Pad-fan system was activated when inside temperature was 10 °C above the outside temperature. Fog system was activated two hours after sunrise and stopped two hours before sunset, at intervals of 10 min.

2.2. Crop system

A tomato crop *(Lycopersicum esculentum* Mill.) of the "*Marenza*" variety (Enza Zaden España S.L., Sta. María del Águila, Spain) was transplanted in April 2013, in coconut fiber and peat bags with a density of 1 plant m^{-2}. The cultural tasks associated with the management of the crop throughout its vegetative development and harvesting were carried out equally in the three greenhouses.

2.3. Photosynthetic activity and production measurements

To determine the influence of the different climate control systems on crop yields, three crop lines (considered as statistical repetitions) were selected. Marketable and non-marketable fruits were weighed with an EKS Premium electronic balance (EKS Spain, SA, Spain), with a measuring range of 0-40 kg and an accuracy of 10 g.

To compare the effect of different climate control systems on the photosynthetic activity of tomato plants, measurements were carried out with an LCI SD photosynthesis analyzer (ADC BioScientific Limited, Hertfordshire, UK) following the methodology used by Jiang *et al*. (2017). It is a portable console with blade clamping chamber, equipped with a CO_2 and H_2O concentration sensor IRGA (infrared gas analysis), with CO_2 measurement ranges of 0-2000 ppm, 0-75 mbar for the H_2O (with accuracy of $\pm$ 2%) and 0-3000 µmol m^{-2} s^{-1} for PAR radiation. From the known airflow in the chamber, the concentrations of CO_2 and water vapor at the entrance and exit of the chamber are measured, calculating the assimilation of CO_2 (photosynthesis) and the rate of transpiration of the leaf.

Data was recorded once or twice a week, depending on the daily weather conditions, since the camera that measures photosynthesis needs clear and sunny days for its proper functioning. Plants were selected randomly during each day of measurement, measuring photosynthesis on the last mature leaves of each selected plant (a total of 12 leaves per sector). The measuring path inside the greenhouses was different each day to prevent distortions on the measurements produced by the position of the sun. In addition, the data was always recorded during the same time interval, between 12:00 and 12:30 hrs.

2.4. Statistical analysis

The statistical analysis of the data was performed with the Statgraphics Centurion XVIII software, using an analysis of variance (considered significant if the *p*-value$\leq$ 0.05), comparing the mean values with Fisher's minimum significant difference (LSD) procedure. Bartlett, Cochran, and Hartley tests were used to determine whether a sector has

similar variation. Where there was a statistically significant difference between standard deviations, parametric analysis was not feasible using analysis of variance. In this case, a nonparametric analysis was performed with Friedman's test, in which each row represents a block (the measurement date), using the box and whisker chart (Statgraphics, 2018).

3. Results and Discussion

3.1. Effect of different climate control systems on the indoor temperature of greenhouses

Average daily temperatures were higher in greenhouse 2 with the fog system for most of the period analysed from April to July (Figure 1). However, the average daily temperatures do not show statistically significant differences between the three greenhouses, being higher than the average daily temperature outside with statistically significant differences. The daily maximum temperature was statistically higher in greenhouse 2 with the fog system and natural ventilation (FS+VN). The minimum temperature was very similar in the three greenhouses with no statistically significant differences (Table 3).
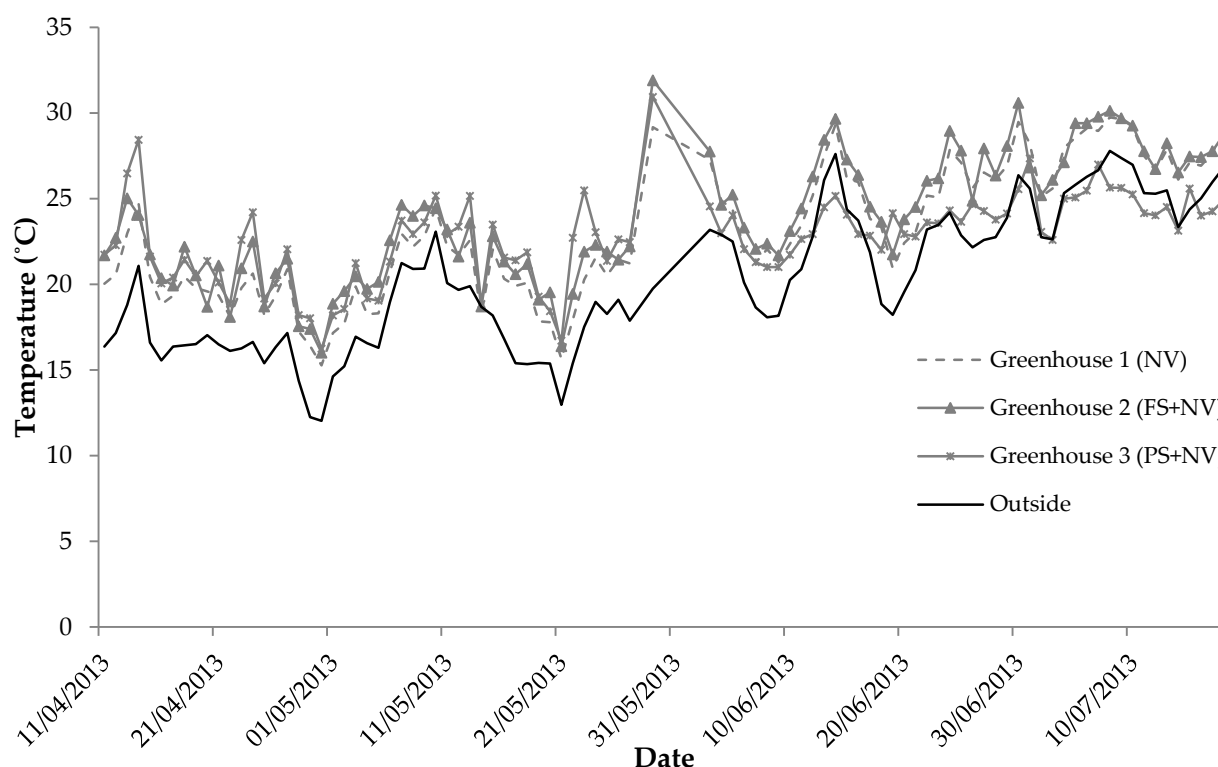
Figure 1. Average daily temperature during the development of the test. Natural ventilation NV, fog system FS and pad-fan system PS.

In the greenhouse 3 equipped with the pad-fan systems crop was less hours above 37 °C (8.9 hours) and in greenhouse 2 with the fog system, the crop was exposed for a greater number of hours (63.6 hours) to excessive temperature (Table 3). The optimal daily temperature for fruit production of tomato crop is about 19-20 °C (Van Ploeg and Heuvelink, 2005). In the case of our test, temperature was exceeded 32 °C during the development of the crop, a temperature at which pollen formation and viability is reduced (Adans *et al.,* 2001; Dominguez, 2005). So, it could be assumed that the development of plants was affected by the high air temperatures described in greenhouses 1 and 2.

Table 3. Mean (± standard deviation) daily temperature T_M, average daily maximum temperature T_{MAX}, average daily minimum temperature T_{MIN} and hours of exposure to temperatures above 37 °C, N_{H37}.

Greenhouse	Cooling systems	T_M (ºC)	T_{MAX} (ºC)	T_{MIN} (ºC)	N_{H37} (hours)
1	Natural ventilation (NV)	23.0b ± 3.9	32.0b ± 4.9	16.3a ± 3.3	44.7
2	Fog systems (FS) + NV	23.8b ± 3.7	34.0c ± 5.3	16.6a ± 3.3	63.7
3	Pad-fan (PS) + NV	22.7b ± 5.9	31.8b ± 5.1	16.7a ± 2.9	8.9
	Outside	20.2a ± 4.0	30.5a ± 4.7	16.1a ± 3.6	0

3.2. Effect of different climate control systems on crop photosynthesis

In this section the values of the photosynthetic activity, PAR radiation that reaches the surface of the leaf, concentration of CO_2 in the environment of the leaf and temperature of the crop during the development of the test will be analyzed.

During the development of the test, the photosynthetic activity was very similar between greenhouse 2 (FS+NV) and the greenhouse equipped only with natural ventilation (greenhouse 1), being slightly higher in the latter although without significant differences (Table 4). In this case the lowest photosynthetic activity was shown in greenhouse 3 (PS+NV) with statistically significant differences with the other two greenhouses.

Table 4. Photosynthetic activity A [μmol CO_2 m^{-2} s^{-1}], radiation PAR R_{PAR} [μmol m^{-2} s^{-1}], concentration of CO_2 C [ppm] and leaf temperature T_L [°C].

Greenhouse	Cooling systems	A	R_{PAR}	C	T_L
1	Natural ventilation (NV)	14.8b ± 4.1	654.2b ±189.3	365.3a ±9.7	33.8a ± 2.4
2	Fog systems (FS) + NV	14.6b ± 2.8	586.0a ± 136.9	364.8a ± 8.3	33.5a ± 2.6
3	Pad-fan (PS) + NV	13.4a ± 2.7	570.6a ± 143.9	361.4a ± 9.6	34.5a ± 2.3

a Values accompanied by different letters are significantly different at the 95.0% confidence level (*p*-value 0.05)

The two main parameters that define photosynthesis capacity are the CO_2 concentration and PAR radiation. Mean CO_2 concentrations measured were statistically similar in the three greenhouses, whereas PAR radiation was statistically higher in the greenhouse 1, as consequence of the different curvature of the roof (wider spans than in greenhouses 2 and 3). As consequence, photosynthesis was greater in greenhouse 1 but without statistical significance.

Temperature measured at the surface of the plants leaf, was higher in greenhouse 3 (PS+NV). The lower values of CO_2 concentration and PAR radiation and the greater leaf temperature observed in greenhouse 3 produced a reduction on photosynthetic activity (Table 4). The increase of plant temperature above the optimum favoring photorespiration reducing photosynthesis (Bar-Tsur *et al.,* 1995).

3.3. Effect of different climate control systems on production

The marketable production harvested in the three greenhouses was very similar (Figure 2), with differences lower than 10%. Greater production was observed in the greenhouse 3 equipped with the pad-fan system, where the exposure of tomato crop to excessive temperatures greater than 37 ºC was significantly lower (Table 3).

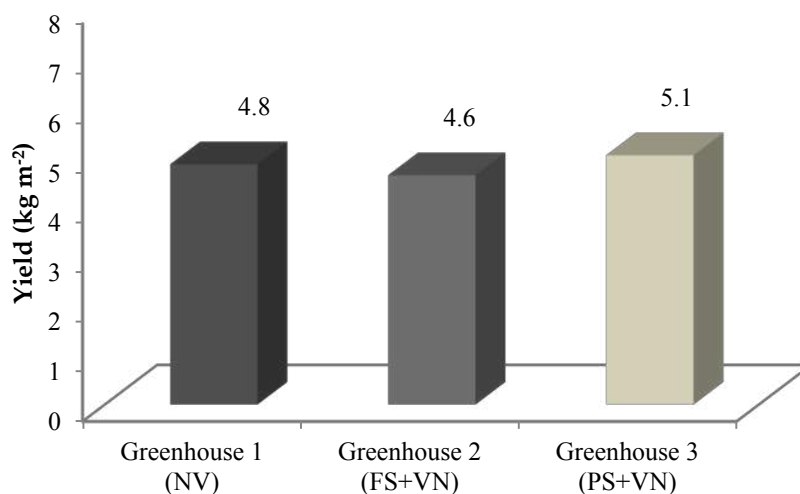Figure 2. Marketable yield obtained in the experimental sectors under the influence of the different cooling systems. Natural ventilation NV, fog system FS and pad-fan system PS.

Tomato production was not significantly increased in greenhouses with the active cooling systems analysed in this work. Even production developed in the greenhouse 1 with wider spans and only natural ventilation was greater than in

greenhouse 2 with fog system, but with lower spans width that reduced PAR radiation. In previous works developed in regions with high relative humidity, water evaporative cooling does not improve the production of tomato crops (Max *et al.,* 2009). In addition, it should be noted that greenhouse 1 has a larger ventilation area and several authors have reported increases in production related to the increase in ventilation surface (Zwart, 1996; Vanthoor *et al.,*2008; Molina-Aiz *et al.,* 2017)

4. Conclusions

In this work the effect of different cooling systems on inside microclimate of greenhouses, tomato production and photosynthetic activity has been analysed. The use of active evaporative cooling systems, pad-fan or fog, combined with natural ventilation was compared to the use of only natural ventilation. From the results obtained the following conclusions can be drawn.

1. Pad-fan cooling systems complementing roof natural ventilation can improve tomato production in spring-summer crop cycles in greenhouses of the Mediterranean area, as consequence of the reduction of the time the crop is exposed to excessive temperature (greater than 37ºC).

2. The increases of span width (from 8 to 9 m) and the ventilation capacity (from 17 to 19% of soil surface) have a similar effect on tomato production that the use of fog cooling system as complement of natural ventilation.

Acknowledgements

References

Adams, S. R., Cockshull, K. E., Cave, C. R. J., 2001. Effect of temperature on the growth and development of tomato fruits. Annals of Botany. 88(5) 869–877. https://doi.org/10.1006/anbo.2001.1524.

Allen Jr., L.H., Amthor, J.S, 1995. *Plant physiological responses to elevated CO₂, temperature, air pollution, and UV-B radiation.* In: Woodwell, G.M., Mackenzie, F.T. (Eds.), Biotic Feedbacks in the Global Climatic System: Will the Warming Feed the Warming? Oxford Univ. Press, Oxford, New York, pp. 51–84.

Arbel, A., Yekutieli, O., Barak, M.,1999. Performance of a fog system for cooling greenhouses. Journal of Agricultural Engineering.2, 129-136. https://doi.org/10.1006/jaer.1998.0351.

Arbel, A., Barak, M., Shklyar, A., 2003.Combination of forced ventilation and fogging systems for cooling greenhouses. Biosystem Engineering. 84 (1),45-55. 10.1016 / S1537-5110 (02) 00216-7.

Bakker, S., Adams, S., Boulard, T., Montero, J.I.,2008. Innovative technologies for an efficient use of energy. Acta Horticulturae.15,25-36. 10.17660 / ActaHortic.2008.801.1.

Bar-Tsur, A., Rudich, J., Bravdo, B.,1995. Pho-tosynthesis, transpiration and stomatal resistance to gasexchange in tomato plants under high temperatures. Hortscience. 60 (3), 405-410. https://doi.org/10.1080/14620316.1985.11515645.

Camejo, D., Rodríguez, P., Morales, M.A., Del´Amico, J.M., Torrecillas, A., Alarcón, J.J., 2005. High tempetature effects on photosynthetic activity of two tomato cultivars with different heat susceptibility. Journal of Plant Physiology. 162,281-289. 10.1016/j.jplph.2004.07.014 .

Ceulemans, R., Taylor, G., Bosac, C., Wilkins, D., Besford, R.T., 1997. Photosynthetic acclimation to elevated CO₂ in poplar grown in glasshouse cabinets or in open top chambers depends on duration of exposure. Journal of Experimental Botany. 48 (314), 1681–1689. 10.1093 / jxb / 48.9.1681.

De Zwart, H.F.,1996. Analyzing energy-saving options in greenhouse cultivation using a simulation model. MS. Thesis, Wageningen University, The Netherlands.

Domínguez, E., Cuartero, J., Fernandez-Muñoz, R., 2005. Breeding tomato for pollen tolerance to low temperatures by gametophytic selection. Euphytica, 142 (3), 253–263. https://doi.org/10.1007/s10681-005-2042-0.

Franco, A., Valera, D.L., Peña, A., Pérez, A.M., 2011. Aerodynamic analysis and CFD simulation of several cellulose evaporative cooling pads used in Mediterranean greenhouses. Computers and Electronics in Agriculture.76, 218–230. 10.1016/j.compag.2011.01.019.

González-Real, M.M, Baille, A., 2006. Plant Response to Greenhouse Cooling. Acta Horticulturae 719, 427-438. 10.17660/ActaHortic.2006.719.48.

Hand, D.W., Warren Wilson, J., Acock, B., 1993. Effects of light and CO_2 on net photosynthetic rates of stands of aubergine and amaranthus. Annals of Botany. 71, 209–216.

Jiang, C., Johkan, M., Hohjo, M., Tsukagoshi, S., Ebihara, M., Nakaminami, A., Maruo, T.,2017. Photosynthesis, plant growth, and fruit production of single-truss tomato improves with supplemental lighting provided from underneath or within the inner canopy. Scientia Horticulturae. 222, 221–229. 10.1016/j.scienta.2017.04.026.

Katsoulas, N., Savvas, D., Tsirogiannis, I. Merkouris, O. Kittas, C., 2009. Response of an eggplant crop grown under Mediterranean summer conditions to greenhouse fog cooling. Scientia Horticulturae.123, 90–98. 10.1016/j.scienta.2009.08.004.

Kim, Y.H., Kozai, T., Kubota, C., Kitaya, Y.,1996. Effects of air current speeds on the microclimate of plug stand under artificial lighting. Acta Horticulturae. 440, 354–359. 10.17660/ActaHortic.1996.440.62.

Kitaya, Y., Shibuya, T., Kozai, T., Kubota, C., 1998. Effects of light intensity and air velocity on air temperature, water vapour pressure and CO_2 concentration inside a plant canopy under an artificial lighting condition. International Journal of Earth Space. 5(2), 199–203.

Kitaya, Y., Tsuruyama, J., Shibuya, T., Yoshida, M., Kiyota, M.,2003. Effects of air current on gas exchange in plant leaves and plant canopies. Annals of Botany. 23 (89), 195–199. 10.1016 / s0273-1177 (02) 00747-0.

Kittas, C., Draoui, B., Boulard, T., 1995. Quantification of the ventilation rate of a greenhouse with a continuous roof opening. Agricultural and Forest Meteorology. 77, 95-111.

Liu, G., Li, J., Du, Q., 2017.Interactive effects of nitrate-ammonium ratios and temperatures on growth, photosynthesis, and nitrogen metabolism of tomato seedlings. Scientia Horticulturae. 214,41-50. https://doi.org/10.1016/j.scienta.2016.09.006.

Luchow, K., Von Zabeltitz, C., 1992. Investigation of a spray cooling system in a plastic-film greenhouse. Journal of Agricultural Engineering Research.52, 1-10. https://doi.org/10.1016/0021-8634(92)80046-U.

Max, J., Horst, W., Mutwiwa, U., Tantau, H.J., 2009. Effects of greenhouse cooling method on growth, fruit yield and quality of tomato (*Solanum lycopersicum* L.) in a tropical climate. Scientia Horticulturae.122, 179–186. https://doi.org/10.1016/j.scienta.2009.05.007.

Molina-Aiz, F.D., López, A., Valera, D.L., 2017. La ventilación natural de invernaderos en climas cálidos (Natural ventilation in greenhouse of warm climates). In I Jornadas de Transferencia HortofrutıCIAMBITAL. Investigación y Experimentación en Ciencias Agroalimentarias en el Sureste Español-2017 (Almeria: Universidad de Almerıa e Investigación CIAIMBITAL), p.13–174.

Montero, J.I., Muñoz, P., Antón, A., Iglesias, N., 2005. Computational Fluid Dynamic modelling of night-time energy fluxes in unheated greenhouses. Acta Horticulturae. 691, 403-409.10.17660/ActaHortic.2005.691.48.

Santiago, J., Mendoza, M., Borrego, F., 1998. Evaluación del tomate (*Lycopersicon esculentum*, Mill) en invernadero: criterios fenológicos y fisiológicos. Agronomía Mesoamericana. 9 (1), 59-65.

Sase, S., 2006. Air movement and climate uniformity in ventilated greenhouses. Acta Horticulturae. 719, 313–323. 10.17660/ActaHortic.2006.719.35.

Shibuya, T., Kozai, T., 1998. Effects of air velocity on net photosynthetic and evapotranspiration rates of a tomato plug sheet under artificial light. Environmental Control in Biology. 36, 131–136. 10.2525/ecb1963.36.131.

Statgraphics Statgraphics®Centurion 18. User Manual. Statgraphics Technologies (https://www.statgraphics.net/wp-content/uploads/2015/03/Centurion-XVI-Manual-Principal.pdf.)

Van Ploeg D., Heuvelink, E.,2005. Influence of sub-optimal temperature on tomato growth and yield: a review. Journal of Horticultural Science and Biotechnology. 80 (6,), 652–659. https://doi.org/10.1080/14620316.2005.11511994.

Valera, D.L., Molina-Aiz, F.D.; Peña, A., 2002. Climatización de invernaderos. Servicio de Publicaciones de la Universidad de Almería, Almería, Spain, 233 p.

Valera, D.L., Belmonte, L.J., Molina, F.D., López, A., 2016. Greenhouse agriculture in Almería. A comprehensive thecno-economic analysis. Cajamar Caja Rural. 2016, 504pp. (Available on line : http://www.publicacionescajamar.es/series-tematicas/economia/greenhouse-agriculture-in-almeria-a-comprehensive-techno-economic-analysis//).

Stanghellini, C., Van Henten, E.J., Gázquez Garrido, J.C., 2008. The combined effects of cover design parameters on tomato production of a passive greenhouse. Acta Horticulturae. 801, 383–392. https://doi.org/10.17660/ActaHortic.2008.801.40.

Wadsworth, F., 1959. Tropical Silviculture. Forest Science. 5 (2), 137. https://doi.org/10.1093/forestscience/5.2.137.

Willits, D.H., Peet, M.M., 2000. Intermittent application of water to an externally mounted, greenhouse shade cloth to modify cooling performance. Transaction of the ASAE, 43 (5) 1247–1252. 10.13031/2013.3018.

Yin, X., Harbinson, J., Struik, P.C., 2009. Mathematical review of literature to assess alternative electron transports and interphotosystem excitation partitioning f steady-state C3 photosynthesis under limiting light. Plant, Cell and Environmental. 29 (9),1771–1782. 10.1111/j.1365-3040.2006. 01554.x.

The 'Manure Shuffle': a System for Frequent Removal of Fine Manure Particles from the Foraging Area of Poultry Houses

Dr. A.P. (Bram) Bos [1] [*], **Ir. Yvo S.M. Goselink** [1], **Dr. Ir. Bastiaan A. Vroegindeweij** [2]

[1] Wageningen Livestock Research, Wageningen, The Netherlands
[2] Livestock Robotics, Ochten, The Netherlands
* Corresponding author: bram.bos@wur.nl

Abstract

Non-cage laying hen houses allow expression of natural behaviours by chicken like foraging and dust-bathing, and are regarded as better for animal welfare than cage systems. An important drawback is their higher indoor concentrations as well as emissions of particulate matter (PM) and ammonia. The use of dried manure as a substrate for these natural behaviours is the main cause. Animal behaviour causes fine manure particles to be released into the air. In addition, manure is a source of ammonia.

We present a novel solution: the 'manure shuffle'. The manure shuffle is a device that moves frequently under a more durable, non-manure substrate suitable for foraging behaviour. Manure will dry and decompose into smaller particles, which percolate through the substrate because of the movement of the manure shuffle, foraging behaviour of the chicken and the larger particle size of the substrate. The small manure particles are collected inside the shuffle through a perforated upper surface and discarded at the end of the barn.

The most important benefit of the manure shuffle is that it removes dry manure from the barn on a daily basis, while still providing a suitable environment for natural behaviours. We expect that the system will have a profound impact on the PM release inside and from the house, since PM is (1) isolated from the behaviour of chickens in and under the substrate, and (2) frequently removed from the living area. Additionally, ammonia emissions might be lower as well because of the lower amount of manure present. Further benefits include the prevention of out-of-nest eggs, a more hygienic living area, and the potential to make a much more engaging foraging area. This may positively impact animal health and welfare.

We describe the way this solution originated from an interactive design process based on the Reflexive Interactive Design-approach (RIO) and was further developed in several iterations to a functioning demo-unit. Furthermore, we report on initial test in a poultry house.

Keywords: Manure removal, poultry, particulate matter

1. Introduction

Particulate matter (PM) is a risk to public health, and for that reason the European Union (European Directives 1996/62/EC, 1999/30/EC, and 2008/50/EC) has set limit values for PM in ambient air. Important sources of PM in the Netherlands are traffic, industry and livestock production. In the case of livestock production, particulate matter will consist of organic matter, to which inflammatory endotoxins may be attached as well. These particles threaten the health of farmers and workers (Eduard et al., 2004, Eduard et al., 2009, Omland, 2002, Seifert et al., 2003) and animals (David et al., 2015) that are chronically exposed inside the barns, and may affect the people living in the vicinity of these barns as well.

Non-cage poultry farms (especially laying hen farms) have a relatively high share in total livestock emission of PM because dried manure is used as a substrate to enable several natural behaviours of chicken, like foraging and dust-bathing. While beneficial for animal welfare, this solution thus has adverse effects on human and animal health. Therefore, the Dutch ministry of Agriculture (LNV) has expressed its ambition to implement binding regulation in the future to reduce PM emissions from poultry houses by 50 to 70%, for existing and newly built farms respectively.

EU regulation prescribes that the living area in non-cage poultry houses is permanently covered by a (litter) substrate for 33% (for laying hens) or 100% (broilers) of the total (indoor) living area. This (litter) substrate is meant to provide an adequate surface to allow for important natural (ethological) behaviours of chicken to be expressed, namely exploration, foraging and dust bathing. The specific material of this (litter) substrate is not prescribed. In almost every poultry farm, the substrate is primarily the (dried) manure of the chickens themselves, since this is the cheapest way to fulfil the requirement. An important drawback of this solution, however is the production and release of particulate matter (PM) and ammonia (NH_3) from the litter bed (Van Harn et al., 2012, Aarnink, 2011 #1532). Ammonia will be formed from the manure below a dry matter (DM) content of around 80%, while particulate matter (also called 'fine dust') $\leq$ PM10 will be present in the (manure) litter if it is dryer. In practice, the (manure) litter bed may however very well consist of a very dry top layer, while having a more humid character below the surface, thus being a source of ammonia and PM at the same time. Ammonia may be released by diffusion alone, but PM is released into the indoor air

predominantly by the scratching behaviour of chicken during day time.

Ammonia, if emitted from the house, is damaging local and regional biodiversity if deposited in natural areas that are or should be nitrogen poor, causing eutrophication of natural habitats, and acidification of surface waters. It furthermore is a precursor for secondary particulate matter. Particulate matter itself is a threat for public health. Because free range systems use dried manure as a foraging substrate, the release in and emission of particulate matter in these housing systems is very high.

An evident solution, that would tackle the problem at its source, would be to regularly remove all manure from the foraging area. However, this would also remove the legally and ethologically required substrate from the surface, thereby necessitating regular replenishment by fresh substrate like wood shavings or lucerne. This would add significant exploitation costs, on top of the required and significant investments in removal systems for large surfaces.

An alternative solution that mitigates a part of the problem is the application of a manure shove or scraper in foraging areas, especially under the housing interior of aviary houses. This shove removes the top layer of the (manure) litter bed to limit its thickness to approximately 3 cm. The manure shove typically consists of a number of V-shaped arms that stretch out when moved forward by a cable, and stretch in when moved back, thus moving the litter to one side of the house, where it can be collected and removed. This manure shove is applied for two reasons: to reduce the amount of manure in the foraging area and to prevent the number of 'out-of-nest-eggs', laid by laying hens in those places instead of the laying nests. This will reduce PM and ammonia emissions by approximately 25-35% (Mosquera et al., 2016), if the source amount is reduced to a thickness of 2-3 cm of manure litter.

We present a different approach to solve this issue, by providing a different and semi-permanent substrate that is suitable for foraging behaviour, and at the same time enables the frequent removal of finer manure particles that result after chicken droppings have been drying and decomposed. The so called 'manure shuffle' is a device to accomplish this manure removal by moving gently under this alternative substrate and transporting the collected manure particles to a deposit.

1.1. Principle of the manure shuffle

The manure shuffle as a device is part of an arrangement that entails a semi-permanent substrate suitable for foraging behaviour (for instance organic material containing a high level of lignine, like small wood chips), with an average diameter of ± 4-6 mm. The substrate layer can have a thickness of 3-10 cm or even more to enable even better animal welfare. The manure shuffle itself is a trapezoid construction of limited height (about 1.5 cm, at least two times lower than the substrate layer itself) that is moved back and forth under the substrate layer several times per day. The manure shuffle has slopes on both sides to lessen the friction in moving through the substrate layer. The top of the manure shuffle is covered with a grate of meshwire, that allows finer particles to fall through, but keeps the substrate particles on top.

Fresh manure deposited by the chicken on the substrate layer will dry in a couple of hours and break into smaller parts by the scratching behaviour of the chickens. Smaller parts will fall down between the larger substrate particles (*percolation*).

The movement back and forth through the substrate layer of the manure shuffle mechanically induces further percolation of the finer (manure) particles through the substrate layer to the bottom, by gently moving and shuffling the substrate when passing.

The finer particles are collected in the space under the manure shuffle, below the grate, and moved along with the manure shuffle itself to a deposit at the end of the track. There the shuffle is emptied, for instance by positioning the shuffle on a grated surface with a storage or conveyor belt underneath. The empty manure shuffle then returns on its track to the other end point.

The most important benefit of the manure shuffle is that it removes dry manure from the house frequently (daily or hourly), while still providing a suitable environment for natural behaviours. In poultry houses, the source of particulate matter is predominantly dry manure. Particles are released from the foraging area into the inside air by chicken behaviours like scratching and dustbathing, and subsequently emitted from the house by the ventilation system. Therefore, we expect that the system will have a significant impact on the PM release inside and subsequent emissions out of the house, since PM is (1) isolated from the behaviour of chickens in and under the substrate, and (2) frequently removed from the living area. Additionally, ammonia emissions can be expected to be lower as well because of the drier litter bed and the lower amount of manure present. Further benefits include the prevention of out-of-nest eggs, a more hygienic living area, and the potential to make a much more engaging foraging area. This may positively impact animal health and welfare.

2. Materials & Methods: the design process

The idea of the manure shuffle originates from an interactive design session in June 2018 with poultry farmers,

manufacturers, an animal welfare activist and scientists. This session followed the approach of Reflexive Interactive Design (RIO, in Dutch), a structured design approach (Elzen and Bos, 2019, Bos et al., 2009, Bos et al., 2011) that is developed in the context of Dutch livestock production science in order to reconcile seemingly conflicting societal, economical and environmental goals. One of the key design challenges was to enable and enhance animal welfare in laying hen houses, while improving indoor air quality, and drastically reducing the emissions of PM and ammonia.

Part of the preparatory work for the design process is a system analysis, and the formulation of a brief of requirements for the most important actors in and around the system, like the farmer, the laying hen and the consumer/citizen. Based on this work it was already known (and presented during the session) that the main source of PM was dry manure (Aarnink et al., 2011, Cambra-López et al., 2011), while the requirements of the laying hen (Van Weeghel et al., 2020) for foraging and dust bathing were also qualitatively and quantitatively defined (see Table 1 for an excerpt). Air quality and labour requirements for the farmer were also known in advance.

Table 1: Excerpt from the Brief of Requirements of the Laying Hen 2020.
Source: Table 4 in (Van Weeghel et al., 2020)

	Need	*Requirement*	*Quantity*
LF4	Foraging substrate	Suitable substrate (quantity)	> 10 cm thick
LF5		Suitable substrate (quality)	Loose particles that can be manipulated by beak and legs

During the session, one of the key functions identified by the participants was to 'remove manure from the foraging area (frequently)'. A number of ideas then originated to perform this function, like frequent removal from the manure litter bed and replacing it with a fresh substrate, frequent removal of a substrate with manure from the house, cleaning it and reintroducing the cleaned substrate into the house, but one young poultry farmer also proposed the idea of isolating the finer manure particles from the bigger ones by providing a layer of plant based organic particles with a larger size (as visualized during the session by a visual designer in Figure 1 - left). The process of distribution of finer and bigger particles over a vertical gradient is known as percolation.
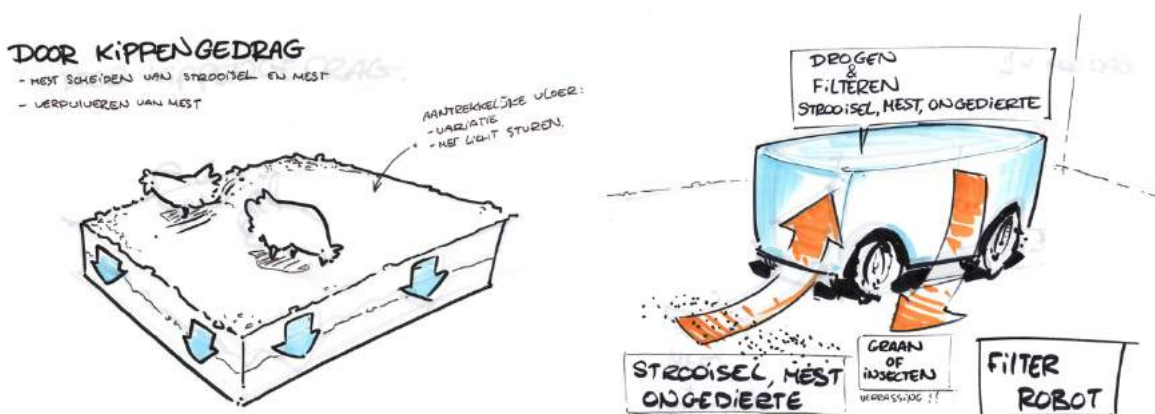
Figure 1. Left: visualisation of the first idea of percolation to vertically separate fine manure particles from another substrate with bigger particles. Right: visualisation of a cleaning robot that could clean a substrate from fine manure particles, while performing other functions like spreading small treats for the animals. Source: Interactive Design Workshop, June 2018.

This would not remove the manure per se, but would block the release into the air by animal behaviour. In a subsequent idea, a cleaning robot (similar to PoultryBot for floor eggs (Vroegindeweij et al., 2018)) would roam around in the substrate to filter out the fine manure particles to be eventually discarded at a special exit point (Figure 1- right).

After the design session, the idea was further elaborated through a more thorough functional analysis of a substrate cleaning system based on the process of percolation, as well as an external substrate cleaning system. Parallel to this, a pilot experiment was performed in a poultry house to test the suitability of different kinds of substrates for foraging behaviour (Neijenhuis et al., 2019), as remarkably little was known about this. It was concluded from the pilot experiment that a variety of materials might be suitable, with a preference for smaller, more easily manipulable and moveable particles on the one hand, and new or interesting materials on the other.

The results of the functional analysis and the pilot experiment were then shared and discussed with a group of poultry farmers during a special session in June 2019. They expressed their preference for an in-house cleaning option, rather than an external one for reasons of simplicity and cost-effectiveness, and pointed out that a moving collecting

structure would be preferred over a fixed separating structure that covers the whole area. It was further suggested to adopt the moving principle of the already known manure scraper, to speed up adoption by farmers, since this technique was already known and applied in practice. A hoover moving under the substrate was suggested as well.
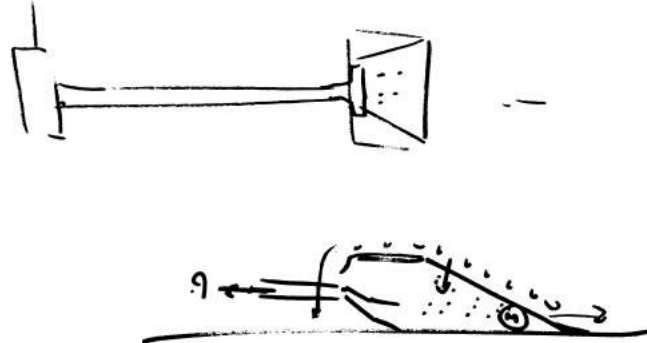
Figure 2: Rough sketch of a filtering device that moves under an alternative substrate and is connected to a hoovering tube. Source: Evaluation workshop with poultry farmers, June 2019.

Based on this input a new iteration of the concept design was made by the authors (Figure 3).

Figure 3: First part of further iteration of the concept design, Nov 2019: a moving structure with a grated top that collects fine particles by moving under a substrate. Source: authors' internal document.

A few months later the principle was tested using wooden boxes of 2x1x0,2m (LxWxH) filled with beech clippings of 6-8 mm in size, and dry manure from a poultry farm applied on top of that (Figure 4). A simple triangular structure of 4x1 cm (LxH) with a grated diagonal (Figure 5) was moved manually under the beech clippings a few times, and then (Figure 6). This showed that the dry manure particles were indeed traveling down through the substrate, facilitated by the agitation induced by the movement of the structure, and were subsequently collected inside the structure.

Figure 4: Wooden box filled with beech clippings and dry manure spread over the top

In order to perform a live test of the principle for a longer time, a mechanized prototype was built, consisting of two units of 4,6 x 0,97 m. (Figure 7). In each unit a manure shuffle was placed (Figure 8), and connected by chains to a drive unit in the middle of the setup. The units allowed for a substrate layer of ± 5 cm thickness. While disposal of the collected manure was originally designed to be done in the middle part, outside the units, this was changed eventually to a grated area at the end of the unit where manure particles could fall down in a separate container.

Figure 5: Detailed view of the first prototype, used to be moved manually under the beech clippings

Figure 6: Prototype is emptied after being moved manually back and forth two times under the beech clippings
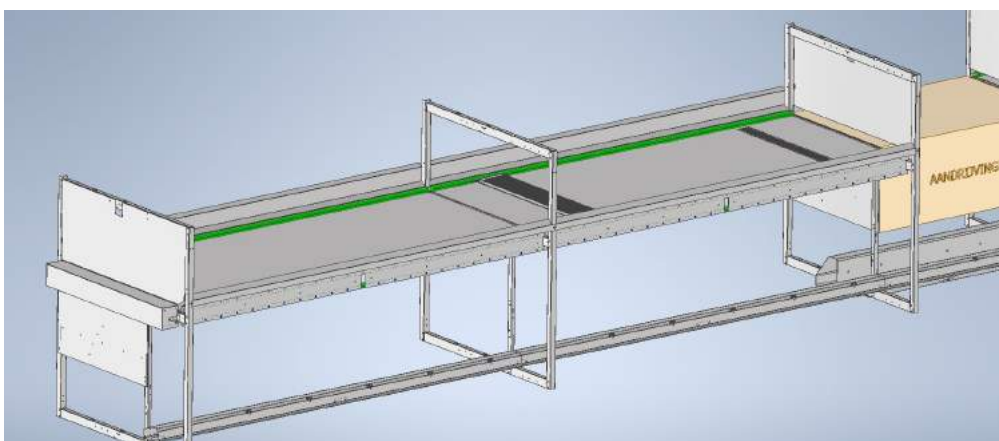
Figure 7: Technical drawing of the left part of the demo unit and the drive train ('aandrijving') in the middle. The dark grey rectangle in the middle is the trapezoid manure shuffle, that is moved back and forth by chains along the long sides. The smaller dark grey rectangle on the right is the grated area in the bottom of the unit where collected manure is deposited.

Figure 8: Close up of the manure shuffle in the demo-unit under the beech clippings (taken from the non-functioning (control) unit, but similar to the one in the functioning unit).

After further adjustment of the mechanics and the controls, the prototype was installed in April 2021 in a small poultry house in Barneveld (the Netherlands) of 2x500 layers for live testing (Figure 9).

Figure 9: Rear view of one of the two units as installed in the pilot farm.

3. Results and Discussion

At the time of submission of this paper (June 2021), the prototype has been tested for 8 weeks. A timer initiated and ended the movement of the manure shuffle for five times during daytime, lasting 4 minutes which allows for 2 complete movements back and forth over the unit. Manure particles collected in the containers below the units were weighed daily during weekdays.

During the first two weeks regular malfunctions to the mechanics occurred, which led to the decision to stop moving the manure shuffle in one of the units, to allow for a more robust functioning in the other one. Thus, the results below pertain to one of the two units in the prototype. The other serves as a control case, to observe the effect of a substrate alone on vertical particle distribution.

We shortly report on the first observed tests results, that are still preliminary and not rigorously case-controlled as the test was primarily meant as a proof-of-principle.

Ambient conditions: During the experiment, ambient temperature varied between 15 and 27 ˚C with an average of 20,7 ˚C. There was a clear daily pattern containing a temperature rise of 2 to 5 degrees in daytime. Relative humidity averaged at 56% and ranged between 40 and 70%, with a less clear daily pattern.

Animal behaviour: laying hens make use of the foraging substrate on the demo-unit at the same densities as they do in the traditional manure-litter (see Figure 10). Behaviours like scraping and pecking are regularly observed. The (young) animals are calm and do not express fear when the shuffle is moving below the substrate. Shuffling of the substrate functions as a trigger for animal foraging, with hens directly exhibiting more of this behaviour during and after activation of the shuffle.

Figure 10: Representative picture of foraging behaviour and animal density on the demo-unit

Manure collection: the shuffle collected dry manure in the container below the functioning unit at one end. Each day an average of 220 gr with a DM of around 90% was harvested.

Drying and disintegration of manure: after eight weeks the substrate still consisted mainly of beech chips, with occasional (almost fresh) manure droppings in between. No build-up of manure in the substrate was detected, nor were there any aggregates of manure and wood chips. Fine particles in both units could be found, but only on the bottom of the substrate.

Manure collection efficiency: after a month samples (425-480 grams each) were taken from the substrate using a cylinder of ø 12,5 cm that was pushed through the substrate to the bottom. Content was isolated by pushing a small piece of metal under the cylinder, and then transferred to a box. This was done three times over the width of the unit, and repeated at three different places over the length of each of the two units. Samples were separated into a fraction with fine particles (< 2 mm) and a fraction with bigger particles. Both fractions were weighed. In the functioning unit the finer particles accounted for 1,4% of the weight, whereas in the non-functioning unit they accounted for 15,1% of the weight. Under the assumption that both units where used in similar intensity by the animals, we can conclude that the manure shuffle was able to collect around 90% of the manure produced over the first month. This percentage will of course likely increase over time, as fine particles will accumulate further in the non-functioning unit.

Dust release: the setting of the demo unit in a larger poultry house made it impossible to test the difference in dust release between laying hens foraging on the substrate and foraging on the traditional manure litter. We plan to test the release potential of the substrate and litter manure, for example by letting a heavy object (500 grams) fall from 0.5 m on the surface, and determine the dust released by the impact. This in accordance with the simulation done by (Derakhshani et al., accepted for publication 2021). However, by the time of submission of this paper this experiment was not executed.

Yet, it is already visually apparent that the top of the substrate layers in both units does not bear any amount of loose fine particles, as is the case in the traditional manure litter in the rest of the house. As (Derakhshani et al., accepted for publication 2021) shows, dust will only be released from the litter bed if an external mechanical force (like a scraping hen's foot) is applied. It thus is rather implausible that dust will be released from the units with the alternative substrate, where the fine particles are removed (functioning unit), or isolated at the bottom (non-functioning unit), but this has to be confirmed in further tests.

4. Conclusions

The principle of the manure shuffle turned out to be working as foreseen in a test with live chicken over 7 weeks. The substrate of beech chips is indeed suitable for enabling foraging behaviour of the chicken, and is actually used for that. The substrate enables percolation of the finer particles to the bottom of the substrate. The comparison between a functioning and a non-functioning unit showed that percolation may be stimulated by the movement of the manure shuffle, but is not dependent on it. In both units manure dried and disintegrated, facilitated by the mechanical forces exerted by the scratching / activity of the chicken, and in both units fine particles travelled down. The manure shuffle was able to collect the fine particles in significant amounts, with a good efficiency of about 90%. The (at least visual) lack of fine particles at the top of the substrate in both units, and the removal efficiency in the functioning one, make it plausible that the manure shuffle will reduce the release of particulate matter into the inside air by the behaviour of the animals, but this has to be further tested in a controlled situation.

The drive train of the demo unit turned out to be quite fragile. In the current setup, the mechanical forces needed to

move the manure shuffle under a load of wood chips are quite high, variable and even unpredictable to some extent, which is due to the wood chips negatively interfering with the functioning of the chains and cogs. We do not see this as a fundamental limitation for the principle, as this can easily be solved by changing to a different type of drive train.

The manure shuffle will be further developed for application in existing poultry farms, on the existing (mostly concrete) floors.

Acknowledgments

References

Aarnink, A.J.A., Cambra-López, M., Lai, H.T.L. & Ogink, N.W.M. 2011. Deeltjesgrootteverdeling en bronnen van stof in stallen. Wageningen/Lelystad: Wageningen UR Livestock Research.

Bos, A.P., Groot Koerkamp, P.W.G., Gosselink, J.M.J. & Bokma, S.J. 2009. Reflexive Interactive Design and its application in a project on sustainable dairy husbandry systems. *Outlook on Agriculture,* 38**,** 137-145.

Bos, A.P., Spoelstra, S.F., Groot Koerkamp, P.W.G., De Greef, K.H. & Van Eijk, O.N.M. 2011. Reflexive design for sustainable animal husbandry: mediating between niche and regime. *In:* Spaargaren, G., Loeber, A. & Oosterveer, P. (eds.) *A transition perspective on sustainable food and agriculture.* London: Routledge.

Cambra-López, M., Hermosilla, T., Lai, H.T.L., Aarnink, A.J.A. & Ogink, N.W.M. 2011. Particulate matter emitted from poultry and pig houses: Source identification and quantification. *Trans. ASABE,* 54**,** 629-642.

David, B., Moe, R.O., Michel, V., Lund, V. & Mejdell, C. 2015. Air quality in alternative housing systems may have an impact on laying hen welfare. Part I—Dust. *Animals,* 5**,** 495-511.

Derakhshani, S.M., Ogink, N.W.M., Bos, A.P. & Groot Koerkamp, P.W.G. accepted for publication 2021. Sensitivity analysis of the spreading of fine dust from litter in poultry houses. *Biosystems Engineering*.

Eduard, W., Douwes, J., Omenaas, E. & Heederik, D. 2004. Do farming exposures cause or prevent asthma? Results from a study of adult Norwegian farmers. *Thorax,* 59**,** 381-386.

Eduard, W., Pearce, N. & Douwes, J. 2009. Chronic bronchitis, COPD, and lung function in farmers: The role of biological agents. *Chest,* 136**,** 716-725.

Elzen, B.E. & Bos, A.P. 2019. The RIO approach: Design and anchoring of sustainable animal husbandry systems. *Technological Forecasting and Social Change,* 145**,** 141-152.

Goselink, Y.S.M., Blaauw, S.K., Bos, A.P. & Derks, M. 2020. *Manure removal device*. EP20193172.2.

Van Harn, J., Ellen, H., Veldkamp, T. & Aarnink, A. 2012. Effects of housing and management on ammonia emissions from laying hen, broiler, turkey and duck houses. Wageningen: Wageningen UR Livestock Research.

Mosquera, J., Van Emous, R., Van Hattum, T., Nijeboer, G., Hol, J.M.G., Van Dooren, H.J. & Ogink, N.W.M. 2016. Effect van strooiselverwijdering bij leghennen in volièrehuisvesting op de emissie van ammoniak, geur, broeikasgassen en fijnstof. Wageningen: Wageningen Livestock Research.

Neijenhuis, F., Van Wijhe-Kiezebrink, M.C. & De Jong, I.C. 2019. Substraat voorkeur voor forageergedrag leghennen: pilot studie. Wageningen: Wageningen Livestock Research.

Omland, Ø. 2002. Exposure and respiratory health in farming in temperate zones - A review of the literature. *Ann. Agric. Environ. Med.,* 9**,** 119-136.

Seifert, S.A., Von Essen, S., Jacobitz, K., Crouch, R. & Lintner, C.P. 2003. Organic dust toxic syndrome: A review. *Clinical Toxicol.,* 41**,** 185-193.

Vroegindeweij, B.A., Blaauw, S.K., Ijsselmuiden, J.M.M. & Van Henten, E.J. 2018. Evaluation of the performance of PoultryBot, an autonomous mobile robotic platform for poultry houses. *Biosystems Engineering,* 174**,** 295-315.

Van Weeghel, H.J.E., De Jong, I.C., Van Niekerk, T.G.C.M. & Bos, A.P. 2020. Programma van Eisen van de leghen 2020: Ontwerpen voor een goed dierenwelzijn. Wageningen: Wageningen Livestock Research.

The D5 Silo of Manganeses de la Lampreana (Zamora): History, Construction Characteristics and Technology

Víctor Marcelo [a,*], José B. Valenciano [b], Javier López [b], Pablo Pastrana [b]

[a] Dpto. Ingeniería y Ciencias Agrarias, Universidad de León, Avda. Astorga S/N, 24401 Ponferrada (León). Spain.

[b] Dpto. Ingeniería y Ciencias Agrarias, Universidad de León, Avda. Portugal 41, 24071 León. Spain.

* Corresponding author. Email: v.marcelo@unileon.es

Abstract

Spain's National Network of Silos and Granaries (NNSG) were built in 1951–1990 building a total de 665 silos and 285 granaries. 20 different typologies of silos were built, highlighting type D over all of them with a total of 389 units. This typology prolonged its construction for 34 years, appearing several subtypes (D1, D2, D3 D4 y D5). The Manganeses de la Lampreana silo (Zamora) is a D5 type silo with 3,350 t of storage capacity, distributed in 24 storage tanks called cells, built in 1968. This silo is a Reception silo whose objective was to be close to the farmers and transfer the cereal from it to the larger Transition and Reserve silos. Architecturally speaking it is a simple and powerful silo. It has a rectangular shape, made up of three rows of square cells, the outer rows of cells rested directly on the ground storey floor and the centre row is raised. Front tower between two cells, being embedded between them in a central position, achieving a compact and robust volume. Together with the D4 subtype it represents the classic image of an NNSG silo. The structure is made up of reinforced concrete pillars at the corners of the cells and the cell walls of reinforce bricks. It is finished off with a flat roof. Technologically speaking it has many similarities with its predecessors, types A and B. Here the elevator receives the grain directly from the reception hopper raising wheat and emptying it onto an upper horizontal belt conveyor, where dampers motorised valves, it is distributed across other tubes to one of the three cells in each bay. The grain is unloaded onto lower horizontal belt conveyors lying at different heights depending on whether the cells stand off (central) or on (side) the floor. From there it is carried to a raised cell for bulk offloading onto a lorry. It also has a cereal cleaning system in case it is necessary. In addition, the silo has vacuum dust collection systems.

Keywords: storage unit, grain store, wheat, industrial architecture, industrial heritage.

1. Introduction

The storage of wheat as a raw material for human consumption has been done since ancient times (Tucci, 2012). A turning point in this type of storage came with the invention of the grain elevator by J. Dart´s in 1843, going from traditional granaries or horizontal storage units (HSU) to silos or vertical storage units (VSU). (Salido, 2011; Fernández-Fernández, 2016). In Spain, in order to ensure the supply of wheat, the state created the Servicio Nacional del Trigo (national wheat service, SNT) (BOE, 1937; Tortella, 1994; Valls et al., 2015) that applied a regulatory and interventionist policy. The SNT around 1945 elaborated the General Plan of the Spain's National Network of Silos and Granaries (NNSG) to build silos and granaries throughout the country where wheat can be stored (SNT, 1947; SNT, 1950; SNT, 1959; SENPA, 1978; SENPA, 1994). Four different groups of silos were built depending on their function:

- • Receipt. Close to the farmer and with less capacity. Includes 11 typologies (A, B, C, D, E, F, GV, H, J, MC and MR).

- • Transition and Reserve. In strategic places, with greater capacity, to receive the cereal from the receipt silos. 6 typologies (TR, TC, TE, TH, TV and TF).

- • Port silos. With functions similar to Transition and Reserve silos located in ports. One typology (P).

- • Seed selection. To select and condition seed for subsequent sowing. Two typologies (SV and SA).

With Spain's accession to the European Economic Community, the use of silos was reduced to a minimum, being 2002 the last year in which many of them were used. The Spain's agricultural guarantee fund, the Fondo Español de Garantía Agraria (FEGA) transferred the responsibilities of the silos to the regional governments (Spain's 'autonomous communities'), recovering control in 2014 (BOE, 2014) causing many to be in a process of abandonment and deterioration. Some of them were leased by farm cooperatives and a number of private companies for grain storage. This is the case of the Silo type D5 of Manganeses de la Lampreana (Zamora). To this day, it is used by the cooperative COBADU store grain or as pick-up sites for onward shipment.

The objective of the work was trace the history of D5 silo of Manganeses de la Lampreana, analyse their construction characteristics and technology. The information gathered is valuable for anyone wishing to learn more about these buildings and would be highly useful for projects designed to conserve and find new applications for this segment of the agro-industrial heritage.

2. Materials and Methods

In the present work, information has been collected from the cereal storage silo belonging to NNSG in Manganeses de la Lampreana (Zamora). Research began with data collection from the FEGA archives in Madrid and data records on file with the regional government of Castilla y León at Valladolid. In the second phase, detailed photographs of the silo were taken and information was collected on its characteristics; which were grouped as follows:

• General features: geolocation, year of construction.

• Architectural features: typology; capacity (t); ground plan and roof shape; tower position; number of cell rows; number of cells; shape of cells; cell material; cell row position relative to the ground.

• Technological facilities: including existence of: weighbridge (t); railway; dust suction system; seed cleaning and selection machinery; thermometric probes; gas dosage system; refrigeration facilities; lift; on-site high-voltage line and substation; and information on; machinery capacity (t/h); No. elevators; No. upper storey horizontal conveyors.

In addition, to supplement the information silo manager were interviewed as described by Fuentes et al. (2015).

3. Results and Discussion

The SNT began the construction of Spain's National Network of Silos and Granaries (NNSG) in 1951. FEGA built the last silo in the NNSG in Valchillón, Córdoba in 1990. In these period (1951–1990) were building a total de 668 silos and 282 granaries. 20 different typologies of silos were built, being the first typologies A (1949-1959), B (mainly in the 50s), C (1952-1956) as well as TR1 (1949), TR2 (1950), TR3 (1950), TR4 (1955-1957) and TR5 (1956-1973) and P (1952-1965) (Fernández-Fernández et al. 2020). Highlighting type D over all of them with a total of 389 units. This typology prolonged its construction for 34 years (1953-1987), appearing several subtypes (D1, D2, D3 D4 y D5).

Subtype D1 has bare façades from the ground to 4 the double-pitch roof. The upper gallery is positioned over the central raw and fitted with mansards for readier access to the outer cells. The tower, built flush against the front façade, features conventional windows (Fernández-Fernández et al. 2020) (Figure 1.1). Subtype D2 is D1 units with an addition on one of the side façades, an arrangement that affords them certain peculiarities (Fernández-Fernández, 2016) (Figure 1.2). The sole subtype D3 silo was built at Barbadillo, Salamanca, it has a single row of 14 six on-the floor cells. It is aesthetically the same as a D1 silo without the two outer rows of cells. The reception hopper and steel canopy are positioned at the rear, opposite the tower (Figure 1.3). Subtype D4 units interiorly to the same on- and off-the-floor row as D1, it differs from that subtype in that it has a parapeted flat roof and its tower has continuous rather than conventional windows. Two small structures attached to either side of the tower house offices and a bulk loading area. The result, an elegantly proportioned building (Fernández-Fernández et al., 2020) (Figure 1.4).

Subtype D5 is a D4 in which the side structures, built up to accommodate cells, flank the tower to the top, providing for a more compact volume than in D4 (Figure 1.4-1.5). The 138 units of this, the most numerous type, were built across a period of years (1957-1987). In 20 cases, primarily in northern Spain where rainfall is heavy, they were fitted with a pitched roof to better evacuate rainwater, detracting from the overall elegance of the design (Fernández-Fernández et al. 2020). Some authors have classified the D5 silos with pitched roofs under a separate subtype, D6 (Azcárate, 2009; Moreno, 2014).
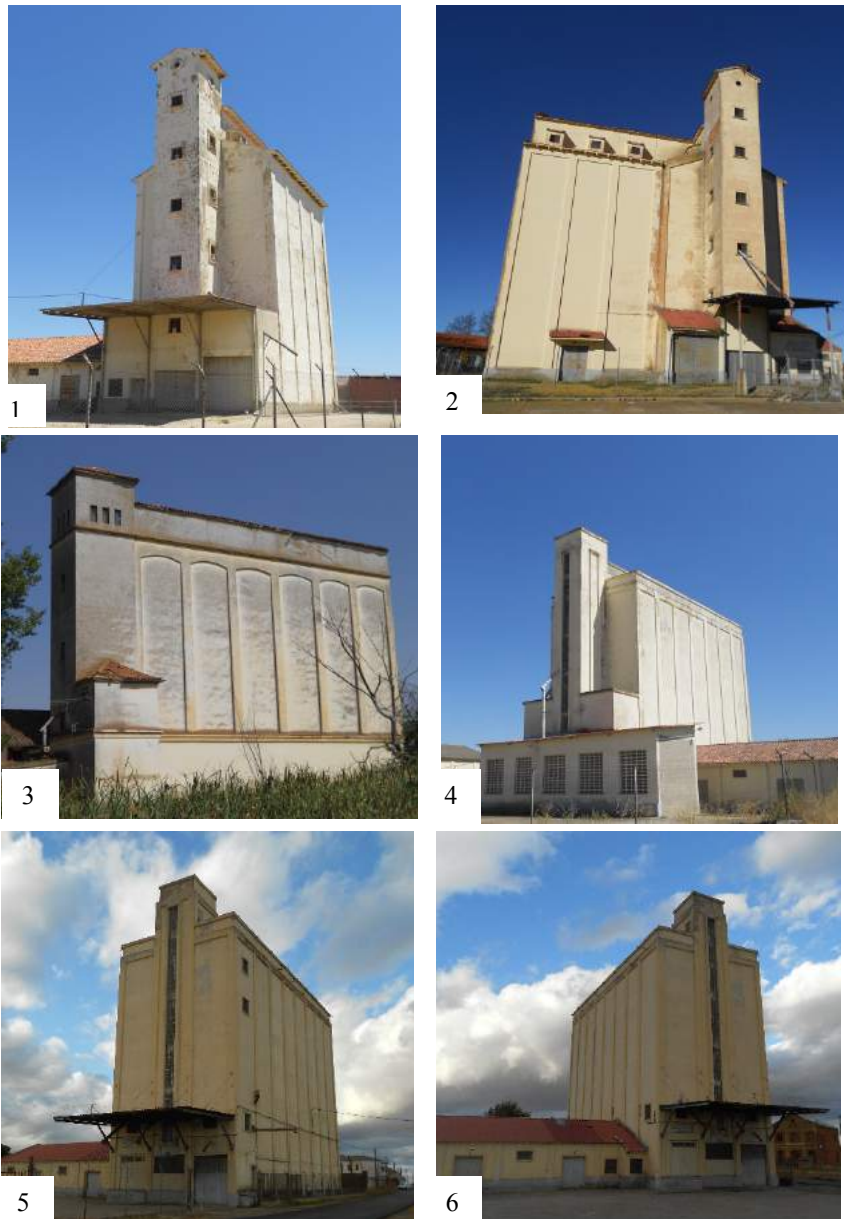
Figure 1. Silo subtypes type A: 1) D_1 at 4 Villardefrades, Valladolid; 2) D_2 at Tábara, Zamora; 3) D_3 at Barbadillo, Salamanca; 4) D_4 at Simancas, Valladolid; 5- 6) D_5 at Manganeses de la Lampreana, Zamora

The Manganeses de la Lampreana silo (Zamora) is a D5 type with 3,350 t of storage capacity, distributed in 24 storage tanks called cells, built in 1968 (Figure 2). Architecturally speaking it is a simple and powerful silo. It has a rectangular shape, made up of three rows of square cells, the outer rows of cells rested directly on the ground storey floor and the centre row is raised. Front tower between two cells, being embedded between them in a central position, achieving a compact and robust volume. The structure is made up of reinforced concrete pillars at the corners of the cells and the cell walls of reinforce bricks. It is finished off with a flat roof. The results of all analysis are listed in Table 1.
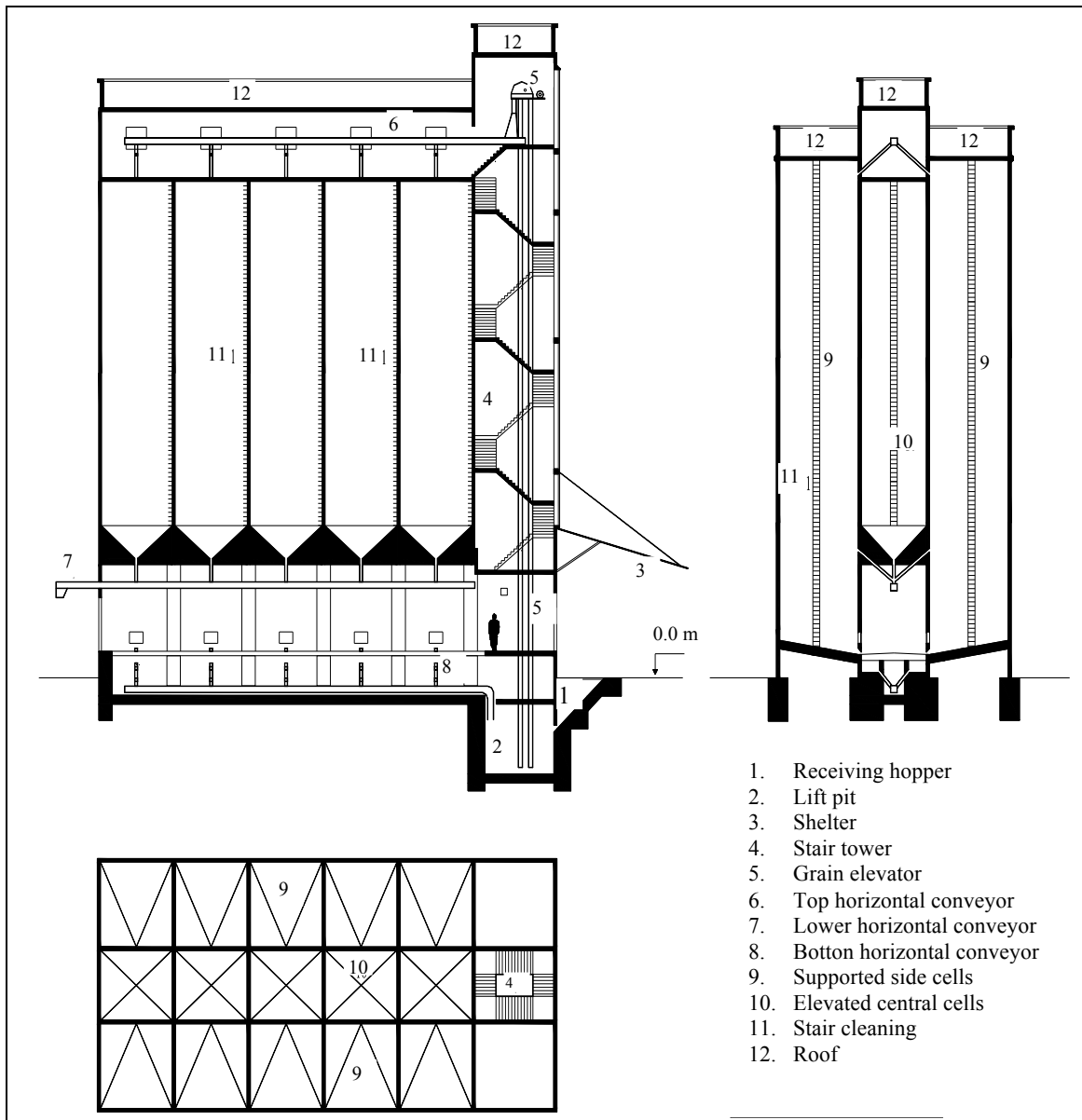
Figure 2. Section and plant of a typical silo type D (SNT, 1947).

1. Receiving hopper
2. Lift pit
3. Shelter
4. Stair tower
5. Grain elevator
6. Top horizontal conveyor
7. Lower horizontal conveyor
8. Botton horizontal conveyor
9. Supported side cells
10. Elevated central cells
11. Stair cleaning
12. Roof

The equipment present in The Manganeses de la Lampreana silo consists in two elevators in the tower. Both receive grain loaded off of trailers or lorries through a reception hopper (Figure 3). The elevators used in the silo have two square section frames inside which a strap carrying small scoops rises on one side and descends on the other (Fernández-Fernández et al. 2020). One of the elevators (grain elevator) raises the grain to the top of the tower where it is emptied onto an upper horizontal belt conveyor, where dampers and motorised valves it is distributed across other tubes to one of the three cells in each bay (Figure 3). The other (cleaning elevator) is only used where necessary to remove impurities, raising and then dropping the grain into the cleaning machinery. The grain is unloaded onto lower horizontal chain-driven belt conveyors lying at different heights depending on whether the cells stand-off (central) or on (side) the floor. Portable telescopic tubes are also installed to redirect the grain back to the elevators if necessary. From there it is carried to a raised cell for bulk offloading onto a lorry. This silo has vacuum dust collection systems similar to the facilities in types A and B (Moreno, 2014).

Table 1. Information collected on the D5 Manganeses de la Lampreana silo (Zamora)

General features	Region	Castilla y León
	Province	Zamora
	Village	Manganeses de la Lampreana
	Geolocation (coordinates ETRS 89 Use 30)	41°45'02.2"N 5°43'13.5"W
	Year construction	1968
Architectural features	Typology	D_5
	Capacity (t)	3 350
	Ground plan	Square
	Roof shape	Flat roof
	Tower position	Front tower between two cells
	Number of cell rows	3
	Number of cells	24
	Shape of cells	Square (3.5 x 3.5 m)
	Cell construction material	Reinforced brick
	Cell row position relative to the ground	Alternating rows of rows resting on and raised off ground storey floor
Technological facilities	Weighbridge (t)	40
	Railway	No
	Dust suction system	Yes
	Seed cleaning and selection machinery	Seed cleaning
	Thermometric probes	No
	Gas dosage system	No
	Refrigeration facilities	No
	Lift	No
	On-site high-voltage line and substation	No
	Machinery capacity (t/h)	25
	No. elevators	2
	No. upper storey horizontal conveyors	1

Figure 3. Detail of hopper area and upper horizontal belt conveyor and distribution tubes in D_5 silo at Manganeses de la Lampreana, Zamora

4. Conclusions

The Manganeses de la Lampreana silo (Zamora) is a D5, built in 1968 type with 3,350 t of storage capacity, distributed in 24 cells. The cells are square made of reinforced brick and the silo has a flat roof.

This silo is a reception silo whose objective was to be close to the farmers and transfer the cereal from it to the larger Transition and Reserve silos.

It is a simple and powerful silo. It has a rectangular shape, made up of three rows of square cells, the outer rows of cells rested directly on the ground storey floor and the centre row is raised. Front tower between two cells, being embedded between them in a central position, achieving a compact and robust volume.

The machinery installed is simpler, essentially consisting in equipment to load the cells at the top and unload the grain at the bottom and to clean it of impurities before or after storage.

References

Azcárate C.A., 2009. *Catedrales olvidadas, La red nacional de silos en España 1949-1990.* T6, Ministerio de Medio Ambiente y Medio Rural y Marino, Madrid, Spain. 555 p.

BOE, 1937. Decreto Ley de 23 de agosto de 1937, de ordenación triguera. Boletín Oficial del Estado (Spain) Nº 309, 25/08/1937. https://www.boe.es/datos/pdfs/BOE//1937/309/A03025-03028.pdf

BOE, 2014. Real Decreto 2/2014, de 10 de enero, por el que se modifica el Estatuto del Fondo Español de Garantía Agraria, aprobado por Real Decreto 1441/2001, de 21 de diciembre. Boletín Oficial del Estado (Spain) Nº 21, 24/01/2014. https://www.boe.es/boe/dias/2014/01/24/pdfs/BOE-A-2014-692.pdf

Fernández-Fernández M.V., 2016. Catalogación de las unidades de almacenamiento vertical de cereales de la red básica de Castilla y León, propuesta de una nueva clasificación y posibilidades de reutilización. MS thesis, Univ. de León, León, Spain.

Fernández-Fernández, M.V., V. Marcelo, José B. Valenciano, F. Javier López, P. Pastrana, 2020. Spain's national network of silos and granaries: architectural and technological change over time. Spanish Journal of Agricultural Research. 18 (3), e0205, 17 pages, https://doi.org/10.5424/sjar/2020183-16250

Fuentes J.M., M. López-Sánchez, A.I. García, F. Ayuga, 2015. Public abattoirs in Spain: History, construction characteristics and the possibility of their reuse. Journal of Cultural Heritage. 16, 632-639. https://doi.org/10.1016/j.culher.2014.12.001

Moreno A, 2014. Un análisis tecnológico sobre la red nacional de silos y graneros desde la ingeniería industrial en el ámbito agrario: ¿con qué maquinaria y cómo funcionaban? In *I Jornadas de Patrimonio Industrial Agrario: silos a debate.* Villanueva del Fresno, Spain, Sept 26-28.

Salido J., 2011. El almacenamiento de cereal en los establecimientos rurales hispanorromanos. In: *Horrea d'Hispanie et de la Méditerranée Romaine.* Casa de Velázquez, Madrid, Spain. Eds., J. Arce, B. Goffaux 127-141.

SENPA, 1978. Red de almacenamiento. Servicio Nacional de Productos Agrarios, Archivo General del Fondo Español de Garantía Agraria (FEGA), Madrid, Spain.

SENPA, 1994. Reordenación y redimensionamiento de la red de silos del SENPA. Servicio Nacional de Productos Agrarios, Archivo General del Fondo Español de Garantía Agraria (FEGA), Madrid, Spain.

SNT, 1947. La red nacional de silos. Servicio Nacional del Trigo, Servicio Nacional de Productos Agrarios, Archivo General del Fondo Español de Garantía Agraria (FEGA), Madrid, Spain. 23

SNT, 1950. Tipos de silos y su construcción. Servicio Nacional del Trigo, Servicio Nacional de Productos Agrarios, Archivo General del Fondo Español de Garantía Agraria (FEGA), Madrid, Spain. 21

SNT, 1959. Ponencia sobre la red nacional de silos en España. Los diversos tipos de silos, su construcción y evolución. Servicio Nacional del Trigo, Servicio Nacional de Productos Agrarios, Archivo General del Fondo Español de Garantía Agraria (FEGA), Madrid, Spain. 14

Tortella G, 1994. *El desarrollo económico de la España contemporánea. Historia económica de los siglos XIX y XX.* Alianza Editorial, Madrid, Spain. 429 p.

Tucci P.L, 2012. La controversa storia della Porticus Aemilia. Archeologia Classica 63, 575-591. https://www.academia.edu/2209356/La_controversa_storia_della_Porticus_Aemilia

Valls A., F. García, M. Ramírez, J. Benlloch, 2015. Understanding subterranean grain storage heritage in the Mediterranean region: The Valencian silos (Spain). Tunnelling and Underground Space Technology. 50, 178-188. https://doi.org/10.1016/j.tust.2015.07.003

Ammonia and Greenhouse Gas Emissions from Norwegian Cattle Buildings— A Field Study

Raphael Kubeba Tabase [a,*], Geir Næss [a], Yngve Larring [b]

[a] Animal science, Production and Welfare Division, Faculty of Biosciences and Aquaculture, Nord Universitet, Steinkjer, Norway

[b] SINTEF, Oslo, Norway

* Corresponding author. raphael.k.tabase@nord.no

Abstract

Ammonia and greenhouse gas (GHG) emissions from cattle buildings are harmful to the environment, public health and wellbeing. Previous studies on NH_3 and GHG emissions of cattle buildings are mostly from the North America and other European countries than Norway. The main objective of this paper is to quantify CH_4, N_2O and NH_3 emissions from different Norwegian cattle buildings under field conditions. Another objective is to compare the measured emissions in this investigation with published emissions from other countries. Continuous 24-hourly gaseous concentrations, as well as air temperature and relative humidity, were measured in a suckler cow and four other dairy cow buildings between 3 and 12 days during autumn, winter and spring. The gaseous concentrations were measured with a portable Fourier Transformed Infrared gas analyser, and ventilation rates were calculated using the CO_2 mass balance method. Indoor air quality was better in the naturally ventilated barn and the barn with the supply-exhaust air mixing system than in the barns with side wall air inlet valves and the cross-flow ventilation design. The reason for this was that the naturally ventilated barn had a higher air exchange rate, whereas the barn with the air mixing system efficiently mixed generated pollutants in the building compared to the other barns. During the measurements, CH_4 emissions from the suckler cow building ranged from 6.8 – 10.4 g h^{-1} LU^{-1}, while CH_4 emissions from the dairy cow buildings ranged from 12.1 – 19.6 g h^{-1} LU^{-1}. The suckler cow building emitted 18.8 – 30.6 mg h^{-1} LU^{-1} of N_2O, while the dairy cow buildings emitted -3.6 – 55.4 mg h^{-1} LU^{-1}. Furthermore, the suckler cow building had NH_3 emissions ranging from 0.8 to 1.9 g h^{-1} LU^{-1}, while the dairy cow buildings had NH_3 emissions ranging from 0.48 to 2.0 g h^{-1} LU^{-1}.

Keywords: Indoor climate and air quality, Dairy and beef cow buildings, NH_3 and Greenhouse emissions, Cold climate, Norway

1. Introduction

Agriculture is a major source of CH_4, N_2O and NH_3 emissions, all of which are harmful to the environment, public health, and well-being. The significance of CH_4 and N_2O is that they are powerful greenhouse gases (GHG) that, when released into the atmosphere, have a long-term impact on global warming via the greenhouse effect. The global warming potential of CH_4 and N_2O at equivalent weight of CO_2 is 28 and 265 times over a 100-year period (IPCC, 2014), respectively. Ammonia emissions, on the other hand, are linked to acidification and eutrophication of ecosystems, and they are a precursor to the formation of secondary particulate matter in the atmosphere (Erisman and Schaap, 2004). According to recent National Inventory Report (NIR) for Norway (The Norwegian Environment Agency et al., 2021), the agricultural sector accounted for 8.8% of the total GHG emissions. Methane production from livestock due to digestive processes (enteric fermentation) was the main source of GHG, accounting for 50.4% of the sector's emissions. Dairy and non-dairy cattle produced 71% of the CH_4 from enteric fermentation. Similarly, among Norwegian livestock, cattle farming produced the most NH_3. The primary source of NH_3 is manure in cattle buildings and storage, which is produced because of urea degradation in cattle excretions.

Norway ratified the Paris Agreement in 2016 and through its National Determined Contribution (NDC) has committed to reducing GHG emissions by at least 50% by 2030 compared to 1990 (NDC, 2020). To track progress toward the NDC, GHG and NH_3 emissions are estimated annually in the Norwegian NIR using the IPCC guideline from 2006. However, there are concerns about the accuracy of the emission factor estimates (VanderZaag et al., 2014). Indeed, despite a recent update to the models for calculating enteric CH_4 from dairy cows (Schwarm et al., 2019), the Norwegian NIR reported a ±28% uncertainty in enteric CH_4 estimates from dairy cows. The uncertainty in the emission factors is due to the wide variation of data used to develop the emission models, which can be attributed to differences in measurement method, animal production and feed characteristics, and local climatic conditions (Ngwabie et al., 2014, Niu et a., 2021). Furthermore, field measurements of GHG and NH_3 emissions from commercial cattle buildings have been reported from Denmark and Sweden, rather than Norway (Zhang et al., 2005, Ngwabie et al., 2011). However, to develop/verify innovative emission abatement techniques and enact emission legislation, national emission inventories require reliable emission models established from accurate emission data representative of local production practices.

Therefore, the main objective of this study is to quantify CH_4, N_2O and NH_3 emissions from Norwegian cattle buildings under field conditions. The measured results are also compared to published emissions from other countries.

In a subsequent study, the measured CH_4 emissions in this study will be compared to calculated CH_4 emissions using the IPPC Tier 2 modelling method. Given that the Norwegian climate has a longer winter season with outdoor temperatures frequently below -10 °C, measurements of indoor climate and gaseous concentrations were also performed to assess the working environment for farmers and animals.

2. Materials and Methods

Measurements were taken in four dairy farms and one suckler cattle farm. Four of the farms were in the county of Trøndelag (central Norway) and the fifth farm was in Oslo (south-eastern Norway). The main building characteristics are shown in table 1. The animal buildings at the farms were divided into feeding alleys, cubicles (with slatted floors and resting areas), and automatic milking parlours in the dairy buildings (figure 1). The resting areas are elevated platforms raised above the slatted floor and equipped with rubber mats. Manure accumulated in the slurry pit and was removed during the spring (April – May) and summer (July – August) seasons, apart from farm IV, which was emptied once a month and stored in a separate outdoor storage. Except for Farm IV, which had an automatic control natural ventilation, the other farms were mechanically ventilated. At the farms, the set-point temperature at the climate controller ranged between 10 and 13 °C. The measurement period was from 23/09/2020 to 18/05/2021 during the autumn, winter, and spring seasons. Table 2 shows the measurement periods and measurement hours at the different farms.

Table 1. Characteristics of the investigated cattle buildings.

Farm	Barn volume (m3)	Manure scrapping (slatted floor)	Manure removal (pit)	Slatted floor (m2)	Resting area (m2)	Feeding area (m2)
I	1212	Manual	Twice a year	291	172	41
II	1666	Robot	Twice a year	340	181	34
III	7193	Robot & manual	Yearly	385	258	120
IV	5818	Robot & manual	Monthly	372	374	173
V	3683	Manual	Twice a year	312	343	149

Table 2. Measurement periods and gaseous concentration measurement hours at the five farms.

Farm	Period			Hours		
	Autumn	Winter	Spring	Autumn	Winter	Spring
I	16/10 - 26/10	18/02 - 22/02	03/05 - 06/05	183	57	54
II	12/10 - 15/10	22/02 - 25/02	27/04 - 02/05	68	61	101
III	02/11 - 05/11	26/02 - 03/03	19/04 - 25/04	71	119	88
IV	23/09 - 08/10	11/02 - 17/02	06/05 - 10/05	295	108	89
V	27/10 - 30/10	01/02 - 11/02	10/05 - 18/05	66	192	184

2.1. Farms

Farm I was located at Inderøy. The farm building was fully-insulated with a flat ceiling and housed dairy cows. Measured from slatted floor, the building had a ceiling height of 3.0 m. There were 7 mechanically controlled air inlet valves facing opposite to each sidewall at the resting section for the dairy cows. The building had glass windows at the section that housed the calves and heifers (figure 1). The openings at this section were manually adjusted by the farmer. There were 3 exhaust fans at the ceiling, one at the resting section for the dairy cows and two at the feeding section of the building.

Farm II was a dairy farm located at Ogndal. The building had a cross-flow ventilation design with two exhaust fans in one of the sidewalls. The other sidewall and the endwalls had glass windows which were manually regulated by the farmer. The building was fully-insulated with a flat ceiling. The height from the slatted floor to the ceiling was 3.0 m. In addition to the room ventilation, the building had a pit ventilation system with two exhaust fans on one of the slurry pit's sidewalls.

Farm III was a dairy farm located in Oslo. The building was insulated with a pitched ceiling. Measured from slatted floor, the building had a ridge height of 10.0 m and an eave height of 3.7 m. The ventilation was by neutral pressure. Three ventilation ducts were used to blow air into and out of the building. Both the supply and exhaust fans were housed in a single housing unit, allowing some of the supply and exhaust air streams to mix (figure 1).
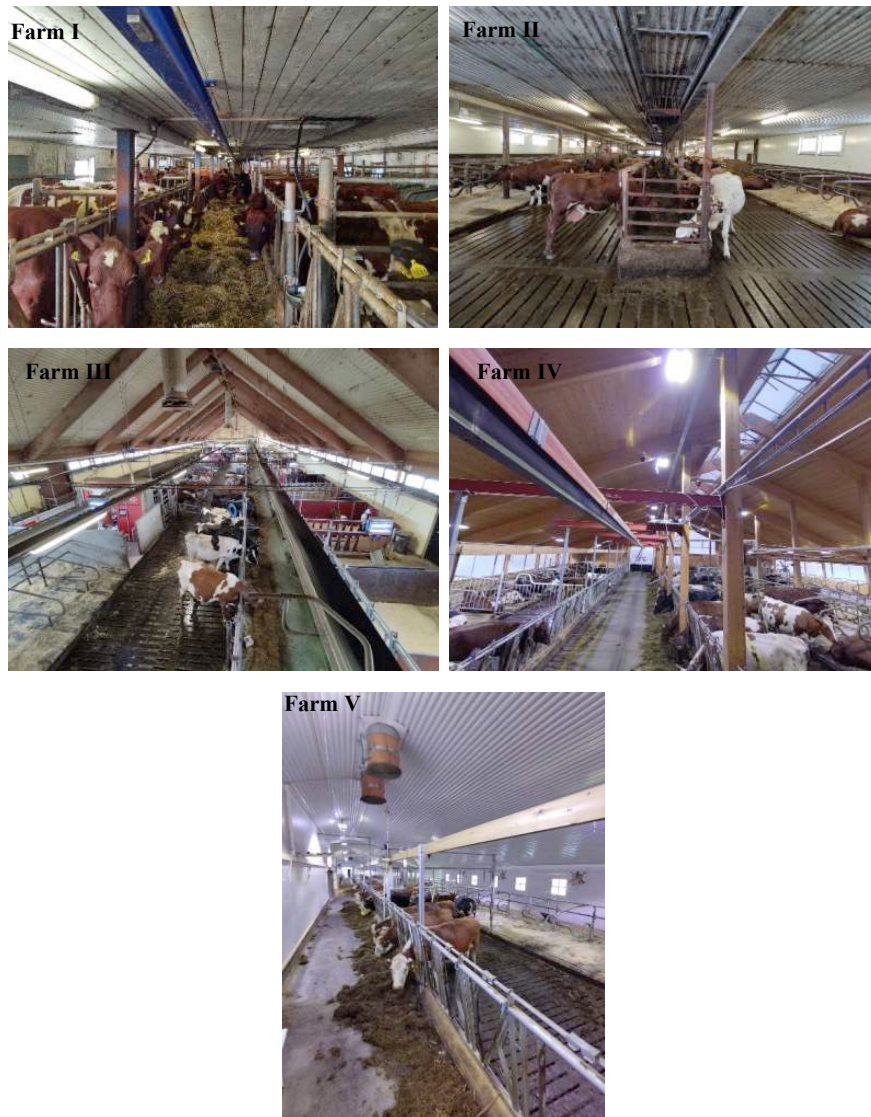
Figure 1. Inside the investigated cattle buildings.

Farm IV was a dairy farm in Mære. The building was semi-insulated and had a pitched ceiling. Measured from slatted floor, the building had a ridge height of 7.8 m, eave height of 2.8 m and sidewall height of 1.2 m. The height of the side wall openings was 1.4 m. The width of the ridge opening was 1.0 m.

Farm V was also in Mære, but the building housed suckler cows. The building was fully-insulated with a pitched ceiling. Measured from the slatted floor, the building had a ridge height of 5.2 m and eave height of 2.6 m. The building had four exhaust fans at the ceiling and 16 mechanically controlled sidewall air inlet valves of size 0.3 m x 0.6 m.

2.2. Production and feed

The dairy cows were Norwegian red (NRF) and the suckler cows were NRF-Limousine cross and Hereford. Cows, heifers, and calves were all housed in the same building. The claves and heifers were 1 week to 24 months old. Table 3 shows the production information at the different farms. The cows were fed roughage, concentrate feed and minerals. Roughage feed include grass silage and barley straw. Concentrate feed composition include milk powder, wheat bran, beet pulp, oats, rapeseed flour, beet molasses, corn, barley, oatmeal flour, soya flour, sugar cane molasses etc. The dairy farms had different feeding schedules for the different category and physiological status of cows (i.e., lactating, dry cows, heifers and calves) with feed delivered 2 - 9 times per day and twice a day at the suckler farm. Dairy cows had concentrate feed at the Automatic Milking Systems (AMS) and additional feed at concentrate feeders. Cattle roughage consumption was not measured during the experiment but concentrate intake by dairy cows was controlled at the AMS and the concentrate feeders. The average daily concentrate intake ranged from 7.6 to 9.7 kg. The animal mass at farms I

and V were estimated with weight tape around the heart girth. The AMS at farm II was equipped with a scale, while the animal weight at farms III and IV were estimated according to Norwegian cattle production information (TINE).

Table 3. Production information at the five cattle farms.

Farm	Animal number			Milk yield (kg/cow/day)	Weight		
	Calves	Heifers	Cows		Calves	Calves	Heifers
I	6	28 - 33	35 - 40	26	90 - 117	348 - 375	600 - 640
II	-	3 - 5	42 - 47	29		535 - 552	623 - 641
III	15 - 33	23 - 52	48 - 55	24	44 - 75	348 - 475	600
IV	-	36 - 58	49 - 57	26	148	348 - 364	600
V*	6 - 17	18 - 24	27 - 39	-	60	320 - 538	650 - 768

Age of calves: < 4 months; Age of heifers: > 4 months to first calving; * 1 bull in farm 5 that was 673 and 880 kg during autumn and winter measurements, respectively.

2.3. Measurements

2.3.1.Climatic data and gases

Air temperature and relative humidity (RH) were measured at different locations inside the cattle buildings. The sensors include 10 HOBO pendant temperature-light data loggers (Onset Computer Corporation, Massachusetts, USA), (Range: -20 to 70 ^{o}C; Accuracy: ± 0.53 ^{o}C) and 5 Tinytag TGU-4500 humidity-temperature data loggers (Gemini Data Loggers Ltd., Chichester, UK) (Range: -25 °C to 85 °C with 0 to 95% RH; Accuracy: ±0.6 °C; ±3 %RH). The weather conditions outside the cattle barns were recorded with an Oregon scientific weather station (Oregon Scientific, Inc., Oregon, USA): (Range: -40°C to 65 ^{o}C, 0% to 99%RH, 0~80m/s; Accuracy +/- 0.5 °C, 3%, +/- 0.9m/s, respectively). Two Tinytag CO_2 data loggers (Gemini Data Loggers Ltd., Chichester, UK) (range: 0 to 5000ppm; Accuracy: ±0.6 °C; Accuracy < ± (50ppm +3% of measuring value) recorded the indoor and outdoor CO_2 concentrations during the winter and spring measurements. All sensor/data loggers measured and logged the data at a sampling frequency of 5 min.

Fourier Transform Infrared Spectrometer (FTIR) gas analyser (GT5000 Terra, Gasmet Technology Oy, Helsinki, Finland) and a multi-point gas YAGA Stream Switcher system (YAGA AS, Ski, Norway) continuously measured the gaseous concentrations at 8 sample points at the farms. Zero-point calibrations were performed using pure N_2 gas before the start and at least every second day during the measurements. The Calcmet software (Gasmet Technology Oy, Helsinki, Finland) and YAGA control program sequentially collected at least 5 gas samples per location every 30 minutes to the gas analyser. At least 1 sample point each in the exhaust duct and at the inlet opening in the mechanically ventilated barns. The remaining sample points were located at different heights from the floor at the resting area and the feeding alley, depending on the layout of the cattle barn. At farm IV, the background gaseous concentration from the FTIR was measured at two sampling points, one at the sidewall opening and the other outside, 10 m from the building. The two Tinytag sensors also measured CO_2 concentrations at the sidewall openings. Similarly, the remaining sample points were located at different heights from the floor at the resting area and the feeding alley in the cattle building. Gas samples to the FTIR were collected using Polytetrafluoroethylene (PTFE) with 1-minute flushing and 2-minute sampling time. During the investigation, multi-location measurements of indoor temperature and relative humidity were also taken.

2.3.2.Ventilation and emission rates

Ventilation rate was calculated on hourly basis using the CO_2 mass balance equation (CIGR, 2020):

$$Q = \frac{10^6 \times P_{CO_2} \times Q_{tot}}{(CO_{2,in} - CO_{2,out})}$$ (1)

where Q is the ventilation rate (m^3 h^{-1}), $CO_{2,in}$ (g m^{-3}) the indoor CO_2 concentration, $CO_{2,out}$ the outdoor CO_2 concentration, PCO_2 is the CO_2 production. This study calculated PCO_2 as 0.2 m^3 h^{-1} per heat production unit (HPU), assuming that the manure pit contributed 10% to the total CO_2 production in the cattle building. Q_{tot} is the total heat production, which was converted from W to heat production unit (HPU), i.e., 1000 W = 1 HPU at an environmental temperature of 20 °C. The Q_{tot} was corrected for the room temperature. Q_{tot} is influenced by factors such as cow category, milk yield, physiological status etc. A detailed description of Q_{tot} for the different category of cows can be found in CIGR (2002). This study analysed all measured parameters (temperature, RH and gases) using their hourly averages and calculated gaseous emission rates (E, g h^{-1}) as the product of the ventilation rate and the gaseous concentrations (Equation 2).

$$E = VR \cdot (C_{in} - C_{out})$$ (2)

where C_{in} and C_{out} (g m^{-3}) represent indoor and outdoor gas concentrations, respectively. The last gas sample,

analysed at every 30 minutes sampling episode from the FTIR in an hour were averaged for the gaseous concentrations at each sample location (section 2.3.1). The calculated emission rates were later converted into g h^{-1} LU^{-1}, where 1 LU (livestock unit) = 500 kg.

3. Results and Discussion

3.1. Indoor climate and gases

Tables 4 and 5 show the average outdoor/indoor temperatures and relative humidity during the measurement, as well as the air exchange rates at the farms. Hourly average minimum and maximum outdoor temperatures were -1.4 to 16 ^{o}C, -18 to 11 ^{o}C and -5 to 19 ^{o}C during the autumn, winter and spring measurement periods. Winter, which had the coldest outdoor temperatures overall, had average indoor temperatures of less than 10 ^{o}C at all farms except farm II, which had temperatures above 15 ^{o}C. This was because at farm II the minimum hourly average outdoor temperature never dipped below 0 ^{o}C. Furthermore, because the inlet openings in this building were manually controlled, the farmer only opened one window to maintain the minimal ventilation and reduce draughts on the cows. Overall, autumn had the warmest indoor temperature at all farms because the outdoor temperature was higher than in spring. Outdoor temperature during the measurements influenced the air temperature in the buildings. As a result, the influence of outdoor temperature (Table 4) on indoor climate was greater in the naturally ventilated building than in mechanically ventilated buildings (table 5).

Moisture in the buildings related to the level of ventilation at the farms. Farms I and IV were the most ventilated while farm V was the least ventilated. During the winter, 94% of the measured hourly RH (table 2) at farm V was greater than 90%. Consequently, during the winter measurements, RH in farm V frequently reached near saturation (99%). This condition was contrary to the recommended maximum indoor RH of less than 80% at an indoor temperature of less than 8 ^{o}C in livestock housing (CIGR, 1984). Furthermore, even though the air exchange rate (ACH) was 3.2 h^{-1} compared to the winter ACH of 1.8 h^{-1}, the RH at farm V was frequently higher than the recommended limit during the autumn measurement. High levels of RH were also recorded at farm II during the winter, but this was due to the farmer closing the inlet openings to keep heat in the building. High levels of moisture in livestock housing during the winter are associated with the risk of condensation, which can deteriorate farm structures and promote pathogen formation (Teye et al., 2008). As a result, CIGR (1984) recommends RH in livestock housing of 40 – 80%.

Table 4. Average (standard deviation) outdoor Temperature and humidity.

Parameter	Season	Farm I	Farm II	Farm III	Farm IV	Farm V
Temperature (^{o}C)	Autumn	4.5 (3.6)	-	-	11.4 (2.9)	2.1 (1.8)
	Winter	1.2 (2.3)	3.5 (2.2)	2.4 (3.2)	-4.5 (3.7)	-10.4 (3.0)
	Spring	5.5 (2.1)	1.4 (2.9)	8.2 (4.1)	4.9 (3.3)	11.0 (3.0)
Humidity (%)	Autumn	84.9 (12.9)	-	-	79.1 (10.7)	-
	Winter	81.8 (9.9)	83.5 (11.9)	87.6 (13.9)	83.7 (11.0)	85.6 (12)
	Spring	56.1 (11.5)	78.3 (14.0)	41.5 (16)	63.9 (14.7)	75.5 (15.7)

Table 5. Average (standard deviation) indoor climate and air exchange rate.

Parameter	Season	Farm I	Farm II	Farm III	Farm IV	Farm V
Temperature (^{o}C)	Autumn	12.5 (0.9)	13.5 (0.5)	13.3 (1.2)	13.5 (2.3)	10.4 (0.5)
	Winter	9.8 (0.8)	15.6 (0.8)	9.7 (1.7)	5.3 (1.8)	7.0 (0.6)
	Spring	11.4 (1.0)	11.6 (0.6)	12.9 (2.3)	9.0 (2.1)	15.6 (1.7)
Humidity (%)	Autumn	82.2 (4.7)	86.8 (5.8)	79.4 (3.9)	75.1 (7.8)	94.6 (2.2)
	Winter	80.3 (4.7)	94.9 (1.3)	80.6 (5.9)	79.5 (6.7)	94.0 (2.9)
	Spring	62.4 (5.6)	75.8 (6.0)	57.2 (8.0)	58.9 (10.4)	76.6 (8.1)
ACH (h^{-1})	Autumn	18.4 (5.8)	10.3 (2.4)	6.1 (1.5)	27.8 (30)	3.2 (0.3)
	Winter	12.1 (3.9)	3.7 (0.5)	2.7 (0.7)	6.1 (3.4)	1.8 (0.2)
	Spring	22.8 (5.1)	7.4 (2.1)	2.8 (0.7)	13.8 (5.1)	4.4 (0.9)

Figure 2 shows the boxplots of the hourly average indoor CO_2, CH_4, N_2O and NH_3 concentrations at the five farms. The hourly average indoor CO_2 concentration at the farms rarely exceeded the maximum exposure limit of 3000 ppm (Mattilsynet, 2020). However, at farms I, II, and V, average indoor NH_3 concentrations exceeded the recommended exposure limit of 10 ppm (Mattilsynet, 2020), but not at farms III and IV. This was due to the later farms' ventilation type, larger volume, and higher ceiling height (figure 1, table 1 and section 2.1). The air supply and exhaust system at farm III efficiently mixed air in the building while the naturally ventilated barn at farm IV efficiently diluted the generated gases due to the higher ACH (table 5). The highest hourly average NH_3 concentrations were measured in the suckler cattle barn (farm V) and farm II. The higher NH_3 concentrations in farm V can be explained by the lower ACH. The lower ACH at the suckler cow barn (farm V), which resulted in the unacceptable indoor RH and NH_3 concentrations (table5, figure 2) during the winter, highlights the dilemma of maintaining a comfortable air temperature for the calves by lowering the ventilation rate versus improving indoor air quality by ventilating more. Either of the two extremes exposes the calves to the risk of diseases. The higher NH_3 concentrations at farm II was probably due to NH_3 boundary layer disturbance from the pit ventilation. Overall, the hourly average CH_4 and N_2O concentrations were within typical concentrations published for cattle buildings at other cold regions (Teye et al., 2008; Ngwabie et al., 2011; Ngwabie et al.,2014; Joo et al., 2015; Cortus et al., 2015; Rzeźnik et al., 2016).

3.2. Emissions

Figure 3 shows boxplots of hourly average CH_4, N_2O, and NH_3 emissions at the farms during the autumn, winter, and spring measurements. Table 6 compares the hourly average emission ranges at the farms during the three seasons to published emissions from five countries. As expected, the suckler cattle building (farm V) emitted the least CH_4 during the three seasons, ranging from 6.8 – 10.4 g h^{-1} LU^{-1}. Farm III had the highest CH_4 emissions, ranging from 15.5 – 19.6 g h^{-1} LU^{-1}. Farms I and II had similar CH_4 emissions, while Farm IV had ~ 2.0 g h^{-1} LU^{-1} lower emissions than farm III. Furthermore, the CH_4 emissions from farms I and II were within the published emission ranges for naturally ventilated dairy barns in Sweden, Canada, and Germany, as well as mechanically ventilated dairy barns in the United States (table 6). The CH_4 emission from farms III and IV were however, greater than these same published emission range in table 6.

The highest CH_4 emission (19.6 g h^{-1} LU^{-1}) occurred in autumn at farm III and in winter at farm IV (17.1 g h^{-1} LU^{-1}). The CH_4 emission from the two naturally ventilated building in USA were lower than the naturally ventilated building at farm IV. Whereas the reported CH_4 emissions from the six naturally ventilated diary buildings in Poland had a wider emission range compared to the current investigation. This was probably because of the uncertainty in estimating ventilation rate in naturally ventilated cattle buildings. The N_2O emissions in this investigation were within the published emission range from dairy cattle buildings (table 6). However, negative hourly average N_2O emissions were recorded at farms II and III during the autumn (figure 3) because the outdoor N_2O concentration was greater than indoor during the field measurement.

In descending order, the least NH_3 emission occurred in autumn, spring and winter (figure 3). Farm III had the lowest overall NH_3 emissions, farm I had the highest emissions in the winter and spring, and farm II had the highest in the autumn (figure 3). Comparing the NH_3 emissions within the same farm for the different seasons in figure 3 revealed no clear seasonal trend in the emissions and would require more detailed statistical analysis. The NH_3 emissions from farms I, II, and IV were greater than the published emission rates from the naturally ventilated dairy buildings in Sweden and Canada (table 6). This was most likely since the measurement seasons at the farms in Sweden and Canada were different from the current investigation. The published NH_3 emissions from Poland and Canada, that included the summer season had higher maximum emissions than the current investigation (table 6). It is generally accepted in the literature that livestock houses emit more NH_3 during the summer than during the colder seasons due to higher ventilation rates and warmer indoor temperatures (Zhang et al., 2005). The reason is that at the emitting surface, NH_3 volatilisation positively correlates with temperature and the air velocity.
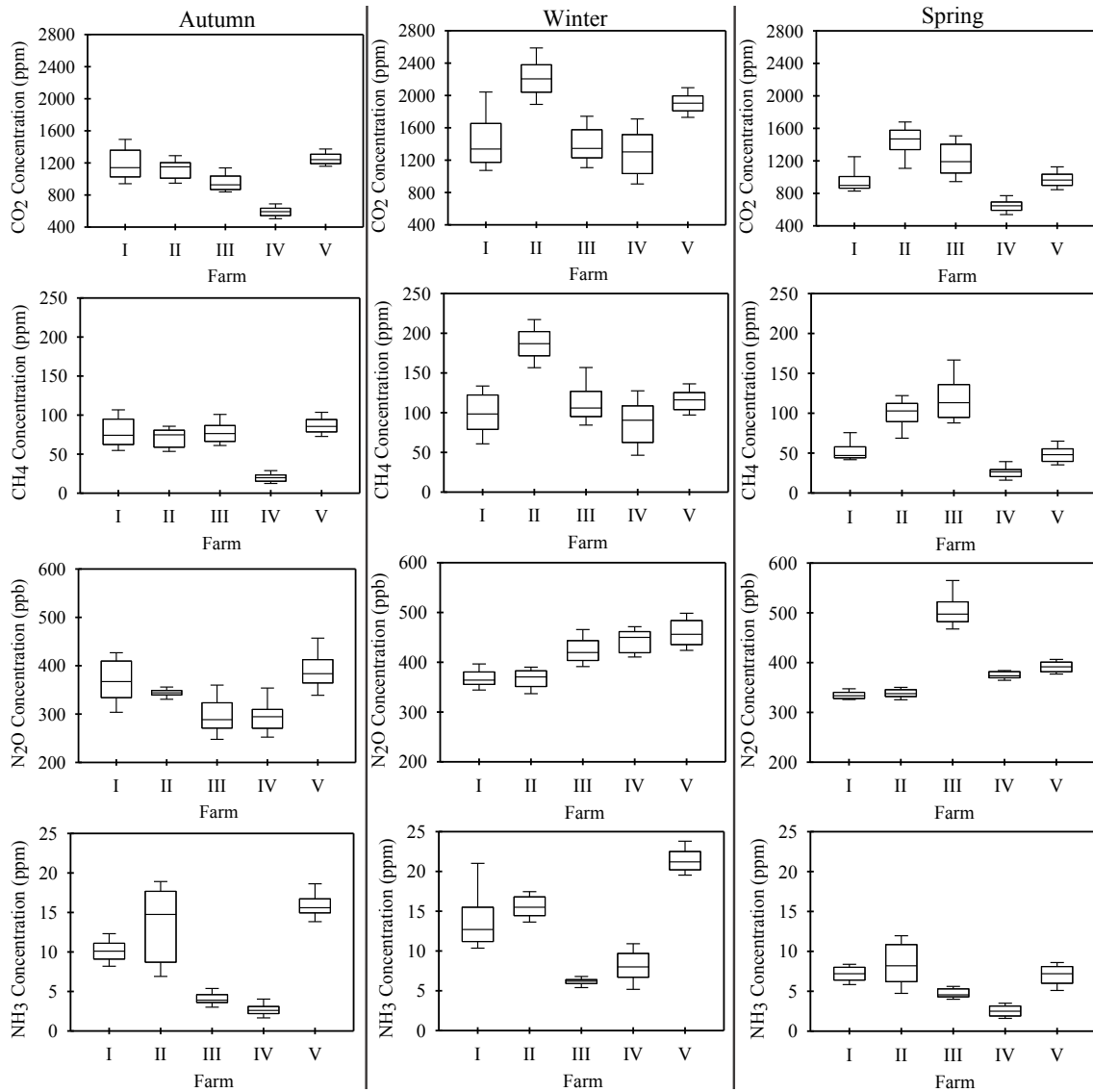
Figure 2. Boxplots of indoor gaseous concentrations at the five farms during the autumn, winter, and spring seasons. The top and bottom of the boxplots represent the first and third quartiles, respectively. The median is indicated by the lines that divide the boxes, and the minimum and maximum values are indicated by the whiskers.
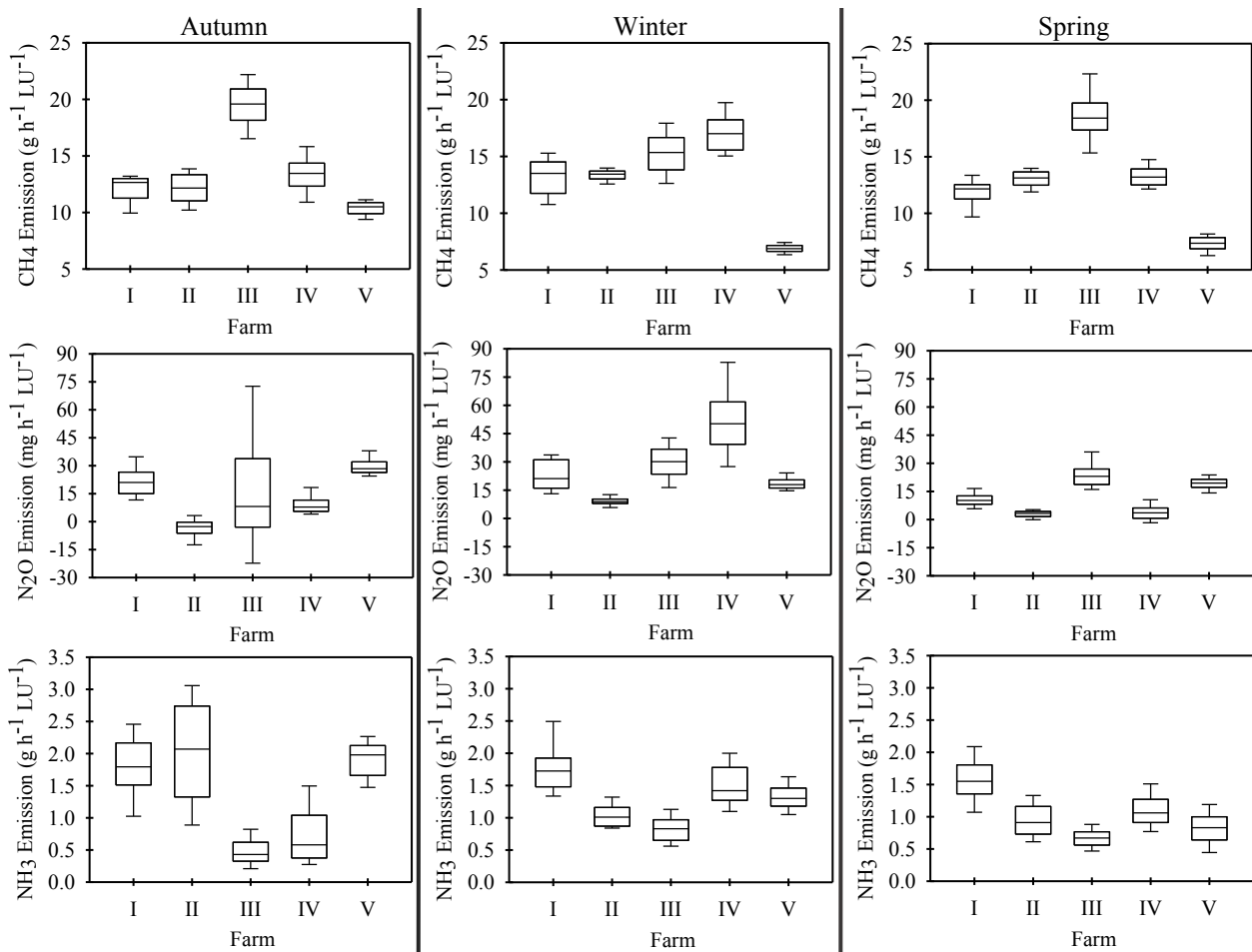
Figure 3. Boxplots of gaseous emission rate at the five farms during the autumn, winter, and spring seasons. The top and bottom of the boxplots represent the first and third quartiles, respectively. The median is indicated by the lines that divide the boxes, and the minimum and maximum values are indicated by the whiskers.

Table 6. Published CH_4, N_2O, and NH_3 emissions compared to current investigation.

Reference	Country	Building (season)	CH_4 (g h^{-1} LU^{-1})	N_2O (mg h^{-1} LU^{-1})	NH_3 (g h^{-1} LU^{-1})
[1] [2]	Sweden	1 NV* (A & B)	7.0 - 15.0		0.40 - 1.50
[3]	Canada	1 NV* (A & D)	12.2 - 13.9	29.4 - 41.3	0.43 - 0.64
[4]	USA	2 NV* (B, C & D)	2.8 - 10.5	12.5 - 104.2	
[5]	USA	2 MV* (19 months)	12.1	28.8	
[6]	Poland	6 NV* (B, C & D)	1.3 – 32.2	2.0 - 336	0.08 – 2.67
[7]	Canada	1 NV* (A, C & D)			0.97 - 3.31
[8]	Canada	1 NV* (A, B, C & D)	9.0 - 12.6	1.8 - 36.0	
[9]	Germany	2 NV* (A, B, C & D)	11.5 - 14.2		
Farm I	*This study*		*12.1 - 13.1*	*10.7 - 22.7*	*1.55 – 1.81*
Farm II	*This study*		*12.2 - 13.3*	*-3.6 – 8.9*	*0.94 - 1.99*
Farm III	*This study*		*15.4 - 19.6*	*17.5 – 29.8*	*0.48 - 0.83*
Farm IV	*This study*		*13.3 - 17.1*	*4.1 – 55.4*	*0.75 - 1.51*
Farm V	*This study*		*6.8 - 10.4*	*18.8 – 30.6*	*0.82 – 1.91*

Ngwabie et al. (2009) **[1];** Ngwabie et al. (2011) **[2]**; Ngwabie et al. (2014) **[3]**; Joo et al. (2015) **[4]**; Cortus et al. (2015) **[5]**; Rzeźnik et al. (2016) **[6]**; Huang & Guo (2017) **[7]**; Huang & Guo (2018) **[8]**; Hempel et al. (2020) **[9]**; *Dairy farm; NV (natural ventilation); MV (mechanical ventilation). Seasons: winter [A], spring [B], summer [C], autumn [D].

4. Conclusions

The following are the findings of this investigation:

The naturally ventilated barn and the barn with the supply-exhaust air mixing system had better indoor air quality than the barns with side wall air inlet valves and the cross-flow ventilation design.

The NH_3 and relative humidity levels in the suckler cattle building frequently exceeded recommended limits of 10 ppm and 80%, respectively, especially during the winter because the air exchange rate in the suckler cattle building was frequently less than 2.0 h^{-1}.

Methane emissions from the suckler cow building ranged between 6.8 – 10.4 g h^{-1} LU^{-1} during the autumn, winter and spring measurement periods. During the same seasons, the mechanically ventilated dairy cow buildings emitted 12.1 – 19.6 g h^{-1} LU^{-1}, whereas the naturally ventilated dairy cow farm emitted 13.3 – 17.1 g h^{-1} LU^{-1}.

The CH_4 emissions from the dairy barns with the side wall air inlet valve and the cross-flow ventilation design were within the published emission ranges for naturally ventilated dairy barns in Sweden, Canada, and Germany, as well as mechanically ventilated dairy barns in the United States. However, the CH_4 emission from the naturally ventilated barn and the barn with the supply-exhaust air mixing system were greater than these same published emission ranges.

The N_2O emissions were from 18.8 – 30.6 mg h^{-1} LU^{-1} at the suckler cow building: -3.6 – 29.8 mg h^{-1} LU^{-1} from the mechanically ventilated dairy cow buildings and 4.1 – 55.4 mg h^{-1} LU^{-1} from the naturally ventilated dairy cow building.

Ammonia emissions from the suckler cow building ranged between 0.8 – 1.9 g h^{-1} LU^{-1}. The mechanically ventilated dairy cow buildings emitted 0.48 – 2.0 g h^{-1} LU^{-1}, whereas the naturally ventilated dairy cow farm emitted 0.75 – 1.51 g h^{-1} LU^{-1}.

In a subsequent study, the measured CH_4 emissions in this study will be compared to calculated CH_4 emissions using the IPPC Tier 2 modelling method. Furthermore, detailed statistical analysis would be performed to investigate the influence of environmental factors, ventilation rate etc. on the gaseous emissions.

Acknowledgements

References

CIGR, 1984. Report of working group on climatization of animal houses. International Commission of Agricultural Engineering. Scottish Farm Buildings Investigation Unit, Aberdeen Scotland.

CIGR, 2002. Heat and moisture production at Animal and House Levels — Report of Working Group Climatization of Animal Houses. CIGR Section II, International Commission of Agricultural Engineering. Research Centre Bygholm, Danish Institute of Agricultural Sciences, Horsens, Denmark. December.

Cortus, E. L., L. D. Jacobson, B. P. Hetchler, A. J. Heber, B. W. Bogan, 2015. Methane and nitrous oxide analyzer comparison and emissions from dairy freestall barns with manure flushing and scraping. Atmospheric Environment. 100, 57-65.

Erisman, J. W., M. Schaap, 2004. The need for ammonia abatement with respect to secondary PM reductions in Europe. Environmental Pollution, 129(1), 159-163.

Hempel, S., D. Willink, D. Janke, C. Ammon, B. Amon, T. Amon, 2020. Methane emission characteristics of naturally ventilated cattle buildings. Sustainability. 12 (10), 4314.

Huang, D., H. Guo, 2017. Diurnal and seasonal variations of odor and gas emissions from a naturally ventilated free-stall dairy barn on the Canadian prairies. Journal of the Air & Waste Management Association. 67(10), 1092-1105.

Huang, D., H. Guo, 2018. Diurnal and seasonal variations of greenhouse gas emissions from a naturally ventilated dairy barn in a cold region. Atmospheric Environment. 172, 74-82.

IPCC, 2014. Climate Change 2014: Synthesis Report. Contribution of Working Groups I, II and III to the Fifth Assessment Report of the Intergovernmental Panel on Climate Change [Core Writing Team, R.K. Pachauri and L.A. Meyer (eds.)]. IPCC, Geneva, Switzerland, 151 pp.

Joo, H. S., P. M. Ndegwa, A. J. Heber, J. Q. Ni, B. W. Bogan, J. C. Ramirez-Dorronsoro, E. Cortus, 2015. Greenhouse gas emissions from naturally ventilated freestall dairy barns. Atmospheric Environment. 102, 384-392.

Mattilsynet, 2010. Veileder til forskrift om hold av storfe. https://www.mattilsynet.no/om_mattilsynet/gjeldende_regelverk/veiledere/veileder_om_hold_av_storfe.1853/binary/Veileder%20om %20hold%20av%20storfe Accessed June 8, 2021.

Ngwabie, N. M., A. Vanderzaag, S. Jayasundara, C. Wagner-Riddle, 2014. Measurements of emission factors from a naturally ventilated commercial barn for dairy cows in a cold climate. Biosystems Engineering. 127, 103-114.

Ngwabie, N. M., K. H. Jeppsson, G. Gustafsson, S. Nimmermark, 2011. Effects of animal activity and air temperature on methane and ammonia emissions from a naturally ventilated building for dairy cows. Atmospheric Environment. 45(37), 6760-6768.

Ngwabie, N. M., K. H. Jeppsson, S. Nimmermark, C. Swensson, G. Gustafsson, 2009. Multi-location measurements of greenhouse gases and emission rates of methane and ammonia from a naturally-ventilated barn for dairy cows. Biosystems Engineering. 103(1), 68-77.

Niu, P., Schwarm, A., Bonesmo, H., Kidane, A., Åby, B. A., Storlien, T. M., Michael Kreuzer, Clementina Alvarez 1,5, Jon K. Sommerseth... & Prestløkken, E. (2021). A Basic Model to Predict Enteric Methane Emission from Dairy Cows and Its Application to Update Operational Models for the National Inventory in Norway.

Norway NDC, 2020. Update of Norway's nationally determined contribution. https://www4.unfccc.int/sites/ndcstaging/PublishedDocuments/Norway%20First/Norway_updatedNDC_2020%20(Updated%20submission).pdf Accessed May 8, 2021.

Rzeźnik, W., P. Mielcarek, I. Rzeźnik, 2016. Pilot study of greenhouse gases and ammonia emissions from naturally ventilated barns for dairy cows. Polish Journal of Environmental Studies. 25(6), 2553-2562.

Schwarm, A., H. Bonesmo, A. Kidane, B. Aspeholen Aby, T. Storlien, M. Kreuzer, C. Alvarez, E. Prestlokken, 2019. Update of methodology for calculation of enteric methane emissions from dairy cows in Norway. In *7th Greenhouse Gas and Animal Agriculture Conference. Proceedings*. Iguassu Falls, Brazil, August 4-8. Embrapa Southeast Livestock. Vol. 135, pp. 180-180.

Teye, F. K., M. Hautala, M. Pastell, J. Praks, I. Veermäe, V. Poikalainen, A. Pajumaägi, T. Kivinen, J. Ahokas, 2008. Microclimate and ventilation in Estonian and Finnish dairy buildings. Energy and Buildings. 40(7), 1194-1201.

The Norwegian Environment Agency, Statistics Norway, Norwegian Institute of Bioeconomy Research, 2021. Greenhouse Gas Emissions 1990-2019, National Inventory Report. The Norwegian Environment Agency.

Zhang, G., J. S. Strøm, B. Li, H. B. Rom, S. Morsing, P. Dahl, C. Wang, 2005. Emission of ammonia and other contaminant gases from naturally ventilated dairy cattle buildings. Biosystems Engineering, 92(3), 355-364.

Structural Design Methodology for Insect Proof Nets of Nethouses Under Snow Load

K. Adamakos [a,*], D. Briassoulis [b]

[a] School of civil engineering, Institute of steel structures, National Technical University of Athens,
9 Iroon Polytechneiou str., Zografou Campus, 15780, Athens, GREECE

[b] Department of Natural Resources & Agricultural Engineering, Agricultural University of Athens,
75, Iera Odos Str., 11855 Athens, Greece

* Corresponding author. E-mail: kadamak@central.ntua.gr

Abstract

The use of Nethouses becomes widespread in Mediterranean regions because of the prevailing mild climatic conditions during a long period of the year, offering a more natural and environmentally friendly cultivation method. Despite the dominant mild weather conditions at the countries where the nethouses are used the most, hailfalls or snowstorms are likely to occur. These actions are not always considered in the nethouse-structural design procedure as design requirement. Nethouses are usually designed for wind, thermal, permanent, crop and operational loads. However, snow loads expected in Mediterranean regions could be more critical than the conventional nethouse design loads. The insect proof nets that cover nethouses behave like tension membranes that exhibit extended deformations to bear the vertical loads. This entails the danger of plastic deformation, failure of the nets and/or damages of the equipment or even the structure in cases that the extensively deformed net encounters other components of the nethouse, like shadow curtains, the crop, or secondary structural elements. The objective of this paper is to produce innovative tools for a safer and accurate design procedure against snow load. For this purpose, elastic numerical analyses with large deformations have been performed to illustrate the structural behavior of the net as an integral structural component of the nethouse. The numerical models include the net as a membrane, but also the cable-based supporting system. Two insect-proof nets with different mechanical properties were investigated and characteristic curves for each net in terms of stress and deflections vs. applied loads were generated. The analysis of the net as a load carrying component of the nethouse is done separately with the use of the design curves that could also simulate the design actions of the nets directly in the numerical model of the nethouse. Hence, the model of the main structure used for the analysis and design of nethouses remains simple and reliable.

Keywords: Nethouse, net, hail, snow, design

1. Introduction

Nethouses are widely used during the last decades and their use is still expanding. The reason is that they offer environmentally friendly cultivation methods, closer to the natural procedure in terms of temperature, radiation, etc., in contrast to the typical greenhouses. Nethouses offer also the control of pests and as a result the farmers use less pesticides and chemical products during the cultivation (Hanafi et al., 2007). The reduction of the need for pesticides makes nethouses ideal for organic growing (Chouinard G., et al, 2016). Moreover, the nethouses have been proven to be more sustainable because of reduced consumption of water and electricity resources (Abdel-Ghany A.M. et al., 2016). However, nethouses are structures used mainly in mild weather conditions and the empirical structural design applied to design such structures ignores critical actions like the snow load. Nevertheless, several failures of greenhouses that are structurally very similar to nethouses have been shown to be caused by snow load (ten cases have been presented by Bartok (2014)). Another detailed review on the collapse of a greenhouse by Briassoulis et al. (2016) showed that the failure of the greenhouse was due to a combination of wind and snow. Nethouses and greenhouses have many similarities and thus the first seem to be also vulnerable to snow loading. The present paper intends to highlight the significance of the snow load in the final structural design of the structure. Nethouses have a deficient normative support, as there is no normative document offering design guidelines for nethouses. Nethouses are designed mainly according to norms that refer to greenhouses such as EN-13031-1 (CEN, 2001) in the EU or NGMA standard (NGMA, 2004) in the USA. Typical nethouses are light weight structures, composed of steel columns, wire ropes (cables) and an insect-proof nets. From the structural point of view the cables and the net act as tension members, a fact that makes the nethouses structurally efficient. The required structural design for such structures is relatively demanding in respect to the one needed for conventional structures. The complexity of this design lies on the membrane behaviour of the net, as well as on the structural coupling of the different components. To overcome this complexity, a separate design of the net is proposed in the present work, that allows for a simpler but reliable model of the nethouse structure, excluding the membrane elements. This also gives the opportunity to the designer to use any commercial software for the design.

2. Structure

The structure of a nethouse is composed of steel columns, primary and secondary cables, anchorage cables and the horizontal net, as it is presented in Figure 1. The cover of a nethouse is composed of parallel net-segments that are indirectly interconnected through common supporting cables. The length of these segments is equal to the total length of the nethouse and the width of each segment is governed by the width of the net that is available by the manufacturer. A typical width is 4 m and subsequently 4 m is also the distance between the parallel primary cables where the net is supported on. Each pair of net-segment is hanging from a common primary cable with the help of independent special connectors, but the neighbored segments are not directly connected to each other. In fact, a small part of each net's longitudinal edge is left free, and these parts are slightly wrapped to each other in order to assure the insect proof character of the structure. Figure 2 shows a typical connector used for the cable-to-net connection. Each connector couples only the two perpendicular to the net edge degrees of freedom (u_Y, u_Z), while the translational degree of freedom (u_X) along the cables direction is free, since the connector can slide along the cables. The net is restrained along the X axis only at the outer transverse cables of the perimeter. Figure 3 highlights the net's boundary conditions.

Figure 3 shows a part of a nethouse and highlights the different areas of a net segment. From the static point of view the net segment is separated into two parts: the internal and the external one. With green is the area that corresponds to the internal part of the segment, while with orange is the external part. The external part exhibits a structural behaviour like a 3-side supported membrane, while the behaviour of the internal parts is a 2-sided simply supported membranes. Since nethouses are longitudinal structures, the internal area of a net-segment appears repeatedly, and it is dominant for the structural behavior.

To perform the structural design of the net, a stress check and a deformation-check should be done regarding the ultimate limit states and the serviceability limit states, regardless of the applied design norm. To investigate the maximum stress and deformations of the net in respect to the applied vertical load a structural simulation of the net is needed. For this purpose, a 5-span model is created. The middle span of this model represents any internal part of the net that repeatedly appears in a longitudinal structure. This span is not affected by the external parts of the net and it saves computing time in comparison to the analysis of a full model with multiple spans.
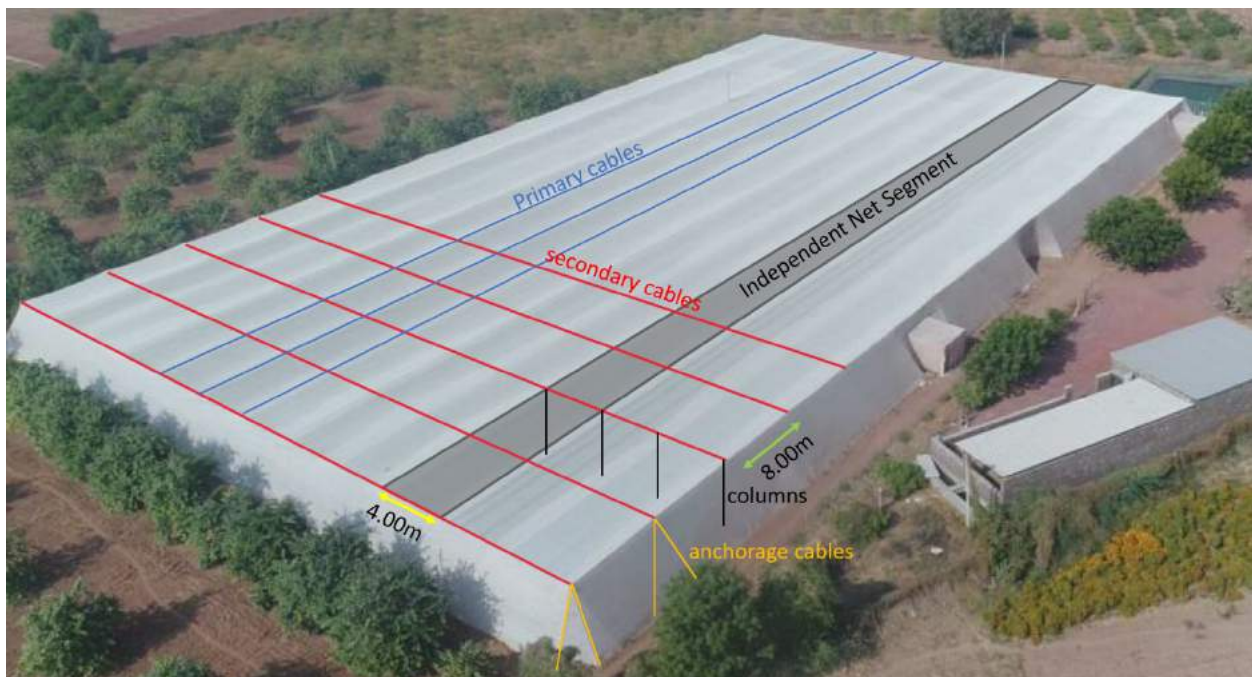

Figure 1 Topology of a typical nethouse
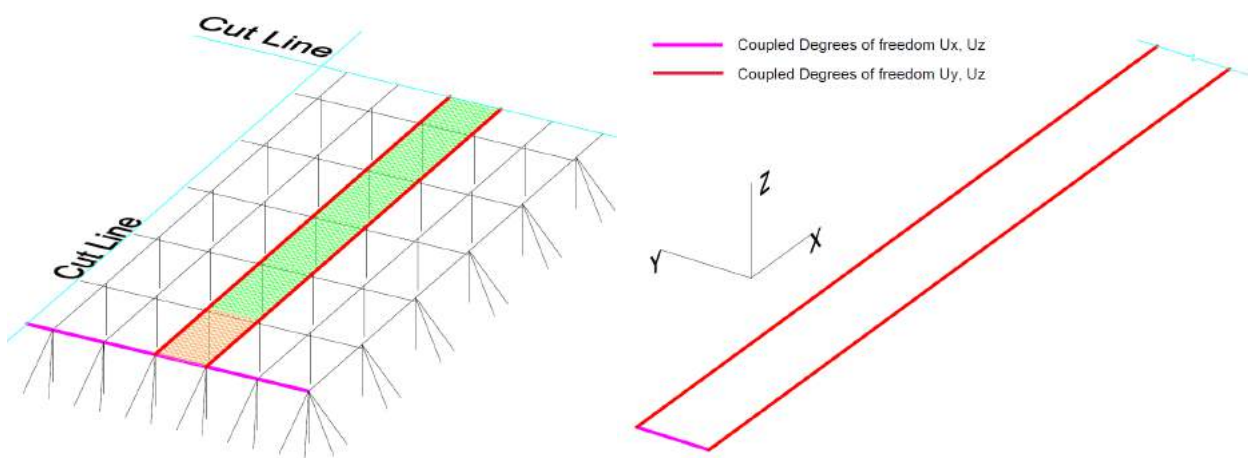
Figure 2 Special Net-to-Cable connector

Figure 3 Clarification of the geometry and support of a net-segment

3. Simulation

The structural model developed includes the primary cables and the net, while the columns, the transverse cables of the perimeter and the neighbored net-segments are simulated as equivalent boundary conditions. The internal secondary cables are ignored, as these are placed in a lower level and are not in direct connection with the net or the primary cables. The primary cables are supported vertically and in plane of the net (u_Z, u_Y) at the column points, however these are free to slide longitudinally (u_X). The cables are hinged at the external column points. The net is connected to the cables by coupling the vertical and transverse degrees of freedom ($u_{i\text{-net}} = u_{i\text{-cable}}$). Moreover, the net is restrained along the short edges (u_X, u_Z) simulating the secondary cables of the perimeter. The primary cables are laterally supported by applying boundary conditions of symmetry, simulating a symmetric (and symmetrically loaded) neighbored net-segment acting on the cable identically but to the opposite direction. Hence, the cable remains laterally in its initial position.

The applied snow load is uniformly distributed to the gravity direction. The load is applied gradually from 0 to 2.0 kN/m^2 a range typical for the snow load in Mediterranean regions. For Mediterranean region according to equation (1) given by Eurocode 1-part 1-3 (CEN, 2003) a typical characteristic value of the snow load at ground level is s_k=1.75 kN/m^2 for zone II and a region at 500 m altitude. Considering the snow load shape coefficient μi=0.8, the exposure coefficient C_e=1 and the thermal coefficient C_t=1, the snow load on the nethouse roof is 1.4 kN/m^2. According to EN13031 (2001) the unfavorable action of snow load is considered with a safety factor of 1.2. Thus, the applied design snow load could be 1.67 kN/m^2.

$$s_k = (0.498Z - 0.209)[1 + (\tfrac{A}{452})^2] \tag{1}$$

where,

s_k is the snow load at the ground level [kN/m^2], Z is the zone number given in the snow maps of the national annexes [values 1÷4], A is the altitude [m]

The analysis is elastic, considering large deformations in order to consider the geometric nonlinearity of such a tension structure. To figure out the influence of some parameters to the structural response, five analyses are performed for the given geometry using different net-material and different values for the cable's diameter and the cable's

prestress. The values of these parameters are given in Table 1. Regarding the material of the net, two nets are used with different mechanical properties. The mechanical properties were determined by Giannoulis et al. (2021) and the test procedure followed the experimental protocol recommended by Briassoulis et al. (2007a, 2007b).

Table 1. Parameter values used in performed analyses.

Analysis ID	Cable diameter [mm]	Net Material Type	Net Ex [MPa]	Net Ey [MPa]	Prestress [kN]	Length [m]	Width [m]	Load [kN/m²]
# 1	8	1	62.7	31.41	-	40	4	0÷2.00
# 2	8	1	62.7	31.41	1	40	4	0÷2.00
# 3	8	1	62.7	31.41	4	40	4	0÷2.00
# 4	8	2	75	50	-	40	4	0÷2.00
# 5	10	1	62.7	31.41	-	40	4	0÷2.00

The cables are made of structural steel, while the net is made of HDPP. The mechanical properties of the structural steel are derived from Eurocode 3-part 1-11 (CEN, 2006) equal to 195 GPa. The corresponding properties of the net have been derived from tensile test in Agricultural University of Athens. Since, the net is an orthotropic material, the elastic modulus E is given differently as E_X and E_Y for directions X and Y, respectively. The stiffer direction of the net is placed parallel to the short side of the net.

The simulation does not include initial prestress of the net itself as it is not recommended for two main reasons, a) the mesh of the net could permanently change size and shape due to an extensive prestress, losing the insect-proofness characteristic and b) the prestress of the independent net-segments at the reality is not easily measurable and implemented.

The analyses are performed with the use of commercial software ANSYS R19.2 (2019). The cables are simulated by elements LINK181, activating the tension only option, and the net by elements SHELL181, activating only their membrane action. The analysis is performed in 100 steps for the sake of convergence. The mesh size for both cable and net elements is 100 mm, selected after a convergence test, at which the relative difference in terms of total maximum displacement with a much finer mesh was less than 0.2%. The results that are monitored are the vertical displacement of the net and cable, the axial force of the primary cables, as well as the maximum principal stress and the equivalent von Mises stress developed in the net.

4. Results

Figure 4 presents the vertical deformation of the system at the last load step (2.00 kN/m²), Figure 5 and Figure 6 show the maximum principal stresses and equivalent von Mises stresses of the net at the last load step, respectively. Figure 7 presents the axial load of the cables at the final load step. It should be noticed that the developed stresses are lower than the expecting maximum tensile strength of the net (16.45 MPa and 25.88 MPa for the net-material 1 and 2, respectively), according to the performed tensile tests by Giannoulis et al. (2021). Figure 8 to Figure 11 display graphically the results for the middle span of the model for all load steps. Thus, these diagrams could be used for any level of snow load in the range of 0-2.00 kN/m².
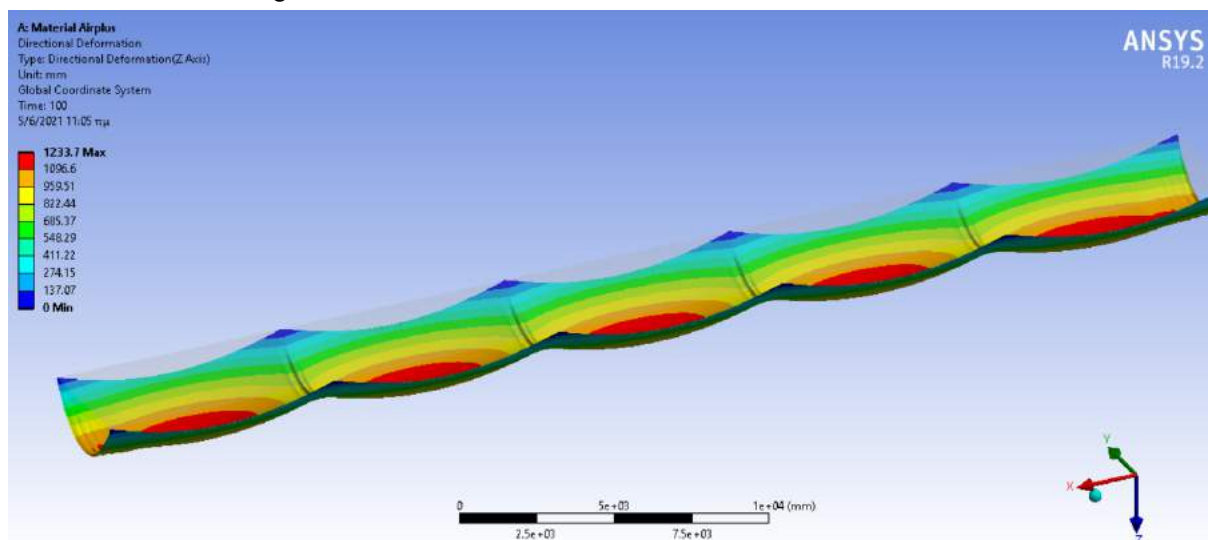

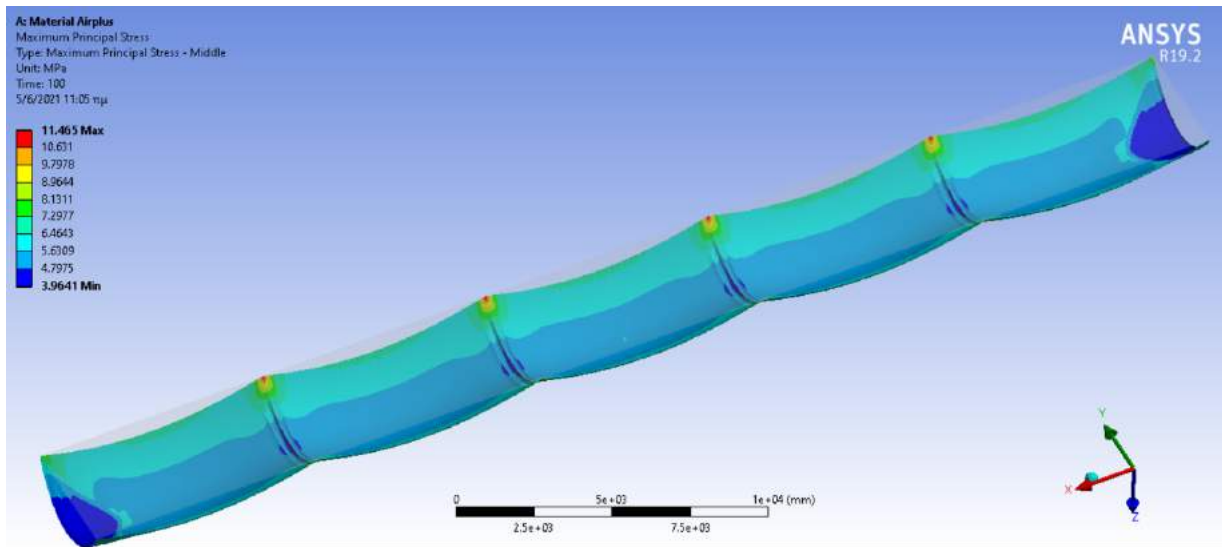Figure 4 Vertical displacements at final load step

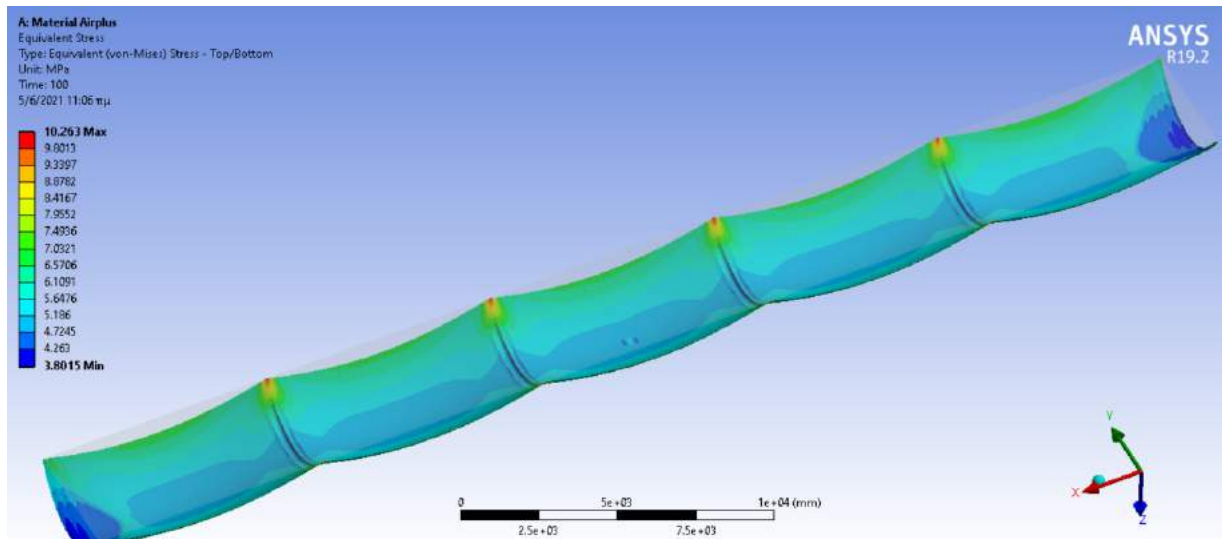Figure 5 Maximum principal stresses at final load step

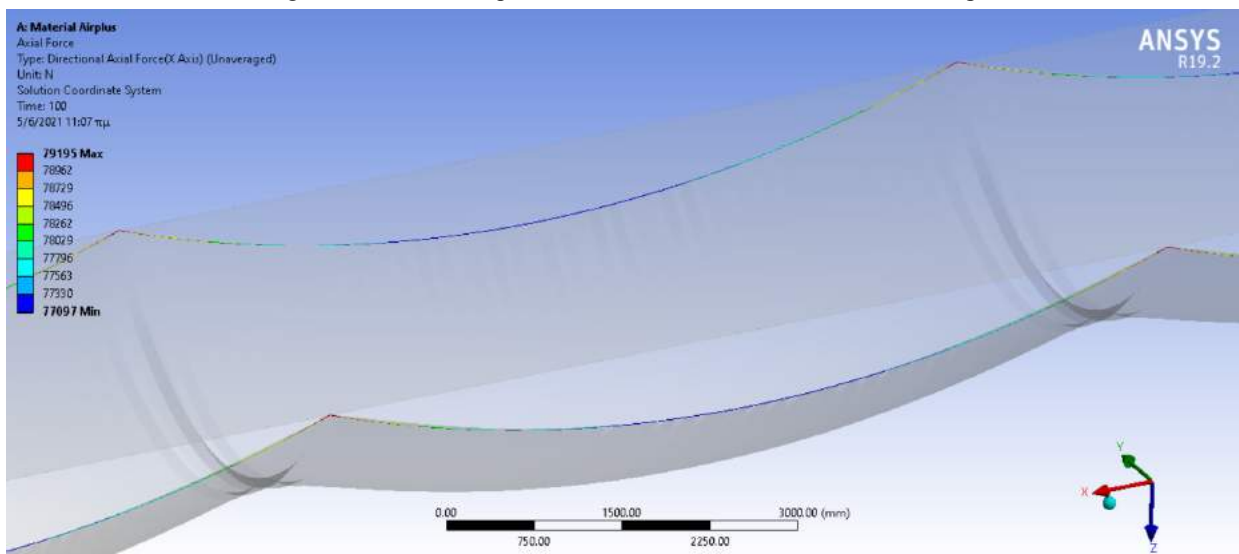Figure 6 Maximum equivalent von-Mises stresses at final load step

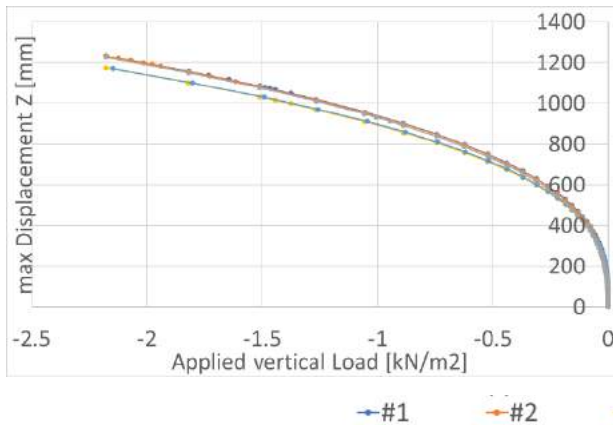Figure 7 Axial load of cables at the final load step

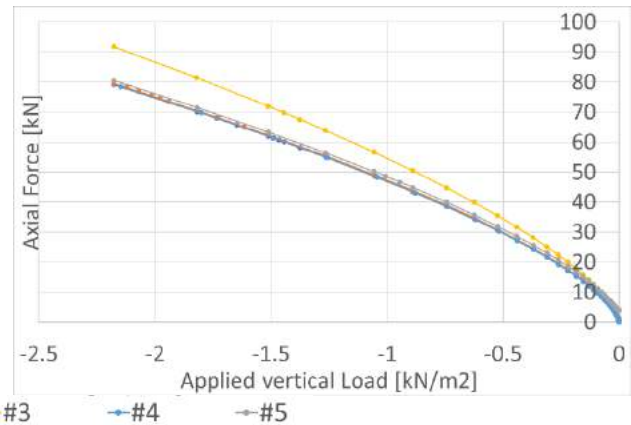Figure 8 Applied vertical load vs. maximum displacement

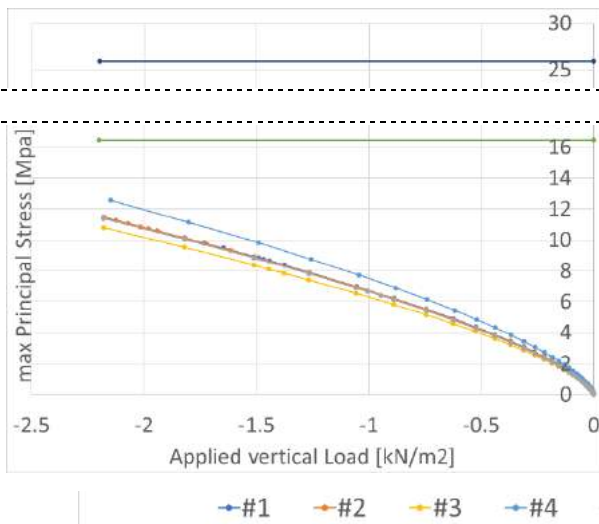Figure 9 Applied vertical load vs. Axial force of the cables

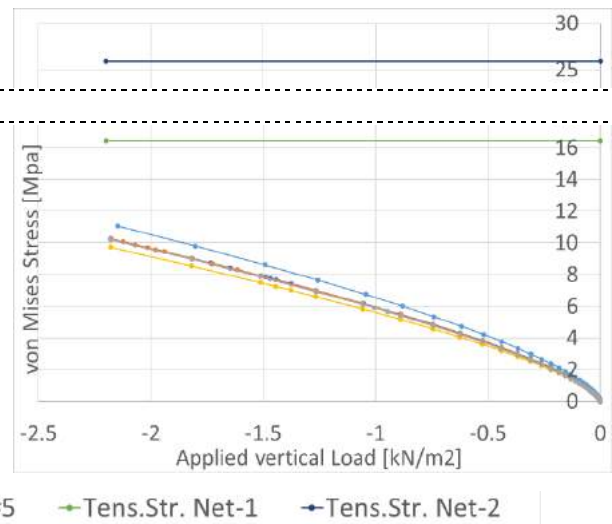Figure 10 Applied vertical load vs. maximum principal stress of the net

Figure 11 Applied vertical load vs. maximum von Mises stress of the net

All four diagrams highlight the nonlinear character of the structural behaviour of the system. Interpretating the results derived from the different parametric analyses the following annotations are made: a) a thicker cable leads to lower stresses in the net, as the stiffer cable carries a higher proportion of the applied load. b) The prestress of the cable does not significantly influence neither the appeared stresses in the net nor the axial forces of the cable. c) a stiffer net-material as well as a thicker cable can slightly only alleviate the maximum displacements of the net. Additionally, the performed analyses show that the displacements under snow load are expected to be so large that are crucial to be considered in the operational design of the nethouse. Deformations around 1000 mm could significantly affect the design, the position, and the functionality of any secondary operating system. Moreover, although the secondary cables of a typical nethouse are placed at a lower level in respect to the primary cables, under such severe deformations of the net the contact of the net to the secondary cables is highly likely to occur. This potential contact could lead to a sudden modification of the static system and subsequently could lead to an unpredictable structural response.

Figure 8 displays a good convergence of the maximum displacement, regardless the values of the different examined parameters. Thus, this diagram could be used at a preliminary design to estimate the maximum displacements of the roof of a nethouse with similar topology and materials. Accordingly, an averaged curve could be derived from Figure 10 and/or Figure 11 in order to estimate the final stress of the net under a given level of snow load. This would be especially useful to decide which type of net is adequate from the static point of view for a specific application. It could also be used as a guide for the possible use of nets reinforced with longitudinal synthetic cables, when no other solution is available.

5. Conclusions

The importance of the snow action as a key design parameter for nethouses is highlighted. Usually, the snow load is ignored because nethouses are mainly developed in regions with low risk of snowfall. However, even in the main territory of Greece, Italy, France, and other Mediterranean countries the snow loads recommended by Eurocodes for conventional structures is a dominant design load in respect to any other design loads of a nethouse. The results of the present analysis prove the magnitude of the expected deformations, as well as the corresponding net-stresses that could reach the tensile strength of the net-material. Furthermore, from the presented results some qualitatively conclusions could be extracted. The developed vertical deformations are large, and this fact should be considered carefully during the design procedure taking into account that a heavy loaded net with such deformations is highly likely to destroy any secondary non-bearing system of the structure, agricultural equipment, or even the crop. These displacements should be limited with innovative solutions. Recommendations on this direction could be the stiffening of the net with the use of longitudinal reinforcing synthetic cables or even a smart release mechanism. A release mechanism could be activated at a specific load-level that is safe for the structure but preventing the structure from overstress in case of an exceptional snowfall and/or excessive deformations.

Acknowledgment

References

Abdel-Ghany, A.M., Al-Helal, I.M., Picuno, P., Shady, M.R. (2016). Modified plastic net-houses as alternative agricultural structures for saving energy and water in hot and sunny regions. Renewable Energy, 93: 332-339. https://doi.org/10.1016/j.renene.2016.02.084

ANSYS, 2019. ANSYS Mechanical documentation, release 19.2, ANSYS Inc., Canonsburg, PA 15317, USA.

Bartok, J. 2014. 10 snow-related causes of greenhouse failure. In Cornell Cooperative Extension. Cornell University. http://cvp.cce.cornell. edu/submission.php?id¼260.

Briassoulis, D., Mistriotis, A., Eleftherakis, D., (2007a). Mechanical behaviour and properties of agricultural HDPE nets, Part I – testing methods. Polymer Testing, 26, 822–832. DOI: 10.1016/j.polymertesting.2007.05.007

Briassoulis, D., Mistriotis, A., Eleftherakis, D., (2007b). Mechanical behaviour and properties of agricultural HDPE nets, part II – analysis. Polymer Testing, 26, 970–984. DOI: 10.1016/j.polymertesting.2007.06.010

Briassoulis, D., Dougka, G., Dimakogianni, D., Vayas, I., 2016. Analysis of the collapse of a greenhouse with vaulted roof. Biosystems Engineering. 151, 495-509. https://doi.org/10.1016/j.biosystemseng.2016.10.018.

CEN., (2001), EN-13031-1: Greenhouses: Design and construction Part 1: Commercial production greenhouses. Brussels: Committee Europeen de Normalisation.

CEN., (2003), EN-1991-1-3: Actions on structures Part 1-3: General actions and Snow loads. Brussels: Committee Europeen de Normalisation.

CEN., (2006), EN-1993-1-11: Design of structures with tension components, 2006, Brussels: Committee Europeen de Normalisation.

Chouinard, G., Firlej, A., Cormier, D., 2016. Going beyond sprays and killing agents: Exclusion, sterilization and disruption for insect pest control in pome and stone fruit orchards. Scientia Horticulturae. 208, 13-27. https://doi.org/10.1016/j.scienta.2016.03.014

Giannoulis, A., Briassoulis, D., Papardaki, N.G., Mistriotis A., 2021. Evaluation of insect-proof agricultural nets with enhanced functionality. Biosystems Engineering. 208, 98-112. DOI: 10.1016/j.biosystemseng.2021.05.012

Hanafi, A., Bouharroud, R., Amouat S., Miftah, S., 2007. Efficiency of Insect Nets in Excluding Whiteflies and Their Impact on Some Natural Biological Control Agents. Proc. VIIIth IS on Protected Cultivation in Mild Winter Climates. Morocco.

NGMA, (2004). Structural design manual. Retrieved 7 22, 2016, from The National Greenhouse Manufacturers Association (NGMA): https://www.ngma.com.

A Full-scale Experimental Analysis of the Microclimate in Two Neighbouring Insect-proof Nethouse Tunnels

Anastasios Giannoulis [a,*], Antonis Mistriotis [a], Demetres Briassoulis [a]

[a] Department of Natural Resources & Agricultural Engineering, Agricultural University of Athens, Athens, Greece

* Corresponding author. Email: agian@aua.gr

Abstract

Insect-proof nethouses are nowadays considered as an efficient means of cultivation protection. They can be an alternative to the -susceptible to environmental hazards- open-field summer cultivations, allowing for significantly increased crop quality and yield. Some mesh configurations of the net cladding materials of such structures have been lately associated to adverse microclimatic conditions at the nethouses interior negatively affecting the crop. The need to protect cultivations from extremely small-sized enemies has led to very dense mesh structures imposing decreased ventilation rates. Net manufacturing companies focus on developing novel types of insect-proof nets to address this issue. A full scale experiment of two neighbouring small tunnel-type nethouses has been carried out in the experimental field of the Agricultural University of Athens. This experiment was aiming to compare the performance of two different types of innovative insect-proof nets as cladding materials. The first net is designed to enhance the airflow through them, while the second to disorient pests by blocking specific radiation wavelengths required for the navigation of the insects. Moreover, the second net offers an additional shading effect that reduces the incoming solar radiation, thus moderating temperature rise during summer. Wind velocity and direction measurements at different locations at the nethouses level allowed for the evaluation of the airflow pattern around and inside the insect-proof structures. Recorded data of temperature and relative humidity inside the nethouses were compared to the open field conditions so that the microclimate developed at their interior could be estimated. Solar radiation was also recorded. Despite shading, measurements indicate that temperatures inside both nethouses are higher as compared to the ambient conditions.

Keywords: insect-proof nethouse, microclimate, airflow pattern, full-scale, enhanced insect-proof nets

1. Introduction

The use of nethouses as a sustainable protected cultivation systems is steadily growing due to their ability to regulate solar radiation (shadenets, photoselective nets, etc.), protect from hail or to exclude harmful insects (insect-proof nets). They enable the implementation of environmentally friendly cultivation practices, producing higher quality produce and higher yields through decreased use of insecticides, limited damages by insects and viruses and reduced irrigation needs. Additionally, their permeable character results in lower wind pressures on the nethouse allowing for the design of light-weight, low-cost and easy to install steel structures.

Insect-proof nethouses use as cladding materials plastic nets able to protect crops from various types of enemies. This can be achieved by means of physical exclusion -insects excluded by adjusting the size of screen holes to the size of the targeted pest – and/or by optical exclusion by blocking their vision (i.e., blocking/absorbing specific ultraviolet [UV]-visible radiation spectra) (Ben-Yakir et al., 2012; Rigakis, 2015).

Insect-proof nets are usually the less porous nets within the market of agricultural nets. The need to exclude significantly small size insects such as aphids, aleyrordidae etc., requires a very dense net structure. It has been reported that the dense mesh configurations of insect-proof nets reduce the air exchange rate with the environment inside the protected space, resulting in a microclimate unfavorable for the protected cultivation (e.g., higher temperature and humidity during the summer period) (Mahmood et al., 2018; Desmarais et al., 1999; Tanny et al., 2003). For this reason, net manufacturers have lately focused on producing novel insect-proof nets with enhanced properties, based on two different types of technologies: manufacturing finer fibers and appropriate mesh configuration for the improvement of the ventilation rates achieved ("Biorete® Air Plus insect screen", 2018; Giannoulis et al., 2021); keeping pests away through the so-called 'optical' exclusion by using radiation absorbing additives at specific wavelengths that interfere with the orientation of the insect's light receptors ("Anti-insect (polysack)nets", 2021; Ben-Yakir et al., 2012; Giannoulis et al., 2021).

This research work presents a full-scale experiment regarding two neighboring tunnel nethouse structures. Insect-proof nets offering enhanced ventilation (finer fibers) and optical exclusion (additives that disorient insects) were used as cladding materials for the nethouses. The air velocities around and inside the nethouses were measured to estimate their air-exchange ability. Microclimatic parameters such as temperature, relative humidity, and irradiance were also recorded inside the nethouses and compared to the ambient conditions. The present study aimed to evaluate the performance of the new types of insect-proof nets. Comparisons between the data acquired for the different cladding materials demonstrate the pros and cons of the new technology insect-proof nets offering a guide for their optimization.

2.   Materials and Methods

2.1. Full-scale experimental setup

The full-scale experiments took place in the experimental field of the Agricultural University of Athens, located in Spata, Attiki, Greece (Figure 1). The area of the field is equal to approximately 4000 m^2. At the NE direction and at 60 m from the location of the experimental setup, a 6 m high tree windbreak exists. Additionally, there is a 4 m high storage facility at the S-SW direction and at approximately 92 m from the experimental setup (Figure 1, left).

Figure 1. The experimental field; Field dimensions (left, Zoom Earth), magnified image (middle, Google Maps), anemometer and wind vane at 4m height

At 10 m from the northern nethouse, a 10 m high mast exists (Figure 1, middle and right). Two rotary cup anemometers (at 10 m and 4 m high) and a wind vane (at 4 m high) were installed at the mast to constantly monitor the wind direction and velocity of the undisturbed flow.

2.2. Insect-proof nethouse structures

The nethouses were low-rise semi-circular steel frame structures (tunnels) with a ridge height of 2 m, a span width of 4 m and length equal to 8 m (Figure 2, left). The insect-proof cladding materials were selected to be the OptiNet 50 mesh (Ginegar, Israel; optical exclusion technology; porosity: 38.7%; OptiNet) and the 3353BT Biorete 50 Mesh AirPlus (Arrigoni, Italy; enhanced ventilation technology; porosity: 53.4%; AirPlus) and they were employed as covering materials on the full scale nethouse tunnel structures. The OptiNet was installed at the northern nethouse structure (OptiNet Nethouse), while the southern nethouse was covered with the AirPlus insect-proof net (AirPlus Nethouse) (Figure 2, right).
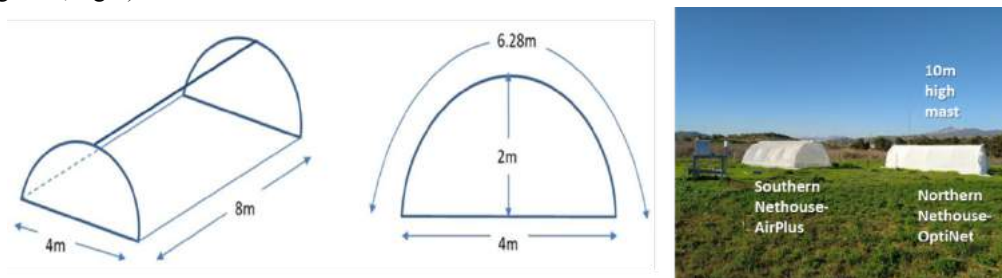
Figure 2. Sketch of the nethouse structure (left) and image of the field (right)

The nethouses were parallel to each other. They were oriented almost perpendicular to the N-S direction, with a small deviation of 4° to the NNE-SSW direction. The nets were fixed through specially designed clips on the frame. The insect-proof nets were installed so that they were stretched on the frame in a way that a strong dynamic behavior is avoided and the net fiber structure remains intact without any deformations.

2.3. Wind velocity measurements

A total 8 anemometers were used for the estimation of the airflow at discrete points windward, leeward and inside the nethouse structures. Two were located on the 10 m high mast at 10 m and 4 m, as aforementioned (M10 and M4 correspondingly). The remaining six anemometers (A1-A6) were located along the centerline of each nethouse (three anemometers at each nethouse) as shown in Figure 3, which presents a detailed sketch of the geometrical configuration of the exact anemometers' locations in the field.

Figure 3. Detailed geometrical configuration of the locations of the rotary cup anemometers

The anemometers inside the nethouses were located exactly at the mid-point of the interior area of the structure, while the outside anemometers were placed 5 m away from the nethouses sides. They were all at the same height of 1.45 m, selected so that the anemometers coul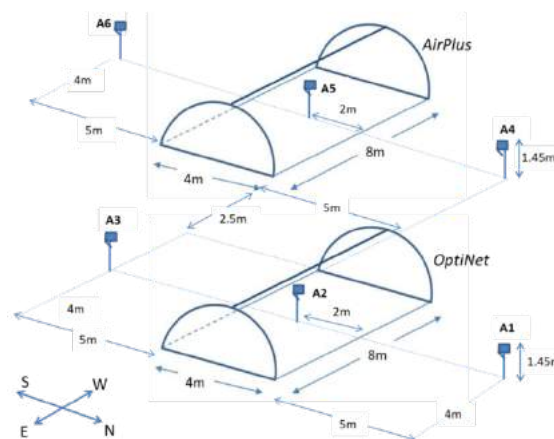d not be close to the ground or the nethouse ridge. The anemometer mounted on the mast at 10 m height, served as the reference anemometer that the rest of the anemometers were correlated to. Wind velocity data were recorded and analyzed only for South wind direction, which is perpendicular to the sides of the nethouses. The existence of the tree windbreak 60 m NE of the nethouses imposed complicated incoming airflow and thus the north wind direction was not considered. The rotary cup anemometers (Vector Instruments, model A100K) were able to measure wind speeds up to 75 m s^{-1}. Their accuracy was 0.1 m s^{-1} and their low operation threshold was 0.2 m s^{-1}. Data were recorded every 15 s and averaged over a 2-minutes period. Analysis of the data was carried out only for winds normal to the nethouse structures sides within a margin of ±10° so that a sufficient amount of data could be recorded and analyzed.

2.4. Wind direction measurements

A potentiometer wind vane was set at 4 m high to constantly monitor the wind direction (Vector Instruments, model W200P). The wind vane was calibrated at the experimental field with its zero set when pointing at the Northern direction. Wind direction measurements were accurate for wind speeds up to 75 m s^{-1}. Its accuracy was ±2° and its low operation threshold was for velocities equal to 0.6 m s^{-1}. The range of the wind vane rotation was 360° (North wind: 0° and 360°; South wind: 180°; after calibration). Data were recorded every 15 s and averaged over a 2-minutes period. The wind vane was mounted on the 10 m high mast through fixed vertical supports (Figure 1, right).

2.5. Temperature and relative humidity measurements

The temperature and relative humidity were monitored by a special probe (LOG32TH, Dostmann Electronic GmbH). The accuracy of the instrument was ±3% for the relative humidity and ±0.5^{o}C for the temperature. The relative humidity measurements ranged between 0 - 99%. The temperature measurements could range between the values of -40 to +70°C. Recordings were collected every minute (1-min recordings) for both the temperature and the relative humidity. Three probes were used. Two of them were inside the nethouse structures and one at the field that would monitor the ambient temperature and relative humidity.

All probes were mounted at the interior of perforated plastic boxes with aluminium foil covering. The boxes served as insulators so that contact with the solar radiation was avoided and only the air temperature was measured. The insulated boxes with the probes at the interior of the nethouses were placed close to the nethouse roofs (hanging), away from ground level so that the measurements are not influenced by the soil conditions. The temperature and relative humidity data recorded at the interior of the nethouses was compared to the measurements of the outside probe.

2.6. Solar radiation measurements

The solar radiation (W m^{-2}) was measured with pyranometers (Kipp & Zonen, model CMP6b). The pyranometers could monitor the solar radiation for the full solar spectrum range (285 nm to 2800 nm) and they have an operating temperature range of -40°C to 80°C. The instrument's accuracy is less than 4% (for temperatures -10°C to 40°C). The maximum irradiance (radiation flux per unit area) value that could be measured was equal to 2000 W m^{-2}. Two pyranometers were available. One was installed in turns at the interior of the nethouse structures, while the second was located outside in order to measure the solar radiation without any disturbances.

3. Results and Discussion

3.1. Air velocity results

Results presented refer to data recorded for the ten (10) days period 1 – 10 February, 2021. During this period the south wind was dominant. The 6 anemometers at the nethouses level were correlated to the data recorded for the reference anemometer M10. At 10 m height the average recorded wind velocity for this period was equal to 4.60 m s^{-1}. Figure 4 presents the correlation between the reference anemometer (M10) and the windward anemometer (A6) as well as with the anemometer located inside the AirPlus nethouse (A5), (Figure 3).
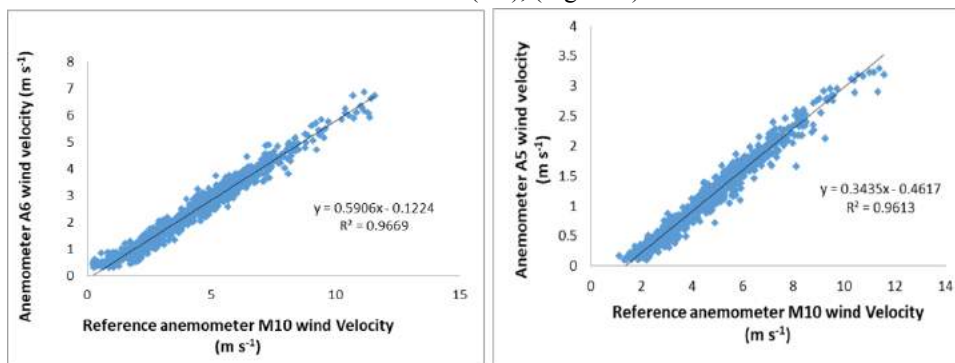

Figure 4. Graphical representation of the correlation of anemometers measurements at the nethouses level with the reference anemometer M10 at 10 m height for south wind

The results of the data presented by the sketch of Figure 5 provide an estimation of the airflow around and at the interior of the nethouses.
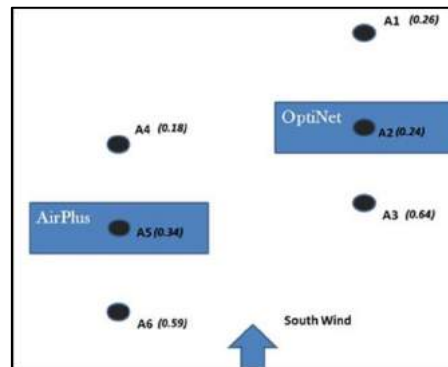

Figure 5. Velocity ratios between the anemometers around the nethouses (A1-A6) and the reference anemometer at 10 m height (M10)

The incoming wind initially interacts with the windward insect-proof nethouse and its windward anemometer (A6). As the wind approaches the most windward anemometer, the velocity ratio A6/M10 is equal to 0.59. A minor increase for the wind velocity was measured for the windward anemometer of the leeward nethouse (A3/M10=0.64) when compared to the windward anemometer A6 of the AirPlus nethouse. This can be attributed to the fact that as the airflow impinges on the windward nethouse (AirPlus), the wind that does not penetrate the net covering, moves away from the nethouse and slightly accelerates towards the A3 anemometer.

Regarding the anemometers at the nethouses interior, there is a substantial velocity drop for both of the nethouses (A5/M10 = 0.34, A2/M10 = 0.24). Results show lower wind velocity drop for the AirPlus insect-proof nethouse. This net covering was manufactured to exhibit enhanced aerodynamic behaviour and allow for better ventilation.

The wind velocity further decreases as the wind passes through the leeward side of the AirPlus nethouse (A4/M10 = 0.18). This was an expected result since the air interacts again with the insect-proof net while exiting the leeward side of the AirPlus nethouse and the velocity drops even further.

For the most leeward anemometer, namely the OptiNet nethouse leeward anemometer (A1/M10 = 0.26) the air velocity ratio was similar to the ratio of the corresponding anemometer at the interior of the nethouse (A2/M10 = 0.24). Additionally, one would expect that for the far leeward anemometer the air velocity reduction would be the highest, but this is not the case. The interaction of the wind with two obstacles close to each other could by itself result in a complicated airflow. Furthermore, the airflow around short length nethouses that use as cladding materials insect-proof

nets with dense mesh as for this study, especially the OptiNet nethouse, could formulate a highly complex pattern. For the leeward airflow and the airflow that does not become bleed flow (pass through the net coverings) turbulent phenomena could become significant and there is even a possibility for recirculations to form at the wake of the nethouses. 3D numerical simulations regarding the field experiment could verify that assumption.

3.2. Temperature and Humidity results

Three temperature and humidity measuring probes (LOG32TH) were available for the simultaneous monitoring of the temperature and relative humidity (%) inside and outside the nethouses. Comparisons provided the temperature and relative humidity (%) differences that occur due to the usage of different properties insect-proof net cladding materials for each nethouse.

Data were recorded for the period 24 April - 10 May, 2021. For this period of the year, the sun rises at 6 a.m. and sets at 8.45 p.m. approximately. For this study, the daytime was assumed to be the time-span from 7 a.m. to 8 p.m., while the night-time from 9 p.m. to 5 a.m. Figure 6 presents the typical daily temperature variations of a sunny day and the temperature difference variations (compared to the ambient temperature) for a specific day that belonged to the aforementioned recording period, namely the 30th of April (average velocity at 10m height = 1.5 m s^{-1}) Temperatures and corresponding temperature differences appear to be higher in the OptiNet nethouse (average daytime temperature: 33.9°C) as compared to the AirPlus (average daytime temperature: 31.7°C) nethouse and the external (average daytime temperature: 27.1°C) measurement. Temperatures during the night are very similar inside and outside the nethouses. This result was expected since at night no solar radiation exists and the air temperature is dominant all over the field and the nethouses interior.
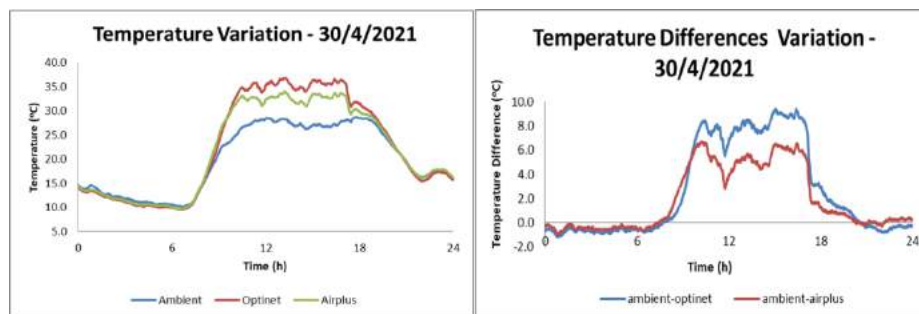

Figure 6. Temperature variation outside and inside the nethouses (left); Temperature difference variation between the nethouses and the outside temperature (right); Date: 30 April 2021

Table 1 presents calculations from the daytime temperature recordings for two different days which represent a regular temperature and windy Spring day (24th of April - average ambient temperature 14.2°C; average velocity at 10m height = 5.2 m s^{-1}) and a hot low wind velocity day (30th of April - average ambient temperature 27.1°C; average velocity at 10m height = 1.5 m s^{-1}) regarding the nethouses interior and the ambient temperature conditions. Specifically, the maximum temperature, the average daytime temperature (for the time-span 9 a.m. to 7 p.m. where temperatures inside the nethouses differ from the ambient temperature) and the maximum temperature difference between each nethouse and the field are presented.

Table 1. Daytime Temperatures and Temperature differences as compared to the ambient conditions

Date	Location	Maximum Temperature (°C)	Average Daytime Temperature (°C)	Maximum Temperature Difference (°C)
24/4/2021	OptiNet	17.6	14.5	1.9
	AirPlus	16.9	14.1	1.0
	Ambient	16.2	14.2	N/A
30/4/2021	OptiNet	36.9	33.9	9.4
	AirPlus	34.1	31.7	6.7
	Ambient	28.7	27.1	N/A

For the daytime measurements, temperatures were observed to be higher in both days at the interior of the OptiNet nethouse. For the 24th of April the temperature difference between the OptiNet and the AirPlus nethouse was low (0.7°C). For a day with moderate temperatures the air convection imposes almost similar temperature values inside and outside the nethouses. However, for the 30th of April (a low wind velocity day) temperature differences were high as shown in Table 1. Even though the OptiNet insect-proof net has an increased shading factor of 43.25%, its denser mesh (porosity: 38.7%) allows for increased temperatures to occur as compared to the ones at the AirPlus Nethouse interior (AirPlus net, shading factor: 7.81%; porosity: 53.8%), (Giannoulis et al., 2021). The average daytime temperature

values also confirm that (OptiNet: 33.9°C, AirPlus: 31.7°C, ambient: 27.1°C).

Table 1 shows that increased temperatures also cause higher temperature differences between the nethouses interior and the field, especially for days that wind velocities are low. For the 30th of April that the maximum temperature exceeds the value of 30°C inside both nethouses, the maximum temperature difference may reach values equal to 9.4°C for the OptiNet and 6.7°C for the AirPlus nethouse. For the same day the average daytime temperature difference is equal to 6.8°C for the OptiNet and 4.6°C. The results confirm that the dense mesh insect-proof nets may lead to the increased temperature at their interior. On the other hand, the AirPlus insect-proof net manufactured to exhibit enhanced air permeability, succeeds to decrease the temperature at its interior.

3.3. Relative Humidity (RH)

In general, RH (%) decreases during daytime because of the temperature increase caused by the existence of the solar radiation. Ventilation is also a significant factor for the reduction of RH (%). Figure 7 presents the RH (%) variation throughout the 5th of May, 2021 for the nethouses and the field and the variation of the difference of the relative humidity (%) between each nethouse and the external RH (%). The average velocity recorded for that day was equal to 1.9 m s^{-1}.

Both the AirPlus (average daytime RH: 32.3%) and the OptiNet (average daytime RH: 34.0%) nethouses RH (%) are lower than the ambient (average daytime RH: 40.1%) for the daytime (time-span from 7 a.m. to 8 p.m.), as depicted in Figure 7. RH (%) recordings for the nethouses do not appear to vary significantly. This was an expected outcome, since in the previous paragraph it was shown that the nethouses temperatures during the daytime are higher than the field temperatures. As a consequence, the nethouses RH (%) decreases. The RH difference (%) between both nethouses and the ambient RH conditions during the daytime may reach a value of 10 – 15% (Figure 7). During the night, RH (%) values inside the nethouses did not show any differences. For the time-span midnight to 6 a.m. the average ambient RH (%) is by 5% lower than inside the nethouses (Figure 7). However, the difference is very small (probe error: ±3%).
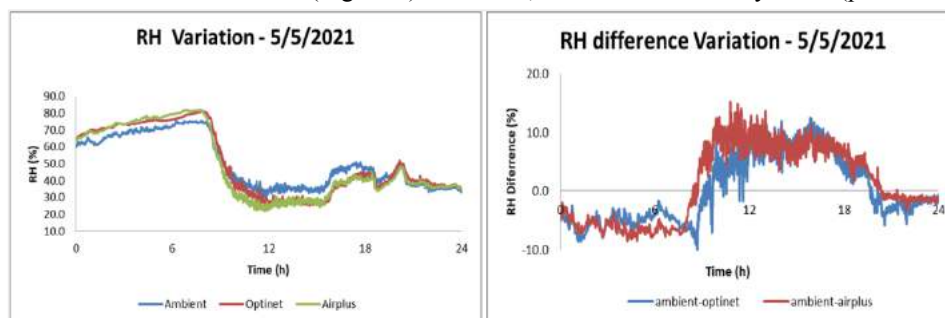

Figure 7. Daily Relative Humidity (%) variation outside and inside the nethouses (left); daily Relative Humidity (%) difference variation between the nethouses and the outside RH (right); Date: 5 May 2021

Table 2 presents calculations regarding the nethouses interior and the ambient RH (%). They correspond to the daytime RH (%) recordings for two different days which represent a low-wind velocity day (5th of May – average daytime ambient temperature = 24.3°C; average velocity at 10m height = 1.9 m s^{-1}) and a windy day (10th of May - maximum ambient temperature = 21.3°C; average velocity at 10m height = 5.9 m s^{-1}). Specifically, the minimum RH (%), the average daytime RH (%) (for the timespan 9 a.m. to 7 p.m. where temperatures inside the nethouses differ from the ambient temperature) and the maximum RH (%) difference between each nethouse and the field are presented.

Table 2. Daytime RH and RH differences to the ambient conditions

Date	Location	Minimum RH (%)	Average Daytime RH (%)	Maximum RH Difference (%)
5/5/2021	OptiNet	24.6	34.0	12.9
	AirPlus	22.1	32.3	15.2
	Ambient	29.8	40.1	N/A
10/5/2021	OptiNet	12.5	26.2	5.4
	AirPlus	10.8	26.1	3.6
	Ambient	10.5	26.5	N/A

For the low-wind velocity day (5th of May) the solar radiation was the dominant factor that affected the RH (%) values. For the AirPlus nethouse (low shading factor: 7.81%), the minimum and average daytime RH (%) are the lowest compared to the OptiNet nethouse and the field conditions. Low wind velocities have an insignificant impact to the RH (%) values. The maximum RH (%) differences reach 15.2 for the AirPlus and 12.9 for the OptiNet nethouse as compared to the field RH (%) values.

For the windy day (10th of May) results show that the RH (%) values (minimum and average) are significantly lower, when compared to the 5th of May recordings, even though for the latter average temperatures are by 3°C higher. It appears that the air convection is a more powerful mechanism regarding the decrease of RH (%) values. The maximum RH (%) difference between the nethouses and the field RH (%) are also lower for this day. High wind velocities during the daytime of the 10th of May affected equally the RH (%) levels inside both nethouses and the field, since the average daytime RH (%) values are very similar, as shown in Table 2. Only the minimum RH (%) value was slightly higher for the OptiNet nethouse (12.5%). This could be attributed to the denser mesh and higher shading factor (43.25%) of the specific nethouse. The AirPlus nethouse and the external measurements showed almost equal minimum RH (%) values.

3.4. Solar Radiation

Two pyranometers were available. One of them remained at the experimental field in order to constantly measure the solar radiation. The second pyranometer was placed in turns at the interior of the two nethouses. For the OptiNet nethouse measurements have been carried out for the period 29 January - 6 February, 2021 (days 29-37), while for the AirPlus nethouse for the period 26 February – 3 March, 2021 (days 57-64). Figure 4 presents the intensity of solar radiation for both pyranometers, inside and outside the OptiNet Nethouse (Figure 4, top) and the AirPlus nethouse (Figure 4, bottom) and their difference for the entire period that data were recorded.

It is evident that for all the days except the Day 32 (very cloudy day), the maxima of the field irradiance (W m^{-2}) are ranging between 565.2 – 686.6 W m^{-2} (average value: 624.73 W m^{-2}) while for the OptiNet nethouse between 331.4 – 421.8 W m^{-2} (average value: 375.94 W m^{-2}). For the cloudy day the maximum irradiance value recorded at the field was equal to 250 W m^{-2} and 150 W m^{-2} at the OptiNet nethouse interior. The ratio of the two averages could provide the radiation transmission at the interior of the OptiNet nethouse, which is equal to 0.601 or 60.1% (shading factor: 0.399 or 39.9%). This result is also verified for the cloudy day (radiation transmission: 150/250 = 0.599 or 59.9%).
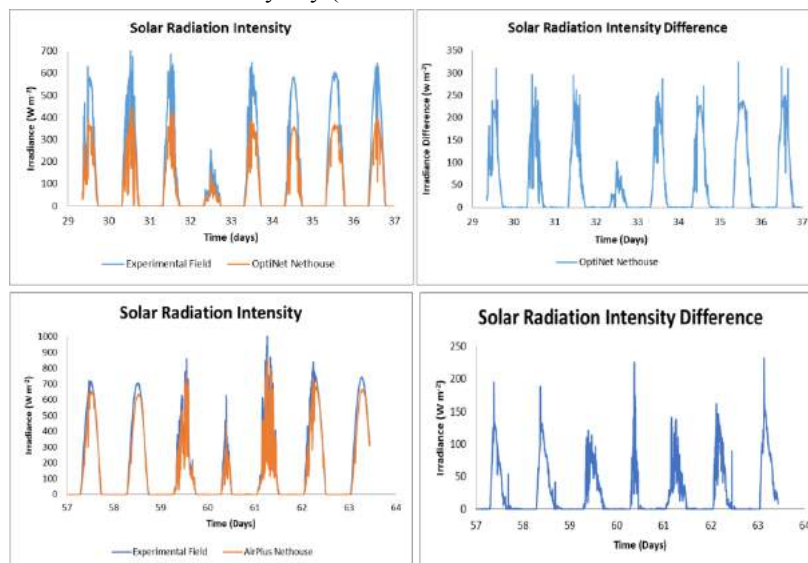

Figure 4. Solar radiation measurements at the experimental field (ambient) compared to the interior of the: OptiNet nethouse (top); AirPlus nethouse (bottom)

The solar radiation intensity at the AirPlus nethouse interior as compared to the ambient solar radiation is presented in Figure 7 (bottom). The measurements of day 63 were not concluded but are shown in Figure 7 (bottom), since the mid-day data were recorded. Days 57, 58 and 63 were very sunny days as the non-fluctuating graphs show. Days 59, 61, and 62 were days of increased solar radiation but with increased cloudiness during the day. Day 60 was mostly cloudy. For this period of measurements (except the cloudy Day 60) the maxima of the field irradiance (W m^{-2}) are ranging between 706 – 1007 W m^{-2} (average value: 810.50 W m^{-2}) while for the OptiNet nethouse between 637.3 – 869 W m^{-2} (average value: 719.63 W m^{-2}). The transmission of the solar radiation regarding the AirPlus nethouse was calculated by the ratio of the previously provided averages and is equal to 0.889 or 88.9% (shading factor: 11.1%). For Day 60 the maximum ambient irradiance was recorded equal to 620.3 W m^{-2} and 449.1 W m^{-2} for the AirPlus nethouse interior, providing a lower solar radiation transmission of 0.724 or 72.4%. The shading of the pyranometers located at the interior of the nethouses may be affected / increased in many cases by the structural elements.

Both insect-proof nets were previously tested through laboratory experiments on their optical properties (Giannoulis et al., 2021). Regarding the PAR range of the spectrum, it was shown that the OptiNet insect-proof net had the lowest solar radiation transmission while the AirPlus net was characterised with the ability to allow increased solar radiation to

penetrate. Table 3 presents the laboratory tests, the full-scale data and the values provided by the manufacturing companies (Ginegar, Israel; Arrigoni, Italy). For the AirPlus insect-proof net the laboratory and full-scale experimental results as well as the company datasheet values are in very good agreement. For the OptiNet, full-scale and laboratory estimations are very similar. The increased shade the specific net imposes as a covering is also indicated by 50-56% shading factor value given by the company.

Table 3. The optical properties of the insect-proof nets covering the pilot nethouses as tested in the field and the laboratory (Giannoulis et al., 2021)

Radiometric Properties			
Net (name)		PAR Radiation Transmission (%)	Shading Factor (%)
AirPlus	*Laboratory Test*	92.09	7.81
	Full scale experiment	88.90	11.10
	Company Datasheet	89.00	11.00
OptiNet	*Laboratory Test*	57.75	43.25
	Full scale experiment	60.10	39.90
	Company Datasheet	44.00-50.00	50.00-56.00

4. Conclusions

A full-scale experiment regarding two low-rise tunnel-type insect-proof nethouses has been carried out for the estimation of the airflow pattern around and inside them, the interior temperatures and relative humidity and the solar radiation transmission. The nethouses were covered with innovative insect-proof nets that either allowed for increased ventilation rates or included additives that could block specific radiation wavelengths so that harmful insects could be disoriented. Both covering materials offer important functional advantages although their design serves different strategies. The more permeable AirPlus allows for better air exchange that reduces air temperature during hot days and could moderate high relative humidity during nights. On the other hand, OptiNet reduces incoming solar radiation by selective shading, thus it possibly protects plants from radiation stress. The current results are indicative but cannot fully predict the effect the tested nets on cultures since plants interact actively with the micro-environment of the nethouse. For this reason, further research is planned to investigate the performance of the two studied nets in the presence of plants.

Acknowledgements

References

Anti-insect (polysack) nets, Ginegar, 2021. https://ginegar.com/product/insect-proof/

Ben-Yakir, D., Antignus, Y., Offir, Y., & Shahak, Y. (2012). Optical manipulations of insect pests for protecting agricultural crops. *Acta Horticulturae*, 956, 609-615. https://doi.org/10.17660/ActaHortic.2012.956.72

Biorete ® Air Plus insect screen, Arrigoni, 2018. http://www.arrigoni.it/agrotextile/notizie/reti-anti-insetto-biorete-air-plus/?lang=en

Desmarais, G., Ratti, C., & Raghavan, G. S. V. (1999). Heat transfer modelling of screenhouses. *Solar Energy*, 65, 271-284. https://doi.org/10.1016/S0038-092X(99)00002-X

Giannoulis, A., Briassoulis, D., Papardaki, N.G., & Mistriotis, A. (2021). Evaluation of insect-proof agricultural nets with enhanced functionality. *Biosystems Engineering,* 208, 98-112. https://doi.org/10.1016/j.biosystemseng.2021.05.012

Mahmood, A., Hu, Y., Tanny, J., & Asante, E. A. (2018). Effects of shading and insect-proof screens on crop microclimate and production: A review of recent advances. *Scientia Horticulturae*, 241, 241-251. https://doi.org/10.1016/j.scienta.2018.06.078

Rigakis, N. (2015). Theoretical and experimental Investigation of Microclimate in screenhouses. PhD Dissertation. N. Ionia, Volos, Greece.

Tanny, J., Cohen, S., & Teitel, M. (2003). Screenhouse microclimate and ventilation: an experimental study. *Biosystems Engineering*, 84, 331-341. https://doi.org/10.1016/S1537-5110(02)00288-X

Development and Testing of an Innovative System to Acidify Animal Slurry with Powdery Sulphur before Mechanical Separation

Elio Dinuccio [a], Jacopo Maffia[a]*, Luca Rollé[a], Fabrizio Gioelli[a], Gianfranco Airoldi[a], Paolo Balsari[a]

[a] Department of Agriculture, Forest and Food Science (DISAFA) University of Torino, Grugliasco, Italy

* Corresponding author. Email: jacopo.maffia@unito.it

Abstract

Slurry acidification is one of the most efficient mitigation strategies to reduce atmospheric emissions of ammonia (NH_3) and greenhouse gases (GHG) from animal slurry. Powdery sulphur (S) has been proposed as an alternative to strong acids to achieve slurry acidification, avoiding safety risks and foam formation. In the context of the Agriclose LIFE Project, a set of lab-scale trials has been carried out to test the effect of S addition to raw pig slurry before mechanical separation on NH_3 and GHG emission during storage of separated (liquid, solid) fractions. Powdery sulphur was added to fresh raw slurry in 2 doses: 0.1% (w/w) and 0.5% (w/w). Ammonia emission rates from raw slurry and separate fractions were reduced on average by up to 28% and 49% respectively. GHG emissions were reduced by 79% and 53%, respectively for raw slurry and the sum of separate fractions. On the basis of the results obtained from lab-scale tests, a full-scale prototype for acidification of pig slurry before mechanical separation has been designed, developed and tested. The prototype adopts a semi-continuous process and is composed of four main parts: a stainless-steel mixing tank provided with a rigid cover and filling sensors, an automatic system for mixing and dosing powdery S to slurry, a volumetric pump to transfer the acidified slurry to a screw press separator, and a control panel. The system automatically adds 0.2 to 1.5 kg S m-3 of slurry, allowing the separator to work at its full capacity (12-15 m^3 h^{-1}). The development of this prototype is a step forward to allow sulphur to be implemented at the farm level, achieving emission reduction and preserving nutrients.

Keywords: slurry treatment, acidification, ammonia emission, mitigation

1. Introduction

Acidification of animal slurry is one of the most promising mitigation strategies available to reduce emission of ammonia (NH_3), which is one of the main anthropogenic pollutant and it is almost entirely ascribable to the agricultural sector (up to 95%). In fact, NH_3 emissions are involved in the formation of particulate matter, water and soil acidification and water eutrophication (Bittman et al., 2014; Erisman & Schaap, 2004). Moreover, high ammonia concentration in barns represent a hazard for farmers and are detrimental for animal health (Baker et al., 2020). Many studies investigated the effects of acidification systems on slurry emissions, in all steps of the manure management chain: housing (Kai et al., 2008), storage (Misselbrook et al., 2016) and field spreading (Seidel et al., 2017). Most acidification systems rely on the use of strong acids, such as sulphuric acid and nitric acid, which are added and mixed into slurry tanks. that the addition of sulphuric acid to stored slurry allows to reduce NH_3 emission by 42-95 % (Seidel et al., 2017; Stevens et al., 1992). Alternative solutions to strong acids and milder acids were tested too (Eriksen et al., 2012; Lefcourt & Meisinger, 2001). In general, acidification of slurry should aim to lower the pH to a level of about 5-6, in order to achieve good emission mitigation results (Fangueiro et al., 2015).

The main issues encountered when applying manure acidification are related to safety concerns, since strong acids are hazardous substances and handling procedure are strictly regulated by national laws, which is one of the reasons why acidification is widely adopted only in certain European countries. Moreover, acid addition to animal slurry induces foam formation, causing handling difficulties.

This study aims to propose alternative acidification technique, relying on the use of powdery sulphur, a refinery industry by-product, to achieve acidification of slurry before its mechanical separation. A farm scale prototype for sulphur acidification was developed and its separation efficiency and working capacity were tested.

2. Materials and Methods

The experiments were carried out in two phases. In the first phase preliminary laboratory experiments were performed to test sulphur acidification mitigation potential, while in the second phase the farm scale prototype was developed and tested.

2.1. Preliminary tests and laboratory emission assessment

Pig slurry, collected from a commercial pig farm, was enriched with powdery sulphur 24 h before performing liquid solid separation in laboratory conditions. Two doses of sulphur were used: 0.1% (S 0.1) and 0.5% (S 0.5) on weight. Mechanical separation of slurry was performed using a lab-scale device, described in Popovic et al. (2017).

The raw slurry (RS), liquid (LF) and solid (SF) fractions were stored for 60 days, in 5 liters glass jars, at room temperature (15.3±2.1°C). The temperature value is comparable with usual outside spring condition in North Italy (temperature monitoring was performed with thermocouples; HOBO, OnSet).

Gaseous emissions during storage were monitored using a dynamic chamber system. Gas concentration measurement were performed using an infrared photoacoustic monitor (IPD; 1412 Multi-gas Monitor, Innova® Air Tech Instruments). The overall dynamic chamber system was described by (Berg et al., 2006). Emissions were monitored from the beginning of the storage period, every 24h for the first 2 weeks of storage and three times per week in the remaining period. The measurement protocol is as described by (Regueiro et al., 2016). Data were analyzed by analysis of variance procedure (ANOVA) followed by Tukey's post hoc test (with the significance level set at $P < 0.05$). The gaseous losses obtained are estimated as CO_2eq using the global warming potentials of 28 for CH_4 and 265 for N_2O, and considering the indirect NH_3 contribution to the N_2O emissions, estimated at 1% (Edenhofer et al., 2015).

2.2. Slurry characterisation

Chemical characteristics of RS, LF and SF at the start of the preliminary experiment and in all stages of the acidification prototype testing were analysed. Dry matter (DM) content, as a percentage of wet weight, was assessed with a precision scale (Kern®, model ABS 220-4) after drying the fresh samples (24h at 105 °C). The volatile solids content (VS) were calculated as loss upon ignition at 550 °C for 5h (VDI 4630, 2006). The pH of the slurry and liquids samples were measured directly using a glass electrode (Hanna instruments® electrode HI 1023). The pH of the solid samples was measured directly using a glass electrode for semi solid (Hanna instruments® electrode HI 1053B). Total nitrogen (N) and ammonium nitrogen (NH_4-N) were measured according to the Kjeldahl method.

2.3. Farm scale prototype development and testing

The farm scale acidification prototype (Figure 1) developed for the Agriclose LIFE project is composed of three main stages: a raw slurry tank a batch acidification system and a screw-press separator. From the raw slurry tank with mixers (1), the slurry is conveyed to a smaller (7 m^3) acidification tank (2), that works as a batch system and is provided with a sulphur dispenser (3) and mixers, finally a volumetric pump makes the acidified slurry flow to a screw-press separator (4), which divides SF and LF. The entire system is controlled from an electric panel.

Working as a batch system, the acidification tank requires a certain amount of time to fill up and perform the acidification before separation can start. The time required to acidify and separate 7 m^3 of slurry was measured and compare with the normal screw-press separator work capacity. Moreover, the Sulphur dosing system (3) was calibrated and tested to evaluate the effect of cochlea rotation speed on sulphur flow rate and the influence of the discharge system opening (which was set to two difference levels: OL1 and OL2).
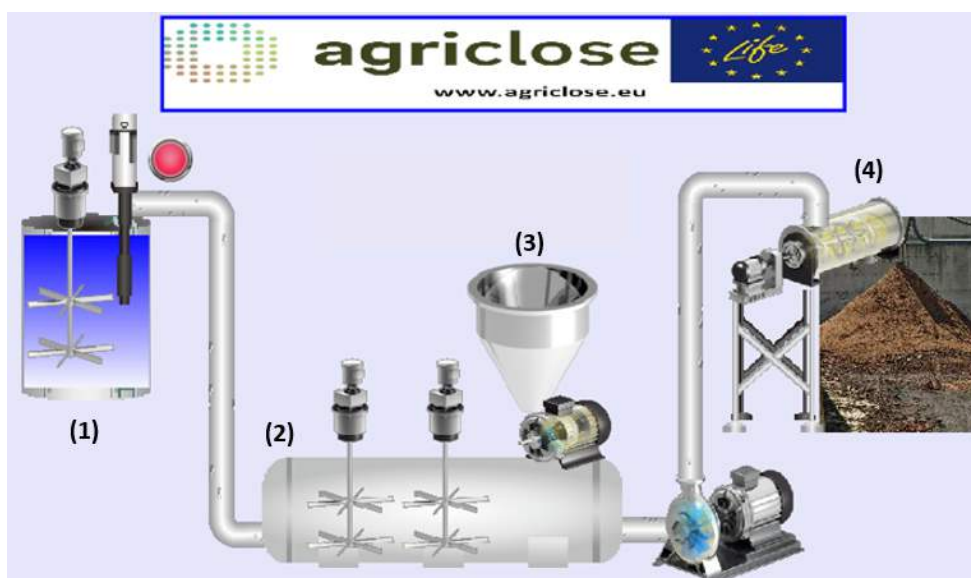

Figure 1. Acidification system prototype with (1) RS tank, (2) acidification tank, (3) sulphur dosing system, (4) screw-press separator.

2.4. Statistical analyses

Statistical analyses were performed using the R software (R core team, 2019). An ANOVA, followed by a Tuckey post hoc test was performed to evaluate differences among non-treated (NT) slurry and acidified ones (S 0.1 and S 0.5) in terms of atmospheric emissions and pH.

3. Results and Discussion

3.1. Slurry characteristics and pH

RS, LF and SF characteristics at the start of preliminary emission tests are presented in Table 1. It was observed that, apart from the difference in DM and VS among fractions, total nitrogen (N_{tot}) and ammonia nitrogen ($N-NH_3$) were more concentrated in SF, after separation. SF also had a higher starting pH. Figure 2 illustrates the pH variations during the experiment in all three thesis (NT, S 0.1 and S 0.5) and in combination with the three manure types. The S 0.5 dose effectively reduced pH for all manures until the end of the experiment, S 0.1, instead, had fewer effects on raw slurry, which was affected only in the first 20 days, and on SF, for which the effect of the S 0.5 dose was almost double the S 0.1 dose one. On LF, the S 0.1 and S 0.5 doses had similar effects. In general, the most promising pH reduction effects were observed on SF.

Slurry characteristics during prototype testing are presented in Table 2. SF DM content is higher than that observed in the preliminary trial, probably due to very low DM content of the slurry, which was three times less than the preliminary trial one.

Table 1. Initial slurry characteristics in the preliminary experiment.

	DM (% on wet mass)	VS (% on DM)	pH	N_{tot} (g kg^{-1})	$N-NH_3$ (%Ntot)
RS	4.62 ± 0.05	3.51 ± 0.03	7.18	1.12 ± 0.10	17.33
LF	2.15 ± 0.03	1.40 ± 0.01	7.29	0.70 ± 0.01	9.33
SF	16.68 ± 0.23	13.78 ± 0.13	8.28	3.26 ± 0.09	21.66
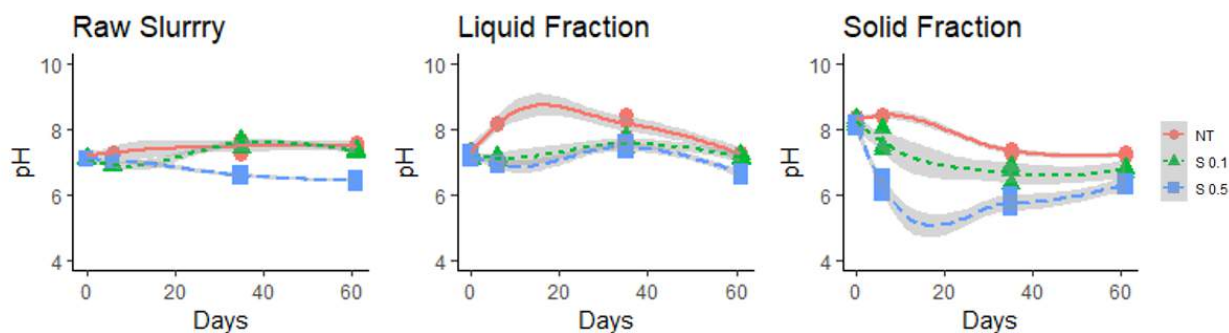
Figure 2. pH trend during simulated storage trial in all three manure types (grey areas indicate 75% confidence levels).

Table 2. Dry matter and Volatile solid content of slurries from prototype testing trial.

	DM (%on wet mass)	SV (% on DM)
RS	1.73 ± 0.01	59.65 ± 0.11
AS*	1.74 ± 0.02	58.24 ± 0.44
LF	1.47 ± 0.00	55.38 ± 0.67
SF	30.84 ± 0.15	83.25 ± 0.09

*Acidified slurry (sampled in the acidification tank).

3.2. Preliminary trial results

Ammonia and CO_2eq emissions observed during the preliminary experiments are presented in Figure 3 and 4, while table 3 reports the results of the post hoc test on total emissions. For all slurry types NH_3 emission reduction were evident and were ascribable to lower emissions in the first 20-40 days of storage. Good mitigation effects were obtained with both S 0.1 and S 0.5 for LF, while in the RS thesis the S 0.1 dose caused a delay in the NH_3 emission but ended up recovering most of the emission potential in the last 20 days of storage. A good emission reduction trend was observed also for SF, but the final emission difference resulted being not significant. Similarly, good mitigation effects were observed for greenhouse gases (GHG) emissions (Figure 4), with both S 0.1 and S0.5 showing good results in RS (S 0.5 had better mitigation effects than S 0.1) and LF (S 0.5 and S 0.1 mitigation effects were statistically similar). For SF only the S 0.5 dose allowed a significant emission reduction. In general, sulphur acidification appears to be an effective mean for emission mitigation of both NH_3 and GHG during slurry storage.
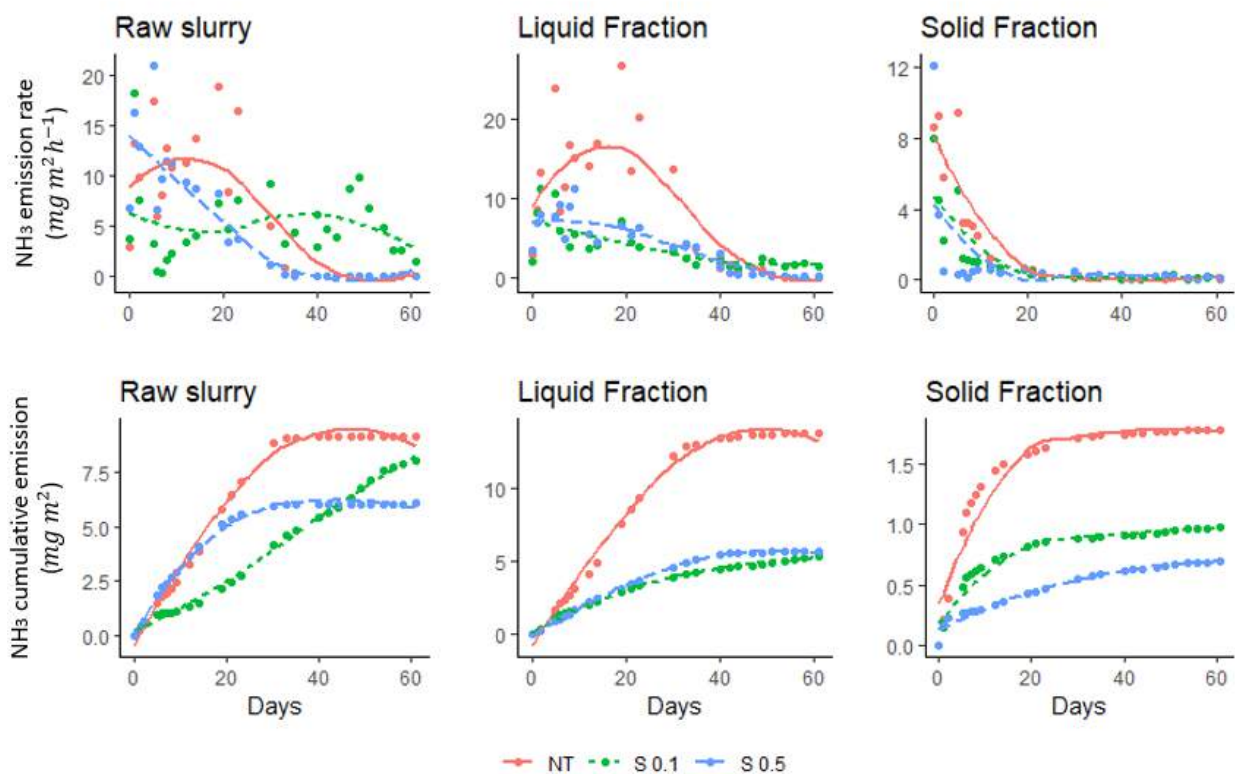
Figure 3. Daily emission trend and cumulative emissions of NH_3 during simulated storage experiment.
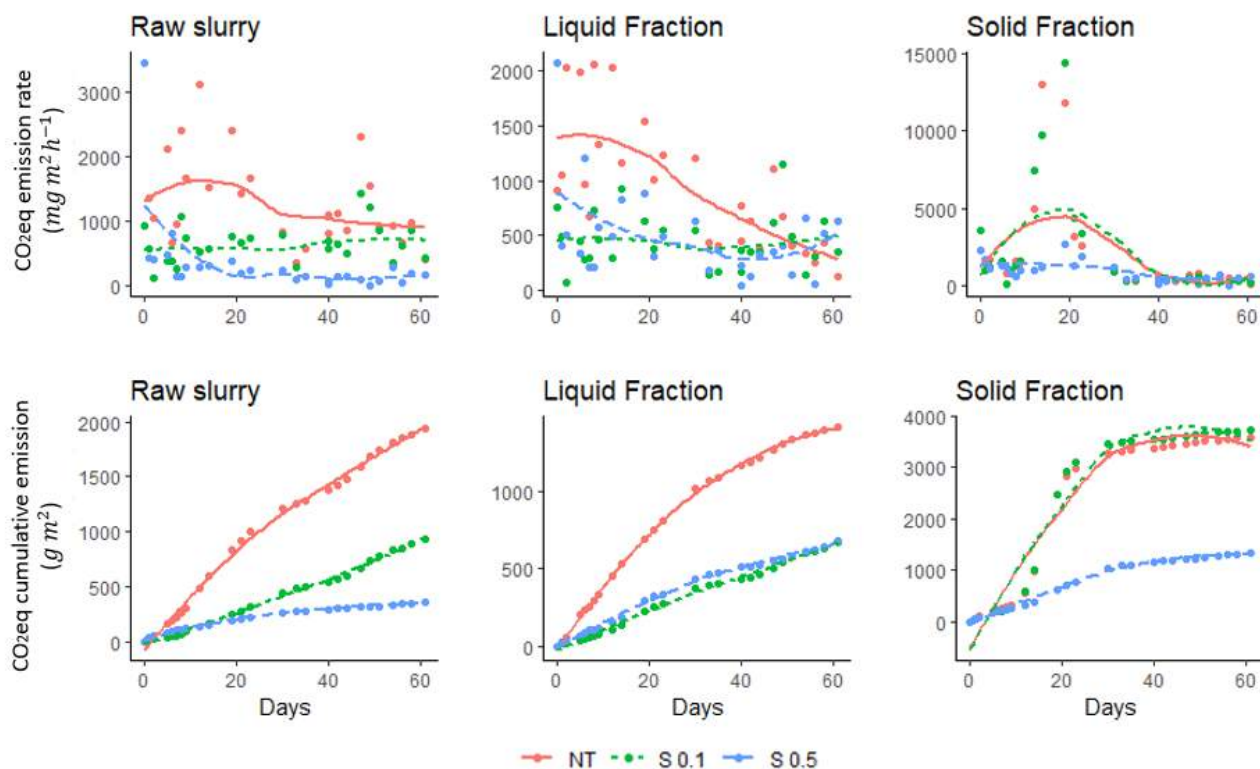
Figure 4. Daily emission trend and cumulative emissions of GHG (in CO$_2$eq) during simulated storage experiment.

Table 3. Total NH$_3$ and GHG emissions occurred during simulated storage experiment (with Tukey's post hoc test results).

			Emissions (g m^{-2})		SEM	N	P
NH$_3$	Liquid fraction	S 0.5	5.6	a			
		S 0.1	5.7	a			
		NT	13.3	b			
	Solid fraction	S 0.5	0.7	a	0.56	3	<0.001
		S 0.1	1.1	a			
		NT	1.9	a			
	Raw slurry	S 0.5	6.3	a			
		S 0.1	8	ab			
		NT	8.9	b			
CO$_2$eq	Liquid fraction	S 0.5	673	a			
		S 0.1	675	a			
		NT	1438	b			
	Solid fraction	S 0.5	1311	a	81.6	3	<0.001
		S 0.1	3677	b			
		NT	3573	b			
	Raw slurry	S 0.5	368	a			
		S 0.1	979	b			
		NT	2001	c			

3.3. Prototype performance and testing

The sulphur dosing mechanism was calibrated and tested to evaluate the rotation speed of cochlea needed to obtain the right S dosages (S 0.1 = 1 kg min^{-1}; S 0.1 = 5 kg min^{-1}), as well as evaluating the best opening level (OL) of the valve at the release point. Figure 5 presents the results of the calibration experiment. The sulphur flow rate increases linearly with incremental rotation speed. The OL2 allowed to reach the S 0.5 dosage in 1 min and, therefore, was chosen as more suited for operation.

Figure 5. Linear regression lines for sulphur dosing calibration.

The DM content of SF was very high (~30 %), highlighting good separation performances. The time required by the prototype to fill the aci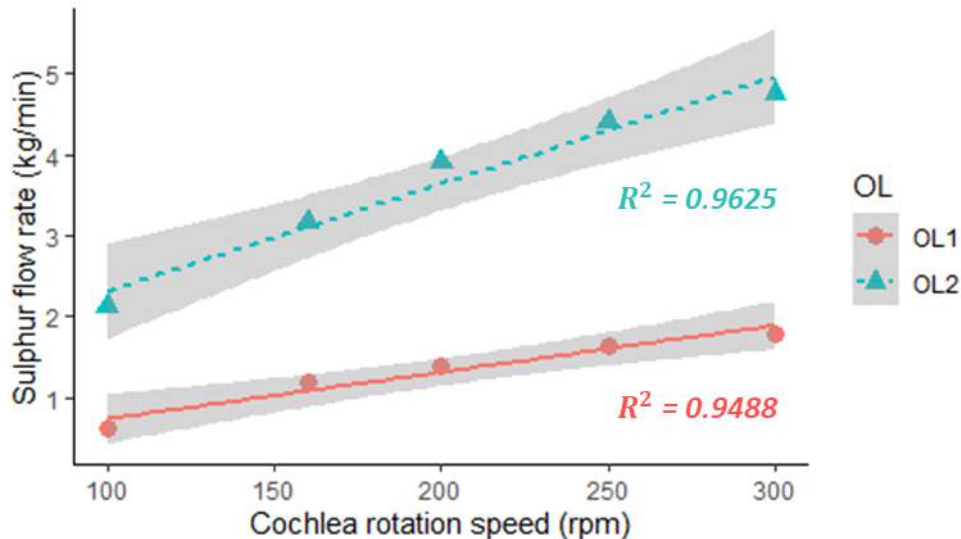dification tank with RS and perform the acidification was of 3 min and 50 ± 10 s, while the time require to separate the acidified slurry into SF and LF and was of 25 min and 8 ± 15 s. The work capacity of the system was calculated to be of 14.5 m^3 h^{-1}, which is only slightly lower than the capacity of the solid-liquid separator itself (15.0 m^3 h^{-1}). The unit cost of sulphur is of about 0.6 € kg^{-1} and, consequently, the cost of the acidification procedure would be of 0.6 and 2.9 € m^{-3} of treated slurry with the S 0.1 and S 0.5 doses respectively. In conclusion, the prototype performed well and allowed to treat the slurry without increasing in a relevant way the separation times.

4. Conclusions

An acidification approach based on the use of powdery sulphur as a mean for slurry acidification was tested in laboratory, obtaining good mitigation results, both on NH$_3$ and GHG emissions. Moreover, a farm-scale prototype for sulphur acidification was developed and tested with good operational results. Sulphur acidification represents an intriguing novelty for manure emission mitigation and treatment, although more studies are needed to assess the possible effects of sulphur on soil and evaluate the economic and energetic feasibility of the system.

Acknowledgements

References

Baker, J., Battye, W. H., Robarge, W., Pal Arya, S., & Aneja, V. P. (2020). Modeling and measurements of ammonia from poultry operations: Their emissions, transport, and deposition in the Chesapeake Bay. Science of The Total Environment, 706, 135290. https://doi.org/10.1016/j.scitotenv.2019.135290

Berg, W., Brunsch, R., & Pazsiczki, I. (2006). Greenhouse gas emissions from covered slurry compared with uncovered during storage. Agriculture, Ecosystems & Environment, 112(2), 129–134. https://doi.org/10.1016/j.agee.2005.08.031

Bittman, S., Brook, J. R., Bleeker, A., & Bruulsema, T. W. (2014). Air Quality, Health Effects and Management of Ammonia Emissions from Fertilizers. In E. Taylor & A. McMillan (Eds.), Air Quality Management: Canadian Perspectives on a Global Issue (pp. 261–277). Springer Netherlands. https://doi.org/10.1007/978-94-007-7557-2_12

Edenhofer, O., Pichs-Madruga, R., Sokona, Y., Minx, J. C., Farahani, E., Kadner, S., Seyboth, K., Adler, A., Baum, I., Brunner, S., Eickmeier, P., Kriemann, B., Savolainen, J., Schlomer, S., Stechow, C. von, Zwickel, T., & Intergovernmental Panel on Climate Change (Eds.). (2015). Climate Change 2014: Mitigation of Climate Change ; Summary for Policymakers Technical Summary ; Part of the Working Group III Contribution to the Fifth Asessment Report of the Intergovernmental Panel on Climate Change. Intergovernmental Panel on Climate Change.

Eriksen, J., Andersen, A. J., Poulsen, H. V., Adamsen, A. P. S., & Petersen, S. O. (2012). Sulfur Turnover and Emissions during Storage of Cattle Slurry: Effects of Acidification and Sulfur Addition. Journal of Environmental Quality, 41(5), 1633–1641. https://doi.org/10.2134/jeq2012.0012

Erisman, J. W., & Schaap, M. (2004). The need for ammonia abatement with respect to secondary PM reductions in Europe. Environmental Pollution, 129(1), 159–163. https://doi.org/10.1016/j.envpol.2003.08.042

Fangueiro, D., Hjorth, M., & Gioelli, F. (2015). Acidification of animal slurry– a review. Journal of Environmental Management, 149, 46–56. https://doi.org/10.1016/j.jenvman.2014.10.001

Kai, P., Pedersen, P., Jensen, J. E., Hansen, M. N., & Sommer, S. G. (2008). A whole-farm assessment of the efficacy of slurry acidification in reducing ammonia emissions. European Journal of Agronomy, 28(2), 148–154. Scopus. https://doi.org/10.1016/j.eja.2007.06.004

Lefcourt, A. M., & Meisinger, J. J. (2001). Effect of Adding Alum or Zeolite to Dairy Slurry on Ammonia Volatilization and Chemical Composition. Journal of Dairy Science, 84(8), 1814–1821. https://doi.org/10.3168/jds.S0022-0302(01)74620-6

Misselbrook, T., Hunt, J., Perazzolo, F., & Provolo, G. (2016). Greenhouse Gas and Ammonia Emissions from Slurry Storage: Impacts of Temperature and Potential Mitigation through Covering (Pig Slurry) or Acidification (Cattle Slurry). Journal of Environmental Quality, 45(5), 1520–1530. https://doi.org/10.2134/jeq2015.12.0618

Popovic, O., Gioelli, F., Dinuccio, E., Rollè, L., & Balsari, P. (2017). Centrifugation of Digestate: The Effect of Chitosan on Separation Efficiency. Sustainability, 9(12), 2302. https://doi.org/10.3390/su9122302

Regueiro, I., Coutinho, J., Gioelli, F., Balsari, P., Dinuccio, E., & Fangueiro, D. (2016). Acidification of raw and co-digested pig slurries with alum before mechanical separation reduces gaseous emission during storage of solid and liquid fractions. Agriculture, Ecosystems & Environment, 227, 42–51. https://doi.org/10.1016/j.agee.2016.04.016

Seidel, A., Pacholski, A., Nyord, T., Vestergaard, A., Pahlmann, I., Herrmann, A., & Kage, H. (2017). Effects of acidification and injection of pasture applied cattle slurry on ammonia losses, N2O emissions and crop N uptake. Agriculture, Ecosystems & Environment, 247, 23–32. https://doi.org/10.1016/j.agee.2017.05.030

Stevens, R. J., Laughlin, R. J., Anderson, R., & Frost, J. P. (1992). Evaluation of separation plus acidification with nitric acid and separation plus dilution to make cattle slurry a balanced, efficient fertilizer for grass and silage. The Journal of Agricultural Science, 119(3), 391–399. Scopus. https://doi.org/10.1017/S0021859600012235

Structural Design and Analysed Methodology for a Flat-roof Nethouse in Greece

Sofia Antonodimitraki [a,*], Anastasios Giannoulis [b], Georgia Dougka [a], Demetres Briassoulis [b], Ioannis Vayas [a]

[a] Institute of Steel Structures, National Technical University of Athens, Athens, Greece

[b] Department of Natural Resources & Agricultural Engineering, Agricultural University of Athens, Athens, Greece

* Corresponding author. Email: santonodimitraki@central.ntua.gr

Abstract

Nethouses are low-cost light-weight structures used for cultivation purposes, protecting plants from meteorological hazards and pests and enhancing internal microclimate naturally. They offer improved crop quality, increased yield, reduction of pesticides requirements and therefore higher profitability when compared to the open field cultivations. Nethouse applications can be effective in hot and mild climate regions and they are found in various geometrical configurations depending on the specific grower's needs and environmental conditions.

The major reason growers in Europe hesitate to invest in nethouses is their empirical, inadequate design, which results in ineffective structures, since the existing Standards do not include provisions for their design and construction. In the present work, conventional nethouse typologies are presented, design requirements are discussed and design parameters are identified.

Finally, the structural design of a steel flat-roof nethouse in south Greece, based on the previous established methodology, is presented. More specifically, the loads acting on the structure are determined according to the European Standards EN 1991 and EN 13031-1 regarding the actions on structures and the design of greenhouses, respectively. Especially, wind loads are calculated through Computational Fluid Dynamic analysis due to the lack of normative provisions concerning the calculation of wind pressures on permeable surfaces. The structural design is realized according to the European Standard for the design of steel structures EN 1993. Results show that following the proposed rational structural analysis and design methodology, a safe and economic nethouse structure can be achieved.

Keywords: nethouses, structural design, CFD, agricultural structures, steel structures

1. Introduction

Nethouses are low-cost agricultural structures used for plant protection purposes offering enhanced microclimate conditions for plant growth over a specific period that extends from the early Spring to the end of Fall. They may be found in a variety of structural shapes, similar to greenhouses, but they are lighter structures covered by nets instead of plastic film. The use of suitable insect-proof nets provides natural protection against harmful insects and viruses and adverse weather conditions minimizing the pesticides requirements and ensuring increased yield, improved crop quality, reduction of irrigation water needs, delay of fruit ripening and therefore higher profitability (Mahmood et al. 2012).

Depending on the size of the cultivation, nethouse structures can be distinguished in two main categories; the low technology improvised rough structures (local-type nethouses, Figure 1a), usually intended for domestic use, and the industrial massively produced structures (standardized nethouses, Figure 1b-d) used for commercial exploitation. Local type nethouses are usually wooden structures. They require low capital, but such structures have several drawbacks such as small lifetime, lack of firmness, low light penetration and lack of adequate ventilation. Standardized nethouses, on the contrary, are prefabricated structures, manufactured massively in crafts and industries. They are, mainly, steel structures made of tubular sections with concrete foundation. Structures with a steel cable roof is also a common solution. Various configurations exist, such as flat roof, arched, duopitch and gothic nethouses. Compared to local-type nethouses, standardized nethouses require a significant investment, but are more cost – effective. They offer more rigid and durable structures, lower maintenance costs, while their prefabrication ensures a steady high-quality level, offering easy assembly and erection solutions, and even a possible relocation of the structure. Furthermore, due to the high resistance of steel, fewer structural elements with smaller cross-sections are needed. This can be advantageous for the functionality of the nethouse allowing for larger spans and high indoors luminance.

Figure 1. Local-type and standardized nethouses: (a) pitched-roof, wooden (Kittas and Katsoulas, 2018), (b) flat-roof, steel (Skytop, Greece), (c) duopitch, steel (Polysack, Israel), (d) gothic (Arrigoni, Italy)

The major problem in the use of nethouses, is the inadequacy of existing International and European standards to cover their design and construction. In contrast to the physical and mechanical properties (Giannoulis et al. 2021) of agricultural nets as well as the control of microclimate conditions (Teitel, 2001) that have been investigated thoroughly, very few studies focus (Briassoulis and Mistriotis, 2010) on the optimal design of nethouse structures from a structural point of view. It is characteristic that although the wind pressure distributions developing on nethouse structures are crucial for their performance there are no relevant provisions of how to define the wind pressure coefficients on these permeable structures. Consequently, the construction of nethouses remains mostly empirical, based on general construction guidelines (but not structural design norms). As a result, the majority of the installed nethouses are either non-safe and inefficient or expensive and overdesigned structures.

This work aims, firstly, to identify the parameters affect the design of nethouse structures and to define the requirements these structures should fulfil. At a second point, the design of a case study is presented following a rational design methodology based on Eurocodes for the structural design and on numerical analyses (CFD) for the determination of wind loads.

2. Design requirements and parameters

Cultivation needs, local climatic conditions (temperature, humidity, solar radiation, precipitation and wind) and latitude of the installation area, growing season, functional requirements of the system as well as financial and legal aspects are the most important parameters to be considered for the construction of an effective Agricultural Protective Structure (Zabeltitz,2011). The geometry and the structural system of a nethouse as well as its orientation influence not only the structural behaviour and capacity of the structure but also its functionality and economy. An overall assessment of each nethouse feature in relation with the design requirements was carried out and the results are summarized Table 1 (Antonodimitraki et al. 2020).

Table 1. Assessment of nethouse design parameters

			Requirements					
			Functionality			Structural capacity		Constructional cost
Design parameters			Light transmissivity	Ventilation	Mechanized works	Snow	Wind	
Structural system		Tensile	+	0	0	-	0[*1]	+
		Arched	--	0	0	++	0[*1]	++
		Framed	-	0	0	+	0[*1]	-
Geometry	Layout	Single-span	+	+	-	+	0[*1]	-
		Multi-span	-	-	+	-	0[*1]	+
	Basic frame shape	Tunnel	-	--	0	+	+	++
		Flat roof	-	+	0	-	+	+
		Pitched roof	+	++	0	++	-	--
		Modified arched	++	-	0	+	+	–
	Sidewalls	Vertical	0	+	-	0	-	0
		Inclined	+	-	+	0	+	0
Dimensions		Length / Width	10 m[*2]	↗+	0	0	4-5 m[*2]	0
		Span	↗+	0	↗+	↗-	0	↗-
		Height	↗+	↗+	↗+	0	↗-	↗-
		Roof slope	↗+	↗+	0	↗+	↗-	↗+

Symbols

++ very good , + sufficient, 0 no effect, - insufficient, -- unfavourable

↗+ favourable with the increase of the relevant dimension, ↗- unfavourable with the increase of the relevant dimension

[*1] All systems can sustain efficiently the wind loads, as long as they are properly designed.   [*2] Optimal values.

A nethouse structure should be able to resist all the possible actions that may act on it during its design working life and at the same time to be functional and cost effective. Regarding functionality, the main requirements refer to the optimum internal microclimate (temperature, humidity, solar radiation), which may be achieved through adequate ventilation and controlled light transmission, and the facilitation of mechanized works. Since internal conditions cannot be controlled artificially due to the permeability of the covering material, their optimization is based on the right

selection of the covering net and the nethouse geometry and dimensions which also affect the convenience of mechanized works. The geometrical configuration of a nethouse structure is defined by the arrangement and the shape of the basic frames and the inclination or not of the sidewalls. Regarding the arrangement of the basic frames, nethouses may be divided into single-span and multi-span structures. The most common shapes of the basic frame are presented in Table 1. Another design parameter of importance is the nethouse structural system. Conventional nethouse structures may be classified according to their structural system in three main categories: tensile, arched and framed structures (Figure 2).
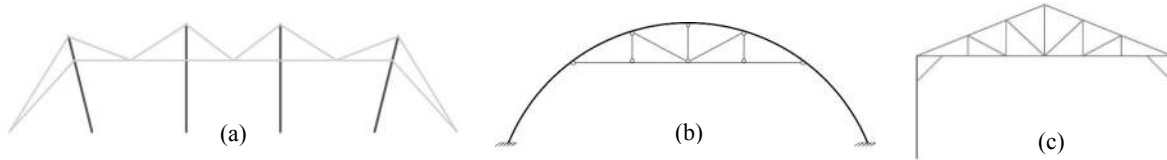

(a)   (b)   (c)

Figure 2. Common structural systems for nethouses: (a) tensile, (b) arched, (c) framed

3. Case study

3.1. Description of the structure

3.1.1.Location and geometry

The nethouse under study is located at the broader area of Tympaki in Heraklion, Crete (altitude: 20 *m* above the sea level, longitude: 24°*E*, latitude 35°*N*). This is a hot, dry region of Greece exposed to strong wind. To eliminate the wind loads on the structure and given that the possibility of a heavy snowfall is very low, a flat-roof structure with inclined sidewalls is selected. More specifically, the examined nethouse is a multi-span structure with dimensions in plan 30 x 38 *m* at the ground level and 24 x 31 *m* at the roof, covering an area of 1140 *m*^{2}. The front and rear walls have an inclination of 41.1^o, while the sidewalls an inclination of 36.8^o. In the main direction there exist five basic frames, at distances of 6 *m*, each one consisting of five bays. The spans of the two pairs of external bays are 6 m, the span of the central bay 7 *m*, while the height of the structure is 4 *m*.

Concerning the structural system, the nethouse is a tensile steel structure consisted of columns, roof and anchorage cables and a trellising system which are covered by insect-proof nets. The geometry of the structure and some structural details are presented in Figure 3. The foundation of the columns is realized by positioning them over dowel tubes which are incorporated into concrete blocks buried in the ground (Figure 3D). Respectively, the foundation of the anchorage cables is realised by connecting their ends with anchors which, as the dowel tubes, are incorporated into buried concrete blocks (Figure 3C).
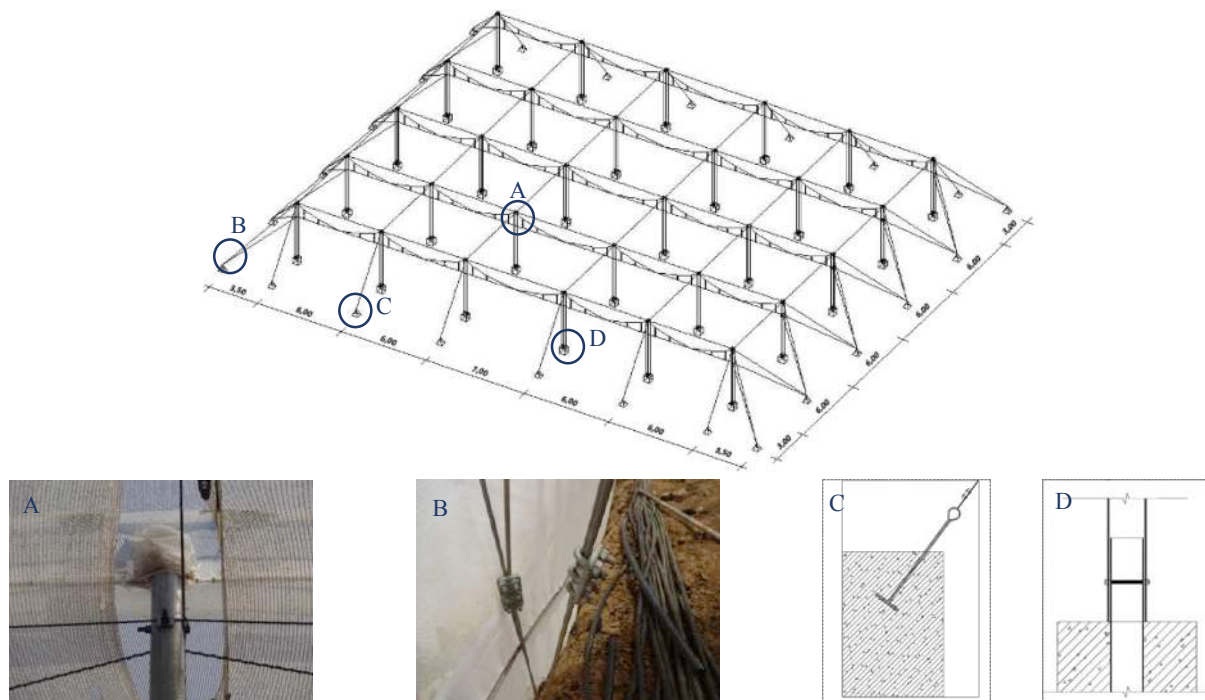

Figure 3. Geometry of the structure and structural details (c)

(c)

3.1.2.Material and cross-sections

The columns are made of galvanized steel standard hot finished Circular Hollow Sections, *CHS 139.7 x 6.3 mm* for the external columns and *CHS 88.9 x 3.2 mm* for the internal ones, steel grade S275 according to EN-1993-1-1. The cables are spiral strands of the PE series of Pfeifer company made of stainless steel, grade Y 1450, and they conform to the European Standard EN 12385. The cross-section of each cable and their characteristics according to the manufacturing company are presented in Table 2. Their modulus of elasticity equals to 130 *GPa*, while the tension resistance of the cables is calculated according to the EN1993-1-11, §6.2 considering a U-bolt grip type of termination (loss   factor ke = 0.8) (Figure 3B). The covering material of the nethouse is an insect-proof net, the OptiNet 50 Mesh from Ginegar company.

Table 2. Cross-sections and characteristics of nethouse cables

Position of cable	Direction	Cross-section	Design strength [kN]	Weight [kg/m]
Roof	X	PE 20	110.8	1.2
	Y	PE 10	57.5	0.7
Anchor	X	PE 20	110.8	1.2
	Y	PE 30	169	1.9
Horizontal – trellising	X	PE 5	26.6	0.3
Suspension - trellising	X	PE 5	26.6	0.3
Anchor – trellising	X	PE 3	15.1	0.2

3.2. Modelling

3.2.1. Structural model

The columns are modelled with beam elements with six degrees of freedom per node and the cables (except the hanger cables of the trellising system) with cable elements. Both columns and cables are discretized into finite elements with a maximum length of 0.2 *m*. The hanger cables of the trellising system are modelled with links which impose the same vertical displacement between the points they connect. The covering nets are not included in the structural model. However, their weight and their function to transfer wind and snow loads to the structural system are taken into consideration by defining load distribution areas at their position. These areas have the property to transfer positive wind loads to all the cables they are in contact, while they transfer negative wind loads only to the cables they are suitably connected to (perimeter roof and corner anchor cables).

Concerning boundary conditions, the supports of the columns are considered fixed, due to the type of foundation, whereas the anchorage cables are considered pinned, since cables are able to transfer only axial forces. The connections between horizontal cables and columns are modelled as rollers, which impose common vertical displacements between the connected members but they permit free movement of the cables in the direction of their longitudinal axis. This type of joint simulates the simple connection depicted in Figure 3A which is commonly used at nethouse structures.

3.2.2.CFD model

A 3D model is created in order to simulate the airflow around the nethouse. The nethouse is simulated as a volume covered by a porous material, perpendicular to the wind flow. The anti-insect nethouse model is placed inside a 3D rectangular wind tunnel. Half of the model is simulated due to symmetry. The model wind tunnel size is 120 *m,* 16 *m* and 36 *m* along the *x, y* and *z* directions respectively (Figure 4).
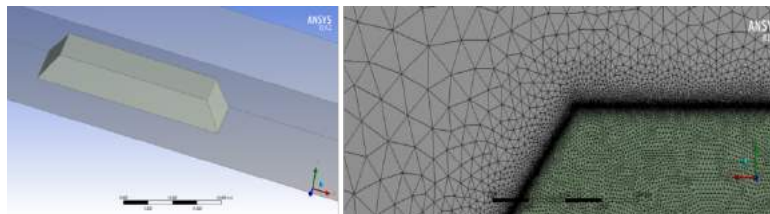
Figure 4. Numerical model geometrical characteristics and mesh formulation

The finite volumes mesh consists of 1.3 million elements. The permeable net domain is modelled as a porous material. 3D tetrahedral elements are used (Figure 4). The mesh is further refined inside and around the nethouse structure where more accurate results are required. As the air interacts with the low porosity insect-proof net small-sized airflow separations may occur.

The pressure drop, *Δp (N/m²)*, across a porous material of thickness *Δx (m)* is expressed by the Forchheimer Equation (Eq. 1).

$$\frac{\Delta p}{\Delta x} = \frac{\mu}{D}V + C\rho V^2 \quad (1) \qquad \Delta p = \beta V + \alpha V^2 \quad (2) \qquad \beta = \frac{\mu}{D}\Delta x, \ \ \alpha = C\rho\Delta x \quad (3)$$

where V $(m\ s^{-1})$ is the velocity of fluid, μ $(kg\ m^{-1}s^{-1})$ is the viscosity, and ρ $(kg\ m^{-3})$ is the density of the fluid. D (m^2) is the specific permeability of the material, and C (m^{-1}) is the aerodynamic resistance coefficient. Eq. (1) can be simplified in the case of a thin permeable material into Eq.2. The factors α $(kg\ m^{-3})$ and β $(kg\ m^{-2}\ s^{-1})$ of Eq.3 describe the air permeability characteristics of the porous material. The selected insect-proof net has an optical porosity of 38.7% while the aerodynamic coefficients α and β are equal to 2.591 $kg\ m^{-3}$ and 2.010 $kg\ m^{-2}\ s^{-1}$ correspondingly.

The wind velocity profile is set to be logarithmic at the inlet of the wind tunnel with a friction length z_0 equal to 0.05 m. The inlet velocity at 10 m high is set equal to 4.2 $m\ s^{-1}$. Inlet boundary conditions included profiles for the turbulent characteristics of the wind, k (m^2/s^2) and ω $(1/s)$ (Richards and Hoxey, 1993. The turbulent model applied for the numerical simulation is the *k-ω SST*. Wall boundary conditions are assumed for the ground surface (no slip conditions). At the outlet of the wind tunnel the pressure is set to zero to simulate the open wind tunnel end. The upper and side walls of the wind tunnel are assumed as frictionless barriers (free slip condition). A symmetry boundary condition is set for the sidewall that the nethouse coincides with the wind tunnel.

3.3. Actions

Assuming that the same type of loads act on nethouses and greenhouses, permanent, variable, accidental and seismic loads have to be taken into consideration according to EN13031. Thermal actions can be neglected, since the length and width of the structure under study are less than 150 m and nethouses may be designated as Class B structures. Similarly, accidental snow actions may be omitted for Greece according to the Annex E of EN13031. Since, nethouses are very flexible structures, inertia forces developed due to seismic displacements are very low. For this reason, seismic actions are not taken into consideration for the present study. Finally, neither a concentrated vertical action nor incidentally-present installation actions are considered for simplicity reasons.

The loads taken into account in the present study are presented in the following paragraphs. The characteristic values of the imposed loads are determined according to the provisions of the European Standards EN13031-1, EN 1991-1-1, EN 1991-1-3 and EN 1991-1-4, considering that the nethouse has a minimum design working life of 15 years.

3.3.1. Permanent actions

The permanent actions involve the following loads:

1. <u>Self-weight (G_{k1})</u>: The specific weight of steel is equal to γ_s = 78.5 $kN/m3$, while the weight of the steel cables depends on their cross-section and for the sections used is: PE 3: 0.2 kg/m, PE 5: 0.3 kg/m, PE 10: 0.7 kg/m, PE 20: 1.2 kg/m and PE 30: 1.9 kg/m for the sections. The self-weight to the net is 1.3 $N/m2$.

2. <u>Prestress (P)</u>: The cables are prestressed in order to increase the stiffness of the structure and support better the load carrying mechanism of the covering net. With the tools used in practice for the construction of nethouses, high prestress forces are difficult to achieve. For this reason, a rather low value of prestress is applied at the cables of the structure, equal to the 20% of the design tension strength of each cable as given in Table 2.

3. <u>Permanently-present installation actions (G_{k2})</u>: They are due to permanently installed equipment and irrigation systems. Assuming a tomato cultivation, the minimum value for crop growing gutters, containers, growing medium, etc. is g_{k2} = 0.13 kN/m2. As the plants are hanged from the trellising system, the permanently-present installation actions are imposed on the horizontal cables of the trellising system as uniformly distributed line loads. Loads from irrigation systems are not considered since they are laid on the ground and not hanged from the structure.

3.3.2. Variable actions

The variable actions involve the following loads:

1. <u>Wind actions (Q_{k1})</u>: Wind loads are calculated according to the methodology described in EN 1991-1-4. The pressure coefficients C_P on the structure are calculated by Eq. (4)

$$c_P = \frac{P}{\frac{1}{2}\rho V_{ref}^2} \qquad (4)$$

where P (Pa) is the average pressure on the studied surface as determined through a numerical simulation analysis (CFD), v_{ref} $(m\ s^{-1})$ is the wind velocity at $z_{ref}(m)$ which is taken equal to the height of the nethouse (h=4.0 m) and ρ $(kg\ m^{-3})$ is the air density. Figure 5(a) presents the wind pressure distribution on the walls. It may be observed that it is almost uniform on the roof, side and leeward walls and that the loading imposed by the impinging air is insignificant for the sidewalls and the flat-roof of the structure. According to EN 1991-1-4 average pressure coefficient C_P values are calculated equal to 0.58 for the windward and 0.18 for the leeward wall and equal to zero for both the roof and the sidewalls of the nethouse.

The characteristic peak velocity pressure (q_p) is calculated considering terrain category *0,* since the installation location is seaside, and the fundamental value of the basic wind velocity is taken equal to $v_{b,0}$ = 33m/s as defined in Greek Annex of EN 1991-1-4 for the Greek islands. The probability factor for the minimum reference period of 15 years equals to c_{prob} = 0.93, therefore the basic wind velocity is calculated

equal to $v_b = 30.7 \ m/s$. The final wind pressures are imposed on the structural model as uniformly distributed area loads on the corresponding load distribution areas as illustrated in Figure 5(b). Since the structure is symmetrical in both directions, only the 0° and 90° wind directions are examined.
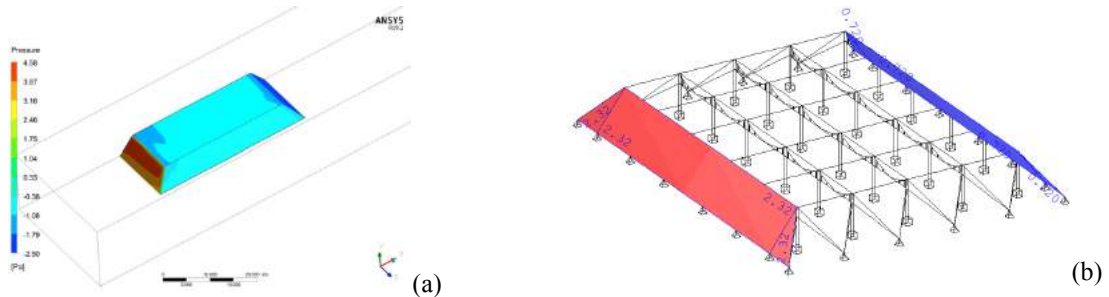

Figure 5. (a) Pressure contours on the nethouse, (b) Distribution of wind loads on the structural model

2. *Snow actions (Q_{k2})*: The calculation of the snow actions is based on the procedure of EN 1991-1-3 in conjunction with the complementary provisions of EN13031 as there is no information available in the international standards or the technical literature on the determination of snow load on permeable structures. The nethouse location is in the snow zone I as defined by the Greek Annex of EN 1991-1-3 and the topography may be classified as windswept. The nets are assumed to be present on the structure all year round firstly for the convenience of the cultivators and additionally because the nethouse may be used during the winter for the protection of a winter cultivation.

   For a return period of 50 years the characteristic value of snow load on the ground at sea level is $s_{k,0} = 0.4 \ kN/m^2$. The exposure coefficient is taken equal to $C_e = 0.8$. The characteristic value of the ground snow load with a return period equal to the design life of the structure (15 years) is determined according to the provisions of Annex E of EN13031 for France and Germany and it equals to $s_n = 0.28 \ kN/m^2$. The snow load shape coefficient is taken as $\mu_1 = 0.8$ (pitch of roof a = 0). Therefore, the snow load on the roof is calculated equal to $s = C_e \cdot \mu_1 \cdot s_n = 0.18 \ kN/m^2$ and it is imposed on the structural model as a uniform distributed area load on the roof.

3. *Crop actions (Q_{k3})*: A tomato cultivation is considered for the present study. According to the revised version of EN13031-1, the minimum value for crop actions is $q_{k3} = 0.2 \ kN/m^2$. Since the plants are hanged from the trellising system, the crop loads are imposed on the structural model as uniformly distributed line loads on the horizontal cables of the trellising system.

The load path for each load case is illustrated in Figure 6.
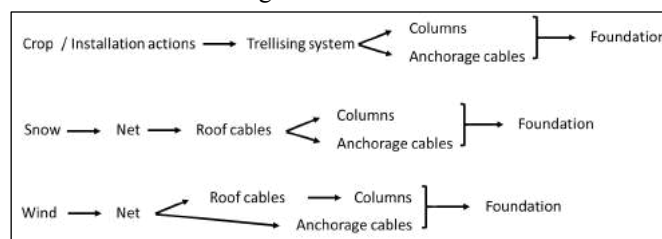
Figure 6. Load paths

3.3.3. Combinations of actions

All the actions that may occur simultaneously are considered in combination with their design values. Class B structures can be designed by considering only Ultimate Limit State (ULS). No verification at Serviceability Limit State (SLS) is required. In total ten different combinations were examined. The most critical between them are the following:

a1: $1.2 \ G_{k1} + 1.2 \ G_{k2} + P + 1.2 \ Q_{k1} + 0.6*1.2 \ Q_{k2} + 1.0*1.2 \ Q_{k3}$

a2: $1.2 \ G_{k1} + 1.2 \ G_{k2} + P + 0.6*1.2 \ Q_{k1} + 1.2 \ Q_{k2} + 1.0*1.2 \ Q_{k3}$

b1: $1.2 \ G_{k1} + P + 1.2 \ Q_{k1}$

3.4. Structural analysis

The analysis and design of the structure is realized with the SOFiSTiK software. The analysis is elastic geometrically nonlinear according to the 3rd order theory (large displacements – large rotations). The results in terms of displacements and internal forces (N, M) are presented indicatively for "a2" combination in Figure 7.

Figure 7. Structural analysis results
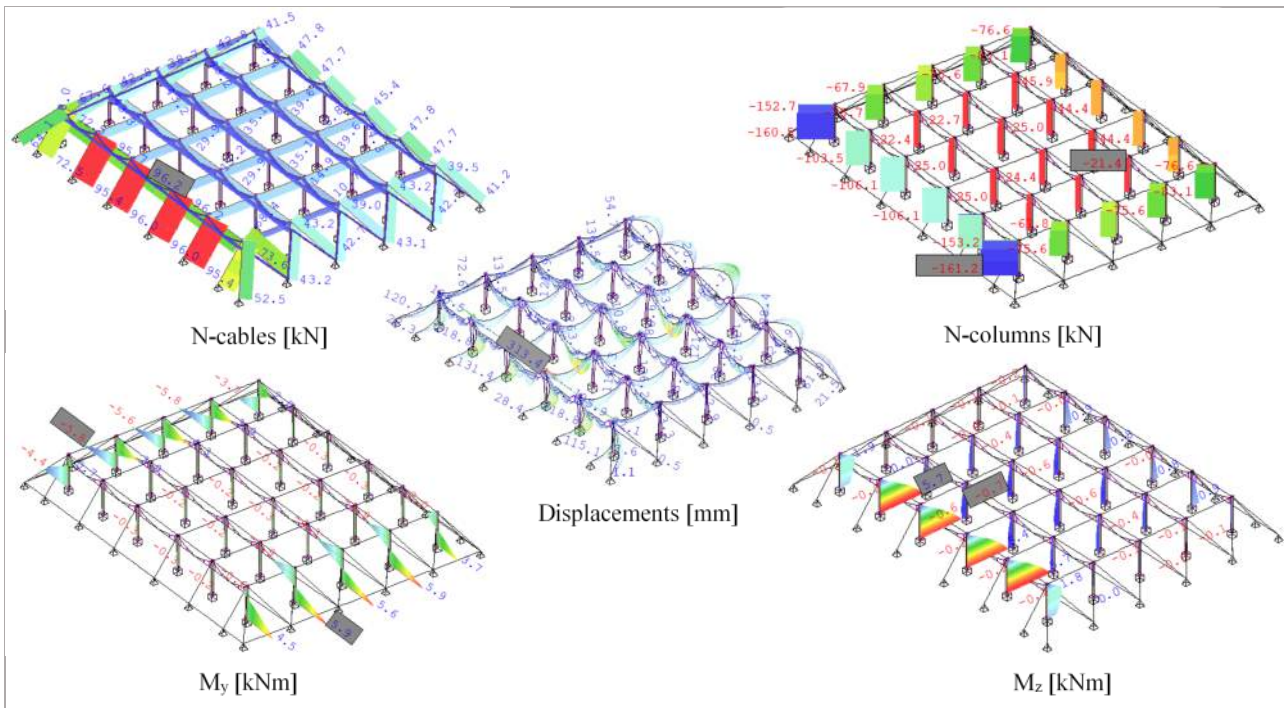
3.5. Structural design

The design of the structure is realised by implementing the provisions of EN1993-1-1 and EN1993-1-11. The cross-sections of all structural member are verified against plastification. Additionally, the columns are verified against buckling. The buckling length factor of the columns is taken equal to 1 since the internal forces are calculated by geometrically nonlinear analysis. The results under the form of utilization factors are presented for the cables in Table 3 and for the columns in Figure 8 (a) and (b), for the cross-sectional and the buckling verification respectively. The critical combinations for the design of the cables are the "a1" and "b1", while the critical combinations for the columns are the "a1" for the external and the "a2" for the internal ones.

Table 3. Utilization factors of cables

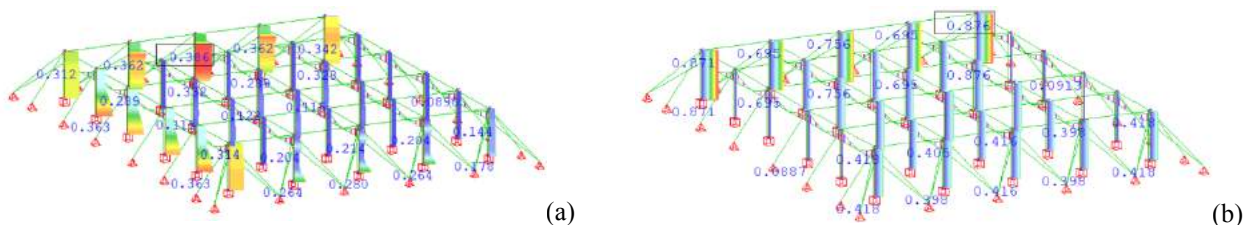| Position of cable	Direction	Utilization factor
Roof	X	0.776
	Y	0.821
Anchor	X	0.893
	Y	0.746
Horizontal – trellising	X	0.711
Suspension - trellising	X	0.613
Anchor – trellising	X	0.656

(a)

(b)

Figure 8. Utilization factors of columns: (a) cross-sectional and (b) buckling verification

4. Conclusions

In the present study the parameters that affect the design of a nethouse structure were identified. The most important between them are the local climate conditions, the functional requirements, the geometry, the dimensions and the structural system and finally financial and legal aspects.

Moreover, the design procedure of a flat-roof tensile nethouse structure at a hot, dry region of south Greece exposed to intense wind loads was presented. For the specific case study, it was found that the wind action dominates the design of the external columns and the cables and the crop action the design of the internal columns. The structural design based on Eurocodes did not display any significant difficulties, therefore, from the structural point of view, tensile nethouses with a flat roof are possible, economical solutions for regions with high wind loads and low snow loads. However, for an overall recommendation, microclimatic conditions should also be evaluated.

Acknowledgements

References

Journal articles:

D. Briassoulis and A. Mistriotis, "Integrated structural design methodology for agricultural protecting structures covered with nets," Biosyst. Eng., vol. 105, no. 2, pp. 205–220, 2010.

A. Giannoulis, D. Briassoulis, N.-G. Papardaki, A. Mistriotis, "Evaluation of insect-proof agricultural nets with enhanced functionality", Biosyst. Eng., vol. 208, pp. 98-112, 2021.

A. Mahmood, Y. Hu, J. Tanny, and E. A. Asante, "Effects of shading and insect-proof screens on crop microclimate and production: A review of recent advances," Sci. Hortic. (Amsterdam)., vol. 241, no. November, pp. 241–251, 2018.

Richards, P.J., Hoxey, R.P., 1993. Appropriate boundary conditions for computational wind engineering models using the k-ε turbulence model. Journal of Wind Engineering and Industrial Aerodynamics 46 & 47, 145-153.

M. Teitel, "The effect of insect- roof screens in roof openings on greenhouse microclimate," Agric. For. Meteorol., vol. 110, pp. 13–25, 2001.

Books:

C. von Zabeltitz, Integrated Greenhouse Systems for Mild Climates, 2011.

Standards:

CEN, "Eurocode 3: Design of steel structures - Part 1-1: General rules and rules for buildings," 2009.

CEN, "Eurocode 3 - Design of steel structures - Part 1-11: Design of structures with tension components Eurocode," 2009.

CEN, "EN 1991-1-3: Eurocode 1: Actions on structures – Part 1-3: General actions – General actions -Snow loads," 2005.

CEN, "EN 1991-1-4: Eurocode 1: Actions on structures – Part 1-4: General actions – Wind actions," 2005.

CEN, "EN-13031-1: Greenhouses: Design and construction Part 1: Commercial production greenhouses," 2001.

CEN, "Draft prEN 13031-1 Greenhouses: Design and Construction - Part 1: Commercial production greenhouses," 2018.

CEN, "EN 12385: Steel wire ropes - safety."

Technical reports:

S. Antonodimitraki et al., "Integrated design methodology for innovative insect-proof nethouse systems for high value horticultural production in Greece", Deliverable 1.1, SmartNethouse, 2020

Internet resources:

K. Kittas and N. Katsoulas, "Nethouses and their contribution to agricultural economy," 2018 in Greek.

Effect of Photoconversion Films Used as Greenhouse Double Roof on the Development of Cucumber Fungal Diseases in Spain

Ávalos-Sánchez E. [a], López-Martínez A. [a *], Molina-Aiz F.D. [a], Lemarié S. [b], Proost Kristof [b], Peilleron F.[b], Moreno-Teruel M.A.[a], Valera D.L. [a].

[a] CIAMBITAL (Centro de Investigación en Agrosistemas Intensivos Mediterráneos y Biotecnología Agroalimentaria), University of Almería, Ctra. Sacramento s/n, 04120 Almería, Spain.

[B] CASCADE SAS, Centre d'Affaires Emergence, 24 rue du Gouverneur Général Eboué, 92130 Issy les Moulineaux, France.

* Corresponding author. Email: fmolina@ual.es

Abstract

The French company CASCADE has developed the 'LIGHT CASCADES®' (LC®) technology that modifies the sunlight spectrum to plant needs. The purpose of this study was to analyse the effect of two double roof covers doped with the LC® technology on the development of fungal diseases on a cucumber crop (*Cucumis sativus*). The study was carried out in Almería (Spain) from September to December 2020 in three multispan greenhouses divided transversally with polyethylene sheets. Greenhouses 1 and 2 were divided into 4 sectors. In each greenhouse, the LC® photoconversion films (named after C1 in the Greenhouse 1 and C2 in the Greenhouse 2) were compared to the reference colourless film (without containing the LC® technology). A third greenhouse was divided in two parts, one with a double roof containing the experimental film C1 and the other one without any double roof. Two different irrigation doses were applied: (i) standard irrigation in the North zone and (ii) 20% of reduction of standard irrigation in the South zone. The study evaluated the development of cucumber fungal diseases, inside each greenhouse using the European and Mediterranean Plant Protection Organization (EPPO) regulation methods (PP 1/57 and PP 1/65). The analysis evaluated 6 cucumber plants with 4 replications in different lines per sector. The development of 3 diseases was noticed, (i) downy mildew (*Pseudoperonospora cubensis*), (ii) powdery mildew (*Podosphaera fuliginia*), and (iii) *Mycosphaerella melonis*. Statistical differences were observed in the case of downy mildew. Less incidence of disease was detected in sectors with the three different double roofs (up to 80% less), than in the sector without any double roof. A similar behaviour was observed for *Mycosphaerrella melonis*. For powdery mildew, less disease incidence was observed in the sectors with the LC® photoconversion films C1 and C2 (up to 50% less), inside the three greenhouses.

Keywords: Sunlight photoconversion film, protected crop, internal impermeable screens, ventilation, fungal infection.

1. Introduction

The province of Almería is the Mediterranean region with the highest concentration of greenhouses in Europe. This type of agriculture is developed under low-cost greenhouses, with passive systems for climate control (Castilla and Montero 2008) basically based on natural ventilation and whitening. Sophisticated systems as the use of heating, forced ventilation, humidification and other active systems are indeed difficult to monetize benefits (Valera *et al*., 2016).

One of the passive climate control techniques, which can be used for off-season crop development, is the use of plastic double roof installed inside of the greenhouses (Bartzanas *et al*., 2005; Cemek *et al*., 2006). Fixed double roofs allow to increase the temperature in cold periods during the night. In addition, double roofs can help to reducing the risk of disease by preventing the fall of condensation water drops on the crop. However, these covers may reduce ventilation and therefore increase humidity in the growing areas and excessively the temperatures during the central hours of the day (Granados *et al*., 2017).

Currently, a significant number of photo-selective materials and coatings are being developed for greenhouses, which differ in their optical properties (Hemming *et al*., 2006), but the best suitable material has not yet been found. An alternative to sunlight modifying films is spectrum photoconversion films that modifies incident solar spectrum to more-active wavelengths for plant photosynthesis (Yoon *et al*., 2020). These films, also known as luminescent solar concentrator (LSC) films can absorb the green-yellow range of the visible solar spectra and shift it to the red light range which is necessary for the photosynthesis process (El-Bashir *et al*., 2016). Spectrum conversion films can help to regulate crops growth, converting the blue–green light (450–550 nm) into the red light (600–700 nm) or the ultraviolet (UV)–violet light (350–450 nm) into the blue–green light range (Hidaka *et al*., 2008). The spectrum photoconversion films can increase photosynthetic rates at plants leaves by 15% (Yoon *et al*., 2020).

The French company CASCADE has developed the LIGHT CASCADE® technology (LC®) that once dispersed into plastic greenhouse films enables to absorb sunlight UV and green wavelengths and reemit into red and blue wavelengths respectively (Lemarié *et al*. 2018). More than 100 trials with LC® films have been performed since 2013 on several crops such as melon and potato (Lemarié *et al*. 2018) but also on red fruits and different vegetables such as tomato, pepper, eggplant. Fruits yields as well as quality have been substantially improved by the LC® films (Lemarié *et al*. 2018).

One of the most well-known fungal diseases in the Mediterranean area are Downy mildew and Powdery mildew. Both diseases are favoured by high temperature and humidity levels that are easily found within greenhouses in warm climates, such as in the Mediterranean area.

Powdery mildew in cucurbits is a serious disease in field crops and greenhouse around the world. The disease has recently been found in crops where it had not previously been observed such as *Cucumis zambianus*, *Cucurbita digitata* and *Melothria scabra* (Rennberger *et al*., 2018; Perez-García *et al*., 2009; Lebeda *et al*., 2016).

Fungal disease growth is visually characterized by the development of white powder on leaves but as well on petioles and stems, and occasionally on fruits. This disease can thus reduce plant growth, induce leave senescence and, consequently, a reduction of the quality and the marketability of fruits. Powdery mildew in cucurbits can develop at the start of crop production and can rapidly colonize plant tissues (Lebeda *et al*.,2016).

Downy mildew (caused by *Pseudoperonospora cubensis*) is one of the most important foliar damaging disease on cucurbits crops, causing significant yield losses in the United States, Europe, China and Israel (Thomas, 1996). The pathogen has a wide geographical distribution and has been reported in more than 70 countries, including areas with climates ranging from semi-arid to tropical. In addition, *Pseudoperonospora cubensis* has a wide range of hosts, infecting approximately 20 different genera of cucurbits (Lebeda and Urban, 2007; Palti and Cohen, 1980).

Downy mildew in cucurbits is easily recognizable by the development of chlorotic lesions on the leaf surface, sometimes with necrotic centres. In both melon and watermelon, foliar lesions are less defined than those of cucumber and are not always bound by leaf veins (Thomas, 1996). As infection progresses, chlorine lesions expand and may become necrotic (Oerke *et al*., 2006). Necrosis occurs more rapidly in warm-dry climates (Cohen and Rotem, 1971c). Leaves colonized by *Pseudoperonospora cubensis* suffer from changes in temperature and transpiration rates, which vary during the course of infection and on the leaf surface (Lindenthal *et al*., 2005; Oerke *et al*., 2006). Low temperatures can delay the development of symptoms and, at the same time, promote the colonization of foliar tissue. Higher temperatures result in faster lesion chlorosis that can inhibit pathogen growth (Cohen, 1977b). As the disease progresses, entire leaves may die within days of the initial infection, as the lesions expand and fuse (Thomas, 1996). A reduced canopy leads to the cessation of fruit development and increases the exposure of the fruits to the sun, which could lead to sunburn and secondary rot (Keinath *et al*., 2007). Ultimately, crop yields and fruit quality are affected (Savory *et al*. 2010).

The purpose of this study is to highlight the effects of double covers, containing sunlight spectrum conversion technologies (named after LC®), on the development of fungal diseases on a cucumber crop under Mediterranean greenhouse conditions.

2. Materials and Methods

2.1. Experimental greenhouses and cropping system

The trials were carried out in three multispan Mediterranean greenhouses, located in the UAL-ANECOOP Experimental Station "*Catedrático Eduardo Fernandez*" of the University of Almería (36º 51' N, 2º 16' W and 87 m.a.s.l.). The greenhouses are divided transversely by polyethylene sheets, constituting isolated sectors with similar cropping conditions. A total of 3 greenhouses have been used during this study.

Divisions at each greenhouse allowed to compare at the same time the two double covers i.e one harbouring the LIGHT CASCADE ® (LC®) technology and the other one the corresponding standard film (without the LC® technology). In order to avoid the possible effects linked to greenhouses orientation, the installation of the double roofs was carried out in the two sectors (i.e. East and West) of the Greenhouses 1 and 2. In Greenhouse 1 four sectors were established: two sectors with double roof with the spectrum conversion film *C1* and two sectors with double roof with the standard transparent film *St* (Table 1).

Table 1. Characteristics of the ten sectors where the spectrum conversion and standard films were installed.

Greenhouse-Sectors	Double roof type	Dimensions	Soil surface S_c [m²]	Openings surface S_V [m²]	S_V/S_c [%]
Greenhouse 1	Transparent film (control) *St*	10 m × 18 m	180	28.5	15.8
West	LC® film *C1*	10 m × 18 m	180	38.0	21.1
Greenhouse 1	Transparent film (control) *St*	10 m × 18 m	180	38.0	21.1
East	LC® film *C1*	15 m × 18 m	270	47.5	17.6
Greenhouse 2	Transparent film (control) *St*	10 m × 22 m	240	22.5	9.4
West	LC® film *C2*	10 m × 22 m	240	30.0	12.5
Greenhouse 2	Transparent film (control) *St*	10 m × 22 m	240	30.0	12.5
East	LC® film *C2*	15 m × 22 m	360	37.5	10.4
G3 - West	LC® film *C1*	20 m × 24 m	480	153.6	32.0
G3 - East	Without any double roof *No*	25 m × 24 m	600	102.0	17.0

The same experimental design has been applied for the Greenhouse 2 testing the LC® film *C2*. In Greenhouse 3 only two sectors were established: a sector with the double roof LC® *C1* with a side vent (maximum opening of 3 m) and the other sector without any double roof but with a standard side vent (maximum opening of 0,9 m). A total of 10 sectors were established (Figure 1).
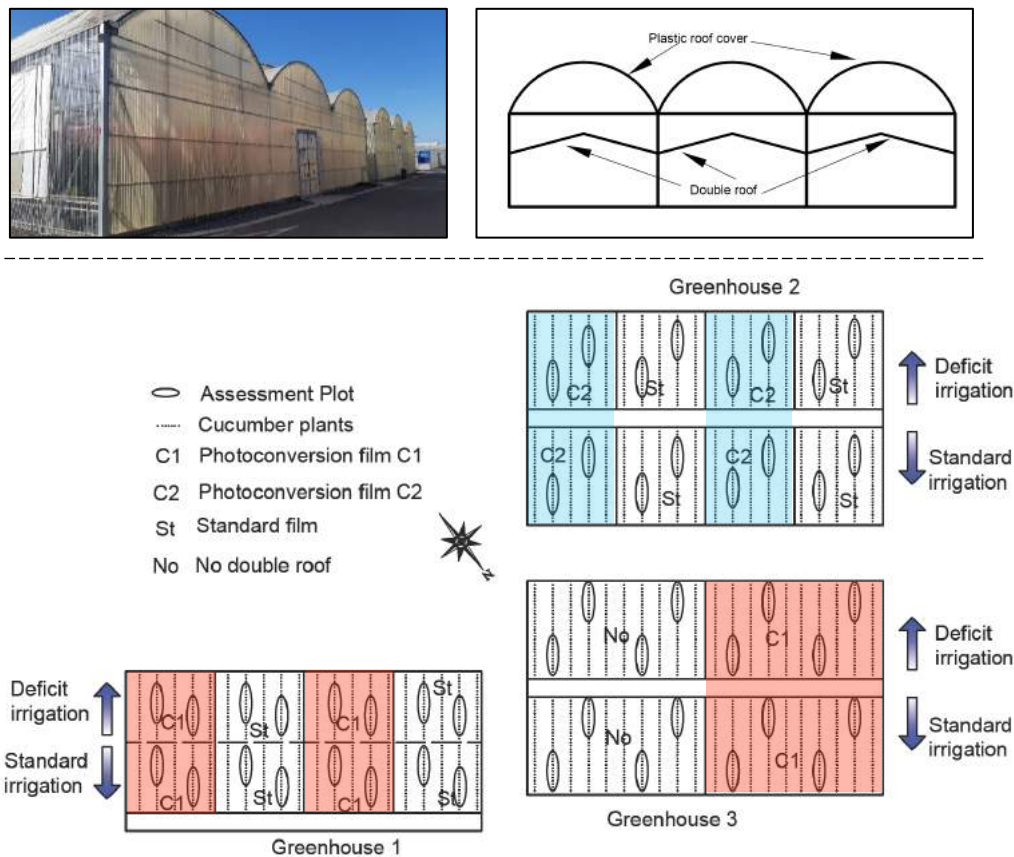

Figure 1. Greenhouse double roof installation, irrigation treatments and plots assessment distribution.

In order to analyse the possible effect of the double roofs in under water deficit stressed plants, two different irrigation doses were applied: (i) in the North zone of the greenhouses standard irrigation was applied (with drippers of 3 l/h and a maximum irrigation of 50 minutes/day) and (ii) in the South zone the water deficit condition was applied which corresponded to 80% of the standard irrigation.

2.2. Plant material

The study was carried out in an autumn-winter cucumber (*Cucumis sativus*) cropping cycle (transplanted the 7th September 2020 and ended the 2nd January 2021), with the commercial variety 'Insula RZ F1' (Rijk Zwaan Ibérica, S.A., Almería, Spain), a long cucumber of indeterminate size. Seeding was carried out on coconut fibre substrate with localized drip irrigation with a plantation density of 1 plant m^{-2}.

2.3. Plant diseases development quantification

For the design of the trial and the evaluation of diseases incidence, the EPPO standards were applied. For Downy mildew and Powdery mildew diseases, EPPO Standard PP 1/181 (Conduct and reporting of Efficacy Evaluation Trials), EPPO Standard PP 1/152 (Design and Analysis of Efficacy Evaluation Trials), EPPO PP 1/57 (Powdery mildews in cucurbits) are applicable and EPPO PP 1/65 (Downey mildew of lettuce and other vegetables, PSPECU).

The percentage of affected leaf area on the upper and lower surfaces of at least four leaves on each plant was evaluated. For each experimental sector of Greenhouses 1 and 2, two assessments plots were established in the North and in the South zone (Figure 1). In Greenhouse 3, in each experimental sector, four assessments plots were established in the North zone and in the South zone (Figure 1). In each assessment plot, 6 plants were evaluated. For each plant analysed, a minimum of 8 uniformly distributed leaves were evaluated (a total of 50 leaves evaluated by each

assessment plot). In total, for each treatment (*C1*, *C2*, *St* and *No*) 200 leaves were analysed in the north zone and 200 leaves in the South zone.

Figure 2 shows an example of quantification of infection percentage index on a cucurbits leaf according to the EPPO regulations. The evaluation of the level of diseases (*Sphaerotheca fuliginea, Pseudoperonospora cubensis* and *Mycosphaerella cucumis*) was carried out every 7 days from the beginning of the disease and until the end of the crop cycle. A final evaluation was performed 7 days before the end of the culture.
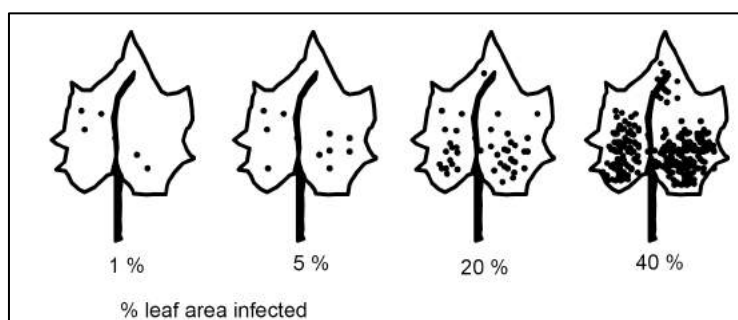

Figure 2. Example assessment % leaf area infected.

2.4. Statistical analysis

The statistical analysis of the data was performed with the software Statgraphics Centurion XVIII, using an analysis of variance (considered significant if *p*-value 0.05), comparing the mean values with the procedure of minimum significant difference (LSD) of Fisher. Bartlett, Cochran and Hartley tests were used to determine whether a sector has a similar variation. For parameters with different variance, we performed a nonparametric analysis with the Friedman test, with each row representing a block (the evaluation date), using averages graphs.

3. Results and discussion

Statistical differences were observed in the case of downy mildew, with lower disease incidence in all sectors where there was double roof in comparison to the sector without any double roof *No* (Table 2). Moreover, the use of spectrum conversion films tends to reduce infection (without any statistical difference) with respect to the standard transparent film in 3 of the 4 cases analysed (Table 2).

Table 2. Mean percentage of infection at the end of the trial (24/12/2021) in the different greenhouses.

Greenhouse	North (standard irrigation)		
Double roof	Powdery mildew *Sphaerotheca fuliginea*	Downy mildew *Pseudoperonospora cubensis*	Mycosphaerella *Mycosphaerella cucumis*
Greenhouse 1 – *C1*	$4.99 \pm 1.67^{\,g}$	$0.35 \pm 0.65^{\,a}$	$0.57 \pm 0.48^{\,def}$
Greenhouse 1 – *St*	$7.23 \pm 1.67^{\,efg}$	$0.51 \pm 0.65^{\,a}$	$0.75 \pm 0.48^{\,cdef}$
Greenhouse 2 – *C2*	$23.92 \pm 1.67^{\,c}$	$0.09 \pm 0.65^{\,a}$	$2.58 \pm 0.48^{\,a}$
Greenhouse 2 – *St*	$27.03 \pm 1.67^{\,bc}$	$0.185 \pm 0.65^{\,a}$	$1.8 \pm 0.48^{\,abcd}$
Greenhouse 3 – *C1*	$33.33 \pm 1.67^{\,a}$	$0.12 \pm 0.65^{\,a}$	$0 \pm 0.48^{\,f}$
Greenhouse 3 – *No*	$33.19 \pm 1.67^{\,a}$	$12.45 \pm 0.65^{\,c}$	$1.56 \pm 0.48^{\,abcde}$
South (20% deficit irrigation)			
Greenhouse 1 – *C1*	$5.63 \pm 1.67^{\,fg}$	$1.52 \pm 0.65^{\,a}$	$1.93 \pm 0.48^{\,abc}$
Greenhouse 1 – *St*	$11.13 \pm 1.67^{\,e}$	$1.67 \pm 0.65^{\,a}$	$1.01 \pm 0.48^{\,bcdef}$
Greenhouse 2 – *C2*	$7.08 \pm 1.67^{\,efg}$	$0.58 \pm 0.65^{\,a}$	$0.96 \pm 0.48^{\,bcdef}$
Greenhouse 2 – *St*	$10.16 \pm 1.67^{\,ef}$	$0.06 \pm 0.65^{\,a}$	$0.90 \pm 0.48^{\,bcdef}$
Greenhouse 3 – *C1*	$16.99 \pm 1.67^{\,d}$	$0.34 \pm 0.65^{\,a}$	$0.25 \pm 0.48^{\,ef}$
Greenhouse 3 – *No*	$30.38 \pm 1.67^{\,ab}$	$5.4 \pm 0.65^{\,b}$	$2.13 \pm 0.48^{\,ab}$

* Different letters indicate statistically significant difference (*p*-value = 0.95).

Globally, regardless the greenhouse considered, and the irrigation treatment applied, the highest percentages of infection have been induced by the powdery mildew (Table 2).

In the sector without double roof, the three diseases occurred at a larger extent in comparison to the three double roofs tested regardless the applied irrigation (Table 2). For Powdery mildew, in the Greenhouse 3, less incidence of

disease was observed in the sectors with the LC® film *C1* combined to ventilation (0.12% in the North Zone and 0.34% in the South Zone respectively), and within sectors with the films *C1*, which obtain the best numerical results (Table 2).

The presence of Downy mildew was the largest in the sector without double roof (Greenhouse 3) in comparison with all the sectors with double roof (Greenhouses 1, 2 and 3), showing statistically significant differences (Table 2).

Mycosphaerrella cucumis disease incidence was globally lower compared to Downy mildew and Powdery mildew, with no such marked difference between the double-roof sectors and the other sectors. The level is so low that the data is not robust enough to tell if the double roof affects or does not affect in the development of the disease.

3.1. Powdery mildew

Powdery mildew (*Sphaerotheca fuliginea*, SPHRFU) symptoms started to be observed on November 2 until the end of the trial. The disease quantification was monitored every 7 days, until December 24, 2020. At this kinetic point, some plots of the trial reached infection rates higher than 30%.

Overall, within each experimental sector, a higher percentage of Powdery mildew incidence has been observed in areas where the standard irrigation was applied (Northern area), compared to areas where the deficit irrigation was applied (Southern area) (Figure 3). The higher level of humidity that is favoured by standard irrigation, compared to a deficit irrigation, may explain the higher disease levels in the Northern area. Higher levels of humidity, in the early stages of development of the disease, favour the infection process and the survival of the spores. Once the mycelium has developed, new spores produced by sporulation and consequently after dispersion may infect new plant tissues. Sporulation and dispersion of Powdery mildew spores are favoured by low humidity, while infection and survival of these spores are favoured by high humidity (Reuveni and Rotem, 1974).
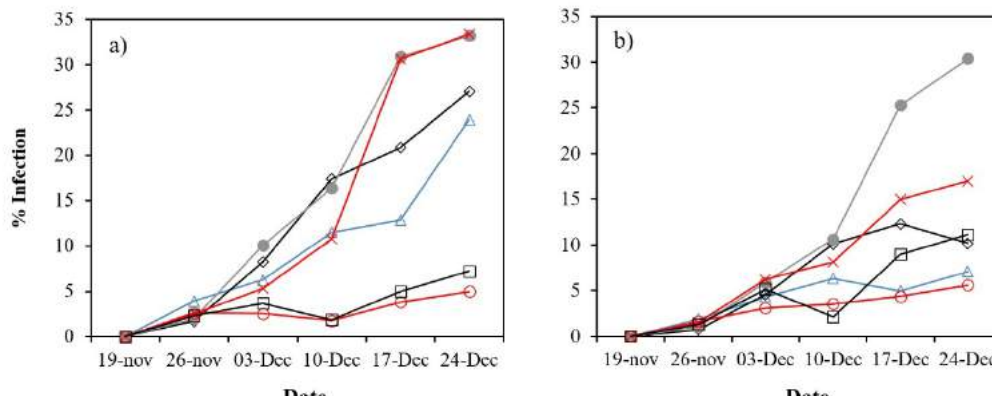

Figure 3. Development of Powdery mildew (*Sphaerotheca fuliginea*) percentage of infection over time, in the sectors with standard (a) and deficit (b) irrigation. Greenhouse 1 with *C1* film (○). Greenhouse 1 with Standard film (□). Greenhouse 2 with Standard film (◊). Greenhouse 2 with *C2* film (△). Greenhouse 3 without double roof (●). Greenhouse 3 with *C1* film (×).

The use of double roof delays the development of Powdery mildew (Figure 3). The highest value in disease intensity was found in the sector of Greenhouse 3 without double roof (with a ventilation surface of 17%), in comparison with the sector with double roof *C1* of greenhouse 3 (with a ventilation surface of 32%).

The disease developed significantly the 10th December 2020 (Figure 3). At this time, the use of the spectrum conversion films *C1* and *C2* reduced the incidence of this disease (inside Greenhouses 1, 2 and 3 under both irrigation treatments), with statistical significance in the greenhouses 2 and 3 for the standard irrigation and in greenhouse 2 for the deficient irrigation (Table 3).

Lower infection rates in the double-roof sectors with both *C1* and *C2* films were observed compared to the sectors with standard plastics in the same greenhouse (Table 3). The minimal disease occurrence was obtained with film *C1*. According to the results obtained at the end of the crop development (Fig. 3), in the sectors with double roof (regardless of the type of plastic tested) the incidence level of *Sphaerotheca fuliginea* has been lower compared to the sector without any double roof, with statistically significant differences. Considering the sectors with deficient irrigation in Greenhouse 3, 40% less incidence has been observed in the sector with double roof with the spectrum conversion film *C1* and large side vents, compared to the sector without any double roof and small ventilation. Indeed, drier environments are conducive to sporulation and dispersion of Powdery mildew spores in Cucurbitaceas (Yarwood, 1957; Aust and Hoyningen-Huene, 1986), and the combination of high humidity at night and at the beginning of the day favour the infection and spores survival during the initial stages of fungus development (Reuveni and Rotem, 1974). Many researchers have reported that high atmospheric humidity (relative humidity 80%) favours the germination, infection and subsequent development of Powdery mildew (Guzman-Plazola *et al*., 2003; Mortensen and Gislerød, 2005; Elad *et al*., 2007; Te Beest *et al*., 2008).

Table 3. Percentage of infection for *Sphaerotheca fuliginea* in the date 10/12/2020.

Greenhouse	*Sphaerotheca fuliginea*	
Double roof	**North** (standard irrigation)	**South** (deficient irrigation)
Greenhouse 1 – *C1*	1,77 ± 1,08 [f]	2,12 ± 1,08 [f]
Greenhouse 1 – *St*	1,88 ± 1,08 [f]	3,55 ± 1,08 [ef]
Greenhouse 2 – *C2*	11,49 ± 1,08 [b]	6,34 ± 1,08 [de]
Greenhouse 2 – *St*	17,38 ± 1,08 [a]	10,11 ± 1,08 [bc]
Greenhouse 3 – *C1*	10,78 ± 1,08 [bc]	8,14 ± 1,08 [cd]
Greenhouse 3 – *No*	16,36 ± 1,08 [a]	10,61 ± 1,08 [bc]

* Different letters indicate statistically significant difference (*p*-value = 0.95).

3.2. Downy mildew

Like Powdery mildew, Downy mildew also naturally appeared during this study. Percentage of incidence has been quantified in a similar manner as the one realised for Powdery mildew. Downy mildew incidence evolution was very similar in both North and South zones. The main statistically significant result here is the high incidence of this disease in the sector without any double roof Greenhouse 3 (Figure 4).
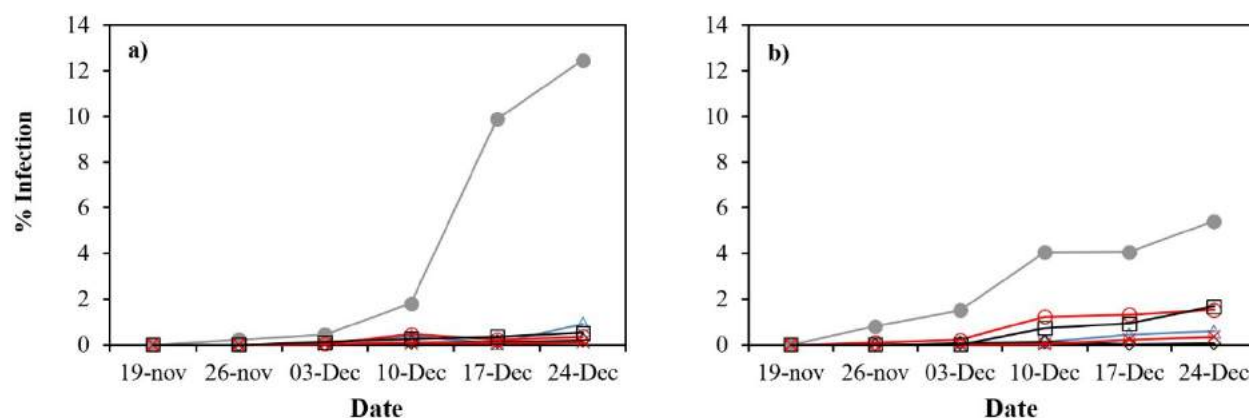

Figure 4. Development of Downy mildew (*Pseudoperonospora cubensis*) percentage of infection over time, in the sectors with standard irrigation (a) and deficit (b) irrigation. Greenhouse 1 with C1 film (○). Greenhouse 1 with Standard film (□). Greenhouse 2 with Standard film (◊). Greenhouse 2 with C2 film (Δ). Greenhouse 3 without any double roof (●). Greenhouse 3 with C1 film (×).

It has been reported that high humidity levels (above 90%) and the presence of water droplets on the leaves favours the development of spores of *Pseudoperonospora cubensis* (Rotem *et al*., 1978). Thus, it can be established that the use of double roofs greatly limits the *Pseudoperonospora cubensis* infection of the crop (Figure 4) preventing the fall of water droplets on the crop (Granados *et al*., 2017).

We observed that there is only a significant incidence of *Pseudoperonospora cubensis* in the sector without any double roof of Greenhouse 3, which was statistically greater than in the other sectors (Table 4).

Table 4. Percentage of infection for *Pseudoperonospora cubensis* at the date 17/12/2020.

Greenhouse	Greenhouse	
Double roof	Double roof	**South** (deficit irrigation)
Greenhouse 1 – *C1*	0,36 ± 0,57 [c]	0,93 ± 0,57 [c]
Greenhouse 1 – *St*	0,22 ± 0,57 [c]	1,31 ± 0,57 [c]
Greenhouse 2 – *C2*	0,07 ± 0,57 [c]	0,44 ± 0,57 [c]
Greenhouse 2 – *St*	0,13 ± 0,57 [c]	0,04 ± 0,57 [c]
Greenhouse 3 – *C1*	0,05 ± 0,57 [c]	0,23 ± 0,57 [c]
Greenhouse 3 – *No*	9,89 ± 0,57 [a]	4,07 ± 0,57 [b]

* Different letters indicate statistically significant difference (*p*-value = 0.95).

4. Conclusions

The use of double roofs in greenhouse reduces the development of fungal diseases on a cucumber crop such as: Downy mildew (*Pseudoperonospora cubensis*)*,* Powdery mildew (*Sphaerotheca fuliginea*) and Mycosphaerella (*Mycosphaerella cucumis*)

Disease incidence has been higher under classic irrigation treatment in comparison to water reduced treatment (by 20%) which can be thus explained by higher humidity levels favourable to disease development.

In the case of *Pseudoperonospora cubensis*, due to the drastic reduction of water droplets on the crop, the use of double roof inside the greenhouse reduces the percentage of infection of Downey mildew and the development.

The use of the two spectrum conversion films *C1* and *C2* for double roof reduced the development of *Sphaerotheca fuliginea*, with respect to the transparent standard double roof.

With the spectrum conversion film *C1* was obtained the lowest percentage of *Sphaerotheca fuliginea* infection.

A good control of ventilation and as well the use of double covers could help to reduce the occurrence of some diseases in Mediterranean greehouses.

References

Aust, F., Hoyningen-Huene, J. v., 1986. Microclimate in relation to epidemics of powdery mildew. Annual Review of Phytopathology, 24, 491–510. https://doi.org/10.1146/annurev.py.24.090186.002423

Castilla, N., Montero, J.I., 2008. Environmental control and crop production in Mediterranean greenhouses. Acta Horticulturae 797, 25–36. https://doi.org/10.17660/ActaHortic.2008.797.1

Cohen, Y., 1981. *Downy mildew of cucurbits. In: The Downy Mildews* (Spencer, D.M., ed.), London: Academic Press. 341–354 p.

Cemek, B., Demir, Y., Uzun, S., 2005. Effects of Greenhouse Covers on Growth and Yield of Aubergine. European journal of horticultural science 70 (1), 16–22. Print. https://doi.org/10.1016/j.energy.2005.08.004

Cohen, Y., Rotem, J., 1971a. Dispersal and viability of sporangia of *Pseudoperonospora cubensis*. Transactions of British Mycological Society. 57, 67–74. https://doi.org/10.1016/S0007-1536(71)80081-5

Cohen, Y., Rotem, J., 1971b. Field and growth chamber approach to epidemiology of *Pseudoperonospora cubensis* on cucumbers. Phytopathology, 61, 736–737. https://doi.org/10.1094/Phyto-61-736

Elad, Y., Messika, Y., Brand,M., Rav David, D., Sztejnberg, A., 2007. Effect of microclimate on *Leveillula taurica* powdery mildew of sweet pepper. Phytopathology, 97, 813–824. https://doi.org/10.1094/PHYTO-97-7-0813

El-Bashir, S.M., Al-Harbi, F.F., Elburaih, H., Al-Faifi, F., Yahia, I.S., 2016. Red photoluminescent PMMA nanohybrid films for modifying the spectral distribution of solar radiation inside greenhouses. Renewable Energy, 85, 928-938. https://doi.org/10.1016/j.renene.2015.07.031.

García Alonso, Y. Espí, E., Salmerón, A., Fontecha, A., Baeza, E.J.,.Pérez Parra, J.J, López, J.C., 2007. *Numerical Simulations of Temperatures in Greenhouse covered with NIR-Reflecting Photoselective Film [Recurso electrónico]*. El Ejido: Estación Experimental de la Fundación de Cajamar, https://indaga.ual.es/permalink/34CBUA_UAL/t0rgfc/alma991001608069704991

Gilardi, G., Gisi U., Garibaldi, A., Gullino, M.L., 2016. Effect of elevated atmospheric CO_2 and temperature on the chemical and biological control of powdery mildew of zucchini and the Phoma leaf spot of leaf beet. European Journal of Plant Pathology. 148, 229–236. https://doi.org/10.1007/s10658-016-1078-4

Granados, M.R., Hernández, J., Bonachela, S., López J.C., Magán, J.J., 2017. Modificación del clima en invernaderos pasivos con pantallas fijas y móviles. Universidad de Almería & Estación Experimental de la Fundación de Cajamar. Actas de Horticultura 77 pages 359-369

Guzman-Plazola, R. A., Davis, R. M., Marois, J. J., 2003. Effects of relative humidity and temperature on spore germination and development of tomato powdery mildew. Crop Protection, 22, 1157–1168. https://doi.org/10.1016/S0261-2194(03)00157-1

Hemming, S., Kempkes, F., van der Braak, N., Dueck, T., Marissen, N., 2006. Greenhouse cooling by NIR-reflection. Acta Horticulturae. 719, 97-106. https://doi.org/10.17660/ActaHortic.2006.719.8

Hernández, J., Bonachela, S., Granados, M.R., López, J.C., Magán, J.J., Montero, J.I., 2017. Microclimate and agronomical effects of internal impermeable screens in an unheated Mediterranean greenhouse. Biosystems Engineering, 163, 66-77. https://doi.org/10.1016/j.biosystemseng.2017.08.012

Hidaka, K., Yoshida, K., Shimasaki, K., Murakami, K., Yasutake, D., Kitano, M., 2008. Spectrum conversion film for regulation of plant growth. Journal of the Faculty of Agriculture, Kyushu University, 53 (2), 549-552. https://doi.org/10.5109/12872

Keinath, A.P., Holmes, G.J., Everts, K.L., Egel, D.S., Langston, D.B., 2007. Evaluation of combinations of chlorothalonil with azoxystrobin, harpin, and disease forecasting for control of downy mildew and gummy stem blight on melon. Crop Protection. 26, 83–88. https://doi.org/10.1016/j.cropro.2006.04.004

Kenyon, D. M., Dixon, G. R., & Helfer, S., 2002. Effects of relative humidity, light intensity and photoperiod on the colony development of *Erysiphe sp.* On *Rhododendron*. Plant Pathology, 51, 103–108. https://doi.org/10.1046/j.0032-0862.2001.x

Lebeda, A., Krístková, E., Sedláková, B., McCreight, J.D., Coffey, M.D., 2016. Cucurbit powdery mildews: methodology for objective determination and denomination of races. European Journal of Plant Pathology 144, 399–410. https://doi.org/10.1007/s10658-015-0776-7

Lebeda, A., Urban, J., 2007. Temporal changes in pathogenicity and fungicide resistance in *Pseudoperonospora cubensis* populations. Acta Horticulturae. 731, 327–336. https://doi.org/10.17660/ActaHortic.2007.731.44

Lindenthal, M., Steiner, U., Dehne, H.W., Oerke, E.C., 2005. Effect of downy mildew development on transpiration of cucumber leaves visualized by digital infrared thermography. Phytopathology, 95, 233–240. https://doi.org/10.1094/PHYTO-95-0233

Lemarié, S., Guérin, V., Jouault, A., Proost, K., Cordier, S., Guignard, G., Demotes-Mainard, S., Bertheloot, J., Sakr, S., Peilleron, F., 2020. Melon and potato crops productivity under a new generation of optically active greenhouse films. Acta Hortic. 1296, 517-526. https://doi.org/10.17660/ActaHortic.2020.1296.67

Mortensen, L. M., Gislerød, H. R., 2005. Effect of air humidity variation on powdery mildew and keeping quality of cut roses. Scientia Horticulturae, 104, 49–55. https://doi.org/10.1016/j.scienta.2004.08.002

Oerke, E.C., Steiner, U., Dehne, H.W., Lindenthal, M., 2006. Thermal imaging of cucumber leaves affected by downy mildew and environmental conditions. Journal of experimental botany. 57, 2121–2132. https://doi.org/10.1093/jxb/erj170

Pérez-García, A., Romero, D., Fernández-Ortuño, D., López-Ruiz, F., De Vicente, A., Torres, J.A., 2009. The powdery mildew fungus *Podosphaera fusca* (synonym *Podosphaera xanthii*), a constant threat to cucurbits. Molecular Plant Pathology 10, 153–60. https://doi.org/10.1111/j.1364-3703.2008.00527.x

Rennberger, G., Keinath, A.P., Kousik, C.S., 2018. First Report of Powdery Mildew on *Cucumis zambianus*, *Cucurbita digitata*, and *Melothria scabra* Caused by *Podosphaera xanthii* in the United States Plant disease. 102(1), 246. https://doi.org/10.1094/pdis-06-17-0916-pdn.

Reuveni, R., Rotem, J., 1974. Effect of humidity on epidemiological patterns of the powdery mildew (*Sphaerotheca fuliginea*) on squash. Phytoparasitica, 2, 25–33. https://doi.org/10.1007/BF02981068

Rotem, J., Cohen, Y., Bashi, E., 1978. Host and environmental influences on sporulation in vivo. Annu. Rev. Phytopathol. 16, 83–101. https://doi.org/10.1146/annurev.py.16.090178.000503

Savory, E.A., Granke, L.L., Quesada-Ocampo, L. M., Varbanova, M., Hausbeck, M.K., Day, B., 2011. The cucurbit downy mildew pathogen *Pseudoperonospora cubensis*. Molecular plant pathology 12 (3), 217–226. https://doi.org/10.1111/j.1364-3703.2010.00670.x

Te Beest, D. E., Paveley, N. D., Shaw, M. W., van den Bosch, F., 2008. Disease-weather relationships for powdery mildew and yellow rust on winter wheat. Phytopathology, 98, 609–617. https://doi.org/10.1094/PHYTO-98-5-0609

Thomas, C.E., 1996. *Downy mildew. In: Compendium of Cucurbit Diseases* (Zitter, T.A., ed.), Ithaca, NY: Cornell University Press. 25–27 p.

Valera, D.L., L.J., Belmonte, F.D., Molina-Aiz, A., López, 2016. *Greenhouse Agriculture in Almería. A Comprehensive Techno-Economic Analysis*. Almería, Spain: Ed. Cajamar Caja Rural. 408 pp. [Available online: http://www.publicacionescajamar.es/series-tematicas/economia/greenhouse-agriculture-in-almeria-a-comprehensive-techno-economic-analysis/ (accessed on 08 April 2020)].

Xu, J., Li, Y., Wang, R., Liu, W., Zhou, P, 2015. Experimental performance of evaporative cooling pad systems in greenhouses in humid subtropical climates. Applied Energy, 138, 291–301. https://doi.org/10.1016/j.apenergy.2014.10.061

Yarwood, C. E., 1957. Powdery mildew. Botanical Review, 23, 235–301. https://doi.org/10.1007/BF02872581

Yoon, H.I., Kim, J.H., Park, K.S., Namgoong, J.W., Hwang, T.G., J.P., Kim, J.E., Son, 2020. Quantitative methods for evaluating the conversion performance of spectrum conversion films and testing plant responses under simulated solar conditions. Hortic. Environ. Biotechnol. 61, 999–1009. https://doi.org/10.1007/s13580-020-00286-y.

Influence of Animal-related Parameters on Emissions of Ammonia and Methane from an Open-sided Free-stall Barn in Hot Mediterranean Climate

Provvidenza Rita D'Urso [a,*], Claudia Arcidiacono [a], Giovanni Cascone [a]

[a] Department of Agriculture, Food and Environment (Di3A), Building and Land Section, University of Catania, Catania, Italy

* Corresponding author. Email: provvidenza.durso@phd.unict.it

Abstract

Increased knowledge on the factors that affect emissions from open-sided dairy buildings may lead to an improvement of the mitigation strategies. The aim of the study was to evaluate emissions of ammonia (NH_3) and methane (CH_4) in an open dairy barn in hot Mediterranean climate and to assess the influence of animal-related parameters on daily emissions.

Measurements were carried out in a cubicle free-stall dairy barn located in the province of Ragusa (Italy) in different weeks of 2016 during spring and summer. Concentrations of NH_3 and CH_4 as well as carbon dioxide (CO_2) were continuously measured by a photo-acoustic analyser. Measurements of climate and microclimate variables were carried out and behavioural activity was monitored by a 24-h video-recording system. Emissions of NH_3 and CH_4 were estimated through the application of the CO_2 mass balance method.

Data collected were organised in specific datasets to carry out different statistical analyses on values of gas emissions in dependence on selected parameters. Application of a one-way Analysis of Variance (ANOVA) tested the equality of the mean values of gas emissions for each group of the parameters analysed during each week. In the post-hoc analysis, the mean values were separated by Tukey's honestly significant difference at P<0.05.

At indoor prevalent air direction, emissions of NH_3 and CH_4 changed in time during the day inside the barn due to the variability of the ratio between the pollutants (i.e., NH_3, and CH_4) and the tracer gas (i.e., CO_2). In the barn under study, the variability of gas emissions was related to the effect of temperature-humidity index (THI) (P<0.05) and cow behaviour and barn management (CBBM) (P<0.05). The highest emissions were recorded during the cleaning procedures for both NH_3 (P<0.001) and CH_4 (P<0.001), whereas the lowest emissions were recorded during the central hours of the day.

Keywords: open structure, cow behaviour, barn management, microclimate conditions.

1. Introduction

The emissions of ammonia (NH_3) and methane (CH_4) from the livestock sector have great environmental impacts. In 2017 manure management from dairy cattle produced the 11% of NH_3 emissions in the EU28 (EEA, 2019), whereas in 2015 the absolute emissions from dairy cattle sector was 1,711.8 million metric tonnes CO_2 equivalent, in particular about 1,100 for CH_4 (FAO, 2019) derived from enteric fermentation and manure management. Increased knowledge on the factors that affect emissions from dairy buildings may lead to an improvement of the mitigation strategies for emissions reduction.

Based on the literature, dairy cows are mainly housed in naturally ventilated (NV) barns (Janke et al. 2020). In these structures, which are characterised by large side openings, outdoor climatic parameters influence the indoor environment due to the high indoor-outdoor air exchange. In fact, the increasing of outdoor temperature during spring and summer seasons in this housing system produces the highest emissions in the barn due to the increasing of indoor temperature.

Since hot climate conditions produce heat stress on the cows, the NV barns are equipped with a cooling system (e.g., fans and sprinklers) to mitigate the effect of heat stress on the cows (Honig et al. 2012; Porto et al. 2017), especially in hot climate Mediterranean regions. Therefore, the indoor microclimatic conditions are determined by the interaction between the outdoor climatic conditions and the management of the cooling system.

In the literature, many studies have been performed to assess the influencing parameters on gas emissions. Saha et al. (2013) found that wind speed and wind direction as well as their interaction had significant influence on air change per hour (ACH) (P < 0.05). Ngwabie et al. (2011) studied the effects of animal activity and air temperature on methane and ammonia emissions. They found that daily CH_4 emissions increased significantly with the activity of the cows (r=0.61) and decreased when indoor air temperature increased (r=-0.84), whereas daily NH_3 emissions increased significantly with the indoor air temperatures (r=0.66). In the meta-analysis carried out by Poteko (2019) in the 'loose housing system with cubicles' category, air temperature influences both NH_3 (p < 0.001) and CH_4 (p < 0.001) emissions. The analysis carried out by Hempel et al. (2016) showed a non-linear temperature dependency of NH_3 and CH_4 emissions as well as the increasing of NH_3 emissions due to higher wind speed and lower relative air humidity

values compared to the night.

According to Bohmanova et al. (2007) the combination of environmental parameters (e.g., temperature, relative humidity, solar radiation, air movement, and precipitation) can cause heat stress in cows with a consequent reduction in milk production. In the study of Hempel et al. (2019), milk yield may decrease by about 2.8% relative to the present European milk yield, and farmers may expect financial losses in the summer season of about 5.4% of their monthly income. Among the main heat stress indicator, the computation of the temperature humidity index (THI) is an indirect parameter based on the values of air temperature and relative humidity (Hoffmann et al., 2020). Heat stress as well as the management of the cooling system significantly influence cow behaviour and time spent at lying or standing (Calegari, et al. 2012; Frazzi et al. 2000; Porto et al. 2017). In the literature, the evaluation of cow behaviour has generally been carried out by using cow behavioural indices, i.e., cow lying index (CLI), cow standing index (CSI), and cow feeding index (CFI) (Bava et al. 2012; Provolo and Riva 2009). These parameters were useful to assess the cow behaviour and barn management (CBBM) in different climatic conditions and cooling sessions.

Although the influence of climatic conditions on emissions as well as the influence of heat stress on cow behaviour has been investigated in the literature, there is a lack in the evaluation of the connections between animal-related parameters (e.g., THI, and cow behavioural indices) and gas emissions in hot climate conditions. Therefore, the aim of the present study is to fill this gap by pursuing the following objectives: (1) evaluating daily emissions of NH_3 and CH_4; (2) studying the influence of THI on gas emissions; (3) assessing the effect of CBBM variations on gas emissions.

2. Materials and Methods

2.1. Experimental barn and period of investigation

The study was conducted in a cubicle free-stall dairy barn located in Pettineo/Pozzilli (37°01'N, 14°32'E) in the province of Ragusa (Italy) for two weeks: week 1 (W1) from 15/06 to 21/06 and week 2 (W2) from 01/07 to 07/07.

The barn facility is about 55.50 m long and 20.80 m wide. The dairy house building is composed of three sides (i.e. the SE, NE, and NW sides) completely open, whereas the SW side is closed by a continuous wall with small openings. The symmetric roof has a central 7 m-high ridge vent and a 4 m-high eave. The natural ventilation system is integrated by two cooling systems, composed of a fogging system with fans, located in the resting area, and a sprinkler system with fans, located in the feeding alley. The barn was composed of three pens on a concrete floor equipped with 64 head-to-head cubicles (Figure 1). The cubicles are arranged in two rows with concrete kerbs, covered with sand.
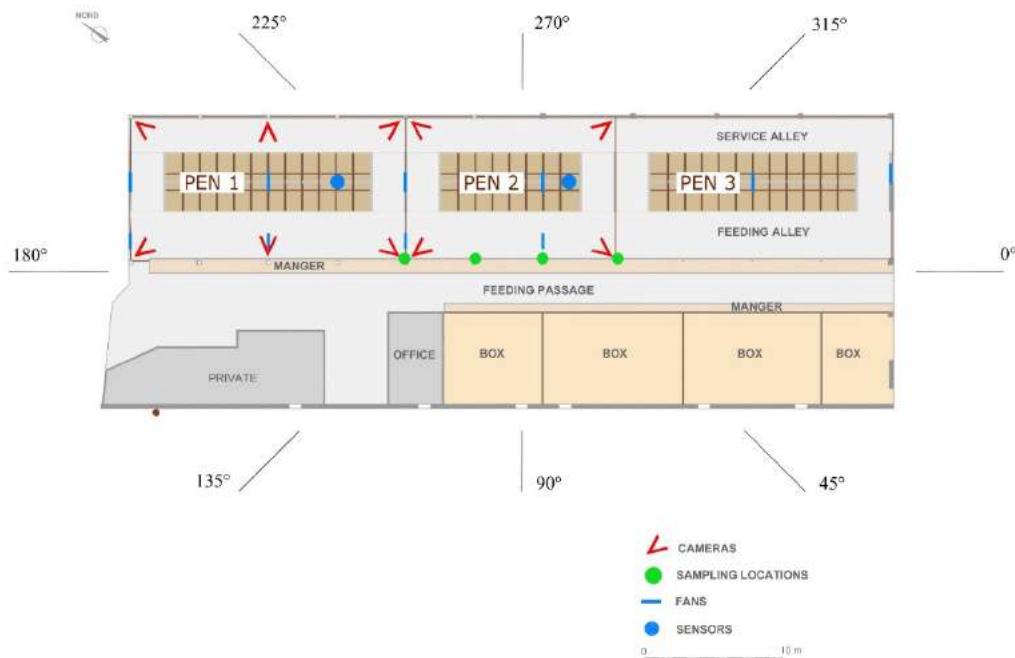
Figure 1. Plan view of the barn and position of sampling locations, cameras, fans, and sensors.

2.2. Measurement of gas concentrations and climatic parameters

Concentrations of NH_3, CH_4 and carbon dioxide (CO_2) were continuously acquired at four sampling locations (SLs) by an INNOVA photo-acoustic analyser composed of a Multigas Monitor mod 1412i and a multipoint sampler 1409/12 (Lumasense Technology A/S). The four inlet channels were made of PTFE (poly-tetrafluoroethylene) tubing to reduce

adsorption of samples. The end of each sampling tube had an air filter to keep the 1409 free of particles. The SLs were located in different areas of the barn. The location of the four indoor SLs was in the central area of the barn at 20 cm from the barn floor. The outdoor SL was located at 3 m above the floor outside the barn to acquire background concentration. Gas concentrations were measured with a sampling frequency of 15 min and a sample integration time of 5 sec. INNOVA analyser was calibrated by the manufacturer just before the measurements.

Climate and microclimate parameters were measured by sensors installed inside the barn at 2.0 m above the floor and outside the barn above the roof along the ridge. Measurements of air temperature and relative humidity, indoor air and wind speed and direction were recorded with a frequency of five seconds by a data-logger CR10X (Campbell, UK) that every five minutes computed the average values and stored them in memory locations. Specific information on the sensors is reported in a previous study by D'Urso et al. 2021.

2.3. Barn management and behavioural activity recordings

The fogging system and the sprinklers with fans were automatically switched on when the indoor temperature exceeded 22° and 27°, respectively. The cooling systems were manually switched off during the milking sessions and the cleaning of the feeding alley. During W2, the sprinklers in the feeding alley were not operated in the framework of another study carried out by D'Emilio et al. (2017).

The daily routine of the cows was characterised by the barn management. The cleaning of the barn was carried out once a day at about 07:30 a.m. by a mechanical tractor with scraper; the milking session was done twice a day at about 5:00 a.m. and 5:00 p.m.; the feed was delivered every day after cleaning and it was moved into the manger before the first and the second milking sessions.

A 24-h video-recording system, composed of ten cameras (Kon.Li.Cor, Perugia, Italy), recorded cow behaviour during the experiment. The visual evaluation of the records allowed application of the scan sampling method (Overton et al. 2002) with a frequency of 15 minutes in order to count the number of cows in a specific behaviour and, therefore, compute the CFI, CLI and CSI.

2.4. Air exchange rate and emissions calculations via indirect method

In this study the estimation of NH_3 and CH_4 emissions was carried out by applying the CO_2 mass balance method that represents the reference method for NV dairy barns (VERA, 2018).

The ventilation rate was calculated as follows (1):

$$Q = \frac{P_{CO2}}{CO2_{in} - CO2_{out}} \times N \qquad (1)$$

where P_{CO2} represents the excretion rate of CO_2 from one cow (g cow^{-1} h^{-1}), N is the number of cows housed inside the building, Q is the ventilation rate calculated according to the CO_2 balance (m^3 h^{-1}), and C_{CO2in} and C_{CO2out} are the hourly average concentrations of the gas inside and outside the building in the prevailing air direction, respectively (gm^{-3}).

Within the CO_2 balance, the CO_2 excretion rate depends on animal heat production. Since in this barn facility without deep litter the CO_2 production from manure is below 4% of the total production (Ngwabie et al. 2009; Ogink et al. 2013), the CO_2 excretion rate was computed as follows (CIGR, 2002):

$$q_t = 5.6 \times m^{0.75} + 1.6 \times 10^{-5} \times p^3 + 22 \times y \qquad (2)$$

$$CF = 4 \times 10^{-5} \times (20 - T_i)^3 + 1 \qquad (3)$$

$$q_{cor} = q_t \times CF \qquad (4)$$

$$P_{CO2} = 0.299 \times q_{cor} \qquad (5)$$

where q_t is the total heat production (W), q_{cor} is the corrected value of the total heat production (W), m is the average mass of the animals (kg cow^{-1}), p is the number of days after insemination (d), y is the milk yield (kg d^{-1}), T_i is the temperature inside the building (°C) and CF is the temperature correction factor. The average weight, milk yield of the cows and contribution of pregnancy were 650 kg cow^{-1}, 32 kg d^{-1} and 135 days, respectively.

The emission rate of a NH_3 and CH_4 was estimated using the following equation:

$$E_t = Q \times (C_{in} - C_{out}) \qquad (6)$$

where E_t is the emission rate of the gas (g h^{-1}), Q is the ventilation rate calculated according to the CO_2 balance method (m^3 h^{-1}), and C_{in} and C_{out} are the average concentrations of the gas inside the barn (i.e., average value of the 4 indoor SLs) and outside the building (i.e., SL07), respectively (g m^{-3}). The weight of the cows and the production may differ from herd to herd. In order to make results comparable with other studies, the emissions E_t are computed as the emissions per livestock unit (LU) in g h^{-1} LU^{-1}, where LU is equivalent to a 500 kg animal mass. The emission rate per LU is estimated as follows:

$$E = \frac{E_t \times LU}{N \times m} \qquad (7)$$

2.5. Data treatment and statistical analyses

Data were analysed by using Microsoft® Excel and Minitab software. Statistical analyses were carried out to assess the influence of THI and CBBM on daily gas emissions. The THI was computed according to Hempel et al. (2018):

$$THI = (1.8{\times}T + 32) - \left[\left(0.55 - \frac{55}{100} {\times}RH\right){\times}(1.8{\times}T - 26)\right] \tag{8}$$

where T is the dry bulb air temperature (°C) and RH is the relative humidity (%).

Gas emissions were subdivided considering the following groups of THI: comfort zone (THI≤72); low risk of thermal stress for cows (72<THI≤78); thermal stress (78<THI<84). Since conditions of emergency for cows (THI≥84) were not recorded in this study, emissions for emergency conditions were not analysed.

The influence of CBBM on gas emissions was analysed by grouping the gas emitted during the following conditions: cow activity, cow lying, and barn cleaning. Cow activity includes gas emissions produced when cows are in standing, feeding, and walking; cow lying consists of gas emitted when cows are resting in the cubicles; barn cleaning refers to the dataset of gas emissions related to the cleaning of the floor.

The statistical analyses on gas emissions were carried out on the values computed for the prevailing air direction (135°-225°). Moreover, the final dataset of gas emissions was composed of the values that excluded gas emissions at complex windy conditions. In detail, CO_2 differences lower than 100 ppm were neglected to reduce biases in the emission values. A one-way analysis of variance (ANOVA) was applied to the above-described groups of NH_3 and CH_4 emissions. The level of significance was defined by a P value of 0.05. If the test resulted significant, the Tukey test post hoc analysis was applied in order to identify differences between groups of gas emissions.

3. Results and Discussion

3.1. Daily NH_3 and CH_4 emissions

Daily variations of NH_3 and CH_4 emissions in both W1 and W2 are shown in Figure 2, whereas Figure 3 shows the difference between indoor and outdoor gas concentrations of gas pollutants (i.e.NH_3, CH_4) and tracer gas (i.e., CO_2) during the day in both weeks.
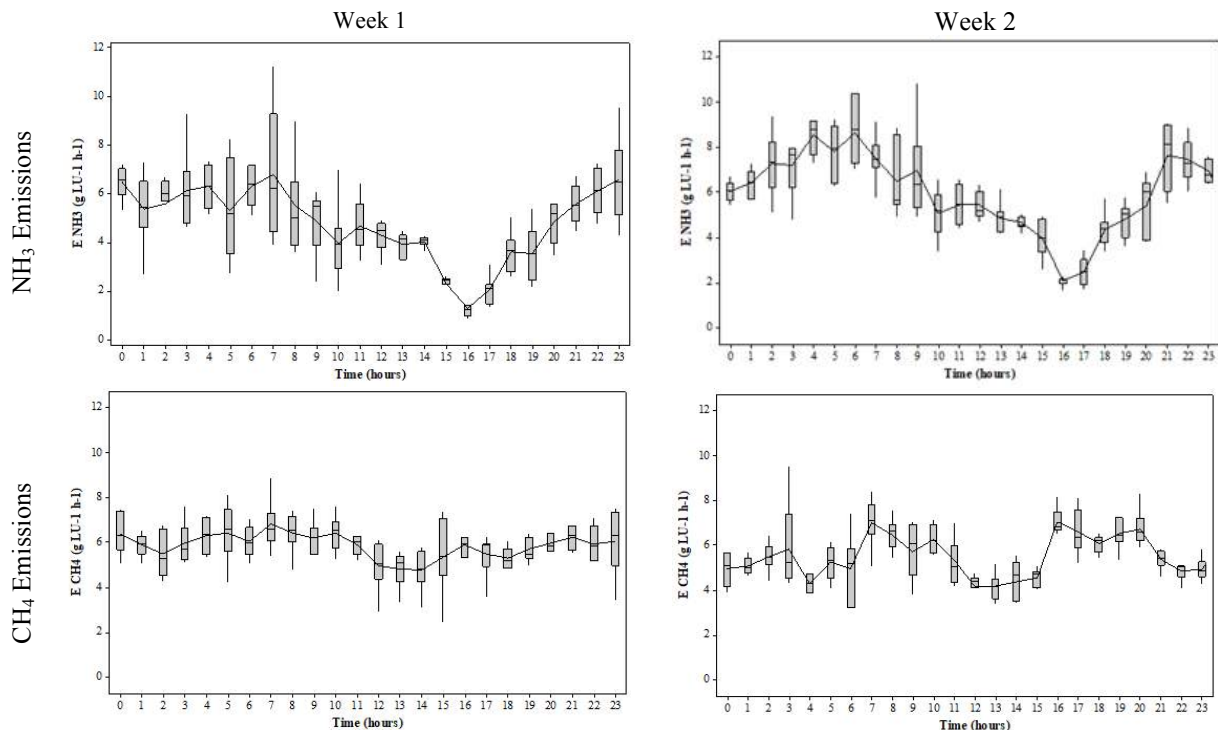

Figure 2. Daily trend of NH_3 and CH_4 emissions during W1 and W2.

In Figure 2, NH_3 emissions reached the highest emissions during the early morning and late afternoon, whereas the lowest value occurred at 4 p.m. in both W1 and W2. The mean NH_3 emission rate in W1 was 4.73 g LU^{-1} h^{-1} with indoor average temperature of 26.3 °C and air velocity of 0.71 m s^{-1}, whereas the mean NH_3 emission rate in W2 was 5.90 g LU^{-1} h^{-1} with indoor average temperature of 27.5 °C and air velocity of 0.69 m s^{-1}. The hourly average NH_3

emissions was 0.85 to 11.25 g LU^{-1} h^{-1} in W1 and 1.64 to 10.86 g LU^{-1} h^{-1} in W2. The values of NH_3 emissions found by other studies (Janke et al. 2020; C. K. Saha et al. 2014) are slightly lower than those found in this study due to the different climate conditions of the countries and the barn management. Based on the results of the one-way ANOVA, NH_3 emissions in W1 were significantly different ($P<0.001$) from those in W2 with higher NH_3 emissions in W2. The higher emissions in W2 can be attributed to the increasing of air temperature between W1 and W2 as it was found in previous studies (Hempel et al. 2016; C. K. Saha et al. 2014).
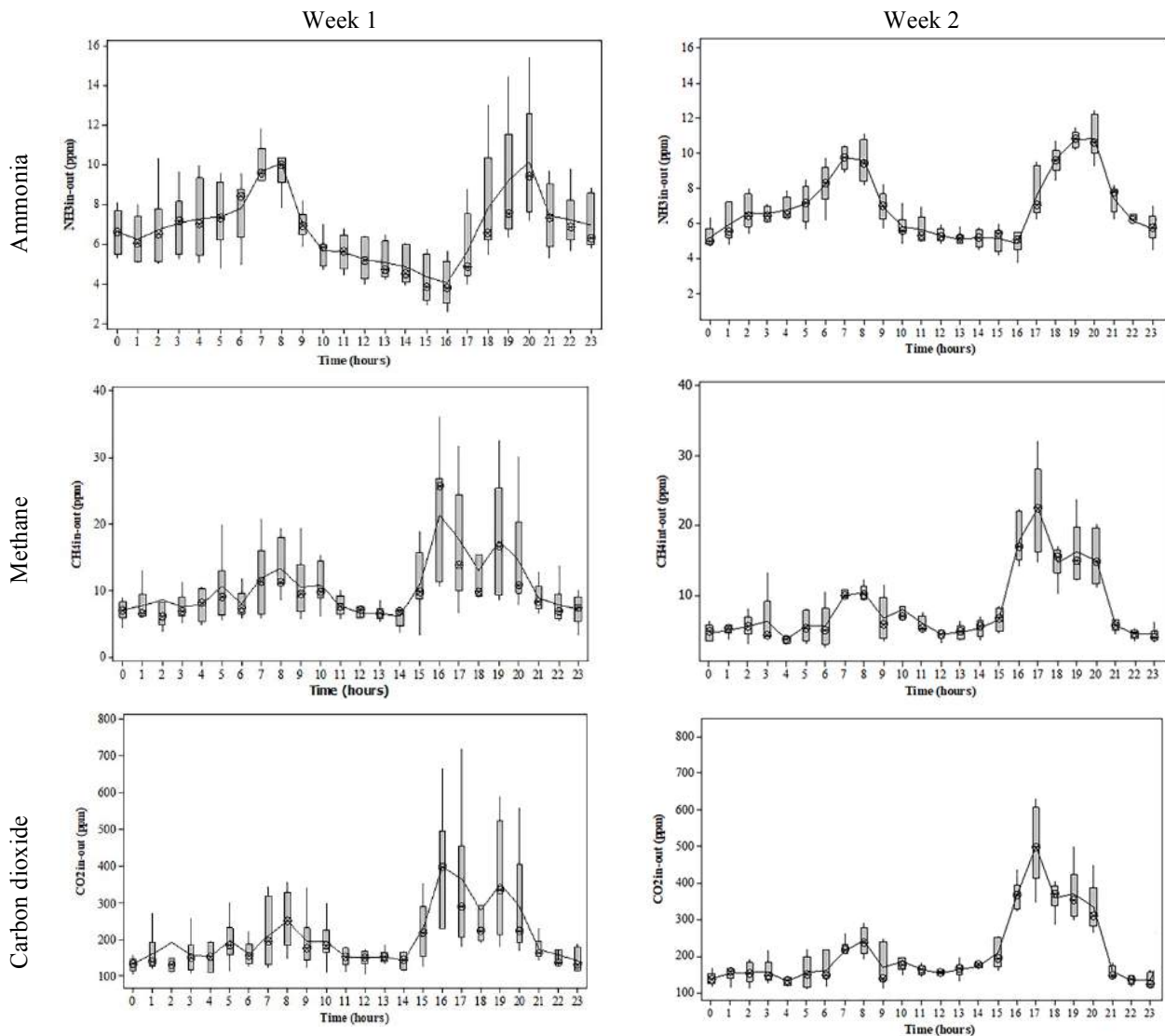

Figure 3. Daily difference between indoor and outdoor gas concentrations of gas pollutants (i.e., NH_3 and CH_4) and tracer gas (i.e. CO_2) during W1 and W2.

The mean CH_4 emission rate was 5.85 g LU^{-1} h^{-1} in W1 and 5.52 g LU^{-1} h^{-1} in W2. The results of the one-way ANOVA showed that there is a significant difference ($P<0.009$) between CH_4 emissions in W1 and CH_4 emissions in W2. The hourly-averaged CH_4 emission values were 2.40 to 8.83 g LU^{-1} h^{-1} in W1 and 2.89 to 9.53 g LU^{-1} h^{-1} in W2. CH_4 emissions showed different peaks during W1 and W2 with lower emissions between 12 a.m. and 3 p.m. The trend of CH_4 emissions in W2 is more variable than in W1 due to the different CH_4 concentrations between W1 and W2 found by D'Urso et al. (2021). In fact, the different management of the cooling system in the feeding alley between W1 and W2 reduced time spent at feeding with a negative effect on dry matter intake (DMI). Therefore, CH_4 concentrations were lower in W2 than in W1. Since the estimation of gas emissions is related to the ratio between concentrations of gas pollutant and tracer gas (Mendes et al. 2015), the reduction of CH_4 emissions in W2 is related to a reduction in CH_4 concentrations.

NH_3 and CH_4 emissions changed hourly during the day where several peaks occurred. Since the estimation of emissions relies on indirect balancing methods, the differences of measured outdoor and indoor concentrations (CO_{2in}-CO_{2out}) and (C_{in} -C_{out}) had a relevant influence on the variability of emissions. For both NH_3 and CH_4 emissions, the daily trends showed the lowest values in the central hours of the day (Figure 2) when air velocity was the highest. In detail, the ratio between (NH_{3in}-NH_{3out}) and (CO_{2in}-CO_{2out}) was low due to the lowering of the NH_3 concentration difference while the CO_2 difference showed a constant trend during the central hours of the day, from about 10 a.m. to 4 p.m. (Figure 3). The same effect was detected for CH_4 yet to a less extend compared to that on NH_3.

3.2. Influence of THI on NH_3 and CH_4 emissions

The results of the one-way ANOVA (Table 2) showed that groups of NH_3 and CH_4 emissions at different THI were significantly different for both W1 and W2. In detail, NH_3 emissions at THI≤72, 72<THI≤78 and 78<THI≤84 were all significantly different. The highest NH_3 emissions occurred when THI was lower than 72, whereas they were the lowest at 78<THI<84. These results are strongly related to the CBBM and can be explained by analysing the emitting source of the gas. In fact, when THI is high during the day, cows are mainly in lying behaviour in the cubicles where the cooling system was operated. Therefore, the chemical process for NH_3 production was reduced due to the presence of water on the floor and the reduced mixing of urea and faces performed by cow activity. Also for CH_4, the lowest emissions occurred at 78<THI<84. The reduction of CH_4 is not related to a direct effect of climatic factors on CH_4 emissions, but to an indirect effect of the animals and their metabolic activity. In the literature Abeni and Galli (2017) found that during heat stress total rumination time decreased. The reduction of CH_4 could be related to the reduced rumination activity even though it was not proved a direct effect of rumination on CH_4 production (Beauchemin 2018).

Table 2. Results of statistical analyses for gas emissions at different groups of THI during W1 and W2.

Gas emissions	P value	W1 Groups	W1 Mean	W1 SD	P value	W2 Groups	W2 Mean	W2 SD
NH_3	0.0001	THI≤72	6.18[a]	1.47	0.0001	THI≤72	7.37[a]	1.31
		72<THI≤78	4.37[b]	1.62		72<THI≤78	5.94[b]	1.88
		78<THI<84	3.02[c]	1.21		78<THI<84	4.44[c]	1.39
CH_4	0.0001	THI≤72	6.19[a]	1.01	0.001	72<THI≤78	6.06[a]	0.96
		72<THI≤78	5.98[a]	0.73		THI≤72	5.33[b]	1.18
		78<THI<84	5.11[b]	1.07		78<THI<84	5.23[b]	1.26

3.3. Influence of CBBM on NH_3 and CH_4 emissions

The statistical analyses at varying CBBM showed a significant difference between groups of gas emissions in both W1 and W2 (Table 3). NH_3 emissions were the highest during barn cleaning due to the high NH_3 concentrations during cleaning. In fact, Figure 3 showed that NH_{3in}-NH_{3out} increased during the cleaning of the barn in the early morning, whereas CO_{2in}-CO_{2out} concentrations varied less. Therefore, NH_3 emissions increased during the floor cleaning. The lowest NH_3 emissions, obtained during cow activity, were attributed to the dilution and flushing effects of the high air velocities during the central hours of the day. These effects contributed to CH_4 emissions reduction during cow lying together with the effect of the frequent cows' sleeping bouts during night hours.

Table 3. Results of statistical analyses for gas emissions at different groups of CBBM during W1 and W2.

Gas emissions	P value	W1 Groups	W1 Mean	W1 SD	P value	W2 Groups	W2 Mean
NH_3	0.0001	cleaning	6.14[a]	2.36	0.0001	cleaning	6.99[a] 1.405
		lying	5.40[a]	1.41		lying	6.37[a] 1.42
		activity	3.73[b]	1.82		activity	5.15[b] 2.29
CH_4	0.008	cleaning	6.61[a]	0.97	0.0001	cleaning	6.73[a] 0.91
		activity	5.85[b]	0.98		activity	5.96[b] 1.14
		lying	5.69[b]	1.01		lying	4.89[c] 0.93

4. Conclusions

A study of the NH_3 and CH_4 emissions was carried out in an open-sided free-stall barn in hot Mediterranean climate. The daily trend of emissions was evaluated in two weeks during spring and summer in order to identify the influence of animal-related parameters. NH_3 emissions were generally higher in W2 than in W1 and a daily variation of emissions was found for both NH_3 and CH_4. NH_3 emissions were characterised by two peaks in the early morning and in the early

afternoon. Daily variation of CH_4 in W1 was less pronounced than in W2 with lower CH_4 emissions in W2 than in W1 due to the different management of the cooling system in the feeding alley. Significant relationships between gas emissions and animal-related parameters were found (P<0.05) for both NH_3 and CH_4. In detail, the highest NH_3 emissions occurred when THI was lower than 72 and during cleaning of the barn, whereas CH_4 emissions were the lowest during cow lying. This study proved that in hot climate conditions emissions varied in response to cow behaviour as affected by microclimate conditions.

References

Abeni, F., Galli, 2017. A. Monitoring cow activity and rumination time for an early detection of heat stress in dairy cow. International Journal of Biometeorology. 61, 417–425. https://doi.org/10.1007/s00484-016-1222-z

Bava, L.; Tamburini, A.; Penati, C.; Riva, E.; Mattachini, G.; Provolo, G.; Sandrucci, 2012. Effects of Feeding Frequency and Environmental Conditions on Dry Matter Intake, Milk Yield and Behaviour of Dairy Cows Milked in Conventional or Automatic Milking Systems. Italian Journal of Animal Science 11(3): 230–35. https://doi.org/10.4081/ijas.2012.e42

Beauchemin, K. A. 2018. Invited Review: Current Perspectives on Eating and Rumination Activity in Dairy Cows. Journal of Dairy Science 101(6): 4762–84. http://dx.doi.org/10.3168/jds.2017-13706

Bohmanova, J., Misztal I., Cole J. B., 2007. Temperature-Humidity Indices as Indicators of Milk Production Losses Due to Heat Stress. Journal of Dairy Science 90(4): 1947–56. https://doi.org/10.3168/jds.2006-513

Calegari, F., Calamari L., and Frazzi E.,. 2012. Misting and Fan Cooling of the Rest Area in a Dairy Barn. International Journal of Biometeorology 56(2): 287–95. https://doi.org/10.1007/s00484-011-0432-7

CIGR, 2002. Climatization of animal houses, in: S. Pedersen, K. Sallvik (Eds.), 4th Report of Working Group: Heat and Moisture Production at Animal and House Levels.

D'Emilio, A., Porto S.M.C., Cascone G., Bella M., Gulino M., 2017. Mitigating Heat Stress of Dairy Cows Bred in a Free-Stall Barn by Sprinkler Systems Coupled with Forced Ventilation. Journal of Agricultural Engineering 48(4): 190–95. https://doi.org/10.4081/jae.2017.691

D'Urso, P.R., Arcidiacono C., Valenti F., Cascone G., 2021. Assessing Influence Factors on Daily Ammonia and Greenhouse Gas Concentrations from an Open-Sided Cubicle Barn in Hot Mediterranean Climate. Animals. 11(5), 1400: 1–17. https://doi.org/10.3390/ani11051400

EEA, 2019. European Union emission inventory report 1990 2017 under the UNECE Convention on Long range Transboundary Air Pollution (LRTAP); EEA Technical Report no. 08/2019.

FAO, 2019. Climate change and the global dairy cattle sector. In The Role ofthe Dairy Cattle Sector in a Low-Carbon Future; Global Agenda for Sustainable Livestock: Manhattan, KS, USA.

Frazzi, E., Calamari, L., Calegari F., and Stefanini, L., 2000. Behavior of Dairy Cows in Response to Different Barn Cooling Systems. Transactions of the American Society of Agricultural Engineers. 43(2): 387–94. https://doi.org/10.13031/2013.2716

Hempel, S., Saha, C.K., Fiedler, M., Berg, W., Hansen, C., Amon, B., Amon, T., 2016. Non-linear temperature dependency of ammonia and methane emissions from a naturally ventilated dairy barn. Biosystems Engineering 145: 10–21. http://dx.doi.org/10.1016/j.biosystemseng.2016.02.006

Hempel, S.; König, M.; Menz, C.; Janke, D.; Amon, B.; Banhazi, T.M.; Estellés, F.; Amon, T., 2018. Uncertainty in the Measurement of Indoor Temperature and Humidity in Naturally Ventilated Dairy Buildings as Influenced by Measurement Technique and Data Variability. Biosystems Engineering. 166: 58–75. https://doi.org/10.1016/j.biosystemseng.2017.11.004

Hempel S., Menz C., Pinto S., Galán E., Janke D., Estellés F., Müschner-Siemens T., Wang X., Heinicke J., Zhang G., Amon B., Del Prado A., Amon T., 2019. Heat Stress Risk in European Dairy Cattle Husbandry under Different Climate Change Scenarios - Uncertainties and Potential Impacts. Earth System Dynamics Discussions: 859–84. https://doi.org/10.5194/esd-10-859-2019

Hoffmann, G.,Herbut P., Pinto S., Heinicke J., Kuhlac B., Amonad T., 2020. Animal-Related, Non-Invasive Indicators for Determining Heat Stress in Dairy Cows. Biosystems Engineering. 199: 83-96 https://doi.org/10.1016/j.biosystemseng.2019.10.017

Honig, H. Miron J., Lehrer, H., Jackoby, S., Zachut M., Zinou, A., Portnick, Y., Moallem, U., 2012. Performance and Welfare of High-Yielding Dairy Cows Subjected to 5 or 8 Cooling Sessions Daily under Hot and Humid Climate. Journal of Dairy Science 95(7): 3736–42. https://doi.org/10.3168/jds.2011-5054

Janke, D., Willink, D., Ammon, C., Hempel, S., Schrade, S., Demeyer, P., Hartung, E., Amon, B., Ogink, N., Amon, T., 2020. Calculation of Ventilation Rates and Ammonia Emissions: Comparison of Sampling Strategies for a Naturally Ventilated Dairy Barn. Biosystems Engineering 198: 15–30. https://doi.org/10.1016/j.biosystemseng.2020.07.011.

Mendes, L., Edouard, N., Ogink, N.W.M., van Dooren H.J.C., Tinôco I.F.F., Mosquera, J., 2015. Spatial Variability of Mixing Ratios of Ammonia and Tracer Gases in a Naturally Ventilated Dairy Cow Barn. Biosystems Engineering 129: 360–69. https://doi.org/10.1016/j.biosystemseng.2014.11.011

Ngwabie, N.M., Jeppsson, K.-H., Nimmermark, S., Swensson, C., Gustafsson, G., 2009. Multi-Location Measurements of Greenhouse Gases and Emission Rates of Methane and Ammonia from a Naturally-Ventilated Barn for Dairy Cows. Biosystems Engineering. 103,1:68-77. https://doi.org/10.1016/j.biosystemseng.2009.02.004

Ngwabie, N., Jeppsson, K.-H.; Gustafsson, G., Nimmermark, S., 2011. Effects of Animal Activity and Air Temperature on Methane and Ammonia Emissions from a Naturally Ventilated Building for Dairy Cows. Atmospheric Environment 45(37): 6760–68. http://dx.doi.org/10.1016/j.atmosenv.2011.08.027.

Ogink, N.W.M., Mosquera J., Calvet S., Zhang G., 2013. Methods for Measuring Gas Emissions from Naturally Ventilated Livestock Buildings: Developments over the Last Decade and Perspectives for Improvement. Biosystems Engineering 116(3): 297–308. https://doi.org/10.1016/j.biosystemseng.2012.10.005

Overton, M.W., Sischo, W.M., Temple, G.D., Moore D. A., 2002. Using Time-Lapse Video Photography to Assess Dairy Cattle Lying Behavior in a Free-Stall Barn." Journal of Dairy Science 85(9): 2407–13. http://dx.doi.org/10.3168/jds.S0022-0302(02)74323-3.

Porto, S.M.C., D'Emilio, A., Cascone, G., 2017. On the Influence of the Alternation of Two Different Cooling Systems on Dairy Cow Daily Activities. Journal of Agricultural Engineering. 48 (1):21. https://doi.org/10.4081/jae.2017.577

Poteko, J., Zahnera, M., Schrade, S., 2019. Effects of Housing System , Floor Type and Temperature on Ammonia and Methane Emissions from Dairy Farming : A Meta-Analysis. Biosystems Engineering 182:16-28. https://doi.org/10.1016/j.biosystemseng.2019.03.012

Provolo, G., and Riva E., 2009. One Year Study of Lying and Standing Behaviour of Dairy Cows in a Frestall Barn in Italy. Journal of Agricultural Engineering 40(2): 27. https://doi.org/10.4081/jae.2009.2.27

Saha, C., Ammon, C., Berg, W., Fiedler, M., Loebsin, C., Sanftleben, P., Brunsch, R., Amon, T., 2014. Seasonal and Diel Variations of Ammonia and Methane Emissions from a Naturally Ventilated Dairy Building and the Associated Factors Influencing Emissions. Science of the Total Environment 468–469: 53–62. https://doi.org/10.1016/j.scitotenv.2013.08.015

Saha, C.K., Ammon, C., Berg, W., Loebsin, C., Fiedler, M., Brunsch, R., Von Bobrutzki, K., 2013. The effect of external wind speed and direction on sampling point concentrations, air change rate and emissions from a naturally ventilated dairy building. Biosystems Engineering. 114, 267–278. https://doi.org/10.1016/j.biosystemseng.2012.12.002

VERA, 2018. Test Protocol for Livestock Housing and Management Systems. Verification of Environmental Technologies for Agricultural Production.

AWARTECH Project: a New Tool of Precision Livestock Farming for Growing-finishing Pigs

Vasco Fitas da Cruz [a,b,*], Fátima Baptista [a,b], José Rico [a,b], Diogo Coelho [a], Teresa Morgado [b], David Botas [c]

[a] Department of Rural Engineering, University of Évora, Évora, Portugal

[b] MED - Mediterranean Institute for Agriculture, Environment and Development, Évora, Portugal

[c] Equiporave Ibérica, Lda., Castanheira do Ribatejo, Portugal

* Vasco Fitas da Cruz. Email: vfc@uevora.pt

Abstract

The world is, day by day, more demanding for high quality food, produced according to animal welfare regulations and ethical principles, and both social and environmental responsibility. This requires a special care with cost rationalization and increased efficiency in the use of production factors and value chains. Intensifying production pursing self-supply or higher competitiveness objectives may decrease animal welfare. Therefore, it's important to monitor the environment inside the swine facilities and the animal welfare conditions. The main objective of the AWARTECH (Animal Welfare Adjusted Real Time Environmental Conditions of Housing) project was to create and develop an innovative precision livestock tool that will support and reinforce the pig value chain, by management solutions based on monitoring, analysis and control of environmental, physiological, behavioural and productive parameters. Environmental data were collected by sensors of temperature, relative humidity, air velocity and gas concentration, which are integrated in an environmental control system (Webisense) and a platform (Nidus). Webisense controlled the ventilation system, the cooling system and the heating system. The physiological data (rectal temperature, surface temperature) were collected manually and automatically. In order to monitor the behaviour of the animals, video cameras were installed. An individual feeding machine equipped with a scale has been installed. That allows, through an RFID system, individual monitoring and control of the amount of food supplied and ingested; number and duration of visits; and animal's weight. The development of AWARTECH platform results from the integration of physiological data manually supplied and real-time data provided by Webisense, Nidus, feeding machine and video analytics, that allow the control of the environmental conditions in order to promote the animal welfare.

Keywords: Animal housing, Environmental control, Animal welfare, Pig.

1. Introduction

It is expected that the world population will increase by about 30% and reach more than 9 billion of habitants by 2050. Consequently, the food demand will increase by about 70% and human consumption of livestock products will double from 258 to 455 million tonnes (Rojas-Downing et al., 2017). In order to find solution for this problem, livestock farming systems need to increase production through intensive systems (Berckmans, 2014). However, intensive production systems, currently face enormous challenges due to environmental impacts and to the public perception opinion, that these systems, characterized by high animal density, reduce animal health and welfare. In this sense, it is important to raise awareness in the animal production sector about the need to accurately monitor animal welfare conditions within the facilities used in the intensive systems.

One of the most important aspects in the definition of animal welfare is the environmental conditions of housing. Environmental control systems in animal housing are a very important tool to provide environmental conditions that allow for adequate levels of productivity and animal welfare (Cruz, 1997; Babot and Revuelta, 2009). However, environmental control of livestock facilities is typically based on rates/balance of heat and moisture production at predetermined ambient temperature levels. This traditional control method cannot reflect the true thermal animal's needs because it does not account some environmental, physiological and behavioural factors (such as air quality, animal surface temperature or animal feed intake).

In this sense, the main challenge for intensive production systems in the future is to monitor and control not only the environmental conditions (microclimate and emissions), but also the growth, behaviour, productivity and health (diseases) of the animals in large groups (Berckmans, 2017; Fournel et al., 2017; Vranken and Berckmans, 2017).

Precision livestock farming (PLF), defined as the application of technology engineering processes in livestock management, is the potential solution to respond to these challenges (Banhazi et al., 2012) once offers many innovative technologies and tools through which the animal response to housing environmental conditions can be continuously observed, monitored and controlled.

Precision livestock farming has used a lot of technological equipment (sensors, microphones and video cameras,

thermographic cameras, automatic scales, automatic feed stations, etc.) since the beginning of the 21th century. The information provided through this equipment can be subject to monitoring, allowing to demonstrate animal's feedback in relation to the environment, which can help farmers to control the productive process and management decisions (Fournel et al., 2017). The use of these technologies can also reduce production costs and make production systems more competitive (Berckmans, 2017), and animal and environment friendly.

The main goal of the AWARTECH was to develop a new tool (AWARTECH Smart Sensing platform) that would respond in real time to the environmental needs of animals through physiological, behavioural and productive indicators using smart-sensing technologies. The development of this tool was based on a facility for growing-finishing pigs.

2. Materials and Methods

The experimental work was developed in an environmental control room. The main goal of this phase was test/validate a set of equipment and parameters in order to develop a technological platform prototype.

After the experimental work the technological platform prototype developed was tested and evaluated in a commercial pig facility, where the animals were subjected to real environmental conditions.

The architecture of the technological component developed in AWARTECH Project (Figure 1) consisted of using different equipment for continually, automatically and real-time collection of environmental, productive, behavioural and physiological data.
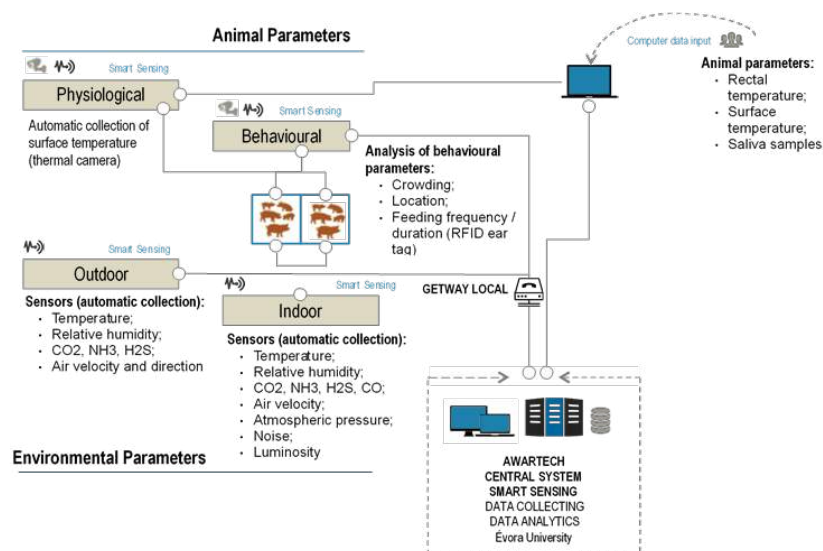

Figure 1. Lay-out of the technological component of Awartech Project

2.1. Structures and Equipment

To develop the platform, a pen with an area of around 12,0 m^2 was installed in the environmental control room. The pen had a manure pit and was equipped with an automatic feed station and two nipple drinking bowl. The floor was partially concrete cover with anti-slip tactile.

Environmental control was carried out through ventilation, heating and cooling systems. Ventilation system was compound by two vertical extractors fans. The air came into the facility through a false ceiling to protect the animals and left through the extractors (negative pressure). The heating system consisted of a conventional gas heater. The cooling of the facility was made by a nebulization system.

The environmental control room was equipped with different equipment and technologies as temperature, relative humidity and gas concentration sensors and video/thermal graphic cameras that allowed to record environmental, behavioural and physiological data.

2.2. Experimental design

In the experimental phase, three trials were carried out in the environmental control room at University of Évora. Three different conditions were set: Winter (W) – cold stress (trial 1), Thermoneutrality (TN) – thermal neutrality

(trial 2) and Summer (S) – hot stress (trial 3) (Table 1).

Table 1. Experimental environment set points

Environmental Conditions	Winter (W)	Thermoneutrality (TN)	Summer (S)
Temperature (ºC)	10 ± 2	18 ± 2	30 ± 2
Relative Humidity (%)	80	70	60

In each trail 8 female pigs of *Piétrain* x *Topigs Norsvin* (TN60) genotype were used whit an initial body weight around of 48 ± 3kg. Each animal had 1,5 m² of area in the pen. The animals were identified with an RFID ear tags system and each trail started after 15 days of habituation period in TN conditions (Tmean = 18 ± 2ºC and RHmean = 70%) and finished when the animals reached a commercial slaughter weight of around 95-105kg live weight.

2.3. Data collection

2.3.1.Environmental measurements

The environmental variables measured were temperature (T), relative humidity (RH), air velocity, gas concentration and noise/luminosity levels. This data collection was made continuously and in real time through an environmental control system (Webisense) and a data collector (Nidus).

2.3.2.Animal measurements

The productive data measured were initial and final body weight (BW) and feed intake (FI). These data were recorded using the electronic feed station, which through the RFID ear tag system, allowed to monitor and control individually, in each feeder access, the amount of food supplied and ingested (grams); number and time of visits to the feed station (h:m:s); and animal's weight (grams). This precision livestock farming tool allowed to calculate the average daily gain (ADG) and feed conversion rate (FCR).

The physiological data were measured manually and automatically. The rectal temperature was collected manually using a digital thermometer. In order to have a non-invasive method to monitor the animal surface temperature a thermal camera was used. The physiological data collection had as methodology the protocol described at Cruz et al., (2021).

The behavioural data was measured through video cameras strategically placed in the environmental room. An algorithm was developed in order to detect abnormal behaviours such as crowding/removal of animals. This algorithm receives video images and process frame by frame. The analyse process occur in two phases. Using a Delaunay triangulation method, the algorithm searches individual or group animal shapes and, after animal identification, records its position in the pen. In a second phase, in function of animal's position, the software calculates the crowding index developed (1 = crowding; 0 = removal).

3. Results and Discussion

3.1.1. Environmental conditions and Animal measurements

The environmental control system helped to control (more or less easily) climatic variations inside the environmental control room.

Inside and outside environmental conditions recorded in the experimental trials are presented in the next Table.

Table 2. Environmental conditions recorded in the experimental trials

	Environmental Conditions								
Conditions	t_0 Average (ºC)	t_0 max (°C)	t_0 min (°C)	t_i Average (ºC)	t_i max (°C)	t_i min (°C)	ΔT (°C)	RH_0 Average (%)	RH_i Average (%)
Winter	10.4	29.7	0.2	12.5	19.4	8.3	2.1	80	75
Thermoneutrality	18.8	44.1	3.7	20.7	24.9	16.0	1.9	65	74
Summer	26.2	45.7	12.0	28.9	33.3	23.2	2.7	56	63

T_0 = Outside temperature; Ti = Inside temperature; RH_0 = Outside relative humidity; RHi = Inside relative humidity.

Table 2 shows that the average temperatures and relative humidity recorded inside the environmental room were in accordance with project goals and represented real winter, thermoneutrality and summer conditions.

Other parameters recorded inside the environmental control room and with particular relevance in the animal welfare are presented in Table 3.

Table 3. Inside environmental parameters recorded in the experimental trials

Conditions	CO_2 (ppm)	Noise level (dB)	Luminosity level (lux)
Winter	882	67	23
Thermoneutrality	1120	65	177
Summer	1704	64	121

According with Table 3, the higher CO_2 concentration occurred in the summer condition. This can be explained because under high temperatures and low humidity levels (Table 2) the animals tends to increase their respiratory rate. Regarding the noise level, these values didn't variate between environmental conditions and wasn't possible to identify stress situations (levels > 85 dB). The luminosity level recorded in the winter was substantially different from the other conditions. It can be explained because in order to increase the thermal insulation at windows level the outside blinds were closed which decreased the light incidence inside the environmental control room.

Productive data recorded in the experimental trials are presented in Table 4:

Table 4. Productive data recorded in the experimental trials

Conditions	$BW_{initial}$ (kg)	BW_{final} (kg)	FI (kg/day)	ADG (kg/day)	FCR (kg/kg)
Winter	45.9	96.0	2.701	0.792	3.41
Thermoneutrality	45.9	103.4	2.560	0.930	2.75
Summer	49.4	98.7	2.310	0.859	2.69

In general, some environmental and productive data allow to understand that the environment had an influence on pig's performance and that animals improved their results under thermal comfort conditions. In addition, environmental control systems have demonstrated their efficiency to simulate environmental conditions and the ability to be a powerful tool to provide adequate housing and welfare conditions.

Physiological data recorded in the experimental trials are presented in the next Table:

Table 5. Rectal and surface temperatures recorded in the experimental trials

Conditions	Rectal temperature (ºC)	Surface temperature (ºC)
Winter	38.7	32.2
Thermoneutrality	39.0	35.9
Summer	39.2	36.9

This table demonstrates that rectal and surface temperatures have higher values in animals housed in summer conditions. These values are in accordance with expectations, since under conditions of high temperatures, pigs have difficulty in dissipating their body heat, which causes an increase in internal and surface temperature (Cruz, 1997). This effect is most evident in surface temperature.

Behavioural data recorded in the experimental trials are presented in the next Graph:
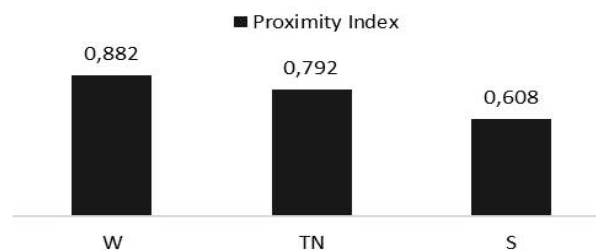
Graph 1. Proximity index recorded in the experimental trials

Based on this graph, it appears that the animals were more close in winter condition. This behaviour is very common in pigs that tend to huddle when subjected to low temperatures, in order to avoid loss of body heat to the surrounding environment. The opposite is verified in the summer condition, since the animals disperse in order to increase the heat exchange with the surroundings and to maintain their body temperature.

3.1.2.Awartech Smart Sensing Platform

The Awartech Smart Sensing Platform is a precision livestock farming tool developed in the AWARTECH Project aim and resulted from the integration in real-time, of data provided by the technological devices used in the experimental trials.

This platform is a WEB-based application used to view and control sensory systems and operates according GRID system. GRID is a data and IoT system that supports many protocols and is available to communicate with different systems/tools (thermal cameras, video cameras, environmental sensors, electronic feed stations, etc.). It allowed to register automatically/manual and continuously many variables related to animals and environment. The different parameters were recorded with variable periodicity and this information could be consulted in real time or in databases due to the ability to store all data over time

All of this information allowed that, according to the animal's feedback, the platform could control the environmental conditions (in real time and automatically) in order to promote the animal welfare.

The platform's automation processes were based on stream processing mechanisms. That is, the sensor data were available in real time when received on the platform. To develop these mechanisms, the Awartech Smart Sensing platform incorporated a rules engine that evaluated the environmental/animal data in real time and, according to the configured rules, could perform one or more actions on the environmental control system (ventilation, heating or cooling).

Automation mechanisms were one of the most difficult tasks to develop during the project due to the complexity of the animal-environment interactions. The major problem with this approach was the interconnectivity between the environmental parameters. As a physical system, when any parameter changed, the environmental conditions also changed. However, in terms of air quality, the results were quite satisfactory and this parameter revelled to be a promising indicator for providing animal welfare conditions.

4. Conclusions

The AWARTECH Project contribute to the scientific and technological advance of the pig sector through the development of a precision livestock farming tool that allows to assist productive systems, contributing to the future sustainable pig production.

The zootechnical results taken from the case study confirm the extraordinary influence that environmental conditions of housing have on animal production and welfare. These results contributed to the development and operation of the Awartech Smart Sensing Platform.

In general, the Awartech Smart Sensing platform operated according to expectations in the experimental trials and in the commercial pig facility. During the project development some expected problems occurred due to the complexity of technologies adopted. However, the tested technologies demonstrated great potential for use in intensive production systems.

Automation process based on animal and environmental real data is a pioneer approach that revelled to be, as expected, a difficult and complex process. However, the AWARTECH Project contributed to develop some technological knowledge that opens doors for future works, in particular the development of a comfort or animal welfare index. This index that will integrate animal and environment information could be the base for balanced actuation rules.

References

Babot, D. and Revuelta, M., 2009. *Ganado Porcino: Diseño de alojamientos e instalaciones*. Servet editorial, Zaragoza, Spain. pp.38-69.

Banhazi, T.M., Lehr, H., Black, J.L., Crabtree, H., Schofield, P., Tscharke, M. and Berckmans, D., 2012. Precision Livestock Farming: an international review of scientific and commercial aspects. International Journal of Agricultural and Biological Engineering 5:1-9. https://doi.org/10.3965/j.ijabe.20120503.001

Berckmans, D., 2014. Precision livestock farming technologies for welfare management in intensive livestock systems. Revue scientifique et technique, 33:189-196. https://doi.org/10.20506/rst.33.1.2273

Berckmans, D., 2017. General introduction to precision livestock farming. Animal Frontiers, 7:6-11. https://doi.org/10.2527/af.2017.0102

Cruz, V. F. (1997). Influência da estação do ano sobre as performances do porco em fase de crescimento e acabamento. Sua relação com a densidade de alojamento e a concentração energética da dieta. PhD thesis, University of Évora, Évora, Portugal.

Cruz, V.F., Rico, J.C. and Coelho, D.J.R., 2021. *E-Manual técnico do Projeto Awartech*. Universidade de Évora, Évora, Portugal.

Fournel, S., Rousseau, A.N. and Laberge, B., 2017. Rethinking environment control strategy of confined animal housing systems through precision livestock farming. Biosystems Engineering 155:96-123. https://doi.org/10.1016/j.biosystemseng.2016.12.005

Rojas-Downing, M.M., Nejadhashemi, A.P., Harrigan, T. and Woznicki, S.A., 2017. Climate change and livestock: Impacts, adaptation, and mitigation. Climate Risk Management, 16:145-163. https://doi.org/10.1016/j.crm.2017.02.001

Vranken, E., and Berckmans, D., 2017. Precision livestock farming for pigs. Animal Frontiers, 7:32-37. https://doi.org/10.2527/af.2017.0106